A Nanofactory Roadmap:

Research Proposal for a Comprehensive Diamondoid Nanofactory Development Program

This document internally DECLASSIFIED in 2025

HISTORICAL NOTE: This document was **completed and privately circulated in 2008**. It was **the first known effort to comprehensively describe one possible experimental technology development pathway that could directly lead to the first working nanofactory** capable of atomically precise manufacturing of products in macroscale quantities. The timescale for nanofactory development was originally estimated to require about 20 years of dedicated and intensive research effort. Elements of this initial proposal were later substantially simplified on the basis of subsequent research.

This document internally DECLASSIFIED in 2025

© 2008, 2025. Robert A. Freitas Jr. and Ralph C. Merkle. All Rights Reserved.

Cite as: Freitas RA Jr., Merkle RC. A Nanofactory Roadmap: Research Proposal for a Comprehensive Diamondoid Nanofactory Development Program. IMM Report No. 58, 2008/2025; http://www.imm.org/Reports/rep058.pdf.

Table of Contents

Mission Statement **8**

1. Executive Summary **9**

1.1 The Nature of the Goal **9**
1.2 Narrowing the Scope **12**
1.3 Disadvantages of Specificity **13**
1.4 A Specific Plan **14**
1.4.1 Phase I: Making Sure It Works 15
1.4.2 Phase II: Making a Production System 17
1.4.3 Phase III: Shrinking the System 17
1.4.4 Phase IV: Speeding Up the Shrunken System 18
1.4.5 Phase V: Assembling Parts at the Nanoscale 19
1.4.6 Phase VI: Getting Rid of the Phase II System 19
1.4.7 Phase VII: Debugging Plate-to-Plate Manufacturing 19
1.4.8 Phase VIII: Exponential Assembly 20
1.4.9 Phase IX: Ten Times Bigger Products and Manipulators 20
1.4.10 Phase X: Increase Mass Throughput by One Thousand-fold 21
1.4.11 Phase XI: Increase Product Size by One Hundred Thousand-fold 22
1.5 Conclusion **23**

2. Nanofactories: Brief Survey of the State-of-the-Art **24**

2.1 Nanofactory-Related Theoretical Work **25**
2.1.1 Merkle-Freitas Hydrocarbon Molecular Assembler (2000-2003) 31
2.1.1.1 Summary Description 31
2.1.1.2 Product Object Extrusion 34
2.1.1.3 Broadcast Architecture for Control 35
2.1.1.4 Hydrocarbon Assembler Subsystems 37
2.1.1.5 Floating Hydrocarbon Assemblers vs. Fixed Nanofactory Configurations 42
2.1.2 Zyvex Exponential Assembly (1999-2000) 42
2.1.3 Drexler Nanofactory (1991-1992) 49
2.2 Nanofactory-Related Experimental Work **57**
2.2.1 Moses Construction Machine (1999-2001) 57
2.2.1.1 Moses Self-Replicating Construction Machine 58
2.2.1.2 Scaling Analysis of the Moses Construction Machine 65
2.2.2 LEGO®-Based Assemblers (2001-present) 67
2.2.2.1 Chirikjian Group Self-Replicating Robots 69
2.2.2.2 Prototype 1 (2001) 69
2.2.2.3 Remote-Controlled Self-Replicating Robots (2002) 73
2.2.2.4 Semi-Autonomous Self-Replicating Robot (2002) 78
2.2.2.5 Chirikjian Group Autonomous Replicators (2002-present) 79
2.2.3 Rapid Prototyping, Solid Printing and 3D Fabbing 88
2.2.3.1 Three-Dimensional Solid Printing 88
2.2.3.2 RepRap, Fab@Home and Related Projects 105
2.2.3.3 3-D Nanostructure Fabrication via Focused-Ion-Beam CVD 113
2.2.4 Zyvex Atomically Precise Manufacturing (2003-present) 119

2.3 Atomically Precise UHV/Tip-Based Molecular Manufacturing 120
2.3.1 Diamondoid Mechanosynthesis (DMS) 123
2.3.2 Designing a Minimal Toolset for DMS 130
2.3.3 Building the First Mechanosynthetic Tools 137
2.3.4 Next Generation Tools and Components 138
2.3.5 Nanofactory Strategies for Molecular Manufacturing 142
2.3.6 Atomically Precise Manufacturing of Macroscale Products 146

3. Nanofactory Development Program Technical Research Milestones 151

3.1 Overview of Major Program Milestones 152

3.2 Phase I: Macroscale Fabrication Workstation (MFW) 155
3.2.1 Description of the MFW 155
3.2.1.1 General Description of the MFW 155
3.2.1.2 High-Precision SPM-Based Tip Positioning Systems 157
3.2.1.3 Repeatable Picometer Positional Accuracy in SPM-Based Systems 163
3.2.1.4 Ultra-Sharp and Atomically Precise SPM Tips 170
3.2.1.5 SPM-Based Multi-Tip and Multi-DOF Systems 182
3.2.1.6 Continuous Sensory Feedback Not Needed by the MFW 192
3.2.1.7 Operation of the MFW 194
3.2.1.8 Reliability of MFW Operation 199
3.2.2 Task I-1: Design and Simulate DMS Tooltips, Surfaces, Reactions, and Reaction Sequences 202
3.2.2.1 Design and Simulation of DMS Tooltips 202
3.2.2.2 Design and Simulation of Tooltip-Workpiece Interactions 203
3.2.2.3 Design and Simulation of Tool-Tool Interactions 204
3.2.2.4 Simulation of Mechanosynthetic Interactions in Realistic Vacuum Environment 204
3.2.2.5 Design and Simulation of DMS Reaction Sequences 205
3.2.2.6 Rearrangement and Reconstruction of Workpiece Surfaces 207
3.2.2.7 Design and Simulation of Molecular Feedstock Presentation Systems for DMS 211
3.2.2.8 Design Procedures for the Experimental Fabrication of DMS Tooltips 211
3.2.2.9 Investigate Availability of Natural Diamondoid Nanoparts for Testing and Fabrication 212
3.2.2.10 Investigate Possible Bulk Chemical Synthesis of Atomically Precise 3D Diamondoid Nanoparts 213
3.2.2.11 Improve Software and Analytical Tools 218
3.2.3 Task I-2: Design, Simulate and Test Automated Reaction Sequence Control Software 222
3.2.3.1 NIST Autonomous Atom Assembler 223
3.2.3.2 EPSRC Matter Compiler Project 225
3.2.4 Task I-3: Demonstrate Simple DMS Reaction Sequences Using Existing SPM 230
3.2.5 Task I-4: Build 1-Tip 3-DOF Picopositioning SPM System to Demonstrate Simple DMS Reaction Sequences 233
3.2.6 Task I-5: Verify Need for 4 Tips and 5 DOFs 235
3.2.7 Task I-6: Add In-Chamber Toolrack to Enable Endogenous Tooltip Changeout 235
3.2.8 Task I-7: Build 1-Tip 4-DOF Picopositioning System and Demonstrate Additional DMS Reaction Sequences 236
3.2.9 Task I-8: Build 2-Tip 5-DOF Picopositioning System and Demonstrate Additional DMS Reaction Sequences 237
3.2.10 Task I-9: Build 4-Tip 5-DOF Picopositioning System and Demonstrate Additional DMS Reaction Sequences 237

3.2.11 Task I-10: Demonstrate Hydrocarbon Product Object Fabrication Integrally on Fabrication Surface using MFW 238
3.2.12 Task I-11: Demonstrate Hydrocarbon-Plus Product Object Fabrication Integrally on Fabrication Surface using MFW 239

3.3 Phase II: Macroscale Manufacturing Workstation (MMW) 241

3.3.1 Description of the MMW 241
3.3.1.1 Operation of the MMW 242
3.3.1.2 MMW Productivity 243
3.3.1.3 Reliability of MMW Operation 244
3.3.2 Task II-1: Establish Standard Registry of Diamondoid Nanomechanical Parts and Processes 245
3.3.2.1 Mission Statement and Rationale 245
3.3.2.2 Parts Registry 248
3.3.2.3 Process Registry 253
3.3.2.4 Initial Registry Set-Up 255
3.3.3 Task II-2: Design Nanoparts and Nanodevices for the Registry 257
3.3.4 Task II-3: Demonstrate DMS Fabrication on a Release Surface 260
3.3.5 Task II-4: Design and Demonstrate Reversible Tip-Mounted Grippers 262
3.3.6 Task II-5: Design and Demonstrate Releasable Rechargeable DMS Toolheads 264
3.3.7 Task II-6: Design and Demonstrate Toolrack for DMS Toolheads 264
3.3.8 Task II-7: Design and Demonstrate Fabrication Sequences for Simple Diamondoid Nanoparts 265
3.3.9 Task II-8: Design and Demonstrate Fabrication Sequences for Complex Diamondoid Nanoparts and Other Specialized Structures 269
3.3.10 Task II-9: Design and Demonstrate Assembly Sequences for Assembling Diamondoid Nanoparts into Nanodevices 271

3.4 Phase III: First-Generation Nanoscale Fabrication Workstation (NFW) 275

3.4.1 Description of the NFW First-Generation Workstation 275
3.4.1.1 Basic Description of the NFW 275
3.4.1.2 Thermal Positional Stability of DMS Manipulators 285
3.4.1.3 Pick-and-Place vs. Sensory Feedback 287
3.4.1.4 Manipulator Speed and NFW Productivity 288
3.4.1.5 Waste Heat Generated by Chemical Transformations During DMS 290
3.4.1.6 Reliability of NFW Manufacture 290
3.4.2 Task III-1: Design and Simulate First-Generation NFW 292
3.4.3 Task III-2: Prepare Multielectrode Assembly Surface 295
3.4.4 Task III-3: Fabricate and Assemble NFW Nanoparts and Nanodevices using Phase II System 304
3.4.5 Task III-4: Assemble First-Generation NFW using Phase II System 305
3.4.6 Task III-5: Operate First-Generation NFW using Phase II System 306

3.5 Phase IV: Second-Generation Nanoscale Fabrication Workstation (NFW-2) 308

3.5.1 Description of the NFW-2 Second-Generation Workstation 308
3.5.1.1 Overall Strategy of the Bulk Feedstock Supply System (BFSS) 309
3.5.1.2 Primary Byproduct Molecule: Molecular Hydrogen 310
3.5.1.3 Primary Hydrocarbon Feedstock Molecule: Ethylene 314
3.5.1.4 Secondary Feedstock or "Vitamin" Molecule: Germane 325
3.5.1.5 Binding Sites for NFW-2 Feedstock and Byproduct Gases 330
3.5.1.6 Conceptual Design of the BFSS 335
3.5.1.7 Operation of the NFW-2 Workstation 344
3.5.1.8 Reliability of NFW-2 Manufacture and Operation 350
3.5.2 Task IV-1: Design and Simulate First-Generation BFSS 352

3.5.3 Task IV-2: Prepare Multielectrode Assembly Surface 353
3.5.4 Task IV-3: Fabricate and Assemble BFSS Nanoparts and Nanodevices using Phase II System 354
3.5.5 Task IV-4: Assemble BFSS using Phase II System..... 355
3.5.6 Task IV-5: Operate First-Generation BFSS using Phase II System 356
3.5.7 Task IV-6: Design and Simulate NFW-2 356
3.5.8 Task IV-7: Fabricate and Assemble NFW-2 Nanoparts and Nanodevices using Phase II System..... 357
3.5.9 Task IV-8: Assemble NFW-2 using Phase II System..... 358
3.5.10 Task IV-9: Operate NFW-2 Endogenously 359
3.5.11 Task IV-10: Win Feynman Grand Prize 361

3.6 Phase V: Nanoscale Assembly Workstation (NAW)..... 363

3.6.1 Description of the NAW 363
3.6.1.1 Basic Description of the NAW 363
3.6.1.2 Thermal Positional Stability of NAW Manipulators 368
3.6.1.3 Manipulator Speed and NAW Productivity 370
3.6.1.4 Reliability of NAW Manufacture 371
3.6.2 Task V-1: Design and Simulate NAW 373
3.6.3 Task V-2: Prepare Multielectrode Assembly Surface 374
3.6.4 Task V-3: Assemble NAW Nanodevices using Phase II System 374
3.6.5 Task V-4: Assemble NAW using Phase II System..... 375
3.6.6 Task V-5: Operate NAW using Phase II System..... 376

3.7 Phase VI: Nanoscale Manufacturing Workstation (NMW)..... 378

3.7.1 Description of the NMW 378
3.7.1.1 Structure of the NMW 379
3.7.1.2 Operation of the NMW 381
3.7.1.3 Productivity of the NMW 381
3.7.1.4 Reliability of NMW Manufacture and Operation 382
3.7.2 Task VI-1: Design and Simulate NMW 384
3.7.3 Task VI-2: Prepare Multielectrode Assembly Surface 385
3.7.4 Task VI-3: Assemble NMW Nanodevices using Phase II System 386
3.7.5 Task VI-4: Assemble NMW using Phase II System..... 386
3.7.6 Task VI-5: Operate NMW Endogenously 388

3.8 Phase VII: Demonstrate Plate/Plate Exponential Manufacturing 390

3.8.1 Description of Plate/Plate Exponential Manufacturing with NMW-2..... 390
3.8.1.1 Plate/Plate Exponential Manufacturing using NMW-2 390
3.8.1.2 Van der Waals and Other Forces Between Plates 393
3.8.1.3 Reliability of NMW-2 Operation..... 398
3.8.2 Task VII-1: Redesign/Simulate NMW for Plate/Plate Replication 402
3.8.3 Task VII-2: Prepare Multielectrode Assembly Surfaces 404
3.8.4 Task VII-3: Build Plate Handler for Precise Parallel Positioning of Two Flat Plate Surfaces 405
3.8.5 Task VII-4: Demonstrate Plate/Plate Mechanical Operations Between Two Parallel Plates..... 408
3.8.6 Task VII-5: Replicate NMW-2 onto Opposing Plate Surface 408
3.8.7 Task VII-6: Shift Opposing Plate Positions, Replicate NMW-2 Again 409
3.8.8 Task VII-7: Increase NMW-2 Productivity by Tenfold 410

3.9 Phase VIII: Exponentially Manufacture 1024 NMW-2 Wafers 412

3.9.1 Description of the NMW-2 Wafer 412
3.9.1.1 Structure of the NMW-2 Wafer 412

3.9.1.2 Operation of the NMW-2 Wafer 414
3.9.1.3 Reliability of NMW-2 Wafer Operation 414
3.9.2 Task VIII-1: Design and Simulate Whole-Wafer Surface and Process 415
3.9.3 Task VIII-2: Prepare Whole-Wafer Multielectrode Assembly Surface 416
3.9.4 Task VIII-3: Replicate NMW-2 on Both Wafers to Full Monolayer Coverage 428
3.9.5 Task VIII-4: Build Additional Plate Handlers and Replicate 1024 NMW-2 Wafers 429

3.10 Phase IX: Micro-Assembler Manipulator (MAM) and Micro-Assembler Array (MAA) 431

3.10.1 Description of the MAM and MAA 431
3.10.1.1 Description of the Micro-Assembler Manipulator (MAM) 431
3.10.1.2 Description of the Micro-Assembler Array (MAA) and Buildout of the MAA Wafer 435
3.10.1.3 Reliability of MAM/MAA Manufacture and Operation 437
3.10.2 Task IX-1: Design and Simulate MAM and MAA 438
3.10.3 Task IX-2: Prepare Multielectrode MAM Test-Assembly Surfaces for Experimentation 441
3.10.4 Task IX-3: Build and Operate First MAM 441
3.10.5 Task IX-4: Prepare Whole-Wafer Multielectrode MAA Wafer Surfaces 442
3.10.6 Task IX-5: Build and Operate One MAA Wafer 442
3.10.7 Task IX-6: Build Out 200 MAA Wafers and 200 MAA Handlers 443
3.10.8 Task IX-7: Modify MAMs and MAA Wafers for High-Frequency Operation 444

3.11 Phase X: First-Generation Nanofactory (FGN) 445

3.11.1 Basic Architecture of the FGN 445
3.11.2 Description of the First Production Layer 448
3.11.2.1 Tanks and Rotors 449
3.11.2.2 Manipulators 449
3.11.2.3 Foundation Blocks 449
3.11.2.4 Power and Control Lines 450
3.11.2.5 Support Frame 459
3.11.2.6 Catacombs 461
3.11.2.7 Ciliary Transport Array (CTA) 463
3.11.2.8 Stovepipes 466
3.11.2.9 Cooling Channels 469
3.11.2.10 Maintaining UHV Inside the FGN During Operation 475
3.11.2.11 Scaling Analysis Summary with Atom Count 475
3.11.3 Description of the Second Production Layer and FGN 476
3.11.3.1 Inspection Plane 477
3.11.3.2 Routing Plane 482
3.11.3.3 Assembly Plane 484
3.11.3.4 Export Plane 490
3.11.3.5 Scaling Analysis Summary with Atom Count 492
3.11.3.6 Reliability of FGN Manufacture and Operation 494
3.11.4 Task X-1: Design, Model and Simulate FGN Components, Operations, and Process of Manufacture 495
3.11.5 Task X-2: Manufacture FGN Base Plate 499
3.11.6 Task X-3: Build 24 Nanotube Wiremaker Wafers 500
3.11.7 Task X-4: Build FGN Assembly System and Vacuum Room 501
3.11.8 Task X-5: Build another 512 NMW-2 Plate Handlers 505
3.11.9 Task X-6: Improve Plate Handling Speed by 50-fold 505

3.11.10 Task X-7: Manufacture and Install 1000 Fabrication Planes and 4 Assembling Planes on FGN Base Plate 505
3.11.10.1 Manufacturing NMW-3 Modules 505
3.11.10.2 Loading the MAAs with NMW-3 Modules 506
3.11.10.3 Loading MAAs into the Inspection Rack 506
3.11.10.4 Unloading the Rack and Installing NMW-3 Parcels 508
3.11.10.5 Assembly of FGN Production Stacks and Total Assembly Time 508
3.11.11 Task X-8: Manufacture, Attach and Test Appurtenant FGN Support Equipment 509
3.11.12 Task X-9: Demonstration of Diamondoid FGN Production 509

3.12 Phase XI: Second-Generation Nanofactory (SGN) 510

3.12.1 SGN Productivity, Products, and Profitability 510
3.12.2 Basic Architecture of the SGN 515
3.12.3 Description of the Third Production Layer and SGN 516
3.12.3.1 Parts Feed Into the Third Production Layer 516
3.12.3.2 Dekamicro-Assembly Manipulator (DAM) Plane 516
3.12.3.3 Hectomicro-Assembly Manipulator (HAM) Plane 517
3.12.3.4 Kilomicro-Assembly Manipulator (KAM) Plane 518
3.12.3.5 Centimeter-Assembly Manipulator (CAM) Plane 519
3.12.3.6 Vacuum Export System (VES) 520
3.12.3.7 SGN Scaling Analysis Summary with Atom Count 523
3.12.3.8 Characteristics and Limitations of SGN-Buildable Products 526
3.12.3.9 Reliability of SGN Manufacture and Operation 530
3.12.4 Task XI-1: Design, Model and Simulate SGN Components, Operations, Process of Manufacture, and Products 531
3.12.5 Task XI-2: Manufacture New FGN with Open Export Plane 532
3.12.6 Task XI-3: Build SGN Assembly System and Vacuum Room 533
3.12.7 Task XI-4: Manufacture and Install 4 Macroassembling Planes and VES on Modified FGN Base 533
3.12.8 Task XI-5: Manufacture, Attach and Test Appurtenant SGN Support Equipment 534
3.12.9 Task XI-6: Demonstration of Diamondoid SGN Production 535
3.12.10 Task XI-7: Design and Build an Efficient Third-Generation Nanofactory (TGN) 535

4. Program Development Timelines 538

4.1 Four Scenarios for Nanofactory Development 538
4.2 An Efficient Timeline for Nanofactory Development 539
4.3 Summary and Conclusions 539

Mission Statement

"If one does not know to which port one is sailing, no wind is favorable."
– Seneca

The long-term program objective of a nanofactory development program would be to design, and ultimately to build, a working diamondoid nanofactory.

The diamondoid nanofactory is a proposed compact molecular manufacturing system, possibly small enough to sit on a desktop, that could build a diverse selection of large-scale atomically precise diamondoid products. The nanofactory is potentially a high quality, extremely low cost, and very flexible manufacturing system for making microscale and macroscale products out of "diamondoid" materials. These materials include crystalline and nanocomposite diamond, graphene structures including fullerenes and carbon nanotubes, polyyne and related strong carbon chain structures, and other similarly hard ceramic materials possibly including silicon carbide, silicon nitride, boron nitride and the like.

Accompanying documents include:

Freitas RA Jr. Molecular Workstation Roadmap I: Survey of Key Technologies Needed to Perform Positionally Controlled Diamondoid Mechanosynthesis using a Molecular Workstation**.** IMM Report No. 59, 2009/2025; http://www.imm.org/Reports/rep059.pdf.

and

Freitas RA Jr. Molecular Workstation Roadmap II: Survey of Single-Atom Tips (SATs) for Diamondoid Mechanosynthesis**.** IMM Report No. 60, 2010/2025; http://www.imm.org/Reports/rep060.pdf.

1. Executive Summary

The purpose of a Diamondoid Nanofactory Development Program is to speed the development of MNT (Molecular Nanotechnology).

In the following we will discuss in more detail what MNT is and what it means to speed its development. We propose not simply a generic goal, but a very specific goal and developmental pathway based on specific assumptions about how best to proceed – assumptions that have only gradually emerged over many years of research in this field.

Before we describe the development pathway in greater detail, we must first address the fundamental question – what is MNT?

1.1 The Nature of the Goal

The general goal of MNT is the ability to inexpensively arrange atoms in most of the ways permitted by physical law. Achieving this general goal involves the ability to control molecular structures involving the approximately 100 elements in the periodic table. While this broad goal is both desirable and appears feasible, directly targeting this objective would require that we develop and analyze a complete set of chemical reactions involving about 100 elements and all the ways they could be added to complex growing molecular structures – and even a small patch of half a dozen atoms on the surface of such a structure could have over $(100)^6$ or about a trillion (10^{12}) different possible arrangements of the various elements.

By contrast, a relatively small subset of the periodic table could be used to build what would be, by today's standards, a truly remarkable range of highly valuable structures (powerful computers, light strong materials, medical nanodevices, and a host of other manufactured products; see Section 2.3.6).

This leads to the following more limited but more tractable goal: pick a small subset of elements that still encompasses structures of great value, analyze the chemical reactions needed to fabricate such structures in full detail, and develop systems to manufacture them.

The present proposal uses only three elements: carbon, hydrogen, and germanium.

The purpose of including carbon and hydrogen is simple: structures made from these two elements include diamond, graphite, fullerenes, buckytubes, lonsdaleite, polyynes (molecular rods), and a bewildering array of variants of these structures. The materials properties of this class of materials are either the best or close to the best in a wide range of categories: strength, lightness, band gap, electron and hole mobility, thermal properties, and others.

The hydrocarbons are also at the heart of the entire field of organic chemistry, a field which includes a remarkable range of structures that have proven their utility in almost every field of human endeavor.

The inclusion of germanium is a bit less obvious, but comes about from the need for the specified subset to include sufficient catalytic flexibility to synthesize the fabrication of its own members.

Synthesizing the full range of hydrocarbons using only other hydrocarbons proved challenging, and the inclusion of germanium proved sufficient to let us develop a full set of reactions.

How to synthesize diamond. Simply settling on a desirable subset of the elements is insufficient. It still remains to discuss the chemical reactions to be used and the context in which those reactions take place. In living systems, the context is liquid water and the chemical reactions must be so arranged that when chance encounters of reactants take place they will react appropriately, and when chance reactions of non-reactants take place, they will not react. Note that this lack of reaction of randomly mixed reactants is crucial to the biological enterprise. Much of chemistry is devoted to avoiding undesired side reactions.

The context for the reactions used in the present approach is very different. This change of context makes the approach seem unfamiliar to those unacquainted with it. The first major change is the way in which we bring reactants into contact with each other, and the way in which we avoid undesired side reactions.

Positionally controlled molecular tools. At this point we introduce the concept of *positional control*. We take it for granted that, when we build things, we use tools. These tools are held, positioned, and applied in a flexible manner. A hammer, for example, is used to pound a nail that has been positioned over a piece of wood into which it is driven. The nail is held in one hand (a positional device) while the hammer is applied with the other (a second positional device). Our hands are able to pick up, put down, and apply a variety of tools and parts, letting us flexibly manufacture many structures. More generally, positional devices that hold parts, move parts, join parts, and modify parts are used in a flexible way to make the vast array of manufactured products in the world around us.

The use of positional control at the molecular scale is still relatively new. At the scale of atoms and molecules we are much more used to the idea of *self assembly*. This process may be likened to building a radio by putting all the parts of a radio into a bag, shaking the bag, and pulling out an assembled radio. While this might sound like a hard way to build a radio, it is a method heavily used at the molecular scale by living systems and in almost all of today's chemistry to assemble finished structures from their component parts.

The concept of building our modern world without hands and without the ability to hold and position parts is one that seems remarkably implausible. The use of positionally controlled tools at the human scale has proven critical to almost all of modern manufacturing. In this proposal we are applying this intuition at the molecular scale. We expect that the use of positionally controlled molecular tools will bring us the same kind of flexibility in fabricating molecular structures that it has brought at the more familiar scale of contemporary manufacturing, and therefore open an entirely new range of possibilities.

More specifically, we propose to use molecular tools synthesized from H, C and Ge to make both more molecular tools and the wide range of hydrocarbons described above. We propose to use these tools in UHV (Ultra High Vacuum), and to position them within a fraction of an atomic diameter with various positional devices. Initially, these positional devices will look like evolutionary improvements of SPMs (Scanning Probe Microscopes), able to position the tools to within a fraction of an atomic diameter. Later, as our abilities develop, we will use molecular positional devices – robotic arms little more than 100 nanometers in size. While these molecular positional devices will be great improvements on the devices we use initially (most dramatically in their speed of operation) they will still carry out the fundamental task of positioning and moving specific molecular tools through specified trajectories.

Which brings us to the obvious question: what are these molecular tools?

The answer is in *A Minimal Toolset for Positional Diamond Mechanosynthesis*[1] by Freitas and Merkle (from which the following discussion is taken).

The proposed tools are illustrated in Figure 1-1, below.

Figure 1-1. A minimal toolset for diamond mechanosynthesis, including primary, auxiliary, and compound tools

(A) HAbst tool	**(B) HDon tool**	**(C) HTrans tool**	**(D) DimerP tool**
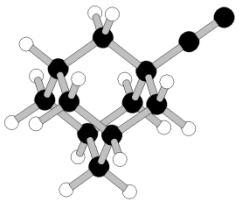	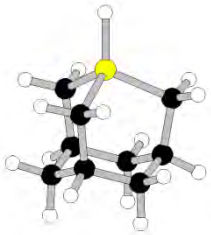	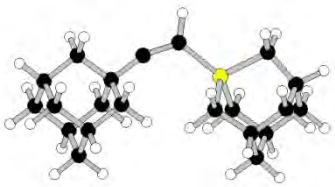	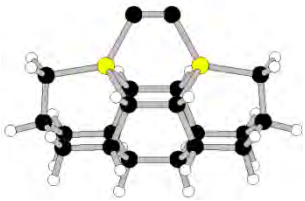

(E) AdamRad Handle	**(F) GeRad Handle**	**(G) Methylene tool**	**(H) Germylmethylene tool**	**(I) Germylene tool**
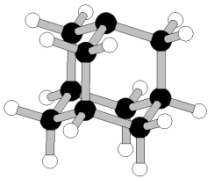	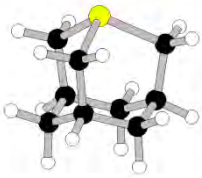	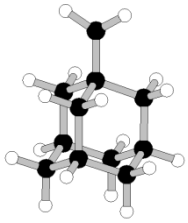	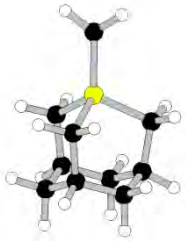	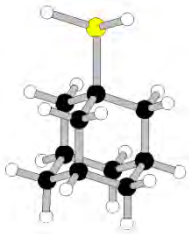

The abstract of that paper says:

Abstract. This paper presents the first theoretical quantitative systems level study of a complete suite of reaction pathways for scanning-probe based ultrahigh-vacuum diamond mechanosynthesis (DMS). A minimal toolset is proposed for positionally controlled DMS consisting of three primary tools – the (1) Hydrogen Abstraction (HAbst), (2) Hydrogen Donation (HDon), and (3) Dimer Placement (DimerP) tools – and six auxiliary tools – the (4) Adamantane radical (AdamRad) and (5) Germyladamantane radical (GeRad) handles, the (6) Methylene (Meth), (7) Germylmethylene (GM), and (8) Germylene (Germ) tools, and (9) the Hydrogen Transfer (HTrans) tool which is a simple compound of two existing tools (HAbst+GeRad). Our description of this toolset, the first to exhibit 100% process closure, explicitly specifies all

[1] Robert A. Freitas Jr., Ralph C. Merkle, "A Minimal Toolset for Positional Diamond Mechanosynthesis," J. Comput. Theor. Nanosci. 5(May 2008):760-861.

reaction steps and reaction pathologies, also for the first time. The toolset employs three element types (C, Ge, and H) and requires inputs of four feedstock molecules – CH_4 and C_2H_2 as carbon sources, Ge_2H_6 as the germanium source, and H_2 as a hydrogen source. The present work shows that the 9-tooltype toolset can, using only these simple bulk-produced chemical inputs: (1) fabricate all nine tooltypes, including their adamantane handle structures and reactive tool intermediates, starting from a flat passivated diamond surface or an adamantane seed structure; (2) recharge all nine tooltypes after use; and (3) build both clean and hydrogenated molecularly-precise unstrained cubic diamond C(111)/C(110)/C(100) and hexagonal diamond surfaces of process-unlimited size, including some Ge-substituted variants; methylated and ethylated surface structures; handled polyyne, polyacetylene and polyethylene chains of process-unlimited length; and both flat graphene sheet and curved graphene nanotubes. Reaction pathways and transition geometries involving 1620 tooltip/workpiece structures were analyzed using Density Functional Theory (DFT) in Gaussian 98 at the B3LYP/6-311+G(2d,p) // B3LYP/3-21G* level of theory to compile 65 Reaction Sequences comprised of 328 reaction steps, 354 unique pathological side reactions and 1321 reported DFT energies. The reactions should exhibit high reliability at 80 K and moderate reliability at 300 K. This toolset provides clear developmental targets for a comprehensive near-term DMS implementation program.

The paper describes not only the tools, but all the reactions involved in fabricating a new tool set from an existing tool set, as well as the reactions involved in fabricating desirable stiff hydrocarbons.

As the reader may have noticed, the ability to use a few molecular tools to build a few molecular structures is not, by itself, going to let us build large numbers of macroscale objects. The issue of scaling up is an integral part of this program proposal, and is discussed below.

1.2 Narrowing the Scope

A *Minimal Toolset for Positional Diamond Mechanosynthesis* provides a very specific answer to the question: "What is the goal of the project?" The answer: to develop and utilize the described molecular tools in a context that permits them to inexpensively fabricate a wide range of manufactured products made from H, C and Ge.

The original definition of MNT was the ability to inexpensively arrange atoms in most of the ways permitted by physical law. This general target still provides ample opportunity for confusion about the precise nature of the goal. We have replaced that general and very broad target with a much more specifically defined target, though a target which is more limited in scope.

(1) Rather than using the full range of elements in the periodic table, we have confined ourselves to three.

(2) Rather than leaving open the nature of the chemical reactions involved in the fabrication process, we have defined an initial set of nine molecular tools and 65 reaction sequences able to fabricate an initial very wide range of structures.

(3) Rather than leaving the fabrication environment unspecified, we specify the use of vacuum and positionally controlled tools.

Given the specificity of the reactions involved, we are now in a position to seek quantitative answers to such questions as: (1) what temperature is required to achieve a given reliability, (2) what accuracy is required of the positional devices, (3) how many degrees of freedom must the positional devices have, (4) what force must the positional devices be able to apply, and (5) a wide range of other critical questions.

And, because the proposed tools are highly reactive ("promiscuous" is a term sometimes used in chemistry for molecules that readily react with many other types of molecules) we have also, by focusing on positional control, explained why these reactive tools do not react with each other and the environment within which they find themselves: they are positionally controlled. Much as a hot soldering iron does not react with the workbench or random parts of a PC board, these highly reactive molecular tools react only when and where desired because the rest of the time they are positioned away from anything that might react with them.

Again, having a specified set of molecular tools and a specified set of reactions for using those tools provides a level of clarity about the goal which is unprecedented. Such clarity is critical in keeping a development program focused on the objective, particularly when that objective is long term.

1.3 Disadvantages of Specificity

While we have focused on the advantages of narrowing the scope, there are disadvantages. The primary disadvantage is that the more we focus on a particular developmental pathway, the greater the risk that a flaw in that particular pathway will disrupt developments. For example, if we set the goal of going from San Francisco to New York and don't specify exactly how we are going to do it, then we're free to consider flying, driving, boating, hitchhiking, or numerous other possible methods. But when we propose to make the trip by driving along a specific route, we can find our plans obstructed by traffic jams, washed-out roads, flat tires, accidents, and other specific problems. Thus, the vaguer claim that travel from San Francisco to New York is feasible is (perhaps surprisingly) more likely to be true than the specific claim that driving along a particular route is feasible. On the other hand, if we want to reach New York we'll eventually have to follow some specific path (with whatever risks that particular path might impose).

While narrowing the scope makes it easier to accomplish the objective, it also leaves open the question of how, once the narrowed objective has been attained, to then broaden the scope to include the original objectives of MNT. While the focus of this proposal is on development of the more specific system involving C, Ge and H (the Phase XI system), once that system has been built the further rapid evolutionary development of MNT is expected (though not described in this document). Having once achieved the ability to fabricate a wide range of stiff hydrocarbons, the incremental addition of additional molecular tools, additional elements, and additional capabilities is expected. The high value of such additions, coupled with the expected profits generated using the initial system, insure that incremental improvements will be eagerly sought and fully funded. By analogy, in today's semiconductor industry incremental improvements in speed, size, reliability, and cost are generally known to be valuable, are pursued vigorously by multiple competing vendors, and occur with remarkable regularity. Once the Phase XI system is in place, we expect that strong financial incentives and competitive pressures will insure its continued improvement in terms of energy efficiency, speed, reliability, diversity of employable chemical elements, and other performance parameters.

Might a pathway to MNT other than the one described here prove superior? While this could be possible, at the present time we're unaware of any alternative proposal that is specified in sufficient detail to permit a meaningful comparison.

1.4 A Specific Plan

Before going into the specific phases of the plan, it is useful to consider some of the basic principles that underlie it.

One of the fundamental principles is that of positional control. Initially, positional control is provided by existing SPMs and devices derived from today's SPMs. These are large (certainly large on the molecular scale) and few in number (one can readily envision a few SPMs, or even a few dozen, but hundreds and thousands of conventional SPMs start to become more expensive – though research using MEMS-based SPM systems is promising in this regard).

Starting in Phase III, these first SPM-like devices are used to build small positional devices. We need small positional devices because we need many of them – by Phase XI we are using well over ten trillion in a single system with the anticipated need for more as the technology progresses further. More specifically, we propose using sub-micron Stewart platforms (or some variant, such as a double tripod) starting in Phase III and continuing through Phase XI. Stewart platforms are attractive because they provide high stiffness (important in reducing positional uncertainty caused by thermal noise) with a smaller atom count (important if we are building them using unit operations that modify one or a few atoms at a time).

Control signals for the electrostatic motors that actuate the Stewart platforms will come from wires. Electronic control is widespread and well understood, and has advantages over other proposals that have been made (acoustic, optical, etc). Wires combine good bandwidth, the ability to use multi-wire bundles to individually control multiple actuators, and a large existing infrastructure both to make very small wires and to provide the complex sequence of control signals needed.

As we increase the number of Stewart platforms, we lay them out in two dimensional planes. This is primarily because the semiconductor industry is expert at producing wafers (which are largely two dimensional) that could provide control signals for our Stewart platforms. In this way, we leverage the ability of the semiconductor industry to manufacture large wafers (tens of centimeters) having small feature sizes (tens of nanometers) which can route complex control signals to multiple Stewart platforms. Each wafer has large numbers of specifically designed sites, each site accommodating a cluster of Stewart platforms and other molecular machines that can act together to build yet more clusters. We call these clusters of molecular machines Nanoscale Manufacturing Workstations, or NMWs.

In general, we propose that large fairly conventional macroscale positional devices build the first atomically precise molecular machines, and eventually build the first atomically precise NMWs. These first NMWs build more NMWs and attach them to specially prepared sites on the surface of a wafer (the wafer being made with bulk technology). The sites on the wafer provide the control signals and power to actuate the new NMWs, which are used to build yet more NMWs which are attached to yet more open sites, and so forth.

Eventually, we have multiple wafers covered with submicron NMWs, able to manufacture tens of grams of atomically precise structures generally similar to diamond, fullerenes, and the like. In

the last two phases, Phase X and Phase XI, we use this ability to replace the (atomically imprecise) wafers with an atomically precise support infrastructure which substantially improves performance.

While this describes the general philosophy for control and power, we must also distribute feedstock molecules to be used by the NMWs in their mechanosynthetic operations.

Initially, we do this by presenting the feedstock as individual molecules bound to a surface. The positional devices can then pick up the feedstock molecules and perform further operations on them.

Starting in Phase IV, we provide feedstock molecules by filling the work environment with gaseous versions of ethylene and germane. Molecular binding sites are required to bind to the feedstock molecules, which are then stored as compressed gas in small (a few hundred nanometer) tanks. The tanks and binding sites are part of the molecular machinery incorporated into each NMW. The work environment is then evacuated or "baked out," leaving a UHV environment suitable for the mechanosynthetic operations which take place in vacuum. The feedstock molecules stored in the tank are removed, molecule by molecule, and bound to an appropriate tool tip on a Stewart platform, at which point they can participate in further mechanosynthetic steps.

Flooding the work environment with gaseous feedstock molecules is a "scalable" process, useful for NMW populations from one workstation up to trillions or more.

Finally, in Phase X, we replace the wafer and the tanks with a more sophisticated support structure that continuously provides feedstock molecules to individual NMWs. This continues in Phase XI, the final phase described in detail in this technology development program.

1.4.1 Phase I: Making Sure It Works

The primary purpose of Phase I is to validate the core assumptions of MNT using the most readily accessible experimental and theoretical approaches.

Today, we cannot build atomically precise three dimensional structures using SPMs (Scanning Probe Microscopes). While experimental work has demonstrated the ability to arrange atoms and molecules on a surface in atomically precise patterns, building three dimensional structures has not been demonstrated. To pursue the approach outlined above, the first and most obvious step is to develop an SPM system able to carry out the basic reactions described in A *Minimal Toolset for Positional Diamond Mechanosynthesis*.

We expect this will be experimentally challenging.

Given the specific reactions outlined, however, we can now initiate a dialog with experimentalists. The paper was published in April 2008, and some initial contacts have already been made. We plan to identify laboratories whose current work seems closest to the desired capabilities, and then discuss with them what is needed to encourage them to pursue specific experimental objectives in directions helpful to our program. This minimizes startup time, reduces the overhead of establishing an experimental facility too early, and makes it easier to identify and support researchers with an established record of excellence.

Three critical reactions are hydrogen abstraction, hydrogen donation, and carbon placement. These would have to take place in UHV (Ultra High Vacuum) on a diamond surface, likely at low temperature (e.g., the temperature of liquid nitrogen (LN_2) or perhaps even lower (LHe)).

While one primary program objective is to demonstrate the feasibility of the basic reactions, a critical supporting requirement is the ability to position the tools accurately enough. In addition, the proposed reactions require at least a five degrees-of-freedom (5-DOF) positional device. Not only must the device be able to position within a fraction of an Angstrom in X, Y and Z, it must also be able to control at least two rotational degrees of freedom.

Although the proposed reactions in the minimal toolset paper assume a 5-DOF capability, the dimer placement tool (whose synthesis was described in the minimal toolset paper, but whose possible use has been studied in other papers) would normally require six degrees of freedom to use. The other tools described in that paper require only 5-DOF. Future tool proposals (e.g., for parts assembly) might also require a full 6-DOF positional device, so the development of a full 6-DOF positional device might prove advantageous, even though 5-DOF appears sufficient at the present time.

There are two avenues of attack in approaching the 5-DOF positional device issue. First, we can demonstrate the capability experimentally. Second, we can analyze the proposed reactions to determine if alternative reaction pathways or motion sequences that might require only a 3-DOF positional device are feasible. If we can simplify the requirements from 5-DOF to 3-DOF, then the design of the positional device becomes simpler. This simplification can only take place, however, if we can develop alternative reaction pathways that don't need rotational degrees of freedom (or which need fewer of them).

At the same time that experimental work is progressing, theoretical work will continue – and is generally less expensive. One of the obvious targets is validation of the existing work. The Minimal Toolset paper[2] describes many reactions, and analyzes them using specific (and rather good) computational chemistry tools. However, computational chemistry tools give more accurate results when more powerful computers can be employed. In addition, expertise in using these tools enhances confidence in the results, as does replication of results by other groups.

As the proposal is now quite specific, it will be relatively easy to contact appropriate computational chemistry groups and request that they: (a) validate the existing results, (b) extend the results in various directions (e.g., by developing reaction pathways that require only 3-DOF positional devices, or by incorporating additional elements that permit the fabrication of a wider range of structures), and (c) model all the reactions that take place in the Phase I system in more detail to provide a deeper computational validation of their feasibility.

At the end of Phase I, we will have demonstrated the ability of four independently controlled tool-positioning devices, working together, to carry out the reactions described in the Minimal Toolset paper. These devices would operate in a small workspace (somewhere between 1 and 10 microns in linear size) in a UHV system, likely (though not certainly) at liquid nitrogen

---

[2] Robert A. Freitas Jr., Ralph C. Merkle, "A Minimal Toolset for Positional Diamond Mechanosynthesis," J. Comput. Theor. Nanosci. 5(May 2008):760-861.

temperature or colder. Carbon and germanium would be transferred into the workspace on two externally prepared surfaces. A third surface would absorb excess hydrogen. Product structures would be fabricated on a fourth diamond working surface (which would also provide hydrogen). At this stage, product structures could not be detached from the surface. The speed of operation would be slow, perhaps one atom added to a growing structure every minute or two. The Phase I system could build modest but atomically precise structures having perhaps 100-1000 atoms.

In short, all the basic mechanosynthetic steps underlying MNT would have been validated both theoretically and experimentally.

1.4.2 Phase II: Making a Production System

With the successful completion of Phase I, the primary issues that then have to be faced involve increasing the size of parts that can be manufactured, the speed of manufacture, the range of parts (e.g., curved parts, strained parts), detaching parts from the work surface, and assembling parts. Phase II provides a basic set of manufacturing capabilities that will be used as a basis for supporting further development throughout Phases III, IV, V and VI.

In short, the objective of Phase II is: yes, mechanosynthesis works in the lab, but now let's make it more useful in practice. The basic approach used in the Phase I system stays the same but a variety of remaining problems that limit the system are dealt with one by one.

At the end of Phase II, we have a system able to make atomically precise molecular structures with 10,000 to 100,000 atoms. These structures would have multiple independent parts that the Phase II system would assemble into the final structure. Anticipated speed of operation is about one second per atom added to the product structure.

1.4.3 Phase III: Shrinking the System

In Phases I and II, most of the manufacturing system is macroscale and not atomically precise. Only the tips and the first tiny products are atomically precise. In Phase III, we start to shrink a significant part of the system, and we also migrate the shrunken system to sit on top of a standard lithographically produced surface that provides electrical control signals (the multielectrode assembly surface) to drive the new nanoscale manufacturing system.

The multielectrode assembly surface is silicon dioxide, with an array of small (perhaps ten nanometer in linear extent) contacts laid out in a grid with about 50 contacts. The surface occupied by the Phase III (Nanoscale Fabrication Workstation (NFW) is somewhat over 100 nanometers in linear extent.

The NFW has, again, four positional devices. However, these positional devices are molecular scale Stewart platforms, able to grasp and release handled tooltips. They are 6-DOF, high accuracy, atomically precise nanoscale manufacturing devices controlled by electrical signals that actuate molecularly precise electrostatic stepper motors.

The Phase III NFW is manufactured by the Phase II workstation. The Phase III NFW still gets its molecular feedstock from the Phase II system, so the Phase II system is still required for operation. In addition, the NFW cannot assemble parts, it can only fabricate them (i.e., by using

the mechanosynthetic reaction steps). The resulting parts are picked up by the Phase II system and assembled.

Because we are using the Phase II system to fabricate the Phase III system, atom counts are important. The Phase II system is limited in its throughput, so we want to keep the atom count for the Phase III system as small as possible. The Phase III system will have somewhat over 500 parts and about 30 million atoms. At one atom per second, it would take about a year to make a single NFW Phase III system if we had only one Phase II workstation to work with – but we'll likely acquire multiple such workstations to speed up the design and development process.

The Phase III NFW would be capable of operating some two orders of magnitude faster than the Phase II system, but remains limited by the speed with which the Phase II system can feed it feedstock molecules. As a consequence, total system productivity remains about the same.

Improving the system speed is the primary objective of the next development step, in Phase IV.

1.4.4 Phase IV: Speeding Up the Shrunken System

The basic purpose of Phase IV is to build an improved NFW – the NFW-2.

The NFW-1 was slow because the Phase II system was providing it with raw materials, and the Phase II system is slow. To eliminate this bottleneck, the Phase IV NFW-2 will get its raw materials in the form of gaseous ethylene and germane. The NFW-2 will operate at a temperature of ~190 K (Kelvins, degrees above absolute zero). This is cold enough to insure adequate reliability of the mechanosynthetic reactions, and ethylene remains gaseous above 169 K.

Note that the Phase IV NFW-2 must operate in UHV so it cannot perform DMS reactions while the feedstock gas is present. To solve this problem, we introduce a bulk tank called the Bulk Feedstock Supply System (BFSS) that gathers and stores the feedstock gas as it is introduced at normal atmospheric pressure. When the tank is full, the external environment is pumped back down to UHV whereupon mechanosynthetic fabrication operations may resume.

The physical design of the Phase IV NFW-2 is similar to the Phase III NFW-1, but includes a tank wrapped around the NFW-1. The macroscale chamber is flooded with ethylene gas (C_2H_4, the carbon feedstock source) which is pumped into the BFSS. The BFSS stores enough ethylene so that the Phase IV NFW-2 can manufacture all the parts needed for another NFW-2 in a single cycle of operation. The ethylene gas is stored at a reasonably high pressure, so the total volume occupied by the gas is roughly similar to the volume occupied by the Phase IV NFW-2. The macroscale chamber is purged of ethylene and the system is baked out. Germane (GeH_4) gas is briefly introduced into the macroscale chamber and a few germane molecules are stored in a separate (and very small) chamber in the BFSS. The system is again baked out.

Even allowing for long bake out times (which are need to purge the system of all residual gas), this approach substantially improves overall efficiency.

Once charged with enough ethylene and a trace of germane, the Phase IV NFW-2 can fabricate all parts for another Phase IV NFW-2 without further input from the Phase II system. The Phase II system is still required to remove parts fabricated by the Phase IV NFW-2 and to assemble them into a replica unit elsewhere, but as there are many fewer parts than feedstock molecules, this is not a rate limiting step.

The total time required to charge the system with feedstock molecules and manufacture the parts for a second Phase IV NFW-2 is up to a few weeks, depending on detailed assumptions about the bake out time. Assembly of the resulting parts using the Phase II system is not a rate limiting step because the number of parts is limited.

1.4.5 Phase V: Assembling Parts at the Nanoscale

Phases III and IV have focused on nanoscale fabrication. Phase V focuses on nanoscale parts assembly. In essence, the design is similar to the Phase III NFW except that it assembles parts instead of fabricating parts, using molecular tools. While the general design is similar, it uses three molecular scale Stewart platforms instead of four. It also operates on a multielectrode assembly surface.

The Phase V Nanoscale Assembly Workstation (NAW) is again assembled by the Phase II system. The primary reason to build the Phase V NAW is to free the nanoscale system from reliance on the Phase II system – which up to this point is still carrying out the assembly operations. Although the use of the Phase II system is not rate limiting, the Phase II system is not scalable to large numbers because it is a macroscale system. Eliminating it from the manufacturing cycle is the key to enabling exponential scaleup of manufacturing capacity in later development phases.

1.4.6 Phase VI: Getting Rid of the Phase II System

Finally, with the availability of the Phase V NAW we are almost freed from dependence on the Phase II system. Integration of the Phase IV NFW-2 and the Phase V NAW produces a molecular scale manufacturing system that can fabricate and assemble another molecular scale system. The assembly of the initial Phase VI NAW is done using the Phase II system. After that, successive Phase VI NAWs can be manufactured without requiring the Phase II system.

A single Phase VI Nanoscale Manufacturing Workstation (NMW) can make another Phase VI NMW on the surface adjacent to it in a few weeks.

1.4.7 Phase VII: Debugging Plate-to-Plate Manufacturing

Now that the entire manufacturing process can be done at the molecular scale on a multielectrode assembly surface, we can start to consider serious scale-up.

The basic idea is to modify the Phase VI NMW so that it can manufacture a new system not on the adjacent surface, but on a facing surface (“above” it).

That is, the Phase VII NMW-2 will operate on a first multielectrode assembly surface, but will manufacture the next Phase VII NMW-2 on a second multielectrode assembly surface that is held about 200 nanometers away from the first surface.

In Phase VII we debug this "plate to plate" manufacturing process, and also tidy up various performance issues (now that the Phase II system no longer limits productivity, squeezing out more performance from the rest of the system is worthwhile).

A critical issue is aligning the two plates with respect to each other very precisely so that the Phase VII NMW-2 will be able to assemble parts on the opposing (second) plate. There is a tradeoff between alignment and molecular workstation complexity – the more accurately the two plates can be aligned, the simpler the workstation design. The current assumption is that high accuracy alignment will be simpler than a more complex molecular work station design that reduces the need for precise alignment. The use of active systems to maintain alignment should work over even a fairly large surface.

The major purpose of plate to plate manufacturing is to allow each Phase VII NMW-2 to manufacture a second Phase VII NMW-2 on the opposing plate. By shifting the plates, each Phase VII NMW-2 can again be positioned opposite an open site on the opposing multielectrode assembly surface. By repeating this cycle, the number of Phase VII NMW-2s can be made to increase exponentially until all available sites on the two opposing plates are occupied. This process is, appropriately enough, called exponential assembly.

In Phase VII we debug this process, manufacturing enough Phase VII NMW-2s to insure that the process is working correctly.

1.4.8 Phase VIII: Exponential Assembly

In this phase, we manufacture about a thousand 10 cm by 10 cm multielectrode assembly plates with 10^{11} worksites per plate. Each worksite can accommodate one Phase VII NMW-2.

We then populate all one thousand plates. The first two plates are populated by plate to plate exponential assembly. The subsequent plates are populated non-exponentially using previously populated plates. The total number of Phase VII NMW-2s that can be manufactured is limited largely by the number of available plate handling mechanisms. With one thousand plates and 10^{11} workstations per plate, the total number of workstations is 10^{14}. At this point, the individual nanoscale Phase VII NMW-2 manufacturing modules are able to build product at about 1,000 atoms per second, so the whole system can collectively manufacture atomically precise products at a rate of 10^{17} atoms/second.

1.4.9 Phase IX: Ten Times Bigger Products and Manipulators

The Phase VII NMW-2's crane arm has a maximum extension of ~0.2 microns. This was sufficient for the assembly tasks it faced. As we prepare for the challenge of building the First-Generation Nanofactory (FGN) we will need robotic arms with a somewhat longer reach to assemble somewhat larger products. A plane of Stewart platforms with a maximum extension of ~2 microns will be able to assemble the somewhat larger structures needed in the next phase. These Stewart platforms are called Micro-Assembler Manipulators (MAMs) and will for the most part have the same design as the NAW-2 crane arms, but scaled up by a factor of 10. The MAMs will be able to assemble parts, but each MAM is a single Stewart platform and does not have any fabrication capability (unlike the NMW series, which can both fabricate and assemble parts).

We continue to use the multielectrode assembly plate as before, to provide control and power to the array of MAMs. Individual worksites occupy 1 micron^2 of surface in a regular grid pattern, letting us put 2 x 10^{11} (200 billion) MAMs on a 40 cm x 50 cm plate. Each MAM has a force sensor which is used to provide simple feedback. The multielectrode assembly plate has conventional semiconductor circuitry to control each MAM, circuitry which interfaces with a conventional external computer control system.

One 40 cm x 50 cm array of MAMs is called a Micro-Assembler Array (MAA) wafer. In Phase IX, 200 MAA wafers are built and will later provide sufficient assembly throughput for building the FGN in the next phase of nanofactory development.

To summarize: In Phase IX we build 200 multielectrode assembly plates each with an array of 2 x 10^{11} Stewart platforms that can now pick up, manipulate, and assemble parts and assemblies made by the 1000 Phase VIII plates, each Phase VIII plate being populated with 10^{11} Phase VII NMW-2s. By bringing a plate and a wafer together, with active surfaces facing each other, the array of micron scale Phase IX Stewart platforms can pick up the parts fabricated by the Phase VII NMW-2s and assemble them, or can reliably install them in a specific pattern to build the first nanofactory, layer by layer, in Phase X.

1.4.10 Phase X: Increase Mass Throughput by One Thousand-fold

The Phase X system – called the First-Generation Nanofactory (FGN) – increases the manufacturing rate to 0.01 kilograms per hour, a thousand-fold improvement over the 0.06 kilogram per year rate achieved by the Phase VIII system.

The basic approach is to adapt the NMW-2 (primarily by eliminating the BFSS) to produce an improved NMW-3, and to increase throughput by building 10^{16} NMW-3s. The infrastructure to support this many NMW-3s, and additional assembly stations to assemble the parts produced by the NMW-3s, and parts handling systems able to move parts from the NMW-3s to the parts assembly and inspection facilities, are all assembled using the Phase IX system and are all atomically precise.

While the BFSS (Bulk Feedstock Supply System) has served us well in previous phases, it has now become a limiting factor in throughput. Rather than loading the BFSS and then purging the entire vacuum system at each cycle, we move to a continuous feed system that continually flows gaseous feedstock to the individual fabrication stations – increasing productivity by a factor of ten. In addition, we increase the areal density of manufacturing modules by decreasing the total area of NMW modules (by eliminating the BFSS) while simultaneously packing more stations into three dimensions. Each 50 cm x 40 cm fabrication plane within the FGN contains 10^{13} NMW-3s (modified versions of the NMW-2, primarily lacking the BFSS). The NMW-3s are also modified to accept feedstock directly from the new continuous flow system, and have various other minor adjustments to accommodate their slightly changed function. The first production layer of the FGN fabricates parts, and includes 1000 fabrication planes which are a total of 10 cm thick. Above the 1000 fabrication planes lies the second production layer, which consists of four additional planes for assembly and inspection that do only assembly work, but no fabrication.

The whole of the 50 cm x 40 cm x 10 cm FGN system is atomically precise, and is manufactured using the Phase VIII and Phase IX systems. More than 99.9% of the volume of the FGN is empty space, providing room both for feedstock/byproduct gases and for the large quantities of cooling fluid that must be continuously pumped through the system. The working manufacturing

machinery of the FGN is still kept in an externally provided UHV environment, and the feedstock and cooling subsystems occupy distinct sealed spaces that are kept entirely separate both from each other and from the externally maintained UHV environment.

The ability to make extensive use of atomically precise manufacturing (including atomically precise supporting infrastructure for the individual NMW-3s) is essential in the productivity increases that are achieved in this phase of nanofactory development.

Basic to Phase X is a large number (~10^{16}) of NMW-3 modules operating in a relatively small volume, along with additional planes of manufacturing machinery devoted entirely to further assembly of larger (micron-scale) product objects. This phase also introduces deterministic ciliary transport using hand-over-hand (bucket-brigade type) movement of parts from one Stewart platform to the next (avoiding the need to design and implement conveyor belt type systems for parts transport).

The FGN can manufacture ~100 cm^3/day (~240 gm/day) of atomically precise microscale product objects having a mean density of ~2.4 gm/cm^3 (i.e., products are ~68% diamond and ~32% vacuum, by volume).

1.4.11 Phase XI: Increase Product Size by One Hundred Thousand-fold

The second generation nanofactory (SGN) has the same mass throughput as the FGN but can manufacture atomically precise macroscale product objects up to 10,000 cm^3 in volume within a 40 cm x 25 cm x 10 cm product dimensional size envelope.

The SGN has the same first and second production levels as in the FGN, but adds a third production level for the purpose of assembling ~5 micron (~100 $micron^3$) parts into macroscale product objects. The SGN measures 50 cm x 40 cm x 44 cm in size, requires ~11 MW to operate (like the FGN), and has a material production cost (excluding capital and human labor costs) of ~$111/gm.

The primary limiting factor in nanofactory productivity is now heat dissipation. Increasing total throughput requires increasing part fabrication rates, but using stepper-motor actuated Stewart platforms guarantees the generation of significant amounts of waste heat when adding a single atom to a growing part. We must subsequently move away from this energy-wasteful approach if we are to increase throughput to the target objective of ~1 kg/hour for atomically precise macroscale products in a feasible technologically-mature molecular manufacturing system. A mill-based low-energy-dissipation nanofabrication system will probably be required to reduce energy usage by 3-4 orders of magnitude to make practical a mature high-throughput ~1 kg/hour diamondoid nanofactory system with a ~1 kW power dissipation as described in Section 2.1.3. If such a system can be designed using a modular architecture for easy assembly, these high-throughput systems could be manufactured very quickly using the SGN because their mass is estimated to lie in the ~1 kg range and the SGN has a mass throughput of ~0.01 kg/hour, giving a build time for a mature diamondoid nanofactory of ~100 hours (~4 days) using the SGN.

1.5 Conclusion

This nanofactory development program is the most specific plan for the realization of MNT that has been proposed to date. The assumptions on which it rests are clearly described, and validating the most critical assumptions is done in Phase I of an eleven-phase development process. Once Phase I is completed (and this is expected to be a multi-year project in itself), serious efforts to raise the possibly multi-billion dollar funding required to complete the remaining ten Phases of the program can begin in earnest.

2. Nanofactories: Brief Survey of the State-of-the-Art

The nanofactory is a proposed compact molecular manufacturing system, possibly small enough to sit on a desktop, that could build a diverse selection of large-scale molecularly precise diamondoid products. This molecular manufacturing system will employ positionally controlled molecular fabrication and assembly techniques that will make possible the creation of fundamentally novel products having the intricate complexity currently found only in biological systems, but operating with greater speed, power, reliability, and, most importantly, entirely under human control. Molecular manufacturing has the potential to be extremely clean, efficient, and inexpensive.

The nanofactory is potentially a high quality, extremely low cost, and very flexible manufacturing system. Our nanofactory will be constructed from diamondoid components of the same sort that it can itself manufacture. While molecular manufacturing systems made from DNA, other biopolymers, or even biological organisms are possible, such systems would be unable to build products that approach the remarkable strength, stiffness, temperature range, lightness, electrical, optical and other properties that can achieved with diamondoid materials. The principal input to a diamondoid nanofactory is simple hydrocarbon feedstock molecules such as natural gas, propane, or acetylene. Small supplemental amounts of a few other simple molecules containing trace atoms of chemical elements such as oxygen, nitrogen or silicon may also be required. The principal output of the first commercial nanofactory will be macroscale quantities of molecularly precise diamondoid products. These products may include nanocomputers, medical nanorobots, products having diverse aerospace and defense applications, devices for cheap energy production and environmental remediation, and a cornucopia of new and improved consumer products. Earlier-generation research nanofactories will produce substantially less complex products but will provide an evolutionary pathway leading from the first simple DMS workstations to more mature commercial systems.

While there have been several preliminary scaling studies and conceptual architecture type studies of nanofactories, no nanofactories capable of manufacturing macroscale products having atomically precise features have yet been built. However, some theoretical studies have looked at architectures for desktop factories capable of manufacturing atomically precise macroscale product objects (Section 2.1),[3] and desktop manufacturing systems capable of producing macroscale products with (albeit atomically imprecise) micron-scale features have been developed and are presently commercially available (Section 2.2). The realization of nanofactories with atomically precise manufacturing capability would vastly expand the quality and range of products that can currently be manufactured using desktop manufacturing systems. We believe that the most capable and economically useful nanofactories will be based on

---

[3] K. Eric Drexler, Nanosystems: Molecular Machinery, Manufacturing, and Computation, John Wiley & Sons, New York, 1992; http://www.zyvex.com/nanotech/nanosystems.html. Robert A. Freitas Jr., Ralph C. Merkle, Kinematic Self-Replicating Machines, Landes Bioscience, Georgetown, TX, 2004; http://www.MolecularAssembler.com/KSRM.htm

positionally controlled diamondoid mechanosynthesis (Section 2.3), and patentable IP is already beginning to be generated in this area.[4]

The current proposal fully complies with the Foresight Guidelines for Responsible Nanotechnology Development.[5] Some previous work on MNT proposed the use of autonomous self-replicating systems, in violation of the Foresight Guidelines. The current proposal does not use such systems. The Foresight Guidelines recommend the use of inherently safe systems, which are used here. The most advanced system analyzed here, the Phase XI nanofactory, cannot function without externally provided power, cooling, ultrahigh vacuum, high purity feedstock molecules (ethylene and germane) and computer control.

2.1 Nanofactory-Related Theoretical Work

Three theoretical nanofactory design efforts are most relevant to the proposed nanofactory development program and will be presented in some detail:

(1) **Merkle-Freitas Hydrocarbon Molecular Assembler** (Section 2.1.1). This was the first complete design (much of it still unpublished) of a stand-alone molecular fabrication unit intended to be capable of using diamondoid mechanosynthesis (DMS) (Section 2.3.1) to manufacture an exact copy of itself. The design provided estimated atom counts, operating speed and energy consumption for all required major subsystems needed to achieve atomically precise diamondoid fabrication – thus represents a valuable reference point in the consideration of the most fundamental level of nanofactory design. An implementation pathway (fabrication using DMS tooltips mounted on scanning probe mechanisms) was suggested but no specific details were provided. The present nanofactory development proposal adopts a similar scheme for molecular fabrication. One limitation of the HC assembler design is that it includes only two opposable 6-DOF manipulators, and more recent analysis[6] suggests that up to four opposable manipulators may be required for diamond-building.

(2) **Zyvex Exponential Assembly** (Section 2.1.2). This was the first worked-out example of the concept of plate/plate replication, which appears to be one of the most efficient methods for bootstrapping large-scale productive systems starting from a small number of stand-alone molecular manufacturing units of the type described in Section 2.1.1. Designs were published for microscale (MEMS-based) but not for nanoscale implementations, and no specific development pathway for a nanoscale version has ever been presented. The present nanofactory

---

[4] Robert A. Freitas Jr., "A simple tool for positional diamond mechanosynthesis, and its method of manufacture," U.S. Provisional Patent Application No. 60/543,802, filed 11 February 2004; U.S. Patent Pending, 11 February 2005; http://www.MolecularAssembler.com/Papers/DMSToolbuildProvPat.htm. Robert A. Freitas Jr., Ralph C. Merkle, "Positional Diamond Mechanosynthesis: Toolset, Reactions, Uses and Products," U.S. Provisional Patent Application No. 60/970,658, filed 7 September 2007.

[5] Foresight Institute, "Molecular Nanotechnology Guidelines: Draft Version 3.7," 4 June 2000; http://www.foresight.org/guidelines/2000june.html.

[6] Robert A. Freitas Jr., Ralph C. Merkle, "A Minimal Toolset for Positional Diamond Mechanosynthesis," J. Comput. Theor. Nanosci. 5(May 2008):760-861.

development proposal adopts a related scheme to make feasible the final buildout of the desktop nanofactory starting from submicron-scale manufacturing modules.

(3) **Drexler Nanofactory** (Section 2.1.3). This was the first published scaling analysis of a complete nanofactory concept. It provided a sketched-out exemplar nanofactory design along with quantified estimates of the mechanisms, productivity, mass and energy usage for each of the ten manufacturing layers comprising the nanofactory. *Nanosystems*[7] presented the first designs for a wide variety of simple nanoparts and nanomachines, but included no systems level designs for a complete manufacturing system and no specific development pathway for building the nanofactory was presented. Nevertheless the present development program proposal has been inspired by this early effort.

Several additional interesting hypothetical nanofactory designs have been published, some providing more detail than others but none providing sufficient details as to the exact implementation pathway that should be followed to actually develop and field a working diamondoid desktop nanofactory. The most notable examples of this genre include the rotary assembler nanofactory design (Figure 2-1)[8] of Forrest Bishop,[9] the molecular manufacturing system design (Figure 2-2)[10] of J. Storrs Hall,[11] the "primitive nanofactory" design (Figure 2-3)[12] of Chris Phoenix,[13] the general purpose "Tattoo" manufacturing system (Figure 2-4) of Tihamer

---

[7] K. Eric Drexler, Nanosystems: Molecular Machinery, Manufacturing, and Computation, John Wiley & Sons, New York, 1992; http://www.zyvex.com/nanotech/nanosystems.html.

[8] Robert A. Freitas Jr., Ralph C. Merkle, Kinematic Self-Replicating Machines, Landes Bioscience, Georgetown, TX, 2004; Section 4.15, p. 136; http://www.MolecularAssembler.com/KSRM/4.15.htm.

[9] "3-D Animations for 'Machines Alive': Rotary Assembler," E-SPACES, 1998; http://www.e-spaces.com/broadcast/assembler/index.html; "Rotary Assembler: Movies," http://www.e-spaces.com/broadcast/assembler/asm.mpg.

[10] Robert A. Freitas Jr., Ralph C. Merkle, Kinematic Self-Replicating Machines, Landes Bioscience, Georgetown, TX, 2004; Section 4.16, pp. 136-138; http://www.MolecularAssembler.com/KSRM/4.16.htm.

[11] J. Storrs Hall, "Architectural considerations for self-replicating manufacturing systems," Nanotechnology 10(1999):323-330; http://www.foresight.org/Conferences/MNT6/Papers/Hall/index.html or http://discuss.foresight.org/~josh/selfrepsys/index.html.

[12] Robert A. Freitas Jr., Ralph C. Merkle, Kinematic Self-Replicating Machines, Landes Bioscience, Georgetown, TX, 2004; Section 4.19, pp. 141-144; http://www.MolecularAssembler.com/KSRM/4.19.htm.

[13] Chris Phoenix, "Design of a Primitive Nanofactory," J. Evol. Technol. 13(October 2003); http://www.jetpress.org/volume13/Nanofactory.htm . See also: "CRN Research: Current Results – Bootstrapping a Nanofactory," 2003; http://CRNano.org/bootstrap.htm.

Toth-Fejel and Chris Phoenix,[14] and the nanofactory animation (Figure 2-49) of John Burch.[15] In 2003, Zyvex Labs briefly described a multiphase development strategy for MNT.[16]

Figure 2-1. Rotary assembler nanofactory design[17] of Forrest Bishop.[18]

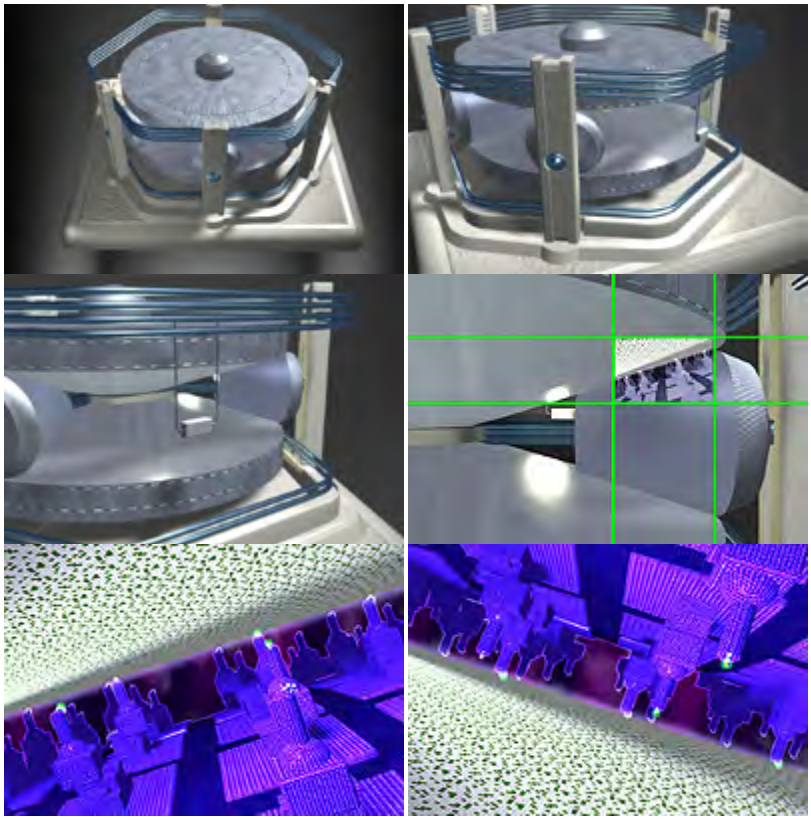

One of the machines that will be possible using the new-found ability to manipulate single molecules and atoms is illustrated here. This vaguely CD-ROM-like machine assembles other nanomechanical systems by means of 5 degrees-of-freedom tips that pick molecules off the upper platter, rotate down and deposit them on the product arrays of the lower platter.

---

[14] Tihamer Toth-Fejel, Chris Phoenix, "Large-Product General-Purpose Design and Manufacturing Using Nanoscale Modules," Technical Proposal for NASA Institute for Advanced Concepts, Phase II: Advanced Aeronautical/Space Concept Studies, NIAC CP 05-02, 2 May 2005.

[15] John Burch nanofactory website, http://www.lizardfire.com/html_nano/nano.html.

[16] Zyvex Labs, "White Paper. Molecular Nanotechnology: A Realistic Treatment," 2003; http://www.zyvexlabs.com/News&Events/WhitePapers/MolecularNanotech.html.

[17] Robert A. Freitas Jr., Ralph C. Merkle, Kinematic Self-Replicating Machines, Landes Bioscience, Georgetown, TX, 2004; Section 4.15, p. 136; http://www.MolecularAssembler.com/KSRM/4.15.htm,

[18] "3-D Animations for 'Machines Alive': Rotary Assembler," E-SPACES, 1998; http://www.e-spaces.com/broadcast/assembler/index.html; "Rotary Assembler: Movies," http://www.e-spaces.com/broadcast/assembler/asm.mpg.

Figure 2-2. Molecular manufacturing system design[19] of J. Storrs Hall.[20] (A) Parts fabricator in Hall factory replicator. (B) Detailed view of the wrist assembly of the parts fabricator. (C) A mobile parts-assembly robot which would assemble parts that had been fabricated by the parts fabricator. (D) Rectangular 3-dimensional framework for parts assembly, which would be used by the mobile parts-assembly robot to provide positional guidance and control.

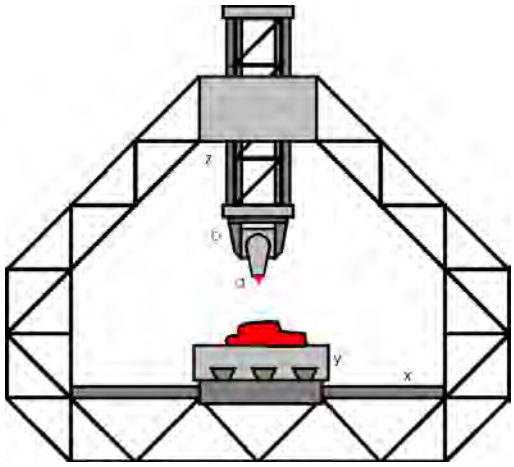

(A)

(B)

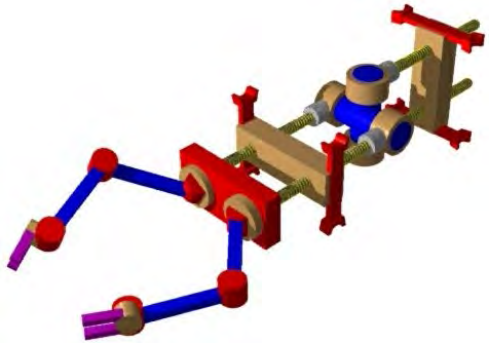

(C)

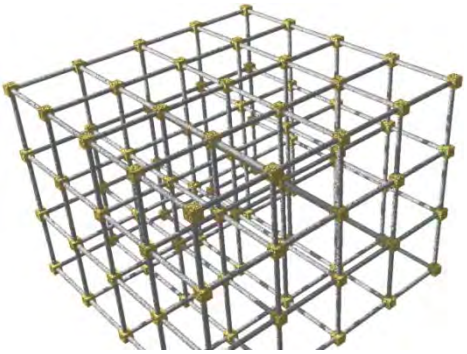

(D)

---

[19] Robert A. Freitas Jr., Ralph C. Merkle, Kinematic Self-Replicating Machines, Landes Bioscience, Georgetown, TX, 2004; Section 4.16, pp. 136-138; http://www.MolecularAssembler.com/KSRM/4.16.htm.

[20] J. Storrs Hall, "Architectural considerations for self-replicating manufacturing systems," Nanotechnology 10(1999):323-330; http://www.foresight.org/Conferences/MNT6/Papers/Hall/index.html or http://discuss.foresight.org/~josh/selfrepsys/index.html.

Figure 2-3. Primitive nanofactory design[21] of Chris Phoenix.[22] Nanofactory workstation grid (top); reliable basic production module (bottom).

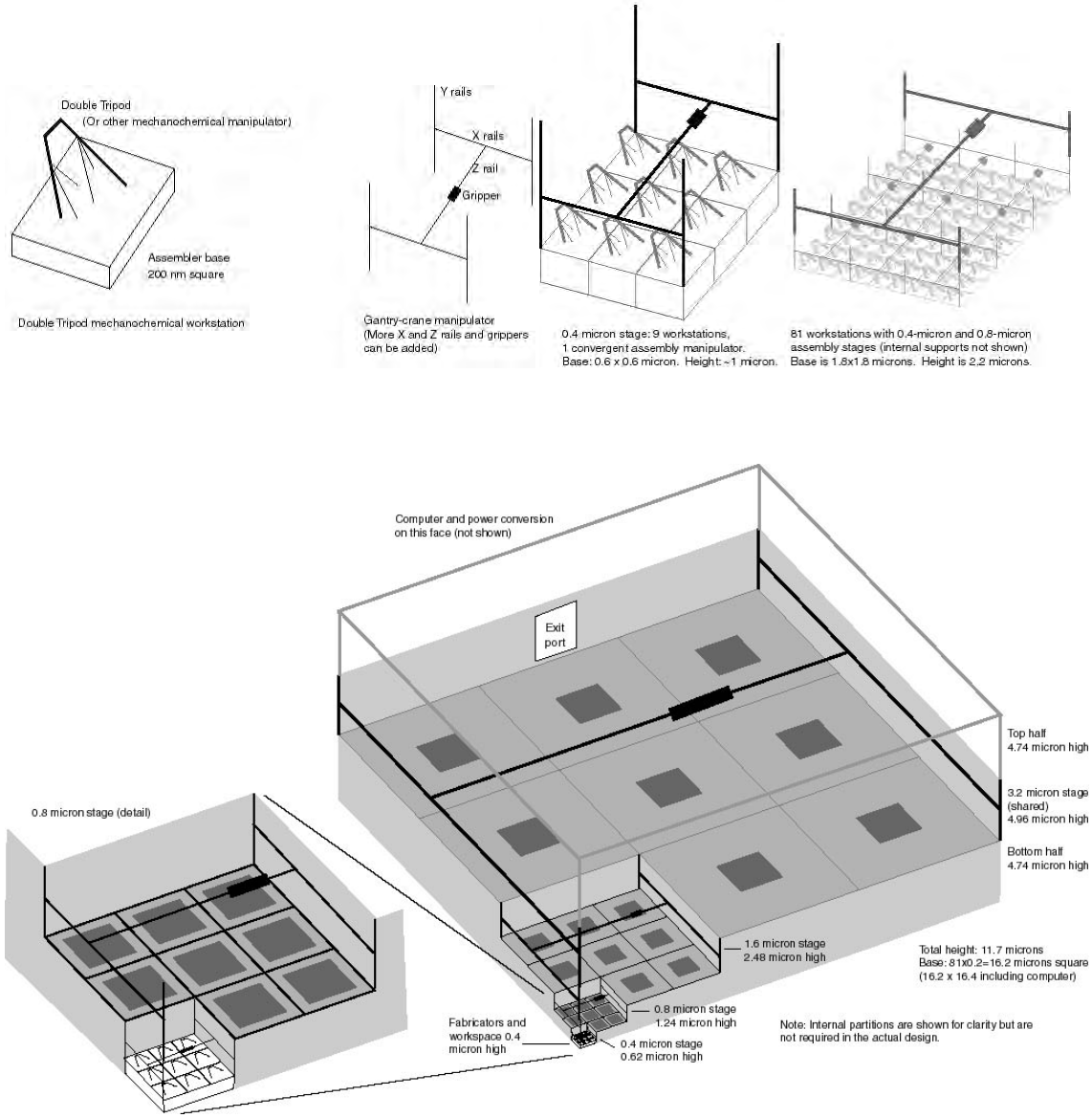

---

[21] Robert A. Freitas Jr., Ralph C. Merkle, Kinematic Self-Replicating Machines, Landes Bioscience, Georgetown, TX, 2004; Section 4.19, pp. 141-144; http://www.MolecularAssembler.com/KSRM/4.19.htm.

[22] Chris Phoenix, "Design of a Primitive Nanofactory," J. Evol. Technol. 13(October 2003); http://www.jetpress.org/volume13/Nanofactory.htm . See also: "CRN Research: Current Results – Bootstrapping a Nanofactory," 2003; http://CRNano.org/bootstrap.htm.

Figure 2-4. General purpose "Tattoo" manufacturing system as a multi-material 3D printer by Tihamer Toth-Fejel and Chris Phoenix.[23] Tattoo needle system uses tip socket to bind nanoblock from fluid environment, implemented using (A) special-purpose configuration tip with a cavity designed block or (B) several blocks to form a cavity followed by post-processing to modify the inner faces. (C) A first-generation "Tattoo" system finishes up a row of second-generation Tattoo machines. (D) A row of third generation addressable probes builds a 2D array of similar probes.

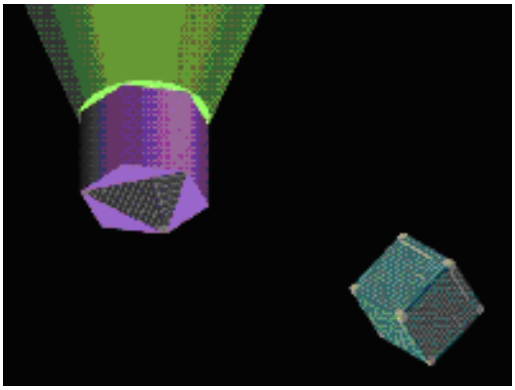

(A)

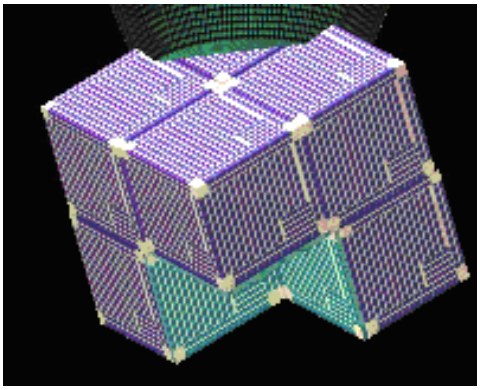

(B)

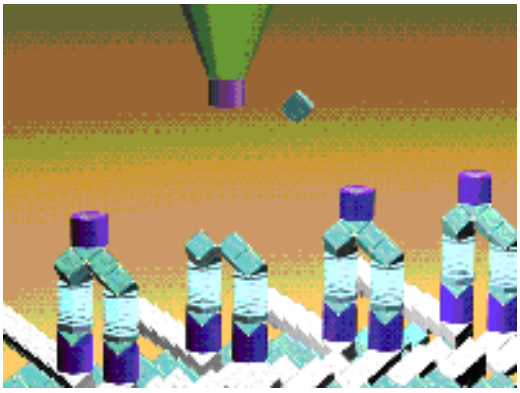

(C)

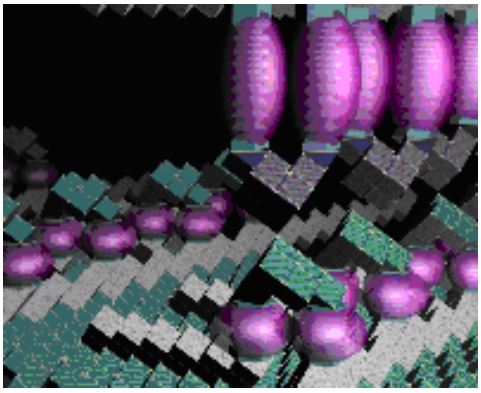

(D)

---

[23] Tihamer Toth-Fejel, Chris Phoenix, "Large-Product General-Purpose Design and Manufacturing Using Nanoscale Modules," Technical Proposal for NASA Institute for Advanced Concepts, Phase II: Advanced Aeronautical/Space Concept Studies, NIAC CP 05-02, 2 May 2005.

2.1.1 Merkle-Freitas Hydrocarbon Molecular Assembler (2000-2003)

A new design for a molecular assembler employing the extruding brick architecture, drawing upon modified elements of earlier designs and introducing new design elements, resulted from a multi-year collaboration between Merkle and Freitas during 2000-2003. The Merkle-Freitas hydrocarbon molecular assembler design[24] repairs all known defects of earlier efforts and addresses additional problems not previously recognized by others. For example, the acoustic power/control piston count is reduced to one, allowing volumetric displacement, power input, efficiency, and reliability to be maximized. The proposed control signal demultiplexor is eliminated in favor of a much simpler control chain concept. The design is further simplified by the elimination of all gases from the interior (substituting a vacuum), by adding a novel "elevator" mechanism, and by eliminating all internal cabling which would be relatively difficult to assemble reliably. The continuous extrusion of daughters is achieved while maintaining full external seal integrity of parental device walls, thus preventing the destruction of parental devices following replication. All waste products – including molecular effluents (e.g., spent parts handles, gases), ruptured casings, and destroyed parental devices – are eliminated, yielding a 100% clean, environment-friendly, zero-waste molecular manufacturing system.

2.1.1.1 Summary Description

The Merkle-Freitas Hydrocarbon Molecular Assembler (Figure 2-5) would be an entry-level molecular manufacturing device which allows the unitary fabrication and extrusion of molecularly precise rigid hydrocarbon product objects, including objects like itself. The Merkle-Freitas assembler is a "minimal assembler" design that requires a minimum of onboard structural complexity so that initial assembler devices can be constructed using the more limited tools and techniques available in a pre-assembler technology environment. Subsequent assembler devices can be conveniently built by the initial assembler device.

The Merkle-Freitas assembler floats in a 2 μm^3 liquid-filled room-temperature microfluidic reaction chamber containing n-octane hydrocarbon solvent in which acetylene feedstock molecules are dissolved. Acetylene molecules are mechanically transported into the device and employed as a source of carbon to construct a product object which is slowly extruded from the device, then released from the device upon completion of manufacture. Solvent molecules of n-octane are also mechanosynthesized and exported as a harmless byproduct to carry off excess hydrogen safely, resulting in a zero-pollution manufacturing system.

A pair of 7-strut Stewart platform manipulators mechanically operate the feedstock molecule import and byproduct molecule export mechanisms, and also manipulate an onboard

---

[24] Robert A. Freitas Jr., Ralph C. Merkle, Kinematic Self-Replicating Machines, Landes Bioscience, Georgetown, TX, 2004; Section 4.11.3, pp. 130-135; http://www.MolecularAssembler.com/KSRM/4.11.3.htm. Robert A. Freitas Jr., Ralph C. Merkle, Kinematic Self-Replicating Machines, Landes Bioscience, Georgetown, TX, 2004; Appendix B, pp. 223-234; http://www.MolecularAssembler.com/KSRM/ AppB.1.htm.

mechanosynthetic tool set[25] to build (1) diamond or other stiff hydrocarbon product objects to molecular precision, and (2) byproduct molecules. The manipulators receive power and step-by-step product/byproduct manufacturing instructions as a series of external pressure pulses broadcast at 10 MHz throughout the solvent fluid. These pulses originate from an acoustic signal generator abutting the microfluidic reaction chamber, and subsequently are transduced by an onboard piston into linear actuation motions which in turn drive manipulator motions coupled through a mechanical control chain system. Tight sliding seals maintain internal vacuum at all times.

---

[25] Jingping Peng, Robert A. Freitas Jr., Ralph C. Merkle, "Theoretical Analysis of Diamond Mechanosynthesis. Part I. Stability of C_2 Mediated Growth of Nanocrystalline Diamond C(110) Surface," J. Comput. Theor. Nanosci. 1(March 2004):62-70; http://www.MolecularAssembler.com/JCTNPengMar04.pdf. Jingping Peng, Robert A. Freitas Jr., Ralph C. Merkle, James R. Von Ehr, John N. Randall, George D. Skidmore, "Theoretical Analysis of Diamond Mechanosynthesis. Part III. Positional C_2 Deposition on Diamond C(110) Surface using Si/Ge/Sn-based Dimer Placement Tools," J. Comput. Theor. Nanosci. 3(February 2006):28-41; http://www.MolecularAssembler.com/Papers/JCTNPengFeb06.pdf. Ralph C. Merkle, Robert A. Freitas Jr., "Theoretical analysis of a carbon-carbon dimer placement tool for diamond mechanosynthesis," J. Nanosci. Nanotechnol. 3(August 2003):319-324; http://www.rfreitas.com/Nano/JNNDimerTool.pdf. See also: Ralph C. Merkle, Robert A. Freitas Jr., "Theoretical analysis of a carbon-carbon dimer placement tool for diamond mechanosynthesis," paper presented at the 10th Foresight Conference on Molecular Nanotechnology, October 2002; http://www.foresight.org/Conferences/MNT10/Abstracts/Merkle/index.html.

Figure 2-5. Physical device specifications for the Merkle-Freitas hydrocarbon molecular assembler.[26]

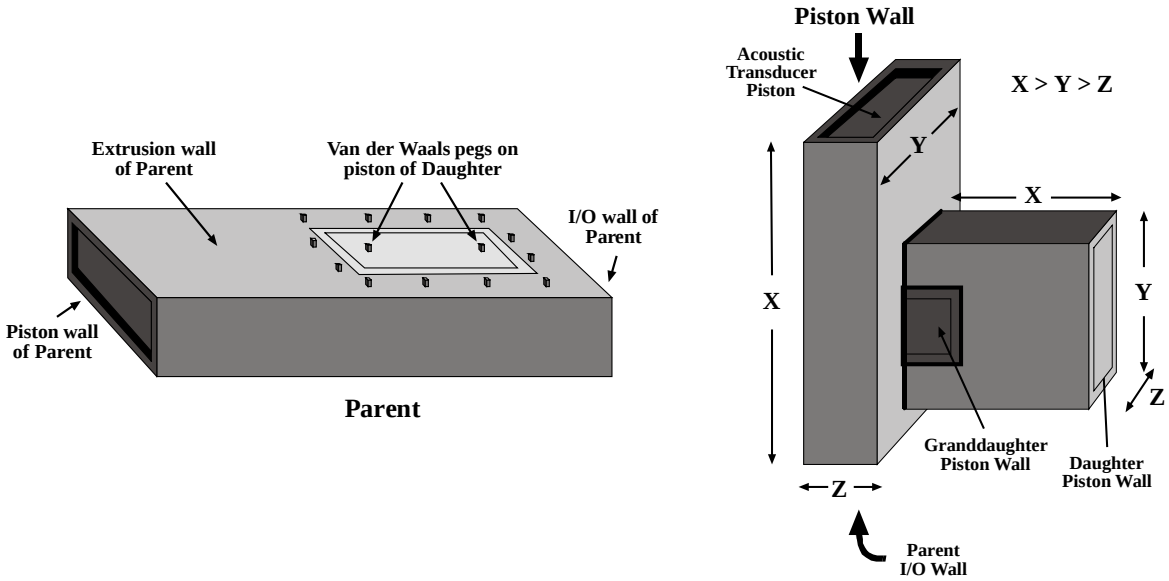

Internal Dimensions (XYZ):	**323.572 nm x 80.00 nm x 40.00 nm**
Internal Volume:	**1,035,430.40 nm^3**
External Dimensions (XYZ):	**333.572 nm x 100.00 nm x 60.00 nm**
External Volume:	**2,001,432.00 nm^3 (~2 mm^3 per trillion devices)**
Initial Mass:	**0.00390826 pg per device**
Initial Atom Count:	**203,908,873 atoms per device**
Initial Molecular Formula:	**$C_{195,231,007}H_{8,677,806}Si_{30}Sn_{30}$**
Carbon Feedstock Molecule:	**C_2H_2 (acetylene)**
Carbon Feedstock Solvent:	**n-C_8H_{18} (n-octane)**
Waste Byproduct:	**n-C_8H_{18} (n-octane)**
Highest Value Assembled Products:	**molecularly precise diamond and other rigid hydrocarbon structures**
Replication Time:	**10^6 seconds (~12 days)**
Power Demand, Single-Band Operation:	**14.2 pW (1-2 atm, 2-3 atm)**
Power Demand, Double-Band Operation:	**56.8 pW (1-3 atm)**
Acoustic Driver Frequency:	**10 MHz**
Instructions per Product Object Atom:	**50,000 bits/atom of product**
Placement Energy per Atom:	**0.073-0.291 pJ/atom C**
Manufacturing Production Rate:	**1 mg/sec per kg of devices**
Energy Cost of Manufacturing:	**$100,000/kg of product**
Manufacturing Defect Rate:	**<10^{-10} per atom of product**

---

[26] Robert A. Freitas Jr., Ralph C. Merkle, Kinematic Self-Replicating Machines, Landes Bioscience, Georgetown, TX, 2004; Section 4.11.3, pp. 130-135; http://www.MolecularAssembler.com/KSRM/4.11.3.htm.

2.1.1.2 Product Object Extrusion

The Merkle-Freitas Hydrocarbon Molecular Assembler includes an interior space and an exterior space, separated by a barrier consisting of a piston attached to an elevator plate. The interior space is a controlled environment where various delicate operations can be performed. The exterior space is a less-controlled environment which provides feedstock and physical support. All manufacturing takes place on the inside, in the controlled vacuum environment. The Merkle-Freitas assembler employs an "extruding brick" architecture which permits the manufacture of objects – whether valuable product or additional assemblers – of sizes smaller than, equal to, or larger than the original manufacturing system, enabling easy scalability. During a replication cycle (Figure 2-6), the parent device extrudes the daughter device, after which both parent and daughter may extrude a subsequent generation, and so on.

Figure 2-6. Replication cycle of Merkle-Freitas assembler.[27]

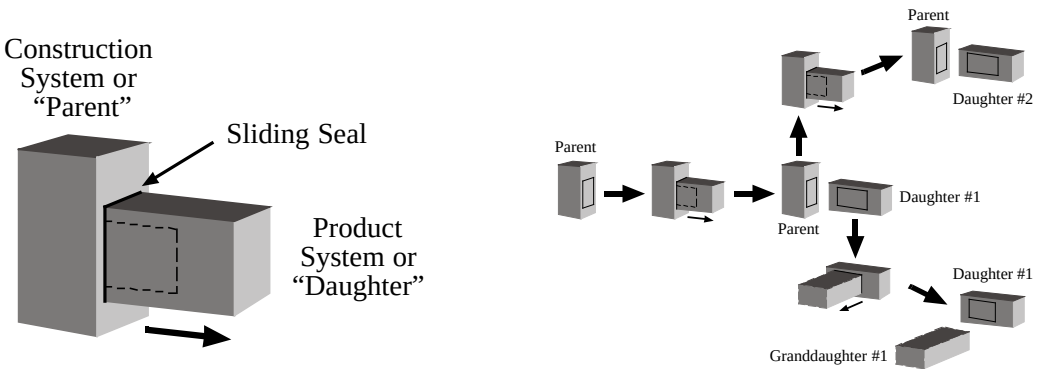

Geometrically, the Merkle-Freitas assembler is essentially a rectangular box. The four large external sidewalls of the daughter device are smooth and parallel as they are extruded. During replication, the four sidewalls establish a tight seal with the inside edges of a rectangular extrusion hole located in the extrusion wall (one of the two largest of the four sidewalls) of the parent.

Initially, the extrusion hole of the parent is plugged with the premanufactured piston end wall (the small YZ face containing the piston that emerges first) of the future daughter. As the daughter is manufactured and extruded, the extrusion hole of the daughter is plugged with the premanufactured piston end wall of the future granddaughter, thus maintaining vacuum inside both parent and daughter.

---

[27] Robert A. Freitas Jr., Ralph C. Merkle, Kinematic Self-Replicating Machines, Landes Bioscience, Georgetown, TX, 2004; Section 4.11.3, pp. 130-135; http://www.MolecularAssembler.com/KSRM/4.11.3.htm.

Each piston end wall lies flush with the sidewall in which it is embedded. When replication resumes, the parent extrudes its daughter with the piston end wall of the future granddaughter already installed in the daughter. The piston end wall of the granddaughter, along with the daughter's four sidewalls, slide in contact with the extrusion hole of the parent while the daughter is being extruded from the parent. Thus five of the six external walls of the device are smooth as they are extruded during the replication cycle. Once a section of the daughter is clear of the parental extrusion hole, this surface smoothness may be modified as required (e.g., pop-out of spring-loaded van der Waals pegs; Section 2.1.1.4(11)). Additionally, after self-replication or extrusion of an improved device, some or all of these smooth walls could in principle be discarded, exposing whatever complex surface might be desired on any face. Similar considerations apply to the extrusion of desired non-self product objects during the analogous product manufacturing cycle.

2.1.1.3 Broadcast Architecture for Control

Von Neumann's proposed architectures for self-replication,[28] the replicating lunar factory designs proposed for NASA[29] in 1980 by Freitas and by von Tiesenhausen and Darbro, Drexler's original assembler proposals in 1986 and 1991,[30] and living systems all carry a complete set of plans for the system onboard the replicating system, in some form of internal memory. This is not a logical necessity in general manufacturing systems, as was observed by the 1980 NASA study (Freitas and Gilbreath,[31] p. 215): "It is quite possible to imagine the lunar factory operating nonautonomously...the in situ computer used simply as a teleoperation-management system for operations controlled directly by Earth-based workers [with] information necessary to accomplish [replication] supplied from outside. An alternative would permit the on-site computer to handle mundane tasks and normal functions with humans retaining a higher-level supervisory role."

Broadcast instructions (teleoperation) can enable system replication without internally stored instructions, an arrangement which has been termed the "broadcast architecture",[32] first described

---

[28] John von Neumann, Theory of Self-Reproducing Automata, A.W. Burks, ed., University of Illinois Press, Urbana IL, 1966.

[29] Robert A. Freitas Jr., William P. Gilbreath, eds., Advanced Automation for Space Missions, NASA Conference Publication CP-2255 (N83-15348), 1982; http://www.islandone.org/MMSG/aasm/.

[30] K. Eric Drexler, Nanosystems: Molecular Machinery, Manufacturing, and Computation, John Wiley & Sons, New York, 1992; http://www.zyvex.com/nanotech/nanosystems.html. K. Eric Drexler, Chris Peterson, Gayle Pergamit, Unbounding the Future: The Nanotechnology Revolution, William Morrow/Quill Books, NY, 1991; http://www.foresight.org/UTF/Unbound_LBW/.

[31] Robert A. Freitas Jr., William P. Gilbreath, eds., Advanced Automation for Space Missions, NASA Conference Publication CP-2255 (N83-15348), 1982; http://www.islandone.org/MMSG/aasm/.

[32] K. Eric Drexler, Nanosystems: Molecular Machinery, Manufacturing, and Computation, John Wiley & Sons, New York, 1992; http://www.zyvex.com/nanotech/nanosystems.html. Ralph C. Merkle, "Self-replicating systems and low cost manufacturing," in M.E. Welland, J.K. Gimzewski, eds., The Ultimate Limits of Fabrication and Measurement, Kluwer, Dordrecht, 1994, pp. 25-32; http://www.zyvex.com/nanotech/selfRepNATO.html. Ralph C. Merkle, "Design-ahead for

in the parallel-operation nanotechnological context in Section 16.3.2(a) of *Nanosystems*[33]: "Broadcast instructions. Replacing computers and stored instructions with broadcast instructions can simplify molecular manufacturing systems. Signals can be broadcast to molecular mechanical systems in several ways, but signaling by modulated pressure via mechanical transducers is both simple and adequate." Similar conclusions have been reached by space technologists who suggest using remote-control procedures (e.g., "teleoperation," "telepresence," "telerobotics," or "teleautonomy")[34] to reduce the high cost of items that would otherwise have to be expensively raised into orbit.

Figure 2-7. Schematic of the broadcast architecture for control.[35]

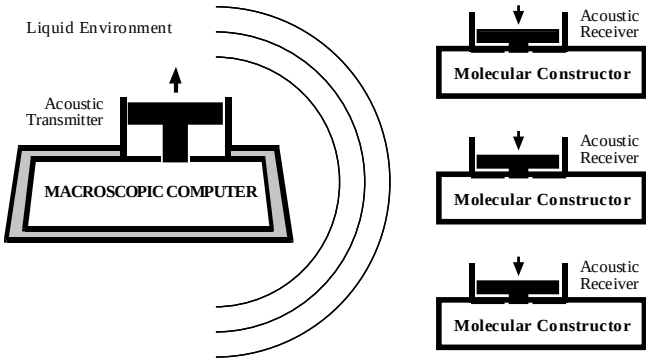

If we separate the "constructor" from the "computer" and allow many individual constructors to receive broadcast instructions from a single central computer, then each constructor need not remember the plans for what it is going to construct.[36] Rather, it can simply be told what to do as it does it (Figure 2-7). This approach eliminates the requirement for an integral repository of

---

nanotechnology," in Markus Krummenacker, James Lewis, eds., Prospects in Nanotechnology: Toward Molecular Manufacturing, John Wiley & Sons, New York, 1995, pp. 23-52.

[33] K. Eric Drexler, Nanosystems: Molecular Machinery, Manufacturing, and Computation, John Wiley & Sons, New York, 1992; http://www.zyvex.com/nanotech/nanosystems.html.

[34] George Bekey, Ivan Bekey, David Criswell, George Friedman, Dan Greenwood, David Miller, Peter Will, "NSF-NASA Workshop on Autonomous Construction and Manufacturing for Space Electrical Power Systems," Final Report, 4-8 April 2000, Arlington VA; http://robot.usc.edu/spacesolarpower/report.doc. See Workshop website at http://robot.usc.edu/spacesolarpower/ or at http://web.archive.org/web/20010821065927/robot.usc.edu/spacesolarpower/.

[35] Robert A. Freitas Jr., Ralph C. Merkle, Kinematic Self-Replicating Machines, Landes Bioscience, Georgetown, TX, 2004; Section 4.11.3, pp. 130-135; http://www.MolecularAssembler.com/KSRM/4.11.3.htm.

[36] Ralph C. Merkle, "Self-replicating systems and low cost manufacturing," in M.E. Welland, J.K. Gimzewski, eds., The Ultimate Limits of Fabrication and Measurement, Kluwer, Dordrecht, 1994, pp. 25-32; http://www.zyvex.com/nanotech/selfRepNATO.html.

plans within the constructor (which is now the only component that must replicate) and also eliminates almost all of the mechanisms involved in decoding and interpreting those plans. This general approach is similar to the SIMD architecture of the Connection Machine,[37] in which a single complex central processor broadcasts instructions to a large number of very simple processors. Storing the program, decoding instructions, and other common activities are the responsibility of the single central processor; while the large number of small processors need only interpret a small set of very simple instructions, thus allowing those small processors to retain comparatively simple structure and function. It is interesting that the living cell also employs the broadcast architecture[38] on a massively-parallel scale, using chemical rather than electrical or acoustic signaling: the DNA-containing nucleus acts as a central computer and data repository that broadcasts chemical instructions in the form of mRNA messenger molecules to up to ten million[39] structurally simpler manufacturing devices distributed throughout the eukaryotic cytoplasm, called ribosomes. Following the instructions received from the messenger molecules, the ribosomes manufacture all cytoplasmic proteins using unidimensional positional assembly.[40]

The specific advantages of the broadcast architecture are that: (1) it reduces the size and complexity of the self-replicating component, (2) it allows the self-replicating component to be rapidly redirected to build something novel, and (3) it is "inherently safe"[41] because the individual constructors lack any capability to function autonomously, a feature that is particularly clear when the central computer is macroscopic and under our direct control. For these reasons we explicitly adopt the broadcast architecture for control in our proposed design for a molecular assembler.

2.1.1.4 Hydrocarbon Assembler Subsystems

The Merkle-Freitas Hydrocarbon Molecular Assembler consists of 12 major subsystems, as illustrated schematically in Figure 2-8, quantified in Table 2-1, and summarized below:

---

[37] Danny Hillis, The Connection Machine, MIT Press, Cambridge, MA, 1986.

[38] Ralph C. Merkle, "Self-replicating systems and low cost manufacturing," in M.E. Welland, J.K. Gimzewski, eds., The Ultimate Limits of Fabrication and Measurement, Kluwer, Dordrecht, 1994, pp. 25-32; http://www.zyvex.com/nanotech/selfRepNATO.html.

[39] Robert A. Freitas Jr., Nanomedicine, Volume I: Basic Capabilities, Landes Bioscience, Georgetown, TX, 1999; http://www.nanomedicine.com/NMI.htm.

[40] Robert A. Freitas Jr., Ralph C. Merkle, Kinematic Self-Replicating Machines, Landes Bioscience, Georgetown, TX, 2004; Section 4.2, pp. 96-101; http://www.MolecularAssembler.com/KSRM/4.2.htm.

[41] Robert A. Freitas Jr., Ralph C. Merkle, Kinematic Self-Replicating Machines, Landes Bioscience, Georgetown, TX, 2004; Section 5.11, pp. 196-199; http://www.MolecularAssembler.com/KSRM/5.11.htm.

Figure 2-8. Schematic view of Merkle-Freitas assembler subsystems.[42]

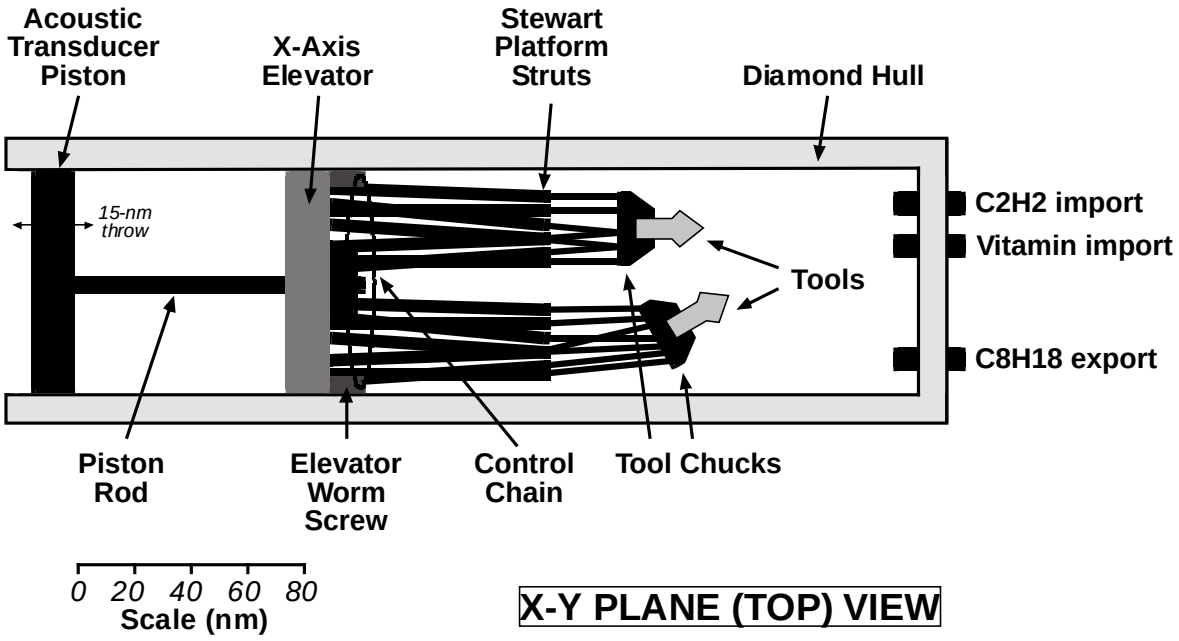

(1) Acetylene Binding Site and Import Mechanism. The acetylene binding site consists of a (9,0) carbon nanotube of open inside diameter 0.7 nm and 2 nm in length, long enough to contain up to 4 molecules of acetylene. The binding site is embedded in a diamond block drawer that can be mechanically slid back and forth through a rectangular hole in the I/O (input-output) wall of the hull while maintaining a tight seal. Once conveyed inside, an acetylene molecule is forced into the receiving chamber by a polyyne rod inserted into the binding site. A di-silicon radical (or other group IV element, possibly Sn,[43] or Ge;[44] further modeling work is required to

---

[42] Robert A. Freitas Jr., Ralph C. Merkle, Kinematic Self-Replicating Machines, Landes Bioscience, Georgetown, TX, 2004; Section 4.11.3, pp. 130-135; http://www.MolecularAssembler.com/KSRM/4.11.3.htm.

[43] Ralph C. Merkle, Robert A. Freitas Jr., "Theoretical analysis of a carbon-carbon dimer placement tool for diamond mechanosynthesis," ***J. Nanosci. Nanotechnol.*** 3(August 2003):319-324; http://www.rfreitas.com/Nano/JNNDimerTool.pdf. See also: Ralph C. Merkle, Robert A. Freitas Jr., "Theoretical analysis of a carbon-carbon dimer placement tool for diamond mechanosynthesis," paper presented at the 10th Foresight Conference on Molecular Nanotechnology, October 2002; http://www.foresight.org/Conferences/MNT10/Abstracts/Merkle/index.html.

[44] Jingping Peng, Robert A. Freitas Jr., Ralph C. Merkle, James R. Von Ehr, John N. Randall, George D. Skidmore, "Theoretical Analysis of Diamond Mechanosynthesis. Part III. Positional C_2 Deposition on Diamond C(110) Surface using Si/Ge/Sn-based Dimer Placement Tools," J. Comput. Theor. Nanosci. 3(February 2006):28-41; http://www.MolecularAssembler.com/Papers/JCTNPengFeb06.pdf.

validate a specific molecular tool) aligned to the acetylene molecule inside the receiving chamber binds the acetylene covalently, whereupon the captured feedstock molecule can be safely transported elsewhere inside the device for further mechanosynthetic processing.

(2) Vitamin Binding Site and Import Mechanism. When product objects consisting entirely of carbon and hydrogen atoms are to be fabricated, no vitamin imports are required during the manufacturing cycle. However, during the fabrication of a daughter device (e.g., self-replication) it is necessary to import 30 atoms each of Si and Sn (or other group IV element, like Ge) so that the mechanosynthetic tool tips of the daughter may be constructed by the assembler. Chemically inert vitamin molecules consisting of an easily disassembled Si- and Sn- (or Ge-) containing hydrocarbon complex are added at a parts-per-billion trace concentration to the external solvent fluid, but only a dozen of these molecules need be imported during the entire 10^6-sec replication cycle of the device.

Table 2-1. Atom count and volume of all major subsystems in the Merkle-Freitas hydrocarbon molecular assembler

Assembler Sub-system (# in M.A.)	**---------- atom counts ----------**					**Total Volume (nm^3)**
	C	**H**	**Si**	**Sn**	**Total Atoms**	
Hull and Piston (1)	180,576,282	6,619,130	0	0	187,195,412	1,026,001.6
Elevator (1)	5,632,000	276,320	0	0	5,908,320	32,000.0
Daughter Downhang	4,928,000	464,720	0	0	5,392,720	28,000.0
Stewrt. Platforms (2)	2,804,751	736,535	0	0	3,541,286	15,936.1
Extrusion Springs	528,000	326,560	0	0	854,560	3,000.0
Piston Rod (1)	225,280	41,197	0	0	266,477	1,280.0
Control Chain (1)	140,800	105,504	0	0	246,304	800.0
Mater. Transport (3)	152,064	45,216	0	0	197,280	864.0
Elevator Screws (4)	138,230	17,408	0	0	155,638	196.3
Tool Tips (30)	105,600	45,216	30	30	150,876	600.0
Internal Vacuum	0	0	0	0	0	892,754.0
TOTALS	**195,231,007**	**8,677,806**	**30**	**30**	**203,908,873**	**2,001,432.0**

(3) Octane Assembly Site and Export Mechanism. n-Octane molecules are mechanosynthesized by combining excess hydrogen atoms with acetylenic precursors in a narrow hydrogen-passivated reaction bay that opens to the external solvent through an exhaust tube (terminating at the I/O wall) just beyond a narrow throat. After final synthesis and release of the n-octane molecule, a carbene rod is inserted into the bay and irreversibly forces the n-octane molecule through the resistive energy barrier at the throat and into the exhaust tube.

(4) Acoustic Transducer. Externally generated pressure pulses between 1-3 atm drive the acoustic transducer through a 15 nm throw, producing a linear rod motion that provides information and mechanical power to the assembler device. The transducer has 3 components: (A) a piston plate (a hydrogen-terminated 10-nm thick rectangular diamond block with 45°-clipped corners to accommodate the legs of the van der Waals cage; see (11) below); (B) a piston rod 4-nm thick attached to the center of the piston plate and extending back through the elevator plate to engage the control chain mechanism that is attached to the other side of the elevator plate, in the assembler interior; and (C) the piston spring, attached to the exterior face of the elevator plate at one end and to the piston rod at the other end, to provide a restoring force.

During replication, the daughter device is manufactured with its piston mechanically locked; slowly cycling through 4 atm unlocks this piston, synchronizing daughter(s) and parent (whose piston is already unlocked) in preparation for the next replicative cycle.

(5) X-Axis Elevator. The 10-nm thick diamond elevator block permits motion of the entire piston-manipulator assembly along the X-axis of the assembler. Movement of the elevator is achieved by four capstan-driven worm screws that engage a linear sequence of shallow slots on the inner face of the hull wall. The control chain mechanism and Stewart platform struts are attached to the interior face of the elevator plate.

(6) Stewart Platform Manipulators. All mechanical manipulations in the interior of the device are performed by either or both of a pair of Stewart platform manipulators.[45] Each manipulator consists of a tool chuck mounted via universal joints to 6 telescoping struts mounted at their base to universal joints affixed to the interior face of the elevator block. Each strut is a matched pair of internally-threaded and externally-threaded tubes, whose capstan-driven relative helical motion extends or retracts the strut. An additional 7th control strut allows interchangeable tool tips to be grasped or released by the tool chuck.

(7) Control Chain. The control chain consists of a single flexible molecular ribbon with a number of graphitic knobs integrally affixed to known positions along its length. A latchlike mechanism at the end of the piston rod engages the chain, converting piston-driven axial rod motion to transverse chain motion and forcing the chain to move. All normal operations use two pressure bands – an upper band from 2-3 atm and a lower band from 1-2 atm. The chain engages latching mechanisms at the control capstans of all elevator worm screws and Stewart platform struts. Cycling across the upper band steps the control chain forward, applying power to successive control capstans. Cycling across the bottom band steps the control chain backwards, but without applying power to any control capstans. Cycling across both bands (from 1-3 atm) causes the control chain to step back and forth over the same control capstan, repeatedly applying power only to that one control capstan.

(8) Tool Garage, Tools, and Tool Tips. A complete set of molecular tool tips[46] sufficient to perform all required mechanosynthetic functions during replication and product manufacturing,

---

[45] K. Eric Drexler, Nanosystems: Molecular Machinery, Manufacturing, and Computation, John Wiley & Sons, New York, 1992; http://www.zyvex.com/nanotech/nanosystems.html. Ilian Bonev, "What is Going on With Parallel Robots," Robotics Online, accessed September 2003; http://www.roboticsonline.com/public/articles/articlesdetails.cfm?id=798.

[46] Jingping Peng, Robert A. Freitas Jr., Ralph C. Merkle, "Theoretical Analysis of Diamond Mechanosynthesis. Part I. Stability of C_2 Mediated Growth of Nanocrystalline Diamond C(110) Surface," J. Comput. Theor. Nanosci. 1(March 2004):62-70; http://www.MolecularAssembler.com/JCTNPengMar04.pdf. Jingping Peng, Robert A. Freitas Jr., Ralph C. Merkle, James R. Von Ehr, John N. Randall, George D. Skidmore, "Theoretical Analysis of Diamond Mechanosynthesis. Part III. Positional C_2 Deposition on Diamond C(110) Surface using Si/Ge/Sn-based Dimer Placement Tools," J. Comput. Theor. Nanosci. 3(February 2006):28-41; http://www.MolecularAssembler.com/Papers/JCTNPengFeb06.pdf. Ralph C. Merkle, Robert A. Freitas Jr., "Theoretical analysis of a carbon-carbon dimer placement tool for diamond mechanosynthesis," J. Nanosci. Nanotechnol. 3(August 2003):319-324; http://www.rfreitas.com/Nano/JNNDimerTool.pdf. See also: Ralph C. Merkle, Robert A. Freitas Jr., "Theoretical analysis of a carbon-carbon dimer placement tool for

including diamond fabrication and deconstruction, hydrogenation and dehydrogenation of surfaces, and tool tip recharge and fabrication are stored in the garage. Graspable jigs for operating molecular import/export mechanisms, controlling extrusion, or extending van der Waals cages are stored in the tool garage, all within reach of the Stewart platform manipulators.

(9) Subassembly Stations. Several areas designated as subassembly stations include wall-mounted active tips, fixed jigs, and other mechanisms by which intermediate structures can be temporarily parked during fabrication, either to allow more efficient execution of manufacturing sequences or to allow more complex assembly operations such as insertion motions.

(10) Extrusion Control System. Manufacture of product object proceeds downward from the extrusion hole towards the opposite floor. When sufficient fabrication has been completed, the workpiece is ratcheted upward a controlled distance by sequentially pulling spring-loaded locking pins out of their staggered complementary pinholes in the exterior face of the workpiece and re-inserting them into the next-lowest pinhole in the workpiece exterior face. This provides a controlled extrusion process, provides mechanical resistance to hydrostatic backpressure and oscillatory acoustic forcing, and ensures that extrusion takes place even if resisted by significant external forces.

(11) Van der Waals Cages and Pegs. Multiple devices whose smooth, flat parallel surfaces approach too closely will be attracted to each other by van der Waals forces, in some cases noncovalently bonding into randomly-ordered aggregates. To prevent such surface bonding and consequent blockage of the I/O wall and the piston wall, two cages of rods configured as wire-frame boxes are extended into the external environment from the I/O and piston walls, as soon as physically possible. Short spring-loaded pegs also deploy from the outer face of the locked piston on extruding daughters and granddaughter devices (or the equivalent face for other product objects) as soon as physically possible, thus geometrically lessening surface attractive forces and reducing any attractive interdevice forces that might resist extrusion.

(12) Passive Hull System. The vast majority (~90%) of all carbon atoms present in the Merkle-Freitas Hydrocarbon Molecular Assembler constitute the 10-nm thick solid diamond hull. This passive hull is penetrated by three openings for materials import/export (I/O wall), by the piston plate at the opposite end (piston wall), by van der Waals cages at either end, and by the extrusion hole in which the daughter device or product object resides while it is being fabricated and extruded.

---

diamond mechanosynthesis," paper presented at the 10th Foresight Conference on Molecular Nanotechnology, October 2002; http://www.foresight.org/Conferences/MNT10/Abstracts/Merkle/index.html. Ralph C. Merkle, "A proposed 'metabolism' for a hydrocarbon assembler," Nanotechnology 8(1997):149-162; http://www.zyvex.com/nanotech/hydroCarbonMetabolism.html.

2.1.1.5 Floating Hydrocarbon Assemblers vs. Fixed Nanofactory Configurations

There are a few arguments favoring floating replicating assemblers over fixed nanofactories, though we do not regard them as sufficiently persuasive. The main arguments favoring standalone fluid-resident assemblers are these:

First, if one floating unit fails, the entire population of working assemblers barely notices. Operations are inherently maximally parallel, since each assembler drops its output into the fluid medium, to float away. In contrast, if a nanofactory production line unit fails, then the whole line fails and must be shut down.

Second, if one free floating assembler fails, it can report to a recycle station, or can raise a flag and be picked up for recycle by scavenger nanorobots that are floating around for just this purpose. Again, operations continue as before. By contrast, a failed unit on a fixed production line is buried deep within the factory structure. It would be very difficult to change it out without halting production in at least a portion of the factory, cracking it open, and lifting the bad item out and inserting a new one – if such repair is even possible.

Third, power may be broadcast omnidirectionally in the case of free-floating units, so wherever the assemblers are floating around they can still receive power and keep working. By contrast, all production units in a factory must be physically tethered to a power supply, either by a wire, a rotating power cable, a chemical feedstock supply line, or some other similar means.

The main advantages of a fixed nanofactory configuration are the ease of scale-up to microscale and macroscale product objects, the ability to operate in a controlled vacuum environment at all times, and the ability to avoid the complexities of interacting with a fluidic environment during feedstock import, product export, power transfer, and the like. The systemic advantages of the floating assemblers in situations where individual units fail may be offset by a sufficient increase in the reliability of nanofactory manufacturing modules.

2.1.2 Zyvex Exponential Assembly (1999-2000)

At the micron scale, using existing MEMS (microelectromechanical systems) technology, Zyvex Corp. has designed simple pick-and-place robotic arms that could pick up relatively complex, planar, micron-scale parts made using lithographic techniques and then assemble those planar parts into simple three-dimensional robotic arms that have the ability to pick up specially designed MEMS parts. In Zyvex's Rotapod™ exponential assembly design,[47] this replicative technology starts with a single robotic arm on a wafer (Figure 2-9) that makes a second robotic

---

[47] George D. Skidmore, Eric Parker, Matthew Ellis, Neil Sarkar, Ralph Merkle, "Exponential assembly," paper presented at the 8th Foresight Conference, Washington DC, November 2000; http://www.foresight.org/Conferences/MNT8/Papers/Skidmore/index.html and http://www.zyvex.com/Publications/papers/exponentialGS.html. See also: "Exponential Assembly", 25 September 2001; http://www.zyvex.com/Research/exponential.html.

arm on a facing surface by picking up miniature parts — carefully laid out in advance in exactly the right locations so the tiny robotic arm can find them — and assembling them (Figure 2-10). The two robotic arms then make two more robotic arms, one on each of the two facing surfaces. These four robotic arms, two on each surface, then make four more robotic arms. This process continues with the number of robotic arms steadily increasing in the pattern 1, 2, 4, 8, 16, 32, 64, etc., until some manufacturing limit is reached (e.g., both surfaces are completely covered with tiny robotic arms). This is an exponential growth rate, hence the name exponential assembly, but the assembly process requires (among other things) lithographically produced parts as well as externally provided power and computer control signals to coordinate the complex motions of the robotic arms. Thus this approach is an example of both the broadcast architecture (for instructions) and the vitamin architecture (for parts and energy) being employed in a single system. As a result, this system is *very* "inherently safe".[48]

While a general purpose robotic arm having six degrees of free movement (like human arms and hands) would be able to pick up parts and position them in any orientation and position desired, such a general purpose arm is harder to make. Zyvex's simpler Rotapod™ design uses robotic arms having only two rotational degrees of freedom and a gripper (Figure 2-10), while offloading three degrees of freedom to the external environment: the surfaces on which the parts are arrayed can be moved in X, Y and Z, providing a total of five degrees of freedom for each robotic arm, with the three translational degrees of freedom being shared across all the robotic arms on a surface. Externally provided power and computer control cause all the robotic arms on a surface to operate synchronously and in parallel.

Figure 2-9. Basic two-component Rotapod™ assembly station from Zyvex Corp.[49]

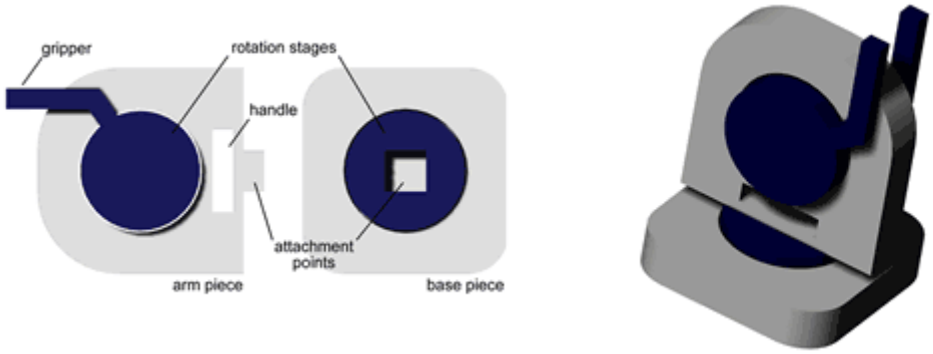

Left: *The rotational stages are labeled as are the gripper, handle, and attachment points.*

Right: *When the two components are assembled, the assembly station is as shown.*

---

[48] Robert A. Freitas Jr., Ralph C. Merkle, Kinematic Self-Replicating Machines, Landes Bioscience, Georgetown, TX, 2004; Section 5.11, pp. 196-199; http://www.MolecularAssembler.com/KSRM/5.11.htm.

[49] George D. Skidmore, Eric Parker, Matthew Ellis, Neil Sarkar, Ralph Merkle, "Exponential assembly," paper presented at the 8th Foresight Conference, Washington DC, November 2000; http://www.foresight.org/Conferences/MNT8/Papers/Skidmore/index.html and http://www.zyvex.com/Publications/papers/exponentialGS.html. See also: "Exponential Assembly", 25 September 2001; http://www.zyvex.com/Research/exponential.html.

Figure 2-10. Sequence of Rotapod™ assembly operations necessary for the first station to assemble the second, from Zyvex Corp.[50]

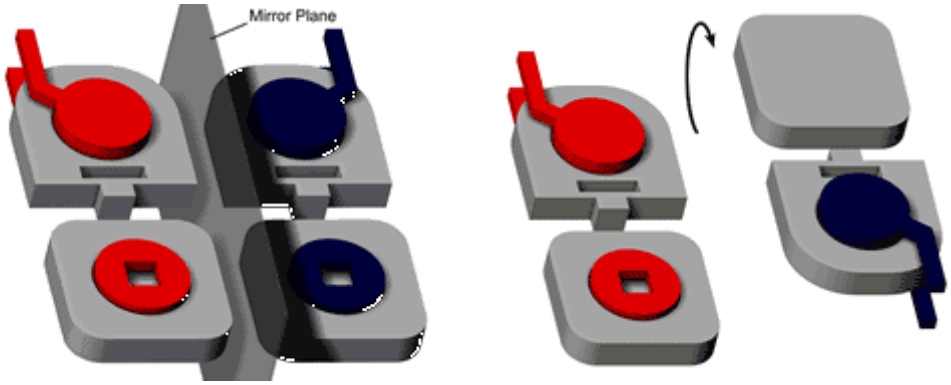

A. *The stations are first shown unassembled.*

B. *After rotating one of the stations, the two are shown facing each other.*

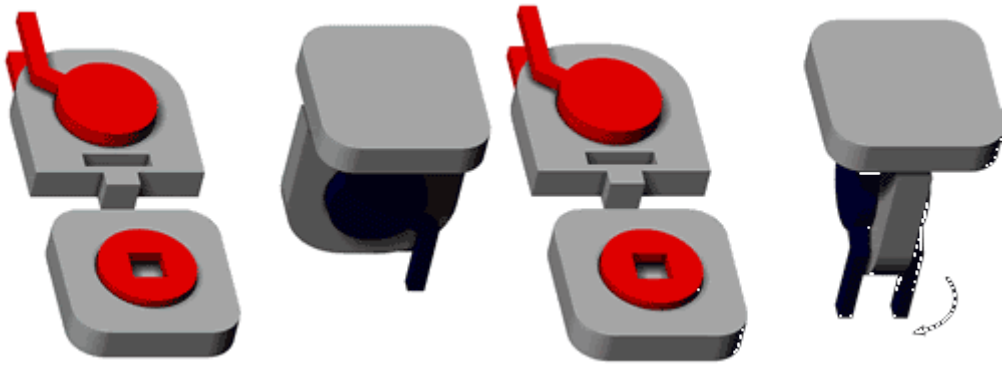

C. *The first is then assembled.*

D. *The assembled station first rotates about the z-axis.*

---

[50] George D. Skidmore, Eric Parker, Matthew Ellis, Neil Sarkar, Ralph Merkle, "Exponential assembly," paper presented at the 8th Foresight Conference, Washington DC, November 2000; http://www.foresight.org/Conferences/MNT8/Papers/Skidmore/index.html and http://www.zyvex.com/Publications/papers/exponentialGS.html. See also: "Exponential Assembly", 25 September 2001; http://www.zyvex.com/Research/exponential.html.

Figure 2-10. (cont'd)

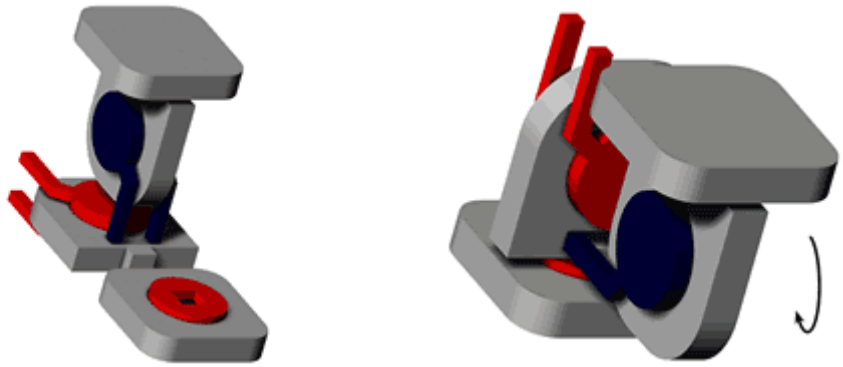

E. *It then translates to grip the component of the other.* ***F.*** *The second rotation stage of station one then rotates 90 degrees and the surface then translates such that the attachment points are aligned with translation.*

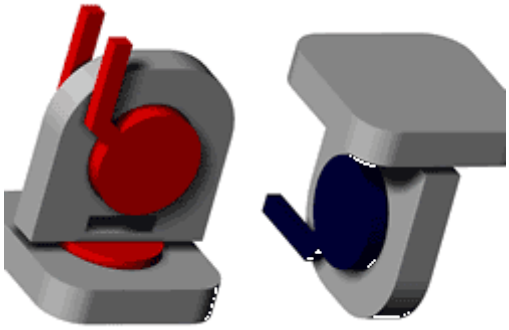

G. *After the attachment is made the gripper releases and the assembly is completed.*

Exponential assembly can be implemented on many different length scales. Given existing manufacturing capabilities, it should be possible to implement exponential assembly using MEMS technology with device sizes measuring tens or hundreds of microns and feature sizes of about one micron. Each rotational degree of freedom could be implemented using a planar rotating stage produced using standard lithographic techniques. Two such rotating stages can be attached at right angles, providing the desired two degrees of rotational freedom for this assembly station. A gripper attached to one rotating stage completes the basic design. Assembly of the first robotic arm could be done manually using Zyvex's MEMbler™ conceptual MEMS assembly station.[51] Having assembled the first robotic arm, the Rotopod™ could then assemble further

---

[51] Animations of MEMS assembly conceptualization; ; http://www.zyvex.com/research/exponential.html. MEMbler TM, see http://www1.zyvex.com:8080/ramgen/videos/mems_adaptive.rm and the RealVideoTM at http://www1.zyvex.com/videos/mems_adaptive.rm.

robotic arms in exponentially increasing numbers (Figure 2-11), as illustrated in an animation.[52] In 2003, a patent "Method and System for Self-Replicating Manufacturing Stations" (#6,510,358) for this manufacturing system was issued to Zyvex by the U.S. Patent Office.[53] A crudely analogous electrophoretic system for stepwise exponential growth of DNA-based chemical replicators using pairs of alternating opposed deposition surfaces has been proposed by von Kiedrowski's group.[54]

---

[52] Animations of exponential assembly; http://www.zyvex.com/research/exponential.html. Rotapod ™ exponential assembly apparatus, see http://www1.zyvex.com:8080/ramgen/videos/roto_adaptive.rm and the RealVideoTM at http://www1.zyvex.com/videos/roto_adaptive.rm.

[53] Ralph C. Merkle, Eric G. Parker, George D. Skidmore, "Method and system for self-replicating manufacturing stations," United States Patent No. 6,510,359, 21 January 2003; http://patft.uspto.gov/netacgi/nph-Parser?Sect1=PTO1&Sect2=HITOFF&d=PALL&p=1&u=/netahtml/srchnum.htm&r=1&f=G&l=50&s1=6,510,359.WKU.&OS=PN/6,510,359.

[54] A. Luther, R. Brandsch, G. von Kiedrowski, "Surface-promoted replication and exponential amplification of DNA analogues," Nature 396(19 November 1998):245-248; B.G. Bag, G. von Kiedrowski, "Stepwise Replication of a Troger's Base Analogue," Angew. Chem. Int. Ed. Engl. 38(16 December 1999):3713-3714; Lars Henning Eckardt, Kai Naumann, Wolf Matthias Pankau, Michael Rein, Markus Schweitzer, Norbert Windhab, Günter von Kiedrowski, "DNA nanotechnology: Chemical copying of connectivity," Nature 420(21 November 2002):286, http://www.nature.com/nlink/v420/n6913/abs/420286a_fs.html; Guenter von Kiedrowski, Lars-Henning Eckardt, Kai Naumann, Wolf Matthias Pankau, Malte Reimold, Michael Rein, "Toward replicatable, multifunctional, nanoscaffolded machines. A chemical manifesto," Pure Appl. Chem. 75(2003):609-619.

Figure 2-11. Result of five generations of Rotapod™ exponential assembly operations (one completed robotic wafer shown, of two), from Zyvex Corp.[55]

In 2001, Zyvex was awarded a $25 million, five-year, National Institute of Standards and Technology (NIST) Advanced Technology Program government contract – to develop prototype microscale assemblers using microelectromechanical systems (MEMS), extend the capabilities to nanometer geometries, and then to develop nanoelectromechanical systems (NEMS) for prototype nanoscale assemblers.[56] Along with its commercial partners and its university collaborators (Rensselaer Polytechnic Institute Center for Automation Technologies,[57] the University of Texas at Dallas, and the University of North Texas), Zyvex hoped to accelerate the production and commercialization of low-cost assemblers for micro- and nanoscale components and subsystems. The ultimate program goal through 2006 was nothing less than automated micro- and nano-manufacturing – the design and construction of "assemblers" capable of

---

[55] George D. Skidmore, Eric Parker, Matthew Ellis, Neil Sarkar, Ralph Merkle, "Exponential assembly," paper presented at the 8th Foresight Conference, Washington DC, November 2000; http://www.foresight.org/Conferences/MNT8/Papers/Skidmore/index.html and http://www.zyvex.com/Publications/papers/exponentialGS.html. See also: "Exponential Assembly", 25 September 2001; http://www.zyvex.com/Research/exponential.html.

[56] "NIST-ATP Project for Assembly of Microsystems," Zyvex Corp., 2003; http://www.zyvex.com/Research/projects.html#NISTProject. Zyvex Corp., "Research and Development Activities," 8 September 2003; http://www.zyvex.com/Research/projects.html.

[57] Center for Automation Technologies, Rensselaer Polytechnic Institute, 2002; http://www.cat.rpi.edu/r&d.htm.

handling thousands of sub-micrometer components at high speed, using MEMS to prototype systems which could then be built at relatively low cost. Zyvex demonstrated[58] a set of 50-micron "snap and lock" building blocks that provides a unique attachment technology to fabricate and assemble MEMS elements into 3D microscale structures (Figure 2-12). The Zyvex/NIST program ended in 2006 having achieved many of the intermediate goals for the automated assembly of microscale components (fabricating using conventional lithography) but without achieving the broader goal of the massively parallel construction of large batches of identical molecular machines simultaneously.

Figure 2-12. (A) Microgrippers are micromachined from single crystal silicon, yielding active end-effectors that can be driven by electrothermal micromachined actuators. (B) The gripper can manipulate microcomponents having features as small as ~1 micron. (C) MEMS components can be detached from a release surface and assembled into 3D "Nanolock™ structures" created using Zyvex's MechTile™ assembly process. Courtesy of Zyvex Corp.[59]

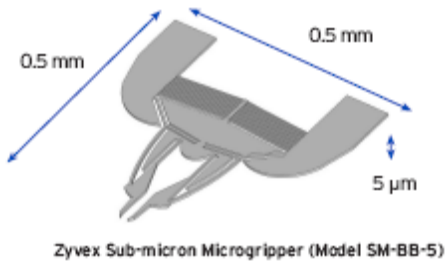

(A)

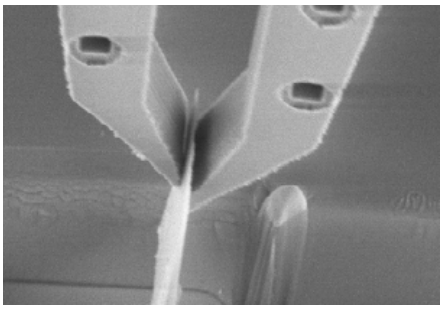

(B)

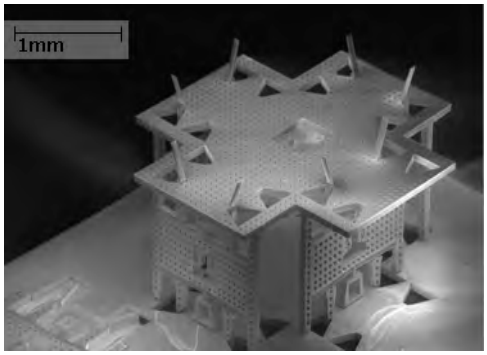

(C)

---

[58] "Zyvex Core Competencies," 2006; http://www.zyvex.com/Products/structures.html.
[59] "Zyvex Core Competencies," 2006; http://www.zyvex.com/Products/structures.html.

2.1.3 Drexler Nanofactory (1991-1992)

In the "unit growth" or factory model, a population of specialist devices, each one individually incapable of self-replication, can collectively fabricate and assemble all necessary components comprising all specialist devices within the system, hence the factory is capable of expanding its size (or of manufacturing duplicate factory systems) indefinitely in an appropriate environment. In Figure 2-13, a molecular manipulator arm (Figure 2-14) performs molecular assembly operations on a passing workpiece attached to a conveyor belt. The workpieces eventually move from one manipulator arm to the next in series, each arm performing specialized tasks, finally resulting in a completed factory component which can be joined with other completed factory components, either to expand the size of the current factory or to replicate another copy of the original factory. Thousands of manipulator arms could fit in the volume of a single cubic micron.

Figure 2-13. Drexler factory replicator[60]

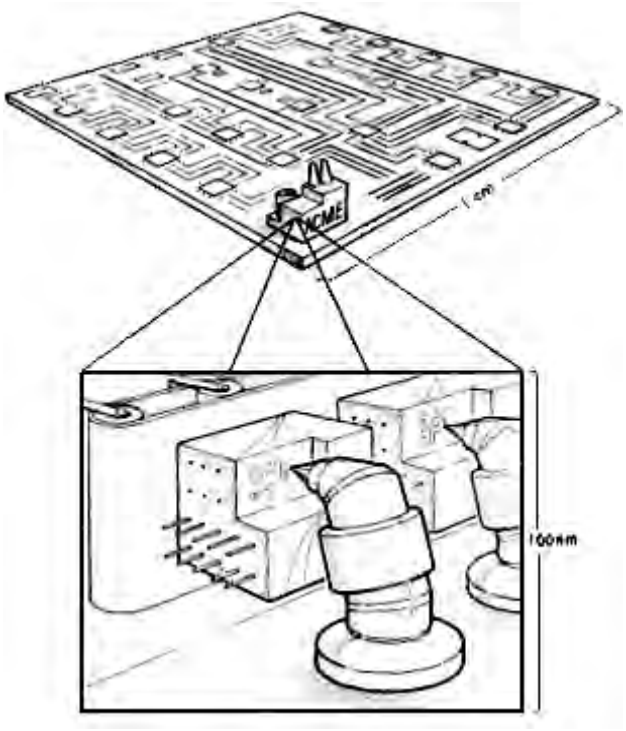

As Drexler describes this approach in an early popular presentation[61] in 1991: "This general-purpose assembler concept resembles, in essence, the factory robots of the 1980s. It is a

---

[60] K. Eric Drexler, Chris Peterson, Gayle Pergamit, Unbounding the Future: The Nanotechnology Revolution, William Morrow/Quill Books, NY, 1991; http://www.foresight.org/UTF/Unbound_LBW/.

[61] K. Eric Drexler, Chris Peterson, Gayle Pergamit, Unbounding the Future: The Nanotechnology Revolution, William Morrow/Quill Books, NY, 1991; http://www.foresight.org/UTF/Unbound_LBW/.

computer-controlled mechanical arm that moves molecular tools according to a series of instructions. Each tool is like a single-shot stapler or rivet gun. It has a handle for the assembler to grab and comes loaded with a little bit of matter – a few atoms – which it attaches to the workpiece by a chemical reaction. Molecular bonds hold things together. In strong, stable materials atoms are either bonded, or they aren't, with no possibilities in between. Assemblers work by making and breaking bonds, so each step either succeeds perfectly or fails completely. In [pre-molecular] manufacturing, parts were always made and put together with small inaccuracies. These could add up to wreck product quality. At the molecular scale, these problems vanish. Since each step is perfectly precise, little errors can't add up. The process either works, or it doesn't. Thermal vibrations can cause mistakes by causing parts to come together and form bonds in the wrong place. Thermal vibrations make floppy objects bend further than stiff ones, and so these assembler arms were designed to be thick and stubby to make them very stiff. Error rates can be kept to one in a trillion [10^{-12}], and so small products can be perfectly regular and perfectly identical. Large products can be almost perfect, having just a few atoms out of place."

Figure 2-14. Cross-section of a stiff molecular manipulator arm, with identification of parts, courtesy of K. Eric Drexler.[62] Copyright © 1992 by John Wiley & Sons, Inc. Used with permission. http://www.zyvex.com/nanotech/nanosystems.html. Image of Fine Motion Controller © IMM, http://www.imm.org. Image of ribosome © PDB http://www.rcsb.org/pdb/newsletter/2000q4/mom.html.

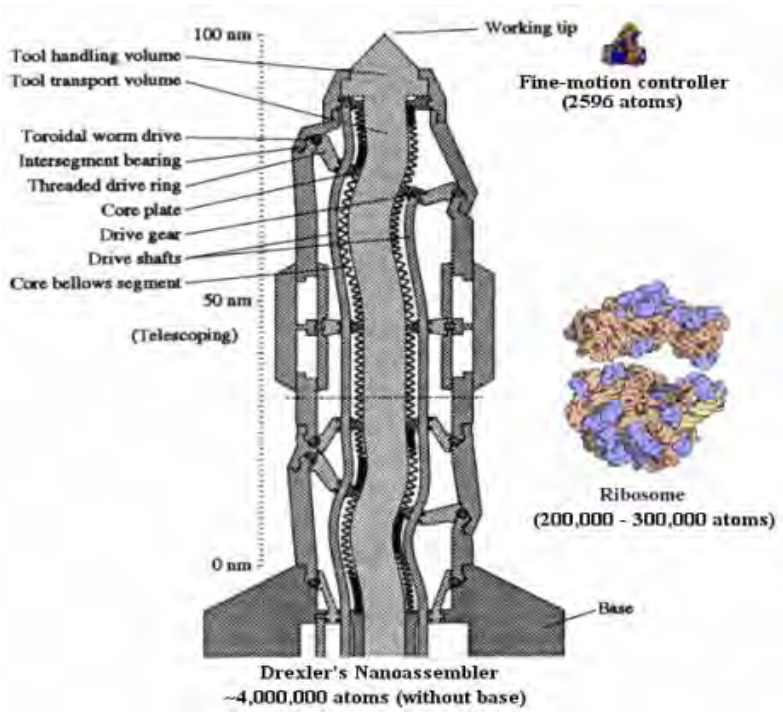

[62] K. Eric Drexler, Nanosystems: Molecular Machinery, Manufacturing, and Computation, John Wiley & Sons, New York, 1992; http://www.zyvex.com/nanotech/nanosystems.html.

In a description of what a microscopic observer would see of this process, from inside a virtual reality simulation, Drexler writes:[63] "One assembler arm is bent over with its tip pressed to a block on the conveyor belt. Walking closer, you see molecular assembly in action. The arm ends in a fist-sized knob with a few protruding marbles, like knuckles. Right now, two quivering marbles – atoms – are pressed into a small hollow in the block. As you watch, the two spheres shift, snapping into place in the block with a quick twitch of motion: a chemical reaction. The assembler arm just stands there, nearly motionless. The fist has lost two knuckles, and the block of nanocomputer is two atoms larger. [A few moments later], the assembler arm has moved by several atom-widths. Through the translucent sides of the arm you can see that the arm is full of mechanisms: twirling shafts, gears, and large, slowly turning rings that drive the rotation and extension of joints along the trunk. The whole system is a huge, articulated robot arm. The arm is big because the smallest parts are the size of marbles, and the machinery inside that makes it move and bend has many, many parts. Inside, another mechanism is at work: the arm now ends in a hole, and you can see the old, spent molecular tool being retracted through a tube down the middle. Within a few minutes, a new tool is on its way back up the tube. Eventually, it reaches the end. Shafts twirl, gears turn, and clamps lock the tool in position. Other shafts twirl, and the arm slowly leans up against the workpiece again at a new site. Finally, with a twitch of motion, more atoms jump across, and the block is again just a little bit bigger. The cycle begins again. This huge arm seems amazingly slow, but the standard simulation settings have shifted speeds by a factor of over 400 million. A few minutes of simulation time correspond to less than a millionth of a second of real time, so this stiff, sluggish arm is completing about a million operations per second."

The molecular manufacturing factory employs the principle of "convergent assembly"[64] to maximize efficiency. Using convergent assembly, molecular assemblers build blocks that go to block assemblers. The block assemblers build block assemblies, which go to system assemblers, which build systems, and so forth. "If a car were assembled by normal-sized robots from a thousand pieces, each piece having been assembled by smaller robots from a thousand smaller pieces, and so on, down and down," Drexler explains,[65] "then only ten levels of assembly process would separate cars from molecules." In Drexler's proposed fractal convergent assembly process (Figure 2-15), the motion of components being assembled traces a tree in space. The trunk corresponds to the path traced by the final workpiece as the final components are assembled, the branches correspond to the paths traced by those components as they are assembled from simpler parts, and so forth – with the final stages resembling the middle and earlier stages, thus creating a

---

[63] K. Eric Drexler, Chris Peterson, Gayle Pergamit, Unbounding the Future: The Nanotechnology Revolution, William Morrow/Quill Books, NY, 1991; http://www.foresight.org/UTF/Unbound_LBW/.

[64] K. Eric Drexler, Nanosystems: Molecular Machinery, Manufacturing, and Computation, John Wiley & Sons, New York, 1992; http://www.zyvex.com/nanotech/nanosystems.html. Ralph C. Merkle, "Convergent assembly," Nanotechnology 8(1997):18-22; http://www.zyvex.com/nanotech/convergent.html.

[65] K. Eric Drexler, Chris Peterson, Gayle Pergamit, Unbounding the Future: The Nanotechnology Revolution, William Morrow/Quill Books, NY, 1991; http://www.foresight.org/UTF/Unbound_LBW/.

fractal progression.[66] Merkle[67] proposed a simpler configuration (Figure 2-16) that retains many of the desirable performance characteristics of Drexler's system.

Figure 2-15. Drexler's exemplar architecture for convergent assembly.[68]

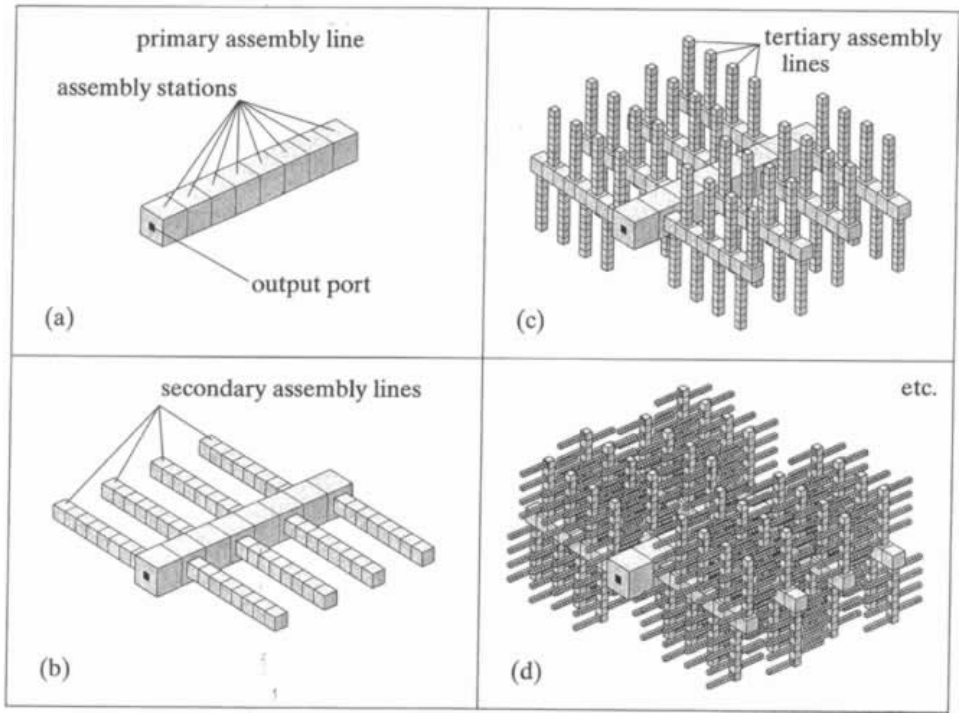

This simple model of a spatial arrangement for a hierarchical convergent assembly process illustrates successively more detailed diagrams of the intended process. In (a), a primary assembly line consisting of a series of 8 assembly stations (drawn as cubes) performs the final 8 assembly operations in a hypothetical manufacturing process. In (b), 8 secondary assembly lines provide parts to the final lines. Panels (c) and (d) illustrate tertiary and quaternary assembly lines. Since each level of lines contains an equal volume, this pattern cannot be indefinitely extended without self-intersection; that is, the maximum radius of expansion is bounded.

---

[66] K. Eric Drexler, Nanosystems: Molecular Machinery, Manufacturing, and Computation, John Wiley & Sons, New York, 1992; http://www.zyvex.com/nanotech/nanosystems.html.

[67] Ralph C. Merkle, "Convergent assembly," Nanotechnology 8(1997):18-22; http://www.zyvex.com/nanotech/convergent.html. Robert A. Freitas Jr., Ralph C. Merkle, Kinematic Self-Replicating Machines, Landes Bioscience, Georgetown, TX, 2004; Section 5.9.4, pp. 191-193; http://www.MolecularAssembler.com/KSRM/5.9.4.htm.

[68] K. Eric Drexler, Nanosystems: Molecular Machinery, Manufacturing, and Computation, John Wiley & Sons, New York, 1992; http://www.zyvex.com/nanotech/nanosystems.html.

Figure 2-16. Merkle's exemplar architecture for convergent assembly[69] used in Drexler's desktop molecular manufacturing appliance.

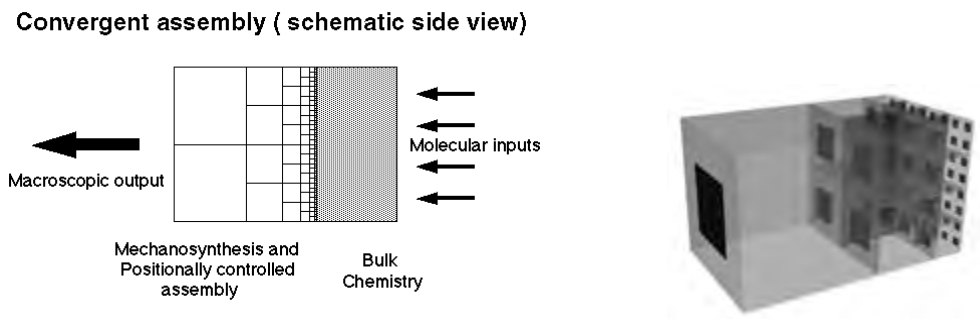

(A) (B)

(A) Schematic side view of convergent assembly in which molecular inputs are combined in parallel into successively larger compound blocks, ultimately reaching the scale of macroscopic output. (B) Three stages of convergent assembly produce a final product of ~1 meter in size from 512 sub-sub-subassemblies each of which is ~0.125 meters in size.[70]

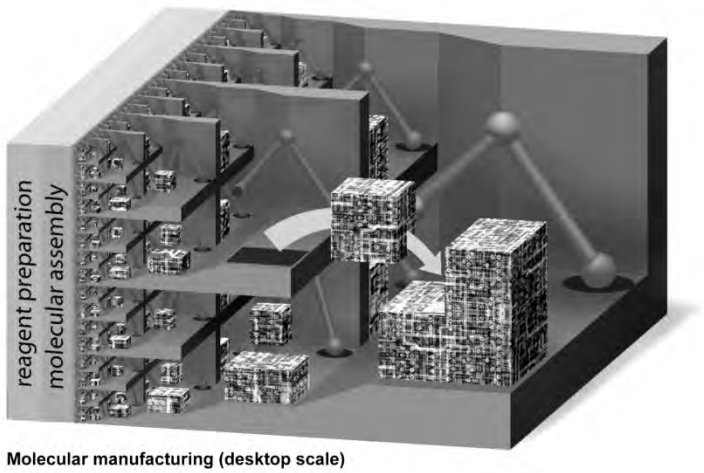

(C) More detailed schematic side view of the convergent assembly of progressively larger compound blocks, ultimately reaching the scale of macroscopic output. Image courtesy of Eric Drexler, www.e-drexler.com

---

[69] K. Eric Drexler, Nanosystems: Molecular Machinery, Manufacturing, and Computation, John Wiley & Sons, New York, 1992; http://www.zyvex.com/nanotech/nanosystems.html.

[70] Robert A. Freitas Jr., Ralph C. Merkle, Kinematic Self-Replicating Machines, Landes Bioscience, Georgetown, TX, 2004; Section 5.9.4; http://www.MolecularAssembler.com/KSRM.htm.

Figure 2-16. (cont'd)

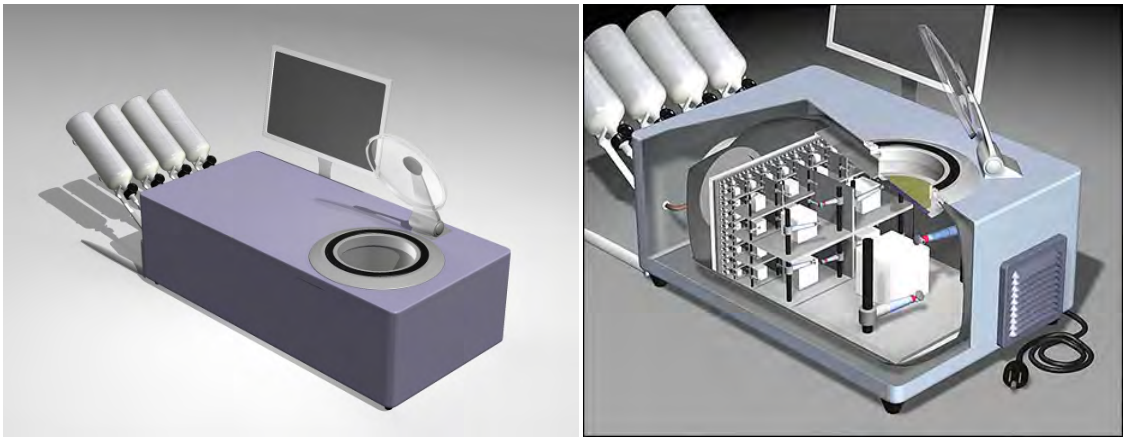

(D) External views of Drexler's proposed desktop molecular manufacturing appliance, outside view (left) and cutaway view of inner mechanisms (right). Images courtesy of John Burch, Lizard Fire Studios (3D Animation, Game Development) http://www.lizardfire.com

In his 1992 technical analysis of this factory approach to molecular manufacturing systems,[71] Drexler outlines an architecture for a system capable of manufacturing macroscopic product objects of mass ~1 kg and ~20 cm dimensions in a cycle time of ~1 hour, starting from a feedstock solution consisting of small organic molecules. The feedstock molecules enter the system through a molecular sorting and orientation mechanism (Figure 2-17), pass through several stages of convergent assembly using mill-style mechanisms (Figure 2-18), and then pass through several more stages of convergent assembly using manipulator-style mechanisms (Figure 2-14). The full system has 10 stages with progressively larger machines assembling progressively larger components at progressively lower frequencies (Table 2-2). Since the manufacturing system can manufacture all of the components of which it is itself composed, Drexler's proposed desktop manufacturing system (system mass ~1 kg) would also be capable of self-replication in about 1 hour (Figure 2-16(D)).

[71] K. Eric Drexler, Nanosystems: Molecular Machinery, Manufacturing, and Computation, John Wiley & Sons, New York, 1992, Section 14.4, pp. 421-428.

Figure 2-17. A molecular sorting rotor for the selective importation of molecular feedstock[72]

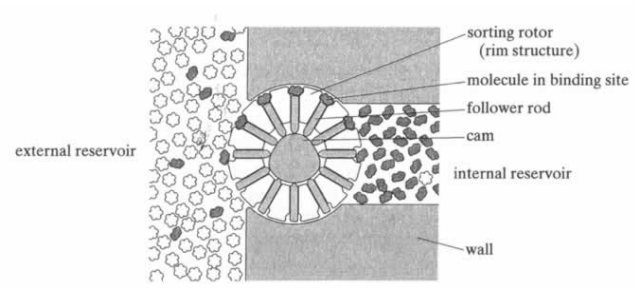

In this sorting rotor based on modulated receptors, a cam surface modulates the position of a set of radial rods. In the binding position (mapping the illustration onto a 12-hour clock dial), the rods form the bottom of a site adapted to bind molecules of the desired type. Between 10:00 and 2:00, the receptors undergo transport to the interior, driven by shaft power (coupling not shown). Between 2:00 and 4:00, the molecules are forcibly ejected by the rods, which are thrust outward by the cam surface. Between 4:00 and 8:00, the sites, now blocked and incapable of transporting molecules, undergo transport to the exterior. Between 8:00 and 10:00, the rods retract, regenerating an active receptor.

Figure 2-18. Schematic diagrams of mill-style reactive encounter mechanisms[73]

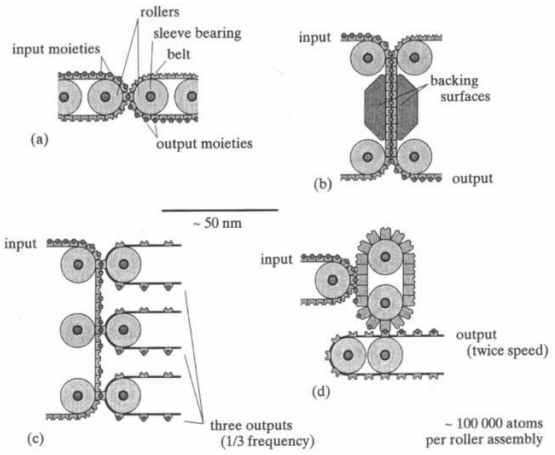

These schematic diagrams show mill-style reactive encounter mechanisms for molecular assembly, including mechanisms designed for: (a) simple contact and separation, (b) prolonged contact with opportunity for substantial cam-driven manipulation, (c) transformation of moiety transit frequency, and (d) transformation of moiety transit speed.

---

[72] K. Eric Drexler, Nanosystems: Molecular Machinery, Manufacturing, and Computation, John Wiley & Sons, New York, 1992; http://www.zyvex.com/nanotech/nanosystems.html.

[73] K. Eric Drexler, Nanosystems: Molecular Machinery, Manufacturing, and Computation, John Wiley & Sons, New York, 1992; http://www.zyvex.com/nanotech/nanosystems.html.

Drexler[74] summarizes as follows: "A wide range of macroscopic products can be made with good efficiency by using mills to make a diverse set of building blocks in the 10^{-7} to 10^{-6} m size range and then using manipulators to assemble them into macroscopic products. Inclusion of a secondary production capability that applies manipulators to smaller building blocks (at the moietal level where necessary) can provide unusual building blocks without requiring a dedicated mill mechanism. The exemplar system...makes the simplifying assumption of a hand-off from mills to manipulators at a single block size, 10^{-6} m [~1 micron]."

Table 2-2. Drexler's exemplar molecular manufacturing system parameters[75]

Level	Number of sets	Number of units per set[a]	Number of inputs per product	Unit operating frequencies (Hz)	Product scale (nm)	Mechanism scale (nm)[b]	Unit radiation-sensitive mass (fg)[c]	Total mass of mechanisms (kg)
Input ordering[d]	1	10^{17}	~1	10^6	0.5	20	0.02	0.002
Reagent prep.[e]	1	10^{17}	~1	10^6	0.5	20	0.06	0.006
Stage 1 mill[f]	10^{15}	100	100	$\leq 10^6$	1	20	0.60	0.06
Stage 2 mill	10^{13}	100	100	$\leq 10^6$	5	20	0.60	<0.01
Stage 3 mill[g]	10^{11}	100	100	$\leq 10^6$	20	100	0.50	<0.01
Stage 4 mill[h]	10^9	100	100	10^4	100	500	–	<0.001
Stage 5 mill	10^6	100	1000	10^4	1000	5000	–	<0.001
Stage 1 manip.[i]	10^9	2	10^6	500	10^5	2×10^5	–	<0.001
Stage 2 manip.	10^4	2	10^5	50	5×10^6	10^7	–	<0.001
Stage 3 manip.	1	2	10^4	5	10^8	2×10^8	–	0.020

[a] All numbers and frequencies are compatible with a ~1 gm/s throughput; within each stage, the combination of radiation-sensitive mass and number of units per redundant set is chosen to permit long operational lifetimes.
[b] Mechanism scale describes (e.g.) the size of a single rotor in a mechanosynthetic device, not of a multi-mechanism unit.
[c] The radiation-sensitive masses of units of each kind are stated in femtograms (1 fg = 10^{-18} kg).
[d] The mass of the input-ordering subsystem is estimated from Section 13.2.2.
[e] The mass of the reagent preparation subsystem is based on Section 13.3.5.
[f] Stage 1, 2 mill units: the mass per encounter mechanism is assumed to be the same as in reagent preparation.
[g] Stage 3 mill units: the moving parts are assumed to be large enough to permit designs tolerant of radiation damage (Section 14.2.2b), and the radiation-sensitive mass is that of product structures in transit through the unit.
[h] Stage 4, 5 mill units: the moving parts and product structures are assumed to be damage tolerant; the number of units per set is large chiefly to permit lower frequencies and speeds.
[i] Manipulator units: the arm structural mass is chosen to permit designs with stiffness >100 N/m, and with all bending-mode frequencies >100 times the unit operating frequency; the arm supporting structures are assumed to be 10 times more massive than the arms themselves.

[74] K. Eric Drexler, Nanosystems: Molecular Machinery, Manufacturing, and Computation, John Wiley & Sons, New York, 1992, Section 14.4, pp. 421-428.

[75] "Table 14.1. Manufacturing system parameters," in: K. Eric Drexler, Nanosystems: Molecular Machinery, Manufacturing, and Computation, John Wiley & Sons, New York, 1992, p. 422. See also in: Robert A. Freitas Jr., Ralph C. Merkle, Kinematic Self-Replicating Machines, Landes Bioscience, Georgetown, TX, 2004; Section 4.9.3 http://www.MolecularAssembler.com/KSRM/4.9.3.htm and Table 4.1 http://www.MolecularAssembler.com/KSRM/Tables/4.1.jpg.

2.2 Nanofactory-Related Experimental Work

Aside from the theoretical studies, some progress has been made on the experimental front that helps lead us toward the goal of a nanofactory in an evolutionary or incremental manner, but to date there have been no experimental programs focused on this objective. The most significant relevant experimental programs to date are the factory-like self-replicating construction machine designed and operated by Matt Moses (Section 2.2.1), the LEGO®-based factories replicators that have been built and operated by various groups, most notably in the Chirikjian lab (Section 2.2.2), the top-down desktop "fabbers" that are either commercially available or are in development, most notably the Rep-Rap project (Section 2.2.3), and the Zyvex Atomically Precise Manufacturing project (Section 2.2.4).

There are also several EU projects – e.g., NanoHand,[76] ROBOSEM[77] and NANORAC[78] – that have partnered the top European laboratories and high-tech companies in robotics, nanomanipulation, microscopy and nanofabrication for the purpose of creating a nanorobotic production system inside of a scanning electron microscope to realize an early version of a primitive nanomanufacturing assembly line by 2009 – although these systems will only be able to manipulate nanometer-sized or larger objects, such as carbon nanotubes.

2.2.1 Moses Construction Machine (1999-2001)

The Moses Construction Machine is the only factory-like positionally-controlled construction system that has been experimentally demonstrated with at least parts-level closure (Section 2.2.1.1). It is a macroscale system, not atomically precise nor even nanoscale, but a basic scaling analysis (Section 2.2.1.2) suggests that if the machine was simply scaled down without modification, it would apparently be accurate enough for nanopart *assembly* work. Unfortunately, there is no analogous system for nanoscale *fabrication* work because Moses posited the manual building of his blocks using processes that are exogenous to the Constructor system.

The description in Section 2.2.1.1 is reproduced verbatim from Section 3.18 of KSRM.[79]

---

[76] NanoHand, accessed April 2008; http://www.nanohand.eu/index.php.

[77] ROBOSEM, accessed April 2008; http://www.robosem.org/Consortium/consortium.html.

[78] "Nano-Robotic for Assembly and Characterisation – NANORAC," accessed April 2008; http://www.amir.uni-oldenburg.de/en/12603.html.

[79] Robert A. Freitas Jr., Ralph C. Merkle, Kinematic Self-Replicating Machines, Landes Bioscience, Georgetown, TX, 2004; Section 3.18, pp. 60-63; http://www.MolecularAssembler.com/KSRM/3.18.htm.

2.2.1.1 Moses Self-Replicating Construction Machine

During 1999-2001, Matt Moses, a graduate student in the Department of Mechanical Engineering at the University of New Mexico, invented a unique set of Lego-like blocks that are especially well-suited for the self-replication task and elaborated some of the detailed kinematic requirements of a machine that can self-replicate or assemble its own duplicate from a stock of components.[80] The Lego-like components were plastic parts that were cast from a polyurethane resin and then used to make a 3-axis Cartesian manipulator which was subsequently shown to be kinematically capable of assembling a duplicate of itself. The machine cannot fabricate its own plastic components and – in addition to mechanical problems that hamper the physical device – the constructor must be controlled by an external entity. To be fully self-replicating, says Moses,[81] the device would have to autonomously control its own actions and would have to possess the instructions necessary for carrying out its duplication. "The ultimate goal of this work is the creation of a machine that can automatically fabricate components from raw materials and then assemble these components into a wide range of useful devices, including duplicates of the original machine."

Figure 2-19(A) shows two exploded views of Moses' "basic component." The component consists of two parts – an upper "handle" and a lower "base". The base contains four compliant snap tangs that are complementary to the four tapered surfaces of the handle. Blocks can be assembled together as shown in Figure 2-19(B), which also shows how the snap tangs of the base will grasp the undercut of the handle of another part. In addition, the convexly tapered surfaces of the base mate with concavely tapered surfaces of the handle in order to provide rigidity with respect to shear and torsion between parts. Most edges on the handle and base are chamfered. The chamfers are important because they allow a certain amount of positioning error during assembly. The tangs and handle also contribute to error tolerance, since they are tapered such that two parts need not be exactly positioned before assembly. The slots cut in each side of the base allow the part to be assembled onto other parts that have reinforcing segments. Depending on the type of loading on the tang, it will bend primarily in either the upper or lower segment of the 'L'. This can be exploited so that parts can be disassembled. In other words, the snap-assembly is reversible. Figure 2-19(C) shows a sequence of sectioned views of two parts during assembly and disassembly.

---

[80] Matt Moses, "A Physical Prototype of a Self-Replicating Universal Constructor," Master's Thesis, Department of Mechanical Engineering, University of New Mexico, 2001; http://www.home.earthlink.net/~mmoses152/SelfRep.doc. Matt Moses, "Self-Replication," 16 December 2002; http://www.home.earthlink.net/~mmoses152/.

[81] Matt Moses, "A Physical Prototype of a Self-Replicating Universal Constructor," Master's Thesis, Department of Mechanical Engineering, University of New Mexico, 2001; http://www.home.earthlink.net/~mmoses152/SelfRep.doc.

Figure 2-19. Moses' "basic component" for self-replicating construction machine (courtesy of Matt Moses)[82]

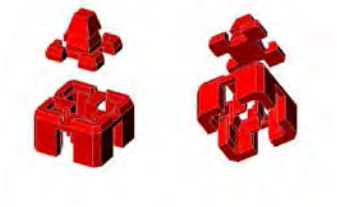

(A) Exploded views of basic component

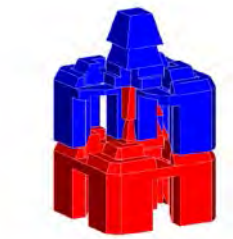

(B) Two assembled components, cutaway view

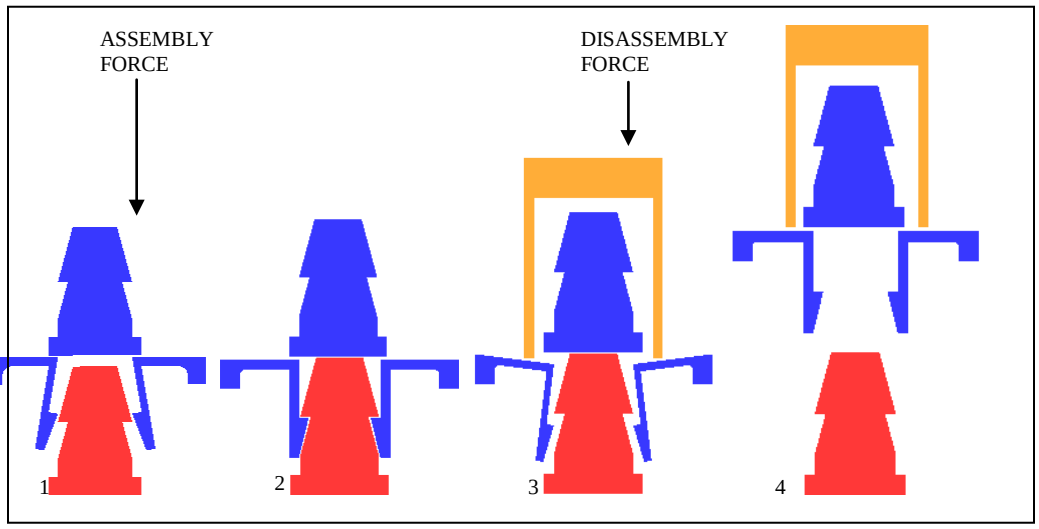

(C) When two parts are assembled, the tangs of one part (blue) bend outward to clear the handle of the other part (red). One way the parts can be disassembled is if a tool (orange) depresses the tangs of a part (blue) so that they can clear the handle of the other part (red).

A plane surface can be tiled by the parts, resulting in a plane covered by periodically spaced handles. The constructing machine described here operates on such a plane. Part type 3 (green in Figure 2-20(A)) is identical to part type 2, except that its top handle has been replaced with a rotary handle. A second type of connection between parts is the handle-slider connection. The slider – a long beam with the same cross section as a snap-tang – allows a part to slide back and forth along the handles of other parts, as in Figure 2-20(B) which shows a rack assembled onto the operating plane. By adding an actuator, forces can be applied to moving parts and their positions can be controlled. In this component set there are two types of motors – a rotary type

---

[82] Matt Moses, "A Physical Prototype of a Self-Replicating Universal Constructor," Master's Thesis, Department of Mechanical Engineering, University of New Mexico, 2001; http://www.home.earthlink.net/~mmoses152/SelfRep.doc.

and a linear type. Racks are actuated by rotary motors. The rotary motors are made by attaching a basic part and a drive gear to an off-the-shelf motor. The rack and the drive gear have self-aligning teeth (the teeth easily mesh) in order to simplify assembly. In Figure 2-20(C), a motor has been added to the assembly.

Figure 2-20. Moses' component assemblies for self-replicating construction machine (courtesy of Matt Moses)[83]

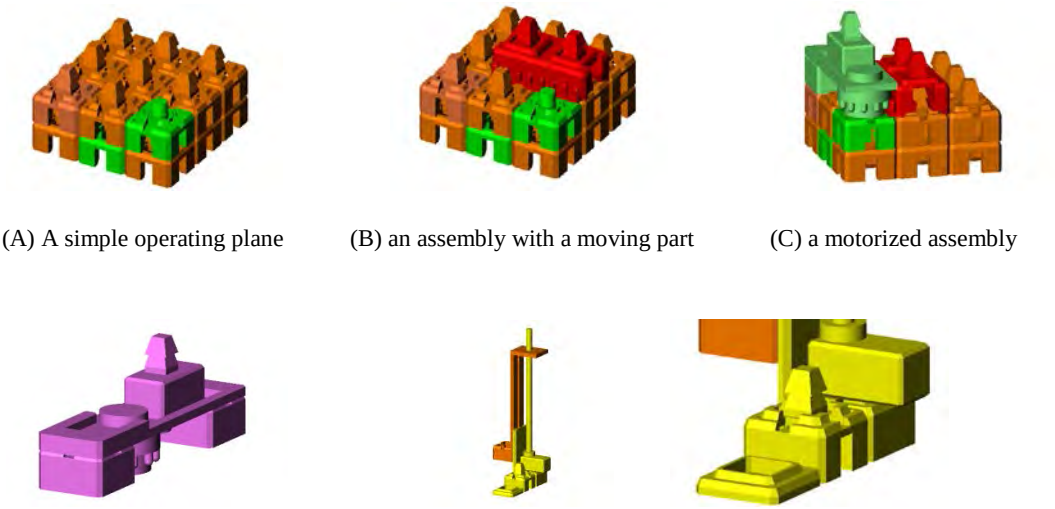

(A) A simple operating plane (B) an assembly with a moving part (C) a motorized assembly

(D) Motor 2 (E) Motor 3 (full view at left, closeup at right)

Moses' constructing machine is built out of 45 parts, including 11 different kinds of parts (all meticulously described in his thesis),[84] as follows: Rack (8 used in constructing machine), Motor 1 (1 used), Anchor (7), Rail (13), Cap (8), Rotary Cap (1), Cross-member (3), Cap with Support (1), Cross-member with Support (1), Motor 2 shown in Figure 2-20(D) (1), and Motor 3 shown in Figure 2-20(E) (1). Five other parts (Basic Part, Plane Element, Rotary Plane Element, Small Gear (11 teeth), and Large Gear (14 teeth)) are not used in the constructor but could be incorporated into devices that the constructor could assemble. Addressing tradeoffs in designing parts sets, Moses explains: "These 'universal' components are not all that universal – some of the parts are used in large numbers, while other special-purpose components are used infrequently. It is possible that an optimally designed component set would contain only a few types of parts, and

---

[83] Matt Moses, "A Physical Prototype of a Self-Replicating Universal Constructor," Master's Thesis, Department of Mechanical Engineering, University of New Mexico, 2001; http://www.home.earthlink.net/~mmoses152/SelfRep.doc.

[84] Matt Moses, "A Physical Prototype of a Self-Replicating Universal Constructor," Master's Thesis, Department of Mechanical Engineering, University of New Mexico, 2001; http://www.home.earthlink.net/~mmoses152/SelfRep.doc.

these parts would find more uniform use in an assembly. Keep in mind, however, that there is a tradeoff between the complexity of the set itself and the complexity of an assembly made from it. Making a given assembly from a set of simple components may necessitate the use of many more parts than would be required when making an equivalent assembly from a set that had an extra few special-purpose components."

Figure 2-21. Functionality matrix for the component set used in the Moses self-replicating construction machine (courtesy of Matt Moses)[85]

	1 Basic Part	2 Plane Element	3 Rotary Plane Element	4 Rack	5 Motor 1	6 Anchor	7 Rail	8 Cap	9 Rotary Cap	10 Cross Member	11 Cap w/ Support	12 Crs Mbr w/ Sprt	13 Motor 2	14 Motor 3	15 Small Gear	16 Large Gear
Column construction unit	●															
Platform construction unit		●	●													
Beam construction unit						●	●	●	●		●					
Sliding X/Y unit (prismatic joint)				●												
Foundation for Sliding X/Y unit	●	●	●	●		●	●	●	●	●	●	●				
Rotating Z unit (pin joint)															●	●
Foundation for Rotating Z unit			●						●							
Z-to-Z power transmission					●								●		●	●
Z-to-X/Y power transmission				●	●								●		●	
Z-axis rotary motor					●								●			
Z-axis linear motor														●		
Gap-spanning unit										●		●				
Overhang support unit											●	●				
Reinforcement for 2 adjacent units						●		●	●		●					
Reinforcement for 2+ adjacent units							●									

[85] Matt Moses, "A Physical Prototype of a Self-Replicating Universal Constructor," Master's Thesis, Department of Mechanical Engineering, University of New Mexico, 2001; http://www.home.earthlink.net/~mmoses152/SelfRep.doc.

Moses continues: "The component set was designed in an iterative process. During this process, there was no clear design for the constructor. New functionalities were simply added to the set until the parts could be made into a suitable manipulator. This aimless wandering through design space is often time-consuming and costly. Suh[86] presents a systematic approach to design wherein a hierarchy of functional requirements (*what* a system must do) and design parameters (*how* it will do it) are evaluated based on two axioms: (1) Maintain the independence of functional requirements. (2) Minimize the information content of the design (keep it simple). The functionality matrix (Figure 2-21) for the component set [makes] clear...that not all functional requirements are independent, and also that in some cases many parts satisfy the same requirement." A functionality matrix can be used to compare structures, components, or features of a design with the functions they perform.

Moses' self-replicating construction machine (Figure 2-22) is a 3-axis Cartesian manipulator made only from parts in the previously described component set that can assemble a wide variety of devices, including duplicates of itself. The machine is kinematically capable of grasping, manipulating, and placing all of the components required for constructing its own duplicate, including the hardware required to manipulate mechanical components but excluding the portion responsible for control. The constructor lacks any type of sensor or onboard control and so must be controlled either by a human operator or a sophisticated external controller. Construction activities include the retrieval of components from a storage site and their subsequent connection to an assembly or operating plane, but components must initially arrive at the storage site through the action of another entity – namely, a human operator. Moses[87] lists the entire sequence of 410 steps (specific operations) that must be executed by the construction machine in order to install each of the 45 parts in its replica, in proper order, proceeding from (A) to (D) in Figure 2-22.

---

[86] N.P. Suh, The Principles of Design, Oxford University Press, Oxford, 1990.

[87] Matt Moses, "A Physical Prototype of a Self-Replicating Universal Constructor," Master's Thesis, Department of Mechanical Engineering, University of New Mexico, 2001; http://www.home.earthlink.net/~mmoses152/SelfRep.doc.

Figure 2-22. Moses' self-replicating construction machine (courtesy of Matt Moses)[88]

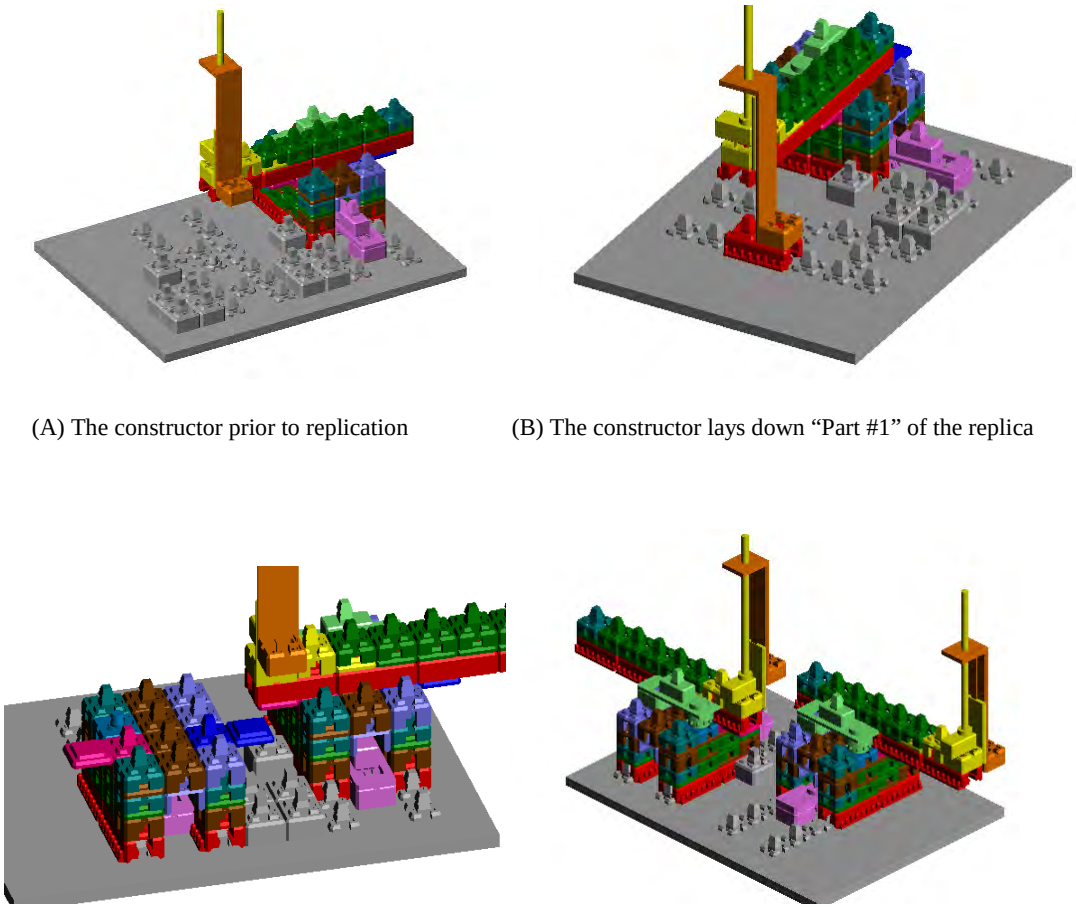

(A) The constructor prior to replication

(B) The constructor lays down "Part #1" of the replica

(C) The base platform is completed

(D) The constructor completes its replica

(For clarity, the storage site for the 45 parts of the duplicate machine is omitted)

In the actual hardware implementation (Figure 2-23), constructor movements were sequenced by a human operator controlling the manipulator through a switch box. Moses candidly admits that "the idea did not work as well in reality as it did in simulation. In order to make a functioning constructor, some of the problems had to be solved by cheating – gluing certain parts together, for example. So the constructor and the device it constructs are not entirely identical. In many cases, the constructor could not develop the necessary force to assemble components. The necessity of strengthening the constructor with methods outside of the allowed fastening techniques can be

---

[88] Matt Moses, "A Physical Prototype of a Self-Replicating Universal Constructor," Master's Thesis, Department of Mechanical Engineering, University of New Mexico, 2001; http://www.home.earthlink.net/~mmoses152/SelfRep.doc.

eliminated in future iterations by producing parts of higher tolerance, revising the part set, or revising the constructor design. Problems with the boom could also be solved by revising the design of the constructor. A gantry-crane manipulator, where the boom is supported at each end, would avoid deflection problems and allow accurate placement of parts. Gantry-cranes are usually wrapped around their workspace, being larger than what they work on. This makes designing a gantry crane that can assemble a duplicate of itself difficult. The problem of running wires to the motors can be solved by laying conductive traces on the plastic parts.... While, kinematically, the design was capable of accessing and connecting the necessary parts to assemble a duplicate of itself, lack of stiffness due to the design of both components and manipulator prevented it from assembling its duplicate in reality." Nevertheless, after an assisted replication both devices were operable.

Figure 2-23. Actual physical implementation of Moses' self-replicating construction machine (courtesy of Matt Moses)[89]

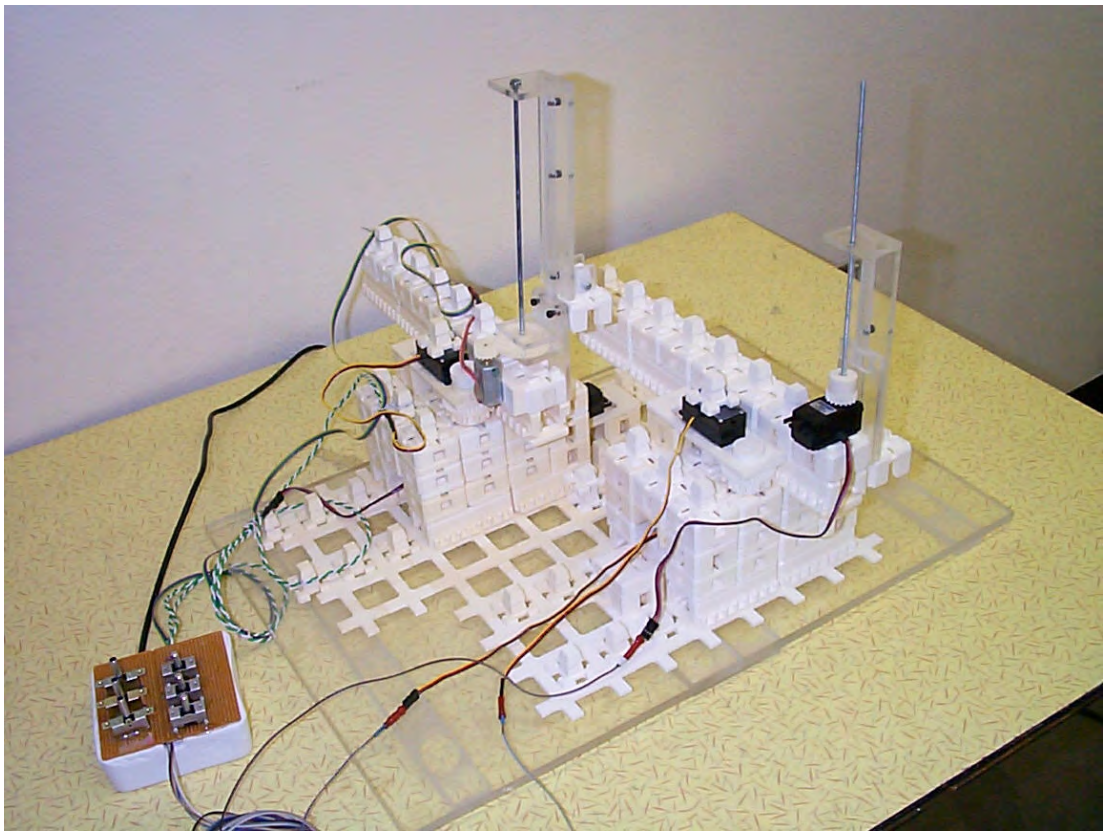

[89] Matt Moses, "A Physical Prototype of a Self-Replicating Universal Constructor," Master's Thesis, Department of Mechanical Engineering, University of New Mexico, 2001; http://www.home.earthlink.net/~mmoses152/SelfRep.doc.

2.2.1.2 Scaling Analysis of the Moses Construction Machine

Moses' constructing machine is built out of 45 parts (Table 2-3), including 11 different kinds of parts (all meticulously described in his thesis),[90] as follows: Rack (8 used in constructing machine), Motor 1 (1 used), Anchor (7), Rail (13), Cap (8), Rotary Cap (1), Cross-member (3), Cap with Support (1), Cross-member with Support (1), Motor 2 shown in Figure 2-20(D) (1), and Motor 3 shown in Figure 2-20(E) (1).

Table 2-3. Component supply for Moses Construction Machine

Nanopart or Nanodevice	Number of Com-ponents	Volume Each (in^3)	# Parts Each	Volume All (in^3)	Total # All Parts
1. Rail	13	1.70	2	22.10	26
2. Rack	8	3.75	4	30.00	32
3. Cap	8	1.70	1	13.60	8
4. Anchor	7	2.50	2	17.50	14
5. Cross-member	3	2.70	2	8.10	6
6. Rotary Cap	1	1.60	1	1.60	1
7. Cap with Support	1	2.50	2	2.50	2
8. Cross-member with Support	1	3.50	3	3.50	3
9. Motor 1	1	5.50	6	5.50	6
10. Motor 2	1	5.75	7	5.75	7
11. Motor 3	1	15.10	12	15.10	12
TOTALS	**45**	**---**	**---**	**125.25 in^3**	**117 parts**

The components are measured in units of 0.875 inches, and the basic part size is 1.5 x 1.5 x 0.875, or 2 x 2 x 1 units. The basic part has a nubbin sticking out on the top and a nubbin-shaped hole underneath it for the neighbor's nubbin to stick in and hold the first part tight, so the net solid volume of the part is almost the solid dimension of the base unit dimensions (Table 2-4). The tool arm connected to Motor 3 has a reach of 7 vertical units, or 6.125 inches. Excluding the vertical tool, the main body of the Constructor fits in a 10.5 x 12.0 x 6.0 box, which is a volume of 756.00 in^3, but there is only 125.25 in^3 of solid volume (16.57% fill). Allowing 17.6 sec per step, the device can follow 410 steps to assemble its own mass in 7200 sec (2 hours).

---

[90] Matt Moses, "A Physical Prototype of a Self-Replicating Universal Constructor," Master's Thesis, Department of Mechanical Engineering, University of New Mexico, 2001; http://www.home.earthlink.net/~mmoses152/SelfRep.doc.

Table 2-4. Component dimensions of the Moses Construction Machine					
Nanopart or Nanodevice	**Width (in)**	**Length (in)**	**Height (in)**	**~Solid Volume (in^3)**	**Number of Parts**
1. Rail	1.50	3.00	0.875	1.70	2
2. Rack	1.50	3.00	0.875	3.75	4
3. Cap	1.50	1.50	0.875	1.70	1
4. Anchor	1.50	3.00	0.875	2.50	2
5. Cross-member	1.50	3.00	1.500	2.70	2
6. Rotary Cap	1.50	1.50	0.875	1.60	1
7. Cap with Support	1.50	3.00	0.875	2.50	2
8. Cross-member with Support	1.50	4.50	1.500	3.50	3
9. Motor 1	1.50	4.50	1.750	5.50	6
10. Motor 2	1.50	5.00	1.750	5.75	7
11a. Motor 3 – Tool Motor	1.50	4.50	10.000	10.60	10
11b. Motor 3 – Tool	1.50	3.00	7.250	4.50	2
Entire Constructor	**10.50**	**12.00**	**6.00**		

If the Moses Construction Machine is simplistically reduced by a scale factor of 2,222,500:1, then its components would be measured in units of 10 nm instead of units of 0.875 inches, and the basic 2 x 2 x 1 unit part size would become 20 x 20 x 10 nm, with a conversion scale factor of 11.428 nm per inch. In that case, a hypothetical nanosize Constructor would fit in a 120.0 x 137.2 x 68.6 nm box, would have a total operating volume of 1,129,432 nm^3, and would have a total solid volume of 187,120 nm^3 or ~32.9 million carbon atoms assuming solid lattice and ignoring H atoms.

These dimensions are similar to the nanoscale assembler (Section 3.6) in the present development program, but it is implausible that the Moses system can be directly scaled down because the Moses design makes extensive use of sliding interfaces which would be more difficult to implement in a nanoscale assembler because they would likely generate larger adhesion forces (i.e., stiction) which probably rules out a simple clone of Moses' design directly into the nanoscale. On the positive side, most of the problems encountered by Moses in getting his design to work involved (1) a lack of perfectly standardized parts dimensions and (2) the impact of gravity loading on a too-weak lever arm. Neither of these issues should be problems at the nanoscale because atomically identical nanoparts can be fabricated and gravity is not an issue at the nanoscale, although greater adhesion between juxtaposed parts might substitute for gravity and overcome the moderate stiffness of a lever arm created from numerous nanoscale blocks. The Moses design might be more appropriate for an intermediate-scale (e.g., 100 micron or 1 millimeter) cube-unit system where gravity is a lesser problem than for 1 inch blocks but where the blocks are large enough that stiction has not yet become a serious problem.

2.2.2 LEGO®-Based Assemblers (2001-present)

An interesting project in 1995-1996 was the development of a computer-controlled LEGO® factory – itself made entirely of LEGO® components – that could build LEGO® cars. The LEGO® factory project was conducted at the CODES Lab in the Electrical and Computer Engineering Department at the University of Massachusetts[91] and began as an Electrical Engineering senior design project inspired by a similar project at Linkoping University, Sweden. The effort was supported by an NSF grant and involved at least 7 students and 5 professors from the University of Massachusetts, Boston University, and Harvard University. The factory (Figure 2-24) was computer-controlled, incorporated up to 16 sensors and a number of motors, and assembled the LEGO® cars in 7 steps. The factory is "an interesting demonstration of a simple, small-scale system capable of handling and assembling the same type of parts that make up the system."[92] The students' future plan[93] was to add "decision-making functionality and the ability to flexibly manufacture multiple products," although the explicit pursuit of self-replication was never stated as a goal before the project ended. The factory itself was not capable of self-replication.[94] A LEGO® model of a steel production factory has also been done in the "Lego Lab" at the University of Aarhus,[95] and there is a U-Tube video[96] of a LEGO®-based factory assembling LEGO®-based cars.

---

[91] "Computer Controlled LEGO® Car Factory," http://vita.bu.edu/cgc/newlego/index.html. See also: C. Cassandras, "Computer Controlled LEGO® Car Factory," University of Massachusetts, 1996; http://web.archive.org/web/20010816195817/http://www.ecs.umass.edu/ece/UG/lego/home.html.

[92] Matt Moses, "A Physical Prototype of a Self-Replicating Universal Constructor," Master's Thesis, Department of Mechanical Engineering, University of New Mexico, 2001; http://www.home.earthlink.net/~mmoses152/SelfRep.doc.

[93] "Computer Controlled LEGO® Car Factory," http://vita.bu.edu/cgc/newlego/index.html. See also: C. Cassandras, "Computer Controlled LEGO® Car Factory," University of Massachusetts, 1996; http://web.archive.org/web/20010816195817/http://www.ecs.umass.edu/ece/UG/lego/home.html.

[94] The first mention of this possibility in the literature appears to have been made by Mitchel Resnick, who concluded his 1987 discussion[*] of LEGO®-based robotic simulated animals with the following comment: "Eventually (and more speculatively), LEGO®/Logo could evolve into a type of universal constructor. One can imagine a LEGO®-based automated factory, in which LEGO® machines construct and program new LEGO® animals – and new LEGO® factory machines. Or, perhaps, the factory machines and the animals should not be viewed as separate categories; perhaps the factory machines are the animals. Obviously, such projects would require complex programs and new types of building materials, including specialized pieces outside of the LEGO® repertoire. Such projects will probably not be feasible for many years – if ever." Just 14 years later, this "not...feasible...ever" project was accomplished experimentally (Section 2.2.2.5, Figure 2-30).
[*] Mitchel Resnick, "LEGO®, Logo, and Life," in Christopher G. Langton, ed., Artificial Life, Santa Fe Institute, Studies in the Science of Complexity, Volume VI, Addison-Wesley, New York, 1989, pp. 397-406.

[95] Thomas Hune, Kim G. Larsen, Paul Pettersson, "Guided Synthesis of Control Programs Using UPPAAL," 20 October 2002, http://www.daimi.au.dk/~baris/CaseStudy/; "A Steel Production Plant Model," LEGO Lab, University of Aarhus, http://legolab.daimi.au.dk/Projects/projects.html.

[96] Lego-based car factory, 31 December 2006; http://www.youtube.com/watch?v=GQ3AcPEPbH0&NR.

Figure 2-24. Computer-controlled LEGO® car factory made entirely from LEGO® components (courtesy of University of Massachusetts)[97]

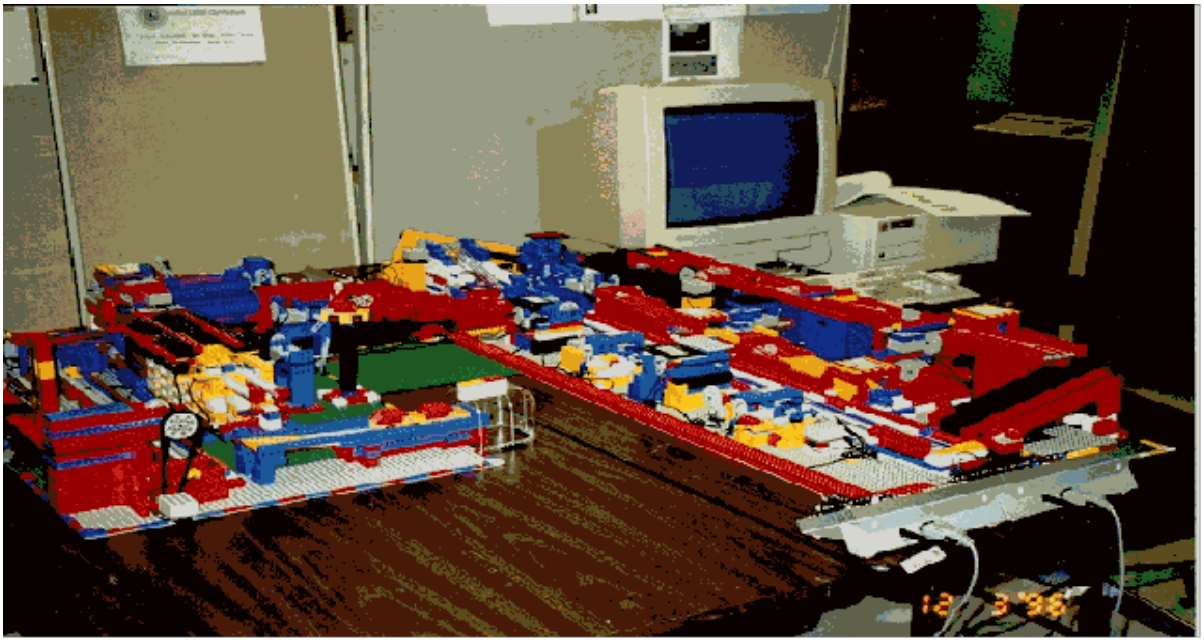

Some of the most interesting experimental work on LEGO®-based machines that can replicate themselves with closure at the compound-part assembly level has been achieved at the Chirikjian laboratory at Johns Hopkins University. (Chirikjian's work is described below in a discussion reproduced verbatim from Section 3.23 of KSRM.[98]) This and the aforementioned LEGO®-based factory work are all positionally controlled manufacturing systems, but they lack complete closure because they are not designed to build themselves from the most primitive parts of which they are comprised, and there is no description of how to build a LEGO®-based block fabricator[99] using these systems. Also, they are not atomically precise.

---

[97] "Computer Controlled LEGO® Car Factory," http://vita.bu.edu/cgc/newlego/index.html. See also: C. Cassandras, "Computer Controlled LEGO® Car Factory," University of Massachusetts, 1996; http://web.archive.org/web/20010816195817/http://www.ecs.umass.edu/ece/UG/lego/home.html.

[98] Robert A. Freitas Jr., Ralph C. Merkle, Kinematic Self-Replicating Machines, Landes Bioscience, Georgetown, TX, 2004; Section 3.23, pp. 69-76; http://www.MolecularAssembler.com/KSRM/3.23.htm.

[99] http://www.news.cornell.edu/stories/Feb07/fabber.ws.html.

2.2.2.1 Chirikjian Group Self-Replicating Robots

Chirikjian's group in the Department of Mechanical Engineering at Johns Hopkins University (JHU) has progressed beyond earlier work[100] on self-reconfiguring systems[101] and now is one of the first laboratories in the world to pursue an active experimental research program on macroscale kinematic self-replicating robots. Gregory Chirikjian and Jackrit Suthakorn, a graduate student in Chirikjian's group, offer a simple operational definition[102] of the subject of their inquiry: "Self-replication is the process of assembling a functional robot from passive components. The robot that is assembled (the replica) is an exact copy of the robot doing the assembling." Suthakorn, Chirikjian and his undergraduate students appear to have built and operated the world's first mobile LEGO®-based self-replicating machines.[103]

2.2.2.2 Prototype 1 (2001)

As recorded in his April 2003 Ph.D. thesis, Suthakorn[104] built his first simple prototype remote-controlled LEGO®-based robot in 2001 to demonstrate that it is mechanically feasible for a robot to produce a copy of itself. "Prototype 1" consisted of 7 subsystems: left motor, right motor, left wheel, right wheel, micro-controller receiver, manipulator wrist, and passive gripper (Figure 2-25(A)). Several passive fixtures were located in the assembly area to assist the robot in assembling its replica. The robot depends for its success on these external passive fixtures, which

---

[100] Gregory S. Chirikjian, "Kinematics of a metamorphic robotic system," Proc. 1994 IEEE Intl. Conf. On Robotics and Automation, San Diego, CA, May 1994, pp. 449-455, http://custer.me.jhu.edu/paper/knm_mtmfic/knm_mtmfic.html; Gregory S. Chirikjian, Amit Pamecha, Imme Ebert-Uphoff, "Evaluating efficiency of self-reconfiguration in a class of modular robots," J. Robotic Systems 13(1996):317-338, http://custer.me.jhu.edu/paper/evaluat/evaluat.html, and see generally http://custer.me.jhu.edu/; A. Pamecha, C. Chiang, D. Stein, G.S. Chirikjian, "Design and implementation of metamorphic robots," in J. McCarthy, ed., Proc. 1996 ASME Design Engineering Technical Conf. and Computers in Engineering Conf., ASME, 1996.

[101] Robert A. Freitas Jr., Ralph C. Merkle, Kinematic Self-Replicating Machines, Landes Bioscience, Georgetown, TX, 2004; Section 3.8, p. 34; http://www.MolecularAssembler.com/KSRM/3.8.htm.

[102] Gregory S. Chirikjian, Jackrit Suthakorn, J. Zhou, "Self-replicating robot: A project in the mechatronics at Johns Hopkins University," JHU, Spring 2002; http://custer.me.jhu.edu/mechatronics/syllabus2002.htm. Gregory S. Chirikjian, Jackrit Suthakorn, "Toward self-replicating robots," Paper #067, Session 8: Design, 9 July 2002, Proc. 8th Intl. Symp. on Experimental Robotics (ISER '02), Italy, 8-11 July 2002; http://caesar.me.jhu.edu/jackritweb/iser2002.pdf or http://www.iser02.unisa.it/papers/67.pdf. Jackrit Suthakorn, "Self-Replicating Robots," http://caesar.me.jhu.edu/html/self_replicating_systems.html.

[103] Jackrit Suthakorn, "Part III: Self-Replicating Robots," in Paradigms of Service Robotics, Ph.D. Dissertation, Department of Mechanical Engineering, Johns Hopkins University, Baltimore, Maryland, February 2003, pp. 167-236; http://caesar.me.jhu.edu/jackritweb/Thesis011403.pdf.

[104] Jackrit Suthakorn, "Part III: Self-Replicating Robots," in Paradigms of Service Robotics, Ph.D. Dissertation, Department of Mechanical Engineering, Johns Hopkins University, Baltimore, Maryland, February 2003, pp. 167-236; http://caesar.me.jhu.edu/jackritweb/Thesis011403.pdf.

are not actuated but are manipulated by the replicator robot. The original robot is remotely controlled to relocate its subsystems from a storage area to the assembly area, whereupon the original robot is guided to perform the assembly process (Figure 2-25(B)) – a process Suthakorn[105] describes as follows:

"The original robot retrieves the left motor subsystem from the storage area and slides it into a motor assembling fixture (this fixture is designed to have a narrow slot so that when the motors are placed in it, they are forced to align with each other). The robot then moves the right motor subsystem from the storage area into the motor-assembling fixture. After both left and right motors are aligned in the fixture, the robot exerts pressure on the subsystems so that they snap together and form one piece. The original robot then manipulates the motor-assembling fixture so as to release the motor subsystem, which completes the first stage of assembling the subsystems. The robot then takes the motor subsystem and slides it into a wheel-assembling fixture which is designed to assist attaching the left and right wheels to the subsystem. After the wheels are successfully attached to the motor subsystem, the robot manipulates the wheel fixture to release the assembled part. The robot continues to perform procedures similar to the previous steps to relocate parts and assemble them. This process leads to the completion of a replica (Figure 2-25(C)) of the original robot."

---

[105] Jackrit Suthakorn, "Part III: Self-Replicating Robots," in Paradigms of Service Robotics, Ph.D. Dissertation, Department of Mechanical Engineering, Johns Hopkins University, Baltimore, Maryland, February 2003, pp. 167-236; http://caesar.me.jhu.edu/jackritweb/Thesis011403.pdf.

Figure 2-25. LEGO®-based teleoperated kinematic replicator: Prototype 1 (courtesy of Jackrit Suthakorn and Gregory Chirikjian, Johns Hopkins University)[106]

(A) Prototype 1, an unassembled set of the replica's components, and environmental fixtures

[106] Jackrit Suthakorn, "Part III: Self-Replicating Robots," in Paradigms of Service Robotics, Ph.D. Dissertation, Department of Mechanical Engineering, Johns Hopkins University, Baltimore, Maryland, February 2003, pp. 167-236; http://caesar.me.jhu.edu/jackritweb/Thesis011403.pdf.

Figure 2-25. (cont'd)

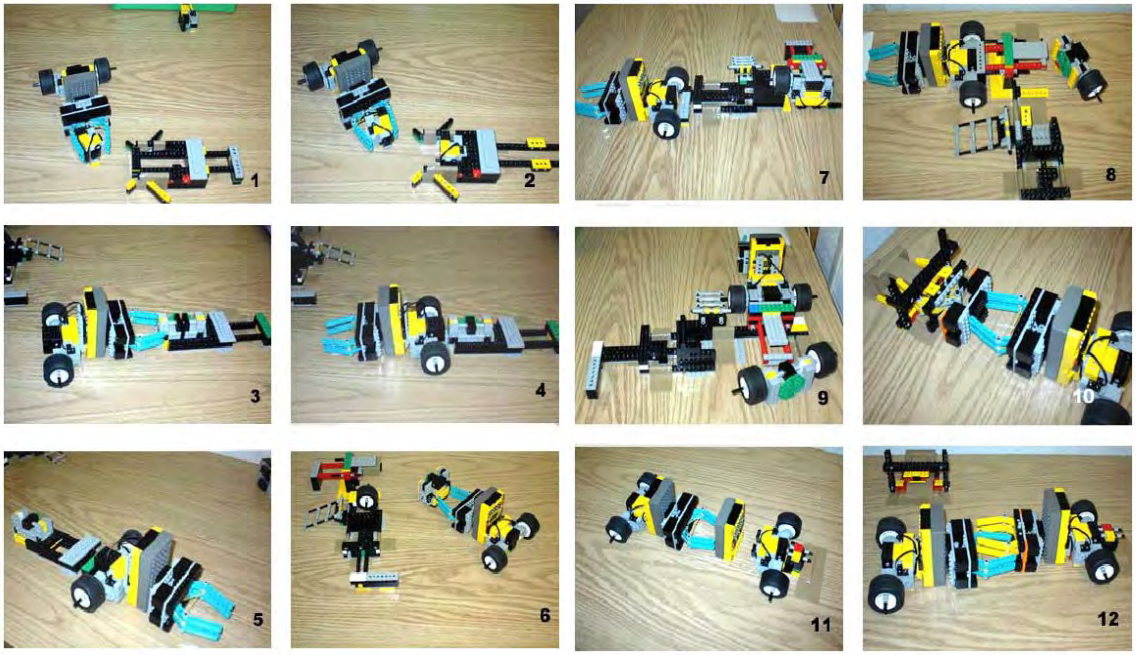

(B) Prototype 1 undergoes self-replication via teleoperation and external fixtures

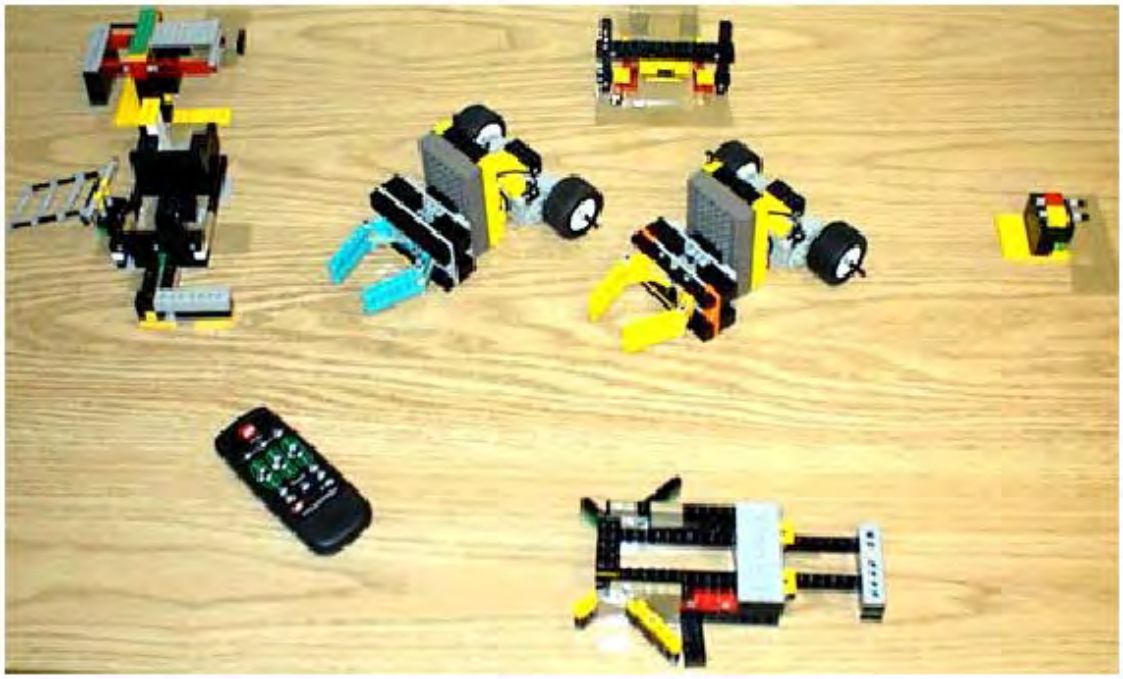

(C) Prototype 1 and its completed replica

2.2.2.3 Remote-Controlled Self-Replicating Robots (2002)

Chirikjian and Suthakorn[107] next describe several prototypes of self-replicating robotic systems that were developed by the undergraduate students and graduate student Yu Zhou during a one-semester mechatronics course taught in the Spring of 2002 at JHU. The students were divided into eight groups to explore designs and implementations of the concept of self-replicating robotic systems. The goal of the course was for each group of students to design a robot with the ability to create an exact functioning replica of itself, starting from a complete set of components or subsystems. A set of rules was established to motivate students to minimize the complexity of each individual subsystem while maximizing the number of subsystems in their designs. The use of LEGO® Mindstorm kits and additional LEGO® parts reduced building time in order to allow students to invest more time in designing and testing the prototypes, and the robots were remote-controlled (teleoperated) rather than autonomous so students could focus on the mechanical issues involved in the design of self-replicating systems. All experiments were conducted in an arena made of wood sheets 1 m^2 in area with walls 30 cm high. The four most distinctive prototypes for self-replicating robotic systems included:

Robot 1: Fixture-Based Design. The first example consists of five subsystems (left part, right part, bumper, controller, and connector). Two fixtures are used: a ramp with a constrained shape which is fitted to the controller and the connector; and a tunnel-like cave with an attached wedge on the ceiling used to physically force the connector in place (Figure 2-26).

Robot 2: Single-Robot-Without-Fixture Design. Robot 2 has five subsystems (left wheel system, right wheel system, left cradle, right cradle, and controller). The original robot has a pair of prongs in the front part to manipulate components and the unfinished replica, and uses the rear part to push the subsystems to the wall in order to compress the subsystems together (Figure 2-27).

---

[107] Gregory S. Chirikjian, Jackrit Suthakorn, J. Zhou, "Self-replicating robot: A project in the mechatronics at Johns Hopkins University," JHU, Spring 2002; http://custer.me.jhu.edu/mechatronics/syllabus2002.htm. Gregory S. Chirikjian, Jackrit Suthakorn, "Toward self-replicating robots," Paper #067, Session 8: Design, 9 July 2002, Proc. 8th Intl. Symp. on Experimental Robotics (ISER '02), Italy, 8-11 July 2002; http://caesar.me.jhu.edu/jackritweb/iser2002.pdf or http://www.iser02.unisa.it/papers/67.pdf. Jackrit Suthakorn, "Self-Replicating Robots," http://caesar.me.jhu.edu/html/self_replicating_systems.html. Jackrit Suthakorn, "Part III: Self-Replicating Robots," in Paradigms of Service Robotics, Ph.D. Dissertation, Department of Mechanical Engineering, Johns Hopkins University, Baltimore, Maryland, February 2003, pp. 167-236; http://caesar.me.jhu.edu/jackritweb/Thesis011403.pdf. Jackrit Suthakorn, Y.T. Kwon, G.S. Chirikjian, "A semi-autonomous replicating robotic system," Proc. 2003 IEEE Intl. Symp. on Computational Intelligence in Robotics and Automation (CIRA), Kobe, Japan, 2003; http://caesar.me.jhu.edu/jackritweb/CIRA2003.pdf. Jackrit Suthakorn, Andrew B. Cushing, Gregory S. Chirikjian, "An autonomous self-replicating robotic system," Proc. 2003 IEEE/ASME Intl. Conf. on Advanced Intelligent Mechatronics (AIM 2003), Kobe, Japan, 2003; http://custer.me.jhu.edu/publication/pdf/auton.pdf or http://caesar.me.jhu.edu/jackritweb/AIM2003.pdf; IEEE/ASME Trans. Mechatronics (submitted December 2003). Jackrit Suthakorn et al, "The intelligence of an autonomous self-replicating robotic system," submitted for review, 2003.

Figure 2-26. LEGO®-based teleoperated kinematic replicator: Robot 1 (courtesy of Chirikjian group, Johns Hopkins University)[108]

(A) Exploded view of Robot 1. Student design team: Jim Bankard, Oprema Ganesan, Oleg Gerovichev, Masaya Kitagawa. Teaching Assistants: Jackrit Suthakorn, Yu Zhou.

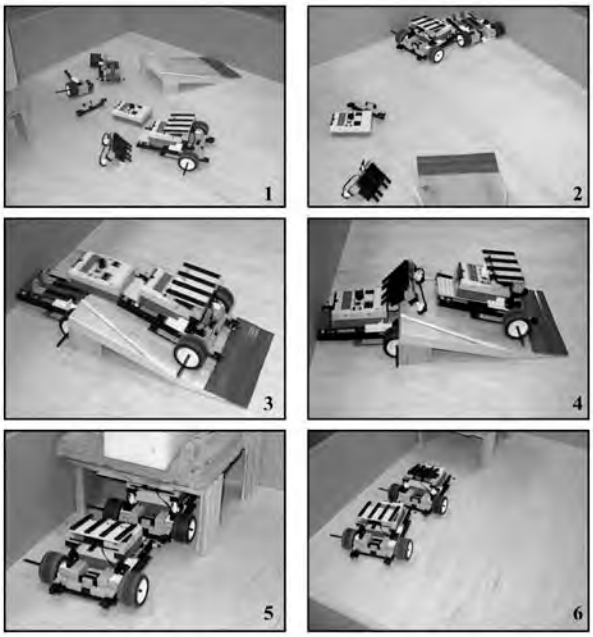

(B) Self-replicating process of Robot 1. The process begins with the original robot dragging the right part (which consists of half of the chassis, the right wheel and the right motor) to a wall. Then the left part (which consists of half of the chassis, the left wheel and the left motor) is pushed to connect with this right part. The left and right parts of the replica are securely merged by adding the bumper which has interlocks to both subsystems. The combined subsystems are moved and oriented to a desired position and orientation next to the ramp. The original robot then pushes the controller up to the ramp, and gently drops and inserts the controller on the top of the previous combination of subsystems. Note that the ramp has a constrained shape to force both controller and connector to be in their places. The connector is fixed in its place in the same fashion. The last step is to physically force the connector to be in contact with the controller by pushing the replica in the tunnel-like area with a wedge on the ceiling. This will force the connector to be in place. After pushing the replica several times, the electronic connectors on the replica finally make contact. The replica is able to operate in the same way as the original does.

---

[108] Gregory S. Chirikjian, Jackrit Suthakorn, "Toward self-replicating robots," Paper #067, Session 8: Design, 9 July 2002, Proc. 8th Intl. Symp. on Experimental Robotics (ISER '02), Italy, 8-11 July 2002; http://caesar.me.jhu.edu/jackritweb/iser2002.pdf or http://www.iser02.unisa.it/papers/67.pdf.

Figure 2-27. LEGO®-based teleoperated kinematic replicator: Robot 2 (courtesy of Chirikjian group, Johns Hopkins University)[109]

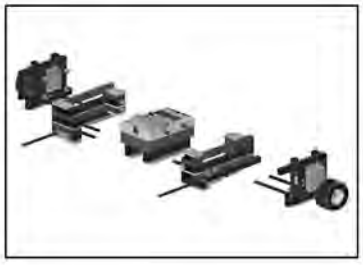

(A) Exploded view of Robot 2. Student design team: Tabish Mustafa, Omar Rivera, Mark Sorensen, Brian Weineler. Teaching Assistants: Jackrit Suthakorn, Yu Zhou.

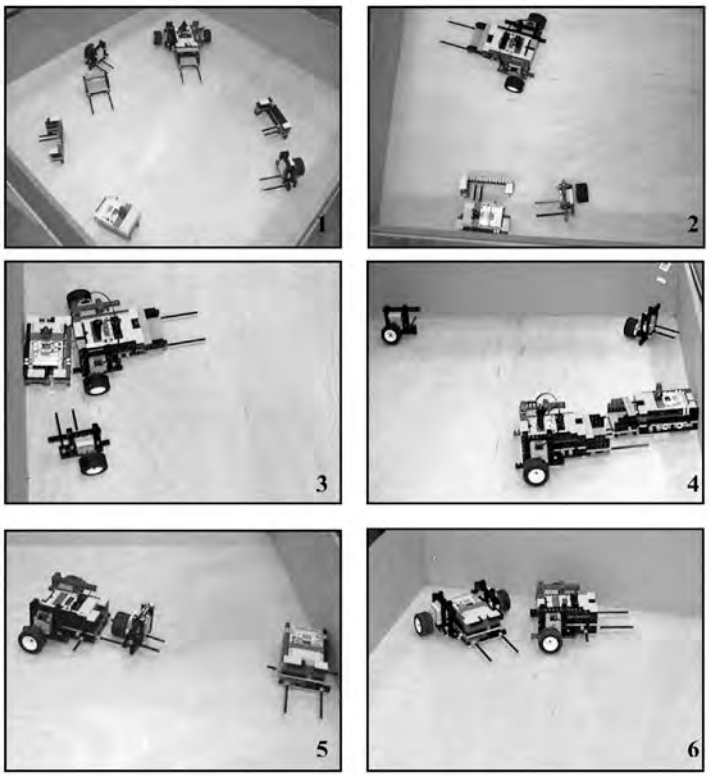

(B) Self-replicating process of Robot 2. The process begins with the original using its prongs to move the controller to a wall. Then the robot brings one side of the cradles to insert into the slot under the controller, and pushes both parts to the wall. The first two subsystems are then connected. The other cradle is combined with the previously combined subsystems in the same way. The left and right wheel systems are then manipulated, and combined to the previously connected subsystems in a similar fashion. The replica is then able to operate.

---

[109] Gregory S. Chirikjian, Jackrit Suthakorn, "Toward self-replicating robots," Paper #067, Session 8: Design, 9 July 2002, Proc. 8th Intl. Symp. on Experimental Robotics (ISER '02), Italy, 8-11 July 2002; http://caesar.me.jhu.edu/jackritweb/iser2002.pdf or http://www.iser02.unisa.it/papers/67.pdf.

Robot 3: Another Fixture-Based Design. This robot consists of three subsystems: the controller; the drive system; and the cage. The cage has a hinge that allows the top part of the cage to open and close to cover the wheel system and controller. The electronic connectors are attached on the top part of the cage. A passive dual linkage is hanging to assist in opening the cage (Figure 2-28).

Figure 2-28. LEGO®-based teleoperated kinematic replicator: Robot 3 (courtesy of Chirikjian group, Johns Hopkins University)[110]

(A) Exploded view of Robot 3. Student design team: James Del Monaco, Paul Stemniski, Sten-Ove Tullbery, Jason Wachs, Chris Wong. Teaching Assistants: Jackrit Suthakorn, Yu Zhou.

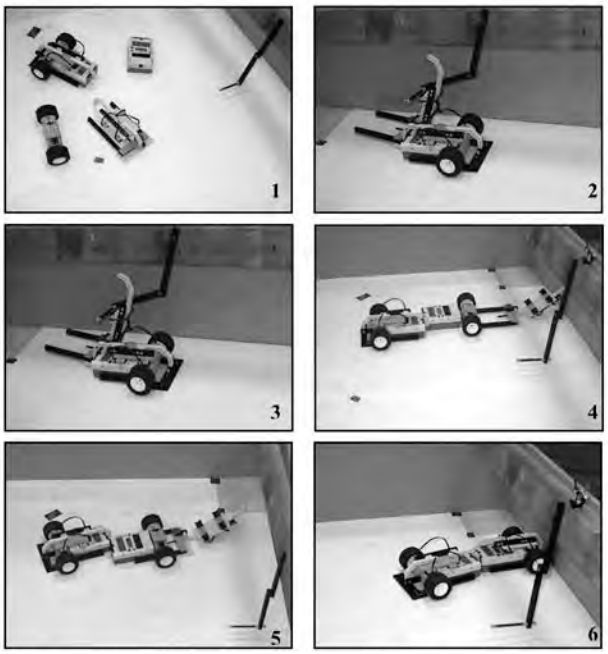

(B) Self-replicating process of Robot 3. The process begins with the original robot pushing the cage to hook with the passive linkage, and then the top part of the cage is opened. The original robot then inserts the drive system and controller into the cage, respectively. The combined but unlocked subsystems are pushed to the wall. Because of the design of the top part of the cage, which is a curved shape, the original robot pushes the cage and the other two subsystems to the wall, and the cage is automatically closed. The replica is then completed.

---

[110] Gregory S. Chirikjian, Jackrit Suthakorn, "Toward self-replicating robots," Paper #067, Session 8: Design, 9 July 2002, Proc. 8th Intl. Symp. on Experimental Robotics (ISER '02), Italy, 8-11 July 2002; http://caesar.me.jhu.edu/jackritweb/iser2002.pdf or http://www.iser02.unisa.it/papers/67.pdf.

Robot 4: Operating Subsystems Assist in the Replication Process. In this design a subsystem is able to operate before finishing the replication process, and hence can assist in the assembly of the complete replica. Robot 4 (Figure 2-29) consists of the controller, the left thread (a long wire with electronic connectors), the right thread, and the gripper subsystem.

Figure 2-29. LEGO®-based teleoperated kinematic replicator: Robot 4 (courtesy of Chirikjian group, Johns Hopkins University)[111]

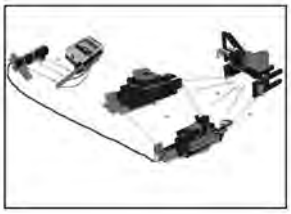

(A) Exploded view of Robot 4. Student design team: Jonathan Lim, Tak Liong, Daniel Moon, Jon Tang, Vincent Wu. Teaching Assistants: Jackrit Suthakorn, Yu Zhou.

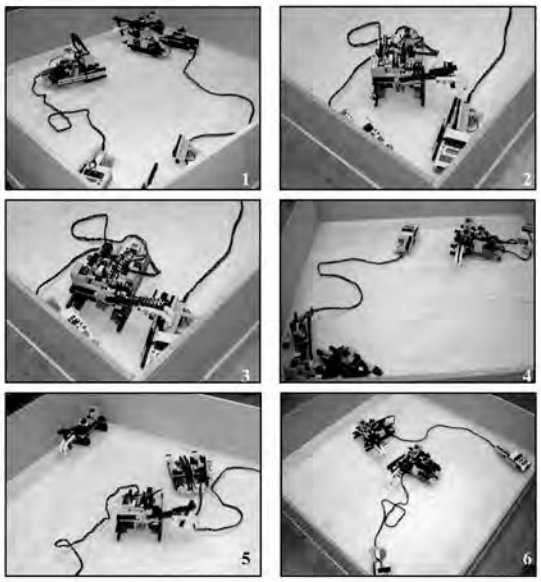

(B) Self-replicating process of Robot 4. The process begins when the original robot uses the gripper to carry the electronic connector (attached to the long wire) to the side of the controller. Then, the original robot uses the gripper to grasp and join the electronic connector to the controller. Once finished joining the electronic connector, the left thread, connected to the end of the wire, is now functioning. A human user is now able to control this subsystem. The original robot still continues moving subsystems next to each other for the next steps. The functioning subsystem is controlled to move to a convenient location for combining other subsystems. Once the left and right threads are aligned, the original robot uses the gripper to compress and join their connectors. The gripper subsystem is a big part. From its structure the gripper is able to slide to the top of the combined left and right threads after the functioning threads are driven into a side of the gripper subsystem. Then, the original robot helps tightening the connectors. The replica is now in a fully stable and operational status.

---

[111] Gregory S. Chirikjian, Jackrit Suthakorn, "Toward self-replicating robots," Paper #067, Session 8: Design, 9 July 2002, Proc. 8th Intl. Symp. on Experimental Robotics (ISER '02), Italy, 8-11 July 2002; http://caesar.me.jhu.edu/jackritweb/iser2002.pdf or http://www.iser02.unisa.it/papers/67.pdf.

The authors[112] concluded: "The study of self-replicating robots is an interesting research area which has not been extensively pursued in recent years. A number of self-replicating robot designs were presented here. The different designs devised by our students has helped us to identify new research problems, and to categorize self-replicating robots. Many challenging issues remain. Our future work will be to develop truly autonomous[113] (rather than remote-controlled) self-replicating robots."

2.2.2.4 Semi-Autonomous Self-Replicating Robot (2002)

Following the Spring 2002 mechatronics course experiments (Section 2.2.2.3), Suthakorn's third project was to design and build a self-replicating system in the manner of a robotic factory.[114] The system consisted of an original robot, subsystems of three fixed-position assembly stations (the factory), and finally a set of complex parts from which replicas of the original robot are assembled. By following painted lines on a 3.75 meter x 3 meter work surface, the robot could move autonomously from station to station along the lines without any human guidance, while still being remotely controlled at each station by a human operator, hence the system is aptly described as semi-autonomous. Feedback sensors were incorporated in each assembly station to automatically activate their functions.

Suthakorn gives an explicit step-by-step replication procedure for the "robot factory".[115] At Station 1 (Chassis Assembly), there is an 8-step procedure; at Station 2 (Motor and Track

---

[112] Gregory S. Chirikjian, Jackrit Suthakorn, "Toward self-replicating robots," Paper #067, Session 8: Design, 9 July 2002, Proc. 8th Intl. Symp. on Experimental Robotics (ISER '02), Italy, 8-11 July 2002; http://caesar.me.jhu.edu/jackritweb/iser2002.pdf or http://www.iser02.unisa.it/papers/67.pdf.

[113] For example: Barry Brian Werger, "Scalable Behavior-Based Multi-Robot Systems," Interaction Lab, University of Southern California, 12 February 2001, http://robotics.usc.edu/~barry/proj-page.html; Gabe Sibley, "SCOWR (Scalable Coordination of Wireless Robots)," University of Southern California, 24 October 2001, http://www-robotics.usc.edu/projects/scowr/; Jens Wawerla, "Collective Construction with Multiple Robots," Robotics Research Labs, University of Southern California, 21 February 2002, http://www-robotics.usc.edu/projects/collectiveconstruction/; Brian P. Gerkey, "Auction-based Multi-Robot Coordination," University of Southern California, 13 February 2003, http://robotics.usc.edu/~gerkey/research/murdoch.html.

[114] Jackrit Suthakorn, "Part III: Self-Replicating Robots," in Paradigms of Service Robotics, Ph.D. Dissertation, Department of Mechanical Engineering, Johns Hopkins University, Baltimore, Maryland, February 2003, pp. 167-236; http://caesar.me.jhu.edu/jackritweb/Thesis011403.pdf. Jackrit Suthakorn, Y.T. Kwon, G.S. Chirikjian, "A semi-autonomous replicating robotic system," Proc. 2003 IEEE Intl. Symp. on Computational Intelligence in Robotics and Automation (CIRA), Kobe, Japan, 2003; http://caesar.me.jhu.edu/jackritweb/CIRA2003.pdf.

[115] Jackrit Suthakorn, "Part III: Self-Replicating Robots," in Paradigms of Service Robotics, Ph.D. Dissertation, Department of Mechanical Engineering, Johns Hopkins University, Baltimore, Maryland, February 2003, pp. 167-236; http://caesar.me.jhu.edu/jackritweb/Thesis011403.pdf.

Assembly), a 12-step procedure; and at Station 3 (Gripper Assembly), a 4-step operational procedure, e.g.,:

1. Ascend backwards on the ramp.
2. Turn 180° on the top of the ramp and dock into position.
3. Operate lift down until gripper slides into the front of the original robot.
4. Descend backwards on the ramp.

The entire self-replication procedure "was conducted several times [and was] generally successful with some disparity of completion time (ranging from 45-75 minutes); however, there were some technical errors, such as battery failure." Several workcells were needed to assist the original robot in the replication process because the robot could not directly build its replicas. Each workcell served as a station in this factory-like replicating system, providing an example of an "indirectly replicating" robot.[116] An AVI video clip is available online.[117]

2.2.2.5 Chirikjian Group Autonomous Replicators (2002-present)

Suthakorn's fourth and final project presented here was to design and build a fully autonomous self-replicating robotic system.[118] This work took place under the direction of professor Gregory Chirikjian; also, Andrew Cushing, a local high school student, assisted in the building of the device. The robot and its replicas each consist of four separate complex parts or "subsystems": controller, left tread, right tread, and gripper/sensor components (Figure 2-30(A)). The prototype device used two light sensors to detect objects and track lines (blue-painted lines and silver spots) for navigation on the 2 meter x 3 meter work surface. Magnets and shape-constraining blocks helped to align and interlock the complex parts during replication (Figure 2-30(B)).

---

[116] Gregory S. Chirikjian, Jackrit Suthakorn, J. Zhou, "Self-replicating robot: A project in the mechatronics at Johns Hopkins University," JHU, Spring 2002; http://custer.me.jhu.edu/mechatronics/syllabus2002.htm. Gregory S. Chirikjian, Jackrit Suthakorn, "Toward self-replicating robots," Paper #067, Session 8: Design, 9 July 2002, Proc. 8th Intl. Symp. on Experimental Robotics (ISER '02), Italy, 8-11 July 2002; http://caesar.me.jhu.edu/jackritweb/iser2002.pdf or http://www.iser02.unisa.it/papers/67.pdf. Jackrit Suthakorn, "Self-Replicating Robots," http://caesar.me.jhu.edu/html/self_replicating_systems.html. Jackrit Suthakorn, "Part III: Self-Replicating Robots," in Paradigms of Service Robotics, Ph.D. Dissertation, Department of Mechanical Engineering, Johns Hopkins University, Baltimore, Maryland, February 2003, pp. 167-236; http://caesar.me.jhu.edu/jackritweb/Thesis011403.pdf.

[117] "A Semi Replicating Robotic System (Summer 2002)," ~33 MB AVI video clip of Suthakorn-Chirikjian semi-self-replicating robots; http://caesar.me.jhu.edu/jackritweb/semisrr.avi.

[118] Jackrit Suthakorn, "Part III: Self-Replicating Robots," in Paradigms of Service Robotics, Ph.D. Dissertation, Department of Mechanical Engineering, Johns Hopkins University, Baltimore, Maryland, February 2003, pp. 167-236; http://caesar.me.jhu.edu/jackritweb/Thesis011403.pdf. Jackrit Suthakorn, Andrew B. Cushing, Gregory S. Chirikjian, "An autonomous self-replicating robotic system," Proc. 2003 IEEE/ASME Intl. Conf. on Advanced Intelligent Mechatronics (AIM 2003), Kobe, Japan, 2003; http://custer.me.jhu.edu/publication/pdf/auton.pdf or http://caesar.me.jhu.edu/jackritweb/AIM2003.pdf; IEEE/ASME Trans. Mechatronics (submitted December 2003).

Figure 2-30. LEGO®-based fully-autonomous kinematic replicator (courtesy of Jackrit Suthakorn and Gregory Chirikjian, Johns Hopkins University)[119]

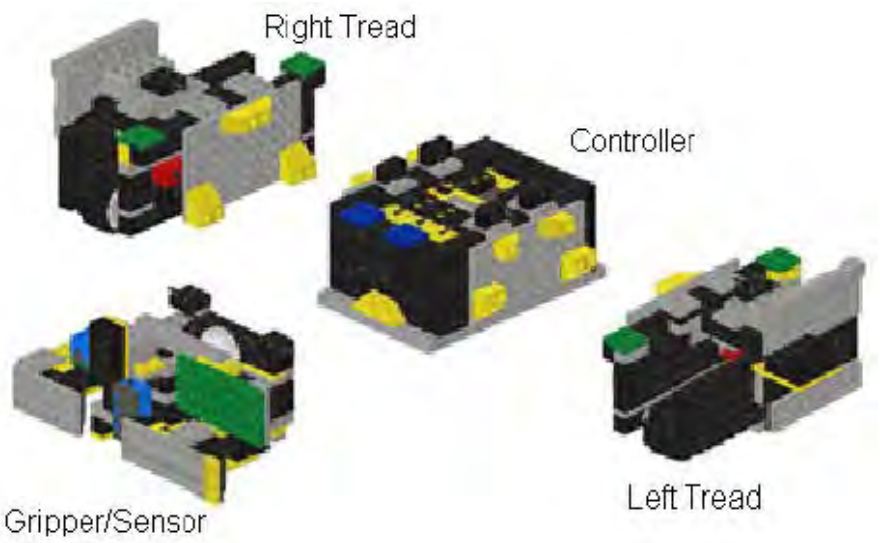

(A) Exploded view of the four complex components comprising the Suthakorn autonomous replicator

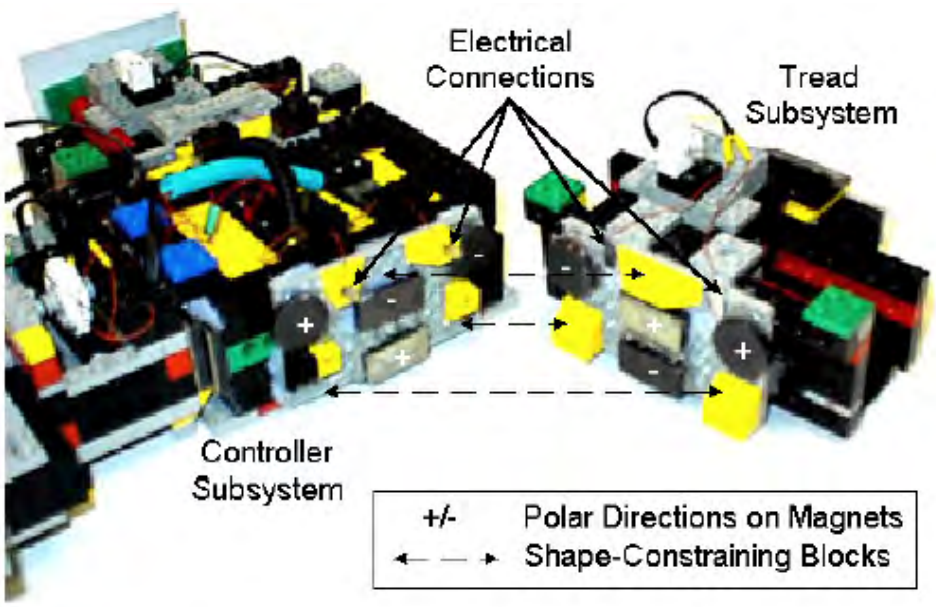

(B) Connections between controller and tread subsystems

---

[119] Jackrit Suthakorn, "Part III: Self-Replicating Robots," in Paradigms of Service Robotics, Ph.D. Dissertation, Department of Mechanical Engineering, Johns Hopkins University, Baltimore, Maryland, February 2003, pp. 167-236; http://caesar.me.jhu.edu/jackritweb/Thesis011403.pdf.

Figure 2-30. (cont'd)

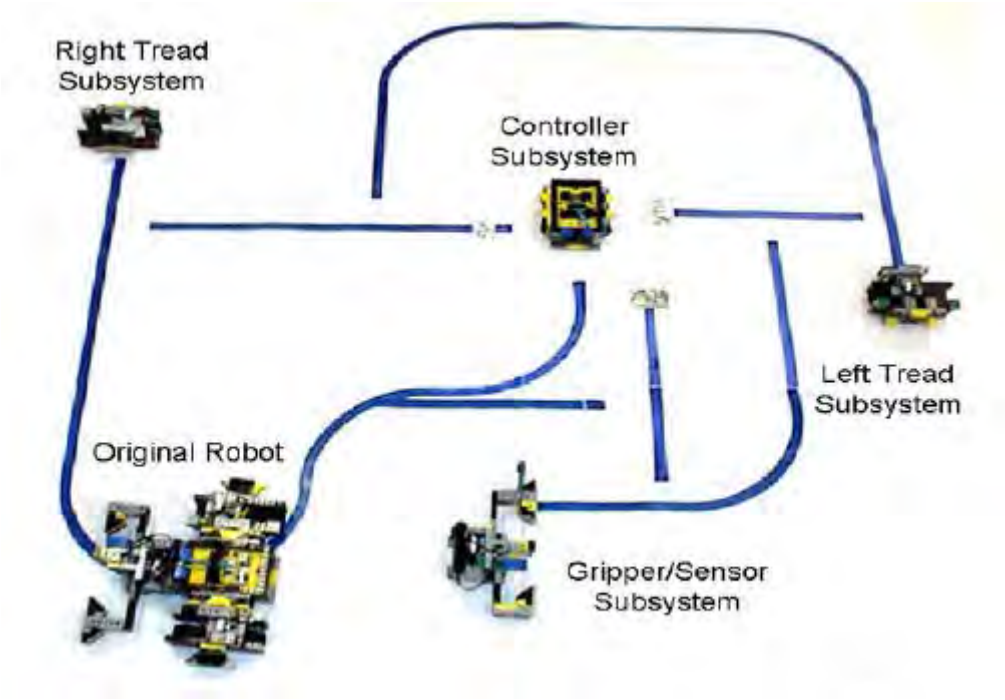

(C) Layout of the experimental area

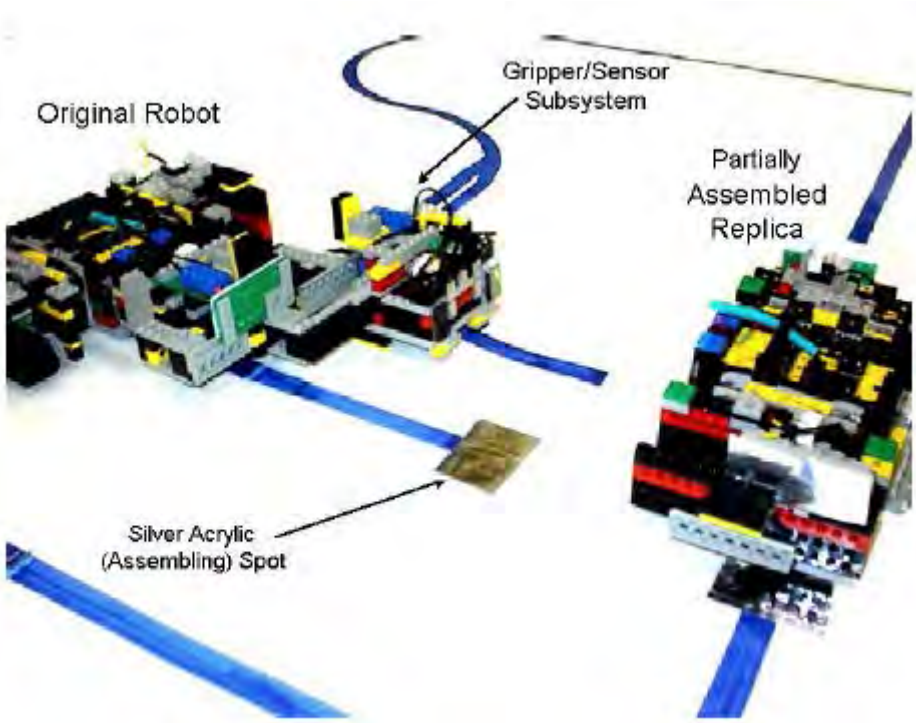

(D) Robot searches for the assembling spot while holding the replica's gripper/sensor part

The replica's parts are prepositioned at known locations and the original robot starts at the initial position (Figure 2-30(C)). The explicit replication procedure is worth quoting verbatim from Suthakorn[120] in its entirety:

(1) The original robot starts following the line from the starting point to the first subsystem (the "right tread" complex part) using sensor No. 1.

(2) Once light sensor No. 2 detects the first subsystem (right tread), the original robot stops and begins the grasping process, then grasps the right tread subsystem.

(3) After the grippers are closed, the original robot will turn to the right until it detects a line.

(4) The original robot will follow the second line until it reaches the assembling spot.

(5) When light sensor No. 1 on the original robot detects the silver acrylic spot (the assembling spot), the robot will stop and begin the attaching process.

(6) The original robot opens the grippers and gives a final push to secure the right tread subsystem (of the replica) to the controller subsystem (of the replica).

(7) The original robot then backs up and turns to the left until it detects a line value on sensor No. 1.

(8) The original robot follows the line until it reaches the left tread subsystem.

(9) Once light sensor No. 2 detects the second subsystem, the robot will stop, and begin the grasping process by closing its gripper around the left tread's wedge.

(10) The original robot turns right until it detects the next line.

(11) The original robot will follow the second line until it reaches the assembling spot.

(12) Once the original robot reaches the assembling spot, it begins the attaching process.

(13) The original robot opens its gripper to release the left tread subsystem.

(14) The original robot gives a final push on the left tread subsystem to help secure it.

(15) The original robot then backs up and turns left until it detects the next line, using sensor No. 1.

(16) The original robot follows the line to the final subsystem.

(17) Once it reaches the gripper/sensor subsystem, it will stop and begin the grasping process.

(18) The original robot closes its gripper and turns right until it detects a line value with sensor No. 1 (Figure 2-30(D)).

(19) The gripper/sensor subsystem is now transferred to the assembling spot.

(20) Once the original robot reaches the assembling spot it will stop and open the gripper.

(21) The original robot backs up and turns left until sensor No. 1 is a line value.

(22) The original robot then follows the line back to the starting point and is ready to replicate the next replica system.

(23) The finished replica robot self-activates 20 seconds after completion and begins following the line to the starting point.

(24) Once each robot reaches the starting point, it begins the replication procedure again.

---

[120] Jackrit Suthakorn, "Part III: Self-Replicating Robots," in Paradigms of Service Robotics, Ph.D. Dissertation, Department of Mechanical Engineering, Johns Hopkins University, Baltimore, Maryland, February 2003, pp. 167-236; http://caesar.me.jhu.edu/jackritweb/Thesis011403.pdf.

Following this cookbook-like procedure, the original robot was capable of automatically assembling its replicas. The replication process took 135 seconds per cycle. While each of the four complex parts had to be placed in known locations, "the errors of positioning and orientation are not highly critical. We found slight errors during the grasping process in a few experiments (out of more than 20 trials) caused by improper placement of the subsystems. Overall, the system is robust and repeatable." An AVI video clip is available online.[121]

In future work, Suthakorn had planned "to build a self-replicating intelligence system[122] such as a circuit controller and a mechanical decoder. This would fill the missing part of the self-replicating robotics research. However, our ultimate goal is to develop a self-replicating robotic system capable of autonomously assembling its replicas from simple components using only electromechanical intelligence, i.e., a mechanical code and transistor-based control circuits. This eliminates complicated electronic components such as programmable micro-controllers, and makes the concept more appropriate for future space systems that can use in-situ resources for self-replication."[123] Pursuing this objective, the syllabus for the Spring 2003 mechatronics course[124] at the JHU Department of Mechanical Engineering, called "the intelligence of self-replicating robots," is described as follows:

"This course is a hands-on, interdisciplinary design project, in which juniors, seniors, and graduate students from all engineering disciplines work together to design, build, and debug robots. This year we continue the exploration of self-replicating robots. Last year, each group built a remote-controlled self-replicating robot. This year our goal is to build autonomous self-replicating electromechanical intelligences. Each group will build a robot consisting of an arm, a control circuit for the arm, and a machine code program to control the arm, among which the circuit and the code should be replicable. The objective is that the arm should be able to implement the same function as before, after being connected to the resulting new circuit and code. The whole system will be built by using LEGO kits. Students are required to build their own logic control circuits which are made up of LEGO pieces embedded with electronic components, such as transistors, resistors, and capacitors. The "program" will also be built with LEGO pieces, and should consist of at least 10 bits but not more than 100 bits."

---

[121] "An Autonomous Self-Replicating Robotic System (Fall 2002)," ~21 MB AVI video clip of Suthakorn-Chirikjian auto-self-replicating robots; http://caesar.me.jhu.edu/jackritweb/autosrr.avi.

[122] Jackrit Suthakorn et al, "The intelligence of an autonomous self-replicating robotic system," submitted for review, 2003.

[123] Jackrit Suthakorn, "Part III: Self-Replicating Robots," in Paradigms of Service Robotics, Ph.D. Dissertation, Department of Mechanical Engineering, Johns Hopkins University, Baltimore, Maryland, February 2003, pp. 167-236; http://caesar.me.jhu.edu/jackritweb/Thesis011403.pdf.

[124] Gregory S. Chirikjian, Yu Zhou, Sangyoon Lee, Jackrit Suthakorn, "Mechatronics: ME 530.421 Spring 2003," Department of Mechanical Engineering, Johns Hopkins University, 2003; http://custer.me.jhu.edu/mechatronics/syllabus2003.htm.

Interestingly, Suthakorn's autonomous replicator passed the "fertility test" recommended by the RSC Team of the 1980 NASA lunar replicator study[125] for their replication feasibility demonstration:[126] "All the replicas were also capable of completing the same replicating process," says Suthakorn.[127] "We believe that this prototype was the world's first fully functional autonomous self-replicating robot."

Matt Moses joined the Chirikjian lab around 2005, and with Chirikjian and six other collaborators by 2007 had demonstrated a simplified version of the earlier replicator design using 7 compound parts comprised of exactly 158 active elements or primitive parts (Figure 2-31).[128]

---

[125] Robert A. Freitas Jr., William P. Gilbreath, eds., Advanced Automation for Space Missions, NASA Conference Publication CP-2255 (N83-15348), 1982; http://www.islandone.org/MMSG/aasm/.

[126] Robert A. Freitas Jr., Ralph C. Merkle, Kinematic Self-Replicating Machines, Landes Bioscience, Georgetown, TX, 2004; Section 3.13.1, pp. 45-46; http://www.MolecularAssembler.com/KSRM/3.13.1.htm.

[127] Jackrit Suthakorn, "Part III: Self-Replicating Robots," in Paradigms of Service Robotics, Ph.D. Dissertation, Department of Mechanical Engineering, Johns Hopkins University, Baltimore, Maryland, February 2003, pp. 167-236; http://caesar.me.jhu.edu/jackritweb/Thesis011403.pdf.

[128] Andrew Liu, Matt Sterling, Diana Kim, Andrew Pierpont, Aaron Schlothauer, Matt Moses, Kiju Lee, Greg Chirikjian, "A Memoryless Robot that Assembles Seven Subsystems to Copy Itself," Paper TuC1.2, Proceedings of the 2007 IEEE International Symposium on Assembly and Manufacturing, Ann Arbor, Michigan, USA, July 22-25, 2007, pp. 264-269.

Figure 2-31. LEGO®-based fully-autonomous kinematic replicator using 7 compound primitive parts (courtesy of Gregory Chirikjian, Johns Hopkins University)[129]

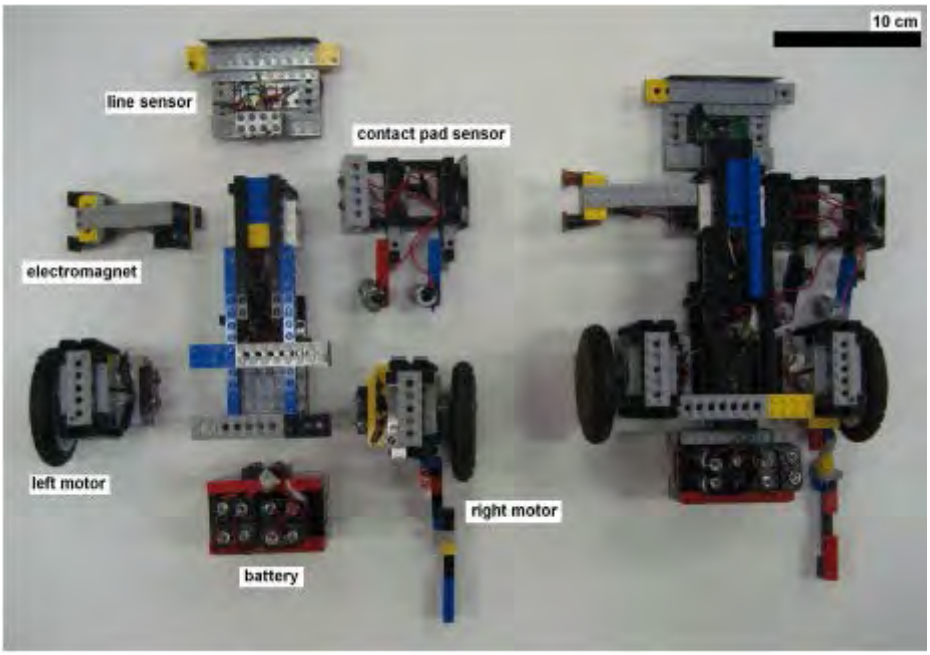

(A) The seven complex components (at left) comprising the autonomous replicator (at right)

Element (value)	CC	LS	RM	LM	CP	EM	BA
support structure (1)	1	1	1	1	1	1	1
magnet (1)	24	4	4	4	4	4	4
motor (4)			1	1			
electromagnet (1)						1	
relay (3)	3						
transistor (1)	2	4					
resistor (1)		4					
IR emitter (1)		2					
IR detector (1)		2					
ball caster (1)		2	2	2	2	1	4
wheel (1)			1	1			
mechanical linkage (1)				2	2		
electrical contact (1)	24	4	4	4	6	4	4
battery pack (1)							2
Total	60	23	16	18	15	11	15

(B) Active element count per component part of the robot

[129] Andrew Liu, Matt Sterling, Diana Kim, Andrew Pierpont, Aaron Schlothauer, Matt Moses, Kiju Lee, Greg Chirikjian, "A Memoryless Robot that Assembles Seven Subsystems to Copy Itself," Paper TuC1.2, Proceedings of the 2007 IEEE International Symposium on Assembly and Manufacturing, Ann Arbor, Michigan, USA, July 22-25, 2007, pp. 264-269.

Figure 2-31. (cont'd)

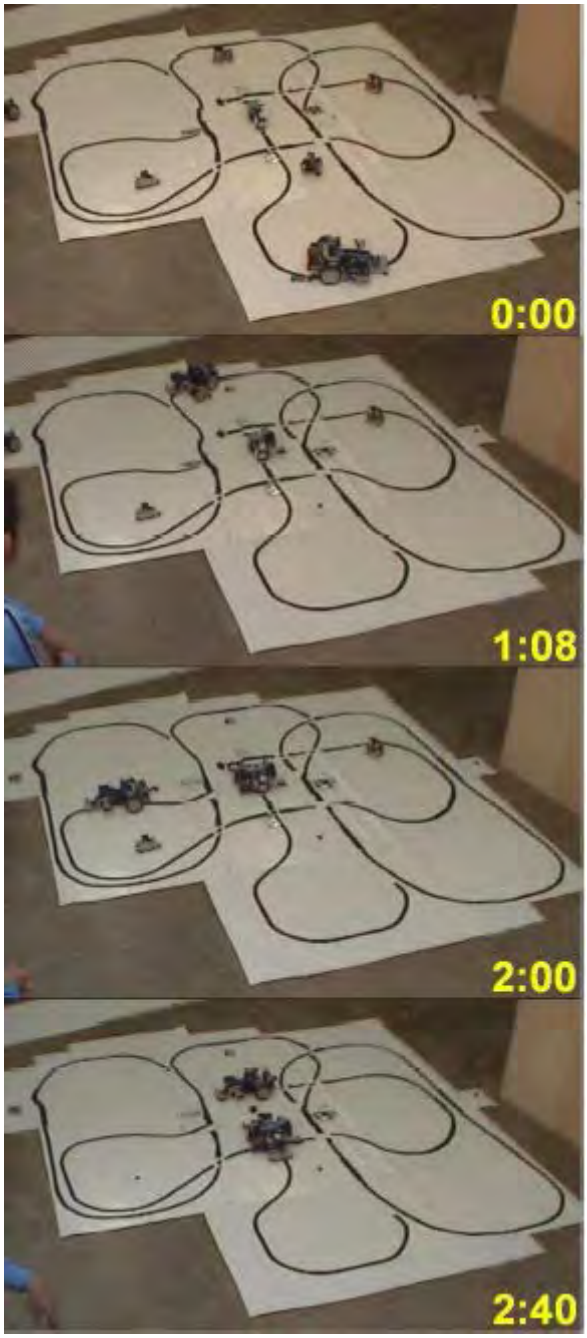

(C) The robot replicates in ~3 min by following the track

Figure 2-31. (cont'd)

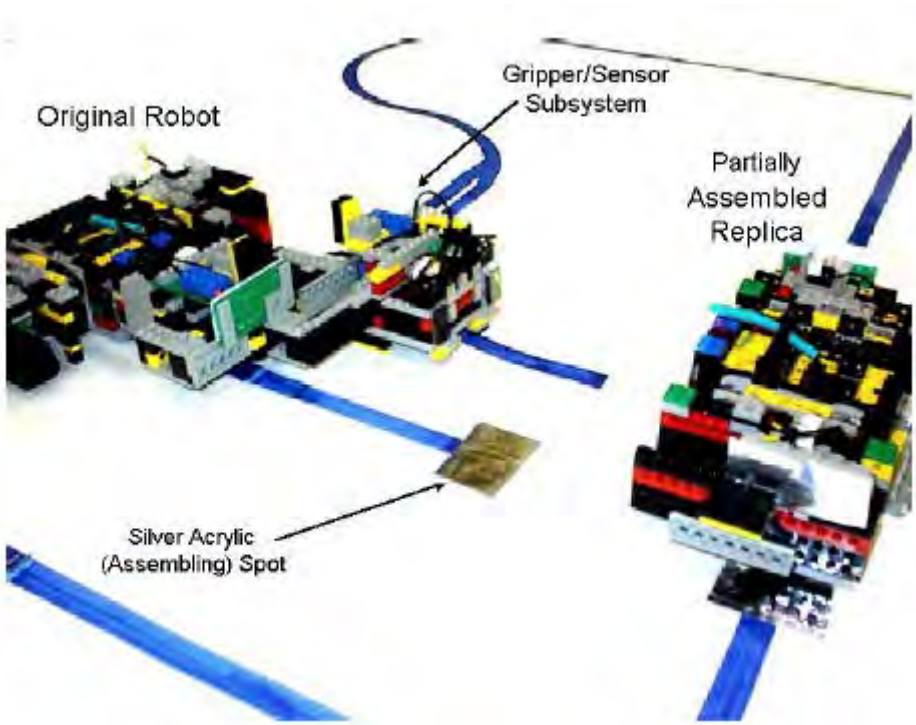

(D) Robot searches for the assembling spot while holding the replica's gripper/sensor part

2.2.3 Rapid Prototyping, Solid Printing and 3D Fabbing

Rapid prototyping systems typically allow an engineer to "print" a 3D copy of a design in polymer or resin – essentially, a desktop factory for manufacturing 3D solid objects. These systems generally lack both closure and full positional control, though they do have some analog-like positional control (e.g., inkjet printer approaches), and they also are neither nanoscale nor atomically precise. This field is briefly summarized below in a discussion reproduced verbatim from Section 3.20 of KSRM[130] (Section 2.2.3.1), followed by a brief description of the much-publicized RepRap, Fab@Home, and related projects (Section 2.2.3.2), and finally a summary of 3D particle-beam-based manufacturing (Section 2.2.3.3) reproduced verbatim from Section 4.7 of KSRM.[131]

2.2.3.1 Three-Dimensional Solid Printing

The GOLEM (Genetically Organized Lifelike Electro Mechanics) Project[132] at Brandeis University, and related earlier efforts in "evolutionary robotics",[133] are an attempt to extend

---

[130] Robert A. Freitas Jr., Ralph C. Merkle, Kinematic Self-Replicating Machines, Landes Bioscience, Georgetown, TX, 2004; Section 3.20, pp. 64-67; http://www.MolecularAssembler.com/KSRM/3.20.htm.

[131] Robert A. Freitas Jr., Ralph C. Merkle, Kinematic Self-Replicating Machines, Landes Bioscience, Georgetown, TX, 2004; Section 4.7, pp. 117-118; http://www.MolecularAssembler.com/KSRM/4.7.htm.

[132] Hod Lipson, Jordan B. Pollack, "Automatic design and manufacture of robotic lifeforms", Nature 406(2000):974-978; http://golem03.cs-i.brandeis.edu/download/naturegolem.pdf. See also: Rodney Brooks, "From robot dreams to reality," Nature 406(31 August 2000):945-947; George Musser, "Robotics replication: Dawn of a new species?" Sci. Amer. 283(November 2000):26; John Whitfield, "Design for living," Nature Science Update, 31 August 2000; http://www.nature.com/nsu/000831/000831-8.html. "The Golem Project," see: http://www.demo.cs.brandeis.edu/golem/, http://golem03.cs-i.brandeis.edu/index.html, http://golem03.cs-i.brandeis.edu/press.html, http://helen.cs-i.brandeis.edu/golem/. Matthew Fordahl, "Computer makes robot offspring," Associated Press, 30 August 2000, http://www.canoe.ca/CNEWSScience0008/30_robot.html; "Robots making robots, with some help," Science News 158(16 September 2000):189, http://golem03.cs-i.brandeis.edu/press/ScienceNews.pdf; Bruce Sterling, "When robots act like rabbits," Wall Street Journal, 6 September 2000, http://golem03.cs-i.brandeis.edu/press/Wsj_a.jpg; Jennifer Viegas, "Robots self-replicate, team up," Discovery.com News, 30 August 2000, http://golem03.cs-i.brandeis.edu/press/discovery.pdf or http://www.discovery.com/news/briefs/20000830/te_robots.html. Jordan B. Pollack, Hod Lipson, "The GOLEM Project: Evolving Hardware Bodies and Brains," Proceedings of the Second NASA/DoD Workshop on Evolvable Hardware (EH'00), 13-15 July 2000, Palo Alto CA, Institute of Electrical and Electronics Engineers, 2000; http://computer.org/proceedings/eh/0762/07620037abs.htm.

[133] Pablo Funes, Jordan Pollack, "Computer evolution of buildable objects," in P. Husbands, I. Harvey, eds., Fourth European Conference on Artificial Life, MIT Press, Cambridge, MA, 1997, pp. 358-367; http://demo.cs.brandeis.edu/papers/ecal97.pdf and http://demo.cs.brandeis.edu/papers/other/cs-97-191.html. Pablo Funes, Jordan Pollack, "Evolutionary body building: Adaptive physical designs for robots," Artificial Life 4(Autumn 1998):337-357; http://demo.cs.brandeis.edu/papers/funpolalife.pdf. Pablo J. Funes, Jordan B. Pollack, "Componential structural simulator," Brandeis University Department of Computer Science, Technical Report CS-98-198, 1998; http://demo.cs.brandeis.edu/papers/cs98-198.pdf. Pablo Funes, Jordan Pollack, "Computer evolution of buildable objects," in P. Bentley, ed., Evolutionary

evolutionary techniques into the physical world by evolving diverse electro-mechanical machines (robots) that can be manufactured by automated fabrication,[134] personal factories,[135] stereolithography (using a UV laser to selectively cure a photopolymerized resin),[136] solid freeform fabrication (SFF),[137] selective laser sintering (SLS) and laser direct metal deposition (DMD),[138] laminated object modeling (LOM) and fused deposition modeling (FDM),[139] or rapid

---

Design by Computers, Morgan Kaufmann, San Francisco, 1999, pp. 387-403; http://demo.cs.brandeis.edu/papers/edc98.pdf. Jordan B. Pollack, Hod Lipson, Sevan G. Ficici, Pablo Funes, Gregory S. Hornby, Richard A. Watson, "Evolutionary techniques in physical robotics," in J. Miller, ed., Evolvable Systems: From Biology to Hardware, Proc. of the Third Intl. Conf. (ICES 2000), Springer, 2000, pp. 175-186 (Lecture Notes in Computer Science, Vol. 1801); http://demo.cs.brandeis.edu/papers/ices00.pdf. Gregory S. Hornby, Hod Lipson, Jordan B. Pollack, "Evolution of generative design systems for modular physical robots," IEEE Intl. Conf. on Robotics and Automation, 2001; http://demo.cs.brandeis.edu/papers/hornby_icra01.pdf. Jordan B. Pollack, Hod Lipson, Pablo Funes, Gregory Hornby, "First three generations of evolved robots," EvoRobots 2001, pp. 62-71. G.S. Hornby, H. Lipson, J.B. Pollack, "Generative representations for the automated design of modular physical robots," IEEE Trans. Robotics and Automation 19(2003):703-719. Jordan B. Pollack, Hod Lipson, Sevan G. Ficici, Pablo Funes, Greg Hornby, Richard A. Watson, "Evolutionary techniques in physical robotics," in Peter J. Bentley, David W. Corne, eds., Creative Evolutionary Systems, Morgan-Kaufmann, San Francisco, 2001, pp. 511-524. Stefano Nolfi, Dario Floreano, Evolutionary Robotics: The Biology, Intelligence, and Technology of Self-Organizing Machines, MIT Press, Cambridge, MA, 2000.

[134] Marshall Burns, Automated Fabrication: Improving Productivity in Manufacturing, Prentice-Hall, 1993. Jerome L. Johnson, Principles of Computer Automated Fabrication, Palatino Press, 1994.

[135] Brock Hinzmann, "The Personal Factory," MCB Internet Conference on Rapid Prototyping, 1996; http://www.ennex.com/~fabbers/publish/199600-Brock-PersonalFactory.asp.

[136] Paul F. Jacobs, Stereolithography and other RP&M Technologies: From Rapid Prototyping to Rapid Tooling, Society of Manufacturing Engineers (SME), 1996; Paul F. Jacobs, Rapid Prototyping and Manufacturing: Fundamentals of StereoLithography, Society of Manufacturing Engineers (SME), 1993.

[137] David S. McKay, Hubert P. Davis, Marshall Burns, "Using fabricators to reduce space transportation costs," Solid Freeform Fabrication Symposium, University of Texas at Austin, 14 August 1995; http://www.ennex.com/publish/199608-MB-SpaceFab.asp. Digital Fabrication Portal "fabbers.com"; http://www.ennex.com/~fabbers/. Arlan Keith Andrews, "Manufacturing magic," Analog 112(September 1992):60-72.

[138] M.L. Griffith, D.M. Keicher, C.L. Atwood, J.A. Romero, J.E. Smugeresky, L.D. Harwell, D.L. Greene, "Freeform Fabrication of Metallic Components Using Laser Engineered Net Shaping (LENS)," in D.L. Bourell, J.J. Beaman, H.L. Marcus, R.H. Crawford, J.W. Barlow, eds., Solid Freeform Fabrication Proceedings, The University of Texas at Austin, August 1996, pp. 125-132. D. Krantz et al., "On-Demand Spares Fabrication During Space Missions Using Laser Direct Metal Deposition," in M.S. El-Genk, Space Technology and Applications International Forum 2001, American Institute of Physics, 2001.

[139] M. Agarwala, A. Bandyopadhyay, R. van Weeren, V. Jamalabad, P. Whalen, N.A. Langrana, A. Safari,, S.C. Danforth, "Fused deposition of ceramics," J. Rapid Prototyping 2(1996):4-19; Dan Qiu, Noshir A. Langrana, Stephen C. Danforth, "Intelligent toolpath for extrusion-based LM process," http://www.caip.rutgers.edu/~danqiu/sff10.html; "An intelligent CAD system for multi-material layered manufacturing," http://www.caip.rutgers.edu/~danqiu/research.html. See also: Laboratory of Solid Freeform Fabrication of Advanced Ceramics at Rutgers University," http://www.caip.rutgers.edu/sff/; Michael Brooks, "Printing dreams," WorldLink, Magazine of the World Economic Forum, 21 March 2001;

prototyping (RP).[140] Lipson and Pollack of the Volen Center for Complex Systems at Brandeis University describe a set of preliminary experiments evolving purely electromechanical systems composed of thermoplastic, linear actuators and "neurons" (evolved artificial neural network) for the task of locomotion, first in simulation and then in reality. Lipson used the FDM technology of Stratasys Inc. which is based on feeding a thermoplastic feedstock wire into a heated nozzle, then positioning the nozzle to deposit the plastic to build a part layer by layer. After 3-D solid printing, these simulation-evolved systems then faithfully reiterate the performance of their virtual ancestors.

Lipson and Pollack start with a set of elementary building blocks (bars, actuators and neurons), and a set of operations that can join building blocks together, take them apart, or modify their dimensions. The first task to be optimized was the speed of locomotion. Virtual robots are initialized empty, each with zero bars, zero actuators and zero neurons. The computer applies design operations to the robots at random. After each operation is carried out, the computer measures the performance of the robot in a simulator. If it is better than average performance (speed, in this case), the computer makes more of it, and if it is less than average, the computer removes it. The computer continues to run all day. In the beginning, most of the virtual robots are just piles of random building blocks and their performance is zero. By chance, after, say, a

---

http://www.worldlink.co.uk/stories/storyReader$632; "3-D printing technology," New Scientist 167(30 September 2000). ToyBuilders.com, a division of Vicale Corp., http://www.toybuilders.com; "Stereolithography (SLA)," http://www.toybuilders.com/stereolithography.htm; "Selective Laser Sintering (SLS)," http://www.toybuilders.com/selective_laser_sintering.htm; "Fused Deposition Modeling (FDM)," http://www.toybuilders.com/fused_deposition_modeling.htm; "Layer Object Manufacturing (LOM)," http://www.toybuilders.com/layer_object_manufacturing.htm; "3 Dimensional Printing (3DP)," http://www.toybuilders.com/3_dimensional_printing.htm. "Fused Deposition Modeling," http://www.quickparts.com/encyclopedia/FDM.pdf; "Info Page: Fused Deposition Modeling," October 1999, http://www-2.cs.cmu.edu/~unsal/research/rapid/fdm.html; "Fused Deposition Modeling," http://www.nitc.qub.ac.uk/divs/adc-fdm.htm; "Fused Deposition Modeling (FDM)," Phoenix Analysis & Design Technologies, 2003, http://www.padtinc.com/rm/fdm/default.htm; "Fused Deposition Modeling," 9 February 2004, http://www.materialise.com/prototypingsolutions/fused_ENG.html.

[140] Paul F. Jacobs, Stereolithography and other RP&M Technologies: From Rapid Prototyping to Rapid Tooling, Society of Manufacturing Engineers (SME), 1996; Paul F. Jacobs, Rapid Prototyping and Manufacturing: Fundamentals of StereoLithography, Society of Manufacturing Engineers (SME), 1993. Lamont Wood, Rapid Automated Prototyping: An Introduction, Industrial Press, Inc., 1993. Ming C. Leu, Handbook of Rapid Prototyping and Layered Manufacturing, Academic Press, New York, 2000. Kenneth G. Cooper, Rapid Prototyping Technology, Marcel Dekker, New York, 2001. S.S. Dimov, Duc Truon Pham, Rapid Manufacturing: The Technologies and Applications of Rapid Prototyping and Rapid Tooling, Springer-Verlag, New York, 2001. L. Lu, J.Y.H. Fuh, Y.S. Wong, Laser-Induced Materials and Processes for Rapid Prototyping, Kluwer Academic Publishers, New York, 2001. I. Gibson, Software Solutions for Rapid Prototyping, Professional Engineering Publishing, 2002. Andreas Gebhardt, Rapid Prototyping, Hanser Gardner Publications, 2003. Chua Chee Kai, Leong Kah Fai, Lim Chu-Sing, Rapid Prototyping: Principles and Applications, Second Edition, World Scientific Publ. Co., New York, 2003. Steve Upcraft, Paul G. Ranky, Rapid Prototyping Solutions, CIMware USA, Inc., 2003. "Functional Rapid Prototyping," Cornell Laboratory for Computational Synthesis; http://www.mae.cornell.edu/ccsl/scm/index.htm. Friedrich B. Prinz et al, "JTEC/WTEC Panel Report on Rapid Prototyping in Europe and Japan," Japanese Technology Evaluation Center, World Technology Evaluation Center, Loyola College in Maryland, March 1997; http://www.wtec.org/loyola/rp/toc.htm.

hundred generations, a particular group of building blocks happens to assemble in such a way that something moves a little. That accidental assembly is then replicated because it has above-average performance.

After many more generations, but essentially the same kind of progress steps, Lipson and Pollack observe the emergence of robots that look like they were designed, but really are just the outcome of this simulated natural selection.[141] The robots are rendered into real physical models using a 3-D printing process (Figure 2-32) that prints solid objects voxel by voxel (though with some multivoxel overlap due to imperfect materials flow) using a raster scan motif, and these robots function largely as expected when built (Figure 2-33). This work demonstrates a complete physical evolution cycle, wherein a robotic system can design and manufacture new robots, but it is not yet self-replication because the machines produced are not as capable as their precursors and the robots require the rather substantial intervention of a 3-D printer machine and human assembly assistance (typically including actuators, power sources and electronic controls) in order to complete their physical instantiation.

Figure 2-32. 3D Systems' ThermoJet 3-D printer allows CAD designers to quickly print a 3-dimensional model to 50-100 micron resolution[142]

Earlier work by Chocron and Bidaud[143] attempted to use a genetic algorithm to evolve both the morphology and inverse kinematics of a modular manipulator composed of prismatic and

---

[141] Karl Sims, "Evolving virtual creatures," Siggraph '94 Proceedings, July 1994, pp.15-22; http://www.genarts.com/karl/papers/siggraph94.pdf. Karl Sims, "Evolving 3-D morphology and behavior by competition," in R. Brooks, P. Maes, eds., Artificial Life IV: Proceedings Fourth Intl. Workshop on the Synthesis and Simulation of Living Systems, MIT Press, Cambridge, MA, 1994, pp. 28-39; http://www.genarts.com/karl/papers/alife94.pdf. Maciej Komosinski, Szymon Ulatowski, "FRAMSTICKS. Artificial Life for real people," Poznan University of Technology; http://www.frams.poznan.pl/.

[142] 3D Systems, "Products"; http://www.3dsystems.com.

[143] O. Chocron, P. Bidaud, "Genetic design of 3-D modular manipulators," Proc. 1997 IEEE Intl. Conf. on Robotics and Automation, Vol. 1, 1997, pp. 223-228.

revolute joints, but their simple serial construction approach precluded the spontaneous emergence of unforeseen or novel solutions. Similarly, Dittrich et al.[144] described a "random morphology robot" which is an arbitrary 2-D structure composed of links and motors; the controller is evolved, then manual changes are applied to the robot to test its behavior with an impaired or mutated body.

Figure 2-33. GOLEM Project[145] uses robotic system to automatically design and manufacture new robots; a computer-designed, 3-D printed robot crawler is shown below.

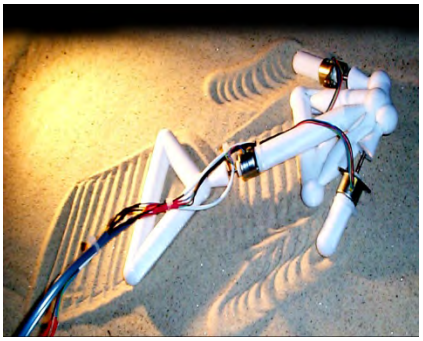

Lipson and Pollack point out that they are a long way from making a 3-D printer that can print another 3-D printer, as would be required for full self-replication. They used the cheapest available technology, a 3-D printer that melts plastic and prints it in layers. Instead of their cheap $50,000 "fab," they note that they could have used a $2M or a $10M "fab" that would build

---

[144] Peter Dittrich, A. Burgel, Wolfgang Banzhaf, "Learning to move a robot with random morphology," in P. Husbands, J.A. Meyer, eds., Evolutionary Robotics: First European Workshop, EvoRobot98, Springer-Verlag, 1998.

[145] Hod Lipson, Jordan B. Pollack, "Automatic design and manufacture of robotic lifeforms", Nature 406(2000):974-978; http://golem03.cs-i.brandeis.edu/download/naturegolem.pdf. See also: Rodney Brooks, "From robot dreams to reality," Nature 406(31 August 2000):945-947; George Musser, "Robotics replication: Dawn of a new species?" Sci. Amer. 283(November 2000):26; John Whitfield, "Design for living," Nature Science Update, 31 August 2000; http://www.nature.com/nsu/000831/000831-8.html. "The Golem Project," see: http://www.demo.cs.brandeis.edu/golem/, http://golem03.cs-i.brandeis.edu/index.html, http://golem03.cs-i.brandeis.edu/press.html, http://helen.cs-i.brandeis.edu/golem/. Matthew Fordahl, "Computer makes robot offspring," Associated Press, 30 August 2000, http://www.canoe.ca/CNEWSScience0008/30_robot.html; "Robots making robots, with some help," Science News 158(16 September 2000):189, http://golem03.cs-i.brandeis.edu/press/ScienceNews.pdf; Bruce Sterling, "When robots act like rabbits," Wall Street Journal, 6 September 2000, http://golem03.cs-i.brandeis.edu/press/Wsj_a.jpg; Jennifer Viegas, "Robots self-replicate, team up," Discovery.com News, 30 August 2000, http://golem03.cs-i.brandeis.edu/press/discovery.pdf or http://www.discovery.com/news/briefs/20000830/te_robots.html. Jordan B. Pollack, Hod Lipson, "The GOLEM Project: Evolving Hardware Bodies and Brains," Proceedings of the Second NASA/DoD Workshop on Evolvable Hardware (EH'00), 13-15 July 2000, Palo Alto CA, Institute of Electrical and Electronics Engineers, 2000; http://computer.org/proceedings/eh/0762/07620037abs.htm.

bigger devices out of stronger material. But Sony Corp. reportedly already uses a robot "fab" for most small consumer electronics. Stereolithography and rapid prototyping[146] enjoy widespread artistic,[147] academic and commercial interest,[148] and machines which can print mechanical, electrical, and electronic logic componentry together on a small scale are under development.[149] (Saul Griffith[150] in Jacobson's group at MIT built a working printer capable of printing in chocolate and beeswax with the LEGO® toolkit – using a simple extrusion chamber based on a

---

[146] Paul F. Jacobs, Stereolithography and other RP&M Technologies: From Rapid Prototyping to Rapid Tooling, Society of Manufacturing Engineers (SME), 1996; Paul F. Jacobs, Rapid Prototyping and Manufacturing: Fundamentals of StereoLithography, Society of Manufacturing Engineers (SME), 1993. Lamont Wood, Rapid Automated Prototyping: An Introduction, Industrial Press, Inc., 1993. Ming C. Leu, Handbook of Rapid Prototyping and Layered Manufacturing, Academic Press, New York, 2000. Kenneth G. Cooper, Rapid Prototyping Technology, Marcel Dekker, New York, 2001. S.S. Dimov, Duc Truon Pham, Rapid Manufacturing: The Technologies and Applications of Rapid Prototyping and Rapid Tooling, Springer-Verlag, New York, 2001. L. Lu, J.Y.H. Fuh, Y.S. Wong, Laser-Induced Materials and Processes for Rapid Prototyping, Kluwer Academic Publishers, New York, 2001. I. Gibson, Software Solutions for Rapid Prototyping, Professional Engineering Publishing, 2002. Andreas Gebhardt, Rapid Prototyping, Hanser Gardner Publications, 2003. Chua Chee Kai, Leong Kah Fai, Lim Chu-Sing, Rapid Prototyping: Principles and Applications, Second Edition, World Scientific Publ. Co., New York, 2003. Steve Upcraft, Paul G. Ranky, Rapid Prototyping Solutions, CIMware USA, Inc., 2003. "Functional Rapid Prototyping," Cornell Laboratory for Computational Synthesis; http://www.mae.cornell.edu/ccsl/scm/index.htm. Friedrich B. Prinz et al, "JTEC/WTEC Panel Report on Rapid Prototyping in Europe and Japan," Japanese Technology Evaluation Center, World Technology Evaluation Center, Loyola College in Maryland, March 1997; http://www.wtec.org/loyola/rp/toc.htm.

[147] "Dimension 3-D Printer Featured as Part of Exploratorium Museum's TeleSculpture 2003 Exhibit," Business Wire, 10 October 2003; http://home.businesswire.com/portal/site/google/index.jsp?ndmViewId=news_view&newsId=20031010005389&newsLang=en.

[148] For example, see: Terry Wohlers, "The World of Rapid Prototyping," Proc. Fourth Intl. Conf. On Desktop Manufacturing, 24-25 September 1992, San Jose, CA, Wohlers Associates, 1992, http://www.wohlersassociates.com/mr.html; "University Rapid Prototyping Programs," http://home.att.net/~castleisland/u_lks.htm; "Rapid Manufacturing Processes at University and R&D Labs," Carnegie Mellon University, Spring 1997, http://www-2.cs.cmu.edu/People/rapidproto/manufacturing/mfguniversity.html; "The Commercial Rapid Prototyping Systems," http://ecoleing.uqtr.uquebec.ca/geniedoc/gmm/productique/rp_systems.htm; "Commercial Rapid Prototyping System Manufacturers," http://home.att.net/~castleisland/com_lks.htm; "Rapid Prototyping Directory," http://mtiac.iitri.org/pubs/rp/rp6.htm; Stratasys Inc., http://www.stratasys.com; Z Corporation, "Industry-Standard Three-Dimensional Printers & Solutions," http://www.zcorp.com; "The Worldwide Rapid Prototyping Directory," http://home.att.net/%7Ecastleisland/links.htm.

[149] Evan Malone, Kian Rasa, Daniel Cohen, Todd Isaacson, Hilary Lashley, Hod Lipson, "Freeform fabrication of 3-D zinc-air batteries and functional electro-mechanical assemblies," Proc. 14th Conference on Solid Freeform Fabrication, Austin TX, Aug 2003, Rapid Prototyping Journal 10(2004):58-69.

[150] Saul Griffith, "Towards Personal Fabricators: Tabletop tools for micron and sub-micron scale functional rapid prototyping," Master's Thesis in Media Arts and Science, Massachusetts Institute of Technology, February 2001, 81pp; http://web.media.mit.edu/~saul/mlmasters/sm_masters.pdf. See also: "Presentation and perspectives on personal fabrication," http://web.media.mit.edu/~saul/pf/pf.ppt.

worm screw and three-axis actuation based on the LEGO® robotics motors and the LOGO programming platform. "A three dimensional printer using programming languages designed for children and low cost consumables has been implemented. One can imagine a new paradigm for children's toys involving the child in the design, production, and then eating! of their own play-things.")

For example, by 2000, Stephen C. Danforth at Rutgers University was printing 3-D electronic components from ceramic materials that can be insulating, semiconducting, or fully conducting, depending on their exact composition.[151] This allowed printing of 3-D electromechanical components such as sensors and actuators with feature sizes as small as 200 microns, which Danforth's group hoped to halve by 2003. By 2002, Joseph Jacobson's group at the MIT Media Lab had printed working inorganic field-effect transistors,[152] radio frequency identification tags,[153] and working three-dimensional machines such as linear drive motors and thermal actuators[154] with feature sizes of ~100 microns (Figure 2-34) by laying down hundreds of layers

---

[151] M. Agarwala, A. Bandyopadhyay, R. van Weeren, V. Jamalabad, P. Whalen, N.A. Langrana, A. Safari,, S.C. Danforth, "Fused deposition of ceramics," J. Rapid Prototyping 2(1996):4-19; Dan Qiu, Noshir A. Langrana, Stephen C. Danforth, "Intelligent toolpath for extrusion-based LM process," http://www.caip.rutgers.edu/~danqiu/sff10.html; "An intelligent CAD system for multi-material layered manufacturing," http://www.caip.rutgers.edu/~danqiu/research.html. See also: Laboratory of Solid Freeform Fabrication of Advanced Ceramics at Rutgers University," http://www.caip.rutgers.edu/sff/; Michael Brooks, "Printing dreams," WorldLink, Magazine of the World Economic Forum, 21 March 2001; http://www.worldlink.co.uk/stories/storyReader$632; "3-D printing technology," New Scientist 167(30 September 2000). ToyBuilders.com, a division of Vicale Corp., http://www.toybuilders.com; "Stereolithography (SLA)," http://www.toybuilders.com/stereolithography.htm; "Selective Laser Sintering (SLS)," http://www.toybuilders.com/selective_laser_sintering.htm; "Fused Deposition Modeling (FDM)," http://www.toybuilders.com/fused_deposition_modeling.htm; "Layer Object Manufacturing (LOM)," http://www.toybuilders.com/layer_object_manufacturing.htm; "3 Dimensional Printing (3DP)," http://www.toybuilders.com/3_dimensional_printing.htm. "Fused Deposition Modeling," http://www.quickparts.com/encyclopedia/FDM.pdf; "Info Page: Fused Deposition Modeling," October 1999, http://www-2.cs.cmu.edu/~unsal/research/rapid/fdm.html; "Fused Deposition Modeling," http://www.nitc.qub.ac.uk/divs/adc-fdm.htm; "Fused Deposition Modeling (FDM)," Phoenix Analysis & Design Technologies, 2003, http://www.padtinc.com/rm/fdm/default.htm; "Fused Deposition Modeling," 9 February 2004, http://www.materialise.com/prototypingsolutions/fused_ENG.html.

[152] Brent A. Ridley, B. Nivi, Joseph M. Jacobson, "All-inorganic field effect transistors fabricated by printing," Science 286(22 October 1999):746-749; http://www.media.mit.edu/molecular/Science10-99.pdf.

[153] Stephen Mihm, "Print your next PC," Technology Review, November/December 2000; http://www.techreview.com/articles/nov00/mihm_printable.htm.

[154] Sawyer B. Fuller, Eric J. Wilhelm, Joseph M. Jacobson, "Ink-jet printed nanoparticle microelectromechanical systems," J. Microelectromechanical Systems 11(January-March 2002):54-60; http://www.media.mit.edu/molecular/IEEE-MEMS2-02.pdf. See also: S. Fuller, J. Jacobson, "Ink jet fabricated nanoparticle MEMS," in Proc. IEEE Microelectromech. Syst. Conf., 2000, pp. 138-141; Joseph Jacobson, Eric Wilhelm, Colin Bulthaup, Brent Ridley, "Nanotectonics: Fabrication of inorganic transistors and micro-electro-mechanical systems from nanoparticle building blocks," paper H8.6, Session H8: Fabrication and Properties of 3D-ordered Nanostructures, Symposium on Three-Dimensional Nanoengineered Assemblies, 1-5 December 2002, Materials Research Society (www.mrs.org) Symposium Proceedings, Vol. 739, 2003. See also: Sawyer B. Fuller, "Ink jet deposition of inorganic nanoparticle

of nanoparticle-based inks using an inkjet printing technique that requires no clean room and temperatures under 300 °C. Several other research groups at Lucent's Bell Labs and Cambridge University (U.K.) have also printed transistors using organic polymers,[155] and there is a growing literature on the ink-jet printing of electronic components.[156] One rumor had it that Hewlett-Packard is planning to sell a personal desktop 3-D printer for as little as $1000.[157]

Figure 2-34. An inkjet printed thermal actuator (from MIT Media Lab)[158]

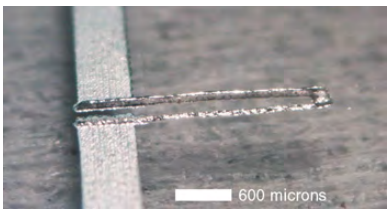

---

materials as a route to desktop fabrication of integrated logic and micromachinery," Thesis, B.S. Mech. Eng., MIT, June 2000.

[155] Stephen Mihm, "Print your next PC," Technology Review, November/December 2000; http://www.techreview.com/articles/nov00/mihm_printable.htm.

[156] K.F. Teng, R.W. Vest, "A microprocessor-controlled ink jet printing system for electronic circuits," IEEE Trans. Indust. Electron. 35(1988):407-412. "Application of ink jet technology on photovoltaic metallization," IEEE Electron Device Lett. 9(November 1988):591-592. T.R. Hebner, C.C. Wu, D. Marcy, M.H. Lu, J.C. Sturm, "Ink-jet printing of doped polymers for organic light emitting devices," Appl. Phys. Lett. 72(1998):519-521. G. Percin, T.S. Lundgren, B.T. Khuri-Yakub, "Controlled ink-jet printing and deposition of organic polymers and solid particles," Appl. Phys. Lett. 73(1998):2375-2377. J. Bharathan, Y. Yang, "Polymer electroluminescent devices processed by inkjet printing: I. Polymer light-emitting logo," Appl. Phys. Lett. 72(1998):2660-2662. D.J. Hayes, W.R. Cox, M.E. Grove, "Microjet printing of polymers and solder for electronics manufacturing," J. Electron. Manufact. 8(1998):209-216. B. Comiskey, J.D. Albert, H. Yoshizawa, J. Jacobson, "An electrophoretic ink for all-printed reflective electronic displays," Nature 394(1998):253-255.

[157] John Markoff, "Innovation at Hewlett Tries to Evade the Ax," The New York Times, 5 May 2003, p. C1; http://www.nytimes.com/2003/05/05/technology/05HEWL.html?th or http://query.nytimes.com/gst/abstract.html?res=F30711FC38580C768CDDAC0894DB404482.

[158] Sawyer B. Fuller, Eric J. Wilhelm, Joseph M. Jacobson, "Ink-jet printed nanoparticle microelectromechanical systems," J. Microelectromechanical Systems 11(January-March 2002):54-60; http://www.media.mit.edu/molecular/IEEE-MEMS2-02.pdf. See also: S. Fuller, J. Jacobson, "Ink jet fabricated nanoparticle MEMS," in Proc. IEEE Microelectromech. Syst. Conf., 2000, pp. 138-141; Joseph Jacobson, Eric Wilhelm, Colin Bulthaup, Brent Ridley, "Nanotectonics: Fabrication of inorganic transistors and micro-electro-mechanical systems from nanoparticle building blocks," paper H8.6, Session H8: Fabrication and Properties of 3D-ordered Nanostructures, Symposium on Three-Dimensional Nanoengineered Assemblies, 1-5 December 2002, Materials Research Society (www.mrs.org) Symposium Proceedings, Vol. 739, 2003. See also: Sawyer B. Fuller, "Ink jet deposition of inorganic nanoparticle materials as a route to desktop fabrication of integrated logic and micromachinery," Thesis, B.S. Mech. Eng., MIT, June 2000. "Printed Machines," http://www.media.mit.edu/molecular/projects.html.

According to John Canny,[159] head of the "flexonics" team at the University of California at Berkeley: "Flexonics could be called macroscopic MEMS, or polymer mechatronics. Our goal is to design fully-functional appliances and human-interfaces from organic materials, and to build them without assembly using 3-D printing techniques." Team members are developing a vocabulary of passive and active mechanical components including flexure, hinge, and rotary joints. Instead of creating an appliance casing and then laboriously filling it with electronic circuit boards, components and switches, says one report,[160] flexonics will allow printing a complete and fully assembled device by setting down layer upon layer of conducting and semiconducting polymers in such a way that the required circuitry is built up as part of the bodywork (Figure 2-35). "When the technique is perfected, devices such as light bulbs, radios, remote controls, mobile phones and toys will be spat out as individual fully functional systems without expensive and labor-intensive production on an assembly line." The Berkeley team has already worked out how to print electronic components such as transistors, capacitors, inductive coils and other semiconductor components.[161] Says Jeremy Risner,[162] a member of Canny's team: "My background is bioengineering and I'd like to develop models based on living designs...Maybe a rather flat insect with wriggling limbs and some actuators." Risner hopes to develop a fully functional, mechanical and electronic device by the end of 2004, using several printer heads to lay circuits, transistors, capacitors, sensors and casing – all printed by one machine in one run, using a multitude of print heads patterning each material in layers.[163] Thin-film printing of electronic devices is already a reality.[164]

---

[159] John Canny's Home Page; http://www.cs.berkeley.edu/~jfc/. John Canny, Jeremy Risner, Vivek Subramanian, "Flexonics: Printable flexure-based mechatronic devices," WAFR, 15-17 December 2002, Nice, France; http://www.cs.berkeley.edu/~risnerj/wafr2002_presentation6.ppt. See also: D. Huang, F. Liao, S. Molesa, D. Redinger, V. Subramanian, "Plastic-compatible low resistance printable gold nanoparticle conductors for flexible electronics," J. Electrochem. Soc. 150(2003):412-417; http://www-device.eecs.berkeley.edu/~viveks/Papers/412ECS150.pdf.

[160] "Gadget printer promises industrial revolution," New Scientist, 8 January 2003; http://www.newscientist.com/news/news.jsp?id=ns99993238.

[161] "Gadget printer promises industrial revolution," New Scientist, 8 January 2003; http://www.newscientist.com/news/news.jsp?id=ns99993238.

[162] Daithi Ohanluain, "3-D Printing's Great Leap Forward," Wired, 11 August 2003; http://wired.com/news/technology/0,1282,59648,00.html.

[163] Daithi Ohanluain, "3-D Printing's Great Leap Forward," Wired, 11 August 2003; http://wired.com/news/technology/0,1282,59648,00.html.

[164] Rolltronics Inc.; http://www.rolltronics.com.

Figure 2-35. Products printed by the 3-D Gadget Printer[165]

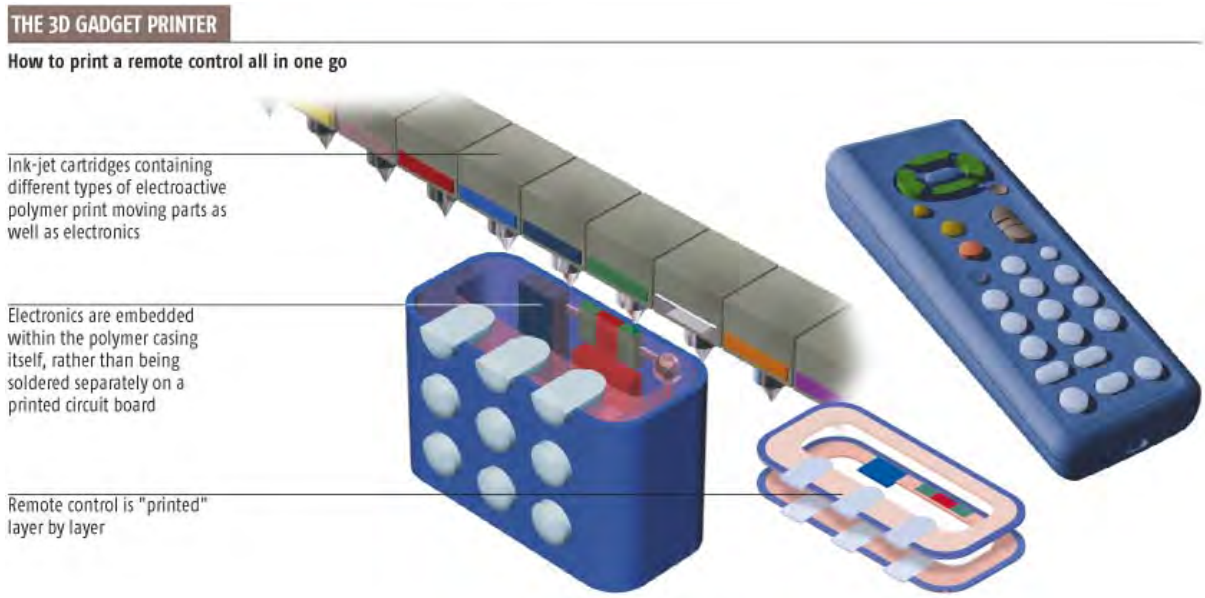

The Thermojet Solid Object Printer[166] manufactured by market leader 3D Systems uses inkjet technology to print solid objects to ~85 micron resolution in X, ~60 microns in Y and ~40 micron resolution in Z (Figure 2-32). According to the product literature, printer volume is 2.57856 m^3 and model build time is ~10^4 sec with a maximum model size of 0.0095 m^3, hence the time to build a printer's volume worth of models is ~2.7 x 10^6 sec, or ~1 month "replication" time for a 499 kg printer. Stratasys is the other market leader in 3D printing systems. According to one observer[167] of these companies: "The projected growth[168] in volume of cheap 3d desktop printers is: (1) sales of hundreds of units in 2008 to a plan of 3500 in 2009; (2) in 2010, a price point of roughly $2,000 and somewhere between 20,000-30,000 units, and (3) in 2011, with a price below $1000 and enter the consumer space. They believe they will sell over a 100,000 units a year and have a business with a quarter of a billion dollars in revenue and a product /consumable margin that's just north of 50%. Consumables will comprise almost 70% of the revenue at that point. We will also have a strong EBITDA margin that's somewhere in the mid 20s. If these targets can be met then perhaps 20% of CAD engineers and hobbyists would own and nearly all would have access to a 3D printer by 2015 and service bureaus (Kinkos) and stores (Walmart, Costco) could

---

[165] "Gadget printer promises industrial revolution," New Scientist, 8 January 2003; http://www.newscientist.com/news/news.jsp?id=ns99993238.

[166] 3D Systems, "Products"; http://www.3dsystems.com.

[167] Brian Wang, "Intermediate systems from now to nanofactories," October 2007; http://advancednano.blogspot.com/2007/10/intermediate-systems-from-now-to.html.

[168] http://www.desktopfactory.com/news/frost_and_sullivan_07_01_07.pdf.

provide access to low and some high end machines. The cost of supplies would need to come down a lot as well from $1 per cubic inch. There would also need to be some common applications for consumers to need to make something frequently using a 3d printer."

The Z406 system built by Z Corporation in cooperation with Hewlett-Packard (prices $20,000-$50,000 as of 2007) offers color inkjet-like 3-D solid printing technology to ~76 micron resolution in Z, with a vertical build speed of 152 microns/minute across a square 203 mm x 254 mm build area, up to a maximum object height of 203 mm.[169] (The product literature gives printer volume as 0.902496 m^3 and model build speed as 1.31 x 10^{-7} m^3/sec, so the build time for a printer volume is 6.9 x 10^6 sec, or ~3 months "replication" time for a 210 kg printer.) Each of the three exterior dimensions of Z Corp.'s smallest solid printer unit, the Z400, are still much larger (740 mm x 910 mm x 1070 mm) than any of the build volume dimensions.[170] Standardization of 3-D descriptive data formats is already under discussion.[171]

Smay, Cesarano and Lewis[172] at the University of Illinois and Sandia Labs use an ink jet printer to deposit colloidal inks carrying tiny particles made of metals, ceramics, plastics, or other materials in a layer-by-layer sequence to directly write desired 3-D patterns with 100 micron features. The robotic deposition or "robocasting" gel must be thick enough to support itself as it spans empty spaces, and must also retain its shape without significant shrinking or sagging as it hardens.

There is already a vast literature[173] on microstereolithography,[174] with applications including microactuators,[175] microbiomedical devices,[176] microelectronics,[177] microelectrophoretics,[178]

---

[169] Z Corporation website; http://www.zcorp.com. See also: Z Corporation Releases Z®406 3D Color Printer," 15 May 2001; http://www.zcorp.com/content/newsroom/print/Z406.html.

[170] Z Corporation website; http://www.zcorp.com. See also: Z Corporation Releases Z®406 3D Color Printer," 15 May 2001; http://www.zcorp.com/content/newsroom/print/Z406.html.

[171] Sara McMains, Jordan Smith, Carlo Sequin, "The evolution of a layered manufacturing interchange format," Proc. 2002 ASME Design Engineering Technical Conferences (DETC02), 29 September 2002, Montreal, Canada, Paper DETC2002/DAC-34136; http://www.me.berkeley.edu/~mcmains/DETC02DAC34136.pdf.

[172] James E. Smay, Joseph Cesarano III, Jennifer A. Lewis, "Colloidal inks for directed assembly of 3-D periodic structures," Langmuir 18(2002):5429-5437; http://colloids.mse.uiuc.edu/research/langmuir_article.pdf. See also: James E. Smay, Jennifer A. Lewis, "Colloidal inks for directed assembly of 3-D periodic structures," Paper SL2, 74th Annual Meeting, The Society of Rheology, October 2002; http://www.rheology.org/sor02a/abstract.asp?PaperID=243.

[173] Vijay K. Varadan, Xiaoning Jiang, Vasundara V. Varadan, Microstereolithography and other Fabrication Techniques for 3-D MEMS, John Wiley & Sons, New York, 2001.

[174] http://dmtwww.epfl.ch/~abertsch/bibliography.html. See also: Charles W. Hull, "Apparatus for production of three-dimensional objects by stereolithography," United States Patent No. 4,575,330, 11 March 1986, http://patft.uspto.gov/netacgi/nph-Parser?Sect1=PTO1&Sect2=HITOFF&d=PALL&p=1&u=/netahtml/srchnum.htm&r=1&f=G&l=50&s1=4,575,330.WKU.&OS=PN/4,575,330; K. Yamaguchi, T. Nakamoto, "Consideration on the optimum conditions to produce micromechanical parts by photo polymerization using direct focused beam writing,"

Proc. 6th Intl. Symp. on Micro Machine and Human Science (MHS'95), 1995, pp. 71-76; T. Nakamoto, K. Yamaguchi, P.A. Abraha, K. Mishima, "Manufacturing of three-dimensional micro-parts by UV laser induced polymerization," J. Micromech. Microeng. 6(1996):240-253; A. Bertsch, S. Zissi, J.Y. Jezequel, S. Corbel, J.C. Andre, "Microstereophotolithography using a liquid crystal display as dynamic mask-generator," Micro. Tech. 3(1997):42-47; M. Cabrera, A. Bertsch, J. Chassaing, J.Y. Jezequel, J.C. Andre, "Microfabrication of very small objects: pushing the limits of stereophotolithography," Mol. Cryst. Liq. Cryst. 315(1998):223-234; C. Ecoffet, A. Espanet, D.J. Lougnot, "Photopolymerization by evanescent waves: a new method to obtain nanoparts," Adv. Mater. 10(1998):411-414; K. Ikuta, S. Maruo, S. Kojima, "New micro stereo lithography for freely movable 3-D micro structure – Super IH Process with submicron resolution," Proc. 11th IEEE Workshop on Micro Electro Mechanical Systems (MEMS'98), 1998, pp. 290-295; S. Maruo, S. Kawata, "Two-photon-absorbed near-infrared photopolymerization for three-dimensional microfabrication," J. Microelectromechanical Syst. 7(1998):411-415; D. Pede, G. Serra, D. De Rossi, "Microfabrication of conducting polymer devices by ink-jet stereolithography," Mater. Sci. Eng. C 5(1998):289-291; X. Zhang, X.N. Jiang, C. Sun, "Micro-stereolithography for MEMS," Micro Electro Mechanical Systems (MEMS) ASME 66(1998):3-9; C.R. Chatwin, M. Farsari, S. Huang, M.I. Heywood, R.C.D. Young, P.M. Birch, F. Clarte-Tournier, J.D. Richardson, "Characterization of epoxy resins for microstereolithographic rapid prototyping," Int. J. Adv. Manuf. Technol. 15(1999):281-286; S. Maruo, K. Ikuta, "Movable microstructures made by two-photon three dimensional microfabrication," Proc. Intl. Symp. on Micromechatronics and Human Science (MHS'99), 1999, pp. 173-178; J.S. Young, S.R. Fox, K.S. Anseth, "A novel device for producing three-dimensional objects," J. Manufacturing Sci. and Eng. – Transactions of the ASME 121(1999):474-477; X. Zhang, X. Jiang, C. Sun, "Micro-stereolithography of polymeric and ceramic microstructures," Sensors and Actuators A 77(1999):149-156; A. Bertsch, P. Bernhard, C. Vogt, P. Renaud, "Rapid prototyping of small size objects," Rapid Prototyping Journal 6(2000):259-266; M. Farsari, F. Clarte-Tournier, S. Huang, C.R. Chatwin, D. Budgett, P.M. Birch, R.C.D. Young, J.D. Richardson, "A novel high-accuracy microstereolithography method employing an adaptive electro-optic mask," J. Mater. Process. Technol. 107(2000):167-172; P. Galajda, O. Pal, "Complex micromachines produced and driven by light," Appl. Phys. Lett. 78(2001):249-251; S. Monneret, C. Provin, H. Le Gall, "Micro-scale rapid prototyping by stereolithography," Proc. 8th IEEE Intl. Conf. on Emerging Technologies and Factory Automation (ETFA 2001) 2(2001):299-304; C. Provin, S. Monneret, "Complex ceramic-polymer composite microparts made by microstereolithography," Proc. Design, Test, Integration and Packaging of MEMS/MOEMS Conf., SPIE 4408(2001):535-542; S. Maruo, K. Ikuta, "Submicron stereolithography for the production of freely movable mechanisms by using single-photon polymerization," Sensors and Actuators A 100(2002):70-76; C. Sun, X. Zhang, "Experimental and numerical investigations on microstereolithography of ceramics," J. Appl. Phys. 92(2002):4796-4802; Dongmin Wu, Nicholas Fang, Cheng Sun, Xiang Zhang, "Adhesion force of polymeric three-dimensional microstructures fabricated by microstereolithography," Appl. Phys. Lett. 81(2002):3963-3965; A. Bertsch, S. Jiguet, P. Bernhard, P. Renaud, "Microstereolithography: a review," Mat. Res. Soc. Symp. Proc. 739(2003):LL1.1.1-LL1.1.11; S. Maruo, K. Ikuta, H. Korogi, "Submicron manipulation tools driven by light in a liquid," Appl. Phys. Lett. 82(2003):133-135; S. Maruo, K. Ikuta, H. Korogi, "Optically driven micromanipulation tools fabricated by two-photon microstereolithography," Mat. Res. Soc. Symp. Proc. 739(2003):H9.4.1-H9.4.6.

[175] A. Bertsch, S. Zissi, M. Calin, S. Ballandras, A. Bourjault, D. Hauden, J.C. Andre, "Conception and realization of miniaturized actuators fabricated by microstereophotolithography and actuated by shape memory alloys," Proc. 3rd France-Japan Congress and 1st Europe-Asia Congress on Mechatronics 2(1996):631-634. S. Ballandras, M. Calin, S. Zissi, A. Bertsch, J.C. Andre, D. Hauden, "Microstereophotolithography and shape memory alloy for the fabrication of miniaturized actuators," Sensors and Actuators A 62(1997):741-747.

[176] K. Ikuta, "Biomedical micro device fabricated by micro stereo lithography (IH process) 'Metabiotic Device' – a synthetic approach for life science," Proc. 6th Intl. Symp. on Micro Machine and Human

microfluidics,[179] microoptics,[180] micropumps,[181] and microrobots,[182] and electrodeposition microfabrication or EFAB™ is well-known.[183] Gas phase SFF (Solid Freeform Fabrication) has also been investigated[184] – laser beams passing through acetylene gas produce solid carbon

---

Science (MHS'95), 1995, pp. 71-76. K. Ikuta, Y. Sasaki, H. Maegawa, S. Maruo, T. Hasegawa, "Micro ultrasonic homogenizer chip made by hybrid microstereolithography," Proc. Micro Total Analysis Systems Conference (MicroTAS'02) 2(2002):745-747.

[177] T.S. Ji, K.J. Vinoy, V.K. Varadan, "Distributed MEMS phase shifters by microstereolithography on silicon substrates for microwave and millimeter wave applications," Smart Materials and Structures 10(2001):1224-1229.

[178] Y. Mizukami, D. Rajniak, M. Nishimura, "An integrated micro-electrophoretic chip fabricated using a new stereolithographic process," Proc. 13th IEEE Intl. Conf. on Micro Electro Mechanical Systems (MEMS 2000), 2000, pp. 751-756.

[179] J. Cooper McDonald, M.L. Chabinyc, S.J. Metallo, J.R. Anderson, G.M. Whitesides, "Prototyping of microfluidic devices in poly(dimethylsiloxane) using solid-object printing," Anal. Chem. 74(2002):1537-1545. Daniel Therriault, Scott R. White, Jennifer A. Lewis, "Chaotic mixing in three-dimensional microvascular networks fabricated by direct-write assembly," Nat. Mater. 2(April 2003):265-271, Nat. Mater. 2(May 2003):347 (erratum); http://www.nature.com/cgi-taf/DynaPage.taf?file=/nmat/journal/v2/n4/abs/nmat863.html (abstract). See also: James E. Kloeppel, "Fabricated microvascular networks could create compact fluidic factories," News Bureau, University of Illinois at Urbana-Champaign, 24 March 2003; http://www.news.uiuc.edu/scitips/03/0324microvascular.html.

[180] S. Maruo, K. Ikuta, T. Ninagawa, "Multi-polymer microstereolithography for hybrid opto-MEMS," Proc. 14th IEEE Intl. Conf. on Micro Electro Mechanical Systems (MEMS 2001), 2001, pp. 151-154.

[181] M.C. Carrozza, N. Croce, B. Magnani, P. Dario, "A piezoelectric-driven stereolithography-fabricated micropump," J. Micromech. Microeng. 5(1995):177-179. D. Accoto, M.C. Carrozza, P. Dario, "Modelling of micropumps using unimorph piezoelectric actuators and ball valves," J. Micromech. Microeng. 10(2000):277-281. V.K. Varadan, V.V. Varadan, "Micro pump and venous valve by micro stereo lithography," Proc. SPIE Smart Structures and Materials 2000: Smart Electronics and MEMS 3990(2000):246-254.

[182] M. Calin, A. Bertsch, N. Chaillet, S. Zissi, S. Ballandras, J. C. Andre, A. Bourjault, D. Hauden, "Microrobots realized by microstereophotolithography and actuated by shape memory alloys," Proc. 1997 IEEE/RSJ International Conference on Intelligent Robot and Systems 3(1997):V33-V34.

[183] John D. Madden, Ian W. Hunter, "3-D Micro-fabrication by localized electrochemical deposition," J. Microelectromechanical Systems 5(January-March 1996):24-32; Ian W. Hunter, Serge R. Lafontaine, John D. Madden, "Three dimensional microfabrication by localized electrodeposition and etching," United States Patent No. 5,641,391, 24 June 1997. "EFAB™: Rapid Batch Manufacturing of True 3-D Micro-Devices," MEMGen Corp., http://www.isi.edu/efab/; "Technology: Imagine Manufacturing Micromachines Directly From CAD In Days, Not Months," MEMGen Corp., http://www.memgen.com/technology/index.htm. "MicroFab: Microfabrication through Electrodeposition," 12 October 1998; http://www.thefirst.org/jefft/microfab/index.html.

[184] Arlan Keith Andrews, "Manufacturing magic," Analog 112(September 1992):60-72. Guishing Zong, "Solid freeform fabrication using gas phase selective area laser deposition," Ph.D. Dissertation, University of Texas at Austin, August 1991. F. Wallenberger, P. Nordine, M. Boman, "Inorganic fibers and

rods.[185] In this manner Westberg et al.[186] have fabricated a 3-turn boron spring 2 mm high and 200 μm wide; Maxwell et al.[187] have formed micro-solenoids and micro-springs from C, W, and TiC fibers as small as 5 μm with horizontal deposition rates >12 cm/sec for high-pressure (11 atm) deposition; and layered microwall[188] and ~300-μm diameter column[189] structures have also been manufactured. (See also Section 2.2.3.3.)

Progress is being made in solid printing at even smaller size scales.[190] For example, in 2001 Satoshi Katawa and colleagues at Osaka University[191] used two-photon micropolymerization in

---

microstructures directly from the vapor phase," Composites Sci. and Technol. 51(1994):193-212; F. Wallenberger, "Inorganic fibers and microfabricated parts by laser assisted chemical vapor deposition (LCVD): Structures and properties," Ceramics Intl. 23(1997):119-126.

[185] L. Nelson, N. Richardson, "Formation of thin rods of pyrolytic carbon by heating with a focused carbon dioxide laser," Materials Res. Bull. 7(1972):971-976.

[186] H. Westberg, M. Boman, S. Johansson, J. Schweitz, "Truly three dimensional structures microfabricated by laser chemical processing," IEEE, May 1991, pp. 516-519; S. Johansson, J. Schweitz, H. Westberg, M. Boman, "Microfabrication of three-dimensional boron structures by laser chemical processing," J. Appl. Phys. 72(15 December 1992):5956-5963.

[187] J. Maxwell, K. Larsson, M. Boman, P. Hooge, K. Williams, P. Coane, "Rapid prototyping of functional three-dimensional microsolenoids and electromagnets by high-pressure laser chemical vapor deposition," Solid Freeform Fabrication, August 1998, pp. 529-536; J. Maxwell, M. Boman, K. Williams, K. Larsson, N. Jaikumar, G. Saiprasanna, "High-speed laser chemical vapor deposition of amorphous carbon fibers, stacked conductive coils, and folded helical springs," SPIE Conf. on Micromachining and Microfabrication Process Technology V, Santa Clara, CA, September 1999, SPIE, Vol. 3874, pp. 227-235; K. Williams, J. Maxwell, K. Larsson, M. Boman, "Freeform fabrication of functional microsolenoids, electromagnets and helical springs using high-pressure laser chemical vapor deposition," IEEE, 1999, pp. 232-237.

[188] D. Messia, J. Pegna, W.H. Lee, "Layered micro-wall structures from gas phase," Proc. Solid Freeform Fabrication Symposium, August 1997, pp. 231-240.

[189] Chad E. Duty, Daniel L. Jean, W. Jack Lackey, "Laser CVD rapid prototyping," Proc. Amer. Ceramic Soc. Meeting, Cocoa Beach, FL, January 1999, pp. 347-354; Daniel L. Jean, Chad E. Duty, Brian T. Fuhrman, W. Jack Lackey, "Precision LCVD system design with real time process control," Proc. Solid Freeform Fabrication Symposium, Austin, TX, August 1999, pp. 59-65; Daniel L. Jean, Chad E. Duty, Brian T. Fuhrman, W. Jack Lackey, "Precision carbon deposition using pyrolytic laser chemical vapor deposition (LCVD)," http://www.me.gatech.edu/Lackey/djsff2000.pdf.

[190] S. Kawata, H.-B. Sun, T. Tanaka, K. Takada, "Finer features for functional microdevices," Nature 412(2001):697-698; W.C. Wilson Jr., T. Boland, "Cell and organ printing 1: Protein and cell printers," Anat. Rec. 272A(June 2003):491-496; T. Boland, V. Mironov, A. Gutowska, E.A. Roth, R.R. Markwald, "Cell and organ printing 2: Fusion of cell aggregates in three-dimensional gels," Anat. Rec. 272A(June 2003):497-502; Vladimir Mironov, Thomas Boland, T. Trusk, G. Forgacs, R.R. Markwald, "Organ printing: computer-aided jet-based 3-D tissue engineering," Trends Biotechnol. 21(April 2003):157-161; Charles Choi, "Ink-jet printing creates tubes of living tissue," New Scientist, 22 January 2003, http://www.newscientist.com/news/print.jsp?id=ns99993292; L.R. Bao, X. Cheng, X.D. Huang, L.J. Guo, S.W. Pang, A.F. Yee, "Nanoimprinting over topography and multilayer three-dimensional printing," J. Vac. Sci. Technol. B 20(2003):2881.

resin to create a 2 micron x 10 micron 3-D sculpture of a bull (Figure 2-36) to a voxel resolution of 120 nm. In the single-beam geometry, a single high numerical aperture objective lens is used to tightly focus the laser light so that two-photon processes are confined to the focal volume – the two-photon absorption cross-section for known materials is quite small, so that the light intensity outside the focal volume is insufficient to launch these reactions, permitting 3-D resolution in a single-beam laser scanning system. The researchers chose the shape of a bull because it has "a very sophisticated 3-D shape with sharp tips and a smooth and rough body," noted Hong-Bo Sun, a team member who says that the same technique might also be used to manufacture microscopic sensors and 3-D computer memories.[192] Marder and Perry[193] at Georgia Tech, also using two-photon 3-D lithography with a two-photon resist, have made 3-D structures of silver, gold, and copper metal as small as 0.170 micron wide and 0.500 micron long, with linear writing speeds up to 100 cm/sec. They believe their process can produce feature sizes as small as 100 nm.

Figure 2-36. A 3-D resin-sculpted bull the size of a red blood cell (2 μm scale bars; photo from S. Kawata et al.[194] and Osaka University)

---

[191] S. Kawata, H.-B. Sun, T. Tanaka, K. Takada, "Finer features for functional microdevices," Nature 412(2001):697-698; W.C. Wilson Jr., T. Boland, "Cell and organ printing 1: Protein and cell printers," Anat. Rec. 272A(June 2003):491-496; T. Boland, V. Mironov, A. Gutowska, E.A. Roth, R.R. Markwald, "Cell and organ printing 2: Fusion of cell aggregates in three-dimensional gels," Anat. Rec. 272A(June 2003):497-502; Vladimir Mironov, Thomas Boland, T. Trusk, G. Forgacs, R.R. Markwald, "Organ printing: computer-aided jet-based 3-D tissue engineering," Trends Biotechnol. 21(April 2003):157-161; Charles Choi, "Ink-jet printing creates tubes of living tissue," New Scientist, 22 January 2003, http://www.newscientist.com/news/print.jsp?id=ns99993292; L.R. Bao, X. Cheng, X.D. Huang, L.J. Guo, S.W. Pang, A.F. Yee, "Nanoimprinting over topography and multilayer three-dimensional printing," J. Vac. Sci. Technol. B 20(2003):2881.

[192] John Whitfield, "Bull wins size prize," Nature Science Update, 16 August 2001; http://www.nature.com/nsu/010816/010816-16.html.

[193] Seth R. Marder, Joseph W. Perry, "Two-photon materials chemistry," 11th Foresight Conference on Molecular Nanotechnology, October 2003; http://www.foresight.org/Conferences/MNT11/Abstracts/Marder/index.html. See also: Focal Point Microsystems LLC.

[194] S. Kawata, H.-B. Sun, T. Tanaka, K. Takada, "Finer features for functional microdevices," Nature 412(2001):697-698.

The successful rapid prototyping of an atomic force microscope (AFM) head was first reported[195] in 2007. The heads perform as well as traditional heads but are not as durable. According to one press report:[196] "The essential part of an AFM is a microscale cantilever with a sharp tip (probe) at its end that is used to scan the specimen surface. The cantilever is typically silicon or silicon nitride with a tip radius of curvature on the order of nanometers. When the tip is brought into proximity of a sample surface, forces between the tip and the sample lead to a deflection of the cantilever according to Hooke's law. A multi-segment photodiode measures the deflection via a laser beam, which is reflected on the cantilever surface. Selective Laser Sintering (SLS – a registered trademark of 3D Systems, Inc.) is an additive rapid manufacturing technique that uses a high powered laser to fuse small particles of plastic, metal, or ceramic powders into a mass representing a desired 3-dimensional object. The laser selectively fuses powdered material by scanning cross-sections generated from a 3-D digital description of the part (e.g. from a CAD file or scan data) on the surface of a powder bed. After each cross-section is scanned, the powder bed is lowered by one layer thickness, a new layer of material is applied on top, and the process is repeated until the part is completed. 'To evaluate the performance of a rapid prototyped AFM, we reprinted one of our aluminum AFM heads with the SLS method in plastic,' Robert Lugmaier, a co-author of the paper,[197] explains. 'To compare the noise and drift values of these AFM heads under equal conditions, the same optical and electrical components were used. The laser diode, the piezoactuator, and the photodetector were identical for the plastic printed as well as the aluminum milled AFM.' "

Many other approaches have been tried. Riehn et al.[198] used near-field optical lithography (a scanning near-field optical microscope (NSOM/SNOM) with a UV laser) to fabricate functional 2-D patterns with 160-nm feature sizes from the conjugated polymer poly(p-phenylene vinylene). Stuke's group[199] has generated 3-D microstructures by rapid laser prototyping, and 3-D

---

[195] Ferdinand Kühner, Robert A. Lugmaier, Steffen Mihatsch, Hermann E. Gaub, "Print your atomic force microscope," Rev. Sci. Instrum. 78(2007):075105, http://dx.doi.org/doi:10.1063/1.2751099. See also: " How to build a Plastic-AFM head," accessed April 2008, http://www.biophysik.physik.uni-muenchen.de/PlasticAFM/.

[196] "Print your atomic force microscope," Nanowerk, 1 August 2007, http://www.nanowerk.com/spotlight/spotid=2304.php; "Make your own plastic-AFM heads and save tens of thousands of dollars," 1 August 2007, http://nextbigfuture.com/2007/08/make-your-own-plastic-afm-heads-and.html.

[197] Ferdinand Kühner, Robert A. Lugmaier, Steffen Mihatsch, Hermann E. Gaub, "Print your atomic force microscope," Rev. Sci. Instrum. 78(2007):075105, http://dx.doi.org/doi:10.1063/1.2751099. See also: " How to build a Plastic-AFM head," accessed April 2008, http://www.biophysik.physik.uni-muenchen.de/PlasticAFM/.

[198] Robert Riehn, Ana Charas, Jorge Morgado, F. Cacialli, "Near-field optical lithography of a conjugated polymer," Appl. Phys. Lett. 82(27 January 2003):526-528; http://www.aidic.it/op2003/opwebpapers/9%20Riehn.pdf. See also: "Nano rapid prototyping advances," TRNmag.com, 18/25 June 2003; http://www.trnmag.com/Stories/2003/061803/Nano_rapid_prototyping_advances_Brief_061803.html.

[199] O. Lehmann, M. Stuke, "Laser-driven movement of three-dimensional microstructures generated by laser rapid prototyping," Science 270(1995):1644-1646; T. Gotz, M. Stuke, "Short pulse UV laser ablation of solid and liquid metals," Appl. Phys. A64(1997):539-543; M.C. Wanke, O. Lehmann, K. Muller, Q.

nanostructure fabrication via focused-ion-beam CVD is described in Section 2.2.3.3. Wilson, Boland, and Mironov et al.[200] have printed 3-D tubes of living tissue using modified desktop printers filled with suspensions of micron-sized cells instead of ink – a first step towards printing protein patterns, complex tissues, or even entire organs. Similarly, Vaidyanathan and Mulligan[201] are solid-printing resorbable implantable bone scaffolds for surgeons, as is the company Therics.[202] Sciperio Inc.[203] is developing a "direct-write tissue deposition apparatus" for the "creation of engineered tissues, or neo-organs" composed of "vascularized 3-D tissue scaffolds and living cells." Mirkin's group[204] has created dip-pen nanolithography arrays that can write 2-D nanoscopic patterns layer by layer on surfaces – a minimum linewidth of 60 nm has been demonstrated using an eight-pen microfabricated probe array. Proteins can be printed with an AFM-based "nanofountainpen".[205] Alexandridis and Docoslis[206] have used electrophoresis to stack latex, silica or graphite microparticles into 3-D structures of prescribed size and

---

Wen, M. Stuke, "Laser rapid prototyping of photonic band-gap microstructures," Science 275(1997):1284-1286.

[200] S. Kawata, H.-B. Sun, T. Tanaka, K. Takada, "Finer features for functional microdevices," Nature 412(2001):697-698; W.C. Wilson Jr., T. Boland, "Cell and organ printing 1: Protein and cell printers," Anat. Rec. 272A(June 2003):491-496; T. Boland, V. Mironov, A. Gutowska, E.A. Roth, R.R. Markwald, "Cell and organ printing 2: Fusion of cell aggregates in three-dimensional gels," Anat. Rec. 272A(June 2003):497-502; Vladimir Mironov, Thomas Boland, T. Trusk, G. Forgacs, R.R. Markwald, "Organ printing: computer-aided jet-based 3-D tissue engineering," Trends Biotechnol. 21(April 2003):157-161; Charles Choi, "Ink-jet printing creates tubes of living tissue," New Scientist, 22 January 2003, http://www.newscientist.com/news/print.jsp?id=ns99993292; L.R. Bao, X. Cheng, X.D. Huang, L.J. Guo, S.W. Pang, A.F. Yee, "Nanoimprinting over topography and multilayer three-dimensional printing," J. Vac. Sci. Technol. B 20(2003):2881.

[201] Duncan Graham-Rowe, "Bad breaks fixed fast by bone 'printer'," NewScientist.com, 20 June 2003, http://www.newscientist.com/news/news.jsp?id=ns99993844; "The Plasti-Bone: A Ceramic Polymer Innovation In Medicine," Office of Naval Research (ONR) Media, 13 June 2003, http://www.onr.navy.mil/media/print_tipoff_display.asp?ID=43 or http://www.sciencedaily.com/releases/2003/06/030616090308.htm.

[202] Therics, Inc.; http://www.therics.com.

[203] Sciperio Inc., "Human Architectural Tool (HAT) Capabilities," 2003; http://www.sciperio.com/bio/hat.html.

[204] Ming Zhang, David Bullen, Sung-Wook Chung, Seunghun Hong, Kee S. Ryu, Zhifang Fan, Chad A. Mirkin, Chang Liu, "A MEMS nanoplotter with high-density parallel dip-pen nanolithography probe arrays," Nanotechnology 13(April 2002):212-217; http://mass.micro.uiuc.edu/publications/papers/72.pdf.

[205] Hesham Taha, Robert S. Marks, Levi A. Gheber, Ittay Rousso, John Newman, Chaim Sukenik, Aaron Lewis, "Protein printing with an atomic force sensing nanofountainpen," Appl. Phys. Lett. 83(2003):1041.

[206] Aristides Docoslis, Paschalis Alexandridis, "One-, two-, and three-dimensional organization of colloidal particles using non-uniform AC electric fields" Electrophoresis 23(2002):2174-2183. See also: John Della Contrada, "UB Engineer Develops Novel Method for Assembly of Nanoparticles. Process may lead to manufacture of nanoscale devices," University at Buffalo, The State University of New York, 21 November 2002; http://www.buffalo.edu/news/fast-execute.cgi/article-page.html?article=59620009.

composition, held together by the electrical field, and it is claimed that the same process could be applied to nanoparticles. Saul Griffith[207] in Jacobson's group has described tabletop "personal fabricators" and several tools for the rapid prototyping of micron-scale feature-sized devices for the manufacture of printed microelectromechanical systems (PEMS). This would include laser-based stereolithography using a rapidly (up to ~4 KHz) switched micromirror array to achieve highly parallel operation.[208] Says Neil Gershenfeld,[209] head of the MIT Center for Bits and Atoms: "We're approaching being able to make one machine that can make any machine. I have a student working on this project who can graduate when his thesis walks out of the printer, meaning that he can output the document along with the functionality for it to get up and walk away."

Lipson and Pollack say that while they are contemplating the conditions necessary for full electromechanical self-replication, this is not a primary goal of their research: "Self-replication is very easy in software and cellular automata. What is harder is to find the 'bootstrap.' Just as a forge, a mill, and a lathe lead to more mills and lathes, and ultimately to the industrial revolution, and just as understanding stored program computers and digital communications lead to all of modern computer science and the internet, our set of robotic technologies could someday lead to a self-sustaining 'bootstrap' and to more complex robotically-designed and robotically-constructed robots." Adds Rodney Brooks,[210] director of the Computer Science and Artificial Intelligence Laboratory at the Massachusetts Institute of Technology, on the Lipson-Pollack work: "This is a long-awaited and necessary step towards the ultimate dream of self-reproducing machines."

2.2.3.2 RepRap, Fab@Home and Related Projects

The purpose of the RepRap (short for "Replicating Rapid-prototyper") project is to create a practical self-copying 3D printer – a macroscale device that can replicate itself under external control. The device is not atomically precise and it is unclear if the existing design could be scaled down to the nanoscale or even to the microscale, but the work is instructive and inspire

---

[207] Saul Griffith, "Towards Personal Fabricators: Tabletop tools for micron and sub-micron scale functional rapid prototyping," Master's Thesis in Media Arts and Science, Massachusetts Institute of Technology, February 2001, 81pp; http://web.media.mit.edu/~saul/mlmasters/sm_masters.pdf. See also: "Presentation and perspectives on personal fabrication," http://web.media.mit.edu/~saul/pf/pf.ppt.

[208] Saul Griffith, "Towards Personal Fabricators: Tabletop tools for micron and sub-micron scale functional rapid prototyping," Master's Thesis in Media Arts and Science, Massachusetts Institute of Technology, February 2001, 81pp; http://web.media.mit.edu/~saul/mlmasters/sm_masters.pdf. See also: "Presentation and perspectives on personal fabrication," http://web.media.mit.edu/~saul/pf/pf.ppt.

[209] "Personal Fabrication: A Talk with Neil Gershenfeld," Edge 123, 24 July 2003; http://www.edge.org/documents/archive/edge123.html or http://www.kurzweilai.net/meme/frame.html?main=/articles/art0601.html.

[210] "Robot learns to reproduce," BBC News, 30 August 2000; http://news.bbc.co.uk/1/hi/sci/tech/903238.stm.

useful thinking about the process of replicative manufacturing. A prototype version of RepRap[211] is shown in Figure 2-37A. Ian Adkins' RepStrap machine[212] is shown in Figure 2-37B, which is virtually identical to RepRap except that all the blue parts are molded resin and not rapid-prototyped. (Ian will shortly be selling all these parts both from his own website and via the RepRap Research Foundation's online store.[213])

Figure 2-37. (A) A prototype RepRap macroscale fabbing machine;[214] (B) a prototype RepStrap machine,[215] which is virtually identical to RepRap except that all the blue parts are moulded resin and not rapid-prototyped.

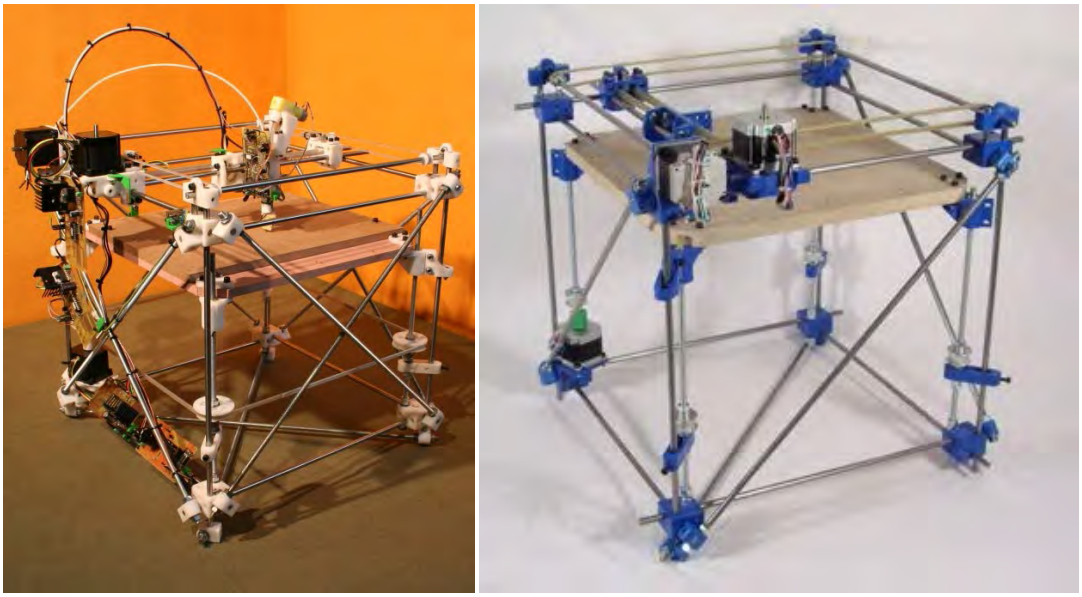

(A) (B)

According to the RepRap website,[216] "the RepRap project became widely known after a large press coverage in March 2005, though the idea goes back to a paper on the web written by [RepRap project leader] Adrian Bowyer.[217] RepRap will make plastic, ceramic, or metal parts, and is itself made from plastic parts, so it will be able to make copies of itself. It is a three-axis robot that moves several material extruders. These extruders produce fine filaments of their

---

[211] http://reprap.org/bin/view/Main/RepRap.
[212] http://builders.reprap.org/2007/11/mould-parts-arrived-at-last.html.
[213] http://parts.rrrf.org/.
[214] http://reprap.org/bin/view/Main/RepRap.
[215] http://builders.reprap.org/2007/11/mould-parts-arrived-at-last.html.

[216] http://reprap.org/.

[217] Adrian Bowyer, 2 February 2004; http://reprap.org/bin/view/Main/BackgroundPage.

working material with a paste-like consistency. If RepRap were making a plastic cone, it would use its plastic extruder to lay down a quickly-hardening filament of molten plastic, drawing a filled-in disc. It would then raise the plastic extrusion head and draw the next layer (a smaller filled disc) on top of the first, repeating the process until it completed the cone. To make an inverted cone it would also lay down a support material under the overhanging parts. The support would be removed when the cone was complete. Conductors can be intermixed with the plastic to form electronic circuits – in 3D even!

"This process is called fused deposition modeling;[218] machines that do this are called 3D printers, rapid prototypers, or fabbers. They are very useful. Unfortunately they are also very expensive – €20,000 or more – and existing models don't self-replicate. The RepRap build cost will be less than €400 for the bought-in materials, all of which have been selected to be as widely available everywhere in the world as possible. Also, the RepRap software will work on all computer platforms for free. Complete open-source instructions and plans are published on this website for zero cost and available to everyone so, if you want to make one yourself, you can. We hope to announce self-replication in 2008, though the machine can be built now – see the 'How-to-build-a-RepRap' link[219]." The project continues to receive positive press.[220]

Another well-known related effort is the Fab@Home project,[221] which has been described as "an open-source 3D printer based on a syringe-squeezing mechanism and pre-cut acrylic sheet panels" (Figure 2-38). This fabber has a single-tip manipulator with three degrees of freedom (DOF), and can move in 15.8 micron steps at a top speed of 25 mm/sec and can apply a maximum force of 120 N at the tip.[222] The positioning resolution of the machine is ~25 microns, but the repeatable accuracy in a typical setup is estimated as ~100 microns.[223] The build volume of the machine – the maximum product size – is an 8-inch cube.[224] It can use a variety of materials, including edibles such as chocolate[225] and table sugar.[226]

---

[218] http://en.wikipedia.org/wiki/Fusion_deposition_modelling.

[219] "How to Build a RepRap," http://reprap.org/bin/view/Main/RepRapOneDarwin.

[220] Ulrika Hedquist, "Open source 3D printer copies itself. Self-replicating printer frees-up 3D printing under GNU," Computerworld, 11 April 2008, http://computerworld.co.nz/news.nsf/tech/2F5C3C5D68A380EDCC257423006E71CD.

[221] "Fab@Home" Wiki homepage, accessed February 2008; http://www.fabathome.org/wiki/index.php?title=Main_Page.

[222] "Fab@Home:Model 1 Overview," accessed February 2008; http://www.fabathome.org/wiki/index.php?title=Fab%40Home:Model_1_Overview.

[223] "Fab@Home:Support," accessed February 2008; http://www.fabathome.org/wiki/index.php?title=Fab%40Home:Support.

[224] "Fab@Home:Support," accessed February 2008; http://www.fabathome.org/wiki/index.php?title=Fab%40Home:Support.

[225] http://www.fabathome.org/wiki/index.php?title=Materials:Chocolate.
[226] http://www.evilmadscientist.com/article.php/candyfab.

Figure 2-38. A Fab@Home fabber.[227] The Fab@Home Model 1 is a 3-axis Cartesian gantry positioning system driven by stepper motors attached to lead screws in a linear stepper motor configuration, with material deposition accomplished using a syringe-based extrusion tool.[228]

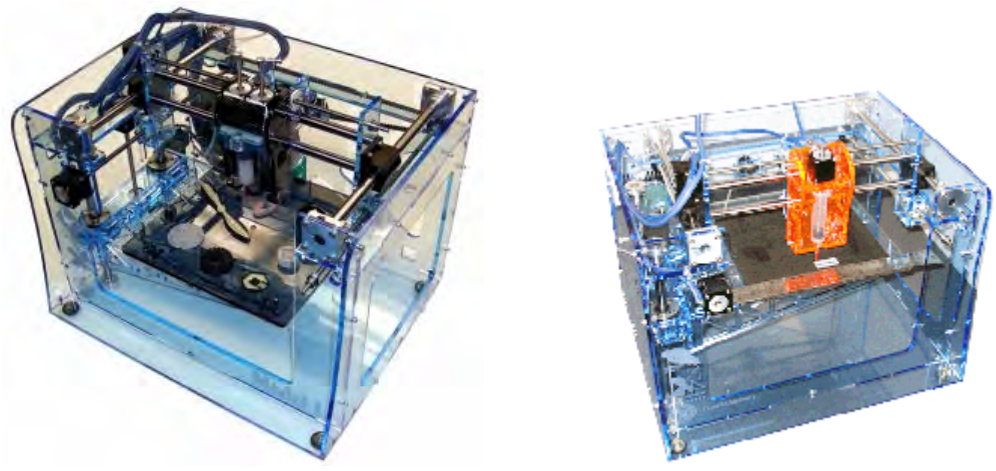

According to the project website: "Fab@Home is a project dedicated to making and using fabbers – machines that can make almost anything, right on your desktop. This website provides everything you need to know to build or buy your own simple fabber, and to use it to print three dimensional objects. The hardware designs and software on this website are free and open-source. Once you have your own fabber, you can also download and print various items, try out new materials, or upload and share your own projects. Advanced users can modify and improve the fabber itself. Fabbers[229] (aka. 3D Printers or rapid prototyping machines) are a relatively new form of manufacturing that builds 3D objects by carefully depositing materials drop by drop, layer by layer. With the right set of materials and a geometric blueprint, you can fabricate complex objects that would normally take special resources, tools and skills if produced using conventional manufacturing techniques. A fabber can allow you to explore new designs, email physical objects to other fabber owners, and most importantly – set your ideas free. Just as MP3s, iPods and the Internet have freed musical talent, we hope that blueprints and fabbers will democratize innovation. Commercial 3D Printers today are limited to one material at a time, and their proprietary technologies limits experimentation. Moreover, their price range – tens of thousands, to hundreds of thousands of dollars – is typically well beyond what an average home user can afford. Our goal with this open-source, multi-material printing is to explore the potential

---

[227] "Fab@Home" Wiki homepage, accessed February 2008; http://www.fabathome.org/wiki/index.php?title=Main_Page.

[228] "Fab@Home:Model 1 Overview," accessed February 2008; http://www.fabathome.org/wiki/index.php?title=Fab%40Home:Model_1_Overview.

[229] "fabbers.com -- Your Digital Fabrication Portal," accessed February 2008; http://www.ennex.com/%7Efabbers/.

of universal fabrication: Machines that can use multiple materials to fabricate complete, active systems."

Fab@Home and RepRap are very similar but have two main differences:[230] (1) RepRap is oriented toward self-replication (trying to make a machine that can make many of its own parts), while Fab@Home attempts only to produce a range of interesting products that will induce more widespread use of fabbers; (2) RepRap has a screw extrusion deposition tool designed for use with polycaprolactone plastic as the intended building material, while Fab@Home uses a syringe tool that allows using a wider variety of materials.

There is growing academic and commercial interest in desktop manufacturing.[231] For example, Fearing et al.[232] at UC Berkeley "plan to build a self-contained desktop rapid prototyping system" combining folding, bonding, and microassembling operations on 100-micron-scale parts to make a fully-automatic, desktop assembly process for millirobots, as part of their laboratory's NSF-supported Desktop Rapid Prototyping Millirobots project[233] and their interest in automated microassembly[234] – though oriented to "minimal bootstrapping for millirobot desktop factories, rather than self-replicating".[235] The Agile Assembly project at Carnegie Mellon University[236] is developing an "agile assembly architecture" applied specifically to tabletop-sized factories or "minifactories" for microassembly including modular elements such as high-precision platens, bridges for mounting modular robotic elements, precision 2-DOF manipulators, 2-DOF couriers,

---

[230] "Fab@Home:Support," accessed February 2008; http://www.fabathome.org/wiki/index.php?title=Fab%40Home:Support.

[231] Tom Shelley, "Manufacturing base keeps on shrinking," 12/06/2007; http://www.eurekamagazine.co.uk/article/9914/Manufacturing-base-keeps-on-shrinking.aspx.

[232] E. Shimada, J.A. Thompson, J. Yan, R.J. Wood, R.S. Fearing, "Prototyping millirobots using dexterous microassembly and folding," Symposium on Microrobotics, ASME Int. Mechanical Engineering Cong. and Exp., Orlando, FL, 5-10 November 2000, DSC-Vol. 69-2, pp. 933-940, http://robotics.eecs.berkeley.edu/~ronf/PAPERS/mumanip.pdf; Ranjana Sahai, Jusuk Lee, Ron Fearing, "Towards automatic assembly of sub-centimeter millirobot structures," Third Intl. Workshop on Microfactories, Minneapolis, MN, 16-18 September 2002, http://robotics.eecs.berkeley.edu/~ronf/PAPERS/autoassemblyv8.pdf.

[233] Ron Fearing, "Desktop Rapid Prototyping Millirobots," http://robotics.eecs.berkeley.edu/~ronf/desktop.html.

[234] J.A. Thompson, R.S. Fearing, "Automating microassembly with ortho-tweezers and force sensing," in IEEE/RSJ Intl. Conf. on Intelligent Robots and Systems (IROS), Maui, HI, 2001.

[235] Ron Fearing, personal communication to Robert A. Freitas Jr., 5 August 2003.

[236] "An Architecture for Agile Assembly," Microdynamic Systems Laboratory, Carnegie Mellon University, August 8, 2002; http://www-2.cs.cmu.edu/afs/cs/project/msl/www/minifactory/minfact_desc.html. R. L. Hollis, J. Gowdy, "Miniature Factories for Precision Assembly," Intl. Workshop on Microfactories, Tsukuba, Japan, 7-9 December 1998, pp. 9-14; http://www-2.cs.cmu.edu/afs/cs/project/msl/www/publications/tsu98.pdf.

and parts feeders, with the assembly of high-density mechatronic equipment as the prototypical application.

Recent research efforts in precision or automated microassembly, desktop manufacturing,[237] microfactories[238] and parallel micromanufacturing are reported at the Agency of Industrial Science and Technology (AIST) (Mechanical Engineering Laboratory),[239] Carnegie Mellon University (Microdynamic Systems Laboratory[240] and Robotics Institute[241]), European IST Program (MiCRoN Project),[242] the Finnish M4 (Micro-Meso Mechanical Manufacturing)[243] project, Innovation On Demand, Inc.,[244] Institute for Machine Tools and Industrial Management (Munich Microassembly Research),[245] Lawrence Livermore National Laboratory (Micro

---

[237] H. Aoyama, F. Iwata, A. Sasaki, "Desktop flexible manufacturing system by movable miniature robots," Proc. Intl. Conf. Robotics and Automation, 1995, pp. 660-665; Y. Hatamura, M. Nakao, T. Sato, "Construction of nano manufacturing world as a desk-top factory," Microsystem Technologies 1(1995):155-162.

[238] "Microfactory Technologies," Advanced Machine Technology, Mechanical Engineering Laboratory, Agency of Industrial Science and Technology (AIST); http://www.mel.go.jp/e/3.html. Antoine Ferreira, "Design of a flexible conveyer microrobot with electromagnetic field-based friction drive control for microfactory stations," J. Micromechatronics 1(September 2000):49-66.

[239] "Microfactory Technologies," Advanced Machine Technology, Mechanical Engineering Laboratory, Agency of Industrial Science and Technology (AIST); http://www.mel.go.jp/e/3.html.

[240] "An Architecture for Agile Assembly," Microdynamic Systems Laboratory, Carnegie Mellon University, August 8, 2002; http://www-2.cs.cmu.edu/afs/cs/project/msl/www/minifactory/minfact_desc.html.

[241] Susan Finger, "Rapid Design Through Virtual and Physical Prototyping," Robotics Institute, Carnegie Mellon University; http://www-2.cs.cmu.edu/~radproto/ and http://www.ri.cmu.edu/projects/project_185.html.

[242] Ramon Estana, "Miniaturised Co-operative Robots advancing towards the Nano range," MiCRoN Project, funded by the Future and Emerging Technologies arm of the IST Programme of the European Commission, 7 February 2002; http://wwwipr.ira.uka.de/~micron/index.html.

[243] Workshop on Micro/Meso-Mechanical Manufacturing (M^4), Northwestern University and NSF, 16-17 May 2000, http://www.mech.nwu.edu/MFG/AML/M4/Start-M4.html; Riku H. Heikkila, Ilpo T. Karjalainen, Jani J. Uusitalo, Asser S. Vuola, Reijo O. Tuokko, "Possibilities of a Microfactory in the Assembly of Small Parts and Products: First Results of the M4-project," IEEE International Symposium on Assembly and Manufacturing, 2007. ISAM'07, 22-25 July 2007, pp. 166-171.

[244] Innovation On Demand, Inc. Website; http://www.innovation-on-demand.com. A.D. Johnson, M. Fanucchi, V. Gupta, V. Martynov, V.Galhotra, K. Clements, "TiNi as a nano-actuator: experimental verification of excitation by electron-beam heating," 2003; http://www.innovation-on-demand.com/Papers/Nanoactuation_Paper.htm.

[245] Institute for Machine Tools and Industrial Management – iwb Munich Microassembly Research; http://www.iwb.tum.de/iwb_lang_en_name_Forschung_page_18.html.

Assembly Automation Laboratory),[246] the MIT Fab Lab project,[247] Nagoya University (Department of Micro System Engineering),[248] Nelson's group,[249] Rensselaer Polytechnic Institute (Center for Automation Technologies),[250] Sandia National Laboratories (Precision Micro Assembly Laboratory),[251] University of California at Berkeley (Robotics and Intelligent Machines Laboratory),[252] University of Minnesota (Advanced Microsystems Laboratory),[253] USATU (Center of High Technologies in Manufacturing Systems),[254] Zyvex Corp. (Assembly of Microsystems),[255] and elsewhere.[256]

---

[246] Micro Assembly Automation Laboratory, Lawrence Livermore National Laboratory, 16 December 1996; http://www.llnl.gov/eng/ee/erd/maal/maalhome.html.

[247] "The MIT Fab Lab project," The Center for Bits and Atoms, MIT, accessed February 2008, http://fab.cba.mit.edu/. See also: Bruce Sterling, "The Dream Factory," Wired, issue 12.12, December 2004, http://www.wired.com/wired/archive/12.12/view.html?pg=4.

[248] Department of Micro System Engineering, Nagoya University; http://www.mech.nagoya-u.ac.jp/MICRO/index-e.html.

[249] S.J. Ralis, B.Vikramaditya, B.J. Nelson, "Micropositioning of a weakly calibrated microassembly system using coarse-to-fine visual servoing strategies," IEEE Trans. on Electr. Packaging Manufacturing 23(2000):123-131; G. Yang, J.A. Gaines, B.J. Nelson, "A flexible experimental workcell for efficient and reliable wafer-level 3-D micro-assembly," IEEE Intl. Conf. on Robotics and Automation (ICRA), Seoul, South Korea, 2001.

[250] Center for Automation Technologies, Rensselaer Polytechnic Institute, 2002; http://www.cat.rpi.edu/r&d.htm.

[251] Precision Micro Assembly Laboratory, The Intelligent Systems & Robotics Center, Sandia National Laboratories, 8 July 2001; http://www.sandia.gov/isrc/precmicroassy.html.

[252] "Microrobotics and Millirobotics Research," Robotics and Intelligent Machines Laboratory, University of California at Berkeley, 26 February 2002; http://robotics.eecs.berkeley.edu/~ronf/milli-robot.html.

[253] Advanced Microsystems Laboratory, University of Minnesota; http://www.me.umn.edu/divisions/design/adv_microsystems/index2.htm.

[254] "Microrobotics and Robotization of Manufacturing Processes," Center of High Technologies in Manufacturing Systems, Ufa State Aviation Technical University (USATU); http://www.ugatu.ac.ru/ugatu.new/DR/eng/english/subject/rarnan/index.htm.

[255] "NIST-ATP Project for Assembly of Microsystems," Zyvex Corp., 2003; http://www.zyvex.com/Research/projects.html#NISTProject. Zyvex Corp., "Research and Development Activities," 8 September 2003; http://www.zyvex.com/Research/projects.html.

[256] A. Mardanov, J. Seyfried, S. Fatikow, "An automated assembly system for a microassembly station," Beitrag in Zeitschrift 38(1999):93-102; S. Fatikow, U. Rembold, "An automated microrobot-based desktop station for micro assembly and handling of micro-objects," Proc. IEEE Conf. on Emerging Technologies and Factory Automation (EFTA '96), Kauai, HI, 18-21 November 1996, pp. 586-592. N. Kawahara, T. Suto, T. Hirano, Y. Ishikawa, T. Kitahara, N. Oyama, T. Ataka, "Microfactories: new applications of micromachine technology to the manufacture of small products," Res. J. Microsystem-Technol. 3(1997):37-41; T. Kitahara, K. Ashida, M. Tanaka, Y. Ishikawa, N. Oyama, Y. Nakazawa, "Microfactory

Other related efforts include Ponoko,[257] described as "the world's first personal manufacturing platform" that provides an "online space for a community of creators and consumers to use a global network of digital manufacturing hardware to co-create, make and trade individualized product ideas on demand"; and Kovio, Inc.,[258] a startup which provides "the world's first all-printed silicon transistor capability" to compete with traditional semiconductor fabbers. In the consumer area, the "CompuCarve" computer-controlled desktop woodworking fabricator (for 3D objects made of wood, plastics, or high-density foam) is being marketed by Craftsman;[259] CarveWright[260] is a 3-D computer-controlled mill/router aimed at serious woodworking hobbyists. In 2007, Desktop Factory[261] began selling a 3D printer for consumer use at $4,995 which were expected to ship in 2008 (Figure 2-39).

---

and microlathe," Proc. Intl. Workshop on Microfactories, 1999, pp. 1-8. International Workshops on Microfactories; http://www.ri.cmu.edu/events/iwmf02/ (2002), http://www-samlab.unine.ch/iwmf2000/ (2000), http://www.aist.go.jp/MEL/keiji/HPiwmf/IWMF98.htm (1998).

[257] Ponoko website, http://www.ponoko.com/, accessed February 2008. See also: http://blog.ponoko.com/2007/10/22/making-the-masses-into-makers-at-maker-faire-austin/ and http://www.technologyreview.com/Biztech/19678/.

[258] Kovio, Inc. website, http://www.kovio.com/, accessed February 2008. See also: R. Colin Johnson, "Silicon circuits made ink-jet printable," EE Times, 13 November 2007, http://www.eetimes.com/news/latest/showArticle.jhtml;jsessionid=3YOOEQDVJJXJOQSNDLSCKHA?articleID=202805929.

[259] See "Craftsman CompuCarve Computer-Controlled Compact Woodworking Machine," http://www.sears.com/shc/s/p_10153_12605_00921754000P?pid=00921754000; "Computerized Carving – from Sears Craftsman" 16 October 2006, http://www.woodworkingonline.com/2006/10/16/computerized-carving-%e2%80%94-from-sears-craftsman/; YouTube video, http://www.youtube.com/watch?v=Dz3_T_8uJ3o.

[260] "CarveWrite Woodworking System," accessed April 2008; http://www.carvewright.com/.

[261] Desktop Factory website, http://www.desktopfactory.com/. See also: Saul Hansell, "Beam It Down From the Web, Scotty," The New York Times, 7 May 2007; http://www.nytimes.com/2007/05/07/technology/07copy.html.

Figure 2-39. In 2007, Desktop Factory started selling a 3D printer for consumer use at $4,995.[262]

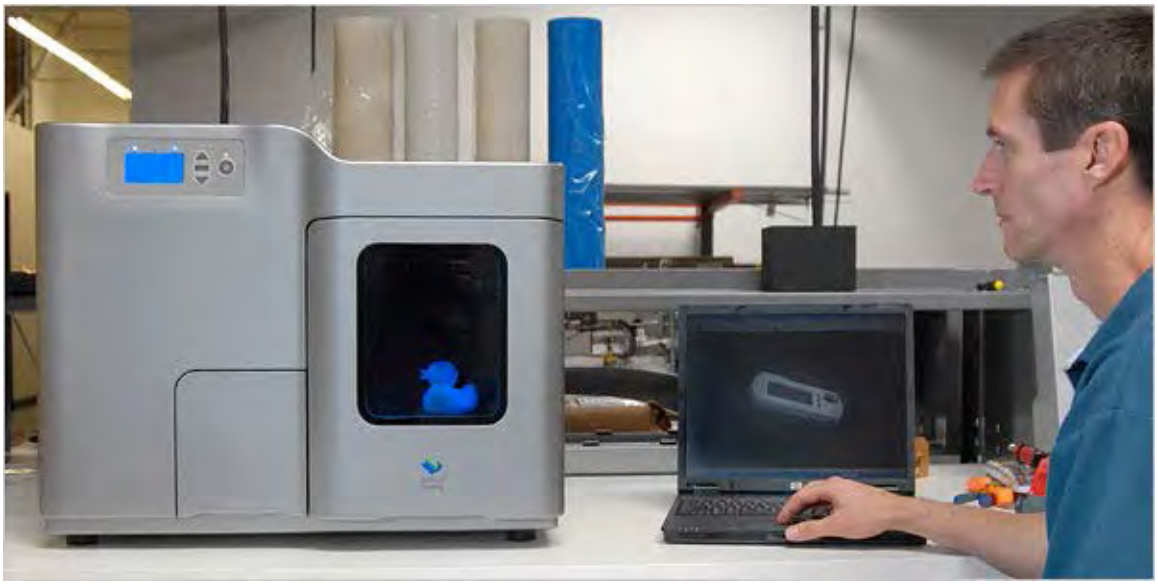

Objects made by the new printer

2.2.3.3 3-D Nanostructure Fabrication via Focused-Ion-Beam CVD

Electron beam induced deposition (EBID) is the process of using a high-intensity electron beam within an electron microscope to induce the formation of structures on the scanned surface.[263]

---

[262] Desktop Factory website, http://www.desktopfactory.com/. See also: Saul Hansell, "Beam It Down From the Web, Scotty," The New York Times, 7 May 2007; http://www.nytimes.com/2007/05/07/technology/07copy.html.

[263] M. Ruhrig, S. Porthun, J.C. Lodder, S. McVitie, L.J. Heyderman, A.B. Johnston, J.N. Chapman, "Electron beam fabrication and characterization of high-resolution magnetic force microscopy tips," J. Appl. Phys. 79(1996):2913-2919. Hans W.P. Koops, Johannes Kretz, Michael Rudolph, Markus Weber,

EBID is a slow but versatile direct-write additive lithography process for the fabrication of mesoscale and nanoscale structures with high lateral accuracies. In this process, the microscope interior is filled with a low pressure precursor gas which is readily broken down under intensive e-beam illumination. For example,[264] $W(CO)_6$ carbonyl gas[265] or WF_6 gas[266] is used to grow tungsten carbide or tungsten wires, $Cr(CO)_6$ and $Re_2(CO)_{10}$ are used to grow chromium and rhenium nanorods,[267] $Al(CH_3)_3$ is used to grow aluminum, $C_7H_7O_2F_6Au$ to grow gold, and (methylcyclopentadientyl)trimethylplatinum is used to grow platinum. In the EBID process, the electron beam is trained on a spot and held there, whereupon the precursor gas breaks down locally, depositing metal atoms only on the spot. As the beam continues to hit the spot, more atoms are deposited and a cylindrical column of metal grows, typically at a rate of ~3-300 nm/minute.[268] By slowly translating the beam position in the XY plane and controlling the substrate angle and the growth conditions, 3-dimensional nanostructures such as atomic force microscopy tips,[269] interconnects,[270] walls,[271] and more complex structures,[272] including a world

---

Gerold Dahm, Kam L. Lee, "Characterization and application of materials grown by electron-beam-induced deposition," Jpn. J. Appl. Phys. 33(30 December 1994):7099-7107.

[264] Marc Madou, Fundamentals of Microfabrication, CRC Press, Boca Raton, FL, 1997.

[265] W.H. Brunger, K.T. Kohlmann, "E-beam induced fabrication of microstructures," Proc. IEEE Microelectromechanical Systems (MEMS'92), Travemunde, Germany, 1992, pp. 168-170. P.C. Hoyle, J.R.A. Cleaver, H. Ahmed, "Electron beam induced deposition from W(CO)6 at 2 to 20 keV and its applications," J. Vac. Sci. Technol. B 14(1996):662. N.A. Kislov, I.I. Khodos, E.D. Ivanov, J. Barthel, "Electron-beam-induced fabrication of metal-containing nanostructures," Scanning 18(1996):114-118.

[266] Hiroshi Hiroshima, Norihito Suzuki, Naomi Ogawa, Masanori Komuro, "Conditions for fabrication of highly conductive wires by electron-beam-induced deposition," Jpn. J. Appl. Phys. 38(30 December 1999):7135-7139.

[267] N.A. Kislov, I.I. Khodos, E.D. Ivanov, J. Barthel, "Electron-beam-induced fabrication of metal-containing nanostructures," Scanning 18(1996):114-118.

[268] F. Cicoira, P. Hoffmann, "Focused electron-beam deposition of three dimensional free standing nanometer structures," Institute of Applied Optics, DMT-IOA, EPFL, CH-1015, Lausanne, Switzerland, June 1999; http://dmtwww.epfl.ch/ioa/reports/Hoffmann/Hoffmann98-2.pdf.

[269] Kam L. Lee, David W. Abraham, F. Secord, L. Landstein, "Submicron Si trench profiling with an electron-beam fabricated atomic force microscope tip," J. Vac. Sci. Technol. B 9(November 1991):3562-3568. P. Boggild, T.M. Hansen, C. Tanasa, F. Grey, "Fabrication and actuation of customized nanotweezers with a 25 nm gap," Nanotechnology 12(September 2001):331-335.

[270] Wolfgang Fritzsche, Konrad J. Bohm, Eberhard Unger, J. Michael Kohler, "Making electrical contact to single molecules," Nanotechnology 9(September 1998):177-183. Wolfgang Fritzsche, J. Michael Kohler, Konrad J. Bohm, Eberhard Unger, Thomas Wagner, Remo Kirsch, Michael Mertig, Wolfgang Pompe, "Wiring of metalized microtubules by electron beam-induced structuring," Nanotechnology 10(September 1999):331-335; http://www.ipht-jena.de/BEREICH_3/abt32/b3/english/molnano/pdf/23.pdf.

[271] Wolfgang Fritzsche, Konrad J. Bohm, Eberhard Unger, J. Michael Kohler, "Making electrical contact to single molecules," Nanotechnology 9(September 1998):177-183.

map printed on a spherical 60-micron resin microsphere with 10 nm features,[273] have been made via "electron beam stereolithography." (See also Section 2.2.3.1.)

Koops notes that objects are readily constructed in vertically free-standing geometric shapes such as Y's, X's, and more complex structures containing internal voids such as arches or closed loops atop columns (i.e., round or square tennis-racquet shapes),[274] including in one case a "three-dimensional build-up with conducting material resembling a field emission electron source, having an emitter tip and an extractor ring around it...[with] a capacitance of 24 aF between the tip and the ring" and in another case an artistic "Micro Coliseum" structure made by "FIB [focused ion beam] assisted deposition using a hydrocarbon precursor gas. The diameter of the structure is 1.8 µm, its height is 0.5 µm, the employed linewidth of the arches constructing the building is 0.08 µm." EBID has also been used to deposit carbonaceous structures,[275] ruthenium nanoparticle chains,[276] and a variety of conducting and nonconducting materials.[277] Conductive

---

[272] T. Ooi, K. Matsumoto, M. Nakao, M. Otsubo, S. Shirakata, S. Tanaka, Y. Hatumura, Proc. MEMS 2000, pp. 580-583.

[273] "Three-Dimensional Nanofabrication Using Electron Beam Lithography – The world's smallest globe with a resolution 100 times higher than previously possible," NTT News Release, 2 February 2004; http://www.ntt.co.jp/news/news04e/0402/040202.html.

[274] Hans W.P. Koops, "Rapid prototyping and structure generation using three-dimensional nanolithography with electron beam induced chemical reactions," Paper No. 5116-52, SPIE Conference 5116, Microtechnologies for the New Millennium 2003, 19-21 May 2003, Maspalomas, Gran Canaria, Canary Islands, Spain, 2003.

[275] Hans W.P. Koops, Johannes Kretz, Michael Rudolph, Markus Weber, Gerold Dahm, Kam L. Lee, "Characterization and application of materials grown by electron-beam-induced deposition," Jpn. J. Appl. Phys. 33(30 December 1994):7099-7107. T. Fujii, M. Suzuki, M. Miyashita, M. Yamaguchi, T. Onuki, H. Nakamura, T. Matsubara, H. Yamada, K. Nakayama, "Micropattern measurement with an atomic force microscope," J. Vac. Sci. Technol. B 9(1991):666; N. Miura, H. Ishii, J.-I. Shirakashi, A. Yamada, M. Konagai, "Electron-beam-induced deposition of carbonaceous microstructures using scanning electron microscopy," Proceedings of the 8th International Conference on Solid Films and Surfaces held in Osaka, Japan, July 1996, Appl. Surf. Sci. 113/114(17 April 1997):269-273; K. Wiesauer, G. Springholza, "Fabrication of semiconductor nanostructures by nanoindentation of photoresist layers using atomic force microscopy," J. Appl. Phys. 88(15 December 2000):7289-7297, http://www.hlphys.uni-linz.ac.at/hl/perskarin/publikat/jap88_7289_00_nano.pdf; Min-Feng Yu, Oleg Lourie, Mark J. Dyer, Katerina Moloni, Thomas F. Kelly, Rodney S. Ruoff, "Strength and breaking mechanism of multiwalled carbon nanotubes under tensile load," Science 287(28 January 2000):637-640; MinFeng Yu, Mark J. Dyer, George D. Skidmore, Henry W. Rohrs, XueKun Lu, Kevin D. Ausman, James R. Von Ehr, Rodney S. Ruoff, "Three-dimensional manipulation of carbon nanotubes under a scanning electron microscope," Nanotechnology 10(September 1999):244-252; P. Boggild, T.M. Hansen, K. Molhave (Mikroelektronik Centret, Technical University of Denmark), "Nanotweezers for manipulation of free-hanging nanowires," abstract FF14, http://www.nbi.dk/dfs/abs2001final/ff14.html; presentation at Physics and Industrial Innovation Session, Chairman F. Grey (Mikroelektronik Centret, Technical University of Denmark), sponsored by Danish Physical Society, 2001, http://www.nbi.dk/dfs/abs2001final/ff00.html.

[276] B.F.G. Johnson, K.M. Sanderson, D.S. Shephard, D. Ozkaya, W. Zhou, H. Ahmed, M.D. R. Thomas, L. Gladden, M. Mantle, "Electron beam induced formation of nanoparticle chains and wires from a ruthenium cluster polymer," Chem. Commun. (2000):1317-1318.

nanostructured devices such as field emission sources have been fabricated[278] – single-atom STM tips can emit up to 10 microamp in field emission mode,[279] although 0.1-1 microamp is more common for field emission from carbon atomic wires.[280] Electron emission from EBID-grown columns or tips has been widely reported in the literature.[281]

EBID resolution is somewhat restricted[282] because electrons scatter quickly in solids, beam electrons are mutually repulsive, and electron wavelengths are typically 20-50 nm. This often limits practical e-beam lithographic resolution to dimensions >10 nm, although resolutions as

---

[277] Hans W. Koops, M. Weber, C. Schoessler, A. Kaja, "Three-dimensional additive electron beam lithography," in Benedykt W. Licznerski, Andrzej Dziedzic, eds., Metal/Nonmetal Microsystems: Physics, Technology, and Applications, SPIE Proceedings Vol. 2780, SPIE – The International Society for Optical Engineering, Bellingham, WA, 1996, Paper #2780-78, pp. 388-395; Ivo Utke, B. Dwir, K. Leifer, F. Cicoira, P. Doppelt, P. Hoffmann, E. Kapon, "Electron beam induced deposition of metallic tips and wires for microelectronics applications," Microelectronics Engineering (2000).

[278] H.W.P. Koops, C. Schoessler, A. Kaya, M. Weber, "Conductive dots, wires, and supertips for field electron emitters produced by electron-beam induced deposition on samples having increased temperature," J. Vac. Sci. Tech. B 14(1996):4105-4109. C. Schoessler, H.W.P. Koops, "Nanostructured integrated electron source," J. Vac. Sci. Technol. B 16(1998):862.

[279] H.W. Fink, "Mono-atomic tips for scanning tunneling microscopy," IBM J. Res. Develop. 30(1986):460-465.

[280] A.G. Rinzler, J.H. Hafner, P. Nikolaev, L. Lou, S.G. Kim, D. Tomanek, P. Nordlander, D.T. Colbert, R.E. Smalley, "Unraveling nanotubes: field emission from an atomic wire," Science 269(15 September 1995):1550-1553.

[281] M. Weber, M. Rudolph, J. Kretz, H.W.P. Koops, "Electron-beam induced deposition for fabrication of vacuum field emitter devices," 7th IVMC, 1994, p. 395; J. Kretz, M. Rudolph. H.W. Koops, "Three dimensional structurization by additive lithography, analysis of deposits using TEM and EDX, and application for field emitter tips," Microelectronic Engineering 23(1994):477-481; M. Takai, H. Morimoto, T. Kishimoto, S. Lipp, L. Frey, H. Ryssel, S. Yura, A. Hosono, S. Okuda, "Electron emission from gated Pt emitters fabricated by electron beam induced deposition," IVMC'96 Technical Digest, 1996, p. 657; Hiroji Morimoto, Takehisa Kishimoto, Mikio Takai, Shinsuke Yura, Akihiko Hosono, Soichiro Okuda, Stephan Lipp, Lothar Frey, Heiner Ryssel, "Electron-beam-induced deposition of Pt for field emitter arrays," Jpn. J. Appl. Phys. 35(30 December 1996):6623-6625; H.W.P. Koops, "Novel field emission devices produced by electron-beam induced deposition," IVESC'98 Session Program, The 2nd International Vacuum Electron Sources Conference, 7-10 July 1998, Tsukuba, Japan; Filip Floreani, H.W.P. Koops, W. Elsabera, "Operation of high power field emitters fabricated with electron beam induced deposition," presented Wednesday, 27 September 2000 at the EuroFE2000 Scientific Program, 25-29 September 2000, Segovia, Spain; http://www.cientifica.com/cientifica/frameworks/generic/public_users/eurofe/EuroFE2k/abstracts/floreani.pdf; J.T.L. Thong, C.H. Oon, "Electron emission from electron beam induced deposition tips," presented at the Second IEEE International Vacuum Electronics Conference, 2-4 April 2001, Noordwijk, The Netherlands.

[282] N. Silvis-Cividjian, C.W. Hagen, P. Kruit, "Resolution limits in electron beam induced deposition (EBID)," Annual Report Nederlandse Vereniging voor Microscopie, 7-8 December 2000, pp. 184-185.

small as 2 nm have been obtained in a few materials,[283] wires 80 nm in diameter have been fabricated with surface roughness below 2-3 nm,[284] tips for AFM/STM work can be made with radii of ~5 nm,[285] and EBID-fabricated carbon supertips have "customizable shapes with features down to below 10 nm".[286] Unlike CVD (chemical vapor deposition), EBID is not a thermal

---

[283] Marc Madou, Fundamentals of Microfabrication, CRC Press, Boca Raton, FL, 1997.

[284] Hans W.P. Koops, "Rapid prototyping and structure generation using three-dimensional nanolithography with electron beam induced chemical reactions," Paper No. 5116-52, SPIE Conference 5116, Microtechnologies for the New Millennium 2003, 19-21 May 2003, Maspalomas, Gran Canaria, Canary Islands, Spain, 2003. Hans W. Koops, "Photonic crystals built by three-dimensional additive lithography enable integrated optics of high density," in Francis T. Yu, Shizhuo Yin, eds., Photorefractive Fiber and Crystal Devices: Materials, Optical Properties, and Applications II, SPIE Proceedings Vol. 2849, SPIE – The International Society for Optical Engineering, Bellingham, WA, 1996, Paper #2849-29, pp. 248-256.

[285] T. Fujii, M. Suzuki, M. Miyashita, M. Yamaguchi, T. Onuki, H. Nakamura, T. Matsubara, H. Yamada, K. Nakayama, "Micropattern measurement with an atomic force microscope," J. Vac. Sci. Technol. B 9(1991):666; N. Miura, H. Ishii, J.-I. Shirakashi, A. Yamada, M. Konagai, "Electron-beam-induced deposition of carbonaceous microstructures using scanning electron microscopy," Proceedings of the 8th International Conference on Solid Films and Surfaces held in Osaka, Japan, July 1996, Appl. Surf. Sci. 113/114(17 April 1997):269-273; K. Wiesauer, G. Springholza, "Fabrication of semiconductor nanostructures by nanoindentation of photoresist layers using atomic force microscopy," J. Appl. Phys. 88(15 December 2000):7289-7297, http://www.hlphys.uni-linz.ac.at/hl/perskarin/publikat/jap88_7289_00_nano.pdf; Min-Feng Yu, Oleg Lourie, Mark J. Dyer, Katerina Moloni, Thomas F. Kelly, Rodney S. Ruoff, "Strength and breaking mechanism of multiwalled carbon nanotubes under tensile load," Science 287(28 January 2000):637-640; MinFeng Yu, Mark J. Dyer, George D. Skidmore, Henry W. Rohrs, XueKun Lu, Kevin D. Ausman, James R. Von Ehr, Rodney S. Ruoff, "Three-dimensional manipulation of carbon nanotubes under a scanning electron microscope," Nanotechnology 10(September 1999):244-252; P. Boggild, T.M. Hansen, K. Molhave (Mikroelektronik Centret, Technical University of Denmark), "Nanotweezers for manipulation of free-hanging nanowires," abstract FF14, http://www.nbi.dk/dfs/abs2001final/ff14.html; presentation at Physics and Industrial Innovation Session, Chairman F. Grey (Mikroelektronik Centret, Technical University of Denmark), sponsored by Danish Physical Society, 2001, http://www.nbi.dk/dfs/abs2001final/ff00.html.

[286] T. Fujii, M. Suzuki, M. Miyashita, M. Yamaguchi, T. Onuki, H. Nakamura, T. Matsubara, H. Yamada, K. Nakayama, "Micropattern measurement with an atomic force microscope," J. Vac. Sci. Technol. B 9(1991):666; N. Miura, H. Ishii, J.-I. Shirakashi, A. Yamada, M. Konagai, "Electron-beam-induced deposition of carbonaceous microstructures using scanning electron microscopy," Proceedings of the 8th International Conference on Solid Films and Surfaces held in Osaka, Japan, July 1996, Appl. Surf. Sci. 113/114(17 April 1997):269-273; K. Wiesauer, G. Springholza, "Fabrication of semiconductor nanostructures by nanoindentation of photoresist layers using atomic force microscopy," J. Appl. Phys. 88(15 December 2000):7289-7297, http://www.hlphys.uni-linz.ac.at/hl/perskarin/publikat/jap88_7289_00_nano.pdf; Min-Feng Yu, Oleg Lourie, Mark J. Dyer, Katerina Moloni, Thomas F. Kelly, Rodney S. Ruoff, "Strength and breaking mechanism of multiwalled carbon nanotubes under tensile load," Science 287(28 January 2000):637-640; MinFeng Yu, Mark J. Dyer, George D. Skidmore, Henry W. Rohrs, XueKun Lu, Kevin D. Ausman, James R. Von Ehr, Rodney S. Ruoff, "Three-dimensional manipulation of carbon nanotubes under a scanning electron microscope," Nanotechnology 10(September 1999):244-252; P. Boggild, T.M. Hansen, K. Molhave (Mikroelektronik Centret, Technical University of Denmark), "Nanotweezers for manipulation of free-hanging nanowires," abstract FF14, http://www.nbi.dk/dfs/abs2001final/ff14.html; presentation at Physics and Industrial

decomposition process, so the purity of the deposit is often much lower unless the substrate is heated.[287] However, a few high-purity free-standing metal nanorods have been made by EBID,[288] and a rapid fabrication process could be achieved by controlling the e-beam spot position with a computer, as demonstrated by Koops et al.,[289] or by employing multiple beams to achieve parallel operation.

Related opportunities for crude atomic or molecular positional assembly may exist with other emerging technologies, as, for example, the beam lithography/nanostencil technique under investigation by IBM Zurich in their "ATOMS" project,[290] neutral molecular beam deposition,[291] 3-D proton beam nanolithography,[292] the manipulation of Bose-Einstein condensates along an "atomic conveyor belt" above a silicon chip,[293] light-driven molecular assembly,[294] atomic holography,[295] and various proposals for quantum mechanical automata.[296] Older techniques of

---

Innovation Session, Chairman F. Grey (Mikroelektronik Centret, Technical University of Denmark), sponsored by Danish Physical Society, 2001, http://www.nbi.dk/dfs/abs2001final/ff00.html.

[287] H.W.P. Koops, C. Schoessler, A. Kaya, M. Weber, "Conductive dots, wires, and supertips for field electron emitters produced by electron-beam induced deposition on samples having increased temperature," J. Vac. Sci. Tech. B 14(1996):4105-4109. M. Weber, M. Rudolph, J. Kretz, H.W.P. Koops, J. Vac. Sci. Technol. B 13(1995):461-464.

[288] N.A. Kislov, I.I. Khodos, E.D. Ivanov, J. Barthel, "Electron-beam-induced fabrication of metal-containing nanostructures," Scanning 18(1996):114-118.

[289] H.W.P. Koops, C. Schoessler, A. Kaya, M. Weber, "Conductive dots, wires, and supertips for field electron emitters produced by electron-beam induced deposition on samples having increased temperature," J. Vac. Sci. Tech. B 14(1996):4105-4109.

[290] IBM Zurich Research laboratory, "Assembly tool for molecular structures," 2001; http://www.zurich.ibm.com/st/nanoscience/assembly.html.

[291] B.K. Dey, M. Shapiro, P. Brumer, "Coherently controlled nanoscale molecular deposition," Phys. Rev. Lett. 85(9 October 2000):3125-3128.

[292] J. A. van Kan, A. A. Bettiol, F. Watt, "Three-dimensional nanolithography using proton beam writing," Appl. Phys. Lett. 83(2003):1629.

[293] W. Hansel, P. Hommelhoff, T.W. Hansch, J. Reichel, "Bose–Einstein condensation on a microelectronic chip," Nature 413(4 October 2001):498-501; http://www.nature.com/cgi-taf/DynaPage.taf?file=/nature/journal/v413/n6855/full/413498a0_fs.html.

[294] Masahiro Muraoka, Thomas W. Bell, Stephen L. Gillett, "Ferrocene intercalation into hydrophobic monolayers: toward light-driven molecular assembly," presentation at the Ninth Foresight Conference on Molecular Nanotechnology, 9-11 November 2001; http://www.foresight.org/Conferences/MNT9/Abstracts/Muraoka/index.html.

[295] Fujio Shimizu, S. Mitake, J. Fujita, "Interferometric modulation of an atomic beam by an electric field: a phase hologram for atoms," Phys. Rev. Lett. 84(1 May 2000):4027-4030; brief summary in Eric J. Lerner, "Holography with Atoms," The Industrial Physicist, October 2000, pp. 10-11, at http://www.aip.org/tip/INPHFA/vol-6/iss-5/p8.pdf. See also: Hilmar Oberst, Shigenori Kasashima, Fujio Shimizu, Victor I. Balykin, "Atomic matter wave scanner," arXiv:physics/0210036v2 (9 October 2002)

automated electrodeposition microfabrication[297] employ a fine-tipped probe in an electroplating solution to locally electrodeposit metals out of solution to form microstructures, such as regularly-spaced arrays of 100-nm tall nickel columns[298] or >100-layer 3-D patterns using layers a few microns thick.[299]

Most recently, Zobelli et al.[300] have shown that electron irradiation in a dedicated scanning transmission electron microscope (STEM) can be used as a nano-electron-lithography technique allowing the controlled reshaping of single walled carbon and boron nitride nanotubes, e.g., by "carving" away small section of nanotubes with ~5 Å spatial resolution, by removing a select number of atoms to locally change the diameter of single-walled organic and inorganic nanotubes, or by removing a line of atoms in a nanotube potentially changing its chirality and thus switching the nanotube from metal to semiconductor or vice versa. The method could also be used to cut graphene layers and produce graphene nanoribbons of well-defined widths.

2.2.4 Zyvex Atomically Precise Manufacturing (2003-present)

In March 2008, Zyvex announced that it had assembled $15 million in funding for its Atomically Precise Manufacturing Consortium. The project includes a mixture of funding from the Defense Advanced Research Projects Agency, the Texas Emerging Technology Fund and cost sharing from the team members. "Increasing the precision of manufacturing has driven both technology and science for the past couple of centuries and what we are doing is just an extension of that drive," said John Randall, vice president of Zyvex Labs, the prime contractor for the research project. "What is revolutionary is having digital control over where we add atoms to a robust

---

http://arxiv.org/pdf/physics/0210036, poster presentation at the 5th Laser Cooling Workshop, 9 January 2003.

[296] D.Z. Albert, "On quantum-mechanical automata," Phys. Lett. 98A(1983):249-252; Seth Lloyd, "A potentially realizable quantum computer," Science 261(17 September 1993):1569-1571.

[297] John D. Madden, Ian W. Hunter, "3-D Micro-fabrication by localized electrochemical deposition," J. Microelectromechanical Systems 5(January-March 1996):24-32; Ian W. Hunter, Serge R. Lafontaine, John D. Madden, "Three dimensional microfabrication by localized electrodeposition and etching," United States Patent No. 5,641,391, 24 June 1997. "EFAB™: Rapid Batch Manufacturing of True 3-D Micro-Devices," MEMGen Corp., http://www.isi.edu/efab/; "Technology: Imagine Manufacturing Micromachines Directly From CAD In Days, Not Months," MEMGen Corp., http://www.memgen.com/technology/index.htm.

[298] "MicroFab: Microfabrication through Electrodeposition," 12 October 1998; http://www.thefirst.org/jefft/microfab/index.html.

[299] "EFAB™: Rapid Batch Manufacturing of True 3-D Micro-Devices," MEMGen Corp., http://www.isi.edu/efab/; "Technology: Imagine Manufacturing Micromachines Directly From CAD In Days, Not Months," MEMGen Corp., http://www.memgen.com/technology/index.htm.

[300] A. Zobelli, A. Gloter, C. P. Ewels, C. Colliex, "Shaping single walled nanotubes with an electron beam," Phys. Rev. B 77(2008):045410; http://link.aps.org/abstract/PRB/v77/e045410.

solid material." In addition to UT Dallas and Zyvex, the research team includes the University of Illinois at Urbana-Champaign, the University of North Texas, the University of Central Florida, the University of Texas at Austin, the National Institute of Standards and Technology, General Dynamics, Molecular Imprints Inc. and Integrated Circuit Scanning Probe Instruments.

The Atomically Precise Manufacturing Project currently consists of three coordinated efforts: MicroAutomation, Molecularly Precise Tools, and Patterned Atomic Layer Epitaxy. The latter initiative is perhaps the most important to our diamondoid nanofactory program: "Atomic layer deposition builds amorphous materials; atomic layer epitaxy (ALE) builds crystalline materials. Start with a protected (passivated) surface: every available bond has a hydrogen atom. If you deprotect the surface, removing the hydrogen, then you can deposit a layer of atoms. If you choose the right precursor gas, you add only one monolayer which is protected as it's added. Then you can deprotect and add exactly one more layer of atoms. There are a number of precursor gases available. There are literally hundreds of systems to grow things with atomic precision in one dimension. Now, if you combine this with the ability to deprotect the surface in selected locations....With a scanning tunneling microscope, you can remove single hydrogen atoms with atomic precision. If you do this layer by layer, you can build 3D structures. Professor Joe Lyding at University of Illinois has done repeated desorption/deposition."

According to a Zyvex website:[301] "The Patterned Atomic Layer Epitaxy Project will combine two known experimental techniques to produce atomically precise nanostructures. In our view, this is the best approach to a molecular assembler that can make reasonable progress before molecularly precise tools are available. We have identified a target process and material system that will be capable of producing complex, atomically precise (in all three dimensions) nanostructures in a robust material. The prototype reactors will not be massively parallel and will be capable of only limited output. We have identified several approaches to massive parallelism that will be evaluated as we develop the prototype tools. The prototype system, even with its limited capabilities, will be able to produce valuable products that require only very small atomically precise structures. When the APM Project produces a superior tip for patterning, this will greatly improve patterned atomic layer epitaxy and enable its scale-up to large parallelism. However, such tools will also enable significant progress in molecular pick and place technology. Zyvex will constantly be evaluating the best path to a massively parallel molecular assembler."

2.3 Atomically Precise UHV/Tip-Based Molecular Manufacturing

One proposed pathway to atomically precise manufacturing is scanning probe diamondoid mechanosynthesis (DMS): employing scanning probe technology for positional control in combination with novel reactive tips to fabricate atomically-precise diamondoid components under positional control. This pathway has its roots in the 1986 book *Engines of Creation*, in which the manufacture of diamondoid parts was proposed as a long-term objective by Drexler,[302] and in the 1989 demonstration by Donald Eigler at IBM that individual atoms could be

---

[301] Zyvex research activities, accessed March 2008; http://www.zyvex.com/Research/activities.html.

[302] K. Eric Drexler, Engines of Creation: The Coming Era of Nanotechnology, Anchor Press/Doubleday, New York, 1986.

manipulated by a scanning tunneling microscope.[303] The proposed DMS-based pathway would skip intermediate technologies proposed by Drexler[304] – these begin with polymeric structures and solution-phase synthesis, though no specific methods for bridging the enormous gap between polymeric and diamondoid structures have ever been proposed[305] – and would instead move toward advanced DMS in a more direct way. As noted in the 2007 Battelle-Foresight nanotechnology roadmap report:[306] "Perhaps the most important contribution of tip-based APM [Atomically Precise Manufacturing] will be to make the atomically precise components required for productive nanosystems....Iterating this process toward higher performance materials leads toward structures (for example, ceramics) that are denser and more stable than biopolymers. APM systems that build products of this sort are envisioned to use flexible tip-based processes, since **biomimetic approaches appear to have limited value in this area**. This anticipated convergence on tip-based inorganic systems suggests that **near-term, tip-based APM methods might be more directly developed in this direction**. The approaches of this kind also involve broadening the range of structures that can be built, leading to nanoscale structures that by themselves provide the central components necessary for APM." (emphasis added)

Although covalent-bonded self-assembly has been demonstrated,[307] complex atomically precise structures ranging from medical nanorobots to macroscale products also cannot be manufactured using the conventional techniques of self-assembly.[308] As noted in the final report[309] of the 2006

---

[303] D.M. Eigler, E.K. Schweizer, "Positioning Single Atoms with a Scanning Tunnelling Microscope," Nature 344(5 April 1990):524-526; http://www.nature.com/nature/journal/v344/n6266/abs/344524a0.html (abstract).

[304] K. Eric Drexler, "Molecular engineering: an approach to the development of general capabilities for molecular manipulation," Proc. Natl. Acad. Sci. (USA) 78(September 1981):5275-5278. K. Eric Drexler, Nanosystems: Molecular Machinery, Manufacturing, and Computation, John Wiley & Sons, New York, 1992, Chapter 16. K. Eric Drexler, "Toward Integrated Nanosystems: Fundamental Issues in Design and Modeling," J. Comput. Theor. Nanosci. 3(February 2006):1-10.

[305] Hamid Ramezani, G. Ali Mansoori, Mohammad-Reza Saberi, "Diamondoids-DNA Nanoarchitecture: From Nanomodules Design to Self-Assembly," J. Comp. Theor. Nanosci. 4(February 2007):96-106.

[306] Productive Nanosystems: A Technology Roadmap, Battelle Memorial Institute and Foresight Nanotech Institute, 2007; http://www.foresight.org/roadmaps/index.html.

[307] Leonhard Grill, Matthew Dyer, Leif Lafferentz, Mats Persson, Maike V. Peters, Stefan Hecht, "Nano-architectures by covalent assembly of molecular building blocks," Nature Nanotechnology 2(2007):687-691, http://dx.doi.org/10.1038/nnano.2007.346.

[308] N. Bowden, A. Terfort, J. Carbeck, G.M. Whitesides, "Self-assembly of mesoscale objects into ordered two-dimensional arrays," Science 276(1997)):233-235; A. Terfort, N. Bowden, G.M. Whitesides, "Three-dimensional self-assembly of millimetre-scale components," Nature 386(1997):162-164; T.L. Breen, J. Tien, S.R.J. Oliver, T. Hadzic, G.M. Whitesides, "Design and self-assembly of open, regular, 3D mesostructures," Science 284(1999):948-951; D.H. Gracias, J. Tien, T.L. Breen, C. Hsu, G.M. Whitesides, "Forming electrical networks in three dimensions by self-assembly," Science 289(2000):1170-1172; G.M. Whitesides. B. Grzybowski, Self-assembly at all scales," Science 295(2002):2418-2421; G.M. Whitesides, M. Boncheva, "Beyond molecules: Self-assembly of mesoscopic and macroscopic components," Proc. Natl. Acad. Sci. (USA) 99(2002):4769-4774; S. Griffith, D. Goldwater, J.M. Jacobson, "Self-replication from random parts," Nature 437(2005):636.

Congressionally-mandated review of the U.S. National Nanotechnology Initiative by the National Research Council (NRC) of the National Academies and the National Materials Advisory Board (NMAB): "For the manufacture of more sophisticated materials and devices, including complex objects produced in large quantities, it is unlikely that simple self-assembly processes will yield the desired results. The reason is that the probability of an error occurring at some point in the process will increase with the complexity of the system and the number of parts that must interoperate." Error detection and correction requires a minimum level of complexity that cannot easily be achieved via thermodynamically-driven self-assembly processes. Self-assembly is not conducive to rapid prototyping because small changes in the final product specification often require major changes in the self-assembly process, and small changes in the process or inputs can often produce large changes in the resulting product. Self-assembly usually produces relatively weak and compliant structures. Self-assembly also violates the principles of sound classical engineering design "because the functional requirements of components are very difficult to separate from each other....Changing one component often requires changing most of the other components also, resulting in a cascade of conflicting requirements that greatly restricts the search space of possible solutions, perhaps even making many sets of requirements unreachable."[310]

The opposite of self-assembly processes is positionally controlled processes, in which the positions and trajectories of all components of intermediate and final product objects are controlled at every moment during fabrication and assembly. For instance, positional control of laser-cooled individual atoms has been demonstrated using laser trapping,[311] and an atomic force microscope (AFM) has been used to manually operate a molecular rack-and-pinion system.[312] Positional processes should allow more complex products to be built with high quality and should enable rapid prototyping during product development. Positional assembly is the norm in conventional macroscale manufacturing (e.g., cars, appliances, houses) but is only recently[313]

---

[309] Committee to Review the National Nanotechnology Initiative, National Materials Advisory Board (NMAB), National Research Council (NRC) (2006) A Matter of Size: Triennial Review of the National Nanotechnology Initiative. The National Academies Press, Washington DC; http://www.nap.edu/catalog/11752.html#toc.

[310] Tihamer Toth-Fejel, Modeling Kinematic Cellular Automata: Final Report, NASA Institute for Advanced Concepts, Phase I: CP-02-02, General Dynamics Advanced Information Systems Contract # P03-0984, 30 April 2004.

[311] Yevhen Miroshnychenko, Wolfgang Alt, Igor Dotsenko, Leonid Forster, Mkrtych Khudaverdyan, Dieter Meschede, Dominik Schrader, Arno Rauschenbeutel, "Quantum engineering: An atom-sorting machine," Nature 442(13 July 2006):151. See also: Frank Luerweg, "Quantum Computer: Laser tweezers sort atoms," PhysOrg.com, 12 July 2006; http://www.physorg.com/news71935118.html.

[312] Franco Chiaravalloti, Leo Gross, Karl-Heinz Rieder, Sladjana M. Stojkovic, André Gourdon, Christian Joachim, Francesca Moresco, "A rack-and-pinion device at the molecular scale," Nature Materials 6(2007):30-33; http://www.nature.com/nmat/journal/v6/n1/abs/nmat1802.html.

[313] T. Kenny, "Tip-Based Nanofabrication (TBN)," Defense Advanced Research Projects Agency (DARPA)/Microsystems Technology Office (MTO), Broad Agency Announcement BAA 07-59, July

starting to be seriously investigated experimentally for nanoscale manufacturing. Of course, we already know that positional fabrication will work in the nanoscale realm. This is demonstrated in the biological world by ribosomes, which positionally assemble proteins in living cells by following a sequence of digitally encoded instructions (even though ribosomes themselves are self-assembled). Lacking this positional fabrication of proteins controlled by DNA-based software, large, complex, digitally-specified organisms would probably not be possible and biology as we know it would not exist.

The most important materials for positional assembly may be the rigid covalent or "diamondoid" solids, since these could potentially be used to build the most reliable and complex nanoscale machinery. Preliminary theoretical studies have suggested great promise for these materials in molecular manufacturing. The NMAB/NRC Review Committee recommended[314] that experimental work aimed at establishing the technical feasibility of positional molecular manufacturing should be pursued and supported: "Experimentation leading to demonstrations supplying ground truth for abstract models is appropriate to better characterize the potential for use of bottom-up or molecular manufacturing systems that utilize processes more complex than self-assembly." Making complex nanorobotic systems requires manufacturing techniques that can build a molecular structure by positional assembly.[315] This will involve picking and placing molecular parts one by one, moving them along controlled trajectories much like the robot arms that manufacture cars on automobile assembly lines. The procedure is then repeated over and over with all the different parts until the final product, such as a medical nanorobot, is fully assembled using a desktop nanofactory.

2.3.1 Diamondoid Mechanosynthesis (DMS)

Theorists believe that the most reliable and durable medical nanorobots will be built using diamondoid materials. What is diamondoid? First and foremost, diamondoid materials include pure diamond, the crystalline allotrope of carbon. Among other exceptional properties, diamond has extreme hardness, high thermal conductivity, low frictional coefficient, chemical inertness, a wide electronic bandgap, and is the strongest[316] and stiffest material presently known at ordinary pressures. Diamondoid materials also may include any stiff covalent solid that is similar to

---

2007; http://www.fbo.gov/spg/ODA/DARPA/CMO/BAA07-59/listing.html. Nanofactory Collaboration website, accessed February 2008; http://www.MolecularAssembler.com/Nanofactory.

[314] Committee to Review the National Nanotechnology Initiative, National Materials Advisory Board (NMAB), National Research Council (NRC) (2006) A Matter of Size: Triennial Review of the National Nanotechnology Initiative. The National Academies Press, Washington DC; http://www.nap.edu/catalog/11752.html#toc.

[315] Robert A. Freitas Jr., "Current status of nanomedicine and medical nanorobotics," J. Comput. Theor. Nanosci. 2(2005):1-25; http://www.nanomedicine.com/Papers/NMRevMar05.pdf.

[316] J.E. Field, "Chapter 9. Strength and Fracture Properties of Diamond," in J.E. Field, ed., The Properties of Diamond, Academic Press, New York, 1979, pp. 281-324; R.H. Telling, C.J. Pickard, M.C. Payne, J.E. Field, "Theoretical Strength and Cleavage of Diamond," Phys. Rev. Lett. 84(May 2000):5160-5163, http://www.tcm.phy.cam.ac.uk/~cjp20/publications/PRL84_5160.pdf.

diamond in strength, chemical inertness, or other important material properties, and possesses a dense three-dimensional network of bonds. Examples of such materials are carbon nanotubes and fullerenes, several strong covalent ceramics such as silicon carbide, silicon nitride, and boron nitride, and a few very stiff ionic ceramics such as sapphire (monocrystalline aluminum oxide) that can be covalently bonded to pure covalent structures such as diamond. Of course, large pure crystals of diamond are brittle and easily fractured. The intricate molecular structure of a diamondoid nanofactory macroscale product will more closely resemble a complex composite material, not a brittle solid crystal. Such products, and the nanofactories that build them, should be extremely durable in normal use.

Mechanosynthesis, involving molecular positional fabrication, is the formation of covalent chemical bonds using precisely applied mechanical forces to build, for example, diamondoid structures. Mechanosynthesis employs chemical reactions driven by the mechanically precise placement of extremely reactive chemical species in an ultra-high vacuum environment. Chemical activation energy is supplied by mechanical force, not by heat.[317] Mechanosynthesis may be automated via computer control, enabling programmable molecular positional fabrication. Molecularly precise fabrication involves holding feedstock atoms or molecules, and a growing nanoscale workpiece, in the proper relative positions and orientations so that when they touch they will chemically bond in the desired manner. In this process, a mechanosynthetic tool is brought up to the surface of a workpiece. One or more transfer atoms are added to, or removed from, the workpiece by the tool. Then the tool is withdrawn and recharged. This process is repeated until the workpiece (e.g., a growing nanopart) is completely fabricated to molecular precision with each atom in exactly the right place. Note that the transfer atoms are under positional control at all times to prevent unwanted side reactions from occurring. Side reactions are also prevented using proper reaction design so that the reaction energetics help us avoid undesired pathological intermediate structures.

The positional assembly of diamondoid structures, some almost atom by atom, using molecular feedstock has been examined theoretically[318] via computational models of diamond

---

[317] Martin Konôpka, Robert Turanský, Joachim Reichert, Harald Fuchs, Dominik Marx, Ivan Štich, "Mechanochemistry and Thermochemistry are Different: Stress-Induced Strengthening of Chemical Bonds," Phys. Rev. Lett. 100(19 March 2008):115503, http://link.aps.org/abstract/PRL/v100/e115503.

[318] Robert A. Freitas Jr., Ralph C. Merkle, "A Minimal Toolset for Positional Diamond Mechanosynthesis," J. Comput. Theor. Nanosci. 5(May 2008):760-861. Jingping Peng, Robert A. Freitas Jr., Ralph C. Merkle, James R. Von Ehr, John N. Randall, George D. Skidmore, "Theoretical Analysis of Diamond Mechanosynthesis. Part III. Positional C_2 Deposition on Diamond C(110) Surface using Si/Ge/Sn-based Dimer Placement Tools," J. Comput. Theor. Nanosci. 3(February 2006):28-41; http://www.MolecularAssembler.com/Papers/JCTNPengFeb06.pdf. Berhane Temelso, C. David Sherrill, Ralph C. Merkle, Robert A. Freitas Jr., "High-level *Ab Initio* Studies of Hydrogen Abstraction from Prototype Hydrocarbon Systems," J. Phys. Chem. A 110(28 September 2006):11160-11173; http://pubs.acs.org/cgi-bin/abstract.cgi/jpcafh/2006/110/i38/abs/jp061821e.html (abstract), http://www.MolecularAssembler.com/Papers/TemelsoHAbst.pdf (paper). Berhane Temelso, C. David Sherrill, Ralph C. Merkle, Robert A. Freitas Jr., "*Ab Initio* Thermochemistry of the Hydrogenation of Hydrocarbon Radicals Using Silicon, Germanium, Tin and Lead Substituted Methane and Isobutane," J. Phys. Chem. A 111(15 August 2007):8677-8688. http://pubs.acs.org/cgi-bin/abstract.cgi/jpcafh/asap/abs/jp071797k.html (abstract), http://www.MolecularAssembler.com/Papers/TemelsoHDon.pdf (paper). Ralph C. Merkle, Robert A.

mechanosynthesis (DMS). DMS is the controlled addition of individual carbon atoms, carbon dimers (C_2), single methyl (CH_3) or like groups to the growth surface of a diamond crystal lattice workpiece in a vacuum manufacturing environment. Covalent chemical bonds are formed one by one as the result of positionally constrained mechanical forces applied at the tip of a scanning probe microscope (SPM) apparatus. Programmed sequences of carbon dimer placement on growing diamond surfaces *in vacuo* appear feasible in theory,[319] as illustrated by the hypothetical DCB6Ge tooltip which is shown depositing two carbon atoms on a diamond surface in Figure 2-40.

The first experimental proof that individual atoms could be manipulated was obtained by IBM scientists in 1989 when they used a scanning tunneling microscope to precisely position 35 xenon atoms on a nickel surface to spell out the corporate logo "IBM" (Figure I-12).[320] However, this feat did not involve the formation of covalent chemical bonds. One important step toward the practical realization of DMS was achieved in 1999 by Ho and Lee,[321] who achieved the first site-

---

Freitas Jr., "Theoretical analysis of a carbon-carbon dimer placement tool for diamond mechanosynthesis," J. Nanosci. Nanotechnol. 3(August 2003):319-324; http://www.rfreitas.com/Nano/JNNDimerTool.pdf. See also: Ralph C. Merkle, Robert A. Freitas Jr., "Theoretical analysis of a carbon-carbon dimer placement tool for diamond mechanosynthesis," paper presented at the 10th Foresight Conference on Molecular Nanotechnology, October 2002; http://www.foresight.org/Conferences/MNT10/Abstracts/Merkle/index.html. Ralph C. Merkle, "A proposed 'metabolism' for a hydrocarbon assembler," Nanotechnology 8(1997):149-162; http://www.zyvex.com/nanotech/hydroCarbonMetabolism.html. K. Eric Drexler, Nanosystems: Molecular Machinery, Manufacturing, and Computation, John Wiley & Sons, New York, 1992, Chapter 8. David J. Mann, Jingping Peng, Robert A. Freitas Jr., Ralph C. Merkle, "Theoretical analysis of diamond mechanosynthesis. Part II. C_2 mediated growth of diamond C(110) surface via Si/Ge-triadamantane dimer placement tools," J. Comput. Theor. Nanosci. 1(March 2004):71-80; http://www.MolecularAssembler.com/JCTNMannMar04.pdf. Damian G. Allis, K. Eric Drexler, "Design and Analysis of a Molecular Tool for Carbon Transfer in Mechanosynthesis," J. Comput. Theor. Nanosci. 2(March 2005):45-55; http://e-drexler.com/d/05/00/DC10C-mechanosynthesis.pdf. Robert A. Freitas Jr., "A simple tool for positional diamond mechanosynthesis, and its method of manufacture," U.S. Provisional Patent Application No. 60/543,802, filed 11 February 2004; U.S. Patent Pending, 11 February 2005; http://www.MolecularAssembler.com/Papers/DMSToolbuildProvPat.htm. Robert A. Freitas Jr., Damian G. Allis, Ralph C. Merkle, "Horizontal Ge-Substituted Polymantane-Based C_2 Dimer Placement Tooltip Motifs for Diamond Mechanosynthesis," J. Comput. Theor. Nanosci. 4(May 2007):433-442; http://www.MolecularAssembler.com/Papers/DPTMotifs.pdf.

[319] Robert A. Freitas Jr., Ralph C. Merkle, "A Minimal Toolset for Positional Diamond Mechanosynthesis," J. Comput. Theor. Nanosci. 5(May 2008):760-861. Jingping Peng, Robert A. Freitas Jr., Ralph C. Merkle, James R. Von Ehr, John N. Randall, George D. Skidmore, "Theoretical Analysis of Diamond Mechanosynthesis. Part III. Positional C_2 Deposition on Diamond C(110) Surface using Si/Ge/Sn-based Dimer Placement Tools," J. Comput. Theor. Nanosci. 3(February 2006):28-41; http://www.MolecularAssembler.com/Papers/JCTNPengFeb06.pdf.

[320] D.M. Eigler, E.K. Schweizer, "Positioning Single Atoms with a Scanning Tunnelling Microscope," Nature 344(5 April 1990):524-526; http://www.nature.com/nature/journal/v344/n6266/abs/344524a0.html (abstract).

[321] Wilson Ho, Hyojune Lee, "Single bond formation and characterization with a scanning tunneling microscope," Science 286(26 November 1999):1719-1722; http://www.physics.uci.edu/~wilsonho/stm-iets.html.

repeatable site-specific covalent bonding operation of a two diatomic carbon-containing molecules (CO), one after the other, to the same atom of iron on a crystal surface, using an SPM – and there have been many other experimental demonstrations of single-molecule chemistry.[322]

Figure 2-40. DCB6Ge tooltip shown depositing two carbon atoms on a diamond surface.[323]

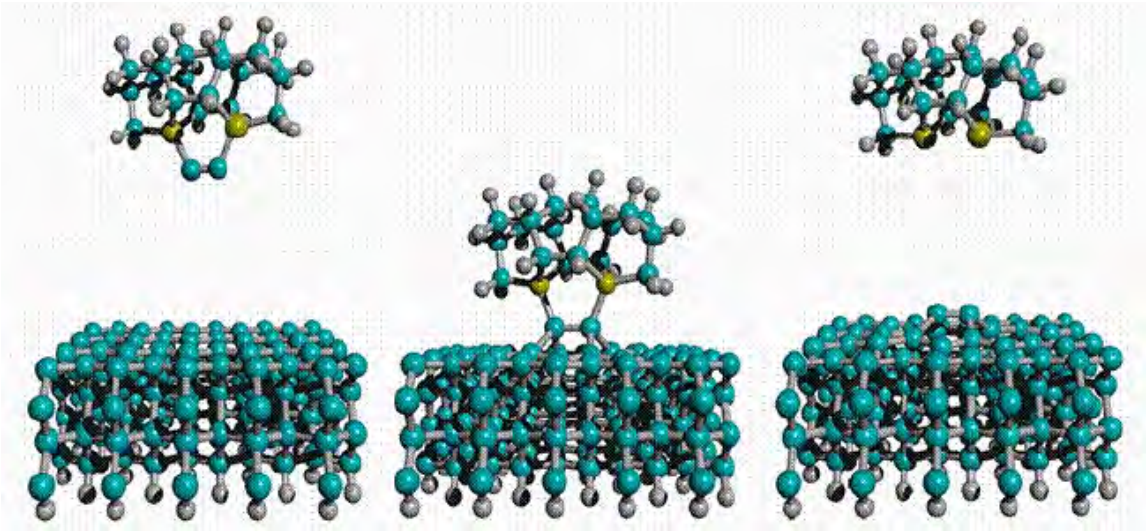

The first experimental demonstration of true mechanosynthesis, establishing covalent bonds using purely mechanical forces – albeit on silicon atoms, not carbon atoms – was reported in 2003 by Oyabu and colleagues[324] in the Custance group. In this landmark experiment, the researchers vertically manipulated single silicon atoms from the Si(111)–(7×7) surface, using a low-temperature near-contact atomic force microscope to demonstrate (1) removal of a selected

---

[322] Saw-Wai Hla, Ludwig Bartels, Gerhard Meyer, Karl-Heinz Rieder, "Inducing All Steps of a Chemical Reaction with the Scanning Tunneling Microscope Tip: Towards Single Molecule Engineering," Phys. Rev. Lett. 85(September 2000):2777-2780; http://prola.aps.org/abstract/PRL/v85/i13/p2777_1 (abstract), http://www.phy.ohiou.edu/~hla/HLA2000-2.pdf (paper). B.C. Stipe et al, Phys. Rev. Lett. 78(1997):4410. J.R. Hahn, W. Ho, Phys. Rev. Lett. 87(2001):166102. Jascha Repp, Gerhard Meyer, Sami Paavilainen, Fredrik E. Olsson, Mats Persson, "Imaging bond formation between a gold atom and pentacene on an insulating surface," Science 312(26 May 2006):1196-1199.

[323] Nanofactory Collaboration website, accessed February 2008; http://www.MolecularAssembler.com/Nanofactory.

[324] Noriaki Oyabu, Oscar Custance, Insook Yi, Yasuhiro Sugawara, Seizo Morita, "Mechanical vertical manipulation of selected single atoms by soft nanoindentation using near contact atomic force microscopy," Phys. Rev. Lett. 90(2 May 2003):176102; http://link.aps.org/abstract/PRL/v90/e176102 (Abstract) http://focus.aps.org/story/v11/st19 (APS story).

silicon atom from its equilibrium position without perturbing the (7×7) unit cell and (2) the deposition of a single Si atom on a created vacancy, both via purely mechanical processes. They later repeated the same feat with a Ge atom.[325]

Following prior theoretical proposals[326] for experimental investigations, participants in the Nanofactory Collaboration[327] began planning work designed to achieve DMS with carbon and hydrogen atoms using an SPM apparatus (Section 2.3.3). (Both positionally controlled surface assembly of DNA-based structures using an AFM tip[328] and protein mechanosynthesis,[329] along with mechanically-augmented[330] and sonomechanically-augmented[331] organic chemical reaction rates, have already been demonstrated experimentally.)

There is a growing realization of the importance of tip-based methods in the field of nanoscale manufacturing. For example, in 2007 DARPA issued a Broad Agency Announcement (BAA) soliciting proposals on Tip-Based Nanofabrication to make nanowires, nanotubes, or quantum dots using functionalized scanning probe tips.[332] Similarly in 2007, Johannes et al.[333] reported

---

[325] N. Oyabu, O. Custance, M. Abe, S. Moritabe, "Mechanical Vertical Manipulation of Single Atoms on the Ge(111)-c(2x8) Surface by Noncontact Atomic Force Microscopy," Abstracts of Seventh International Conference on non-contact Atomic Force Microscopy, Seattle, Washington, USA, 12-15 September, 2004, p.34; http://www.engr.washington.edu/epp/afm/abstracts/15Oyabu2.pdf.

[326] Robert A. Freitas Jr., Ralph C. Merkle, "A Minimal Toolset for Positional Diamond Mechanosynthesis," J. Comput. Theor. Nanosci. 5(May 2008):760-861. Robert A. Freitas Jr., "A simple tool for positional diamond mechanosynthesis, and its method of manufacture," U.S. Provisional Patent Application No. 60/543,802, filed 11 February 2004; U.S. Patent Pending, 11 February 2005; http://www.MolecularAssembler.com/Papers/DMSToolbuildProvPat.htm.

[327] Nanofactory Collaboration website, accessed February 2008; http://www.MolecularAssembler.com/Nanofactory.

[328] S.K. Kufer, E.M. Puchner, H. Gumpp, T. Liedl, H.E. Gaub, "Single-Molecule Cut-and-Paste Surface Assembly," Science 319(1 February 2008):594-596.

[329] T.P. Sullivan, M.L. Van Poll, P.Y. Dankers, W.T. Huck, "Forced Peptide Synthesis in Nanoscale Confinement under Elastomeric Stamps," Angew. Chem. Int. Ed. Engl. 43(13 August 2004):4190-4193.

[330] F. Kersey, W.C. Yount, S.L. Craig, "Single Molecule Force Spectroscopy of Bimolecular Reactions: System Homology in the Mechanical Activation of Ligand Substitution Reactions," J. Am. Chem. Soc. 128(2006):3886-3887, http://pubs.acs.org/cgi-bin/abstract.cgi/jacsat/2006/128/i12/abs/ja058516b.html; see also http://www.sciencemag.org/cgi/reprint/311/5767/1525c.pdf.

[331] C.R. Hickenboth, J.S. Moore, S.R. White, N.R. Sottos, J. Baudry, S.R. Wilson, "Biasing reaction pathways with mechanical force," Nature 446(22 March 2007):423-427.

[332] T. Kenny, "Tip-Based Nanofabrication (TBN)," Defense Advanced Research Projects Agency (DARPA)/Microsystems Technology Office (MTO), Broad Agency Announcement BAA 07-59, July 2007; http://www.fbo.gov/spg/ODA/DARPA/CMO/BAA07-59/listing.html.

[333] Matthew S. Johannes, Daniel G. Cole, Robert L. Clark, "Three-dimensional design and replication of silicon oxide nanostructures using an atomic force microscope," Nanotechnology 18(2007):345304.

using an AFM to draw patterns of local anodic oxidation on a silicon substrate, yielding 3D silicon dioxide structures with ~100 nm features in the shapes of circles, triangles, and stars (Figure 2-41). Note, however, that neither method specifies sufficient positional resolution to accomplish atomically precise manufacturing (Table 2-5).

Figure 2-41. Design and replication of select 3D nanostructures: (a) CAD design of desired features; (b)-(d) contact AFM height images of resulting structures. The sample structures are about 100 nm in feature size, using silicon oxide.[334]

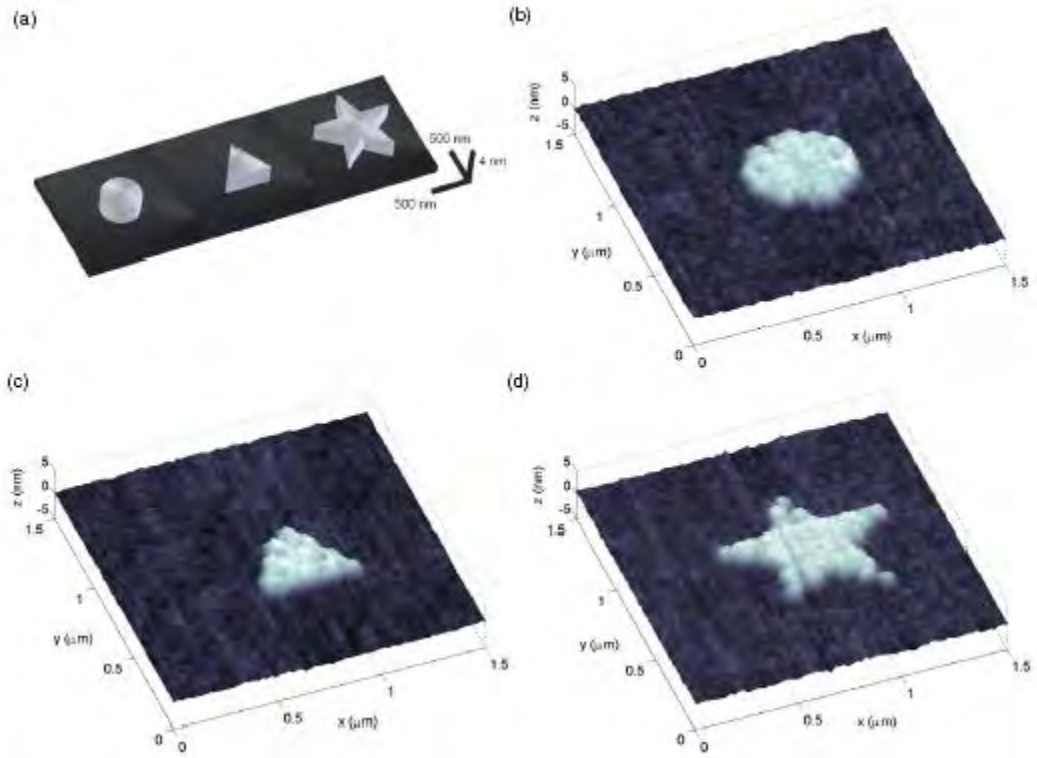

[334] Matthew S. Johannes, Daniel G. Cole, Robert L. Clark, "Three-dimensional design and replication of silicon oxide nanostructures using an atomic force microscope," Nanotechnology 18(2007):345304.

Table 2-5. Metrics in DARPA BAA for Tip-Based Nanomanufacturing[335]				
Metric	**Unit**	***Phase I***	***Phase II***	***Phase III***
Feature Position Control	nm	50	25	5
Feature Size Control	% of dimension	10%	3%	1%
Heterogeneity		2 values of one parameter	5 values of 2 parameters	Continuous control over 2 parameters
Feature Rate		1/min Single tip	5/min/tip 5-tip array	60/min/tip 30-tip array
Tip Shape Variation	% of dimension	Height < 10% Radius < 20% 100 operations	Height < 10% Radius < 20% 10^3 operations	Height < 10% Radius < 20% 10^6 operations
Tip Height Sensing	nm	20 nm	10 nm	2 nm

Two-handed coordinated micromanipulation under the view of an SEM was demonstrated in 1993,[336] followed by the first microscale AFM in 1995.[337] In 1998, Zyvex demonstrated the first simultaneous coordinated operation of three independently controlled AFM tips within the same workspace at different orientations;[338] Zyvex's custom piezoelectric vacuum manipulator achieved positional resolutions comparable to SPMs along with the ability to manipulate objects along one rotational and three linear degrees of freedom with 0.1 nm spatial resolution, allowing the simultaneous coordinated operation of three independently controlled AFM tips within the same workspace, at different orientations. A successor 4-tip system was designed as early as 1999 and finally offered as a commercial product starting in 2003. Recent work has proceeded to even more tooltips[339] and degrees of freedom (Section 3.2.1.5).

---

[335] T. Kenny, "Tip-Based Nanofabrication (TBN)," Defense Advanced Research Projects Agency (DARPA)/Microsystems Technology Office (MTO), Broad Agency Announcement BAA 07-59, July 2007; http://www.fbo.gov/spg/ODA/DARPA/CMO/BAA07-59/listing.html.

[336] Hiroshi Morishita, Yotaro Hatamura, "Development of Ultra Micro Manipulator System Under Stereo SEM Observation," Proc. 1993 IEEE/RSJ Intl. Conf. on Intelligent Robots and Systems, 26-30 July 1993, Yokohama, Japan, Volume 3, pp. 1717-1721.

[337] Y. Xu, N.C. MacDonald, S.A Miller, "Integrated micro-scanning tunneling microscope," Appl. Phys. Lett. 67(1995):2305-2307.

[338] MinFeng Yu, Mark J. Dyer, George D. Skidmore, Henry W. Rohrs, Xue Kun Lu, Kevin D. Ausman, James Von Ehr, Rodney S. Ruoff, "3 dimensional manipulation of carbon nanotubes under a scanning electron microscope," 6th Foresight Nanotechnology Conference, November 1998; http://www.foresight.org/Conferences/MNT6/Papers/Yu/index.html. Robert F. Service, "AFMs wield parts for nanoconstruction," Science 282(27 November 1998):1620-1621.

[339] Jason J. Gorman, Yong-Sik Kim, András E. Vladár, Nicholas G. Dagalakis, "Design of an on-chip microscale nanoassembly system," Int. J. Nanomanufacturing 1(2007):710-721.

2.3.2 Designing a Minimal Toolset for DMS

It is already possible to synthesize bulk diamond today. In a process somewhat reminiscent of spray painting, layer after layer of diamond can be built up by holding a cloud of reactive hydrogen atoms and hydrocarbon molecules over a deposition surface. When these molecules bump into the surface they change it by adding, removing, or rearranging atoms. By carefully controlling the pressure, temperature, and the exact composition of the gas in this process – called chemical vapor deposition or CVD – conditions can be created that favor the growth of diamond on the surface. But randomly bombarding a surface with reactive molecules does not offer fine control over the growth process and lacks atomic-level positional control. To achieve molecularly precise fabrication, the first challenge is to make sure that all chemical reactions will occur at precisely specified places on the surface. A second problem is how to make the diamond surface reactive at the particular spots where we want to add another atom or molecule. A diamond surface is normally covered with a layer of hydrogen atoms. Without this layer, the raw diamond surface would be highly reactive because it would be studded with unused (or "dangling") bonds from the topmost plane of carbon atoms. While hydrogenation prevents unwanted reactions, it also renders the entire surface inert, making it difficult to add carbon (or anything else) to it.

To overcome these problems, we're trying to use a set of molecular-scale tools that would, in a series of well-defined steps, prepare the surface and create hydrocarbon structures on a layer of diamond, atom by atom and molecule by molecule. A mechanosynthetic tool typically has two principal components – a chemically active tooltip and a chemically inert handle to which the tooltip is covalently bonded. The tooltip is the part of the tool where chemical reactions are forced to occur. The much larger handle structure is big enough to be grasped and positionally manipulated using an SPM or similar macroscale instrumentality. At least three types of basic mechanosynthetic tools (Figure 2-42) have already received considerable theoretical (and some experimental) study[340] and are likely among those required to build molecularly precise diamond via positional control:

---

[340] "Annotated Bibliography on Diamond Mechanosynthesis," Nanofactory Collaboration website, accessed February 2008; http://www.MolecularAssembler.com/Nanofactory/AnnBibDMS.htm.

Figure 2-42. Examples of three basic mechanosynthetic tooltypes that are required to build molecularly precise diamond via positional control (black = C atoms, yellow = Ge atoms, white = H atoms).[341]

(A) Hydrogen Abstraction Tool	(B) Hydrogen Donation Tool	(C) Carbon Placement Tool
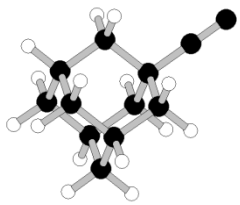	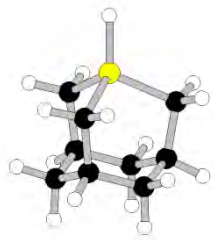	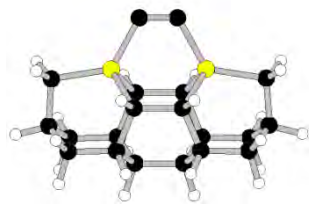

(1) **Hydrogen Abstraction Tools**. The first step in the process of mechanosynthetic fabrication of diamond might be to remove a hydrogen atom from each of two specific adjacent spots on the diamond surface, leaving behind two reactive dangling bonds. This could be done using a hydrogen abstraction tool[342] that has a high chemical affinity for hydrogen at one end but is elsewhere inert (Figure 2-42(A)). The tool's unreactive region serves as a handle or handle attachment point. The tool would be held by a molecular positional device, initially perhaps a scanning probe microscope tip but ultimately a molecular robotic arm, and moved directly over particular hydrogen atoms on the surface. One suitable molecule for a hydrogen abstraction tool is the acetylene or "ethynyl" radical, comprised of two carbon atoms triply bonded together. One carbon of the two serves as the handle connection, and would bond to a nanoscale positioning tool through a much larger handle structure perhaps consisting of a lattice of adamantane cages as shown in Figure 2-43. The other carbon of the two has a dangling bond where a hydrogen atom would normally be present in a molecule of ordinary acetylene (C_2H_2). The working environment around the tool would be inert (e.g., vacuum or a noble gas such as neon).

---

[341] Robert A. Freitas Jr., Ralph C. Merkle, "A Minimal Toolset for Positional Diamond Mechanosynthesis," J. Comput. Theor. Nanosci. 5(May 2008):760-861.

[342] Berhane Temelso, C. David Sherrill, Ralph C. Merkle, Robert A. Freitas Jr., "High-level *Ab Initio* Studies of Hydrogen Abstraction from Prototype Hydrocarbon Systems," J. Phys. Chem. A 110(28 September 2006):11160-11173; http://pubs.acs.org/cgi-bin/abstract.cgi/jpcafh/2006/110/i38/abs/jp061821e.html (abstract), http://www.MolecularAssembler.com/Papers/TemelsoHAbst.pdf (paper).

Figure 2-43. Recyclable DCB6Ge tooltip with "Xtip" crossbar handle motif[343] (left), which is then inverted and mounted on a massive diamond rod handle structure (right).

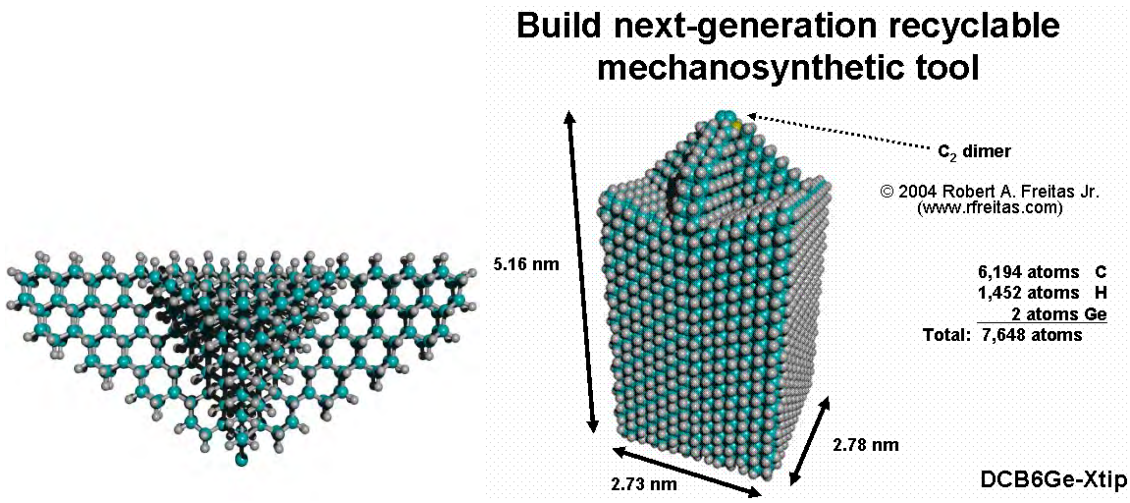

(2) **Hydrogen Donation Tools**. After a molecularly precise structure has been fabricated by a succession of hydrogen abstractions and carbon depositions, the fabricated structure must be passivated to prevent additional unplanned reactions. While the hydrogen abstraction tool is intended to make an inert structure reactive by creating a dangling bond, the hydrogen donation tool[344] does the opposite. It makes a reactive structure inert by terminating a dangling bond. Such a tool would be used to stabilize reactive surfaces and help prevent the surface atoms from rearranging in unexpected and undesired ways. The key requirement for a hydrogen donation tool is that it include a weakly attached hydrogen atom. Many molecules fit that description, but the bond between hydrogen and germanium is sufficiently weak so that a Ge-based hydrogen donation tool (Figure 2-42(B)) should be effective.

(3) **Carbon Placement Tools**. After the abstraction tool has created adjacent reactive spots by selectively removing hydrogen atoms from the diamond surface but before the surface is

---

[343] Jingping Peng, Robert A. Freitas Jr., Ralph C. Merkle, James R. Von Ehr, John N. Randall, George D. Skidmore, "Theoretical Analysis of Diamond Mechanosynthesis. Part III. Positional C_2 Deposition on Diamond C(110) Surface using Si/Ge/Sn-based Dimer Placement Tools," J. Comput. Theor. Nanosci. 3(February 2006):28-41; http://www.MolecularAssembler.com/Papers/JCTNPengFeb06.pdf.

[344] Berhane Temelso, C. David Sherrill, Ralph C. Merkle, Robert A. Freitas Jr., "*Ab Initio* Thermochemistry of the Hydrogenation of Hydrocarbon Radicals Using Silicon, Germanium, Tin and Lead Substituted Methane and Isobutane," J. Phys. Chem. A 111(15 August 2007):8677-8688. http://pubs.acs.org/cgi-bin/abstract.cgi/jpcafh/asap/abs/jp071797k.html (abstract), http://www.MolecularAssembler.com/Papers/TemelsoHDon.pdf (paper).

re-passivated by hydrogen, carbon placement tools may be used to deposit carbon atoms at the desired reactive surface sites. In this way a diamond structure would be built on the surface, molecule by molecule, according to plan. The first *complete* tool ever proposed for this carbon deposition function is the "DCB6Ge" dimer placement tool[345] – in this example, a carbon (C_2) dimer having two carbon atoms connected by a triple bond with each carbon in the dimer connected to a larger unreactive handle structure through two germanium atoms (Figure 2-42(C)). This dimer placement tool, also held by a molecular positional device, is brought close to the reactive spots along a particular trajectory, causing the two dangling surface bonds to react with the ends of the carbon dimer. The dimer placement tool would then withdraw, breaking the relatively weaker bonds between it and the C_2 dimer and transferring the carbon dimer from the tool to the surface, as illustrated in Figure 2-40. A positionally controlled dimer could be bonded at many different sites on a growing diamondoid workpiece, in principle allowing the construction of a wide variety of useful nanopart shapes. As of 2008, the DCB6Ge dimer placement tool remains the most intensively studied of any mechanosynthetic tooltip to date,[346] having had more than 150,000 CPU-hours of computation invested thus far in its analysis, and it remains the only DMS tooltip motif that has been successfully simulated and validated for its intended function on a full 200-atom diamond surface model.[347] Other proposed dimer (and

---

[345] Ralph C. Merkle, Robert A. Freitas Jr., "Theoretical analysis of a carbon-carbon dimer placement tool for diamond mechanosynthesis," J. Nanosci. Nanotechnol. 3(August 2003):319-324; http://www.rfreitas.com/Nano/JNNDimerTool.pdf. See also: Ralph C. Merkle, Robert A. Freitas Jr., "Theoretical analysis of a carbon-carbon dimer placement tool for diamond mechanosynthesis," paper presented at the 10th Foresight Conference on Molecular Nanotechnology, October 2002; http://www.foresight.org/Conferences/MNT10/Abstracts/Merkle/index.html.

[346] Robert A. Freitas Jr., Ralph C. Merkle, "A Minimal Toolset for Positional Diamond Mechanosynthesis," J. Comput. Theor. Nanosci. 5(May 2008):760-861. Jingping Peng, Robert A. Freitas Jr., Ralph C. Merkle, James R. Von Ehr, John N. Randall, George D. Skidmore, "Theoretical Analysis of Diamond Mechanosynthesis. Part III. Positional C_2 Deposition on Diamond C(110) Surface using Si/Ge/Sn-based Dimer Placement Tools," J. Comput. Theor. Nanosci. 3(February 2006):28-41; http://www.MolecularAssembler.com/Papers/JCTNPengFeb06.pdf. Ralph C. Merkle, Robert A. Freitas Jr., "Theoretical analysis of a carbon-carbon dimer placement tool for diamond mechanosynthesis," J. Nanosci. Nanotechnol. 3(August 2003):319-324; http://www.rfreitas.com/Nano/JNNDimerTool.pdf. See also: Ralph C. Merkle, Robert A. Freitas Jr., "Theoretical analysis of a carbon-carbon dimer placement tool for diamond mechanosynthesis," paper presented at the 10th Foresight Conference on Molecular Nanotechnology, October 2002; http://www.foresight.org/Conferences/MNT10/Abstracts/Merkle/index.html. David J. Mann, Jingping Peng, Robert A. Freitas Jr., Ralph C. Merkle, "Theoretical analysis of diamond mechanosynthesis. Part II. C_2 mediated growth of diamond C(110) surface via Si/Ge-triadamantane dimer placement tools," J. Comput. Theor. Nanosci. 1(March 2004):71-80; http://www.MolecularAssembler.com/JCTNMannMar04.pdf. Robert A. Freitas Jr., "A simple tool for positional diamond mechanosynthesis, and its method of manufacture," U.S. Provisional Patent Application No. 60/543,802, filed 11 February 2004; U.S. Patent Pending, 11 February 2005; http://www.MolecularAssembler.com/Papers/DMSToolbuildProvPat.htm. Robert A. Freitas Jr., Damian G. Allis, Ralph C. Merkle, "Horizontal Ge-Substituted Polymantane-Based C_2 Dimer Placement Tooltip Motifs for Diamond Mechanosynthesis," J. Comput. Theor. Nanosci. 4(May 2007):433-442; http://www.MolecularAssembler.com/Papers/DPTMotifs.pdf.

[347] Jingping Peng, Robert A. Freitas Jr., Ralph C. Merkle, James R. Von Ehr, John N. Randall, George D. Skidmore, "Theoretical Analysis of Diamond Mechanosynthesis. Part III. Positional C_2 Deposition on

related carbon transfer) tooltip motifs[348] have received less extensive study but are also expected to perform well.

In 2007, Freitas and Merkle[349] completed a three-year project to computationally analyze a comprehensive set of DMS reactions and an associated minimal set of 9 tooltips (Figure 2-44) that could be used to build basic diamond, graphene (e.g., carbon nanotubes), and all of the tools themselves including all necessary tool recharging reactions. The research defined 65 DMS reaction sequences incorporating 328 reaction steps, with 354 pathological side reactions analyzed and with 1,321 unique individual DFT-based (Density Functional Theory) quantum chemistry reaction energies reported. (These mechanosynthetic reaction sequences range in length from 1-13 reaction steps (typically 4) with 0-10 possible pathological side reactions or rearrangements (typically 3) reported per reaction step.) One typical sequence – used to recharge a spent hydrogen abstraction tool – is Reaction Sequence RS5, illustrated in Figure 2-45. For the first time, this toolset provides clear developmental targets for a comprehensive near-term DMS implementation program – specifically, the nanofactory development program that is presented in this proposal.

Diamond C(110) Surface using Si/Ge/Sn-based Dimer Placement Tools," J. Comput. Theor. Nanosci. 3(February 2006):28-41; http://www.MolecularAssembler.com/Papers/JCTNPengFeb06.pdf.

[348] Robert A. Freitas Jr., Ralph C. Merkle, "A Minimal Toolset for Positional Diamond Mechanosynthesis," J. Comput. Theor. Nanosci. 5(May 2008):760-861. Ralph C. Merkle, Robert A. Freitas Jr., "Theoretical analysis of a carbon-carbon dimer placement tool for diamond mechanosynthesis," J. Nanosci. Nanotechnol. 3(August 2003):319-324; http://www.rfreitas.com/Nano/JNNDimerTool.pdf. See also: Ralph C. Merkle, Robert A. Freitas Jr., "Theoretical analysis of a carbon-carbon dimer placement tool for diamond mechanosynthesis," paper presented at the 10th Foresight Conference on Molecular Nanotechnology, October 2002; http://www.foresight.org/Conferences/MNT10/Abstracts/Merkle/index.html. Ralph C. Merkle, "A proposed 'metabolism' for a hydrocarbon assembler," Nanotechnology 8(1997):149-162; http://www.zyvex.com/nanotech/hydroCarbonMetabolism.html. K. Eric Drexler, Nanosystems: Molecular Machinery, Manufacturing, and Computation, John Wiley & Sons, New York, 1992, Chapter 8. Damian G. Allis, K. Eric Drexler, "Design and Analysis of a Molecular Tool for Carbon Transfer in Mechanosynthesis," J. Comput. Theor. Nanosci. 2(March 2005):45-55; http://e-drexler.com/d/05/00/DC10C-mechanosynthesis.pdf. Robert A. Freitas Jr., Damian G. Allis, Ralph C. Merkle, "Horizontal Ge-Substituted Polymantane-Based C_2 Dimer Placement Tooltip Motifs for Diamond Mechanosynthesis," J. Comput. Theor. Nanosci. 4(May 2007):433-442; http://www.MolecularAssembler.com/Papers/DPTMotifs.pdf.

[349] Robert A. Freitas Jr., Ralph C. Merkle, "A Minimal Toolset for Positional Diamond Mechanosynthesis," J. Comput. Theor. Nanosci. 5(May 2008):760-861.

Figure 2-44. A minimal toolset for diamond mechanosynthesis, including primary, auxiliary, and compound tools.[350] Only tooltips are shown. In an actual DMS toolhead, the tooltips would be mounted on a large diamond rod handle structure as shown in Figure 2-43.

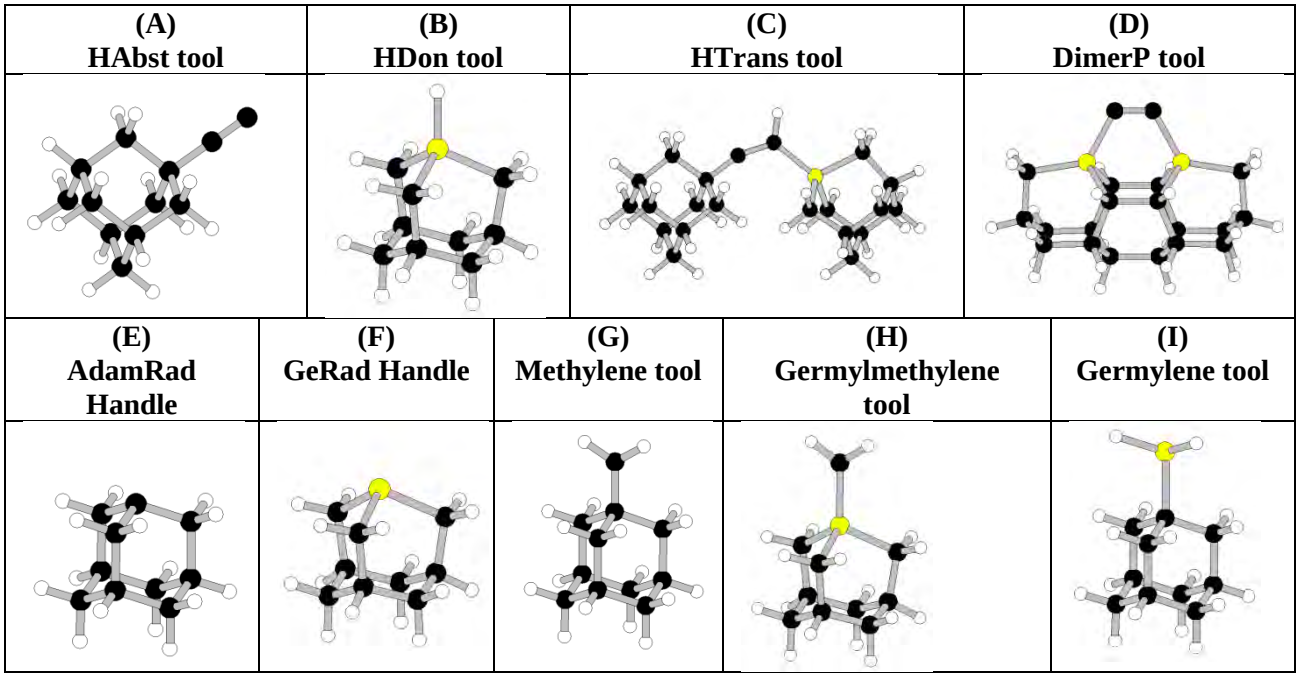

[350] Robert A. Freitas Jr., Ralph C. Merkle, "A Minimal Toolset for Positional Diamond Mechanosynthesis," J. Comput. Theor. Nanosci. 5(May 2008):760-861.

Figure 2-45. Reaction Sequence RS5: Recharging the hydrogen abstraction tool.[351]

RS5: Recharge HAbst tool
***and* recharge HDon tool from GeRad tool (Step 2)**
[full cage models illustrated]

Step 1	Step 2	Step 3

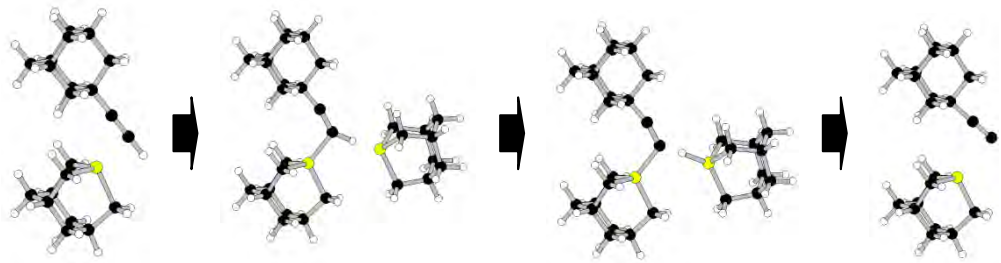

Step	Description of Reaction	Mult.	Ener. (eV)	Barr. (eV)
1	**Join GeRad tool to apical C atom of HAbstH tool**			
	R: HAbstH (ACC0A/28) + GeRad (ACC0A/25)	S+D		
	P: C15FCcis (ACC0A/53) **[≡ HTrans tool]**	D	**-0.43** [a]	
	T: Barrier map minimum from Tarasov et al (2008)			**+0.10** [b]
	P: C15FCtrans (ACC0A/53)	D	-0.55	
	R: CH33Ge (ACC0A/13) + ClusterHAbH (ACC0A/16)	D+S		
	T: R1415Trans-QST3 (ACC1A/29)	D		**+0.27** [b]
1B1	H steal from HAbstH workpiece to GeRad tool			
	R: HAbstH (ACC0A/28) + GeRad (ACC0A/25)	S+D		
	P: HAbst (ACC0A/27) + HDon (ACC0A/26)	D+S	+2.19	
1D1	H migrates to radical site from adjacent CH in chain on HTrans			
	R: C15FCcis (ACC0A/53)	D		
	P: C15FCp2 (ACC0A/53)	D	-0.13	
	T: C15FCp2TS (ACC1A/53)	D		+1.66
1F6	H dissociates from -C●=CH- group on HTrans tool			
	R: S15cis (ACC0A/11)	D		
	P: S16Run0 (ACCCA/10) + H (ACC0A/1)	S+D	+2.68	
2	**Abstract apical H from HAbstH using GeRad tool**			
	R: S15cis (ACC0A/11) + GeRad (ACC0A/25)	D+D		
	P: S16Run0 (ACCCA/10) + HDon (ACC0A/26)	S	**-0.83** [cd]	
	R: S15trans (ACC0A/11) + GeRad (ACC0A/25)	D+D		
	P: S16Run0 (ACCCA/10) + HDon (ACC0A/26)	S	**-0.84** [c]	
2F6	H dissociates from GeRad handle of HDon tool			
	R: HDon (ACC0A/26)	S		
	P: GeRad (ACC0A/25) + H (ACC0A/1)	D+D	+3.51	
2H	Ge● radical bonds to C● adjacent to target CH group			
	R: Cluster15cis (ACC1A/29) + CH33Ge (ACC0A/13)	D+D		
	P: Cluster28cis (ACC0A/42)	S	**-2.66** [e]	
2^1	**Abstract apical H from HAbstH using AdamRad tool**			
	R: S15cis (ACC0A/11) + AdamRad (ACC0A/25)	D+D		
	P: S16Run0 (ACCCA/10) + Adam (ACC0A/26)	S	**-1.43** [c]	

[351] Robert A. Freitas Jr., Ralph C. Merkle, "A Minimal Toolset for Positional Diamond Mechanosynthesis," J. Comput. Theor. Nanosci. 5(May 2008):760-861.

2^1F6	H dissociates from Adam bridgehead site R: HDon (ACC0A/26) P: GeRad (ACC0A/25) + H (ACC0A/1)	 S D+D	 +4.12	
3	**Detach GeRad handle from workpiece** R: C16FC-2 (ACC0A/52) P: HAbst (ACC0A/27) + GeRad (ACC0A/25) *Rotationally constrained:* R: S16Run10 (ACCCA/10) (CC-GeRad angle = 180°) P: CH3CC (ACC0A/6) + GeH3 (ACC0A/4) R: S16Run0 (ACCCA/10) (CC-GeRad angle = 124°) P: CH3CC (ACC0A/6) + GeH3 (ACC0A/4)	 S D+D S D+D S D+D	 +4.81 +4.83 +3.62	
3C4	C≡C steal from workpiece by departing GeRad handle R: C16FC-2 (ACC0A/52) P: AdamRad (ACC0A/25) + GeRadCC (ACC0B/27)	 S D+D	 **+5.06** [f]	

[a] This energy improves to -0.50 eV using an optimal tool approach trajectory as reported by Tarasov et al (2007).
[b] The minimum barrier height improves to +0.10 eV using an optimal tool approach trajectory with full-cage positionally-constrained models producing only a ~0.3 Å deflection at the HAbstH tip prior to bonding, as reported by Tarasov et al (2008).
[c] Deletion of apical H from S15cis (doublet) structure, followed by single point evaluation of the resulting structure either as singlet S16initS (ACC0S/10) or triplet S16initT (ACC1S/10), indicates singlet (C≡C) is significantly preferred (by -2.21 eV) to triplet (●C=C●).
[d] This energy may improve to -1.62 eV using constrained optimally-positioned full-cage models as reported by Tarasov et al (2008), but our more conservative figure is used in the present paper pending a more detailed analysis of the HTrans tool in future work.
[e] This highly exoergic pathology is easily avoided by positional control because the H and C● are 2.07 Å apart, well in excess of the assumed 0.50 Å positional uncertainty.
[f] Even though the reaction energy for pathology 3C4 is only +0.25 eV above the main reaction, this dimer transfer pathology will not occur because C-C bonds (dimer to Adam handle) can withstand greater tensile loads (~5.53 nN) than C-Ge bonds (dimer to GeRad handle) can tolerate (~3.64 nN).

2.3.3 Building the First Mechanosynthetic Tools

The first practical proposal for building a DMS tool experimentally was published by Freitas in 2005 and was the subject of the first mechanosynthesis patent ever filed.[352] According to this proposal, the manufacture of a complete DCB6Ge positional dimer placement tool would require four distinct steps: synthesizing a capped tooltip molecule, attaching it to a deposition surface, attaching a handle to it via CVD, then separating the tool from the deposition surface. The workability of the proposed process has already received valuable criticism from the scientific community and may be sufficiently viable to serve as a vital stepping-stone to more sophisticated DMS approaches.

---

[352] Robert A. Freitas Jr., "A simple tool for positional diamond mechanosynthesis, and its method of manufacture," U.S. Provisional Patent Application No. 60/543,802, filed 11 February 2004; U.S. Patent Pending, 11 February 2005; http://www.MolecularAssembler.com/Papers/DMSToolbuildProvPat.htm.

An even simpler practical proposal for building DMS tools experimentally, also using only experimental methods available today, was published in 2007 by Freitas and Merkle as part of their minimal toolset work[353] (Section 2.3.2). Processes (currently under patent application) are identified for the experimental fabrication of a hydrogen abstraction tool, a hydrogen donation tool, and two alternative carbon placement tools (the Methylene and Germylmethylene tooltips), and these processes and tools are part of the second mechanosynthesis patent ever filed and the first to be filed by the Nanofactory Collaboration.[354] At this writing, Nanofactory Collaboration participants are undertaking preparatory steps (including equipment assessment and securing of funding) leading to direct experimental tests of these proposals to begin in 2008 (Section 3.2.4).

2.3.4 Next Generation Tools and Components

After the ability to fabricate the first primitive DMS tooltips has been demonstrated experimentally and repeatable sub-Angstrom positional placement accuracy for SPM tips has been developed, then-existing primitive tooltips could be manipulated to build the next generation of more precise, more easily rechargeable, and generally much improved mechanosynthetic tools. These more capable tools may include more stable handles of standardized dimensions, such as the rechargeable DCB6Ge dimer placement tool with the more reliable crossbar design[355] shown in Figure 2-43, or tools with more complex handles incorporating moving components (Figure 2-46). The end result of this iterative development process will be a mature set of efficient, positionally controlled mechanosynthetic tools that can reliably build molecularly precise diamondoid structures – including more DMS tools.

---

[353] Robert A. Freitas Jr., Ralph C. Merkle, "A Minimal Toolset for Positional Diamond Mechanosynthesis," J. Comput. Theor. Nanosci. 5(May 2008):760-861.

[354] Robert A. Freitas Jr., Ralph C. Merkle, "Positional Diamond Mechanosynthesis: Toolset, Reactions, Uses and Products," U.S. Provisional Patent Application No. 60/970,658, filed 7 September 2007.

[355] Jingping Peng, Robert A. Freitas Jr., Ralph C. Merkle, James R. Von Ehr, John N. Randall, George D. Skidmore, "Theoretical Analysis of Diamond Mechanosynthesis. Part III. Positional C_2 Deposition on Diamond C(110) Surface using Si/Ge/Sn-based Dimer Placement Tools," J. Comput. Theor. Nanosci. 3(February 2006):28-41; http://www.MolecularAssembler.com/Papers/JCTNPengFeb06.pdf.

Figure 2-46. Mechanosynthetic tooltip incorporating moving components, courtesy of Damian Allis.[356]

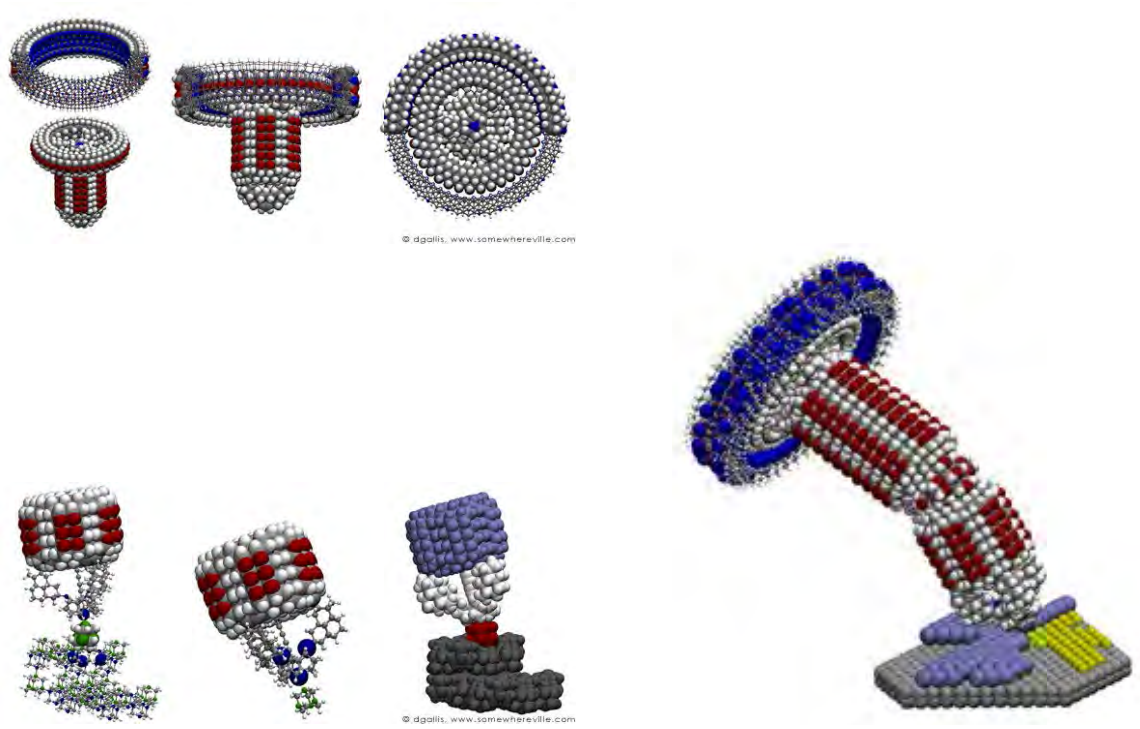

These more sophisticated tools also will be designed to allow building more complex components such as the all-hydrocarbon diamond logic rod (Figure 2-47(A)), a hydrocarbon bearing (Figure 2-47(B)) and a diamond universal joint (Figure 2-47(C)). Once mechanosynthetic tooltips are developed for additional element types, a still wider variety of nanomachines can be fabricated incorporating atoms other than hydrogen, carbon and germanium (e.g., silicon, oxygen, and sulfur). Examples of these diamondoid nanomachines include the speed reduction gear (Figure 2-48(A)), in which the train of gears reduces the speed from the high-speed one on the left to the half-speed one on the right, and the differential gear (Figure 2-48(B)) that smoothly converts mechanical rotation in one direction into mechanical rotation in the opposite direction. The largest molecular machine model that had been simulated as of 2008 using molecular dynamics was the worm drive assembly (Figure 2-48(C)), consisting of 11 separate components and over 25,000 atoms; the two tubular worm gears progress in opposite directions, converting rotary into linear motion. Note that the magnitude of quantum effects is only ~10% of the classical (nonquantum) magnitudes for ~1 nm objects at 300 K, and even less significant for larger objects.[357]

---

[356] Damian Allis, Nanotechnology Gallery; http://www.somewhereville.com/?page_id=10.

[357] K. Eric Drexler, Nanosystems: Molecular Machinery, Manufacturing, and Computation, John Wiley & Sons, New York, 1992, Figure 5.9.

Figure 2-47. Some simple diamond nanoparts and nanodevices: (A) hydrocarbon logic rod, (B) hydrocarbon bearing, and (C) hydrocarbon universal joint.[358]

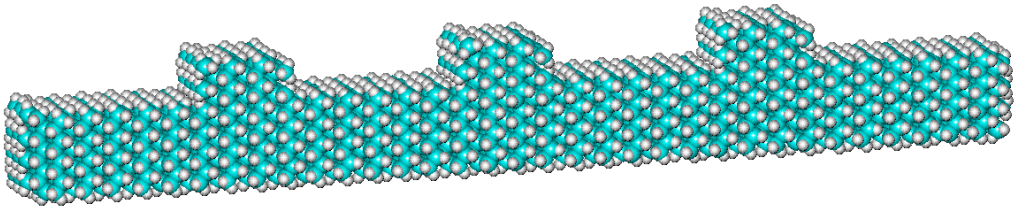

(A)

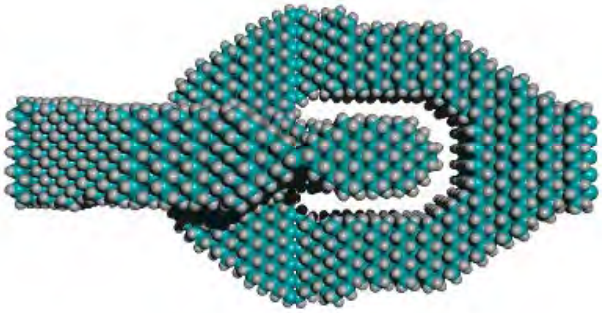

(B) (C)

[358] Nanofactory Collaboration website, accessed February 2008; http://www.MolecularAssembler.com/Nanofactory.

Figure 2-48. More complex mechanical nanodevices: (A) speed reduction gear, above left; (B) interior workings of differential gear, above right; (C) worm drive, below (grey = silicon, white = hydrogen, yellow = sulfur, red = oxygen). Images courtesy of Nanorex.[359]

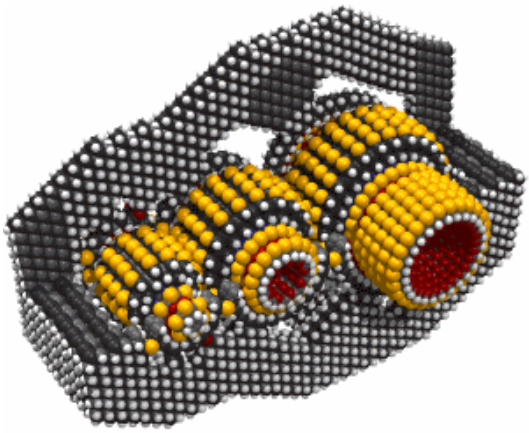

(A)

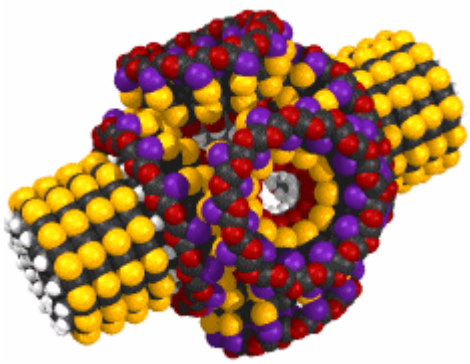

(B)

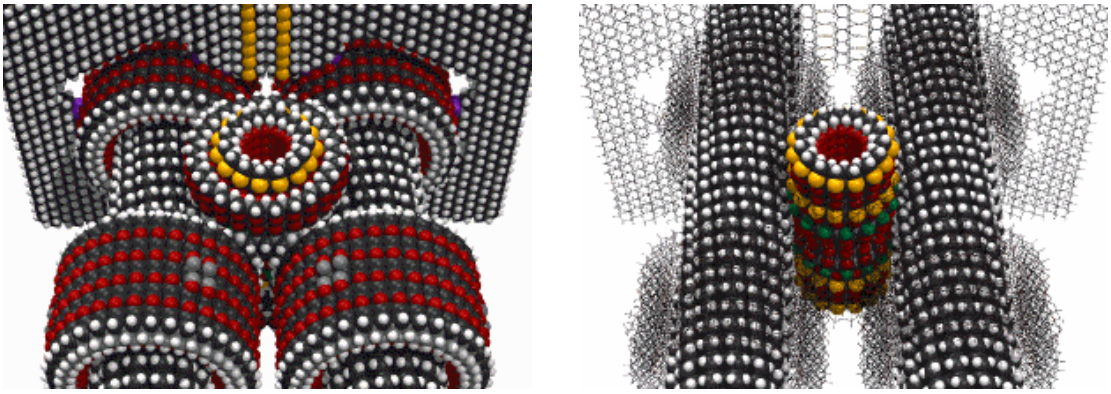

(C)

Using computer-automated tooltips performing positionally-controlled DMS in lengthy programmed sequences of reaction steps, we should be able to fabricate simple diamondoid nanomechanical parts such as bearings, gears, struts, springs, logic rods and casings to atomic precision. Early tools would progress from single DMS tools manipulated by SPM-like mechanisms, to more complex multitip tools and jigs which the simple tools could initially fabricate, one at a time. In a factory production line (Figure 2-49), individual DMS tooltips can be affixed to rigid moving support structures and guided through repeated contact events with workpieces, recharging stations, and other similarly-affixed opposable tooltips. These "molecular mills" could then perform repetitive fabrication steps using simple, efficient mechanisms. Such

---

[359] http://www.nanoengineer-1.com; accessed January 2008.

mills can, in principle, be operated at high speeds – with positionally constrained mechanosynthetic encounters possibly occurring at up to megahertz frequencies.

Figure 2-49. Fabrication of nanoparts using DMS tooltips affixed to rigid moving support structures and guided through repeated contact events with workpieces under computer control in a nanofactory production line. Image courtesy of John Burch.[360]

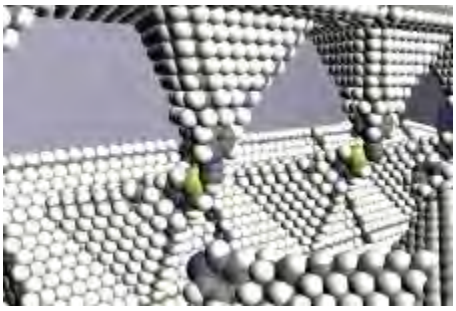

The Nanofactory Collaboration has identified a large number of technical challenges[361] that must be solved before we can progress to building the kinds of complex nanoscale machinery described above. Among the theoretical and design challenges are: (1) nanopart gripper design, (2) nanopart manipulator actuator design, (3) design and simulation of nanopart feedstock presentation systems, (4) design and simulation of workpiece release surfaces, (5) design and simulation of nanopart assembly sequences, and (6) atomic rearrangements in juxtaposed nanoparts. Some experimental challenges include: (1) development of SPM technology to enable nanopart assembly work, (2) fabrication and testing of workpiece release surfaces, and (3) experimental proof-of-principle and early positional assembly demonstration benchmarks.

2.3.5 Nanofactory Strategies for Molecular Manufacturing

The ultimate goal of molecular nanotechnology is to develop a manufacturing technology able to inexpensively manufacture most arrangements of atoms that can be specified in molecular detail – including complex arrangements involving millions or billions of atoms per product object, as in the hypothesized medical nanorobots and other atomically precise macroscale products. This will provide the ultimate manufacturing technology in terms of precision, flexibility, and low cost. But to be practical, molecular manufacturing must also be able to assemble very large numbers of identical nano- or microstructures very quickly. Two central technical objectives thus form the core of our current strategy for diamondoid molecular manufacturing: (1) programmable positional assembly including fabrication of diamondoid structures using

---

[360] John Burch nanofactory website, http://www.lizardfire.com/html_nano/nano.html.

[361] "Remaining technical challenges for achieving positional diamondoid molecular manufacturing and diamondoid nanofactories," Nanofactory Collaboration website, accessed February 2008; http://www.MolecularAssembler.com/Nanofactory/Challenges.htm

molecular feedstock, as discussed above, and (2) massive parallelization of all fabrication and assembly processes, briefly described below.

Molecular manufacturing nanofactory systems capable of massively parallel fabrication[362] might employ, at the lowest level, large arrays of DMS-enabled scanning probe tips all building similar diamondoid product structures in unison. Analogous approaches are found in present-day larger-scale systems. For example, simple mechanical ciliary arrays consisting of 10,000 independent microactuators on a 1 cm^2 chip have been made at the Cornell National Nanofabrication Laboratory for microscale parts transport applications, and similarly at IBM for mechanical data storage applications.[363] Active probe arrays of 10,000 independently-actuated microscope tips have been developed by Mirkin's group at Northwestern University for dip-pen nanolithography[364] using DNA-based "ink". Almost any desired 2D shape can be drawn using 10 tips in concert. A million-tip DPN array has been fabricated by the Micro Nano Technology

---

[362] Robert A. Freitas Jr., Ralph C. Merkle, Kinematic Self-Replicating Machines, Landes Bioscience, Georgetown, TX, 2004; Section 5.7, pp. 182-184; http://www.MolecularAssembler.com/KSRM/5.7.htm.

[363] "1000 Tips for Ultrahigh-Density Data Storage," IBM News, Zurich Research Lab, 11 October 1999, http://www.zurich.ibm.com/news/99/millipede.html; IBM Research: Millipede, http://domino.research.ibm.com/Comm/bios.nsf/pages/millipede.html; P. Vettiger, G. Cross, M. Despont, U. Drechsler, U. Duerig, B. Gotsmann, W. Haeberle, M. Lantz, H. Rothuizen, R. Stutz, G. Binnig, "The Millipede – nanotechnology entering data storage," Technical Report, IBM Zurich Research Lab; http://domino.research.ibm.com/Comm/bios.nsf/pages/millipede.html/$FILE/pv7201-preprint.pdf; also published in: Vettiger P, Cross G, Despont M et al., "The Millipede – nanotechnology entering data storage," IEEE Trans Nanotechnol 1(June 2002):39-55.

[364] Seunghun Hong, Chad A. Mirkin, "A nanoplotter with both parallel and serial writing capabilities," Science 288(9 June 2000):1808-1811; http://www.nanotechnology.northwestern.edu/press/Science%20.Vol288.9june2000.pdf; Ming Zhang, David Bullen, Kee S. Ryu, Chang Liu, S. Hong, S. Chung, Chad Mirkin, "Passive and active probes for dip pen nanolithography," First IEEE Conference on Nanotechnology, 28-30 October 2001, Maui, HI; http://mass.micro.uiuc.edu/publications/papers/64.pdf; D. Bullen, M. Zhang, C. Liu, "Thermal-mechanical optimization of thermally actuated cantilever arrays," Smart Electronics, MEMS, and Nanotechnology Conference (4700), SPIE's 9th Annual International Symposium on Smart Structures and Materials, 17-21 March 2002, San Diego, CA; http://mass.micro.uiuc.edu/publications/papers/70.pdf; Ming Zhang, David Bullen, Sung-Wook Chung, Seunghun Hong, Kee S. Ryu, Zhifang Fan, Chad A. Mirkin, Chang Liu, "A MEMS nanoplotter with high-density parallel dip-pen nanolithography probe arrays," Nanotechnology 13(April 2002):212-217; http://mass.micro.uiuc.edu/publications/papers/72.pdf; X. Wang, D. Bullen, J. Zou, K. Ryu, C. Liu, S.W. Chung, C. Mirkin, "Linear probe arrays for dip-pen nanolithography," Intl. Conf. on Micro & Nano Systems (ICMNS 2002), 11-14 August 2002, Kunming, China; http://mass.micro.uiuc.edu/publications/papers/74.pdf; D. Bullen, S. Chung, X. Wang, J. Zou, C. Liu, Chad Mirkin, "Development of parallel dip pen nanolithography probe arrays for high throughput nanolithography," (Invited) Symposium LL: Rapid Prototyping Technologies, Materials Research Society Fall Meeting, Boston, MA, Proceedings of the MRS, Vol. 758, 2-6 December 2002; http://mass.micro.uiuc.edu/publications/papers/84.pdf; D. Bullen, X. Wang, J. Zou, S. Hong, S. Chung, K. Ryu, Z. Fan, C. Mirkin, C. Liu, "Micromachined arrayed dip pen nanolithography probes for sub-100 nm direct chemistry patterning," Proc. 16th IEEE International Micro Electro Mechanical Systems Conference, MEMS 2003, Kyoto, Japan, 19-23 January 2003; http://mass.micro.uiuc.edu/publications/papers/86.pdf; Jun Zou, David Bullen, Xuefeng Wang, Chang Liu, Chad A. Mirkin, "Conductivity-based contact sensing for probe arrays in dip-pen nanolithography," Appl. Phys. Lett. 83(2003):581.

Research Group at the University of Illinois,[365] and another microcantilever array manufactured by Protiveris Corp. has millions of interdigitated cantilevers on a single chip.[366] Martel's group has investigated using fleets of independently mobile wireless instrumented microrobot manipulators called NanoWalkers to collectively form a nanofactory system that might be used for positional manufacturing operations.[367] Zyvex Corp. (www.zyvex.com) of Richardson TX received a $25 million, five-year, National Institute of Standards and Technology (NIST) contract to develop prototype microscale assemblers using microelectromechanical systems.[368]

At the end of a carefully focused development program, this kind of research can lead to the design of production lines in a nanofactory, both for diamondoid mechanosynthesis and for component assembly operations. Ultimately, medical nanorobots and other atomically precise macroscale products will be manufactured in desktop nanofactories efficiently designed for this purpose. The nanofactory system will include a progression of fabrication and assembly mechanisms at several different physical scales (Figure 2-50). In one conceivable design, at the smallest scale molecular mills could manipulate individual molecules to fabricate successively larger submicron-scale building blocks. These would be passed to larger block assemblers that assemble still larger microblocks, which would themselves be passed to even larger product assemblers that put together the final product. The microblocks could be placed in a specific pattern and sequence following construction blueprints created using a modern "design for assembly" and "Design for Manufacturability" (DFM) philosophy. As plane after plane is completed, the product would extrude outward through the surface of the nanofactory output platform (Figure 2-51).

---

[365] "MNTR Research Focus Slide Show: Passive Parallel DPN Array," 2006, http://mass.micro.uiuc.edu/research/current/nanolithography/2006-focus-intro/slide11.html.

[366] "Microcantilever Arrays," Protiveris Corp., 2003; http://www.protiveris.com/cantilever_tech/microcantileverarrays.html.

[367] S. Martel, I. Hunter, "Nanofactories based on a fleet of scientific instruments configured as miniature autonomous robots," Proc 3rd Intl Workshop on Microfactories; 16-18 Sep 2002; Minneapolis MN, pp. 97-100.

[368] Robert A. Freitas Jr., Ralph C. Merkle, Kinematic Self-Replicating Machines, Landes Bioscience, Georgetown, TX, 2004; Section 4.20, p. 144; http://www.MolecularAssembler.com/KSRM/4.20.htm.

Figure 2-50. Assembly of nanoparts into larger components and product structures using mechanical manipulators at various size scales on interconnected production lines inside a diamondoid nanofactory. Images courtesy of John Burch.[369]

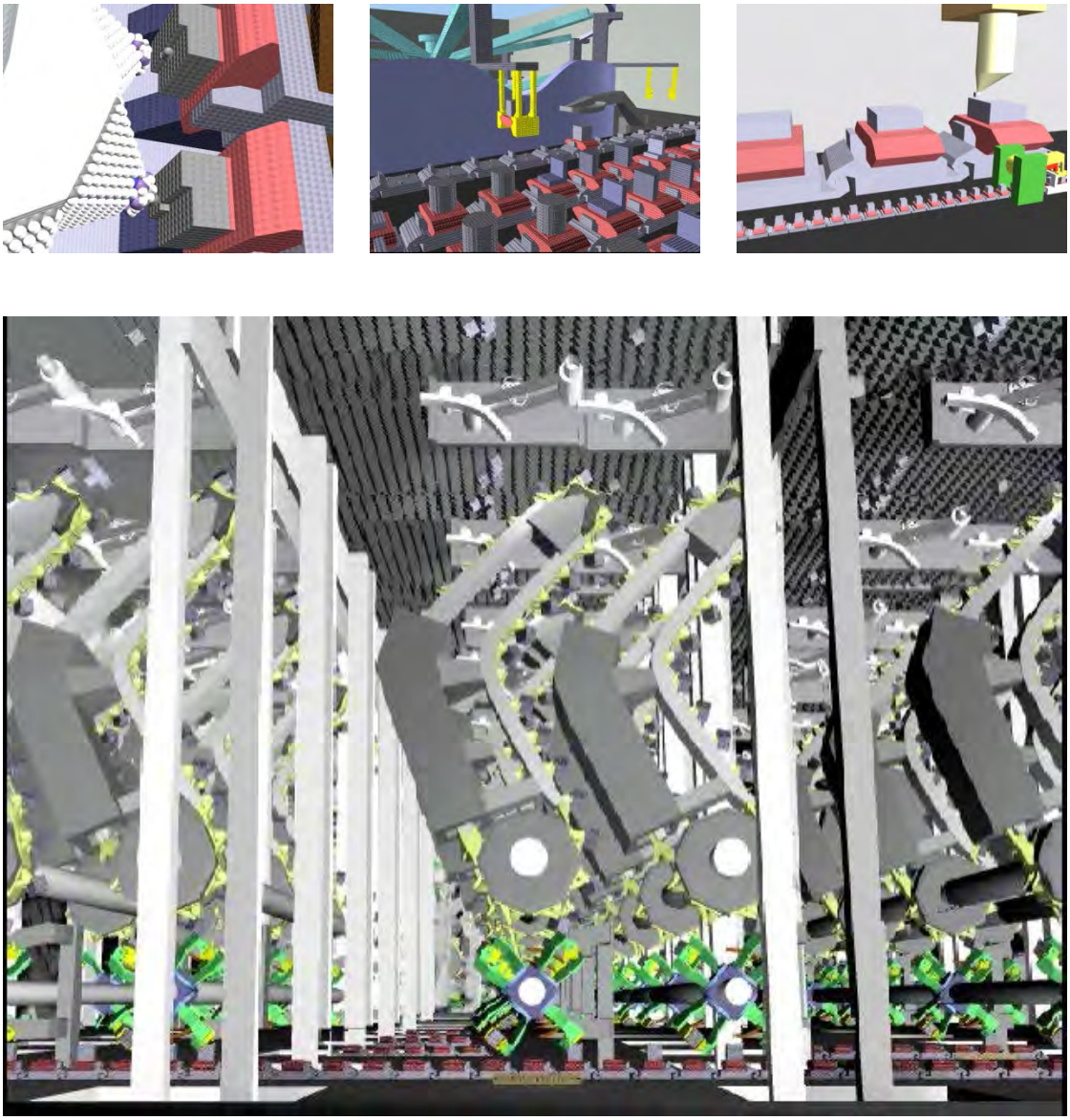

[369] John Burch nanofactory website, http://www.lizardfire.com/html_nano/nano.html.

Figure 2-51. Diamondoid desktop nanofactory. Images courtesy of John Burch.[370]

2.3.6 Atomically Precise Manufacturing of Macroscale Products

The end result of the nanofactory development program proposed here will be molecular manufacturing systems capable of producing macroscale quantities of atomically precise diamondoid structures. Nanofactories will make possible the manufacture of fundamentally novel products having the intricate complexity currently found only in biological systems, but operating with greater speed, power, reliability, and, most importantly, entirely under human control. Ultimate product manufacturing costs on the order of ~$1/kg appear plausible.[371] Here are a few examples:

Molecular Electronics and Molecular Computers. The manufacture of computer chips for data storage and computation will undergo a profound change. There are fundamental limits to further improvements in conventional lithography, the current process for chip manufacture. If improvements to computer hardware are to continue at the present pace, in a decade or so lithography must be replaced by some new manufacturing technology. Designs for computer logic elements composed of fewer than 1,000 atoms have already been suggested – but each atom in such a small device has to be in exactly the right place. Nanofactories or molecular assemblers could build these devices. A 1 cm^3 block of diamond contains more than 10^{23} carbon atoms, enough to build and connect more than 10^{18} computer logic elements. With machine-phase nanotechnology, we should be able to build mass storage devices that can store about 100 billion billion (~10^{20}) bits of information (~1 million copies of the Library of Congress) in a volume the size of a sugar cube – a billion times more storage capacity than that possessed by desktop computers in 2008. Massively parallel computers with a 1 cm^3 core (if properly cooled) should

---

[370] John Burch nanofactory website, http://www.lizardfire.com/html_nano/nano.html.

[371] Robert A. Freitas Jr., "Economic Impact of the Personal Nanofactory," Nanotechnology Perceptions: A Review of Ultraprecision Engineering and Nanotechnology 2(May 2006):111-126; http://www.rfreitas.com/Nano/NoninflationaryPN.pdf.

likewise deliver about 1000 billion billion instructions per second – a trillion times more than desktop computers in 2008. Both achievements would represent a phenomenal acceleration of the standard Moore's Law curve by many orders of magnitude.

Diamond is an excellent electronic material. It outperforms silicon in several key respects. For one thing, electrons move faster in diamond than in silicon. More importantly, as chips get faster and faster, their performance is limited by the need to dissipate heat generated in the circuitry – and diamond can work better than silicon at high temperatures. Diamond has this advantage for two reasons. First, diamond has greater thermal conductivity than silicon, allowing heat to exit a diamond transistor more quickly. Second, the "bandgap" of diamond (5.5 electron volts) is larger than that of silicon (1.1 electron volts). The bandgap is the minimum amount of energy required to boost an electron from its relatively immobile state into the semiconductor's conduction band, where the electron moves freely under the influence of a voltage. As temperature increases, more electrons gain the energy needed to jump into the conduction band. When too many electrons do this, the device changes from a semiconductor into a conductor; the transistor shorts out and stops working. Diamond's higher bandgap means that it shorts out at a higher temperature.

Quantum computing is another area where molecular precision in the manufacturing process is likely to be essential. Quantum computers, if they prove feasible, will let us solve certain types of problems in a few days that conventional computers couldn't solve in billions of years. Of greatest interest is factoring, a problem at the heart of modern cryptographic systems that has great commercial and national security implications. While it is still too early to say which of the many competing proposals for a quantum computer will prove most successful, it seems likely that the winning approach will benefit from greater precision in the manufacturing process. There is already one proposal which requires individual phosphorus atoms to be placed at specific lattice sites in a silicon or diamond crystal – something that today's technology can't easily do.[372] Machine-phase nanotechnology is the obvious way to inexpensively build such remarkably precise structures.

Nanomedicine and Medical Nanorobotics. Once we learn how to design and construct complete artificial nanorobots using strong diamondoid materials, nanometer-scale parts, and onboard subsystems including sensors, motors, manipulators, power plants, and molecular computers, the practice of medicine will be forever changed.[373] One example is the artificial mechanical red cell

---

[372] J.L. O'Brien, S.R. Schofield, M.Y. Simmons, R.G. Clark, A.S. Dzurak, N.J. Curson, B.E. Kane, N.S. McAlpine, M.E. Hawley, and G.W. Brown, "Scanning tunnelling microscope fabrication of arrays of phosphorus atom qubits for a silicon quantum computer", Smart Materials and Structures 11(2002):741.

[373] Robert A. Freitas Jr., Nanomedicine, Volume I: Basic Capabilities, Landes Bioscience, Georgetown, TX, 1999; http://www.nanomedicine.com/NMI.htm. K. Eric Drexler, Engines of Creation: The Coming Era of Nanotechnology, Anchor Press/Doubleday, New York, 1986. Robert A. Freitas Jr., "Chapter 15. Comprehensive Nanorobotic Control of Human Morbidity and Aging," in Gregory M. Fahy, Michael D. West, L. Stephen Coles, and Steven B. Harris, eds, The Future of Aging: Pathways to Human Life Extension, Springer, New York, 2008. Robert A. Freitas Jr., Nanomedicine, Volume IIA: Biocompatibility, Landes Bioscience, Georgetown, TX, 2003; http://www.nanomedicine.com/NMIIA.htm.

called a respirocyte[374] (Figure 2-52). Still entirely theoretical, the respirocyte would be a micron-wide spherical nanorobot made of 18 billion atoms precisely arranged in a diamondoid structure to form a tiny tank for compressed gas, that can be safely pressurized up to 1,000 atmospheres. Several billion molecules of oxygen and carbon dioxide can be absorbed or released from the tank in a controlled manner using computer-controlled molecular pumps powered by glucose and oxygen. External gas concentration sensors would allow respirocytes to mimic the action of the natural hemoglobin-filled red blood cells, with oxygen released and carbon dioxide absorbed in the tissues, and vice versa in the lungs. Each respirocyte could hold 236 times more gas per unit volume than a natural red cell, so a few cubic centimeters injected into the human bloodstream would exactly replace the gas carrying capacity of the patient's entire 5.4 liters of blood. A half-liter dose could keep a patient's tissues safely oxygenated for up to 4 hours in the event that a heart attack caused the heart to stop beating. Or this large dose would enable a healthy person to sit quietly at the bottom of a swimming pool for four hours, holding his breath, or to sprint at top speed for at least 15 minutes without breathing.

Figure 2-52. Artificial red cell (respirocyte, left) and artificial white cell (microbivore, right).

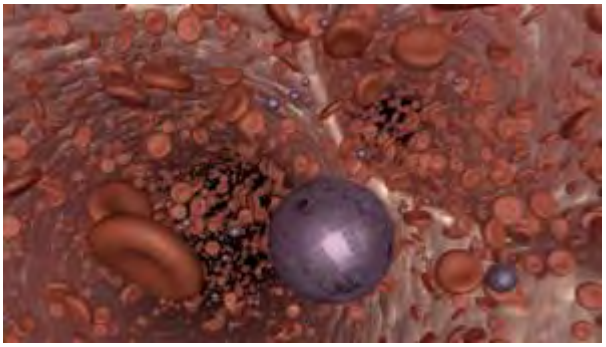

http://www.foresight.org/Nanomedicine/Respirocytes.html (Designer Robert Freitas, Artist PhleschBubble; © 2001 PhleschBubble)

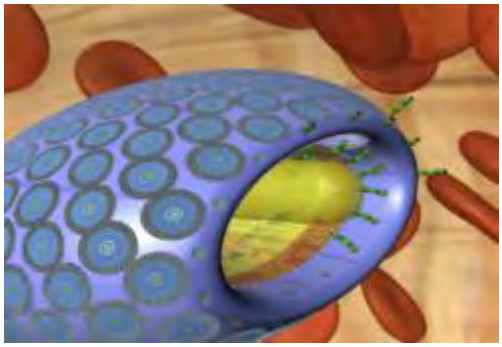

http://www.jetpress.org/volume14/freitas.html (Designer Robert Freitas, additional design Forrest Bishop; © 2002 Zyvex)

Other proposed medical nanorobots potentially offer equally astonishing performance improvements over nature. For instance, nanorobotic phagocytes (artificial white cells) called microbivores[375] (Figure 2-52) could patrol the human bloodstream, seeking out and digesting unwanted pathogens including bacteria, viruses, or fungi. Each one of these nanorobots could

---

[374] Robert A. Freitas Jr., "Exploratory Design in Medical Nanotechnology: A Mechanical Artificial Red Cell," Artificial Cells, Blood Substitutes, and Immobil. Biotech. 26(1998):411-430; http://www.foresight.org/Nanomedicine/Respirocytes.html.

[375] Robert A. Freitas Jr., "Microbivores: Artificial Mechanical Phagocytes using Digest and Discharge Protocol," J. Evol. Technol. 14(April 2005):1-52; http://www.jetpress.org/volume14/freitas.html.

completely destroy one pathogen in just 30 seconds – about 100 times faster than natural leukocytes or macrophages – releasing a harmless effluent of amino acids, mononucleotides, fatty acids and sugars. It will not matter that a bacterium has acquired multiple drug resistance to antibiotics or to any other traditional treatment. The microbivore will remove it anyway, achieving complete clearance of even the most severe septicemic infections in minutes to hours, as compared to weeks or even months for antibiotic-assisted natural white cell defenses – and without increasing the risk of sepsis or septic shock. Related nanorobots could be programmed to recognize and digest cancer cells, or to mechanically clear circulatory obstructions in a time scale on the order of minutes, thus quickly rescuing the stroke patient from ischemic damage.

Medical nanorobots will also be able to intervene at the cellular level, performing *in vivo* cytosurgery.[376] The most likely site of pathological function in the cell is the nucleus – more specifically, the chromosomes. In one simple cytosurgical procedure, a nanorobot controlled by a physician would extract existing chromosomes from a diseased cell and insert new ones in their place. This is called chromosome replacement therapy.[377] The replacement chromosomes will be manufactured to order, outside of the patient's body in a clinical benchtop production device that includes a molecular assembly line, using the patient's original individual genome as the blueprint. The replacement chromosomes would be appropriately methylated, thus expressing only the appropriate exons that are active in the cell type to which the nanorobot has been targeted. If the patient chooses, inherited defective genes could be replaced with nondefective base-pair sequences, permanently curing a genetic disease – possibly including aging.[378]

Aerospace and Defense. Natural diamond is expensive, can't be formed into arbitrary desired shapes, and readily shatters. Nanofactories will allow the inexpensive fabrication of shatterproof diamond (e.g., diamond fibers) in exactly the shapes we want. This would allow the design and construction of a space shuttle with a structural mass just 1/50th of today's version without any sacrifice of strength. Made-to-order diamondoid assemblies would benefit all load-bearing structures, and most of the mass in most of our products is load bearing. Beams, struts, buildings, cars, planes, boats and almost all other products would benefit – for example, automobiles could weigh less than the weight of their passengers, and 1-kilogram bicycles would delight racers. The most dramatic improvements are possible for rockets, where the strength-to-weight ratio and the cost of components are critical. Personal ground-to-orbit vehicles the size of a station wagon with launch costs of ~$1/kg to orbit should be feasible, allowing easy personal access to space.

Arrays of molecular sensors on airborne nanorobots and other surveillance devices should allow immediate detection and response to chemical and biological warfare attacks, as well as a defense

---

[376] Robert A. Freitas Jr., "Nanotechnology, Nanomedicine and Nanosurgery," Intl. J. Surgery 3(December 2005):1-4; http://www.nanomedicine.com/Papers/IntlJSurgDec05.pdf.

[377] Robert A. Freitas Jr., "The Ideal Gene Delivery Vector: Chromallocytes, Cell Repair Nanorobots for Chromosome Replacement Therapy," J. Evol. Technol. 16(June 2007):1-97; http://jetpress.org/v16/freitas.pdf.

[378] Robert A. Freitas Jr., "Chapter 15. Comprehensive Nanorobotic Control of Human Morbidity and Aging," in Gregory M. Fahy, Michael D. West, L. Stephen Coles, and Steven B. Harris, eds, The Future of Aging: Pathways to Human Life Extension, Springer, New York, 2008.

against a variety of biological and nuclear terrorism threats. Once detected, malicious chemical, biological, and nuclear agents can be rapidly analyzed and neutralized. Machine-phase nanotechnology has a wide range of both defensive and offensive applications. Admiral David E. Jeremiah, USN (Ret), former Vice Chairman of the Joint Chiefs of Staff, has said: "Military applications of molecular manufacturing have even greater potential than nuclear weapons to radically change the balance of power."

Environment. Nanofactories are the ultimate "green" technology. Clean assembler-based factories using molecularly-precise feedstocks would eliminate the pollution typically produced by traditional bulk manufacturing and would allow complete recycling of previously manufactured molecular structures. Products could be manufactured and used without generating wastes or noxious effluents, with high process efficiency and lighter materials thus reducing both material and energy consumption. Forced flow of polluted water through nanopore filters, possibly using simple mechanical power supplied by people or animals, could provide a cheap source of fresh potable water for impoverished third-world populations.

Energy. Low cost solar cells and batteries produced by molecular manufacturing could replace coal, oil and nuclear fuels with clean, cheap and abundant solar power. Humanity currently consumes about 10 terawatts of power, but over 100,000 terawatts of solar energy continuously fall on the Earth, most of it unused directly by man. Nanofactories could radically alter the economics of energy production. We already know how to make efficient solar cells. Nanotechnology could cut costs, finally making solar power economical. Here we need not make new or technically superior devices – just by making inexpensively what we already know how to make expensively, we would move solar power into the mainstream.

3. Nanofactory Development Program Technical Research Milestones

Developing the first working diamondoid nanofactory will require a very long term, complex, and comprehensive program to achieve this objective. An exhaustive list of subgoals and requirements cannot be definitively enumerated at this time. The specifics tasks comprising this program, especially those describing the latter stages of the program, will be modified over time as more resources are dedicated to the task and as more information becomes available. However, it is already possible to set forth a clear, step-by-step research and development roadmap that should lead to the desired result.

In this Section we describe the major Phases of a diamondoid nanofactory development program and the essential component Tasks necessary to achieve each milestone. There are 11 distinct program Phases and the completion of each Phase is an important milestone in the program. Each Phase requires the completion of a number of key Tasks, with specific research projects supporting and enabling the completion of each Task. Tasks are arranged in the logical order of completion in order to most efficiently achieve each major Phase. Successive Tasks and Phases build upon the successes of previously completed Tasks and Phases to achieve the next major milestone. Each Phase that is achieved represents both an important step toward fulfillment of the program goal to build a working diamondoid nanofactory and the development of a unique standalone molecular manufacturing capability that could have significant commercial utility and value. Achievement of all 11 Phases completes the ultimate program objective of building a working diamondoid nanofactory.

An overview of nanofactory development program Phases (Section 3.1) is followed by a more detailed summary of Phases and Tasks necessary to support the achievement of each major program milestone (Section 3.2 through Section 3.12).

3.1 Overview of Major Program Milestones

This Section provides a brief overview of the principal milestones of the proposed comprehensive diamondoid nanofactory development program. These milestones are expected to be achieved as the research proceeds and new capabilities are sequentially developed. To summarize our program, we propose first to build a macroscale scanning probe based atomically precise manufacturing capability (Phases I-II), then to use this capacity to build a standalone self-replicable nanoscale workstation again yielding an atomically precise manufacturing capability (Phases III-VI), then to use this capacity to exponentially build a massively parallel nanoscale manufacturing capability (Phases VII-IX), and finally to use this capacity to build the first desktop nanofactories (Phases X-XI).

The following is a thumbnail description of the strategy and sequencing of the proposed nanofactory development program.

We first build a macroscale workstation that is capable of nanoscale atomically precise manufacturing, albeit at a very slow rate. This capability is used to build a nanoscale fabrication system that is capable of the exact same nanoscale atomically precise fabrication as the macroscale system. However, this nanoscale system is slow because it must be provided with feedstock molecules and assembly services by the comparatively ponderous macroscale system. To remove the need for the macroscale system to provide feedstock to the nanoscale system, we add an *in situ* feedstock supply using cyclically-filled gas tanks to the nanoscale workstation, which increases nanoscale productivity. To remove the need for the macroscale system to provide assembly operations for the nanoscale system, we next add an *in situ* assembly subsystem to the nanoscale workstation which again increases nanoscale productivity. We now have a self-contained nanoscale manufacturing workstation that has all the capabilities of the macroscale manufacturing, but is much smaller, more efficient and more productive. We next use plate/plate replication to build vast numbers (~10^{11}) of nanoscale manufacturing workstations that can be operated as a massively parallel array on a single 100 cm^2 wafer, and we additionally replicate a large number (~1000) of these arrays. This provides enough manufacturing capacity to build the first layer of the nanofactory using a micron-scale manipulator array which is also built using the nanoscale workstation arrays. Since the delays in operating the cyclically-filled gas tanks are now the sole remaining significant productivity bottleneck, we eliminate the gas tanks by installing continuous feedstock gas supply for the first layer of the nanofactory. The result is a completed working diamondoid nanofactory that can manufacture macroscale quantities of atomically precise diamondoid product objects.

The diamondoid nanofactory development program is organized into eleven distinct Phases of activity, with the completion of each Phase representing a major program milestone marking the development of a significant new capability in atomically precise massively parallel molecular manufacturing.

The eleven nanofactory development Phases (the completion of each of which is a major program milestone) are as follows:

Phase I: Macroscale Fabrication Workstation (MFW) (Section 3.2)

The key objective of Phase I is to build a macroscale workstation (MFW) for diamondoid mechanosynthetic fabrication on a flat working surface. (~0.01 atom/sec for MFW; T = cryogenic)

Phase II: Macroscale Manufacturing Workstation (MMW) (Section 3.3)

The key objective of Phase II is to build a macroscale manufacturing workstation (MMW) that can nonintegrally fabricate diamondoid nanoparts from molecular feedstock primitives on a reversible fabrication surface (from which the manufactured nanoparts may be easily detached), and then pick up and assemble those diamondoid nanoparts into multi-nanopart diamondoid product objects on a reversible assembly surface. (~1 atom/sec for MMW; T = cryogenic)

Phase III: First-Generation Nanoscale Fabrication Workstation (NFW) (Section 3.4)

The key objective of Phase III is to build, on an atomically precise multi-electrode assembly surface, the first-generation nanoscale fabrication workstation (NFW) – a set of individually controlled nanoscale manipulators and toolheads capable of performing diamondoid mechanosynthesis inside a UHV workspace chamber, powered by electrical control signals passed through the assembly surface via electrical surface contact points, with material feedstock provided via manual handoff from the macroscale MMW workstation developed in Phase II. (~1 atom/sec for MMW-limited NFW; $T \leq 195$ K)

Phase IV: Second-Generation Nanoscale Fabrication Workstation (NFW-2) (Section 3.5)

The key objective of Phase IV is the design and manufacture of the automated Bulk Feedstock Supply System (BFSS) and its subsequent integration with the existing NFW system developed in Phase III to create an upgraded, more nearly self-contained second-generation NFW system that no longer needs to be hand-fed its molecular feedstock by the Phase II MMW manipulator system, thus enabling the NFW-2 to operate at ~100-fold faster production rates. (~100 atoms/sec for NFW-2; $T \leq 190$ K)

Phase V: Nanoscale Assembly Workstation (NAW) (Section 3.6)

The key objective of Phase V is to build the first-generation nanoscale assembly workstation (NAW) – a set of individually controlled nanoscale manipulators and toolheads inside a UHV workspace chamber that is capable of acquiring fabricated nanoparts and assembled nanodevices by handoff from the Phase II MMW system, assembling these components into more complex nanodevices, and then using them to construct a working nanosystem on the multi-electrode assembly surface immediately adjacent to the NAW. (~100 atoms/sec for NFW-2-limited NAW; $T \leq 193$ K)

Phase VI: Nanoscale Manufacturing Workstation (NMW) (Section 3.7)

The key objective of Phase VI is the design and manufacture of the first self-contained nanoscale manufacturing workstation (NMW) that is capable of fully endogenous operation with no assistance from the macroscale Phase II system. (~100 atoms/sec for NMW; T ~ 185 K)

Phase VII: Demonstrate Plate/Plate Exponential Manufacturing (Section 3.8)

The key objective of Phase VII is the design, manufacture, and operational demonstration of a second-generation nanoscale manufacturing workstation (NMW-2) that is capable of assembling an atomically exact working copy of itself on an opposing surface under full endogenous operation. (~10^3 atoms/sec for NMW-2; T = 118-127 K)

Phase VIII: Exponentially Manufacture 1024 NMW-2 Wafers (Section 3.9)

The key objective of Phase VIII is the exponential manufacture of 1024 wafers full of NMW-2 units, a quantity sufficient to fabricate and assemble atomically precise product objects up to the ~100-nm scale at a ~10^{17} atom/sec build rate, enabling the massively parallel manufacture of additional NMW-2 molecular manufacturing units. (~10^{14} atoms/sec per NMW-2 wafer, assuming 10^{11} NMW-2 units/wafer; T = 118-127 K)

Phase IX: Micro-Assembler Manipulators and Micro-Assembler Array (Section 3.10)

The key objective of Phase IX is to build a massively parallel array of micron-scale manipulators capable of reliably assembling void-free solid planes of submicron-scale product objects. (~10^{15} parts assembly operations/sec per MAA wafer at 120 MHz, assuming 2 x 10^{11} MAMs/wafer; T = 118-127 K)

Phase X: First-Generation Nanofactory (Section 3.11)

The key objective of Phase X is to eliminate the Bulk Feedstock Supply System (BFSS) system in favor of a macroscale bulk feedstock supply system and to build a first-generation nanofactory (FGN) capable of mass-producing micron-scale atomically precise diamondoid product objects at ~0.01 kg/hour production rates. (~10^{20} atoms/sec for FGN; T = 109 K)

Phase XI: Second-Generation Nanofactory (Section 3.12)

The key objective of Phase XI is to build out the first desktop nanofactory capable of manufacturing atomically precise diamondoid macroscale product objects up to ~10,000 cm^3 in volume at ~0.01 kg/hour production rates. (~10^{20} atoms/sec for SGN; T = 109 K)

In the following Sections, we provide a concise description of each milestone manufacturing system that is created, followed by a more detailed technical description of each Task that must be successfully completed in order to complete the given Phase of activity and thus to reach the indicated major milestone. Each Task description includes the research needed to be performed, scaling issues, and references to existing supporting research. The proposed system designs are sufficiently robust that an increase by twofold or more in total atom count in each Phase should still yield a feasible development pathway. Achievement of each program milestone yields a real, working, operational atomically precise manufacturing system representing great IP value with potentially significant licensing and other commercial potential.

3.2 Phase I: Macroscale Fabrication Workstation (MFW)

The key objective of Phase I is to build a macroscale workstation for diamondoid mechanosynthetic fabrication on a flat working surface. The workstation includes a 4-tip 5-DOF (degrees of freedom) picopositioner system capable of performing diamondoid mechanosynthesis (DMS) (Section 2.3.1) on an bulk-prepared surface inside a vibration-isolated UHV workspace chamber, powered by electrical control signals that energize piezoelectric actuators to drive the positioning tips, with material feedstock provided on presentation surfaces accessible to the scanning probe tip-mounted tooltips. The Phase I system could create the basis for the world's first commercial diamondoid product fabrication workstation providing a limited capacity for positionally controlled diamondoid mechanosynthesis using a small set of mechanosynthetic tooltips that could be employed to fabricate small, simple, but atomically precise diamondoid nanostructures.

The macroscale DMS fabrication workstation is described in Section 3.2.1 and illustrated in Figure I-1. This is followed by an enumeration of the specific sequence of tasks leading to an operational fabrication workstation, which include: design and simulation of DMS tooltips, surfaces, reactions, and reaction sequences (Section 3.2.2), the design, simulation and testing of automated reaction sequence control software (Section 3.2.3), demonstration of simple DMS reaction sequences using existing SPM (Section 3.2.4), building a 1-tip 3-DOF picopositioning SPM system to demonstrate basic DMS reaction sequences (Section 3.2.5), verifying the need for 4 tips and 5 DOFs (Section 3.2.6), adding an in-chamber toolrack to enable endogenous tooltip changeout (Section 3.2.7), building a 1-tip 4-DOF system to demonstrate additional DMS reaction sequences (Section 3.2.8), building a 2-tip 5-DOF system to demonstrate additional DMS reaction sequences (Section 3.2.9), building a 4-tip 5-DOF system to demonstrate additional DMS reaction sequences (Section 3.2.10), the fabrication of diamondoid product objects containing only hydrocarbon atoms on a surface (Section 3.2.11), and the fabrication of diamondoid product objects including atoms in addition to carbon and hydrogen on a surface (Section 3.2.12).

3.2.1 Description of the MFW

The structure and basic function of the macroscale fabrication workstation (MFW) is described in this Section.

3.2.1.1 General Description of the MFW

The macroscale fabrication workstation (MFW) is a scanning probe microscopy (SPM) based system for fabricating relatively small diamondoid nanostructures (i.e., up to 100-1000 atoms) on a flat bulk-prepared diamondoid fabrication surface using the techniques of diamondoid mechanosynthesis (Section 2.3.1). The final MFW scanning probe system (Figure I-1) will employ 4 tips whose structure is either atomically precise or is characterized to atomic precision and whose operational envelopes include simultaneous and collisionless access both to the other tips and to the diamondoid fabrication surface and other adjacent workspace surfaces (i.e., two

feedstock presentation surfaces and a hydrogen dump)[379] within an (up to) 100 micron x 100 micron area. Each tip will be capable of motion in all three Cartesian dimensions (XYZ) to a repeatable precision of 0.2-0.5 Å (20-50 picometers) over 10-100 micron path lengths (as corrected for hysteresis effects). Each tip probably must also be capable of motion in at least two rotational directions (pitch and yaw) in ~1 degree angular increments, subject to the principle design constraint that such rotations must not destroy the precision of the motions in the three Cartesian directions. (Rotation stages with 5 µrad (0.0003 deg) rotational increments with 240 µrad (0.014 deg) of backlash are commercially available.)[380] The picopositioner probe system will be ensconced within a UHV chamber in a vibration-isolated environment and should be capable of operating at room temperature (~300 K) or at liquid nitrogen temperature (~80 K); operations at colder temperatures are currently believed to be unnecessary.

Figure I-1. Schematic layout of the Phase I Macroscale Fabrication Workstation (MFW). (Scanning probe tip rack not shown)

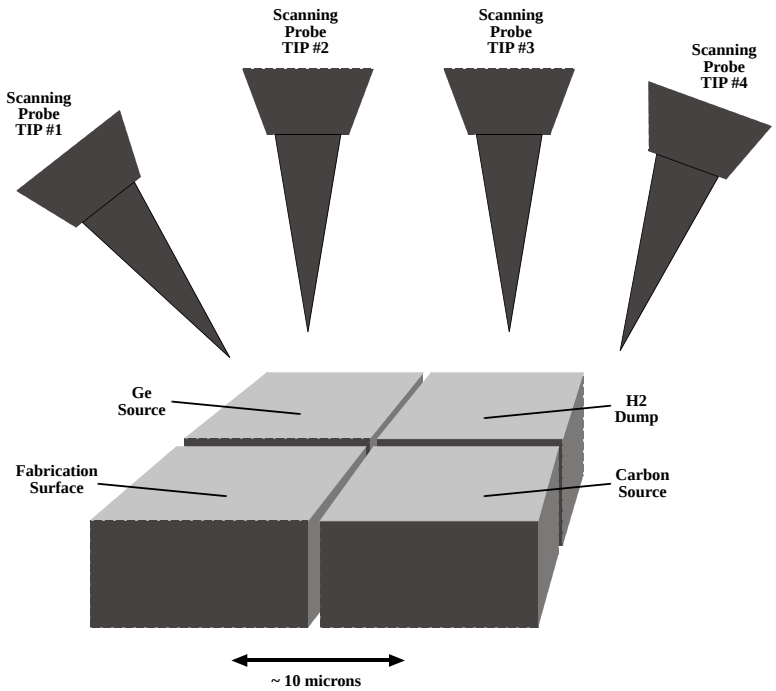

[379] Robert A. Freitas Jr., Ralph C. Merkle, "A Minimal Toolset for Positional Diamond Mechanosynthesis," J. Comput. Theor. Nanosci. 5(May 2008):760-861.

[380] Physik Instrumente, "M-060 · M-061 · M-062, Series Rotation Stages with Worm Gear Drive," accessed January 2008, http://www.physikinstrumente.com/en/products/prdetail.php?sortnr=703100; see also http://www.physikinstrumente.com/en/pdf/M060_Datasheet.pdf.

3.2.1.2 High-Precision SPM-Based Tip Positioning Systems

The scanning probe microscopy-based picopositioner system described in Section 3.2.1.1 has not yet been experimentally demonstrated but is believed to lie within the existing or developable state-of-the-art. Given the recognized importance of developing a high-precision measurement infrastructure for nanotechnology, many national metrology institutes worldwide have already initiated ongoing efforts in the development of high-quality SPM-based metrology instruments.[381] The metrological performance of many of these SPM systems was compared by Breil et al.[382] in a study that included both standard and special metrological SPMs and clearly showed the need for active metrology sensors to achieve the necessary measurement accuracy. Most of the instruments surveyed operate over sub-millimeter ranges, but there are a few large-range (≥25 mm) interferometer-based SPM metrology instruments and stages that have also been developed.[383]

---

[381] J. Schneir, T.H. McWaid, J. Alexander, B.P. Wilfley, "Design of an atomic force microscope with interferometric position control," J. Vac. Sci. Technol. B 12(1994):3561-3566; F. Meli, R. Thalmann, "Long-range AFM profiler used for accurate pitch measurements," Meas. Sci. Technol. 9(1998):1087-1092; M. Bienias, S. Gao, K. Hasche, R. Seemann, K. Thiele, "A metrological scanning force microscope used for coating thickness and other topographical measurements," Appl. Phys. A 66(1998):S837-S842; S. Gonda, T. Doi, T. Kurosawa, Y. Tanimura, N. Hisata, T. Yamagishi, H. Fujimoto, H. Yukawa, "Real-time, interferometrically measuring atomic force microscope for direct calibration of standards," Rev. Sci. Instrum. 70(1999):3362-3368; R.K. Leach, J. Haycocks, K. Jackson, A. Lewis, S. Oldfield, A. Yacoot, "Advances in traceable nanometrology at the National Physical Laboratory," Nanotechnology 12(2001):R1-R6; G.B. Picotto, M. Pisani, "A sample scanning system with nanometric accuracy for quantitative SPM measurements," Ultramicroscopy 86(2001):247-254; I. Misumi, S. Gonda, T. Kurosawa, K. Takamasu, "Uncertainty in pitch measurements of one-dimensional grating standards using a nanometrological atomic force microscope," Meas. Sci. Technol. 14(2003):463-471; Andrew Yacoot, Ludger Koenders, "From nanometre to millimetre: a feasibility study of the combination of scanning probe microscopy and combined optical and x-ray interferometry," Meas. Sci. Technol. 14(2003):N59-N63; M. Bisi, E. Massa, A. Pasquini, G. B. Picotto, M. Pisani, "Nanometrology at the IMGC", in: Günter Wilkening, Ludger Koenders, eds., Nanoscale Calibration Standards and Methods, Wiley-VCH Verlag GmbH & Co. KGaA, 2005; H.-U. Danzebrink, L. Koenders, G. Wilkening, A. Yacoot, H. Kunzmann, "Advances in Scanning Force Microscopy for Dimensional Metrology," CIRP Annals - Manufacturing Technology 55(2006):841-878; K.R. Koops, M.G.A. van Veghel, G.J.W.L. Kotte, M.C. Moolmanration, "Strategies for scanning probe metrology," Meas. Sci. Technol. 18(January 2007):390-394; M. Ritter, T. Dziomba, A. Kranzmann, L. Koenders, "A landmark based 3D calibration strategy for SPM," in: Measurement Science and Technology, IOP, Bristol, 2007, pp. S404-S414.

[382] R. Breil, T. Fries, J. Garnaes, J. Haycocks, D. Huser, J. Joergensen, W. Kautek, L. Koenders, N. Kofod, K.R. Koops, R. Korntner, B. Lindner, W. Mirande, A. Neubauer, J. Peltonen, G.B. Picotto, M. Pisani, H. Rothe, M. Sahre, M. Stedman, G. Wilkening, "Intercomparison of scanning probe microscopes," Precis. Eng. 26(July 2002):296-305.

[383] M. Holmes, R. Hocken, D. Trumper, "The long-range scanning stage: a novel platform for scanned-probe microscopy," Precis. Eng. 24(2000):191-209; "Nano Positioning and Nano Measuring Machine," SIOS Messtechnik, GmbH, http://www.sios.de; G. Dai, L. Jung, F. Pohlenz, H.-U. Danzerbrink, R. Krueger-Sehm, K. Hasche, G. Wilkening, "Measurement of micro-roughness using a metrological large range scanning force microscope," Meas. Sci. Technol. 15(2004):2039-2046.

One good example of a high-performance state-of-the-art metrology instrument is the Molecular Measuring Machine (M^3) project[384] at the National Institute of Standards and Technology (NIST), the details of which are both illuminating and representative of such systems and thus will be presented here at length. M^3 is a 1-tip 3-DOF (degrees of freedom) SPM- and Michelson interferometer-based metrology instrument designed to achieve 1 nanometer measurement uncertainty for point-to-point measurements over a 50 mm x 50 mm working area, and thus "to achieve sub-nanometer-scale metrology over centimeter-scale areas...[and] to be able to repeatably locate any specific atom within the 50 mm by 50 mm measurement area, and measure the distance between it and any other atom." According to a description[385] of M^3 published in 2005 by John Kramar, leader of the NIST Nanoscale Metrology Group:

"Key design requirements that must be accentuated because of the large range-over-resolution goal are vibration isolation, machine stiffness and low noise in the control electronics, which together are needed to minimize the positional noise. For measurement accuracy, care must also be taken to design for motion accuracy and repeatability, and high-stability temperature control to minimize measurement uncertainty due to thermal expansion effects. In addition, we have chosen to operate in a vacuum environment, both to reduce sample contamination and adsorbed overlayers, and to remove measurement errors in the interferometers due to changes in the refractive index of the ambient air."

"For the basic machine core structure, a spherical geometry was chosen to maximize stiffness and symmetry, which also gives improved thermal uniformity and stability. The core is 350 mm in diameter, made out of pure copper, again for thermal uniformity and for long-term creep stability. The planar motion is generated separately as one-dimensional (1D) motions of the sample relative to the core (X-axis carriage), and orthogonally, of the probe relative to the core (Y-axis carriage) (Figure I-2). Avoiding stacked stages avoids position-dependent cross-talk between the axes, simplifying the error mapping of the planar motion into two 1D maps. To achieve the desired range over resolution, each axis of motion is a combination of a coarse motion and fine motion stage. Here stacked stages are used, but the small range of the fine motion stage, and the resulting limited mass shift, is small enough that the effect on the attitude of the coarse motion stage should be negligible. For repeatability, the coarse motion stages are guided by slideways. The motion is generated by linear piezoceramic stepper motors, from which sub-micrometer position control is readily achieved over the 50 mm linear range. The piezoceramic motors also have a decided advantage over electromagnetic stepper motors in terms of minimal heat generation. The fine motion stages are guided by parallel flexure elements and have a range of about 10 microns. They are driven directly by piezoceramics, with any parasitic lateral drive motion somewhat decoupled by means of a flexible coupling element. The fine stage resolution is limited only by the noise on the control electronics and high voltage amplifiers, and for highest resolution work, the noise can be scaled down by scaling down the motion range."

---

[384] John A. Kramar, "Nanometre resolution metrology with the Molecular Measuring Machine," Meas. Sci. Technol. 16(2005):2121-2128.

[385] John A. Kramar, "Nanometre resolution metrology with the Molecular Measuring Machine," Meas. Sci. Technol. 16(2005):2121-2128.

Figure I-2. Illustration of the Molecular Measuring Machine (M^3) project: Cut-away view of the Molecular Measuring Machine.[386] Courtesy of John Kramar.

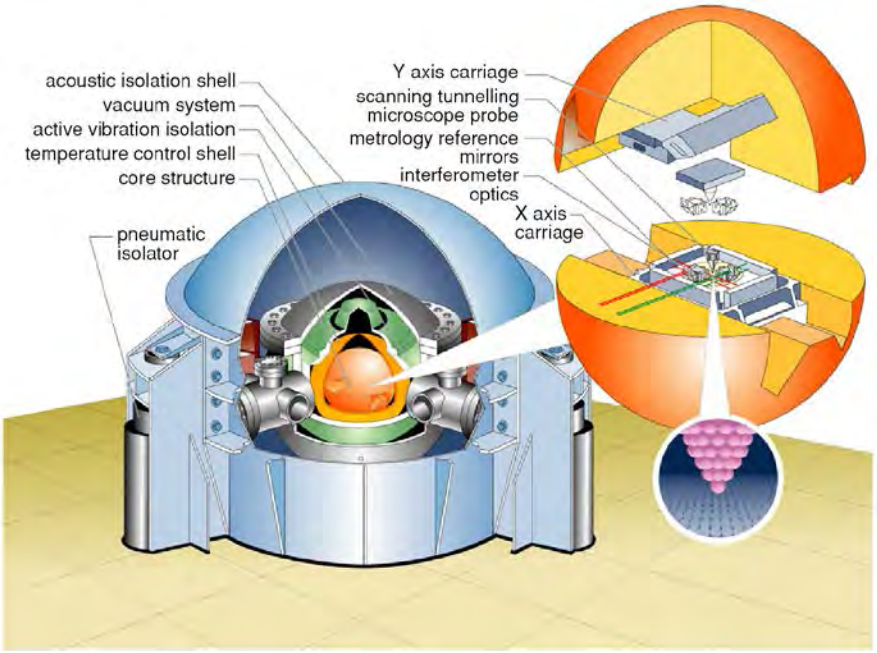

"The relative motion of the upper and lower fine motion stages, carrying the probe and sample respectively, is measured using a 2D displacement measuring interferometer system (Figure I-3). The interferometers measure differentially the combined motion of the coarse and fine stages, giving a continuous metric independent of what portion of the total motion was generated by the fine or coarse stages. (For error mapping, the position of each fine motion stage is also measured relative to its coarse motion stage, using a capacitance gauge.) The reference mirrors for the interferometer are the inside surfaces of a highly accurate, low-expansion-coefficient metrology box, inside of which lies the sample. The interferometer beam-splitter optic assemblies are carried by the upper carriage on the same mounting plate that carries the probe system, suspended inside the metrology box.

[386] John A. Kramar, "Nanometre resolution metrology with the Molecular Measuring Machine," Meas. Sci. Technol. 16(2005):2121-2128.

Figure I-3. Illustration of the Molecular Measuring Machine (M^3) project: Differential interferometer beam path view – the position of the central assembly is measured with respect to the metrology box, with the input and output beams directed along the motion axis of the central assembly.[387] Courtesy of John Kramar.

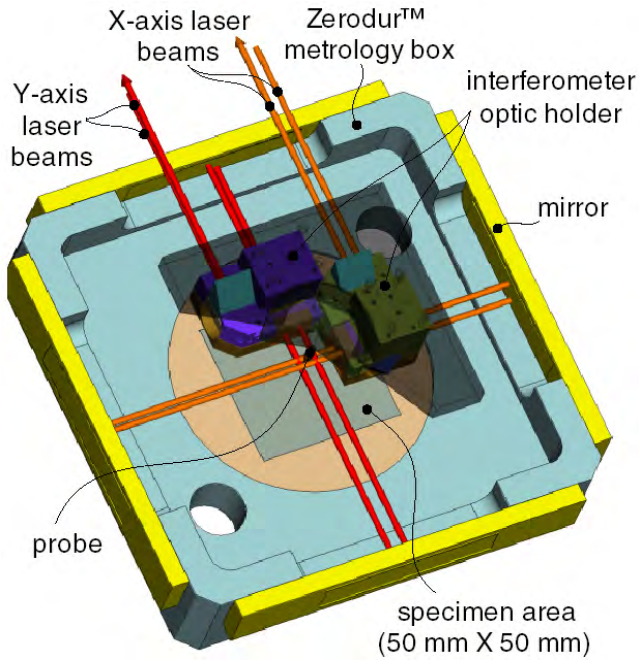

"A scanning probe microscope is used as the sample imaging probe system for M^3. The probe system is comprised of coarse and fine motion stages, a capacitance gauge position sensor, and the probe itself (Figure I-4). It was in-house designed to meet the various constraints, notable among them the very limited available space. The coarse motion stage is a cylindrical piezoceramic linear stepper motor that operates in the vertical axis with a 3 mm range. The grounded or open circuit clamping force is sufficient to keep the motor slug from sliding down when the power is removed. Built into this motor slug is the vertical, 5 micron range fine motion stage, having flexure-guided motion, and driven by a piezoceramic through a decoupling mechanism of a ball between two flats. The elements of the fine motion stage had to be folded back through the coarse motion stage to accommodate the space constraints. There is no horizontal (scan) motion built into the probe system, because any such motion would not be measured by the interferometer system; all horizontal scanning either drives the metrology box containing the sample or drives the entire upper assembly that includes the probe system along with the interferometer optics, as already described. The vertical fine motion is measured relative to the vertical coarse motion stage using a capacitance gauge that is calibrated *ex situ* against an interferometer. For a given measurement, the vertical range is limited to that provided by the

---

[387] John A. Kramar, "Nanometre resolution metrology with the Molecular Measuring Machine," Meas. Sci. Technol. 16(2005):2121-2128.

guided fine motion stage. The vertical coarse motion is only crudely guided by the cylindrical housing in which the motor slug runs, and is not considered to be sufficiently characterized or repeatable to use during measurements, since it is within the metrology loop.

Figure I-4. Illustration of the Molecular Measuring Machine (M^3) project: Probe actuator assembly exploded views, showing separately the detail of the coarse and fine motion mechanisms: The coarse motion is a linear piezo stepping motor; the fine motion is a folded, piezo-driven, flexure-guided system, with a capacitance gauge sensor.[388] Courtesy of John Kramar.

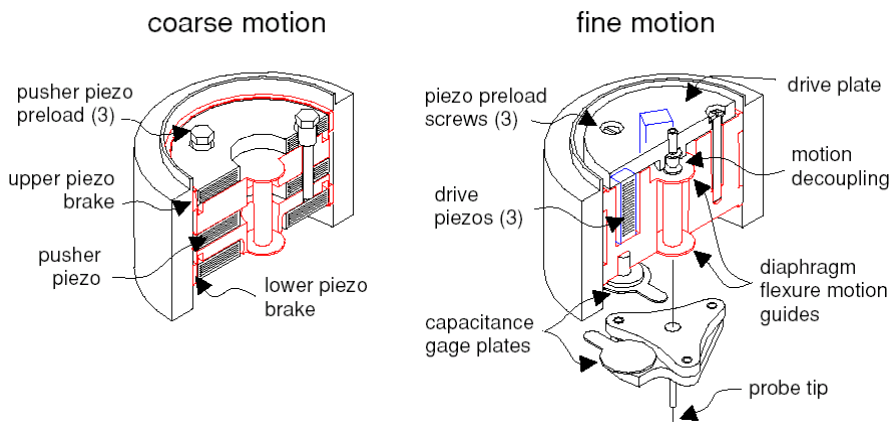

"The machine core assembly is enclosed in layers of environmental isolation and control, as illustrated in (Figure I-2). The first layer is a temperature control shell. This is a gold-coated copper sphere about 50 mm larger in diameter than the machine core, spiral-wrapped with polyimide-insulated copper wire at a 6 mm spacing. The shell has three doors on rails to allow the removal and replacement of the coarse motion carriages. To maintain a stable temperature at 20 ^{o}C, the room is kept at 17 ^{o}C ± 0.01 ^{o}C, and the current through the heater shell wire is controlled. There are several thermocouples distributed about the temperature control shell and the machine core to monitor the temperature, as well as platinum resistance thermometers on the probe mounting plate and near the sample. The control scheme is to maintain stability through thermal inertia and by keeping a constant heat load. Between the large thermal mass of the copper core and the weak coupling between it and the temperature control shell, the temperature rise time for the system is on the order of one day. Temperature stability of ±0.001 ^{o}C has been demonstrated.

"The next layer of environmental control is an active vibration isolation system. For this, the payload is suspended inside an outer shell, kinematically constrained by means of six actuator

---

[388] John A. Kramar, "Nanometre resolution metrology with the Molecular Measuring Machine," Meas. Sci. Technol. 16(2005):2121-2128.

rods in the Mallock suspension configuration,[389] each actuator having an accompanying accelerometer mounted as nearly as possible coaxially, on the suspended inner mass. Different vibration compensation control algorithms have been implemented using a digital signal processor (DSP),[390] which have good effect when the vibration environment is noisy, for example when the turbomolecular pump is operating. In the quieter environment in which we more typically operate, the performance of the active system is limited by the sensor noise, and is less useful. The entire instrument described to this point is contained in a vacuum system equipped with a turbo pump for roughing and eight symmetrically placed ion pumps for quiet operation. Several of the machine components will not withstand the bake out temperatures needed to achieve ultra-high vacuum levels; a typical base pressure reached is 10^{-5} Pa. The vacuum system is contained in an environmental control chamber that can be hermetically sealed to provide further acoustic isolation. This chamber is supported by pneumatic isolators having level control and a damped natural resonance of about 1 Hz.

"We have recently moved this instrument to our new Advanced Metrology Laboratory.[391] The new laboratory space is in a building that is completely underground. The laboratory is a class 100 clean room with ±0.01 ^{o}C temperature control, and yet is acoustically quiet. The instrument rests on a pneumatically supported concrete slab that is in a pit under the walk-on floor. Most of the electronics and power supplies that drive the instrument are located in an adjacent control room. The control system for M^3 runs on multiple DSPs on a VME (Versa Module Europa) backplane. The VME processor cards each have mezzanine input/output boards for reading from and controlling the instrument. The overall system control is done from a desktop computer that communicates with the VME through a bus adaptor. Code for the DSPs is developed on the desktop computer. User interface and top level control is done in the Matlab programming environment on the desktop computer. Our closed-loop positioning control has some noise at the few tenths of nanometers [~300 pm] level and at relatively low bandwidth due in part to what we believe to be a second-order effect caused by laser pointing instability due to turbulence. In order to decrease this source of noise in the interferometer measurements, we are currently developing a system for delivering the laser beams to the in-vacuum interferometer using fibre optics."

Note that the M^3 system has a far greater range of motion (50 mm range) that is required for the successful completion of at least the first six phases of this program (1-100 micron range). A different version of the M^3 system that reduces the range of motion 1000-fold should be able to improve the repeatable positional accuracy by just 20-50 fold, which is all that we require.

---

[389] R.S. Whipple, "The design and construction of scientific instruments," Trans. Opt. Soc. Lond. 22(1921):35-52.

[390] K.-J. Lan, J.-Y. Yen, J.A. Kramar, "Active vibration isolation for a long range scanning tunneling microscope," Asian J. Control 6(2004):179-186; K.-J. Lan, J.-Y. Yen, J.A. Kramar, "Sliding mode control for active vibration isolation of a long range scanning tunneling microscope," Rev. Sci. Instrum. 75(2004):4367-4373.

[391] Advanced Measurement Laboratory 2004; http://www.nist.gov/public affairs/amlbrochure.htm; The National Institute of Standards and Technology Advanced Measurement Laboratory, Gaithersburg, MD; http://www.nanobuildings.com/projects/nist/.

3.2.1.3 Repeatable Picometer Positional Accuracy in SPM-Based Systems

What positional accuracy is required for reliable DMS work? Distances between neighboring competing radical sites are ~1.54 Å on C(110) for displacements across the dimer row, ~1.64 Å on C(100) for displacements in the cross-row direction, and ~2.50 Å on C(111) between neighboring surface sites. A tooltip which is mispositioned by more than half of the mean lateral distance between competing reactive sites (e.g., ~0.77 Å (77 pm) for C(110), ~0.82 Å (82 pm) for C(100), ~1.25 Å (125 pm) for C(111)) will be more likely to bond to the neighboring incorrect site than to the targeted correct site. (The presence of potentially abstractable passivating atoms ringing the perimeter of a depassivated target site, and other factors, greatly complicates this analysis.) Despite initial suggestions in *Nanosystems*[392] that positional placement accuracies on the order of one C-C bondlength (~1.54 Å, ~154 pm) may suffice for reliable DMS, subsequent studies and simulations have determined that reliable DMS operations such as hydrogen abstraction,[393] hydrogen donation,[394] and carbon dimer placement on the most positionally demanding C(110) diamond surface[395] will apparently require better than one-third of a C-C bondlength of positional placement accuracy, typically 0.2-0.5 Å (20-50 pm). This requirement for 20-50 picometer positional accuracy in SPM-based systems appears to be at or very near the current state of the art – both for positioning resolution and for positioning repeatability (Figure I-5).

---

[392] K. Eric Drexler, Nanosystems: Molecular Machinery, Manufacturing, and Computation, John Wiley & Sons, New York, 1992, Section 8.3.3.f, pp. 204-206.

[393] Berhane Temelso, C. David Sherrill, Ralph C. Merkle, Robert A. Freitas Jr., "High-level *Ab Initio* Studies of Hydrogen Abstraction from Prototype Hydrocarbon Systems," J. Phys. Chem. A 110(28 September 2006):11160-11173; http://pubs.acs.org/cgi-bin/abstract.cgi/jpcafh/2006/110/i38/abs/jp061821e.html (abstract), http://www.MolecularAssembler.com/Papers/TemelsoHAbst.pdf (paper).

[394] Berhane Temelso, C. David Sherrill, Ralph C. Merkle, Robert A. Freitas Jr., "*Ab Initio* Thermochemistry of the Hydrogenation of Hydrocarbon Radicals Using Silicon, Germanium, Tin and Lead Substituted Methane and Isobutane," J. Phys. Chem. A 111(15 August 2007):8677-8688. http://pubs.acs.org/cgi-bin/abstract.cgi/jpcafh/asap/abs/jp071797k.html (abstract), http://www.MolecularAssembler.com/Papers/TemelsoHDon.pdf (paper).

[395] Jingping Peng, Robert A. Freitas Jr., Ralph C. Merkle, "Theoretical Analysis of Diamond Mechanosynthesis. Part I. Stability of C_2 Mediated Growth of Nanocrystalline Diamond C(110) Surface," J. Comput. Theor. Nanosci. 1(March 2004):62-70; http://www.MolecularAssembler.com/JCTNPengMar04.pdf. Jingping Peng, Robert A. Freitas Jr., Ralph C. Merkle, James R. Von Ehr, John N. Randall, George D. Skidmore, "Theoretical Analysis of Diamond Mechanosynthesis. Part III. Positional C_2 Deposition on Diamond C(110) Surface using Si/Ge/Sn-based Dimer Placement Tools," J. Comput. Theor. Nanosci. 3(February 2006):28-41; http://www.MolecularAssembler.com/Papers/JCTNPengFeb06.pdf. Denis Tarasov, Natalia Akberova, Ekaterina Izotova, Diana Alisheva, Maksim Astafiev, Robert A. Freitas Jr., "Optimal Tooltip Trajectories in a Hydrogen Abstraction Tool Recharge Reaction Sequence for Positionally Controlled Diamond Mechanosynthesis," J. Comput. Theor. Nanosci. 5(2008). In preparation.

Figure I-5. At left: Image of the Physik Instrumente PicoCube P-363 XYZ Nanopositioner[396] and E-536 Controller,[397] which can provide 0.5 A (50 pm) positioning accuracy with 5 A (500 pm) repeatability across a 1 micron round-trip pathway. At right: Image of the Queensgate NPS-XYZ-100A/15A XYZ Nanopositioner,[398] which can provide 2.5 A (250 pm) positioning accuracy with 1 A (100 pm) repeatability across a 1 micron round-trip pathway.

Table I-1 is a survey of commercially available high-precision positioning components or systems. The "repeatability" columns report the positional hysteresis or linearity for each system, assuming a 1 micron round-trip excursion with a return to the original position. The table shows that at least three commercial positioning systems have 0.5 Å (50 pm) step accuracy but only with 5-10 Å (500-1000 pm) repeatability across 0.4 micron paths in closed-loop mode; one positioning system has 1 Å (100 pm) repeatability over a 1-micron round trip path but does not simultaneously possess high step accuracy.

---

[396] Physik Instrumente, "PicoCube™ Ultra-Fast, XY and XYZ NanoPositioning and Scanning Stages," accessed January 2008, http://www.pionline.it/html/schede/PicoCube.pdf; see also http://www.physikinstrumente.de/pdf/P363_Datasheet.pdf.

[397] "E-536 PicoCube® Piezo Controller," accessed January 2008; http://www.physikinstrumente.com/en/products/prdetail.php?sortnr=602950. See also: "XYZ-Piezo-Scanner for AFM Provides 25 Picometers Resolution," 4 June 2007; http://www.lambdaphoto.co.uk/press_releases/200642.

[398] Queensgate Instruments Ltd., "NPS-XYZ-100A/15A Technical Specification," accessed June 2004, http://www.nanopositioning.co.uk/products/NanoMechanisms/NPS-XYZ-100A-15A/specification.aspx; model NPS-XYZ-100A/15H has the same parameters, http://www.nanopositioning.co.uk/products/NanoMechanisms/NPS-XYZ-100A-15H/specification.aspx; Queensgate Instruments Ltd., "NPS-XYZ-100A/15A Technical Specification," accessed January 2008, http://www.nanopositioning.co.uk/catalogue/line.aspx?lne_id=6dfca5f5-4a3c-49cb-afaa-ae4b4acb558a.

Table I-1. Experimentally Attainable Positioning Precision for Commercially Available Systems (1 Å = 100 pm)

Nanopositioning System Manufacturer	Nanopositioning Model	**Resolution (Å)**			**Repeatability* (Å)**		
		X	Y	Z	X	Y	Z
Veeco	Dimension 3100[399]	60	60	0.5 [a]	100 [b]	100 [b]	*n/a*
Zyvex Corp.	S-100 Nanomanipulator[400]	50	50	50	*n/a*	*n/a*	*n/a*
Klocke Nanotechnik	XYZ-Manipulator[401]	100	100	100	*n/a*	*n/a*	*n/a*
	NMT-Modules[402]	20	20	20	*n/a*	*n/a*	*n/a*
	Nanomanipulator[403]	10	10	–	10 [c]	10 [c]	–
Danish MicroEngineer	95-200 AFM Scanner[404]	10	10	5	*n/a*	*n/a*	50 [d]
Asylum Research	MFP-3D™ AFM[405]	6	6	3	50 [e]	50 [e]	20 [f]
Attocube Systems	ANSxyz100 XYZ-scanner[406]	~5	~5	~5	500 [s]	500 [s]	500 [s]
PiezoMax/nPoint	XY40Z25 3-axis stage[407]	3	3	2	2 [g]	2 [g]	2 [g]

---

[399] Veeco, "Dimension 3100 Datasheet," accessed June 2004, http://www.veeco.com/html/datasheet_d3100.asp.

[400] Zyvex Corp., "S100 Nanomanipulator Specifications," accessed June 2004, http://www.zyvex.com/Products/S100_Spec.html; "Zyvex's S100 Nanomanipulator System," accessed June 2004, http://www.zyvex.com/Products/S100_Faq.html.

[401] Klocke Nanotechnik, "XYZ – Manipulator: Orthogonal Movement with High Resolution," accessed June 2004, http://www.nanomotor.de/n_xyz_manipulator.htm.

[402] Klocke Nanotechnik, "SEM-Manipulators: Comparison of Different Systems," accessed June 2004, http://www.nanomotor.de/pdf/Compare_e_lo.pdf; "The Nanomanipulator: A Universal Tool With One Nanometer Resolution," accessed June 2004; http://www.nanomotor.de/pdf/nanoman_e_lo.PDF.

[403] Klocke Nanotechnik, "Manipulators: Univeral Tools with 1 Nanometer Resolution," June 2004, http://www.nanomotor.de/p_nanomanipulator.htm; "Processing Material in Electron Microscopes: Nanomanipulation With Several D.O.F.," accessed June 2004, http://www.nanomotor.de/aa_processing.htm.

[404] Danish Micro Engineering (DME), "DME AFM scanners: Technical specifications for 95-200 AFM scanner,' accessed June 2004, http://www.dme-spm.dk/Products/AFMScanner.htm.

[405] Asylum Research, "MFP-3D™ Atomic Force Microscope: Power and Flexibility in One Complete System," accessed June 2004, http://www.asylumresearch.com/Products/Mfp3D/Mfp3D.pdf.

[406] Attocube Systems, "ANSxyz100 large range xyz-scanner," accessed January 2008, http://attocube.com/nanoPOSITIONING/ANSxyz100/Specifications_ANSxyz100.pdf.

Mad City Labs	Nano-F100 positioner[408]	2	–	–	*n/a*	–	–
	Nano-M350 XYZ positioner[409]	1	1	0.5	*n/a*	*n/a*	*n/a*
	Nano-T Series XYZ positioner[410]	2	2	0.4	*n/a*	*n/a*	*n/a*
Pacific Nanotechnology	Nano-R[411]	1	1	1	20 [h]	20 [h]	*n/a*
	Nano-I[412]	2	2	2	20 [h]	20 [h]	*n/a*
Concern Nanoindustry	Base system[413]	1	1	–	*n/a*	*n/a*	–
Queensgate Instruments	NPS-X-15A, 1-axis[414]	0.5 [i]	–	–	1 [j]	–	–
	NPS-XY-100A, 2-axis[415]	1 [k]	1 [k]	–	0.5 [j]	0.5 [j]	–
	NPS-XYZ-100A/15A[416]	2.5 [l]	2.5 [l]	0.5 [m]	1 [j]	1 [j]	1 [j]

---

[407] PiezoMax/nPoint, "Specification Table: XY40Z25 3-axis stage," accessed June 2004, http://www.piezomax.com/dnld/spec/spec-XY40Z25_3715109.pdf.

[408] Mad City Labs, Inc., "Nano-F Series," accessed January 2008, http://www.madcitylabs.com/nanofseries.html.

[409] Mad City Labs, Inc., "Nano-M350," accessed January 2008, http://www.madcitylabs.com/nanom350.html.

[410] Mad City Labs, Inc., "Nano-T Series," accessed January 2008, http://www.madcitylabs.com/nanotseries.html.

[411] Pacific Nanotechnology, Inc., "The Nano-R™ Atomic Force Microscope," accessed June 2004, http://pacificnanotech.com/nano-r-afm_nano-r-specifications.html.

[412] Pacific Nanotechnology, Inc., "The Nano-I™ Atomic Force Microscope," accessed June 2004, http://pacificnanotech.com/nano-i-afm_nano-i-specifications.html.

[413] Concern Nanoindustry, "Nanotechnological System," accessed June 2004, http://www.nanotech.ru/cn/e/tech6.php.

[414] Queensgate Instruments Ltd., "NPS-X-30A Technical Specification," accessed June 2004, http://www.nanopositioning.co.uk/products/NanoMechanisms/NPS-X-30A/specification.aspx; Queensgate Instruments Ltd., "Nano Mechanisms-NPS-X-15A Technical Datasheet," accessed January 2008, http://www.nanopositioning.co.uk/catalogue/line.aspx?lne_id=1b7c9a8d-6bca-4003-a880-ceabbc029c17.

[415] Queensgate Instruments Ltd., "NPS-XY-100B Technical Specification," accessed June 2004, http://www.nanopositioning.co.uk/products/NanoMechanisms/NPS-XY-100B/specification.aspx; Queensgate Instruments Ltd., "NPS-XY-100A Technical Datasheet," accessed January 2008, http://www.nanopositioning.co.uk/catalogue/line.aspx?lne_id=400ed857-5446-4fb9-a622-c91483b290ab.

[416] Queensgate Instruments Ltd., "NPS-XYZ-100A/15A Technical Specification," accessed June 2004, http://www.nanopositioning.co.uk/products/NanoMechanisms/NPS-XYZ-100A-15A/specification.aspx; model NPS-XYZ-100A/15H has the same parameters, http://www.nanopositioning.co.uk/products/NanoMechanisms/NPS-XYZ-100A-15H/specification.aspx; Queensgate Instruments Ltd., "NPS-XYZ-100A/15A Technical Specification," accessed January 2008, http://www.nanopositioning.co.uk/catalogue/line.aspx?lne_id=6dfca5f5-4a3c-49cb-afaa-ae4b4acb558a.

Physik Instrumente (PI)	PicoCube P-363 XYZ[417]	0.5 [n]	0.5 [n]	0.5 [n]	10 [o]	10 [o]	20 [o]
	PicoCube P-363 XY[418]	0.5 [n]	0.5 [n]	–	5 [o]	5 [o]	–
	P.C. P-363 + E-536 Controller[419]	0.25 [n]	0.25 [n]	–	5 [o]	5 [o]	–
	Capacitive Position Sensors[420]	0.1	–	–	0.3 [p]	–	–
	N-310 NEXACT® PiezoWalk[421]	0.25	–	–	0.25 [c]	–	–
NanoWave	NW SPPE[422]	0.13 [q]	–	–	10 [r]	–	–
Minimum needed to achieve controlled DMS:		***0.5***	***0.5***	***0.5***	***0.5***	***0.5***	***0.5***

[417] Physik Instrumente, "PicoCube™ Ultra-Fast, XY and XYZ NanoPositioning and Scanning Stages," accessed January 2008, http://www.pionline.it/html/schede/PicoCube.pdf; see also http://www.physikinstrumente.de/pdf/P363_Datasheet.pdf.

[418] Physik Instrumente, "PicoCube™ Ultra-Fast, XY and XYZ NanoPositioning and Scanning Stages," accessed January 2008, http://www.pionline.it/html/schede/PicoCube.pdf; see also http://www.physikinstrumente.de/pdf/P363_Datasheet.pdf.

[419] "E-536 PicoCube® Piezo Controller," accessed January 2008; http://www.physikinstrumente.com/en/products/prdetail.php?sortnr=602950. See also: "XYZ-Piezo-Scanner for AFM Provides 25 Picometers Resolution," 4 June 2007; http://www.lambdaphoto.co.uk/press_releases/200642.

[420] Physik Instrumente, "Capacitive Position Sensors / Controllers, Featuring Sub-Nanometer Resolution," accessed January 2008, http://nanotechweb.org/buyers/index.cfm?action=viewcomp&id=698.

[421] Physik Instrumente, "N-310 Compact NEXACT® OEM Piezo Stepping Drives with Long Travel Ranges," accessed January 2008, http://www.physikinstrumente.com/en/pdf/N310_Datasheet.pdf.

[422] Physik Instrumente, "Characteristics of Capacitive Position Sensors: Stability and Linearity of PI Capacitive Position Sensors," accessed June 2004, http://www.physikinstrumente.de/products/prdetail.php?secid=5-6. NanoWave, Inc., "NanoWave Inc. Breakthrough – Attains Picometer-Resolution Position Measurement System for True NanoScale Manufacturing," June 2003 Press Release, accessed June 2004, http://www.nanowave.com/news_FAQs/news_PR_02.html.

* positional hysteresis or linearity, assuming 1 µm round-trip excursion with return to original position
Open loop control = dead reckoning with no sensory feedback; closed loop control = motion guided by sensory feedback

[a] "RMS Z-noise, in appropriate environment"
[b] "XY nonlinearity 1%"
[c] "with no backlash"
[d] "Z-linearization: 0.5% on full-scale scan"
[e] "sensor nonlinearity 0.5% full travel, closed-loop all 3 axes"
[f] "sensor nonlinearity 0.2% full travel, closed-loop all 3 axes"
[g] "typical linearity and hysteresis 0.02% at slew rate of 8 mm/sec"
[h] "scan linearity 1%"
[i] "position noise (1 sigma) at slowest slew rate of 1.0 mm/sec"
[j] typical linearity error is 0.005%-0.01%, "percent error over the full range of motion"; 0.01% hysteresis error peak-to-peak, "hysteresis specification for a displacement of less than 1 µm amplitude is 0.1 nm"
[k] "position noise (1 sigma) at slowest slew rate of 0.5 mm/sec"
[l] "position noise (1 sigma) at slowest slew rate of 0.5 mm/sec"
[m] "position noise (1 sigma) at slowest slew rate of 0.5 mm/sec"
[n] "open-loop resolution"
[o] "typical closed loop P-363 repeatability" (across 0.4 µm of travel)
[p] "When used with PI digital controllers (which use 4th order polynomial linearization techniques), positioning linearity up to 0.003% is achievable"[423]
[q] "NanoWave Scanning Probe Position Encoder demonstrated approximately 13 picometers resolution"
[r] "precision/repeatability"
[s] linearity "typically 5-10%"

Research systems have exhibited better performances in specific areas but these advances have not yet been integrated into commercially available manipulator systems. For example, in imaging, isolated SPM-based positioning systems have achieved high-resolution imaging scans – one demonstrated by a German group at Augsburg University[424] showing features of 0.77 Å (77 pm) and another by an ORNL group[425] showing 0.6 Å (60 pm) features. A UCSB team[426] has reported the record-breaking detection of ~0.023 pm deflections in a 250-nm-wide beam of GaAs

---

[423] NanoWave, Inc., "Technology/capabilities," accessed June 2004, http://www.nanowave.com/technology_applications/tech_cap.html.

[424] Stefan Hembacher, Franz J. Giessibl, Jochen Mannhart, "Force Microscopy with Light-Atom Probes," Science 305(16 July 2004):380-383. See also: Belle Dumé, "Microscopy Moves to the Picoscale," PhysicsWeb.org, 10 June 2004; http://physicsweb.org/article/news/8/6/6.

[425] P.D. Nellist, M.F. Chisholm, N. Dellby, O.L. Krivanek, M.F. Murfitt, Z.S. Szilagyi, A.R. Lupini, A. Borisevich, W.H. Sides, Jr., S.J. Pennycook, "Direct Sub-Angstrom Imaging of a Crystal Lattice," Science 305(17 September 2004):1741. See also: "ORNL Microscope Pushes Back Barrier of 'How Small'," 19 September 2004; http://www.nanotechnology.com/news/?id=5025.

[426] Robert G. Knobel, Andrew N. Cleland, "Nanometer-scale displacement sensing using a Single-Electron Transistor," Nature 424(17 July 2003):291-293. See also: Jyllian Kemsley, "Device Measures Femtometers: Nanoscale sensor couples transistor with crystal to approach quantum limit," Chemical & Engineering News 81(21 July 2003):6; http://pubs.acs.org/cen/topstory/8129/8129notw5.html.

at a temperature of 3 millikelvins. FEI Company's Titan 80-300 High-Resolution Scanning-Transmission Electron Microscope (HR-STEM) can image diamond C(110) surface at 0.9 Å (90 pm) resolution and germanium Ge(112) surface at 0.81 Å (81 pm) resolution,[427] and the TEAM 0.5 transmission electron achromatic microscope (the world's most powerful transmission electron microscope can produce images with ~0.5 Å (50 pm) resolution.[428] In metrology, Chassagne's group in France has designed a positioning control system with repeatable 0.53 Å (53 pm) precision over 1 micron of travel[429] and another control system with repeatable 5 Å (500 pm) precision over 5 mm of travel.[430] A NIST group[431] reported operating a vacuum chamber-based laser-based device able to measure 25 millimeter distances to 0.1 Å (10 pm) accuracy in 2005. In 2006, Robert Celotta (also of NIST) reported[432] the ability to stabilize an STM to 0.002 Å (0.2 pm).

We conclude from this survey that all of the components likely to be needed to construct a reliable 0.2-0.5 Å (20-50 pm) 1-tip 3-DOF (degrees of freedom) picomanipulator are presently in existence, and that to build such a system only will require sufficient dedicated resources and a well-focused research effort. It is possible that feature-oriented scanning methodologies might assist the fine positioning task.[433]

---

[427] FEI Company, "Titan™ 80-300," accessed January 2008; http://www.feicompany.com/Portals/_default/PDFs/content/2007_10_TitanFamily_pb.pdf.

[428] "0.5 Angstrom transmission electron microscope," 22 January 2008; http://nextbigfuture.com/2008/01/05-angstrom-transmission-electron.html.

[429] Luc Chassagne, Suat Topcu, Yasser Alayli, Patrick Juncar, "Highly accurate positioning control method for piezoelectric actuators based on phase-shifting optoelectronics," Meas. Sci. Technol. 16(2005):1771-1777.

[430] L. Chassagne, M. Wakim, S. Xu, S. Topçu, P. Ruaux, P. Juncar, Y. Alayli, "A 2D nano-positioning system with sub-nanometric repeatability over the millimetre displacement range," Meas. Sci. Technol. 18(2007):3267-3272; http://www.iop.org/EJ/abstract/0957-0233/18/11/001.

[431] J.R. Lawall, "Fabry-Perot metrology for displacements up to 50 mm," J. Optical Soc. Amer. A (December 2005). See also: "Physicists measure 'long' distances with picometer accuracy," 2 December 2005; http://www.physorg.com/news8668.html.

[432] Robert Celotta, "Enabling Nanotechnology: An Introduction to NIST's New Center for Nanoscale Science & Technology," presentation at the SME Conference: "The Next Industrial Revolution: Nanotechnology & Manufacturing," Oak Ridge, TN, 24 August 2006; http://www.sme.org/cgi-bin/get-evdoc.pl?&&001640&000007&020104&&SME&.

[433] Rostislav V. Lapshin, "Feature-oriented scanning methodology for probe microscopy and nanotechnology," Nanotechnology 15(September 2004):1135-1151; http://www.nanoworld.org/homepages/lapshin/publications.htm#feature2004.

3.2.1.4 Ultra-Sharp and Atomically Precise SPM Tips

Ultrasharp, and preferably atomically precise, scanning probe tips are needed to reliably perform positionally controlled mechanosynthetic reactions. Atomically-precise diamondoid pyramidal tooltip geometries (Figure I-11) as described in Section 3.2.1.5 – that may require atomically precise molecular manufacturing to fabricate – will allow the close tooltip proximation required for DMS, but current scanning probe tips with a sub-nanometer radius of curvature should allow 2-tip operations in free space and may allow multi-tip operations near surfaces. A 2008 survey (Table I-2) of available ultra-sharp tips – generally defined as having a radius of curvature of 10-20 nm (~50-100 carbon atoms) or less – revealed that sub-nanometer tips are already available in many materials, including diamond and CNTs, and that three-atom and one-atom tungsten tips[434] have been fabricated (though tungsten has a tendency to oxidize). Especially noteworthy is the NT-MDT[435] diamond-like carbon (DLC) spike-probe tip with an asperity that is only a few carbon atoms wide at the tip. This tip has been used by Klinov et al.[436] to scan short poly(dG)-poly(dC) DNA fragments deposited on modified HOPG (highly oriented pyrolytic graphite), enabling them to detect single-stranded regions in double-stranded poly(dG)-poly(dC) and double-stranded and single-stranded regions in poly(dG)-poly(dG)-poly(dC) triplexes, as well as to resolve the helical pitch of the triplex molecules (Figure I-6). Thus it appears that sufficient tip sharpness is already available to undertake Phase I efforts which will require single-molecule bonding to the tips.

---

[434] Moh'd Rezeq, Jason Pitters, Robert Wolkow, "Tungsten nanotip fabrication by spatially controlled field-assisted reaction with nitrogen," J. Chem. Phys. 124(28 May 2006):204716; http://www.aip.org/png/2006/264.htm (image), http://www.phys.ualberta.ca/~wolkow (movie).

[435] NT-MDT (Molecular Devices and Tools for Nanotechnology, Moscow, Russia, http://www.ntmdt.com), "Super sharp Diamond_Like Carbon (DLC) tips," from their "SPM Probe and Accessories" catalog, 2008; http://www.ntmdt.com/download/accessories_catalog.pdf.

[436] Dmitry Klinov, Benjamin Dwir, Eli Kapon, Natalia Borovok, Tatiana Molotsky, Alexander Kotlyar, "High-resolution atomic force microscopy of duplex and triplex DNA molecules," Nanotechnology 18(6 June 2007):225102.

Figure I-6. Probe sharpness determines resolution. DNA strand diameter (~2 nm) can be resolved[437] using a ~1 nm DLC spike-probe tip.[438] Small unwound single-strand DNA fragments can be seen (bold arrow on scan) and even the helical pitch of the DNA molecule can be resolved (thin arrows).

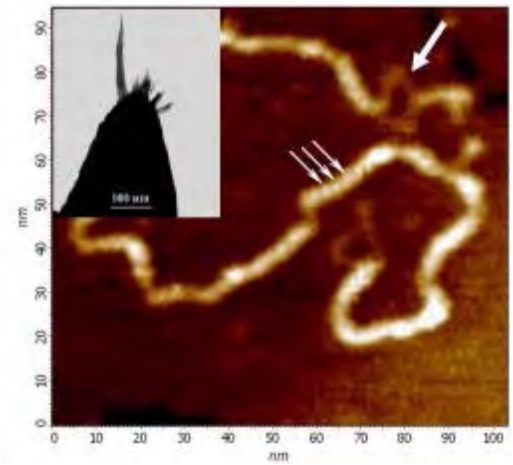

[437] "DNA in nanotechnology," 2007; http://www.nanovip.com/node/4971. Dmitry Klinov, Benjamin Dwir, Eli Kapon, Natalia Borovok, Tatiana Molotsky, Alexander Kotlyar, "High-resolution atomic force microscopy of duplex and triplex DNA molecules," Nanotechnology 18(6 June 2007):225102.

[438] NT-MDT (Molecular Devices and Tools for Nanotechnology, Moscow, Russia, http://www.ntmdt.com), "Super sharp Diamond_Like Carbon (DLC) tips," from their "SPM Probe and Accessories" catalog, 2008; http://www.ntmdt.com/download/accessories_catalog.pdf.

Table I-2. Experimentally Attainable or Commercially Available Ultra-Sharp Probe Tips for Scanning Probe Microscopy			
Probe Tip Manufacturer or Experimentalist Group	**Probe Tip Product**	**Probe Tip Radius**	**Image of Tip**
Silicon			
Tao et al.[439]	experimental tip	< 20 nm	
Park Systems[440]	HART0-#-05	10 nm	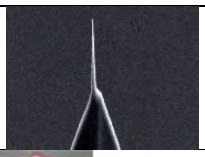
Nanochip[441]	data storage cantilever tips	10 nm	
Park et al.[442]	experimental tip	< 10 nm	

[439] Y. Tao, R. J. Fasching, F. B. Prinz, "Ultra-sharp High-aspect-ratio Probe Array for SECM and AFM Analysis," 2003, http://www-rpl.stanford.edu/goto-publication/138; Ye Tao, Rainer J. Fasching, Fritz B. Prinz, "Ultrasharp high-aspect-ratio probe array for SECM and AFM Analysis," Proceedings of SPIE, Vol. 5389, Smart Structures and Materials 2004: Smart Electronics, MEMS, BioMEMS, and Nanotechnology, Vijay K. Varadan, ed., July 2004, pp. 431-442.

[440] Park Systems (http://www.parkafm.com/) SPM Tool Box; HART0-#-05, http://www.psiastore.com/product.sc?categoryId=11&productId=98.

[441] Kevin Bullis, "Higher-Capacity Memory: A new type of memory could soon be available to device makers," Technology Review, 12 February 2008; http://www.technologyreview.com/Nanotech/20192/. See also Nanochip website: http://www.nanochipinc.com/.

[442] Jaehong Park, Kidong Park, Byoungdoo Choi, Kyo-In Koo, Seung-Joon Paik, Sangjun Park, Jongpal Kim, Dong-Il Dan Cho, "A novel fabrication process for ultra-sharp, high-aspect ratio nano tips using (111) single crystalline silicon," 12th International Conference on Transducers, Solid-State Sensors, Actuators and Microsystems, 2003, Vol. 2, 8-12 June 2003, pp. 1144-1145.

Nanosensors[443]	Pointprobe® Silicon-SPM-Sensors	< 10 nm	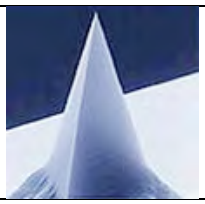
Innovative Solutions[444]	ISB-BudgetSensors	< 10 nm	
NanoWorld®[445]	AR5-NCHR Cantilevers	< 10 nm	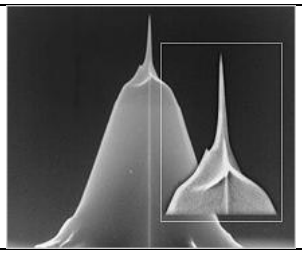
ASM[446]	various tips	< 10 nm	
Applied NanoStructures[447]	HART0-1	< 10 nm	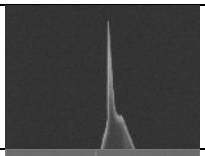
Veeco[448]	Super Cone Probes	< 10 nm	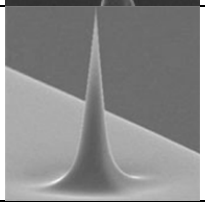

[443] Nanosensors™ Probes, Pointprobe® Silicon-SPM-Sensors http://www.nano-tools.com/php/cantilever.php?g_id=2&t_id=18.

[444] Innovative Solutions Bulgaria (ISB-BudgetSensors) Sofia, Bulgaria.

[445] NanoWorld® POINTPROBE® sensors, https://ssl.jpk.com/cantilevers/images/ar5.jpg; Type AR5-NCHR Cantilevers, https://ssl.jpk.com/cantilevers/csc_article_details.php?nPos=0&saArticle[ID]=29&VID=NyVAykQ2RMEgcnrx.

[446] Advanced Surface Microscopy, Inc. (ASM) Indianapolis, IN.

[447] Applied NanoStructures, high aspect ratio probe tips, HART0-1; http://www.2spi.com/catalog/spec_prep/high-aspect-ratio-AFM-probe-tips.shtml.

[448] IBMSC – Super Cone Probes; https://www.veecoprobes.com/probe_detail.asp?ClassID=28.

Park Systems[449]	FORTA-10	5-6 nm	
Park Systems[450]	SICONA-10	5-6 nm	
Park Systems[451]	ACLA-10	5-6 nm	
MikroMasch[452]	GP AFM probe STING probe (DP14)	5-10 nm	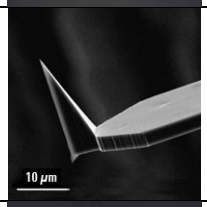
Park Systems[453]	ACTA-10	5-6 nm	
Park Systems[454]	NCHR (610-#051)	2-5 nm	

[449] Park Systems (http://www.parkafm.com/) SPM Tool Box; FORTA-10, http://www.psiastore.com/product.sc?categoryId=7&productId=95.

[450] Park Systems (http://www.parkafm.com/) SPM Tool Box; SICONA-10, http://www.psiastore.com/product.sc?categoryId=6&productId=94.

[451] Park Systems (http://www.parkafm.com/) SPM Tool Box; ACLA-10, http://www.psiastore.com/product.sc?categoryId=4&productId=92.

[452] MikroMasch http://www.spmtips.com/, GP AFM probe http://www.spmtips.com/products/cantilevers/datasheets/gp, DP14/GP series http://www.spmtips.com/dp140/gp.

[453] Park Systems (http://www.parkafm.com/) SPM Tool Box; ACTA-10, http://www.psiastore.com/product.sc?categoryId=4&productId=93.

[454] Park Systems (http://www.parkafm.com/) SPM Tool Box; NCHR (610-#051), http://www.psiastore.com/product.sc?categoryId=4&productId=102.

Veeco[455]	TESP-SS - ESP Series Probes - Super Sharp Tip	2-5 nm	
NanoScience Instruments[456]	ACL-SS Super Sharp Dynamic Mode AFM Probes	2-3 nm	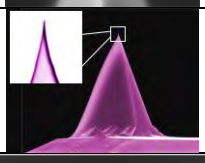
Nanosensors[457]	SuperSharpSilicon™	< 2 nm	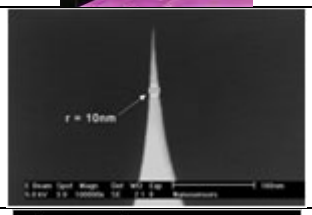
NanoWorld®[458]	SSS-NCH Cantilevers	< 2 nm	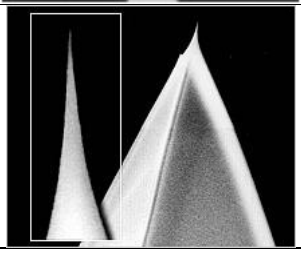
Marcus et al.[459]	experimental tip	~1 nm	
Ding et al.[460]	field emission tip	~0.75 nm	

---

[455] TESP-SS - ESP Series Probes - Super Sharp Tip; https://www.veecoprobes.com/probe_detail.asp?ClassID=111.

[456] NanoScience Instruments, "ACL-SS Super Sharp Dynamic Mode AFM Probes" AC / tapping mode - 225 micron Long cantilever - Super Sharp tip; http://store.nanoscience.com/store/pc/viewCategories.asp?idCategory=83.

[457] Nanosensors http://www.nanosensors.com/ , http://www.nanosensors.com/products_overview.html, SuperSharpSilicon™ http://www.nanosensors.com/products_overview.html#SSS (Image) Writeup on SSS is at: http://www.nanosensors.com/SuperSharpSilicon.pdf.

[458] NanoWorld®, Tip shape: Super Sharp, https://ssl.jpk.com/cantilevers/images/sss.jpg Type SSS-NCH Cantilevers https://ssl.jpk.com/cantilevers/csc_article_details.php?nPos=0&saArticle[ID]=45&VID=NyVAykQ2RMEgcnrx.

[459] R.B. Marcus, T.S. Ravi, T. Gmitter, K. Chin, D. Liu, W.J. Orvis, D.R. Ciarlo, C.E. Hunt, J. Trujillo, "Formation Of Silicon Tips with < 1 nm Radius," Appl. Phys. Lett. 56(15 January 1990):236-238; http://www.ece.ucdavis.edu/HuntGroup/Publications/APL_Marcus_AtomSharp.pdf. See also: Yongxia Zhang, Yanwei Zhang, T.S. Sriram, R.B. Marcus, "Formation of single tips of oxidation-sharpened Si," Appl. Phys. Lett. 69(30 December 1996):4260.

Tungsten			
Fujita et al.[461]	experimental tip	5 nm	
Guise et al.[462]	electrochemical etch	5 nm	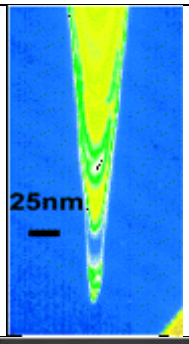
Lucier[463]	three-atom apex W(111) tip	< 0.6 nm	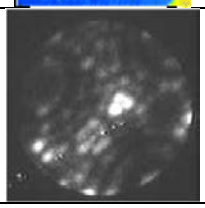
Chen[464] and Binh[465]	single-atom "Teton tip"	~0.3 nm (single-atom tip)	

---

[460] Ding Meng, Sha Guobin, A.I. Akinwande, "Silicon field emission arrays with atomically sharp tips: turn-on voltage and the effect of tip radius distribution," IEEE Transactions on Electron Devices 49(December 2002):2333-2342.

[461] Jun-ichi Fujita, Yuta Ikeda, Satoshi Okada, Kodai Higashi, Shotaro Nakazawa, Masahiko Ishida, Shinji Matsui, "In-situ Visualization of Local Field Enhancement in an Ultra Sharp Tungsten Emitter under a Low Voltage Scanning Transmission Electron Microscope," Japanese Journal of Applied Physics 46(2007):L498-L501; http://jjap.ipap.jp/link?JJAP/46/L498/.

[462] Olivier L. Guise, Joachim W. Ahner, Moon-Chul Jung, Peter C. Goughnour, John T. Yates Jr., "Reproducible Electrochemical Etching of Tungsten Probe Tips," Nano Letters 2(2002):191-193; http://pubs.acs.org/cgi-bin/abstract.cgi/nalefd/2002/2/i03/abs/nl010094q.html.

[463] Anne-Sophie Lucier, "Preparation and Characterization of Tungsten Tips Suitable for Molecular Electronics Studies," M.S. Thesis, Center for the Physics of Materials, Department of Physics, McGill University, Montreal, Quebec, Canada, February 2004; http://www.physics.mcgill.ca/~peter/theses/lucier.pdf.

[464] C.J. Chen, Introduction to Scanning Tunneling Microscopy, Oxford University Press, 1993.

[465] V.T. Binh, "In Situ Fabrication and Regeneration of Microtips for Scanning Tunnelling Microscopy," J. Microsc. 152(November 1988):355-361.

Rezeq et al.[466]	single-atom tip (FIM image)	~0.3 nm (inside centermost ring)	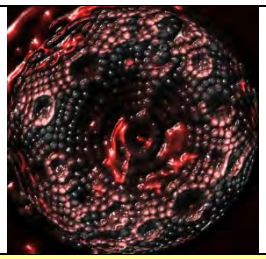
Diamond/DLC			
Wang et al.[467]	solid diamond	< 50 nm	
Nanosensors[468]	diamond-coated silicon	10 nm	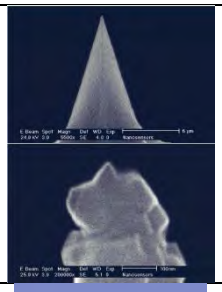
Nanotools[469]	T-EAR M* 8-40 (high dense carbon over silicon nitride)	~10 nm	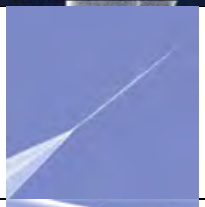
Nanotools[470]	Universal Type U3 (high dense carbon over silicon nitride)	~10 nm	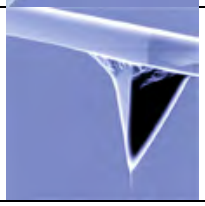

[466] Moh'd Rezeq, Jason Pitters, Robert Wolkow, "Tungsten nanotip fabrication by spatially controlled field-assisted reaction with nitrogen," J. Chem. Phys. 124(28 May 2006):204716, http://www.aip.org/png/2006/264.htm (image), http://www.phys.ualberta.ca/~wolkow (movie).

[467] Zongli Wang, Changzhi Gu, Junjie Li, Zheng Cui, "A novel method for making high aspect ratio solid diamond tips," Microelectronic Engineering 78-79(March 2005):353-358.

[468] Nanosensors: Diamond Coated Silicon-SPM-Sensors Pointprobe®; http://www.nanosensors.com/Diamond.pdf.

[469] Nanotools Scanning Probes, "Supersharp Probes," http://www.nano-tools.com/.

[470] Nanotools Scanning Probes, "Supersharp Probes," http://www.nano-tools.com/.

Advanced Diamond Technologies, Inc.[471]	NaDiaProbe™ (ultrananocrystalline (~5 nm) diamond)	7-12 nm	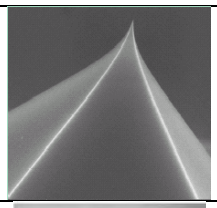
Mesa & Magonov[472]	solid diamond experimental tips	5 nm	
Nanotools[473]	Supersharp (high dense carbon over silicon nitride)	2-3 nm	
Veeco[474]	Diamond-Like Carbon Spike Probe	1 nm *(asperity)* 5 nm *(tip)*	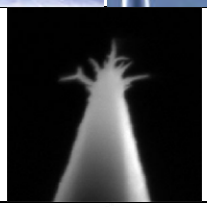
NT-MDT[475]	Super sharp Diamond-Like Carbon (DLC) tips	≤ 1 nm	
Carbon Nanotube Tips			
Dai et al.[476]	MWCNT	5-20 nm	

[471] Advanced Diamond Technologies, Inc., "NaDiaProbe™ – Monolithic Diamond AFM Probes," accessed March 2008; http://www.thindiamond.com/downloads/NaDiaProbe.pdf.

[472] Bernard Mesa, Sergei Magonov, "Novel diamond/sapphire probes for scanning probe microscopy applications," Journal of Physics: Conference Series 61(2007):770-774; http://www.microstartech.com/index/mesa-magonov.pdf.

[473] Nanotools Scanning Probes, "Supersharp Probes," http://www.nano-tools.com/.

[474] "Diamond-Like Carbon Spike Probes," https://www.veecoprobes.com/probe_detail.asp?ClassID=12.

[475] NT-MDT (Molecular Devices and Tools for Nanotechnology, Moscow, Russia, http://www.ntmdt.com), "Super sharp Diamond_Like Carbon (DLC) tips," from their "SPM Probe and Accessories" catalog, 2008; http://www.ntmdt.com/download/accessories_catalog.pdf.

NanoScience Instruments[477]	Carbon Nanotube AFM Tips	5-15 nm	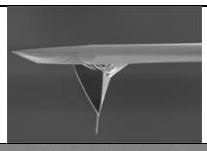
Xidex[478]	MWCNT	~10 nm	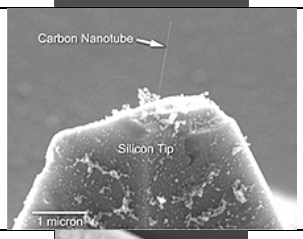
Cheung et al.[479]	MWCNT	3-8 nm	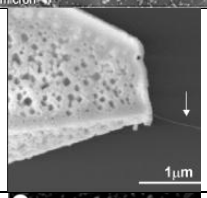
Zhang et al.[480]	tubular graphite cones	2-10 nm	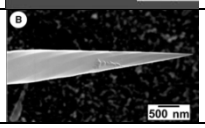
Lieber et al.[481]	MWCNT	3-5 nm	

---

[476] Hongjie Dai, Jason H. Hafner, Andrew G. Rinzler, Daniel T. Colbert, Richard E. Smalley, "Nanotubes as Nanoprobes in Scanning Probe Microscopy," Nature 384(1996):147-151; http://web.archive.org/web/20020609154706/http://cnst.rice.edu/TIPS_rev.htm.

[477] NanoScience Instruments, "Carbon Nanotube AFM Tips," CNTek™ AFM Probes; http://www.nanoscience.com/products/carbon_nanotube_probes.html.

[478] "AMRC Research Leads to Promising Nanotechnology Application for Chip Industry," (23 February, 2005), Advanced Materials Research Center, SEMATECH; http://www.amrctx.org/news/20050223.htm.

[479] Chin Li Cheung, Jason H. Hafner, Charles M. Lieber, "Carbon nanotube atomic force microscopy tips: Direct growth by chemical vapor deposition and application to high-resolution imaging," Proc. Natl. Acad. Sci. (USA) 97(11 April 2000):3809-3813; http://www.pubmedcentral.nih.gov/articlerender.fcgi?artid=18098.

[480] Guangyu Zhang, Xin Jiang, Enge Wang, "Tubular Graphite Cones," Science 300(18 April 2003):472-474; http://www.scienceonline.org/cgi/content/full/300/5618/472.

[481] Charles M. Lieber, Adam T. Woolley, Jong-in Hahm, David Housman, "Direct haplotyping using carbon nanotube probes," United States Patent 20020146714, 10/10/2002, http://freepatentsonline.com/20020146714.html; see also (WO/2002/022889) Direct Haplotyping Using Carbon Nanotube Probes, http://www.wipo.int/pctdb/en/wo.jsp?IA=US2001042138&DISPLAY=DESC.

Martinez et al.[482]	MWCNT sharpened to SWCNT radius	~0.9 nm	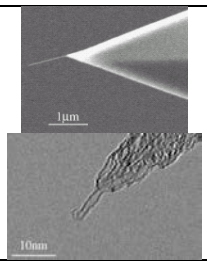
Nguyen et al.[483]	SWCNT	0.7 nm	
Hafner et al.[484]	SWCNT	0.5-1.4 nm	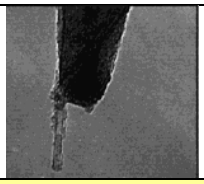
Other			
Zhu et al.[485]	Fe_2O_3 nanoflakes	12-22 nm	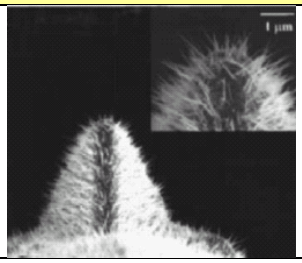
Lee et al.[486]	ZnO piezo tip	< 15 nm	

[482] J. Martinez, T.D. Yuzvinsky, A.M. Fennimore, A. Zettl, R. Garcia, C. Bustamante, "Length control and sharpening of atomic force microscope carbon nanotube tips assisted by an electron beam," Nanotechnology 16(2005):2493-2496; http://socrates.berkeley.edu/~tyuz/pub/nanotechnology16.pdf.

[483] Cattien V. Nguyen, Kuo-Jen Chao, Ramsey M.D. Stevens, Lance Delzeit, Alan Cassell, Jie Han, M. Meyyappan, "Carbon nanotube tip probes: stability and lateral resolution in scanning probe microscopy and application to surface science in semiconductors," Nanotechnology 12(September 2001):363-367; http://www.iop.org/EJ/abstract/0957-4484/12/3/326/.

[484] J.H. Hafner, C.L. Cheung, T.H. Oosterkamp, C.M. Lieber, "High-Yield Assembly of Individual Single-Walled Carbon Nanotube Tips for Scanning Probe Microscopies," J. Phys. Chem. B. 105(2001):743-746; http://cmliris.harvard.edu/publications/2000s/2001/jPCB105_743.pdf.

[485] Y.W. Zhu, T.Yu, C.H. Sow, Y.J. Liu, A.T.S. Wee, X.J. Xu, C.T. Lim, J.T.L. Thong, "Efficient field emission from -Fe_2O_3 nanoflakes on an atomic force microscope tip,"Appl. Phys. Lett. 87(2005):023103; http://www.ntu.edu.sg/home/yuting/papers/APL_Fe2O3%20on%20AFM%20tip.pdf.

[486] S.H. Lee, S.S. Lee, J.-J. Choi, J.U. Jeon, K. Ro, "Fabrication of a ZnO piezoelectric micro cantilever with a high-aspect-ratio nano tip," Microsystem Technologies 11(June 2005):416-423..

Asylum Research[487]	aluminum tip	< 15 nm	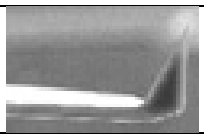
Libioulle et al.[488]	platinum tip	~5 nm	
Ermanoski et al.[489]	faceted clean iridium	~0.3 nm (single-atom tip; schematic at lower right)	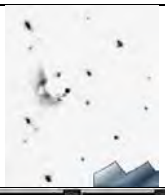
Fu et al.,[490] Madey et al.,[491] Kuo et al.,[492] Itagaki et al.[493]	Pd-coated tungsten	~0.3 nm (single-atom tip)	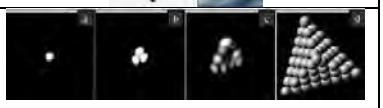

Another important consideration is that these early tips (the ultra-sharps) must also have an adequate aspect ratio – that is, they need to be sufficiently long and pointed. A good range of "high aspect ratio" tips are commercially available, with some providing ratios as high as 20:1 (especially the nanotube-based tips). For example, Ahner et al.[494] used ultra-sharp tungsten

---

[487] Asylum Research, AC160BN, High Aspect Ratio, AC Mode; http://www.asylumresearch.com/Products/Levers/AC160BN.shtml.

[488] L. Libioulle, Y. Houbion, J.-M. Gilles, "Very sharp platinum tips for scanning tunneling microscopy," Rev. Sci. Instrum. 66(January 1995):97.

[489] Ivan Ermanoski, Kalman Pelhos, Wenhua Chen, Jamie S. Quinton, Theodore E. Madey, "Oxygen-induced nano-faceting of Ir(210)," Surf. Sci. 549(10 January 2004):1-23.

[490] T.-Y. Fu, L.C. Cheng, C.H. Nien, T.T. Tsong, "Method of creating a Pd-covered single-atom sharp W pyramidal tip: Mechanism and energetics of its formation," Phys. Rev. B 64(15 September 2001):113401.

[491] Theodore E. Madey, Kalman Pelhos, Qifei Wu, Robin Barnes, Ivan Ermanoski, Wenhua Chen, Jacek J. Kolodziej, John E. Rowe, "Nanoscale surface chemistry," Proc. Nat. Acad. Sci. USA 99(2002):6503-6508; http://www.physics.rutgers.edu/~wchen/Madey_page/Full_Publications/PDF/madey_PNAS_2002.pdf.

[492] H.S. Kuo, I.S. Hwang, T.-Y. Fu, J.Y. Wu, C.C. Chang, T.T. Tsong, "Preparation and characterization of single-atom tips," Nano Lett. 4(December 2004):2379-2382.

[493] T. Itagaki, E. Rokuta, H.-S. Kuo, K. Nomura, T. Ishikawa, B.-L. Cho, I.-S. Hwang, T.T. Tsong, C. Oshima, "Stabilities in field electron emissions from noble-metal covered W nano-tips: apex structure dependence," Surface and Interface Analysis 39(2006):299-303.

[494] Joachim Ahner, Olivier Guise, Hubertus Marbach, Jeremy Levy, Jr. Yates, "The Nanoworkbench: Electron transport on Ge/Silicon Surfaces. First Results," [N14.005] Session N14 - Microscopic Techniques. ORAL session, Wednesday morning, March 05, Room 8C, Austin Convention Center, APS Meeting March 2003, http://flux.aps.org/meetings/YR03/MAR03/baps/abs/S4940.html.

tips[495] to place four independent probes on the facet faces of selected single Ge nanodots, and on various assemblies of dots, with a positional accuracy of better than 5 nm. Olbrich et al.[496] have fabricated high aspect ratio (7:1) diamond tips using focused ion beam methods, although the tip radius rather large (~30 nm) and milling of the tip left a 10-20 nm thick nonconducting amorphous carbon layer that had to be etched away by pure HNO_3 to expose the diamond surface. As tips get very long and narrow, the amplitude of their lateral vibrations increases, injecting more uncertainty into the apex position; as tips get shorter, their aspect ratio declines which increases the risk of handle collision during close proximation. The optimum technical tradeoff must be determined in order to select the best tips for the Phase I efforts.

It should be noted that while atomically precise tooltips (Figure I-11) are needed in Phase II and beyond, such tooltips are not strictly required to undertake Phase I. However, such tooltips will be a product of Phase I. That is, we don't need atomically precise tips to complete Phase I, but once we've completed Phase I, we'll be able to build atomically precise tips.

3.2.1.5 SPM-Based Multi-Tip and Multi-DOF Systems

A minimum of three independent high-precision SPM-based picopositioners are needed to perform many of the diamondoid mechanosynthesis (DMS) reaction sequences that have been identified[497] for building diamond nanostructures. Manipulators having multiple degrees of freedom (DOF), including tip translation in all three Cartesian dimensions and at least one – and often two – rotational dimensions, also (very conservatively) appear to be required to consummate all foundational DMS reactions[498] (Table I-3) and likely most Phase II nanoassembly operations as well (Section 3.3). Hence a multi-tip 5-DOF SPM-based manipulator system[499] may ultimately be required to build a sufficiently functional MFW system and successfully complete Phases I and II. Our plan is to start with a 1-tip 3-DOF system early in Phase I, then upgrade to systems with more tips and perhaps more DOF, possibly culminating with a 4-tip 5-DOF system later in Phase I or in Phase II.

---

[495] Olivier L. Guise, Joachim W. Ahner, Moon-Chul Jung, Peter C. Goughnour, John T. Yates Jr., "Reproducible Electrochemical Etching of Tungsten Probe Tips," Nano Letters 2(2002):191-193; http://pubs.acs.org/cgi-bin/abstract.cgi/nalefd/2002/2/i03/abs/nl010094q.html.

[496] A. Olbrich, B. Ebersberger, C. Boit, Ph. Niedermann, W. Hänni, J. Vancea, H. Hoffmann, "High aspect ratio all diamond tips formed by focused ion beam for conducting atomic force microscopy," J. Vac. Sci. Tech. B 17(July 1999):1570-1574; http://link.aip.org/link/?JVTBD9/17/1570/1.

[497] Robert A. Freitas Jr., Ralph C. Merkle, "A Minimal Toolset for Positional Diamond Mechanosynthesis," J. Comput. Theor. Nanosci. 5(May 2008):760-861.

[498] Robert A. Freitas Jr., Ralph C. Merkle, "A Minimal Toolset for Positional Diamond Mechanosynthesis," J. Comput. Theor. Nanosci. 5(May 2008):760-861.

[499] Shuji Hasegawa, "Chapter 12. Multiprobe SPM," in: Seizo Morita, ed., Roadmap of Scanning Probe Microscopy, Springer Berlin Heidelberg, 2007, pp. 95-100.

Table I-3. Number of Freitas-Merkle[500] Reaction Sequences* Nominally Executable Using a Given Multiplicity of Independent Positionally-Controlled Tooltips with a Given Number of Degrees of Freedom (DOF)

Degrees of Freedom per Tooltip	**Number of Available Tooltips**				Totals for All Tooltips
	1 tooltip	2 tooltips	3 tooltips	4 tooltips	
1 DOF	RS59 (2)				1 (2)
2 DOF					0 (0)
3 DOF	RS1,RS2,RS46 (47)	RS47,RS48 (5)			5 (53)
4 DOF	RS12,RS13,RS14, RS20b,RS24,RS25, RS26,RS27,RS37, RS40,RS49,RS50, RS51 (34)	RS3,RS4,RS9, RS10b,RS11b,RS15, RS20a,RS21,RS22, RS23,RS28b,RS38, RS39,RS42,RS52 (113)	RS16b (1)		29 (152)
5 DOF		RS7,RS19,RS29, RS30,RS31,RS32, RS45,RS63 (33)	RS5,RS6,RS8, RS10a,RS11a,RS17, RS28a,RS33,RS34, RS35,RS41,RS44, RS53,RS54,RS55, RS58,RS61,RS62, RS64,RS65 (71)	RS16a,RS18,RS36, RS43,RS56,RS57, RS60 (9)	35 (113)
6 DOF					0 (0)
Totals for All DOFs	17 (83)	25 (151)	21 (77)	7 (9)	70 (320)

* Reaction Sequences are designated as: a = workpiece on tooltip/manipulator, b = workpiece on fabrication surface. (The number of individual reactions that can be executed with a given tip/DOF capability are given in parens.)

Building a multi-tip system (Figure I-7) is more challenging than a single-tip system in terms of system geometry and stability. Experimentally, the first opposable STM tip pair was fabricated by MacDonald's group in 1991 using the Cornell Nanofabrication Facility,[501] and two-handed coordinated micromanipulation under the view of an SEM was reported in 1993.[502] In 2005, Xidex reported opposable AFM dual-tip calipers for metrology, with each cantilever probe tiltable in up to three rotational degrees of freedom allowing tips to touch each other's apices and to access vertical and re-entrant feature sidewalls, using tips with 10 nm radius of curvature and a

[500] Robert A. Freitas Jr., Ralph C. Merkle, "A Minimal Toolset for Positional Diamond Mechanosynthesis," J. Comput. Theor. Nanosci. 5(May 2008):760-861.

[501] J. Jason Yao, Susanne C. Arney, Noel C. MacDonald, "Fabrication of high frequency two-dimensional nanoactuators for scanned probe devices," J. Microelectromech. Syst. 1(March 1992):14-22.

[502] Hiroshi Morishita, Yotaro Hatamura, "Development of ultra micro manipulator system under stereo SEM observation," Proc. 1993 IEEE/RSJ Intl. Conf. on Intelligent Robots and Systems, 26-30 July 1993, Yokohama, Japan, Volume 3, pp. 1717-1721.

10° cone angle but without closed-loop control.[503] In 2005 a dual probe system available from Nanonics allowed two tips to approach within 10 nm of each other,[504] and other dual-tip SPM systems have been described in the experimental literature.[505] In 1998, Zyvex demonstrated the first simultaneous coordinated operation of three independently controlled AFM tips within the same workspace at different orientations;[506] a successor 4-tip system was designed as early as 1999 and finally offered as a commercial product starting in 2003. A three-probe AFM was employed experimentally in 2001 by Watanabe et al.[507] A 4-tip STM was used for conductivity measurements in 2005.[508] In 2006, Nanonics introduced the MV4000 Multiprobe SPM to allow four SPM tips to be brought to within 10 nm of each other throughout a volume of 160 microns x 160 microns in XY and 130 microns in Z,[509] and four-tip SPM systems are now being reported in

---

[503] V. Mancevski, P.F. McClure, "Development of a dual-probe Caliper™ CD-AFM for near model-independent nanometrology," Proc. of the SPIE. Metrology, Inspection and Process Control for Microlithography XVI, 4-7 March 2003 Vol. 4689, pp. 83-91; http://www.xidex.com/Xidex%20Caliper%20CD%20AFM%20SPIE%202002.pdf. P.F. McClure, V. Mancevski, "Calibration of a dual-probe NanoCaliper™ AFM for CD metrology," SPIE Microlithography 2005 Conference, San Jose California, February 27-March 4, 2005; http://www.xidex.com/Xidex%20SPIE%205752-100.pdf.

[504] "The MultiView 3000," Nanonics Imaging Ltd., 2005; http://www.nanonics.co.il/main/prod_item.php?ln=en&item_id=146&cat=5&sub_cat=22.

[505] H. Grube, B.C. Harrison, J.F. Jia, J.J. Boland, "Stability, resolution, and tip imaging by a dual-probe scanning tunneling microscope," Rev. Sci. Instr. 72(December 2001):4388-4392. H. Okamoto, D.M. Chen, "An ultrahigh vacuum dual-tip scanning tunneling microscope operating at 4.2 K," Rev. Sci. Instr. 72(December 2001):4398-4403. K. Takami, J. Mizuno, M. Akai-kasaya, A. Saito, M. Aono, Y. Kuwahara, "Conductivity measurement of polydiacetylene thin films by double-tip scanning tunneling microscopy," J. Phys. Chem. B 108(2004):16353-16356.

[506] MinFeng Yu, Mark J. Dyer, George D. Skidmore, Henry W. Rohrs, Xue Kun Lu, Kevin D. Ausman, James Von Ehr, Rodney S. Ruoff, "3 dimensional manipulation of carbon nanotubes under a scanning electron microscope," 6th Foresight Nanotechnology Conference, November 1998; http://www.foresight.org/Conferences/MNT6/Papers/Yu/index.html. Robert F. Service, "AFMs wield parts for nanoconstruction," Science 282(27 November 1998):1620-1621.

[507] H. Watanabe, C. Manabe, T. Shigematsu, K. Shimotani, M. Shimizu, "Single molecule DNA device measured with triple-probe atomic force microscope," Appl. Phys. Lett. 79(2001):2462.

[508] Olivier Guise, Hubertus Marbach, John T. Yates, Jr., Moon-Chul Jung, Jeremy Levy, Joachim Ahner, "Development and performance of the nanoworkbench: A four tip STM for conductivity measurements down to submicrometer scales," Rev. Sci. Instrum. 76(2005):045107, http://www.nanotechnik.com/fileadmin/public/publications/ahner_rsi2005.pdf.

[509] "Nanonics' MultiView 4000 Multi-Probe Scanned Probe Microscopy (SPM) Systems," Nanonics Imaging Ltd., 3 September 2008, http://www.nanonics.co.il/new-product-announcement-the-multiview-4000-multiprobe-.html; Alexander Kirkwood, "Nanonics Imaging Ltd - MV4000 multiprobe SPM," Microscopy and Analysis, 1 September 2006; http://www.microscopy-analysis.com/cgi-bin/item.cgi?id=356; see image at http://www.photonics.com/images/spectra/newprods/2006/October/Nanonics_FourTowers2.jpg.

the experimental literature[510] and by other manufacturers such as Omicron[511] and RHK Technology[512] (Figure I-7). By 2008, Zyvex had expanded their 3-DOF nanomanipulator line[513] to 4-probe (S100 and sProber™), 6-probe (dProber™) and 8-probe (nProber™) systems, and MultiProbe's AFP II Nanoprober system[514] allows up to six MP II probe heads to be placed with 100 nm of each other in a sample area of dimension ~10 cm. In 2008, Gorman et al.[515] described a design for a 4-tip microscale assembly system, to be fabricated on a single chip, that includes four MEMS-based nanomanipulators (each composed of an XYZ nanopositioning mechanism with an attached nanoprobe) positioned around a centrally located port for introducing nanostructure samples (Figure I-8). The prototype manipulator demonstrated sequences of 50 nm steps with ±7 nm resolution; open-loop nanopositioning control can presently achieve this precision only for ±1 micron tip excursions, but a closed-loop controller is being developed that should significantly improve repeatability.[516]

---

[510] Shinya Yoshimoto, Yuya Murata, Keisuke Kubo, Kazuhiro Tomita, Kenji Motoyoshi, Takehiko Kimura, Hiroyuki Okino, Rei Hobara, Iwao Matsuda, Shin-ichi Honda, Mitsuhiro Katayama, Shuji Hasegawa, "Four-Point Probe Resistance Measurements Using PtIr-Coated Carbon Nanotube Tips," Nano Lett. 7(2007):956-959; http://www-surface.phys.s.u-tokyo.ac.jp/papers/2007/Yoshimoto07-NanoLetters.pdf.

[511] "UHV Nanoprobe," Omicron Vacuumphysik GmbH, Taunusstein, Germany; http://www.omicron.de/products/spm/multi_technique_spms/uhv_nanoprobe/index.html.

[512] "QuadraProbe 4 Probe System," RHK Technology, 2008; http://www.rhk-tech.com/4probe.php.

[513] "S100", http://www.zyvex.com/Products/S100_Features.html; "sProber™", http://www.zyvex.com/Products/sProber_Features.html; "dProber™", http://www.zyvex.com/Products/dProber_Features.html; "nProber™", http://www.zyvex.com/Products/nProber_Features.html.

[514] MultiProbe, Inc., "AFP II Core System," accessed January 2008, http://www.multiprobe.com/products/.

[515] Jason J. Gorman, Yong-Sik Kim, András E. Vladár, Nicholas G. Dagalakis, "Design of an on-chip microscale nanoassembly system," Int. J. Nanomanufacturing 1(2007):710-721.

[516] Jason J. Gorman, Yong-Sik Kim, András E. Vladár, Nicholas G. Dagalakis, "Design of an on-chip microscale nanoassembly system," Int. J. Nanomanufacturing 1(2007):710-721.

Figure I-7. Multiprobe SPM-based systems commercially available from Nanonics, Omicron, and Zyvex.

Nanonics MV4000 Multi-Probe SPM

Zyvex S100 Nanomanipulator

Zyvex dProber™

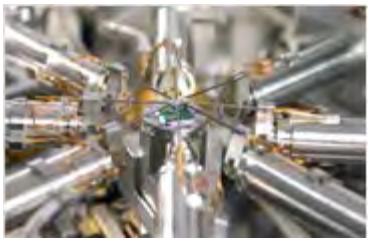

Zyvex nProber™

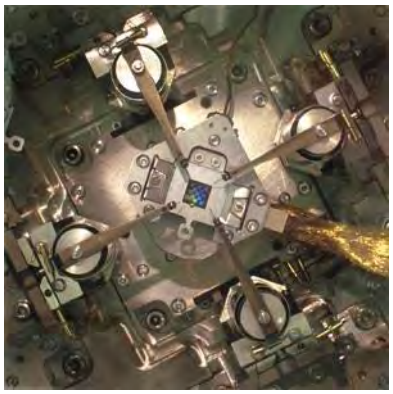

Omicron UHV Nanoprobe

RHK Technology QuadraProbe

Figure I-8. Schematic representations of: (A) microscale nanoassembly cell with 2 × 2 array of XYZ nanomanipulators; (B) multiple nanoprobes working in a shared workspace; and (C) an actual fabricated microscale XYZ nanomanipulator prototype. Images from Gorman et al.[517]

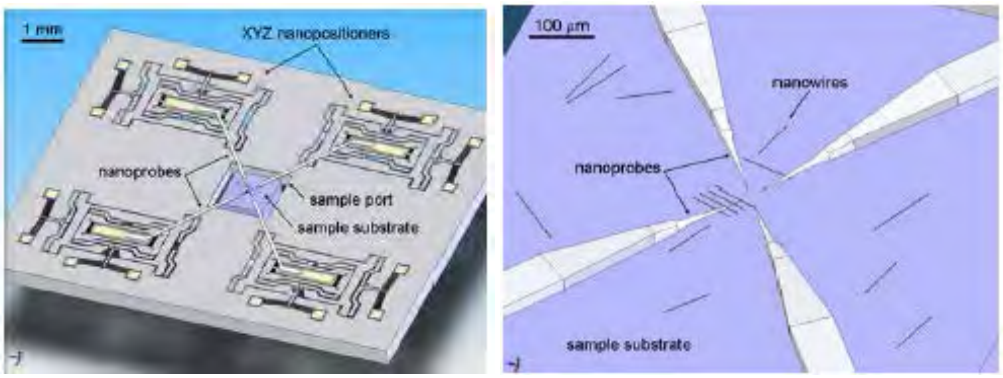

(A) (B)

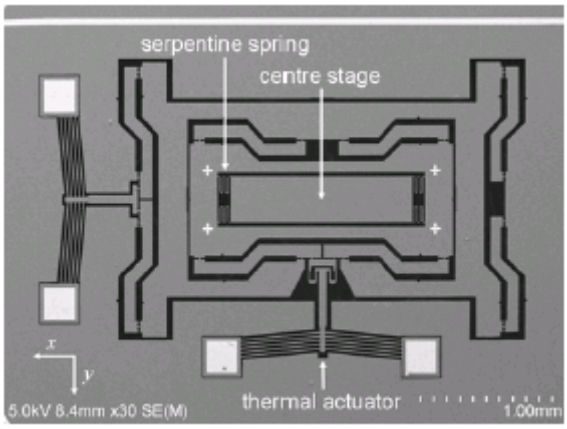

(C)

Building a 4-DOF or a 5-DOF system will also be more challenging than building a 3-DOF system. The smallest 6-DOF SPM-based nanopositioner system may be the 6-axis Piezo Nanopositioning P-587 (Figure I-9A) manufactured by Physik Instrumente.[518] The P-587 has an

---

[517] Jason J. Gorman, Yong-Sik Kim, András E. Vladár, Nicholas G. Dagalakis, "Design of an on-chip microscale nanoassembly system," Int. J. Nanomanufacturing 1(2007):710-721.

[518] Physik Instrumente, "P-587 6-Axis, Long-Travel Piezo Nanopositioning / Scanning Stage with Parallel Metrology," accessed January 2008, http://www.physikinstrumente.com/en/products/prdetail.php?sortnr=201600 and datasheet at http://www.physikinstrumente.com/en/pdf/P587_Datasheet.pdf.

800 x 800 x 200 micron linear range with a resolution of ~10^{-5} x travel range (e.g., 80 Å or 8000 pm over 800 microns of linear travel) – with XY linearity of 0.004% (0.4 Å or 40 pm over 1 micron of linear travel) and Z linearity of 0.01% (1 Å or 100 pm over 1 micron of linear travel) – and rotation ranges of 3 mrad, 3 mrad, and 10 mrad (~0.6 deg) with a typical closed-loop linearity in rotation of 0.2% (~2 μrad). Rotation stages with 5 μrad (0.0003 deg) rotational increments with 240 μrad (0.014 deg) of backlash are commercially available.[519] A few microscale 6-axis mechanisms comprised of rigid links and sliding bearings have been built,[520] but while these devices may achieve work volumes comparable to their size, bearing friction and bearing/joint gaps limit the achievable positional resolution to several microns.

Hexapod or Stewart-platform type nanomanipulators are generally rare in commercial systems, probably due to limited demand, but there appear to be no fundamental technical barriers to substantial improvements in resolution and repeatability in such systems. Physik Instrumente's vacuum-compatible M-824 six-axis parallel-kinematics hexapod[521] is a coarser 6-DOF manipulator (Figure I-9B) with a travel range of 45 mm and 25° of rotation, and with 7 nm resolution but a minimum incremental motion of 300 nm and a repeatability of only ±500 nm, the related 6-DOF M-840 six-axis hexapod (Figure I-9C) has an actuator resolution of 16 nm but a repeatability of only ±2000 nm.[522] 6-DOF micromanipulators have been described in the literature,[523] including one medical micromanipulator with a 20 micron movement range and a 20 nm resolution,[524] Stewart platform micromanipulators,[525] and a 6-DOF dual micromanipulator system.[526]

---

[519] Physik Instrumente, "M-060 · M-061 · M-062, Series Rotation Stages with Worm Gear Drive," accessed January 2008, http://www.physikinstrumente.com/en/products/prdetail.php?sortnr=703100; see also http://www.physikinstrumente.com/en/pdf/M060_Datasheet.pdf.

[520] B. Jokiel, G.L. Benavides, L.F. Bieg, J.J. Allen, "Planar and spatial three degree-of-freedom micro-stages in silicon MEMS," in: Proceedings of the 2001 Annual Meeting of the American Society for Precision Engineering, 2001, pp. 32-35. H. Bamberger, M. Shoham, "A new configuration of a six degree-of-freedom parallel robot for MEMS fabrication," in: Proceedings of the 2004 IEEE International Conference on Robotics and Automation, 2004, pp. 4545-4550.

[521] Physik Instrumente, "M-824 Compact 6-Axis Parallel Kinematics Microrobot," accessed January 2008, http://www.physikinstrumente.com/en/products/prdetail.php?sortnr=700815 and datasheet at http://www.physikinstrumente.com/en/pdf/M824_Datasheet.pdf.

[522] Physik Instrumente, "M-840 HexaLight™ 6-Axis-Parallel Kinematics Microrobot," accessed January 2008, http://www.physikinstrumente.com/en/products/prdetail.php?sortnr=700810 and datasheet at http://www.physikinstrumente.com/en/pdf/M840_Datasheet.pdf.

[523] Eric Pernette, Simon Henein, Ivo Magnani, Reymond Clavel, "Design of parallel robots in microrobotics," Robotica 15(1997):417-420; Quan Zhou, Petteri Korhonen, Jukka Laitinen, Sami Sjövall, "Automatic dextrous microhandling based on a 6-DOF microgripper," Journal of Micromechatronics 3(September 2006):359-387.

[524] S. Guo, J. Wang, "A New Human-Scale Tele-Operating System For Biomedical Applications," International Journal of Robotics and Automation 22(2007), #206-1008.

[525] Feng Gao, Zhang Jianjun, Chen Yulong, Jin Zhenlin, "Development of a new type of 6-DOF parallel micro-manipulator and its control system," Robotics, Intelligent Systems and Signal Processing 2(8-13

Figure I-9. (A) At left: Image of Physik Instrumente's P-587 piezo-driven nanopositioning/scanning stage with 6-axis digital controller, which is perhaps the smallest known 6-DOF SPM-based nanopositioner system.[527] (B) At middle: Image of Physik Instrumente's vacuum-compatible M-824 compact 6-Axis Parallel Kinematics hexapod nanopositioner.[528] (C) At right: Image of Physik Instrumente's M-840 HexaLight™ 6-axis micropositioning system.[529]

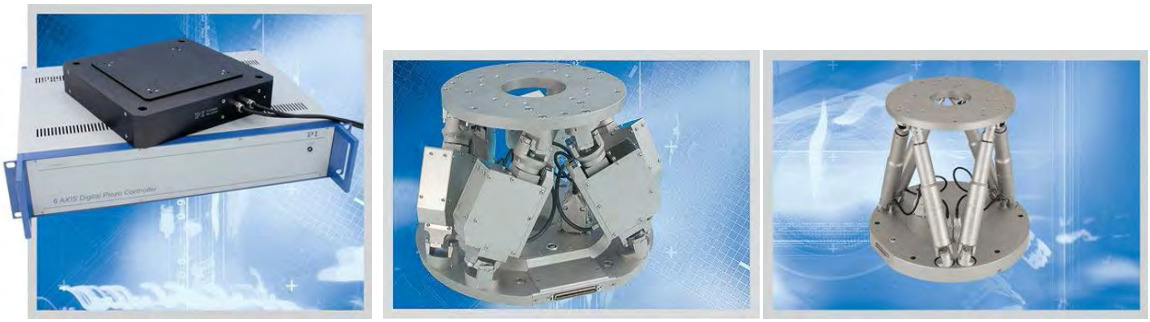

(A) (B) (C)

Another related system is the 6-axis μHexFlex microscale nanopositioner demonstrated by Chen and Culpepper.[530] Their 3-mm prototype (Figure I-10A) proved capable of 8.4 micron x 12.8 micron x 8.8 micron translational displacements (with a ~20-30 nm noise level) and 19.2 mrad x

---

October 2003):715-720; http://ieeexplore.ieee.org/xpls/abs_all.jsp?tp=&arnumber=1285672&isnumber=28679.

[526] Gilgueng Hwang, Peter Tamas Szemes, Noriaki Ando, Hideki Hashimoto, "A Realization of Autonomous Rectilinear Movement on 6 D.O.F Parallel Micromanipulator," Nippon Kikai Gakkai Robotikusu, Mekatoronikusu Koenkai Koen Ronbunshu 2004: 1A1-H-44; Gilgueng Hwang, Peter Tamas Szemes, Noriaki Ando, Hideki Hashimoto, "Development of a single-master multi-slave tele-micromanipulation system," Advanced Robotics 21(March 2007):329-349.

[527] Physik Instrumente, "P-587 6-Axis, Long-Travel Piezo Nanopositioning / Scanning Stage with Parallel Metrology," accessed January 2008, http://www.physikinstrumente.com/en/products/prdetail.php?sortnr=201600 and datasheet at http://www.physikinstrumente.com/en/pdf/P587_Datasheet.pdf.

[528] Physik Instrumente, "M-824 Compact 6-Axis Parallel Kinematics Microrobot," accessed January 2008, http://www.physikinstrumente.com/en/products/prdetail.php?sortnr=700815 and datasheet at http://www.physikinstrumente.com/en/pdf/M824_Datasheet.pdf.

[529] Physik Instrumente, "M-840 HexaLight™ 6-Axis-Parallel Kinematics Microrobot," accessed January 2008, http://www.physikinstrumente.com/en/products/prdetail.php?sortnr=700810 and datasheet at http://www.physikinstrumente.com/en/pdf/M840_Datasheet.pdf.

[530] S.-C. Chen, M.L. Culpepper, "Design of a six-axis micro-scale nanopositioner – μHexFlex," Precision Engineering 30(2006):314-324; http://pcsl.mit.edu/2_72/documents/microHexFlex.pdf.

17.5 mrad x 33.2 mrad (1.1^o x 1.0^o x 1.9^o) angular displacements. Although its angular range is quite limited, the modular design might readily lend itself for use in close-packed 4-tip systems.

Figure I-10. (A) Closeup of 6-axis µHexFlex microscale nanopositioner and (B) the 6-DOF nanopositioner shown with its electrical connections. Alternative conceptual schemes for this general manipulator motif include: (C) parallel flexures, (D) series flexures, and (E) amplifying bow flexures. Images from Chen and Culpepper.[531]

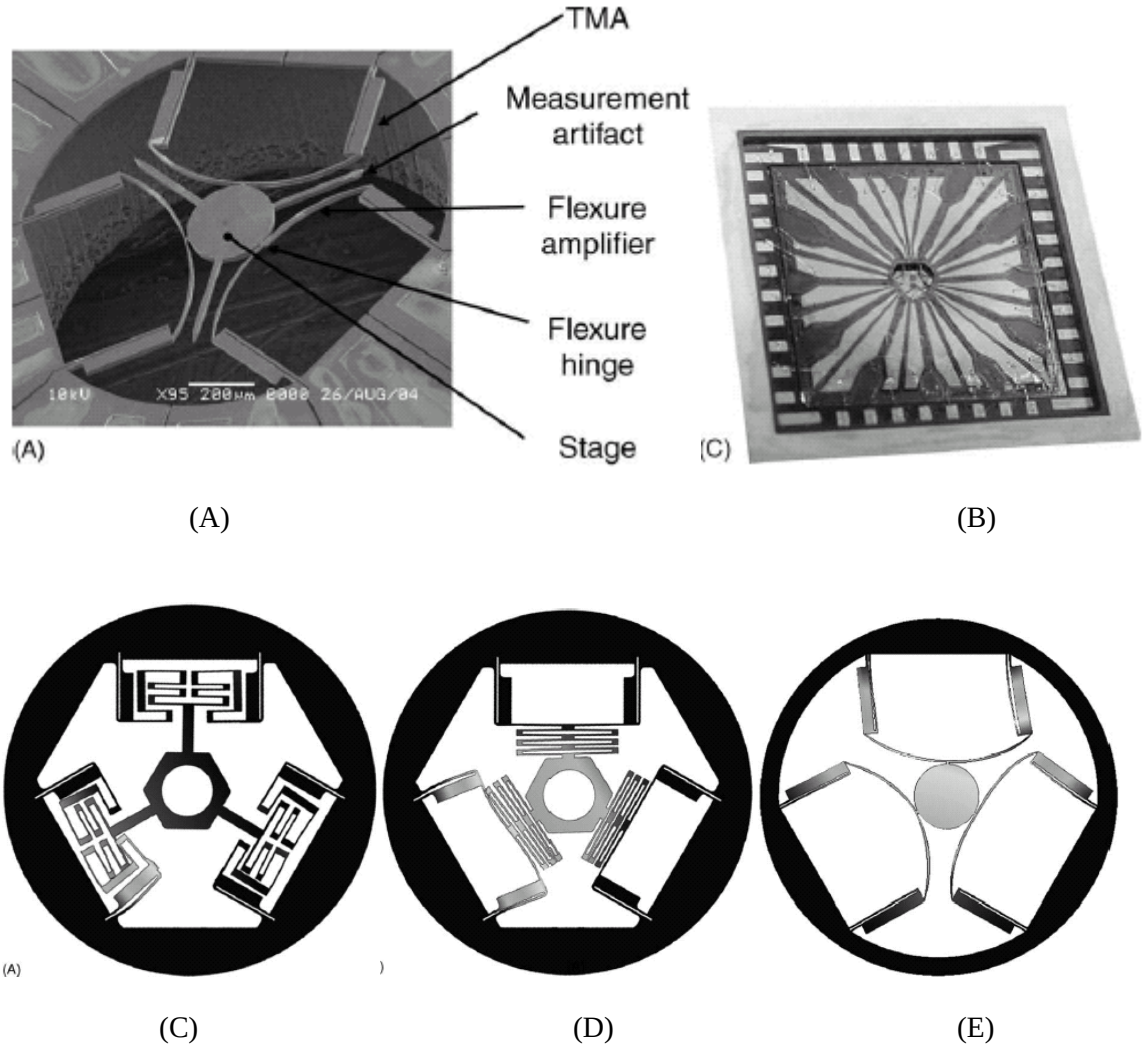

[531] S.-C. Chen, M.L. Culpepper, "Design of a six-axis micro-scale nanopositioner – µHexFlex," Precision Engineering 30(2006):314-324; http://pcsl.mit.edu/2_72/documents/microHexFlex.pdf.

We conclude that a 5-DOF three-nanomanipulator system is probably also within the state of the art but may require considerably greater development effort than a 3-DOF system, which is why the 4-DOF and 5-DOF systems are broken out as separate Tasks in Phase I, in case these are determined (during Task I-5) to be absolutely required.

Any multitool SPM system must provide adequate clearance when juxtaposed near a workpiece. With two exceptions, all primary and auxiliary tools in the minimal DMS toolset[532] are mounted on simple pyramidal diamond handles consisting of stacked planes of adamantane cages. The simplest 1, 2, 3,... adamantane stack (Figure I-11A) has an aspect angle of ~60°, which may be considered typical for most tooltypes in our toolset. The two exceptions are the DimerP tool, essentially a fused double GeRad tool, which requires a handle with a ~60° aspect angle in the common dimension and ~140° in the transverse dimension, and the two-handled HTrans tool, similarly at ~60-90° x ~140-160°, adjustable by manipulating the component HAbst and GeRad handles independently.

For tool operations in free space, the 360° of available planar angle can conservatively accommodate at most four proximated tools (4 x 60° = 240°), again occupying only 2/3 of available planar angle. However, tools arranged tetrahedrally rather than coplanarly use only half of the effectively available 120° tetrahedral angle between each pair, leaving extra room for positional and rotational adjustments during mechanosynthetic operations. A tetrahedral arrangement of 4 tooltips on a single workpiece may be regarded as 3 coplanar tools at 120° separation with any single tool positioned above the plane, with that single tool having much of an entire hemisphere of free space in which to maneuver. Purely for illustrative purposes, the most severe geometry (Figure I-11B) occurs when four proximated DimerP tools whose C_2 dimer payloads are shown bonded in an energetically unstable cubane configuration (while the addition of the fourth DimerP tool is exoergic by -1.03 eV, subsequent retraction of this tool retrieves the donated C_2 dimer because such retrieval is strongly exoergic compared to C_2 deposition).

For tool operations in the proximity of a flat surface, the 180° of available planar angle can conservatively accommodate at most two proximated tools (60° + 60° = 120°), occupying only 2/3 of available planar angle, since three proximated tools would occupy the entire 180° planar angle, leaving no room for positional or rotational adjustments during mechanosynthetic operations. The most severe instance is again illustrated by two proximated DimerP tools on a flat C(110) surface. In Figure I-11C, the two tools are very close (~5° relative angle), yielding an estimated van der Waals intertool attraction of ~1.3 nN which is reduced to ~0.4 nN when the tools are tipped to a ~30° relative angle as in Figure I-11D. (Adhesive force is crudely estimated by integrating the Israelachvili relation[533] for opposed planar surfaces across the entire tool height for the two nearest tipped central planes taken as the width of 3 adamantane cages on each tool, and taking the Hamaker constant as ~3.4 x 10^{-19} J for diamond surface.)

---

[532] Robert A. Freitas Jr., Ralph C. Merkle, "A Minimal Toolset for Positional Diamond Mechanosynthesis," J. Comput. Theor. Nanosci. 5(May 2008):760-861.

[533] Jacob N. Israelachvili, Intermolecular and Surface Forces, Second Edition, Academic Press, NY, 1992.

Figure I-11. (A) Adam tooltip mounted on pyramidal handle, (B) four DimerP tooltips forced into unstable cubane geometry in free space, and two handled DimerP tools in close (C) and more distant (D) apposition on a workpiece surface.

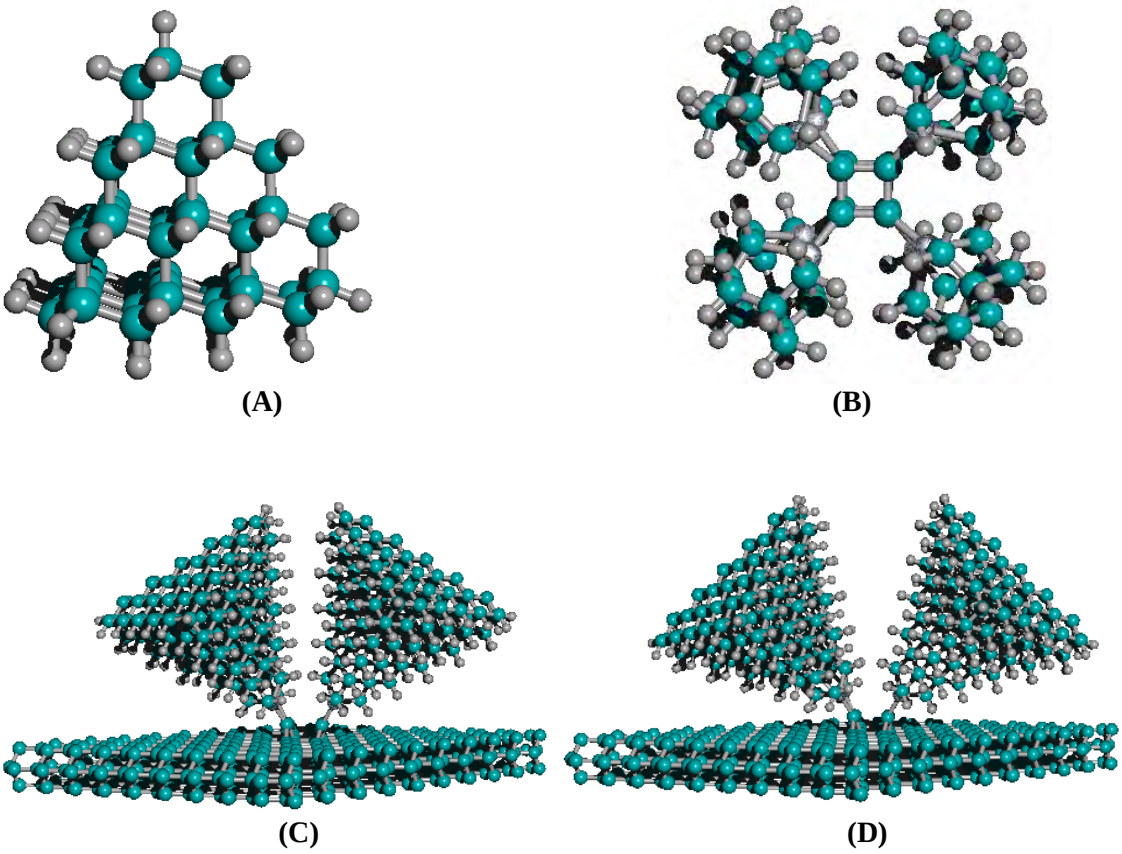

3.2.1.6 Continuous Sensory Feedback Not Needed by the MFW

It has been observed that it may be difficult to separate successful trials from failures, and to elucidate the failure mechanisms of the failures, unless adequate sensor-based feedback can be employed at the tooltip during the fabrication of nanoscale parts. Unlike biological evolution, which proceeds by random variations in ensembles of organisms combined with deterministic reproduction/extinction as a selection process to achieve great complexity after billions of years (a set of mechanisms which Richard Dawkins has referred to as a “blind watchmaker”), deliberate design and positionally controlled fabrication of nanoscale mechanisms requires a means other than reproduction/extinction to winnow successes from failures in proceeding from simplicity to complexity. Similarly, macroscale factories are commonly constructed and operated by human engineers using continuous sensory feedback provided by eyes, ears, and hands.

While there are sensory advantages present at the macroscale compared to the limited sensorium available at the nanoscale (termed "sensory blight" by some critics),[534] proposals for positionally controlled nanoscale mechanosynthetic fabrication systems employ dead reckoning of tooltips combined with reliable reaction sequence design to ensure reliable results, hence a limited tooltip sensorium is no handicap (Section 3.2.1.8). For example, reaction-by-reaction sensor-validated discrimination among the three possible outcomes of an attempted dimer placement – deposition at the correct location, deposition at the wrong location, and failure to place the dimer at all – is unnecessary because the proposal is to position the tooltip by dead reckoning, with the proper reaction assured by designing appropriate chemical energetics and relative bond strengths for the tooltip-surface interaction. In a macroscale factory, possible mechanical failure modes for each component mechanism are numerous (in part because macroscale components have poor quality control at the atomic scale), requiring significant sensory feedback to discriminate among them and diagnose the problem. In a nanoscale DMS workstation employing single-molecule tip-based chemical reactions, possible failure modes for each properly designed reaction are few (in part because nanoscale components can have excellent quality control at the atomic scale, being made of a small number of absolutely identical atoms), requiring minimal diagnostic sensory feedback to discriminate among them.

If future experiments show that positional errors from dead reckoning may accumulate to unacceptable levels after some number of full-range tooltip motions, protocols for tooltip positional registration involving, e.g., in-theater fiducial markers,[535] scanning probe registration marks,[536] etc., can be re-executed as often as necessary to ensure continuous reliability of DMS reactions. Similar considerations apply to the positional assembly of small nanoparts (e.g., Section 3.3.10). (See also Sections 3.4.1.3 and 3.8.1.3.) For closed-loop operation, encoders commercially available in 2008 already have ~nanometer precision.[537]

Regarding nonbiological methods for winnowing successes from failures, nanopart and nanofactory design evolution should occur deterministically and strictly under human control, using the conventional engineering paradigm of modeling, design, prototyping, testing, analysis, and redesign. In this case the limited sensorium is no handicap because, for example, prototype nanoparts and every one of their stable (or stabilizable) intermediate structures can be fabricated via dead reckoning using positionally controlled chemically active tooltips, then characterized by chemically inactive scanning probe tooltips or other technical means, with errors corrected or design changes sequentially implemented in the next prototyping iteration. Once

---

[534] "New version of Productive Nanosystems film released," Nanodot, 28 March 2006; http://www.foresight.org/nanodot/?p=2188/Anonimouse5Apr06.htm#comment-8448.

[535] F.J. Rueb, L. Oberbeck, K.E.J. Goh, M.J. Butcher, E. Gauja, A.R. Hamilton, M.Y. Simmons, "The use of etched registration markers to make four-terminal electrical contacts to STM-patterned nanostructures," Nanotechnology 16(2005):2446-2449.

[536] A.W. Dunn, B.N. Cotier, A. Nogaret, P. Moriarty, P.H. Beton, S.P. Beaumont, "Molecular scale alignment strategies: An investigation of Ag adsorption on patterned fullerene layers," Appl. Phys.Lett. 71(1997):2937.

[537] ACS Motion Control, "Nanometer Positioning & High Velocity," http://www.acs-tech80.com/Solutions/AdvancedFeatures/Nanometerpositioninghighvelocity/tabid/226/Default.aspx.

mechanosynthetic tooltips and related positionally-controlled molecular tools are fabricated, the same technology will permit convenient prototyping, testing, and rework of failed designs.

3.2.1.7 Operation of the MFW

To operate the macroscale fabrication workstation (MFW), the workspace chamber containing the ultimate 4-tip 5-DOF nanomanipulator system with repeatable 20-50 pm positioning accuracy over 1-100 micron round-trip excursions (independently for all four tips), as described in Sections 3.2.1.2-3.2.1.4, is first pumped down to ultra-high vacuum (UHV) conditions.

UHV is generally defined as an ambient gas pressure lower than about 10^{-7} Pa (i.e., 100 nanopascals; aka. ~10^{-9} torr, 10^{-12} atm, 10^{-12} bar or 10^{-9} mbar) which is 2.45 x 10^{13} molecules/m^3 at 300 K or 9.17 x 10^{13} molecules/m^3 at 80 K for an ideal gas). At this threshold pressure, about the same as in low-Earth orbit at ~300 km or ~185 miles altitude, the mean free path for a gas molecule at 300 K is ~230 km and the molecules are colliding with the chamber walls many times before colliding with each other. A 34.4 micron cubic box (40,800 $micron^3$) containing gas at 10^{-12} atm and 300 K contains, on average, a single gas molecule. UHV is considered to range from ~10^{-12}-10^{-15} atm. The minimum lifetime of a radical site ($t_{radical}$) on a diamondoid mechanosynthesis (DMS) tooltip that is exposed to a 10^{-12} atm threshold-UHV environment may be estimated as the time required for a binding event to occur (as a function of the molecular impingement rate), which is given, analogously for binding sites,[538] by: $t_{radical} \sim (N_{encounters} / A_{radical}\ n_{gas})\ (\pi\ MW_{kg} / 2\ k_B T\ N_A)^{1/2}$ = 19,325 sec (~5 hours), where $A_{radical}$ = active receptor cross-sectional area ~ 0.0237 nm^2 for a carbon radical site in a diamond matrix, n_{gas} = 2.45 x 10^{13} molecules/m^3 for ideal gas molecules at 10^{-12} atm and T = 300 K, $N_{encounters}$ ~ 10 random molecule-radical encounters required for a binding event, MW_{kg} = 0.002 kg/mole for H_2 to give the most conservative result, k_B = 1.381 x 10^{-23} J/K (Boltzmann constant), and N_A = 6.023 x 10^{23} molecules/mole (Avogadro's number). Radical site lifetime can be increased to ~2.2 days by dropping ambient UHV operating pressure from 10^{-12} atm to 10^{-13} atm – the same pressure to which vacuum tubes are typically pumped (i.e., 10^{-10}-10^{-13} atm). Operation on the lunar surface (~10^{-14} atm) would increase $t_{radical}$ to ~22 days; at the lowest pressures currently achievable in the laboratory (~10^{-16} atm,[539] ~10^{-17} atm,[540] ~10^{-18} atm[541]), $t_{radical}$ would increase to 6-600 years. (The

---

[538] Robert A. Freitas Jr., Nanomedicine, Volume I: Basic Capabilities, Landes Bioscience, Georgetown, TX, 1999; Section 4.2.1, p. 94; http://www.nanomedicine.com/NMI/4.2.1.htm.

[539] H. Ishimaru, "Ultimate Pressure of the Order of 10^{-13} Torr in an Aluminum Alloy Vacuum Chamber," J. Vac. Sci. Technol. **7(**1989**):**2439-2442. H. Akimichi, M. Hirata, "Generation and pressure measurement of extremely high vacuum (XHV) using a TiN coated chamber," Metrologia 42(2005):S184-S186, http://www.iop.org/EJ/abstract/0026-1394/42/6/S08; "Non-Evaporable Getter (NEG) Thin Film Coatings," CERN Technology Transfer DSU-TT, 2008, http://technologytransfer.web.cern.ch/TechnologyTransfer/en/Technology/NEG.html; Marcy Stutzman, Philip Adderley, "Vacuum at CEBAF: Seminar for Accelerator Operators," 17 January 2006, http://www.jlab.org/accel/inj_group/docs/2006/Operator_Vacuum_Talk.ppt; Marcy Stutzman, Philip Adderley, Matt Poelker, "Extreme High Vacuum: The Need, Production, and Measurement," Thomas Jefferson National Accelerator Facility, 14 November 2006,

pressure range of 10^{-13} torr (~10^{-16} atm) and below is often called the XHV (Extremely High Vacuum)[542] region; interplanetary space is ~10^{-18} atm, interstellar space ~10^{-19} atm.) Cooling the external system to <54 K will cause all major atmospheric constituents to freeze out on the chamber walls, reducing the ambient concentration of likely contaminant gases by several orders of magnitude (Table I-4).

Next, four workspace surfaces are transferred into the UHV workspace chamber from an adjacent transfer chamber which has also been pumped down to UHV conditions, fully pre-degassing the four surfaces. The four workspace surfaces are:[543]

(1) a diamondoid fabrication surface, which in the initial setup will consist of a fully hydrogen-passivated diamond C(111), C(110) or C(100) surface depending upon the product nanostructures that are desired to be fabricated;

(2) a hydrogen dump consisting of a fully depassivated stable diamond C(110) surface (which will not reconstruct at any normal operating temperature) or C(100) surface (which reconstructs in the same known manner, whether hydrogenated or not);

(3) a carbon source consisting of a depassivated germanium Ge(111) or Ge(100) surface that has been partially methylated (i.e., decorated with CH_3 groups) or has been deposited with a partial monolayer of C_2 dimers; and

(4) a germanium source consisting of a post-annealing depassivated and reconstructed Ge(111)-c(2x8) surface that has been partially germylated (i.e., decorated with GeH_3 groups).

---

http://www.jlab.org/accel/inj_group/docs/2006/XHV.ppt. P. Chiggiato, "Production of extreme high vacuum with non evaporable getters," Phys. Scr. T71(1997):9-13; http://www.iop.org/EJ/abstract/1402-4896/1997/T71/002/.

[540] Dr.-Ing. K. Busch GmbH, "What is vacuum?" Busch Vacuum Pumps and Systems, 2002; http://www.busch.com.au/whatisvacuum.htm. (~10^{-14} torr was achieved during a test by IBM Thomas J. Watson Research Center, New York, USA, October 1976, in a cryogene system using cryopumping at ~4 K with an outer guard vacuum; also reported in 1994 Guinness Book of Records.) P. Chiggiato, "Production of extreme high vacuum with non evaporable getters," Phys. Scr. T71(1997):9-13; http://www.iop.org/EJ/abstract/1402-4896/1997/T71/002/.

[541] "Vacuum Pumps," in: McGraw Hill Encyclopedia of Science and Technology, 7th Edition, 1992, Vol. 19, p. 128. Also mentioned in http://hypertextbook.com/facts/1998/RobertSaronson.shtml.

[542] H. Akimichi, M. Hirata, "Generation and pressure measurement of extremely high vacuum (XHV) using a TiN coated chamber," Metrologia 42(2005):S184-S186, http://www.iop.org/EJ/abstract/0026-1394/42/6/S08; "Non-Evaporable Getter (NEG) Thin Film Coatings," CERN Technology Transfer DSU-TT, 2008, http://technologytransfer.web.cern.ch/TechnologyTransfer/en/Technology/NEG.html; Marcy Stutzman, Philip Adderley, "Vacuum at CEBAF: Seminar for Accelerator Operators," 17 January 2006, http://www.jlab.org/accel/inj_group/docs/2006/Operator_Vacuum_Talk.ppt; Marcy Stutzman, Philip Adderley, Matt Poelker, "Extreme High Vacuum: The Need, Production, and Measurement," Thomas Jefferson National Accelerator Facility, 14 November 2006, http://www.jlab.org/accel/inj_group/docs/2006/XHV.ppt.

[543] Robert A. Freitas Jr., Ralph C. Merkle, "A Minimal Toolset for Positional Diamond Mechanosynthesis," J. Comput. Theor. Nanosci. 5(May 2008):760-861.

Table I-4. Pressure Reduction Achieved by Freezing Out Normal Atmospheric Constituent Gases[544] at Progressively Lower Temperatures (excluding the highly variable H_2O content which is also frozen out; typical air concentration ~7.75 x 10^{-2} atm)

Atmos-pheric Gas	Freeze Temp (K)	Partial Pressure (atm)	Cumulative P_{atm} (atm)	Atmos-pheric Gas	Freeze Temp (K)	Partial Pressure (atm)	Cumulative P_{atm} (atm)
HCO_2H	281.55	1 x 10^{-14}	1	CH_3Cl	176.15	7 x 10^{-10}	0.999639676
H_2O_2	272.74	2 x 10^{-10}	1	COF_2	159.15	1 x 10^{-14}	0.999639676
NO_2	261.95	2.3 x 10^{-11}	1	HCl	158.35	1 x 10^{-9}	0.999639675
HCN	259.15	1.7 x 10^{-10}	1	PH_3	139.65	1 x 10^{-20}	0.999639675
HNO_3	231.15	5 x 10^{-11}	1	OCS	135.15	6 x 10^{-10}	0.999639674
SF_6	222.65	1 x 10^{-14}	1	NO	109.55	3 x 10^{-10}	0.999639674
HI	222.35	3 x 10^{-12}	1	CH_4	90.67	1.7 x 10^{-6}	0.999637974
CO_2	216.55	3.6 x 10^{-4}	0.99964	C_2H_6	90.35	2 x 10^{-9}	0.999637972
SO_2	200.45	3 x 10^{-10}	0.999639999	Ar	83.95	9.3 x 10^{-3}	0.990337972
NH_3	195.45	5 x 10^{-11}	0.999639999	O_3	80.45	2.66 x 10^{-8}	0.990337945
C_2H_2	191.35	3 x 10^{-10}	0.999639999	CO	74.15	1.5 x 10^{-7}	0.990337795
HF	190.05	1 x 10^{-14}	0.999639999	N_2	63.29	7.81 x 10^{-1}	0.209337795
H_2S	187.65	1 x 10^{-14}	0.999639999	O_2	54.75	2.09 x 10^{-1}	0.000337795
HBr	184.65	1.7 x 10^{-12}	0.999639999				
N_2O	182.35	3.2 x 10^{-7}	0.999639679	*and:*			
H_2CO	181.15	2.4 x 10^{-9}	0.999639677	H_2O	273.15	*(variable)*	< 0.0001

The four workspace surfaces total at least 1-100 micron^2 of surface area and are transported on separate sample carriers inside the UHV workspace chamber to allow the surfaces to be positioned in close proximity – e.g., a "four-corners" juxtaposition of four squares (Figure I-1). (Multiple juxtaposed samples is a widely-used technique, e.g., by Boland et al.[545] in low temperature tunneling spectroscopy where a diamond and a metal substrate are mounted side by side on an SPM sample holder.) The temperature of the sample carriers and their payload surfaces can be regulated as necessary for specific reactions – most importantly, for the storage and occasional retrieval of a GeH_3 feedstock molecule from the germanium source which may require one positionally controlled reaction step to be performed at ≤150 K to avoid unscheduled GeH_3 decomposition.[546] The passivated diamondoid fabrication surface can also serve as a source of hydrogen atoms and as a neutral test surface during one possible scheme for fabricating

---

[544] "Major Concentration of Gases in the Atmosphere," NOAA S/T 76-1562, 1976; "AFGL Atmospheric Constituent Profiles (0-120 km)," AFGL-TR-86-0110, 1986; U.S. Standard Atmosphere, 1962 and 1976, Supplement 1966, U.S. Govt. Printing Office, Washington DC, 1976.

[545] B. Naydenov, P. Ryan, L.C. Teague, John J. Boland, "Measuring the Force of Interaction between a Metallic Probe and a Single Molecule," Phys. Rev. Lett. 97(2006):098304.

[546] Robert A. Freitas Jr., Ralph C. Merkle, "A Minimal Toolset for Positional Diamond Mechanosynthesis," J. Comput. Theor. Nanosci. 5(May 2008):760-861.

the GM tool.[547] We also require a small annex chamber (located adjacent to the main workspace chamber) that can accept at least one sample carrier into its interior, then be (1) hermetically sealed off from the main chamber, (2) pressurized to ~6300 atm with H_2 gas in the case of a few rare DMS reactions[548] that may occasionally be necessary (Section 3.2.2.5(B)), and (3) pumped back down to UHV, after which the sample carrier with its attached workspace surface may be returned to the main chamber.

The four workspace surfaces are juxtaposed, leveled flat and adjusted as close as possible to the same mutual altitude to ensure adequate vertical registration, then scanned and mapped: (1) to measure relative surface flatness and surface tilt, (2) to identify the regions of unbroken passivation and depassivation, and (3) to map the locations of all feedstock molecules. (AFMs can discriminate the chemical identity of individual atoms on a surface, even at room temperature.[549]) This procedure, which allows positional parameters for fabrication reaction sequences to be adjusted to actual local geometries, should be repeated every time the relative positions of workspace surfaces are disturbed. At least one of the workspace surfaces should include a metrological fiducial ledge structure at least a few atomic layers high to allow convenient tip alignment.

A set of macroscale SPM tips should be stored in a tool rack inside the main UHV chamber (Figure I-1). The MFW must be able to replace its SPM tips under UHV conditions while the equipment is being operated and without breaking the vacuum seal. Once replaced, the precise location of the distal end of the new tip must be measured by comparison to a fiducial feature also present nearby within the workspace chamber. To prevent DMS radical tip poisoning, all chemically active tooltips which may be fabricated on the distal end of an SPM tip can be stored either in hydrogenated (unreactive) condition and then depassivated by H abstraction just prior to use, or possibly in tip-tip pairs that are easily pulled apart (e.g., GeRad-HAbst, GeRad-GeRad, GeRad-Meth, GeRad-AdamRad)[550] if the challenge of maintaining two-tooltip positional stability can be overcome. The compound HTrans tool should be assembled only when needed.

After mapping and sequence adjustment, the four 5-DOF manipulators in the workspace chamber are maneuvered and operated so as to effectuate the various reactions and reaction sequences

---

[547] Robert A. Freitas Jr., Ralph C. Merkle, "A Minimal Toolset for Positional Diamond Mechanosynthesis," J. Comput. Theor. Nanosci. 5(May 2008):760-861.

[548] Robert A. Freitas Jr., Ralph C. Merkle, "A Minimal Toolset for Positional Diamond Mechanosynthesis," J. Comput. Theor. Nanosci. 5(May 2008):760-861.

[549] Yoshiaki Sugimoto, Pablo Pou, Masayuki Abe, Pavel Jelinek, Rubén Pérez, Seizo Morita, Óscar Custance, "Chemical identification of individual surface atoms by atomic force microscopy," Nature 446(1 March 2007):64-67. See also: David Shiga, "Microscope discerns atoms of different elements," NewScientist.com, 28 February 2007, http://www.newscientisttech.com/article/dn11272-microscope-discerns-atoms-of-different-elements.html.

[550] Robert A. Freitas Jr., Ralph C. Merkle, "A Minimal Toolset for Positional Diamond Mechanosynthesis," J. Comput. Theor. Nanosci. 5(May 2008):760-861.

previously described by Freitas and Merkle[551] to build a variety of simple diamond nanostructures on the diamondoid fabrication surface. The cycle of operation might include: grab a new SPM tip, measure tip position against the fiducial feature, transport the tip to the fabrication area on the fabrication surface, perform the DMS operation (perhaps in concert with 1-2 other tooltips), then withdraw the spent tip. In the most primitive system, SPM tips may be one-use throwaways, in which case the spent tip may be transported to a dump area (perhaps a section of tool rack). There the spent SPM tip is detached (e.g., by loosening mechanical fasters or sliding magnetic fasteners apart), after which the SPM tip holder is moved away and then attached to a new tip to begin the next cycle. In a less primitive system, the SPM tips will be rechargeable; in this scenario, the SPM tip holder later returns and regrasps the spent tip, then participates in a subsequent recharge cycle[552] following which the recharged tip may be returned to service.

To estimate MFW net productivity, we start by assuming (as detailed in Section 3.4.1.4) that ~6 mechanosynthetic operations per atom may typically be required to add each carbon atom to a growing diamond workpiece via DMS, or to add C and H atoms to a hydrogen-passivated diamond surface, including feedstock acquisition, tool operation, tool recharge, and toolrack exchange. We further assume that each operation requires a round-trip tip excursion of the maximum possible ~200 microns using interferometric counting increments of ~0.2 Å that are countable at a ~1 MHz rate, yielding a precision-trackable tip motion velocity of ~20 microns/sec. In this case the MFW can be operated at a rate of ~10 sec per round-trip tip excursion or ~10 sec/operation, yielding a gross productivity of 1 atom per ~60 sec taking ~6 operations required per atom. Assuming a 60% duty cycle for translational tip motions to allow various non-translational motions (e.g., tooltip changeouts) during 40% of the time, the net productivity of the macroscale Phase I MFW system is ~0.01 atom/sec (~0.01 Hz) for nanostructures fabricated on the diamondoid fabrication surface. This speed may be achieved under automated control (Section 3.2.3), but manually controlled MFW operations will undoubtedly go much slower.

Note that in the first primitive experiment by Eigler and Schweizer[553] at IBM Almaden, an STM was used to drag 35 individual xenon atoms across a nickel surface to spell out the corporate logo "IBM" (Figure I-12) in 22 hours of continuous manual effort,[554] giving an effective atom build rate of 0.00044 atom/sec – about 20-fold slower than the 0.01 atom/sec rate estimated for the MFW.

---

[551] Robert A. Freitas Jr., Ralph C. Merkle, "A Minimal Toolset for Positional Diamond Mechanosynthesis," J. Comput. Theor. Nanosci. 5(May 2008):760-861.

[552] Robert A. Freitas Jr., Ralph C. Merkle, "A Minimal Toolset for Positional Diamond Mechanosynthesis," J. Comput. Theor. Nanosci. 5(May 2008):760-861.

[553] D.M. Eigler, E.K. Schweizer, "Positioning Single Atoms with a Scanning Tunnelling Microscope," Nature 344(5 April 1990):524-526; http://www.nature.com/nature/journal/v344/n6266/abs/344524a0.html (abstract).

[554] Malcolm Ritter, "World's smallest moving job shifts just one atom at a time," Sacramento Bee, Thursday, 5 April 1990, p. A8.

Figure I-12. IBM logo spelled out using 35 xenon atoms arranged on a nickel surface via scanning probe microscopy in 1989.[555]

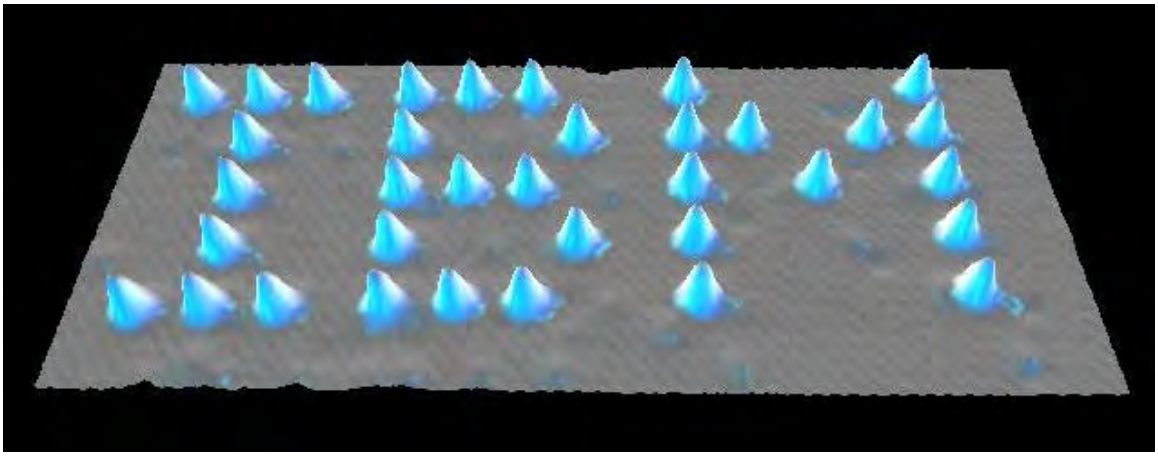

3.2.1.8 Reliability of MFW Operation

All manufacturing processes create defective product objects at some measurable rate. Molecular manufacturing processes will also have a measurable error rate. In each Phase of the nanofactory development program, it is important to ensure that the manufacturing error rate will be low enough to satisfy the stated productivity requirements of that Phase. Error can simultaneously accumulate from many sources and each major source must be accounted for in estimating the total likely error rate of a given sequence of manufacturing operations.

In Section 3.2.1.6, we asserted that reaction-by-reaction sensor-validated discrimination among possible outcomes of an attempted positionally-controlled mechanosynthetic reaction would be unnecessary for the MFW because the proposal is to position the tooltip by dead reckoning. Implicit to this assertion is the requirement that the picopositioning system (e.g., Task I-4, and see Section 3.2.1.3) must be designed with sufficient repeatable placement accuracy to ensure the required number of error-free round trip excursions of the positionally controlled DMS tooltip(s). For the Phase I MFW system, we have a target productivity rate of ~0.01 atom/sec with ~6 mechanosynthetic operations required for placement of each atom in the growing workpiece structure (Section 3.2.1.7), and a target workpiece size of up to 100-1000 atoms for each fabricated diamondoid nanostructure (Section 3.2.1.1). Building the largest 1000-atom structure thus requires ~6000 mechanosynthetic operations, so to avoid even a single misplacement error the picopositioner system must be capable of delivering a minimum of ~6000 error-free round

---

[555] D.M. Eigler, E.K. Schweizer, "Positioning Single Atoms with a Scanning Tunnelling Microscope," Nature 344(5 April 1990):524-526; http://www.nature.com/nature/journal/v344/n6266/abs/344524a0.html (abstract).

trip excursions of the positionally controlled DMS tooltips. A highly reliable picopositioner system is clearly required, and additional steps for increasing positioning reliability are mentioned in Section 3.2.1.6.

Another source of intrinsic manufacturing error arises from the reliability of the DMS reactions themselves. In Section 3.2.1.6 we noted that a proper reaction would be assured by designing appropriate chemical energetics and relative bond strengths for the tooltip-surface interaction. The DMS reaction sequences provisionally employed in this program proposal are based on the set of reactions described by Freitas and Merkle[556] in which net reaction exoergicities and energy barriers to accessible pathologies are no less than 0.40 eV (~64.1 zJ, ~9.2 kcal/mole).

As noted in that paper:[557] "Minimum acceptable reaction energies were guided by reaction reliability requirements. If the absolute value of an energy barrier or reaction exoergicity is E_{react}, then the Boltzmann population of the examined product structure may be approximated as $P_{react} \sim \exp(-E_{react}/k_B T)$ with $k_B = 1.381 \times 10^{-23}$ J/K and T = temperature in K. At T = 300 K, a reaction exoergicity of $E_{react} = 0.40$ eV gives $P_{react} = 2 \times 10^{-7}$ for the failed reaction, reliable enough for products requiring <~10^7 reaction steps for fabrication (e.g., products containing ~10^6 heavy atoms, assuming ~10 steps are required per heavy atom), at room temperature. At T = 80 K (LN_2 temperature), $E_{react} = 0.40$ eV gives $P_{react} = 5 \times 10^{-26}$ at 0.40 eV), indicating extreme reliability for fabricating products with very high atom counts at low temperature. Likewise, a barrier of E_{react} = 0.40 eV that blocks formation of an unwanted pathological structure along a second reaction pathway that competes with the desired more exoergic main reaction pathway gives $P_{react} = 2 \times 10^{-7}$ at T = 300 K for the unwanted structure, yielding similar reliability estimates as before. For these reasons, all proposed reactions have minimum energy barriers (blocking an undesired outcome) or relative exoergicities (favoring a desired outcome) of ~0.40 eV."

Table I-5 gives the probability of misreaction at various relevant operating temperatures, assuming a defect energy threshold of 0.40 eV. At room temperature (~300 K) the misreaction probability per mechanosynthetic operation is 1.91×10^{-7}, conservatively assuming that all reactions have the minimum defect energy threshold of 0.40 eV (most have higher thresholds than this, hence are much less error prone), so the probability of finding a single erroneous atom placement in the largest 1000-atom workpiece after ~6000 mechanosynthetic operations is at most ~0.11%. If any workpiece having one or more erroneous atom placements is considered defective, then the room temperature DMS defect rate will be at most ~10^{-3} for 1000-atom product objects and ~10^{-4} for 100-atom product objects fabricated using this set of DMS reactions, hence room temperature operation appears feasible in Phase I. At near liquid nitrogen temperatures (~80 K), the DMS-related error rate using reaction sequences with a defect energy threshold of 0.40 eV falls to ~4×10^{-22} for a 1000-atom product object, completely negligible for Phase I purposes.

---

[556] Robert A. Freitas Jr., Ralph C. Merkle, "A Minimal Toolset for Positional Diamond Mechanosynthesis," J. Comput. Theor. Nanosci. 5(May 2008):760-861.

[557] Robert A. Freitas Jr., Ralph C. Merkle, "A Minimal Toolset for Positional Diamond Mechanosynthesis," J. Comput. Theor. Nanosci. 5(May 2008):760-861.

Table I-5. Probability of DMS Misreaction as a Function of Temperature, for Reactions Having Minimum Exoergicities and Minimum Barriers to Accessible Pathologies of 0.40 eV.[558]

Operating Temperature (K)	Physical State of Feedstock Molecules	Probability of Misreaction (P_{react})
300.00	room temperature	1.91×10^{-7}
273.15	mp of water-ice	4.18×10^{-8}
194.65	dry ice (solid CO_2)	4.42×10^{-11}
185.00	C_2H_4 gas, GeH_4 gas	1.28×10^{-11}
184.00	C_2H_4 gas, GeH_4 liquid	1.11×10^{-11}
170.00	C_2H_4 gas, GeH_4 liquid	1.39×10^{-12}
169.00	C_2H_4 liquid, GeH_4 liquid	1.19×10^{-12}
118.00	C_2H_4 liquid, GeH_4 liquid	8.32×10^{-18}
109.00	C_2H_4 liquid, GeH_4 liquid	3.23×10^{-19}
104.00	C_2H_4/GeH_4 both solid	4.18×10^{-20}
80.00	C_2H_4/GeH_4 solid, near LN_2	6.41×10^{-26}
77.35	LN_2	8.79×10^{-27}
20.00	approaching liquid helium	1.69×10^{-101}

Another major source of error is radical poisoning by contaminants in an imperfect UHV environment. At a target productivity rate of ~0.01 atom/sec for the Phase I MFW system, the largest 1000-atom product object will require $t_{fab} \sim 10^5$ sec (~1 day) to fabricate. Assuming that a radical site susceptible to poisoning is exposed to the imperfect UHV environment for a fraction $f_{vac} \sim 50\%$ of the time, then the maximum tolerable UHV pressure that will permit one defect-free 1000-atom product object to be fabricated is $P_{UHV} \leq (N_{encounters}\ T / n_{contam}\ A_{radical}\ f_{vac}\ t_{fab})\ (\pi\ MW_{kg} / 2\ k_B T\ N_A)^{1/2} \sim 10^{-12}$ atm, where $n_{contam} = 7.34 \times 10^{27}$ molecules-K/m^3-atm (= N_A/R_{gas}) for ideal gas (contaminant) molecules and T = 300 K, with the other quantities as previously defined in Section 3.2.1.7. If any workpiece having one or more erroneous atom placements is considered defective, then in a UHV environment maintained at ~10^{-16} atm (~10 million contaminant molecules present in a 5-liter UHV work volume; currently achievable experimentally, Section 3.2.1.7) the radical-poisoning defect rate at 300 K will be ~10^{-4} for 1000-atom product objects and ~10^{-5} for 100-atom product objects. If H_2 contaminant is determined not to be a serious radical poisoning risk or can be rigorously excluded from the workspace, then taking MW_{kg} = 0.014 kg/mole for N_2 raises the required P_{UHV} by a factor of ~2.6; conversely, operation at 80 K lowers the required P_{UHV} by a factor of ~2.

Other manufacturing errors are due to environmental conditions that have nothing to do with the operation of the MFW tooltips or the immediate vacuum workspace. For example, without impractical masses of shielding radiation induced errors cannot be avoided in small systems that are exposed to ordinary conditions found on the surface of the Earth. This sets a lower bound on

[558] Robert A. Freitas Jr., Ralph C. Merkle, "A Minimal Toolset for Positional Diamond Mechanosynthesis," J. Comput. Theor. Nanosci. 5(May 2008):760-861.

error rates. Early studies[559] of radiation-induced enzyme inactivation found that ~1.06 x 10^{-17} J of absorbed radiation was required to produce one inactivating hit, yielding a failure condition of $\kappa_{fail} \sim 10^{15}$ hits/kg-rad. Conservatively assuming[560] a rather high value for background photonic and particulate radiation of $I_{rad} \sim 0.5$ rad/yr, the mean time τ_{rad} between radiation-disabling hits on a mostly-carbon 1000-atom diamondoid workpiece (or tooltip) of mass $m_{target} = 2 \times 10^{-23}$ kg is $\tau_{rad} \sim (\kappa_{fail}\, m_{target}\, I_{rad})^{-1} \sim 10^{8}$ years (conservatively assuming that one such hit will cause the workpiece or tooltip to fail with 100% certainty), a negligible error rate.

3.2.2 Task I-1: Design and Simulate DMS Tooltips, Surfaces, Reactions, and Reaction Sequences

Task I-1 is to design and simulate the tooltips, the positionally-controlled reactions, and the reaction sequences needed to perform diamondoid mechanosynthesis (DMS), and to perform computational simulations and other theoretical studies on the thermal stability and propensity to reconstruct of diamondoid surfaces, DMS tooltips, and small diamondoid product objects. The first systematic study of DMS reaction sequences was published by Freitas and Merkle in 2008.[561]

Specific theoretical studies to be completed during Phase I will include the following subtasks, presented in outline form.

3.2.2.1 Design and Simulation of DMS Tooltips

(A) Need design and computational simulations of new mechanosynthetic tooltips – e.g., we should check out the several unexplored variants of the hydrogen donation tool from our previous work.[562]

(B) Need design and computational simulations of tooltip handle structures having high aspect ratios which will permit close proximation of workpiece reaction sites and (possibly multiple) tooltips juxtaposed near a reaction site.

---

[559] G.R. Kepner, R.I. Macey, "Membrane enzyme systems: Molecular size determination from radiation inactivation," Biochim. Biophys. Acta 163(1968):188-203.

[560] K. Eric Drexler, Nanosystems: Molecular Machinery, Manufacturing, and Computation, John Wiley & Sons, New York, 1992, Section 6.6 "Radiation Damage," pp. 154-156.

[561] Robert A. Freitas Jr., Ralph C. Merkle, "A Minimal Toolset for Positional Diamond Mechanosynthesis," J. Comput. Theor. Nanosci. 5(May 2008):760-861.

[562] Robert A. Freitas Jr., Ralph C. Merkle, "Hydrogen Donation Tools for Diamond Mechanosynthesis," 16 November 2005 (unpublished working document).

3.2.2.2 Design and Simulation of Tooltip-Workpiece Interactions

(A) Need simulations of tooltip-workpiece interactions with diamond surfaces (e.g., VASP[563] or equivalent software recommended). Enough surface must be included in these simulations to provide an accurate representation of the model system. (Long-range effects are known to be chemically important in pi-bonded chains of the sort found in organic conductors and some diamond surfaces such as C(110). Pi-bonded carbon chains often show bond-length alternation due to the Peierls instability that propagates the effects of perturbations, so long-range interaction energies in these systems can be larger than those seen in, e.g., Friedel oscillations on metal surfaces. This effect (even if unperturbed C(110) chains don't show alternation) gives a good motivation for extending model structures relatively far along the pi-chain direction.)

(B) Need analysis of optimal tool-workpiece approach trajectories, optimal relative positional configurations of tools and workpiece, and mapping of tooltip work envelopes relative to experimentally controllable parameters such as tooltip rotational state, tooltip-workpiece angles, and tooltip-workpiece distances, possibly leading to revised tooltip designs, configurations, and trajectories. The first study of optimal tooltip trajectories is currently being completed by Tarasov et al.[564] This methodology should be extended at least to all major reaction sequences specified within the minimal toolset[565] framework.

(C) Need analytic and statistical assessments of whether the basic DMS mechanochemistry is reliable enough to proceed without error checking.

(D) Need a comprehensive assessment of the potential for electron poisoning of radical-based tooltips during use, and possible methods for avoiding this. For example, the hydrogen abstraction tool, which is chemically very similar to the ethynyl radical, has a high affinity for electrons (~3 eV). If the abstraction tool attracts a stray electron and is converted to the negative anion, then it would be unable to abstract hydrogen, thus fail in its intended function. This can be prevented by either (a) insuring that electrons are unavailable to migrate to the radical or (b) providing other sites (other hydrogen abstraction tools, or a positively charged wire) to which the stray electron could migrate. At present, the probability of observing this failure mode appears low. Diamond, for instance, has a band gap of ~5.5 eV so electrons in the valence band could only gain access to the conduction band after gaining ~5.5 eV of energy, hence the probability of thermal activation at room temperature or colder would be vanishingly small. Similarly, the ionization potential for other organic compounds is usually multiple electron volts, implying that they too are an unlikely source of such an electron even in a structure which is not purely

---

[563] G. Kresse, J. Furthmuller, Vienna Ab-initio Simulation Package (VASP): The Guide, VASP Group, Institut fur Materialphysik, Universitat Wien, Sensengasse 8, A-1130 Wien, Vienna, Austria, 2003. See also VASP website: http://cms.mpi.univie.ac.at/vasp/.

[564] Denis Tarasov, Natalia Akberova, Ekaterina Izotova, Diana Alisheva, Maksim Astafiev, Robert A. Freitas Jr., "Optimal Tooltip Trajectories in a Hydrogen Abstraction Tool Recharge Reaction Sequence for Positionally Controlled Diamond Mechanosynthesis," J. Comput. Theor. Nanosci. 5(2008). In preparation.

[565] Robert A. Freitas Jr., Ralph C. Merkle, "A Minimal Toolset for Positional Diamond Mechanosynthesis," J. Comput. Theor. Nanosci. 5(May 2008):760-861.

diamond. Electrons in the conduction band would not be available unless deliberate action had been taken to create them (e.g., the use of dopants in the diamond lattice, or the injection of electrons into the conduction band). If it is found that some mechanism creates a low probability that an electron would occupy the radical site, then providing adjacent sacrificial radical sites would reduce the risk that the primary site was occupied. In this case, during a hydrogen abstraction the abstracting tool would function correctly even if initially occupied by an electron because that electron would, during the abstraction process, find it energetically favorable to migrate to the unoccupied radical site, thus reducing the energy of the system by abstracting the hydrogen to the first (or primary) site while allowing the electron to migrate to a secondary site.

3.2.2.3 Design and Simulation of Tool-Tool Interactions

Need focused studies of possible steric congestion among proximated tooltips (Figure I-11C/D). For example, many groups who are working on dual probe scanning probe systems have encountered fundamental limits on how close together two probes may be placed, due to the finite radius of curvature of existing scanning probe tips. DMS failure modes thus may include steric hindrance of desired reactions, possible atomic reconstruction of tooltip handle structures that are brought too closely together, and outright mechanical damage due to tip clash. The ideal tooltip/handle combination will have a high aspect ratio to allow maximum proximation of tooltips. The boundaries of the operating envelopes of closely juxtaposed tooltips must be quantified both theoretically and experimentally.

3.2.2.4 Simulation of Mechanosynthetic Interactions in Realistic Vacuum Environment

(A) Need simulations and studies examining tooltips with exposed radical sites that are placed in realistic experimental vacuum environments. Need assessment of the risk of radical site poisoning due to stray contaminants, and estimates of the expected lifetime of these exposed radical sites in such vacuum environments. What level of vacuum is the minimum required for adequate tooltip lifetimes to allow feasible DMS processes? Are some likely contaminants worse than others?

(B) Need simulations and studies examining workpieces and diamondoid surfaces with exposed radical sites that are placed in realistic experimental vacuum environments. Need assessment of the risk of radical site poisoning due to stray contaminants, and estimates of the expected lifetime of these exposed radical sites in such vacuum environments. What level of vacuum is the minimum required for adequate workpiece or diamondoid surface lifetimes to allow feasible DMS processes? Are some likely contaminants worse than others?

(C) Need a survey of existing vacuum systems and availability of ultra-high vacuums. What levels of vacuum are available, what volumes can be placed in vacuum, how long can vacuum be maintained, and what are the cost/performance tradeoffs? Need an assessment of likely increase in risk of workspace contamination (poisoning of the vacuum) from sources other than tooltips and workpieces, particularly outgassing (desorption) of contaminant molecules from surfaces, tooltip handles, seals, or other mechanisms that might be present inside the workspace volume.

3.2.2.5 Design and Simulation of DMS Reaction Sequences

(A) Need design and simulation of DMS reaction sequences, extending existing work,[566] that minimize workpiece, tooltip, and intermediate structure reconstructions, and that maintain adequate passivation of intermediate workpiece structures.

(B) The 65 reaction sequences described by Freitas and Merkle[567] include 4 sequences that have rate-limiting steps because they require bulk pressurized H_2 to be applied to the workpiece to hydrogenate it. Although SPM-based site-specific bond breaking followed by same-site rehydrogenation using H_2 gas has been demonstrated experimentally,[568] application of pressurized bulk gas is not a tip-based positionally controlled process. The four Reaction Sequences in which these rate-limiting steps occur are not required for methylation or for building diamond cages and thus are not critical-path reactions. Nevertheless, additional studies should be undertaken to determine if and how all four rate limited steps can be eliminated. These four steps[569] include: (a) Step 6 of RS35 for building the germano-adamantane (GeRad) cage (which will only be used very rarely), (b) Step 5 of RS42 while initially acquiring the GeH_3 feedstock molecule (which will only be used very rarely), and (c) Step 6 of RS47 and Step 5 of RS48 which are ethylation sequences on specific diamond surfaces (although substitutes for RS47 and RS48 are available using the existing toolset).

(C) Need to design and simulate tooltip recharge procedures for discharged tooltips.[570]

(D) Need concise definition of minimal toolsets and minimal reaction sets for basic hydrocarbon DMS, including specific diamond-building reaction sequences, that are necessary and sufficient to build simple diamond structures. Reaction sequences using acetylene and digermane as described by Freitas and Merkle[571] must be extended to explicitly include equivalent sequences involving ethylene and germane, since these will be the preferred feedstock molecules employed for nanoscale DMS operations in Phase III and beyond.

---

[566] Robert A. Freitas Jr., Ralph C. Merkle, "A Minimal Toolset for Positional Diamond Mechanosynthesis," J. Comput. Theor. Nanosci. 5(May 2008):760-861.

[567] Robert A. Freitas Jr., Ralph C. Merkle, "A Minimal Toolset for Positional Diamond Mechanosynthesis," J. Comput. Theor. Nanosci. 5(May 2008):760-861.

[568] Satoshi Katano, Yousoo Kim, Masafumi Hori, Michael Trenary, Maki Kawai, "Reversible Control of Hydrogenation of a Single Molecule," Science 316(29 June 2007):1883-1886.

[569] Robert A. Freitas Jr., Ralph C. Merkle, "A Minimal Toolset for Positional Diamond Mechanosynthesis," J. Comput. Theor. Nanosci. 5(May 2008):760-861.

[570] Robert A. Freitas Jr., Ralph C. Merkle, "A Minimal Toolset for Positional Diamond Mechanosynthesis," J. Comput. Theor. Nanosci. 5(May 2008):760-861.

[571] Robert A. Freitas Jr., Ralph C. Merkle, "A Minimal Toolset for Positional Diamond Mechanosynthesis," J. Comput. Theor. Nanosci. 5(May 2008):760-861.

(E) Need to design tools, reactions, reaction sequences, and specific procedures for the positionally controlled fabrication of concave, curved, and strained-shell diamondoid structures.

(F) Need to extend and elaborate existing minimal toolsets to allow DMS using atoms other than C and H (beyond pure hydrocarbons) and Ge – ideally ensuring a combination of close-to-zero dangling bond density, high diffusion barriers, and directional covalent bonds. More specifically, we need to design and simulate DMS tooltips and reactions to allow the placement or donation of atoms of all first- and second-row elements in the Periodic Table. The first study of non-HC DMS tooltips for all first- and second-row elements is currently being completed by Allis et al.[572] Extension of our capabilities beyond hydrocarbons is insurance against possible constraints on nanomechanical system design using purely diamond gears, bearings and related mechanical components, which have limited geometrical diversity as compared to the somewhat wider range of nanocomponent sizes and configurations that may be available using other atoms in addition to C and H. This also argues for an early start to the Registry project (Section 3.3.2) which entails assembling comprehensive libraries of possible nanomachinery designs to quantitatively assess the impact of element choice in molecular machine system design. Another driver for extension to nonhydrocarbon elements may arise during the design of the Stewart platform in Task II-2(H) and Task III-1, or during other focused design efforts that we will be undertaking. However, unless a strong need for elements beyond C/Ge/H can be identified, our efforts in this direction should be limited to a handful of exploratory efforts that consume a minimum of computational and human resources, as befitting an "insurance policy."

(G) Investigate possible methods for effective electron spin control in the context of DMS, e.g., employing the experimentally confirmed spin-orbit coupling of electrons in carbon nanotubes[573] or using electric-field modulated spin rotation (i.e., Rabi oscillations)[574] or spin currents[575] which may provide new ways to manipulate electron spin, thus enabling previously unreliable DMS reaction pathways.

(H) Need comprehensive enumeration and assessment of all pathological states which the workpiece may adopt during a DMS reaction. This analysis must include reaction endo-/exoergicity relative to the desired state, barriers to pathological states, and pathological

---

[572] Damian G. Allis, Robert A. Freitas Jr., Ralph C. Merkle, "Single-Atom Radical-Exchange Mechanosynthetic Transfer Reactions for Period 1,2,3,4 Elements using Monosubstituted Adamantane Tools and Workpieces," J. Comput. Theor. Nanosci. (2008); in preparation.

[573] F. Kuemmeth, S. Ilani, D.C. Ralph, P.L. McEuen, "Coupling of spin and orbital motion of electrons in carbon nanotubes," Nature 452(27 March 2008):448-452. See also: "Electron spin and orbits in carbon nanotubes are coupled," PhysOrg.com, 26 March 2008; http://www.physorg.com/news125767527.html.

[574] K.C. Nowack, F.H.L. Koppens, Yu.V. Nazarov, L.M.K. Vandersypen, "Coherent Control of a Single Electron Spin with Electric Fields," Science 318(30 November 2007):1430-1433, http://www.sciencemag.org/cgi/content/abstract/1148092.

[575] O.M.J. van 't Erve, A.T. Hanbicki, M. Holub, C.H.Li, C. Awo-Affouda, P.E. Thompson, B.T. Jonker, "Electrical injection and detection of spin-polarized carriers in silicon in a lateral transport geometry," Appl. Phys. Lett. 91(19 November 2007):212109, http://link.aip.org/link/?APPLAB/91/212109/1.

intermediate/transitional states that the workpiece may adopt during the DMS reaction or after the DMS reaction is complete. Workpiece defect densities must be controlled and eliminated.

(I) Need to develop and validate a new reaction sequence to produce H_2 using the methods of positionally controlled DMS. The result of this investigation must be made available well before the design work for Phase IV begins, in case such a reaction sequence proves difficult to design (requiring the byproduct gas to be switched from H_2 to CH_4, C_2H_6, or some other hydrogen-rich hydrocarbon).

3.2.2.6 Rearrangement and Reconstruction of Workpiece Surfaces

(A) Are the small diamondoid structures commonly envisioned for nanomechanical parts (and their intermediate structures during and after each DMS reaction in the fabrication process) structurally stable, or do they rearrange? Recent research on "nanodiamond" rearrangements[576] will be instructive and should be extensively reviewed, along with the literature describing effects of H passivation/depassivation and temperature on the nature and frequency of surface reconstructions. (Semi-empirical[577] and first principles[578] methods have shown that the phase transition between "onion" and "nanodiamond" forms is initiated by the presence of the C(111) surface and does not occur on the C(100) or C(110) surfaces,[579] but there is apparently no transition to the delaminated "onion" form in hydrogenated nanodiamonds.[580])

(B) Studies have already been published reporting simulations of various numbers of carbon dimers placed adjacently in a single layer on a C(110) surface, and the stability of such arrangements.[581] Additional DFT studies are needed in which 3D stacks of dimers and other

---

[576] Jean-Yves Raty, Giulia Galli, "Ultradispersity of diamond at the nanoscale," Nature Materials 2(December 2003):792-795.

[577] V.L. Kuznetsov, I.L. Zilberberg, Y.V. Butenko, A.L. Chuvilin, B. Seagall, "Theoretical study of the formation of closed curved graphite-like structures during annealing of diamond surface," J. Appl. Phys. 86(1999):863-870.

[578] A.S. Barnard, S.P. Russo, I.K. Snook, "First principles investigations of diamond ultrananocrystals," Int. J. Mod. Phys. B 17(2003):3865-3879, http://www.worldscinet.com/cgi-bin/details.cgi?id=pii:S0217979203020752&type=html.

[579] S.P. Russo, A.S. Barnard, I.K. Snook, "Hydrogenation of nanodiamond surfaces: Structure and effects on crystalline stability," Surf. Rev. Lett. 10(April/June 2003):233-239, http://www.worldscinet.com/cgi-bin/details.cgi?id=pii:S0218625X03004998&type=html.

[580] S.P. Russo, A.S. Barnard, I.K. Snook, "Hydrogenation of nanodiamond surfaces: Structure and effects on crystalline stability," Surf. Rev. Lett. 10(April/June 2003):233-239, http://www.worldscinet.com/cgi-bin/details.cgi?id=pii:S0218625X03004998&type=html. A.S. Barnard, S.P. Russo, I.K. Snook, "Visualization of Hybridization in Nanocarbon Systems," J. Comput. Theor. Nanosci. 2(March 2005):68-74.

[581] Jingping Peng, Robert A. Freitas Jr., Ralph C. Merkle, "Theoretical Analysis of Diamond Mechanosynthesis. Part I. Stability of C_2 Mediated Growth of Nanocrystalline Diamond C(110) Surface,"

related structures are modeled and simulated to test their stability and reconstruction characteristics. Such a study would also examine the stability of simple dimer-built geometrical shapes, both in planar (2D) and vertically stacked (3D) forms. How high can stacks be built? Does sidewall passivation eliminate reconstruction? Can 3D structures also be stacked on the C(100) surface?

(C) If small diamondoid structures rearrange, is the rearrangement regular and reliable, or random and multistructural? Can the rearrangement be reversed, e.g., by repassivation of the reconstructed surface, as with the diamond C(111) surface? Can the rearrangement be ignored, as in the case of a tooltip handle that rearranges in a known but relatively harmless manner after it is fabricated (i.e., in a way that does not affect the reliability of the positionally controlled chemistry that takes place at the tip)? For example, in early studies of the DCB6Ge dimer placement tooltip interacting with the diamond surface[582] the C(110) surface was chosen because it does not reconstruct whether H-passivated or not, hence allows the study of pure dimer deposition without any complicating factors. Adding carbon dimers to the C(100) or C(111) diamond surfaces will require either: (i) leaving the diamond surface H-passivated during fabrication on that surface, using an H abstraction tool to depassivate just two or a few sites in the immediate vicinity of the proposed deposition prior to the DMS operation, then using an H deposition tool to repassivate after the DMS operation, thus avoid reconstruction; or (ii) taking the reconstructions into account in planning the DMS fabrication reaction sequence – e.g., by offsetting laterally or rotationally the incoming dimer to be deposited, in an appropriate manner to ensure bonding in the desired location – if the reconstruction always occurs in the same way and is predictable and reliable. In some cases a reconstruction may be reversible, as occurs during hydrogenation and heating of a reconstructed C(111) surface to restore the original passivated unreconstructed surface structure.

(D) Need a literature review and supplemental theoretical studies on the propensity of diamondoid surface to undergo graphitization, and the conditions under which this structural pathology may occur.

(E) Need a literature review and supplemental theoretical studies on the propensity and rate of migration of adspecies across the three principal diamond surfaces, including also migrations along ledge and corner structures, around hole rims, and across convex and concave regions, as a function of adspecies type and system temperature. These studies should include an analysis and quantification of any barriers to surface desorption, surface diffusion and migration,

---

J. Comput. Theor. Nanosci. 1(March 2004):62-70; http://www.MolecularAssembler.com/JCTNPengMar04.pdf. M. Sternberg, M. Kaukonen, R.M. Nieminen, Th. Frauenheim, "Growth of (110) diamond using pure dicarbon," Phys. Rev. B 63(April 2001):165414.

[582] Jingping Peng, Robert A. Freitas Jr., Ralph C. Merkle, "Theoretical Analysis of Diamond Mechanosynthesis. Part I. Stability of C_2 Mediated Growth of Nanocrystalline Diamond C(110) Surface," J. Comput. Theor. Nanosci. 1(March 2004):62-70; http://www.MolecularAssembler.com/JCTNPengMar04.pdf. Jingping Peng, Robert A. Freitas Jr., Ralph C. Merkle, James R. Von Ehr, John N. Randall, George D. Skidmore, "Theoretical Analysis of Diamond Mechanosynthesis. Part III. Positional C_2 Deposition on Diamond C(110) Surface using Si/Ge/Sn-based Dimer Placement Tools," J. Comput. Theor. Nanosci. 3(February 2006):28-41; http://www.MolecularAssembler.com/Papers/JCTNPengFeb06.pdf.

and other relevant issues relating to hydrogen diffusion through diamond surfaces.[583] Surface migrations are important in two contexts: (1) tooltip poisoning, and (2) workpiece poisoning – the two entities which exhibit exposed radical sites during DMS fabrication processes. Barriers to surface migration are generally fairly high on diamond. For instance, the barrier to H migration on the clean C(111) shuffle plane is estimated by Heggie et al.[584] as $E_{mig} \sim 2.8$ eV. The reaction time per surface site can then be estimated using the following approximation from transition-state theory:[585] $t_{migrate}^{-1} \sim (k_B T/h) \exp(-E_{mig}/k_B T)$, where $t_{migrate}$ is the mean migration time for any given H adatom (or dangling bond) and $h = 6.63 \times 10^{-34}$ J-sec (Planck's constant). At T = 300 K, $t_{migrate} \sim 5 \times 10^{34}$ sec, and so the probability of H adatom (or dangling bond) migration on the C(111) diamond surface appears negligible at room temperature and virtually vanishes at lower temperatures.

(F) Need a study of the extent to which photoexcitation leads to misreaction and rearrangement of these structures (and their intermediates during fabrication). Misreaction and rearrangement effects due to photoexcitation can usually be avoided by keeping the workspace in darkness. This study should also examine other likely forms of radiation-induced damage.[586]

(G) Need a study of the extent to which the presence and geometric distribution of strained bonds, and the degree of strain, influences the reconstruction of small diamondoid nanoparts and their intermediate structures.

(H) Proper quantum chemistry calculations (e.g., *ab initio*, Density Functional Theory) are needed to determine the structural and chemical stability of target diamondoid machine parts – yielding the stable structure at equilibrium (the structure with the overall lowest free energy). Molecular mechanics simulations alone cannot accurately determine this because these structures have a great deal of surface (increasing the probability of unwanted reactivity or proneness to rearrangement) and typically include a large number of strained bonds (molecular mechanics models are not especially reliable for such bonds).

(I) Molecular dynamics simulations employing quantum chemistry (e.g., AIMD) are needed to probe the kinetic stability of metastable structures. Metastable structures are structures that are not at equilibrium but which have a low enough probability of transforming to the

---

[583] Oren Hershcovitz, "Computational Study of Hydrogen in Nanodiamond," Ph.D. Thesis, Computational Physics Group, Department of Physics, Technion Israel Institute of Technology; http://phycomp.technion.ac.il/~oren/thesis/thesis.html.

[584] Malcolm I. Heggie, Christopher D. Latham, Bob Jones, Patrick R. Briddon, "Local density functional modeling of diamond growth and graphitization," in K.V. Ravi, J.P. Dismukes, eds., Proceedings of the Fourth International Symposium on Diamond Materials, The Electrochemical Society, Pennington NJ, 1995, pp. 643-648. See also: M.I. Heggie, G. Jungnickel, C.D. Latham, "The theory of CVD diamond growth," Diam. Relat. Mater. 5(1996):236-241.

[585] J.I. Steinfeld, J.S. Francisco, W.L. Hase, Chemical Kinetics and Dynamics, Prentice-Hall, Englewood Cliffs NJ, 1989.

[586] Roger V. Lloyd, Silvio DiGregorio, Louis DiMauro, David E. Wood, "Radical Formatlon and Radiation Damage in Adamantane," J. Phys. Chem. 84(1980):2891-2895; http://dx.doi.org/10.1021/j100459a013.

(undesired) more stable state that they can still be useful for practical nanoengineering purposes. Assessing the utility of metastable structures requires calculation of the energy barrier that prevents reconstruction and ensuring that the energy available in the system (whether thermal, mechanical, or other) is insufficient to push the metastable system over that barrier. Tooltips and nanoparts should be carefully searched for the existence of metastable configurations.

(J) Only a very small subset of unterminated surfaces don't reconstruct. Need a review of all surfaces (both passivated and unpassivated) that are known not to reconstruct. This will provide an early target list for experimental attempts at DMS. The best-known example of a non-reconstructing surface is the diamond C(110) surface. A subsequent broader review of the general phenomenon of surface reconstruction would help to prioritize the secondary target list for future mechanosynthetic experimentation, including surfaces containing elements other than C and H. For this broader study, there should be an analytic emphasis on stiff covalent ceramics and related solids, and on nanoclusters <10 nm in size which are most directly analogous to proposed mechanical nanoparts such as gears and bearings that may contain up to ~10^4 atoms each.

(K) Need a definitive study to determine whether or not the clean (nonpassivated) C(111) surface will spontaneously reconstruct at or below room temperature (~300 K), and to determine below what temperature threshold, if any, it will not reconstruct.

(L) Need to quantify the impact on DMS reliability and repeatability of surface relaxation phenomena, as distinct from surface reconstruction phenomena.[587] Relaxation effects can be significant in many diamondoid materials, most notably in the case of sapphire (alumina, Al_2O_3) where surface oxygen ion relaxations can reach ~50% of the layer spacing on the hexagonal (0001) face.

(M) Need a review of the experimental literature and any necessary supplemental experimental work to completely characterize the behavior of the C(111), C(110) and C(100) diamond surfaces under various conditions likely to be encountered during DMS (including intermediate states of hydrogenation/dehydrogenation, partially-completed workpiece structures, etc.).

---

[587] Andrew Zangwill, Physics at Surfaces, Cambridge University Press, 1988, http://www.amazon.com/gp/product/0521347521; M. Prutton, Introduction to Surface Physics, Oxford University Press, 1994, http://www.amazon.com/gp/product/0198534752; D.P. Woodruff, T.A. Delchar, Modern Techniques of Surface Science, Cambridge University Press, 1994, http://www.amazon.com/gp/product/0521424984; John A. Venables, Introduction to Surface and Thin Film Processes, Cambridge University Press, 2000, http://www.amazon.com/gp/product/0521785006; Hans Luth, Solid Surfaces, Interfaces, and Thin Films, 4th edition, Springer, 2001, http://www.amazon.com/gp/product/3540423311.

3.2.2.7 Design and Simulation of Molecular Feedstock Presentation Systems for DMS

(A) Need to design and simulate the presentation of feedstock molecules tethered to fixed surfaces, for easy pickup by mechanosynthetic deposition tools, as well as the range of motions and procedures for acquiring feedstock molecules onto a positionally controlled tooltip from a feedstock molecule presentation surface.

(B) For future Phases, the binding, transport through barrier surfaces, and positioning of initially positionally unconstrained liquid or gaseous feedstock molecules (e.g., acetylene (C_2H_2), ethylene (C_2H_4), germane (GeH_4), methane (CH_4), molecular hydrogen (H_2), etc.) should begin to be explored with a view toward the design of binding sites based mainly on molecular steric (shape) properties that can be flexibly engineered for use in molecular manufacturing systems.

3.2.2.8 Design Procedures for the Experimental Fabrication of DMS Tooltips

(A) Need proposals (and critiques of proposals) describing how to build mechanosynthetic tooltips with appropriate handle structures, using techniques that are experimentally accessible today. (Later-generation systems may employ atomically precise tooltips to make replica tooltips, a far quicker and more efficient process.)

(B) Need methods to characterize tooltips, once they have been fabricated, without destroying or inactivating them. This will be especially important in the early stages of DMS experimentation when our experience with (and understanding of) such systems is at its lowest ebb.

(C) Need an analysis of the utility of conditional testing of intermediate states of the workpiece during DMS fabrication, and of the most appropriate methods for doing this. Is tooltip/workpiece registration, combined with positional and force feedback measurements during a DMS reaction step, sufficient to ensure reliable DMS operations? Or is conditional testing and workpiece reaction site characterization between each step necessary to achieve acceptable DMS reliability? It is believed that testing of intermediate workpiece states may be essential in the early stages of DMS experimentation. As experience with these systems grows and knowledge is accumulated about the normal range of responses during tooltip-workpiece interactions, it may be possible to largely eliminate step-by-step testing, substituting end-product testing and spot-checking for quality-control purposes. The elimination of step-by-step testing is key for massive parallelization and scaleup of DMS-based fabrication systems.

(D) Need to analyze the utility and difficulty of DMS on re-entrant structures (i.e., modification of a covalent structure that has already been built). Our current view is that re-entrant operations are both difficult and unnecessary with adequate positional control of the original fabrication process, but this assumption should be challenged or defended with definitive studies of the issue. The presumption in this program proposal is that with good positional control, fabrication errors will rarely occur, but if they do occur, the ruined product object should be discarded, not repaired.

3.2.2.9 Investigate Availability of Natural Diamondoid Nanoparts for Testing and Fabrication

(A) It would be useful to have a complete library of naturally-occurring adamantane structures, cataloged according to size, geometric structure, atom count, bonding/connectivity, availability after extraction from natural petroleum,[588] and so forth. This would tell us what naturally-occurring "parts" might be readily available in large quantities for further processing into more complex nanostructures such as bearings, gears, and the like, or for testing the performance of early stage experimental manipulator systems. Additionally, fabrication of atomically precise diamondoid building blocks, nanoparts, or even simple nanodevices using purely non-positional techniques (e.g., conventional bulk chemical synthesis (Section 3.2.2.10(B)), patterned ALE (Section 3.2.2.10(C)), supramolecular chemistry, DNA nanotechnology-assisted self-assembly, chemical vapor deposition (CVD), etc.) could accelerate the completion of Phase I and Phase II by providing a convenient supply of ready-made diamondoid components suitable for further assembly as part of a more complete positionally-controlled nanomanufacturing system.

(B) The possibility of constructing diamondoid nanoparts starting with adamantane building block primitives, via positionally controlled manipulation, should be investigated. If it proves possible, this could reduce some of the need for precision DMS to be employed in the manufacture of the basic cage frameworks of diamondoid nanoparts. However, precision DMS would still be required for the addition or modification of essential nanopart surface features and for the covalent joining of adamantane primitives into larger aggregates during the diamondoid nanopart fabrication process. Use of adamantane building blocks as primitives would require designing binding sites to acquire and hold in a preferred orientation the target adamantane cage molecule, followed by attachment of a block-grabbing tool using two bonding sites to maintain positional control of the molecule and prevent uncontrolled rotation. Other non-diamondoid building-block primitives have been proposed[589] but would yield products of inferior stiffness and strength compared to diamondoid.

---

[588] J.E. Dahl, S.G. Liu, R.M.K. Carlson, "Isolation and Structure of Higher Diamondoids, Nanometer-Sized Diamond Molecules," Science 299(3 January 2003):96-99; http://moleculardevices.org/diamond-isol.pdf and http://dx.doi.org/10.1126/science.1078239. See also: http://moleculardevices.org/diamond-intro.pdf and http://moleculardevices.org/diamond-suppl.pdf. Jeremy E. P. Dahl, J. Michael Moldowan, Torren M. Peakman, Jon C. Clardy, Emil Lobkovsky, Marilyn M. Olmstead, Paul W. May, Tim J. Davis, John W. Steeds, Ken E. Peters, Andy Pepper, Andy Ekuan, Robert M. K. Carlson, "Isolation and Structural Proof of the Large Diamond Molecule, Cyclohexamantane ($C_{26}H_{30}$)," 42(2003):2040-2044, http://www3.interscience.wiley.com/cgi-bin/abstract/104531060.

[589] Ralph C. Merkle, "Molecular building blocks and development strategies for molecular nanotechnology," Nanotechnology 11(2000):89-99, http://www.zyvex.com/nanotech/mbb/mbb.html. Jesper Wengel, "Nucleic acid nanotechnology – towards Angstrom-scale engineering," Org. Biomol. Chem. 2(2004):277-280; http://www.rsc.org/CFmuscat/intermediate_abstract.cfm?FURL=/ej/OB/2004/b313986g.PDF.

3.2.2.10 Investigate Possible Bulk Chemical Synthesis of Atomically Precise 3D Diamondoid Nanoparts

(A) Atomically-precise 222-carbon-atom graphene sheets[590] and 10-nm wide graphene nanoribbons (GNRs)[591] have been prepared by bulk (solution-phase) chemical synthesis, and it may be possible to cut graphene nanoribbons of defined chirality with ~5 Å spatial resolution from graphite sheets via STEM techniques (e.g., Zobelli et al.;[592] Section 2.2.3.3). A chemical synthesis of C_{60} fullerene has been reported,[593] though the final step requires flash vacuum pyrolysis at 1100 ^{o}C and 0.01 torr, and the yield is only 0.1-1%; other C_{60} chemical synthesis schemes have also been proposed.[594] Half-closed "buckybowls",[595] graphite crystals,[596] and

---

[590] C.D. Simpson, J.D. Brand, A.J. Berresheim, L. Przybilla, H.J. Rader, K. Mullen, "Synthesis of a giant 222 carbon graphite sheet," Chemistry 8(15 March 2002):1424-1429, http://www.ncbi.nlm.nih.gov/entrez/query.fcgi?cmd=Retrieve&db=PubMed&list_uids=11921226&dopt=Abstract. See also: C. Gunther, N. Karl, J. Pflaum, R. Strohmaier, B. Gompf, W. Eisenmenger, M. Muller, K. Mullen, "LEED, STM, and TDS studies of ordered thin films of the rhombus-shaped polycondensed aromatic hydrocarbon $C_{54}H_{22}$, on MoS_2, GeS, and graphite," Langmuir 21(18 January 2005):656-665; Q. Song, C.W. Lebeis, X. Shen, D.M. Ho, R.A. Pascal Jr., "Polyphenyl macrocyclic oligophenylenes," J. Am. Chem. Soc. 127(5 October 2005):13732-13737; L. Zhi, J. Wu, K. Mullen, "Star-shaped hexa-peri-hexabenzocoronene 'heptamer': synthesis and self-assembly," Org. Lett. 7(22 December 2005):5761-5764.

[591] Xiaolin Li, Xinran Wang, Li Zhang, Sangwon Lee, Hongjie Dai, "Chemically derived, ultrasmooth graphene nanoribbon semiconductors," Science 319(29 February 2008):1229-1232. See also: Hannes C. Schniepp, Je-Luen Li, Michael J. McAllister, Hiroaki Sai, Margarita Herrera-Alonso, Douglas H. Adamson, Robert K. Prud'homme, Roberto Car, Dudley A. Saville, Ilhan A. Aksay, "Functionalized single graphene sheets derived from splitting graphite oxide," J. Phys. Chem. B 110(2006):8535-8539, http://pubs3.acs.org/acs/journals/doilookup?in_doi=10.1021/jp060936f; S. Stankovich, R.D. Piner, S.T. Nguyen, R.S. Ruoff, "Synthesis and exfoliation of isocyanate-treated graphene oxide nanoplatelets," Carbon 44(2006):3342-3347; Aiping Yu, Palanisamy Ramesh, Mikhail E. Itkis, Elena Bekyarova, Robert C. Haddon, "Graphite nanoplatelet-epoxy composite thermal interface materials," J. Phys. Chem. C 111(2007):7565-7569.

[592] A. Zobelli, A. Gloter, C. P. Ewels, C. Colliex, "Shaping single walled nanotubes with an electron beam," Phys. Rev. B 77(2008):045410; http://link.aps.org/abstract/PRB/v77/e045410.

[593] Lawrence T. Scott, Margaret M. Boorum, Brandon J. McMahon, Stefan Hagen, James Mack, Jarred Blank, Hermann Wegner, Armin de Meijere, "A Rational Chemical Synthesis of C_{60}," Science 295(22 February 2002):1500-1503; Lawrence T. Scott, "Methods for the Chemical Synthesis of Fullerenes," Angewandte Chemie International Edition 43(2004):4994-5007.

[594] Ayumu Yasuda, "Chemical synthesis scheme for a C_{60} fullerene," Carbon 43(2005):889-892.

[595] Andrzej Sygula, Renata Sygula, Peter W. Rabideau, "The First Buckybowl Aryne. Corannulyne: A Nonplanar Benzyne," Org. Lett. 7(2005):4999-5001.

[596] Svetlana Dimovski, Alexei Nikitin, Haihui Ye, Yury Gogotsi, "Synthesis of graphite by chlorination of iron carbide at moderate temperatures," J. Mater. Chem. 14(2004):238-243.

"cubic graphite" (a hollow graphene box)[597] have been chemically synthesized. The self-assembly of curved pentagonal hydrocarbon (corannulene skeleton, $C_{20}H_{10}$) spherical segments into ~3-nm icosahedral spherical containers using hydrogen bonding, metal binding, or disulfide covalent bonding has been investigated theoretically.[598] These materials should be investigated as possible sources of prefabricated input nanoparts for positionally controlled constructions as envisioned in this proposal.

(B) The potential for bulk chemical synthesis of simple diamondoid nanoparts should be investigated as a possible shortcut if some way to impose positional control on the reaction site can be found. Past investigations of the bulk chemical synthesis of diamondoid materials, which may inform and inspire future efforts, include:

(**i**) the chemical synthesis of 1-cage adamantane,[599] 2-cage biadamantane,[600] 2-cage diamantane,[601] 3-cage triamantane[602] and 4-cage tetramantane[603] (but since 4-cage to

---

[597] Q. Song, C.W. Lebeis, X. Shen, D.M. Ho, R.A. Pascal Jr., "Polyphenyl macrocyclic oligophenylenes," J. Am. Chem. Soc. 127(5 October 2005):13732-13737.

[598] Arthur J. Olson, Yunfeng H. E. Hu, Ehud Keinan, "Chemical mimicry of viral capsid self-assembly," PNAS 104(26 December 2007):20731-20736, http://tc2tc.mojolingo.xuite.net/m2m-0000/www.pnas.org/cgi/reprint/0709489104v1.

[599] Paul von R. Schleyer, "A simple preparation of adamantane," J. Am. Chem. Soc. 79(1957):3292; Paul von R. Schleyer, Malcolm M. Donaldson, "The relative stability of bridged hydrocarbons. II. Endo- and exo-trimethylenenorborane," J. Am. Chem. Soc. 82(5 September 1960):4645-4651; D.E. Johnston, M.A. McKervey, J.J. Rooney, "Preparation of diamondoid hydrocarbons by rearrangement employing a chlorinated platinum-alumina catalyst," J. Am. Chem. Soc. 93(2 June 1971):2798-2799.

[600] S. Landa, S. Hala, Chem. Listy. 51(1957):2325; H.F. Reinhardt, "Biadamantane and some of its derivatives," J. Org. Chem. 27(September 1962):3258-3261; Paul von Rague Schleyer, "My thirty years in hydrocarbon cages: From adamantane to dodecahedrane," in George A. Olah, ed., Cage Hydrocarbons, John Wiley & Sons, New York, 1990, pp. 1-38.

[601] Chris A. Cupas, Paul von R. Schleyer, David J. Trecker, "Congressane," J. Am. Chem. Soc. 87(20 February 1965):917-918; Tamara M. Gund, Van Zandt Williams, Jr., Eiji Osawa, Paul v.R. Schleyer, "A convenient, high-yield preparation of diamantane (congressane)," Tetrahedron Lett. (1970):3877-3880; D. Faulkner, R.A. Glendinning, D.E. Johnston, M.A. McKervey, "Functionalisation reactions of diamantane," Tetrahedron Lett. (1971):1671-1674; E. Boelema, J. Strating, Hans Wynberg, "Spiro[adamantane-2,2'-adamantane]," Tetrahedron Lett. 12(1972):1175-1177; W.D. Graham, P. von R. Schleyer, "Diamond lattice hydrocarbons: spiro[adamantane-2,2'-adamantane]," Tetrahedron Lett. 12(1972):1179-1180; T. Courtney, D.E. Johnston, M.A. McKervey, J.J. Rooney, "The chemistry of diamantane. Part 1. Synthesis and some functionalization reactions," J. Chem. Soc. Perkin Trans. 1(1972):2691-2696; Tamara M. Gund, W. Thilecke, Paul v.R. Schleyer, Org. Synth. 53(1973):30; W. David Graham, Paul von R. Schleyer, Edward W. Hagaman, Ernest Wenkert, "[2]Diadamantane, the first member of a new class of diamondoid hydrocarbons," J. Am. Chem. Soc. 95(22 August 1973):5785-5786.

[602] Van Zandt Williams, Jr., Paul von R. Schleyer, Gerald Jay Gleicher, Lynn B. Rodewald, "Triamantane," J. Am. Chem. Soc. 88(20 August 1966):3862-3863; William Burns, M. Anthony McKervey, John J. Rooney, "New synthesis of triamantane involving a novel rearrangement of a polycyclic olefin in the gas phase on platinum," Chem. Commun. (1975):965-966; Fredric S. Hollowood, M. Anthony McKervey,

11-cage diamondoids occur naturally in oil,[604] some relatively simple but as yet unidentified natural chemical process must exist to synthesize them);

(**ii**) chemical functionalization[605] and kink-site functionalization[606] of fullerenes, and chemical functionalization of higher diamondoids up to pentamantanes;[607]

(**iii**) cycloaddition reactions to C(100) surfaces,[608] Si(100) surfaces,[609] Ge(100) surfaces,[610] other semiconductor surfaces,[611] and fullerene[612] and carbon nanotube[613] walls;

Robert Hamilton, John J. Rooney, "Synthesis of triamantane," J. Org. Chem. 45(21 November 1980):4954-4958.

[603] William Burns, Thomas R.B. Mitchell, M. Anthony McKervey, John J. Rooney, George Ferguson, Paul Roberts, "Gas-phase reactions on platinum. Synthesis and crystal structure of anti-tetramantane, a large diamondoid fragment," J. Chem. Soc. Chem. Commun. (1976):893-895; William Burns, M. Anthony McKervey, Thomas R.B. Mitchell, John J. Rooney, "A new approach to the synthesis of diamondoid hydrocarbons: synthesis of anti-tetramantane," J. Am. Chem. Soc. 100(1978):906-911.

[604] J.E. Dahl, S.G. Liu, R.M.K. Carlson, "Isolation and Structure of Higher Diamondoids, Nanometer-Sized Diamond Molecules," Science 299(3 January 2003):96-99; http://moleculardevices.org/diamond-isol.pdf and http://dx.doi.org/10.1126/science.1078239. See also: http://moleculardevices.org/diamond-intro.pdf and http://moleculardevices.org/diamond-suppl.pdf.

[605] R. Taylor, D.R.M. Walton, "The chemistry of fullerenes," Nature 363(1993):685; F. Diederich, C. Thilgen, "Covalent fullerene chemistry," Science 271(19 January 1996):317-323; B. Ni, S.B. Sinnott, "Chemical functionalization of carbon nanotubes through energetic radical collisions," Phys. Rev. B 61(2000):R16343-R16346; J.L. Bahr, J.P. Yang, D.V. Kosynkin, M.J. Bronikowski, R.E. Smalley, J.M. Tour, "Functionalization of carbon nanotubes by electrochemical reduction of aryl diazonium salts: A bucky paper electrode," J. Am. Chem. Soc. 123(2001):6536-6542, http://smalley.rice.edu/rick's publications/JACS123-6536.pdf; Sarbajit Banerjee, Stanislaus S. Wong, "Functionalization of Carbon Nanotubes with a Metal-Containing Molecular Complex," Nano Letters 2(2002):49-53; Frank J. Owens, Zafar Iqbal, "Electrochemical Functionalization Of Carbon Nanotubes With Hydrogen," 23rd Army Science Conference, Session L Poster Summaries: Nanotechnology, LP-11, 2002, http://www.asc2002.com/summaries/l/LP-11.pdf; S.B. Sinnott, "Chemical Functionalization of Carbon Nanotubes: A Review," J. Nanosci. Nanotechnol. 2(2002):113-123; Keun Soo Kim, Kyung Ah Park, Hyun Jin Kim, Dong Jae Bae, Seong Chu Lim, Young Hee Lee, Jae Ryong Kim, Ju-Jin Kim, Won Bong Choi, "Band Gap Modulation of a Carbon Nanotube by Hydrogen Functionalization," J. Korean Phys. Soc. 42(February 2003):S137-S142, http://nanotube.skku.ac.kr/data/paper/KSKim_JKPS.pdf; Sarbajit Banerjee, Michael G.C. Kahn, Stanislaus S. Wong, "Rational Chemical Strategies for Carbon Nanotube Functionalization," Chem. Eur. J. 9(2003):1898-1908.

[606] Kevin D. Ausman, Henry W. Rohrs, MinFeng Yu, Rodney S. Ruoff, "Nanostressing and mechanochemistry," Nanotechnology 10(September 1999):258-262.

[607] Boryslav A. Tkachenko, Natalie A. Fokina, Lesya V. Chernish, Jeremy E. P. Dahl, Shenggao Liu, Robert M. K. Carlson, Andrey A. Fokin, Peter R. Schreiner, "Functionalized Nanodiamonds Part 3: Thiolation of Tertiary/Bridgehead Alcohols," Org. Lett., 8(2006):1767-1770, http://dx.doi.org/10.1021/ol053136g; Andrey A. Fokin, Peter R. Schreiner, Natalie A. Fokina, Boryslav A. Tkachenko, Heike Hausmann, Michael Serafin, Jeremy E. P. Dahl, Shenggao Liu, Robert M. K. Carlson, "Reactivity of [1(2,3)4]Pentamantane (Td-Pentamantane): A Nanoscale Model of Diamond," J. Org. Chem. 71(2006):8532-8540, http://dx.doi.org/10.1021/jo061561x.

(**iv**) hydrosilylation of adamantane molecules onto silicon surfaces;[614]

---

[608] J.S. Hovis, S.K. Coulter, R.J. Hamers, M.P.D'Evelyn, J.N. Russell Jr., J.E. Butler, "Cycloaddition Chemistry at Surfaces: Reaction of Alkenes with the Diamond(001)-2 x 1 Surface," J. Am. Chem. Soc. 122(2000):732-733, http://hamers.chem.wisc.edu/papers/pdf/hovis_diamond.pdf; X. Lu, X. Xu, N. Wang, Q. Zhang, "A DFT study of the 1,3-dipolar cycloadditions on the C(100)-2x1 surface," J. Org. Chem. 67(25 January 2002):515-520.

[609] M.J. Bozack, P.A. Taylor, W.J. Choyke, J.T. Yates Jr., "Chemical activity of the C=C double bond on silicon surfaces," Surf. Sci. 177(1986):L933-L937; R.J. Hamers, J.S. Hovis, S. Lee, H. Liu, J.J. Shan, "Formation of Ordered, Anisotropic Organic Monolayers on the Si(001) Surface," Phys. Chem. B 101(1997):1489-1492, http://hamers.chem.wisc.edu/papers/pdf/hamers_cyclopentene.pdf; R. Konecny, D.J. Doren, "Theoretical prediction of a facile Diels-Alder reaction on the Si(100)-2x1 surface," J. Am. Chem. Soc. 119(1997):11098-11099; A.V. Teplyakov, M.J. Kong, S.F. Bent, "Vibrational spectroscopic studies of Diels-Alder reactions with the Si(100)-2x1 surface as a dienophile.," J. Am. Chem. Soc. 119(1997):11100-11101; Jennifer S. Hovis, Hongbing Liu, Robert J. Hamers, "Cycloaddition Chemistry of 1,3-Dienes on the Silicon(001) Surface: Competition between [4 + 2] and [2 + 2] Reactions," J. Phys. Chem. B 102(1998):6873-6879, http://hamers.chem.wisc.edu/papers/pdf/hovis_diels-alder.pdf; A.V. Teplyakov, M.J. Kong, S.F. Bent, "Diels-Alder reactions of butadienes with the Si(100)-2x1 surface as a dienophile: vibrational spectroscopy, thermal desorption and near edge X-ray absorption fine structure studies," J. Chem. Phys. 108(1998):4599-4606.

[610] A.V. Teplyakov, P. Lal, Y.A. Noah, S.F. Bent, "Evidence for a Retro-Diels-Alder Reaction on a Single Crystal Surface: Butadienes on Ge(100)," J. Am. Chem. Soc. 120(1998):7377-7378; R.J. Hamers, J.S. Hovis, C.M. Greenlief, D.F. Padowitz, "Scanning Tunneling Microscopy of Organic Molecules on Monolayers on Silicon (001) Surfaces," Jpn. J. Appl. Phys. 38(1999):3879-3887, http://hamers.chem.wisc.edu/papers/pdf/hamers_jjap.pdf; Sang Won Lee, Jennifer S. Hovis, Sarah K. Coulter, Robert J. Hamers, C. Michael Greenlief, "Cycloaddition chemistry on germanium(001) surfaces: the adsorption and reaction of cyclopentene and cyclohexene," Surface Science 462(2000):6-18, http://hamers.chem.wisc.edu/papers/pdf/lee_cyclopentene_germanium.pdf.

[611] R.J. Hamers, S.K. Coulter, M.D. Ellison, J.S. Hovis, D.F. Padowitz, M.P. Schwartz, C.M. Greenlief, J.N. Russell Jr., "Cycloaddition chemistry of organic molecules with semiconductor surfaces," Acc. Chem. Res. 33(September 2000):617-624, http://hamers.chem.wisc.edu/papers/pdf/hamers_acr.pdf.

[612] Steven H. Hoke, Jay Molstad, Dominique Dilettato, Mary Jennifer Jay, Dean Carlson, Bart Kahr, R. Graham Cooks, "Reaction of Fullerenes and Benzyne," J. Org. Chem. 57(11 September 1992):5069-5071; M.S. Meier, G.W. Wang, R.C. Haddon, C.P. Brock, M.A. Lloyd, J.P. Selegue, "Benzyne adds across a closed 5-6 ring fusion in C_{70}: Evidence for bond delocalization in fullerenes," J. Am. Chem. Soc. 120(1998):2337-2342.

[613] R.W. Hoffmann, Dehydrobenzene and Cycloalkynes, Verlag Chemie-Academic Press, New York, 1967; Richard Jaffe, Jie Han, Al Globus, "Formation of Carbon Nanotube Based Gears: Quantum Chemistry and Molecular Mechanics Study of the Electrophilic Addition of o-Benzyne to Fullerenes, Graphene, and Nanotubes," First Electronic Molecular Modeling & Graphics Society Conference, 1996, http://www.nas.nasa.gov/Groups/Nanotechnology/publications/MGMS_EC1/quantum/paper.html; Al Globus, Richard Jaffe, "NanoDesign: Concepts and Software for a Nanotechnology Based on Functionalized Fullerenes," First Electronic Molecular Modeling & Graphics Society Conference, 1996, http://www.nas.nasa.gov/Groups/Nanotechnology/publications/MGMS_EC1/NanoDesign/paper.html.

[614] L. Giraud, V. Huber, T. Jenny, "2,2-Divinyladamantane: a new substrate for the modification of silicon surfaces," Tetrahedron 54(1998):11899-11906; E. Leroy, O. M. Kuttel, L. Schlapbach, L. Giraud, T.

(**v**) liquid-phase diamond synthesis via electrolysis of solutions of ammonium acetate in liquid acetic acid;[615]

(**vi**) liquid-phase diamond synthesis in boiling benzene and in molten lead;[616]

(**vii**) a 2% yield of diamond from carbon tetrachloride in liquid sodium at 700 ^{o}C;[617]

(**viii**) electrochemical growth of diamond films below 50 ^{o}C in liquid ethanol;[618]

(**ix**) hydrothermal synthesis of diamond;[619]

(**x**) carbon nanotubes prepared chemically from supercritical CO_2;[620]

(**xi**) laser heating of solid CO_2 at 30-80 GPa pressure which causes the molecule to decompose into oxygen and diamond, revealing a new region of the CO_2 phase diagram with a boundary having a negative P-T slope;[621]

(**xii**) conversion of SiC to microcrystalline diamond-structured carbon up to 1000 ^{o}C;[622] and

(**xiii**) hydrogen abstraction from passivated diamond surface in liquid phase.[623]

(C) Patterned ALE or PALE (Sections 2.2.4 and 3.4.3) can in principle be used to produce rectilinear nanoparts with atomic precision in all three dimensions. Currently envisioned buildable nanoparts include regular lattices of pure silicon and germanium that are fabricated as a

---

Jenny, "Chemical vapor deposition of diamond growth using chemical precursor," Appl. Phys. Lett. 73(24 August 1998):1050-1052; Anne Giraud, Titus Jenny, Eric Leroy, Olivier M. Kuttel, Louis Schlapbach, Patrice Vanelle, Luc Giraud, "Chemical nucleation for CVD diamond growth," J. Am. Chem. Soc. 123(2001):2271-2274.

[615] P. Aublanc, V.P. Novikov, L.V. Kuznetsova, M. Mermoux, "Diamond synthesis by electrolysis of acetates," Diam. Rel. Mater. 10(March-July 2001):942-946.

[616] C.V. Burton, "Artificial diamonds," Nature 72(24 August 1905):397.

[617] Yadong Li, Yitai Qian, Hongwei Liao, Yi Ding, Li Yang, Cunyi Xu, Fangqing Li, Guien Zhou, "A reduction-pyrolysis-catalysis synthesis of diamond," Science 281(10 July 1998):246-247.

[618] Yoshikatsu Namba, "Attempt to grow diamond phase carbon films from an organic solution," J. Vac. Sci. Technol. A 10(September/October 1992):3368-3370.

[619] S. Feng, R. Xu, "New materials in hydrothermal synthesis," Acc. Chem. Res. 34(March 2001):239-247.

[620] H. Sowa, E. Koch, "A proposal for a transition mechanism from the diamond to the lonsdaleite type," Acta Crystallogr. A 57(July 2001):406-413.

[621] O. Tschauner, H.K. Mao, R.J. Hemley, "New transformations of CO(2) at high pressures and temperatures," Phys. Rev. Lett. 87(13 August 2001):075701.

[622] Y. Gogotsi, S. Welz, D.A. Ersoy, M.J. McNallan, "Conversion of silicon carbide to crystalline diamond-structured carbon at ambient pressure," Nature 411(17 May 2001):283-287.

[623] T. Tsubota, O. Hirabayashi, S. Ida, S. Nagaoka, M. Nagata, Y. Matsumoto, K. Kusakabe, S. Morooka, "Hydrogen abstraction reaction of hydrogenated diamond surface in liquid phase by radical initiators used in polymer synthesis," Nippon Kagaku Kaishi 11(2001):631-636.

stack of single-atom-thick layers without internal voids whose perimeters are delineated with atomic precision by a direct-write tip-based process, giving access to a wide range of parts shapes similar to those accessible via solid printing technologies (Section 2.2.3), but at the nanoscale. Since diamond is ten times stronger, less chemically reactive, and less prone to surface reconstruction pathologies than silicon, the possibility of diamond PALE is of interest as a potential shortcut to diamondoid nanoparts fabrication. Progress toward this end should be closely monitored. Theoretical simulations[624] and experimental investigations[625] of low-temperature diamond ALE using alternating fluxes of halocarbons and atomic hydrogen have been conducted with only limited success, and further research will be required to extend these or related techniques to atomically precise patterned ALE for diamond.

3.2.2.11 Improve Software and Analytical Tools

(A) Need to develop new software tools for design, modeling, simulation, analysis, and experimentation. For example, the possibility of automated retrosynthesis and the computer-aided design/analysis of reaction sequences,[626] including methods involving artificial intelligence

---

[624] M.G. Wensell, Z. Zhang, J. Bernholc, "Fluorine-Based Mechanisms for Atomic-Layer-Epitaxial Growth on Diamond (110)," Phys. Rev. Lett. 74(June 1995):4875-4878; T.I. Hukka, T.A. Pakkanen, M.P.D'Evelyn, "CF_3 radicals as growth precursors and halogen-assisted growth on diamond (100)2 x 1: An ab initio study," Surface Science 359(1 July 1996):213-226.

[625] T.I. Hukka, R.E. Rawles, M.P. D'Evelyn, "Novel method for chemical vapor deposition and atomic layer epitaxy using radical chemistry," Thin Solid Films 225(1993):212-218; Roy Gat, Terttu I. Hukka, Robin E. Rawles, Mark P. D'Evelyn, "Progress Toward Atomic Layer Epitaxy of Diamond: Diamond Films Grown One Layer at a Time," Technical Report 16, ADA265530, 4 May 1993, http://handle.dtic.mil/100.2/ADA265530; S.F. Komarov, J.-J. Lee, J.B. Hudson, M.P. D'Evelyn, "Self-limiting diamond growth from alternating CFx and H fluxes," Diamond and Related Materials 7(August 1998):1087-1094. Mark Hammond, Keith Jamison, "Diamond Atomic Layer Epitaxy," Report Number A765882, 6 October 1994, http://www.stormingmedia.us/76/7658/A765882.html; Andrew Freedman, Gary N. Robinson, David D. Neison Jr., Paul L. Kebabian, Mark S. Zahniser, "Atomic Layer Epitaxy of Thin Diamond Films," Report Number A316203, November 1995, http://www.stormingmedia.us/31/3162/A316203.html; Max N. Yoder, "Apparatus for and a method of growing thin films of elemental semiconductors," 6 July 1993, U.S. Patent 5225366, http://www.wikipatents.com/5225366.html; Max N. Yoder, "Atomic layer epitaxy (ALE) apparatus for growing thin films of elemental semiconductors," 25 January 1994, U.S. Patent 5281274, http://www.freepatentsonline.com/5281274.html.

[626] E.J. Corey, M. Ohno, R.B. Mitra, P.A. Vatakencherry, "Total synthesis of longifolene," J. Amer. Chem. Soc. 86(1964):478-485, LHASA homepage http://lhasa.harvard.edu/, LHASA publications http://lhasa.harvard.edu/LHASApublications.htm; E.J. Corey, W.T. Wipke, "Computer-Assisted Design of Complex Organic Syntheses," Science 166(1969):178-192; H.L. Gelernter, A.F. Sanders, D.L. Larsen, K.K. Agarwal, R.H. Boivie, G.A. Spritzer, J.E. Searleman , "Empirical explorations of SYNCHEM," Science 197(9 September 1977):1041-1049; W.T. Wipke et al., "SECS - Simulation and Evaluation of Chemical Synthesis: Strategy and Planning," in: W.T. Wipke, W.J. House, eds., Computer-Assisted Organic Synthesis, ACS, Washington, 1977, p. 97; P.N. Judson, "Industrial Collaboration in Computer Aided Synthesis Design," LHASA U.K. Kemia-Kemi 12(1985):150-152; E.J. Corey, A.K. Long, S.D. Rubenstein, "Computer-assisted analysis in organic synthesis," Science 228(26 April 1985):408-418; J.B. Hendrickson, "Organic Synthesis in the Age of Computers," Angew. Chem. Intl. Ed. 29(1990):1286-1295;

such as neural networks,[627] should be investigated. In the nanomachinery design area, the NanoEngineer-1 software from Nanorex[628] enables the easy computer-aided design and modeling of atomically precise nanoparts up to 10^4-10^5 atoms in size using desktop computers, and template-filling[629] or genetic algorithms[630] could also be used to design nanoparts, using

---

W.L. Jorgensen, E.R. Laird, A.J. Gushurst, J.M. Fleischer, S.A. Gothe, H.E. Helson, G.D. Paderes, S. Sinclair, "CAMEO: A Program for the Logical Prediction of the Products of Organic Reactions," Pure Appl. Chem. 62(1990):1921-1932, http://www.iupac.org/publications/pac/1990/pdf/6210x1921.pdf; P.N. Judson, "Industrial and Academic Researchers Open Second Decade of Collaboration on LHASA Program," Chemical Design Automation News 5(1990):6-7; P.P. Mager, "Computer-assisted series design in chemical synthesis of bioactive compounds," Med. Res. Rev. 11(July 1991):375-402; L. Matyska, J. Koca, "MAPOS: a computer program for organic synthesis design based on synthon model of organic chemistry," J. Chem. Inf. Comput. Sci. 31(August 1991):380-386; J.B. Hendrickson, "Descriptions of Reactions: their logic and applications," Rec. Trav. Chim. Pays-Bas 111(1992):323-334; A.P. Johnson, C. Marshall, P.N. Judson, "Starting Material Oriented Retrosynthetic Analysis in the LHASA Program," J. Chem. Inf. Comput. Sci. 32(1992):411-417; J.B. Hendrickson, "Systematic Synthesis design: The SynGen program," in: Working Notes of the AAAI Spring Symposium on Systematic Methods of Scientific Discovery, AAAI Press, Stanford CA, 1995, pp. 13-17, homepage http://squirrel.bio.brandeis.edu/faculty/hendrickson.html; R. Fick, "Konzepte zur Syntheseplanung: Strukturelle Ähnlichkeit und strategische Bindungen," Ph.D. Thesis, 25 June 1996, http://www2.chemie.uni-erlangen.de/services/dissonline/data/dissertation/Ralf_Fick/html/Titel.doc4.html; M.G. Bures, Y.C. Martin, "Computational methods in molecular diversity and combinatorial chemistry," Curr. Opin. Chem. Biol. 2(June 1998):376-380; S.L. Schreiber, "Target-oriented and diversity-oriented organic synthesis in drug discovery," Science 287(17 March 2000):1964-1969; J.B. Hendrickson, "The SynGen program for organic synthesis design," 21 May 2001, http://syngen2.chem.brandeis.edu/syngen.html; A. Bartolozzi, P.H. Seeberger, "New approaches to the chemical synthesis of bioactive oligosaccharides," Curr. Opin. Struct. Biol. 11(October 2001):587-592; M.D. Burke, S.L. Schreiber, "A planning strategy for diversity-oriented synthesis," Angew. Chem. Int. Ed. Engl. 43(January 2004):46-58; S. Hanessian, "Man, machine and visual imagery in strategic synthesis planning: computer-perceived precursors for drug candidates," Curr. Opin. Drug Discov. Devel. 8(November 2005):798-819; C. Portal, M. Bradley, "Approaches to high throughput physical organic chemistry," Org. Biomol. Chem. 5(21 February 2007):587-592; R.M. Wilson, S.J. Danishefsky, "Pattern recognition in retrosynthetic analysis: snapshots in total synthesis," J. Org. Chem. 72(8 June 2007):4293-4305; John Figueras, "SynTree v3.0: A Program for Exploring Organic Synthesis," Trinity Software, accessed April 2008, http://www.trinitysoftware.com/orgchem5/syntree7.html.

[627] P.M. Agrawal, A.N.A. Samadh, L.M. Raff, M.T. Hagan, S.T. Bukkapatnam, R. Komanduri, "Prediction of molecular-dynamics simulation results using feedforward neural networks: Reaction of a C_2 dimer with an activated diamond (100) surface," J. Chem. Phys. 123(2005):1-11. E. Tafeit, W. Estelberger, R. Horejsi, R. Moeller, K. Oettl, K. Vrecko, G. Reibnegger, "Neural networks as a tool for compact representation of ab initio molecular potential energy surfaces," J. Mol. Graphics 14(1996):12-18; H. Gassner, M. Probst, A. Lauenstein, K. Hermansson, "Representation of intermolecular potential functions by neural networks," J. Phys. Chem. A 102(1998):4596-4605; S. Hobday, R. Smith, J. Belbruno, "Applications of genetic algorithms and neural networks to interatomic potentials," Nuclear Instruments and Methods in Physics Research, Section B: Beam Interactions with Materials and Atoms 153(1999):247-263; S. Lorenz, A. Groay, M. Scheffler, "Representing high-dimensional potential-energy surfaces for reactions at surfaces by neural networks," Chem. Phys. Lett. 395(2004):210-215.

[628] http://www.nanoengineer-1.com; accessed January 2008.

[629] Markus Krummenacker, "Cavity Stuffer," 1993; see at: http://www.ai.sri.com/~kr/nano/cavstuf/cavstuf.html.

molecular mechanics – but higher-level ab DFT simulations are to be preferred. Haptic interfaces could allow hands-on design of molecular structures, such as the high performance haptic controller and virtual reality interface at the California Nanotechnology Institute or the Posey interface (Figure I-13A) created at Carnegie Mellon for desktop computing,[631] and visualization could be greatly improved using high-performance systems such as the Hyperwall (Figure I-13B) at NASA/Ames[632] and related systems developed by the Collaboratory for Advanced Computing and Simulations (CACS) at the University of Southern California[633] for visualization of billion-atom systems.[634] Widely-available systems such as VMD readily visualize structures containing millions of atoms (but this apparently requires 4-8 GB or RAM). In the experimental area, the Nt_STM software from Nanotimes simulates scanning probe experiments or images to help "authenticate or forecast SPM results for surface treatments, molecule adsorptions, atom deposits, single molecule electron transport, molecular circuit modeling, or molecular electronics".[635]

---

[630] Al Globus, Madhu Menon, Deepak Srivastava, "JavaGenes: Evolving Molecular Force Field Parameters with Genetic Algorithm," Computer Modeling in Engineering and Science 3(2002):557-574; T. McKendree, R.A. Freitas Jr., A. Globus, M. Levit, C. Sherrill, M. Li, R.C. Merkle, "Challenges of Molecular Nanotechnology for Space Exploration," AIAA-2005-6814, AIAA Space 2005 Conference, Long Beach, CA, 30-31 August 2005, http://www.rfreitas.com/Nano/McK68141.pdf. Jordan B. Pollack, "Dynamical & Evolutionary Machine Organization," Department of Computer Science, Volen National Center for Complex Systems, Brandeis University, accessed April 2008, http://www.demo.cs.brandeis.edu/; see also "Automated Modular Design" and "Computer Evolution of Buildable Objects" at http://www.demo.cs.brandeis.edu/pr/robotics.html.

[631] Mason Inman, "Smart 'Lego' conjures up virtual 3D twin," NewScientist.com, 31 January 2008; http://technology.newscientist.com/article/dn13261-smart-lego-conjures-up-virtual-3d-twin.html.

[632] http://www.nas.nasa.gov/Groups/VisTech/hyperwall/.
[633] http://cacs.usc.edu/.

[634] Ashish Sharma, Xinlian Liu, Paul Miller, Aiichiro Nakano, Rajiv K. Kalia, Priya Vashishta, Wei Zhao, Timothy J. Campbell, Andy Haas, "Immersive and Interactive Exploration of Billion-Atom Systems," IEEE Virtual Reality Conference 2002 (VR 2002), Proc. IEEE Virtual Reality 2002, IEEE CS Press, 2002, pp. 217-223.

[635] http://www.nanotimes-corp.com; accessed January 2008.

Figure I-13. (A) <u>Top:</u> Posey[636] construction kit for PCs can sense its position and makes a 3D virtual double, with physical additions or adjustments immediately reproduced on-screen (left image); can be used to build molecular representations (right image). (B) <u>Middle:</u> NASA/Ames Research Center 128-node cluster Hyperwall[637] is a unique high-performance visualization tool that can display multiple independent, but related, images and provides useful means for composing and controlling these image sets. (C) <u>Bottom:</u> The NanoManipulator[638] couples the microscope to a virtual-reality interface that gives the scientist virtual telepresence on the surface, scaled by a factor of about a million to one.

[636] Mason Inman, "Smart 'Lego' conjures up virtual 3D twin," NewScientist.com, 31 January 2008; http://technology.newscientist.com/article/dn13261-smart-lego-conjures-up-virtual-3d-twin.html.

[637] http://www.nas.nasa.gov/Groups/VisTech/hyperwall/.

[638] Center for Computer Integrated Systems for Microscopy and Manipulation; http://www.cs.unc.edu/Research/nano/cismm/nm/ and http://www.nanomanipulator.org.

AFMs can also be operated using a visual-haptic interfaces[639] such as the nanoManipulator (Figure I-13C) developed at the University of North Carolina at Chapel Hill[640] and other related haptic-controlled systems for real-time nanoscale manipulation.[641] New types of software needed for massively parallel computing are being developed at the Pervasive Parallelism Lab.[642]

(B) Need to conduct studies and analysis to elucidate formal design rules for engineering nanoparts, nanodevices, and nanosystems. Need to specify metrics for measuring progress and value – e.g., cost per kilogram to fabricate product; reliability metrics; standard tooltip design, development and testing protocols (i.e., design rules for tooltips); extension of design rules to nanoparts and nanodevices; error rate metrics for manufacturing systems; and metrics to measure and compare the energy usage and the time required to fabricate a nanopart.

(C) Need a study of tooltip and handle mechanisms subjected to high-speed motion. The dynamic response of such mechanisms is critical to their performance during nanomanipulation because their frequency response determines the fastest rate at which the nanomanipulator can move without suffering resonant vibrations.

3.2.3 Task I-2: Design, Simulate and Test Automated Reaction Sequence Control Software

Task I-2 is to develop fabrication procedures and tooltip control software to enable the DMS fabrication process to be automated. The software must integrate physical models of the fabrication surfaces and mechanosynthetic tooltips with realistic experimental operating parameters to permit accurate simulation of a proposed process, then must be able to drive the

---

[639] A. Ferreira, C. Mavroidis, "Virtual reality and haptics for nanorobotics," Robotics & IEEE Automation Magazine 13(September 2006):78-92. See also http://www.coe.neu.edu/Research/robots/papers/Tcn_40.pdf and http://www.coe.neu.edu/Research/robots/papers/ROBIO05_1.pdf.

[640] Center for Computer Integrated Systems for Microscopy and Manipulation; http://www.cs.unc.edu/Research/nano/cismm/nm/ and http://www.nanomanipulator.org.

[641] R.M. Taylor, M. Falvo, "Pearls Found on the Way to the Ideal Interface for Scanned-probe Microscopes," IEEE Visualization Conference, 1997; S. Horiguchi et al., "Virtual Reality User Interface for Teleoperated Nanometer Scale Object Manipulation," Proceedings of the 7th International IEEE Workshop on Robot and Human Communication," ROMAN'98, Takamatsu, Japan, 1998, pp. 142-147; A. Nakano et al., IEEE Comput. Sci. Eng. 3(2001):56; Aydin Varol, Ihsan Gunev, Cagatay Basdogan, "A Virtual Reality Toolkit for Path Planning and Manipulation at Nano-scale," Proceedings of the IEEE Conference on Virtual Reality, IEEE Computer Society, Washington DC, 2006, p. 114, also in HAPTICS: Proceedings of the Symposium on Haptic Interfaces for Virtual Environment and Teleoperator Systems (HAPTICS'06), 2006; Ning Xi, Guangyong Li, Jiangbo Zhang, "Nano Robotic Manipulation and Assembly," IARP'06, 2006, http://iarp06.robot.jussieu.fr/Papers/Xi/Nano-Robotics-AFM_Ning_Xi.pdf.

[642] "Race Is on to Advance Software for Chips," New York Times, 30 April 2008; http://www.kurzweilai.net/email/newsRedirect.html?newsID=8571&m=40924.

tooltips and other positioning devices through all necessary motions and activities necessary to fabricate a target product object. Task I-2 is expected to continue throughout the balance of Phase I and Phase II, as new systems with new capabilities are fielded and also need to be automated.

3.2.3.1 NIST Autonomous Atom Assembler

Perhaps the best-known and earliest example of such a system is the Autonomous Atom Assembler (AAA) project[643] sponsored by the National Institute of Standards and Technology (NIST) and the Office of Naval Research (ONR). Until the AAA, atomic manipulation had been performed manually (or with rudimentary computer assistance), with the experimentalist essentially moving the scanning probe tip by hand through a sequence of steps. For example, in 1989 Eigler and Schweizer[644] at IBM Almaden used an STM to position 35 individual xenon atoms on a nickel surface to spell out the corporate logo "IBM" (Figure I-12). To accomplish this, a bias voltage was applied to weaken the adsorption of each atom to its nickel substrate, then each atom was dragged, one by one, to the desired locations at a speed of ~0.4 nm/sec to build a meaningful pattern.[645] It took 22 hours to make the entire logo, or ~38 min/atom. The experiment had to be carried out at 4 K (i.e., liquid helium temperatures) because the arrangement would have been unstable at room temperature.

As the number of atoms involved in an assembly process grows, the time consumption becomes prohibitive unless the process can be automated. The NIST AAA was intended as a first step toward accomplishing this. The AAA is described[646] as "an instrument capable of assembling a desired nanostructure from an unknown random collection of atoms without human intervention." The AAA instrument is based on a low-temperature STM system with various hardware and software extensions. "In operation, a dilute coverage of adsorbate atoms is deposited on a clean, flat substrate. The AAA then instructs the STM to image the random adsorbate pattern, identifies the position of each adsorbate atom relative to the substrate lattice, and plans a series of moves to place the available atoms at positions specified in a previously entered diagram. The plan minimizes construction time, follows a set of extensible rules, and allows for error correction. The AAA then instructs the STM to execute the plan and, upon completion, provide an image of the final assembled nanostructure. In our initial trials, Co atoms were deposited at sub-monolayer coverage on a Cu(111) at 7K in UHV and subsequent STM measurements were performed at a 4.3 K sample temperature," producing the image shown in Figure I-14. A major limitation of the AAA was that it could only push around non-covalently bonded atoms on a cold surface. In part,

---

[643] "Autonomous Atom Assembly," NIST, July 2004; http://cnst.nist.gov/epg/Projects/STM/aaa_proj.html.

[644] D.M. Eigler, E.K. Schweizer, "Positioning Single Atoms with a Scanning Tunnelling Microscope," Nature 344(5 April 1990):524-526; http://www.nature.com/nature/journal/v344/n6266/abs/344524a0.html (abstract).

[645] Malcolm Ritter, "World's smallest moving job shifts just one atom at a time," Sacramento Bee, Thursday, 5 April 1990, p. A8..

[646] "Autonomous Atom Assembly," NIST, July 2004; http://cnst.nist.gov/epg/Projects/STM/aaa_proj.html.

this limitation was due to the lack of experimental success (until recently)[647] of demonstrated covalent bond-making and bond-breaking via mechanosynthesis, and in part due to the lack of experimental[648] or theoretical[649] procedures for performing even short sequences of single-molecule covalent bonding operations that could in principle be capable of being automated.

Figure I-14. NIST logo with cobalt atoms on a copper surface produced in the NIST Nanoscale Physics Facility using the Autonomous Atom Assembler.[650] "The ripples in the background are due to electrons in the fluid-like layer at the copper surface bouncing off the cobalt atoms, much like the patterns produced when pebbles are dropped in a pond."

---

[647] Noriaki Oyabu, Oscar Custance, Insook Yi, Yasuhiro Sugawara, Seizo Morita, "Mechanical vertical manipulation of selected single atoms by soft nanoindentation using near contact atomic force microscopy," Phys. Rev. Lett. 90(2 May 2003):176102; http://link.aps.org/abstract/PRL/v90/e176102 (Abstract) http://focus.aps.org/story/v11/st19 (APS story).

[648] Wilson Ho, Hyojune Lee, "Single bond formation and characterization with a scanning tunneling microscope," Science 286(26 November 1999):1719-1722; http://www.physics.uci.edu/~wilsonho/stm-iets.html. Saw-Wai Hla, Ludwig Bartels, Gerhard Meyer, Karl-Heinz Rieder, "Inducing All Steps of a Chemical Reaction with the Scanning Tunneling Microscope Tip: Towards Single Molecule Engineering," Phys. Rev. Lett. 85(September 2000):2777-2780; http://prola.aps.org/abstract/PRL/v85/i13/p2777_1 (abstract), http://www.phy.ohiou.edu/~hla/HLA2000-2.pdf (paper).

[649] Robert A. Freitas Jr., Ralph C. Merkle, "A Minimal Toolset for Positional Diamond Mechanosynthesis," J. Comput. Theor. Nanosci. 5(May 2008):760-861.

[650] "Autonomous Atom Assembly," NIST, July 2004; http://cnst.nist.gov/epg/Projects/STM/aaa_proj.html.

3.2.3.2 EPSRC Matter Compiler Project

Most recently, a formal project has begun in the U.K. to extend automated molecular-scale fabrication to sequences of covalent bonding and debonding operations. This effort grew out of an interactive workshop[651] called "Software Control of Matter" directed by Richard Jones that involved 20 scientists from various disciplines who initially met for one week to think through new and innovative approaches to making nanomaterials and devices. The workshop was part of the Ideas Factory program funded by the UK's government funding agency for engineering and the physical sciences (EPSRC: Engineering and Physical Sciences Research Council) that provided ~$3M to fund the most successful ideas. The group was given the following charge: "Can we design and construct a device or scheme that can arrange atoms or molecules according to an arbitrary, user-defined blueprint? This is at the heart of the idea of the software control of matter – the creation, perhaps, of a "matter compiler" which will interpret software instructions to output a macroscopic product in which every atom is precisely placed."

One team proposed and received funding for the "Matter Compiler" project, which Jones describes[652] as follows: "An ambition to assemble molecules and materials under atomically precise control demands a big leap forward in control engineering and computer science. Is it possible to anticipate the properties and needs of a 'nano-assembler'? If so, there is a need for a high level instruction language and a computer compiler that translates commands in this language into instructions for the 'nano-assembler'. This development will require a breakthrough in understanding of chemical synthesis that must embrace the radically new 'pick and place' assembly method which is now possible in scanning probe microscopy (SPM). The Matter Compiler project is thus both an exercise in foresight, to anticipate developments in this area, and a prototype implementation for the engineering control and computer science aspects of directed molecular assembly. It has as inputs data from SPM experiments of collaborators, energy landscapes for 'pick and place' reactions and the vast knowledge base of classical synthetic chemistry, including methodologies such as retrosynthesis. This will be supplemented by reaction schemes for 'pick and place' reactions deduced from first principles quantum chemistry calculations and the technology of object oriented databases and inference engines." The Matter Compiler team is led by Dr Harris Makatsoris (Engineering, Brunel University) and comprises Professor Malcolm Heggie (Chemistry, University of Sussex), Dr Nick Holliman (Computer Science, University of Durham), Dr Helen Wright (Computer Science, University of Hull), Professor Jeremy Ramsden (Advanced Materials, Cranfield University), and Professor Philip Moriarty (Physics, University of Nottingham).

Directly supporting Nanofactory Collaboration objectives, the focus of the Matter Compiler project is on hydrogen-passivated diamond. While we expect to be able to perform DMS operations without the need for sensory feedback (Section 3.2.1.6) and without the possibility of "repairing" an erroneous placement operation, the Matter Compiler project makes the more

---

[651] "EPSRC Sandpit - Software Control Of Matter At The Atomic Or Molecular Scale", 22 December 2006; http://ideasfactory.wordpress.com/2006/12/22/.

[652] "The Matter Compiler," 17 January 2007; http://ideasfactory.wordpress.com/2007/01/17/the-matter-compiler/.

conservative assumption that workpiece defects must be "routinely and reliably classified," after which the defects must be repaired, and that we will therefore need "protocols and a planning algorithm for determining how to repair the defects and guide the tip to carry out these repairs" using site-specific chemistry "to reliably repair defects."

In their proposal[653] for a subsequent round of EPSRC funding in late 2007, the Matter Compiler project team described their work as follows: "This project focuses on the development of novel software and a set of advanced protocols for automated matter compilation. Of key significance, we will validate those protocols by ensuring strong feedback between the simulation/computational aspects of the project and a prototypical atom manipulation experiment. At the heart of the project is the development of an integrated control system (including autonomous characterisation and error-checking routines) which is capable of instructing the tip of a scanning probe microscope (SPM) to synthesize an arbitrary nanostructure comprising pre-defined arrangements of atoms/vacancies on a hydrogen-passivated diamond surface. The proposed project builds on the original and (and ongoing) Matter Compiler project (EP/F009801/1).

"The manipulation of single atoms and molecules with atomic precision is a powerful emerging tool in nanoscience and condensed matter physics and will enable future breakthrough applications in MEMS/NEMS and device fabrication. However, if SPM-based nanofabrication is to fulfill its potential, it is essential that tip structure and dynamics are controlled precisely and reproducibly. It is the introduction of high level control and characterisation protocols for the probe – in addition to, as is conventionally the case in SPM, the sample surface – which represents an important experimental target of this application. As described in more detail below, tip-based nanofabrication is currently attracting substantial support from funding agencies in the U.S.; our proposal therefore represents a timely mechanism for the UK to build on its strengths in atomic/molecular manipulation and to establish a world-leading position in this area.

"**The concept of computer-directed molecular level chemistry was first described by Drexler,[654] but, despite being demonstrably valid for a number of well-chosen adsorbate-substrate systems, has been heavily criticized,[655] not least because of the absence of essential technical details.** Drexler focuses on 'diamondoid' structures throughout *Nanosystems*.[656] At the core of his approach lies the idea that hydrogen is abstracted from passivated surfaces to form

---

[653] Malcolm Heggie, Nick Holliman, Harris Makatsoris, Philip Moriarty, Jeremy Ramsden, Helen Wright, "The Matter Compiler++: Towards Automated 'Machine-Phase' Synthesis," Joint Reference G593402, December 2007.

[654] K. Eric Drexler, "Molecular engineering: an approach to the development of general capabilities for molecular manipulation," Proc. Natl. Acad. Sci. (USA) 78(September 1981):5275-5278.

[655] R.A.L. Jones, Soft Machines, Oxford University Press, 2004. See also the Letters section of Physics World, Oct. 2004 and the following discussion: http://www.softmachines.org/wordpress/?p=60. R.E. Smalley, "Nanotechnology," Chemical and Engineering News 81(2003):37-42. P. Moriarty, http://www.softmachines.org/wordpress/?p=70.

[656] K. Eric Drexler, Nanosystems: Molecular Machinery, Manufacturing, and Computation, John Wiley & Sons, New York, 1992; http://www.zyvex.com/nanotech/nanosystems.html.

radical centres, or dangling bonds, using an appropriately functionalised 'molecular tool' driven by mechanical forces. Although Drexler's work lacks detail, Jones[657] and others[658] have pointed out that it is not easy to identify fundamental flaws in the concept, although there are evident practical challenges associated with the development of macroscopic products from a sequence of single atom placements, the ultimate outcome of mechanosynthesis. **Peer-reviewed papers involving sophisticated DFT calculations of mechanosynthetic reactions have been published {by Freitas and Merkle.[659]** Furthermore, two examples of atomic extraction involving purely mechanical forces have been carried out to date.[660] Both were carried out by the same group, Oyabu et al. at Osaka University, although in both experiments the tip was not specifically functionalised to drive the extraction chemistry in a manner described in

---

[657] R.A.L. Jones, Soft Machines, Oxford University Press, 2004. See also the Letters section of Physics World, Oct. 2004 and the following discussion: http://www.softmachines.org/wordpress/?p=60.

[658] R.E. Smalley, "Nanotechnology," Chemical and Engineering News 81(2003):37-42. P. Moriarty, http://www.softmachines.org/wordpress/?p=70. R.A.L. Jones, http://www.softmachines.org/wordpress/?p=80.

[659] Jingping Peng, Robert A. Freitas Jr., Ralph C. Merkle, "Theoretical Analysis of Diamond Mechanosynthesis. Part I. Stability of C_2 Mediated Growth of Nanocrystalline Diamond C(110) Surface," J. Comput. Theor. Nanosci. 1(March 2004):62-70; http://www.MolecularAssembler.com/JCTNPengMar04.pdf. Jingping Peng, Robert A. Freitas Jr., Ralph C. Merkle, James R. Von Ehr, John N. Randall, George D. Skidmore, "Theoretical Analysis of Diamond Mechanosynthesis. Part III. Positional C_2 Deposition on Diamond C(110) Surface using Si/Ge/Sn-based Dimer Placement Tools," J. Comput. Theor. Nanosci. 3(February 2006):28-41; http://www.MolecularAssembler.com/Papers/JCTNPengFeb06.pdf. Berhane Temelso, C. David Sherrill, Ralph C. Merkle, Robert A. Freitas Jr., "High-level *Ab Initio* Studies of Hydrogen Abstraction from Prototype Hydrocarbon Systems," J. Phys. Chem. A 110(28 September 2006):11160-11173; http://pubs.acs.org/cgi-bin/abstract.cgi/jpcafh/2006/110/i38/abs/jp061821e.html (abstract), http://www.MolecularAssembler.com/Papers/TemelsoHAbst.pdf (paper). Berhane Temelso, C. David Sherrill, Ralph C. Merkle, Robert A. Freitas Jr., "*Ab Initio* Thermochemistry of the Hydrogenation of Hydrocarbon Radicals Using Silicon, Germanium, Tin and Lead Substituted Methane and Isobutane," J. Phys. Chem. A 111(15 August 2007):8677-8688. http://pubs.acs.org/cgi-bin/abstract.cgi/jpcafh/asap/abs/jp071797k.html (abstract), http://www.MolecularAssembler.com/Papers/TemelsoHDon.pdf (paper).

[660] Noriaki Oyabu, Oscar Custance, Insook Yi, Yasuhiro Sugawara, Seizo Morita, "Mechanical vertical manipulation of selected single atoms by soft nanoindentation using near contact atomic force microscopy," Phys. Rev. Lett. 90(2 May 2003):176102; http://link.aps.org/abstract/PRL/v90/e176102 (Abstract) http://focus.aps.org/story/v11/st19 (APS story). N. Oyabu, O. Custance, M. Abe, S. Moritabe, "Mechanical Vertical Manipulation of Single Atoms on the Ge(111)-c(2x8) Surface by Noncontact Atomic Force Microscopy," Abstracts of Seventh International Conference on non-contact Atomic Force Microscopy, Seattle, Washington, USA, 12-15 September, 2004, p.34; http://www.engr.washington.edu/epp/afm/abstracts/15Oyabu2.pdf. Noriaki Oyabu, Pablo Pou, Yoshiaki Sugimoto, Pavel Jelinek, Masayuki Abe, Seizo Morita, Rubén Pérez, Óscar Custance, "Single Atomic Contact Adhesion and Dissipation in Dynamic Force Microscopy," Phys. Rev. Lett. 96(15 March 2006):106101; http://link.aps.org/doi/10.1103/PhysRevLett.96.106101 (abstract), http://netserver-alt.aip.org/epaps/phys_rev_lett/E-PRLTAO-96-034611/AdditionalInformation.pdf (paper).

Nanosystems.[661] It is particularly important to note, however, that the U.S. National Academy of Sciences, in a recent review of the National Nanotechnology Initiative, suggests[662] that there is scope for "defining and focusing on basic experimental steps that are critical to advancing long-term goals" and for funding "experimental demonstrations that link to abstract models and guide long-term vision". Moreover, the NAS report has recently been followed by a call from DARPA for proposals in the area of tip-based nanofabrication.[663]

"**Aim and Objectives.** The project will **demonstrate for the first time the deterministic automated synthesis of matter at the atomic scale from a predefined blueprint**. This entails the development of the Matter Compiler system into a truly integrated controller for computer directed nanofabrication and its experimental validation. This will be achieved by:

1. Designing and implementing an advanced process controller. This entails novel feedback strategies, algorithms and protocols for automated detection, characterisation and repair of errors that can occur in a scanning probe manipulation. Such defects can occur at the work surface, in the product(s), and, importantly, at the tip. In addition it includes a compiler of instructions to drive the actual process by converting the steps predicted by the Matter Compiler for synthesis, manipulation or error correction into motion control instructions for a standard SPM to execute. These will be captured and implemented in a software component to drive automation.
2. Modeling and simulation (using DFT) to drive matter compilation predictions for the systems under consideration, in particular for hydrogen passivated diamond surfaces.
3. Producing a novel image processing/computer vision system that determines the current state of the assembly process and providing input to the control system on the location of defects.
4. Developing a visualization interface providing to the operator insight into the status of the nanoassembly process, allowing operator intervention in the event that they identify errors.
5. Integrating all components into one coherent prototype system.
6. Validating the system experimentally by performing SPM tip driven reactions on hydrogenated diamond surfaces.

"**The Integrated System.** The second phase of the Matter Compiler, MC++, and explores the requirements of automation – replacing human vision, understanding and motor control with computer vision and robotic control. Human supervision is achieved by an advanced visual interface with the possibility of tactile feedback. This extremely demanding agenda must be tightly coupled to experiment and the experiment must be operational from the start. We have

---

[661] K. Eric Drexler, Nanosystems: Molecular Machinery, Manufacturing, and Computation, John Wiley & Sons, New York, 1992; http://www.zyvex.com/nanotech/nanosystems.html.

[662] Committee to Review the National Nanotechnology Initiative, National Materials Advisory Board (NMAB), National Research Council (NRC) (2006) A Matter of Size: Triennial Review of the National Nanotechnology Initiative. The National Academies Press, Washington DC; http://www.nap.edu/catalog/11752.html#toc.

[663] T. Kenny, "Tip-Based Nanofabrication (TBN)," Defense Advanced Research Projects Agency (DARPA)/Microsystems Technology Office (MTO), Broad Agency Announcement BAA 07-59, July 2007; http://www.fbo.gov/spg/ODA/DARPA/CMO/BAA07-59/listing.html.

thus geared the computational work to the SPM manipulation of atoms on a diamond surface and included a small amount of resourcing for this experiment. This approach supports and extends the Matter Compiler project and requires the execution of the following tasks:

1. Motion control to achieve assembly.
2. Image analysis (inferring the atomic geography).
3. Solid representation of this analysis.
4. Image updating from tip information during motor operations.

"**Experimental validation of the system.** The objectives of the MC++ project lead us to focus on the simplest systems and operations – ones which could prove useful in themselves and as precursors to more complex, molecular assembly operations. We fix the terrain as a diamond surface (C(100) for example) and limit ourselves in the first instance to H atom addition and removal, and surface atom dimerization. In particular the following "proof of principle" experiment will be pursued which focuses on the tip driven abstraction of a row of hydrogen from a hydrogenated diamond surface. The "path planning" and positioning of the tip on specific locations of the surface will be predicted by the system and these will then be converted into detailed control instructions.

1. Initially the Translator executes a DFT calculation on the dimer row structure to calculate electronic density of states, a prediction of the electronic structure, estimates of energy barriers, transition states and the overall potential energy surface. The calculation will be used to design the optimal pathway for achieving the specified structure.

2. A hydrogen-passivated diamond surface is scanned with a UHV STM-AFM to ensure there are no defects in the work area (for example, 10 x 10 nm^2). This, in itself, is a process that raises significant challenges for automation. In particular *how are defects routinely and reliably classified? Once identified, how can the defects be repaired?* An image analysis and pattern recognition algorithm will be used for defect classification. In addition, protocols and a planning algorithm for determining how to repair the defects and guide the tip to carry out these repairs will also be explored in this project. Site-specific chemistry is required to reliably repair defects arising from missing hydrogen atoms (in the surface area representing the "work piece"). Although **a number of elegant strategies for purely force-driven hydrogen abstraction and donation using scanning probes have very recently been put forward by Freitas and Merkle**,[664] developing these on the [too-limited] timescale and budget of the MC++ project is not credible. We will therefore use well-established protocols for hydrogen abstraction and donation based on field-induced diffusion.[665]

3. Once a defect-free region has been identified/prepared, a hydrogen atom is abstracted.

4. A key question now arises: *how can it be made certain that the correct reaction has been carried out?* Automated defect-checking algorithms using spectroscopic techniques, as explained in the Methodology section below, will be explored for both STM and AFM, in addition to identifying the correct spectral signatures to consider. These will be integrated into

---

[664] Robert A. Freitas Jr., Ralph C. Merkle, "A Minimal Toolset for Positional Diamond Mechanosynthesis," J. Comput. Theor. Nanosci. 5(May 2008):760-861.

[665] D.H. Huang, Y. Yamamoto, "Physical mechanism of hydrogen deposition from a scanning tunneling microscopy tip," Appl. Phys. A 64(April 1997):R419-R422; C. Thirstrup, M. Sakurai, T. Nakayama, M. Aono, "Atomic scale modifications of hydrogen-terminated silicon 2 x 1 and 3 x 1 (001) surfaces by scanning tunneling microscope," Surf. Sci. 411(1998):203-214.

the matter compiler system. Furthermore, protocols to correct these errors will be developed. We will monitor both the conservative and non-conservative components of the force (via a qPlus sensor, see below) and the tunnel current as this process is carried out. A key element of the automation will be to ensure that the correct spectral signature has been obtained, indicating that the H abstraction event has occurred. This process is repeated automatically until the H abstraction event has successfully occurred.

5. Repeat from Step 2 moving along to the next (blueprint-defined) atomic site on the surface, and repeat to form the user-defined pattern."

As of early 2008, a dedicated 120 m^2 laboratory hosted Makatsoris' research team and a mini Grid for computational and prototyping work. The team had access to an AFM-STM instrument and larger computational resources as well as widely used DFT codes and molecular modeling software. Brunel University has complemented the Matter Compiler (MC) project with a funded PhD student from the DTA account working full time in this ongoing project. An Omicron low-temperature (4 K) UHV STM-AFM system in the Nottingham group's laboratories, equipped with tuning fork (qPlus) AFM capability, was to be used for the proof-of-principle MC experiment, with hydrogen-passivated diamond surfaces to be supplied via an existing collaboration between Moriarty and Pakes (La Trobe University, Melbourne); Pakes has extensive experience of the preparation and characterization of hydrogen-passivated diamond surfaces. Tunneling electron-induced hydrogen desorption will be used to create radical (dangling bond) centers and supplemented with probe-driven lateral atomic/molecular manipulation,[666] electric field-induced diffusion,[667] and tunnel current-induced reactions.[668] The expanded MC++ effort was scheduled to commence in May 2008.

3.2.4 Task I-3: Demonstrate Simple DMS Reaction Sequences Using Existing SPM

Task I-3 is to achieve an experimental laboratory demonstration of a few simple representative positionally-controlled diamondoid mechanosynthesis reactions. These experiments will use existing UHV SPM/AFM systems (e.g., Table I-1) with commercially available or experimentally realized tooltips (e.g., Table I-2). For Task I-3, tooltips may be changed out manually if necessary to avoid complicating the task. For simplicity and of relevance to later Tasks in Phase I, likely mechanosynthetic targets include: (1) the abstraction of individual hydrogen atoms from

---

[666] P. Moriarty, Y.-R. Ma, M.D. Upward, P.H. Beton, "Translation, rotation and removal of C60 on Si(100)-(2x1) using anisotropic molecular manipulation," Surf. Sci. 407(1998):27-35.

[667] Joseph A. Stroscio, D.M. Eigler, "Atomic and Molecular Manipulation with the Scanning Tunneling Microscope," Science 254(29 November 1991):1319-1326.

[668] Wilson Ho, Hyojune Lee, "Single bond formation and characterization with a scanning tunneling microscope," Science 286(26 November 1999):1719-1722; http://www.physics.uci.edu/~wilsonho/stm-iets.html. Saw-Wai Hla, Ludwig Bartels, Gerhard Meyer, Karl-Heinz Rieder, "Inducing All Steps of a Chemical Reaction with the Scanning Tunneling Microscope Tip: Towards Single Molecule Engineering," Phys. Rev. Lett. 85(September 2000):2777-2780; http://prola.aps.org/abstract/PRL/v85/i13/p2777_1 (abstract), http://www.phy.ohiou.edu/~hla/HLA2000-2.pdf (paper).

specific individual sites on a hydrogen-passivated diamond surface; (2) the donation of hydrogen atoms to specific individual radical sites that have been created on a previously hydrogen-passivated surface from which H atoms have been abstracted on a site-specific basis; (3) the donation of hydrogen atoms to specific individual radical sites that remain on a depassivated diamond surface, either before or after that surface has reconstructed (if it reconstructs); and (4) the placement of a positionally-controlled tip-bound carbon-containing reactive moiety (e.g., single-carbon payloads such as CH_2 or two-carbon payloads such as C_2H_4 or C_2) to specific individual radical sites on a diamond surface prepared as described in (2) or (3) above.

Due to the relatively poor positional repeatability of existing SPM systems and the availability of sub-nanometer tips that are only poorly characterized at the level of individual atoms, Task I-3 is expected to require a great deal of trial and error. Successful early experimental results are likely to be dearly won and only after numerous attempts because the process initially will be highly unreliable. Experiments will undoubtedly have to be performed at low temperature (at least 80 K, but probably 4 K) to achieve adequate stability and repeatability, using a single-tip system with only 3-DOF (degrees of freedom) positional control in Cartesian translational directions, resulting in an extremely primitive – but nonetheless seminal – mechanosynthetic fabrication capability.

Philip Moriarty, an internationally respected scanning probe experimentalist at the University of Nottingham (UK), has stepped forward with a specific suggestion for addressing Task I-3. Moriarty, also a Nanofactory Collaboration participant, has submitted a grant proposal[669] in which he starts by asking: "Can one realise a 'deterministic epitaxy' where each atom, rather than adsorbing from the gas phase and subsequently (randomly) diffusing to a reactive site, is placed in position via a deterministic, computer-controlled trajectory? Is the automated atom-by-atom assembly of three-dimensional nanoparticles (or, indeed, mesoscopic/microscopic structures) possible? More succinctly, what are the ultimate limits of scanning probe technology in assembling matter from its component atoms/molecules?" The purpose of his work would be "to develop single atom/molecule manipulation protocols capable of autonomous generation of atomically precise (and likely kinetically-hindered) two-dimensional and three-dimensional nanostructures." This will involve developing new techniques for mechanosynthesis, mechanoepitaxy, and tip engineering.

More specifically, Moriarty proposes to "focus on hydrogen-passivated diamond surfaces throughout and on achieving two key milestones: (i) the demonstration of computer-controlled epitaxy of a line of carbon dimers, five to ten units long, on an otherwise hydrogen-terminated C(100) surface; (ii) the synthesis of a three-dimensional, covalently-bonded diamond island on C(100). Our focus on H:C(100) surfaces is motivated in part by Freitas and Merkle's recent completion[670] of a lengthy and comprehensive density functional theory (DFT) study of a toolset for diamond mechanosynthesis (Figure 2-44). Importantly, the precise tip structures, and, moreover, the detailed reaction pathways required to drive the mechanochemistry have been considered in depth and subjected to high level DFT calculations (involving the B3LYP

---

[669] Philip Moriarty, "Digital Matter?: Towards Mechanised Mechanosynthesis," Leadership Fellowships 2008: Outline Application, December 2007, pp. 1-3; personal communication to R. Freitas.

[670] Robert A. Freitas Jr., Ralph C. Merkle, "A Minimal Toolset for Positional Diamond Mechanosynthesis," J. Comput. Theor. Nanosci. 5(May 2008):760-861.

functional with a 6-311+G(2d,p) basis set). For the first time, Freitas and Merkle explicitly specify all reaction steps and reaction pathologies for the system. The toolset employs three element types (C, Ge, and H) and requires inputs of four 'feedstock' molecules – CH_4 and C_2H_2 as carbon sources, Ge_2H_6 (digermane) as the Ge source (Ge is used to drive strain-mediated directional transfer of C atoms), and H_2 as a hydrogen source. A particularly exciting result of this study is the proposal of an experimentally viable route towards the generation of a set of *rechargeable* tools which can, amongst a variety of other processes, extract hydrogen from H:C(100), deposit C dimers, and donate hydrogen to an unpassivated diamond surface. In addition to mapping out the potential energy landscape associated with the mechanosynthetic reactions, Freitas and Merkle have also calculated the dominant vibrational frequencies associated with the tip tools they propose. This information will be of especial importance when attempting to experimentally verify the tip termination (via, for example, inelastic tunneling spectroscopy).

"Throughout the research programme the applicant will collaborate closely with Freitas et al. to ensure high level computational chemistry support for the experimental programme. Furthermore, a collaboration (initiated via the Software Control of Matter sandpit; Section 3.2.3.2) with Heggie (Sussex), an expert on modeling of diamond systems, will prove invaluable. A third, equally important, collaboration involves Pakes et al. at the University of La Trobe, experts in the generation and characterisation of hydrogen-passivated diamond surfaces. A recently funded Australian Research Council grant application (AU$370K) will bolster links between La Trobe and Nottingham.

"In the US, DARPA has very recently announced a call for proposals[671] in the area of tip-based nanofabrication with a particular focus on functionalised AFM cantilevers on tips. Similarly, a U.S. National Academies report[672] on site-specific chemistry highlighted the need to fund proof-of-principle studies of mechanosynthetic reactions. Moreover, a major project headed by J.A. Stroscio[673] at NIST has as its objective autonomous atomic-level assembly (AAA) (Section 3.2.3.1). The Fellowship project we propose moves far beyond the AAA strategy to merge, in a radical new technology, probe-driven chemistry, advanced atomic level tip characterisation, and the computerised synthesis of 3D structures."

Moriarty's project would run for approximately five years, occupying 62.5% of his allocated time and also requiring one full-time 5-year post-doctoral resident assistant, one full-time 4-year PhD student, and a dedicated commercially-available low-temperature (LHe, ~5 K) UHV STM-AFM

---

[671] T. Kenny, "Tip-Based Nanofabrication (TBN)," Defense Advanced Research Projects Agency (DARPA)/Microsystems Technology Office (MTO), Broad Agency Announcement BAA 07-59, July 2007; http://www.fbo.gov/spg/ODA/DARPA/CMO/BAA07-59/listing.html.

[672] Committee to Review the National Nanotechnology Initiative, National Materials Advisory Board (NMAB), National Research Council (NRC) (2006) A Matter of Size: Triennial Review of the National Nanotechnology Initiative. The National Academies Press, Washington DC; http://www.nap.edu/catalog/11752.html#toc.

[673] Joseph A. Stroscio, D.M. Eigler, "Atomic and Molecular Manipulation with the Scanning Tunneling Microscope," Science 254(29 November 1991):1319-1326.

system with tuning fork capability.[674] The work would include an attempt to fabricate the ethynyl-based hydrogen abstraction tool (which can also serve as a C_2 dimer placement tool)[675] in the manner proposed by Freitas and Merkle.[676]

3.2.5 Task I-4: Build 1-Tip 3-DOF Picopositioning SPM System to Demonstrate Simple DMS Reaction Sequences

Task I-4 is to design, develop, and demonstrate a high-precision UHV scanning probe picopositioning system, using piezo or electrostatic actuators and position sensing using interferometry and capacitive sensors, which can achieve 20-50 pm repeatable placement precision over 1-100 micron round trip excursions of the fixed SPM tip. The system is envisioned as a single-tip, 3-DOF (degrees of freedom) manipulator similar to the Molecular Measuring Machine (M^3) high-performance state-of-the-art metrology instrument[677] developed at NIST (National Institute of Standards and Technology). In private discussion,[678] John Kramar (Group Leader of the Nano-Scale Metrology Group in the Precision Engineering Division at NIST) has informally opined that the system required for the successful completion of Task I-4 might be buildable in the course of a dedicated 3-5 year development project, starting from the M^3 design or other comparable relevant metrology systems that are known to him, if sufficient funding is provided.

Once completed, the Task I-4 system can repeat the achievements of Task I-3, but now with much higher reliability and repeatability, possibly at a faster processing speed per reaction step, and probably at higher operating temperatures (e.g., 80 K). The Task I-4 system should be much more amenable to control automation (Section 3.2.3.2) because of the enhanced precision and repeatability of its movements. This system can also be used as a testbed to develop the more advanced manipulator systems that are envisioned for subsequent Tasks within Phase I. The ability to perform in-chamber tooltip changeouts is not required for Task I-4 and is deferred to Task I-5.

---

[674] Franz J. Giessibl, "Advances in atomic force microscopy," Rev. Mod. Phys. 75(July 2003):949-983. See also: F.J. Giessibl, "Atomic resolution on Si(111)-(7×7) by noncontact atomic force microscopy with a force sensor based on a quartz tuning fork," Appl. Phys. Lett. 76(2000):1470-1472.

[675] Robert A. Freitas Jr., Ralph C. Merkle, "A Minimal Toolset for Positional Diamond Mechanosynthesis," J. Comput. Theor. Nanosci. 5(May 2008):760-861.

[676] Robert A. Freitas Jr., Ralph C. Merkle, "A Minimal Toolset for Positional Diamond Mechanosynthesis," J. Comput. Theor. Nanosci. 5(May 2008):760-861.

[677] John A. Kramar, "Nanometre resolution metrology with the Molecular Measuring Machine," Meas. Sci. Technol. 16(2005):2121-2128.

[678] John A. Kramar; personal communication to Robert A. Freitas Jr., 10 October 2007.

Some generic single-tip UHV picopositioner design and construction challenges include:

(A) The most urgently needed new experimental capability is the development of a low-noise SPM positioning system with highly repeatable sub-Angstrom (0.2-0.5 Å) positioning accuracy over 1-100 micron round-trip paths, coupled with a sub-nanometer precision coordinate system spanning at least tens of microns.

(B) Need a positioning system that minimizes hysteresis and backlash, or which at minimum performs in a sufficiently repeatable manner as to guarantee tooltip placement accuracy to 0.2-0.5 Å. Are expensive interferometer-feedback based systems (Section 3.2.1.3) absolutely required, or might improved but less-expensive encoder multiplier systems[679] be usable instead?

(C) Ultraclean UHV environments having minimal contamination must be provided. A typical UHV vacuum of ~10^{-9} torr would give the experimenter, on average, ~4000 seconds before poisoning of an exposed radical site might occur due to an impingement of stray contaminant atoms, ions, and molecules (Section 3.2.1.7). The ability to work inside small volumes would help. For example, a vacuum of 1 nanotorr inside an enclosed 10,000 cubic micron box contains, on average, far less than one contaminant molecule – usually making, in effect, a perfect vacuum.

(D) Computer control of trajectories, rotations, and positioning must be studied, with the ultimate objective of fully automating the DMS process so that nanostructures may be fabricated according to a particular blueprint (Section 3.2.3.2).

Other challenges that are more specific to single-tip picopositioning systems for DMS include:

(E) Need new methods of positional registration and alignment of the tooltip relative to the target reaction site on the workpiece. Even an extremely small mismatch in the alignment of the tooltip can result in unwanted bond formation. In the case of a multitool tip, each tool must be capable of precision alignment and positioning over the proper workpiece reactive site. Traditional methods include alignment marks on the sample stage as well as the sample.

(F) Need repeatable positional registration and alignment of a new or returning repositioned tooltip, relative to a workpiece site previously visited by a tooltip, with sufficient accuracy to enable low-error DMS.

(G) In subsequent Phase I Tasks, we may need repeatable tooltip rotation and tilt of a new or returning tooltip, relative to a workpiece reactive site, with sufficient accuracy to enable low-error DMS. Small changes in tooltip tilt are predicted to alter reaction exoergicity, reaction barriers, and reaction reliability.

(H) Need to devise methods for positional registration of proximated multiple tooltips. How does one locate one tool, relative to another, to carry out a mechanosynthetic step requiring

---

[679] ACS Motion Control, "Nanometer Positioning & High Velocity," http://www.acs-tech80.com/Solutions/AdvancedFeatures/Nanometerpositioninghighvelocity/tabid/226/Default.aspx.

the coordinated action of two or more tooltips? This issue applies both to relative tooltip positions and (in future Phase I Tasks) relative tooltip rotations.

(I) Experimental capability for multi-tip tooltip changeout will be required for DMS demonstration system in subsequent Phase I Tasks. The Task I-4 system should be designed to anticipate the need for tooltip changeout and to accommodate the geometric requirements of an in-chamber toolrack as will be added in Task I-5 (Section 3.2.6).

3.2.6 Task I-5: Verify Need for 4 Tips and 5 DOFs

Task I-5 is to examine the computational simulations of Reaction Sequences undertaken in Task I-1 as reported in Freitas and Merkle,[680] concentrating on those reactions that appear to require one or more rotational degrees of freedom (DOF), with the objective of definitively determining the minimum number of independent manipulators and rotational DOFs that are required to successfully perform all critical reactions needed to build diamond and related hydrocarbon structures. If possible, this study should be extended to include any additional Reaction Sequences and DMS tooltips needed to fabricate non-hydrocarbon diamondoid structures.

Based on the published initial 65 Reaction Sequences,[681] the most conservative analysis is that 4 manipulators and 5 DOF (including two rotational DOF) are minimally required to execute all necessary reactions. However, if these reactions turn out to be sufficiently exoergic and reliable even in the absence of the additional rotational DOFs, then it might be possible to skip one or both of Tasks I-7 and I-8, thus saving the program time, money, and other resources. Additionally, it may be possible to avoid the need for ultrastable tip rotations to be performed in the immediate vicinity of the workpiece, in some cases allowing necessary tip rotations to be performed at macroscale distances from the workpiece in the absence of tip-workpiece bonds during the rotations.

The possibility of reducing the number of manipulators and DOFs by altering the existing Reaction Sequences should also be explored in Task I-5.

3.2.7 Task I-6: Add In-Chamber Toolrack to Enable Endogenous Tooltip Changeout

Task I-6 is to add a toolrack inside the UHV workspace chamber to hold at least 4, and possibly up to 20, detachable scanning probe tips. The manipulator system developed in Task I-4 should be modified so that the manipulator can physically access the toolrack, and can withdraw or deposit scanning probe tips while the equipment is being operated without having to break

---

[680] Robert A. Freitas Jr., Ralph C. Merkle, "A Minimal Toolset for Positional Diamond Mechanosynthesis," J. Comput. Theor. Nanosci. 5(May 2008):760-861.

[681] Robert A. Freitas Jr., Ralph C. Merkle, "A Minimal Toolset for Positional Diamond Mechanosynthesis," J. Comput. Theor. Nanosci. 5(May 2008):760-861.

vacuum inside the workspace UHV chamber. The manipulator geometry should be modified as required to permit convenient docking with a tip handle, securing of the tip handle to the manipulator, and withdrawal of the tip from the rack, and also the ability to reverse these steps – inserting the tip back into the toolrack and releasing it – after the operator has used the tip to perform various mechanosynthetic operations. The toolrack and manipulator kinematic trajectories should be designed to ensure that tips cannot scrape the interior walls as they are inserted or extracted from the toolrack.

The toolrack should have openings at the top to admit each detachable tip but should otherwise be a sealed unit. When a tip is stored in the rack, the tip terminus should be maintained in an in-rack vacuum environment that does not communicate with the exterior chamber vacuum. Since the in-rack vacuum will be very small in volume and getters can be provided, the expectation is that the in-rack vacuum will be a near-perfect vacuum while the tip is stored (Section 3.2.5(C)), thus allowing tips to be stored almost indefinitely without high probability of tip poisoning. For additional protection, tips will generally be stored in passivated condition to further extend their storage lifetime; Section 3.2.1.7).

Once replaced, the precise absolute location of the distal end of the new tip must be measured by comparison to a fiducial feature also present nearby within the workspace chamber, using the existing capabilities of the high-precision Task I-4 system. Thus each tip can be positionally re-registered after each changeout operation.

3.2.8 Task I-7: Build 1-Tip 4-DOF Picopositioning System and Demonstrate Additional DMS Reaction Sequences

Task I-7 is to design, develop, and demonstrate a high-precision UHV scanning probe picopositioning system with the same capabilities as the Task I-4 system (Section 3.2.5), but with (if necessary) one rotation degree of freedom (DOF) added to the tip manipulator motion, yielding a 1-tip 4-DOF picopositioning system. According to the conservative analysis in Table I-3, the addition of one rotational degree of freedom to the system gives access to 17 Reaction Sequences (out of the total of 65) and a total of 83 individual reactions (out of the total of 320) that were defined for elementary DMS operations by Freitas and Merkle.[682] Included among the accessible Reaction Sequences are the ability to build the Methylene tool (using RS40) and the Germylmethylene tool (using RS40 with Step 4') – the two principal carbon transfer tooltypes in the minimal toolset (Section 2.3.2). As previously noted in Section 3.2.1.5, positioning systems with 1-3 rotational DOFs are available commercially, though no complete system with the rotational precision that we require presently exists. We believe this is attributable to a lack of development effort, primarily due to lack of current commercial interest, rather than to any fundamental technical barriers to substantial improvements in resolution and repeatability in such systems.

---

[682] Robert A. Freitas Jr., Ralph C. Merkle, "A Minimal Toolset for Positional Diamond Mechanosynthesis," J. Comput. Theor. Nanosci. 5(May 2008):760-861.

If adding one rotational DOF to the existing three translational DOFs proves to be excessively challenging experimentally, alternative strategies might be pursued. For example, reaction sequences could be redesigned to allow successful execution without needing the extra degree of rotational freedom. (A study of the operational envelopes of moving tooltips in reactions already specified might reveal that these reactions can remain sufficiently exoergic even when bond angles are altered from the ideal minimum energy configurations.) As another possibility, note that for many Reaction Sequences the tooltip rotation is not required to take place while the rotating tooltip is in bonded contact with the workpiece or even while the rotating tooltip is in the immediate vicinity of the workpiece. In such cases, a relatively coarse rotational DOF may suffice, since the tooltip can be pre-rotated into the required position far from the workpiece and then be locked down (in the rotational dimension). Tooltip registration techniques can then be employed to re-calibrate the exact new positional and rotational orientation of the tooltip, after which the Reaction Sequence can be successfully performed using only the remaining three translational DOFs while the tooltip is in close proximity to the workpiece or other tooltips.

3.2.9 Task I-8: Build 2-Tip 5-DOF Picopositioning System and Demonstrate Additional DMS Reaction Sequences

Task I-8 is to design, develop, and demonstrate a high-precision UHV scanning probe picopositioning system with the same capabilities as the Task I-7 system (Section 3.2.8), but with (if necessary) one rotation degree of freedom (DOF) added to the tip manipulator motion, and a second tip manipulator set installed in the same workspace chamber, yielding a 2-tip 5-DOF picopositioning system. According to the analysis in Table I-3, the addition of one extra positionable tooltip and one extra rotational degree of freedom to the system now gives access to 42 Reaction Sequences (out of the total of 65) and a total of 234 individual reactions (out of the total of 320) that were defined for elementary DMS operations by Freitas and Merkle.[683]

If adding one rotational DOF to the existing three translational DOFs proves to be excessively challenging experimentally, alternative strategies might be pursued as previously described in Section 3.2.8. However, adding the second tooltip picopositioning manipulator appears essential both to accessing additional reactions and to continued progress toward developing the final macroscale fabrication workstation (MFW) system (Section 3.2.1).

3.2.10 Task I-9: Build 4-Tip 5-DOF Picopositioning System and Demonstrate Additional DMS Reaction Sequences

Task I-9 is to design, develop, and demonstrate a high-precision UHV scanning probe picopositioning system with the same capabilities as the Task I-8 system (Section 3.2.9), but with two additional tip manipulator sets installed in the same workspace chamber, yielding a 4-tip 5-DOF picopositioning system. According to the analysis in Table I-3, the addition of two extra positionable tooltips to the system now gives access to all 65 Reaction Sequences and all 320

---

[683] Robert A. Freitas Jr., Ralph C. Merkle, "A Minimal Toolset for Positional Diamond Mechanosynthesis," J. Comput. Theor. Nanosci. 5(May 2008):760-861.

individual reactions that were defined for elementary DMS operations by Freitas and Merkle.[684] Adding the second pair of tooltip picopositioning manipulators appears essential to accessing all remaining required reactions for building diamond and graphene structures on a fabrication surface, and completes the development of the macroscale fabrication workstation (MFW) system described in Section 3.2.1.

While it is believed that a 5 DOF system (including two rotational degrees of freedom) should suffice to experimentally realize all 65 minimal toolset reaction sequences, the possible benefits and costs of adding a third rotational degree of freedom – yielding a 4-tip 6-DOF picopositioning system – should be investigated and fully evaluated to determine if 6 DOF might produce significantly better multi-tip alignment, and whether adding this capability would be worth the extra cost and effort. The results of this analysis will also inform the subsequent Phase II and Phase III design efforts.

3.2.11 Task I-10: Demonstrate Hydrocarbon Product Object Fabrication Integrally on Fabrication Surface using MFW

Task I-10 is to use the macroscale fabrication workstation (MFW) completed in Task I-9 (Section 3.2.10) to fabricate, under precise positional control, a variety of basic hydrocarbon structures including adamantane cages and extended cage structures (to form any of the three principle diamond surfaces), tabbed structures, polyyne or hydrocarbon chain structures, and graphene nanotube or fullerene structures. The structures will be constructed integral to the fabrication surface. By integrally fabricated, we mean that the product is fabricated with covalent bonds directly into the fabrication surface, using a bonding pattern that is congruent with the existing diamondoid cage structure of the fabrication surface. In Phase I, it is not intended for the product object to ever become separated from the surface upon which it is fabricated. Product objects are to remain permanently affixed to their fabrication surface.

If necessary, the MFW may be slightly reconfigured to serve as a well-integrated atomically precise hydrocarbon workstation with efficient feedstock supply processes, an efficient flow-through design, a convenient user interface, a reliable UHV pumping system, and a convenient means for tooltip introduction or replacement into and out of the UHV working environment. This workstation would only be able to build hydrocarbon structures using carbon and hydrogen atoms, plus a limited range of additional atomically precise structures incorporating germanium atoms. The set of buildable structures would be very narrow – e.g., unstrained hydrocarbon cage arrays, carbon-rich cables, carbon nanotubes and fullerene cages. All product objects are built as one-offs with no parallelization.

---

[684] Robert A. Freitas Jr., Ralph C. Merkle, "A Minimal Toolset for Positional Diamond Mechanosynthesis," J. Comput. Theor. Nanosci. 5(May 2008):760-861.

Experimental proof-of-principle and DMS demonstration benchmarks for MFW development should include at minimum the following sequence:

(A) an experimental demonstration of purely mechanosynthetic (i.e., mechanical forces only, no electric fields involved) H abstraction, preferably on a diamond surface.

(B) an experimental demonstration of purely mechanosynthetic H donation, preferably on a diamond surface.

(C) an experimental demonstration of purely mechanosynthetic C_2 dimer (or other simple hydrocarbon moiety, like CH_3) placement, preferably on a diamond surface.

(D) an experimental demonstration of a purely mechanosynthetic sequence of two or more DMS reactions on or near the same reactive site on the same workpiece – for example, two adjacent H abstractions on a diamond surface, or a C_2 dimer placement on C(110) followed by H donation onto the previously-placed C_2 dimer.

(E) an experimental demonstration of the ability to perform a repeatable sequence of DMS operations on a diamond surface, resulting in the verifiable fabrication of a new diamondoid structure on that surface.

(F) an experimental demonstration of a purely mechanosynthetic fabrication of a significant 3D diamondoid nanostructure, such as a square rod, a solid prism, triangular objects, rods with gaps or holes, gear-shaped objects, and so forth.

3.2.12 Task I-11: Demonstrate Hydrocarbon-Plus Product Object Fabrication Integrally on Fabrication Surface using MFW

Task I-11 is to use the macroscale fabrication workstation (MFW) to fabricate, under precise positional control, a variety of atomically precise diamondoid structures that may contain atoms in addition to carbon, hydrogen and germanium. Modifications to the input streams, tooltypes, reaction sequences and fabrication surfaces employed in the MFW would be made in order to accommodate the new element types, potentially considerably broadening the range of buildable structures. As noted in Section 3.2.2.5, extension of our capabilities beyond hydrocarbons is insurance against possible constraints on nanomechanical system design using purely diamond gears, bearings and related mechanical components, which have limited geometrical diversity as compared to the wider range of nanocomponent sizes and configurations that may be available using other atoms in addition to C and H. As in Task I-10, all multi-element product objects are built as one-offs with no parallelization.

Additional theoretical work (starting in Task I-1; Section 3.2.2.5(E)) will be needed to identify minimal toolsets and reaction sequences for building diamondoid cages, chains, and surfaces using atoms other than C/Ge/H, possibly to include all noninert elements in the first two rows of the Periodic Table. Later-generation more advanced workstations would then be able to build simple diamondoid cage, graphene nanotube, and other basic diamondoid structures out of elements other than C/H/Ge, in addition to using those elements. Task I-11 thus should be viewed as a ongoing parallel research effort that may continue throughout Phase II (and some later Phases) as required, and serves as an “insurance policy” against the remote possibility that

the additional configurational diversity provided by non-hydrocarbon elements might be necessary to complete the development program proposed here.

3.3 Phase II: Macroscale Manufacturing Workstation (MMW)

The key objective of Phase II is to build a macroscale manufacturing workstation (MMW) that can nonintegrally fabricate diamondoid nanoparts from molecular feedstock primitives on a reversible fabrication surface (from which the manufactured nanoparts may be easily detached), and then pick up and assemble those diamondoid nanoparts into multi-nanopart diamondoid product objects on a reversible assembly surface. The MMW will be derived from the 4-tip 5-DOF picopositioning system implemented inside a vibration-isolated UHV workspace chamber that was created as the macroscale fabrication workstation (MFW) during Phase I. The Phase II system will represent the world's first commercializable diamondoid product fabrication and assembly workstation that provides a general capacity for manufacturing a variety of atomically precise complex diamondoid product objects as one-off structures up to 10^4-10^5 atoms, composed of nanoparts and multipart nanodevices.

The macroscale manufacturing workstation is described in Section 3.3.1 and illustrated in Figure II-1. This is followed by an enumeration of the specific sequence of tasks leading to an operational manufacturing workstation comprising both fabrication and assembly capabilities, which tasks include: establishment of the Standard Registry of Diamondoid Nanomechanical Parts and Processes (Section 3.3.2), population of the Registry with relevant nanopart and nanodevice designs (Section 3.3.3), experimental demonstration of DMS nanopart fabrication on a release surface (Section 3.3.4), design and experimental demonstration of reversible tip-mounted nanopart grippers (Section 3.3.5), design and experimental demonstration of releasable rechargeable DMS toolheads (Section 3.3.6), design and experimental demonstration of a toolrack for DMS toolheads (Section 3.3.7), design and experimental demonstration of fabrication sequences for simple diamondoid nanoparts (Section 3.3.8), design and experimental demonstration of fabrication sequences for complex diamondoid nanoparts and other specialized structures (Section 3.3.9), and design and experimental demonstration of assembly sequences for assembling diamondoid nanoparts into multipart nanodevices (Section 3.3.10).

3.3.1 Description of the MMW

The macroscale manufacturing workstation (MMW) (Figure II-1) has the same infrastructure, features and basic components as the macroscale fabrication workstation (MFW) previously described in Section 3.2.1. However, the MMW has several additional system components that enable it to perform atomically precise diamondoid fabrication on release surfaces and also to mechanical assemble nanoparts. These additional system components include:

(1) a reversible release surface (Section 3.3.4), perhaps bonded to the fabrication surface previously described in Phase I (Section 3.2.1.7), upon which diamondoid nanoparts can be fabricated and then released;

(2) a reversible assembly surface (Section 3.3.10), perhaps also bonded to the fabrication surface described in Phase I (Section 3.2.1.7), upon which diamondoid parts can be parked and then retrieved at a later time (thus serving as a convenient depot area), or which can provide a mechanical barrier to assist in assembly (e.g., during press-fit operations);

(3) an actuator-enabled gripper (Section 3.3.5) permanently mounted on the apex of a bulk probe tip of the sort used in Phase I, that enables the picopositioning manipulator to reversibly pick up or set down reusable nanoscale toolheads in a toolrack without requiring changeout of the bulk probe tooltip containing the gripper as in Phase I, also eliminating the need for positional re-registration after each toolhead exchange as was likewise required in Phase I;

(4) a toolrack for reusable nanoscale toolheads (Section 3.3.7)); and

(5) atomically precise reusable nanoscale toolheads (Section 3.3.6) which may be used for DMS fabrication, for nanopart assembly, or as jigs or other specialized tools to support either activity.

Figure II-1. Schematic layout of the Phase II Macroscale Manufacturing Workstation (MMW).

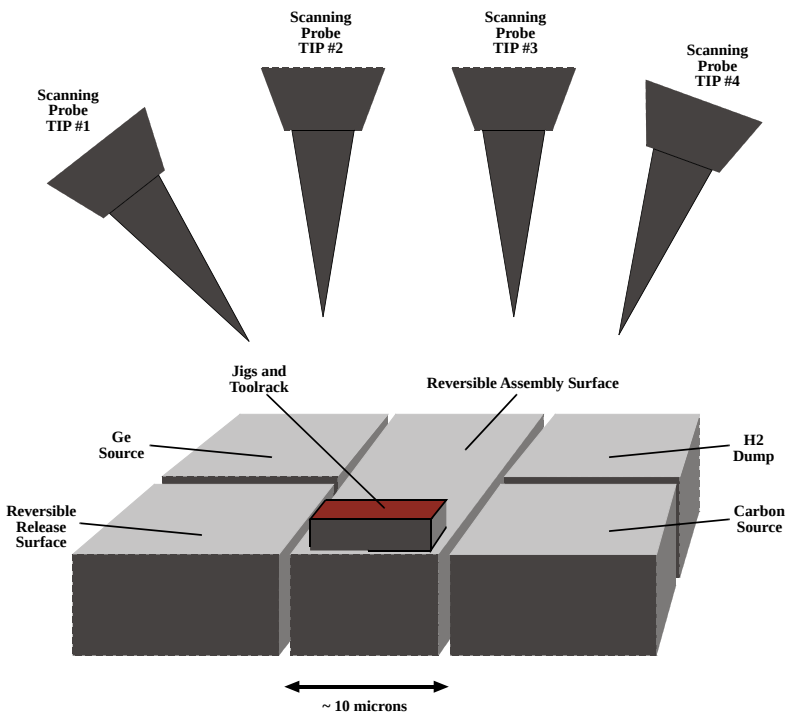

3.3.1.1 Operation of the MMW

The operation of the MMW proceeds in much the same way as for the MFW, including vacuum pumpdown, insertion and alignment of the workspace surfaces, followed by mapping and sequence adjustment (Section 3.2.1.7). Nanopart fabrication proceeds similarly, except that each of the four manipulators is installed with a probe tip to which has been affixed a reversible toolhead gripper mechanism. Manipulator registration is required only once, at the beginning, because unless the probe tip is unstable or breaks during use, it is never again changed out until the operations are finished and therefore it should never lose its original registration if the nanopositioning system is operating correctly. (It may nevertheless be advisable to periodically re-verify the probe registration, especially during early experiments while gaining experience with a novel system. Sensory feedback can readily be added to the Phase I/II programs if necessary to ensure reliable operation because the Phase I/II systems need no scalability, e.g., to other sizes or to greater numbers.) DMS operations proceed as before, with the probe-mounted gripper picking up atomically precise toolheads from the toolrack, using them, possibly recharging them, then replacing them in the toolrack.

3.3.1.2 MMW Productivity

To estimate MMW net productivity, we start by assuming (as detailed in Section 3.4.1.4) that ~6 mechanosynthetic operations per atom may typically be required to add each carbon atom to a growing diamond workpiece via DMS, or to add C and H atoms to a hydrogen-passivated diamond surface, including feedstock acquisition, tool operation, tool recharge, and toolrack exchange. We further assume that the toolrack has been more conveniently placed within 10 microns of the fabrication release surface so that each operation typically requires a round-trip tip excursion of ~20 microns using interferometric counting increments of ~0.2 Å. Laser interferometry with electronic fringe-counting at rates up to 10 MHz were first described in 1964[685] and was considered commonplace by the 1990s,[686] but higher counting rates of 15 MHz,[687] 25 MHz,[688] 30 MHz,[689] 43 MHz,[690] 50 MHz,[691] and even up to 300 MHz[692] (near the characteristic cutoff frequency of silicon diode detector elements) have been reported or discussed in the literature. Conservatively assuming that fringes are reliably countable at a ~10 MHz rate, this yields a precision-trackable tip motion velocity of ~200 microns/sec when counting increments of ~0.2 Å are employed. In this case the MMW can be operated at a rate of ~0.1 sec per round-trip tip excursion or ~10 operations/sec, yielding a gross productivity of ~1.7 atoms/sec taking ~6 operations required per atom. Assuming a 60% duty cycle for translational

---

[685] F.T. Arrechi, G. Lepre, A. Sona, Alfa Frequenza 33(1964):534-541. See also: S.J. Bennett, W.R.C. Rowley, "Automatic compensation for changes of signal level in laser interferometry," J. Phys. E: Sci. Instrum. 6(1973):963-964.

[686] Michael J. Downs, "Single-frequency bidirectional fringe-counting interferometer," United States Patent 5546184, US Patent Issued on August 13, 1996.

[687] Scott E. Pollack, "Analytic and Interferometric Techniques for the Laser Interferometer Space Antenna," PhD Thesis, Department of Physics, University of Colorado, 2005; http://jilawww.colorado.edu/pubs/thesis/pollack/.

[688] R.S. Eng, K.A. Langdon, W.A. Richardson, J. Lapato, "High-speed laser interferometry applied to transient vibration measurements," Appl. Opt. 23(1984):2956-2960; http://www.opticsinfobase.org/abstract.cfm?URI=ao-23-17-2956.

[689] A.G. Basden, C.A. Haniff, C.D. Mackay, M.T. Bridgeland, D.M.A. Wilson, J.S. Young, D.F. Buscher, "A new photon counting spectrometer for the COAST," Proceedings of SPIE -- Volume 5491, New Frontiers in Stellar Interferometry, Wesley A. Traub, ed., October 2004, pp. 677-688; ftp://ftp.mrao.cam.ac.uk/pub/coast/spie-5491-78.pdf.

[690] Graham Flint, "Integration Of Ife Beamlet Alignment, Target Tracking And Beam Steering: Bistatic Target Tracking Concept," 3 March 2005, accessed February 2008; http://www-ferp.ucsd.edu/HAPL/MEETINGS/0503-HAPL/flint.ppt.

[691] Laser Metric Systems, Inc., "Sub-Fringe Position Reading Modules for Laser Interferometers", accessed February 2008; http://laser-metric-systems.com/products/prm/index.html.

[692] Frank Eugene Goodwin, Dana Simonson, "3-Dimensional vision system utilizing coherent optical detection," European Patent EP0283222, Filing Date 03/11/1988; http://www.freepatentsonline.com/EP0283222B1.html.

tip motions to allow various non-translational motions (e.g., tooltip changeouts) during 40% of the time, the net productivity of the macroscale Phase II MMW system may be estimated as ~1 atom/sec (~1 Hz) for nanostructures fabricated on the diamondoid fabrication surface. This is about 100-fold faster than the Phase I system when used for DMS fabrication. When used for nanoparts assembly, we conservatively assume a working assembly frequency of only ~0.01 nanoparts/sec (~0.01 Hz) to allow plenty of time for larger travel distances, binding and unbinding operations from release surfaces, slow and gentle press fitting operations, and deployment and stowage of any special jigs that may be required.

3.3.1.3 Reliability of MMW Operation

For the Phase II MMW system, we have a target productivity rate of ~1 atom/sec with ~6 mechanosynthetic operations required for placement of each atom in the growing workpiece structure (Section 3.3.1.2), and a target workpiece size of up to 10^4-10^5 atoms for each fabricated diamondoid nanostructure (Section 3.3). Building the largest 10^5-atom structure thus requires ~600,000 mechanosynthetic operations, so to avoid even a single misplacement error the picopositioner system must be capable of delivering a minimum of ~600,000 error-free round trip excursions of the positionally controlled DMS tooltips – a design requirement to better the minimum performance of the Phase I system (see Section 3.2.1.3 and Section 3.2.1.8) by ~100-fold.

Another source of intrinsic manufacturing error arises from the reliability of the DMS reactions themselves, as previously discussed in Section 3.2.1.8. Table I-5 gives the probability of misreaction at various relevant operating temperatures, assuming a defect energy threshold of 0.40 eV. At room temperature (~300 K) the misreaction probability per mechanosynthetic operation is 1.91×10^{-7}, conservatively assuming that all reactions have the minimum defect energy threshold of 0.40 eV (most have higher thresholds than this, hence are much less error prone), so the probability of finding a single erroneous atom placement in the largest 10^5-atom workpiece after ~600,000 mechanosynthetic operations is at most ~11% at 300 K. If any workpiece having one or more erroneous atom placements is considered defective, then the room temperature DMS defect rate will be at most $\sim 10^{-1}$ for 10^5-atom product objects and $\sim 10^{-2}$ for 10^4-atom product objects fabricated using this set of DMS reactions, hence room temperature operation appears feasible in Phase II. At near liquid nitrogen temperatures (~80 K), the DMS-related error rate using reaction sequences with a defect energy threshold of 0.40 eV falls to $\sim 4 \times 10^{-20}$ for a 10^5-atom product object, completely negligible for Phase II purposes.

Another major source of error is radical poisoning by contaminants in an imperfect UHV environment. At a target productivity rate of ~1 atom/sec for the Phase II MMW system, the largest 10^5-atom product object will require $t_{fab} \sim 10^5$ sec (~1 day) to fabricate. Assuming that a radical site susceptible to poisoning is exposed to the imperfect UHV environment for a fraction $f_{vac} \sim 50\%$ of the time, then the maximum tolerable UHV pressure that will permit one defect-free 10^5-atom product object to be fabricated is $P_{UHV} \leq (N_{encounters}\, T / n_{contam}\, A_{radical}\, f_{vac}\, t_{fab})\, (\pi\, MW_{kg} / 2\, k_B T\, N_A)^{1/2} \sim 10^{-12}$ atm, where $n_{contam} = 7.34 \times 10^{27}$ molecules-K/m^3-atm (= N_A/R_{gas}) for ideal gas (contaminant) molecules and T = 300 K, with the other quantities as previously defined in Section 3.2.1.7. If any workpiece having one or more erroneous atom placements is considered defective, then in a UHV environment maintained at $\sim 10^{-16}$ atm (~10 million contaminant molecules present in a 5-liter UHV work volume; currently achievable experimentally, Section 3.2.1.7) the radical-poisoning defect rate at 300 K will be $\sim 10^{-4}$ for 10^5-atom product objects and $\sim 10^{-5}$ for 10^4-atom product objects. If H_2 contaminant is determined not to be a serious radical

poisoning risk or can be rigorously excluded from the workspace, then taking $MW_{kg} = 0.014$ kg/mole for N_2 raises the required P_{UHV} by a factor of ~2.6; conversely, operation at 80 K lowers the required P_{UHV} by a factor of ~2.

As for radiation damage rates, assuming a failure condition of $\kappa_{fail} \sim 10^{15}$ hits/kg-rad and an $I_{rad} \sim$ 0.5 rad/yr background the mean time τ_{rad} between radiation-disabling hits on a mostly-carbon 10^5-atom diamondoid workpiece (or tooltip) of mass $m_{target} = 2 \times 10^{-21}$ kg is $\tau_{rad} \sim (\kappa_{fail}\, m_{target}\, I_{rad})^{-1} \sim 10^6$ years (conservatively assuming that one such hit will cause the workpiece or tooltip to fail with 100% certainty), a negligible error rate.

When used for assembly work rather than for fabrication, the Phase II system neither creates nor destroys chemically active radical sites, hence its operations are not subject to DMS-related error rates and are only weakly subject to vacuum poisoning effects. Hence MMW reliability during assembly operations is governed chiefly by its ability to correctly execute a small number of non-covalent parts assembly operations and by error rates in nanopart gripping/releasing mechanisms, and these error rates are assumed to be small in comparison with the DMS-related error rates.

3.3.2 Task II-1: Establish Standard Registry of Diamondoid Nanomechanical Parts and Processes

Task II-1 is to perform nanopart and nanodevice design-ahead by setting up a Standard Registry for parts and for the processes to be used in building them. We need to establish nanopart libraries to be catalogued, if possible, in CAD-usable formats. Nanoparts and nanoassemblies should employ "design for assembly," "Design for Manufacturability" (DFM), and "design for analysis and validation" philosophies. Establishment of the Registry will make it possible to conduct a comprehensive analysis of proposed nanodevices and nanosystems to determine how many distinct nanoparts and materials surfaces will be needed to constitute a complete set of low-level structural and functional components sufficient for molecular manufacturing.

The following material is modified from the original Nanofactory Collaboration Project Proposal for the "Standard Registry of Diamondoid Nanomechanical Parts and Processes" (Version 1.9, 29 November 2007).

3.3.2.1 Mission Statement and Rationale

In order to organize and systematize the design and analysis results generated by Nanofactory Collaboration efforts, and to lay the foundation for the component design efforts to be undertaken by the Collaboration in later phases of nanofactory development, we will create a uniform database of standardized nanoparts, nanodevices, and nanosystems, and standardized reaction or fabrication sequences, assembly sequences, and manufacturing processes for diamondoid materials.

There are at least five reasons for undertaking this effort:

(1) to collect in one place all of the design and analysis work that has been done to date, to illuminate gaps and to suggest immediate future areas where this work should be expanded, since no one else is currently concentrating effort on this (i.e., if we don't do it, it won't get done);

(2) to begin to create a standardized compilation of processes and validated parts that could be used as input structures by a future nanoCAD/CAM system for the design of more complex processes and components, including future automated nanodesign systems;

(3) to seed efforts to involve professional researchers, and even the interested amateur public (consistent with our intent to create a "hard-science" registry with entries reviewed and approved via a professional review process), in contributing to this line of development by providing a focal point for such efforts, and by providing an easy way to participate in furthering Collaboration objectives;

(4) to begin the process of standardizing nanoparts, nanodevices and nanosystems, and also standardizing processes, including relevant nomenclature, with the view to creating a future rigorous discipline of nanosystems engineering and design; and

(5) to respond directly to the call by the Foresight/Battelle 2007 Technology Roadmap for Productive Nanosystems[693] to create "catalogues of atomically precise building blocks (organic or inorganic, natural or synthetic) organized by functional properties" to spur development of "productive nanosystems," particularly diamondoid nanofactories; and to the call by the National Research Council (NRC) of the National Academies and the National Materials Advisory Board (NMAB) in their Congressionally-mandated 2006 review[694] of the U.S. National Nanotechnology Initiative to encourage and support "experimentation leading to demonstrations supplying ground truth for abstract models...to better characterize the potential for use of bottom-up or molecular manufacturing systems that utilize processes more complex than self-assembly."

The Registry will be restricted to "diamondoid" parts and processes. For the purposes of this Registry, "diamondoid" will refers to strong stiff materials containing dense 3D networks of covalent bonds, formed chiefly from first and second row atoms with a valence of 3 or more. Examples typically include lattices involving carbon, such as diamond, graphene (e.g., nanotubes and fullerenes) and polyyne structures (e.g., carbyne rods), but also include other strong covalently bonded ceramic materials such as silicon nitride, silicon carbide, boron nitride, and so forth. Strong ionic solids such as sapphire are also considered to be diamondoid materials. Diamondoid lattices may be terminated using atoms of valence 3 or lower. Precursors of diamondoid parts may also be included in the Registry.

Where do we draw the precise boundaries for "diamondoid" materials? This may evolve with time, but the key criterion is whether or not a component or process made of the proposed material may be useful in the construction of a strong, rigid molecular machine system having strength and rigidity comparable to nanomachines made of diamond or diamondlike materials.

---

[693] Productive Nanosystems: A Technology Roadmap, Battelle Memorial Institute and Foresight Nanotech Institute, 2007; http://www.foresight.org/roadmaps/index.html.

[694] Committee to Review the National Nanotechnology Initiative, National Materials Advisory Board (NMAB), National Research Council (NRC) (2006) A Matter of Size: Triennial Review of the National Nanotechnology Initiative. The National Academies Press, Washington DC; http://www.nap.edu/catalog/11752.html#toc.

For example, some organometallic molecules might qualify for inclusion if, for instance, they are attached to an adamantane base and can clearly be envisioned as comprising a component that could be part of a rigid molecular machine structure and would give to that structure some particular desired characteristic that would be relevant to nanomachinery operating in a vacuum environment. As another example, both oxygen-terminated silicon and fused quartz (silica cage framework) are diamondoid materials, as are rigidly covalently bonded silsesquioxane cages (direct cage-cage bonds, not using relatively weak linker molecules) formed into rods or shell structures (e.g., to make bearings or gears) would be considered "diamondoid" and thus relevant for inclusion in the Registry, but highly cross-linked polymers would not qualify. As the Registry is set up, a specific list of materials and objects that qualify as "diamondoid" will be assembled. Qualification of a material as "diamondoid" may include a formal materials strength requirement within one order of magnitude of diamond – i.e., a Young's modulus of at least 10^{11} N/m^2 plus a failure strength either in tension or compression of at least 10^{10} N/m^2. Other considerations might include the chemical stability and reactivity of the material, especially as they relate to the mechanical, electrical, etc. operation of components in nanodevices fabricated from that material.

The Parts Registry will consist primarily of nanoparts, nanodevices and nanosystems intended to be used, and having their main function, as mechanical components in larger mechanical systems. The function of a mechanical component is to transmit force to other mechanical components, prevent the transmission of such force, or to act as barriers (e.g., walls serving to separate volumes containing different constituents, to shield radiation, etc.). The Parts Registry will also include mechanosynthetic tools and tooltips, the atomic-scale equivalent of machine tools. The Registry may include nanoparts, nanodevices and nanosystems whose primary function is electronic, optical, or other, but the primary focus will be on mechanical components and systems.

The Process Registry will consist primarily of methods for fabricating and assembling nanoparts, nanodevices and nanosystems. In this Registry, "fabrication" refers to construction of a component structure using only covalent or ionic bonding patterns, whereas "assembly" refers to the construction of a structure using a process that additionally makes use of noncovalent bonding such as van der Waals forces or hydrogen bonding. Fabrication processes typically accept the most primitive molecular feedstock as their inputs and produce simple nanoparts as their output, while assembly processes typically accept simple nanoparts as their inputs and produce compound nanoparts (nanodevices) or complex nanosystems as their output. The precise distinction between fabrication and assembly will be further clarified as the Registry accumulates more information over time.

It is envisioned that the Registry will evolve in response to new results and to developing user needs in the growing molecular CAD/CAM research community. Formal procedures must be defined for the addition of new parts and processes to the Registry from sources outside of the Nanofactory Collaboration, possibly including a requirement for at least one peer-reviewed published research paper describing the proposed new part or process. Trivial variations of an existing part or process design that involve no new design principles but represent simple extensions of prior work might be admissible subject to internal peer review. In the event that progress in the addition of parts or processes steps beyond the time limits of the academic peer review process, the possibility exists for extending the Parts Registry by way of an open journal dedicated to the reporting of newly developed Registry content, such as has been established for a number of research fields as part of the Open Library of Science (http://www.plos.org/).

Regarding involvement of the interested amateur public, the intent is to create a "hard-science" registry with entries reviewed and approved by a professional review process.

Component and process nomenclature will initially be used that is consistent with conventional terminology commonly used in present-day mechanical and molecular engineering. Further refinements in nomenclature are expected to occur over time, with input from – and the assistance of – Society of Manufacturing Engineers (SME) members and other technical participants.

The Registry itself initially will be organized in four major parts.

3.3.2.2 Parts Registry

In the Parts Registry, each object entry may be accessed via a user-friendly Object Page containing all available details of the object. A master parts table will summarize all objects, with links to individual Object Pages. Master summary parts table entries will be arranged as a sequential listing of object types, with all entries within each object type listed in descending order of validation, possibly into the following broad object validation categories:

Class A: Validated experimentally;
Class B: Validated theoretically only, using *ab initio* or DFT methods;
Class C: Validated theoretically only, using semi-empirical methods;
Class D: Validated theoretically only, using molecular mechanics methods; and
Class F: Invalidated either theoretically or experimentally.

Class A will include any component that has any sort of experimental validation. Degrees of experimental validation will need to be defined as this classification is populated in the years ahead, e.g., what degrees of partial validation (of part of an object) will count, what experimental methods were used, whether experimental validation of a closely related or analogous system will count, and so forth.

Class B includes components validated using only or up to (*ab initio* and DFT methods outranking semi-empirical and molecular mechanics calculations) *ab initio* or DFT quantum chemistry methods but that are not yet validated experimentally. This also includes QM/MD (quantum mechanical (*ab initio* or Density Functional Theory) molecular dynamics) studies. Components within an object type are listed in the Registry in descending quality order, with analyses using larger basis sets ranked higher than those with smaller basis sets, and so forth.

Class C includes components validated using only or up to (semi-empirical methods outranking molecular mechanics calculations) semi-empirical methods but that are not yet validated experimentally.

Class D includes components validated using only molecular mechanics methods, including molecular dynamics studies using molecular mechanics force fields, but that are not yet validated experimentally. The minimum standard for inclusion of a component in the Registry is that a model consisting of a full set of atomic coordinates has been created and energy-minimized using a molecular mechanics package, and has been checked to ensure elementary quality standards such as correct element bond numbers, bond types, and no improper valences.

Class F includes components that have been invalidated by one or more methods, either theoretical or experimental. The primary purpose of this category is to serve as an organizational memory to avoid repetition of past mistakes. A policy decision must be made regarding the

limits of inclusion for the "invalidated" category – will it include all design failures, or just objects that were validated at one level but then later found to be invalid at a higher level of analysis? Further, the retention of previously studied components within this class enables their reinvestigation at higher levels of theory when it can be determined that the theoretical invalidation may be a result of limits within the employed theoretical model, and potentially would enable CAD systems to check, e.g., trial system designs for parts that had been used on the basis of tentative validation but were subsequently invalidated. Objects may be moved from one category to another as warranted by new results.

The Registry should make clear which theoretical methods give results more likely to be accurate, providing a key that indicates which methods should be more highly ranked. The accompanying textbook might serve this function. Links should be included to relevant software so people can learn how to use it. Links to instructions or brief tutorials on how to run these programs might be added, if the textbook material to be provided online will not suffice, perhaps including an online discussion group because the Registry cannot directly offer "tech support" services for operating these programs.

Parts Registry items should include direct links to relevant items in the Process Registry wherever possible.

The Object Page for each object listed in the Parts Registry will include the following object attributes:

(1) chemical and/or common name(s);

(2) elements used (include isotope specification if relevant);

(3) total atom count;

(4) physical dimensions (length > width > height) and volume (while summation over van der Waals radii is the most useful form of calculated molecular volume, the issue of "solvent accessibility," or inner-component access by small molecules, results in a possible need to differentiate between "component volume" (generated by, for instance, a bounding box) and "surface volume" (generated by only calculating volume from the sum of non-overlapping atomic van der Waals volumes);

(5) stoichiometric and structural chemical formulas;

(6) atomic structure files (e.g., pdb, hin, mmp, etc.; investigate possible inclusion of other file types that might be useful to the mechanical engineering community);

(7) molecular weight and mass;

(8) bulk physical characteristics at relevant temperatures if known (e.g., density, melting/boiling point, vapor pressure, etc.);

(9) an MSDS spec sheet if available;

(10) known commercial suppliers and purities available (including cost and potential delivery delays);

(11) object type (e.g., nanopart (rod, gear), nanodevice (bearing), etc.) – consider setting this up as a selection from a predefined list, the point being to avoid the problem where people are using different names for the same thing (e.g., "tube" and "pipe" are not synonyms for mechanical engineers, so we may need guidelines about such things for the non-ME's; an extensible list managed by the Registry personnel would seem most appropriate);

(12) inventor or discoverer (include name, contact information, company, etc.);

(13) date of invention or discovery;

(14) accession date (date when added to Registry) and the identity of the person who added it;

(15) patent information on the object;

(16) trademark information on the object;

(17) copyright information on the object;

(18) images of the object (e.g., jpg images; models or actual) and sources;

(19) videos of the object (animations or actual) and sources;

(20) object description (brief textual description of the structure and function of the object, and any other pertinent information not included elsewhere);

(21) part-specific structure information (e.g., if a screw, the pitch angle of the threads; if a gear, the tooth number; if a SWCNT, the (n,m) chirality; if a bearing, the commensurability ratio of the interface; etc. – some of this requires standardization or it will be hard for the CAD programs to make use of it);

(22) indication of whether the object is still theoretical or has actually been fabricated;

(23) indication of whether the object occurs naturally, can be chemically synthesized, or can only be positionally fabricated;

(24) computational validation (e.g., software used (Gaussian, GAMESS, etc.), method used (MM, AM1, DFT), basis sets used, convergence criteria used, frequency analysis or not, etc., plus links to relevant print/online technical papers or webpages);

(25) experimental validation (e.g., hardware used, method used, partial/complete object validated, direct/analogous validation, plus links to relevant print/online technical papers or webpages);

(26) Registry Part Number, or accession number, or some other standardized designation;

(27) indication of whether a fabrication or assembly pathway to create the object has already been specified in the Process Registry, and if so, the links to those pathway(s) or processes;

(28) parts topology (overall geometry, with certain structures and structural motifs important to specific applications, or for use with specified components within the Registry);

(29) parts interoperability (chemical, vibrational, thermal, electronic, etc., compatibility of a structure or a specific material with other structures or materials in a developed "interaction chart" format);

(30) some indication of the weakest class of validation for any nanodevice or nanosystem involving multiple nanoparts (i.e., what is the weakest link), to help clarify where additional validation work might be most useful;

(31) a true/false tag indicating whether the object is considered a fullerene object, or if it contains fullerene components;

(32) the validation history of the object should be retained for future reference; and

(33) if known, the various "mechanical isomers" of a mechanical system should be described individually (e.g., a hinge mechanism might possess two or more global or local energy minima ("resting positions") at, say, 90 deg and 180 deg, or at some other set of angles).

The Parts Registry will consist of the following five Sections:

Section A. Registry of Diamondoid Feedstock Molecules and Accessory Structures

This will consist of a compilation of simple hydrocarbon and other "vitamin" molecules that may be used for positionally-controlled diamondoid mechanosynthesis, primarily for the fabrication of simple diamondoid nanoparts. Items will be restricted to molecules consisting solely of covalent and/or ionic bonded atoms that can be produced via traditional bulk synthetic chemistry processes and can be obtained in macroscale (e.g., gram+) quantities. These items will include synthetically-accessible feedstocks that can be prepared using scalable synthesis processes already published in the technical literature or can be obtained from commercial vendors (e.g., the Sigma-Aldrich catalog). Also included are accessory structures, such as atomically flat depassivated diamond or germanium surfaces, and SPM tips that can be prepared using

conventional bulk methods and which may assist in DMS tool fabrication or in the initiation of a workpiece seed structure.

Categories of diamondoid feedstock molecules may include the following: molecular hydrogen, acetylene, ethylene, methane, or digermane.

Categories of diamondoid accessory structures may include the following: atomically flat passivated or depassivated diamond or germanium bulk surfaces, surfaces with step ledges or troughs, surfaces with holes, and so forth. "Accessory structures" should probably be displayed in a separate subsection from the more typical single-molecule feedstocks.

Section B. Registry of Diamondoid Nanoparts

A diamondoid nanopart is a nanoscale object consisting solely of covalent and/or ionic bonded atoms that requires no van der Waals or hydrogen bonding to maintain its shape, structure, or significant physical characteristics. Nanoparts are the most primitive nanomechanical objects used in constructing molecular machine systems and will often contain no "moving parts". Tooltips and their handle structures will also be included in the nanoparts registry. Nanoparts may be fabricated either by conventional techniques of bulk chemical synthesis or by new techniques of positionally-controlled mechanosynthesis as described in the Process Registry (Section 3.3.2.3).

Categories of diamondoid nanoparts may include the following: adamantanes, polymantanes, plates, rods, prisms, rings, tubes, screws, gears, binding sites, levers, wires, and mechanosynthetic tooltips.

Section C. Registry of Diamondoid Nanodevices

A diamondoid nanodevice is a nanoscale object consisting of two or more nanoparts joined together either strongly by covalent bonds (e.g., two planar nanoparts joined through single-atom covalent bonds to make a hinge) or relatively weakly by van der Waals or hydrogen bonds (e.g., two ring-shaped nanoparts pressed together to make a bearing), or which are otherwise mechanically not separable (e.g., interlocking rings). Nanodevices may be regarded as complex nanoparts in the construction of molecular machine systems and generally will perform a single function (e.g., two rotational nanoparts fitted together to make a bearing or simple neon pump, a dozen nanoparts fitted together inside a housing to make a planetary gear assembly, several dozen nanoparts comprising a telescoping manipulator arm, etc.). Nanodevices will usually be assembled using techniques of positionally-controlled fabrication and assembly as described in the Process Registry (Section 3.3.2.3), although assembly via conventional techniques of bulk chemical synthesis or self-assembly will not be excluded from the Registry. In some cases the definitional dividing line between "nanodevice" and "nanopart" may be somewhat arbitrary and so the object classification may be chosen primarily for convenience of discussion, analysis, or categorization.

Note that all nanodevices are composite objects assembled from smaller components already described in Sections A or B. All such composite objects should explicitly link to their components (and vice versa), and all nanodevices should include both an explicit atomic description (containing atomic coordinates for every atom in the nanodevice structure) and a more abstract nanoparts-level description (describing the nanodevice in terms of the positions and

orientations of the various nanoparts of which it is comprised, shedding light on the actual underlying structure and composition of the device). Providing one large file of single-atom coordinates will almost always be necessary because nanoparts, once fitted together into a nanodevice, will normally experience numerous forces that significantly displace the relative positions of atoms within each such nanopart.

Categories of diamondoid nanodevices may include the following: bearings, gear trains, complex gears (e.g., planetary gears, speed reduction gears, worm gears, toroidal gears), transmissions, hinges, joints, springs, ratchets, rack and pinion, reversible binding sites, sorting rotors, nanosensors, actuators, acoustic transducers, motors, power generation and storage devices, power/control distribution cables/junctions, pumps, mechanical grippers, mechanical manipulators (e.g., telescoping arms, Stewart platforms), nanocomputer components (e.g., gates, registers, data transmission lines, logic arrays, hydrofluorocarbon tape memories). Nanodevices listed in Section C of the Registry should be comprised of nanoparts listed in Section B and/or nanodevices listed in Section C.

Section D. Registry of Diamondoid Nanosystems

A diamondoid nanosystem is an object consisting of a large set of nanoparts and/or nanodevices that operate together as a complex nanomechanical system to perform a complex multifunctional task. The macroscale products of molecular manufacturing will commonly consist of complex nanosystems, not isolated simple nanodevices or nanoparts. Nanosystems will usually be assembled using techniques of positionally-controlled assembly as described in the Process Registry (Section 3.3.2.3). In some cases the definitional dividing line between “nanosystem” and “nanodevice” may be somewhat arbitrary and so the object classification may be chosen primarily for ease of discussion, analysis, or categorization.

Note that all nanosystems are composite objects assembled from smaller components already described in Sections A, B, or C. All such composite objects should explicitly link to their components (and vice versa), and all nanosystems may include both an explicit atomic description (containing atomic coordinates for every atom in the nanosystem structure) and more abstract nanoparts- and nanodevices-level descriptions (describing the nanosystem in terms of the positions and orientations of the various nanoparts and nanodevices of which it is comprised, shedding light on the actual underlying structure and composition of the system). Providing one large file of single-atom coordinates might not always be necessary because nanodevices, once fitted together into a nanosystem, may not experience significant distortions in atomic positions down at the nanopart level, and because nanodevices will already incorporate atomic level descriptions of stressed nanopart structures; thus in these cases, the nanosystem can be specified to atomic precision by specifying links to previously described components.

Categories of diamondoid nanosystems may include the following: manipulator arrays, power distribution systems, nanocomputers, nanofabrication systems, nanoassembly systems, component transport systems, nanofactories, nanorobots, nanoproducts. Nanosystems listed in Section D of the Registry should be comprised of nanoparts listed in Section B and/or nanodevices/nanosystems listed in Sections C/D.

Section E. Registry of Fullerene Nanomachines

Because of the widespread interest in nanotube- and fullerene-based systems, and to create greater visibility for the Registry among fullerene researchers, a distinct registry will be created for fullerene mechanical systems. Despite creating some redundancy, such a unique registry is deemed desirable for at least three reasons: (1) many potentially useful theoretical designs already exist, (2) fullerene and nanotube systems are currently experimentally accessible and are the subject of great experimental interest, and (3) we would like to capitalize upon and stimulate more activity among researchers who are trying to design simple systems (providing opportunities for cross-pollination).

For the purposes of this registry, "fullerenes" will be broadly defined as structures composed of closed surfaces of 2D networks of atoms that are joined together solely by strong covalent bonds. Fullerenes may be composed of carbon atoms, but related structures involving other elements such as boron-nitrogen nanotubes would also be included. Since objects populating this registry may consist of feedstock molecules, nanoparts, nanodevices, or nanosystems, all entries in Section E will also be listed at the appropriate place in Sections A-D of the Standard Registry. Within the fullerene registry, the same nanopart/nanodevice/nanosystem is used as in the main Registry.

3.3.2.3 Process Registry

In the Process Registry, each process entry may be accessed via a user-friendly Process Page containing all available details of the process. A master process table will summarize all processes, with links to individual Process Pages. Master summary process table entries will be arranged as a sequential listing of process types, with entries of each type grouped into the same validation categories as previously described in Section 3.3.2.2. Process Registry items should include direct links to relevant items in the Parts Registry wherever possible.

The Process Page for each process listed in the Process Registry will include the following process attributes:

(1) brief title describing the nature and purpose of the process;

(2) list of input nanoparts or nanodevices involved in the process (including intra-Registry links to the nanoparts or nanodevices used);

(3) total count of atoms, nanoparts and nanodevices involved in the process;

(4) links to the atomic structure files of input and output structures as previously defined in the Parts Registry (e.g., incorporating pdb, hin, mmp, or other file types useful to the mechanical engineering community);

(5) process type (e.g., mechanosynthetic reaction sequence, assembly sequence, etc.; we probably want an extensible list managed by Registry personnel here too, so categories don't proliferate or become ambiguous);

(6) inventor or discoverer (include name, contact information, company, etc.);

(7) date of invention or discovery;

(8) accession date (date when added to Registry) and the identity of the person who added it;

(9) patent information on the process;

(10) trademark information on the process;

(11) copyright information on the process;

(12) images of the process (e.g., jpg images; models or actual) and sources;

(13) videos of the process (animations or actual) and sources;

(14) process description (brief textual description of the details of the process, a tabular presentation of accessible fabrication/assembly pathologies,[695] and any other pertinent information not included elsewhere, including links to papers);

(15) process-specific information (e.g., tooltip trajectories analyses,[696] translational and rotational requirements for fabrication[697] and assembly operations, etc. At present, we have a relative paucity of such information.[698] As more information accumulates, we'll probably need to devise new file formats that can concisely describe such processes – including methods for describing tooltip trajectories,[699] allowed tolerances,[700] and the like – since a mere list of inputs and outputs is unlikely to be sufficient);

(16) indication of whether the process is still theoretical or has actually been experimentally verified;

(17) indication of whether the process occurs naturally, can be achieved via conventional chemical synthesis, or can only be executed via positionally-controlled fabrication or assembly manipulations;

(18) computational validation of the process (e.g., software used (Gaussian, GAMESS, etc.), method used (MM, AM1, DFT), basis sets used, convergence criteria used, frequency analysis or not, etc., plus links to relevant print/online technical papers or webpages);

(19) experimental validation of the process (hardware used, method used, partial/complete object validated, direct/analogous validation, links to relevant papers or webpages);

(20) Registry Process Number, or accession number, or some other standardized designation;

(21) indication of which objects in the Parts Registry (Section 3.3.2.2) can be fabricated or assembled by the given process, and if so, the links to those object(s);

(22) known failure modes or limitations of the process, provided as a means of identifying under which design constraints the process is appropriate or most efficient for use;

(23) some indication of the weakest class of validation for any multi-step process (i.e., what is the weakest link), to help clarify where additional validation work might be most useful;

(24) known allowable physical constraints on the process (e.g., temperature, pressure, gas/vacuum/liquid, presence/absence of light, chemical environment, etc.); and

(25) the validation history of the process should be retained for future reference.

The Process Registry will consist of the following two Sections:

Section A. Registry of Fabrication Processes for Diamondoid Nanoparts

This Registry will include fabrication processes for diamondoid nanoparts that consist solely of covalent and/or ionic bonded atoms and require no van der Waals or hydrogen bonding to

---

[695] http://www.molecularassembler.com/Nanofactory/AnnBibDMS.htm#FreitasMerkle07.
[696] http://www.molecularassembler.com/Nanofactory/AnnBibDMS.htm#Tarasov08.
[697] http://www.molecularassembler.com/Nanofactory/AnnBibDMS.htm#Peng06.
[698] http://www.molecularassembler.com/Nanofactory/AnnBibDMS.htm#FreitasMerkle07.
[699] http://www.molecularassembler.com/Nanofactory/AnnBibDMS.htm#Tarasov08.
[700] http://www.molecularassembler.com/Nanofactory/AnnBibDMS.htm#Peng06.

maintain its shape, structure, or significant physical characteristics. Fabrication processes will primarily involve positionally-controlled making and breaking of strong covalent or ionic bonds, typically by applying chemically reactive tools to workpieces under UHV conditions, e.g., tip-based fabrication via diamondoid mechanosynthesis. The use of van der Waals forces or hydrogen bonding may occur as incidentals to the fabrication processes but the transaction of strong bonds between constituent atoms of the object, being fabrication, is the primary focus. Fabrication processes may include published reaction sequences or may be drawn from other reliable sources, and will only make use of components that are described in the Parts Registry (Section 3.3.2.2). Nanopart fabrication processes may also include conventional bulk synthetic methods not involving positional control, but examples of this are expected to be relatively few in number.

Section B. Registry of Assembly Processes for Diamondoid Nanodevices and Nanosystems

This Registry will include assembly processes for diamondoid nanodevices that consist of two or more nanoparts joined together either strongly by covalent bonds or relatively weakly by van der Waals or hydrogen bonds, or that consist of two or more nanodevices joined together. Assembly processes may include positionally-controlled making or breaking of strong covalent or ionic bonds, but more typically will involve assembly sequences in which nanoparts and/or nanodevices are grasped by manipulators and moved through space along positionally-controlled trajectories and then mechanically joined either with other nanoparts and/or nanodevices, or are added to a growing workpiece, whose physical structure is maintained via van der Waals forces between closely-fitted components. The use of strong covalent bonds may occur as an incidental to an assembly process but the transaction of van der Waals forces or hydrogen bonding between constituent nanoparts comprising the object that is being assembled is the primary focus. Assembly processes may include published assembly sequences or may be drawn from other reliable sources, but will only make use of tools and components including or comprised of nanoparts and/or nanodevices that are described in the Parts Registry (Section 3.3.2.2).

3.3.2.4 Initial Registry Set-Up

Subject to further discussion, the Registry will be initially set up as a Wiki, with password-protected access to the ability to access or to modify any pages. After initial set-up, password-protected viewing access may be relaxed to allow unfettered public reading (but not editing) of the Wiki. At a later stage, members of the public may be allowed to add comments but not to alter content. Blank templates will be provided for Object Pages, Process Pages, and all compositional elements within these pages including graphics, lists, tables, references, and so forth, in order to ensure compositionally uniform additions to the site by disparate authorized users; but only fully authorized users with passwords will be allowed to view or download the blank templates.

Future versions of the Registry might employ a non-Wiki format, perhaps more akin to a formal custom database, but for the first-generation Registry a Wiki format seems to be the most convenient of various possibilities. Although a Wiki may not be the ideal long-term format for the Registry, the Nanofactory Collaboration needs to get a database up and running as quickly as possible to support our Research Proposal development activities in 2008. The initial Registry must be easy to understand, simple to use, quick and convenient to modify, able to ensure all necessary restrictions on authorized use, and that employs a widely familiar technology in case

the number of nanoworkers must be expanded or replenished. A Wiki seems to best satisfy all of these goals. It is important to ensure that each Registry entry has its own unique URL, so that users can refer to them and bookmark them. These URLs should not change even if components are somehow reclassified or reorganized – stability of URLs is an important design feature.

Once the initial Registry has been set up and is populated with significant numbers of useful items, the nature and dimensions of the future "ideal" system should become clearer and we can begin planning for it. (For example, one potentially useful database from which we can perhaps derive inspiration and useful features are the curated BioCyc metabolic pathway databases,[701] since the interplay between nanoparts and processes in our Registry has some similarities to reactions that convert small molecules[702] which can be chained into larger pathways[703] – in the latter case, the flowcharts with arrows and clickable component items are an attractive mode of visualization and their Pathway Tools software[704] is freely available for research purposes.) But until then, our judgment is that we need to establish a strong coastal beachhead before venturing deeper into the dark continent of molecular machine design.

The Registry will be operated as a Collaboration project but will be established with the advice and consultation of the Society of Manufacturing Engineers, who will join the Nanofactory Collaboration as an affiliated organization through the efforts of Tihamer Toth-Fejel, Chairman of the SME Nanomanufacturing Technical Group.[705]

Long-term responsibility for Registry maintenance and page review/repair will need to be assigned to an individual or committee consisting of participants in the Nanofactory Collaboration to ensure stylistic and substantive consistency. Our "nanoworkers" will initially set up and maintain the site, with a small group of Collaboration technical participants (chiefly Freitas, Merkle, Allis and Toth-Fejel at the outset) providing initial technical content and "curation" approval of major decisions on features, etc. All contributors to the setup and maintenance effort should be acknowledged somewhere on the site.

The initial group of volunteer "nanoworkers" will be established and will organize their own cooperative activities as they implement this proposal. This organization should include sufficient redundancy so that the departure or arrival of existing or future volunteers will not jeopardize the Wiki's ability to keeping functioning. The nanoworkers will be given administrative site access and will be responsible for setting up the initial Wiki as described in this document, including its large-scale structure and page-specific formats, the "look and feel" of the Registry, the connectivity between pages, the templates, and so forth. One conceptual exemplar of a useful registry Wiki is the Standard Registry for Biological Parts (SRBP).[706] We may want to borrow many of the useful features found in the SRBP. However, our Registry has many different objectives, methods, and requirements, so the SRBP should not be slavishly

---

[701] http://biocyc.org/.
[702] http://biocyc.org/ECOLI/NEW-IMAGE?type=REACTION-IN-PATHWAY&object=PHOSGLYPHOS-RXN.
[703] http://biocyc.org/ECOLI/NEW-IMAGE?type=PATHWAY&object=GLYCOLYSIS&detail-level=2.
[704] http://bioinformatics.ai.sri.com/ptools/.
[705] http://www.sme.org/nano.
[706] http://parts.mit.edu/registry/index.php/Main_Page.

followed but rather should be improved upon and hopefully exceeded – resulting in a professional-looking format that is easier to understand and to use than the SRBP. On 5 November 2007, Freitas reserved for exclusive Registry use the domain name http://www.NanopartRegistry.com and established an ISP account for the future website.

Complete Libraries

Additionally, we need to add complete libraries including the following basic structures:

(1) cylindrical rods of a full range of diameters;
(2) polygonal rods (prisms) of triangular, square/rectangular, or hexagonal cross-section;
(3) cylindrical screws with various pitch angles, thread spacings, etc.;
(4) comprehensive systematic libraries of gear and bearing designs;
(5) single-walled carbon nanotubes of all (n,m) chiralities (this library may already exist online somewhere, and we may need to seek permission to incorporate), including carbon-only as well as BN and other relevant systems; and
(6) adamantane and polymantane structures, both functionalized and nonfunctionalized, that could reasonably be considered as potentially useful nanoparts.

Formal limits may need to be established to restrict which "nanopart" molecules can be included in the Registry to avoid mission creep leading toward effective inclusion of the entire PubChem database or the whole of the Beilstein chemical structure catalog. On the other hand, we do want to include in the Registry every rigid structure that could legitimately be considered a valid diamondoid nanopart, especially since some of these objects might already be accessible via conventional bulk synthetic pathways and thus readily available for experimentation in gram+ quantities.

Analysis of Registry Use Cases

It would be interesting to think about the several most typical "use cases" for the Registry and make sure that the system supports them. One example of a primary use case might include searches for examples of a particular class of part or process (e.g., all examples of bearings) to provide guidance and inspiration in designing a new object of that particular class, or searches through descriptive textual material looking for particular words, phrases, or synonyms (this may require a separate definitional page of words, phrases, acronyms and synonyms. Other use cases (such as searching for all parts of a given type having certain dimensions, element types, and so forth) may be addressed in the future. Ideally we will try to make sure from the outset that as many field values as possible have been sufficiently formalized for future users to do effective searches.

3.3.3 Task II-2: Design Nanoparts and Nanodevices for the Registry

Task II-2 is to populate the Registry (Section 3.3.2) with thoroughly analyzed designs for nanoparts that are specifically relevant to Phase II development. This would include designs for DMS fabrication release surfaces (Section 3.3.4) and assembly surfaces (Section 3.3.10), DMS toolheads (Section 3.3.5), reversible grippers capable of mechanically grasping both toolheads and nanoparts (the requirement for grippability may affect nanopart design) (Section 3.3.6), toolracks (Section 3.3.7), and any special jigs that might be needed for nanopart assembly (Section 3.3.10).

We also need to begin populating the Registry with design-ahead structures and systems that are relevant to future development Phases, or even (with somewhat lesser urgency) to structures and systems that may be relevant to future atomically precise products. These structures and systems might include:

(1) nanoparts such as plates, rods, beams, prisms, rings, tubes, pipes, screws, simple gears, wheels, axles, binding sites, levers, wires, and additional mechanosynthetic tooltips or specialized jigs;

(2) nanodevices such as bearings,[707] gear trains, complex gears (e.g., planetary gears, speed reduction gears, worm gears, toroidal gears), molecular cables in sheaths,[708] transmissions, hinges, joints, springs,[709] ratchets, rack and pinion, reversible binding sites, sorting rotors, nanosensors, actuators, valves, acoustic transducers, motors, power generation and storage devices, power/control distribution cables/junctions, pumps, mechanical grippers, mechanical manipulators (e.g., telescoping arms, Stewart platforms), or nanocomputer components (e.g., gates, registers, data transmission lines, logic arrays, hydrofluorocarbon tape memories); and

(3) nanosystems such as manipulator arrays, power distribution systems, nanocomputers, nanofabrication systems, nanoassembly systems, component transport systems, nanofactories, nanorobots, nanoproducts. Nanosystems listed in Section D of the Registry should be comprised of nanoparts listed in Section B and/or nanodevices/nanosystems listed in Sections C/D.

In each case these designs need to be conceptualized, modeled, then tested with successively more powerful simulation methods to create the highest possible confidence that the structure or system would work as intended, if manufactured. Later in Phase II, theory will be tested against experiment by actually building some of these designed nanoparts and physically measuring their stability, reliability, and kinematic performance. Amateur efforts in diamondoid molecular machine design[710] should be encouraged and integrated into the nanofactory development program if possible.

Additional nanopart- and nanodevice-related studies will include:

(A) Need an analysis of bonding interfaces between dissimilar materials, in particular diamond and sapphire, and diamond and silica (O-terminated silicon).

---

[707] John Cumings, A. Zettl, "Low-friction nanoscale linear bearing realized from multiwall carbon nanotubes," Science 289(28 July 2000):602-604.

[708] G.C. McIntosh, D. Tomanek, Y.W. "Park Energetics and electronic structure of a polyacetylene chain contained in a carbon nanotube," Phys. Rev. B 67(2003):125419.

[709] John Cumings, A. Zettl, "Low-friction nanoscale linear bearing realized from multiwall carbon nanotubes," Science 289(28 July 2000):602-604.

[710] http://machine-phase.blogspot.com/.

(B) Need a study of atomic defect tolerance within nanoparts. This would involve a series of simulations in which random changes are imposed one at a time, while observing which ones affect nanopart performance most strongly and by how much. Changes may involve mispositioning, misbonding, element substitutions, or pathological rearrangements in the nanopart.

(C) Need a detailed design for a nanomotor (Section 3.4.1.1), with atomistic simulations of at least the key components. Materials must be specified and the chemical stability of the resulting structures must be tested. An electrostatic stepper motor intended for use in an electrically-driven Stewart platform (or related manipulator system) should be the primary focus here, though other motor types could be considered. The use of any kind of metal may raise serious surface stability issues and failure might occur due to the adhesion of contacting surfaces, but metallic graphenes, doped diamond or other relevant stiff covalent materials might be used instead. Exquisite precision in positioning may also be required due to the exponential dependence of tunneling current with separation.

(D) Need a detailed design for a molecule-selective pump, with atomistic simulations of at least the key components, especially the binding sites and drive mechanisms. One useful target might be a molecular level design of a selective valve or pump system based on rigid diamondoid materials that admits a chosen molecule while excluding, say, oxygen and nitrogen with nearly 100% efficiency. Design-ahead of sorting rotor systems specifically targeted at ethylene (C_2H_4), germane (GeH_4), and molecular hydrogen (H_2) are needed by Phase IV.

(E) Investigate the need for a CML (Chemical Markup Language)[711] specification suitable for representing nanomechanical parts and devices for molecular machine systems.

(F) Need to develop software for computer-aided nanodevice design, possibly including automated design of subassemblies of nanoparts comprising nanodevices and the ability to test those designs in simulation against relevant dimensional specifications, constraints, and performance/tradeoff criteria. We should try to work towards a system that can maintain an appropriate hierarchy of levels of abstraction, imposing some manner of consistency while designers work at various different levels. Microprocessors are designed in this way – e.g., CPU, functional units, register level, gate level, logic level, component level – and nanofactory design will require a similar ability to deal with multiple levels of design abstraction. According to one software engineer:[712] "The electronics industry really runs off a language called VHDL. It was originally designed as a variant of Ada for designing and testing highly complex (50K devices back then) integrated circuits. But the huge advantage was the ability to set up a hierarchy of design levels and to work at any particular level. (And of course, if a company announces a new IC, the first thing they ship is the VHDL model, possibly at several design levels.) Is VHDL the perfect language for developing nanotech? No. The problem is that VHDL is sort of 2 1/2 dimensional. Two dimensions are used for layout, and the third dimension is used for both layering and abstraction levels. You could say that this fits well with the way components and

---

[711] Peter Murray-Rust, Henry S. Rzepa, "Chemical Markup Language. A Position Paper," 2001-04-10; http://cml.sourceforge.net/historical/position.html.

[712] Robert I. Eachus, newsgroup communication, 5 October 2003.

printed circuit boards are designed, or you could say that the language affects the way electronic systems are designed and built. For nanotech, we really need a 3 1/2 dimensional language – in other words, a design language that lets you think in terms of three dimensional components, then flip through stacks of abstraction levels. The picture of your design as electric fields, atoms, components, subassemblies, subsystems, etc., needs to be different views of the same (software and eventually hardware) object."

(G) Once preliminary designs for nanoparts and for their assembly sequences into multi-nanopart nanodevices have been specified, the number of DOF that are minimally required to perform all essential assembly sequences must be assessed. The possible need for a 6 DOF assembly manipulator must be evaluated, taking into account the possibility of using specialized jigs to offset the need for an extra rotational degree-of-freedom. If 5 DOF will not suffice and 6 DOF are required, then the Phase II system must be upgraded to 6 DOF if this has not already been done.

(H) Need a detailed atomically precise design for a Stewart platform (or related)[713] manipulator system of the kind that will be employed in Phase III (e.g., Task III-1, Section 3.4.2) and in later Phases of this development program. This design should include specification of all nanoparts comprising a diamond Stewart platform, including the electrostatic stepper motors, along with validating simulations. This manipulator design effort must be preceded by a range-of-motion study to validate that Stewart platforms have a large enough work envelope to meet all operational needs. This preceding effort will require a complete layout of the workspace and an analysis of the motions involved.

3.3.4 Task II-3: Demonstrate DMS Fabrication on a Release Surface

Task II-3 is to design and build a "release surface" for nanopart fabrication, atop the bulk surface (e.g., H-passivated diamond) previously employed in Phase I, then demonstrate that nanoparts can be fabricated on the release surface and then can be conveniently removed from that surface purely mechanically and in a continuously and fully positionally controlled manner – e.g., using the tip-mounted grippers developed in Task II-4. Tasks II-3 and II-4 should be pursued in tandem for this reason.

In Phase I, DMS fabrication via UHV scanning probe methods created structures integrally bonded to the fabrication surface. In Phase II, improved DMS fabrication methods will create structures that need not be integrally bonded to the fabrication surface, but which may instead be released from that surface. A releasable fabrication surface is a surface upon which diamondoid nanostructures may be positionally fabricated and then mechanically removed without destroying either the release surface or the fabricated nanostructure. Numerous concepts for release surfaces are currently being investigated, for example:

(1) Build structures on a hydrogenated C(111) surface which is punctuated by an occasional Ge-substituted bridgehead atom, making an array of well-separated "weakly sticky

---

[713] Ralph C. Merkle, "A New Family of Six Degree Of Freedom Positional Devices," Nanotechnology 8(June 1997):47-52, http://www.zyvex.com/nanotech/6dof.html.

points" from which parts may be readily separated. A rigid structure under construction will need at least two such attachment points to prevent it from spinning, and possibly a third attachment point to prevent rocking, during the performance of positionally controlled DMS reaction sequences. Van der Waals forces between nanopart and passivated surface can be reduced by elevating the Ge radical sites to the apexes of low pyramidal piers having the same surface number density.

(2) Use shaped H-terminated diamond "pits" or "cups" to hold single-adamantane molecules or related molecular precursors via predominantly van der Waals forces, upon which larger nanostructures are then constructed, then pulled out of the cup. A single Ge substituent atom in the base of the cup may provide a weak covalent anchor point for the growing structure. In a more sophisticated system, the cup may be in two halves that are pressed together to apply mechanical restraint to the precursor molecule, and the halves may be pre-shaped to provide large barriers to rotation of the trapped molecule (especially if the molecule has significant geometric asymmetries and/or the experiments are conducted at reduced temperatures). The halves can also be used to detach the finished nanostructure from the surface.

(3) Build nanopart structures directly onto the chemically active apexes of multiple repositionable radical-tipped jigs or auxiliary manipulators that will hold the growing nanopart. Once the nanopart is finished and fixture detachment is required, the jigs or manipulators can be pulled off of the finished part one by one in the right sequence and at the right angles, and the revealed radical sites on the nanopart passivated as soon as they appear. The key advance here is to demonstrate that we can start with a simple non-cage diamondoid seed structure – e.g., a methyl group on the end of a GM tool – and build up a whole cage structure just from that, effectively eliminating the need for a formal fabrication release surface.

The design, modeling, simulation, fabrication and physical testing of workpiece release surfaces and the nanoparts to be built upon those surfaces should address the following key technical issues:

(A) Need to design nanoparts to allow easy gripping and manipulation.

(B) Need efficient parts presentation schemes.

(C) Need to devise complete DMS fabrication sequences to build nanoparts and/or their intermediate structures on piers or detachable surfaces, and then pick them up.

(D) Need to verify that nanoparts may be held sufficiently rigidly on the release surface during DMS fabrication steps (e.g., to within the required 0.2-0.5 Å positional accuracy limits),[714] while allowing convenient and nondestructive removal of the nanopart from the surface once fabrication is complete.

(E) Investigate the possibility of controlled or reversible parts adhesivity during positionally controlled assembly.

---

[714] Robert A. Freitas Jr., Ralph C. Merkle, "A Minimal Toolset for Positional Diamond Mechanosynthesis," J. Comput. Theor. Nanosci. 5(May 2008):760-861.

(F) Investigate possible schemes for nanopart palletization (transport jigs of standardized shape and size to permit standardized handling, but that can easily release the affixed nanopart).

(G) As a low priority effort (because it somewhat diverges from our current critical development pathway which emphasizes positional control at all times), investigate the possibility of DMS-based nanopart fabrication on a sacrificial surface which is dissolved away, releasing nanoparts into a carrier fluid. (The nanopart-bearing fluid could then be evaporated onto an assembly surface, after which the nanopart residue could be scanned, mapped, and identified, with the deposited nanoparts then grasped and carried off for assembly into nanodevices elsewhere.)

3.3.5 Task II-4: Design and Demonstrate Reversible Tip-Mounted Grippers

Task II-4 is to demonstrate the ability to build an active (actuated) atomically precise end-effector or "gripper" directly onto the apex of a bulk-manufactured scanning probe tip (as was employed in Phase I), with the gripper able to be actuated into closed (gripping) or open (nongripping) states. The gripping state must be mechanically strong enough: (1) to hold an atomically precise nanopart without slip during DMS operations or (2) to remove a nanopart or toolhead from the release surface described in Section 3.3.4 or from the toolrack described in Section 3.3.7. (Tasks II-3 and II-4 should be pursued in tandem for this reason.) Micromechanical grippers with multiple independently-actuated fingers have already been experimentally demonstrated with positional control of a few nanometers at each fingertip.[715]

One conceptual design for a reversible gripper might employ a T-shaped member that slides along a race on the bottom leg of a second larger L-shaped member, with a two-position latch corresponding to gripped and ungripped states. The design would include a mechanical barrier preventing movement away from either state, once occupied, with said barrier surmountable by laterally pushing the traveling member to the left (from the right side) to open the gripper, or to the right (from the left side) to close the gripper. The mechanical sliding force to overcome the barrier could be supplied either (1) by using the manipulator to which the gripper is attached to press against a nubbin or protrusion in the workspace environment (e.g., near or attached to the toolrack), or (2) by using a second manipulator to press against the first at the appropriate location and direction to trigger a change of mechanical state in the gripper. Gripping of an object would be mediated entirely by van der Waals forces, but the gripper surface contours could be design to maximally positionally constrain the gripped nanopart by having cavities and protrusions that are shape-complementary to the nanopart intended to be gripped. Another concept using weak covalent bonds might employ a two-site radical-based gripper analogous to a

---

[715] Sandeep Krishnan, Laxman Saggere, "A multi-fingered micromechanism for coordinated micro/nano manipulation," J. Micromech. Microeng. 17(March 2007):576-585, http://www.iop.org/EJ/abstract/0960-1317/17/3/021. See also: "Micromanipulator makes its debut", 21 February 2007, http://nanotechweb.org/articles/news/6/2/19/1.

discharged DCB6Ge tool;[716] this might make a nice 2-point gripper that could relatively easily be pulled away from a diamondoid part, but getting more than two workable pullaway connection points using this concept will be hard to do.

The design, modeling, simulation, fabrication and physical testing of gripper mechanisms (and the nanoparts which they will be capable of gripping) will address several key technical issues. Theoretical analyses of nanopart gripper design should include:

(A) Positionally controlled grippers must be designed that can grab and then manipulate finished nanoparts, whether to transport them elsewhere or to further manipulate them in a series of assembly steps, such as a parts insertion operation (a peg pushed into a complementary hole) or other similar assembly operation, in which small parts are mechanically combined to make larger compound nanoparts which include van der Waals bonding.

(B) The grippers must be able to firmly and reliably grip toolheads. Handled tools intended to be used for the purpose of constructing compound nanomachines from their component parts might be significantly different in design from handled tools intended to be used for mechanosynthesis. For example, mechanosynthetic tooltips will usually have almost exclusively covalent-bond-forming reactivity, whereas tooltips intended to be used for assembly work may employ primarily van der Waals or other weak bonding systems for parts gripping, though weak covalent bonding (e.g., dative bonds, Sn-C bonds, etc.) might also be used.

(C) Need methods for attaching the actuated gripper mechanism to the picopositioning system (e.g., via a bulk-made scanning probe tip) while provably retaining rigidity and an ability to actuate the gripper.

Experimental work to demonstrate a working nanopart gripper should include:

(D) Development of SPM technology to enable nanopart assembly work.

(E) Need a reversible nanopart gripper as an end-effector on an SPM tip. The gripper should be capable of remote and/or conditional actuation. The gripper should be able to grab a nanopart and hold it with at least 3-point contact so that the nanopart is translationally and rotationally fully constrained while it is being gripped.

(F) SPM systems to be used for assembly work may require less positional placement precision but an ability to apply greater forces, and in more complex directions (e.g., twisting motions that apply circular or helical torques, threading/insertion motions. etc.). Making an atomically precise product out of nanometer-scale nanoparts does not necessarily require atomic

---

[716] Ralph C. Merkle, Robert A. Freitas Jr., "Theoretical analysis of a carbon-carbon dimer placement tool for diamond mechanosynthesis," J. Nanosci. Nanotechnol. 3(August 2003):319-324; http://www.rfreitas.com/Nano/JNNDimerTool.pdf. See also: Ralph C. Merkle, Robert A. Freitas Jr., "Theoretical analysis of a carbon-carbon dimer placement tool for diamond mechanosynthesis," paper presented at the 10th Foresight Conference on Molecular Nanotechnology, October 2002; http://www.foresight.org/Conferences/MNT10/Abstracts/Merkle/index.html.

precision in nanopart positioning, but rather only enough positional precision to distinguish the desired assembly structure from adjacent pathological assembly structures.

(G) Must develop an actuation methodology that can potentially be controlled in parallel and is potentially scalable.

(H) Need a specific experimental demonstration in which the gripper mechanism is fabricated onto (or otherwise mated with) a bulk scanning probe tip, and then the tip is actuated so as to grab a nanopart off of the release surface demonstrated in Task II-3, and then setting it down in a different place on the surface.

3.3.6 Task II-5: Design and Demonstrate Releasable Rechargeable DMS Toolheads

Task II-5 is to design, build and demonstrate releasable rechargeable toolheads for both fabrication and assembly operations. Such toolheads consist of a working tip structure mounted on a relatively inert handle structure (e.g., Figure 2-43). The handle is of a size and shape that can be securely grasped by the Task II-4 gripper mechanism, and also may includes specialized features (such as a raised circumferential stop ledge) that permit the toolhead to be inserted into a hole in a toolrack, forming an airtight seal once inserted and keeping the active tooltip physically separated from the toolrack floor to prevent unwanted interactions there. Existing computational design, modeling and simulation software as described elsewhere (Section 3.2.2.11, Section 3.4.2) can be used for this purpose.

Completion of Task II-5 requires a demonstration that toolheads can be reliably grasped and released by the gripper, that toolheads (in both charged and discharged condition) can be reliably removed from and inserted into the toolrack without misalignment or other misadventure, and that the toolheads can be recharged via DMS processes previously described.

3.3.7 Task II-6: Design and Demonstrate Toolrack for DMS Toolheads

Task II-6 is to design and build a toolrack inside the UHV workspace chamber to hold at least 20 atomically precise toolheads of the type that will be manufactured in Task II-5. The toolrack should also be able to hold any fabrication/assembly jigs or other specialized assembly tools that might be required. The toolrack and manipulator kinematic trajectories should be designed to ensure that tips cannot scrape the interior walls as they are inserted or extracted from the toolrack.

The toolrack should have openings at the top to admit each toolhead but should otherwise be a sealed unit. When a toolhead is stored in the rack, the tooltip should be maintained in an in-rack vacuum environment that does not communicate with the exterior chamber vacuum. Since the in-rack vacuum will be very small in volume, the expectation is that the in-rack vacuum will be a near-perfect vacuum while the toolhead is stored, thus allowing toolheads to be stored almost indefinitely without high probability of tooltip poisoning. To further prevent DMS radical tip poisoning and to extend storage lifetime, all chemically active tooltips could be stored either in

hydrogenated (unreactive/passivated) condition and then depassivated by H abstraction just prior to use, or possibly in tip-tip pairs that are easily pulled apart (e.g., GeRad-HAbst, GeRad-GeRad, GeRad-Meth, GeRad-AdamRad),[717] with the compound HTrans tool assembled only when needed.

One additional design objective is that storage of toolheads in the toolrack should be sufficiently rigid to maintain toolhead registration to the required positional accuracy. If this objective cannot be achieved, then the precise absolute location of the distal end of a replaced toolhead can be measured by comparison to a fiducial feature also present nearby within the workspace chamber, using the existing capabilities of the high-precision (e.g., Task I-4) system. Thus each toolhead can be positionally re-registered after each changeout operation.

3.3.8 Task II-7: Design and Demonstrate Fabrication Sequences for Simple Diamondoid Nanoparts

Task II-7 is to design and experimentally demonstrate diamondoid mechanosynthesis (DMS) fabrication sequences for manufacturing simple diamondoid nanoparts, using the toolheads (Task II-5), grippers (Task II-4) and release surfaces (Task II-3) developed earlier in Phase II.

Building on the existing literature on DMS fabrication sequences[718] and related similar efforts in Phase I (e.g., Task I-9; Section 3.2.10), these fabrication sequences will start with molecular primitives as feedstock and will result in the efficient fabrication of adamantane cages and extended cage structures (to form any of the three principle diamond surfaces) and tabbed structures, and simple linear nanoparts such as cubes, rods, prisms, L-shapes, Y-shapes, square hoops, and the like. This will make heavy use of previous experience with automated DMS operations developed earlier in Phase I, but using the new tools developed in Phase II as efficiently as possible. It may become necessary to redesign some toolheads or nanoparts to make it possible to fabricate them more efficiently.

This experimental effort should be supported by some theory (and possibly software development work) in the simulation of nanoparts, nanomachines, and nanomachine operations as follows:

(A) Need software that can reliably model and simulate the kinematic operation of diamondoid machine parts. The availability (or current ability to develop) software capable of doing DFT-based quantum chemistry simulations on structures up to several thousands of atoms on desktop computers (or small clusters of such computers) should be investigated, along with other methods using simplified DFT-based simulations on up to millions of atoms (Section 3.4.2).

(B) Need to develop a CAD/simulation system capable of performing molecular dynamics simulation of numerous interacting parts, and of accurately predicting the reliability

---

[717] Robert A. Freitas Jr., Ralph C. Merkle, "A Minimal Toolset for Positional Diamond Mechanosynthesis," J. Comput. Theor. Nanosci. 5(May 2008):760-861.

[718] Robert A. Freitas Jr., Ralph C. Merkle, "A Minimal Toolset for Positional Diamond Mechanosynthesis," J. Comput. Theor. Nanosci. 5(May 2008):760-861.

and physical characteristics of their interactions. One approach might include a Q-SMAKAS type analysis, starting with some small bearings or gear assemblies. For example, the analysis might start with AM1, since the atomic structure models will have too many atoms for conventional DFT or *ab initio* simulation software to handle, even using a stripped down STO-3G basis set. Simulations might be done at each of 5-10 rotational positions corresponding to progressive gear tooth/position rotational positions to make sure all possible relative gear positions (tool rotational states) are covered. This might be followed by a series of runs in which one component is pressed into the other component starting at zero force (free running) and going up in lateral and longitudinal stress (simulating various stress vectors that might be placed on the component during actual use). We should run these stress forces up until we observe the gear start to fail. Any failures found using AM1 could be investigated in more detail using DFT with smaller models incorporating just a piece of the structure(s) involved.

(C) Prior theoretical work[719] lays out a general framework for estimating the effects of thermal noise, which is then applied to one engineering design in a calculation of positional uncertainty at the tip of a molecular positioner. This shows that the positional uncertainty can be made to be less than an atomic diameter – a necessary, if perhaps not sufficient, condition for such devices to work. But we also need a broader range of molecular dynamics simulations of more complex nanomachines operated at liquid nitrogen and room temperatures, in which both the mechanism itself and its mountings are subject to thermal noise.

(D) Need a review of the new body of recent experimental and simulation work on nanotribology (nanoscale friction), followed by an assessment of its implications for the performance of nanoscale machinery. For example, superlubricity[720] of incommensurate graphite and incommensurate graphene sliding surfaces has been demonstrated experimentally.[721] MD simulations and SPM experiments have investigated tip sliding friction on commensurate H-terminated C(111) and C(100) diamond surfaces.[722] However, the AFM experiments[723] used

---

[719] K. Eric Drexler, Nanosystems: Molecular Machinery, Manufacturing, and Computation, John Wiley & Sons, New York, 1992; http://www.zyvex.com/nanotech/nanosystems.html.

[720] M. Hirano, K. Shinjo, "Atomistic locking and friction," Phys. Rev. B 41(June 1990):11837-11851; http://prola.aps.org/abstract/PRB/v41/i17/p11837_1.

[721] Ali Erdemir, Jean-Michel Martin, eds., Superlubricity, Elsevier B.V.,2007; http://www.science-direct.com/science/book/9780444527721.

[722] Guangtu Gao, Rachel J. Cannara, Robert W. Carpick, Judith A. Harrison, "Atomic-Scale Friction on Diamond: A Comparison of Different Sliding Directions on (001) and (111) Surfaces Using MD and AFM," Langmuir 23(2007):5394-5405; http://pubs.acs.org/cgi-bin/abstract.cgi/langd5/2007/23/i10/abs/la062254p.html. Geoffrey J. Germann, Sidney R. Cohen, Gabi Neubauer, Gary M. McClelland, Hajime Seki, D. Coulman, "Atomic scale friction of a diamond tip on diamond (100) and (111) surfaces," J. Appl. Phys. 73(1 January 1993):163-167; http://content.aip.org/JAPIAU/v73/i1/163_1.html.

[723] Guangtu Gao, Rachel J. Cannara, Robert W. Carpick, Judith A. Harrison, "Atomic-Scale Friction on Diamond: A Comparison of Different Sliding Directions on (001) and (111) Surfaces Using MD and AFM," Langmuir 23(2007):5394-5405; http://pubs.acs.org/cgi-bin/abstract.cgi/langd5/2007/23/i10/abs/la062254p.html.

amorphous hydrocarbon tips that gave irregular stick-slip behavior consistent with the presence of surface inhomogeneities and single-asperity interfacial friction that would not occur in an atomically precise nanodevice such as a bearing or gear (because opposed surfaces in these devices would be homogeneous and would have no asperities); the MD simulations[724] used an irregularly-stepped tip, treated the tip as a rigid body, ignored van der Waals forces, and employed contact loading pressures up to ~100 times the largest expected values for loaded sleeve bearings[725] – at the lowest loading pressures, MD-calculated friction between opposed flat surfaces almost falls to zero (see Fig. 8 in Gao et al.[726]). Earlier work by the same group investigating sliding friction between opposed C(111) surfaces[727] also involved commensurate surfaces, hence is also of limited direct relevance to estimates of frictional losses between atomically engineered incommensurate surfaces.[728] Interestingly, a 50 nm-radius tip dragged across a deuterium-terminated single-crystal diamond surface exhibits reduced nanoscale friction than for H-terminated surfaces[729] – D atoms have a larger atomic mass and a lower natural vibration frequency hence collide less frequently with the sliding tip, slowing energy dissipation at the contact area. Sinusoidally oscillating vibrations imposed normal to an interfacial surface can also reduce frictional losses by 100-fold,[730] and almost frictionless operation of sliding

---

[724] Guangtu Gao, Rachel J. Cannara, Robert W. Carpick, Judith A. Harrison, "Atomic-Scale Friction on Diamond: A Comparison of Different Sliding Directions on (001) and (111) Surfaces Using MD and AFM," Langmuir 23(2007):5394-5405; http://pubs.acs.org/cgi-bin/abstract.cgi/langd5/2007/23/i10/abs/la062254p.html.

[725] "Section 10.4.4. Properties of loaded bearings," in: K. Eric Drexler, Nanosystems: Molecular Machinery, Manufacturing, and Computation, John Wiley & Sons, New York, 1992, pp. 288-289.

[726] Guangtu Gao, Rachel J. Cannara, Robert W. Carpick, Judith A. Harrison, "Atomic-Scale Friction on Diamond: A Comparison of Different Sliding Directions on (001) and (111) Surfaces Using MD and AFM," Langmuir 23(2007):5394-5405; http://pubs.acs.org/cgi-bin/abstract.cgi/langd5/2007/23/i10/abs/la062254p.html.

[727] J.A. Harrison, C.T. White, R.J. Colton, D.W. Brenner, "Molecular-dynamics simulations of atomic-scale friction of diamond surfaces," Phys. Rev. B 46(October 1992):9700-9708.

[728] A.N. Kolmogorov, V.H. Crespi, "Smoothest bearings: interlayer sliding in multiwalled carbon nanotubes," Phys. Rev. Lett. 85(27 November 2000):4727-4730.

[729] Rachel J. Cannara, Matthew J. Brukman, Katherine Cimatu, Anirudha V. Sumant, Steven Baldelli, Robert W. Carpick, "Nanoscale Friction Varied by Isotopic Shifting of Surface Vibrational Frequencies," Science 318(2 November 2007):780-783; http://lib.bioinfo.pl/pmid:17975061. See also: " 'Heftier' Atoms Reduce Friction At The Nanoscale, Study Reveals," ScienceDaily, 2 November 2007; http://www.sciencedaily.com/releases/2007/11/071101170719.htm.

[730] Anisoara Socoliuc, Enrico Gnecco, Sabine Maier, Oliver Pfeiffer, Alexis Baratoff, Roland Bennewitz, Ernst Meyer, "Atomic-Scale Control of Friction by Actuation of Nanometer-Sized Contacts," Science 313(14 July 2006):207-210. See also: "Towards frictionless nanomachines," PhysicsWorld.com, 14 July 2006, http://physicsworld.com/cws/article/news/25348.

MEMS components has been observed using 1-pentanol as a "lubricant" molecule.[731] Further insight into the scale of the problem and any specific design constraints it might impose should be obtained by quantitative molecular dynamic simulations of simple, driven nanomechanical systems. Even modest values of friction could compromise nanomachine operation by generating high levels of local heating which might lessen the chemical stability of such devices. Leakage of energy from the driving modes of the machines into the random, higher frequency vibrational modes that constitute heat may occur whenever the chemical bonds are stretched beyond the range over which they are well approximated by a harmonic potential (i.e., obeying Hooke's law), though it appears possible to design systems where the desired modes and the dissipative modes are sufficiently decoupled to allow 99%+ efficiency, far superior to analogous macroscale systems. The degree of C-H surface polarization[732] could also affect adhesion forces by enhancing electrostatic interactions.[733]

(E) Need literature review, definitive simulations, and a comprehensive assessment of radiation damage effects on the reliability of diamondoid mechanical structures and operations. Molecular dynamics simulations[734] indicate that the damage threshold energy needed to displace a single atom is well above simple estimates based on the diamond cohesive energy, and other estimates of radiation damage rates for diamond have been published.[735]

---

[731] D.B. Asay, M.T. Dugger, S.H. Kim, "In-situ Vapor-Phase Lubrication of MEMS," Tribol. Lett. 29(2008):67-74, http://www.springerlink.com/content/h54162x11560v171/?p=340ce184268046a9bb959a68d3caa814&pi=7 ; D.B. Asay, M.T. Dugger, J.A. Ohlhausen, S.H. Kim, "Macro- to Nano-scale Wear Prevention via Molecular Adsorption," Langmuir 24(2008):155-159, http://pubs.acs.org/cgi-bin/abstract.cgi/langd5/2008/24/i01/abs/la702598g.html. See also: Rachel Courtland, "Helping a micromachine to work," Nature News, 7 April 2008, http://www.nature.com/news/2008/080407/full/news.2008.740.html.

[732] J. Urban, unpublished results cited in: Guangtu Gao, Rachel J. Cannara, Robert W. Carpick, Judith A. Harrison, "Atomic-Scale Friction on Diamond: A Comparison of Different Sliding Directions on (001) and (111) Surfaces Using MD and AFM," Langmuir 23(2007):5394-5405, http://pubs.acs.org/cgi-bin/abstract.cgi/langd5/2007/23/i10/abs/la062254p.html.

[733] Guangtu Gao, Rachel J. Cannara, Robert W. Carpick, Judith A. Harrison, "Atomic-Scale Friction on Diamond: A Comparison of Different Sliding Directions on (001) and (111) Surfaces Using MD and AFM," Langmuir 23(2007):5394-5405; http://pubs.acs.org/cgi-bin/abstract.cgi/langd5/2007/23/i10/abs/la062254p.html.

[734] W. Wu, S. Fahy, "Molecular-dynamics study of single-atom radiation damage in diamond," Phys. Rev. B 49(February 1994):3030-3035.

[735] David Saada, Joan Adler, R. Kalish, "Computer simulation of damage in diamond due to ion impact and its annealing," Phys. Rev. B 59(March 1999):6650-6660.

3.3.9 Task II-8: Design and Demonstrate Fabrication Sequences for Complex Diamondoid Nanoparts and Other Specialized Structures

Task II-8 is to design and experimentally demonstrate diamondoid mechanosynthesis (DMS) fabrication sequences for manufacturing complex diamondoid nanoparts, using the toolheads (Task II-5), grippers (Task II-4) and release surfaces (Task II-3) developed earlier in Phase II, building on the experience previously gained by completing Task II-7.

There are two general classes of nanoparts to be fabricated. First, path-critical nanoparts consisting of components needed to build and operate a nanoscale manipulation system such as the one that will be introduced in Phase III (Section 3.4) – such as nanoparts needed to build nanomotors, nanomanipulator mechanisms, DMS tooltips for fabrication, and the tooltip end-effectors for assembly – are of highest priority and should be demonstrated first. We also need designs and procedures for fabricating nanoscale actuators. (These designs should be generated in contemplation of the need for future large-scale integration of the actuators into nanoscale machinery, and should include consideration of possible future multi-actuator systems.) Second, non-critical nanoparts consisting of components needed to build and operate a more generalized manufacturing system such as nanoparts for sorting rotors and nanopumps, are of lower priority and may be demonstrated later. Some of these structures may require assembly to complete, hence Task II-8 should probably be performed in tandem with Task II-2 and Task II-9.

An experimental demonstration of the fabrication of several additional specialized diamondoid structures (that may also be required to complete our development program) are more challenging and will require further study to successfully construct,[736] including:

(A) **Concave structures**. Highly concave structures, such as inside corners or cavities inside blocks, might be difficult for tools in the existing minimal toolset[737] to reach due to steric constraints. This may include nanoparts having concave features suitable for mechanically interlocking adhesive interfaces. However, it may be possible to build most such structures by judicious design of the fabrication sequence, with fabrication proceeding in successive planar layers to incorporate concavities and other necessary inclusions while avoiding the premature creation of sterically inaccessible locations. Also, the proposed minimal toolset is sufficiently versatile to fabricate additional tools, including specialized asymmetrical tool structures that could afford access to otherwise inaccessible geometries or processes, and in principle also a wider toolset capable of manipulating atoms other than C/Ge/H.

(B) **Thin-walled structures**. In the limit of highly cribriform, foamy, or fenestrated zeolite-like diamondoid structures (e.g., Figure II-2),[738] it may be difficult to apply the necessary

---

[736] Robert A. Freitas Jr., Ralph C. Merkle, "A Minimal Toolset for Positional Diamond Mechanosynthesis," J. Comput. Theor. Nanosci. 5(May 2008):760-861.

[737] Robert A. Freitas Jr., Ralph C. Merkle, "A Minimal Toolset for Positional Diamond Mechanosynthesis," J. Comput. Theor. Nanosci. 5(May 2008):760-861.

[738] "NanoDiamond" website, accessed March 2008; http://www.domaindirections.com/members/nanodiamond/introduction.html.

forces without disrupting the thin walls (perhaps 1-2 atomic layers thick) of neighboring cells. Such thin-walled structures (e.g., a graphene sheet stretched across a concave void) may also be subject to rearrangements as normally occur on the clean or hydrogenated C(100) or the clean C(111) diamond surfaces. In many cases, these changes might be only transitional if adding additional bonds to build a successive layer can restore the original desired underlying crystal structure. Weak-force Ge-based handles might also be employed as temporary jigs to enhance stiffness during fabrication, then later be removed with minimal disruption.

Figure II-2. "NanoDiamond" – an example of fenestrated zeolite-like diamondoid structures. Courtesy of Michael Richards.[739]

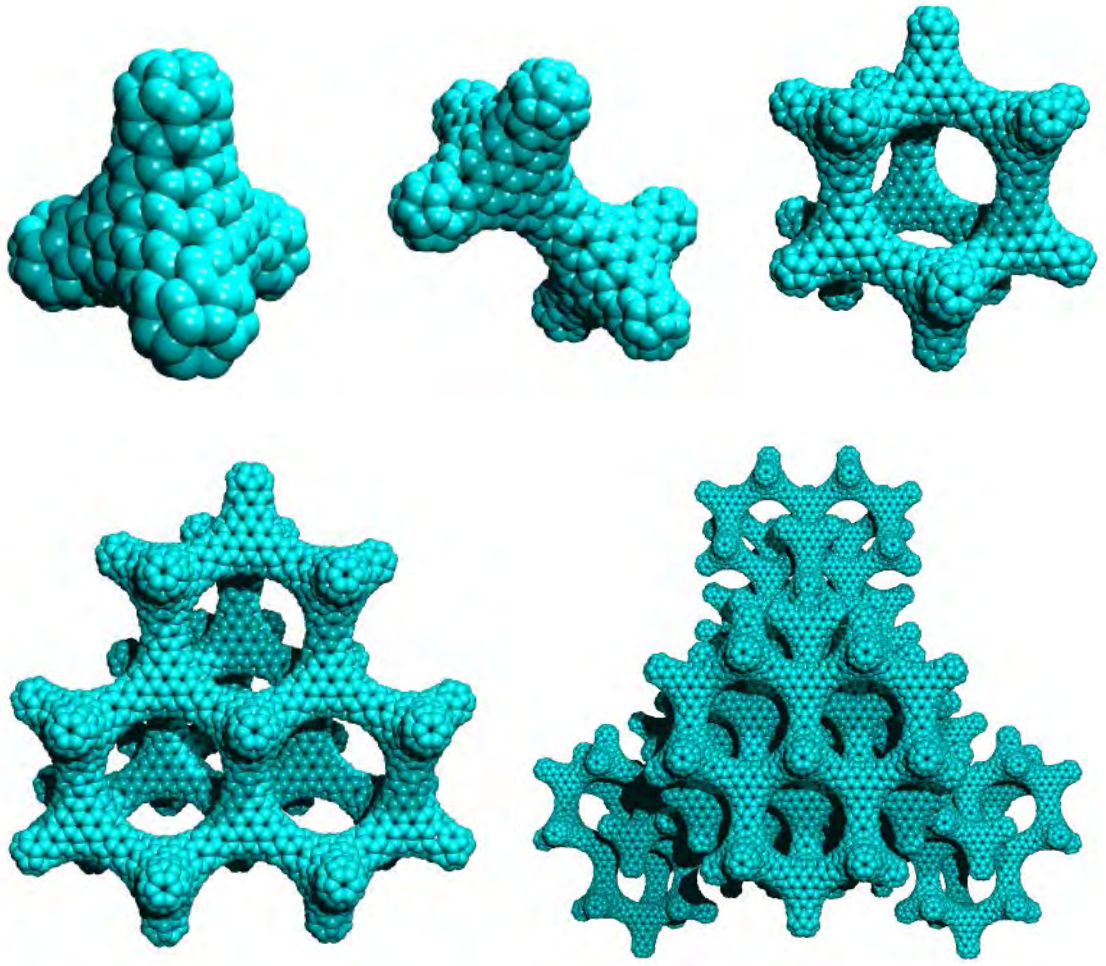

[739] "NanoDiamond" website, accessed March 2008; http://www.domaindirections.com/members/nanodiamond/introduction.html.

(C) **Curved shell structures**. Curved shell diamond structures incorporating carefully targeted crystal dislocations to relieve internal strain will be challenging to build because of competing lattice rearrangements at almost every step, and the addition of Ge atoms to diamond structures will enable even more complex potentially pathological rearrangements. The extent of all rearrangements that may occur during a given construction sequence must be taken into account during fabrication sequence planning.

(D) **Strained-shell structures**. Strained-shell structures, including rotationally symmetric structures useful for bearings and gears, may require specialized restraints, jigs, and other tools, whether to maintain constant strain during fabrication or to apply temporary strain to a partially completed structure. Such operations may create complex strain gradients throughout the workpiece that may alter the effectiveness of the forces applied by mechanosynthetic tools, and may require the creation of new tools that can apply greater or lesser forces during specified operations in particular geometries. Detailed simulations will be required for each reaction step.

(E) **Detachable and embedded nonbonded structures**. Structures such as isolated nanoparts that are intended to be fabricated on a surface, then detached from that surface and transported elsewhere for further mechanosynthetic processing or for assembly into larger multipart mechanical systems, must be fabricated on jigs or surfaces that allow for convenient release of the finished nanopart without disturbing its molecular structure. Provision must also be made for additional tools that are capable of securely grasping the finished nanopart, transporting the nanopart to its remote destination, maintaining the nanopart in the preferred orientation at all times during transport, and releasing the transported nanopart once it has reached its destination. Unitary fabrication of nonbonded embedded components (e.g., a freely rotating bearing inside a race) will also require further study.

3.3.10 Task II-9: Design and Demonstrate Assembly Sequences for Assembling Diamondoid Nanoparts into Nanodevices

Task II-9 is to assemble from nanoparts the multipart nanodevices that have been designed, simulated, and validated in the Standard Registry (Section 3.3.2), possibly using a revised gripper. Here we must demonstrate the ability to assemble mechanical nanoparts fabricated earlier in Phase I/II into multipart nanodevices as one-offs (no parallelization). This may require the extension or redesign of existing actuated gripper end-effectors that are used to reversibly grip multiple types of nanoparts and to hold them rigidly enough to be able to reliably fit them together mechanically to make simple multi-part nanodevices.

There are two general classes of nanodevices to be assembled from their constituent nanoparts. First, path-critical nanodevices consisting of components needed to build and operate a nanoscale manipulation system such as the one that will be introduced in Phase III (Section 3.4) – such as multipart nanodevices needed to build nanomotors, nanomanipulator mechanisms, and the tooltip end-effectors for assembly – are of highest priority and should be demonstrated first. We also need designs and procedures for assembling nanoscale actuators. (These designs should be generated in contemplation of the need for future large-scale integration of the actuators into nanoscale machinery, and should include consideration of possible future multi-actuator systems.) Second, non-critical nanodevices consisting of components needed to build and operate a more generalized manufacturing system such as nanodevices for sorting rotors and nanopumps, are of lower priority and may be demonstrated later. The requirements for efficient assembly may

require redesign of some nanoparts, hence Task II-9 should probably be performed in tandem with Task II-2 and Task II-8.

A general program for defining methods for nanoscale assembly operations might involve designing specific manipulation primitives and developing simulation models for verifying manipulation strategies.[740] A number of problems must be solved including the development of repeatable manipulation maneuvers using multiple nanoprobes and precision motion control, including multiprobe manipulation strategies that are needed to properly constrain a nanostructure during assembly.[741] With three nanoprobes available, two can be used to grip a nanostructure while the third is used to rotate the nanostructure about the gripping point.[742] Current research on these and related issues is still in its infancy. For instance, Sitti and Hashimoto[743] have modeled the mechanical interactions between an AFM tip and nanoparticles during manipulation on a substrate, and used these results to improve manipulation – an approach that has also been extended by the Requicha group to include the assembly of polymer nanoparticles and their subsequent thermal bonding.[744] Another approach to AFM nanomanipulation uses a sharp-tipped nanoprobe that can be positioned with nanometer resolution for micromanipulation,[745] wherein the manipulation of nanostructures (e.g., pushing with the tip of a sharp probe) is visualized via SEM without the occlusion that normally occurs using cantilever-type probes. Zyvex[746] and others[747] (see Section 2.2.3.2) have experimented

---

[740] Jason J. Gorman, Yong-Sik Kim, András E. Vladár, Nicholas G. Dagalakis, "Design of an on-chip microscale nanoassembly system," Int. J. Nanomanufacturing 1(2007):710-721.

[741] Jason J. Gorman, Yong-Sik Kim, András E. Vladár, Nicholas G. Dagalakis, "Design of an on-chip microscale nanoassembly system," Int. J. Nanomanufacturing 1(2007):710-721.

[742] Jason J. Gorman, Yong-Sik Kim, András E. Vladár, Nicholas G. Dagalakis, "Design of an on-chip microscale nanoassembly system," Int. J. Nanomanufacturing 1(2007):710-721.

[743] M. Sitti, H. Hashimoto, "Controlled pushing of nanoparticles: modeling and experiments," IEEE/ASME Transactions on Mechatronics 5(2000):199-211.

[744] E. Harel, S.E. Meltzer, A.A.G. Requicha, M.E. Thompson, B.E. Koel, "Fabrication of polystyrene latex nanostructures by nanomanipulation and thermal processing," Nanoletters 5(2005):2624-2629.

[745] T. Kasaya, H.T. Miyazaki, S. Saito, K. Koyano, T. Yamaura, T. Sato, "Image-based autonomous micromanipulation system for arrangement of spheres in a scanning electron microscope," Rev. Sci. Instrum. 75(2004):2033-2042.

[746] G. Skidmore, M. Ellis, A. Geisberger, K. Tsui, R. Saini, A. Mercanzini, N. Sarkar, R. Folaron, J. Randall, "MEMS Tools That Enable Precision Automated Microassembly," Sensors Expo and Conference, Chicago IL, June 2003; K. Kim, A. Geisberger, M. Chiew, K. Bray, K. Tham, M. Ellis, G. Skidmore, T. Khoury, H. Lu, S. Park, J-B. Lee, "Development of metallic microgrippers as end-effectors for micro/nano assembler," 5th Intl. Workshop on High Aspect Ratio Microstructure Technology, Monterey CA, June 2003; K. Tsui, A. Geisberger, M. Ellis, G. Skidmore, "Calibration Systems and Techniques for Automated Microassembly," Proc. InterPack2003, 2003 International Electronic Packaging Technical Conferences and Exhibition, Maui, Hawaii, July 2003; Ho Lee Woo, Hun Kang Byoung, Seok Oh Young, H. Stephanou, A.C. Sanderson, G. Skidmore, M. Ellis, "Micropeg manipulation with a compliant microgripper," Proc. ICRA '03, IEEE International Conference on Robotics and Automation, September 2003; George D. Skidmore, Matthew Ellis, Aaron Geisberger, Ken Tsui, Kimberly Tuck, Rahul Saini, Tushar Udeshi,

with software and techniques for automated microassembly – the automated assembly of MEMS components into larger multicomponent microscale structures.

Early experimental proof-of-principle and subsequent positional assembly demonstration benchmarks include:

(A) Need experimental demonstration of ability to accurately find and retrieve input nanoparts from a parts presentation (assembly) surface or parts depot.

(B) Need experimental demonstration of purely mechanical joining of two or more nanoparts into a more complex product object.

(C) Need experimental demonstration of ability to stably place finished assembled product objects onto a product storage surface or product depot, in a known location and orientation.

(D) Need experimental demonstration of purely nanomechanical insertion and/or threading operation.

(E) Need experimental demonstration of the ability to acquire two product objects and join them together to form a more complex product object.

(F) Need development and manufacture of actuated tip end-effector structures able to reversibly grip multiple types of nanoparts and to hold them rigidly enough to be able to fit them together mechanically to make simple multi-part nanodevices.

(G) Need to design and build an assembly surface. We need a reversible assembly surface: (1) upon which nanoparts and nanodevices can be stored/parked/warehoused until needed for some other purpose and then easily picked up off that surface, or (2) which can act as a jig during an assembly sequence, in effect constraining the motion of one part while another part is forced into mechanical contact with it (e.g., to press-fit an axle into a ring bearing). Both of these abilities of the assembly surface must be designed and then demonstrated experimentally on specific examples of interest.

Michael Nolan, James von Ehr, "Assembly Technology Across Multiple Length Scales From the Micro-scale to the Nano-scale," IEEE MEMS 2004 Technical Digest, pp 588-592; Kenneth Tsui, Aaron A. Geisberger, Matt Ellis, George D. Skidmore, "Micromachined end-effector and techniques for directed MEMS assembly," J. Micromech. Microeng. 14 (2004):542-549, http://dx.doi.org/10.1088/0960-1317/14/4/015; K. Kim, E. Nilsen, T. Huang, A. Kim, M. Ellis, G. Skidmore, J.-B. Lee, "Metallic microgripper with SU-8 adaptor as end-effectors for heterogeneous micro/nano assembly applications," Microsystem Technologies 10(December 2004):689-693; N. Sarkar, D. Yan, E. Horne, H. Lu, M. Ellis, J.B. Lee, R. Mansour, A. Nallani, G. Skidmore, "Microassembled tunable MEMS inductor," MEMS 2005, 18th IEEE International Conference on Micro Electro Mechanical Systems, pp. 183-186.

[747] D.O. Popa, H.E. Stephanou, "Micro- and Meso-Scale Robotic Assembly", SME J. Manufacturing Processes 6(2004):52-71; J. Sin, H.E. Stephanou, "A Parallel Micromanipulation Method for Microassembly," SPIE Conference on Micromachining and Microfabrication, 2001, pp.158-164.

(H) Design and simulation of nanopart feedstock presentation systems. Need to design and simulate the presentation of nanoparts tethered to fixed surfaces, for easy pickup by assembly tools, as well as the range of motions and procedures for acquiring nanoparts onto a positionally controlled assembly tool from a nanopart presentation surface.

(I) Design and simulation of nanopart assembly sequences. Need to design the sequences of assembly steps required to assemble a specific collection of parts into a specific assembled object, per blueprint plan. This includes should include motions relevant to parts acquisition and stowage of finished product object in depot areas.

(J) Atomic rearrangements and pathologies in juxtaposed nanoparts. Need quantum chemistry and molecular dynamics analyses of possible reconstructions (and chemical stability) of moving nanoparts that are placed in intimate contact with other moving nanoparts during assembly operations.

(K) Principles of “design automation,” “design for assembly” and “Design for Manufacturability” (DFM) should be explicitly incorporated into the aforementioned subtasks and objectives.

Successful accomplishment of Task II-9 (and all previous Phase II Tasks) completes the development of the Phase II macroscale manufacturing workstation (MMW).

3.4 Phase III: First-Generation Nanoscale Fabrication Workstation (NFW)

The key objective of Phase III is to build, on an atomically precise multi-electrode assembly surface, the first-generation nanoscale fabrication workstation (NFW) – a set of individually controlled nanoscale manipulators and toolheads capable of performing diamondoid mechanosynthesis inside a UHV workspace chamber, powered by electrical control signals passed through the assembly surface via electrical surface contact points, with material feedstock provided via manual handoff from the macroscale MMW workstation developed in Phase II. Note that the DMS fabrication of nanoparts does not take place on the silica surface but on the Phase II release surface, with nanoparts and assembled nanodevices later assembled into a working NFW unit on the silica surface – this SiO_2 surface is an assembly surface, not a fabrication surface. The Phase III system should provide a general capacity for fabricating atomically precise complex diamondoid product objects roughly as complex as itself, up to ~31 million atoms (e.g., see Table III-2), as one-off structures composed of nanoparts and multipart nanodevices.

The NFW is described in Section 3.4.1 and illustrated in Figure III-1. This is followed by an enumeration of the specific tasks required to manufacture an NFW which include: design and simulation of the first-generation NFW (Section 3.4.2), preparation of a multielectrode assembly surface (Section 3.4.3), fabrication of needed nanoparts and assembly of needed multipart nanodevices using the Phase II system (Section 3.4.4), the manual assembly of the first NFW using the Phase II system (Section 3.4.5), and finally the demonstrated successful operation of the first-generation NFW using the Phase II System (Section 3.4.6).

3.4.1 Description of the NFW First-Generation Workstation

The structure and basic function of the first-generation nanoscale fabrication workstation (NFW) is described in this Section.

The function of a completed diamondoid NFW is to fabricate nanoparts using a set of individually controlled nanoscale manipulators grasping DMS toolheads capable of performing diamondoid mechanosynthesis. The NFW builds diamondoid nanoparts starting from basic feedstock molecules presented to it via manual handoff from the macroscale workstation developed in Phase II. In this phase of the program we initially assume that all atomically precise components will be comprised solely of carbon (C), hydrogen (H), or germanium (Ge) atoms. Relaxing this constraint to allow the use of additional chemical elements would change a few specific details of this program but should not significantly alter the overall system design which incorporates numerous general-purpose features that are equally applicable to structures employing additional chemical elements.

3.4.1.1 Basic Description of the NFW

The basic NFW is contained within a volume measuring ~10^6 nm^3 and is assumed in the baseline design to occupy a square footprint measuring 100 nm x 100 nm = 10,000 nm^2 in area on an atomically precise multi-electrode assembly surface. To perform all diamondoid mechanosynthesis (DMS) reaction sequences as described by Freitas and Merkle[748] the NFW requires a minimum of three independent positionally controlled DMS manipulators capable of atomically precise tooltip placement to 0.2-0.5 Å repeatable accuracy and with at least 5 DOF (degrees of freedom). The manipulators must also be able to reversibly grasp and release a DMS toolhead (Section 3.3.6), and must be able to acquire toolheads from, and stow toolheads in, an airtight toolrack. A fourth manipulator with slightly longer reach is used to hold the workpiece steady while mechanosynthetic operations are being performed on it, to pass completed diamondoid nanoparts out of the local DMS work volume to an exogenous manipulator or to place completed nanoparts in an open space on the adjacent silica assembly surface for later retrieval, to manually operate mechanical switches appurtenant to the NFW, and for other support functions. Electrical power and control signals are applied to NFW mechanisms via carbon nanotube wires that connect conductive silver terminals on the atomically smooth silica assembly surface (see Section 3.4.3) to electrostatic motors that actuate the manipulators.

Figure III-1. Schematic illustration of the Nanoscale Fabrication Workstation (NFW), showing four Stewart platform manipulators mounted on a foundation block adjacent to a 20-tip toolrack.

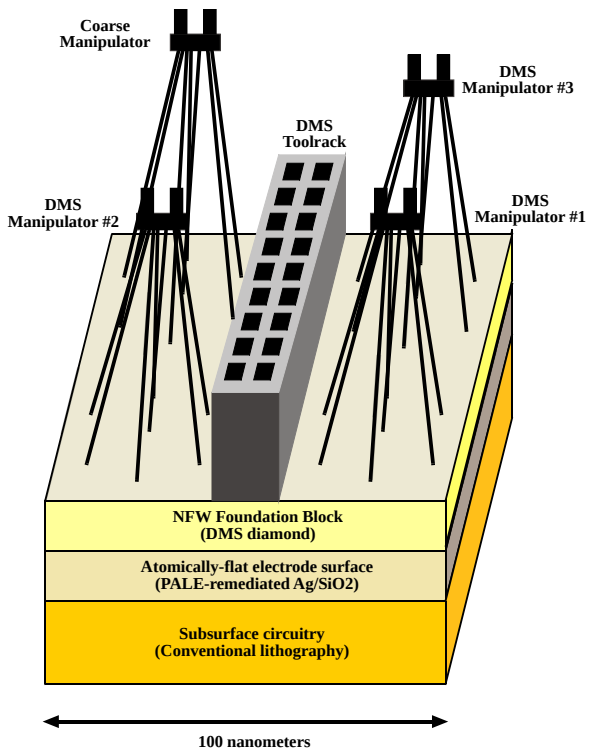

[748] Robert A. Freitas Jr., Ralph C. Merkle, "A Minimal Toolset for Positional Diamond Mechanosynthesis," J. Comput. Theor. Nanosci. 5(May 2008):760-861.

Figure III-2. A generic schematic illustration of a nanoscale Stewart platform (from Drexler, *Nanosystems*[749]). The Stewart platforms in this proposal use threaded cylindrical extensible struts instead of the square rods shown here.

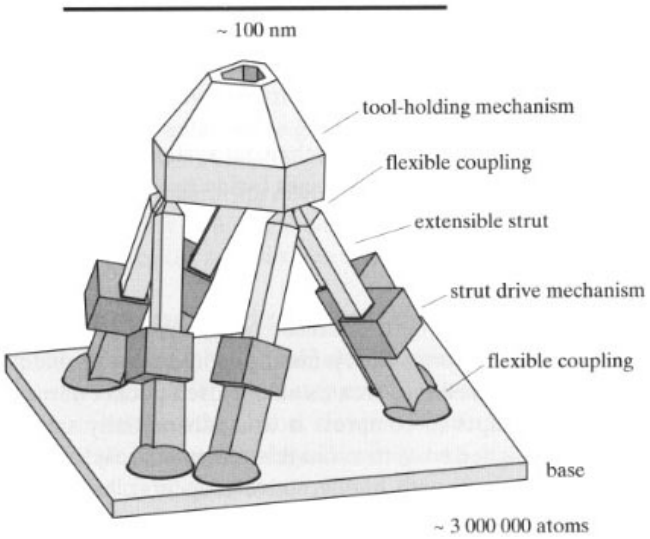

Each of the three DMS manipulators is a Stewart platform (Figure III-2) capable of ~0.2 Å incremented motions at the tip (with smaller motion increments potentially available if needed by mechanically arranging for only the first electrical drive pulse of a pulse train to always trigger a half-step movement in either the extension or retraction directions but not both.) Each DMS manipulator consists of a tool chuck mounted via universal joints to 6 telescoping struts which in turn are mounted at their base to universal joints affixed to the foundation block which lies atop the assembly surface floor (Figure III-3), allowing each DMS manipulator 6 DOF (3 translational, 3 rotational) mobility. The tool chuck has just two states – closed (to grasp) and open (to release) – and a 7th telescoping strut is used to control this simple end effector, allowing interchangeable toolheads to be grasped or released by the tool chuck.

Each telescoping strut is a matched pair of internally-threaded and externally threaded tubes. (Examples of molecular screw drives (Figure III-4) are well-known in biology.[750]) A rotary

---

[749] K. Eric Drexler, Nanosystems: Molecular Machinery, Manufacturing, and Computation, John Wiley & Sons, New York, 1992; http://www.zyvex.com/nanotech/nanosystems.html.

[750] C. Chen, P. Guo, "Sequential action of six DNA-packaging pRNA during phage phi29 genomic DNA translocation," J. Virology 71(1997):3864-3871, http://jvi.asm.org/cgi/reprint/71/5/3864?view=long&pmid=9094662; D. Shu, L. Huang, S. Hoeprich, P. Guo, "Construction of phi29 DNA-packaging RNA (pRNA) Monomers, Dimers and Trimers With Variable Sizes and Shapes as Potential Parts for Nano-devices," J. Nanosci. Nanotechnol. 3(2003):1-8, http://www.vet.purdue.edu/PeixuanGuo/papers/shu2003nanodevices.pdf.

stepper motor drives relative helical motion by turning one tube to extend or retract the strut. Each strut has a forward and a reverse rotary motor; power applied to either motor drives motion in one direction only (either extension or retraction of the strut), with operation of either one of the motor pair mechanically disengaging the other motor in the pair, allowing the tubes to slide freely in the new direction. The chuck control strut uses a single motor which operates the chuck gripper as a bistable switch between open and closed positions. Since movement of the platform involves rotation that could in principle trigger an undesired change of state in the gripper due to relative motion between the platform and the gripper control strut, the strut/gripper linkage will be designed so that a full 360° of strut rotation is necessary to trigger a gripper state change, making accidental triggering impossible because the platform cannot be continuously rotated through 360°. (Rather than two mutually threaded tubes, the chuck control strut may more resemble a nonthreaded trombone with a coaxial slot and pin.) Each DMS manipulator therefore requires (6 x 2) + 1 = 13 rotary motors to control all manipulator actions.

Figure III-3. Schematic illustration of the NFW assembly surface. An array of silver electrodes are embedded in an insulating silicon dioxide surface layer that has been remediated by PALE processing to atomically smoothness. The electrodes connect to multiple layers of electronic circuitry below the topmost insulating layer, which are fabricating using conventional lithographic techniques.

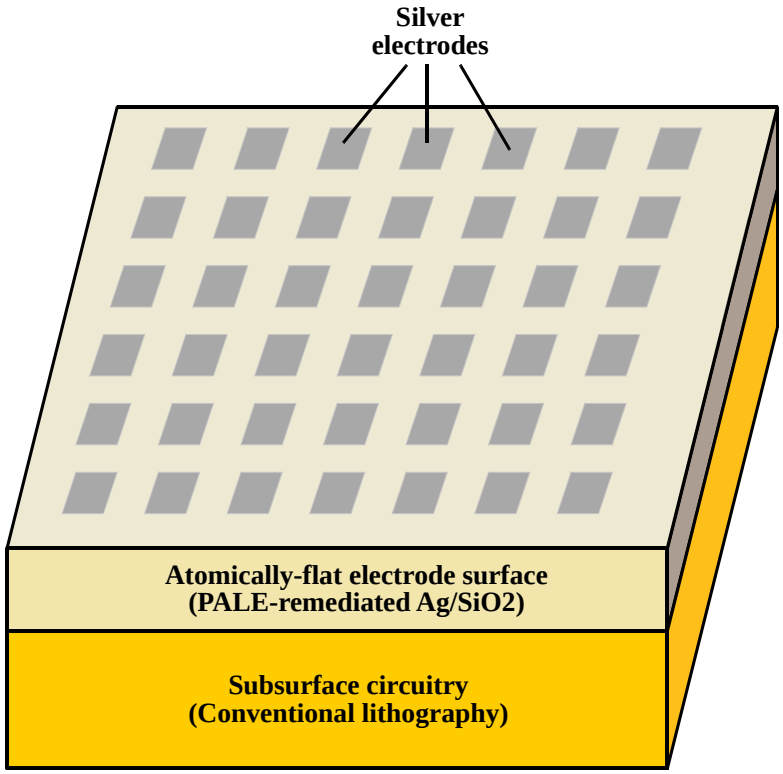

Figure III-4. The ø29 motor (yellow) compresses coiled lengths of DNA into the viral capsid to 6,000 times its normal volume, creating pressure 10 times as powerful as that inside a champagne bottle. Image credit: Carlos Bustamante of Berkeley Lab's Physical Biosciences Division.

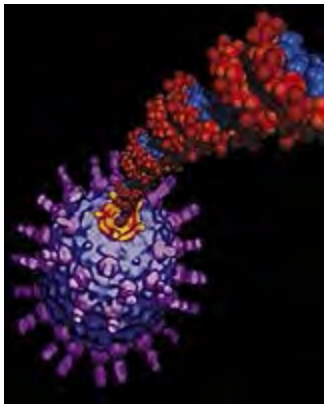

For scaling purposes, the externally threaded tube at the distal end of each strut is taken as a cylindrical rod 5 nm wide and 50 nm long (982 nm^3 of solid diamondoid material volume, 825 nm^2 passivated diamondoid surface area), surrounded near the base by an internally threaded tube at the proximal end of each strut which is taken as a 10 nm external diameter and 5 nm internal diameter annular cylindrical strut sheath into which the distal rod may be screwed, measuring 50 nm long with 50% material cutout (1473 nm^3 of solid diamondoid material volume, ~2474 nm^2 passivated diamondoid surface area) allowing a reach extension range for the strut (composed of sheath + rod) of 50-90 nm for 0%-80% extension. Each screw thread is assumed to have a 10:1 helix, with rotation through a π(5 nm) ~ 16 nm circumferential distance producing ~1.6 nm of forward motion of the screw.

Each strut is electrically driven by one or two rotary stepper motors. For scaling purposes, each rotary motor is assumed to consist of four parts (rotor, stator, output gear, and housing) and to fit within a box requiring a solid diamondoid material volume of ~200 nm^3 and ~500 nm^2 of passivated diamondoid surface area per motor. We envision using an electrostatic motor nominally comprised of charged nested nanotubes. Electrostatically-driven carbon nanotube-based nanomotors have been fabricated and demonstrated experimentally[751] including arrays of

---

[751] A.M. Fennimore, T.D. Yuzvinsky, Wei-Qiang Han, M.S. Fuhrer, J. Cumings, A. Zettl, "Rotational actuators based on carbon nanotubes," Nature 424(24 July 2003):408-410; http://socrates.berkeley.edu/~tyuz/pub/nature424.pdf. T.D. Yuzvinsky, A.M. Fennimore, A. Kis, A. Zettl, "Controlled placement of highly aligned carbon nanotubes for the manufacture of arrays of nanoscale torsional oscillators," *Nanotechnology 17(2006):*434-438; http://socrates.berkeley.edu/~tyuz/pub/nanotechnology17.pdf. Amelia Barreiro, Riccardo Rurali, Eduardo R. Hernández, Joel Moser, Thomas Pichler, Laszlo Forro, Adrian Bachtold, "Subnanometer Motion of Cargoes Driven by Thermal Gradients Along Carbon Nanotubes," ScienceExpress, 10 April 2008; http://www.sciencemag.org/cgi/rapidpdf/1155559v1.pdf. B. Bourlon, D.C. Glattli, C. Miko, L. Forro, A. Bachtold, "Carbon Nanotube Based Bearing for Rotational Motions," Nano Lett. 4(2004):709; http://www.nanocat.org/dataeng/recerca/qnepriv/images/nanoletter.pdf. S.J. Papadakis, A.R. Hall, P.A. Williams, L. Vicci, M.R. Falvo, R. Superfine, S. Washburn, "Resonant Oscillators with carbon-nanotube

such nanomotors[752] (Figure III-5); related experimental demonstrations include nanotube switches,[753] mass conveyors,[754] and nanotube-based resonators operating at nearly ~200 MHz[755] and even 1-4 GHz[756] frequencies. Current-carrying carbon nanotubes possess extraordinary thermal stability.[757]

Figure III-5. Examples of experimentally proven electrically-driven carbon nanotube-based nanomotors.[758]

---

torsion springs," Phys. Rev. Lett. 93(2004):146101; http://www.physics.unc.edu/~falvo/papers/2004_MWNToscillators-PRL.pdf.

[752] T.D. Yuzvinsky, A.M. Fennimore, A. Kis, A. Zettl, "Controlled placement of highly aligned carbon nanotubes for the manufacture of arrays of nanoscale torsional oscillators," *Nanotechnology 17(2006):*434-438; http://socrates.berkeley.edu/~tyuz/pub/nanotechnology17.pdf.

[753] V.V. Deshpande, H.-Y. Chiu, H.W. Ch. Postma, C. Mikó, L. Forró, M. Bockrath, "Carbon Nanotube Linear Bearing Nanoswitches," Nano Lett. 6(June 2006):1092-1095; http://nanoscale.caltech.edu/publications/pdf/deshpandeetal.pdf.

[754] B.C. Regan, S. Aloni, R.O. Ritchie, U. Dahmen, A. Zettl, "Carbon nanotubes as nanoscale mass conveyors," Nature 428(2004):924-927; http://www.physics.berkeley.edu/research/zettl/projects/mass_conveyor/nature02496.pdf or http://leitl.org/docs/nano/nature02496.pdf. K. Svensson, H. Olin, E. Olsson, "Nanopipettes for Metal Transport," Phys. Rev. Lett. 93(2004):145901; http://isis.ku.dk/kurser/blob.aspx?feltid=29300. D. Golberg, P.M.F.J. Costa, M. Mitome, C. Mueller, S. Hampel, A. Leonhardt, Y. Bando, "Copper-filled carbon nanotubes: rheostat-like behavior and femtogram copper mass transport," Adv. Mat. 19(2007):1937-1942.

[755] Vera Sazonova, Yuval Yaish, Hande Üstünel, David Roundy, Tomás A. Arias, Paul L. McEuen, "A tunable carbon nanotube electromechanical oscillator," Nature (London) 431(2004):284-287; https://www.andrew.cmu.edu/user/asurie/15398/nt-oscillator.pdf.

[756] H.B. Peng, C.W. Chang, S. Aloni, T.D. Yuzvinsky, A. Zettl, "Ultrahigh frequency nanotube resonators," Phys. Rev. Lett. 97(2006):087203; http://socrates.berkeley.edu/~tyuz/pub/prl97.pdf. H.B. Peng, C.W. Chang, S. Aloni, T.D. Yuzvinsky, A. Zettl, "Microwave electromechanical resonator consisting of clamped carbon nanotubes in an abacus arrangement," Phys. Rev. B 76(2007):035405; http://socrates.berkeley.edu/~tyuz/pub/prb76.pdf.

[757] G.E. Begtrup, K.G. Ray, B.M. Kessler, T.D. Yuzvinsky, H. Garcia, A. Zettl, "Extreme thermal stability of carbon nanotubes," Physica Status Solidi B 244(2007):3960; http://socrates.berkeley.edu/~tyuz/pub/pssb244.pdf.

[758] A.M. Fennimore, T.D. Yuzvinsky, Wei-Qiang Han, M.S. Fuhrer, J. Cumings, A. Zettl, "Rotational actuators based on carbon nanotubes," Nature 424(24 July 2003):408-410; http://socrates.berkeley.edu/~tyuz/pub/nature424.pdf. T.D. Yuzvinsky, A.M. Fennimore, A. Kis, A. Zettl, "Controlled placement of highly aligned carbon nanotubes for the manufacture of arrays of nanoscale torsional oscillators," Nanotechnology 17(2006):434-438; http://socrates.berkeley.edu/~tyuz/pub/nanotechnology17.pdf. Amelia Barreiro, Riccardo Rurali, Eduardo R. Hernández, Joel Moser, Thomas Pichler, Laszlo Forro, Adrian Bachtold, "Subnanometer Motion of Cargoes Driven by Thermal Gradients Along Carbon Nanotubes," ScienceExpress, 10 April 2008;

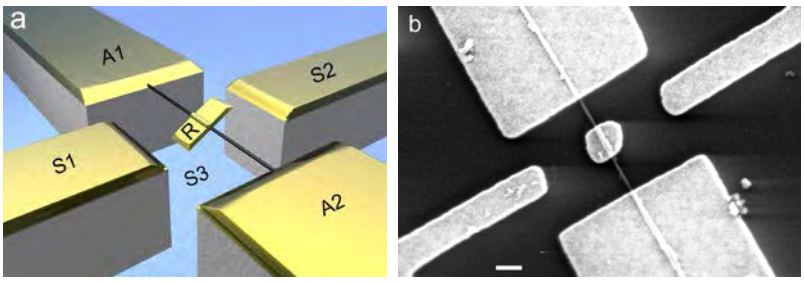

Nanotube-based rotational actuator (Fennimore et al.[759])

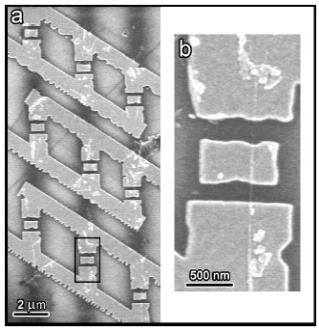

Array of nanotube actuators (Yuzvinsky et al.[760])

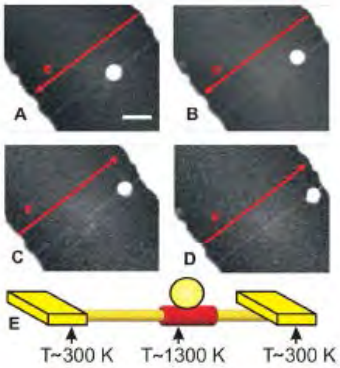

Gold cargo translating on nanotube via electrothermal actuation (Barreiro et al.[761])

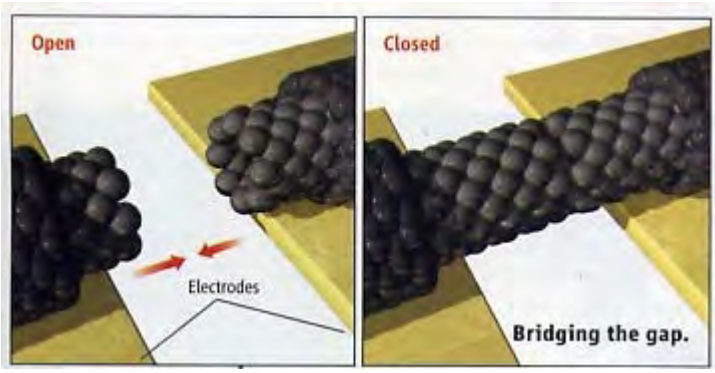

Raising voltage between opposed multiwall carbon nanotubes from 4.5 V (at left) to 5-10 V (at right) produces a charge-induced sliding of the inner tubes through the outer shells and across the gap (Deshpande et al.[762])

---

http://www.sciencemag.org/cgi/rapidpdf/1155559v1.pdf. V.V. Deshpande, H.-Y. Chiu, H.W. Ch. Postma, C. Mikó, L. Forró, M. Bockrath, "Carbon Nanotube Linear Bearing Nanoswitches," Nano Lett. 6(June 2006):1092-1095; http://nanoscale.caltech.edu/publications/pdf/deshpandeetal.pdf.

[759] A.M. Fennimore, T.D. Yuzvinsky, Wei-Qiang Han, M.S. Fuhrer, J. Cumings, A. Zettl, "Rotational actuators based on carbon nanotubes," Nature 424(24 July 2003):408-410; http://socrates.berkeley.edu/~tyuz/pub/nature424.pdf.

[760] T.D. Yuzvinsky, A.M. Fennimore, A. Kis, A. Zettl, "Controlled placement of highly aligned carbon nanotubes for the manufacture of arrays of nanoscale torsional oscillators," Nanotechnology 17(2006):434-438; http://socrates.berkeley.edu/~tyuz/pub/nanotechnology17.pdf.

[761] Amelia Barreiro, Riccardo Rurali, Eduardo R. Hernández, Joel Moser, Thomas Pichler, Laszlo Forro, Adrian Bachtold, "Subnanometer Motion of Cargoes Driven by Thermal Gradients Along Carbon Nanotubes," ScienceExpress, 10 April 2008; http://www.sciencemag.org/cgi/rapidpdf/1155559v1.pdf.

In the absence of a specific motor design, purely for energy scaling purposes in this proposal we will assume the analogy of a simple mechanical dielectric drive motor[763] that involves drawing a dielectric slab of area A_{slab} and dielectric constant κ_{slab} into a gap d_{gap} between the plates of a charged capacitor at voltage V_{cap} producing a field-dependent force F_{motor}. Applying a time-varying input voltage of frequency ν_d (Hz) produces a mechanical output power of $P_{motor} = (\varepsilon_0 A_{slab} / 2 d_{gap}) (1 - \kappa_{slab}^{-1}) \nu_d V_{cap}^2 \sim 0.2$ pW (power density ~10^{12} watts/m^3), taking $\varepsilon_0 = 8.85 \times 10^{-12}$ coul/N-m^2 (vacuum permittivity constant), $A_{slab} = 100$ nm^2, $d_{gap} = 0.5$ nm, $V_{cap} = 1$ volt, $\kappa_{slab} = 5.7$ for diamond at 300 K, and $\nu_d \sim 1.2$ MHz (Section 3.4.1.4). The force generated on the slab during $\Delta x = 2$ Å displacements is therefore $F_{motor} = P_{motor} / (\Delta x\ \nu_d) \sim 1$ nN, with each control pulse rotating the threaded screw through a circumferential distance of 2 Å. This rotation produces ~0.2 Å of forward motion of the screw (per pulse) with a force of 10 nN applied to the strut (due to the 10:1 mechanical advantage), or a maximum of ~60 nN for all 6 power struts in an ideal geometry, exceeding up to tenfold the maximum mechanical force of ~5.53 nN required to effectuate DMS tooltip reactions.[764] Note also that a ~0.2 pW motor operated at ~1.2 MHz is applying a per pulse energy of ~2×10^{-19} J or ~50 k_BT/pulse at 300 K or ~200 k_BT/pulse at 80 K, which seems sufficient to ensure adequate reliability. The current delivered to each motor is $I_{motor} = P_{motor} / V_{cap} \sim 2 \times 10^{-13}$ amp.

Each motor housing is affixed to a foundation block and its output gear is attached to a universal joint which in turn connects to the base of the sheath of each strut: rotating the sheath extends or retracts the strut. For scaling purposes, each universal joint (Figure 2-47(C)) is assumed to consist of 2 parts and ~40 nm^3 of solid diamond structure with ~80 nm^2 of passivated diamondoid surface area, and the foundation blocks are allocated the equivalent of (40 nm)^2 x 10 nm thick, but using a honeycomb structure to eliminate 75% of mass, this adds 4,000 nm^3 of solid structure and ~2000 nm^2 of passivated diamondoid surface – though in the actual NFW, these blocks need not be either square or arranged coplanar. The triangular tool chuck is assumed to be a half-square of area (1/2) (20 nm)^2 at its base, 10 nm thick, and to include three integral nanoparts (housing with fixed backstop, a moving rack-mounted gripper plate, and a drive gear), adding 2500 nm^3 of solid structure and ~3000 nm^2 of passivated diamondoid surface. Electrical leads connecting control lines to each motor are 2 nm diameter unpassivated and uninsulated single-walled carbon nanotubes that are 50 nm long, adding ~314 nm^2 x ~0.154 nm thickness ~ 48 nm^3 of unpassivated carbon nanotube wire solid volume, or 96 nm^3 for each hot/ground wire pair; atom count is ~314 nm^2 x ~31 C atoms/nm^2 ~ 9734 C atoms per wire pair, with all grounding lines connected to a single common ground line of assumed equivalent length. (Bilayer graphene

---

[762] V.V. Deshpande, H.-Y. Chiu, H.W. Ch. Postma, C. Mikó, L. Forró, M. Bockrath, "Carbon Nanotube Linear Bearing Nanoswitches," Nano Lett. 6(June 2006):1092-1095; http://nanoscale.caltech.edu/publications/pdf/deshpandeetal.pdf.

[763] Robert A. Freitas Jr., Nanomedicine, Volume I: Basic Capabilities, Landes Bioscience, Georgetown, TX, 1999; Section 6.3.5, p. 155; http://www.nanomedicine.com/NMI/6.3.5.htm.

[764] Robert A. Freitas Jr., Ralph C. Merkle, "A Minimal Toolset for Positional Diamond Mechanosynthesis," J. Comput. Theor. Nanosci. 5(May 2008):760-861.

nanoribbons suppress electrical noise that arises due to Hooge's rule.[765]) Allowing an additional 907 nm^3 for unallocated diamond lattice structure gives the results for each of the three smaller manipulators as shown in Table III-1.

Table III-1. Volume and Parts Estimate for DMS Manipulator in First-Generation NFW

Nanopart or Nanodevice	Number of Com-ponents	Solid Volume each (nm^3)	# Parts / Com-ponent	Solid Volume All (nm^3)	Total # of All Parts
Strut Rods	7	982	1	6874	7
Strut Sheaths	7	1473	1	10311	7
Rotary motors	13	200	4	2600	52
Electrical leads	13	96	2	1248	26
Universal joints	14	40	2	560	28
Foundation blocks	1	4000	1	4000	1
Tool chuck	1	2500	3	2500	3
Unallocated structure	1	933	1	907	1
TOTALS	**57**			**29,000 nm^3**	**125 parts**

The fourth manipulator is a Stewart platform of similar design to the first three, but it is a coarser-incremented (~0.5 Å) manipulator capable of larger movements with longer reach, intended to be used for workpiece positioning and other ancillary tasks. For scaling purposes, the fourth manipulator is assumed to have double the solid volume but $2^{1/3}$ ~26% longer reach (63-113 nm reach at 80% extension, allowing it to reach beyond the 100 nm envelope of the NFW), and thus includes 125 parts and 58,000 nm^3 of solid diamondoid volume.

Freitas and Merkle[766] define a minimal toolset of 9 DMS tooltips (the ninth tooltip is a temporary compound of two of the other eight) (Figure 2-44) to allow mechanosynthesis of C/H/Ge diamondoid lattice and pure carbon graphene surfaces, but for scaling purposes a multiple-redundant total of 20 DMS toolheads must be included in the NFW scaling design to accommodate nonproductive tooltip recharging activities. Each toolhead to be used for DMS operations measures ~$(4\ nm)^2$ x 8 nm including tooltip plus tool handle, yielding a solid diamondoid volume of 128 nm^3 (and ~160 nm^2 of passivated diamondoid surface) per toolhead, or 2560 nm^3 and 3200 nm^2 for all 20 toolheads. The toolrack has a footprint area of $(5\ nm)^2$ x 20 toolheads = 500 nm^2 (20 nm x 25 nm) and it is 8 nm deep (4000 nm^3 of solid diamondoid

---

[765] Yu-Ming Lin, Phaedon Avouris, "Strong suppression of electrical noise in bilayer graphene nanoribbons," Nano Letters, 26 February 2008; http://pubs.acs.org/cgi-bin/abstract.cgi/nalefd/asap/abs/nl080241l.html. See also: Michael Loughran, "IBM Scientists 'Quiet' Unruly Electrons in Atomic Layers of Graphite: Atomic-Sized Graphene Double Layer Holds Nanoelectronics Promise," IBM press release, 6 March 2008; http://www-03.ibm.com/press/us/en/pressrelease/23648.wss.

[766] Robert A. Freitas Jr., Ralph C. Merkle, "A Minimal Toolset for Positional Diamond Mechanosynthesis," J. Comput. Theor. Nanosci. 5(May 2008):760-861.

volume, ~1720 nm^2 passivated surface), but it has 20 holes in it measuring $(4\ nm)^3$ or 64 nm^3 each (subtracting 1280 nm^3 solid volume and adding 1280 nm^2 passivated surface for all 20 toolhead slots), giving a total solid diamondoid volume of 2720 nm^3 and a total passivated surface of ~3000 nm^2 for the toolrack. The total solid diamondoid volume of the 20 toolheads plus the toolrack is 5280 nm^3 with 6200 nm^2 of passivated diamondoid surface, and there are a total of 21 parts. The toolrack may be attached to one or more foundation blocks to mechanically stabilize and stiffen the NFW system. The toolrack is positioned so that all three DMS manipulators can access it to remove or replace any of the 20 toolheads stored therein.

Allocating ~176 C atoms/nm^3 for diamondoid lattice and ~31 H atoms per nm^2 to passivate diamondoid surface and assuming a maximum of 10 Ge atoms required in the 20-tool NFW toolset (Section 2.3.2), the scaling results for the entire NFW (Figure III-1) are obtained as shown in Table III-2.

Table III-2. Estimated Atom Counts for First-Generation NFW

NFW Nanopart or Nanodevice	# of Nano-parts	Total Solid Volume (nm^3)	Total Passiv. Area (nm^2)	# of C Atoms*	# of H Atoms	# of Ge Atoms	Total # of Atoms
3 Small DMS Manipulators	375	87,000	107,139	15,032,682	3,321,309	0	18,353,991
1 Large Manipulator†	125	58,000	56,691	10,186,894	1,757,421	0	11,872,315
20 DMS Toolheads	20	2560	3200	450,560	99,200	10	549,770
1 DMS Toolrack	1	2720	3000	478,720	93,000	0	571,720
TOTALS	521	150,280	170,030	26,076,856	5,270,930	10	31,347,796

* The C count uses the direct estimate of C atom count for the electrical nanotube wires (9734 C atoms per wire pair x 13 pairs = 126,542 C atoms) which is 93,106 fewer C atoms than the 1248 nm^3 x 176 C/nm^3 = 219,648 C volumetric estimate for the 13 pairs of electrical leads.

† Passivation area of large manipulator taken as $2^{2/3}$ ~ 1.5874 times the passivation area of smaller manipulator.

This atom count is manufacturable (Section 3.4.4 and Section 3.4.5) using the available Phase II system. We further allocate 849,720 nm^3 of empty space to allow for clearance between struts and room for movement of manipulators, tools, workpieces and feedstock, giving a total operational volume for the NFW of 1,000,000 nm^3 approximating a $(100\ nm)^3$ cube having a ~10,000 nm^2 (~100 nm x ~100 nm) footprint on the chip surface, with a total atom count of ~31,347,796 atoms (83.2% C atoms, 16.8% H atoms), a total mass of 5.28 x 10^{-19} kg, and a total nanopart count of 521. The average nanopart in the NFW has a volume of ~288 nm^3 (a ~6.6 nm cube) and is composed of ~60,169 atoms. There are 52 actuators (individually controlled electrostatic motors) in the NFW, so we need 52 separate control lines (plus one common ground line for a total of 53) to avoid multiplexing and allow direct control of each individual actuator, the conceptually simplest approach. Note that the current load on each common ground line is only ~52 I_{motor} ~ 1.04 x 10^{-11} amp, well below the current-carrying capacity experimentally

observed[767] for individual 10-50 nm long single-walled "metallic" carbon nanotubes which can conduct 25-100 x 10^{-6} amp/wire electrical currents before failing, and a burnout threshold of 1000 x 10^{-6} amp/wire reported by others.[768]

3.4.1.2 Thermal Positional Stability of DMS Manipulators

The required positional placement accuracy for tooltips on a mechanosynthetic manipulator system performing reliable DMS is apparently in the range of 0.2-0.5 Å (Section 3.2.1.3).[769] There are at least three potential sources of positional uncertainty due to thermal displacements that could apply to the NFW Stewart platform manipulators: transverse displacement of the tip, positional stability of the foundation blocks, and thermal expansion due to localized heating.

First, the extent of thermally-driven transverse displacements of the strut terminus at minimum strut extension may be crudely estimated by treating the two nested tubes as a single rod. The transverse stiffness k_{trans} for a simple cantilevered rod of length L_{rod} for which a lateral deflection force $F_{deflect}$ produces a transverse deflection $d_{deflect}$ at the tip is given by $k_{trans} = F_{deflect} / d_{deflect} = 3 E_{rod} I_{rod} / L_{rod}^3$, where $E_{rod} = 1.05 \times 10^{12}$ N/m^2 is Young's modulus for diamond rod material and $I_{rod} = \pi r_{rod}^4 / 4$ is the second moment of area (also known as the moment of inertia of the area) for a rod of circular cross-section.[770] The lateral positional uncertainty of the tip of the rod is the square root of the positional variance[771] as given by $\Delta x = (k_B T / k_{trans})^{1/2}$, where $k_B = 1.381 \times 10^{-23}$

---

[767] Ali Javey, Pengfei Qi, Qian Wang, Hongjie Dai, "Ten- to 50-nm-long quasi-ballistic carbon nanotube devices obtained without complex lithography," PNAS 101(14 September 2004):13408-13410; http://www.pnas.org/cgi/content/abstract/101/37/13408.

[768] Hongjie Dai, Eric W. Wong, Charles M. Lieber, "Probing Electrical Transport in Nanomaterials: Conductivity of Individual Carbon Nanotubes," Science 272(26 April 1996):523-526; Stefan Frank, Philippe Poncharal, Z.L. Wang, Walt A. de Heer, "Carbon Nanotube Quantum Resistors," Science 280(12 June 1998):1744-1746.

[769] Jingping Peng, Robert A. Freitas Jr., Ralph C. Merkle, "Theoretical Analysis of Diamond Mechanosynthesis. Part I. Stability of C_2 Mediated Growth of Nanocrystalline Diamond C(110) Surface," J. Comput. Theor. Nanosci. 1(March 2004):62-70; http://www.MolecularAssembler.com/JCTNPengMar04.pdf. Jingping Peng, Robert A. Freitas Jr., Ralph C. Merkle, James R. Von Ehr, John N. Randall, George D. Skidmore, "Theoretical Analysis of Diamond Mechanosynthesis. Part III. Positional C_2 Deposition on Diamond C(110) Surface using Si/Ge/Sn-based Dimer Placement Tools," J. Comput. Theor. Nanosci. 3(February 2006):28-41; http://www.MolecularAssembler.com/Papers/JCTNPengFeb06.pdf. Denis Tarasov, Natalia Akberova, Ekaterina Izotova, Diana Alisheva, Maksim Astafiev, Robert A. Freitas Jr., "Optimal Tooltip Trajectories in a Hydrogen Abstraction Tool Recharge Reaction Sequence for Positionally Controlled Diamond Mechanosynthesis," J. Comput. Theor. Nanosci. 5(2008). In preparation.

[770] S.A. Wainwright, W.D. Biggs, J.D. Currey, J.M. Gosline, Mechanical Design in Organisms, John Wiley & Sons, New York, 1976.

[771] K. Eric Drexler, Nanosystems: Molecular Machinery, Manufacturing, and Computation, John Wiley & Sons, New York, 1992; http://www.zyvex.com/nanotech/nanosystems.html.

J/K (Boltzmann constant) and T is temperature. At minimum strut extension, L_{rod1} = 50 nm and r_{rod1} = 5 nm yielding $I_{rod1} = 4.91 \times 10^{-34}$ m^4 and k_{trans1} = 12.4 N/m, hence Δx_{MinExt} = 0.18 Å at 300 K and 0.09 Å at 80 K per strut, either of which is excellent for reliable DMS work.

To estimate the strut terminus displacement at maximum strut extension we must add to Δx_{MinExt} the additional positional uncertainty due to thermal displacements of the smaller 80% extended rod, which thus has L_{rod2} = 40 nm and r_{rod2} = 2.5 nm yielding $I_{rod2} = 3.07 \times 10^{-35}$ m^4 and k_{trans2} = 1.51 N/m, hence Δx_2 = 0.52 Å at 300 K and 0.27 Å at 80 K, implying a total uncertainty of $\Delta x_{MaxExt} = \Delta x_{MinExt} + \Delta x_2$ = 0.70 Å at 300 K and 0.36 Å at 80 K for each strut. However, each Stewart platform has 6 active struts mechanically joined at the tool chuck base so the stiffnesses of all 6 struts must be combined to determine the stiffness of the overall manipulator system at the toolchuck. Adding the compliances of the two tubes gives a net k_{trans3} for the extended strut of 1.35 N/m, which for 6 linked struts gives a combined stiffness of order $k_{transAll} \sim 6\ k_{trans3}$ = 8.1 N/m, hence $\Delta x_{MaxExtAll}$ = 0.23 Å at 300 K and 0.12 Å at 80 K, either of which is acceptable for reliable DMS work. Note that a manipulator system with net overall stiffness of ~10 N/m will deflect by ~1 Å when it applies a lateral force of ~1 nN.

Second, the foundation blocks that anchor the telescoping struts must be stiff enough to provide an adequately stable base for positioning the Stewart platform to within the required thermal displacement uncertainty limits. To assess the magnitude of this effect, we consider the bending stiffness of a clamped square plate of thickness h_{plate} and edge length L_{plate} which is given[772] by $k_{bending} = E_{plate}\ h_{plate}^3 / (12\ L_{plate}^2\ (1 - k_{pois}^2))$ and the positional uncertainty[773] of the plate surface due to thermal noise which is $\Delta x_{bending} \sim (k_B T / k_{bending})^{1/2}$. Taking $E_{plate} = 1.05 \times 10^{12}$ N/m^2, h_{plate} = 10 nm, Poisson's ratio $k_{pois} \sim 0.1$ for diamond[774] and L_{plate} ~40 nm, then $k_{bending}$ = 55.2 N/m and $\Delta x_{bending}$ ~ 0.09 Å at 300 K and 0.04 Å at 80 K, a minor contribution to positional uncertainty at the tool chuck. Stiffness scales as the cube of the wall thickness, so a small increase in plate thickness would be sufficient to compensate either for the uncertainties in this estimate or to increase stiffness and further reduce positional uncertainty if this proves necessary.

Third, thermal expansion due to energy dissipation during mechanical operations and positionally controlled exothermic chemical reactions could produce unacceptable thermal expansion in the manipulator struts. If all Stewart platform struts and the tool chuck are continuously fully actuated simultaneously (13 motors running at 0.2 pW/motor; Section 3.4.1.1) then each Stewart platform can consume at most ~2.6 pW for mechanical operations, roughly the same order as the telescoping manipulator described elsewhere.[775] The exoergic making of ~100 bonds/sec of C-C

---

[772] Prof. Dr.-Ing. Kai-Uwe Bletzinger, "Theory of Plates, Part II: Plates in bending," Lehrstuhl fur Statik, Technische Universitat Munchen, Lecture Notes, Winter Semester 2000/2001; http://www.statik.bauwesen.tu-muenchen.de/vorlesungen/plates.dir/plates_part2.pdf.

[773] K. Eric Drexler, Nanosystems: Molecular Machinery, Manufacturing, and Computation, John Wiley & Sons, New York, 1992; http://www.zyvex.com/nanotech/nanosystems.html.

[774] K. Eric Drexler, Nanosystems: Molecular Machinery, Manufacturing, and Computation, John Wiley & Sons, New York, 1992; http://www.zyvex.com/nanotech/nanosystems.html.

[775] K. Eric Drexler, Nanosystems: Molecular Machinery, Manufacturing, and Computation, John Wiley & Sons, New York, 1992; http://www.zyvex.com/nanotech/nanosystems.html.

bonds each having energy of ~3.4 eV/bond generates a negligible additional 0.00005 pW of waste heat for a maximum possible total power dissipation of 10.4 pW for all four manipulators in continuous operation at the 1.2 MHz control pulse frequency. If the 0.2 pW dissipation from each motor is directed along the thinnest (5 nm wide) strut member, this initiates a longitudinal thermal power flux of $I_{thermal}$ = 10,200 W/m^2 transiting a strut of length L_{strut} ~ 50 nm that is composed mostly of diamond having thermal conductivity $K_{diamond}$ = 2000 W/m-K and heat capacity C_V ~ 1.82 x 10^6 J/m^3-K that produces a tiny equilibrium temperature differential of $\Delta T \sim I_{thermal} L_{strut} / K_{diamond} \sim 3 \times 10^{-7}$ K in an equilibration time of $t_{EQ} \sim L_{strut}^2 C_V / K_{diamond} = 2 \times 10^{-12}$ sec and a linear thermal expansion in diamond rod (expansion coefficient $\alpha_{diamond} = 8 \times 10^{-7}$ K^{-1}) that cannot be larger than $\Delta L_{strut} \sim L_{strut} (\alpha_{diamond} \Delta T) \sim 10^{-10}$ Å, which is negligible.

3.4.1.3 Pick-and-Place vs. Sensory Feedback

It appears that the positional uncertainties of the tooltips of the four interacting manipulators are sufficiently low to allow blind pick-and-place operation even at room temperature (Section 3.4.1.2). If future simulations or experimental results employing these devices invalidates this assumption, due to larger than expected positioning errors after repeated operation of the manipulators, positional uncertainty can readily be halved by moving from room temperature operation (~300 K) to operation at LN_2 temperatures (~80 K). During later Phases which involve the transfer of feedstock gases, this change in procedure may require shifting between warmer and colder temperatures within a single manufacturing cycle, somewhat increasing cycle length but not significantly altering the course of the proposed nanofactory development program; or operations may occur in the colder all-fluid regime). An additional halving of uncertainty is obtained by moving to operation at ~20 K, and still another halving (now totaling three halvings or 12.5%) by moving to ~5 K (~LHe temperatures), although this latter option would be more expensive and inconvenient.

Besides lowering the operating temperature, a second approach for dealing with unexpectedly large tip uncertainties during repetitive operations is to add a single force sensor (see also Sections 3.4.3, 3.6.1.2, 3.8.1.3 and 3.8.4) to one of the four manipulators, thus allowing self-registration of the four manipulators at the beginning of operations and as often thereafter as deemed necessary. Adding such a sensor to the existing design would add negligibly to the total atom count and parts count, hence would not appreciably alter the current design. To be scalable to massive parallelization in later Phases, the sensing mechanism should incorporate only localized feedback and correction that did not need to be directly monitored and controlled by the external (human or computer) operator. In the ideal case the operator would instruct the manipulators to execute a standardized registration procedure, after which the manipulators would be left in a known and precisely re-aligned state from which further DMS operations could reliably proceed. (See also Sections 3.2.1.6 and 3.8.1.3.)

A simple force sensor that produces a mechanical output signal when a predetermined force has been applied may consist of a flexible rod that is restrained from bending by a restoring spring force that trips a mechanical latch when the rod deflection exceeds a certain distance, indicating that a threshold force has been detected by the sensor. The probability of erroneous measurement (P_{err}) by a cantilever force sensor that deflects by δ in distinguishing two applied forces differing

by ΔF newtons is approximated[776] by $P_{err} \sim \exp(-\delta\, \Delta F / 4\, k_B T)$. Each Stewart platform manipulator can apply up to 60 nN in an ideal orientation but we assume ~5 nN can reliably be applied in any orientation (Section 3.4.1.1). Taking $\Delta F \sim 1$ nN (mechanical nanosensors can be designed to reliably measure forces as small as ~10 pN),[777] T = 300 K, and $P_{err} \leq 10^{-20}$ to ensure flawless operation in Phase VIII for 10^{14} NMW-2 units on 1024 wafers operated for 10^6 sec (Section 3.9.5) assuming once force measurement per second, then $\delta \leq 1$ nm to operate the latch. A cantilever rod with length L_{rod} ~10 nm, Young's modulus $E_{rod} = 1.05 \times 10^{12}$ N/m^2 for diamond, and cross section area ~2 nm^2 (circular rod radius r_{rod} ~0.8 nm) to which a lateral force of ΔF ~1 nN is applied at the tip produced a tip deflection[778] of $\delta = 4\, L_{rod}^3\, \Delta F / 3\, \pi\, E_{rod}\, r_{rod}^4 \sim 1$ nm as required, using a ~20 nm^3 rod. Assuming that a latch mechanism and any necessary support housing can be constructed with a solid volume of ~30 nm^3, insertion of a ~50 nm^3 sensor into the design would add only ~9000 carbon atoms and ~9000 atoms of surface-passivating hydrogen.

Our presumption is that pick-and-place operations will be sufficiently reliable to eliminate the need for detailed inspection of finished product objects (nanoparts) prior to their use in subsequent fabrication or assembly processes. Should such inspection be deemed necessary, exterior atomic-scale defects are readily detected by touch. Buried atomic scale defects may be detected: (1) by testing dynamic functionality, (2) by measuring various static properties such as surface profile or charge distribution (since a bonding defect inserts a static strain field into the workpiece that modifies these properties), or (3) by measuring variations in vibrational properties (e.g., an acoustic traveling wave with an initial phase distribution shaped to converge on a possible defect should be able to sense internal defects down to roughly a wavelength or ~1 bondlength, though there will be attenuation from processes that thermalize the acoustic energy and decoupling where intervening soft internal layers or voids can't transmit the high frequency waves needed to see small internal defects, and the presence of carbon isotopes will introduce random scattering that attenuates diagnostic acoustic waves and puts a "noise floor" on how small a signature we can use to detect defects, even with zero temperature and an infinite integration time[779]).

3.4.1.4 Manipulator Speed and NFW Productivity

How fast can DMS manipulators be operated within an NFW? A basic DMS methylation reaction sequence (RS) typically requires 4 reaction steps, or 5 steps if we count a subsequent H abstraction to reduce the added CH_3 group to the CH_2 group it will possess in the completed

---

[776] K. Eric Drexler, Nanosystems: Molecular Machinery, Manufacturing, and Computation, John Wiley & Sons, New York, 1992, Section 11.2.2, p. 322.

[777] Robert A. Freitas Jr., Ralph C. Merkle, Kinematic Self-Replicating Machines, Landes Bioscience, Georgetown, TX, 2004; Section 4.4.1, p. 102; http://www.MolecularAssembler.com/KSRM/4.4.1.htm.

[778] Robert A. Freitas Jr., Ralph C. Merkle, Kinematic Self-Replicating Machines, Landes Bioscience, Georgetown, TX, 2004; Section 9.3.1.2, pp. 286-287; http://www.MolecularAssembler.com/KSRM/9.3.1.2.htm.

[779] Jeffrey P. Soreff, newsgroup communication, 22 August 2001.

adamantane cage unit of the diamond lattice,[780] plus ~3 more steps may be required to recharge a spent tooltip after each operation (e.g., RS5).[781] Hence the net atom placement rate is ~ (5 placement steps per methyl group) x (3 recharge steps per placement step) / (3 atoms (one C and two H) laid down) ~ 5 steps/atom. Hydrogen atoms are most often placed onto the workpiece along with the carbon atom as part of a methyl group. For pure carbon deposition, C_2 dimer placement lays down two C atoms at once and requires just 1 reaction step (e.g., RS4),[782] although positionally controlled acquisition of, say, ethylene feedstock and recharge of a DCB6Ge dimer placement tool may require 5 reaction steps (e.g., one to bind the C_2H_4 followed by four H abstraction reactions); hence the net atom placement rate is ~ 1 placement step per C_2 dimer group x 5 recharge steps per placement step / 2 C atoms ~ 2.5 steps/atom. Taking the same C:H ratio of 5:1 as in Section 3.4.1.1 and doubling the number of steps to allow for toolhead exchanges at the toolrack, we estimate that 2((5)(2.5)+(1)(5))/6 ~ 6 mechanosynthetic operations per atom may typically be required to add each carbon atom to a growing diamond workpiece via DMS, or to add C and H atoms to a hydrogen-passivated diamond surface, including feedstock acquisition, tool operation, tool recharge, and toolrack exchange. All four manipulators have separate control channels and thus can be operated in parallel if necessary during each mechanosynthetic operation.

A mechanosynthetic operation that typically requires one half-range round trip between 50 nm to 90 nm extension and then back again, or a round trip of 40 nm in 0.2 Å increments, needs 2000 increments per round trip. In this case, placement of each new atom requires 2000 increments/operation x 6 operations = 12,000 increments/atom. If power/control signals are applied at a ~1.2 MHz frequency, thus driving manipulator tips at a top speed of ~24 microns/sec, this enables the NFW to fabricate structures at a (1.2×10^6 increments/sec) / (1.2×10^4 increments/atom) ~ 100 atom/sec rate when presentation of feedstock molecules is not a time-limiting factor, allowing the NFW to replicate its own mass in ~3.13×10^5 sec (~3.6 days). Assuming one bit to describe each increment, a complete replication cycle thus requires up to (31,347,796 atoms)(12,000 increments/atom-actuator)(1 bit/increment)(52 actuators) ~ 1.96×10^{13} bits of replication process data.

In the actual Phase III setup proposed here, the NFW will operate about 2 orders of magnitude slower than this (Section 3.4.6) – that is, at a ~1 atom/sec rate – because it must be fed its molecular feedstock by the Phase II macroscale SPM system at a process-limiting ~1 Hz supply rate (Section 3.3.1). That's why adding the scalable bulk feedstock supply capability to upgrade the NFW in Phase IV is the next most urgent development priority.

---

[780] Robert A. Freitas Jr., Ralph C. Merkle, "A Minimal Toolset for Positional Diamond Mechanosynthesis," J. Comput. Theor. Nanosci. 5(May 2008):760-861.

[781] Robert A. Freitas Jr., Ralph C. Merkle, "A Minimal Toolset for Positional Diamond Mechanosynthesis," J. Comput. Theor. Nanosci. 5(May 2008):760-861.

[782] Robert A. Freitas Jr., Ralph C. Merkle, "A Minimal Toolset for Positional Diamond Mechanosynthesis," J. Comput. Theor. Nanosci. 5(May 2008):760-861.

3.4.1.5 Waste Heat Generated by Chemical Transformations During DMS

As already noted (Section 3.4.1.2), the waste heat generated by chemical transformations during positionally controlled DMS chemical reactions taking place at the tooltips will be very small compared to energy consumed by NFW motors in generating tooltip motions. For example, to methylate an adamantane sidewall site using a germylmethylene (GM) tooltip in four steps (e.g., Reaction Sequence RS7),[783] the site must first be dehydrogenated using an HAbst tool, costing an irreversible 1.58 eV energy loss; the GM tool is then bonded to the radical site, releasing another 3.09 eV from this exoergic reaction; detaching the now-empty GM handle is endoergic, thus requiring the input of mechanical energy but not producing any additional chemical energy losses; then the remaining radical site is hydrogenated using an HDon tool, another exoergic reaction costing an irreversible 0.67 eV energy loss. Hence the total irreversible chemical energy loss during RS7 is 5.34 eV or ~8.6 x 10^{-19} J. This represents an energy loss on the order of ~10^{7} J/kg, near the theoretical limit for conventional irreversible chemical processes that may become available in a mature nanofactory (Phase XI).

In contrast, the NFW will require at least 0.04 sec to perform Reaction Sequence RS7 operating at a ~100 atom/sec rate (Section 3.4.1.4). Assuming a total power dissipation of 10.4 pW for all four NFW manipulators in continuous operation at the 1.2 MHz control pulse frequency (Section 3.4.1.2), then 0.04 sec of NFW operation will generate 4.16 x 10^{-13} J of irreversible mechanical energy loss. This represents a manufacturing energy loss on the order of ~10^{13} J/kg, which is very energy inefficient and is at least six orders of magnitude higher than the theoretical limit for conventional irreversible chemical processes. As we progress through subsequent Phases of nanofactory development, effort should be made to improve energy efficiency, perhaps eventually approaching the theoretical limit as the final Task in Phase XI.

3.4.1.6 Reliability of NFW Manufacture

The Phase III first-generation NFW is never operated as a production system, so the issue of reliability in Phase III arises only in connection with the use of the Phase II system to construct the NFW. It is intended that about one dozen Phase II systems will be duplicated and brought online, then operated in parallel to build the NFW and successor nanoscale systems (Section 3.4.4). A Phase II system has a target productivity rate of ~1 atom/sec with ~6 mechanosynthetic operations required for placement of each atom in the growing workpiece structure (Section 3.3.1.2). The target product object is the NFW which has ~31 x 10^{6} atoms (Table III-2), so building the NFW requires ~186 x 10^{6} mechanosynthetic operations or ~16 x 10^{6} operations for each of 12 Phase II systems working in parallel. Thus to avoid even a single misplacement error the picopositioner system must be able to deliver a minimum of ~16 x 10^{6} error-free round trip excursions of the positionally controlled DMS tooltips – a ~30-fold more stringent design requirement for the MMW that at the conclusion of the Phase II effort (Section 3.3.1.3). The

---

[783] Robert A. Freitas Jr., Ralph C. Merkle, "A Minimal Toolset for Positional Diamond Mechanosynthesis," J. Comput. Theor. Nanosci. 5(May 2008):760-861.

potential ability of computer controllers to reliably deliver such lengthy data sequences with low error, and the ability of simple mechanical actuators to reliably execute such lengthy sequences of mechanical actuations with low error, is discussed in Section 3.8.1.3.

Another source of intrinsic manufacturing error arises from the reliability of the DMS reactions themselves, as previously discussed in Section 3.2.1.8. Table I-5 gives the probability of misreaction at various relevant operating temperatures, assuming a defect energy threshold of 0.40 eV. The misreaction probability per mechanosynthetic operation may be as high as 1.91 x 10^{-7} at 300 K, conservatively assuming that all reactions have the minimum defect energy threshold of 0.40 eV, producing ~36 erroneous atom placements in the ~31 x 10^6-atom NFW product object after ~186 x 10^6 mechanosynthetic operations, hence room temperature fabrication of the NFW by the Phase II system appears impractical. The expected error rate falls to <1 erroneous atom placement below 244 K, ~10^{-2} at dry-ice temperature (~195 K), or ~10^{-3} at 179 K for a ~31 x 10^6-atom product object fabricated using the original set[784] of DMS reactions, hence operation at $T \leq 195$ K appears feasible in Phase III. At near liquid nitrogen temperatures (~80 K), the DMS-related error rate using reaction sequences with a defect energy threshold of 0.40 eV falls to ~10^{-17} for a ~31 x 10^6-atom product object, completely negligible for Phase III purposes.

Another major source of error is radical poisoning by contaminants in an imperfect UHV environment. At a target productivity rate of ~1 atom/sec for the Phase II system, the ~31 x 10^6-atom NFW will require t_{fab} ~ 2.6 x 10^6 sec (~1 month) for 12 MMW systems to fabricate, working in parallel. Assuming that a radical site susceptible to poisoning is exposed to the imperfect UHV environment for a fraction f_{vac} ~ 50% of the time, then the maximum tolerable UHV pressure that will permit all nanoparts for one defect-free ~31 x 10^6-atom NFW to be fabricated is $P_{UHV} \leq (N_{encounters}\ T / n_{contam}\ A_{radical}\ f_{vac}\ t_{fab})\ (\pi\ MW_{kg} / 2\ k_B T\ N_A)^{1/2}$ ~ 1.2 x 10^{-14} atm, where n_{contam} = 7.34 x 10^{27} molecules-K/m^3-atm (= N_A/R_{gas}) for ideal gas (contaminant) molecules and T = 195 K, with the other quantities as previously defined in Section 3.2.1.7. If any workpiece having one or more erroneous atom placements is considered defective, then in a UHV environment maintained at ~10^{-16} atm (~10 million contaminant molecules present in a 5-liter UHV work volume; currently achievable experimentally, Section 3.2.1.7) the radical-poisoning defect rate at 195 K will be ~10^{-2} for NFW product objects or ~10^{-1} for all 12 MMWs taken together, which is probably acceptable. If H_2 contaminant is determined not to be a serious radical poisoning risk or can be rigorously excluded from the workspace, then taking MW_{kg} = 0.014 kg/mole for N_2 raises the required P_{UHV} by a factor of ~2.6, lowering the 12-MMW defect production rate from 50% to 19% per manufacturing cycle.

As for radiation damage rates, assuming a failure condition of κ_{fail} ~ 10^{15} hits/kg-rad and an I_{rad} ~ 0.5 rad/yr background the mean time τ_{rad} between radiation-disabling hits on a mostly-carbon ~31 x 10^6-atom NFW of mass m_{target} = 5.28 x 10^{-19} kg is $\tau_{rad} \sim (\kappa_{fail}\ m_{target}\ I_{rad})^{-1}$ ~ 3788 years (conservatively assuming that one such hit will cause the workpiece or tooltip to fail with 100% certainty), still a negligible error rate (~10^{-5} per replication cycle).

---

[784] Robert A. Freitas Jr., Ralph C. Merkle, "A Minimal Toolset for Positional Diamond Mechanosynthesis," J. Comput. Theor. Nanosci. 5(May 2008):760-861.

When used for assembly work rather than for fabrication, the Phase II system neither creates nor destroys chemically active radical sites, hence its operations are not subject to DMS-related error rates and are only weakly subject to vacuum poisoning effects. Hence MMW reliability during assembly operations is governed chiefly by its ability to correctly execute a small number of non-covalent parts assembly operations and by error rates in nanopart gripping/releasing mechanisms, and these error rates are assumed to be small in comparison with the DMS-related error rates.

3.4.2 Task III-1: Design and Simulate First-Generation NFW

Task III-1 is to design and simulate the entire NFW, specifying all component nanoparts and nanodevices (assemblies of nanoparts) and also specifying all fabrication and assembly processes that will be required to complete the manufacturing operations of: (1) nanopart fabrication, (2) nanodevice assembly from nanoparts, (3) NFW assembly from nanoparts and nanodevices, and (4) to verify correct NFW operation, if properly assembled. Of critical importance is a study of the available work envelope of the Stewart platforms, to make sure that it is sufficient for all tasks assigned to them. If the Stewart platform work envelope is not sufficient, we can use a double tripod[785] or a related system instead. Determination of the most efficient manipulator system is a key design effort that should be undertaken as soon as possible – and should begin in Phase II (e.g., Task II-2, Section 3.3.3(H)) or earlier. In an efficient development effort, the first generation NFW should also be designed to be interoperable with the bulk feedstock supply system to be designed in Task IV-1 (Section 3.5.2). Hence greater efficiencies may be attained in the design process if Task II-2(H), Task III-1, and Task IV-1 are undertaken simultaneously or at least in close coordination.

Design and simulation of the typical NFW nanopart will require at minimum a molecular mechanics / molecular dynamics (MM/MD) level analysis of a nanopart having (31,347,796 atoms)/(521 nanoparts) ~ 60,169 atoms/nanopart (Table III-2). Such modeling and simulation could be performed using the NanoEngineer-1 software package that was available in 2007, running on commonplace personal computers that were available in 2008. The typical nanodevice consists of 2-4 nanoparts (Table III-1), increasing the simulation software capacity requirement to 120,338-240,676 atoms/nanodevice for basic modeling and validation of proper operation. Following Moore's Law assuming an 18-month doubling time and conservatively assuming traditional $\sim N_{atom}^2$ scaling with atom count for MM/MD algorithms, a 240,676-atom nanodevice could be simulated using NanoEngineer-1 on a single commonplace personal computer that would be available in 2013, or on a 16-CPU computer cluster that might be available in 2008. Additional software and computing capacity will need to be acquired if higher levels of analysis are deemed necessary for these nanoparts and nanodevices (in light of results from earlier Phases), such as semi-empirical or density-functional (DFT) levels of theory.

MM/MD modeling and simulation of the entire 31,347,796-atom NFW at the full atomistic level is well beyond the current ability of NanoEngineer-1 executing on a desktop PC or on a small computer cluster and will require specialized software running on highly parallel supercomputers. The ability to perform highly parallelized or "scalable" computations on cluster supercomputers

---

[785] Ralph C. Merkle, "A New Family of Six Degree Of Freedom Positional Devices," Nanotechnology 8(June 1997):47-52, http://www.zyvex.com/nanotech/6dof.html.

comprised of hundreds up to literally tens of thousands of networked CPUs has contributed to a kind of "Moore's Law" of simple exponential growth in computational simulation capabilities. The number of atoms that MD simulations (of all types) can handle has approximately doubled every 15 months since 1985 (Figure III-6). By the year 2005 a classical MD simulation on 40 billion Lennard-Jones atoms had been performed on the LLNL Blue Gene parallel computer using 65,536 processors.[786] The dashed line shows the comparatively meager improvement in conventional *ab initio*/DFT simulations, but new breakthroughs in linear-scaling (i.e., runtime ~ N^1, not N^3) DFT algorithms for parallel computers such as the embedded divide-and-conquer (EDC-DFT) method of Nakano et al.[787] has allowed advances in AIMD to keep pace with those in classical MD. If these trends continue, by 2015 we could see practical supercomputer-based Lennard-Jones MD simulations up to 10 trillion atoms, classical MD simulations up to 100 billion atoms, semiempirical AIMD up to 10 billion atoms, and DFT-based AIMD up to 1 billion atoms using 10 petaflop computing machines. This will allow nanoengineers at the research forefront to undertake high-quality AIMD simulations of very complex nanomachine systems and classical MD simulations of entire nanorobotic systems (typically 10-100 billion atoms for 1-3 micron nanorobots[788]).

Figure III-6. "Moore's law" in molecular dynamics simulations on highly parallel supercomputers.

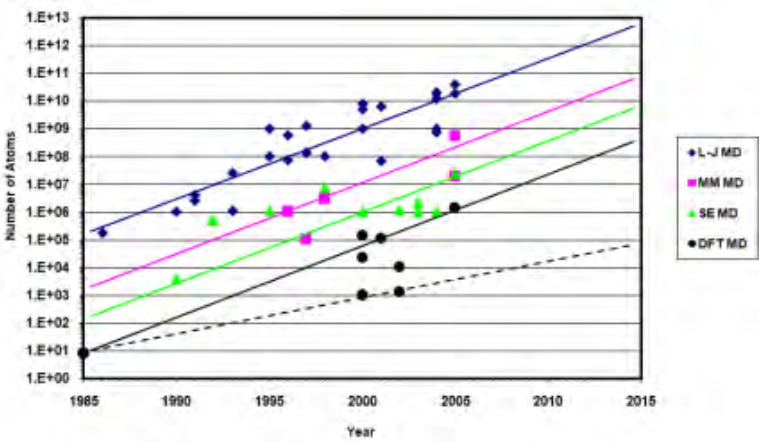

[786] "LAMMPS, Large-scale Atomic/Molecular Massively Parallel Simulator," 3 June 2005; http://www.cs.sandia.gov/~sjplimp/lammps.html. See also: "LAMMPS Benchmarks," http://www.cs.sandia.gov/%7Esjplimp/lammps/bench.html.

[787] Aiichiro Nakano, Martina E. Bachlechner, Rajiv K. Kalia, Elefterios Lidorikis, Priya Vashishta, George Z. Voyiadjis, Timothy J. Campbell, Shuji Ogata, Fuyuki Shimojo, "Multiscale Simulation of Nanosystems," Computing in Science & Engineering 3(July/August 2001):56-66.

[788] Robert A. Freitas Jr., "Exploratory Design in Medical Nanotechnology: A Mechanical Artificial Red Cell," Artificial Cells, Blood Substitutes, and Immobil. Biotech. 26(1998):411-430; http://www.foresight.org/Nanomedicine/Respirocytes.html. Robert A. Freitas Jr., "Microbivores: Artificial Mechanical Phagocytes using Digest and Discharge Protocol," J. Evol. Technol. 14(April 2005):1-52; http://www.jetpress.org/volume14/freitas.html.

A snapshot of the relative computation time required per MD time step using a cluster of 1024 Cray T3E processors in the year 2000 is shown in Figure III-7. Using this particular computer resource, one time step of a classical MD simulation of a 1.02 billion atom silica structure required 26.4 sec with a parallel efficiency of 97%.[789] With access to this same resource in 2008 assuming no improvements since 2000, simulation of the entire 31,347,796-atom NFW at the full atomistic level at the MM/MD level of theory would consume ~0.8 second of cluster time per MD step, allowing calculation of ~100,000 MM/MD time steps per day of cluster computing time, or ~1 nanosecond of NFW operation per week of cluster computing time (assuming 10^{-15} sec step sizes). Applying Moore's Law assuming an 18-month doubling time in capability, by 2012 (8 doubling times from 2000) an upgraded equivalent computing resource could calculate ~30,000,000 MM/MD time steps per day of cluster computing time, or ~1 microsecond of NFW operation per month of cluster computing time. This is sufficient time to simulate the entire NFW running through one entire atom addition transaction, which includes ~12,000 stepper-motor increments comprising 6 separate tool cycle operations (Section 3.4.1), plausibly running the NFW at 1 MHz rather than 100 Hz inside the simulation. The upgraded computer resource could also calculate ~10 MD time steps per day of cluster computing time at the DFT level of theory, or ~1 picosecond of NFW operation in ~3 months of cluster computing time. An MD simulation of the Stewart platform could help to demonstrate that the energy barriers preventing motion reversal are high enough to prevent the mechanism from, say, taking a few steps forward and then one step back, thus ruining the digital precision of the actuation sequence.

Figure III-7. Computation time of MD and QM algorithms as a function of the number of atoms on 1,024 Cray T3E processors: (circles) classical MD based on many-body inter-atomic potentials; (squares) environment-dependant, variable-charge MD; (triangles) QM calculation based on the tight-binding method; and, (diamonds) self-consistent DFT-QM.[790]

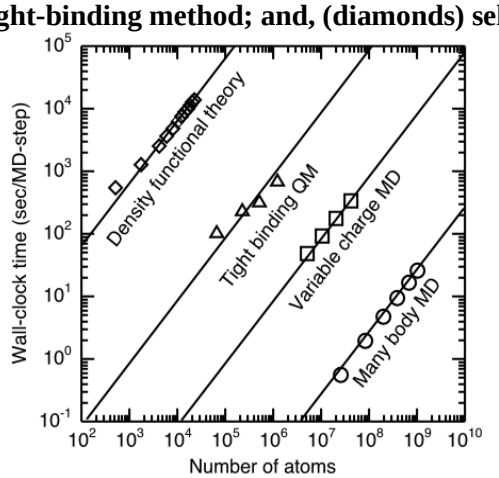

[789] Aiichiro Nakano, Martina E. Bachlechner, Rajiv K. Kalia, Elefterios Lidorikis, Priya Vashishta, George Z. Voyiadjis, Timothy J. Campbell, Shuji Ogata, Fuyuki Shimojo, "Multiscale Simulation of Nanosystems," Computing in Science & Engineering 3(July/August 2001):56-66.

[790] Aiichiro Nakano, Martina E. Bachlechner, Rajiv K. Kalia, Elefterios Lidorikis, Priya Vashishta, George Z. Voyiadjis, Timothy J. Campbell, Shuji Ogata, Fuyuki Shimojo, "Multiscale Simulation of Nanosystems," Computing in Science & Engineering 3(July/August 2001):56-66.

Design, modeling and simulation of fabrication and assembly processes using the Phase II system (Section 3.3) will probably require mixed-model techniques in which noncritical atoms are modeled using MM and a much smaller number of critical atoms (presumably those in apposition or contact, or directly covalently bonded to such atoms) using DFT, giving a MM/DFT mixed model, for testing crucial moments of various fabrication and assembly sequences. An even more simplified continuum model for bulk atoms combined with MM for interfacial (and related) atoms may allow simulation of the entire sequence of NFW fabrication and assembly, and simulation and validation of all NFW operations needed to fabricate all of its own parts.

3.4.3 Task III-2: Prepare Multielectrode Assembly Surface

Task III-2 is to prepare an atomically flat surface (Figure III-3) upon which the first NFW can be physically constructed and debugged. Electrical power and control signals will be applied to NFW mechanisms via carbon nanotube wires that connect conductive silver (or aluminum) terminals on the atomically smooth assembly surface to electrostatic motors that actuate the manipulators. Recent work[791] suggests that the intrinsic resistivity of graphene is lower than that of copper and comparable to that of silver, and that graphene's electron mobility is superior to the best-known inorganic semiconductors, e.g., InSb. Nanotube wires from the NFW are joined to the silver electrodes by simple van der Waals attraction,[792] or if this is insufficient then by nanotube impalement of the softer metal,[793] by e-beam spot welding,[794] by using designed

---

[791] J. H. Chen, C. Jang, S. Xiao, M. Ishigami, M. S. Fuhrer, "'Intrinsic and Extrinsic Performance Limits of Graphene Devices on SiO_2," Nature Nanotechnology (23 March 2008), http://www.nature.com/nnano/journal/vaop/ncurrent/abs/nnano.2008.58.html. See also: "Physicists Show Electrons Can Travel More Than 100 Times Faster in Graphene," University of Maryland press release, 24 March 2008; https://www.newsdesk.umd.edu/scitech/release.cfm?ArticleID=1621.

[792] Myounggu Park, Baratunde A. Cola, Thomas Siegmund, Jun Xu, Matthew R. Maschmann, Timothy S. Fisher, Hyonny Kim, "Effects of a carbon nanotube layer on electrical contact resistance between copper substrates," Nanotechnology 17(2006):2294-2303; http://docs.lib.purdue.edu/cgi/viewcontent.cgi?article=1003&context=nanopub.

[793] E.M. Yunus, J.W. McBride, S.M. Spearing, "The relationship between contact resistance and contact force on Au coated carbon nanotube surfaces," Proceedings of The 53rd IEEE Holm Conference on Electrical Contacts., The Institute of Electrical and Electronics Engineers, 2007, pp. 167-174; http://eprints.soton.ac.uk/48464/.

[794] MinFeng Yu, Mark J. Dyer, George D. Skidmore, Henry W. Rohrs, Xue Kun Lu, Kevin D. Ausman, James Von Ehr, Rodney S. Ruoff, "3 Dimensional Manipulation of Carbon Nanotubes under a Scanning Electron Microscope," paper presented at the Sixth Foresight Nanotechnology Conference, November 1998; see also: Robert F. Service, "AFMs Wield Parts for Nanoconstruction," Science 282(27 November 1998):1620-1621; and http://www.foresight.org/Conferences/MNT6/Papers/Yu/index.html.

mateable connectors, or by other means.[795] Note also that carbon nanotube based multi-electrode arrays have been created experimentally via CVD[796] and conductive nanoscale islands on nonconductive surfaces have been created experimentally via SPM.[797] Most recently, Cen et al.[798] report the creation and erasure of nanoscale conducting regions at the interface between two insulating oxides using an AFM tip to draw conducting lines with widths of ~3 nm (considerably narrower than the lines that can be drawn using electron beam lithography) and arrays of conducting islands with number density $>10^{13}/cm^2$ (mean separation ~2.5 nm).

The assembly surface will have a foundation based on single-crystal silicon – but probably including multiple submerged layers of silicon circuitry fabricated via conventional lithography – topped with a moderately thick (~50 nm) overlayer of silicon dioxide embedded with a multitude of metallic power lines to energize and control the NFW. The silica overlayer will include 100-1000 well-defined square-area worksites on each semiconductor assembly surface chip which should be a sufficient number for NFW experimentation and testing in Phase III. A set of 53 silver electrodes (Section 3.4.1.1) will be fabricated into the silica overlayer in each 10,000 nm^2 NFW worksite to allow direct electrical contact to be established between the future NFW and the chip assembly surface. For an evenly spaced Cartesian grid of $N_{electrode} = 53$ square electrodes each of edge length $l_{electrode} = 10$ nm with center-to-center nearest-neighbor separation of $(l_{electrode} + d_{electrode}) = 15$ nm, the footprint of the electrode array has area $A_{array} = N_{electrode} (l_{electrode} + d_{electrode})^2 = 11{,}925$ nm^2, only slightly larger than the nominal 10,000 nm^2 worksite perimeter, with the electrodes occupying only $f_{electrode} = l_{electrode}^2 / (l_{electrode} + d_{electrode})^2 = 44\%$ of the electrode surface area. If the electrodes are operated at ~1 volt then the electric field strength across the $d_{electrode} = 5$ nm silicon dioxide insulator gap separating the electrodes is $\sim 2 \times 10^8$ V/m, well below the $\sim 10^9$ V/m breakdown field usually cited in the literature[799] for silicon dioxide (with 1.7×10^9 V/m measured experimentally for 2.0-2.5 nm silica thin layers[800]) and very close to the onset of

---

[795] B.M. Quinn, S.G. Lemay, "Single-Walled Carbon Nanotubes as Templates and Interconnects for Nanoelectrodes," Advanced Materials 18(7 March 2006):855-859; http://www3.interscience.wiley.com/cgi-bin/fulltext/112474877/PDFSTART.

[796] Tamir Gabay, Moti Ben-David, Itshak Kalifa, Raya Sorkin, Ze'ev R. Abrams, Yael Hanein, Eshel Ben-Jacob, "Electro-chemical properties of carbon nanotube based multi-electrode arrays," http://www.eng.tau.ac.il/~hanein/papers/CNT_EC_final.pdf.

[797] K. Matsushigea, H. Yamada, H. Tada, T. Horiuchi, X.Q. Chen, "Nanoscopic Molecular Memories," Annals N.Y. Acad. Sci. 852(1998):290-305.

[798] C. Cen, S. Thiel, G. Hammerl, C. W. Schneider, K. E. Andersen, C. S. Hellberg, J. Mannhart, J. Levy, "Nanoscale control of an interfacial metal–insulator transition at room temperature," Nature Materials (2 March 2008), doi:10.1038/nmat2136; http://www.nature.com/nmat/journal/vaop/ncurrent/abs/nmat2136.html.

[799] S.M. Sze, Semiconductor Devices: Physics and Technology, Wiley, New York, 1985.

[800] Tero Majamaa, "Ultrahigh Vacuum Plasma Oxidation in the Fabrication of Ultrathin Silicon Dioxide Films," PhD Dissertation, Helsinki University of Technology (Espoo, Finland), 20 October 2000; http://www.micronova.fi/units/epg/publications/publications2000/Reports24.pdf.

"soft breakdown"[801] at ~10^8 V/m which appears as a sudden increase in film conductivity but is rarely destructive. (If "soft breakdown" proves problematic, the operating voltage can be reduced or the electrode spacing increased without major alteration to the present NFW design architecture.) Note that tunneling through the oxide becomes significant only at a thickness $d_{electrode} \leq 3$ nm.[802] At ~2 x 10^8 V/m for a 3.0 nm SiO_2 layer, the measured tunneling current density is ~0.00125 amp/cm^2 for a 3 nm SiO_2 layer[803] or ~4.5 amp/m^2 for a 5 nm SiO_2 layer using the ~$d_{electrode}^{-2}$ theoretical dependency,[804] giving a leakage current of ~0.002 pA through the 10 nm x 50 nm sidewalls of the silica-embedded silver electrode columns which is 100-fold smaller than the primary ~0.2 pA electrode current flow (see below).

Due to their wide use in microelectronic applications, single-crystal silicon wafers of high purity are commercially available and relatively inexpensive – while the most common surface orientations are Si(100) and Si(111), other Si(hkl) orientations are known.[805] Upon exposure to air, single-crystal silicon rapidly becomes coated with a ~2 nm native oxide layer that can be removed chemically with fluoride ion or thermally under UHV conditions.[806] Atomically flat areas of monohydride ≡Si-H termination can be achieved by treating a commercial Si(111)-oriented wafer for 4-6 min with degassed 40% aqueous NH_4F.[807] The bulk-prepared hydride-terminated silicon surface typically has excellent chemical homogeneity (>99% H termination). The Si-H-terminated surface has a propensity to oxidize in the presence of oxygen, though such

---

[801] M. Depas, T. Nigam, M.M. Heyus, "Soft breakdown of ultra-thin gate oxide layers," IEEE Transactions on Electron Devices 43(September 1996):1499-1504; http://ieeexplore.ieee.org/xpl/freeabs_all.jsp?arnumber=535341.

[802] Tero Majamaa, "Ultrahigh Vacuum Plasma Oxidation in the Fabrication of Ultrathin Silicon Dioxide Films," PhD Dissertation, Helsinki University of Technology (Espoo, Finland), 20 October 2000; http://www.micronova.fi/units/epg/publications/publications2000/Reports24.pdf.

[803] Tero Majamaa, "Ultrahigh Vacuum Plasma Oxidation in the Fabrication of Ultrathin Silicon Dioxide Films," PhD Dissertation, Helsinki University of Technology (Espoo, Finland), 20 October 2000; http://www.micronova.fi/units/epg/publications/publications2000/Reports24.pdf.

[804] M. Lenzlinger, E.H. Snow, "Fowler-Nordheim tunneling into thermally grown SiO_2," J. Appl. Phys. 40(1969):278-283; S.M. Sze, Semiconductor Devices: Physics and Technology, Wiley, New York, 1985.

[805] H.N. Waltenburg, J.T. Yates, "Surface Chemistry of Silicon," Chem. Rev. 95(1995):1589-1673; R.J. Hamers, Y. Wang, "Atomically-Resolved Studies of the Chemistry and Bonding at Silicon Surfaces," Chem. Rev. 96(20 June 1996):1261-1290, http://www.ncbi.nlm.nih.gov/pubmed/11848789; D.Q. Hu, C.D. MacPherson, K.T. Leung, Surf. Sci. 273(1992):21; C.D. MacPherson, D.Q. Hu, M. Doan, K.T. Leung, "Catalytic dehydrogenation and thermal chemistry of cyclohexene and 1-methyl-1,4-cyclohexadiene on Si(111) 7x7 surfaces," Surf. Sci. 310(1994):231-242.

[806] Jillian M. Buriak, "Organometallic Chemistry on Silicon and Germanium Surfaces," Chem. Rev. 102(2002):1271-1308; http://pubs.acs.org/cgi-bin/article.cgi/chreay/2002/102/i05/pdf/cr000064s.pdf.

[807] G.S. Higashi, Y.J. Chabal, G.W. Trucks, K. Raghavachari, "Ideal Hydrogen Termination of the Si(111) Surface," Appl. Phys. Lett. 56(1990):656. G.S. Higashi, R.S. Becker, Y.J. Chabal, A.J. Becker, "Comparison of Si(100) Surfaces Prepared using Aqueous Solutions of NH_4F versus HF," Appl. Phys. Lett. 58(1991):1656. T.A. Newton, J.A. Boiani, M.A. Hines, Surf. Sci. 430(1999):67.

surfaces can easily be handled in air for minutes to tens of minutes without measurable degradation.[808] However, pure silicon has a breakdown voltage of only ~3 x 10^7 V/m,[809] and thus would be an inappropriate NFW assembly surface material.

Each silver electrode provides power and control to a single motor in a single NFW. As a very crude estimate using standard electrical formulas,[810] each motor requires up to P_w ~ 0.2 pW of power to drive it (Section 3.4.1.1) so each motor draws $I_{motor} = P_w / E_{motor}$ ~ 0.2 pA of current at E_{motor} = 1 volt. The electrical resistance of a 10-nm square (A_w = 100 nm^2) 50 nm tall column (L_{Ag} = 50 nm) of silver is $R_w = \rho_e L_{Ag} / A_w \sim 10^4$ ohms taking silver resistivity as $\rho_e = 1.59 \times 10^{-8}$ ohm-m, giving a negligible heat loss of $P_{loss} = I_{motor}^2 R_w$ ~ 0.4 zW (~0.1 k_BT/sec at 300 K) and a negligible voltage drop of $E_{motor} = I_{motor} R_w \sim 2 \times 10^{-9}$ V across the silver electrode. Resistance and joule heating are also low in nanotube wires: individual single-walled "metallic" carbon nanotubes 10-50 nm in length have been experimentally observed[811] to conduct large 25-100 microamp electrical currents before failing. Simple electrical contacts to carbon nanotubes can exhibit significant contact resistance[812] but contact area enlargement and van der Waals interactions reduce contact resistance between nanotube and metal surfaces,[813] so we do not anticipate a large resistance (typically one quantum unit or $R_c \sim h/2e^2$ ~ 12,949 ohms, with ~0.2 pA of NFW motor current producing a negligible ~3 x 10^{-9} volt drop across the contact) or heat loss ($P_{loss} = I_{motor}^2 R_c$ ~ 0.5 zW) across the nanotube/electrode contact area. The current density through the silver electrode is ~I_{motor} / A_w = 2000 amp/m^2 which lies far below the electromigration-limited ~10^{10} amps/m^2 limit for bulk aluminum[814] and even farther below the peak current densities of 10^{10}-10^{11} amps/m^2 in the 0.2-6.0 volt range in nanotubes[815] and >10^{14} amps/m^2 that has been pulled through a single chain of carbon atoms.[816]

---

[808] Jillian M. Buriak, "Organometallic Chemistry on Silicon and Germanium Surfaces," Chem. Rev. 102(2002):1271-1308; http://pubs.acs.org/cgi-bin/article.cgi/chreay/2002/102/i05/pdf/cr000064s.pdf.

[809] M. Lenzlinger, E.H. Snow, "Fowler-Nordheim tunneling into thermally grown SiO_2," J. Appl. Phys. 40(1969):278-283; S.M. Sze, Semiconductor Devices: Physics and Technology, Wiley, New York, 1985. Also: http://www.ioffe.rssi.ru/SVA/NSM/Semicond/Si/electric.html.

[810] Robert A. Freitas Jr., Nanomedicine, Volume I: Basic Capabilities, Landes Bioscience, Georgetown, TX, 1999; Section 6.4.3.1, p. 166; http://www.nanomedicine.com/NMI/6.4.3.1.htm.

[811] Ali Javey, Pengfei Qi, Qian Wang, Hongjie Dai, "Ten- to 50-nm-long quasi-ballistic carbon nanotube devices obtained without complex lithography," PNAS 101(14 September 2004):13408-13410; http://www.pnas.org/cgi/content/abstract/101/37/13408.

[812] J. Tersoff, "Contact resistance of carbon nanotubes," Appl. Phys. Lett. 74(12 April 1999):2122-.

[813] Myounggu Park, Baratunde A. Cola, Thomas Siegmund, Jun Xu, Matthew R. Maschmann, Timothy S. Fisher, Hyonny Kim, "Effects of a carbon nanotube layer on electrical contact resistance between copper substrates," Nanotechnology 17(2006):2294-2303; http://docs.lib.purdue.edu/cgi/viewcontent.cgi?article=1003&context=nanopub.

[814] Robert A. Freitas Jr., Nanomedicine, Volume I: Basic Capabilities, Landes Bioscience, Georgetown, TX, 1999; Section 6.4.3.1, p. 166; http://www.nanomedicine.com/NMI/6.4.3.1.htm.

[815] Hongjie Dai, Eric W. Wong, Charles M. Lieber, "Probing Electrical Transport in Nanomaterials: Conductivity of Individual Carbon Nanotubes," Science 272(26 April 1996):523-526; Stefan Frank,

The electrically active atomically rough multiple basement layers can be made using conventional lithography. According to the ITRS semiconductor industry roadmap,[817] 20 nm feature widths (corresponding to the conductor strip widths) should be available by 2009 for MPU physical gate lengths and by 2011 for ASIC physical gate lengths. However, the electrically active atomically smooth single topmost layer will be made using a combination of conventional lithography and patterned atomic layer epitaxy (PALE), which is a positionally-controlled variant of atomic layer deposition (ALD) or atomic layer epitaxy (ALE). ALE is a cyclic Chemical Vapor Deposition (CVD) type process that deposits a monolayer (or a well defined fraction of a monolayer) per ALE cycle. (ALE is a special case of ALD: the focus of ALE is depositing epitaxial layers, meaning perfect crystal structure, whereas ALD seeks to deposit one layer at a time with the focus on film uniformity, not single crystal structure.)

To fabricate the topmost layer, the surface is first coarsely patterned lithographically. Note that silver has the lowest electrical resistivity (1.59 μΩcm) of the known nonsuperconducting materials and the highest thermal conductivity, and is preferred to gold in ALD because it provides a stable atomic surface and does not exhibit reconstruction phenomena.[818] To make the electrodes, the standard semiconductor industry technology roadmap (ITRS) anticipates 10 nm feature widths (corresponding to the size of the electrode squares) with ±1 nm manufacturing error at the 3-sigma level by 2015 in production wafers,[819] but since the 1990s electron beam

---

Philippe Poncharal, Z.L. Wang, Walt A. de Heer, "Carbon Nanotube Quantum Resistors," Science 280(12 June 1998):1744-1746.

[816] Robert A. Freitas Jr., Nanomedicine, Volume I: Basic Capabilities, Landes Bioscience, Georgetown, TX, 1999; Section 6.4.3.1, p. 166; http://www.nanomedicine.com/NMI/6.4.3.1.htm. A.G. Rinzler, J.H. Hafner, P. Nikolaev, L. Lou, S.G. Kim, D. Tomanek, P. Nordlander, D.T. Colbert, R.E. Smalley, "Unraveling Nanotubes: Field Emission from an Atomic Wire," Science 269(15 September 1995):1550-1553.

[817] International Technology Roadmap for Semiconductors (ITRS), 2006 Update. "Overview and Working Group Summaries," Tables 1a (Product Generations and Chip Size Model Technology Trend Targets—Near-term Years) and 1b (Product Generations and Chip Size Model Technology Trend Targets—Long-term Years), p.3; http://www.itrs.net/Links/2006Update/FinalToPost/00_ExecSum2006Update.pdf; see also in "Lithography," pp. 7-8; http://www.itrs.net/Links/2006Update/FinalToPost/08_Lithography2006Update.pdf.

[818] M. Innocenti, G. Pezzatini, F. Loglio, M.L. Foresti, "Overview on the ultrathin films formation of II-VI compound semiconductors on silver by electrochemical atomic layer epitaxy," in: Manuel P. Soriaga et al., eds, Thin Films: Preparation, Characterizatin, Applications; Kluwer Academic/Plenum Publishers, 2002, pp. 95-135.

[819] International Technology Roadmap for Semiconductors (ITRS), 2006 Update. "Overview and Working Group Summaries," Tables 1a (Product Generations and Chip Size Model Technology Trend Targets—Near-term Years) and 1b (Product Generations and Chip Size Model Technology Trend Targets—Long-term Years), p.3; http://www.itrs.net/Links/2006Update/FinalToPost/00_ExecSum2006Update.pdf; see also in "Lithography," pp. 7-8; http://www.itrs.net/Links/2006Update/FinalToPost/08_Lithography2006Update.pdf.

stereolithography[820] and other[821] technologies have been able to create ~10 nm metallic (e.g., W, Cr, Re, Al, Au) features, with ~5 nm feature resolutions becoming available in the 2000s.[822] However, either method produces a surface that is coarse, not atomically smooth. Thus we propose to use ALD/PALE to remediate the electronically active coarse surface into perfect atomic smoothness such that the resulting surface contains no significant occurrences of steps or ledge features across each 10,000 nm^2 worksite area, and secondarily, if necessary, to remediate the final surface electrode geometries into more perfect square shapes.

Notes Aaltonen:[823] "ALD is a gas phase thin film deposition method which can be regarded as a special modification of the more widely used chemical vapor deposition (CVD) technique. In ALD, the precursors are led into the reaction chamber in alternate pulses while in CVD, the precursors are led into the reaction chamber simultaneously. The alternate precursor pulses in ALD are separated by inert gas purging (in flow type reactors) or by evacuation of the reactor (in high-vacuum type reactors). The precursors react with the surface groups on the substrate, or chemisorb on the substrate surface. In properly chosen process conditions, the surface reactions are self-limiting, which leads to highly controlled film growth. If the surface reactions become saturated, a constant film growth rate is obtained over the whole substrate surface, and films with excellent conformality and good large-area uniformity are obtained. The set of successive pulses of two or more precursors, separated by purge periods, is called an ALD cycle. The film growth rate is usually measured as the film thickness obtained during one ALD cycle. The film thickness can be easily and accurately controlled by the number of the applied growth cycles."

---

[820] Robert A. Freitas Jr., Ralph C. Merkle, Kinematic Self-Replicating Machines, Landes Bioscience, Georgetown, TX, 2004; Section 4.7; http://www.MolecularAssembler.com/KSRM/4.7.htm; N.A. Kislov, I.I. Khodos, E.D. Ivanov, J. Barthel, "Electron-beam-induced fabrication of metal-containing nanostructures," Scanning 18(1996):114-118; Marc Madou, Fundamentals of Microfabrication, CRC Press, Boca Raton, FL, 1997; Hiroshi Hiroshima, Norihito Suzuki, Naomi Ogawa, Masanori Komuro, "Conditions for fabrication of highly conductive wires by electron-beam-induced deposition," Jpn. J. Appl. Phys. 38(30 December 1999):7135-7139; Hans W.P. Koops, "Rapid prototyping and structure generation using three-dimensional nanolithography with electron beam induced chemical reactions," Paper No. 5116-52, SPIE Conference 5116, Microtechnologies for the New Millennium 2003, 19-21 May 2003, Maspalomas, Gran Canaria, Canary Islands, Spain, 2003.

[821] Cheng-Chung Lee et al., "Ion-assisted deposition of silver thin films," Thin Solid Films 359(January 2000):95-97.

[822] In-Bok Baek, Jong-Heon Yang, Won-Ju Cho, Chang-Geun Ahn, Kiju Im, Seongjae Lee, "Electron beam lithography patterning of sub-10 nm line using hydrogen silsesquioxane for nanoscale device applications," Journal of Vacuum Science & Technology B: Microelectronics and Nanometer Structures 23(November 2005):3120-3123.

[823] Titta Aaltonen, "Atomic Layer Deposition of Noble Metal Thin Films", Academic Dissertation, Helsinki 2005; http://www.cambridgenanotech.com/theses/Atomic%20Layer%20Deposition%20of%20Noble%20Metal%20Thin%20Films.pdf.

Atomic layer epitaxy technologies for Si on Si substrate,[824] insulating SiO_2 on Si substrate,[825] P/B doping on SiGe,[826] Si on Ge,[827] and semiconductor on silver substrate[828] are well known, but the ALD of metals on Si and SiO_2 substrates has traditionally been quite challenging. Even so, by 2005 a large number of metallic elements (Al, Co, Cu, Fe, Ir, Mo, Ni, Pd, Pt, Rh, Ru, Ta, Ti, W) had been deposited either by using a thermally activated process or with additional activation.[829] Silver was successfully deposited via a low-temperature REALD (Radical Enhanced ALD) process for the first time in 2006.[830] The silver films were successfully deposited on both silicon and glass (SiO_2) substrates. A saturated growth of 0.12 nm/cycle was obtained at 140 °C using a 3 second silver precursor pulse followed by a 7 second hydrogen radical pulse. The films were also relatively pure, containing only 4.0 atom-% phosphorous, 5.0 atom-% hydrogen and 1.0 atom-% carbon. (Exclusion of these elements from high-purity feedstock gases for ALE should greatly improve film purity.) The high purity was also evident in the low film resistivity (only 6 μΩcm for a 40 nm thick film) which also verified that the films were continuous even on a

---

[824] Eiji Hasunuma, Satoshi Sugahara, Shinji Hoshino, Shigeru Imai, Keiji Ikeda, Masakiyo Matsumura, "Gas-phase-reaction-controlled atomic-layer-epitaxy of silicon," J. Vac. Sci. & Technol. A: Vacuum, Surfaces, and Films 16(1998):679-684.

[825] Ofer Sneh, Steven M. George, "Thermal Stability of Hydroxyl Groups on a Well-Defined Silica Surface," J. Phys. Chem. 99(1995):4639-4647; http://pubs.acs.org/cgi-bin/abstract.cgi/jpchax/1995/99/i13/f-pdf/f_j100013a039.pdf?sessid=6006l3. S. Morishita, Y. Uchida, M. Matsumura, "Atomic-Layer Chemical-Vapor-Deposition of SiO_2 by Cyclic Exposures of $CH_3OSi(NCO)_3$ and H_2O_2," Jpn. J. Appl. Phys. 34(1995):5738-5742; http://jjap.ipap.jp/link?JJAP/34/5738. O. Sneh, M.L. Wisem A.W. Ott, L.A. Okada, S.M. George, "Atomic layer growth of SiO_2 on Si(100) using $SiCl_4$ and H_2O in a binary reaction sequence," Surf. Sci. 334(1995):135-152.. J.W. Klaus, A.W. Ott, J.M. Johnson, S.M. George, "Atomic layer controlled growth of SiO_2 films using binary reaction sequence chemistry," Appl. Phys. Lett. 70(3 March 1997):1092; http://link.aip.org/link/?APPLAB/70/1092/1. Kei-ichi Yamaguchi, Shigeru Imai, Naoto Ishitobi, Masashi Takemoto, Hidejiro Miki, Masakiyo Matsumura, "Atomic-layer chemical-vapor-deposition of silicon dioxide films with an extremely low hydrogen content," Applied Surface Science 130-132(June 1998):202-207. Eva Aro, Suvi Haukka, Marko Tuominen, "Atomic-Layer-Chemical-Vapor-Deposition of Films That Contain Silicon Dioxide," European Patent EP1248865, Filing Date 12/04/2000; www.freepatentsonline.com/EP1248865.html.

[826] B. Tillack, "Atomic layer doping of SiGe," Journal de Physique IV: Proceedings (1999), Proceedings of the Twelfth European Conference on Chemical Vapour Deposition, 1999, Vol. 1, pp. 295-305.

[827] Keiji Ikeda, Satoshi Sugahara, Yasutaka Uchida, Tomonori Nagai, Masakiyo Matsumura, "Formation of an atomically abrupt Si/Ge hetero-interface," Japanese Journal of Applied Physics 37(1998):1311-1315.

[828] M. Luisa Foresti, Francesca Forni, Massimo Innocenti, Francesca Loglio, Giovanni Pezzatini, "Deposition and characterization of ultrathin layers of compound semiconductors on Ag(111)," Abstr. Papers, Am. Chem. Soc. (2001), 221st COLL-345.

[829] Antti Niskanen, Radical Enhanced Atomic Layer Deposition of Metals and Oxides, Academic Dissertation, Helsinki, 2006; https://oa.doria.fi/dspace/bitstream/10024/2729/1/radicale.pdf. See also: A. Niskanen, T. Hatanpää, K. Arstila, M. Leskelä, M. Ritala, "Radical Enhanced Atomic Layer Deposition of Metallic Silver Films," submitted to Mater. Chem. 2006.

[830] Antti Niskanen, Radical Enhanced Atomic Layer Deposition of Metals and Oxides, Academic Dissertation, Helsinki, 2006; https://oa.doria.fi/dspace/bitstream/10024/2729/1/radicale.pdf.

macroscopic scale and visually mirror-like. On close inspection the depositions were polycrystalline and as a result very rough (Figure III-8), albeit growing conformally despite the high roughness. It should be possible to obviate the surface roughness by employing the REALD approach (in which only radicals are allowed to reach the substrate) in a scanning-probe-based PALE process for depositing silver, and for the silicon or nonconducting portions of the assembly surface as well.

Figure III-8. A cross-sectional SEM image of a 40 nm thick silver film deposited on a patterned trench substrate.[831] Left: A close-up of the top of a trench. Middle: An overview of the trench substrate. Right: A close-up of the bottom of a trench.

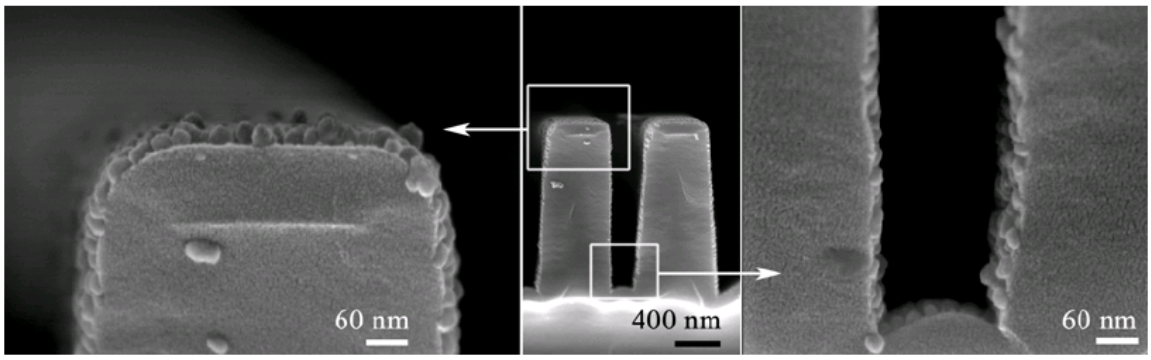

PALE, which has been proposed by researchers at Zyvex[832] (Section 2.2.4), is an extension of ALD or ALE in which scanning probe technology is employed for positional control to selectively deprotect specific atomic sites on a surface (Figure III-9), after which atomic layer epitaxy is used to add a single atomic layer of a second material from the vapor phase at the positionally selected depassivated sites in a CVD-type reaction with an ambient gas. Repeating this process can allow atomically precise three-dimensional structures to be built up one atomic layer at a time. For example, Lyding's group at the Beckman Institute has successfully grown silicon nanostructures by selectively depassivating a hydrogen-terminated silicon surface at atomically precise locations using Feedback Controlled Lithography,[833] then depositing silicon

---

[831] Antti Niskanen, Radical Enhanced Atomic Layer Deposition of Metals and Oxides, Academic Dissertation, Helsinki, 2006; https://oa.doria.fi/dspace/bitstream/10024/2729/1/radicale.pdf.

[832] J.N. Randall et al, "Patterned atomic layer epitaxy," United States Patent 20050223968, 13 October 2005. See also: Mikko Ritala, Markku Leskelä, "Atomic layer epitaxy – a valuable tool for nanotechnology?" Nanotechnology 10(March 1999):19-24.

[833] M.C. Hersam, G.C. Abeln, J.W. Lyding, "An approach for efficiently locating and electrically contacting nanostructures fabricated via UHV-STM lithography on Si(100)," Microelectronic Engineering 47(June 1999):235-237. See also: Mark C. Hersam, Nathan P. Guisinger, and Joseph W. Lyding, "Silicon-Based Molecular Nanotechnology," Seventh Foresight Conference on Molecular Nanotechnology, 15-17 Oct. 1999, Santa Clara, CA. http://www.foresight.org/conferences/mnt7/Papers/Hersam/index.html.

onto the sites from the gas phase, demonstrating that atomically precise deprotection is possible with an STM tip that is not itself atomically precise.

Figure III-9. (a) The feedback {z} and tunneling current {I} signals are monitored as a function of time while patterning at 3V, 2 nA; hydrogen atom desorption is clearly observed as a ~1.5 Å step in z and occurs in ~0.005 sec.[834] (c) 3 x 3 array of individual dangling bonds nanopatterned with feedback controlled lithography on Si(100)-2x1:H in ultra-high vacuum.[835]

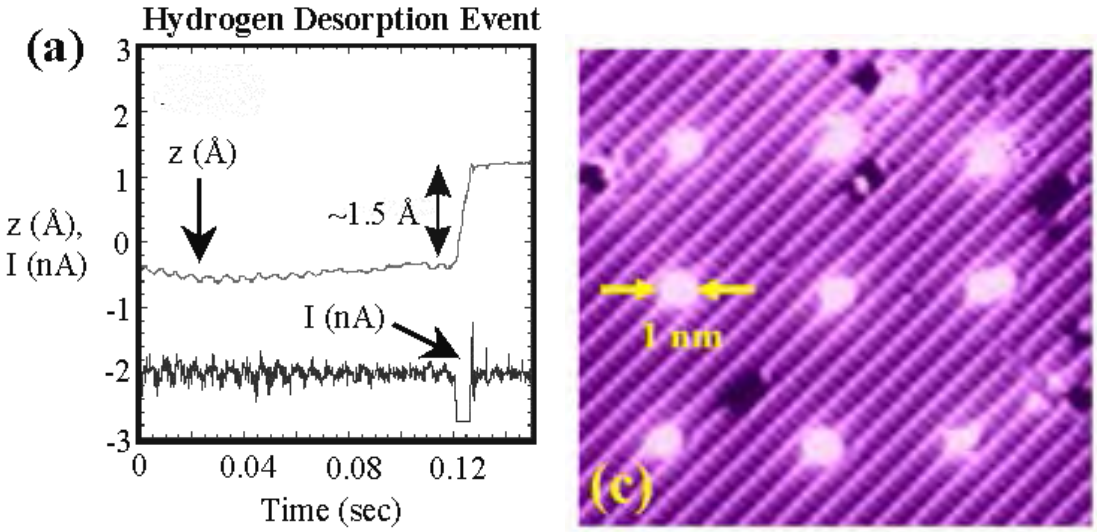

To eliminate the roughness of the coarse surface, the surface is scanned to identify topographical low spots within each designated workspace area on the chip. The PALE process is then employed to fill in the low areas, one layer at a time, until all surfaces within each 10,000 nm^2 workspace area have been raised to the same height, resulting in an atomically smooth surface upon which an NFW can be assembled during Task III-4. Hydrogen desorption occurs in ~0.005 sec[836] which is conservatively consistent with at least ~200 Hz operation, corresponding to a 17-

---

[834] M.C. Hersam, G.C. Abeln, J.W. Lyding, "An approach for efficiently locating and electrically contacting nanostructures fabricated via UHV-STM lithography on Si(100)," Microelectronic Engineering 47(June 1999):235-237. See also: Mark C. Hersam, Nathan P. Guisinger, and Joseph W. Lyding, "Silicon-Based Molecular Nanotechnology," Seventh Foresight Conference on Molecular Nanotechnology, 15-17 Oct. 1999, Santa Clara, CA. http://www.foresight.org/conferences/mnt7/Papers/Hersam/index.html.

[835] Mark Hersam, "Conductive Scanning Probe Microscopy Nanopatterning," The Hersam Research Group: Single Molecule Sensing, Characterization, and Actuation, 2007; http://www.hersam-group.northwestern.edu/nanopatterning.html.

[836] M.C. Hersam, G.C. Abeln, J.W. Lyding, "An approach for efficiently locating and electrically contacting nanostructures fabricated via UHV-STM lithography on Si(100)," Microelectronic Engineering

29 nm^2/tip-sec depassivation rate at surface atom densities of 6.8 (100), 9.6 (110) and 11.8 (111) atoms/nm^2 for the three principal Si crystal faces. This yields a reasonable estimated scan time of 340-590 sec (5-10 min) per layer for each 10,000 nm^2 worksite surface using just a single depassivating tip. Remediating an average of 5 full layers on ~1000 worksites would thus require a total scan time of 20-40 days using a single tip.

It should be noted that the addition of a few sensors to the NFW design (at a very small cost in number of atoms and additional assembly surface electrodes; Section 3.8.1.3) might allow the operator to compensate for any remaining minor irregularities in the assembly surface by appropriately adjusting the program parameters, or by providing some measure of self-correcting feedback.

3.4.4 Task III-3: Fabricate and Assemble NFW Nanoparts and Nanodevices using Phase II System

Task III-3 is to use the macroscale manufacturing system created during Phase II (Section 3.3) to fabricate all necessary nanoparts, and then to assemble some of these nanoparts into all necessary nanodevices, that are needed to build a complete working nanoscale fabrication workstation (NFW) that is itself capable of performing all fabrication steps previously demonstrated by the macroscale system developed in Phase II.

Assuming the availability of a 1 Hz deposition frequency for DMS fabrication in which one atom of nanopart structure can be placed onto a workpiece each second by the Phase II system (Section 3.3.1), then one Phase II macroscale workstation can fabricate (from primitive feedstock molecules) all 521 nanoparts needed to build one NFW, comprised of 31,347,796 atoms, in ~3.13 x 10^7 sec (~363 days or ~1 year). This build time may be significantly reduced by employing multiple Phase II macroscale workstations operated simultaneously, each building different sets of nanoparts for the one NFW. For example, the simultaneous use of 12 Phase II systems would reduce NFW nanopart build time from 1 year to just 1 month. The use of multiple workstations is also advisable to permit more rapid prototyping and experimentation with new nanopart designs, and to perform quality control testing on fabricated nanoparts. Note that build time cannot be reduced by increasing pulse frequency in Phase III because fabrication operations are limited by the operating rate of the Phase II system (during manual transport of feedstock molecules).

Assuming the availability of a conservative 0.01 Hz operating frequency for nanopart assembly operations in which one nanopart can be added to a multipart nanodevice workpiece every 100 seconds (Section 3.3.1), and conservatively assuming that on average each nanopart must be handled once to be fitted into a nanodevice workpiece, then one Phase II macroscale workstation could assemble nanoparts into all necessary nanodevices needed to build one NFW, comprised of 521 nanoparts, in no more than (~521 nanoparts / 0.01 Hz) ~ 5.21 x 10^4 sec (~15 hours). Since this time requirement is a thousandfold less than the time required for nanopart fabrication, and

---

47(June 1999):235-237. See also: Mark C. Hersam, Nathan P. Guisinger, and Joseph W. Lyding, "Silicon-Based Molecular Nanotechnology," Seventh Foresight Conference on Molecular Nanotechnology, 15-17 Oct. 1999, Santa Clara, CA. http://www.foresight.org/conferences/mnt7/Papers/Hersam/index.html.

since nanodevice assembly can take place both during and after nanopart fabrication, the total production time required to build all nanoparts and nanodevices comprising an NFW is driven almost exclusively by nanopart fabrication time.

All manufactured components including both individual nanoparts and multipart nanodevices should be laid out on one Phase II workstation release surface in a specific pattern of positions and orientations to allow blind pick-and-place to be employed during final assembly of the NFW in Task III-4. The longest dimension of any nanopart described in Section 3.4.1.1 is 50 nm, so conservatively allocating a 50 nm x 50 nm area for warehousing each of the 521 nanoparts would occupy an area of 1,302,500 nm^2 (equivalent to a 1.14 x 1.14 micron square area) on the Phase II system release surface. If multiple Phase II macroscale workstations are used for nanopart fabrication as recommended above, then an additional subtask here is the consolidation of all nanoparts and nanodevices manufactured in the several workstations into one workstation, by transferring all NFW components onto a single Phase II workstation release surface in a specific pattern of positions and orientations that will allow blind pick-and-place to be employed during final assembly of the NFW in Task III-4. Both Phase II and Phase III surfaces are either free of step edges and other irregularities, or else these irregularities will have been previously mapped and the blind pick-and-place assembly sequence modified accordingly.

3.4.5 Task III-4: Assemble First-Generation NFW using Phase II System

Task III-4 is to manually assemble the first-generation nanoscale fabrication workstation (NFW) as a one-off (no parallelization) at a designated worksite on the atomically smooth assembly surface of the multielectrode chip created during Task III-2 (Section 3.4.3), using the macroscale manufacturing system created during Phase II (Section 3.3) to build an NFW that is itself capable of performing all fabrication steps previously demonstrated by the macroscale system developed in Phase I.

The first step toward the completion of Task III-4 is to insert the multielectrode multiworksite chip created during Task III-2 into the Phase II apparatus, there to be properly positioned and aligned relative to the Phase II release surface upon which the component nanoparts and nanodevices were originally pre-positioned during Task III-3. The juxtaposition and calibration of both surfaces may require the addition of a piezopositioner capable of translating the visiting chip surface so that it can be aligned and made flush with the Phase II release surface. This will allow the Phase II system to most readily assemble objects at a worksite on the more distant visiting chip surface.

Because fabricated nanoparts and assembled nanodevices must be transferred from the Phase II system release surface to a specific worksite on the surface of the multielectrode chip created during Task III-2, to be assembled there into the NFW, assembly at the worksite might take longer than on the Phase II release surface because of the extra transport time. However, some

high-accuracy nanopositioning systems[837] can achieve high-velocity slew rates up to 1 mm/sec. Coarse transport of NFW components requiring the Phase II manipulator to translate across a distance of ~100 microns at a slew speed of 100-1000 micron/sec is fully consistent with an assembly operating frequency of ~0.01-1 Hz. However, the assumed operating frequency is not a crucial quantity in the present context because the successful completion of Task III-4 in a reasonable elapsed time is relatively insensitive (by many orders of magnitude) to the assembly frequency.

We conservatively assume the availability of a 0.01 Hz operating frequency for nanopart assembly operations using the Phase II system in which one nanopart may be transported from one surface to the other and then added to the NFW workpiece every 100 seconds (Section 3.3.1). The four NFW manipulators each consist of 57 assemblable components (Table III-1); combining this with the 20 toolheads and 1 toolrack (Table III-2) gives a total of 249 components to be assembled to make the first generation NFW. Conservatively assuming that on average each component must be handled once to be installed onto the growing NFW workpiece at the designated 10,000 nm^2 53-electrode worksite, then the Phase II macroscale workstation can assemble the entire first-generation NFW, comprised of 249 assemblable components, in no more than (~249 components / 0.01 Hz) ~ 2.49 x 10^4 sec (~7 hours). Construction of the first-generation NFW is done as a one-off with no parallelization at the assembly stage.

3.4.6 Task III-5: Operate First-Generation NFW using Phase II System

Task III-5 is to validate the design of the first-generation nanoscale fabrication workstation (NFW) by experimentally demonstrating its basic functionality.

To operate the completed NFW, the Phase II macroscale workstation is used to acquire feedstock from its own native feedstock presentation surface and manually transfer each feedstock molecule to DMS manipulators requiring feedstock as material input for the NFW. Aside from this exogenous supply source, the NFW is operated as a standalone nanoscale workstation by sending appropriate current pulses through the 53 electrodes which provide both power and control. These control pulses are synchronized with the actions of the Phase II manipulator to achieve a smoothly running nanofabrication system. Finished nanoparts are carried off by the Phase II system.

The NFW must demonstrate its complete functionality by fabricating at least one instance of each of the 16 different nanopart types (Tables III-1 and III-2) previously fabricated in greater numbers using the Phase II system during Task III-3. This will prove that the NFW can fabricate all nanoparts needed to make a copy of itself from externally supplied feedstock, power, and control signals, demonstrating 100% nanoparts closure for the NFW system design. The Phase II system is used to remove each completed nanopart from the NFW and transport it back to its own

---

[837] Luc Chassagne, Suat Topcu, Yasser Alayli, Patrick Juncar, "Highly accurate positioning control method for piezoelectric actuators based on phase-shifting optoelectronics," Meas. Sci. Technol. 16(2005):1771-1777.

working area for storage and further characterization. Assuming ~60,169 atoms/nanopart (Section 3.4.2), then fabricating 16 such parts will require the placement of ~10^6 atoms. Further assuming that the Phase II system can present feedstock molecules to the NFW at ~1 Hz, then NFW productivity is feedstock-limited to ~1 Hz (Section 3.4.1) and fabricating the 16 exemplar nanoparts will require ~10^6 sec (~12 days), concluding the required demonstration.

An absolutely rigorous demonstration of functionality would additionally require the NFW to prove its ability to build all 521 of its own nanoparts, which would then be acquired by the Phase II system and used to assemble a replica NFW on an adjacent 10,000 nm^2 worksite, with the replica then required to demonstrate its ability to fabricate at least one instance of each of the 16 different nanopart types comprising the NFW. This would definitively prove replication fidelity[838] of the NFW. However, insisting on this proof could add more than a year's delay to the program without providing significant useful information unavailable by other means such as by direct characterization and validation of nanopart structure for the 16 nanoparts produced by the first NFW. For this reason we recommend that this secondary demonstration should be shelved until Phase IV (Section 3.5.10) in favor of faster validation methods. (A tertiary demonstration involving the production of a granddaughter NFW by the daughter NFW, needed to prove offspring fertility,[839] would add yet another year of delay and should also be shelved for similar reasons until Phase IV (Section 3.5.10).)

It may be necessary to iterate Tasks III-1, III-3, III-4, and III-5 to fully debug the NFW design and to successfully achieve the desired results.

---

[838] Robert A. Freitas Jr., Ralph C. Merkle, Kinematic Self-Replicating Machines, Landes Bioscience, Georgetown, TX, 2004; Sections 5.1.9(L2) and 5.1.9(L4); http://www.MolecularAssembler.com/KSRM/5.1.9.L.htm.

[839] Robert A. Freitas Jr., Ralph C. Merkle, Kinematic Self-Replicating Machines, Landes Bioscience, Georgetown, TX, 2004; Sections 5.1.9(L2) and 5.1.9(L4); http://www.MolecularAssembler.com/KSRM/5.1.9.L.htm.

3.5 Phase IV: Second-Generation Nanoscale Fabrication Workstation (NFW-2)

The second-generation nanoscale fabrication workstation (NFW-2) is a set of individually controlled nanoscale manipulators and toolheads capable of performing diamondoid mechanosynthesis on a multi-electrode assembly surface inside a UHV workspace chamber, powered by electrical control signals passed through the assembly surface via electrical surface contact points, with material feedstock provided from a Bulk Feedstock Supply System (BFSS) installed adjacent to the workstation on the same assembly surface.

The key objective of Phase IV is the design and manufacture of the automated BFSS and its subsequent integration with the existing NFW system developed in Phase III to create an upgraded, more nearly self-contained second-generation NFW system that no longer needs to be hand-fed its molecular feedstock by the Phase II MMW manipulator system, thus enabling the NFW-2 to operate at ~100-fold faster production rates. For this phase of the program we continue to assume that all atomically precise components will be comprised solely of C, H, or Ge atoms.

The second-generation NFW is described in Section 3.5.1 and illustrated in Figure IV-1. This is followed by an enumeration of the specific tasks required to manufacture the NFW-2 which include: design and simulation of the first-generation BFSS (Section 3.5.2), preparation of a multielectrode assembly surface (Section 3.5.3), fabrication of needed BFSS nanoparts and assembly of needed BFSS multipart nanodevices using the Phase II system (Section 3.5.4), manual assembly of the first-generation BFSS using the Phase II system (Section 3.5.5), operation of the first-generation BFSS using the Phase II system (Section 3.5.6), design and simulation of the NFW-2 second-generation workstation (Section 3.5.7), fabrication of needed NFW-2 nanoparts and assembly of needed NFW-2 multipart nanodevices using the Phase II system (Section 3.5.8), manual assembly of the NFW-2 using the Phase II system (Section 3.5.9), demonstration of successful endogenous operation of the NFW-2 without needing the Phase II system to assist in feedstock presentation, byproduct disposal, or other fabrication-related functions (Section 3.5.10), and finally the winning of the Feynman Grand Prize (Section 3.5.11).

3.5.1 Description of the NFW-2 Second-Generation Workstation

The structure and basic function of the second-generation nanoscale fabrication workstation (NFW-2) is described in this Section.

The function of a completed second-generation NFW is to fabricate nanoparts using a set of individually controlled nanoscale manipulators grasping DMS toolheads capable of performing diamondoid mechanosynthesis. The NFW-2 builds diamondoid nanoparts starting from basic feedstock molecules that it acquires from a Bulk Feedstock Supply System (BFSS) installed adjacent to the workstation on the same assembly surface. The structure and basic function of the BFSS is also described in this Section, followed by a description of the operation of the NFW-2, which includes purging and recharging the BFSS prior to each manufacturing cycle.

Figure IV-1. Schematic illustration of the second-generation Nanoscale Fabrication Workstation (NFW-2), showing four Stewart platform manipulators mounted on a foundation block adjacent to a 20-tip toolrack, surrounded by the Bulk Feedstock Supply System (BFSS) graphene storage tank (BFSS appurtenant structures not shown).

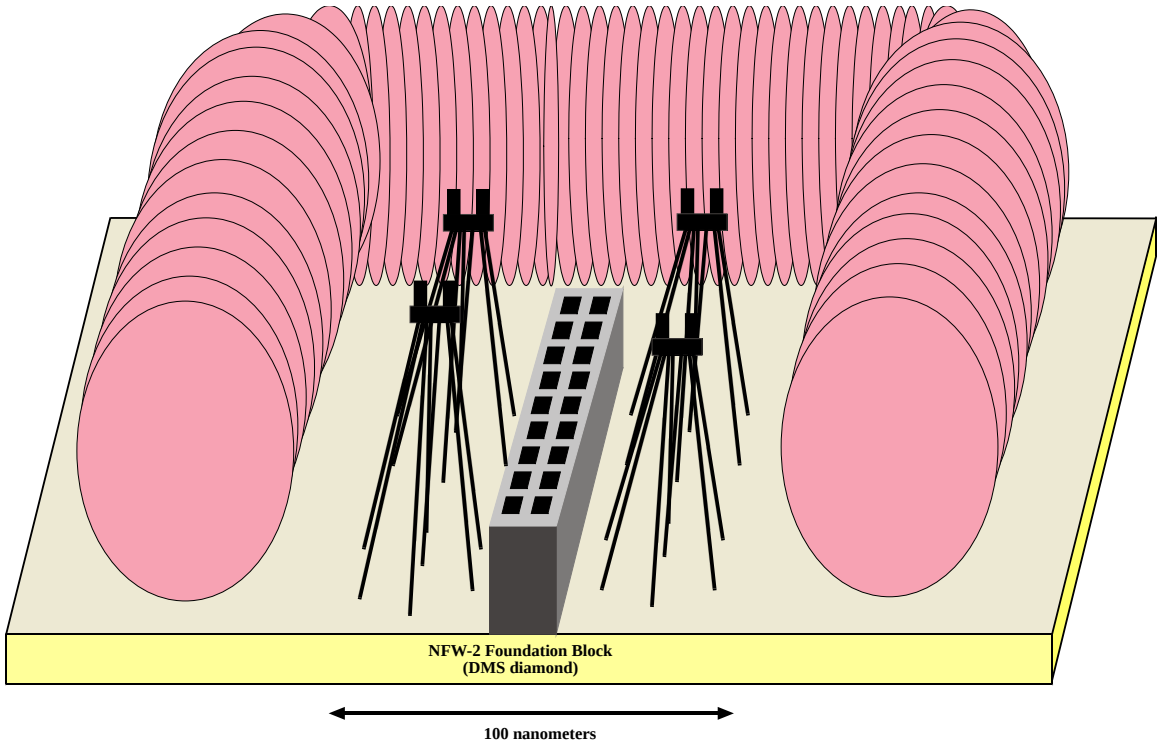

3.5.1.1 Overall Strategy of the Bulk Feedstock Supply System (BFSS)

The purpose of the BFSS is to directly supply the NFW with all feedstock gases and to remove byproduct (waste) gases, without requiring any intervention during NFW operation by macroscale instrumentalities such as the Phase II system, thus providing a highly scalable feedstock delivery system that can itself be replicated along with the NFW and can supply the NFW with feedstock molecules at high speed. Addition of the BFSS to the NFW allows NFW-2 to be operated at much faster mass throughput rates for building nanoparts.

The strategy underlying the design of the BFSS is driven by the insight that the only chemically reactive entities present inside the UHV workspace chamber, other than one or two transitory unpassivated sites on a workpiece in progress, are the active mechanosynthetic toolheads which have exposed radicals at their tooltips. These toolheads are held by an end effector (tool chuck) at the distal terminus of each manipulator. The toolheads are detachable from the manipulators and are stowed in an airtight toolrack. This allows the workspace chamber to be periodically flooded, then purged, of various gases without poisoning the DMS tooltips – by keeping reactive radicals and gas molecules separated in time, rather than separated in space via a solid barrier

wall as in earlier molecular assembler designs.[840] All other exposed surfaces inside the workspace chamber are chemically nonreactive nanomachinery having passivated surfaces from which the feedstock and byproduct gases are readily purged (Section 3.5.1.7).

If further study defines a serious risk in which pre-purge feedstock or byproduct molecules are able to jam a mechanism, or form covalent bonds across or inside concave openings in structures, or physisorb across two moving parts and oppose their relative movement, then the NFW-2 system can be redesigned to allow tool chucks and other workstation components that gas molecules might invade to be temporarily stowed inside small protective flanges or garages during the gas flooding phase of operation (analogous to the toolrack in which reactive tooltips are parked).

Other strategies for supplying feedstock gases – including subsurface piping, on-surface piping, vertically-lowered gas pipe arrays, and free-rolling gas tanks such as gated gas-filled fullerenes – were considered and rejected as inferior to the method chosen.

3.5.1.2 Primary Byproduct Molecule: Molecular Hydrogen

One important function of the BFSS is to sequester byproduct gases which carry away unneeded feedstock atoms. A hydrocarbon feedstock molecule will generate negligible materials waste when the elemental composition of the feedstock exactly matches the elemental composition of the products being manufactured using that feedstock – that is, when $N_{H,feedstock}/N_{C,feedstock} = N_{H,product}/N_{C,product}$, where $N_{H,feedstock}$ and $N_{C,feedstock}$ are, respectively, the number of hydrogen or carbon atoms per feedstock molecule, and where $N_{H,product}$ and $N_{C,product}$ are the number of hydrogen or carbon atoms in each product object. If $N_{H,feedstock}/N_{C,feedstock} > N_{H,product}/N_{C,product}$, then

---

[840] K. Eric Drexler, Engines of Creation: The Coming Era of Nanotechnology, Anchor Press/Doubleday, New York, 1986. K. Eric Drexler, Chris Peterson, Gayle Pergamit, Unbounding the Future: The Nanotechnology Revolution, William Morrow/Quill Books, NY, 1991; http://www.foresight.org/UTF/Unbound_LBW/. K. Eric Drexler, Nanosystems: Molecular Machinery, Manufacturing, and Computation, John Wiley & Sons, New York, 1992. Ralph C. Merkle, "Self replicating systems and molecular manufacturing," J. Brit. Interplanet. Soc. 45(1992):407-413; http://www.zyvex.com/nanotech/selfRepJBIS.html. Ralph C. Merkle, "Design considerations for an assembler," Nanotechnology 7(1996):210-215; http://www.zyvex.com/nanotech/nano4/merklePaper.html. Ralph C. Merkle, "Casing an assembler," Nanotechnology 10(1999):315-322; http://www.zyvex.com/nanotech/casing. Robert A. Freitas Jr., Ralph C. Merkle, Kinematic Self-Replicating Machines, Landes Bioscience, Georgetown, TX, 2004; Section 4.9.1; http://www.MolecularAssembler.com/KSRM/4.9.1.htm; Section 4.9.2, http://www.MolecularAssembler.com/KSRM/4.9.2.htm; Section 4.9.3, http://www.MolecularAssembler.com/KSRM/4.9.3.htm; Section 4.10.1, http://www.MolecularAssembler.com/KSRM/4.10.1.htm; Section 4.10.2, http://www.MolecularAssembler.com/KSRM/4.10.2.htm; Section 4.11.1, http://www.MolecularAssembler.com/KSRM/4.11.1.htm; Section 4.11.2, http://www.MolecularAssembler.com/KSRM/4.11.2.htm; Section 4.11.3, http://www.MolecularAssembler.com/KSRM/4.11.3.htm and Appendix B http://www.MolecularAssembler.com/KSRM/AppB.1.htm; Section 4.18, pp. 140-141, http://www.MolecularAssembler.com/KSRM/4.18.htm.

the feedstock is hydrogen-rich relative to the manufactured product, and hydrogen byproduct will be generated as waste material requiring discharge. If $N_{H,feedstock}/N_{C,feedstock} < N_{H,product}/N_{C,product}$, then the feedstock is carbon-rich relative to the manufactured product, and carbon byproduct will be generated. Taking the proposed NFW as the product to be manufactured (Table III-2), the ideal target ratio would be $N_{H,feedstock}/N_{C,feedstock} = N_{H,product}/N_{C,product} = N_{H,NFW}/N_{C,NFW} \sim 0.20$. A survey of the likely major classes of hydrocarbon feedstock molecules (Table IV-1) suggests that – excepting pure carbon molecules (which would require supplemental hydrogen feedstock to be provided separately), unstable hydrocarbon radicals (which would recombine if transferred in bulk), and partially hydrogenated fullerenes (which are nongaseous and would be relatively difficult to supply and disassemble reliably) – all available hydrocarbons have an $N_{H,feedstock}/N_{C,feedstock}$ ratio significantly higher than 0.20, hence are all hydrogen-rich. This implies that regardless of which hydrocarbon is chosen as the primary feedstock molecule, excess hydrogen will have to be disposed of as the primary byproduct.

Table IV-1. Possible Hydrocarbon Feedstock Molecules

Feedstock Molecule Candidate	**Formula**	**$N_{H,feedstock}/N_{C,feedstock}$**
Fullerenes	C_{20}, C_{22},...,C_{60},...	0
Carbon nanotubes	$C_{n\ (large)}$	0
Cyclic polyynes[841]	C_{18}	0
Carbon clusters (radicals)	C_4, C_6, C_8, C_{10}	0
Polyacetylene radicals	C_2H - $C_{11}H$	0.09-0.50
Partially hydrogenated fullerenes	$C_{240}H_2$	0.01
	$C_{48}H_2$	0.04
	$C_{34}H_2$	0.06
	$C_{60}H_6$	0.10
Polycyclic Aromatic Hydrocarbons (planar rings)		
Benzene (1 ring)	C_6H_6	1.00
Naphthalene (2 rings)	$C_{10}H_8$	0.80
Phenalene (3 rings)	$C_{13}H_9$	0.69
Pyrene (4 rings)	$C_{16}H_{10}$	0.63
Perylene (5 rings)	$C_{20}H_{12}$	0.60
Benzoperylene (6 rings)	$C_{22}H_{12}$	0.55
Coronene (7 rings)	$C_{24}H_{12}$	0.50
Dibenzocoronene (9 rings)	$C_{30}H_{14}$	0.47
Ovalene (10 rings)	$C_{32}H_{14}$	0.44
Circumcoronene (19 rings)	$C_{54}H_{18}$	0.36
Prismanes (cage hydrocarbons)		
Triangulane	C_6H_6	1.00
Cubane	C_8H_8	1.00
Hexagonane	$C_{12}H_{12}$	1.00
Adamantanes		

[841] F. Diederich, Y. Rubin, C.B. Knobler, R.L. Whetten, K.E. Schriver, K.N. Houk, Y. Li, "All-carbon molecules: Evidence for the generation of cyclo[18]carbon from a stable organic precursor," Science 245(1989):1088-1090; F. Diederich, Y. Rubin, "Synthetic Approaches toward Molecular and Polymeric Carbon Allotropes," Angew. Chem. Int. Ed. Engl. 31(1992):1101-1123; F. Diederich, "Carbon scaffolding: building acetylenic all-carbon and carbon-rich compounds," Nature 369(19 May 1994):199-207, http://www.nature.com/nature/journal/v369/n6477/abs/369199a0.html; Dietmar A. Plattner, K.N. Houk, "C18 is a polyyne," J. Am. Chem. Soc. 117(1995):4405-4406.

Triamantane	$C_{18}H_{24}$	1.33
Tetramantane	$C_{22}H_{28}$	1.27
Pentamantane	$C_{26}H_{32}$	1.23
Hexamantane	$C_{30}H_{36}$	1.20
Iceanes (hexagonal diamond)	$C_{6n}H_{6n}$	1.00
Radialenes[842]	C_nH_n	1.00
	$C_{2n}H_n$	0.50
	$C_{3n}H_n$	0.33
Alkynes (C≡C)		
Propyne (methylacetylene)	C_3H_4	1.33
Butenyne (vinylacetylene)	C_4H_4	1.00
Ethyne (acetylene)	C_2H_2	1.00
Pentadiyne	C_5H_4	0.80
Phenylacetylene	C_8H_6	0.75
Octatriyne	C_8H_6	0.75
Benzyne	C_6H_4	0.67
Butadiyne (diacetylene)	C_4H_2	0.50
Triacetylene	C_6H_2	0.33
Alkenes and Cumulenes (C=C)		
Ethylene (ethene)	C_2H_4	2.00
Propylene (propene)	C_3H_6	2.00
Butene	C_4H_8	2.00
Butadiene	C_4H_6	1.50
Propadiene (allene)	C_3H_4	1.25
Butatriene	C_4H_4	1.00
Cyclooctatetraene	C_8H_8	1.00
Pentatetraene	C_5H_4	0.80
Acenaphthylene	$C_{12}H_8$	0.67
Alkanes (C–C)		
Methane	CH_4	4.00
Ethane	C_2H_6	3.00
Propane	C_3H_8	2.67
Butane	C_4H_{10}	2.50

The most efficient primary byproduct molecule in a hydrocarbon NFW is pure molecular hydrogen (H_2) because it requires no carbon atom mediation (but see Section 3.5.1.6). Thus H_2 has been provisionally selected as the primary byproduct gas for hydrogen removal for the second-generation nanoscale fabrication workstation. Neither silver[843] nor silicon dioxide[844]

---

[842] Henning Hopf, Gerhard Maas, "Preparation and properties, reactions, and applications of radialenes," Angew. Chem. Int. Ed. Engl. 31(August 1992):931-954; Armen M. Boldi, Francois Diederich, "Expanded radialenes: A novel class of cross-conjugated macrocycles," Angew. Chem. Int. Ed. Engl. 33(1994):468-471.

[843] G.K. Boreskov, I.V. Lokhova, A.V. Khasin, "Adsorption isotherm of oxygen on silver," Reaction Kinetics and Catalysis Letters 16(June 1981):167-170.

[844] Arthur T. Hubbard, Encyclopedia of Surface and Colloid Science, CRC Press, 2002.

surfaces chemisorb molecular hydrogen, though weak physisorption of H_2 on Ag surface is observed at ~20 K;[845] silica surfaces are also inert to methane.[846]

If the disposal of pure H_2 proves problematic (perhaps due to the molecule's small size and consequent propensity to leak), Table IV-2 suggests that the best alternative would be methane (CH_4), the hydrocarbon with the highest $N_{H,byproduct}/N_{C,byproduct}$ ratio – a highly desired characteristic for the ideal carbon-containing byproduct gas with which to efficiently export the largest amount of hydrogen per diverted carbon atom. (Free-floating hydrogen-entrained diamondoid or polyethylene nanotanks and fullerenes do not permit easy and reliable continuous positional control and thus are not a convenient or scalable solution; their use would tend to increase system complexity with size.) However, even using methane in preference to other hydrocarbons as the byproduct molecule would still require the diversion of a significant number of carbon atoms from the product stream, hence mandating correspondingly larger BFSS storage tanks with resulting longer buildout times during the first half of the nanofactory development program.

Table IV-2. Possible Byproduct Molecules for Hydrogen Disposal

Byproduct Molecule Candidate	**Formula**	$N_{H,byproduct}/N_{C,byproduct}$
Pure molecular hydrogen	H_2	∞
H_2-entrained fullerenes		
20.1 nm diameter spheroid	$50{,}000H_2$ @ $C_{20,000}$	5.00
2.2 nm diameter spheroid	$50H_2$ @ C_{240}	0.41
1.1 nm diameter spheroid	$5H_2$ @ C_{60}	0.17
0.8 nm diameter spheroid	H_2 @ C_{30}	0.07
H_2-entrained polyethylene nanotanks (10 nm radius, 200 nm long, 1 nm wall, 100 atm)	$140{,}000H_2$ @ $C_{550,000}H_{1,100,000}$	2.50
H_2-entrained diamond nanotanks (10 nm radius, 200 nm long, 1 nm wall, 10,000 atm)	$1{,}300{,}000H_2$ @ $C_{2,300,000}$	1.10
Alkanes (C–C)		
Methane	CH_4	4.00
Ethane	C_2H_6	3.00
Propane	C_3H_8	2.67
Butane	C_4H_{10}	2.50
Pentane	C_5H_{12}	2.40
Hexane	C_6H_{14}	2.33
Octane	C_8H_{18}	2.25
Decane	$C_{10}H_{22}$	2.20
Eicosane	$C_{20}H_{42}$	2.10
Polyethylene	$\sim(CH_2)_n$	2.00

[845] J.E. Demuth, D. Schmeisser, Ph. Avouris, "Resonance Scattering of Electrons from N_2, CO, O_2, and H_2 Adsorbed on a Silver Surface," Phys. Rev. Lett. 47(October 1981):1166-1169; http://prola.aps.org/abstract/PRL/v47/i16/p1166_1.

[846] J. Kong, H. Soh, A. Cassell, C.F. Quate, H. Dai, "Synthesis of Single Single-Walled Carbon Nanotubes on Patterned Silicon Wafers," Nature 395(1998):878-881.

3.5.1.3 Primary Hydrocarbon Feedstock Molecule: Ethylene

The principal function of the BFSS is to store carbon-rich feedstock molecules for presentation to the NFW. Ethylene (aka. ethene, acetene; C_2H_4 or $H_2C{=}CH_2$) has been provisionally selected as the primary feedstock gas and C/H source for the second-generation nanoscale fabrication workstation. Historically, ethylene – a volatile, flammable, colorless gas at room temperature with a faint, sweet odor – was once used as an anesthetic.[847] As with acetylene (HC≡CH), ethylene contains an unsaturated carbon-carbon bond (i.e., C=C) which conveniently may allow a radical-site-tipped DMS tool to capture the molecule via secure covalent bonding with only a change in bond order without altering the atom population of the feedstock molecule (e.g., via a relatively simple positionally controlled chemical reaction). Since ethylene is readily dehydrogenated to acetylene by applying two successive positionally controlled hydrogen abstraction reactions, all of the positionally controlled mechanosynthetic reactions identified in Freitas and Merkle[848] for acetylenic precursors are also accessible using ethylene.

Figure IV-2 lists some physical properties and gives a pressure-temperature phase diagram[849] for ethylene.[850] Unlike acetylene, ethylene can be stably stored at very high pressures, and at – or somewhat above – room temperature. Ethylene is often shipped in cylinders or in tube trailers as a compressed gas at 81.6-85.0 atm (8.27-8.62 MPa, or 1200-1250 psig) and 21.1 ^{o}C, or as a refrigerated liquid in tankers at normal atmospheric pressure and -104 ^{o}C.[851] The majority of ethylene produced in the United States and Western Europe is transported and stored in integrated, underground pipeline systems in which ethylene is transported as a pressurized gas at 49-56 atm (5-5.7 MPa).[852]

---

[847] K.M. Sundaram et al., "Ethylene," in: Kirk-Othmer Encyclopedia of Chemical Technology, John Wiley and Sons, 2005; http://www.mrw.interscience.wiley.com/kirk/kirk_search_fs.html. Heinz Zimmermann, Roland Walzl, "Ethylene," in: Ullmann's Encyclopedia of Industrial Chemistry, 7th Edition, John Wiley and Sons, 2005, http://www.mrw.interscience.wiley.com/ueic/ueic_search_fs.html and http://media.wiley.com/product_data/excerpt/55/35273038/3527303855.pdf. Compressed Gas Association, "Ethylene," in: Handbook of Compressed Gases, 4th edition, Kluwer Academic Publishers, 1999, pp. 351-356.

[848] Robert A. Freitas Jr., Ralph C. Merkle, "A Minimal Toolset for Positional Diamond Mechanosynthesis," J. Comput. Theor. Nanosci. 5(May 2008):760-861.

[849] A. L. Kovarskii, High-Pressure Chemistry and Physics of Polymers, CRC Press, 1994.

[850] J. Smukala, Roland Span, Wolfgang Wagner, "New Equation of State for Ethylene Covering the Fluid Region for Temperatures From the Melting Line to 450 K at Pressures up to 300 MPa," J. Phys. Chem. Ref. Data 29(September 2000):1053-1121.

[851] "Ethylene," ChemInfo Chemical Profiles, Canadian Centre for Occupational Health and Safety, 8 November 2005; http://www.intox.org/databank/documents/chemical/ethylene/cie89.htm.

[852] K.M. Sundaram et al., "Ethylene," in: Kirk-Othmer Encyclopedia of Chemical Technology, John Wiley and Sons, 2005; http://www.mrw.interscience.wiley.com/kirk/kirk_search_fs.html. Heinz Zimmermann, Roland Walzl, "Ethylene," in: Ullmann's Encyclopedia of Industrial Chemistry, 7th Edition, John Wiley and Sons, 2005, http://www.mrw.interscience.wiley.com/ueic/ueic_search_fs.html and http://media.wiley.com/product_data/excerpt/55/35273038/3527303855.pdf.

Figure IV-2. Ethylene pressure-temperature phase diagram[853] and physical properties.[854]

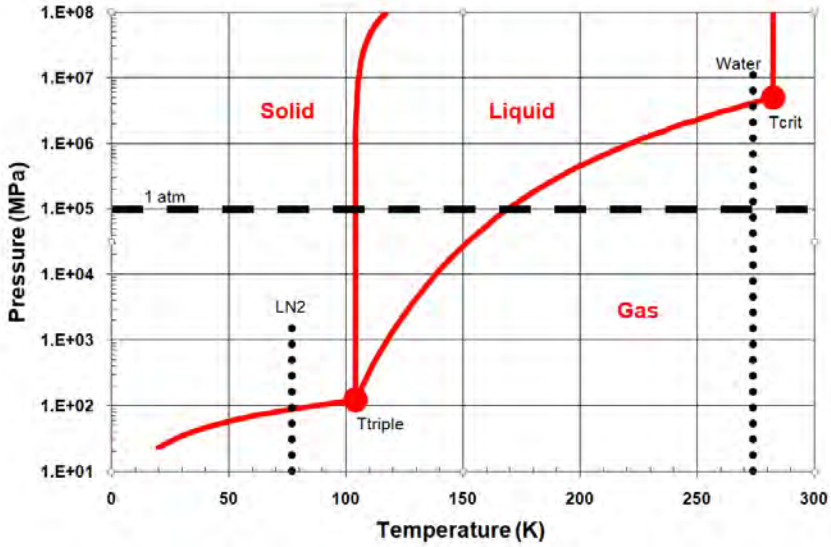

---

[853] A. L. Kovarskii, High-Pressure Chemistry and Physics of Polymers, CRC Press, 1994.

[854] A. L. Kovarskii, High-Pressure Chemistry and Physics of Polymers, CRC Press, 1994. V. Vladimirovich Sychev, Thermodynamic Properties of Ethylene; Thermodynamic Properties Of Ethylene (National Standard Reference Data Service of the USSR: A Series of Property Tables), Taylor & Francis; first edition, 1 April 1987. Ethylene: Product Stewardship Guidance Manual, Olefins Panel Ethylene Product Stewardship Task Group, American Chemistry Council, December 2004; http://www.lyondell.com/lyondell/techlit/techlit/Handbooks%20and%20Manuals/ACC_Ethylene_Manual.pdf. K.M. Sundaram et al., "Ethylene," in: Kirk-Othmer Encyclopedia of Chemical Technology, John Wiley and Sons, 2005; http://www.mrw.interscience.wiley.com/kirk/kirk_search_fs.html. Heinz Zimmermann, Roland Walzl, "Ethylene," in: Ullmann's Encyclopedia of Industrial Chemistry, 7th Edition, John Wiley and Sons, 2005, http://www.mrw.interscience.wiley.com/ueic/ueic_search_fs.html (subscription required) and http://media.wiley.com/product_data/excerpt/55/35273038/3527303855.pdf. Compressed Gas Association, "Ethylene," in: Handbook of Compressed Gases, 4th edition, Kluwer Academic Publishers, 1999, pp. 351-356. "Ethylene," CAS No. 74-85-1, OECD Screening Information Dataset (SIDS) High Production Volume Chemicals, UNEP Publications, October 1998; http://www.inchem.org/documents/sids/sids/74851.pdf. Syracuse Research Corporation, The Physical Properties Database (PHYSPROP), Interactive PhysProp Database Demo; http://www.syrres.com/esc/physdemo.htm. "Odor thresholds for chemicals with established occupational health standards," American Industrial Hygiene Association, 1989, pp. 19, 58. Emergency Action Guide for Ethylene, Association of American Railroads, January 1988. J.A. Dean, Lange's Handbook of Chemistry, 15th edition, McGraw-Hill, New York, 1999, pp. 1.217, 5.4 to 5.5, 5.116, 5.143, 6.149. "Ethylene (liquid, refrigerated)," in: Chemical Safety Sheets: Working Safely With Hazardous Chemicals, Kluwer Academic Publishers, 1991, p. 401. H. Haase, Electrostatic Hazards: Their Evaluation and Control, translated by M. Wald, Verlag Chemie, 1997, p. 108. P.M. Holland, B.E. Eaton, H.J.M. Hanley, "A Correlation of the Viscosity and Thermal Conductivity Data of Gaseous and Liquid Ethylene," J. Phys. Chem. Ref. Data 12(1983):917-932; http://www.nist.gov/srd/PDFfiles/jpcrd235.pdf. B.A. Younglove, "Thermophysical Properties of Fluids. 1. Argon, Ethylene, Parahydrogen, Nitrogen, Nitrogen Trifluoride, and Oxygen," J. Phys. Chem. Ref. Data 11(1982):1-368; http://www.nist.gov/srd/PDFfiles/jpcrdS1Vol11.pdf.

Physical Property of Ethylene	Data Value
Chemical formula	C_2H_4
Structural formula	$H_2C{=}CH_2$
Molecular weight	28.0538 gm/mole
Annual global production capacity, bulk gas	79.3 x 10^6 metric tons (1996)
Melting point	104.00 K
Boiling point	169.409 K
Triple point	103.986 K @ 121.295 Pa
Critical point temperature (T_{crit})	282.3428 K
Critical point pressure	49.905 atm (5.0404 MPa)
Critical point density	214.6 kg/m^3
Critical compressibility factor	0.281
Density of liquid at 109 K	648.5 kg/m^3
Density of liquid @ boiling point	570 kg/m^3
Density of liquefied gas @ 0 ^oC	340 kg/m^3
Density of gas @ STP (1 atm, 0 ^oC)	1.2603 kg/m^3
Vapor pressure @ -150 ^oC	0.02 atm (0.002 MPa)
Vapor pressure @ b.p.	1.0 atm (0.102 MPa)
Vapor pressure @ -50 ^oC	10.9 atm (1.100 MPa)
Vapor pressure @ 0 ^oC	42.3 atm (4.270 MPa)
Heat capacity of liquid @ 109 K (C_V)	9.702 x 10^5 J/m^3-K
Heat capacity of liquid @ 9.90 ^oC (T_{crit})	5.171 J/gm-^oC
Heat capacity of ideal gas at 21.1 ^oC	1.517 J/gm-^oC
Specific heat of liquid @ boiling point	2.63 x 10^3 J/kg-K
Specific heat of gas @ 9.90 ^oC (T_{crit})	1.55 x 10^3 J/kg-K
Thermal conductivity of liquid @ 109 K	0.2645 W/m-K
Thermal conductivity of gas @ 0 ^oC	1.77 x 10^{-2} W/m-K
Thermal conductivity of gas @ 100 ^oC	2.94 x 10^{-2} W/m-K
Thermal conductivity of gas @ 400 ^oC	8.05 x 10^{-2} W/m-K
Heat of formation, ideal gas @ 25 ^oC	1.8718 x 10^6 J/kg
Enthalpy of formation	5.232 x 10^3 J/mole
Entropy	220 J/mole-K
Heat of fusion, ethylene ice	1.195 x 10^5 J/kg, 6.81 x 10^7 J/m^3
Heat of vaporization @ boiling point	4.88 x 10^5 J/kg
Heat of vaporization @ 0 ^oC	1.91 x 10^5 J/kg
Heat of sublimation	6.7674 x 10^5 J/kg
Heat of combustion	4.7183 x 10^7 J/kg
Dynamic viscosity of liquid @ m.p.	0.73 mPa-sec (0.73 centipoise)
Dynamic viscosity of liquid @ 109 K	5.82 x 10^{-4} kg/m-sec
Dynamic viscosity of liquid @ b.p.	0.17 mPa-sec (0.17 centipoise)
Dynamic viscosity of liquid @ 0 ^oC	0.07 mPa-sec (0.07 centipoise)
Dynamic viscosity of gas @ m.p.	3.6 x 10^{-6} Pa-sec
Dynamic viscosity of gas @ 0 ^oC	9.3 x 10^{-6} Pa-sec
Dynamic viscosity of gas @ 150 ^oC	1.43 x 10^{-5} Pa-sec
Speed of sound in liquid @ 109 K	1726.3 m/sec
Surface tension @ -104 ^oC (liquefied gas)	16.5 mN/m (16.5 dynes/cm)
Surface tension @ 0 ^oC (liquefied gas)	1.1 mN/m (1.1 dynes/cm)
Henry's law constant (water solubility @ 298 K)	2.64 x 10^{24} molecules/m^3-atm
Refractive index (n_D) @ 25°C	1.3632
Odor threshold – detection	270-600 ppm (310-690 mg/m^3)

Odor threshold – recognition	418 ppm (480 mg/m^3)
Flash point	-136 ^{o}C
Lower flammable (explosive) limit (LFL/LEL)	2.7% @ 25 ^{o}C
Upper flammable (explosive) limit (UFL/UEL)	36% @ 25 ^{o}C
Minimum ignition energy	0.07 millijoules
Autoignition temperature, best value	490 ^{o}C
Autoignition temperature, reported range	425-542.8 ^{o}C

Six potential risk factors have been identified and evaluated, none of which appears to prevent the use of ethylene as the principal carbon-rich molecular feedstock as envisioned in the present research proposal:

(1) **Polymerization**. In the presence of significant impurities, ethylene can polymerize at temperatures ≥373 K and pressures ≥1000 atm (100 MPa).[855] Using initiators, ethylene polymerizes at ≥413 K and ≥700 atm, or at ≥403 K and ≥1300 atm in the presence of 3.7 x 10^{-4} mol/l of tetramethyltetrazene initiator producing polymers with lots of chain branching, or at 325-333 K and 3500-10,000 atm producing true linear polymers essentially free from chain branching,[856] and especially effective catalysts can induce ethylene polymerization at low pressures of 1-200 atm,[857] e.g., rare earths at 140 atm.[858] A typical commercial polyethylene reactor might operate at 493-568 K and 1335 atm.[859] In the absence of catalysts or significant impurities, pure ethylene will not thermally polymerize at temperatures ≤403-423 K and pressures ≤2500-3200 atm.[860] Besides eliminating impurities, compressed ethylene in the BFSS should be shielded from deep UV photons (at 250-200 nm) that can induce

---

[855] A. Michels, M. Geldermans, "Isotherms of ethylene up to 3000 atmospheres between 0° and 150°C," Physica 9(1942):967-973.

[856] A. L. Kovarskii, High-Pressure Chemistry and Physics of Polymers, CRC Press, 1994.

[857] K.M. Sundaram et al., "Ethylene," in: Kirk-Othmer Encyclopedia of Chemical Technology, John Wiley and Sons, 2005; http://www.mrw.interscience.wiley.com/kirk/kirk_search_fs.html. Heinz Zimmermann, Roland Walzl, "Ethylene," in: Ullmann's Encyclopedia of Industrial Chemistry, 7th Edition, John Wiley and Sons, 2005, http://www.mrw.interscience.wiley.com/ueic/ueic_search_fs.html and http://media.wiley.com/product_data/excerpt/55/35273038/3527303855.pdf.

[858] A. L. Kovarskii, High-Pressure Chemistry and Physics of Polymers, CRC Press, 1994.

[859] Hee-Jong Lee, Yeong-Koo Yeo, Jin Yang Chang, "Modeling of Industrial High Pressure Autoclave Polyethylene Reactor Including Decomposition Phenomena," Korean J. Chem. Eng. 17(2000):223-229; http://www.cheric.org/PDF/KJChE/KC17/KC17-2-0223.pdf.

[860] A. L. Kovarskii, High-Pressure Chemistry and Physics of Polymers, CRC Press, 1994. V. Vladimirovich Sychev, Thermodynamic Properties of Ethylene; Thermodynamic Properties Of Ethylene (National Standard Reference Data Service of the USSR: A Series of Property Tables), Taylor & Francis; first edition, 1 April 1987. A. Michels, M. Geldermans, "Isotherms of ethylene up to 3000 atmospheres between 0° and 150°C," Physica 9(1942):967-973.

photopolymerization.[861] Gamma rays can also initiate polymerization at 293-363 K between 17-400 atm;[862] assuming a conservative single-hit polymerization failure model with a failure condition of ~10^{15} hits/kg-rad (Section 3.8.1.3) and an average measured background of terrestrial gamma radiation in urban areas of ~0.09 rad/yr,[863] the mean time between radiation-induced polymerization events in a tank of compressed ethylene in the BFSS containing ~24 million molecules of C_2H_4 gas (taking BFSS pressurized volume as ~2.79×10^6 nm^3) of mass 1.1×10^{-18} kg is ~10,000 years or a mean failure rate of ~3×10^{-12} sec^{-1} of BFSS operation.

(2) **Carbonization**. At elevated temperatures and pressures[864] ethylene can decompose to carbon and methane in an exothermic reaction that releases heat, further fueling the decomposition.[865] The higher the pressure, the lower the temperature needed to initiate the decomposition reaction: For pressures ≤300 atm, no carbonization occurs at temperatures ≤773 K,[866] and there is no carbonization at temperatures ≤422 K even at elevated pressures.[867] Unless immediate steps are taken to halt decomposition (e.g., depressuring, removing heat, lowering temperature), an elevating temperature can cause the containment vessel to fail with consequent release of unreacted ethylene. Examples of events that can initiate an ethylene decomposition include: (1) Sudden pressurization of a vessel or pipeline with ethylene, or of one containing ethylene; (2) heat (steam, flame) added to a vessel or pipeline containing ethylene, such as a flame impinging on a pipeline or vessel containing ethylene under elevated pressure; (3) polymerization of ethylene in a pressurized vessel, without adequate heat removal, can generate sufficient heat to initiate the decomposition reaction; or (4) heat of adsorption from addition of ethylene to an adsorbent bed (where the adsorbent has pore size sufficient to adsorb ethylene)

---

[861] "Selective Hydrophobic and Hydrophilic Texturing of Surfaces Using Photolithographic Photodeposition of Polymers," Center for Integrated Sensors and Circuits, Department of Electrical Engineering, University of Michigan, Ann Arbor, accessed January 2008; http://www.eecs.umich.edu/chm-group/publications/pdf/darren/SPIE98.pdf.

[862] A. L. Kovarskii, High-Pressure Chemistry and Physics of Polymers, CRC Press, 1994.

[863] J. Koperski, "Exposure of Urban Populations to Natural Gamma Background in Poland," Radiation Protection Dosimetry 8(1984):163-171; http://rpd.oxfordjournals.org/cgi/content/abstract/8/3/163.

[864] Laurence G. Britton, D. Alex Taylor, Donald C. Wobser, "Thermal Stability of Ethylene at Elevated Pressures," Plant/Operations Progress 5(October 1986).

[865] Ethylene: Product Stewardship Guidance Manual, Olefins Panel Ethylene Product Stewardship Task Group, American Chemistry Council, December 2004; http://www.lyondell.com/lyondell/techlit/techlit/Handbooks%20and%20Manuals/ACC_Ethylene_Manual.pdf.

[866] A. L. Kovarskii, High-Pressure Chemistry and Physics of Polymers, CRC Press, 1994.

[867] Ethylene: Product Stewardship Guidance Manual, Olefins Panel Ethylene Product Stewardship Task Group, American Chemistry Council, December 2004; http://www.lyondell.com/lyondell/techlit/techlit/Handbooks%20and%20Manuals/ACC_Ethylene_Manual.pdf.

under elevated pressure can release sufficient heat to initiate an ethylene decomposition.[868] Decomposition can also occur at lower temperatures and pressures in the presence of high energy initiators (e.g. hot wire plus gun cotton, exploding wire, or electric).[869]

(3) **Dehydrogenation**. Various nondiamond metal surfaces including cobalt,[870] nickel,[871] palladium[872] and vanadium[873] can induce the thermal decomposition via dehydrogenation of C_2H_4 to C_2H_2 and/or the subsequent decomposition of C_2H_2 to simpler species, or even to pure carbon.[874] In the case of silver (the selected electrode material), silver metal (e.g., the Ag(110) surface)[875] catalyzes the formation of ethylene oxide from ethylene and oxygen, underscoring the need to exclude gaseous molecular oxygen from the NFW workspace. More specifically:

On the Ag(110) surface, between 110-160 K pure ethylene weakly physisorbs to metallic Ag(110) and related silver oxide surfaces without decomposition.[876] (Ethylene oxide also only weakly adsorbs and does not decompose on Ag(110) surface.[877])

---

[868] Ethylene: Product Stewardship Guidance Manual, Olefins Panel Ethylene Product Stewardship Task Group, American Chemistry Council, December 2004; http://www.lyondell.com/lyondell/techlit/techlit/Handbooks%20and%20Manuals/ACC_Ethylene_Manual.pdf.

[869] L. Bretherick, Handbook of Reactive Chemical Hazards, 4th edition, Butterworth-Heinemann Ltd., Boston MA, 1990, p. 260; see also: P.G. Urben, ed., Bretherick's Reactive Chemical Hazards Database [CD-ROM], 6th edition, Version 3.0, Butterworth-Heinemann Ltd., 1999.

[870] P. Tiscione, G. Rovida, "Adsorption and decomposition of ethylene and acetylene on cobalt," Surf. Sci. 154(1985):L255-L260.

[871] Mimi E. Lam, Russell J. Boyd, H.J. Kreuzer, "Mechanism of C_2H_2 dehydrogenation to C_2H_2 on the Ni(111) surface," Chem. Phys. Lett. 253(1996):129-134. F. Zaera, R.B. Hall, "High-resolution electron energy loss spectroscopy and thermal programmed desorption studies of the chemisorption and thermal decomposition of ethylene and acetylene on Ni(100) single-crystal surfaces," J. Phys. Chem. 91(1987):4318-4323.

[872] L.L. Kesmodel, "Acetylene decomposition on Pd(100) and Pd(111): EELS evidence for CCH formation," J. Vac. Sci. Technol. A 2(April-June 1984):1083-1084.

[873] Dae Bok Kang, Alfred B. Anderson, "Adsorption and decomposition of acetylene on vanadium (100), (110), and (111) surfaces: The effect of large d orbitals," Surf. Sci. 165(1986):221-233.

[874] F. Zaera, R.B. Hall, "High-resolution electron energy loss spectroscopy and thermal programmed desorption studies of the chemisorption and thermal decomposition of ethylene and acetylene on Ni(100) single-crystal surfaces," J. Phys. Chem. 91(1987):4318-4323.

[875] Shiwu Gao, J.R. Hahn, W. Ho, "Adsorption induced hydrogen bonding by CH group," J. Chem. Phys. 119(22 September 2003):6232-6236; http://scitation.aip.org/getabs/servlet/GetabsServlet?prog=normal&id=JCPSA6000119000012006232000001.

[876] Masato Akita, Shuji Hiramoto, Naoki Osaka, Koichi Itoh, "Adsorption Structures of Ethylene on Ag(110) and Atomic Oxygen Precovered Ag(110) Surfaces: Infrared Reflection-Absorption and Thermal

On the Ag(100) surface, pure surface ethylene is known to be physisorbed in multilayers which desorb above 85 K.[878] DFT studies show that ethylene binds only very weakly (i.e., 0.08-0.13 eV binding energy[879]) to the perfect Ag(100) surface (with ethylene molecular geometry almost unchanged upon adsorption[880]), even if precovered with oxygen[881] – the perfect Ag(100) surface is not able to form a strong chemical bond with the ethylene molecule.[882] However, the binding energy increases considerably near steps and adatoms[883] removing a barrier to ethylene adsorption into a covalent π-bonded state on Ag(100), allowing chemisorption to occur, in the special cases of Ag(210) and Ag(410), vicinal surfaces of Ag(100) characterized by a high density of open (110)-like steps and narrow (100) terraces.[884] The sticking probability decreases with increasing translational energy (corresponding to higher temperatures), indicating non-

---

Desorption Spectroscopic Studies," J. Phys. Chem. B 103(1999):10189-10196; http://pubs.acs.org/cgi-bin/abstract.cgi/jpcbfk/1999/103/i46/abs/jp992025u.html.

[877] Charles T. Campbell, M.T. Paffett, "The adsorption of ethylene oxide on Ag(110) and Pt(111): Relevance to selective olefin oxidation," Surface Science 177(1 December 1986):417-430.

[878] D. Arvantis, K. Baberschke, L. Wenzel, U. Dober, "Experimental study of the chemisorbed state of C_2H_2 , C_2H_4 , and C_2H_6 on noble-metal surfaces," Phys. Rev. Lett. 57(December 1986):3175-3178; L. Vattuone, U. Valbusa, M. Rocca, "Influence of Rotational Energy on Adsorption Probability for a Physisorbed System: C_2H_4 on Ag(001)," Phys. Rev. Lett. 82(June 1999):4878-4881.

[879] Anton Kokalj, Andrea Dal Corso, Stefano de Gironcoli, Stefano Baroni, "The Interaction of Ethylene with Perfect and Defective Ag(001) Surfaces," J. Phys. Chem. B 106(2002):9839-9846; http://people.sissa.it/~dalcorso/publications/JPCB-106-9839-2002.pdf.

[880] Anton Kokalj, Andrea Dal Corso, Stefano de Gironcoli, Stefano Baroni, "The Interaction of Ethylene with Perfect and Defective Ag(001) Surfaces," J. Phys. Chem. B 106(2002):9839-9846; http://people.sissa.it/~dalcorso/publications/JPCB-106-9839-2002.pdf.

[881] Anton Kokalj, Andrea Dal Corso, Stefano de Gironcoli, Stefano Baroni, "Co-adsorption of ethylene and oxygen on the Ag(001) surface," Surface Science 532-535(2003):191-197; http://people.sissa.it/~dalcorso/publications/SS-532-191-2003.pdf.

[882] Anton Kokalj, Andrea Dal Corso, Stefano de Gironcoli, Stefano Baroni, "The Interaction of Ethylene with Perfect and Defective Ag(001) Surfaces," J. Phys. Chem. B 106(2002):9839-9846; http://people.sissa.it/~dalcorso/publications/JPCB-106-9839-2002.pdf.

[883] Anton Kokalj, Andrea Dal Corso, Stefano de Gironcoli, Stefano Baroni, "The Interaction of Ethylene with Perfect and Defective Ag(001) Surfaces," J. Phys. Chem. B 106(2002):9839-9846; http://people.sissa.it/~dalcorso/publications/JPCB-106-9839-2002.pdf.

[884] L. Savio, L. Vattuone, M. Rocca, "Interaction of ethylene and oxygen with stepped Ag surfaces," Journal of Electron Spectroscopy and Related Phenomena 129(June 2003):157-164. L. Vattuone, L. Savio, M. Rocca, "Coverage dependence of the dynamics of ethylene adsorption on Ag(210)," J. Phys.: Condens. Matter 16(9 July 2004):S2929-S2936; http://www.iop.org/EJ/abstract/0953-8984/16/29/008.

activated adsorption.[885] Such chemisorption events can likely be avoided if the silver electrodes on the NFW assembly surface are fabricated atomically flat with no terraces (Section 3.4.3).

On the Ag(111) surface, pure ethylene physisorbs only below 128 K in a flat geometry through a weak bond involving pi electrons with no detectable carbon hybridization, with a 0.33 eV desorption energy.[886] There is some experimental evidence that the silver (111) oxide surface can adsorb ethylene and chemically interact in the 230-300 K temperature range, possibly yielding ethylidyne and hydroxyl species[887] – another reason to exclude free oxygen species from the NFW workspace.

Unpassivated and thus highly reactive silicon surfaces can also induce the thermal decomposition via dehydrogenation of C_2H_4 to C_2H_2.[888] In particular, no ethylene decomposition is observed on silica support material,[889] or on SiO_2 with no catalyst present,[890] or on quartz walls[891] even at high CVD temperatures,[892] and ethylene driven off during ALE of SiO_2 does not re-react with the deposited silica.[893] (Thermal decomposition of ethylene would also not be

---

[885] L. Vattuone, L. Savio, M. Rocca, "Coverage dependence of the dynamics of ethylene adsorption on Ag(210)," J. Phys.: Condens. Matter 16(9 July 2004):S2929-S2936; http://www.iop.org/EJ/abstract/0953-8984/16/29/008.

[886] M.-L. Bocquet, A.M. Rappe, H.-L. Dai, "A density functional theory study of adsorbate-induced work function change and binding energy: Olefins on Ag(111)," Molecular Physics 103(20 March-April 2005):883-890; http://lorax.chem.upenn.edu/Research/pubs091505/Papers/Bocquet05p883.pdf.

[887] Kai Wu, Xuming Wei, Yuming Cao, Dezheng Wang, Xiexian Guo, "Oxidation of Cl-modified Ag(111) under UHV conditions and ethylene adsorption on the oxidized surface," Catalysis Letters 26(March 1994):109-121; http://www.springerlink.com/content/w26141472422jp30/.

[888] M. Nishijima, J. Yoshinobu, H. Tsuda, M. Onchi, "The adsorption and thermal decomposition of acetylene on Si(100) and vicinal Si(100)9°," Surf. Sci. 192(1987):383-397. J.W. Kim, T.U. Kampen, K. Horn, M.-C. Jung, "Thermal decomposition of ethylene on Si(1 1 1): Formation of the Si(111) √3 x √3:carbon structure," Surf. Sci. 601(1 February 2007):694-698.

[889] J.-F. Colomer, G. Bister, I. Willems, Z. Kónya, A. Fonseca, G. Van Tendeloo, J. B. Nagy, "Synthesis of single-wall carbon nanotubes by catalytic decomposition of hydrocarbons," Chem. Commun. (1999):1343-1344.

[890] M. Radosavljevic, M. Freitag, K.V. Thadani, A.T. Johnson, "Non-volatile molecular memory elements based on ambipolar nanotube field effect transistors," 20 June 2002, arXiv:cond-mat/0206392 v1, http://arxiv.org/pdf/cond-mat/0206392 and R. Sant, D.J. Kaul, E.E. Wolf, "Transient studies and kinetic modeling of ethylene oxidation on platinum/silicon dioxide," AIChEJ 35(1989):267-278.

[891] J.-F. Colomer, G. Bister, I. Willems, Z. Kónya, A. Fonseca, G. Van Tendeloo, J. B. Nagy, "Synthesis of single-wall carbon nanotubes by catalytic decomposition of hydrocarbons," Chem. Commun. (1999):1343-1344.

[892] Tamir Gabay, Moti Ben-David, Itshak Kalifa, Raya Sorkin, Ze'ev R. Abrams, Yael Hanein, Eshel Ben-Jacob, "Electro-chemical properties of carbon nanotube based multi-electrode arrays," http://www.eng.tau.ac.il/~hanein/papers/CNT_EC_final.pdf.

[893] T.A. Jurgens-Kowal, J.W. Rogers Jr., "Pyrolysis of Tetraethoxysilane on Mo(100) at Low Temperatures," J. Phys. Chem. B 102(1998):2193-2206.

expected to occur on fully hydrogen-passivated silicon surfaces because such surfaces do not react with alkenes[894] (and see Section 3.4.3), alkanes, or molecular hydrogen at room temperature.) Since gaseous O_2 can react with ethylene to cause dehydrogenation, we must ensure that: (1) assembly surface SiO_2 cannot de-gas O_2 into the UHV chamber, or can be pumped out if O_2 degassing from the silica does occur; and (2) the PALE process used to grow the SiO_2 does not oxidize the silver surface, since silver oxide could then dehydrogenate ethylene.

(4) **Combustion and Explosion**. Bulk ethylene is classified as a flammable gas by OSHA and DOT. It poses a significant fire and explosion hazard based on its physical properties (e.g., -136 ^{o}C flashpoint, high vapor pressure, low boiling point) which allow it to readily form explosive mixtures in air at concentrations between 2.3% and 32.3%.[895] Such mixtures can produce fire or explosion at any temperature if an ignition source is present; even if no ignition source (e.g., flame, spark) is present this material can autoignite at temperatures of $\geq$723 K.[896] Thus oxygen should be rigorously excluded from the NFW workspace. Ethylene is not shock sensitive, but forcing it in bulk through 5 Å molecular sieves at high pressure can produce exothermic reaction and explosion.[897]

(5) **Spontaneous Chemical Reaction**. Since the assembly surface upon which the NFW is assembled and operates includes metallic electrodes, it is of interest that (a) olefin complexes can form between C_2H_4 and ions including Ag^+, Cu^+, Pt^{2+}, Pd^{2+} and Hg^{2+}; (b) ethylene can react explosively with chlorine ~300 K over the oxides of silver or mercury;[898] (c) ethylene is catalyzed to relatively unstable ethylene oxide in the presence of a surplus of oxygen gas and a silver oxide catalyst at high temperature (>400 K), believed to be initiated by the production of

---

[894] Jillian M. Buriak, "Organometallic Chemistry on Silicon and Germanium Surfaces," Chem. Rev. 102(2002):1271-1308; http://pubs.acs.org/cgi-bin/article.cgi/chreay/2002/102/i05/pdf/cr000064s.pdf. G.C. Abeln, M.C. Hersam, D.S. Thompson, S.-T. Hwang, H. Choi, J.S. Moore, J.W. Lyding, "Approaches to nanofabrication on Si(100) surfaces: Selective area chemical vapor deposition of metals and selective chemisorption of organic molecules," J. Vac. Sci. & Technol. B: Microelectronics and Nanometer Structures 16(November 1998):3874-3878; G.C. Abeln, M.C. Hersam, D.S. Thompson, S.-T. Hwang, H. Choi, J.S. Moore, J.W. Lyding, J. Vac. Sci. Technol. B 16(1998):3874.

[895] Ethylene: Product Stewardship Guidance Manual, Olefins Panel Ethylene Product Stewardship Task Group, American Chemistry Council, December 2004; http://www.lyondell.com/lyondell/techlit/techlit/Handbooks%20and%20Manuals/ACC_Ethylene_Manual.pdf.

[896] Ethylene: Product Stewardship Guidance Manual, Olefins Panel Ethylene Product Stewardship Task Group, American Chemistry Council, December 2004; http://www.lyondell.com/lyondell/techlit/techlit/Handbooks%20and%20Manuals/ACC_Ethylene_Manual.pdf.

[897] L. Bretherick, Handbook of Reactive Chemical Hazards, 4th edition, Butterworth-Heinemann Ltd., Boston MA, 1990, p. 260; see also: P.G. Urben, ed., Bretherick's Reactive Chemical Hazards Database [CD-ROM], 6th edition, Version 3.0, Butterworth-Heinemann Ltd., 1999.

[898] "Ethylene," ChemInfo Chemical Profiles, Canadian Centre for Occupational Health and Safety, 8 November 2005; http://www.intox.org/databank/documents/chemical/ethylene/cie89.htm

Ag^+ sites via atomic oxygen attack on a silver oxide surface;[899] and (d) the polymerization and decomposition of ethylene in the presence of metallic copper can become violent at temperatures ≥673 K and pressures ≥54 atm with much carbon being deposited.[900] None of these conditions should be present in the NFW workspace.

(6) **Chemical Corrosivity**. Ethylene is not corrosive to ordinary metals, nor does it attack plastics like Teflon, nylon, rigid polyurethane, or high-density polyethylene (HDPE),[901] or elastomers like nitrile Buna N (NBR), butyl rubber (isobutylene isoprene), Viton A, polyurethane, chlorosulfonated polyethylene (CSM), low-density polyethylene (LDPE), Teflon, or Kalrez (perfluorinated elastomer).[902] However, ethylene does attack the plastic polyvinyl chloride (PVC)[903] and the elastomers ethylene propylene (EP and EPDM), styrene butadiene (SBR), silicone, and Fluoraz (fluorinated copolymer).[904] Ethylene physisorbs with minimal molecular distortion and apparently without chemically attacking ordinary silicon or germanium semiconductor surfaces[905] or the Ag(110) silver surface.[906]

Bulk polymer-grade ethylene is commonly sold up to 99.95% purity, but high-purity ethylene is readily commercially available at 4N (99.99%) from Air Liquide[907] and at "research grade" 5N purity (99.999%) from Matheson Tri-Gas, Praxair, Saudi Industrial Gas Company Ltd. (SIGAS),

---

[899] C. Stegelmann, N. C. Schiødt, C. T. Campbell, P. Stoltze, "Microkinetic modeling of ethylene oxidation over silver," Journal of Catalysis 221(25 January 2004):630-649.

[900] L. Bretherick, Handbook of Reactive Chemical Hazards, 4th edition, Butterworth-Heinemann Ltd., Boston MA, 1990, p. 260; see also: P.G. Urben, ed., Bretherick's Reactive Chemical Hazards Database [CD-ROM], 6th edition, Version 3.0, Butterworth-Heinemann Ltd., 1999.

[901] K.M. Pruett, Chemical Resistance Guide For Plastics: A Guide To Chemical Resistance Of Engineering Thermoplastics, Fluoroplastics, Fibers And Thermoset Resins, Compass Publications, 2000, pp. 182-193.

[902] K.M. Pruett, Chemical Resistance Guide For Elastomers II: A Guide To Chemical Resistance Of Rubber And Elastomeric Compounds, Compass Publications, 1994, pp. C-146 to C-151.

[903] K.M. Pruett, Chemical Resistance Guide For Plastics: A Guide To Chemical Resistance Of Engineering Thermoplastics, Fluoroplastics, Fibers And Thermoset Resins, Compass Publications, 2000, pp. 182-193.

[904] K.M. Pruett, Chemical Resistance Guide For Elastomers II: A Guide To Chemical Resistance Of Rubber And Elastomeric Compounds, Compass Publications, 1994, pp. C-146 to C-151.

[905] R. Miotto, A.C. Ferraza, G.P. Srivastava, "Comparative study of the adsorption of C_2H_4 on the Si(001) and Ge(001) surfaces," Surface Science 507-510(June 2002):12-17. M. Rahmani, M.-A. Zaïbi, J.-P. Lacharme, "Interaction of ethylene with cleaved silicon surface," Vacuum 77(18 February 2005):323-328.

[906] C.G.P.M. Bernardo, J.A.N.F. Gomes, "The adsorption of ethylene on the (110) surfaces of copper, silver and platinum: a DFT study," J. Molec. Structure: Theochem 582(22 April 2002):159-169.

[907] "Ethylene, Research Grade," December 2007; http://www.us.airliquide.com/en/medias/pdf/business/industry/laboratories/analyses/SpecialtyGasCatalog.pdf.

Scott Specialty Gases, and Wesco Gas.[908] Limited quantities of even higher purity hydrocarbon gases reportedly have been prepared in special circumstances, such as 6N acetylene (C_2H_2) by Koatsu Gas Kogyo Co., Ltd., in Osaka, Japan in 1988,[909] and other targeted purifications including ~7N ethylene by Praxair[910] and another instance of ethylene with at least the acetylene impurity reduced to the ~8N level.[911] It is worth noting that Ge[912] and Ga[913] are commercially available at 8N purity; also available at even higher purity are Au,[914] Cu,[915] H_2,[916] Hg,[917] and the five principal noble gases[918] at 9N purity, H_2O at 10N purity,[919] and Si at 11N purity.[920] The

---

[908] https://www.mathesontrigas.com/pdfs/products/Ethylene-Pure-Gas.pdf; http://praxair.com/praxair.nsf/0/96F351569A7B5B6B8525655300802B67/$file/Sec+C+-+PAGE+C-21.pdf; http://www.sigas1.com/en/pdf/pure_gases_12.pdf; http://www.scottecatalog.com/ScottPur.nsf/74923c9ec562a6fb85256825006eb87d/7c934415f689a7ff85256863006ccb1f?OpenDocument; http://www.wesco-gas.com/products/gas/pureinfo.html.

[909] Koatsu Gas Kogyo Co., Ltd., Osaka, Japan, 1988; http://www.koatsugas.co.jp/english/index.htm.

[910] Robert Denyszyn, "Impurities going undetected?" 2002; http://www.chemicalprocessing.com/articles/2002/107.html; Brian Thompson, "Determination of sub-ppm concentrations of CO and CO_2 in ethylene and propylene," Varian Application Note Number 26 (GC26:0794R), downloaded 12 November 2007; http://www.varianinc.com/image/vimage/docs/products/chrom/apps/gc26.pdf.

[911] E.M. Beyer, "C(2)H(4): Its Purification for Biological Studies," Plant Physiol. 55(May 1975):845-848; http://www.plantphysiol.org/cgi/reprint/55/5/845 or http://www.pubmedcentral.nih.gov/articlerender.fcgi?tool=pubmed&pubmedid=16659178.

[912] Novotech, Inc., http://www.novotechinc.com/products/GE%20ZR.html ; http://www.boftec.gov.cn/company/ymie/e_html/e_ym6.html.

[913] Deborah A. Kramer, "Gallium," 1995, http://minerals.usgs.gov/minerals/pubs/commodity/gallium/460495.pdf ; MCP Group, http://www.mcp-group.com/metals/mc_gal.html.

[914] "Nine nines fine," http://www.word-detective.com/back-f.html.

[915] http://www.evidenceaudio.com/nav/design.html.

[916] Sigma Aldrich, "Aeronex Gatekeeper Purifiers, Model 35K and Model 500K Product Specification," http://www.sigmaaldrich.com/sp_acrobat/497021.pdf.

[917] Electronic grade mercury, http://www.ophram.com/usvente.htm.

[918] Sigma Aldrich, "Aeronex Gatekeeper Purifiers, Model 35K and Model 500K Product Specification," http://www.sigmaaldrich.com/sp_acrobat/497021.pdf.

[919] Sahana Singh, "Ultrapure water – a challenge for perfectionists," Asian Water, January 2001, http://www.eti.org.sg/news0101asianwater.htm.

[920] Ara Philipossian, "Single Crystal Silicon Wafers," Univ. of Arizona, Dept. of Chemical and Environmental Engineering, CHEE415 & 515, 2001, http://arizona.edu/virtualcampus/ece415/SILICON.PDF; Bruce Ramsey, "Silicon made for world's

semiconductor industry has developed gas- and fluid- handling techniques that can maintain the extreme purity of these materials throughout a complex manufacturing process.

Ethylene physisorbs only relatively weakly to graphene surface (-0.17 eV at 276 K for C_2H_4,[921] and -0.13 eV at 300 K for CH_4;[922] experimental values on graphite) as may be found on the graphene wires and the in-tank bladder sheet (Section 3.5.1.6) of the NFW-2. The H-passivated diamond surfaces of the NFW-2 are also chemically inert and the physisorption of neutral molecules relies predominantly on van der Waals forces, producing only weak bonding (e.g., -0.24 eV for C_2H_2 at 83 K;[923] experimental value). The SiO_2-based multi-electrode assembly surface is naturally hydrophilic so strongly hydrophobic hydrocarbon molecules such as ethylene should not strongly physisorb.

3.5.1.4 Secondary Feedstock or "Vitamin" Molecule: Germane

Digermane (Ge_2H_6) is often used in atomic layer epitaxy[924] and was specified as the sole germanium source in the basic DMS reaction sequences investigated by Freitas and Merkle.[925] That study assumed that digermane would be flowed over a clean Ge surface at low temperatures, causing the molecule to chemisorb as two separate surface-bound germyl groups (GeH_3) which can then be extracted separately from the surface by subsequent single-tool operations. Specifically, when digermane is flowed over a depassivated (clean) Ge(111) surface the molecule

---

electronics," Seattle Post-Intelligencer, 3 September 1996, (Advanced Silicon Inc., http://www.portofmoseslake.com/p970903b.htm ; "Electronic Grade Silicon (EGS)," http://et.nmsu.edu/ETCLASSES/vlsi/files/MANUF.HTM ; Mitsubishi Materials Silicon Corp., http://wwwmsil.mmc.co.jp/english/laboratory/laboratory001.html and http://www.mmc.co.jp/english/business/semicon.html ; Shin-Etsu, http://www.shinetsu.co.jp/english/profile/division/sem-div/main.html. Tyler W. Norton, Richard T. Dailey, "The impact of a new high technology manufacturing facility on the small business sector of a rural community: A case study," Univ. of Montana; http://www.sbaer.uca.edu/DOCS/2000icsb/024DAI.PDF.

[921] A.V. Kiselev, D.P. Poshkus, "Molecular-statistical calculation of the thermodynamic characteristics of adsorption of saturated and unsaturated hydrocarbons on graphitized thermal carbon black," J. Chem. Soc. Faraday Trans. II 72(1976):950-966.

[922] Moti Lal, D. Spencer, "Interactions of alkanes with graphite," J. Chem. Soc. Faraday Trans. II 70(1974):910-919.

[923] H.-C. Chang, J.-C. Lin, "Structure and bonding of C_2H_2 on diamond C(111)-1x1:H: Infrared spectroscopy and exciton calculations," J. Phys. Chem. 100(1996):7018-7025.

[924] Kuang-Hsin Huang, Tsai-Shian Ku, Deng-Sung Lin, "Growth process of Ge on Si(100)-(2 x 1) in atomic-layer epitaxy from Ge_2H_6," Phys. Rev. B 56(15 August 1997):4878-4886.

[925] Robert A. Freitas Jr., Ralph C. Merkle, "A Minimal Toolset for Positional Diamond Mechanosynthesis," J. Comput. Theor. Nanosci. 5(May 2008):760-861.

predominantly physisorbs below 120 K,[926] but the molecule dissociates via Ge-Ge bond scission to form chemisorbed GeH_3 between 120-150 K; yields chemisorbed surface germyl (GeH_3), germylene (GeH_2), and germylidyne (GeH) species when flowed at 200 K; and produces only chemisorbed GeH_2 and GeH when flowed at 300 K and 400 K, with a much lower concentration of GeH_2 at 400 K; surface GeH_2 and GeH species are also generated by the successive decomposition of GeH_3 upon heating.[927] (Similar results are observed on the bare (unpassivated) Si(100)-2x1 surface.[928]) Just as reactive alkenes do not react with hydride-terminated silicon surfaces,[929] gaseous digermane molecules presented to a fully hydrogenated silicon surface likely would not lose their H atoms to that surface and decompose, thus those molecules would not be chemisorbed but instead would form a nondecomposed noncovalently bonded (i.e., physisorbed) partial or whole monolayer. In the case of the NFW SiO_2 assembly surface, the atomically flat worksites on the semiconductor surface also will not be "clean" (i.e., lacking passivation) but rather will be oxygen-terminated (see below).

Digermane decomposes at 215 ^{o}C and germane (GeH_4) at 350 ^{o}C,[930] though the MSDS's for both gases[931] recommend storage at temperatures no higher than 55 ^{o}C. This property potentially limits the temperature to which the assembly surface can be heated during bake-out (Section 3.5.1.6). However, the MSDS for digermane also recommends storage no lower than 0 ^{o}C to prevent liquefaction because bulk liquid digermane liquefies at 29 ^{o}C and has been observed to deflagrate without air (decompose to hydrogen and germanium) without an obvious source of initiation,[932] whereas germane does not liquefy down to -88.4 ^{o}C (m.p. -165.9 ^{o}C). Both materials

---

[926] Guangquan Lu, John E. Crowell, "The adsorption and thermal decomposition of digermane on Ge(111)," J. Chem. Phys. 98(15 February 1993):3415-3421.

[927] Guangquan Lu, John E. Crowell, "The adsorption and thermal decomposition of digermane on Ge(111)," J. Chem. Phys. 98(15 February 1993):3415-3421.

[928] D.A. Klug, W. Du, C.M. Greenlief, "Adsorption and Decomposition of Ge_2H_6 on Si(100)," J. Vac. Sci. Technol. A 11(1993):2067-2072. Deng-Sung Lin, Kuang-Hsin Huang, Tun-Wen Pi, Rong-Tzong Wu, "Coverage-dependent thermal reactions of digermane on Si(100)-(2×1)," Phys. Rev. B (Condensed Matter) 54(15 December 1996):16958-16964.

[929] Jillian M. Buriak, "Organometallic Chemistry on Silicon and Germanium Surfaces," Chem. Rev. 102(2002):1271-1308; http://pubs.acs.org/cgi-bin/article.cgi/chreay/2002/102/i05/pdf/cr000064s.pdf. G.C. Abeln, M.C. Hersam, D.S. Thompson, S.-T. Hwang, H. Choi, J.S. Moore, J.W. Lyding, "Approaches to nanofabrication on Si(100) surfaces: Selective area chemical vapor deposition of metals and selective chemisorption of organic molecules," J. Vac. Sci. & Technol. B: Microelectronics and Nanometer Structures 16(November 1998):3874-3878; G.C. Abeln, M.C. Hersam, D.S. Thompson, S.-T. Hwang, H. Choi, J.S. Moore, J.W. Lyding, J. Vac. Sci. Technol. B 16(1998):3874.

[930] Robert C. Weast, Handbook of Chemistry and Physics, 49th edition, CRC Press, Cleveland OH, 1968.

[931] Material Safety Data Sheet for Digermane, Voltaix, Inc., 1994; http://www.voltaix.com/images/doc/Msge010_Digermane.pdf. Material Safety Data Sheet for Germane, Voltaix, Inc., 1994; http://www.voltaix.com/images/doc/Msge000_Germane.pdf.

[932] Material Safety Data Sheet for Digermane, Voltaix, Inc., 1994; http://www.voltaix.com/images/doc/Msge010_Digermane.pdf.

have a pungent odor, are poisonous hemolytic chemicals, and have a propensity to ignite on exposure to air (yielding GeO_2 and H_2O, with higher germanes increasingly reactive) and to react with oxidizers and halogens – so such exposures should be avoided. Digermane is also reported as incompatible with finely divided metals[933] whereas germane is not[934] – though evidently neither reacts with polished silver metal surfaces (analogous to the NFW electrodes) at least at low temperatures.[935]

Given the foregoing considerations, germane (GeH_4) has been provisionally selected as the secondary feedstock gas and Ge source for the second-generation nanoscale fabrication workstation. Germane is considered a "vitamin molecule" since only a tiny number of Ge atoms are required to replicate the NFW (Table III-2). The vapor pressure of germane is 44 atm[936] and the gas does not metalize until compressed up to ~500,000 atm.[937] Just 25 molecules of germane gas could be stored at 10 atm pressure in ~100 nm^3, a volume easily made available inside the germane sorting rotor housing of the BFSS (Section 3.5.1.5). Germane at 5N or 99.999% "semiconductor" purity (i.e., one impurity molecule per 100,000 germane molecules) is available from Matheson Tri-Gas[938] and elsewhere.

GeH_4 is sometimes used to deposit Ge onto an SiO_2 surface, with two surface silica molecules in effect chemically reduced by one GeH_4 molecule.[939] However, for this reaction to proceed the germane must first be thermally "cracked" over a hot filament[940] near the germane decomposition temperature of ~600-700 K, and this reaction also apparently requires initiation by the presence

---

[933] Material Safety Data Sheet for Digermane, Voltaix, Inc., 1994; http://www.voltaix.com/images/doc/Msge010_Digermane.pdf.

[934] Material Safety Data Sheet for Germane, Voltaix, Inc., 1994; http://www.voltaix.com/images/doc/Msge000_Germane.pdf.

[935] William Carrier, Weijun Zheng, Yoshihiro Osamura, Ralf I. Kaiser, "Infrared spectroscopic identification of digermene, Ge2H4(X1Ag), and of the digermenyl radical, Ge2H3(X2A″), together with their deuterated counterparts in low temperature germane matrices," Chemical Physics 330(8 November 2006):275-286. See also: http://www.spacegrant.hawaii.edu/reports/15_FA05-SP06/Carrier_William_FA.pdf.

[936] Material Safety Data Sheet for Germane, Voltaix, Inc., 1994; http://www.voltaix.com/images/doc/Msge000_Germane.pdf.

[937] Zhi Li, Wen Yu, Changqing Jin, "First-principles calculation on phase stability and metallization in GeH_4 under pressure," Solid State Communications 143(August 2007):353-357.

[938] "Germane," Matheson Tri-Gas, December 2007; https://www.mathesontrigas.com/pdfs/products/EGG/germane.pdf.

[939] Yasuo Takahasi, Hiromu Ishii, Kiyohisa Fujinaga, "Reduction reaction of native oxide at the initial stage of GeH_4 chemical vapor deposition on (100)Si," Appl. Phys. Lett. 57(6 August 1990):599-601.

[940] Scott K. Stanley, Shawn S. Coffee, John G. Ekerdt, "Influence of Thermal Treatments on the Chemistry and Self-Assembly of Ge Nanoparticles on SiO_2 Surfaces," MRS Proceedings, 2004 Fall, Symposium D; http://www.mrs.org/s_mrs/sec_subscribe.asp?CID=2687&DID=114512&action=detail.

of other reactive gases in the mix such as disilane and diborane.[941] GeH_4 diluted with H_2 will deposit Ge on quartz but only at elevated temperatures, e.g., ~523 K.[942] Apparently, temperature and surface conditions that would allow GeH_4 feedstock gas to attack the SiO_2-based multi-electrode assembly surface during the BFSS recharge operation of each NFW activity cycle at or below room temperature will not occur in the proposed NFW architecture. Of course, unpassivated and thus highly reactive silicon surfaces can induce the dissociative chemisorption of GeH_4, e.g., involving scission of a Ge-H bond with hydrogen atom transfer onto the Si(100)-2x1[943] or Si(111)-7x7[944] surface as adatom. (GeH_4 also dissociatively adsorbs onto clean Ge(100) surface.[945]) However, even a half-hydrogenated silicon surface has higher barriers to GeH_4 adsorption than the clean surface[946] and decomposition of germane should not occur at all on fully hydrogen-passivated silicon or diamond surfaces because there are no available surface sites to receive an H adatom.

It is unknown whether or under what conditions GeH_4 might irreversibly chemisorb to silver surfaces. Some concern arises because silane is known to dissociatively chemisorb to Cu(111) surface at 90-150 K[947] and to W(110) surface at 350 K,[948] though only slightly to Ni(111) at 110

---

[941] Fujioka, Hiroshi, "Process for forming germanium-containing layer on oxygen-containing insulation layer," European Patent EP0484056, filing date 10/24/1991, http://www.freepatentsonline.com/EP0484056.html; and D.W. Kim, S.B. Hwang, T.F. Edgar, S. Banerjee, "Characterization of SiGe quantum dots on SiO2 and HfO2 grown by rapid thermal chemical deposition for nanoelectronic devices," J. Electrochemical Soc. 150(2003):G240-G243, http://www.cheric.org/research/tech/periodicals/vol_view.php?seq=412552.

[942] T. Sakata, H. Murakami, S. Higashi, S. Miyazaki, "Growth of Crystallized Ge Films from VHF Inductively-Coupled Plasma of H_2-Diluted GeH_4," Proc Int Symp Dry Process 5(2005):233-234.

[943] Chia-Liang Cheng, Dah-Shyang Tsai, Jyh-Chiang Jiang, "DFT study on dissociative adsorption of SiH_4 and GeH_4 on SiGe(100)-2×1 surface," Surface Science 600(15 August 2006):3194-3201.

[944] J. Braun, H. Rauscher, R.J. Behm, "Mechanism of GeH_4 dissociation on Si(111)-(7×7)," Surface Science 531(1 June 2003):265-271.

[945] Jyh Shing Lin, Wen-Chi Chou, "The dependence of dynamic variables on gas-surface reactivity during direct dissociative adsorption of GeH_4 onto Ge(001) surface," Surface Science 560(1 July 2004):79-87.

[946] Chia-Liang Cheng, Dah-Shyang Tsai, Jyh-Chiang Jiang, "DFT study on dissociative adsorption of SiH_4 and GeH_4 on SiGe(100)-2×1 surface," Surface Science 600(15 August 2006):3194-3201.

[947] B.C. Wiegand, S.P. Lohokare, R.G. Nuzzo, "Si-H bond activation on Cu : reaction of silane on Cu(111)," J. Phys. Chem. 97(1993):11553-11562; E.M. McCash, M.A. Chesters, P. Gardner, S.F. Parker, "The adsorption and decomposition of silane on Cu(111)," Surface Science 225(1990):273-280. I.G. Shuttleworth, W. Allison, "The adsorption and desorption processes accompanying the chemical vapour deposition of silane on Cu(111) And Ni(111)," Surface Review and Letters (SRL) 8(December 2001):613-620; http://www.worldscinet.com/cgi-bin/details.cgi?id=pii:S0218625X01001567&type=html.

[948] A.G. Sault, D.W. Goodman, "Reactions of silane with the W(110) surface," Surface Science 235(1990):28; http://www.chem.tamu.edu/rgroup/goodman/pdf%20files/099_ss_235_90_28.pdf.

K.[949] On the other hand, silane is generally more reactive than germane and heating silylated Cu(111) to 400 K regenerates ~16% of the clean copper surface.[950] Only a few theoretical[951] or experimental[952] studies have looked at the growth of incommensurate Ge layers on silver surface, e.g., on Ag(111),[953] Ag(110),[954] or Ag(100).[955] The Ge-Ag system shows a large miscibility gap

---

[949] I.G. Shuttleworth, W. Allison, "The adsorption and desorption processes accompanying the chemical vapour deposition of silane on Cu(111) And Ni(111)," Surface Review and Letters (SRL) 8(December 2001):613-620; http://www.worldscinet.com/cgi-bin/details.cgi?id=pii:S0218625X01001567&type=html.

[950] I.G. Shuttleworth, W. Allison, "The adsorption and desorption processes accompanying the chemical vapour deposition of silane on Cu(111) And Ni(111)," Surface Review and Letters (SRL) 8(December 2001):613-620; http://www.worldscinet.com/cgi-bin/details.cgi?id=pii:S0218625X01001567&type=html.

[951] S. Sawaya, J. Goniakowski, G. Tréglia, "Local-density approximation study of semiconductor/metal adsorption characteristics: Ge/Ag(100)," Phys. B 59(1999):15337-15345, http://prola.aps.org/pdf/PRB/v59/i23/p15337_1.

[952] H. Oughaddou, B. Aufray, J.M. Gay, "Ge/Ag(111): surface alloy of a semiconductor on a metal," Surface Review and Letters (SRL) 6(October 1999):929-934, http://www.worldscinet.com/cgi-bin/details.cgi?id=pii:S0218625X99001001&type=html; H. Oughaddou, S. Sawaya, J. Goniakowski, B. Aufray, G. Le Lay, J.M. Gay, G. Tréglia, J.P. Bibérian, N. Barrett, C. Guillot, A. Mayne, G. Dujardin, "Ge/Ag(111) semiconductor-on-metal growth: Formation of an Ag2Ge surface alloy," Phys. Rev. B 62(2000):16653-16656, http://prola.aps.org/pdf/PRB/v62/i24/p16653_1. See also: http://www-hasylab.desy.de/science/annual_reports/1999_report/part1/contrib/43/1608.pdf. C. Leandri, H. Oughaddou, J.M. Gay, B. Aufray, G. Le Lay, O. Bunk, R.L. Johnson, "Structural study of the Ge/Ag(110) C(4x2) reconstruction by synchrotron radiation XRD," Paper J-I.4, E-MRS 2002 Spring Meeting, Symposium J, Tuesday, 18 June 2002. See also: J.-M. Gay, B. Aufray, G. Le Lay, C. Leandri, H. Oughaddou, O. Bunk, R.L. Johnson, "Structural study of the Ge/Ag(110) C(4x2) superstructure," IHP-Contract HPRI-CT-1999-00040, European Commission; http://www-hasylab.desy.de/science/annual_reports/2001_report/part1/contrib/43/5299.pdf. H. Oughaddou, J.-M. Gay, B. Aufray, L. Lapena, G. Le Lay, O. Bunk, G. Falkenberg, J.H. Zeysing, R.L. Johnson, "Ge tetramer structure of the p(2sqrt[2]×4sqrt[2])R45° surface reconstruction of Ge/Ag(001): A surface x-ray diffraction and STM study," Phys. Rev. B 61(2000):5692-5697, http://prola.aps.org/pdf/PRB/v61/i8/p5692_1.

[953] H. Oughaddou, B. Aufray, J.M. Gay, "Ge/Ag(111): surface alloy of a semiconductor on a metal," Surface Review and Letters (SRL) 6(October 1999):929-934, http://www.worldscinet.com/cgi-bin/details.cgi?id=pii:S0218625X99001001&type=html; H. Oughaddou, S. Sawaya, J. Goniakowski, B. Aufray, G. Le Lay, J.M. Gay, G. Tréglia, J.P. Bibérian, N. Barrett, C. Guillot, A. Mayne, G. Dujardin, "Ge/Ag(111) semiconductor-on-metal growth: Formation of an Ag2Ge surface alloy," Phys. Rev. B 62(2000):16653-16656, http://prola.aps.org/pdf/PRB/v62/i24/p16653_1. See also: http://www-hasylab.desy.de/science/annual_reports/1999_report/part1/contrib/43/1608.pdf.

[954] C. Leandri, H. Oughaddou, J.M. Gay, B. Aufray, G. Le Lay, O. Bunk, R.L. Johnson, "Structural study of the Ge/Ag(110) C(4x2) reconstruction by synchrotron radiation XRD," Paper J-I.4, E-MRS 2002 Spring Meeting, Symposium J, Tuesday, 18 June 2002. See also: J.-M. Gay, B. Aufray, G. Le Lay, C. Leandri, H. Oughaddou, O. Bunk, R.L. Johnson, "Structural study of the Ge/Ag(110) C(4x2) superstructure," IHP-Contract HPRI-CT-1999-00040, European Commission; http://www-hasylab.desy.de/science/annual_reports/2001_report/part1/contrib/43/5299.pdf.

[955] H. Oughaddou, J.-M. Gay, B. Aufray, L. Lapena, G. Le Lay, O. Bunk, G. Falkenberg, J.H. Zeysing, R.L. Johnson, "Ge tetramer structure of the p(2sqrt[2]×4sqrt[2])R45° surface reconstruction of Ge/Ag(001): A surface x-ray diffraction and STM study," Phys. Rev. B 61(2000):5692-5697,

in the bulk phase and the surface tension of germanium is lower than that of silver.[956] However, a thinly germylated silver surface – if one arose – should be easily penetrable mechanically by nanotube wire and ought not to significantly inhibit electrical connectivity.

3.5.1.5 Binding Sites for NFW-2 Feedstock and Byproduct Gases

To reliably transport and handle each of the three gases that are transacted by the NFW-2, high-affinity binding sites must be designed. Since the gases will be pure once they are sequestered in their isolated storage compartments (Section 3.5.1.6), high competitive binding specificity of these sites may be less essential. In this proposal it is initially assumed that satisfactory binding sites for all three gas molecules can be made using only C/Ge/H atoms. If the affinity of all-hydrocarbon binding sites is too low, additional sorting rotor stages can be added to the BFSS design to achieve the required feedstock purity for a very small additional cost in atom count and without major alteration to the existing NFW design architecture, or alternatively one or more new element types could be incorporated into the design.

Ethylene Binding Sites. Binding sites for ethylene (C_2H_4) are very well known because the gas is an important plant hormone that regulates a multitude of plant processes, ranging from seed germination and ripening time to stress responses and organ senescence. Figure IV-3 shows a typical member of the high-affinity ethylene receptor (ETR) family in which a single Cu(I) ion is coordinated within electron rich hydrophobic pockets formed by membrane-spanning alpha-helices of the hydrophobic domain of the ETR1 protein from *Arabidopsis*,[957] with an unusually

---

http://prola.aps.org/pdf/PRB/v61/i8/p5692_1. S. Sawaya, J. Goniakowski, G. Tréglia, "Local-density approximation study of semiconductor/metal adsorption characteristics: Ge/Ag(100)," Phys. B 59(1999):15337-15345, http://prola.aps.org/pdf/PRB/v59/i23/p15337_1.

[956] H. Oughaddou, B. Aufray, J.M. Gay, "Ge/Ag(111): surface alloy of a semiconductor on a metal," Surface Review and Letters (SRL) 6(October 1999):929-934, http://www.worldscinet.com/cgi-bin/details.cgi?id=pii:S0218625X99001001&type=html; H. Oughaddou, S. Sawaya, J. Goniakowski, B. Aufray, G. Le Lay, J.M. Gay, G. Tréglia, J.P. Bibérian, N. Barrett, C. Guillot, A. Mayne, G. Dujardin, "Ge/Ag(111) semiconductor-on-metal growth: Formation of an Ag2Ge surface alloy," Phys. Rev. B 62(2000):16653-16656, http://prola.aps.org/pdf/PRB/v62/i24/p16653_1. See also: http://www-hasylab.desy.de/science/annual_reports/1999_report/part1/contrib/43/1608.pdf. C. Leandri, H. Oughaddou, J.M. Gay, B. Aufray, G. Le Lay, O. Bunk, R.L. Johnson, "Structural study of the Ge/Ag(110) C(4x2) reconstruction by synchrotron radiation XRD," Paper J-I.4, E-MRS 2002 Spring Meeting, Symposium J, Tuesday, 18 June 2002. See also: J.-M. Gay, B. Aufray, G. Le Lay, C. Leandri, H. Oughaddou, O. Bunk, R.L. Johnson, "Structural study of the Ge/Ag(110) C(4x2) superstructure," IHP-Contract HPRI-CT-1999-00040, European Commission; http://www-hasylab.desy.de/science/annual_reports/2001_report/part1/contrib/43/5299.pdf.

[957] A.B. Bleecker, J.J. Esch, A.E. Hall, F.I. Rodríguez, B.M. Binder, "The ethylene-receptor family from *Arabidopsis*: structure and function," Philos. Trans. R. Soc. Lond. B Biol. Sci. 353(29 September 1998):1405-1412. Fernando I. Rodriguez, Jeffrey J. Esch, Anne E. Hall, Brad M. Binder, G. Eric Schaller, Anthony B. Bleecker, "A Copper Cofactor for the Ethylene Receptor ETR1 from Arabidopsis," Science 283(12 February 1999):996-998; http://www.sciencemag.org/cgi/reprint/283/5404/996.pdf

stable ethylene/receptor complex having a half-life for dissociation of ~11 hours.[958] The binding of ethylene to the transition metal in the ethylene binding domain[959] induces a conformational change in the sensor domain that is propagated to the cytoplasmic transmitter domain of the protein.[960] Ethylene binding has been studied in many other plants including *Phaseolus vulgaris* (Canadian Wonder cotyledons),[961] tobacco,[962] and tomato.[963]

Reversible ethylene binding in an inorganic crystal lattice has also been demonstrated for the copper halide compound $CuAlCl_4$ in which ethylene ligands are bound to Cu(I) primarily through a sigma-interaction, resulting in reversible olefin binding,[964] and for other copper complexes.[965] Ligand atoms other than copper can also bind ethylene, including metal ions such as silver Ag(I)[966] and gold[967] and nonmetal atoms such as sulfur.[968] Further research is required to

---

[958] G.E. Schaller, A.B. Bleecker, "Ethylene-Binding Sites Generated in Yeast Expressing the Arabidopsis ETR1 Gene," Science 270(15 December 1995):1809-1811; http://www.sciencemag.org/cgi/reprint/270/5243/1809.pdf.

[959] W. Wang, J.J. Esch, S.H. Shiu, H. Agula, B.M. Binder, C. Chang, S.E. Patterson, A.B. Bleecker, "Identification of important regions for ethylene binding and signaling in the transmembrane domain of the ETR1 ethylene receptor of *Arabidopsis*," Plant Cell 18(December 2006):3429-3442.

[960] A.B. Bleecker, J.J. Esch, A.E. Hall, F.I. Rodríguez, B.M. Binder, "The ethylene-receptor family from *Arabidopsis*: structure and function," Philos. Trans. R. Soc. Lond. B Biol. Sci. 353(29 September 1998):1405-1412.

[961] C.J.R. Thomas, A.R. Smith, M.A. Hall, "The effect of solubilisation on the character of an ethylene-binding site from *Phaseolus vulgaris* L. cotyledons," Planta 160(April 1984):474-479; http://www.springerlink.com/content/l5q122g0qh11/?p=de4f210441dd4b4a88ea4b7046ee2c8e&pi=0.

[962] E.C. Sisler, "Measurement of Ethylene Binding in Plant Tissue," Plant Physiol. 64(October 1979):538-542; http://www.pubmedcentral.nih.gov/articlerender.fcgi?tool=pubmed&pubmedid=16661005.

[963] R.C. O'Malley, F.I. Rodriguez, J.J. Esch, B.M. Binder, P. O'Donnell, H.J. Klee, A.B. Bleecker, "Ethylene-binding activity, gene expression levels, and receptor system output for ethylene receptor family members from *Arabidopsis* and tomato," Plant J. 41(March 2005):651-659.

[964] R.M. Sullivan, H. Liu, D.S. Smith, J.C. Hanson, D. Osterhout, M. Ciraolo, C.P. Grey, J.D. Martin, "Sorptive reconstruction of the CuAlCl(4) framework upon reversible ethylene binding," J. Am. Chem. Soc. 125(10 September 2003):11065-11079; M.D. Capracotta, R.M. Sullivan, J.D. Martin, "Sorptive reconstruction of $CuMCl_4$ (M = Al and Ga) upon small-molecule binding and the competitive binding of CO and ethylene," J. Am. Chem. Soc. 128(18 October 2006):13463-13473.

[965] J.S. Thompson, R.L. Harlow, J.F. Whitney, "Copper(1)-Olefin Complexes. Support for the Proposed Role of Copper in the Ethylene Effect in Plants?" J. Am. Chem. Soc. 105(1983):3522-3527, http://pubs.acs.org/cgi-bin/abstract.cgi/jacsat/1983/105/i11/f-pdf/f_ja00349a026.pdf?sessid=6006l3; M. Munakata, S. Kitagawa, S. Kosome, A. Asahara, "Studies of Copper(1) Olefin Complexes. Formation Constants of Copper Olefin Complexes with 2,2'-Bipyridine, 1,10-Phenanthroline, and Their Derivatives," Inorg. Chem. 25(1986):2622-2627, http://pubs.acs.org/cgi-bin/abstract.cgi/inocaj/1986/25/i15/f-pdf/f_ic00235a027.pdf?sessid=6006l3.

[966] Elmo M. Beyer Jr., "A Potent Inhibitor of Ethylene Action in Plants," Plant Physiol. 58(1976):268-271; http://www.pubmedcentral.nih.gov/articlerender.fcgi?artid=542228.

determine if serviceable ethylene binding sites can be designed using purely C/H/Ge-based diamondoid materials or if one additional element type might be needed to make a high-affinity ethylene binding site structure.

Figure IV-3. Model of ethylene binding site.[969] (A) Copper loading of ethylene receptors by RAN1. RAN1 is a copper transporting ATPase. Copper is bound to RAN1 by two aminoterminal metal-binding motifs and then transported across the membrane. Copper is delivered to the ethylene receptor apoproteins. One copper ion is coordinated per receptor homo-dimer. Upon coordinating copper, the ethylene receptors are competent for ethylene binding. (B) Transmembrane structure of ethylene binding site. There is one copper binding site and consequently one ethylene-binding site per receptor homodimer. Each monomer of the receptor homodimer contains three transmembrane segments. Cys65 and His69 coordinate the copper ion within the second transmembrane domains of each monomer.

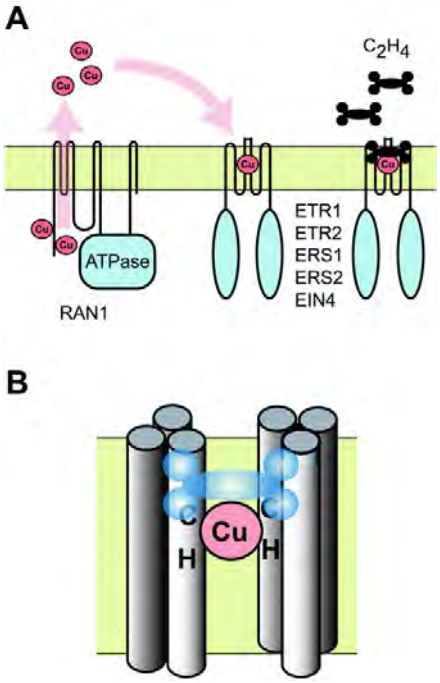

---

[967] B.M. Binder, F.I. Rodriguez, A.B. Bleecker, S.E. Patterson, "The effects of Group 11 transition metals, including gold, on ethylene binding to the ETR1 receptor and growth of *Arabidopsis thaliana*," FEBS Lett. 581(30 October 2007):5105-5109.

[968] D.J. Harrison, A.J. Lough, N. Nguyen, U. Fekl, "Push-pull molybdenum trisdithiolenes allow rapid nonconventional binding of ethylene at ligand sulfur atoms," Angew. Chem. Int. Ed. Engl. 46(2007):7644-7647.

[969] Model of Ethylene Binding Site; http://www.bioone.org/perlserv/?request=display-figures&name=i1543-8120-12-1-1-f07&ct=1

Hydrogen Binding Sites. Binding sites for molecular hydrogen (H_2) are well known. Carbons and many hybrid metal/organic compounds are examples of materials that store H_2 simply by physisorption.[970] The interaction between H_2 and carbon is via weak van der Waals forces, so significant binding only occurs at relatively low temperatures and binding energies are typically < 0.1 eV.[971] At the other extreme, dissociative chemical binding of H_2 occurs in materials such as metal hydrides,[972] so-called complex hydrides,[973] and in other chemical systems such as aminoborane,[974] but these tend to be irreversible processes typically having binding energies of 3-4 eV or higher. The desire to create reversible hydrogen storage for use in the automotive industry and elsewhere in the energy economy has stimulated major commercial interest in searches for materials with intermediate hydrogen-binding properties – e.g., materials capable of binding molecular hydrogen by strong chemical interactions instead of weak nonbonded interactions, but where the chemical interaction is insufficient to break the dihydrogen chemical bond, thus leaving the H_2 molecule reversibly bonded and intact.

Many new H_2 binding sites have been found since the first demonstration of molecular hydrogen chemisorption in 2001,[975] for example at unsaturated Ni(II) sites showing a chemisorption energy of -0.11 eV with the H_2 desorbing at 140-160 K.[976] By late 2007, the binding affinity record for

---

[970] A recent summary can be found in Andreas Züttel, "Hydrogen storage methods," Naturwissenschaften 91(April 2004):157-172; http://pubs.acs.org/cgi-bin/crossref/10.1007/s00114-004-0516-x. See also: Jesse L. C. Rowsell, Omar M. Yaghi, "Strategies for Hydrogen Storage in Metal-Organic Frameworks," Angew. Chem. Int. Ed. 44(2005):4670-4679; http://pubs.acs.org/cgi-bin/crossref/10.1002/anie.200462786.

[971] Steven S. Kaye, Jeffrey R. Long, "The role of vacancies in the hydrogen storage properties of Prussian blue analogues," Catalysis Today 120(2007):311-316; http://alchemy.cchem.berkeley.edu/jeff/paper71.pdf.

[972] J. Huot, J.F. Pelletier, G. Liang, M. Sutton, R. Schultz, "Structure of nanocomposite metal hydrides," J. Alloys Comp. 330-332(17 January 2002):727-731; http://dx.doi.org/10.1016/S0925-8388(01)01662-0.

[973] F. Schüth, B. Bogdanović, M. Felderhoff, "Light metal hydrides and complex hydrides for hydrogen storage," Chem. Commun. (2004):2249-2258; http://pubs.acs.org/cgi-bin/crossref/10.1039/b406522k.

[974] A. Gutowska, L. Li, Y. Shin, C.M. Wang, X.S. Li, J.C. Linehan, R.S. Smith, B.D. Kay, B. Schmid, W. Sahw, M. Gutowski, T. Autrey, "Nanoscaffold Mediates Hydrogen Release and the Reactivity of Ammonia Borane," Angew. Chem., Int. Ed. 44(2005):3578-3582; http://pubs.acs.org/cgi-bin/crossref/10.1002/anie.200462602.

[975] B.L. Mojet, J. Eckert, R. van Santen, A. Albinati, R. Lechner, "Evidence for chemisorbed molecular hydrogen in Fe-ZSM5 from inelastic neutron scattering," J. Am. Chem. Soc. 123(2001):8147-8148; http://www.hmi.de/pubbin/oai_publication?ID=-1296.

[976] Paul M. Forster, Juergen Eckert, Brandon D. Heiken, John B. Parise, Ji Woong Yoon, Sung Hwa Jhung, Jong-San Chang, Anthony K. Cheetham, "Adsorption of Molecular Hydrogen on Coordinatively Unsaturated Ni(II) Sites in a Nanoporous Hybrid Material," J. Am. Chem. Soc. 128(2006):16846-16850; http://pubs.acs.org/cgi-bin/sample.cgi/jacsat/2006/128/i51/html/ja0649217.html.

molecular hydrogen was reported for a copper ZSM5 zeolite[977] that was found to exhibit a calculated H_2 binding energy of -0.58 eV[978] (Figure IV-4). Even higher binding energies will likely be found by further research in this very active field, providing a wider selection of H_2 binding site motifs with affinities perhaps up to 2-3 eV. (The energy required to dissociate a free H_2 molecule into two unbonded H atoms has been calculated using Gaussian98 as +4.49 eV with DFT at the B3LYP/6-311+G(2d,p)//B3LYP/3-21G* level of theory.) Binding sites for atomic hydrogen (H) have been studied in a variety of inorganic (e.g., ZnO)[979] and organic (e.g., enzyme)[980] substrates, and even in diamond.[981]

Figure IV-4. A molecular hydrogen binding site in a copper ZSM5 zeolite.[982]

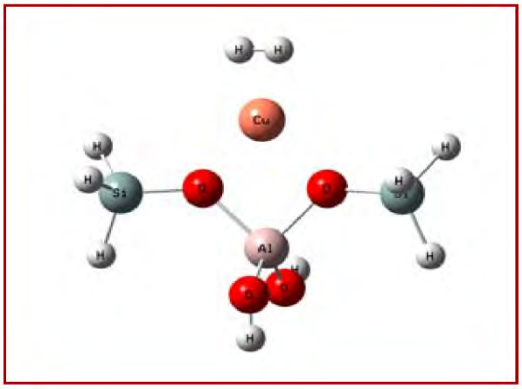

[977] P.A. Georgiev, A. Albinati, B.L. Mojet, J. Ollivier, J. Eckert, "Observation of exceptionally strong binding of molecular hydrogen in a porous material: Formation of an eta(2)-H-2 complex in a Cu-exchanged ZSM-5 zeolite," J. Am. Chem. Soc. 129(4 July 2007):8086-8087.

[978] A.J. Ramirez-Cuesta, P.C.H. Mitchell, "Hydrogen adsorption in a copper ZSM5 zeolite An inelastic neutron scattering study," Catalysis Today 120(28 February 2007):368-373.

[979] Sukit Limpijumnong, S. B. Zhang, "Resolving hydrogen binding sites by pressure -- a first-principles prediction for ZnO," Appl. Phys. Lett. 86(2005):151910; http://physics.sut.ac.th/~mai/paper/01ISI/2005_znoh-APL/APL_86_151910.pdf.

[980] S.P.J. Albracht, K.A. Bagley, E.C. Duin, R.P. Happe, E. Muumlnck, N. Ravi, W. Roseboom, T. van der Spek, W.H. Woodruff, "The hydrogen binding site(s) in nickel hydrogenases," J. Inorg. Biochem. 59(August 1995):635.

[981] S.P. Mehandru, Alfred B. Anderson, John C. Angus, "Hydrogen binding and diffusion in diamond," J. Mater. Res. 7(March 1992):689-695; http://www.mrs.org/s_mrs/bin.asp?CID=3136&DID=187287&DOC=FILE.PDF.

[982] A.J. Ramirez-Cuesta, P.C.H. Mitchell, "Hydrogen adsorption in a copper ZSM5 zeolite An inelastic neutron scattering study," Catalysis Today 120(28 February 2007):368-373.

As for the alternate byproduct molecule: methane (CH_4) binding sites also are known in methanotrophic bacteria such as the *Methylococcus capsulatus (Bath)* bacterium,[983] e.g., in MMO (methane monooxygenase enzyme) component A, the methane-binding protein whose active site contains copper.[984]

Germane Binding Sites. Binding sites for germane (GeH_4) have been only lightly studied because they are nonessential in biology and commerce. Nevertheless, GeH_4 binding sites could be based on known metal-germane complexes – e.g., the calculated binding energy of GeH_4 to the RuH[2](H[2])(PH[3])[2] fragment of one ruthenium complex is a quite respectable -0.92 eV[985] – though it remains unknown whether germane binding sites can be designed using purely diamondoid materials or if at least one metal atom must be included in the binding site structure. Peptides that preferentially bind to germania (GeO_2)[986] (or to the chemically analogous silica (SiO_2)[987]) are also known.

3.5.1.6 Conceptual Design of the BFSS

The design of the first-generation bulk feedstock supply system (BFSS) for the second-generation nanoscale fabrication workstation (NFW-2) is dominated by the primary storage tank that holds the primary feedstock and byproduct gases. This tank is roughly cylindrical in shape and wraps around the perimeter of three of the four edges of the square ~10,000 nm^2 footprint of the NFW (Section 3.4.1.1).

As internal gas pressure rises to critical levels in a tank, a hemispherically capped cylinder blows out first through the walls, not through the endcaps, so cylinder length is not a burst-relevant

---

[983] N. Ward et al., "Genomic insights into methanotrophy: the complete genome sequence of *Methylococcus capsulatus (Bath)*," PLoS Biol. 2(October 2004):e303; http://www.pubmedcentral.nih.gov/articlerender.fcgi?tool=pubmed&pubmedid=15383840.

[984] R.L. Lieberman, A.C. Rosenzweig, "Crystal structure of a membrane-bound metalloenzyme that catalyses the biological oxidation of methane," Nature 434(10 March 2005):177-182.

[985] Ridha Ben Said, Hussein Khansaa, Bahoueddine Tangour, Sylviane Sabo-Etienne, Jean-Claude Barthelat, "A DFT study of germane activation in ruthenium complexes: σ-coordination versus oxidative addition," New Journal of Chemistry 27(2003):1385-1391.

[986] Maureen R. Regan, Ipsita A. Banerjee, "Immobilization of invertase in germania matrix and a study of its enzymatic activity," Journal of Sol-Gel Science and Technology 43(July 2007):27-33; Ipsita Atin Banerjee, Maureen R. Regan, "Preparation of gold nanoparticle templated germania nanoshells," Materials Letters 60(April 2006):915-918; Matthew B. Dickerson, Rajesh R. Naik, Morley O. Stone, Ye Cai, Kenneth H. Sandhage, "Identification of peptides that promote the rapid precipitation of germania nanoparticle networks via use of a peptide display library," Chem. Commun. (2004):1776-1777.

[987] K. Taniguchi K. Nomura, Y. Hata, T. Nishimura, Y. Asami, A. Kuroda, "The Si-tag for immobilizing proteins on a silica surface," Biotechnol. Bioeng. 96(15 April 2007):1023-1029; R.R. Naik, L.L. Brott, S.J. Clarson, M.O. Stone, "Silica-precipitating peptides isolated from a combinatorial phage display peptide library," J. Nanosci. Nanotechnol. 2(February 2002):95-100.

parameter. For a hemispherically-capped cylinder of radius R, cylinder segment length L, wall thickness t_{wall}, and wall material failure strength $\sigma_w = 10^{10}$ N/m^2 for diamond or fullerene (at a *very* conservative[988] 20% of minimum failure strength), the maximum tolerable gas storage pressure P_{max} is given by: $P_{max} = t_{wall}\ \sigma_w / R$. Tanks are scaled such that all BFSS working gases (ethylene, germane, and hydrogen or methane) can be safely stored up to P_{max} = 1000 atm and 300 K. The enclosed volume of the cylindrical tank is approximately $V_{tank} = \pi R^2 L + (4/3)\ \pi R^3$, adding the volume of two hemispherical caps to the cylinder volume. The surface area of the tank is $S_{tank} = 2\pi RL + 4\pi R^2$, the cylinder area plus two hemispherical cap areas. Hence the volume of the tank walls is $V_{wall} = t_{wall}\ S_{tank}$, and so the number of carbon atoms in the tank walls, assuming they're diamond at n_{diam} = 176 C atoms/nm^3, is $N_{WallC} = n_{diam}\ V_{wall}$. The number of gas molecules contained inside the pressure tank is obtained by applying the van der Waals equation for compressed gases[989] and amounts to 8.61 molecules/nm^3 for ethylene gas at 1000 atm and 300 K (7.60 molecules/nm^3 at 400 atm), taking van der Waals constants A = 4.47 x 10^{-6} m^6-atm/mole^2 and B = 5.71 x 10^{-5} m^3/mole for ethylene.[990]

An interesting scaling issue arises when deciding whether H_2 or CH_4 is the better byproduct gas to use. The particle number densities in the gas are much higher for H_2 (12.3 molecules/nm^3) or CH_4 (10.5 molecules/nm^3) at 1000 atm than for ethylene at either 400 atm or 1000 atm, so we can be assured that with proper design, tank volume vacated by withdrawn ethylene feedstock molecules will not be overfilled by byproduct hydrogen or methane molecules placed inside the same tank. Note that when using H_2 as the byproduct gas, 2 byproduct gas molecules are created per feedstock molecule consumed which requires that the feedstock gas pressure must be cut roughly in half (~400 atm) to leave enough room in the tank to fill it with byproduct gas at 1000 atm, with the result that the feedstock tank volume must be roughly doubled to provide sufficient feedstock. On the other hand, when using CH_4 as the byproduct gas, only 1 byproduct gas molecule is created per feedstock molecule consumed. But in this case only one of the two feedstock carbon atoms remains available for manufacturing (since the other C must be thrown away in the byproduct gas molecule), with the result that twice as many feedstock molecules will be needed for the same manufacturing capacity, again requiring feedstock tank volume roughly to double. Hence the most persuasive reason for choosing H_2 as the byproduct molecule is not its maximized H/C ratio *per se* as argued in Section 3.5.1.2 (since this benefit is largely offset by its increased molecular volume compared to CH_4), but rather its comparative ease of disposal using the minimum number of available DMS reaction sequences (see below), as compared to CH_4.

A linear cylindrical tank that is bent into three equal segments forming a square-U shape has critical weak spots at the two bend sites. A slight tank wall thickening along the bend site seam

---

[988] An experimental study[*] of the bursting strength of a single-walled (10,10) carbon nanotube treated as a pressure-holding vessel found P_{max} = 40 GPa (400,000 atm) for an R = 0.77 nm tube, which yields a true failure strength of $\sigma_w = 2 \times 10^{11}$ N/m^2 taking t_{wall} ~ 0.15 nm.
[*] L. Sun, F. Banhart, A.V. Krasheninnikov, J.A. Rodriguez-Manzo, M. Terrones, P.M. Ajayan "Carbon nanotubes as high-pressure cylinders and nanoextruders," Science 312(26 May 2006):1199-1202.

[989] Robert A. Freitas Jr., Nanomedicine, Volume I: Basic Capabilities, Landes Bioscience, Georgetown, TX, 1999; Section 10.3.2, p. 354; http://www.nanomedicine.com/NMI/10.3.2.htm.

[990] Robert C. Weast, Handbook of Chemistry and Physics, 49th edition, CRC Press, Cleveland OH, 1968.

should provide a blowout-proof gas-tight seal and a 45° bevel-cut bearing across the seam interface would additionally allow the two distal segments to be rotated into place after installation; neither method would add much to BFSS mass or atom count, or would significantly alter the design. Since the present analysis already assumes t_{wall} = 0.45 nm tank walls – nearly three times as thick as required by the conservative bursting formula given above – we have not added any additional diamondoid atoms to reinforce the seams in the present design. It should be noted that total BFSS atom count is directly proportional to t_{wall}, hence if tank wall thickness had to be increased for reasons other than prevention of tank bursting (e.g., for puncture resistance, transwall diffusion prevention, vibration resistance, etc.) this could significantly increase the total atom count – though such an increase is not currently believed to be necessary.

Additionally, for convenience in the present design the tank contains an internal bladder structure to divide the tank into separate ethylene and hydrogen compartments. This is a conservative design feature intended in part to help prevent H_2 leakage through the C_2H_4 sorting rotors if the two gas were allowed to become mixed in the same tank. (A sliding piston could also be use to maintain two separate compartments of variable volume, but the bladder sheet strategy appears to use fewer atoms.) Chemically, mixing the gases is allowable because noncatalytic hydrogenation of ethylene to ethane at 300 K (e.g., in a mixed-gas tank) would require H_2 pressurized to ~20,800 atm,[991] hence this unwanted reaction should not happen at P_{max} ~ 1000 atm. The bladder membrane consists of a single-atom thick sheet of graphene through which even the small H_2 byproduct molecules cannot diffuse at 1000 atm and 300 K. This barrier property is confirmed by computer simulations[992] and experimentally with room temperature gases at ~1300 atm[993] and with argon gas at ~600 atm[994] stably trapped inside carbon nanotubes; helium atoms at energies up to ~5 eV (~800 zJ) also cannot penetrate a graphene sheet. The internal bladder sheet is assumed to be a single flexible sheet of graphene at 31.4 C atoms/nm^2 with a surface area approximating half the surface area of the tank (~S_{tank}/2) that is bonded to the interior tank walls and allows the hydrogen compartment to expand as feedstock gases are removed from the (contracting) ethylene compartment during NFW-2 operations.

The storage tank is sized by applying the simple criterion that the number of C atoms present in the feedstock gas molecules contained within the tank must be equal to the number of C atoms

---

[991] Robert A. Freitas Jr., Ralph C. Merkle, "A Minimal Toolset for Positional Diamond Mechanosynthesis," J. Comput. Theor. Nanosci. 5(May 2008):760-861.

[992] Farida Darkrim, Dominique Levesque, "Monte Carlo simulations of hydrogen adsorption in single-walled carbon nanotubes," J. Chem. Phys. 109(1998):4980-4984; Ifadat Ali Khan, K.G. Ayappa, "Density distributions of diatoms in carbon nanotubes: A grand canonical Monte Carlo study," J. Chem. Phys. 109(1998):4576; Qinyu Wang, J. Karl Jonhson, "Molecular simulation of hydrogen adsorption in single-walled carbon nanotubes and idealized carbon slit pores," J. Chem. Phys. 110(1999):577-586; Qinyu Wang, J. Karl Johnson, "Computer Simulations of Hydrogen Adsorption on Graphite Nanofibers," J. Phys. Chem. B 103(1999):277-281.

[993] D. Ugarte, A. Chatelain, W.A. de Heer, "Nanocapillarity and Chemistry in Carbon Nanotubes," Science 274(13 December 1996):1897-1899.

[994] G.E. Gadd, M. Blackford, S. Moricca, N. Webb, P.J. Evans, A.M. Smith, G. Jacobsen, S. Leung, A. Day, Q. Hua, "The World's Smallest Gas Cylinders?" Science 277(15 August 1997):933-936.

present in the structures of the NFW-2 (= BFSS + NFW). That is, we require that $N_{gasC} = N_{BFSS} + N_{NFW}$, where $N_{BFSS} = N_{WallC} + N_{bladderC} + N_{NonWallC}$ and $N_{NonWallC}$ is the C atom count for the rest of the BFSS excluding the storage tank and the graphene bladder sheet. To obtain $N_{NonWallC}$ we must describe the nontank components of the BFSS, all of which are confined to a single manifold accessible to the three DMS manipulators in the NFW, as follows:

(1) **Exhaust Valve**. A gated valve in the tank wall allows gas to flow out of the tank. This requires one actuator that is operated as a simple on/off switch, and one physical valve that can be cranked open or closed by the actuator motor. When the valve is opened, the contents of both feedstock and byproduct compartments within the tank are vented into the external environment. The valve is assumed to include a ring-shaped housing and a mechanically actuated flap, together comprising a solid disk shaped mass measuring 20 nm in diameter and 5 nm thick, or 1571 nm^3 solid mass and ~1885 nm^2 of passivated diamondoid surface area. The switch consists of a ~200 nm^3 and ~500 nm^2 4-part motor with a ~200 nm^3 electrical control lead attached to it.

(2) **Sorting Rotors**. One sorting rotor (Figure IV-5) set is nominally required for each feedstock or byproduct molecule type, but the current design conservatively includes one additional feedstock and byproduct rotor set, giving a total of 5 rotor sets to handle all necessary gas transactions. At present only 3 rotor sets are specified: one for ethylene, one for germane, and one for molecular hydrogen.

Figure IV-5. A molecular sorting rotor.[995]

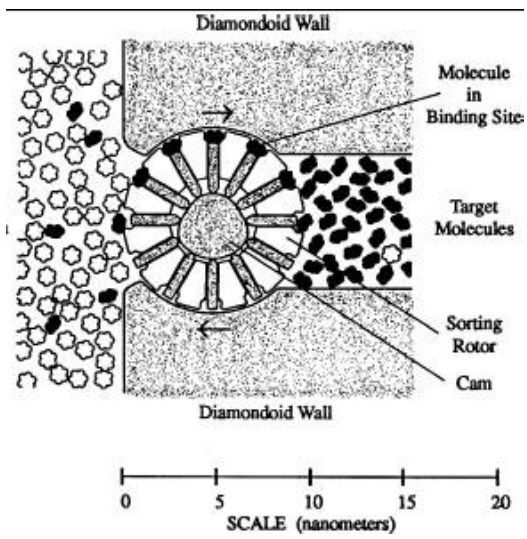

[995] Robert A. Freitas Jr., Nanomedicine, Volume I: Basic Capabilities, Landes Bioscience, Georgetown, TX, 1999; Figure 3.7, p. 81; http://www.nanomedicine.com/NMI/Figures/3.7.jpg.

During tank recharge at the beginning of an NFW-2 production cycle, the workspace will first be filled with ethylene at ~1 atm pressure and ~300 K. The transfer unit door in front of the ethylene sorting rotor is opened, allowing feedstock molecules in the workspace to freely impinge upon the ethylene binding sites in the rotor as the rotor turns. The molecular impingement rate will be sufficient to keep the sorting rotor binding sites loaded with ethylene molecules at all times. The frequency $\nu_{binding}$ at which binding events occur is given[996] by: $\nu_{binding} \sim (A\ c_{ligand} / N_{encounters})\ (2\ k_B T\ N_A / \pi\ MW_{kg})^{1/2} = 6.1$ MHz consistent with an eventual future megahertz rotor operation rate, where A = active receptor cross-sectional area ~ 0.1 nm^2 for ethylene gas molecules, c_{ligand} = 0.0245 molecules/nm^3 for ethylene gas at 1 atm and T = 300 K, $N_{encounters}$ = number of random ligand-receptor encounters required for a binding event, conservatively taken as 100 attempts,[997] MW_{kg} = 0.026 kg/mole for C_2H_4, k_B = 0.01381 zJ/K (Boltzmann constant), and $N_A = 6.023 \times 10^{23}$ molecules/mole (Avogadro's number).

Once an ethylene molecule has been captured in the binding site, it will almost always stay captured during the fraction of a second required to rotate the rotor site to its release position inside the tank. Taking the biological binding site performance as typical for an ethylene binding site, an 11-hour half-life for dissociation in *Arabidopsis*[998] implies a dissociation constant[999] of $k_d = 1.75 \times 10^{-5}\ sec^{-1}$ and the ethylene-binding site from *Phaseolus vulgaris* in raw unsolubilized form has a reported rate constant of association[1000] of $k_a \sim 10^3\ M^{-1}\ s^{-1}$ or $1.66 \times 10^3\ nm^3$/molecule-sec,[1001] yielding an estimated equilibrium constant[1002] of $K_d = k_d / k_a = 1.05 \times 10^{-8}$ molecules/nm^3 for the presumptive ethylene binding site. The ratio of probabilities that the binding site is unoccupied (P_{unocc}) vs. occupied (P_{occ}) is only $P_{unocc}/P_{occ} = K_d/c_{ligand} = 4.29 \times 10^{-7}$, indicating an extremely low likelihood that a site, once occupied, will become unoccupied.

---

[996] Robert A. Freitas Jr., Nanomedicine, Volume I: Basic Capabilities, Landes Bioscience, Georgetown, TX, 1999; Section 4.2.1, p. 94; http://www.nanomedicine.com/NMI/4.2.1.htm.

[997] K. Eric Drexler, Nanosystems: Molecular Machinery, Manufacturing, and Computation, John Wiley & Sons, New York, 1992; http://www.zyvex.com/nanotech/nanosystems.html.

[998] G.E. Schaller, A.B. Bleecker, "Ethylene-Binding Sites Generated in Yeast Expressing the Arabidopsis ETR1 Gene," Science 270(15 December 1995):1809-1811; http://www.sciencemag.org/cgi/reprint/270/5243/1809.pdf.

[999] Robert A. Freitas Jr., Nanomedicine, Volume I: Basic Capabilities, Landes Bioscience, Georgetown, TX, 1999; Section 3.5.2, p. 85; http://www.nanomedicine.com/NMI/3.5.2.htm.

[1000] Robert A. Freitas Jr., Nanomedicine, Volume I: Basic Capabilities, Landes Bioscience, Georgetown, TX, 1999; Section 3.5.2, p. 85; http://www.nanomedicine.com/NMI/3.5.2.htm.

[1001] C.J.R. Thomas, A.R. Smith, M.A. Hall, "The effect of solubilisation on the character of an ethylene-binding site from *Phaseolus vulgaris* L. cotyledons," Planta 160(April 1984):474-479; http://www.springerlink.com/content/l5q122g0qh11/?p=de4f210441dd4b4a88ea4b7046ee2c8e&pi=0.

[1002] Robert A. Freitas Jr., Nanomedicine, Volume I: Basic Capabilities, Landes Bioscience, Georgetown, TX, 1999; Section 3.5.2, p. 85; http://www.nanomedicine.com/NMI/3.5.2.htm.

After the main tank is full of ethylene at 400 atm pressure, the ethylene transfer unit door is closed and the germane inventory is refilled via a similar process. Note that just a small number of GeH_4 molecules are needed for an entire NFW production cycle, and this gas can be stored at ~10 atm inside ~100 nm^3 (Section 3.5.1.4) of the germane sorting rotor housing.

After the GeH_4 is loaded, the germane transfer unit door is closed, and the workspace is pumped down, the NFW-2 will undertake a complete production cycle during which the ethylene and germane feedstock molecules are removed from storage by the sorting rotors until the storage is nearly empty. As these rotors turn, they transfer gas molecules one by one from the interior of the tank through the tank wall into a small single-molecule transfer unit, from which the DMS tooltips can directly bind the feedstock molecule in a controlled confined volume and then transport the molecule to its next destination to begin chemical processing using established DMS reaction sequences.[1003] Byproduct hydrogen is discharged possibly by juxtaposing two HTrans tooltips[1004] each bearing a weakly bound H atom and mechanically forcing these H atoms into the close vicinity of an H_2 binding site on a sorting rotor disk inside a sealed transfer unit. (To maintain adequate geometric clearance this will require the design of a single-handle HTrans tool to replace the current two-handle version.[1005]) The formation of H_2 from the two HTrans tooltips is endoergic by +0.87 eV but an engineered H_2 binding site having an exoergic binding affinity of -1.27 eV or more (Section 3.5.1.5) should overcome this barrier and reliably (i.e., reaction delta = -0.40 eV) extract the two H atoms from the tooltips. The byproduct H_2 is then conveyed into the main tank and sequestered there until vented in bulk from the NFW-2 after the production cycle is finished. (One alternative but more complex approach might employ the classical radical fragmentation-based method for ethane cracking in hydrocarbon chemistry. In this theoretical scheme, two ethane byproduct molecules would be trapped inside a transfer unit. An H abstraction tool would remove a single H atom from one of them, producing an ethyl radical which promptly decomposes to an H atom and an ethylene molecule. The H then abstracts another H from the other ethane, forming molecular H_2 and a second ethylene radical which also decomposes to H and a second ethylene molecule. Exposure of transfer box contents to a spent H donation tool chemisorbs the H and recharges that tool, leaving two ethylene molecules which can be recycled as feedstock and a free H_2 molecule to be rotored out.)

Each of the 5 sorting rotor sets needs a motor to drive it, connected by a wire pair (hot + ground) to its own power/control line. Each sorting rotor is assumed to require 120,736 C atoms because it occupies a mostly solid space of 7 x 7 x 14 nm (~686 nm^3 solid volume and ~700 nm^2 passivated surface area), and is composed of 16 parts (12 rods, 1 cam, 1 drive shaft with clutch, 1 perforated disk, and 1 housing). Each rotary motor that drives one rotor set is assumed, as elsewhere, to be electrically driven, to consist of four parts (rotor, stator, output gear, and housing), and to fit within a box requiring a solid volume of ~200 nm^3 and ~500 nm^2 of

---

[1003] Robert A. Freitas Jr., Ralph C. Merkle, "A Minimal Toolset for Positional Diamond Mechanosynthesis," J. Comput. Theor. Nanosci. 5(May 2008):760-861.

[1004] Robert A. Freitas Jr., Ralph C. Merkle, "A Minimal Toolset for Positional Diamond Mechanosynthesis," J. Comput. Theor. Nanosci. 5(May 2008):760-861.

[1005] Robert A. Freitas Jr., Ralph C. Merkle, "A Minimal Toolset for Positional Diamond Mechanosynthesis," J. Comput. Theor. Nanosci. 5(May 2008):760-861.

passivated diamondoid surface area per motor. It is assumed that the electrical ground is at zero voltage; applying a positive voltage steps a rotor set forward, whereas applying a negative voltage steps it in the reverse direction. Electrical leads connecting control lines to each motor are 2 nm diameter unpassivated single-walled carbon nanotube x 50 nm long, adding ~314 nm^2 x ~0.154 nm thickness ~ 48 nm^3 of unpassivated carbon nanotube wire solid volume, or 96 nm^3 for each hot/ground pair of wires. Here we conservatively assume 200 nm^3 for each unpassivated carbon nanotube wire pair, which includes a ground line to each motor with all grounding lines connected to a single common ground line of assumed equivalent length.

If the feedstock being introduced into the workspace was absolutely pure, then the use of a single sorting rotor for each of the 5 sets could guarantee that the storage volumes contained only pure gases. But if as expected the starting material has some impurities, then using a multistage rotor system with reverse transport paths for impurities[1006] can help guarantee that only pure gases reach the final storage spaces, and also can allow the use of cheaper feedstock of lesser purity at negligible additional cost. Conservatively assuming that each sorting rotor stage can achieve a 1000:1 purification ratio[1007] and recognizing that the NFW-2 will consume ~3.2 x 10^7 C_2H_4 molecules per feed cycle (i.e., one tankful of ethylene feedstock), then to ensure that not a single impurity molecule is stored in the BFSS tank requires an impurity rate at or below $(3.2 \times 10^7)^{-1} \sim 3 \times 10^{-8}$. To achieve this modest objective starting with commercially available 5N purity ethylene feedstock (Section 3.5.1.3) thus requires 10^{-5} (5N purified feedstock) x 10^{-3} (1st rotor pair) ~ 10^{-8} (going into the tank), so we need just one rotor pair for ethylene. In the case of germane, we require an impurity rate at or below ~$(25\ GeH_4\ \text{molecules})^{-1} \sim 4 \times 10^{-2}$ which is easily achieved using a single rotor with no counterflow assuming 5N (i.e., 10^{-5} impurities) germane feedstock is available (Section 3.5.1.3). (Note that a slightly larger germane storage volume could allow the germane reloading process to be skipped during one or more feedstock recharging cycles.) No withdrawals are made from the H_2 compartment, so storage purity is not a concern and a single rotor will suffice. Since only the ethylene rotor set must be a paired set, a total of 2+1+1+1+1 = 6 sorting rotors will suffice in the first-generation BFSS.

(3) **Transfer Units**. There are 5 single-molecule transfer units sealing off a volume of space in the immediate vicinity of the exposed (reversible) binding site(s) of each sorting rotor set. The transfer unit is a hollow box with a sliding door that may be engaged and operated by the DMS manipulators using an empty tool chuck. Each transfer unit is assumed to include 2 parts and to resemble a rectangular 5 x 5 x 10 nm box with 5 nm thick walls, giving a solid volume of 5(4(50)+2(25)) = 1250 nm^3 of solid volume and ~500 nm^2 of passivated surface area each.

(4) **Other Structure**. An additional 663 nm^3 of solid volume is included in the design as unallocated structure to account for structural mass which might include housings, extra features on the struts, stabilizing brackets between foundation blocks, and so forth.

[1006] K. Eric Drexler, Nanosystems: Molecular Machinery, Manufacturing, and Computation, John Wiley & Sons, New York, 1992; http://www.zyvex.com/nanotech/nanosystems.html

[1007] K. Eric Drexler, Nanosystems: Molecular Machinery, Manufacturing, and Computation, John Wiley & Sons, New York, 1992; http://www.zyvex.com/nanotech/nanosystems.html

None of these non-wall components scale with tank size so all may be treated as constants during scaling design iterations. Table IV-3 summarizes the non-wall components of the BFSS. Note that there are 6 motors to be controlled (5 rotor motors + 1 valve motor), so the entire BFSS is controlled with just 6 electrical lines. Adding 52 control lines for the NFW (Section 3.4.1.1) and 6 control lines for the BFSS yields a total of 58 control lines (plus 1 common ground line for a total of 59) for the NFW-2. Note that the current load on each common ground line is only ~58 I_{motor} ~ 1.16 x 10^{-11} amp, well below the current-carrying capacity experimentally observed[1008] for individual 10-50 nm long single-walled "metallic" carbon nanotubes which can conduct 25-100 x 10^{-6} amp/wire electrical currents before failing, and a burnout threshold of 1000 x 10^{-6} amp/wire reported by others.[1009]

Table IV-3. Volume and Parts Estimate for Non-Wall Components of First-Generation Bulk Feedstock Supply System (BFSS) in Second-Generation NFW-2

Nanopart or Nanodevice	Number of Com-ponents	Solid Volume each (nm^3)	# Parts / Com-ponent	Solid Volume All (nm^3)	Total # of All Parts
Tank valve	1	1571	2	1571	2
Valve motor	1	200	4	200	4
Valve wire pair	1	200	1	200	1
Sorting rotors	6	686	16	4116	96
Rotary motors	5	200	4	1000	20
Power/control wires	5	200	1	1000	5
Transfer units	5	1250	2	6250	10
Unallocated structure	1	663	1	663	1
TOTALS	**25**			**15,000 nm^3**	**139 parts**

Allocating ~176 C atoms/nm^3 for diamondoid lattice and ~31.4 H atoms per nm^2 to passivate diamondoid surface and assuming a maximum of 25 Ge atoms required in the BFSS germane sorting rotor storage volume, the scaling results for the entire NFW-2 are obtained as shown in Table IV-4. The main storage tank scales out as 40 nm in radius, 568 nm in length, with H-passivated diamond walls 0.45 nm thick and wrapping around 3 edges of the NFW or ~79% of the total perimeter. The NFW-2 covers an area of 56,040 nm^2 on the assembly surface and has an excluded solid volume of 4.91 x 10^6 nm^3, while the graphene bladder sheet is 81,430 nm^2 in surface area. There are ~24 million ethylene gas molecules in the tank at 400 atm when it is full at the beginning of a replication or production cycle, and ~38 million H_2 byproduct molecules in

[1008] Ali Javey, Pengfei Qi, Qian Wang, Hongjie Dai, "Ten- to 50-nm-long quasi-ballistic carbon nanotube devices obtained without complex lithography," PNAS 101(14 September 2004):13408-13410; http://www.pnas.org/cgi/content/abstract/101/37/13408.

[1009] Hongjie Dai, Eric W. Wong, Charles M. Lieber, "Probing Electrical Transport in Nanomaterials: Conductivity of Individual Carbon Nanotubes," Science 272(26 April 1996):523-526; Stefan Frank, Philippe Poncharal, Z.L. Wang, Walt A. de Heer, "Carbon Nanotube Quantum Resistors," Science 280(12 June 1998):1744-1746.

the tank at 1000 atm at the end of a replication or production cycle when all the ethylene has been consumed. The unloaded NFW-2 system has a total atom count of ~64,898,035 atoms (72% C atoms, 28% H atoms), a total mass of 9.65 x 10^{-19} kg, and a total nanopart count of 662. Excluding the main tank and bladder sheet, the average NFW-2 nanopart has 55,543 atoms (43,511 atoms of C and 12,032 atoms of H).

Table IV-4. Estimated Atom Counts for Second-Generation Workstation (NFW-2)

NFW Nanopart or Nanodevice	# of Nano parts	Total Solid Volume (nm^3)	Total Passiv. Area (nm^2)	# of C Atoms	# of H Atoms	# of Ge Atoms	Total # of Atoms
Main tank wall	1	73,287	325,720	15,455,429	10,227,618	0	25,683,047
Bladder sheet	1	8126	0	2,556,905	0	0	2,556,905
Tank valve	2	1571	1885	276,496	59,189	0	335,685
Valve motor	4	200	500	35,200	15,700	0	50,900
Valve wire pair	1	200	0	35,200	0	0	35,200
Sorting rotors	96	4116	67,200	724,416	2,110,080	0	2,834,496
Rotary motors	20	1000	10,000	176,000	314,000	0	490,000
Power/control wire + ground	5	1000	0	176,000	0	0	176,000
Transfer units	10	6250	5000	1,100,000	157,000	0	1,257,000
Unallocated structure	1	663	456	116,688	14,318	0	131,006
BFSS Subtotals	141	96,413	410,761	20,652,334	12,897,905	0	33,550,239
NFW	521	150,280	170,030	26,076,856	5,270,930	10	31,347,796
NFW-2 (Empty)	662	246,693	580,791	46,729,190	18,168,835	10	64,898,035
Feedstock gases	----	3,123,162	----	47,478,470	94,956,940	25	142,435,435
NFW-2 (Filled)	662	3,369,855	580,791	94,207,660	113,125,775	35	207,333,470

Since the BFSS tank is relatively flexible due to its thinner walls, concern may arise that its expansion during filling and contraction during emptying might produce positioning error during blind pick-and-place gas molecule handling operations by NFW-2 manipulators. Of course, if sorting rotors and transfer units are rigidly affixed to a foundation block, then movements of the more flexible tank structure cannot significantly enhance the positioning error between manipulators and rotor binding sites. However, rotors mounted on the tank wall alone might have more freedom to move. In this case, the fractional change in BFSS tank surface area during tank filling and emptying can be estimated as $\Delta A_{tank}/A_{tank} \sim \Delta P / K_{tank} \sim 1.2 \times 10^{-3}$ where tank wall area compressibility K_{tank} is approximated by the 5 x 10^{10} N/m^2 failure strength for diamond[1010] and ΔP = 600 atm when tank pressure cycles between 400 atm (BFSS full of C_2H_4; Section 3.5.1.6)

[1010] Robert A. Freitas Jr., Nanomedicine, Volume I: Basic Capabilities, Landes Bioscience, Georgetown, TX, 1999; Table 9.3, p. 295; http://www.nanomedicine.com/NMI/Tables/9.3.jpg.

and 1000 atm (BFSS full of H_2; Section 3.5.1.6). Thus the worst-case full-cycle variation of the position of a binding site mounted on the tank wall located a maximum of $2R_{tank} \sim 80$ nm from a foundation block approximates $\Delta L_{site} \sim R_{tank} \cdot (\Delta A_{tank}/A_{tank})^{1/2} = 28$ Å, or ≥140 times the acceptable variation of ≤0.2 Å that would not significantly contribute to manipulator positioning error. The tank wall stretching varies with pressure in a predictable manner, so the manipulator control code can incorporate ≥140 minor positional parameter adjustments (one per every ≤464,000 atoms processed) during each production cycle to keep the manipulator reliably going to the right place.

3.5.1.7 Operation of the NFW-2 Workstation

The second-generation nanoscale fabrication workstation (NFW-2) (Figure IV-1) fabricates nanoparts using a set of individually controlled nanoscale manipulators grasping DMS toolheads capable of performing diamondoid mechanosynthesis virtually identical to the system already described for the NFW (Section 3.4.1.1). The NFW-2 builds diamondoid nanoparts starting from basic feedstock molecules that it acquires from the BFSS (Section 3.5.1.6) installed adjacent to the workstation on the same assembly surface. Finished nanoparts are still carried off by the macroscale Phase II system.

After the NFW-2 has been constructed in UHV on the atomically smooth electrode-rich assembly surface, the workstation may be operated as follows. At the beginning of the work cycle, all sensitive NFW-2 components (e.g., any tooltips with exposed radical sites) are protectively stowed within gastight housings. The workspace UHV chamber is flooded with (5N+ purity) ethylene gas, the primary feedstock molecule, pressurized to 1 atm. Control signals and power are sent through the surface electrodes to operate the BFSS sorting rotor pair that pumps the feedstock gas into the BFSS main tank until a 400 atm storage pressure is reached (Section 3.5.1.6). Although the ethylene rotors could be operated up to a $\sim 10^6$ molecule/sec transport rate (Section 3.5.1.6), using a more conservative 10^5 molecule/sec transport rate still allows the BFSS tank to be filled with ~24 million C_2H_4 molecules in only ~2400 sec (~0.03 day). The ethylene gas is then purged from the workspace chamber, and the chamber and its contents are pumped down to UHV conditions (see below). A similar process is then repeated with (5N+ purity) germane gas, the secondary feedstock molecule, using one sorting rotor to pump a small number of GeH_4 molecules into the sorting rotor plenum at ~10 atm storage pressure (Section 3.5.1.4). All germane gas is then purged from the workspace chamber, and the chamber and its contents are once again pumped down to UHV conditions (see below). Employing two separate feedstock gas loading cycles reduces the demand for high specificity in the sorting rotor binding sites for each gas by minimizing the number of alternative molecule types competing for the same binding site. If ethylene and germane binding sites of sufficiently high specificity can be designed, it may be possible to reduce the number of feedstock gas loading cycles from two to one.

The NFW-2 is unstowed for use in UHV conditions, then operated much like the first-generation NFW to build nanoparts (Section 3.4.6), but drawing feedstock molecules from the BFSS instead of being hand-fed feedstock via the Phase II system and delivering byproduct molecules directly to the BFSS for disposal rather than to the Phase II system. At the end of the production cycle, the BFSS main tank is essentially empty of ethylene feedstock molecules but has been filled to ~1000 atm with H_2 byproduct molecules (Section 3.5.1.6). All sensitive NFW-2 components are again protectively stowed within gastight housings, then the contents of the main tank (mostly molecular hydrogen plus a small amount of unused ethylene) are vented into the workspace

chamber which is again pumped down to UHV conditions (see below). The first NFW-2 manufacturing cycle is then complete and a new cycle may be initiated.

During workspace chamber pumpdown after BFSS gas loading or byproduct gas venting, feedstock and byproduct molecules will be weakly physisorbed to the exposed silica, hydrogenated diamond, graphene and silver surfaces comprising the NFW-2 system. These gases can be quickly and fully desorbed by employing both thermal and nonthermal means:

(1) **Thermal Desorption**. Practical bakeout protocols at T < 548 K are known to reliably desorb hydrocarbons from Ge/Si photodetector surfaces,[1011] but we require room temperature desorption to avoid post-loading ethylene decomposition inside the BFSS main tank. Ethylene physisorbs only relatively weakly to graphene surface (0.17 eV binding energy at 276 K)[1012] and to silica,[1013] and the heat of vaporization of C_2H_4 is 0.0555 eV/molecule at 273 K.[1014] Under approximate conditions of negligible readsorption (i.e., very high vacuum), the Arrhenius equation for the one-step thermal desorption rate, $k_1 \sim \nu \exp(-E_d / k_B T)$, may be used to crudely approximate the canonical residence time for a molecule physisorbed to a working surface heated to temperature T, where T = 300 K and the pre-exponential attempt rate is $\nu \sim k_B T/h \sim 6 \times 10^{12}$ sec^{-1} ($h = 6.63 \times 10^{-34}$ J-sec) as typically used for thermally migrating hydrocarbons on diamond surfaces (the precise value of which does not sensitively influence the conclusion). Hence the ethylene vaporization time for $E_d \sim 0.0555$ eV is $k_1^{-1} \sim 10^{-12}$ sec, and for desorbing ethylene from graphene at T ~ 300 K ($E_d \sim 0.17$ eV), $k_1^{-1} \sim 10^{-10}$ sec. The binding energy of germane for physisorption on relevant surfaces has not yet been measured experimentally, though it is expected to also be rather weak.

(2) **Nonthermal Stimulated Desorption**. Stimulated desorption[1015] is used as an additional nonthermal means to help ensure complete desorption of physisorbed feedstock and

---

[1011] Prabhakar Bandaru, Subal Sahni, Eli Yablonovitch, Hyung-Jun Kim, Ya-Hong Xie, "The fabrication of p-Ge/n-Si photodetectors, compatible with back-end Si CMOS processing, by low temperature (< 400 ^oC) molecular beam epitaxy and electron-beam evaporation," Mat. Res. Soc. Symp. Proc. Vol. 796, Materials Research Society, 2004, V2.8.1-6; http://www.mrs.org/s_mrs/bin.asp?CID=2637&DID=61421&DOC=FILE.PDF.

[1012] A.V. Kiselev, D.P. Poshkus, "Molecular-statistical calculation of the thermodynamic characteristics of adsorption of saturated and unsaturated hydrocarbons on graphitized thermal carbon black," J. Chem. Soc. Faraday Trans. II 72(1976):950-966.

[1013] G. A. Nesterov, V. M. Mastikhin, O. B. Lapina, V. A. Zakharov, "NMR studies of ethylene adsorption on supported zirconium catalysts for polymerization of olefins," Reaction Kinetics and Catalysis Letters 19(March 1982):175-179.

[1014] Heinz Zimmermann, Roland Walzl, "Ethylene," in: Ullmann's Encyclopedia of Industrial Chemistry, 7th Edition, John Wiley and Sons, 2005, http://www.mrw.interscience.wiley.com/ueic/ueic_search_fs.html (subscription required) and http://media.wiley.com/product_data/excerpt/55/35273038/3527303855.pdf

[1015] John F. O'Hanlon, "Gas Release from Solids," in John F. O'Hanlon, ed., A User's Guide to Vacuum Technology, John Wiley & Sons, New York, 2003, pp. 57-78; http://www3.interscience.wiley.com/cgi-bin/bookhome/109855969/.

byproduct gases from workspace surfaces and to facilitate the evacuation of these gases from the workspace chamber. The most common form of stimulated desorption is **laser-induced surface desorption** *in vacuo* which allows mass spectrometry measurements without breaking the chemical bonds in the desorbed species[1016] while inducing relatively insignificant bulk reaction[1017] (e.g., as in the pump-probe scheme used in ultrafast photoionization spectroscopy).[1018] In particular, infrared laser radiation impinging onto a molecule adsorbed on a solid surface can resonantly excite the admolecular internal vibrational/rotational modes or deposit photon energy in the adbond with which the molecule is bound to the surface.[1019] For example, it has been shown experimentally[1020] that SF_6 and CH_3F molecules adsorbed on NaCl surfaces at low temperatures can be desorbed by the resonant excitation of the adsorbate internal vibration (the ν_3 mode). Other studies showed: (1) desorption of organics from silver metal

---

[1016] T. Gonthiez, T. Gibert, P. Brault, C. Boulmer-Leborgne, C. Olivero, M.C. Castex, "VUV laser photoionization of laser-stimulated desorbed species," Appl. Phys. A Materials Science & Processing 69(December 1999):171-173.

[1017] Wayne P. Hess, Alan G. Joly, Daniel P. Gerrity, Kenneth M. Beck, Peter V. Sushko, Alexander L. Shluger, "Selective laser desorption of ionic surfaces: Resonant surface excitation of KBr," J. Chem. Phys. 115(22 November 2001):9463-9472.

[1018] D. von der Linde, H.-P. Ludescher, "Measurement of ultrafast surface processes using laser photoionization," in Charles M. Miller, James E. Parks, eds., Resonance Ionization Spectroscopy, CRC Press, 1992, pp. 249-254; M.J. Pellin, K.R. Lykke, P. Wurz, D.H. Parker, "Molecular surface analysis by laser ionization of desorbed molecules," in Charles M. Miller, James E. Parks, eds., Resonance Ionization Spectroscopy, CRC Press, 1992, pp. 167-172; W. Kaiser, ed., Ultrashort Laser Pulses: Generation and Applications, Second Edition, Springer-Verlag, 1993.

[1019] X.Y. Huang, T.F. George, J.M. Yuan, L.M. Narducci, "Phase-dissipative mechanisms for laser-induced surface desorption/dissociation processes," J. Phys. Chem. 88(1984):5772-5774; http://pubs.acs.org/cgi-bin/abstract.cgi/jpchax/1984/88/i24/f-pdf/f_j150668a005.pdf. M.S. Slutsky, T.F. George, "Quantum theory of laser-stimulated desorption," Chem. Phys. Lett. 57(1978):474-476; J. Lin, T.F. George, "Dynamical model of selective vs. nonselective laser-stimulated surface processes. 2. Analytical methods and applications to surface rate processes," J. Phys. Chem. 84(30 October 1980):2957-2968, http://dx.doi.org/10.1021/j100459a025; Jui-teng Lin, Thomas F. George, "Classical model of laser-stimulated surface processes: Energy-absorption profiles via the Langevin equation," Phys. Rev. B 24(1981):64-75; D. Lucas, G.E. Ewing, "Spontaneous desorption of vibrationally excited molecules physically adsorbed on surfaces," Chem. Phys. 58(1981):385-393; Z.W. Gortel, H.J. Kreuzer, P. Piercy, R. Teshima, "Theory of photodesorption of molecules by resonant laser-molecular vibrational coupling," Phys. Rev. B 27(1983):5066-5083, http://prola.aps.org/pdf/PRB/v27/i8/p5066_1.

[1020] J. Heidberg, H. Stein, A. Nestmann, E. Hoefs, I. Hussla, in S.D. Ferris, H.J. Leamy, J.M. Poate, eds., Laser-Solid Interactions and Laser Processing, AIP Conference Proceedings, Vol. 50, American Institute of Physics, New York, 1979, pp. 49-54; J. Heidberg, H. Stein, E. Riehl, "Resonance, Rate, and Quantum Yield of Infrared-Laser-Induced Desorption by Multiquantum Vibrational Excitation of the Adsorbate CH_3F on NaCl," Phys. Rev. Lett. 49(1982):666-669, http://prola.aps.org/pdf/PRL/v49/i9/p666_1; J. Heidberg, H. Stein, E. Riehl, Z. Szilágyi, H. Weiss, "Vibrational Predesorption," Surf. Sci. 158(1985):553-578; J. Heidberg, H. Stein, H. Weiss, "Vibrational Predesorption of Carbon Monoxide from Sodium Chloride at 20 K Induced by Resonant Infrared Laser Excitation," Surf. Sci. 184(1987):L431-L438.

surface;[1021] (2) desorption of ammonia from copper metal surface;[1022] (3) desorption of neutral Na atoms from Na clusters deposited on mica substrates when irradiated with a pulsed laser beam in the 2-3 eV energy range,[1023] which raised the substrate surface temperature by just 10 K;[1024] (4) photolysis of adsorbed aluminum compounds;[1025] (5) rare gas atom desorption from metal surfaces; [1026] (6) low fluence laser irradiation of cleaved KBr crystals, near the calculated surface exciton energy of 6.2 eV, produces hyperthermal Br atom emission without a significant thermal component;[1027] and, of course, (7) photon-stimulated H desorption from diamond C(111) surface.[1028] (**Ion-induced desorption** has been experimentally demonstrated to release Na^+ from NaCl(100),[1029] and **electron-stimulated desorption** of hydrogen[1030] and electron-beam desorption of halocarbons from polycrystalline tungsten[1031] has also been shown.)

[1021] T.J. Chuang, H. Seki, "Resonantly Stimulated Desorption of Pyridine from Silver Surfaces by Polarized Infrared Laser Radiation," Phys. Rev. Lett. 49(1982):382-386; http://prola.aps.org/pdf/PRL/v49/i6/p382_1.

[1022] T.J. Chuang, Ingo Hussla, "Time-Resolved Mass-Spectrometric Study on Infrared Laser Photodesorption of Ammonia from Cu(100)," Phys. Rev. Lett. 52(1984):2045-2048; http://prola.aps.org/pdf/PRL/v52/i23/p2045_1.

[1023] J. R. Manson M. Renger, H.-G. Rubahn, "Subthermal Kinetic Energy Distributions of Neutral Atoms Photodesorbed from Na Cluster Surfaces," Max Planck Institut fur Stromungsforschung, 25 August 1996; http://www.ces.clemson.edu/surfphys/papers/93.ps.gz.

[1024] F. Balzer, H.-G. Rubahn, "Size effects and the determination of absolute temperature increases in laser heating of dielectrics," Chem. Phys. Lett. 233(1995):75-80.

[1025] G.S. Higashi, "The chemistry of alkyl-aluminum compounds during laser-assisted chemical vapor deposition," Appl. Surf. Sci. 43(2 December 1989):6-10; http://dx.doi.org/10.1016/0169-4332(89)90182-7.

[1026] John C. Tully, "Dynamics of gas-surface interactions: Thermal desorption of Ar and Xe. from platinum," Surf. Sci. 111(2 November 1981):461-478; http://dx.doi.org/10.1016/0039-6028(81)90402-7.

[1027] Wayne P. Hess, Alan G. Joly, Daniel P. Gerrity, Kenneth M. Beck, Peter V. Sushko, Alexander L. Shluger, "Selective laser desorption of ionic surfaces: Resonant surface excitation of KBr," J. Chem. Phys. 115(22 November 2001):9463-9472.

[1028] B.B. Pate, M.H. Hecht, C. Binns, I. Lindau, W.E. Spicer, "Photoemission And Photon-Stimulated Ion Desorption Studies Of Diamond(111): Hydrogen," J. Vac. Sci. Technol. 21(1982):364-367.

[1029] Z. Postawa, R. Maboudian, M. El-Maazawi, M.H. Ervin, M.C. Wood, N. Winograd, "Electronic and Nuclear Effecs in Ion-Induced Desorption from NaCl(100)," J. Chem. Phys. 96(1992):3298-3305; http://nxw.chem.psu.edu/nxw/pdf%5C177.pdf.

[1030] Fumio Watanabe, Maki Suemitsu, "Separation of electron-stimulated-desorption neutrals from outgassing originating from the grid surface of emission-controlled gauges: Studies with a heated-grid gauge," J. Vac. Sci. Technol. A: Vacuum, Surfaces, and Films 17(November 1999):3467-3472; Fumio Watanabe, "Investigation and reduction of spurious peaks caused by electron-stimulated desorption and outgassing by means of a grid heating method in a hot-cathode quadrupole residual gas analyzer," J. Vac. Sci. Technol. A: Vacuum, Surfaces, and Films 20(July 2002):1222-1229.

[1031] Mario Antonio Bica de Moraes, "Electron stimulated desorption studies of some halocarbons ($CC1_2F_2$, $C_2H_2F_2$ and C_2F_6) adsorbed on polycrystalline tungsten," Ph.D. Thesis (QC 1000.M827x), UWM Masters

Equally compelling as proofs of concept are the many known examples of **laser cleaning** – e.g., IR laser induced desorption of water and hydrocarbon molecules[1032] from optical surfaces, various adsorbate molecules from silicon surfaces,[1033] and other particles[1034] and molecules[1035] from other surfaces. In the case of ethylene, there are 12 normal-mode infrared frequencies including two at 1428 cm^{-1} (4.28 x 10^{13} Hz) and 1711 cm^{-1} (5.13 x 10^{13} Hz) that seem to correspond mostly to C=C stretching with the least amount of C-H stretching, as calculated using Gaussian98 with DFT at the B3LYP/6-311+G(2d,p)//B3LYP/3-21G* level of theory. A published paper[1036] gives a similar IR frequency of ~3200 cm^{-1} for C≡C stretching in acetylene molecules physisorbed on diamond C(111) surface. This spectral feature is reported as having an extremely narrow bandwidth (only ~2 cm^{-1}) which should allow a precisely tuned IR laser inside the workspace chamber to selectively excite that one vibrational mode and nothing else to induce surface desorption of the physisorbed hydrocarbon molecule while causing negligible collateral surface heating.

Phonon-assisted desorption of physisorbed molecules on surfaces has also been reported,[1037] including Rayleigh surface acoustic wave desorption of O_2 from NiO surfaces,[1038] desorption of other species by surface waves excited by ultrasonic SAW,[1039] and liquid-phase

---

& Doctoral Dissertations, Physics, University of Wisconsin at Milwaukee, 1978; http://www.uwm.edu/Libraries/guides/theses/qc1000.html.

[1032] S.D. Allen, J.O. Porteus, W.N. Faith, "Infrared laser-induced desorption of H_20 and hydrocarbons from optical surfaces," Appl. Phys. Lett. 41(1982):416-418; S.D. Allen, J.O. Porteus, W.N. Faith, J.B. Franck, "Contaminant and defect analysis of optical surfaces by infrared laser induced desorption," Appl. Phys. Lett. 45(1984):997-999.

[1033] V. Dobler, R. Oltra, J.P. Boquillon, M. Mosbacher, J. Boneberg, P. Leiderer, "Surface acceleration during dry laser cleaning of silicon," Appl. Phys. A 69(1999):S335-S339.

[1034] A. Miller, S.J. Lee, S.D. Allen, "Laser assisted particle removal 'dry' cleaning of critical surfaces," Mater. Sci. Eng. B 49(1997):85-88.

[1035] A.C. Tam, H.K. Park, C.P. Grigoropoulos, "Laser Cleaning of Surface Contaminants," Appl. Surf. Sci. 127-129(1998):721-725; P.T. Leung, N. Do, Leander Klees, W.P.Leung, Frank Tong, L.Lam, W. Zapka, A.C. Tam, "Transmission studies of explosive vaporization of a transparent liquid film on an opaque solid surface induced by excimer-laser-pulsed irradiation," J. Appl. Phys. 72(1992):2256-2263.

[1036] H.-C. Chang, J.-C. Lin, "Structure and bonding of C_2H_2 on diamond C(111)-1x1:H: Infrared spectroscopy and exciton calculations," J. Phys. Chem. 100(1996):7018-7025.

[1037] Gert Due Billing, Dynamics of Molecule Surface Interaction, Wiley-Interscience, 1999.

[1038] H. Nishiyama, N. Rattana, N. Saito, K. Sato, Y. Inoue, "Effects of Rayleigh Surface Acoustic Wave upon Adsorptive and Surface Properties of a Thin NiO Film," J. Phys. Chem. B 104(2000):10602-10607.

[1039] Charles Krischer, David Lichtman, "Ultrasonic Surface Wave-Induced Desorption," 2nd Intl. Conf. Solid Surfaces, Kyoto (1974), Japanese Journal of Applied Physics 2(1974):469-470 (Suppl. 2-2); http://jjap.ipap.jp/link?JJAPS/2S2/469/.

ultrasonic desorption of organic molecules such as trichloroethylene[1040] and chlorophenol[1041] (e.g., at 516 KHz)[1042] from activated carbon substrates wherein the nonthermal dominate the thermal effects.

The raw productivity of the NFW-2 system should be identical to the maximum theoretical capacity of the NFW of ~100 atoms/sec as estimated in Section 3.4.1.4. Addition of the BFSS means that the NFW is no longer process-limited by the ~1 Hz capacity of the Phase II system to present feedstock molecules to the NFW and to carry away byproduct molecules, but can now run at the full 100 Hz rate with ~100 atoms/sec fabricated into nanoparts (Section 3.4.1.4). Note that fabrication time could now be reduced by increasing pulse frequency because fabrication operations are no longer limited by the operating rate of the Phase II system.

One BFSS tankful of ethylene feedstock gas allows the NFW-2 to fabricate roughly its own mass of nanoparts. This requires the acquisition of ~24 million C_2H_4 gas molecules from the BFSS, followed by the fabrication of nanoparts composed of ~47 million carbon atoms plus ~18 million H atoms that are installed along with the carbon atoms, giving a total of ~65 million atoms in the fabricated nanoparts (Table IV-4) requiring ~0.65 million seconds or ~7.5 days. Note that although 76.8 million surplus H atoms must be disposed of via ~38.4 million DMS operations (in which two H atoms at a time are disposed as H_2 molecules), each such operation (Section 3.5.1.6) effectively recharges two HTrans tools at the same time and thus these operations are already counted in the ~6 step/atom calculation from Section 3.4.1.4 – which estimates that ~390 million steps are needed to emplace all ~65 million atoms, of which only ~38 million steps are involved in handling H_2 disposal.

However, the net productivity of the NFW-2 is reduced by the necessity for multiple pumpdowns to UHV conditions – possibly including two such excursions to load the ethylene and germane feedstock molecules separately and a third such excursion to pump the workspace chamber free of byproduct gases at the end of each cycle. Taking a ~7 day UHV pumpdown time for typical present-day laboratory setups,[1043] the NFW-2 could fabricate its own mass of nanoparts in a total

---

[1040] Jae-Lim Lim, Mitsumasa Okada, "Regeneration of granular activated carbon using ultrasound," Ultrasonics Sonochemistry 12(March 2005):277-282.

[1041] O. Hamdaoui, E. Naffrechoux, J. Suptil, C. Fachinger, "Ultrasonic desorption of p-chlorophenol from granular activated carbon," Chemical Engineering Journal 106(15 February 2005):153-161; Oualid Hamdaoui, Emmanuel Naffrechoux, "An investigation of the mechanisms of ultrasonically enhanced desorption," Amer. Inst. Chem. Eng. Journal 53(2007):363-373; http://www3.interscience.wiley.com/cgi-bin/abstract/114034329/ABSTRACT.

[1042] O. Hamdaoui, E. Naffrechoux, J. Suptil, C. Fachinger, "Ultrasonic desorption of p-chlorophenol from granular activated carbon," Chemical Engineering Journal 106(15 February 2005):153-161; Oualid Hamdaoui, Emmanuel Naffrechoux, "An investigation of the mechanisms of ultrasonically enhanced desorption," Amer. Inst. Chem. Eng. Journal 53(2007):363-373; http://www3.interscience.wiley.com/cgi-bin/abstract/114034329/ABSTRACT.

[1043] Richard Hurley, "Vacuum Tutorial #1: Outgassing Of Stainless Steel And Pumping For UHV Systems," Richard Hurley's Vacuum Pages, 2004; http://vacuumtunes.co.uk/vtut1.html.

cycle time of ~((3)(7) + 7.5) ~ 28.5 days. The gas loading time might be dramatically reduced by several means:

(1) **Single-Cycle Operation.** Simply performing all feedstock loading in a single cycle might reduce NFW-2 replication time to ~22 days.

(2) **Aggressive Desorption and Gettering.** Applying desorption techniques (described above) more aggressively may be coupled with cold traps and the extensive use of nanomechanical getters analogous to non-evaporable getters (NEGs).[1044] Such getters can include NFW-fabricated arrays of binding sites for the feedstock, byproduct, and contaminant molecules, with the sites installed on sorting rotor mechanisms embedded in wands (having internal gas exhaust channels) that can be inserted into the workchamber space to rapidly mechanically outpump all gases.

(3) **Operation in Space.** Moving all operations off-Earth into the orbital space environment could facilitate pumpdown via simple venting into the hard vacuum of space. (Molecular manufacturing in space[1045] offers additional benefits including vibration isolation, access to ultralow temperatures and thermal control, and low transport costs for low-mass high-value products.)

These and related methods might reduce the pumpdown time to ~1 day thus decreasing NFW-2 nanopart replication time to as little as ~8 days per cycle. At the completion of Phase IV, the Phase II system is only needed to remove finished nanoparts from the NFW-2 system which can occur at a relatively leisurely pace.

Again assuming ~12,000 increments to place each atom of carbon and one bit to describe each increment (Section 3.4.1.4), a complete replication cycle for the NFW-2 system requires up to (64,898,035 atoms)(12,000 increments/atom-actuator)(1 bit/increment)(58 actuators) ~ 4.52 x 10^{13} bits of replication process data.

3.5.1.8 Reliability of NFW-2 Manufacture and Operation

Regarding the use of the Phase II system to construct the Phase IV NFW-2 system, the NFW-2 has about twice as many atoms (~65 million atoms; Table IV-4) as the NFW (~31 million atoms; Table III-2), mostly due to the extra mass of the BFSS. Doubling the atom count to be built by the Phase II system gives substantially similar reliability estimates for building the Phase IV system as for the Phase III system. In particular: the Phase II system must correctly execute 390 million mechanosynthetic operations, or 32.5 million operations for each of the 12 MMWs; a DMS reaction error rate of <1 below 235 K, ~10^{-2} near dry-ice temperature at ~190 K, ~10^{-3} at 174 K, or ~10^{-17} at 80 K for a ~65 x 10^{6}-atom product object fabricated using the original set of

---

[1044] P. Chiggiato, "Production of extreme high vacuum with non evaporable getters," Phys. Scr. T71(1997):9-13; http://www.iop.org/EJ/abstract/1402-4896/1997/T71/002/.

[1045] T. McKendree, R. Freitas, A. Globus, M. Levit, C. Sherrill, M. Li, R. Merkle, "Challenges of Molecular Nanotechnology for Space Exploration," AIAA-2005-6814, AIAA Space 2005 Conference, Long Beach, CA, 30-31 August 2005; http://www.rfreitas.com/Nano/McK68141.pdf.

DMS reactions,[1046] completely negligible for Phase IV purposes; minimum vacuum pressure P_{UHV} falls about twofold for Phase IV at 190 K (8 x 10^{-15} atm), compared to Phase III at 195 K (1.2 x 10^{-14} atm); and the radiation damage time is $\tau_{rad} \sim (\kappa_{fail}\ m_{target}\ I_{rad})^{-1} \sim 2073$ years for a mostly-carbon ~65 x 10^6-atom NFW-2 of mass m_{target} = 9.65 x 10^{-19} kg, still a negligible error rate. An operating temperature of T ≤ 190 K thus seems appropriate.

The Phase IV second-generation NFW-2 is then operated as a standalone fabrication system in Task IV-9. For this Phase IV NFW-2 fabrication system, we have a target productivity rate of ~100 atom/sec (Section 3.5.1.7) with ~6 mechanosynthetic operations required for placement of each atom in the growing workpiece structure (Section 3.4.1.4), and a target product object size consisting of all 662 nanoparts comprising an entire 64,898,035-atom NFW-2 replica (which are later assembled by the Phase II system). Building the NFW-2 replica using the original NFW-2 unit thus requires ~390 million mechanosynthetic operations, so to avoid even a single misplacement error the NFW-2 manipulators must be able to deliver a minimum of ~390 million error-free round trip excursions of the positionally controlled DMS tooltips. The potential ability of computer controllers to reliably deliver such lengthy data sequences with low error, and the ability of simple mechanical actuators to reliably execute such lengthy sequences of mechanical actuations with low error, is discussed in Section 3.8.1.3.

Another source of intrinsic manufacturing error arises from the reliability of the DMS reactions themselves as previously discussed (Section 3.2.1.8 and Section 3.4.1.6). Table I-5 gives the probability of misreaction at various relevant operating temperatures, assuming a defect energy threshold of 0.40 eV. The misreaction probability per mechanosynthetic operation may be as high as 1.91 x 10^{-7} at 300 K, conservatively assuming that all reactions have the minimum defect energy threshold of 0.40 eV, producing ~75 erroneous atom placements in the ~65 x 10^6-atom NFW-2 replica product object after ~390 x 10^6 mechanosynthetic operations, hence endogenous room temperature fabrication of the NFW-2 replica by the original NFW-2 system appears infeasible. The expected error rate falls to <1 erroneous atom placement below 235 K, ~10^{-2} near dry-ice temperature at ~190 K, or ~10^{-3} at 174 K for a ~31 x 10^6-atom product object fabricated using the original set of DMS reactions.[1047] Ethylene remains a gas above 170 K, and while GeH_4 liquefies below 185 K enough germane should remain in the vapor state to permit gaseous feedstock operation throughout the 174-190 K temperature range. At near liquid nitrogen temperatures (~80 K), the DMS-related error rate using reaction sequences with a defect energy threshold of 0.40 eV would fall to ~10^{-17} for a ~65 x 10^6-atom product object, completely negligible for Phase IV purposes. Note that the error rate due to feedstock gas impurities is zero because feedstock molecules are sufficiently purified during transfer into the BFSS to remove all contaminants (Section 3.5.1.6(2)).

Another major source of error is radical poisoning by contaminants in an imperfect UHV environment. At a target productivity rate of ~100 atoms/sec for the Phase IV system, the original ~65 x 10^6-atom NFW-2 will require t_{fab} ~ 6.5 x 10^5 sec (~8 days) to fabricate the ~65 x

---

[1046] Robert A. Freitas Jr., Ralph C. Merkle, "A Minimal Toolset for Positional Diamond Mechanosynthesis," J. Comput. Theor. Nanosci. 5(May 2008):760-861.

[1047] Robert A. Freitas Jr., Ralph C. Merkle, "A Minimal Toolset for Positional Diamond Mechanosynthesis," J. Comput. Theor. Nanosci. 5(May 2008):760-861.

10^6-atom NFW-2 replica. Assuming that a radical site susceptible to poisoning is exposed to the imperfect UHV environment for a fraction f_{vac} ~ 50% of the time, then the maximum tolerable UHV pressure that will permit all nanoparts for one defect-free ~65 x 10^6-atom NFW-2 replica to be fabricated is $P_{UHV} \leq (N_{encounters}\ T / n_{contam}\ A_{radical}\ f_{vac}\ t_{fab})\ (\pi\ MW_{kg} / 2\ k_B T\ N_A)^{1/2}$ ~ 5 x 10^{-14} atm, where n_{contam} = 7.34 x 10^{27} molecules-K/m^3-atm (= N_A/R_{gas}) for ideal gas (contaminant) molecules and T = 190 K, with the other quantities as previously defined in Section 3.2.1.7. If any workpiece having one or more erroneous atom placements is considered defective, then in a UHV environment maintained at ~10^{-16} atm (~10 million contaminant molecules present in a 5-liter UHV work volume; currently achievable experimentally, Section 3.2.1.7) the radical-poisoning defect rate at 190 K will be a quite acceptable ~10^{-3} for replica NFW-2 product objects. If H_2 contaminant is determined not to be a serious radical poisoning risk or can be rigorously excluded from the workspace, then taking MW_{kg} = 0.014 kg/mole for N_2 raises the required P_{UHV} by a factor of ~2.6.

As for radiation damage rates, assuming a failure condition of κ_{fail} ~ 10^{15} hits/kg-rad and an I_{rad} ~ 0.5 rad/yr background the mean time τ_{rad} between radiation-disabling hits on a mostly-carbon ~65 x 10^6-atom NFW of mass m_{target} = 9.65 x 10^{-19} kg is $\tau_{rad} \sim (\kappa_{fail}\ m_{target}\ I_{rad})^{-1}$ ~ 2073 years (conservatively assuming that one such hit will cause the workpiece or tooltip to fail with 100% certainty), still a negligible error rate (~10^{-5} per replication cycle).

When used for assembly work rather than for fabrication, the Phase II system neither creates nor destroys chemically active radical sites, hence its operations are not subject to DMS-related error rates and are only weakly subject to vacuum poisoning effects. Hence MMW reliability during assembly operations is governed chiefly by its ability to correctly execute a small number of non-covalent parts assembly operations and by error rates in nanopart gripping/releasing mechanisms, and these error rates are assumed to be small in comparison with the DMS-related error rates.

3.5.2 Task IV-1: Design and Simulate First-Generation BFSS

Task IV-1 is to design and simulate the entire BFSS, specifying all component nanoparts and nanodevices (assemblies of nanoparts) and also specifying all fabrication and assembly processes required to build the BFSS and to validate the BFSS functional operations of: (1) feedstock gas inloading into main tank and germane rotor plenum, (2) single-molecule delivery of feedstock molecules to appropriate tooltips, (3) importation of molecular hydrogen byproduct, including a theoretical analysis of making H_2 gas using available DMS procedures, and (4) end-of-cycle gas venting. The first-generation BFSS design should accommodate the existing NFW design (Section 3.4.2) and should be designed to cleanly interface with the existing NFW work envelope. Greater efficiencies may be attainable in the design process if Task III-1 and Task IV-1 are undertaken simultaneously.

Design and simulation of the typical BFSS nanopart will require at minimum a molecular mechanics / molecular dynamics (MM/MD) level analysis of a non-tankwall nanopart having (5,310,287 atoms)/(139 nanoparts) ~ 38,203 atoms/nanopart (Table IV-4), excluding the main tank and bladder sheet. Such modeling and simulation could be performed using the NanoEngineer-1 software package that was available in 2007, running on commonplace personal computers that were available in 2007. Excepting the sorting rotors which have ~16 nanoparts, the typical nanodevice consists of 2-4 nanoparts (Table IV-3), increasing the simulation software capacity requirement to 76,000-153,000 atoms/nanodevice for basic modeling and validation of proper operation, and the tank and bladder sheet are much larger. Following Moore's Law

assuming an 18-month doubling time and conservatively assuming traditional ~N_{atom}^2 scaling with atom count for MM/MD algorithms, a 153,000-atom nanodevice could be simulated using NanoEngineer-1 on a single commonplace personal computer that would be available in 2011, or on a 16-CPU computer cluster that might be available in 2008. Additional software and computing capacity will need to be acquired to simulate these nanodevices, or to simulate still larger sorting rotor assemblies, main tank and bladder sheet, or if higher levels of analysis (i.e., semi-empirical or density-functional (DFT) levels of theory) are deemed necessary for these nanoparts and nanodevices.

MM/MD modeling and simulation of the entire 33,550,239-atom BFSS at the full atomistic level is well beyond the current ability of NanoEngineer-1 executing on a desktop PC or on a small computer cluster and will require specialized software running on highly parallel supercomputers as described earlier in Section 3.4.2.

We will also need a literature review, definitive simulations, and comprehensive assessment of the possibility of hydrogen diffusion through diamondoid surfaces (including graphene and thin diamondoid sheets) and bulk diamondoid crystal.

3.5.3 Task IV-2: Prepare Multielectrode Assembly Surface

Task IV-2 is to prepare an atomically flat surface upon which the first BFSS can be physically constructed and debugged. Electrical power and control signals are applied to BFSS mechanisms via carbon nanotube wires that connect conductive silver terminals on the atomically smooth assembly surface to electrostatic motors that actuate the rotors and valve. Nanotube wires from the BFSS are joined to the ~59 silver electrodes per worksite by simple van der Waals attraction, or if this is insufficient then by nanotube impalement of the softer metal, by e-beam spot welding,[1048] by using designed mateable connectors, or by other means. The assembly surface material is again silicon dioxide and will include 100-1000 worksites each of area ~56,040 nm^2 (Section 3.5.4) on each semiconductor chip which should be a sufficient number for experimentation and testing, as described earlier in Section 3.4.3, probably requiring a total scan time of 20-40 days using a single tip.

The electrode array surface should be of the appropriate configuration to accommodate the addition of the NFW to the BFSS in Task IV-8 (Section 3.5.9).

[1048] MinFeng Yu, Mark J. Dyer, George D. Skidmore, Henry W. Rohrs, Xue Kun Lu, Kevin D. Ausman, James Von Ehr, Rodney S. Ruoff, "3 Dimensional Manipulation of Carbon Nanotubes under a Scanning Electron Microscope," paper presented at the Sixth Foresight Nanotechnology Conference, November 1998; see also: Robert F. Service, "AFMs Wield Parts for Nanoconstruction," Science 282(27 November 1998):1620-1621; and http://www.foresight.org/Conferences/MNT6/Papers/Yu/index.html.

3.5.4 Task IV-3: Fabricate and Assemble BFSS Nanoparts and Nanodevices using Phase II System

Task IV-3 is to use the macroscale manufacturing system created during Phase II (Section 3.3) to fabricate all necessary nanoparts, and then to assemble some of these nanoparts into all necessary nanodevices, that are needed to build a complete working bulk feedstock supply system (BFSS) that is itself capable of performing all feedstock gas import and byproduct gas export steps previously demonstrated for the macroscale system developed in Phase II. All manipulation tasks are performed via blind pick-and-place.

Assuming the availability of a 1 Hz deposition frequency for DMS fabrication in which one atom of nanopart structure can be placed onto a workpiece each second (Section 3.3), then one Phase II macroscale workstation can fabricate (from primitive feedstock molecules) all 141 nanoparts needed to build one BFSS, comprised of 33,550,239 atoms, in ~3.36×10^7 sec (~389 days or ~1.1 years). This includes 297 days (~76% of total build time) to build the tank, ~30 days (~8%) to build the bladder sheet, and just 62 days (~16%) to build the non-tankwall components. This build time may be significantly reduced by employing multiple Phase II macroscale workstations operated simultaneously, each building different sets of nanoparts for the one BFSS. For example, the simultaneous use of 12 Phase II systems would reduce BFSS nanopart build time from ~1.1 years to ~1 month. The use of multiple workstations is also advisable to permit more rapid prototyping and experimentation with new nanopart designs, and to perform quality control testing on fabricated nanoparts.

Assuming the availability of a conservative 0.01 part/sec operating frequency for nanopart assembly operations in which one nanopart can be added to a multipart nanodevice workpiece every 100 seconds (Section 3.3.1), and conservatively assuming that on average each nanopart must be handled once to be fitted into a nanodevice workpiece, then one Phase II macroscale workstation could assemble nanoparts into all necessary nanodevices needed to build one BFSS, comprised of 141 nanoparts, in no more than (~141 nanoparts / 0.01 Hz) ~ 1.41×10^4 sec (~4 hours). Since this time requirement is more than a thousandfold less than the time required for nanopart fabrication, and since nanodevice assembly can take place both during and after nanopart fabrication, then with one exception the total production time required to build all nanoparts and nanodevices comprising a BFSS should be driven almost exclusively by nanopart fabrication time. The one exception is the rather large nanotank component which may require special handling to avoid rupturing the tank walls.

All manufactured components including both individual nanoparts and multipart nanodevices should be laid out on one Phase II workstation release surface in a specific pattern of positions and orientations to allow blind pick-and-place to be employed during final assembly of the BFSS in Task IV-4. The longest dimension of any non-tankwall nanopart described in Section 3.5.1.6 is 50 nm, so conservatively allocating a 50 nm x 50 nm area for warehousing each of the 139 non-tankwall nanoparts would occupy an area of 1,302,500 nm^2. The tank and graphene bladder sheets are of length ~568 nm and add another ~45,440 nm^2 and ~81,430 nm^2 in resting cross-sectional surface area, raising the total to 1,429,370 nm^2 which is equivalent to a 1.2 x 1.2 micron square area on the Phase II system release surface.

If multiple Phase II macroscale workstations are used for nanopart fabrication as recommended above, then an additional subtask here is the consolidation of all nanoparts and nanodevices manufactured in the several workstations into one workstation, by transferring all BFSS components onto a single Phase II workstation release surface in a specific pattern of positions

and orientations that will allow blind pick-and-place to be employed during final assembly of the BFSS in Task IV-4.

3.5.5 Task IV-4: Assemble BFSS using Phase II System

Task IV-4 is to manually assemble the first-generation bulk feedstock supply system (BFSS) as a one-off (no parallelization) at a designated worksite on the atomically smooth assembly surface of the multielectrode chip created during Task IV-2 (Section 3.5.3), using the macroscale manufacturing system created during Phase II (Section 3.3). All manipulation tasks are performed via blind pick-and-place.

The first step toward the completion of Task IV-4 is to insert the multielectrode multiworksite chip created during Task IV-2 into the Phase II apparatus, there to be properly positioned and aligned relative to the Phase II release surface upon which the component nanoparts and nanodevices were originally pre-positioned during Task IV-3. The juxtaposition and calibration of both surfaces may require the addition of a piezopositioner capable of translating the visiting chip surface so that it is can be aligned and made flush with the Phase II release surface. This will allow the Phase II system to most readily assemble objects at a worksite on the more distant visiting chip surface.

Because fabricated nanoparts and assembled nanodevices must be transferred from the Phase II system release surface to a specific worksite on the surface of the multielectrode chip created during Task IV-2, to be assembled there into the BFSS, assembly at the worksite might take longer than on the Phase II release surface because of the extra transport time. However, some high-accuracy nanopositioning systems[1049] can achieve high-velocity slew rates up to 1 mm/sec. Coarse transport of BFSS components requiring the Phase II manipulator to translate across a distance of ~100 microns at a slew speed of 100-1000 micron/sec is fully consistent with an assembly operating frequency of ~0.01-1 parts/sec. However, the assumed operating frequency is not a crucial quantity in the present context because the successful completion of Task IV-4 in a reasonable elapsed time is relatively insensitive (by many orders of magnitude) to the assembly frequency.

We conservatively assume the availability of a 0.01 parts/sec operating frequency for nanopart assembly operations using the Phase II system in which one nanopart may be transported from one surface to the other and then added to the BFSS workpiece every 100 seconds (Section 3.3.1). Only 25 assemblable components must be put together to make the first-generation BFSS. Conservatively assuming that on average each component must be handled once to be installed onto the growing BFSS workpiece at the designated 56,040 nm^2 and ~59-electrode worksite, then the Phase II macroscale workstation can assemble the entire first-generation BFSS, comprised of 25 assemblable components, in no more than (~25 components / 0.01 Hz) ~ 2500 sec (~0.7 hour). Construction of the first-generation BFSS is done as a one-off with no parallelization at the assembly stage. Total BFSS final assembly time will probably be dominated by placement of the

---

[1049] Luc Chassagne, Suat Topcu, Yasser Alayli, Patrick Juncar, "Highly accurate positioning control method for piezoelectric actuators based on phase-shifting optoelectronics," Meas. Sci. Technol. 16(2005):1771-1777.

rather large nanotank component which may require special handling to achieve precise positioning on the assembly surface and to avoid rupturing the tank walls during deployment.

3.5.6 Task IV-5: Operate First-Generation BFSS using Phase II System

The purpose of Task IV-5 is to validate the design of the first-generation bulk feedstock supply system (BFSS) by experimentally demonstrating its basic functionality using the Phase II system and the workspace chamber gas import and pumpdown systems.

To operate the completed BFSS, the Phase II macroscale workstation is used to acquire feedstock one molecule at a time from the ethylene and germane sorting rotors using toolheads of the same type as are included in the NFW design. Tests using the Phase II system should be conducted to confirm that a single feedstock molecule has been transferred in each case, that the feedstock remained under adequate positional control during and after transfer, and that no gas leakage from the BFSS has occurred. Subsequently, the Phase II system is operated so as to transfer two hydrogen atoms into the BFSS, wherein these two atoms are combined into a single H_2 molecule and reliably transferred into the main BFSS tank without leakage or other mishap.

Aside from using the Phase II system, the ability to recharge and vent the BFSS must also be demonstrated by operating the BFSS through a complete cycle of bulk feedstock gas inloading into the main tank and into the germane rotor plenum, along with workspace chamber pumpdown and end-of-cycle bulk gas venting. For most of these demonstrations the BFSS is operated as a standalone nanoscale nanosystem by sending appropriate current pulses through the ~59 electrodes which provide both power and control. These control pulses are synchronized with the actions of the Phase II manipulator to achieve a smoothly running nanofabrication system.

It may be necessary to iterate Tasks IV-1, IV-3, IV-4, and IV-5 to fully debug the BFSS design and to successfully achieve the desired results.

3.5.7 Task IV-6: Design and Simulate NFW-2

Task IV-6 is to design and simulate the second generation nanoscale fabrication workstation (NFW-2), specifying all component nanoparts and nanodevices (assemblies of nanoparts) and also specifying all fabrication and assembly processes that will be required to complete the manufacturing operations of: (1) nanopart fabrication, (2) nanodevice assembly from nanoparts, (3) NFW-2 assembly from nanoparts and nanodevices, and (4) to verify correct BFSS and NFW operation, if properly assembled, when operated in tandem.

Simulations should also begin to explore the limits to increasing operating frequency for the fabrication workstation, starting with an analysis of the impact on NFW-2 design, if any, of increasing pulse frequency 10-100 fold from 1.2 MHz to 12-120 MHz. This is an advance study only – operation of a physical manufacturing system at these faster speeds is deferred until Phase VII. As a reality check, note that the Servo Halbeck DMC-16x0 CompactPCI DMC-1600 motion

controller[1050] already allows for high speed servo control up to 12 million encoder counts/sec (12 MHz) with step motor control up to 3 million steps per second (3 MHz).

If the first generation NFW has already been designed to allow it to transact feedstock and byproduct gas molecules directly from the BFSS, then the present task is completed and development may proceed to Task IV-7. If not, or if previous iterations have resulted in design changes to the BFSS that render it incompatible with the original NFW design, then the NFW must be redesigned by reiterating Task III-1 (Section 3.4.2) to allow the NFW to accept feedstock from the BFSS and to allow the transfer of byproduct molecules from the NFW to the BFSS.

3.5.8 Task IV-7: Fabricate and Assemble NFW-2 Nanoparts and Nanodevices using Phase II System

Task IV-7 is to use the macroscale manufacturing system created during Phase II (Section 3.3) to fabricate all necessary nanoparts, and then to assemble some of these nanoparts into all necessary nanodevices, providing the complete set of nanoparts and nanodevices that are needed to build a complete working second-generation nanoscale fabrication workstation (NFW-2) that is itself capable of performing all fabrication steps previously demonstrated by the first-generation NFW developed in Phase III and by the macroscale system developed in Phase II.

If the first-generation NFW and BFSS have already been designed to be compatible, then Task IV-7 requires the manufacture of a complete set of NFW (Task III-3; Section 3.4.4) and BFSS (Task IV-3; Section 3.5.4) nanoparts and nanodevices using the Phase II system. If the first-generation NFW and BFSS are not compatible, requiring NFW redesign in Task IV-6 (Section 3.5.7), then the components comprising the revised NFW and the BFSS must be manufactured using the Phase II system as previously described.

In either case, assuming the availability of a 1 Hz deposition frequency for DMS fabrication in which one atom of nanopart structure can be placed onto a workpiece each second (Section 3.3.1), then one Phase II macroscale workstation can fabricate (from primitive feedstock molecules) all 662 nanoparts needed to build one NFW-2 (Table IV-4), comprised of 64,898,035 atoms, in ~6.49×10^7 sec (~751 days or ~25 months). This build time can be cut in half if a new NFW can be assembled directly onto the existing site of a working BFSS, thus eliminating the component build time for a duplicate BFSS. The total build time may also be significantly reduced by employing multiple Phase II macroscale workstations operated simultaneously, each building different sets of nanoparts for the one NFW-2 system. For example, the simultaneous use of 10 Phase II systems would reduce NFW-2 nanopart build time from 2.1 years to just 76 days. The use of multiple workstations is also advisable to permit more rapid prototyping and experimentation with new nanopart designs, and to perform quality control testing on fabricated nanoparts.

Assuming the availability of a conservative 0.01 part/sec operating frequency for nanopart assembly operations in which one nanopart can be added to a multipart nanodevice workpiece

---

[1050] http://www.servo-halbeck.com/html/controller_pages_10.html.

every 100 seconds (Section 3.3), and conservatively assuming that on average each nanopart must be handled once to be fitted into a nanodevice workpiece, then one Phase II macroscale workstation could assemble nanoparts into all necessary nanodevices needed to build one NFW-2, comprised of 662 nanoparts, in no more than (~662 nanoparts / 0.01 Hz) ~ 6.62 x 10^4 sec (~18 hours). Since this time requirement is more than a thousandfold less than the time required for nanopart fabrication, and since nanodevice assembly can take place both during and after nanopart fabrication, then with one exception the total production time required to build all nanoparts and nanodevices comprising an NFW-2 should be driven almost exclusively by nanopart fabrication time. The one exception is the rather large nanotank component of the BFSS which may require special handling to avoid rupturing the tank walls.

All manufactured components including both individual nanoparts and multipart nanodevices should be laid out on one Phase II workstation release surface in a specific pattern of positions and orientations to allow blind pick-and-place to be employed during final assembly of the NFW-2 in Task IV-8. Combining the NFW layout area of 1,302,500 nm^2 (Section 3.4.4) with the BFSS layout area of 1,429,370 nm^2 (Section 3.5.4) gives a total layout area of 2,731,870 nm^2 which is equivalent to a 1.65 x 1.65 micron square area on the Phase II system release surface.

If multiple Phase II macroscale workstations are used for nanopart fabrication as recommended above, then an additional subtask here is the consolidation of all nanoparts and nanodevices manufactured in the several workstations into one workstation, by transferring all NFW-2 components onto a single Phase II workstation release surface in a specific pattern of positions and orientations that will allow blind pick-and-place to be employed during final assembly of the NFW-2 in Task IV-8.

3.5.9 Task IV-8: Assemble NFW-2 using Phase II System

Task IV-8 is to manually assemble the second-generation nanoscale fabrication workstation (NFW-2) as a one-off (no parallelization) at a designated worksite on the atomically smooth assembly surface of the multielectrode chip created during Task IV-2 (Section 3.5.3), using the macroscale manufacturing system created during Phase II (Section 3.3). All manipulation tasks are performed via blind pick-and-place.

The first step toward the completion of Task IV-8 is to insert the multielectrode multiworksite chip created during Task IV-2 into the Phase II apparatus, there to be properly positioned and aligned relative to the Phase II release surface upon which the component nanoparts and nanodevices were originally pre-positioned during Task IV-7. The juxtaposition and calibration of both surfaces may require the addition of a piezopositioner capable of translating the visiting chip surface so that it is can be aligned and made flush with the Phase II release surface. This will allow the Phase II system to most readily assemble objects at a worksite on the more distant visiting chip surface.

Because fabricated nanoparts and assembled nanodevices must be transferred from the Phase II system release surface to a specific worksite on the surface of the multielectrode chip created during Task IV-2, to be assembled there into the NFW-2, assembly at the worksite might take

longer than on the Phase II release surface because of the extra transport time. However, some high-accuracy nanopositioning systems[1051] can achieve high-velocity slew rates up to 1 mm/sec. Coarse transport of NFW-2 components requiring the Phase II manipulator to translate across a distance of ~100 microns at a slew speed of 100-1000 micron/sec is fully consistent with an assembly operating frequency of ~0.01-1 parts/sec. However, the assumed operating frequency is not a crucial quantity in the present context because the successful completion of Task IV-8 in a reasonable elapsed time is relatively insensitive (by many orders of magnitude) to the assembly frequency.

We conservatively assume the availability of a 0.01 parts/sec operating frequency for nanopart assembly operations using the Phase II system in which one nanopart must be transported from one surface to the other and then added to the NFW-2 workpiece every 100 seconds (Section 3.3.1). Only 274 assemblable components (including 25 from the BFSS (Section 3.5.5) and 249 from the NFW (Section 3.4.5)) must be put together to make the second-generation NFW-2. Conservatively assuming that on average each component must be handled once to be installed onto the growing NFW-2 workpiece at the designated 56,040 nm^2 and ~59-electrode worksite, then the Phase II macroscale workstation can assemble the entire second-generation NFW-2, comprised of 274 assemblable components, in no more than (~274 components / 0.01 Hz) ~ 2.74 x 10^4 sec (~8 hours). Construction of the NFW-2 is done as a one-off with no parallelization at the assembly stage. Total NFW-2 final assembly time will probably be dominated by placement of the rather large nanotank component of the first-generation BFSS which may require special handling to achieve precise positioning on the assembly surface and to avoid rupturing the tank walls during deployment.

3.5.10 Task IV-9: Operate NFW-2 Endogenously

Task IV-9 is to validate the design of the second-generation nanoscale fabrication workstation (NFW-2) by experimentally demonstrating its basic functionality.

To experimentally validate the completed NFW-2, the NFW must be operated as a standalone nanoscale workstation as described in Section 3.5.1.7 by sending appropriate current pulses through the ~59 worksite electrodes which provide both power and control. Unlike the NFW which relied entirely on the Phase II system for feedstock and byproduct molecule transactions, the NFW-2 can acquire feedstock from its own BFSS module and can thus endogenously transfer each feedstock molecule to DMS manipulators requiring feedstock as material input for the NFW. Byproduct molecules can be endogenously disposed of via the BFSS as well. NFW-2 control pulses are synchronized with the actions of the Phase II manipulator which now serves only to accept handoffs of finished nanoparts from the NFW-2 system.

As before in Task III-5 (Section 3.4.6), the NFW-2 must demonstrate its complete functionality by endogenously fabricating at least one instance of each of the 46 different non-tankwall nanopart types (Tables III-1, III-2, and IV-3) previously fabricated in greater numbers using the

---

[1051] Luc Chassagne, Suat Topcu, Yasser Alayli, Patrick Juncar, "Highly accurate positioning control method for piezoelectric actuators based on phase-shifting optoelectronics," Meas. Sci. Technol. 16(2005):1771-1777.

Phase II system during Tasks III-3, IV-3, and IV-7, and perhaps also manufacturing a representative section of the tank structure and graphene bladder wall previously fabricated by the Phase II system in Task IV-3. This will prove that the NFW-2 can fabricate all nanoparts needed to make a copy of itself from externally supplied feedstock, power, and control signals, demonstrating 100% materials and nanoparts closure for the NFW-2 system design. The Phase II system is used only to remove each completed nanopart from the NFW-2 and transport the nanopart back to the Phase II system's working area for storage and further characterization. Assuming ~55,543 atoms/nanopart (36,658,083 non-tankwall atoms and 660 non-tankwall nanoparts, for the NFW-2 (Section 3.5.1.6), then fabricating 46 such parts will require the placement of ~2.55 x 10^6 atoms. Assuming that the NFW-2 can fabricate nanoparts at a 100 atom/sec rate, then fabrication of 46 typical nanopart types by the NFW-2 should require ~2.55 x 10^4 sec (~7 hours), quickly concluding the required demonstration.

An absolutely rigorous demonstration of functionality requires the NFW-2 to prove its ability to build all 662 of its own nanoparts, which would then be acquired by the Phase II system and used to assemble a replica NFW-2 on an adjacent 56,040 nm^2 worksite on the assembly surface, with the replica NFW-2 (the "daughter" unit) then required to demonstrate its ability to fabricate at least one instance of each of the 16 different nanopart types comprising the NFW-2. This would definitively prove replication fidelity[1052] of the NFW-2. Whereas in Phase III such a test would have been prohibitively expensive, in Phase IV this test is practical because of the 100-fold increase in fabrication system productivity. Specifically, fabricating all 662 nanoparts comprising an entire 64,898,035-atom NFW-2 replica, using an operational NFW-2 system, should require only 6.49 x 10^5 sec (~7.5 days), to which must be added the feedstock/byproduct gas handling and chamber pumpdown cycle times (1-21 days; Section 3.5.1.7). The daughter NFW-2 can then fabricate another set of 662 nanoparts comprising a third "granddaughter" NFW-2 unit in another ~7.5 days (plus 1-21 days for pumpdown cycles), thus definitively proving offspring replicative fertility.[1053] In other words, the validated NFW-2 unit is already partially scalable and thus can be used for practical replication with limited parallelization of production lines. However, the Phase II system must still be employed for assembly work and this constitutes a remaining production bottleneck when more than 10-100 descendant NFW-2 systems are operated in parallel.

It may be necessary to iterate Tasks IV-6, IV-7, IV-8, and IV-9 to fully debug the NFW-2 design and to successfully achieve the desired results.

[1052] Robert A. Freitas Jr., Ralph C. Merkle, Kinematic Self-Replicating Machines, Landes Bioscience, Georgetown, TX, 2004; Sections 5.1.9(L2) and 5.1.9(L4); http://www.MolecularAssembler.com/KSRM/5.1.9.L.htm.

[1053] Robert A. Freitas Jr., Ralph C. Merkle, Kinematic Self-Replicating Machines, Landes Bioscience, Georgetown, TX, 2004; Sections 5.1.9(L2) and 5.1.9(L4); http://www.MolecularAssembler.com/KSRM/5.1.9.L.htm.

3.5.11 Task IV-10: Win Feynman Grand Prize

In an effort to stimulate scientific and engineering interest in constructing the first nanoassembler, in November 1995 the Foresight Nanotech Institute created the $250,000 Feynman Grand Prize,[1054] with major funding contributed by Zyvex founder James R. von Ehr II and St. Louis venture capitalist Marc E. Arnold. The prize will be awarded to the individual or group that first achieves both of two significant nanotechnology breakthroughs – first, the design and construction of a functional nanometer-scale robotic arm, and second, the design and construction of a functional 8-bit adder computing nanodevice.

According to Grand Prize rules, the robotic nanomanipulator must fit entirely inside a 100-nm cube, carry out actions directed by input signals of specified types, be able to move to a directed sequence of positions anywhere within a 50-nm cube, complete all directed actions with a positioning accuracy of 0.1 nanometer or better, and perform at least 1,000 accurate, nanometer-scale positioning motions per second for at least 60 consecutive seconds. The adder must fit entirely within a 50-nm cube, and must be capable of adding accurately any pair of 8-bit binary numbers, discarding overflow, accepting input signals of specified types, and producing its output as a pattern of raised nanometer-scale bumps on an atomically precise and level surface. (J.S. Hall notes that a conventional 8-bit adder may be constructed using a total of 94 AND, OR, and NOT gates; using XOR gates, the total may be reduced to 37 gates.) Both devices may accept inputs from acoustic, electrical, optical, diffusive chemical, or mechanical means, although any mechanical driving mechanism used for input must be limited to a single linkage that either slides or rotates on a single axis. To demonstrate the capacity for mass-production, at least 32 copies of each device must be provided for analysis and destructive testing by judges. The device does not need to demonstrate self-replication to qualify for the Grand Prize.

Task IV-10 is to win the Feynman Grand Prize (if it has not yet been won by anyone else) by meeting all three Prize requirements, as follows:

(1) The first Prize requirement is to construct a robotic nanomanipulator, which can be satisfied by building a copy of the larger fourth manipulator designed for the NFW (Section 3.4.1.1) which has an operating envelope spanning exactly the required 50 nm (range of 63-113 nm; Section 3.4.1.1) with 0.5 Å precision (Section 3.4.1.1), better than the required 0.1 nm (1 Å), and fitting entirely within a 100 nm cube when retracted. With a pulse frequency of 1.2 MHz, manipulator tips can be driven at ~60 microns/sec (Section 3.4.1.4), allowing a rapid sequence of 60 nm round-trip motions at the required repetition rate of 1000 sec^{-1}. This manipulator has a total of 11,872,315 atoms (Table III-2).

(2) The second Prize requirement is to build a functional half-adder, which will require manufacturing a total of 37 mechanical XOR gates (see above). At ~16 nm^3 of diamond per interlock (gate) in a tightly packed array including support components,[1055] the total gate volume

---

[1054] Foresight Nanotech Institute, "Feynman Grand Prize," accessed January 2008; http://www.foresight.org/GrandPrize.0.html.

[1055] K. Eric Drexler, Nanosystems: Molecular Machinery, Manufacturing, and Computation, John Wiley & Sons, New York, 1992; "Volume per interlock", Section 12.3.8(a), p. 354.

is 592 nm^3; allowing 108 nm^3 for the base structure and another 300 nm^3 for I/O mechanisms that can be manipulated by the robotic nanomanipulator (itself controlled electrically via the assembly surface electrode system) gives a 1000 nm^3 product object which could be a cube 10 nm on an edge, easily fitting within a 50 nm cube as required by Prize rules. Such a product object contains up to ~176,000 carbon atoms in the solid bulk of the device, ~5000 passivating hydrogen atoms on the outer surface, and ~1200 passivating H atoms on each of the 37 gates, a total of ~225,400 atoms or just 2% of the atoms contained in the much large robotic nanomanipulator.

(3) The third Prize requirement is to manufacture 32 copies of both the robotic nanomanipulator and the mechanical half-adder (neither of which must be self-replicating, nor participate in their own manufacture), which implies building a total of ~(32 copies)(11,872,315 atoms + 225,400 atoms) = 387,126,880 atoms. All nanoparts for all 32 copies can be fabricated by the NFW-2 operating endogenously at the 100 atom/sec rate (Section 3.5.10) in 3.87 x 10^6 sec of NFW-2 runtime, to which must be added ~6 feedstock/byproduct gas handling and chamber pumpdown cycle times (1-21 days/cycle; Section 3.5.1.7), or ~42 days assuming a midrange gas handling + pumpdown cycle length of ~7 days. To this must be added another 5.28 x 10^5 sec to assemble 32 copies of the combined 165 nanoparts comprising both product objects (125 parts for the robotic nanomanipulator (Table III-1) and ~40 nanoparts for the half-adder) at the 0.01 parts/sec rate using the macroscale Phase II system (Section 3.3), giving a total manufacturing time of 8,026,800 sec (~93 days) to win the Feynman Grand Prize at the end of Phase IV.

3.6 Phase V: Nanoscale Assembly Workstation (NAW)

The key objective of Phase V is to build the first-generation nanoscale assembly workstation (NAW) – a set of individually controlled nanoscale manipulators and toolheads inside a UHV workspace chamber that is capable of acquiring fabricated nanoparts and assembled nanodevices by handoff from the Phase II MMW system, assembling these components into more complex nanodevices, and then using them to construct a working nanosystem on the multi-electrode assembly surface immediately adjacent to the NAW. Like the previously developed NFW and NFW-2 systems, the NAW will be powered by electrical control signals passed through the assembly surface via electrical surface contact points. The set of nanosystem product objects that can be assembled by the NAW on the adjacent assembly surface must include, at minimum, the NFW-2 (i.e., the first-generation BFSS and second-generation NFW developed in Phase IV) and the NAW itself.

The NAW is described in Section 3.6.1 and illustrated in Figure V-1. This is followed by an enumeration of the specific tasks required to manufacture an NAW which include: design and simulation of the NAW (Section 3.6.2), preparation of a multielectrode assembly surface (Section 3.6.3), assembly of NAW multipart nanodevices using the Phase II system (Section 3.6.4), assembly of the NAW using the Phase II system (Section 3.6.5), and finally the demonstrated successful operation of the NAW using the Phase II System (Section 3.6.6).

3.6.1 Description of the NAW

The structure and basic function of the first-generation nanoscale assembly workstation (NAW) is described in this Section.

The NAW will consist of three externally controlled mechanical manipulator systems and is an approximate functional analog (at the nanoscale) of the macroscale Matt Moses Construction Machine[1056] (Section 2.2.1). The Moses machine has ~45 parts and requires 410 assembly steps to replicate itself in the adjacent space on the same surface using an externally provided source of its own parts.

3.6.1.1 Basic Description of the NAW

The basic NAW is contained within a volume measuring ~10^6 nm^3 and is assumed in the baseline design to occupy a square footprint measuring 100 nm x 100 nm = 10,000 nm^2 in area on the assembly surface.

[1056] Robert A. Freitas Jr., Ralph C. Merkle, Kinematic Self-Replicating Machines, Landes Bioscience, Georgetown, TX, 2004; Section 3.18, pp. 60-63; http://www.MolecularAssembler.com/KSRM/3.18.htm. Matt Moses, "A Physical Prototype of a Self-Replicating Universal Constructor," Master's Thesis, Department of Mechanical Engineering, University of New Mexico, 2001; http://www.home.earthlink.net/~mmoses152/SelfRep.doc. Matt Moses, "Self-Replication," 16 December 2002; http://www.home.earthlink.net/~mmoses152/.

A key design issue is the accuracy to which positional control must be repeatably maintained throughout the nanopart assembly process. As of 2007 there had only been one published theoretical study of the misplacement tolerance for nanoparts during an assembly process. In 1998, Tuzun et al.[1057] calculated the requirements for the successful coaxial docking of two single-walled carbon nanotubes of different diameters to form a near-frictionless molecular bearing of the type first proposed by Drexler[1058] and later demonstrated experimentally by Cumings and Zettl.[1059] Tuzun et al. looked at bearings formed from nanotubes 11 rings long, with the shaft of the bearing composed of a nanotube with 10 carbons per ring (i.e., nanotube diameter ~5 Å to atomic centers) and the sleeve of the bearing composed of a nanotube with either 30 or 34 carbons per ring (i.e., nanotube diameters ~13 Å or ~15 Å to atomic centers).

Figure V-1. Schematic illustration of the Nanoscale Assembly Workstation (NAW), showing three Stewart platform manipulators mounted on a foundation block.

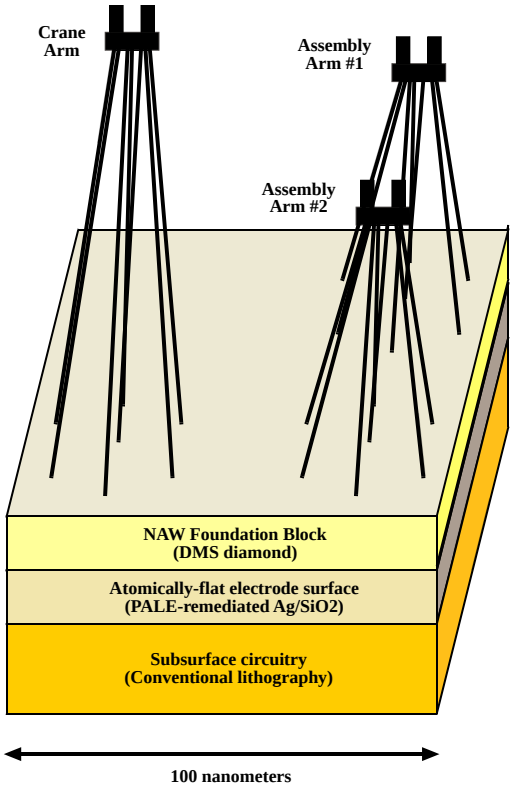

[1057] Robert E. Tuzun, Karl Sohlberg, Donald W. Noid, Bobby G. Sumpter, "Docking envelopes for the assembly of molecular bearings," Nanotechnology 9(March 1998):37-48.

[1058] K. Eric Drexler, Nanosystems: Molecular Machinery, Manufacturing, and Computation, John Wiley & Sons, New York, 1992; http://www.zyvex.com/nanotech/nanosystems.html.

[1059] John Cumings, A. Zettl, "Low-friction nanoscale linear bearing realized from multiwall carbon nanotubes," Science 289(28 July 2000):602-604.

For these molecular dynamics simulations, the sleeve of the bearing was positioned in space along the z axis and the shaft was then imparted a small initial velocity in a roughly coaxial direction towards the sleeve. The simulations found that a perfectly aligned shaft would fall straight into the potential well formed from the van der Waals attraction between shaft and sleeve but a displaced or misoriented shaft would bounce off the edge of the sleeve if the positioning error was large enough. The docking envelopes for the molecular dynamics calculations and for the rigid body calculations had essentially the same shape but with slightly different sizes. For the atomistic calculation, a ~5 Å diameter shaft aligned parallel to a ~13 Å diameter sleeve could be laterally displaced by 2.6 Å before it failed to dock, compared to a 1.6 Å maximum tolerable displacement using the rigid body calculation. Some tilting error was also tolerable, with the authors noting that "if an end of the shaft points closely enough to the center of the sleeve, it will fall into the nonbonded potential energy well and the two nanotubes will dock." These calculations suggest that the maximum displacement tolerance for the fundamental assembly operation of inserting a round peg into a round hole is on the order of about half of the diameter of the peg. While many additional studies are needed of the specific assembly operations described in the present proposal, for our initial scaling analysis here we will conservatively assume that the most primitive NAW assembly operations must be performed to a repeatable accuracy of ~1 Å.

A minimum of three independent positionally controlled manipulators capable of end-effector placement to ~1.0 Å repeatable accuracy and with 6 DOF (degrees of freedom) are required for the NAW. Three manipulators will allow two separate objects to be inserted into a third object at the same time, and other similarly complex motions, and will allow greater forces to be applied than one or two manipulators alone. All three manipulators must be able to reversibly grasp and release nanoparts and nanodevices which they have been tasked to assemble, and grasping must be done in a way that maintains the repeatable positioning accuracy of mateable surfaces to within the specified ~1.0 Å repeatable accuracy. Additionally, one of the three manipulators must be able to reach out at least 150 nm from the NAW center, or 200 nm from an edge if reaching across a 100 nm square area (depending on the specific NAW design that is chosen). Hence for the baseline NAW design we shall include two smaller high-strength manipulator arms to forcefully jam two parts together during assembly, and one larger crane arm that can be used (1) for long-distance transport when fully extended and (2) for relatively stiffly holding a workpiece in close quarters when fully retracted. Electrical power and control signals are applied to NFW mechanisms via carbon nanotube wires that connect conductive silver terminals on the atomically smooth assembly surface (see Section 3.4.2) to electrostatic motors that actuate the manipulators.

Each of the two smaller assembly arm manipulators is a Stewart platform capable of ~1 Å incremented motions at the tip and are of similar design as the manipulators previously described in Section 3.4.1.1 and summarized in Table III-1, employing 7 telescoping legs and a simple end-effector device for grasping nanoscale components. The smallest nanopart size to be manipulated may have a few thousand atoms in it and may be a few nanometers in size, and will need to be graspable by at least one, and possible two, manipulators depending on the assembly operation that is required to be performed. This may require a slight redesign of the "tool chuck" end-effector described in Section 3.4.1.1. Each of these smaller manipulators has a nominal 50-90 nm reach for 0%-80% extension (Section 3.4.1.1), giving them a 60-100 nm maximum reach when the 10 nm thick tool chuck is included.

The larger crane arm manipulator must be capable of larger movements across 200 nm of reach to allow it to assemble its replica on an adjacent worksite on the assembly surface. This requires a

larger number of strut segments than the two segments employed for the smaller assembly arm manipulators. The design tradeoff is that the greater the number of strut segments, the shorter the length of each of the strut segments but the wider the segments in diameter and hence the larger the manipulator footprint on the NAW floor. For example, the minimum strut footprint is obtained by using just 2 strut segments with f = 80% overlap, yielding a sheath that is 111 nm long and a rod that is 89 nm long, in which case the manipulator can only collapse down to 111 nm which is larger than the desired 100 nm x 100 nm footprint, hence more segments are necessary. With 7 segments, the longest segment would be of length $200 / (1 + f^1 + f^2 + f^3 + f^4 + f^5 + f^6) = 50.61$ nm (again assuming f = 0.80) and the crane manipulator could now collapse down to the same length as the fully retracted assembly manipulators, but at the cost of increasing the bottommost strut diameter to 35 nm and the minimum possible diameter of the bundle of 7 struts to a width of 105 nm which again exceeds the desired 100 nm x 100 nm footprint on the NAW floor.

A workable design compromise appears to be the use of four segments for each of the 7 Stewart platform struts, yielding a longest segment of length $200 / (1 + f^1 + f^2 + f^3) = 67.75$ nm (f = 0.80). The four segments are then of length ~68 nm, ~68 nm (54.1 nm extended, with f = 79.6%), ~54.4 nm (43.3 nm extended, with f = 79.6%), and ~43.5 nm (34.6 nm extended, with f = 79.5%), which sums to 200.0 nm when fully extended, 68.0 nm when fully retracted. To maximize manipulator stiffness the four segments are deployed from the wide base first, with the 4th and thinnest segment deployed only when the longest possible reach is required. Reaching the far end of travel causes the next segment outward to become unlatched, allowing it to rotate, and locks the previous segment, so that it cannot rotate; during retraction, the lock/unlock sequence mechanically reverses. This allows the entire stack to be driven by a single drive motor at the base of the stack.

For the four crane arm segments, the 4th segment is a cylinder 5 nm wide and ~43.5 nm long (solid volume = 854 nm^3, passivation surface area = 723 nm^2); the 3rd segment is an annulus 10 nm wide of length ~54.4 nm with radii 2.5 nm and 5.0 nm (volume = 3204 nm^3, passivation surface area = 2681 nm^2); the 2nd segment is an annulus 15 nm wide of length ~68 nm with radii 5 nm and 7.5 nm (volume = 6676 nm^3, passivation surface area = 5537 nm^2); and the 1st segment is an annulus 20 nm wide of length ~68 nm with radii 7.5 nm and 10 nm (volume = 9346 nm^3, passivation surface area = 7752 nm^2). This means the minimum footprint of a hexagonal strut pattern with the 7th strut placed in the middle would be ~3 x 20 nm ~ 60 nm wide or ~2800 nm^2; we conservatively allow 4000 nm^2 for the foundation block for the crane arm manipulator.

Each segment-driving rotary motor (Section 3.4.1.1) is assumed to be electrically driven, to consist of four parts (rotor, stator, output gear, and housing) and to fit within a box requiring a solid diamondoid material volume of ~200 nm^3 and ~500 nm^2 of passivated diamondoid surface area per motor. Each motor is fixed to a foundation block and attached to the universal joint which in turn connects to the base of the sheath (the 1st segment) of each strut; rotating the sheath extends or retracts the other three segments comprising the strut. There is one locking latch (assumed volume ~50 nm^3 and ~100 nm^2 each, or 200 nm^3 and 400 nm^2 for all 4 on each strut) for each of the 4 segments comprising each strut. Each universal joint (Figure 2-47(C)) is assumed to consist of 2 parts and ~40 nm^3 of solid diamond structure with ~80 nm^2 of passivated diamondoid surface area. Foundation blocks are allocated 4000 nm^2 x 10 nm thick, but using a honeycomb structure to eliminate 75% of mass, this adds 10,000 nm^3 of solid structure and 10,530 nm^2 of passivated surface; in the actual NAW, these blocks need not be either square or arranged coplanar, though that is the simplest arrangement. The triangular tool chuck is assumed to be a half-square of area (1/2) $(20\ nm)^2$ at its base, 10 nm thick, and to include three integral nanoparts (housing with fixed backstop, a moving rack-mounted gripper plate, and a drive gear),

adding 2500 nm^3 of solid structure and ~3000 nm^2 of passivated diamondoid surface. Electrical leads connecting control lines to each motor are 2 nm diameter unpassivated single-walled carbon nanotube x 50 nm long, adding ~314 nm^2 x ~0.154 nm thickness ~ 48 nm^3 of unpassivated carbon nanotube wire solid volume, or 96 nm^3 for each hot/ground pair of wires; atom count is ~314 nm^2 x ~31 C atoms/nm^2 ~9734 C atoms per wire pair. Allowing an additional 2132 nm^3 of material volume and 2400 nm^2 of passivated surface area for unallocated diamond lattice structure gives the results for the crane arm manipulator as shown in Table V-1.

Table V-1. Volume and Parts Estimate for Crane Arm Manipulator in NAW

Nanopart or Nanodevice	Number of Com-ponents	Solid Volume each (nm^3)	# Parts / Com-ponent	Solid Volume All (nm^3)	Total # of All Parts
Strut Segment 4	7	854	1	5978	7
Strut Segment 3	7	3204	1	22428	7
Strut Segment 2	7	6676	1	46732	7
Strut Segment 1	7	9346	1	65422	7
Locking Latches	28	50	1	1400	28
Rotary motors	13	200	4	2600	52
Electrical leads	13	96	2	1248	26
Universal joints	14	40	2	560	28
Foundation block	1	10000	1	10000	1
End-effector	1	2500	3	2500	3
Unallocated structure	1	2132	1	2132	1
TOTALS	**99**			**161,000 nm^3**	**167 parts**

Allocating ~176 C atoms/nm^3 for diamondoid lattice and ~31 H atoms per nm^2 to passivate diamondoid surface gives the scaling results for the entire NAW (Figure V-1) as shown in Table V-2. We further allocate 779,000 nm^3 of empty space to allow for clearance between struts and room for movement of manipulators and workpieces, giving a total operational volume for the NAW of 1,000,000 nm^3 approximating a $(100\ nm)^3$ cube having a ~10,000 nm^2 (~100 nm x ~100 nm) footprint on the chip surface, with a total atom count of ~45,642,437 atoms (85.2% C atoms, 14.8% H atoms), a total mass of 7.89 x 10^{-19} kg, and a total nanopart count of 418. The average nanopart in the NAW has a volume of ~529 nm^3 (an ~8.1 nm cube) and is composed of ~109,192 atoms. There are 39 actuators (individually controlled electrostatic motors) in the NAW, so we need 39 separate control lines (plus one common ground line for a total of 40) to avoid multiplexing and allow direct control of each individual actuator, the conceptually simplest approach. Note that the current load on each common ground line is only ~39 I_{motor} ~ 0.78 x 10^{-11} amp, well below the current-carrying capacity experimentally observed[1060] for individual 10-50 nm long single-walled "metallic" carbon nanotubes which can conduct 25-100 x 10^{-6} amp/wire

[1060] Ali Javey, Pengfei Qi, Qian Wang, Hongjie Dai, "Ten- to 50-nm-long quasi-ballistic carbon nanotube devices obtained without complex lithography," PNAS 101(14 September 2004):13408-13410; http://www.pnas.org/cgi/content/abstract/101/37/13408.

electrical currents before failing, and a burnout threshold of 1000 x 10^{-6} amp/wire reported by others.[1061]

Table V-2. Estimated Atom Counts for the NAW							
NAW Nanopart or Nanodevice	**# of Nano-parts**	**Total Solid Volume (nm^3)**	**Total Passiv. Area (nm^2)**	**# of C Atoms**	**# of H Atoms**	**# of Ge Atoms**	**Total # of Atoms**
2 Assembly Arm Manipulators	250	58,000	71,426	10,208,000	2,214,206	0	12,422,206
1 Crane Arm Manipulator	167	161,000	143,201	28,336,000	4,439,231	0	32,775,231
Other Misc. Structure	1	2000	3000	352,000	93,000	0	445,000
TOTALS	418	221,000	217,627	38,896,000	6,746,437	0	45,642,437

3.6.1.2 Thermal Positional Stability of NAW Manipulators

If the most primitive NAW assembly operations must be performed to a repeatable accuracy of ~1 Å (Section 3.6.1.1), can the existing manipulator designs meet or exceed this requirement? The two assembly arm manipulators have already been determined to meet a more stringent 0.2-0.5 Å requirement (Section 3.4.1.2), so it remains only to estimate the uncertainty at the tip of the crane arm manipulator at various states of its extension or retraction.

Following the same analysis as in Section 3.4.1.2, we treat the manipulator struts as rods. The transverse stiffness k_{trans} for a simple cantilevered rod of length L_{rod} for which a lateral deflection force $F_{deflect}$ produces a transverse deflection $d_{deflect}$ at the tip is given by $k_{trans} = F_{deflect} / d_{deflect} = 3 E_{rod} I_{rod} / L_{rod}^3$, where $E_{rod} = 1.05 \times 10^{12}$ N/m^2 is Young's modulus for diamond rod material and $I_{rod} = \pi (r_{out}^4 - r_{in}^4) / 4$ is the second moment of area (also known as the moment of inertia of the area) for a circular cylinder of inner radius r_{in} and outer radius r_{out}.[1062] The lateral positional uncertainty of the tip of the rod is the square root of the positional variance[1063] as given by $\Delta x = (k_B T / k_{trans})^{1/2}$, where $k_B = 1.381 \times 10^{-23}$ J/K (Boltzmann constant) and T is temperature.

[1061] Hongjie Dai, Eric W. Wong, Charles M. Lieber, "Probing Electrical Transport in Nanomaterials: Conductivity of Individual Carbon Nanotubes," Science 272(26 April 1996):523-526; Stefan Frank, Philippe Poncharal, Z.L. Wang, Walt A. de Heer, "Carbon Nanotube Quantum Resistors," Science 280(12 June 1998):1744-1746.

[1062] S.A. Wainwright, W.D. Biggs, J.D. Currey, J.M. Gosline, Mechanical Design in Organisms, John Wiley & Sons, New York, 1976.

[1063] K. Eric Drexler, Nanosystems: Molecular Machinery, Manufacturing, and Computation, John Wiley & Sons, New York, 1992; http://www.zyvex.com/nanotech/nanosystems.html.

Each of the 4 strut segments will have a separate uncertainty which we can sum to approximate the total uncertainty at the tip of a single Stewart platform strut at a given temperature of operation. Assuming that the uncertainties of each segment are additive, the results for various states of extension of the struts comprising the crane arm manipulator (Table V-3) indicate that the design should meet the minimum stiffness requirement, even at full extension, when operated at either 80K or 300 K. A more realistic calculation would take account of the greatly increased stiffness that 7 struts ganged together would provide compared to just a single strut. (If needed, stiffness can be increased dramatically by increasing the segment radii slightly, since stiffness ~ I ~ r^4.) The other sources of tip uncertainty reviewed in Section 3.4.1.2 should be even less problematic for the crane arm manipulator.

Thus it appears that the positional uncertainties all three interacting manipulators should be sufficiently low to allow blind pick-and-place operation even at room temperature. If future simulations or experimental results employing these devices invalidates this assumption, due to larger than expected positioning errors after repeated operation of the manipulators, positional uncertainty can readily be reduced either by switching to lower temperature operation or by adding at least one force sensor (at negligible cost in terms of atoms or parts count) as previously described in Section 3.4.1.3. For assembly operations, additional ameliorative measures may be undertaken, e.g., adding tapered alignment pegs at key locations on the surfaces of nanoparts requiring assembly to increase the viable operating envelope of the existing manipulator system.

Table V-3. Estimated Positional Uncertainty at the Tip of a Single Strut Comprising the 7-Strut NAW Crane Arm Manipulator, as a Function of the Number of Strut Segments Extended and the Manipulator Operating Temperature

Crane Arm Manipulator Segments	**Length (nm)**	**Inner Radius r_{in} (nm)**	**Outer Radius r_{out} (nm)**	**Second Moment of Area I_{rod} (m^4)**	**k_{trans} (N/m)**	**Δx @ 80K**	**Δx @ 300K**
Individual Segment:							
4	34.6	0.0	2.5	3.07×10^{-35}	2.33	0.22 Å	0.42 Å
3	43.3	2.5	5.0	4.60×10^{-34}	17.85	0.15 Å	0.10 Å
2	54.1	5.0	7.5	1.99×10^{-33}	39.60	0.08 Å	0.06 Å
1	68.0	7.5	10.0	5.37×10^{-33}	106.84	0.05 Å	
						0.03 Å	
w/Segments Extended:							
1	68.0					0.03 Å	0.06 Å
1+2	122.1					0.08 Å	0.16 Å
1+2+3	165.4					0.16 Å	0.31 Å
1+2+3+4	200.0					0.38 Å	0.75 Å

Note that "assembly operations" as envisioned here will usually not involve the making or breaking of covalent bonds as during "fabrication operations," but generally will involve only the fitting together of hydrogen-terminated nanoparts into nanodevices consisting of two or more unbonded nanoparts – with nanodevices therefore containing numerous internal nonbonded interfaces. If it is desired to covalently bond two nanoparts so as to eliminate the passivated interface between them, this can be done in certain limited circumstances (Section 3.12.3.8). However, such an assembly operation is exoergic and will release waste heat as cross-interface C-C bonds are formed (Section 3.12.3.8(4)). The flow and proper disposal of this heat must be incorporated into the NAW system design.

3.6.1.3 Manipulator Speed and NAW Productivity

How fast can assembly manipulators be operated within an NAW? A basic insertion operation conservatively may require a nanopart acquisition step (possibly performed simultaneously by up to three manipulators), an insertion step, and a post-assembly stowage step (a step which might often be omitted if the assembled output component is an input component for the next assembly step). In a typical scenario, each one of N_{parts} nanoparts that make up a product object might be handled once, hence the number of manipulator operations needed to assemble the product object is ~$3N_{parts}$. Note that all three manipulators have separate control channels and thus can be operated in parallel if necessary during each assembly operation.

Assuming 1 Å step increments across a maximum 400 nm round-trip travel distance for the tip of the crane manipulator, each manipulator operation takes at most ~(400 nm / 1 Å) ~ 4000 pulse increments applied to the electric stepper motors, hence the number of pulse increments needed to assemble the product object is ~$12000N_{parts}$. If power/control signals are applied at a ~1.2 MHz frequency, thus driving manipulator tips at a top speed of ~120 microns/sec, this enables the NAW to fabricate structures at a (1.2×10^6 increments/sec) / (1.2×10^4 increments/part) ~ 100 parts/sec rate when presentation of finished nanoparts and nanodevices (as assembly process inputs) is not a time-limiting factor. Under such conditions the NAW could assemble its own mass of nanoparts (418 nanoparts; Table V-2) in ~4.18 sec, or the 1080 nanoparts comprising both the NFW-2 (662 nanoparts; Table IV-4) and the NAW in ~10.8 sec. Assuming one bit to describe each increment, a complete replication cycle for the NAW thus requires up to (418 nanoparts)(12,000 increments/nanopart-actuator)(1 bit/increment)(39 actuators) ~ 1.96×10^8 bits of replication process data.

In the actual Phase V setup proposed here, the NAW will operate about 4 orders of magnitude slower than this (Section 3.6.6) because it must be fed its nanocomponent inputs by the macroscale Phase II system at a process-limiting ~0.01 parts/sec supply rate (Section 3.3.1). Here we assume that the nanoparts have previously been accumulated on the Phase II work surface so that transfer rates are limited only by Phase II manipulator speed and not by NFW nanopart fabrication speed. At a slow 0.01 Hz nanopart supply rate, the replication time for the NAW from prefabricated parts increases to ~41,800 sec (~12 hours).

Note that the NAW can assemble product objects from nanoparts at a much faster per-atom rate than the NFW-2 can fabricate nanoparts from atoms. More specifically, the NFW-2 can fabricate nanoparts at ~100 atoms/sec and the average nanopart in the NFW-2 plus NAW combination is ~(110,540,472 atoms / 1080 nanoparts) ~ 102,352 atoms in size, so a single NFW-2 operating endogenously can produce one average nanopart in ~1024 sec, yielding a ~0.001 Hz parts fabrication rate per NFW-2 unit. This is a tremendous mismatch of capabilities because the

NAW can assemble nanoparts at a tenfold-faster ~0.01 Hz parts assembly rate even when supplied with input nanoparts by the relatively slow macroscale Phase II system, or up to a ~100 Hz parts assembly rate if nanoparts could be presented in a non-time-limiting manner. The mismatch could be eliminated by feeding each NAW with nanoparts fabricated by 100,000 simultaneously operating NFW-2 systems, since a 100,000 NFW-2 array could collectively produce nanoparts matching the unrestricted 100 Hz input rate of the NAW – but at the cost of having to engineer a complex scalable nanoparts distribution subsystem to efficiently and reliably transport the components from their site of fabrication to the input of the NAW. This would be a relatively challenging task but fortunately is not necessary because the productivity per unit area of surface in the NFW-2 + NAW system developed in Phase VI (Section 3.7) only falls by a factor of 2 even if the productivity of the NAW subsystem is minimal compared to the NFW-2 subsystem, a relatively small penalty for not eliminating this inefficiency. Hence the mismatch between fabrication and assembly rates is acceptable because a significant increase in manufacturing capability is nonetheless achieved despite the mismatch-related production inefficiency.

If operated at full capacity the NAW power usage would be similar to the estimate for the NFW previously presented in Section 3.4.3. However, NAW power will usually be far lower than this because the NAW operates at a much lower duty cycle compared to the NFW (Section 3.6.1.3).

3.6.1.4 Reliability of NAW Manufacture

The NAW Phase V system is never operated as a standalone production system, so the issue of reliability in Phase V arises only in connection with the use of the Phase IV system to fabricate all the nanoparts comprising the NAW and the use of the Phase II system to assemble the NAW from its nanoparts. Since there are only 418 nanoparts to assemble into a NAW the reliability of such assembly is not a serious concern, so the principle reliability issues concern the nanoparts fabrication operations using the Phase IV system. The Phase IV fabrication system has a target productivity rate of ~100 atom/sec (Section 3.5.1.7) with ~6 mechanosynthetic operations required for placement of each atom in the growing workpiece structure (Section 3.4.1.4), and a 45,642,437-atom target product object size consisting of all 418 nanoparts of the NAW (which are later assembled by the Phase II system). Building the NAW replica using the Phase IV NFW-2 fabrication system thus requires ~274 million mechanosynthetic operations, so to avoid even a single misplacement error the NFW-2 manipulators must be able to deliver a minimum of ~274 million error-free round trip excursions of the positionally controlled DMS tooltips. The potential ability of computer controllers to reliably deliver such lengthy data sequences with low error, and the ability of simple mechanical actuators to reliably execute such lengthy sequences of mechanical actuations with low error, is discussed in Section 3.8.1.3.

Another source of intrinsic manufacturing error arises from the reliability of the DMS reactions themselves, as previously discussed in Section 3.2.1.8. Table I-5 gives the probability of misreaction at various relevant operating temperatures, assuming a defect energy threshold of 0.40 eV. The misreaction probability per mechanosynthetic operation may be as high as 1.91 x 10^{-7} at 300 K, conservatively assuming that all reactions have the minimum defect energy threshold of 0.40 eV, producing ~52 erroneous atom placements in the ~46 x 10^{6}-atom NAW

product object after ~274 x 10^6 mechanosynthetic operations, hence room temperature fabrication of the NAW by the Phase IV system appears impractical. The expected error rate falls to <1 erroneous atom placement below 239 K, ~10^{-2} near dry-ice temperature at ~193 K, or ~10^{-3} at 176 K for a ~46 x 10^6-atom product object fabricated using the original set of DMS reactions,[1064] hence operation at T ≤ 193 K appears feasible in Phase V. At near liquid nitrogen temperatures (~80 K), the DMS-related error rate using reaction sequences with a defect energy threshold of 0.40 eV falls to ~10^{-17} for a ~46 x 10^6-atom product object, the latter completely negligible for Phase V purposes.

Another major source of error is radical poisoning by contaminants in an imperfect UHV environment. At a target productivity rate of ~100 atom/sec for the Phase IV system, the ~46 x 10^6-atom NAW will require t_{fab} ~ 4.6 x 10^5 sec (~5 days) for the NFW-2 system to fabricate. Assuming that a radical site susceptible to poisoning is exposed to the imperfect UHV environment for a fraction f_{vac} ~ 50% of the time, then the maximum tolerable UHV pressure that will permit all nanoparts for one defect-free ~46 x 10^6-atom NAW to be fabricated is $P_{UHV} \leq (N_{encounters}\ T / n_{contam}\ A_{radical}\ f_{vac}\ t_{fab})\ (\pi\ MW_{kg} / 2\ k_B T\ N_A)^{1/2}$ ~ 7 x 10^{-14} atm, where n_{contam} = 7.34 x 10^{27} molecules-K/m^3-atm (= N_A/R_{gas}) for ideal gas (contaminant) molecules and T = 193 K, with the other quantities as previously defined in Section 3.2.1.7. If any workpiece having one or more erroneous atom placements is considered defective, then in a UHV environment maintained at ~10^{-16} atm (~10 million contaminant molecules present in a 5-liter UHV work volume; currently achievable experimentally, Section 3.2.1.7) the radical-poisoning defect rate at 193 K will be ~10^{-3} for one NAW product object. If H_2 contaminant is determined not to be a serious radical poisoning risk or can be rigorously excluded from the workspace, then taking MW_{kg} = 0.014 kg/mole for N_2 raises the required P_{UHV} by a factor of ~2.6, thus lowering the defect rate from 0.14% to 0.05% per manufacturing cycle.

As for radiation damage rates, assuming a failure condition of κ_{fail} ~ 10^{15} hits/kg-rad and an I_{rad} ~ 0.5 rad/yr background the mean time τ_{rad} between radiation-disabling hits on a mostly-carbon ~31 x 10^6-atom NFW of mass m_{target} = 7.89 x 10^{-19} kg is $\tau_{rad} \sim (\kappa_{fail}\ m_{target}\ I_{rad})^{-1}$ ~ 2535 years (conservatively assuming that one such hit will cause the workpiece or tooltip to fail with 100% certainty), still a negligible error rate (~10^{-5} per replication cycle).

When operated in test mode to validate its capabilities, the NAW neither creates nor destroys chemically active radical sites, hence its operations are not subject to DMS-related error rates and are only weakly subject to vacuum poisoning effects. Hence NAW reliability is governed chiefly by its ability to correctly execute a small number of non-covalent parts assembly operations and by error rates in nanopart gripping/releasing mechanisms, and these error rates are assumed to be small in comparison with the DMS-related error rates.

[1064] Robert A. Freitas Jr., Ralph C. Merkle, "A Minimal Toolset for Positional Diamond Mechanosynthesis," J. Comput. Theor. Nanosci. 5(May 2008):760-861.

3.6.2 Task V-1: Design and Simulate NAW

Task V-1 is to design and simulate the entire NAW, specifying all component nanoparts and nanodevices (assemblies of nanoparts) and also specifying all fabrication and assembly processes that will be required to complete the manufacturing operations of: (1) nanopart fabrication, (2) nanodevice assembly from nanoparts, (3) NAW assembly from nanoparts and nanodevices, and (4) to verify correct NAW operation, if properly assembled. Of critical importance is a study of the available work envelope of the Stewart platforms, to make sure that it is sufficient for all tasks assigned to them. If the Stewart platform work envelope is not sufficient, we can use a double tripod[1065] or a related system instead. Determination of the most efficient manipulator system is a key design effort that should be undertaken as soon as possible. In an efficient development effort, the first generation NAW will be designed: (a) to be interoperable with the NFW-2 system with which the NAW will be mated in Phase VI, and (b) to cleanly interface with the NFW-2 work envelope. Hence greater efficiencies may be attained in the design process if Task V-1 and Task VI-1 are undertaken simultaneously.

Simulations should also begin to explore the limits to increasing operating frequency for the assembly workstation, starting with an analysis of the impact on NAW design, if any, of increasing pulse frequency 10-100 fold from 1.2 MHz to 12-120 MHz. This is an advance study only – operation of a physical manufacturing system at these faster speeds is deferred until Phase VII.

Design and simulation of the typical NAW nanopart will require at minimum a molecular mechanics / molecular dynamics (MM/MD) level analysis of a nanopart having (45,642,437atoms)/(418 nanoparts) ~ 109,192 atoms/nanopart (Table V-2. Such modeling and simulation could be performed using the NanoEngineer-1 software package that was available in 2007, running on a personal computer that should be available in 2009. The typical NAW nanodevice consists of 2-4 nanoparts (Table III-1 and Table V-1), increasing the simulation software capacity requirement to 218,000-437,000 atoms/nanodevice for basic modeling and validation of proper operation of nanodevices. Following Moore's Law assuming an 18-month doubling time and conservatively assuming traditional ~N_{atom}^2 scaling with atom count for MM/MD algorithms, a 437,000-atom nanodevice could be simulated using NanoEngineer-1 on a single commonplace personal computer that would be available in 2016, or on an 80-CPU computer cluster that might be available in 2008. Additional software and computing capacity will need to be acquired to simulate these nanodevices, or if higher levels of analysis (i.e., semi-empirical or density-functional (DFT) levels of theory) are deemed necessary for these nanoparts and nanodevices.

MM/MD modeling and simulation of the entire 45,642,437-atom NAW at the full atomistic level is well beyond the current ability of NanoEngineer-1 executing on a desktop PC or on a small computer cluster and will require specialized software running on highly parallel supercomputers as described earlier in Section 3.4.2.

[1065] Ralph C. Merkle, "A New Family of Six Degree Of Freedom Positional Devices," Nanotechnology 8(June 1997):47-52, http://www.zyvex.com/nanotech/6dof.html.

3.6.3 Task V-2: Prepare Multielectrode Assembly Surface

Task V-2 is to prepare an atomically flat surface upon which the first NAW can be physically constructed and debugged. Electrical power and control signals are applied to NAW mechanisms via carbon nanotube wires that connect conductive silver terminals on the atomically smooth assembly surface to electrostatic motors that actuate the manipulators. Nanotube wires from the NAW are joined to the ~40 silver electrodes per NAW worksite by simple van der Waals attraction, or if this is insufficient then by nanotube impalement of the softer metal, by e-beam spot welding,[1066] by using designed mateable connectors, or by other means. The NAW assembly surface is silicon dioxide and will include 100-1000 worksites each of area ~10,000 nm^2 (Section 3.6.1.1) on each semiconductor chip which should be a sufficient number for experimentation and testing, as described earlier in Section 3.4.3, probably requiring a total scan time of 20-40 days using a single tip.

If convenient, the electrode array surface should be of the appropriate configuration to accommodate the addition of the NFW-2 to the NAW in Phase VI (Section 3.7).

Theoretical studies and simulations examining ways of accelerating the PALE processing of semiconductor assembly surfaces – especially by increasing the tip scanning rate and the number of processing tips involved – should begin, aiming toward actual implementation no later than Phase VIII.

3.6.4 Task V-3: Assemble NAW Nanodevices using Phase II System

Task V-3 is to fabricate all necessary NAW nanoparts using the NFW-2 that was created during Phase IV (Section 3.5), and then to use the macroscale manufacturing system that was created during Phase II (Section 3.3) to assemble some of these nanoparts into all necessary NAW nanodevices, providing the complete set of nanoparts and nanodevices that are needed to build a complete working first-generation nanoscale assembly workstation (NAW) that is itself capable of performing all assembly steps previously demonstrated by the macroscale Phase II system.

Assuming the availability of a 100 Hz nanopart fabrication frequency using the NFW-2 system (Section 3.5.1.7), then one NFW-2 workstation could fabricate (from primitive feedstock molecules) all 418 nanoparts needed to build one NAW (Table V-2), comprised of 45,642,437 atoms, in ~456,425 sec (~5.3 days). Assuming the availability of a conservative 0.01 Hz operating frequency for nanopart assembly operations in which one nanopart can be added to a multipart nanodevice workpiece every 100 seconds (Section 3.3), and conservatively assuming that on average each nanopart must be handled once to be fitted into a nanodevice workpiece, then one macroscale Phase II system could assemble nanoparts into all necessary nanodevices needed to build one NAW, comprised of 418 nanoparts, in no more than (~418 nanoparts / 0.01

[1066] MinFeng Yu, Mark J. Dyer, George D. Skidmore, Henry W. Rohrs, Xue Kun Lu, Kevin D. Ausman, James Von Ehr, Rodney S. Ruoff, "3 Dimensional Manipulation of Carbon Nanotubes under a Scanning Electron Microscope," paper presented at the Sixth Foresight Nanotechnology Conference, November 1998; see also: Robert F. Service, "AFMs Wield Parts for Nanoconstruction," Science 282(27 November 1998):1620-1621; and http://www.foresight.org/Conferences/MNT6/Papers/Yu/index.html.

Hz) ~ 4.18 x 10^4 sec (~12 hours). Since this time requirement is about 10-fold less than the time required for nanopart fabrication, and since nanodevice assembly can take place both during and after nanopart fabrication, the total production time required to build all nanoparts and nanodevices comprising an NAW is driven almost exclusively by nanopart fabrication time. The faster build times available in Phase V will permit more rapid prototyping and experimentation with new nanopart, nanodevice, and overall workstation designs, and to perform quality control testing on fabricated nanoparts and nanoassemblies.

All manufactured components including both individual nanoparts and multipart nanodevices should be laid out on one Phase II workstation release surface in a specific pattern of positions and orientations to allow blind pick-and-place to be employed during final assembly of the NAW in Task V-4. The longest dimension of any nanopart described in Section 3.6.1.1 is 68 nm, so conservatively allocating a 68 nm x 68 nm area for warehousing each of the 418 nanoparts would occupy an area of 1,932,832 nm^2 (equivalent to a 1.39 x 1.39 micron square area) on the Phase II system release surface.

3.6.5 Task V-4: Assemble NAW using Phase II System

Task V-4 is to manually assemble the first-generation nanoscale assembly workstation (NAW) as a one-off (no parallelization) at a designated worksite on the atomically smooth multielectrode silica assembly surface created during Task V-2 (Section 3.6.3), using the macroscale manufacturing system created during Phase II (Section 3.3). All manipulation tasks are performed via blind pick-and-place.

The first step toward the completion of Task V-4 is to insert the multielectrode multiworksite chip created during Task V-2 into the Phase II apparatus, there to be properly positioned and aligned relative to the Phase II release surface upon which all NAW component nanoparts and nanodevices were originally pre-positioned during Task V-3 (Section 3.6.4). The juxtaposition and calibration of both surfaces probably requires the addition of a piezopositioner capable of translating the visiting chip surface so that it is can be aligned and made flush with the Phase II release surface, allowing the Phase II system to most readily assemble objects at a worksite on the more distant visiting chip surface, as previously accomplished during Task IV-4 (Section 3.5.5).

Because fabricated nanoparts and assembled nanodevices must be transferred from the Phase II system release surface to a specific worksite on the surface of the multielectrode chip created during Task V-2, to be assembled there into the NAW, assembly at the worksite might take longer than on the Phase II release surface because of the extra transport time. However, some high-accuracy nanopositioning systems[1067] can achieve high-velocity slew rates up to 1 mm/sec. Coarse transport of NAW components requiring the Phase II manipulator to translate across a distance of ~100 microns at a slew speed of 100-1000 micron/sec is fully consistent with an assembly operating frequency of ~0.01-1 parts/sec. However, the assumed operating frequency is not a crucial quantity in the present context because the successful completion of Task V-4 in a

---

[1067] Luc Chassagne, Suat Topcu, Yasser Alayli, Patrick Juncar, "Highly accurate positioning control method for piezoelectric actuators based on phase-shifting optoelectronics," Meas. Sci. Technol. 16(2005):1771-1777.

reasonable elapsed time is relatively insensitive (by many orders of magnitude) to the assembly frequency.

We conservatively assume the availability of a 0.01 parts/sec operating frequency for nanopart assembly operations using the Phase II system in which one nanopart may be transported from one surface to the other and then added to the NAW workpiece every 100 seconds (Section 3.3.1). Only 214 assemblable components (including 114 from the two assembly arm manipulators (Table III-1), 99 from the crane arm manipulator (Table V-1), and 1 unassigned component (Table V-2)) must be put together to make the first-generation NAW. Conservatively assuming that on average each component must be handled once to be installed onto the growing NAW workpiece at the designated 10,000 nm^2 and ~40-electrode worksite, then the Phase II macroscale workstation can assemble the entire second-generation NAW, comprised of 214 assemblable components, in no more than (~214 components / 0.01 Hz) ~ 2.14×10^4 sec (~6 hours). Construction of the NAW is done as a one-off with no parallelization at the assembly stage.

3.6.6 Task V-5: Operate NAW using Phase II System

Task V-5 is to validate the design of the first-generation nanoscale assembly workstation (NAW) by experimentally demonstrating its basic functionality.

To operate the completed NAW, the macroscale Phase II workstation is used to acquire a series of assemblable nanoparts and nanodevices from its own native presentation surface (which has been prestocked with components as in Task V-4) and then to manually transfer each component to NAW manipulators as material inputs for the NAW. Aside from this exogenous supply source, the NAW is operated as a standalone nanoscale workstation by sending appropriate current pulses through the 40 electrodes which provide both power and control. These control pulses are synchronized with the actions of the Phase II manipulator to achieve a smoothly running nanoassembly system.

The NAW must demonstrate its minimal functionality by assembling at least one instance of each of the half-dozen different nanopart assemblies (Table V-1) from nanoparts previously fabricated in greater numbers using the NFW-2 system during Task V-3. This will prove that the NAW can assemble all multicomponent nanodevices needed to make a copy of itself from externally supplied nanoparts, power, and control signals, demonstrating 100% nanoassembly closure for the NAW system design. The Phase II system is used to supply nanoparts to the NAW and to collect completed assemblies at the end of each assembly sequence. Even if the assembly tests require 100 sec per operation (i.e., ~0.01 Hz assembly rate), all these tests can be concluded in less than an hour once the input nanoparts have been fabricated by the NFW-2 system and pre-positioned on the native presentation surface of the Phase II system.

An absolutely rigorous demonstration of replicative functionality would additionally require the NAW to prove its ability to assemble all 418 of its own nanoparts (to be fed to the NAW by the Phase II system) into larger assemblies – up to and including a finished replica NAW to be

assembled on an adjacent 10,000 nm^2 worksite, thus definitively proving replication fidelity[1068] of the NAW. With nanoparts being fed to the NAW at a 0.01 Hz rate, this demonstration may be completed in ~41,800 sec (~12 hours). If desired, the daughter NAW could then assemble another set of 418 nanoparts comprising a third "granddaughter" NAW unit in another ~12 hours of NAW runtime, thus definitively proving offspring replicative fertility.[1069]

It would also be useful for the NAW to demonstrate one additional closely-related capability that will serve as preparation to confront the challenges of Phase VI (Section 3.7.2). When premanufactured nanoparts are delivered to a depot area adjacent to the NAW on the electrode surface using the macroscale Phase II system, the NAW shows that it can acquire those nanoparts from the on-surface depot without having to be handed these parts directly by the Phase II system, and then, using these components, assemble all multi-nanopart nanodevices previously demonstrated in Task V-3, placing the finished product nanodevices in a product depot adjacent to the NAW on the workspace surface.

It may be necessary to iterate Tasks IV-1, IV-3, IV-4, and IV-5 to fully debug the NAW design and to successfully achieve the desired results.

[1068] Robert A. Freitas Jr., Ralph C. Merkle, Kinematic Self-Replicating Machines, Landes Bioscience, Georgetown, TX, 2004; Sections 5.1.9(L2) and 5.1.9(L4); http://www.MolecularAssembler.com/KSRM/5.1.9.L.htm.

[1069] Robert A. Freitas Jr., Ralph C. Merkle, Kinematic Self-Replicating Machines, Landes Bioscience, Georgetown, TX, 2004; Sections 5.1.9(L2) and 5.1.9(L4); http://www.MolecularAssembler.com/KSRM/5.1.9.L.htm.

3.7 Phase VI: Nanoscale Manufacturing Workstation (NMW)

Manufacturing typically may require both fabrication and assembly operations to be performed. The purpose of this phase of the nanofactory development program is to combine both functions in a single nanoscale system.

The key objective of Phase VI is the design and manufacture of the first self-contained nanoscale manufacturing workstation (NMW) that is capable of fully endogenous operation with no assistance from the macroscale Phase II system. The NMW is the first complete molecular manufacturing module, incorporating the ability of the NFW-2 (Phase IV; Section 3.5) to fabricate nanoparts from molecular feedstock and the ability of the NAW (Phase V; Section 3.6) to assemble those nanoparts into multipart nanodevices and more complex nanosystems, including nanosystems at least as complex as itself.

The NMW is described in Section 3.7.1 and illustrated in Figure VI-1. This is followed by an enumeration of the specific tasks required to manufacture the NMW which include: design and simulation of the NMW (Section 3.7.2), preparation of a multielectrode assembly surface (Section 3.7.3), fabrication of needed NMW nanoparts and assembly of needed NMW multipart nanodevices using the Phase II system (Section 3.7.4), manual assembly of the NMW using the Phase II system (Section 3.7.5), demonstration of fully endogenous operation of the NMW without using the macroscale Phase II system and successful endogenous replication of the NMW (Section 3.7.6).

3.7.1 Description of the NMW

The basic structure of the NMW includes one copy of a nanoscale assembly workstation (NAW), as developed in Phase V (Section 3.6), which is positioned on the multielectrode assembly surface immediately adjacent to one copy of an NFW-2 as developed in Phase IV (Section 3.5) but having a larger second-generation bulk feedstock supply system (BFSS-2). The BFSS-2 differs from the BFSS developed in Phase IV (Section 3.5.1.6) primarily in the size of the main storage tank, which again wraps around three of the four sides of the now-combined 100 nm x 100 nm NFW and the 100 nm x 100 nm NAW subsystems, a larger (100 nm x 200 nm) rectangular footprint than before. The BFSS-2 is large enough to contain sufficient molecular feedstock for one complete replication cycle of the NMW. The function of the NMW is to combine the ability of the NFW-2 (Section 3.5) to fabricate nanoparts from molecular feedstock with the ability of the NAW (Section 3.6) to assemble those nanoparts into multipart nanodevices and more complex nanosystems, including nanosystems at least as complex as itself. Large product objects including NMW replicas can be assembled on the assembly surface along the one edge of the four-edge footprint rectangle that is not partially blocked by the three-edge main tank structure.

Figure VI-1. Schematic illustration of the first-generation Nanoscale Manufacturing Workstation (NMW), showing four Stewart platform manipulators comprising the DMS fabrication machinery (NFW-2) adjacent to three Stewart platform manipulators comprising the nanocomponent assembly machinery (NAW) mounted on a foundation block adjacent to a 20-tip toolrack, surrounded by the Bulk Feedstock Supply System (BFSS) graphene storage tank (BFSS appurtenant structures not shown).

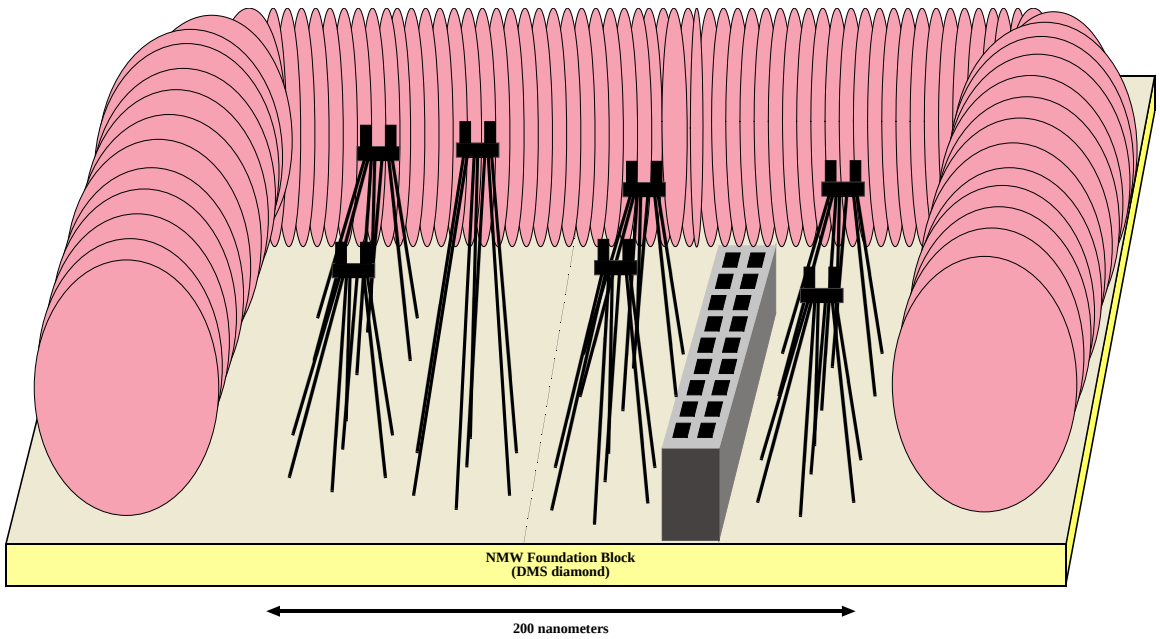

3.7.1.1 Structure of the NMW

Preliminary scaling results for a compromise NMW design are shown in Table VI-1. Main tank cylindrical radius increases from 40 nm in the BFSS (Section 3.5.1.6) to 55 nm in the BFSS-2, tank length increases from 568 nm (~79% of NFW perimeter) in the BFSS to 660 nm (~63% of NFW+NAW perimeter) in the BFSS-2, and BFSS-2 tank pressure is lowered to 250 atm to make sufficient room in the tank to hold the additional byproduct molecular hydrogen that will be generated during a single cycle of operation of the larger NMW system. The H-passivated diamond tank wall thickness stays at 0.45 nm (more than three times the nominal thickness conservatively required to forestall tank bursting) while the graphene bladder sheet surface area increases from 81,430 nm^2 in the BFSS to 133,046 nm^2 in the BFSS-2 to accommodate the larger tank size. The maximum ethylene storage pressure in the BFSS-2 is reduced from 400 atm to 250 atm to make room for the additional H_2 byproduct molecules.

Table VI-1. Estimated Atom Counts for the NMW							
NMW Nanopart or Nanodevice	**# of Nano-parts**	**Total Solid Volume (nm^3)**	**Total Passiv. Area (nm^2)**	**# of C Atoms**	**# of H Atoms**	**# of Ge Atoms**	**Total # of Atoms**
BFSS-2 tank	1	119,742	532,186	21,074,592	16,710,634	0	37,785,226
BFSS-2 bladder	1	13,277	0	4,177,658	0	0	4,177,658
BFSS-2 nontank	139	31,252	85,041	5,500,352	2,670,287	0	8,170,639
NFW	521	150,280	170,030	26,076,856	5,270,930	10	31,347,796
NAW	418	221,000	217,627	38,896,000	6,746,437	0	45,642,437
Other Misc. Structure	20	10,000	10,000	1,761,080	310,000	0	2,071,080
NMW (Empty)	1100	545,551	1,014,884	97,486,538	31,708,288	10	129,194,836
Feedstock gases	----	6,969,100	----	97,801,486	195,602,972	25	293,404,483
NMW (Filled)	1100	7,514,651	1,014,884	195,288,024	227,311,260	35	422,599,319

The NMW incorporates roughly twice the number of carbon atoms as the NFW-2 system. Conservatively assuming that each sorting rotor stage can achieve a 1000:1 purification ratio[1070] and recognizing that the NFW subsystem in the NMW will consume ~4.89 x 10^7 C_2H_4 molecules per feed cycle (i.e., one tankful of ethylene feedstock), then to ensure that not a single impurity molecule is stored in the BFSS-2 tank requires an impurity rate at or below $(4.89 \times 10^7)^{-1} \sim 2 \times 10^{-8}$. To achieve this modest objective starting with commercially available 5N purity ethylene feedstock (Section 3.5.1.3) thus requires 10^{-5} (5N purified feedstock) x 10^{-3} (1st rotor pair) ~ 10^{-8} (going into the tank), so we still need just one rotor pair for ethylene in the BFSS-2. Applying the conservative 10^5 molecule/sec transport rate for ethylene sorting rotors (Section 3.5.1.7) allows the BFSS-2 tank to be filled with ~48.9 million C_2H_4 molecules in only ~4890 sec (~0.06 day).

The NMW tankage and machinery covers an area of 93,200 nm^2 on the assembly surface and has an inferred excluded solid volume of 10.7 x 10^6 nm^3 (1.6 x 10^6 nm^3 of which is empty space to allow free movement of tools and workpieces; Sections 3.4.1.1 and 3.6.1.1). There are ~49 million ethylene gas molecules in the tank at 250 atm when it is full at the beginning of a replication or production cycle, and ~85 million H_2 byproduct molecules in the tank at 1000 atm at the end of a replication or production cycle when all the ethylene has been consumed. The unloaded NMW system has a total atom count of ~129,194,836 atoms (75% C atoms, 25% H atoms), a mass of 1,202,634,445 amu (assuming natural isotopic mix for C and Ge) or 2.01143 x 10^{-18} kg, and a total nanopart count of ~1100. Excluding the main tank and bladder sheet, the average NMW nanopart has 79,446 atoms (65,787 atoms of C and 13,659 atoms of H). There is also ~6800 nm^2 of free space on the assembly surface for nanopart depoting between the NFW and NAW if needed, giving a ~100,000 nm^2 footprint for each NMW on the assembly surface.

[1070] K. Eric Drexler, Nanosystems: Molecular Machinery, Manufacturing, and Computation, John Wiley & Sons, New York, 1992; http://www.zyvex.com/nanotech/nanosystems.html.

The NMW requires 58 control lines to operate the NFW-2 subsystem (Section 3.5.1.6) and 39 control lines to operate the NAW subsystem (Section 3.6.1.1), plus 1 common ground wire and two spares for a total of 100 control lines needed at each NMW worksite on the assembly surface. Note that the current load on each common ground line is only ~100 I_{motor} ~ 2 x 10^{-11} amp, well below the current-carrying capacity experimentally observed[1071] for individual 10-50 nm long single-walled "metallic" carbon nanotubes which can conduct 25-100 x 10^{-6} amp/wire electrical currents before failing, and a burnout threshold of 1000 x 10^{-6} amp/wire reported by others.[1072]

3.7.1.2 Operation of the NMW

After the NMW has been constructed by the macroscale Phase II system in UHV on the atomically smooth electrode-rich assembly surface, the workstation may be operated as follows. Feedstock/byproduct gas handlers and NFW-2 manipulators are operated as previously described in Section 3.5.1.7, consuming the ethylene feedstock during the fabrication of nanoparts comprised of up to ~98 million carbon atoms and a surfeit of passivating hydrogen atoms. Finished nanoparts are either (1) depoted on the assembly surface between the NFW and NAW subsystems for future use, or (2) passed to the NAW for assembly into multipart components, which themselves may be depoted or installed (along with recently fabricated or previously depoted nanoparts) into a more complex product object positioned adjacent to the NMW footprint on the assembly surface.

The end result of Phase VI is to create an externally controlled planar nanoscale manufacturing workstation able to manufacture, and deliver to arbitrary nearby depots on the workspace surface, continuous (until the BFSS-2 tank is empty) quantities of individual nanoparts and nanodevices as products, and also to assemble an exact copy of its own structure, adjacent to itself on the workspace surface, following assembly commands fed to it from an external source. NMW power usage is similar to estimates for the NFW previously presented in Section 3.4.3 because the NAW operates at a much lower duty cycle compared to the NFW (Section 3.6.1.3).

3.7.1.3 Productivity of the NMW

Due to the significant productivity mismatch between the NFW and NAW (Section 3.6.1.3), the NMW is fabrication-limited and thus is restricted to the output rate of the endogenously operated NFW-2 system (Section 3.5.1.7) which is ~100 atoms/sec (using a ~1.2 MHz electrical control

---

[1071] Ali Javey, Pengfei Qi, Qian Wang, Hongjie Dai, "Ten- to 50-nm-long quasi-ballistic carbon nanotube devices obtained without complex lithography," PNAS 101(14 September 2004):13408-13410; http://www.pnas.org/cgi/content/abstract/101/37/13408.

[1072] Hongjie Dai, Eric W. Wong, Charles M. Lieber, "Probing Electrical Transport in Nanomaterials: Conductivity of Individual Carbon Nanotubes," Science 272(26 April 1996):523-526; Stefan Frank, Philippe Poncharal, Z.L. Wang, Walt A. de Heer, "Carbon Nanotube Quantum Resistors," Science 280(12 June 1998):1744-1746.

pulse rate) for fully assembled nanosystems. If operated endogenously, during each production cycle (in which one tankful of ethylene feedstock is consumed) the NMW could fabricate its own mass of nanoparts in ~(129,194,836 atoms) / (100 atoms/sec) ~ 1.29 x 10^6 sec (~15 days), and then assemble them into finished multipart product objects – including itself, on an adjacent worksite – in an additional nanodevice assembly time of ~1.10 x 10^4 sec (Section 3.7.4) plus an NMW assembly time (from constituent nanoparts and nanodevices) of 5.08 x 10^4 sec (Section 3.7.5), giving a serial NMW manufacturing time of 1.35 x 10^6 sec (~15.6 days) – an in-cycle atom-assembly rate of 95.7 atoms/sec (which ignores chamber pumpdown time).

Assuming we need one bit to describe each manipulator increment in the NMW and ~12,000 increments to add either one atom during fabrication (Section 3.4.1.4) or one nanopart during assembly (Section 3.6.1.3), then a complete replication cycle for the NMW requires up to (129,194,836 atoms)(12,000 increments/atom-actuator)(1 bit/increment)(58 actuators) ~ 8.99 x 10^{13} bits of replication process data for fabrication and (1100 nanoparts)(12,000 increments/nanopart-actuator)(1 bit/increment)(39 actuators) ~ 5.15 x 10^8 bits of replication process data for assembly.

3.7.1.4 Reliability of NMW Manufacture and Operation

Regarding the use of the NFW-2 Phase IV system to fabricate nanoparts for the NMW Phase VI system, the NMW has about twice as many atoms (~129 million atoms; Table VI-1) as the NFW-2 (~65 million atoms; Table IV-4), mostly due to the extra mass of the NAW. Doubling the atom count to be built by the Phase IV system gives substantially similar reliability estimates for building the Phase VI system as for building the replica of the Phase IV system using the Phase IV system (Task IV-9). In particular: the NFW-2 Phase IV system must correctly execute (129,194,836 atoms)(6 operations/atom) ~ 775 million mechanosynthetic operations; there is a DMS reaction error rate of <1 below 227 K, ~10^{-2} near dry-ice temperature at ~185 K, ~10^{-3} at 170 K, or ~10^{-17} at 80 K for a ~129 x 10^6-atom product object fabricated using the original set of DMS reactions,[1073] the latter completely negligible for Phase VI purposes; minimum vacuum pressure P_{UHV} falls about twofold for Phase VI at 185 K (2.5 x 10^{-14} atm), compared to Phase IV at 190 K (5 x 10^{-14} atm); and the radiation damage time is $\tau_{rad} \sim (\kappa_{fail}\, m_{target}\, I_{rad})^{-1}$ ~ 995 years for a mostly-carbon ~129 x 10^6-atom NMW of mass m_{target} = 2.01 x 10^{-18} kg, still a negligible error rate. An operating temperature of T ~ 185 K seems appropriate. The Phase II system is then used to assemble the relatively small number of fabricated nanoparts. In this task, MMW reliability will be governed chiefly by its ability to correctly execute a small number of non-covalent parts assembly operations and by error rates in nanopart gripping/releasing mechanisms, and these error rates are assumed to be small in comparison with the DMS-related error rates.

The NMW is then operated as a standalone manufacturing system in Task VI-5 to build a replica of itself. For this Phase VI manufacturing system, we have a target productivity rate of ~100 atom/sec (Section 3.7.1.3) with ~6 mechanosynthetic operations required for placement of each atom in the growing workpiece structure (Section 3.7.1.3), and a target product object size

---

[1073] Robert A. Freitas Jr., Ralph C. Merkle, "A Minimal Toolset for Positional Diamond Mechanosynthesis," J. Comput. Theor. Nanosci. 5(May 2008):760-861.

consisting of all 1100 nanoparts comprising an entire 129,194,836-atom NMW replica (Table VI-1) which are later assembled by the NMW system as well. Building the NMW replica using the original NMW unit requires ~775 million mechanosynthetic operations, so to avoid even a single misplacement error during an entire replication cycle the NMW manipulators must be able to deliver a minimum of ~775 million error-free round trip excursions of the positionally controlled DMS tooltips. The potential ability of computer controllers to reliably deliver such lengthy data sequences with low error, and the ability of simple mechanical actuators to reliably execute such lengthy sequences of mechanical actuations with low error, is discussed in Section 3.8.1.3.

Another source of intrinsic manufacturing error arises from the reliability of the DMS reactions themselves as previously discussed (Section 3.2.1.8 and Section 3.4.1.6). Table I-5 gives the probability of misreaction at various relevant operating temperatures, assuming a defect energy threshold of 0.40 eV. The misreaction probability per mechanosynthetic operation may be as high as 1.91×10^{-7} at 300 K, conservatively assuming that all reactions have the minimum defect energy threshold of 0.40 eV, producing ~148 erroneous atom placements in the ~129×10^6-atom NMW replica product object after ~775×10^6 mechanosynthetic operations, hence endogenous room temperature fabrication of the NMW replica by the original NMW system appears infeasible. The expected error rate falls to <1 erroneous atom placement (per replication cycle) below 227 K, ~10^{-2} near dry-ice temperature at ~185 K, or ~10^{-3} at 170 K for a ~129×10^6-atom product object fabricated using the original set of DMS reactions.[1074] Ethylene remains a gas above 170 K, and while GeH_4 liquefies below 185 K enough germane should remain in the vapor state to permit gaseous feedstock operation throughout a 170-185 K temperature range. At near liquid nitrogen temperatures (~80 K), the DMS-related error rate using reaction sequences with a defect energy threshold of 0.40 eV would fall to ~10^{-16} for a ~129×10^6-atom product object, completely negligible for Phase VI purposes.

Another major source of error is radical poisoning by contaminants in an imperfect UHV environment. At a target productivity rate of ~100 atoms/sec for the Phase VI system, the original ~129×10^6-atom NMW will require $t_{fab} \sim 1.29 \times 10^6$ sec (~15 days) to fabricate the ~129×10^6-atom NMW replica. Assuming that a radical site susceptible to poisoning is exposed to the imperfect UHV environment for a fraction $f_{vac} \sim 50\%$ of the time, then the maximum tolerable UHV pressure that will permit all nanoparts for one defect-free ~129×10^6-atom NMW replica to be fabricated is $P_{UHV} \leq (N_{encounters}\ T / n_{contam}\ A_{radical}\ f_{vac}\ t_{fab})\ (\pi\ MW_{kg} / 2\ k_B T\ N_A)^{1/2} \sim 2.5 \times 10^{-14}$ atm, where $n_{contam} = 7.34 \times 10^{27}$ molecules-K/m^3-atm (= N_A/R_{gas}) for ideal gas (contaminant) molecules and T = 185 K, with the other quantities as previously defined in Section 3.2.1.7. If any workpiece having one or more erroneous atom placements is considered defective, then in a UHV environment maintained at ~10^{-16} atm (~10 million contaminant molecules present in a 5-liter UHV work volume; currently achievable experimentally, Section 3.2.1.7) the radical-poisoning defect rate at 185 K will be an acceptable ~0.4% for replica NMW product objects. If H_2 contaminant is determined not to be a serious radical poisoning risk or can be rigorously excluded from the workspace, then taking $MW_{kg} = 0.014$ kg/mole for N_2 raises the required P_{UHV} by a factor of ~2.6.

[1074] Robert A. Freitas Jr., Ralph C. Merkle, "A Minimal Toolset for Positional Diamond Mechanosynthesis," J. Comput. Theor. Nanosci. 5(May 2008):760-861.

As for radiation damage rates, assuming a failure condition of $\kappa_{fail} \sim 10^{15}$ hits/kg-rad and an $I_{rad} \sim$ 0.5 rad/yr background the mean time τ_{rad} between radiation-disabling hits on a mostly-carbon ~129 x 10^6-atom NMW of mass $m_{target} = 2.01 \times 10^{-18}$ kg is $\tau_{rad} \sim (\kappa_{fail}\, m_{target}\, I_{rad})^{-1} \sim 995$ years (conservatively assuming that one such hit will cause the workpiece or tooltip to fail with 100% certainty), still a negligible error rate (~10^{-4} per replication cycle).

The NMW system is then used to assemble the relatively small number of fabricated nanoparts to complete its replica. In this task, NMW reliability will be governed chiefly by its ability to correctly execute a small number of non-covalent parts assembly operations and by error rates in nanopart gripping/releasing mechanisms, and these error rates are assumed to be small in comparison with the DMS-related error rates.

3.7.2 Task VI-1: Design and Simulate NMW

Task VI-1 is to design and simulate the entire NMW, specifying all component nanoparts and nanodevices (assemblies of nanoparts) and also specifying all fabrication and assembly processes that will be required to complete the manufacturing operations of: (1) nanopart fabrication, (2) nanodevice assembly from nanoparts, (3) NMW assembly from nanoparts and nanodevices, and (4) to verify correct NMW operation, if properly assembled. The major design changes include a approximate doubling of the atom count of the BFSS main tank and modifications to the NFW and NAW work envelopes to allow (a) reliable handoff of nanoparts directly between NFW and NAW subsystems and (2) reliable placement to or retrieval from adjacent surface depots of nanoparts or larger nanoassemblies by either NFW or NAW subsystems (as previously mentioned in Section 3.6.6). In an efficient design effort, the NMW will be designed in conjunction with the first-generation NAW, with Tasks V-1 and VI-1 undertaken simultaneously.

Simulations should continue to explore the limits to increasing operating frequency for the assembly workstation, completing a full analysis of the impact on NMW design, if any, of increasing pulse frequency 10-100 fold from 1.2 MHz to 12-120 MHz. Particular attention should be paid to power consumption, electrode current-carrying capacity, and system reliability as a function of operating frequency. (Note that the ITRS semiconductor industry roadmap[1075] anticipates ~40 GHz chip speeds by 2015-2017.) Any structural changes believed necessary to enable future NMW operation at 12-120 MHz should be incorporated into the design at this stage. However, operation of a physical manufacturing system at these faster speeds is deferred until Task VII-7 in Phase VII.

Design and simulation of the typical NMW nanopart will require at minimum a molecular mechanics / molecular dynamics (MM/MD) level analysis of a nanopart having (87,231,952

[1075] International Technology Roadmap for Semiconductors (ITRS), 2006 Update. "Overview and Working Group Summaries," Tables 1a (Product Generations and Chip Size Model Technology Trend Targets—Near-term Years) and 1b (Product Generations and Chip Size Model Technology Trend Targets—Long-term Years), p.3; http://www.itrs.net/Links/2006Update/FinalToPost/00_ExecSum2006Update.pdf; see also in "Lithography," pp. 7-8; http://www.itrs.net/Links/2006Update/FinalToPost/08_Lithography2006Update.pdf.

atoms)/(1098 nanoparts) ~ 79,446 atoms/nanopart (Table VI-1) for nontank nanoparts. Such modeling and simulation could be performed using the NanoEngineer-1 software package that was available in 2007, running on a personal computer available in 2008. The typical NMW nanodevice consists of 2-4 nanoparts (Tables III-1 and V-1), increasing the simulation software capacity requirement to 159,000-318,000 atoms/nanodevice for basic modeling and validation of proper operation of nanodevices. Following Moore's Law assuming an 18-month doubling time and conservatively assuming traditional ~N_{atom}^2 scaling with atom count for MM/MD algorithms, a 318,000-atom nanodevice could be simulated using NanoEngineer-1 on a single commonplace personal computer that would be available in 2015, or on a 40-CPU computer cluster that might be available in 2008. Additional software and computing capacity will need to be acquired to simulate these nanodevices, or if higher levels of analysis (i.e., semi-empirical or density-functional (DFT) levels of theory) are deemed necessary for these nanoparts and nanodevices.

MM/MD modeling and simulation of the entire 129,194,836-atom NMW at the full atomistic level is well beyond the current ability of NanoEngineer-1 executing on a desktop PC or on a small computer cluster and will require specialized software running on highly parallel supercomputers as described earlier in Section 3.4.2.

3.7.3 Task VI-2: Prepare Multielectrode Assembly Surface

Task VI-2 is to prepare an atomically flat surface upon which the first NMW can be physically constructed and debugged. Electrical power and control signals are applied to NMW mechanisms via carbon nanotube wires that connect conductive silver terminals on the atomically smooth assembly surface to electrostatic motors that actuate the manipulators. Nanotube wires from the NMW are joined to the ~100 silver electrodes per NMW worksite by simple van der Waals attraction, or if this is insufficient then by nanotube impalement of the softer metal, by e-beam spot welding,[1076] by using designed mateable connectors, or by other means. The NMW assembly surface is silicon dioxide and will include 100-1000 worksites each of area ~100,000 nm^2 (e.g., a ~420 nm x ~240 nm rectangular footprint; Section 3.7.1) on each semiconductor chip which should be a sufficient number for experimentation and testing, as described earlier in Section 3.4.3, probably requiring a total scan time of 20-40 days using a single tip.

Theoretical studies and simulations examining ways of accelerating the PALE processing of semiconductor assembly surfaces – especially by increasing the tip scanning rate and the number of processing tips involved – should continue, aiming toward actual implementation no later than Phase VIII.

[1076] MinFeng Yu, Mark J. Dyer, George D. Skidmore, Henry W. Rohrs, Xue Kun Lu, Kevin D. Ausman, James Von Ehr, Rodney S. Ruoff, "3 Dimensional Manipulation of Carbon Nanotubes under a Scanning Electron Microscope," paper presented at the Sixth Foresight Nanotechnology Conference, November 1998; see also: Robert F. Service, "AFMs Wield Parts for Nanoconstruction," Science 282(27 November 1998):1620-1621; and http://www.foresight.org/Conferences/MNT6/Papers/Yu/index.html.

3.7.4 Task VI-3: Assemble NMW Nanodevices using Phase II System

Task VI-3 is to fabricate all necessary nanoscale manufacturing workstation (NMW) nanoparts using the NFW-2 that was created during Phase IV (Section 3.5), and then to use the macroscale manufacturing system that was created during Phase II (Section 3.3) to assemble some of these nanoparts into all necessary NMW nanodevices, providing the complete set of nanoparts and nanodevices that are needed to build a complete working first-generation NMW workstation that will itself be capable of performing all fabrication and assembly steps previously demonstrated by the macroscale Phase II system.

Assuming the availability of a 100 Hz nanopart fabrication frequency using the NFW-2 system (Section 3.5.1.7), then one NFW-2 workstation can fabricate (from primitive feedstock molecules) all 1100 nanoparts needed to build one NMW (Table VI-1), comprised of 129,194,836 atoms, in ~1.29 x 10^6 sec (~15 days). Assuming the availability of a conservative 0.01 Hz operating frequency for nanopart assembly operations in which one nanopart can be added to a multipart nanodevice workpiece every 100 seconds using a Phase II system (Section 3.3), and conservatively assuming that on average each nanopart must be handled once to be fitted into a nanodevice workpiece, then one macroscale Phase II system could assemble nanoparts into all necessary nanodevices needed to build one NMW, comprised of 1100 nanoparts, in no more than (~1100 nanoparts / 0.01 Hz) ~ 1.10 x 10^4 sec (~31 hours). Since this time requirement is about 100-fold less than the time required for nanopart fabrication, and since nanodevice assembly can take place both during and after nanopart fabrication, the total production time required to build all nanoparts and nanodevices comprising an NMW is driven almost exclusively by nanopart fabrication time.

All manufactured components including both individual nanoparts and multipart nanodevices should be laid out on one Phase II workstation release surface in a specific pattern of positions and orientations to allow blind pick-and-place to be employed during final assembly of the NMW in Task VI-4. The longest dimension of any non-tankwall nanopart described in Sections 3.4.1.1, 3.5.1.6 and 3.6.1.1 is 68 nm, so conservatively allocating a 68 nm x 68 nm area for warehousing each of the 1098 nanoparts would occupy an area of 5,077,152 nm^2. The tank and graphene bladder sheets are of length ~660 nm and add another ~72,600 nm^2 and ~133,046 nm^2 in resting cross-sectional surface area, raising the total to 5,282,798 nm^2 which is equivalent to a 2.3 x 2.3 micron square area on the Phase II system release surface.

3.7.5 Task VI-4: Assemble NMW using Phase II System

Task VI-4 is to manually assemble the first-generation nanoscale manufacturing workstation (NMW) as a one-off (no parallelization) at a designated worksite on the atomically smooth multielectrode assembly surface created during Task VI-2 (Section 3.7.3), using the macroscale manufacturing system created during Phase II (Section 3.3). All manipulation tasks are performed via blind pick-and-place.

The first step toward the completion of Task VI-4 is to insert the multielectrode multiworksite chip created during Task VI-2 into the Phase II apparatus, there to be properly positioned and aligned relative to the Phase II release surface upon which all NMW component nanoparts and nanodevices were originally pre-positioned during Task VI-3 (Section 3.7.4). The juxtaposition and calibration of both surfaces probably requires the addition of a piezopositioner capable of translating the visiting chip surface so that it is can be aligned and made flush with the Phase II

release surface, allowing the Phase II system to most readily assemble objects at a worksite on the more distant visiting chip surface, as previously accomplished during Task IV-4 (Section 3.5.5).

Because fabricated nanoparts and assembled nanodevices must be transferred from the Phase II system release surface to a specific worksite on the surface of the multielectrode chip created during Task VI-2, to be assembled there into the NMW, assembly at the worksite might take longer than on the Phase II release surface because of the extra transport time. However, some high-accuracy nanopositioning systems[1077] can achieve high-velocity slew rates up to 1 mm/sec. Coarse transport of NMW components requiring the Phase II manipulator to translate across a distance of ~100 microns at a slew speed of 100-1000 micron/sec is fully consistent with an assembly operating frequency of ~0.01-1 Hz. However, the assumed operating frequency is not a crucial quantity in the present context because the successful completion of Task VI-4 in a reasonable elapsed time is relatively insensitive (by many orders of magnitude) to the assembly frequency.

We conservatively assume the availability of a 0.01 Hz operating frequency for nanopart assembly operations using the Phase II system in which one nanopart may be transported from one surface to the other and then added to the NMW workpiece every 100 seconds (Section 3.3). At most only 508 assemblable components – including 274 components for the NFW-2 (Section 3.5.9), 214 for the NAW (Section 3.6.5), and 20 unassigned components in the NMW (Table VI-1) – must be put together to make the first-generation NMW. Conservatively assuming that on average each component must be handled once to be installed onto the growing NMW workpiece at the designated ~100,000 nm^2 and ~100-electrode worksite, then the Phase II macroscale workstation can assemble the entire first-generation NMW, comprised of 508 assemblable components, in no more than (~508 components / 0.01 Hz) ~ 5.08×10^4 sec (~14 hours). Construction of the NMW is done as a one-off with no parallelization at the assembly stage.

It is worth noting that the above estimates for the number of manufacturing steps are in line with those of other non-nanoscale manufacturing industries. For example, a 1 MB DRAM with 1 micron features required 200 manufacturing steps;[1078] a 16 MB DRAM required 400 steps (including 57 layers deposited (e.g., SiO_2 (14 times), Si_3N_4, Al, ...), 73 etching steps (54 with "plasma etching", 19 with wet chemistry), 19 lithography steps with masks (including deposition of the resist, exposure, and development), 12 high temperature processes (including several oxidations), 37 dedicated cleaning steps that are built in (wet chemistry occurs 150 times altogether) and 158 process validation measurements);[1079] a 63 MB DRAM with 0.35 micron features needed 500 steps;[1080] and ~1000 steps for the 0.13 micron technology.[1081] In the

---

[1077] Luc Chassagne, Suat Topcu, Yasser Alayli, Patrick Juncar, "Highly accurate positioning control method for piezoelectric actuators based on phase-shifting optoelectronics," Meas. Sci. Technol. 16(2005):1771-1777.

[1078] http://ipomaven.123jump.com/rep/v/veco.php3.
[1079] http://www.techfak.uni-kiel.de/matwis/amat/elmat_en/kap_4/backbone/r4_2_1.html.
[1080] http://ipomaven.123jump.com/rep/v/veco.php3.

[1081] R.T. "Tets" Maniwa, "IC Fabs: What Does It Take to Be on the Leading Edge? A look at the issues defining deep-submicron wafer processing," Integrated System Design Magazine, 1997; http://www.isdmag.com/editorial/1997/tetsarticle9709.html.

electromechanical area, Seiko Epson's LQ100 printer had 53 manufacturing steps using 38 assembly stages, 7 inspection stages, and 8 packaging stages, of which 5 assembly operations were manual;[1082] in the automotive area, exactly 2,146 precision welds were made by robots in each Nissan Maxima automobile manufactured in 2001;[1083] and in the consumer products area, in 2000 a complex sneaker (footwear) required 128-136 manufacturing steps.[1084]

3.7.6 Task VI-5: Operate NMW Endogenously

Task VI-5 is to validate the design of the first-generation nanoscale manufacturing workstation (NMW) by experimentally demonstrating its basic functionality.

To experimentally validate the completed NMW, the system must be operated as a standalone nanoscale workstation as described in Section 3.7.1 by sending appropriate current pulses through the ~100 worksite electrodes which provide both power and control. Unlike the NFW which relied entirely on the Phase II system for feedstock and byproduct molecule transactions, the NFW-2 subsystem within the NMW can acquire feedstock from its own BFSS-2 module and can thus endogenously transfer each feedstock molecule to DMS manipulators requiring feedstock as material input for the NFW-2. Byproduct molecules can be endogenously disposed of via the BFSS-2 as well. Similarly, unlike the NAW which relied entirely on the Phase II system for nanopart-handling transactions, the NAW subsystem within the NMW can acquire nanoparts directly from its NFW-2 module or from internal depots and can thus endogenously transfer each nanopart and multipart nanodevice to the appropriate assembly manipulators thus allowing all fabrication and assembly operations to be completed endogenously. The Phase II system has no further role in NMW operations.

An absolutely rigorous demonstration of full functionality first requires the NMW to prove its ability to build all 1100 of its own nanoparts, which would be passed from the NFW-2 subsystem to the NAW subsystem which in turn would assemble a working replica NMW on an adjacent ~100,000 nm^2 worksite on the assembly surface. Nanopart fabrication time is ~1.29×10^6 sec (Section 3.7.4), nanodevice assembly time is ~1.10×10^4 sec (Section 3.7.4), and NMW assembly time (from constituent nanoparts and nanodevices) is 5.08×10^4 sec (Section 3.7.5), giving a serial NMW manufacturing time of 1.35×10^6 sec (~15.6 days), to which must be added the feedstock/byproduct gas handling and chamber pumpdown cycle times (1-21 days; Section 3.5.1.7). The replica NMW (the "daughter" unit) is then required to demonstrate its ability to fabricate a third "granddaughter" NMW unit, thus definitively proving both replication fidelity

---

[1082] "Japan's Automated Electronics Assembly Demonstrated," information on NEC and Seiko Epson by David Kahaner of the Office of Naval Research, Tokyo; http://itri.loyola.edu/ep/c5s4.htm.

[1083] Luisa Kroll, "Speed bump," Forbes 167(30 April 2001):113, 115.

[1084] http://www.iwvaluechain.com/Features/articles.asp?ArticleId=1053.

and offspring replicative fertility[1085] of the NMW in another 16-37 day experimental run. For a 129,194,836-atom NMW unit, this represents a 40-93 atom/sec net build rate. So we now have an operational NMW nanopart fabrication and assembly system that can manufacture nanoparts, nanodevices, and small nanosystems from feedstock atoms at an atom placement frequency of up to ~100 Hz. The NMW is fully scalable and can be used for practical replication on an assembly surface with exponential parallelization of production lines – which is the main objective of Phases VII and VIII.

It would also be useful for the NMW to demonstrate the additional closely-related ability to endogenously manufacture, and deliver to arbitrary nearby depots on the workspace surface, quantities of individual nanoparts and various nanodevices as products. These components should include: (1) critical nanoparts and nanodevices of which the NMW is itself constructed; (2) non-critical nanoparts and nanodevices of which the NMW is not constructed, but which are likely to be required for the manufacture of post-Phase VI systems, particularly nanofactory modules (as trial designs for these components become available); and (3) other nanoparts and nanodevices believed to be useful, either for nanoscale manufacturing or as products (or components of products) in their own right (e.g., respirocyte[1086] or microbivore[1087] nanorobot components). The end result is an NMW that can demonstrably: (1) assemble a wide range of nanodevices from nanoparts that it can fabricate by itself (demonstrating useful production), and (2) assemble a copy of itself from nanoparts fabricated by itself and from nanodevices assembled by itself from nanoparts fabricated by itself (demonstrating self-replication) which confirms 100% nanopart and nanodevice closure along with 100% fabrication and assembly process closure, excepting only the exogenous information inputs.

It may be necessary to iterate Tasks VI-1, VI-3, VI-4, and VI-5 to fully debug the NMW design and to successfully achieve the desired results.

[1085] Robert A. Freitas Jr., Ralph C. Merkle, Kinematic Self-Replicating Machines, Landes Bioscience, Georgetown, TX, 2004; Sections 5.1.9(L2) and 5.1.9(L4); http://www.MolecularAssembler.com/KSRM/5.1.9.L.htm.

[1086] Robert A. Freitas Jr., "Exploratory Design in Medical Nanotechnology: A Mechanical Artificial Red Cell," Artificial Cells, Blood Substitutes, and Immobil. Biotech. 26(1998):411-430; http://www.foresight.org/Nanomedicine/Respirocytes.html.

[1087] Robert A. Freitas Jr., "Microbivores: Artificial Mechanical Phagocytes using Digest and Discharge Protocol," J. Evol. Technol. 14(April 2005):1-52; http://www.jetpress.org/volume14/freitas.html.

3.8 Phase VII: Demonstrate Plate/Plate Exponential Manufacturing

Massive parallelization of the manufacturing process is required to achieve practical molecular manufacturing of macroscale quantities of atomically precise product.

The key objective of Phase VII is the design, manufacture, and operational demonstration of a second-generation nanoscale manufacturing workstation (NMW-2) that is capable of assembling an atomically exact working copy of itself on an opposing surface under full endogenous operation. This ability will then enable the massively parallel manufacture of additional NMW-2 molecular manufacturing modules in Phase VIII. Because the functioning of the NMW no longer depends on the slow Phase II system for any aspect of its functioning (Section 3.7.6), and because the NMW has already been redesigned to allow operation at a much higher 12-120 MHz control pulse frequency (Section 3.7.2), the operating frequency is increased from 1.2 MHz for the NMW to 12-120 MHz for the NMW-2 at the end of Phase VII (Section 3.8.8).

The NMW-2 is described in Section 3.8.1 and illustrated in Figure VII-1. This is followed by an enumeration of the specific tasks required to manufacture the NMW-2 which include: design and simulation of the NMW-2 for plate/plate replication (Section 3.8.2), preparation of a multielectrode assembly surface (Section 3.8.3), construction of a macroscale plate handling system to allow precise parallel positioning of two flat plate surfaces (Section 3.8.4), demonstration of plate/plate mechanical operations by NMW-2 units installed on two separate parallel plates (Section 3.8.5), demonstration of fully endogenous replication of the NMW-2 onto an opposing plate surface (Section 3.8.6), demonstration of a second successful endogenous double-replication of the two NMW-2 units after the plates have laterally shifted position (Section 3.8.7), and finally a re-demonstration of the previous three tasks when the system is operated so as to achieve tenfold higher productivity (Section 3.8.8).

3.8.1 Description of Plate/Plate Exponential Manufacturing with NMW-2

The structure and basic function of the second-generation nanoscale manufacturing workstation (NMW-2), operated using a plate/plate exponential manufacturing strategy (Section 2.1.2), is described in Section 3.8.1.1, followed by a discussion of the forces that may arise between closely juxtaposed plates (Section 3.8.1.2) and a summary of error rates and reliability issues in the operation of NMW-2 modules (Section 3.8.1.3).

3.8.1.1 Plate/Plate Exponential Manufacturing using NMW-2

The basic strategy of plate/plate exponential manufacturing has previously been described in Section 2.1.2. In the context of this proposal, the strategy involves bringing into close juxtaposition – but not physical contact – two parallel plates each containing electrode-rich silica assembly surfaces fabricated as previously described in Section 3.4.3. Specialized macroscale plate handling machines are constructed for this purpose (Section 3.8.4). The exponential manufacturing process begins with the construction of a single “seed” workstation on one of the two plates, which are then juxtaposed such that their atomically smooth assembly surfaces face each other and are actively maintained at a 220 nm separation distance.

Figure VII-1. Schematic illustration of the second-generation Nanoscale Manufacturing Workstation (NMW-2) module, showing four Stewart platform manipulators comprising the DMS fabrication machinery (NFW-2) adjacent to three Stewart platform manipulators comprising the nanocomponent assembly machinery (NAW) mounted on a foundation block adjacent to a 20-tip toolrack, surrounded by the Bulk Feedstock Supply System (BFSS) graphene storage tank (BFSS appurtenant structures not shown).

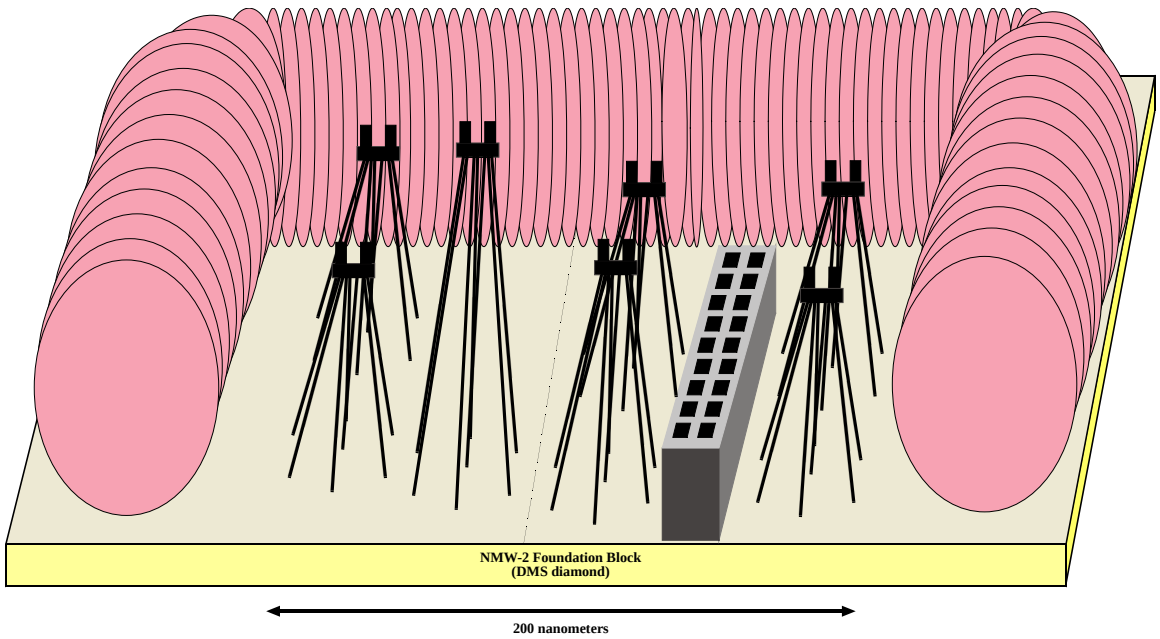

In the first production cycle, the seed workstation on one plate constructs its replica on the opposing second plate. The relative positions of the two plates are then shifted so that both copies lie adjacent to empty worksites, whereupon the original workstation and its replica each construct daughter replicas of themselves upon the empty worksites, resulting in a total of four workstations, two on each plate, at the end of the second production cycle, concluding the Phase VII effort. But this process may be repeated indefinitely (Figure VII-2) until all worksites on both plates are fully built out with replica workstations, thus achieving massively parallel exponential manufacturing using two plates (to be demonstrated in Phase VIII). Note that Task VI-5 already demonstrated the ability of an NMW to assemble a working replica on an adjacent ~100,000 nm^2 worksite on the assembly surface. But assembling 10^{11} copies in this manner (Phase VIII) would result in a too-slow non-exponential growth in the number of NMW units because interior units would become landlocked after a single replication cycle and because growth could occur only along the slowly expanding perimeter line, thus would require a prohibitively long ~10^5 production cycles (400-40,000 years) to populate the entire wafer in Phase VIII.

Figure VII-2. Schematic illustration of a succession of plate/plate replication cycles on a wafer, using the NMW-2 modules. Starting from a single NMW-2 module, eight NMW-2 modules have been manufactured after three plate/plate replication cycles are completed.

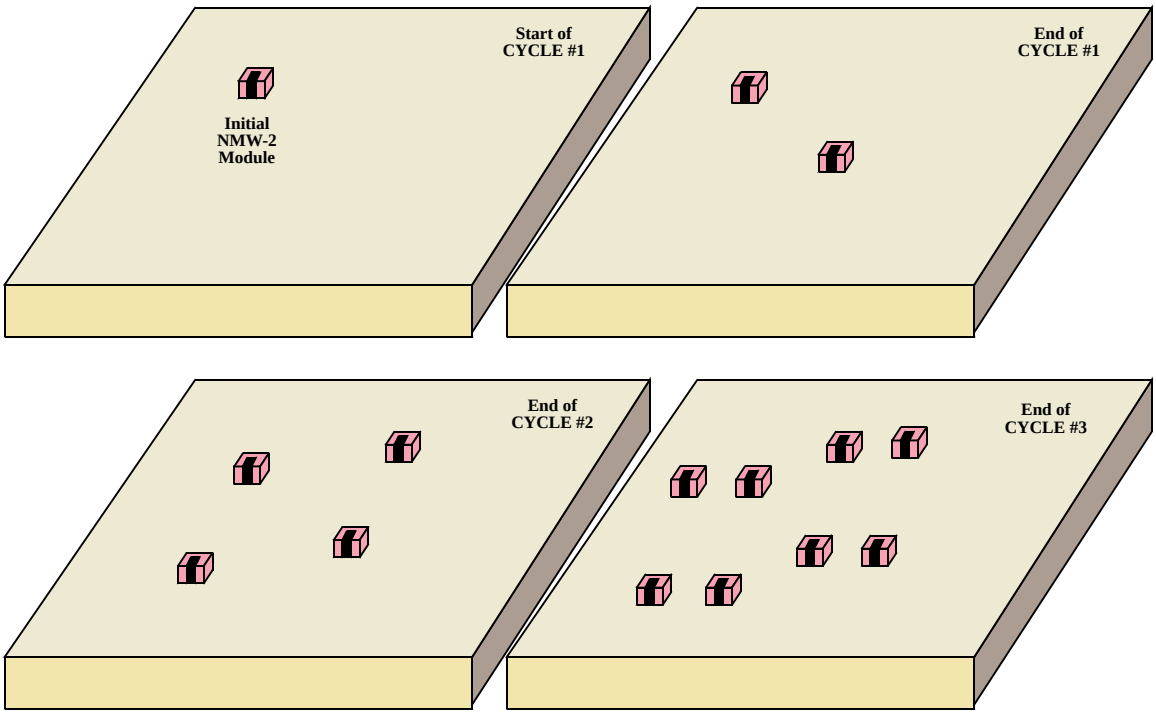

The NMW (Section 3.7.1) has cylindrical feedstock tanks that are 55 nm in radius or 110 nm in diameter, hence when two NMW units face each other on two opposing plates, the plate surfaces must be separated by at least 220 nm to avoid bringing the upper surfaces of the opposing tank surfaces into adhesive contact. The crane arm within the NAW subsystem of the NMW has a vertical reach of 200 nm (Section 3.6.1.1). Hence a crane arm that rests upon a 10 nm thick foundation block and holds a second 10 nm thick foundation block (by a gripping nub mounted on the large upper surface of the second block) must traverse only a 200 nm gap which lies within the work envelope of the crane arm. Other machinery to be installed by the crane arm on top of the foundation blocks on the opposing plate will require less that 200 nm clearance and thus also lie within the work envelope of the crane arm. Finally, the feedstock tanks (of the BFSS-2 subsystem) can be installed on the opposing plate surface with a clearance of only 100 nm (= 220 nm – 10 nm – 110 nm), which lies within the 68-200 nm work-reach envelope of the NAW crane arm (Section 3.6.1.1) and also within the 60-100 nm reach of the two assembly manipulators when the 10 nm thick tool chuck is included (Section 3.4.1.1), possibly allowing them to assist in tank installation.

Note that plate separation is a design choice and can be increased if necessary to provide larger clearances without major alterations to the NFW-2 design or wafer handling architecture. For example, an extra 20 nm of clearance between tank tops on opposing wafers is readily obtained by decreasing BFSS-2 tank diameter from 110 nm to 100 nm while increasing tank length from

660 nm to 868 nm (now wrapping 87% of perimeter, not 63%); this design change would also increase total NMW-2 atom count by 6,591,501 atoms (~5% of total) and increase the NMW-2 footprint on the wafer surface from 93,200 nm^2 to 107,400 nm^2.

The second-generation nanoscale manufacturing workstation (NMW-2) is essentially identical to the NMW, including using 100-electrode worksites, but with the assembly sequences redesigned to allow construction of product objects on an empty worksite on an opposing plate, rather than on an adjacent empty worksite on the same plate as described in Section 3.7.6. The control pulse frequency is also increased from 1.2 MHz to 12-120 MHz, as this capability has previously been incorporated into the NMW design (Section 3.7.2). Achieving this additional functionality may also require some structural design adjustments in the NMW to increase work envelopes of the manipulators, plate separation distance, tank size, and so forth, resulting in a slightly modified NMW-2 design. For the purposes of this scaling analysis the NFW-2 will be assumed to be identical in structure to the NMW, and also to contain 129,194,836 atoms (Table VI-1). The in-cycle productivity (ignoring pumpdown and plate changeout times) of the NFW-2 should scale the same as for the NMW (Section 3.7.1): an in-cycle ~95.7 atom/sec atom-assembly rate (using a ~1.2 MHz electrical control pulse rate) for complex atomically precise product objects (including the NMW-2 itself) and a serial NMW-2 replication time of 1.35 x 10^6 sec (~15.6 days), or an in-cycle ~9570 atom/sec atom-assembly rate and a serial NMW-2 replication time of 1.35 x 10^4 sec (~4 hours) using the fastest ~120 MHz electrical control pulse rate.

3.8.1.2 Van der Waals and Other Forces Between Plates

In vacuum environments, adhesion forces between two plates separated by ~100 nm or less are normally dominated by van der Waals interactions.[1088] For two parallel plates of equal interfacial area A_{plate} and uniform vertical separation z_{sep}, the van der Waals force is approximated[1089] by $F_{vdW} \sim H_{plate}A_{plate} / 24 \pi z_{sep}^3$, where H_{plate} is the Hamaker constant for the plate material (e.g., ~0 zJ for vacuum or dry air, 65 zJ for silicon dioxide, 260-275 zJ for silicon, 340 zJ for diamond, and 344 zJ for silver)[1090] and the Hamaker constant for two plates of different materials embedded in a dielectric medium is estimated as $H_{plate} \sim (H_{plate1}^{1/2} - H_{medium}^{1/2})(H_{plate2}^{1/2} - H_{medium}^{1/2})$. Hence the attractive pressure between two silica plates separated by z_{sep} = 220 nm in vacuum would be $F_{vdW} / A_{plate} \sim 0.081$ N/m^2 (~0.8 x 10^{-6} atm), and the pressure would only rise to 0.428 N/m^2 (~4 x 10^{-6} atm) between two plates dominated by diamond or silver surfacing. The attractive force changes by ±14% if plate separation is varied by ±10 nm around the 220 nm target separation distance (i.e., to ~0.071-0.093 N/m^2 in the silica/silica case). Note that the related Casimir force[1091] (the

---

[1088] Jacob N. Israelachvili, Intermolecular and Surface Forces, Second Edition, Academic Press, NY, 1992.

[1089] Kevin Kendall, "Adhesion: Molecules and Mechanics," Science 263(25 March 1994):1720-1725.

[1090] Robert A. Freitas Jr., Nanomedicine, Volume I: Basic Capabilities, Landes Bioscience, Georgetown, TX, 1999; Table 9.1, p. 276; http://www.nanomedicine.com/NMI/Tables/9.1.jpg.

[1091] H.B.G. Casimir, "On the attraction between two perfectly conducting plates," Proc. K. Ned. Akad. Wet. 60(1948):793-795.

retarded limit of the van der Waals force)[1092] between two perfectly conducting metal plates is given by $F_{casimir} = -\pi^2 \hbar c A_{plate} / 240 z_{sep}^4$, where $\hbar = h / 2\pi = 1.056 \times 10^{-34}$ J-sec (h = Planck's constant) and $c = 3 \times 10^8$ m/sec (speed of light); at $z_{sep} = 220$ nm, $F_{casimir}/A_{plate} = 0.55$ N/m^2 (~5 x 10^{-6} atm). Casimir forces act between metals, insulators and semiconductors.

Holding two plates perfectly parallel at submicron separations is experimentally challenging[1093] but has been accomplished by researchers seeking to make precise measurements of Casimir forces.[1094] For example, in one MEMS experiment at Bell Labs[1095] a 500-micron-square, 3.5-micron thick silicon plate was suspended $z_{sep} = 2000$ nm above and parallel to the surface of a silicon wafer (Figure VII-3A); the plate pivots like a seesaw on two rods, with electrodes embedded in the wafer able to measure a mere ~0.001 degree tilt (~6 x 10^{-6} radian) away from horizontal in the plate (a ~4 nm vertical movement at the plate edge) by the change in capacitance on either side of the tilting plate. Another experiment proposed by the same authors[1096] would employ a flat 40 micron diameter calcite disk suspended in vacuum above a flat barium titanate plate at a distance of $z_{sep} = 100$ nm which is calculated to produce a ~0.5 nN attractive force, corresponding to an interplate pressure of ~0.4 N/m^2 (~0.000004 atm). (A resistive torque of ±100 x 10^{-20} N-m is also predicted to arise between these two plates when they are rotated through π radians around a vertical axis, since these optically anisotropic (birefringent) materials are at lowest energy when their optical axes are aligned.)

[1092] E.M. Lifshitz, "The theory of molecular attractive forces between solids," Sov. Phys.-JETP 2(1 January 1956):73-83.

[1093] M.J. Sparnaay, "Attractive forces between flat plates," Nature 180(1957):334; M.J. Sparnaay, "Measurements of attractive forces between flat plates," Physica 24(1958):751-764.

[1094] Federico Capasso, Jeremy N. Munday, Davide Iannuzzi, H.B. Chan, "Casimir Forces and Quantum Electrodynamical Torques: Physics and Nanomechanics," IEEE Journal of Selected Topics in Quantum Electronics 13(2007):400; http://www.seas.harvard.edu/capasso/publications/Capasso_STJQE_13_400_2007.pdf. G. Bressi, G. Carugno, R. Onofrio, G. Ruoso, "Measurement of the Casimir force between Parallel Metallic Surfaces," Phys. Rev. Lett. 88(15 January 2002):041804; http://link.aps.org/abstract/PRL/v88/e041804 and http://arxiv.org/PS_cache/quant-ph/pdf/0203/0203002v1.pdf.

[1095] H.B. Chan,, V.A. Aksyuk, R.N. Kleinman, D.J. Bishop, F. Capasso, "Quantum mechanical actuation of microelectromechanical systems by the Casimir force," Science 291(2001):1941-1944; http://www.seas.harvard.edu/capasso/publications/Chan_Science_291_1941_2001.pdf; H.B. Chan, V.A. Aksyuk, R.N. Kleinman, D.J. Bishop, F. Capasso, "Nonlinear micromechanical Casimir oscillator," Phys. Rev. Lett. 87(2001):211801; http://www.seas.harvard.edu/capasso/publications/Chan_PRL_87_211801_2001.pdf See also: Eric Smalley, "Quantum effect moves machine," TRNmag.com, 14 February 2001; http://www.trnmag.com/Stories/021401/Quantum_effect_moves_machine_021401.html.

[1096] J.N. Munday, D. Iannuzzi, Y. Barash, F. Capasso, "Torque on birefringent plates induced by quantum fluctuations," Phys. Rev. A 71(2005):042102.
Jeremy N. Munday, Davide Iannuzzi, Yuri Barash, Federico Capasso, "Torque on birefringent plates induced by quantum fluctuations." Phys. Rev. A 71(2005):042102; http://www.seas.harvard.edu/capasso/publications/Munday_PRA_71_042102_2005.pdf.

Figure VII-3. (A) At left, MEMS-based (500 micron)^2 silicon plate suspended over silicon surface to measure Casimir force.[1097] (B) At right, two parallel plates (upper half of image) of size 1.9 cm × 1.2 mm are separated by 500-3000 nm to measure the Casimir force.[1098]

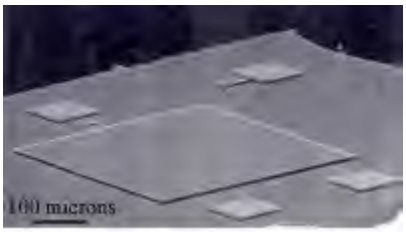

This half-millimeter-square plate pivots like a seesaw. The quantum-mechanical Casimir effect causes the end of the plate to tip up toward a sphere lowered to within 300 nanometers of the plate.

Source: Bell Labs

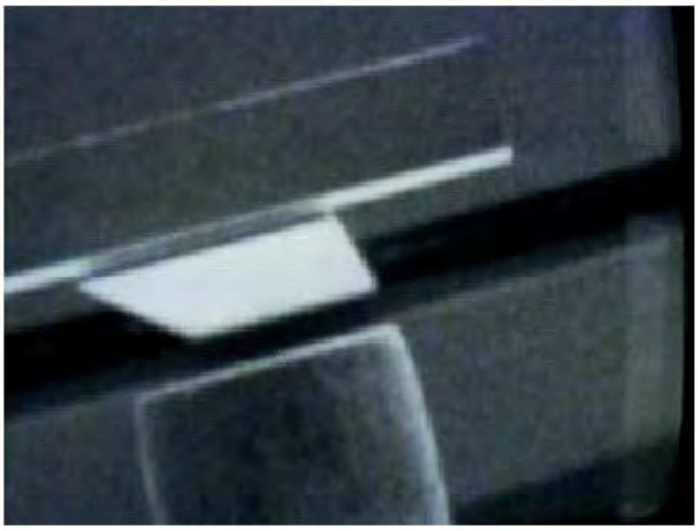

In another important experiment in 2001,[1099] the Casimir force was measured between two parallel plates separated by z_{sep} = 500-3000 nm (Figure VII-3B). A very large rectangular silicon cantilever of size 1.9 cm × 1.2 mm × 47 µm thick with optically flat (~10 nm roughness) surfaces covered with a 50 nm thick chromium layer was held 500-3000 nm distant from another Cr-coated silicon beam of size 1.9 cm × 1.2 mm × 500 µm thick. Using an ac bridge sensitivity of ~0.4 pF and a formula describing capacitance between non-parallel plates the authors could align the plates to a parallelism better than 30 nm over the 1.2 mm plate width, equivalent to an angular deviation of ~0.005 deg (~3 x 10^{-5} radians). Achieving only 0.1 nm divergence from parallelicity

---

[1097] H.B. Chan,, V.A. Aksyuk, R.N. Kleinman, D.J. Bishop, F. Capasso, "Quantum mechanical actuation of microelectromechanical systems by the Casimir force," Science 291(2001):1941-1944; http://www.seas.harvard.edu/capasso/publications/Chan_Science_291_1941_2001.pdf; H.B. Chan, V.A. Aksyuk, R.N. Kleinman, D.J. Bishop, F. Capasso, "Nonlinear micromechanical Casimir oscillator," Phys. Rev. Lett. 87(2001):211801; http://www.seas.harvard.edu/capasso/publications/Chan_PRL_87_211801_2001.pdf See also: Eric Smalley, "Quantum effect moves machine," TRNmag.com, 14 February 2001; http://www.trnmag.com/Stories/021401/Quantum_effect_moves_machine_021401.html.

[1098] G. Bressi, G. Carugno, R. Onofrio, G. Ruoso, "Measurement of the Casimir force between Parallel Metallic Surfaces," Phys. Rev. Lett. 88(15 January 2002):041804; http://link.aps.org/abstract/PRL/v88/e041804 and http://arxiv.org/PS_cache/quant-ph/pdf/0203/0203002v1.pdf.

[1099] G. Bressi, G. Carugno, R. Onofrio, G. Ruoso, "Measurement of the Casimir force between Parallel Metallic Surfaces," Phys. Rev. Lett. 88(15 January 2002):041804; http://link.aps.org/abstract/PRL/v88/e041804 and http://arxiv.org/PS_cache/quant-ph/pdf/0203/0203002v1.pdf.

across a 10 cm plate will require new techniques to obtain four orders of magnitude improvement (to ~10^{-9} radians) in the capability demonstrated in the 2001 experiment.

The theoretical Casimir force between two silicon plates[1100] increases slightly under UV irradiation because this generates free charge carriers inside the silicon.[1101] Corrugations,[1102] surface roughness[1103] and temperature[1104] in opposed surfaces inject additional complexities into the calculation of plate/plate forces. (Thermal fluctuations also produce radiation pressure and can increase the measured Casimir force than expected – e.g., the force between two plane mirrors 7 microns apart is twice as large at room temperature than at absolute zero – though thermal fluctuations at room temperature are only important at plate separations >1 micron, below which the wavelength of the fluctuations is too large to fit inside the cavity.[1105])

A complete calculation of the van der Waals forces between opposed plates is beyond the scope of the present analysis but several key design requirements for the macroscale plate handling system (Section 3.8.4) must be addressed:

(1) **Tilted plate surfaces.** The two opposed plates may be tilted relative to each other. The plate handling mechanism (Section 3.8.4) should measure and adjust plate separation to eliminate this positioning error.

(2) **Unflat plate surfaces.** A clean vacuum environment should allow the production of detritus-free atomically flat plates. Plates can be manufactured atomically flat using ALE processes (Section 3.4.3), and such processes regularly produce flat surfaces over very large areas, e.g., on 5 cm x 5 cm glass (silica) or silicon substrates.[1106] Changes in overall plate

---

[1100] G.L. Klimchitskaya, U. Mohideen, V.M. Mostepanenko, "Pulsating Casimir force," J. Phys. A: Math. Theor. 40(24 August 2007):F841-F847..

[1101] Norio Inui, "Change in the Casimir force between semiconductive bodies by irradiation," J. Phys.: Conf. Ser. 89(2007):012018; http://www.iop.org/EJ/abstract/1742-6596/89/1/012018.

[1102] R. Buscher, T. Emig, "Geometry and spectrum of Casimir forces," Phys. Rev. Lett. 94(2005):133901.

[1103] A. Gusso, G.J. Delben, "Influence of the Casimir force on the pull-in parameters of silicon based electrostatic torsional actuators," Sensors and Actuators A 135(15 April 2007):792-800; http://linkinghub.elsevier.com/retrieve/pii/S0924424706005693.

[1104] A. Gusso, G.J. Delben, "Influence of the Casimir force on the pull-in parameters of silicon based electrostatic torsional actuators," Sensors and Actuators A 135(15 April 2007):792-800; http://linkinghub.elsevier.com/retrieve/pii/S0924424706005693. V.S Bentsen, R. Herikstad, S. Skriudalen, I. Brevik, J.S. Høye, "Calculation of the Casimir force between similar and dissimilar metal plates at finite temperature," J. Phys. A: Math. Gen. 38(2005):9575-9588. C. Genet, A. Lambrecht, S. Reynaud, "Temperature dependence of the Casimir force between metallic mirrors," Phys. Rev. A 62(2000):012110; http://link.aps.org/abstract/PRA/v62/e012110.

[1105] "Understanding the Casimir force," Physics World, 1 September 2002; http://physicsworld.com/cws/article/print/9747.

[1106] Antti Niskanen, Radical Enhanced Atomic Layer Deposition of Metals and Oxides, Academic Dissertation, Helsinki, 2006; https://oa.doria.fi/dspace/bitstream/10024/2729/1/radicale.pdf. See also: A.

temperature or variation in plate temperature between opposite sides of a plate can cause differential thermal expansion or contraction and also distort the plate geometry (Section 3.4.1.2).

(3) **Nonuniform distribution of machinery on plate surface.** As the NMW and related machinery are built on each plate surface, the machinery will present an uneven distribution of high spots and low spots to the opposing plate (which has similar irregularities) and these must be accounted for in the mutual force calculation.

(4) **Time varying distribution of objects on plate surfaces.** As NMW and related machinery are built out across a plate surface, the geometry of the surface irregularities shifts with time. On a shorter time scale, the surface irregularities also vary as manipulator arms are extended and retracted, changing the attractive forces between the plates.

(5) **Plate flexing due to mechanical operations.** Interplate mechanical operations involving NMW manipulators on one plate reaching across to an opposing plate and applying mechanical forces to it could cause both plates to flex away each other and from the desired position. A crane manipulator on a ~10^5 nm^2 NMW worksite that applies a point force of 10 nN that is distributed across a similar ~10^5 nm^2 NMW footprint on the opposing plate is applying a ~10^5 N/m^2 (~1 atm) pressure to the opposing plate. However, the mean elapsed time between plate/plate assembly operations by crane manipulators is approximated by the serial NMW manufacturing time of 1.35 x 10^6 sec (Section 3.7.6) divided by the ~508 assemblable components comprising an NMW (Section 3.7.5) on the opposite plate, or ~2657 sec/operation, but each plate/plate assembly operation actually requires only ~0.01 sec at the ~100 Hz parts assembly rate (Section 3.6.1.3), giving a mean duty cycle of (0.01 sec / 2657 sec) ~ 4 x 10^{-6}, reducing the instantaneous pressure applied across the entire opposed plate to just ~4 x 10^{-6} atm.

This subjects each plate to an oscillating pressure load which may cause each wall to bow out of plane. Each plate may be analyzed mechanically[1107] by analogy to a rectangular 1.5:1 clamped plate[1108] or to a >2:1 clamped strip plate.[1109] The maximum out-of-plane deflection at the center of a rectangular plate of shortest edge L_{plate}, thickness h_{plate}, and Young's modulus E_{plate}, when clamped on all four sides and loaded by uniform normal pressure ΔP_{plate}, is given by $\delta_{plate} = k_{plate} (\Delta P_{plate} L_{plate}^4 / E_{plate} h_{plate}^3)$, where k_{plate} is a constant of order ~0.1.[1110] The worst deflection

---

Niskanen, T. Hatanpää, K. Arstila, M. Leskelä, M. Ritala, "Radical Enhanced Atomic Layer Deposition of Metallic Silver Films," submitted to Mater. Chem. 2006.

[1107] Stephen P. Timoshenko, Theory of Plates and Shells, McGraw-Hill/United Engineering Trustees, New York, 1940; Ansel C. Ugural, Stresses in Plates and Shells, Second Edition, McGraw-Hill Higher Education, New York, 1998.

[1108] Samuel Levy, Samuel Greenman, "Bending with large deflection of a clamped rectangular plate with length-width ratio of 1.5 under normal pressure," National Advisory Committee for Aeronautics (NACA), Washington DC, Technical Note 853, 1942; http://naca.larc.nasa.gov/reports/1942/naca-tn-853/.

[1109] Prof. Dr.-Ing. Kai-Uwe Bletzinger, "Theory of Plates, Part II: Plates in bending," Lehrstuhl fur Statik, Technische Universitat Munchen, Lecture Notes, Winter Semester 2000/2001; http://www.statik.bauwesen.tu-muenchen.de/vorlesungen/plates.dir/plates_part2.pdf.

[1110] Prof. Dr.-Ing. Kai-Uwe Bletzinger, "Theory of Plates, Part II: Plates in bending," Lehrstuhl fur Statik, Technische Universitat Munchen, Lecture Notes, Winter Semester 2000/2001;

occurs in the very largest plate envisioned here, where L_{plate} = 10 cm and E_{plate} = 1.8 x 10^{11} N/m^2 for single-crystal silicon. Taking the net applied uniform pressure pulse as $\Delta P_{plate} \sim 4 \times 10^{-6}$ atm across the entire plate and allowing a maximum deflection of $\delta_{plate} \leq 0.1$ nm (~1 Å, the minimum positioning accuracy for assembly; Section 3.6.1.1), then $h_{plate} \geq 6.1$ mm which seems acceptable; for L_{plate} = 1 cm, $h_{plate} \geq 0.28$ mm.

(6) **Excitation of mechanical resonances due to mechanical operations.** Interplate mechanical operations involving numerous NMW manipulators on one plate reaching across to an opposing plate and applying mechanical forces to it, either in synchrony or in a regular repeating pattern (as where numerous NMWs are operated in gangs) could excite resonant vibrations in the plates or in NMW components present on the plate surfaces.

(7) **Suppression of electrostatics.** The opposing plates must be maintained in an uncharged state at all times. Plates that accumulate charge may experience mutual attractive or repulsive electrostatic forces; an NMW manipulator may experience unexpected forces if it accumulates charge and then approaches another charged object on the native or opposed plate surface; and charge buildup can lead to electrostatic discharge between components, causing electrical or mechanical damage.

3.8.1.3 Reliability of NMW-2 Operation

To simplify the designs in this proposal we have generally assumed the use of open-loop operations largely without sensor-driven feedback (Sections 3.2.1.6 and 3.4.1.3). This eliminates the need for sensors, conditional operations, repetition of unsuccessful operations, and clean-up strategies to deal with the undesired results of unsuccessful operations, but it also implies the need for low error rates to ensure high reliability of operation.

Any manufacturing process will have some characteristic error rate. The number of steps in the manufacture of a module will depend on the error rate that can be achieved. If a high error rate must be tolerated, module size must be small to insure an adequate yield. For example, ribosomes have an error rate of approximately 10^{-3}-10^{-4} for every amino acid in the protein that they fabricate.[1111] It is therefore not surprising that proteins usually have many fewer than 10,000 amino acids, which ensures that the manufactured proteins have a high probability of being exactly correct. This is a biological example of the general principle that the modules being constructed are typically small enough that they can be manufactured in good yield with a high probability of being error free.

---

http://www.statik.bauwesen.tu-muenchen.de/vorlesungen/plates.dir/plates_part2.pdf. Samuel Levy, Samuel Greenman, "Bending with large deflection of a clamped rectangular plate with length-width ratio of 1.5 under normal pressure," National Advisory Committee for Aeronautics (NACA), Washington DC, Technical Note 853, 1942; http://naca.larc.nasa.gov/reports/1942/naca-tn-853/.

[1111] J.D. Watson, N.H. Hopkins, J.W. Roberts, J.A. Steitz, A.M. Weiner, Molecular Biology of the Gene, Fourth Edition, Benjamin/Cummings, Menlo Park, CA, 1987.

If the error rate can be made small, then larger module sizes can be used while maintaining a satisfactory yield. Experience in manufacturing suggests that driving error rates to the lowest feasible value is usually the best approach. It simplifies the manufacturing process and increases the yield of correct parts.

Some errors are due to environmental conditions that have nothing to do with the operation of the machine. For example, without impractical masses of shielding radiation induced errors cannot be avoided in small systems that are exposed to ordinary conditions found on the surface of the Earth. This sets a lower bound on error rates. For instance, early studies[1112] of radiation-induced enzyme inactivation found that ~1.06 x 10^{-17} J of absorbed radiation was required to produce one inactivating hit, yielding a failure condition of $\kappa_{fail} \sim 10^{15}$ hits/kg-rad. Conservatively assuming[1113] a rather high value for background photonic and particulate radiation of $I_{rad} \sim 0.5$ rad/yr, the mean time τ_{rad} between radiation-disabling hits on a 129,194,836-atom NMW-2 unit of mass $m_{target} = 2 \times 10^{-18}$ kg (Section 3.7.1) is $\tau_{rad} \sim (\kappa_{fail}\, m_{target}\, I_{rad})^{-1} \sim 1000$ years or a mean failure rate of ~3 x 10^{-11} sec^{-1} of NMW-2 operation (conservatively assuming that one such hit will cause the NMW-2 to fail with 100% certainty). At the original ~1.2 MHz electrical control pulse rate, NMW-2 replication time is 1.35 x 10^6 sec (Section 3.8.1.1), giving an NMW-2 radiation-induced error rate of $\varepsilon \sim (3 \times 10^{-11}\ sec^{-1})(1.35 \times 10^6\ sec) \sim 10^{-5}$; at the accelerated ~120 MHz electrical control pulse rate introduced in Task VII-7 (Section 3.8.8), NMW-2 replication time is reduced to 1.35 x 10^4 sec (Section 3.8.1.1), giving an NMW-2 radiation-induced error rate of $\varepsilon \sim (3 \times 10^{-11}\ sec^{-1})(1.35 \times 10^4\ sec) \sim$ **10^{-7}**.

Gamma ray hits on the BFSS may induce polymerization events at a ~tenfold lower rate up to ~3 x 10^{-12} sec^{-1} of BFSS operation (Section 3.5.1.3). Other error mechanisms are a function of one or more environmental variables that can be controlled, and therefore can be reduced in magnitude below the error rates induced by radiation. For example, photochemical damage can be avoided by operating the system only in darkness. Intel recently received a patent[1114] for the idea of building cosmic ray detectors into every semiconductor chip to correct radiation-induced errors.

Other errors depend on the particular nanosystem design and its mode of mechanical operation. In the case of the NMW-2, during one replication cycle the unit undergoes ~10^{12} control pulse cycles. In each cycle, an electrical pulse may be transmitted over one or all of 100 control lines, giving a maximum possible number of ~10^{14} electrical control pulses needed to complete a single replication cycle of the NMW-2 unit. This gives rise to two main sources of error.

[1112] G.R. Kepner, R.I. Macey, "Membrane enzyme systems: Molecular size determination from radiation inactivation," Biochim. Biophys. Acta 163(1968):188-203.

[1113] K. Eric Drexler, Nanosystems: Molecular Machinery, Manufacturing, and Computation, John Wiley & Sons, New York, 1992, Section 6.6 "Radiation Damage," pp. 154-156.

[1114] "Should every computer chip have a cosmic ray detector?" NewScientist blog, 7 March 2008, http://www.newscientist.com/blog/technology/2008/03/do-we-need-cosmic-ray-alerts-for.html. See Intel patent at: http://patft.uspto.gov/netacgi/nph-Parser?Sect1=PTO1&Sect2=HITOFF&d=PALL&p=1&u=%2Fnetahtml%2FPTO%2Fsrchnum.htm&r=1&f=G&l=50&s1=7,309,866.PN.&OS=PN/7,309,866&RS=PN/7,309,866.

First, the $\leq 10^{14}$ control signals must be electronically generated by an external control computer with 100% accuracy, to be transmitted into the NMW-2 unit. Such levels of accuracy are readily achieved in modern computer systems. For instance, although possible variability in CPU program execution has been noted,[1115] a ~1 GHz CPU comprised of tens of millions of transistors can quite reasonably normally operate for a week or longer with no errors – an implied error rate of 10^{-21} sec^{-1} or less than one error in 10^{21} switching operations (assuming each transistor switches 10% of the time), which – if this can be achieved in our nanomechanical manufacturing system – would give an error rate per NMW-2 replication cycle of ~**10^{-7}**. Digital computing has provided six decades of ongoing experience with a requirement for perfect performance of long sequences of data-based operations. Noted von Neumann[1116] in a 1948 lecture: "I am not aware of any other field of human effort where the result really depends on a sequence of a billion (10^9) steps in any artifact, and where, furthermore, it has the characteristic that every step actually matters – or, at least, may matter with a considerable probability. Yet, precisely this is true for computing machines – this is their most specific and most difficult characteristic."

Second, the $\leq 10^{14}$ mechanical operations (almost exclusively: single steps of an electrostatic rotary stepper motor; Section 3.4.1.1) that are actuated by receipt of the $\leq 10^{14}$ control signals during a single NMW-2 replication cycle must also be 100% fault-free. Here again there is solid evidence that such levels of reliability are readily achievable in microscopic mechanical systems. In 1998, Douglass and Sontheimer of Texas Instruments reported[1117] the results of an ongoing series of performance tests on the Digital Micromirror Device (DMD) – an all-digital chip-mounted ~1 cm^2 projection display consisting of an array of >500,000 square micromirrors each measuring 16 microns on an edge. The receipt of an electrical control pulse actuates an individual micromirror, causing it to twist through $\pm 10^o$ of angle and allowing the tilted surface to reflect colored light onto a screen. The performance test on a small number of DMD units cycled all mirrors on and off at 50 KHz, ten times the normal rate, eventually accumulating a total of 2×10^{18} mechanical mirror switching cycles without failure while showing no evidence of hinge fatigue. This is a demonstrated micromechanical actuation error rate of $<5 \times 10^{-19}$ for the individual MEMS actuators, the equivalent of an error rate per NMW-2 replication cycle of $\sim 5 \times 10^{-5}$.

For very small cost in number of atoms (Section 3.4.1.3) and additional assembly surface electrodes we could add one or more sensors to the NMW-2 design to provide self-correcting

---

[1115] Hugues Berry, Daniel Gracia Pérez, Olivier Temam, "Chaos in computer performance," 14 December 2005, http://arxiv.org/abs/nlin/0506030v2.

[1116] John von Neumann, "The general and logical theory of automata," in L.A. Jeffress, ed., Cerebral Mechanisms in Behavior – The Hixon Symposium, John Wiley & Sons, New York, 1951, pp. 1-31. See also in A.H. Taub, ed., John von Neumann: Collected Works, Volume V: Design of Computers, Theory of Automata and Numerical Analysis, Pergamon Press, New York, 1963, pp. 288-329. (Slightly edited version of von Neumann's paper that was read at the Hixon Symposium on 20 September 1948 in Pasadena, California.)

[1117] Mike Douglass, Andrew Sontheimer, "Identifying and eliminating Digital Light Processing failure modes through accelerated stress testing," TI Technical Journal (July-September 1998):128-136; http://www.bbe-group.com/plus/titj14.pdf or http://www.dlp.com/dlp/resources/whitepapers/pdf/titj14.pdf.

feedback for the manipulators. This might increase NMW-2 error tolerance by 3-5 orders of magnitude to 10^{-10}-10^{-12} per replication cycle – e.g., in mechanical hard drives, the recovered read error rate is typically 10^{-9}, compared to a 10^{-12} error rate for recovery after multiple reads with full error correction and 10^{-14} for unrecoverable read errors even with full error correction[1118] – again, a 3-5 orders-of-magnitude improvement using error recovery. (The data miscorrection rate[1119] for mechanical disk drives is ~10^{-21}.) In view of the above, we shall assume that a mechanical/control error rate of ~**10^{-7}** per replication cycle (equivalent to a ~10^{-21} error rate for mechanical actuation operations) is achievable for the NMW-2.

The DMS-related error rate must also be accounted for. Since the operation of the NMW-2 is virtually identical to that of the NMW (except that a replica is assembled on an opposing plate surface, rather than at an adjacent site on the same plate), the DMS-related reliability estimates are substantially the same as previously given for NMW (Section 3.7.1.4). In order to complete a single replication cycle, the NMW-2 Phase VII system must correctly execute (129,194,836 atoms)(6 operations/atom) ~ 775 million mechanosynthetic operations. There is a DMS reaction error rate of $\varepsilon \sim 1$ per replication cycle below $T_\varepsilon \sim (-(k_B / 0.40\ \text{eV}) \ln(\varepsilon / 775 \times 10^6))^{-1} \sim 227$ K, ~10^{-2} near dry-ice temperature at ~185 K, ~10^{-3} at 170 K (the lowest temperature permitting gaseous feedstock operation), ~10^{-7} at 127 K, ~6.4×10^{-9} at 118 K, or $\varepsilon \sim 2.5 \times 10^{-10}$ at 109 K (the lowest temperature permitting liquid feedstock operation) for a ~129×10^6-atom product object fabricated using the original set of DMS reactions.[1120] For standalone operation, an operating temperature of $T_\varepsilon \sim 170$-185 K seems adequate and allows gaseous feedstock operation of the NMW-2. However, a lower operating temperature will be required to achieve a ~10^{-7} DMS-related error rate (or better) similar to the ~10^{-7} mechanical/control error rate estimated above. Such a lower operating temperature will in turn require switching to liquid feedstock operation for NMW-2 wafer operations during plate/plate replication. This can be accomplished by loading the BFSS with gaseous feedstock at higher temperature, then operating the NMW-2 at a lower temperature using feedstock gases that have now liquefied in the tank. (Detailed simulations and design work are needed to determine if a minor BFSS tank redesign will be required to maintain a continuous feedstock molecule supply to the sorting rotors.) Operating the NMW-2 in this manner at $T_\varepsilon = 109$-127 K holds the DMS-related error rate to the desired $\varepsilon \sim$ **10^{-10}-10^{-7}** level. Note that compressed ethylene remains in liquid form up to 1000 atm (the highest pressure encountered inside the BFSS tank) at ~118 K or warmer (below which temperature it solidifies; Figure IV-2), and up to 400 atm (the starting fill pressure of the BFSS; Section 3.5.1.6) at ~109 K or warmer. Operating the BFSS at 118 K or warmer ensures that conditions are unlikely to arise in which ethylene can solidify inside the tank; further study is required to determine if the BFSS can be operated all the way down to 109 K.

[1118] Charles M. Kozierok, "Read Error Severities and Error Management Logic," The PC Guide, Reference Guide – Hard Disk Drives, 1997-2000; http://www.storagereview.com/guide2000/ref/hdd/geom/errorRead.html.

[1119] Charles M. Kozierok, "Read Error Severities and Error Management Logic," The PC Guide, Reference Guide – Hard Disk Drives, 1997-2000; http://www.storagereview.com/guide2000/ref/hdd/geom/errorRead.html.

[1120] Robert A. Freitas Jr., Ralph C. Merkle, "A Minimal Toolset for Positional Diamond Mechanosynthesis," J. Comput. Theor. Nanosci. 5(May 2008):760-861.

Another major source of error is radical poisoning by contaminants in an imperfect UHV environment. At a target serial atom-assembly rate of ~10,000 atoms/sec for the accelerated Phase VII system after the completion of Task VII-7 (Section 3.8.8), the original ~129 x 10^6-atom NMW-2 will require t_{fab} ~ 1.29 x 10^4 sec (~4 hours) to fabricate the ~129 x 10^6-atom NMW-2 replica. Assuming that a radical site susceptible to poisoning is exposed to the imperfect UHV environment for a fraction f_{vac} ~ 50% of the time, then the maximum tolerable UHV pressure that will permit all nanoparts for one defect-free ~129 x 10^6-atom NMW-2 replica to be fabricated is $P_{UHV} \leq (N_{encounters}\ T / n_{contam}\ A_{radical}\ f_{vac}\ t_{fab})\ (\pi\ MW_{kg} / 2\ k_B T\ N_A)^{1/2}$ ~ 2 x 10^{-12} atm, where n_{contam} = 7.34 x 10^{27} molecules-K/m^3-atm (= N_A/R_{gas}) for ideal gas (contaminant) molecules and T = 127 K, with the other quantities as previously defined in Section 3.2.1.7. If H_2 contaminant is determined not to be a serious radical poisoning risk or can be rigorously excluded from the workspace, then taking MW_{kg} = 0.014 kg/mole for N_2 raises the required P_{UHV} by a factor of ~2.6, yielding $P_{UHV} \leq 5 \times 10^{-12}$. If any workpiece having one or more erroneous atom placements is considered defective, then in a UHV environment maintained at ~10^{-18} atm (~100,000 contaminant molecules present in a 5-liter UHV work volume; currently achievable experimentally (Section 3.2.1.7) but a hundredfold better than assumed in previous Phases) the radical-poisoning defect rate at 127 K will fall to **~10^{-7}** for a replica NMW-2 product object.

Taking a total error rate of **~10^{-7}** per replication cycle from all sources for NMW-2 operation at the 120 MHz pulse rate (Section 3.8.8) and T = 127 K, then on average ~10^4 NMW-2 units on a built-out wafer (Section 3.9.1) containing 10^{11} NMW-2 units will experience a single error during a single whole-wafer replication cycle. Since each NMW-2 replica consists of ~129,194,836 atoms, the ~10^{-7} error rate per replication cycle is equivalent to a net per-atom error rate of **~10^{-15}** for DMS-based molecular manufacturing at T = 127 K.

3.8.2 Task VII-1: Redesign/Simulate NMW for Plate/Plate Replication

Task VII-1 is to design and simulate the second-generation workstation (NMW-2), specifying all component nanoparts and nanodevices (assemblies of nanoparts) and also specifying all fabrication and assembly processes that will be required to complete the manufacturing operations of: (1) nanopart fabrication, (2) nanodevice assembly from nanoparts, (3) NMW-2 assembly from nanoparts and nanodevices, and (4) to verify correct NMW-2 operation, if properly assembled, up to a 120 MHz operating frequency. The NMW-2 is essentially identical to the NMW (Section 3.7.6), but with the assembly sequences redesigned to allow the workstation to construct product objects on an empty worksite on an opposing plate, rather than on an adjacent empty worksite on the same plate. This may require some slight structural design adjustments in the NMW to increase work envelopes of the manipulators, plate separation distance, or tank size, but for the purposes of this scaling analysis the NMW-2 is assumed to be identical in structure to the NMW, also containing 129,194,836 atoms (Table VI-1).

As already noted in Section 3.7.2, design and simulation of the typical NMW-2 nanopart will require at minimum a molecular mechanics / molecular dynamics (MM/MD) level analysis of a nanopart having ~79,446 atoms/nanopart (Table VI-1) for nontank nanoparts. Such modeling and simulation could be performed using the NanoEngineer-1 software package that was available in 2007, running on a personal computer available in 2008. The typical NMW-2 nanodevice consists of 2-4 nanoparts (Table III-1 and Table V-1), increasing the simulation software capacity requirement to 159,000-318,000 atoms/nanodevice for basic modeling and validation of proper operation of nanodevices. Following Moore's Law assuming an 18-month doubling time and conservatively assuming traditional ~N_{atom}^2 scaling with atom count for MM/MD algorithms, a

318,000-atom nanodevice could be simulated using NanoEngineer-1 on a single commonplace personal computer that would be available in 2015, or on a 40-CPU computer cluster that might be available in 2008. Additional software and computing capacity will need to be acquired to simulate these nanodevices, or if higher levels of analysis (i.e., semi-empirical or density-functional (DFT) levels of theory) are deemed necessary for these nanoparts and nanodevices. MM/MD modeling and simulation of the entire 129,194,836-atom NMW-2 at the full atomistic level is well beyond the current ability of NanoEngineer-1 executing on a desktop PC or on a small computer cluster and will require specialized software running on highly parallel supercomputers as described earlier in Section 3.4.2.

An important part of the NMW-2 design process will be the modeling and simulation of plate/plate exponential manufacturing, which may include simulations of the wafer surfaces, the NMW-surface interactions, and plate shifting operations – not just the internal workings of the NMW-2 nanomachinery alone. A typical simulation might include two 129,194,836-atom NMW-2 units each resting on a ~10^5 nm^2 surface having ~1.5 x 10^7 silicon and silver atoms and ~4 x 10^6 passivating O atoms for a 1 nm thick simulated slab of silica assembly surface, giving a total of 294,389,672 atoms for two empty NMW-2 units or 881,198,638 atoms for two feedstock-charged NMW-2 units. As noted in Section 3.4.2, by 2015 we could see practical supercomputer-based Lennard-Jones MD simulations up to 10 trillion atoms, classical MD simulations up to 100 billion atoms, semiempirical AIMD up to 10 billion atoms, and DFT-based AIMD up to 1 billion atoms using 10 petaflop computing machines. This will allow nanoengineers at the research forefront to undertake high-quality AIMD simulations of a complete two-plate NMW-2 replication cycle to validate the lack of pathological mechanochemical interactions between major system components, and classical MD or Lennard-Jones MD simulations for all major mechanical interactions in the two-plate system.

Employing the same estimation method as described in Section 3.4.2, we benchmark the computational requirement using a more modest cluster of 1024 Cray T3E processors that were used to perform a ~1 billion atom MD simulation (similar in size to the 881,198,638-atom two-plate NMW-2 system) in the year 2000, requiring 26.4 sec for a single time step of the simulation.[1121] Applying Moore's Law assuming an 18-month doubling time in capability, by 2018 (12 doubling times from 2000) an upgraded equivalent computing resource could calculate each time step 4096 times faster, yielding ~13 million MM/MD time steps per day (~13 nanosec of operating time per day of cluster computing, assuming 1 fs time steps) or ~0.4 microsecond of actual two-plate NMW-2 operating time per month of cluster computing time.

Design, modeling and simulation of all major fabrication and assembly processes can also be undertaken using mixed-model techniques in which noncritical atoms are modeled using MM and a much smaller number of critical atoms (presumably those in apposition or contact, or directly covalently bonded to such atoms) using DFT, giving a MM/DFT mixed model, for testing crucial moments of various fabrication and assembly sequences. An even more simplified continuum model for bulk atoms combined with MM for interfacial (and related) atoms may allow

---

[1121] Aiichiro Nakano, Martina E. Bachlechner, Rajiv K. Kalia, Elefterios Lidorikis, Priya Vashishta, George Z. Voyiadjis, Timothy J. Campbell, Shuji Ogata, Fuyuki Shimojo, "Multiscale Simulation of Nanosystems," Computing in Science & Engineering 3(July/August 2001):56-66.

simulation of the entire sequence of NFW fabrication and assembly, and simulation and validation of all NFW operations needed to fabricate all of its own parts.

At this point it would also be useful to begin the following important additional theoretical studies in advance of actual nanofactory design, which are intended to carry through the next several phases in anticipation of need in Phase X:

(a) a design analysis of the utility of, and requirements for, incorporating various levels of redundancy into massively parallel manufacturing systems;

(b) the design of control systems for parallel-operated billion-workstation parts assembly arrays, including implementation of positionally controlled actuation systems;

(c) an analysis of the reliability and error rates in large parts assembly systems, including studies of fault tolerant design for massively parallel manufacturing systems;

(d) development of simulation software for massively parallel manufacturing systems, including software capable of multilevel integrated simulations of major subsystems and systems of nanofactories; and

(e) the development of workflow planning software for massively parallel assembly systems.

3.8.3 Task VII-2: Prepare Multielectrode Assembly Surfaces

Task VII-2 is to prepare a number of atomically flat surfaces upon which NMW-2 units can be physically constructed and debugged. Electrical power and control signals are applied to NMW-2 mechanisms via carbon nanotube wires that connect conductive silver terminals on the atomically smooth assembly surface to electrostatic motors that actuate the manipulators. Nanotube wires from the NMW-2 are joined to the ~100 silver electrodes per NMW-2 worksite by simple van der Waals attraction, or if this is insufficient then by nanotube impalement of the softer metal, by e-beam spot welding,[1122] by using designed mateable connectors, or by other means. Each NMW-2 assembly surface is a single-crystal silicon wafer with silicon dioxide top layers and may include up to 100-1000 worksites each of area ~100,000 nm^2 (e.g., a ~420 nm x ~240 nm rectangular footprint; Section 3.7.1) which should be a sufficient number for experimentation and testing, as described earlier in Section 3.4.3, probably requiring a total scan time of 20-40 days using a single tip. Each wafer is a macroscale semiconductor wafer up to 10 cm x 10 cm in size that can be manipulated and precisely positioned using the plate handling system developed in Task VII-3 (Section 3.8.4), which most efficiently should be pursued in concert with Task VII-2.

Theoretical studies and simulations examining ways of accelerating the PALE processing of semiconductor assembly surfaces – especially by increasing the tip scanning rate and the number of processing tips involved – should continue, aiming toward actual implementation no later than Phase VIII.

[1122] MinFeng Yu, Mark J. Dyer, George D. Skidmore, Henry W. Rohrs, Xue Kun Lu, Kevin D. Ausman, James Von Ehr, Rodney S. Ruoff, "3 Dimensional Manipulation of Carbon Nanotubes under a Scanning Electron Microscope," paper presented at the Sixth Foresight Nanotechnology Conference, November 1998; see also: Robert F. Service, "AFMs Wield Parts for Nanoconstruction," Science 282(27 November 1998):1620-1621; and http://www.foresight.org/Conferences/MNT6/Papers/Yu/index.html.

3.8.4 Task VII-3: Build Plate Handler for Precise Parallel Positioning of Two Flat Plate Surfaces

Task VII-3 is to prepare design and build a plate handling system that can hold two atomically flat electrode-rich semiconductor wafer surfaces precisely parallel to each other at a uniform separation of ~220 microns with a variation of 1 Å or less in separation across the entire area. One design for such an apparatus might include two plateholders mounted on a very stiff rack and pinion positioner that could move the plates rapidly in coarse motion, coupled with a piezo-based fine positioning system for each plate that would allow either plate to be edge-tilted in ~0.5 Å increments to achieve ≤1 Å divergence from parallelicity across an (up to) 10 cm wide plate using an interferometric system to accurately measure the plate separation. Researchers have already demonstrated,[1123] almost a decade ago, the ability to align millimeter-scale plates to a parallelism better than 30 nm over the 1.2 mm plate width, equivalent to an angular deviation of ~0.005 deg (~3 x 10^{-5} radians) using relatively simple techniques.

It is almost certain that direct sensory feedback coupled with active flexure control will be required to maintain the plates at such a precise separation across an entire ~100 cm^2 wafer surface. Consequently, the NMW plus the Phase II system (used as an assembly device) should be employed to build sensor crane arms on the NMW-2 wafer. Sensor crane arms will have a simple force-measuring deflection sensor at their tips (Section 3.4.1.3). These arms will be used to reach out and touch the opposing wafer plate as it approaches, continuously reporting back to the operating system the exact plate/plate separation distance at its position on the wafer. Sensor cranes may be located at 1-3 cm intervals across the wafer in a square grid pattern, hence there are 10-100 of them across the face of a 10 cm x 10 cm wafer surface. Each sensor crane occupies its own special multielectrode worksite. An array of 10-20 piezopositioners could be attached to the side of the plateholder rack opposite the face to which the wafer is attached, allowing the piezos to apply minute corrective forces to the backside of the wafer which are driven by sensory feedback from the field of sensor cranes. Thus the wafer surface may be flexed in real time in response to actual measurements of the plate/plate separation at up to 100 sample points across the surface of the wafer, helping to maintain the required ≤1 Å divergence from parallelicity.

It is worth noting that an analogous method is already used to maintain perfect parabolic shapes in the deformable optical mirrors of very large astronomical telescopes such as the 8-10 meter VLT and Keck optical telescopes. In astronomical systems, one common technology is to bond a thin deformable mirror faceplate to an array of piezoelectric actuators (Figure VII-4A), yielding a large macroscale deformable mirror (Figure VII-4C). Another approach is the bimorph mirror which consists of two piezoelectric wafers bonded together and oppositely polarized with an array of electrodes deposited between the two wafers and with the front surface acting as a mirror – when a voltage is applied to an electrode, one wafer contracts and the opposite wafer expands, producing a localized bending (Figure VII-4B).

[1123] G. Bressi, G. Carugno, R. Onofrio, G. Ruoso, "Measurement of the Casimir force between Parallel Metallic Surfaces," Phys. Rev. Lett. 88(15 January 2002):041804; http://link.aps.org/abstract/PRL/v88/e041804 and http://arxiv.org/PS_cache/quant-ph/pdf/0203/0203002v1.pdf.

Figure VII-4. (A) At top left, schematic of a thin mirror faceplate bonded to an array of piezoelectric actuators.[1124] (B) At top right, schematic of a bimorph curvature mirror consisting of two oppositely polarized piezoelectric wafers bonded together with an array of electrodes deposited between the two wafers to induce localized bending.[1125] (C) Below, front and back images of a deformable mirror used in astronomical applications, manufactured by Xinetics.[1126]

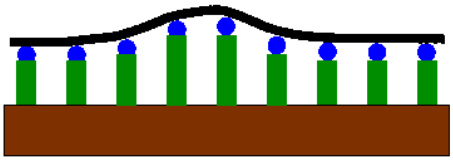

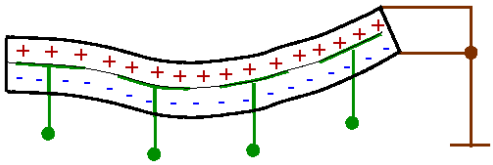

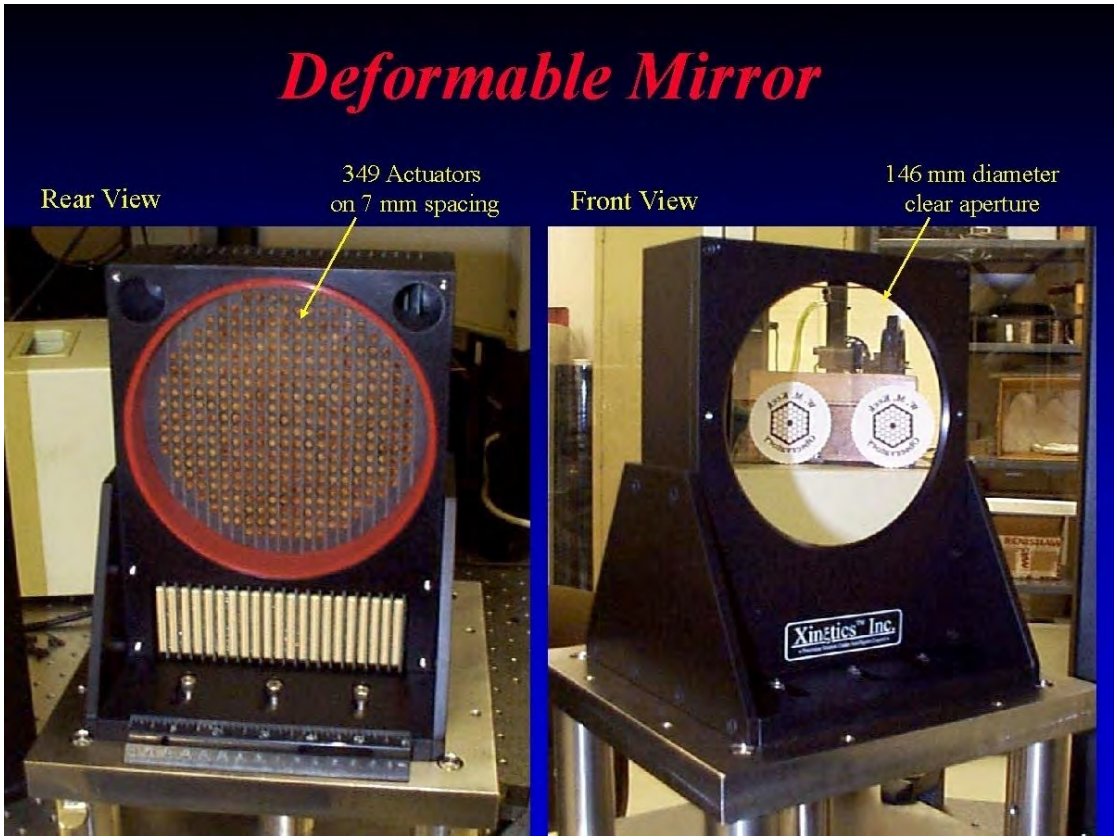

[1124] "Adaptive optics tutorial at CTIO. Correcting the turbulence: Deformable Mirrors," accessed January 2008; http://www.ctio.noao.edu/~atokovin/tutorial/part2/dm.html.

[1125] "Adaptive optics tutorial at CTIO. Correcting the turbulence: Deformable Mirrors," accessed January 2008; http://www.ctio.noao.edu/~atokovin/tutorial/part2/dm.html.

[1126] Xinetics Deformable Mirror; http://www.tiac.net/users/xinetics/Mirrors.html.

Adaptive optics systems are also used for optical wavefront control in MEMS-based deformable mirrors for communications applications (Figure VII-5), in which, for example, a ~1 cm^2 mirror membrane is supported by an underlying 1024-actuator array with each actuator in the array able to be individually deflected 1.5 microns by electrostatic actuation to achieve the desired pattern of deformation.[1127] Although each crane arm manipulator has ~32,775,231 atoms (Table V-2), we will assume that a sensor crane (which requires significantly less functionality than a 6-DOF assembly manipulator) can be designed using only ~10,000,000 atoms, hence 10 sensor crane arms may be manufactured in a single 129,194,836-atom (Table VI-1) production cycle lasting 47-87 days (Section 3.8.5) by a single NMW-2 unit.

Additionally, the plate handling system must be able to translate the two wafers in the lateral plane parallel to the plates, then re-establish (1) wafer parallelicity to within ~10^{-9} radians, (2) the 220 nm wafer separation, and (3) the relative plate positioning in the lateral plane, all to ~1 Å repeatable accuracy. The spacing of the sensor crane arms must be designed to accommodate these periodic wafer-shifting motions, and they can be used to report back the actual relative positions (both lateral and plate separation) of the two plates after they have finished moving. This information could be used either to correct the plate positioning or to modify the software parameters driving NMW-2 operations to accommodate slightly mispositioned wafers, possibly somewhat relaxing the performance constraints on the macroscale plate handling system.

Wafer flexing due to the mechanical operations of the NMW-2 units should maintain a deflection of $\delta_{plate} \leq 0.1$ nm (~1 Å, the minimum positioning accuracy for assembly; Section 3.6.1.1) for a 10-cm wide silicon plate of thickness $h_{plate} \geq 6$ mm, or for a 1-cm wide silicon plate of thickness then $h_{plate} \geq 0.3$ mm (Section 3.8.1.2(5)). The plate handler design must also address all design requirements previously enumerated in Section 3.8.1.2.

Figure VII-5. A MicroElectroMechanical Systems (MEMS) deformable mirror manufactured by Boston Micromachines.[1128]

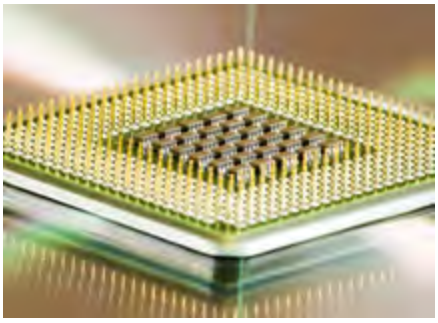

[1127] http://www.bostonmicromachines.com/products_kilodm.htm and http://www.bostonmicromachines.com/technology.htm.

[1128] http://www.bostonmicromachines.com/products_kilodm.htm and http://www.bostonmicromachines.com/technology.htm.

The plate handling system must provide electrical connectivity to each of the opposing semiconductor assembly surfaces and must be designed to operate in the workspace chamber environment which alternates between 1 atm feedstock gases (during BFSS recharge) and UHV (during fabrication and assembly operations).

A compact plate handler design should allow the entire mechanism to fit within a ~20 cm cubic volume.

3.8.5 Task VII-4: Demonstrate Plate/Plate Mechanical Operations Between Two Parallel Plates

Task VII-4 is to use the plate handling system developed in Task VII-3 to demonstrate the first plate/plate mechanical operations between two separate plates (each of which contains at least one active manipulator system on its assembly surface).

The first step is to construct a new NMW-2 unit on an assembly surface on one wafer, then another NMW-2 unit on an assembly surface on another opposed wafer – using the new NMW-2 design created in Task VII-1, the assembly surfaces created in Task VII-2, and the procedures for building an NMW developed during Task VI-3 and Task VI-4 of Phase VI. Given the serial NMW manufacturing time of 1.35×10^6 sec (~15.6 days; Section 3.7.6) at the conservative 1.2 MHz control pulse frequency, to which must be added the feedstock/byproduct gas handling and chamber pumpdown cycle times (1-21 days; Section 3.5.1.7) and conservatively allowing ~2 weeks for one plate changeout operation in this early Phase, the total build time for two NMW-2 units on separate plates is approximately 47-87 days.

The two plates are then mounted in the plate handler, electrical connections are established between handler and plates, and the two plates are parallelized at the desired 220 nm separation. The NMW-2 units on each plate are operated to fabricate and assemble a variety of nanoparts, nanodevices and nanosystems which are then mechanically transported and installed on a vacant worksite on the opposing plate. The ability to perform plate/plate installation or assembly operations should be demonstrated, along with the ability to insert contact wires into the silver electrodes and other key operations that will be required in subsequent Phase VII tasks during NMW-2 replication (Section 3.8.6). After testing two plates with opposed simple manipulator arms, further tests should include successful parts transfers and plate/plate assembly operations. The plate handler should also demonstrate the ability to adequately resist variation in wafer separation when maximum forces are applied to the opposing wafer that are similar in magnitude and direction to those that will be applied during plate/plate replication of one or more NMW-2 units.

It may be necessary to iterate Tasks VII-1, VII-2, VII-3, and VII-4 to successfully achieve the desired results.

3.8.6 Task VII-5: Replicate NMW-2 onto Opposing Plate Surface

Task VII-5 is to validate the design of the second-generation nanoscale manufacturing workstation (NMW-2) working in concert with the plate handling system developed in Task VII-

3 by experimentally demonstrating the ability of the NMW-2 on one wafer to construct a replica of itself on the opposing wafer.

As in Task VII-4, the first step is to construct a new NMW-2 unit on each of two assembly surfaces on two different wafers, requiring a total build time of about 47-87 days at the conservative 1.2 MHz control pulse frequency (Section 3.8.5). The two wafers are mounted in the plate handler, electrical connections are established between handler and plates, and the two wafers are parallelized at the desired 220 nm separation. The NMW-2 units on each wafer are then operated (1) to fabricate all 1100 nanoparts comprising the NMW-2, (2) to assemble from these nanoparts all needed nanodevices comprising the NMW-2, and finally (3) to mechanically transport all components and install a working replica NMW-2 unit on a vacant worksite on the opposing wafer. It may be prudent to attempt a single NMW-2 unit replication first, to be followed by a simultaneous double-replication of a new NMW-2 unit on each of two assembly surfaces on two different wafers (thus demonstrating plate/plate mechanical operations originating from both plates at the same time) in Task VII-6. Each replication cycle should require about 16-37 days at the conservative 1.2 MHz control pulse frequency (Section 3.8.5).

3.8.7 Task VII-6: Shift Opposing Plate Positions, Replicate NMW-2 Again

Task VII-6 is to validate the ability of daughter replicas of the two original "seed" NMW-2 units to again replicate themselves, thus definitively proving both replication fidelity and offspring replicative fertility[1129] of the NMW-2 in another 16-37 day experimental run at the conservative 1.2 MHz control pulse frequency (Section 3.8.6). To complete this task, the plate handling system is used to shift the two wafers (as they exist at the conclusion of Task VII-5) so that both replica NMW-2 units lie adjacent to empty worksites. The original workstation and its replica then each construct daughter replicas of themselves upon the empty worksites, resulting in a total of four workstations, two on each wafer, concluding the Phase VII effort.

It would also be useful for the NMW-2 to demonstrate the additional closely-related ability to endogenously manufacture, and deliver to depots on the opposing wafer surface, quantities of individual nanoparts and various nanodevices as products. These components should include: (1) critical nanoparts and nanodevices of which the NMW-2 is itself constructed; (2) non-critical nanoparts and nanodevices of which the NMW-2 is not constructed, but which are likely to be required for the manufacture of post-Phase VII systems, particularly nanofactory modules (as trial designs for these components become available); and (3) other nanoparts and nanodevices believed to be useful, either for nanoscale manufacturing (e.g., manipulator arrays such as the 10^7-tip "multitool" required in Phase VIII; Section 3.9.3) or as products (or components of products) in their own right (e.g., respirocyte[1130] or microbivore[1131] nanorobot components).

[1129] Robert A. Freitas Jr., Ralph C. Merkle, Kinematic Self-Replicating Machines, Landes Bioscience, Georgetown, TX, 2004; Sections 5.1.9(L2) and 5.1.9(L4); http://www.MolecularAssembler.com/KSRM/5.1.9.L.htm.

[1130] Robert A. Freitas Jr., "Exploratory Design in Medical Nanotechnology: A Mechanical Artificial Red Cell," Artificial Cells, Blood Substitutes, and Immobil. Biotech. 26(1998):411-430; http://www.foresight.org/Nanomedicine/Respirocytes.html.

3.8.8 Task VII-7: Increase NMW-2 Productivity by Tenfold

In the presently-defined NFW-2 system as operated at the conservative 1.2 MHz control pulse frequency, the total per-cycle replication time of 16-37 days (Section 3.8.6) represents up to a ~100 atom/sec net build rate for a 129,194,836-atom NMW-2 unit. The expeditious completion of the next program phase (Phase VIII) requires the productivity of the NFW-2 to be increased approximately tenfold. To accomplish this, three modifications to the existing processing systems should be made.

First, the electrical control pulse frequency driving the NMW-2 is increased 100-fold from 1.2 MHz to 120 MHz – per previous design, simulation, and theoretical validation (Section 3.7.2). The 100-fold higher operating frequency increases manipulator power consumption 100-fold while maintaining the same applied force (Section 3.4.1.1), produces negligible increase in thermal expansion of manipulator struts (Section 3.4.1.2), harmlessly increases NFW subsystem manipulator tip speed from 24 microns/sec (Section 3.4.1.4) to 2.4 mm/sec and NAW crane manipulator tip speed from a top speed of ~120 microns/sec (Section 3.6.1.3) to 1.2 cm/sec, increases electrode voltage and current draw by tenfold which seems acceptable (Section 3.4.3), has no effect on sorting rotor operation (Section 3.5.1.6(2)), and leaves the manipulator plate/plate duty cycle unchanged (Section 3.8.1.2(5)). Operating at 120 MHz reduces the serial NMW-2 replication time from ~15.6 days to 1.35×10^4 sec (~4 hours; Section 3.8.1.1) and boosts the serial atom-assembly rate to ~10,000 atoms/sec (though the overall in-cycle rate is tenfold lower; see below).

Second, the aggressive chamber evacuation measures previously described in Section 3.5.1.7 but not yet employed are now applied to reduce the feedstock/byproduct gas handling and chamber pumpdown cycle times from the stated 1-21 day range to ~1 day.

Third, the efficiency of plate changeout operations is streamlined to reduce handling times from ~2 weeks to ~8 hours, possibly by constructing a larger vacuum chamber or adding removable chamber annexes to the main workspace chamber.

Tasks VII-4, VII-5 and VII-6 are then repeated and iterated until successful demonstrations are achieved for all tasks. For Task VII-4, these increases in productivity reduce the total build time for two NMW-2 units on separate wafers to ~2.6 days, which is the sum of two 1.35×10^4 sec replication times, two ~1 day pumpdown times, and one ~8 hour plate changeout time. For Tasks VII-5 and VII-6, each replication cycle now requires 128,700 sec (~1.5 days) at the 120 MHz control pulse frequency, including pumpdown and plate changeout. For a 129,194,836-atom NMW-2 unit, this represents a ~1000 atom/sec in-cycle build rate – achieving the required tenfold increase in NMW-2 productivity. Unless further reductions in chamber evacuation and plate changeout times can be made, achieving significant further productivity gains would probably require major redesign of the BFSS subsystem.

[1131] Robert A. Freitas Jr., "Microbivores: Artificial Mechanical Phagocytes using Digest and Discharge Protocol," J. Evol. Technol. 14(April 2005):1-52; http://www.jetpress.org/volume14/freitas.html.

At a target in-cycle productivity rate of ~1000 atoms/sec for the accelerated Phase VII system, the original ~129 x 10^6-atom NMW-2 will require t_{fab} ~ 1.29 x 10^5 sec (~1.5 days) to fabricate a ~129 x 10^6-atom NMW-2 replica.

3.9 Phase VIII: Exponentially Manufacture 1024 NMW-2 Wafers

The successful design, manufacture, and demonstration of a second-generation nanoscale manufacturing workstation (NMW-2) capable of efficiently assembling an atomically exact working copy of itself on an opposing surface under full endogenous operation in Phase VII now enables the massively parallel manufacture of additional NMW-2 molecular manufacturing units. This is the key objective of Phase VIII: the exponential manufacture of 1024 wafers full of NMW-2 units, a quantity sufficient to fabricate and assemble atomically precise product objects up to the ~100-nm scale at a ~10^{17} atom/sec build rate. This assumes a ~1000 atom/sec net build rate per NMW-2 unit with 10^{11} NMW-2 units/wafer on 1024 wafers, with a ~10^{14} atom/sec build rate per wafer. A ~10^{17} atom/sec build rate is equivalent to ~0.06 kg/year of carbon atoms. A hypothetical mature MNT desktop nanofactory with a ~1 kg/hour output rate may be comprised of ~0.06 kg of diamondoid nanomachinery[1132] (Table 2-2), so a population of 1024 NMW-2 wafers should enable (when combined with other systems) the manufacture of the first ~0.053 kg desktop nanofactory (e.g., the FGN; Section 3.11.3.5) within ~1 year.

The fully built-out NMW-2 wafer is briefly described in Section 3.9.1 and illustrated in Figure VIII-1. This is followed by an enumeration of the specific tasks required to exponentially manufacture a large number of NMW-2 wafers which include: design and simulation of the whole-wafer surface and process (Section 3.9.2), preparation of a whole-wafer multielectrode assembly surface (Section 3.9.3), exponential manufacture of NMW-2 units on a single wafer to full monolayer coverage (Section 3.9.4), and finally the construction of additional plate handling systems and 1024 full-monolayer NMW-2 wafers (Section 3.9.5).

3.9.1 Description of the NMW-2 Wafer

3.9.1.1 Structure of the NMW-2 Wafer

The NMW-2 wafer is a plate of single-crystal ultrapure silicon that is approximately 10 cm x 10 cm square and at least ~6 mm thick (Section 3.8.1.2(5)), upon which multiple layers of electronic circuitry have been deposited using 10-nm lithography (anticipated by the semiconductor industry in 2015-2017 for production wafers)[1133] or using other methods (Section 3.4.3). The topmost

---

[1132] "Table 14.1. Manufacturing system parameters," in: K. Eric Drexler, Nanosystems: Molecular Machinery, Manufacturing, and Computation, John Wiley & Sons, New York, 1992, p. 422. See also in: Robert A. Freitas Jr., Ralph C. Merkle, Kinematic Self-Replicating Machines, Landes Bioscience, Georgetown, TX, 2004; Section 4.9.3 http://www.MolecularAssembler.com/KSRM/4.9.3.htm and Table 4.1 http://www.MolecularAssembler.com/KSRM/Tables/4.1.jpg.

[1133] International Technology Roadmap for Semiconductors (ITRS), 2006 Update. "Overview and Working Group Summaries," Tables 1a (Product Generations and Chip Size Model Technology Trend Targets—Near-term Years) and 1b (Product Generations and Chip Size Model Technology Trend Targets—Long-term Years), p.3; http://www.itrs.net/Links/2006Update/FinalToPost/00_ExecSum2006Update.pdf; see also in

layers consist of atomically flat silicon dioxide interrupted only by 10 nm x 10 nm atomically flat silver electrodes arranged in adjacent 100,000 nm^2 worksites. At 100 electrodes per worksite, the electrodes cover ~10% of the wafer surface.

Figure VIII-1. Schematic illustration of a completely built-out NMW-2 wafer, containing ~10^{11} active NMW-2 modules on a PALE-remediated atomically-smooth Ag/SiO_2 wafer surface. Plate handling mechanisms, electrical connections, and other appurtenant structures are not shown. Not to scale.

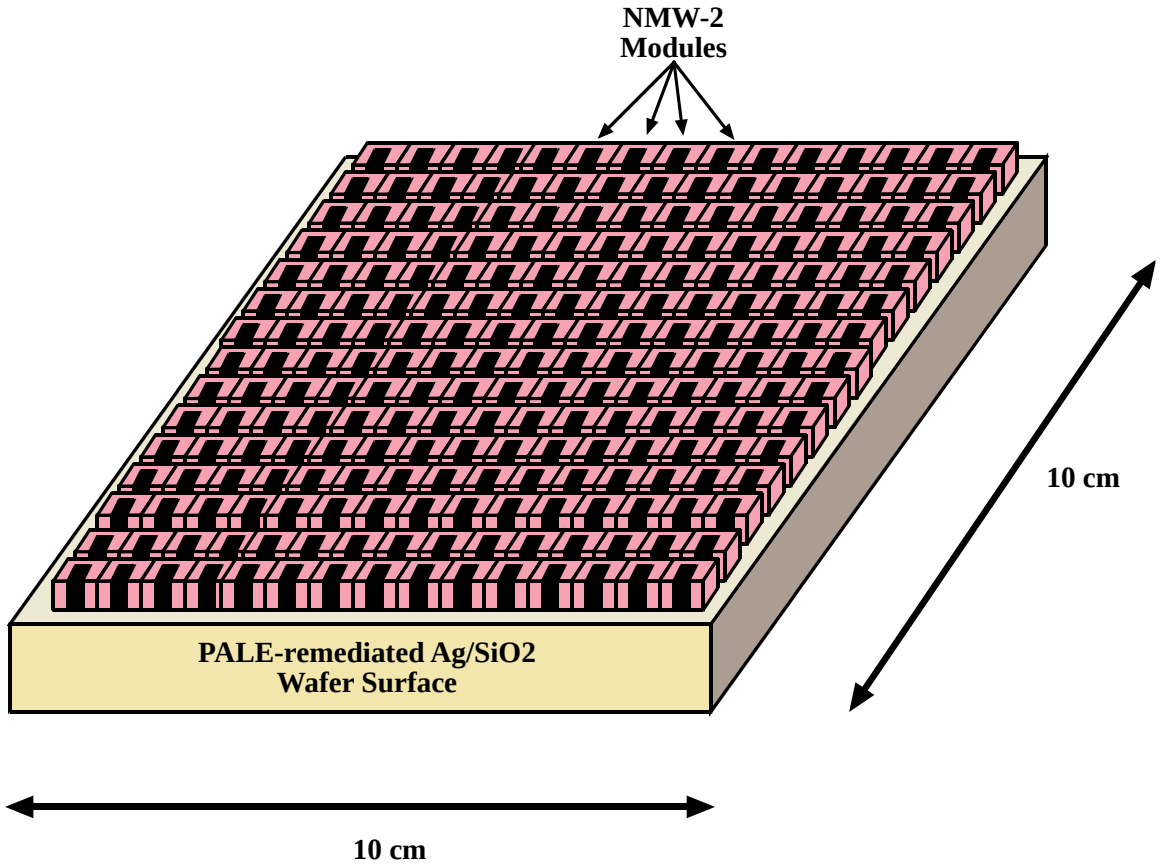

Since each worksite is ~0.1 $micron^2$ in area, a ~100 cm^2 (10^{10} $micron^2$) wafer surface can accommodate up to ~10^{11} individual second-generation nanoscale manufacturing workstation (NMW-2) worksites, with ~10^{13} silver electrodes present on each wafer. This is in line with the ITRS semiconductor industry roadmap[1134] which anticipates a SRAM transistor density of ~10^{12}

"Lithography," pp. 7-8;
http://www.itrs.net/Links/2006Update/FinalToPost/08_Lithography2006Update.pdf.

[1134] International Technology Roadmap for Semiconductors (ITRS), 2006 Update. "Overview and Working Group Summaries," Tables 1a (Product Generations and Chip Size Model Technology Trend Targets—Near-term Years) and 1b (Product Generations and Chip Size Model Technology Trend Targets—Long-term Years), p.3;

transistors per 100 cm^2 of chip surface by 2015-2017. Each of the SRAM transistors will be addressable individually, so it should also be possible to design an NMW-2 wafer in which each worksite is individually addressable, though it may be desirable to operate large groups of individual NMW-2 units in parallel using a single control source.

3.9.1.2 Operation of the NMW-2 Wafer

A fully built-out NMW-2 wafer will have one working NMW-2 unit installed at each of the 10^{11} individual worksites on the wafer, giving a total of 10^{11} installed NMW-2 units per wafer. The wafer will be controlled by electrical connections leading from the wafer through the plate handling system to an external source of control and power signals (e.g., a macroscale benchtop computer controller). Virtually all of the active duty cycle (~99% of manufacturing time, excluding pumpdown and plate changeout times; Section 3.7.1) of an NMW-2 unit is consumed by fabrication operations using the NFW subsystem (Section 3.5), which has four manipulators. Assuming a maximum possible total power dissipation of 1040 pW for all four manipulators in continuous operation (Sections 3.4.1.1 and 3.4.1.2) at the 120 MHz control pulse frequency, the maximum power draw for the entire 10^2 cm^2 NMW-2 wafer is ~104.0 watts. This is dwarfed by the maximum allowable power of ~6387 watts per 10^2 cm^2 wafer area for the electronic circuitry on high performance chips with heatsinks (198 watts per 3.1 cm^2 chip area) that is anticipated for 2015-2017 by the semiconductor industry.[1135]

3.9.1.3 Reliability of NMW-2 Wafer Operation

As previously detailed in Section 3.8.1.3, a total error rate of ~10^{-7} per replication cycle from all sources for NMW-2 operation at the 120 MHz pulse rate (Section 3.8.8) implies that, on average, ~10^4 NMW-2 units on a built-out wafer containing 10^{11} NMW-2 units will experience a single error during a single whole-wafer replication cycle. Such single errors can be as small as a single-step manipulator displacement error (e.g., a single missed 0.2 Å step in an NFW-2 cycle) or as large as a missed or incorrect atom placement that results in a pathological product surface structure, or even a jammed or nonfunctioning manipulator. Failures such as these must be enumerated, categorized, and analyzed in detail, after which systemic design changes must be implemented to allow the early detection of – and the minimization of replica shortfall and damage cascade effects from – every class of commonly occurring failure. (See further

---

http://www.itrs.net/Links/2006Update/FinalToPost/00_ExecSum2006Update.pdf; see also in "Lithography," pp. 7-8; http://www.itrs.net/Links/2006Update/FinalToPost/08_Lithography2006Update.pdf.

[1135] International Technology Roadmap for Semiconductors (ITRS), 2006 Update. "Overview and Working Group Summaries," Tables 1a (Product Generations and Chip Size Model Technology Trend Targets—Near-term Years) and 1b (Product Generations and Chip Size Model Technology Trend Targets—Long-term Years), p.3; http://www.itrs.net/Links/2006Update/FinalToPost/00_ExecSum2006Update.pdf; see also in "Lithography," pp. 7-8; http://www.itrs.net/Links/2006Update/FinalToPost/08_Lithography2006Update.pdf.

discussion in Section 3.9.2, below.) Since each NMW-2 replica consists of ~129,194,836 atoms, the ~10^{-7} error rate per replication cycle is equivalent to a net per-atom error rate of ~10^{-15} for DMS-based molecular manufacturing (Section 3.8.1.3).

Note that the error rate due to feedstock gas impurities remains ~zero because feedstock molecules are sufficiently purified during transfer into the BFSS to remove all contaminants, effectively achieving ~19N purity (Section 3.9.2).

3.9.2 Task VIII-1: Design and Simulate Whole-Wafer Surface and Process

Task VIII-1 is to design and simulate the whole-wafer surface and wafer buildout processes which have already been detailed at the single NMW-2 unit level during Task VII-1 (Section 3.8.2). Since NMW-2 units do not interact with each other but only with the assembly surface and a growing passive daughter structure on the opposing plate, detailed atomistic simulations are no longer required. Finite-element and other continuum models should suffice to explore the mechanical responses of wafer plates and machine components to mechanical operations performed by a growing population of NMW-2 units. These forces will grow in magnitude as the number of working NMW-2 units increases toward the full complement of 10^{11} units on each wafer. Substantial resonance vibrations might develop if all NMW-2 units are operated in unison; however, while control issues would be considerably more complex, in principle all 10^{11} NMW-2 units on each wafer could be operated uniquely out of unison with all other units because a train of ~10^{12} control pulse cycles (Section 3.7.1) is needed to replicate an NMW-2 unit.

Another important modeling and simulation effort will be required to design and analyze the optimum shift patterns to be executed by the plate handling system during wafer buildout. Buildout of 10^{11} NMW-2 units starting from a single unit will require $\log_{10}(10^{11})/\log_{10}(2) \sim 37$ replicative generations to fill one 10^4 cm^2 NMW-2 wafer. Therefore buildout of each wafer requires at least 35 plate-shift operations to build out the next generation of NMW-2 units on the wafer. The exact sequence of plate-shift operations should be designed and simulated so that the entire wafer is filled using the minimum possible number of plate shifts which wastes the minimum number of unit replication cycles. (An NMW-2 unit positioned over an already-built daughter that was manufactured in an earlier generation must sit out the cycle, producing nothing.)

On each wafer, some number of NMW-2 units will be unreliable or nonfunctional and must be permanently shut down, producing replicative "dead spots" on the NMW-2 wafer. (Semiconductor wafers typically have 80-90% yields of good chips using current lithographic techniques.)[1136] Each wafer will have its own unique pattern of dead spots and the number of

---

[1136] International Technology Roadmap for Semiconductors (ITRS), 2006 Update. "Overview and Working Group Summaries," Tables 1a (Product Generations and Chip Size Model Technology Trend Targets—Near-term Years) and 1b (Product Generations and Chip Size Model Technology Trend Targets—Long-term Years), p.3; http://www.itrs.net/Links/2006Update/FinalToPost/00_ExecSum2006Update.pdf; see also in "Lithography," pp. 7-8; http://www.itrs.net/Links/2006Update/FinalToPost/08_Lithography2006Update.pdf.

dead spots will slowly increase over time as existing functional NMW-2 units cease proper functioning and are shut down. The dead spot map for each wafer can be recorded and updated electronically on each wafer with each use. Thus the optimal shift pattern for any pair of wafers will be unique (given their unique patterns of opposing dead spots) and must be calculated prior to commencing the plate/plate manufacturing operation. Simulations may be performed to help develop the most efficient algorithms for generating quick solutions to the optimal shift pattern problem.

Note that an operating error rate of ~10^{-7} per replication cycle for the NMW-2 implies that ~10^4 randomly-chosen NMW-2 units on a built-out wafer containing 10^{11} NMW-2 units will experience a single error during a single whole-wafer replication cycle (Section 3.9.1.3). If we conservatively assume that these randomly-placed single production errors result in a nonfunctional daughter NMW-2 unit, then these nonfunctional daughters can be detected at the end of the replication cycle, marked as dead spots and permanently deactivated. If the operating errors were truly random they most likely will not occur again in the same NMW-2 unit during the next replication cycle. However, conservatively the error-producing units should be tentatively marked as "suspect" for the next cycle, and if a "suspect" NMW-2 unit repeats another production error it can then be judged as unreliable and permanently shut down, adding further to the list of dead spots.

Again conservatively assuming that each sorting rotor stage in the BFSS-2 (Section 3.7.1) can achieve a 1000:1 purification ratio via rotored counterflows of impurities[1137] and recognizing that an entire wafer of NMW-2 units will consume ~4.89 x 10^{18} C_2H_4 molecules per feed cycle (i.e., 10^{11} tankfuls of ethylene feedstock per whole-wafer production cycle, at ~4.89 x 10^7 C_2H_4 molecules per tankful), then to ensure that not a single impurity molecule is stored in any BFSS-2 tank in any NMW-2 unit on an entire built-out wafer will require an impurity rate at or below $(4.89 \times 10^{18})^{-1} \sim 2 \times 10^{-19}$ or 19N purity. Sending commercially available 5N purity ethylene feedstock (Section 3.5.1.3) through four additional rotor pair stages would yield a net impurity rate of 10^{-5} (5N purified feedstock) x 10^{-3} (1st rotor pair) x 10^{-3} (2nd rotor pair) x 10^{-3} (3rd rotor pair) x 10^{-3} (4th rotor pair) x 10^{-3} (5th rotor pair) ~ 10^{-20} (going into the tank). An upgraded BFSS would therefore need a total of five ethylene rotor pairs to exceed the 19N purity objective at a cost of ~5500 nm^3 or ~10^6 atoms, which is less than 1% of NMW-2 structure.

3.9.3 Task VIII-2: Prepare Whole-Wafer Multielectrode Assembly Surface

Task VIII-2 is to prepare a 10^{13}-electrode wafer using an upgraded lithography-PALE process (Section 3.4.3) to create a remediated atomically smooth surface. PALE typically occurs at ~10 sec per atomic layer for the actual deposition process. If we have a 100 cm^2 wafer and can remediate ~10^6 nm^2/sec-tip (e.g., typical atomic-resolution SPM scan rate is ~10 KHz for a 10 nm x 10 nm ~ 100 nm^2 area, a much higher rate than was assumed for the initial process first

---

[1137] K. Eric Drexler, Nanosystems: Molecular Machinery, Manufacturing, and Computation, John Wiley & Sons, New York, 1992; http://www.zyvex.com/nanotech/nanosystems.html.

described in Section 3.4.3), and if we need 100 passes (e.g., ~100 atomic layers or ~20 nm thick) to completely remediate a wafer surface, and if we employ a 10-million-tip PALE scanning tool, the "multitool," then the remediation for each wafer would take ~((10^{-2} m^2/wafer-pass) (~100 passes)) / ((~10^{-12} m^2/sec-tip) (~10^7 tips)) = 10^5 sec/wafer ~ 1 day/wafer. Preparing 1024 wafers for Task VIII-4 (Section 3.9.5) thus would require ~1024 days using a single wafer processing system but only ~64 days (approximately matching the maximum 1024-wafer total buildout time of 73.4 days; Section 3.9.5) using 16 wafer processing systems operated in tandem.

In earlier program phases, multielectrode assembly surfaces included only 100-1000 worksites and could be fabricated in a reasonable time using a single PALE process scanning tip. In later phases, we began studying ways to accelerate the PALE processing of semiconductor assembly surfaces in part by increasing the number of processing tips involved. Up to now we've been fabricating wafers with up to ~100 electrodes per station and 100-1000 stations per wafer, or 10^4-10^5 electrodes on each wafer. In Phase VIII, we must fabricate a whole-wafer multielectrode assembly surface which involves 10^{11} worksites and 10^{13} electrodes on each wafer. As a result, single-tip PALE processing is no longer feasible and we must upgrade to a multi-tip processing approach (unless alternative massively parallel schemes such as nanopantography[1138] can be made to work).

Regarding the need for PALE multitip arrays for parallel surface patterning, Randall[1139] notes that "because each tip will need atomic precision capability, it is unlikely that a fixed array of tips can be scanned in unison. There will be the need to make at least small individual adjustments to assure each tip is on some grid that is commensurate with the lattice that it is patterning, but independent scanning capabilities for each tip can also be used to improve throughput and flexibility in patterning. To maximize throughput, flexibility, and reliability, the requirement is for closed loop 3-DOF (XYZ) positioners with at least 1 Å precision....If possible the tip should be replaceable. Each scanner should be independently operable. Control of the potential of the tip is also required."

To implement such a multi-tip processing approach in Phase VIII, the single-tip tool employed in previous phases will be replaced with a 10 million tip multitool which can perform assembly surface remediation writing operations at 10^7 surface sites simultaneously. A single DMS manipulator as developed in Phase III (Section 3.4.1.1) includes a total of 6,117,997 carbon and hydrogen atoms (Table III-2). We shall assume that a greatly simplified manipulator requiring just 3 electrode contacts and having ~5,000,000 atoms can serve as a PALE surface-remediation tooltip and could be produced in ~5000 sec by a single NMW-2 unit operating at a ~1000 atom/sec manufacturing rate (Section 3.8.8).

[1138] Economou, Donnelly and Ruchhoeft, 10 September 2007; http://advancednano.blogspot.com/2007/09/nanopantography-can-scale-ion-beam.html. See: Nanopantography: A New Method for Massively Parallel Nanopatterning over Large Areas, http://pubs.acs.org/cgi-bin/abstract.cgi/nalefd/2005/5/i12/abs/nl051976i.html.

[1139] John Randall, "Patterned ALE Path Phases," Technical Report 03, in: Productive Nanosystems: A Technology Roadmap, Battelle Memorial Institute and Foresight Nanotech Institute, 2007; http://www.foresight.org/roadmaps/index.html.

The multitool can be manufactured on a wafer using the NMW-2 units previously constructed in Phase VII (Section 3.8.7) as follows. Iterating Task VII-6 (Section 3.8.7) twelve additional times at the accelerated processing rates demonstrated in Task VII-7 (Section 3.8.8) fills out an 8,192-worksite assembly surface with 8,192 copies of NMW-2 units in ~(12)(128,700 sec) = 1.54 x 10^6 sec (~18 days) with a combined production capacity of ~8.192 x 10^6 atoms/sec. A 3 x 10^7-electrode assembly surface (equivalent to an assembly surface with 300,000 NMW worksites) sufficient to host 10 million 3-electrode manipulators as previously described could then be prepared in the usual manner (e.g., Section 3.8.3), taking ~20 days. The 8192-unit NMW-2 array would then be employed to build 10 million 3-electrode manipulators on the 10^7-electrode assembly surface in ~6.1 x 10^6 sec (~71 days), completing the manufacture of the 10^7-tip PALE multitool. This 10^7-tip multitool could then be used to produce 1 wafer/day having 10^{13} electrodes/wafer as described above.

Using 16 wafer processing systems would allow 16 wafers/day to be produced enabling faster buildout (see above), but this would require building 16 multitools. To accomplish this, we first build 16 array handlers and 16 PALE processing systems, which can presumably be done over the course of ~1 year. Once these are in place, the first 8192-unit NMW-2 array is replicated four times, yielding sixteen 8192-unit NMW-2 arrays in a build time of ~(4)(128,700 sec) = 5.15 x 10^5 sec (~6 days). Sixteen copies of a 3 x 10^7-electrode assembly surface (equivalent to an assembly surface with 300,000 NMW worksites) sufficient to host 10 million 3-electrode manipulators as previously described could then be prepared in the usual manner (e.g., Section 3.8.3), taking ~20 days when manufactured in parallel using the 16 duplicate PALE processing systems. The 16 arrays are then employed to build 10 million 3-electrode manipulators on each of sixteen copies of the 10^7-electrode assembly surface in ~6.1 x 10^6 sec (~71 days), completing the manufacture of sixteen copies of the 10^7-tip PALE multitool in 18 days + 6 days + 20 days + 71 days = 115 days. These sixteen 10^7-tip multitools could then be used to produce 16 wafers/day each having 10^{13} electrodes/wafer, completing 1024 wafers in an additional ~64 days as described above.

Simple precursors to such extremely sophisticated tip arrays already exist in current technologies that are found in massively parallel scanning probe microscope (SPM) arrays[1140] and microscale SPMs.[1141] Force-sensing devices such as piezoelectric,[1142] piezoresistive,[1143] and capacitive[1144]

[1140] Aristides A.G. Requicha, "Massively parallel nanorobotics for lithography and data storage," Intl. J. Robotics Res. 18(March 1999):344-350; http://www-lmr.usc.edu/~lmr/publications/ijrr98/; K.E. Drexler, "Molecular tip arrays for molecular imaging and nanofabrication," J. Vac. Sci. Technol. B 9(1991):1394-1397.

[1141] Thomas R. Albrecht, Shinya Akamine, Mark J. Zdeblick, Calvin F. Quate, "Microfabrication of integrated scanning tunneling microscope," J. Vac. Sci. Technol. A 8(January/February 1990):317-318; M.I. Lutwyche, Y. Wada, "Observation of a vacuum tunnel gap in a transmission electron microscope using a micromechanical tunneling microscope," Appl. Phys. Lett. 66(22 May 1995):2807-2809; D.A. Walters, J.P. Cleveland, N.H. Thomson, P.K. Hansma, M.A. Wendman, G. Gurley, V. Elings, "Short cantilevers for atomic force microscopy," Rev. Sci. Instrum. 67(October 1996):3583-3590; D. Lange, M. Zimmermann, C. Hagleitner, O. Brand, H. Baltes, "CMOS 10-cantilever array for constant-force parallel scanning AFM," Technical Digest, Transducers '01, Vol. 2, 2001, pp. 1074-1077.

[1142] T. Itoh, T. Suga, "Development of a force sensor for atomic force microscopy using piezoelectric thin films," Nanotechnology 4(1993):218-224. See also: T. Itoh, T. Suga, "Scanning force microscope using a piezoelectric microcantilever," J. Vac. Sci. Technol. B 12(1994):1581-1585; T. Itoh, T. Ohashi, T. Suga,

microcantilevers made it possible to construct microscale atomic force microscopes (AFMs) on chips without an external deflection sensor. (We exclude fixed-tip arrays[1145] in the following discussion.) In 1995, Itoh and colleagues[1146] at the University of Tokyo fabricated an experimental piezoelectric ZnO_2-on-SiO_2 microcantilever array of ten tips on a single silicon chip. Each cantilever tip lay ~70 microns from its neighbor, and measured 150 microns long, 50 microns wide and 3.5 microns thick, or ~26,000 micron^3/device, and each of the devices could be operated independently in the Z-axis (e.g., vertically) up to near their mechanical resonance frequencies of 145-147 KHz at an actuation sensitivity of ~20 nm/volt – for instance, 0.3-nm resolution at 125 KHz.

Parallel probe scanning and lithography was first achieved by Quate's group at Stanford, which progressed from simple piezoresistive microcantilever arrays with 5 tips spaced 100 microns apart and 0.04-nm resolution at 1 KHz but only one z-axis actuator for the whole array,[1147] to arrays with integrated sensors and actuators that allow parallel imaging and lithography with feedback and independent control of each of up to 16 tips, with scanning speeds up to 3 mm/sec using a piezoresistive sensor.[1148] By 1998, Quate's group had demonstrated[1149] arrays of 50-100

"Scanning force microscope using piezoelectric excitation and detection," IEICE Trans. Electron. E78-C(1995):146-151; Toshihiro Itoh et al, "Independent parallel scanning force microscopy using Pb(Zr, Ti)O3 microcantilever array," Proc. MEMS'97, Nagoya, Japan, 1997.

[1143] M. Tortonese, H. Yamada, R.C. Barrett, C.F. Quate, "Atomic force microscopy using a piezoresistive cantilever," Digest of Technical Papers, Sixth Intl. Conf. Solid-State Sensors and Actuators (Transducers '91), San Francisco, CA, 24-28 June 1991, pp. 448-451. See also: M. Tortonese, R.C. Barrett, C.F. Quate, "Atomic resolution with an atomic force microscope using piezoresistive detection," Appl. Phys. Lett. 62(22 February 1993):834-836.

[1144] N. Blanc, J. Brugger, N.F. de Rooji, U. Durig, "Scanning force microscopy in the dynamic mode using microfabricated capacitive sensors," paper presented at the 8th Intl. Conf. Scanning Tunneling Microscopy/Spectroscopy and Related Techniques, STM '95, Snowmass Village, CO, 23-28 July 1995. See also: J. Brugger, R.A. Buser, N.F. de Rooij, "Micromachined atomic force microprobe with integrated capacitive readout," J. Micromech. Microeng. 2(1992):218-220.

[1145] Fumiya Watanabe, Makoto Arita, H. Murayama, Teruaki Motooka, Ken Okano, Takatoshi Yamada, "Diamond tip arrays for parallel processing of microelectromechanical systems," Japan J. Appl. Phys. 37(1998):L562-L564; S.-J. Park, J. Chen, C. Liu, J.G. Eden, "Silicon microdischarge devices having inverted pyramidal cathodes: Fabrication and performance of arrays", Appl. Phys. Lett. 78(22 January 2001):419-421; http://mass.micro.uiuc.edu/publications/papers/50.pdf.

[1146] Toshihiro Itoh, Takahiro Ohashi, Tadatomo Suga, "Piezoelectric cantilever array for multiprobe scanning force microscopy," MEMS-9, 1996, pp. 451-455.

[1147] S.C. Minne, Ph. Flueckiger, H.T. Soh, C.F. Quate, "Atomic force microscope lithography using amorphous silicon as a resist and advances in parallel operation," J. Vac. Sci. Technol. B 13(May/June 1995):1380-1385.

[1148] S.C. Minne, S.R. Manalis, C.F. Quate, "Parallel atomic force microscopy using cantilevers with integrated piezoresistive sensors and integrated piezoelectric actuators," Appl. Phys. Lett. 67(1995):3918-3920; S.R. Manalis, S.C. Minne, C.F. Quate, "Atomic force microscopy for high speed imaging using cantilevers with an integrated actuator and sensor," Appl. Phys. Lett. 68(1996):871-873.

independently controllable AFM probe tips mounted in 2-D patterns with 60 KHz resonances, including a 10 x 10 cantilevered tip array fabricated in closely spaced rows using throughwafer interconnects on a single chip, and this work continues.[1150]

MacDonald's group at the Cornell Nanofabrication Facility pursued similar goals. In 1991, the team fabricated their first submicron stylus, driven in the XY plane using interdigitating MEMS comb drives,[1151] including the first opposable tip pair. By 1993, they had produced a 25-tip array on one XYZ actuator,[1152] and by 1995 a complete working micro-STM (including XY comb drives) measuring 200 microns on an edge and a micro-AFM measuring 2 mm on an edge including a 1-mm long cantilever with a 20-nm diameter integrated tip on a 6-micron high by 1-micron diameter support shaft.[1153] MacDonald's group then demonstrated tip arrays with 5 micron spacings, exploiting the same process used to make the working micro-STM.[1154] With the

---

[1149] S.R. Manalis, S.C. Minne, A. Atalar, C.F. Quate, "Interdigital cantilevers for atomic force microscopy," Appl. Phys. Lett. 69(1996):3944-3946; K. Wilder, H.T. Soh, S.C. Minne, S.R. Manalis, C.F. Quate, "Cantilever arrays for lithography," Naval Research Reviews 49(1997):35-48; C.F. Quate, "Scanning probes as a lithography tool for nanostructures," Surf. Sci. 386(1997):259-264; S.C. Minne, S.R. Manalis, A. Atalar, C.F. Quate, "Independent parallel lithography using the atomic force microscope," J. Vac. Sci. Technol. B 14(1997):2456-2461; S.C. Minne, G. Yaralioglu, S.R. Manalis, J.D. Adams, J. Zesch, A. Atalar, C.F. Quate, "Automated parallel high speed atomic force microscopy," Appl. Phys. Lett. 72(4 May 1998):2340-2342; http://www.nano.unr.edu/adams/papers/auto_par.pdf; Kathryn Wilder, Calvin F. Quate, Bhanwar Singh, David F. Kyser, "Electron beam and scanning probe lithography: A comparison," J. Vac. Sci. Technol. B 16(November/December 1998):3864-3873; K. Wilder, D. Adderton, R. Bernstein, V. Elings, C.F. Quate, "Noncontact nanolithography using the atomic force microscope," Appl. Phys. Lett. 73(1998):2527-2529; S.C. Minne, J.D. Adams, G. Yaralioglu, S.R. Manalis, A. Atalar, C.F. Quate, "Centimeter scale atomic force microscope imaging and lithography," Appl. Phys. Lett. 73(21 September 1998):1742-1744; http://www.nano.unr.edu/adams/papers/cmscale.pdf

[1150] K. Wilder K, H.T. Soh, A. Atalar, C.F. Quate, "Nanometer-scale patterning and individual current-controlled lithography using multiple scanning probes", Rev. Sci. Instr. 70(1999):2822-2827; E.M. Chow, H.T. Soh, H.C. Lee, J.D. Adams, S.C. Minne, G. Yaralioglu, A. Atalar, C.F. Quate, T.W. Kenny, "Integration of through-wafer interconnects with a two-dimensional cantilever array", Sensors and Actuators A 83(2000):118-123; T. Sulchek, R.J. Grow, G.G. Yaralioglu, S.C. Minne, C.F. Quate, S.R. Manalis, A. Kiraz, A. Aydiner, A. Atalar, "Parallel atomic force microscopy with optical interferometric detection", Appl. Phys. Lett. 78(2001):1787-1789.

[1151] J. Jason Yao, Susanne C. Arney, Noel C. MacDonald, "Fabrication of high frequency two-dimensional nanoactuators for scanned probe devices," J. Microelectromech. Syst. 1(March 1992):14-22.

[1152] Z. Lisa Zhang, Noel C. MacDonald, "A RIE process for submicron, silicon electromechanical structures," J. Micromech. Microeng. 2(March 1992):31-38; Z. Lisa Zhang, N.C. MacDonald, "Integrated silicon process for micro-dynamic vacuum field emission cathodes," J. Vac. Sci. Technol. B 11(November/December 1993):2538-2543.

[1153] Y. Xu, N.C. MacDonald, S.A. Miller, "Integrated micro-scanning tunneling microscope," Appl. Phys. Lett. 67(16 October 1995):2305-2307; Kaigham J. Gabriel, "Engineering microscopic machines," Sci. Amer. 273(September 1995):150-153.

[1154] S. Arney, N.C. MacDonald, "Formation of submicron silicon on insulator structures by lateral oxidation of substrate-silicon islands," J. Vac. Sci. Technol. B 6(January/February 1988):341-345; J.P.

same technology tips or small arrays of tips could be spaced 25-50 microns apart and integrated with individual Z-axis microactuators, so that one XY-axis manipulator could support many tips with each tip having a separate Z-actuator. By 1997, the group[1155] had built and tested an array of micro-STMs on the surface of an ordinary silicon chip, with each tip on a cantilever 150 microns long with 3-D sensing and control. The largest prototype array had 144 probes,[1156] arranged in a square consisting of 12 rows of 12 probes each, with individual probe needles about 200 microns apart (Figure VIII-2). Further development was to focus on increasing the range of movement and on fitting more and smaller probes into the same space.

Figure VIII-2. An array of 144 scanning probe microscope tips.[1157]

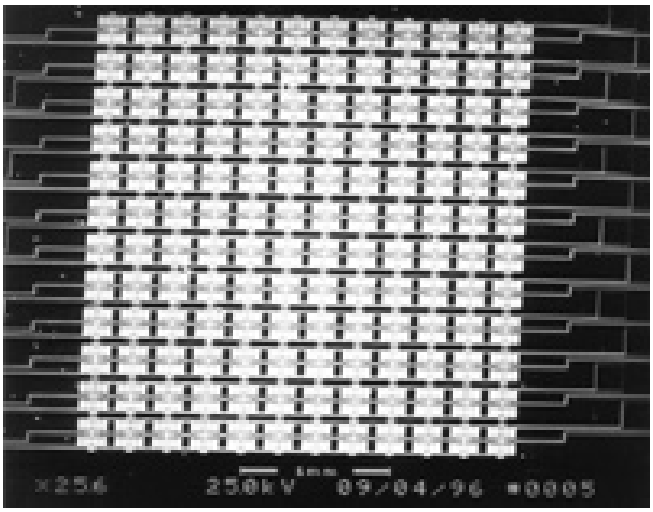

Spallas, N.C. MacDonald, "Self-aligned silicon field emission cathode arrays formed by selective, lateral thermal oxidation of silicon," J. Vac. Sci. Technol. B 11(March/April 1993):437-440.

[1155] Scott A. Miller, Kimberly L. Turner, Noel C. MacDonald, "Microelectromechanical scanning probe instruments for array architectures," Rev. Sci. Instrum. 68(November 1997):4155-4162. See also: http://www.news.cornell.edu/releases/March98/nanoprobe.bs.html

[1156] Robert F. Service, "Meeting Briefs: Atomic Landscapes Beckon Researchers. Scanning scopes go parallel," Science 274(1 November 1996):723; http://www.sciencemag.org/cgi/content/full/sci;274/5288/723.

[1157] Robert F. Service, "Meeting Briefs: Atomic Landscapes Beckon Researchers. Scanning scopes go parallel," Science 274(1 November 1996):723; http://www.sciencemag.org/cgi/content/full/sci;274/5288/723.

Figure VIII-3. Millipede concept of IBM Zurich Research Laboratory – schematic of cantilever tip array on a chip positioned over a flat surface indented with data-carrying Braille-like pits, shown at left; actual images of a fabricated array shown at right (courtesy of IBM).[1158]

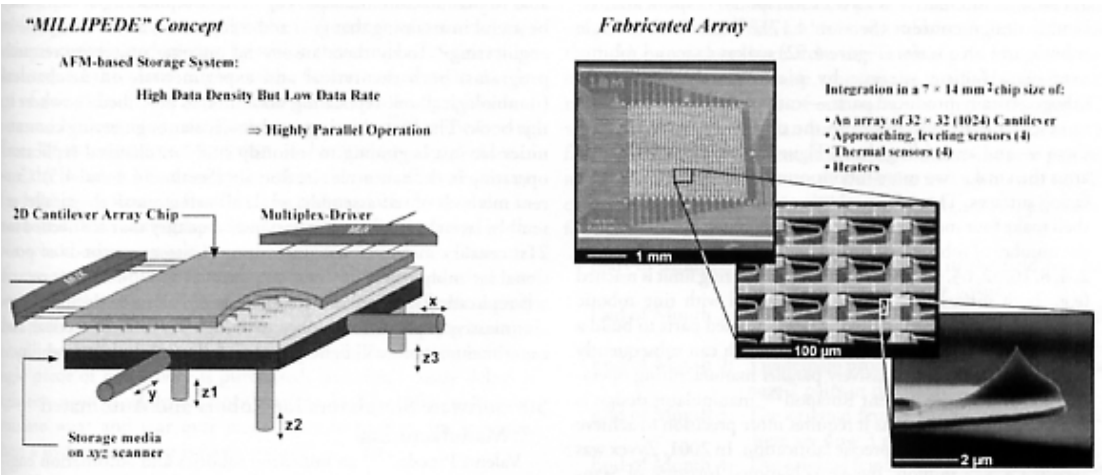

Using conventional microlithography, researchers in the Millipede project at IBM's Zurich Research Laboratory[1159] have fabricated scanning probe tip arrays of up to 1024 individual tips (Figure VIII-3) to achieve terabit-per-square-inch data storage densities.[1160] Simpler mechanical

---

[1158] "1000 Tips for Ultrahigh-Density Data Storage," IBM News, Zurich Research Lab, 11 October 1999, http://www.zurich.ibm.com/news/99/millipede.html; IBM Research: Millipede, http://domino.research.ibm.com/Comm/bios.nsf/pages/millipede.html; P. Vettiger, G. Cross, M. Despont, U. Drechsler, U. Duerig, B. Gotsmann, W. Haeberle, M. Lantz, H. Rothuizen, R. Stutz, G. Binnig, "The Millipede – nanotechnology entering data storage," Technical Report, IBM Zurich Research Lab; http://domino.research.ibm.com/Comm/bios.nsf/pages/millipede.html/$FILE/pv7201-preprint.pdf; also published in: Vettiger P, Cross G, Despont M et al., "The Millipede – nanotechnology entering data storage," IEEE Trans Nanotechnol 1(June 2002):39-55.

[1159] "1000 Tips for Ultrahigh-Density Data Storage," IBM News, Zurich Research Lab, 11 October 1999, http://www.zurich.ibm.com/news/99/millipede.html; IBM Research: Millipede, http://domino.research.ibm.com/Comm/bios.nsf/pages/millipede.html; P. Vettiger, G. Cross, M. Despont, U. Drechsler, U. Duerig, B. Gotsmann, W. Haeberle, M. Lantz, H. Rothuizen, R. Stutz, G. Binnig, "The Millipede – nanotechnology entering data storage," Technical Report, IBM Zurich Research Lab; http://domino.research.ibm.com/Comm/bios.nsf/pages/millipede.html/$FILE/pv7201-preprint.pdf; also published in: Vettiger P, Cross G, Despont M et al., "The Millipede – nanotechnology entering data storage," IEEE Trans Nanotechnol 1(June 2002):39-55.

[1160] "IBM's 'Millipede' Project Demonstrates Remarkable Trillion-Bit Data Storage Density," IBM Press Release, 11 June 2002; http://www-916.ibm.com/press/prnews.nsf/jan/F37FD677741C778A85256BD5004871CF; M.I. Lutwyche, M. Despont, U. Drechsler, U. Durig, W. Haberle, H. Rothuizen, R. Stutz, R. Widmer, G.K. Binnig, P. Vettiger,

ciliary arrays consisting of 10,000 independent microactuators on a 1 cm^2 chip have been fabricated at the Cornell National Nanofabrication Laboratory for microscale parts transport applications,[1161] and other ciliary array systems for parts presentation in microscale manufacturing have been reported by many others including the Fujita group,[1162] Bohringer and colleagues,[1163] Will's group,[1164] Darling, Suh and Kovacs,[1165] and others.[1166] Microcantilever

---

"Highly parallel data storage system based on scanning probe arrays," Appl. Phys. Lett. 77(13 November 2000):3299-3301.

[1161] K.F. Bohringer, B.R. Donald, N.C. MacDonald, "Single-crystal silicon actuator arrays for micro manipulation tasks," Proc. IEEE 9th Intl. Workshop on Micro Electro Mechanical Systems (MEMS'96), San Diego CA, 11-15 February 1996, pp. 7-12; http://www.cs.cornell.edu/home/karl/MicroActuators; Dan Reznik, Stan Brown, John Camy, "Dynamic simulation as a design tool for a microactuator array," Proc. 1997 IEEE International Conference on Robotics and Automation, 20-25 April 1997, IEEE Robotics and Automation Society, pp. 1675-1680; http://www.cs.berkeley.edu/~jfc/dreznik/Pubs/icra97.pdf.

[1162] N. Takeshima, H. Fujita, "Polyimide bimorph actuators for a ciliary motion system," ASME WAM, Symp. Micromech. Sensors, Actuators, and Systems, 1991; M. Ataka, A. Omodaka, H. Fujita, "A biometric micro system – a ciliary motion system," Tech. Digest, 7th Intl. Conf. Solid-State Sensors and Actuators (Transducers'93), Yokohama, Japan, 7-10 June 1993, pp. 38-41; H. Fujita, "Group Work of Microactuators," Intl. Advanced Robot Program Workshop on Micromachine Technologies and Systems, Tokyo, Japan, October 1993, pp. 24-31; Manabu Ataka, Akito Omodaka, Naohiro Takeshima, Hiroyuki Fujita, "Fabrication and operation of polyimide bimorph actuators for a ciliary motion system," J. Microelectromech. Syst. 2(December 1993):146-150; Y. Mita, S. Konishi, H. Fujita, "Two dimensional micro conveyance system with through holes for electrical and fluidic interconnection," Tech. Digest, 9th Intl. Conf. on Solid-State Sensors and Actuators (Transducers '97), Chicago, IL, 1997; Y. Mita, A. Kaiser, B. Stefanelli, P. Garda, M. Milgram, H. Fujita, "A distributed microactuator conveyance system with integrated controller," 1999 IEEE Intl. Conf. on Systems, Man and Cybernetics (SMC '99), 12-15 October 1999, Tokyo, Japan; http://www.ee.t.u-tokyo.ac.jp/~mita/SMC99/.

[1163] K.F. Bohringer, B.R. Donald, R. Mihailovich, N.C. MacDonald, "A theory of manipulation and control for microfabricated actuator arrays," Proc. IEEE Workshop on Micro Electro Mechanical Systems (MEMS), Oiso, Japan, January 1994, pp. 102-107; http://www.cs.cornell.edu/home/karl/MicroActuators; K.F. Bohringer, B.R. Donald, R. Mihailovich, N.C. MacDonald, "Sensorless manipulation using massively parallel microfabricated actuator arrays," Proc. IEEE Intl. Conf. Robotics and Automation (ICRA), San Diego, CA, May 1994, pp. 826-833; http://www.cs.cornell.edu/home/karl/MicroManipulation; K.F. Bohringer, B.R. Donald, N.C. MacDonald, "Upper and lower bounds for programmable vector fields with applications to MEMS and vibratory plate parts feeders," in J.P. Laumond, M. Overmars, eds., Intl. Workshop on Algorithmic Foundations of Robotics (WAFR), Toulouse, France, July 1996, A.K. Peters, Wellesley, Mass., 1997, pp. 255-276; http://www.cs.cornell.edu/home/karl/MicroManipulation; Karl F. Bohringer, Bruce R. Donald, Noel C. MacDonald, Gregory T.A. Kovacs, John W. Suh, "Computational methods for design and control of MEMS micromanipulator arrays," IEEE Computational Science & Engineering 4(January-March 1997):17-29; http://www.cs.dartmouth.edu/~brd/cse97/cse97.html; Karl Fredrich Bohringer, John W. Suh, Bruce Randall Donald, Gregory T.A. Kovacs, "Vector fields for task-level distributed manipulation: experiments with organic micro actuator arrays," Proc. 1997 IEEE Intl. Conf. on Robotics and Automation (ICRA), Albuquerque, New Mexico, 20-25 April 1997, IEEE Robotics and Automation Society, pp. 1779-1786; http://www.ee.washington.edu/faculty/karl/Publications/ICRA97.pdf; K.F. Bohringer, B.R. Donald, N.C. MacDonald, "Programmable vector fields for distributed manipulation, with applications to MEMS actuator arrays and vibratory parts feeders," Intl. J. Robotics Research 18(February 1999):168-200; http://www.ee.washington.edu/faculty/karl/Publications/IJRR98.pdf; John W. Suh, R. Bruce Darling, Karl F. Bohringer, Bruce R. Donald, Henry Baltes, Gregory T.A. Kovacs, "CMOS integrated ciliary actuator

array as a general-purpose micromanipulation tool for small objects," J. MEMS 8(December 1999):483-496; http://www.cs.dartmouth.edu/~brd/papers/jmems99.pdf or http://www.ee.washington.edu/faculty/karl/DistrManipulation/Papers/donald.pdf; Karl Friedrich Bohringer, Bruce Randall Donald, Lydia E. Kavraki, Florent Lamiraux, "Part orientation with one or two stable equilibria using programmable force fields," IEEE Trans. Robotics and Automation 16(April 2000):157-170; http://www-mtl.mit.edu/research/mems-salon/nick_fieldassemblyadvance.pdf; K.F. Bohringer, H. Choset, eds., Distributed Manipulation, Kluwer Academic Publishers, Norwell, MA, 2000; http://www.electrostatic.com/Bohringer.htm; J. Suh, R. B. Darling, K.F. Bohringer, H. Baltes, Bruce Randall Donald, G. Kovacs, "Fully programmable MEMS ciliary actuator arrays for micromanipulation tasks," IEEE Intl. Conf. on Robotics and Automation (ICRA) San Francisco, CA, April 2000, pp. 1101-1108; http://www.cs.dartmouth.edu/~brd/papers/karl-cmos-icra00.pdf; Karl Bohringer, Bruce Darling, Bruce Donald, Greg Kovacs, John Suh, "Micromanipulation with cilia arrays"; http://www.cs.dartmouth.edu/~brd/Research/MEMS/ciliaarrays.html.

[1164] C. Liu, T. Tsai, Y.C. Tai, Peter Will, C.M. Ho, "A micromachined permalloy magnetic actuator array for micro robotics assembly systems," Tech. Digest, 8th Intl. Conf. on Solid-State Sensors and Actuators/Eurosensors IX (Transducers '95), Stockholm, Sweden, 25-29 June 1995, pp. 328-331; Peter Will, Wenheng Liu, "Parts manipulation on a MEMS intelligent motion surface," ISI Research Report ISI/RR-94-391, Marina del Rey, CA, May 1994; Wenheng Liu, Peter Will, "Parts manipulation on an intelligent motion surface," Human Robot Interaction and Cooperative Robots, Proc. IEEE/RSJ Intl. Conf. on Intell. Robots and Systems (IROS), Pittsburgh, PA, Vol. 3, August 1995, pp. 399-404; Wenheng Liu, Peter Will, Michael Pottenger, "Modeling and simulation of an intelligent motion surface in MEMS," First Intl. Conf. on Simulation and Design of Microsystems and Microstructures, Southampton, England, September 1995; Murilo G. Coutinho, Peter M. Will, P. Selvan Viswanathan, "The Intelligent Motion Surface: A hardware/software tool for the assembly of meso-scale devices," Proc. 1997 IEEE Intl. Conf. on Robotics and Automation, 20-25 April 1997, IEEE Robotics and Automation Society, pp. 1755-1760; Murilo Coutinho, Peter Will, "CILIA: a programmable, task-level planning, 2-D simulation software for arrays of manipulators," Intl. Workshop on Intelligent Robotics, Brasilia, Brazil, August 1997; Murilo G. Coutinho, Peter M. Will, "A general theory for positioning and orienting 2-D polygonal or curved parts using intelligent motion surfaces," Proc. IEEE Intl. Conf. on Robotics and Automation (ICRA), Leuven, Belgium, May 1998.

[1165] J.W. Suh, S.F. Glander, R.B. Darling, C.W. Storment, G.T.A. Kovacs, "Combined organic thermal and electrostatic omnidirectional ciliary microactuator array for object positioning and inspection," Tech. Digest, Solid-State Sensors and Actuator Workshop, Hilton Head, SC, June 1996, pp. 168-173; J.W. Suh, S.F. Glander, R.B. Darling, C.W. Storment, G.T.A. Kovacs, "Organic thermal and electrostatic ciliary microactuator array for object manipulation," Sensors and Actuators A 58(1997):51-60; R.B. Darling, J.W. Suh, G.T.A. Kovacs, "Ciliary microactuatory array for scanning electron microscope positioning state," Vac. Sci. & Technol. A 16(1998):1998-2002.

[1166] H. Nakazawa, Y. Watanabe, O. Morita, "The two-dimensional micro conveyor: Principles and fabrication process of the actuator," Tech. Digest, 9th Intl. Conf. on Solid-State Sensors and Actuators (Transducers '97), Chicago, IL, 1997; L. Kavraki, "Part orientation with programmable vector fields: two stable equilibria for most parts," Proc. IEEE Intl. Conf. Robotics and Automation (ICRA), Albuquerque, NM, April 1997; H. Nakazaw, Y. Wantanabe, O. Morita, M. Edo, E. Yonezawa, "The two-dimensional micro conveyer," Tech. Digest, 9th Intl. Conf. Solid-State Sensors and Actuators (Transducers'97), Chicago, IL, 16-19 June 1997, pp. 33-36; Thorbjorn Ebefors, Johan Ulfstedt Mattsson, Edvard Kelvesten, Goran Stemme, "A robust micro conveyor realized by arrayed polyimide joint actuators," Proc. 12th IEEE Intl. Micro Electro Mechanical System Conf. (MEMS'99), Orlando, FL, 17-21 January 1999, pp. 576-581; J. Micromech. Microeng. 10(2000):1-13; http://www.s3.kth.se/mst/research/publications/pdf/2000/tejm00preprint.pdf; Jonathan Luntz, William

arrays for "electronic nose"[1167] and other applications[1168] have also been constructed, in at least one case having millions of interdigitated cantilevers on a single chip.[1169] A probe-array-based

---

Messner, "Dynamics and control of discrete distributed manipulation," CCA 2001; http://lims.mech.nwu.edu/~lynch/cca2001/INV-CCA-5-4.pdf; T.D. Murphey, J.W. Burdick, "Smooth feedback control algorithms for distributed manipulators," Intl. Conf. on Robotics and Automation (ICRA), 2003; http://www.mech.nwu.edu/lims/people/murphey/murpheyicra2003b.pdf.

[1167] R. Berger, H.P. Lang, E. Delamarche, Ch. Gerber, J.K. Gimzewski, C. Andreoli, J. Brugger, M. Despont, P. Vettiger, "Integration of silicon micromechanical arrays with molecular monolayers for miniaturized sensor systems," in A.T. Augousti, N.M. White, eds., Sensors and their Applications, Vol. 8, IOP, London, 1997, p. 71; http://monet.physik.unibas.ch/nose/rz2926.pdf; R. Berger, H.P. Lang, J.P. Ramseyer, F. Battiston, J.H. Fabian, L. Scandella, C. Andreoli, J. Brugger, M. Despont, P. Vettiger, E. Meyer, H.J. Guntherodt, Ch. Gerber, J.K. Gimzewski, "Transduction principles and integration of chemical sensors into a micromechanical array device," in A. van den Berg, P. Bergveld, eds., Sensor Technology in the Netherlands: State of the Art, Kluwer, Dordrecht, 1998, p. 33; http://monet.physik.unibas.ch/nose/rz2986.pdf; H.P. Lang, R. Berger, C. Andreoli, J. Brugger, M. Despont, P. Vettiger, Ch. Gerber, J.K. Gimzewski, J.P. Ramseyer, E. Meyer, H.J. Guntherodt, "Sequential position readout from arrays of micromechanical cantilever sensors," Appl. Phys. Lett. 72(19 January 1998):383-385; http://monet.physik.unibas.ch/~lang/pub/APL72383.pdf; H.P. Lang, R. Berger, C. Andreoli, J. Brugger, M. Despont, P. Vettiger, F. Battiston, J.P. Ramseyer, E. Meyer, T. Mezzacasa. L. Scandella, H.J. Guntherodt, Ch. Gerber, J.K. Gimzewski, "A chemical sensor based on a micromechanical cantilever array for the identification of gases and vapors," Appl. Phys. A 66(1998):S61-S64; http://www.chem.ucla.edu/dept/Faculty/gimzewski/pub/APA66S61.pdf; H.P. Lang, F.M. Battiston, M.K. Baller, R. Berger, J.P. Ramseyer, P. Fornaro, E. Meyer, H.J. Guntherodt, C. Andreoli, J. Brugger, M. Despont, P. Vettiger, J.H. Fabian, T. Mezzacasa, L. Scandella, Ch. Gerber, J.K. Gimzewski, "An electronic nose based on a micromechanical cantilever array" in D.J. Harrison, A. van den Berg, eds., Micro Total Analysis Systems, Kluwer, Dordrecht, 1999, pp. 57-60; http://monet.physik.unibas.ch/nose/UTAS.pdf; H.P. Lang, M.K. Baller, F.M. Battiston, J. Fritz, R. Berger, J.P. Ramseyer, P. Fornaro, E. Meyer, H.J. Guntherodt, J. Brugger, U. Drechsler, H. Rothuizen, M. Despont, P. Vettiger, Ch. Gerber, J.K. Gimzewski, "The nanomechanical NOSE," 12th IEEE Intl. Conf. on Micro Electro Mechanical Systems, 1999, pp. 9-13; http://www.chem.ucla.edu/dept/Faculty/gimzewski/pub/mems99.pdf; H.P. Lang, M.K. Baller, R. Berger, Ch. Gerber, J.K. Gimzewski, F.M. Battiston, P. Fornaro, J.P. Ramseyer, E. Meyer, H.J. Guntherodt, "An artificial nose based on a micromechanical cantilever array," Analytica Chimica Acta 393(1999):59-65; http://monet.unibas.ch/nose/rz3068.pdf; M.K. Baller, H.P. Lang, J. Fritz, Ch. Gerber, J.K. Gimzewski, U. Drechsler, H. Rothuizen, M. Despont, P. Vettiger, F.M. Battiston, J.P. Ramseyer, P. Fornaro, E. Meyer, H.J. Guntherodt, "A cantilever array based artificial nose," Ultramicroscopy 82(2000):1-9; http://monet.physik.unibas.ch/nose/ult821.pdf; F.M. Battiston, J.P. Ramseyer, H.P. Lang, M.K. Baller, Ch. Gerber, J.K. Gimzewski, E. Meyer, H.J. Guntherodt, "A chemical sensor based on a microfabricated cantilever array with simultaneous resonance-frequency and bending readout," Sensors and Actuators B 77(2001):122-131; http://monet.physik.unibas.ch/nose/battiston.pdf; B.H. Kim, F.E. Prins, D.P. Kern, S. Raible, U. Weimar, "Multicomponent analysis and prediction with a cantilever array based gas sensors," Sensors and Actuators B 78(2001):12-18.

[1168] K.M. Hansen, H.F. Ji, G. Wu, R. Datar, R. Cote, A. Majumdar, T. Thundat, "Cantilever-based optical deflection assay for discrimination of DNA single-nucleotide mismatches," Anal. Chem. 73(1 April 2001):1567-1571; Guanghua Wu, Ram H. Datar, Karolyn M. Hansen, Thomas Thundat, Richard J. Cote, Arun Majumdar, "Bioassay of prostate-specific antigen (PSA) using microcantilevers," Nat. Biotechnol. 19(1 September 2001):856-860; R. McKendry, J. Zhang, Y. Arntz, T. Strunz, M. Hegner, H.P. Lang, M.K. Baller, U. Certa, E. Meyer, H.-J. Güntherodt, Ch. Gerber, "Multiple label-free biodetection and quantitative DNA-binding assays on a nanomechanical cantilever array," Proc. Nat. Acad. Sci. (USA) 99(2002):9783-9787; http://monet.physik.unibas.ch/~lang/pub/pnas2002.pdf; Y. Arntz, J.D. Seelig, H.P. Lang, J. Zhang,

"micro-factory" for site-specific deposition of desired molecular feedstock moieties from gas phase onto a planar workpiece surface has been proposed.[1170]

Active probe arrays for dip-pen nanolithography using DNA-based "ink" have been developed by Mirkin's group.[1171] At a Materials Research Society meeting in late 2002,[1172] Mirkin reported that his group had constructed an array of 10,000 microscope tips, each capable of acting independently from the others. By using 10 tips in concert they can draw essentially any desired shape. "The goal is to use dip pen nanolithography to generate [DNA-based] templates on surfaces that guide the assembly of nanoscale building blocks," Mirkin says. "It opens the door to placing electronic particles right where you want them. We think it's ultimately going to be a production tool....This is not going to stop at 10,000. We can make arrays of arrays." By 2008,

---

P. Hunziker, J.-P. Ramseyer, E. Meyer, M. Hegner, Ch. Gerber, "Label-free protein assay based on a nanomechanical cantilever array ," Nanotechnology 14(2003):86-90; http://monet.physik.unibas.ch/nose/t30119.pdf.

[1169] "Microcantilever Arrays," Protiveris Corp., 2003; http://www.protiveris.com/cantilever_tech/microcantileverarrays.html.

[1170] Massood Tabib-Azar, Morton Litt, "Silicon wafer-scale micro-fabrication factory using scanning probe micro-robots," presentation at the Fifth Foresight Conference on Molecular Nanotechnology, 1997; http://www.foresight.org/Conferences/MNT05/Abstracts/Tabiabst.html.

[1171] Seunghun Hong, Chad A. Mirkin, "A nanoplotter with both parallel and serial writing capabilities," Science 288(9 June 2000):1808-1811; http://www.nanotechnology.northwestern.edu/press/Science%20.Vol288.9june2000.pdf; Ming Zhang, David Bullen, Kee S. Ryu, Chang Liu, S. Hong, S. Chung, Chad Mirkin, "Passive and active probes for dip pen nanolithography," First IEEE Conference on Nanotechnology, 28-30 October 2001, Maui, HI; http://mass.micro.uiuc.edu/publications/papers/64.pdf; D. Bullen, M. Zhang, C. Liu, "Thermal-mechanical optimization of thermally actuated cantilever arrays," Smart Electronics, MEMS, and Nanotechnology Conference (4700), SPIE's 9th Annual International Symposium on Smart Structures and Materials, 17-21 March 2002, San Diego, CA; http://mass.micro.uiuc.edu/publications/papers/70.pdf; Ming Zhang, David Bullen, Sung-Wook Chung, Seunghun Hong, Kee S. Ryu, Zhifang Fan, Chad A. Mirkin, Chang Liu, "A MEMS nanoplotter with high-density parallel dip-pen nanolithography probe arrays," Nanotechnology 13(April 2002):212-217; http://mass.micro.uiuc.edu/publications/papers/72.pdf; X. Wang, D. Bullen, J. Zou, K. Ryu, C. Liu, S.W. Chung, C. Mirkin, "Linear probe arrays for dip-pen nanolithography," Intl. Conf. on Micro & Nano Systems (ICMNS 2002), 11-14 August 2002, Kunming, China; http://mass.micro.uiuc.edu/publications/papers/74.pdf; D. Bullen, S. Chung, X. Wang, J. Zou, C. Liu, Chad Mirkin, "Development of parallel dip pen nanolithography probe arrays for high throughput nanolithography," (Invited) Symposium LL: Rapid Prototyping Technologies, Materials Research Society Fall Meeting, Boston, MA, Proceedings of the MRS, Vol. 758, 2-6 December 2002; http://mass.micro.uiuc.edu/publications/papers/84.pdf; D. Bullen, X. Wang, J. Zou, S. Hong, S. Chung, K. Ryu, Z. Fan, C. Mirkin, C. Liu, "Micromachined arrayed dip pen nanolithography probes for sub-100 nm direct chemistry patterning," Proc. 16th IEEE International Micro Electro Mechanical Systems Conference, MEMS 2003, Kyoto, Japan, 19-23 January 2003; http://mass.micro.uiuc.edu/publications/papers/86.pdf; Jun Zou, David Bullen, Xuefeng Wang, Chang Liu, Chad A. Mirkin, "Conductivity-based contact sensing for probe arrays in dip-pen nanolithography," Appl. Phys. Lett. 83(2003):581.

[1172] Robert F. Service, "Nanotechnology: Biology Offers Nanotechs a Helping Hand," 20 December 2002; http://www.sciencemag.org/cgi/content/full/298/5602/2322?etoc.

Mirkin's group reported[1173] the ability to write 1 molecule thick dots with a diameter of 100 ±20 nm and a spacing of 400 nm, using a 55,000-tip array of gold-coated Si_3N_4 cantilevers to write complex dot patterns (Figure VIII-4), and they "have discovered a way to fabricate arrays that consist of over one million cantilevers." (A million-tip DPN array (Figure VIII-5) has been fabricated by the Micro Nano Technology Research Group at the University of Illinois.)[1174] However, none of these existing microcantilever systems is atomically precise.

Figure VIII-4. A 55,000-pen array[1175] can create patterns on Au or glass substrates using a 1-octadecanethiol (ODT) ink. Arrays consisting of Au-coated Si_3N_4 cantilevers, having sharp tips at one end, are used as pens to fabricate surface patterns in parallel on a massive scale. The arrays are organized over a 1 cm^2 area with cantilever spacings of 90 µm and 20 µm in the *x* and *y* directions, respectively. The 55,000 pens can fabricate approximately 88 million, 1 molecule high ODT dots with a diameter of 100 ± 20 nm and a spacing of 400 nm. An image of Thomas Jefferson is reproduced 55,000 times in under 30 minutes by holding the probe array in contact with a substrate for 0.08 sec and then traveling between specific points at a scan speed of 60 microns/sec.

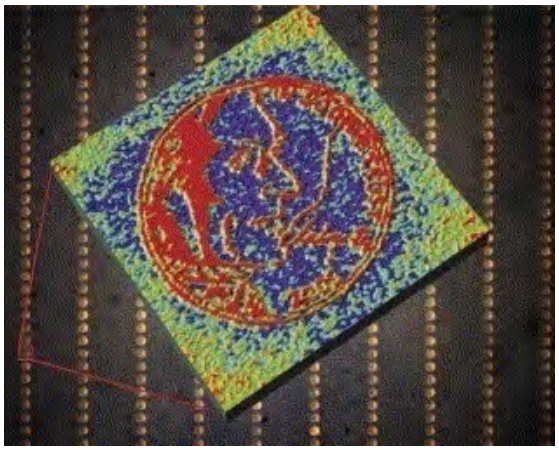

[1173] K. Salaita, Y. Wang, C.A. Mirkin, "Massively Parallel Dip-Pen Nanolithography with 55,000 Two-Dimensional Arrays," Angew. Chem. Int. Edit. 45(2006):7220-7223. See also: Katerina Busuttil, "Thomas Jefferson is spotted in large numbers Surface patterning," NanoToday 1(November 2006)10; http://www.sciencedirect.com/science?_ob=ArticleURL&_udi=B82X8-4M97WHX-5&_user=10&_coverDate=11%2F30%2F2006&_rdoc=1&_fmt=&_orig=search&_sort=d&view=c&_acct=C000050221&_version=1&_urlVersion=0&_userid=10&md5=4fe038c67c68e5df6e206ecb317cfc59.

[1174] "MNTR Research Focus Slide Show: Passive Parallel DPN Array," 2006, http://mass.micro.uiuc.edu/research/current/nanolithography/2006-focus-intro/slide11.html.

[1175] K. Salaita, Y. Wang, C.A. Mirkin, "Massively Parallel Dip-Pen Nanolithography with 55,000 Two-Dimensional Arrays," Angew. Chem. Int. Edit. 45(2006):7220-7223. See also: Katerina Busuttil, "Thomas Jefferson is spotted in large numbers Surface patterning," NanoToday 1(November 2006)10; http://www.sciencedirect.com/science?_ob=ArticleURL&_udi=B82X8-4M97WHX-5&_user=10&_coverDate=11%2F30%2F2006&_rdoc=1&_fmt=&_orig=search&_sort=d&view=c&_acct=C000050221&_version=1&_urlVersion=0&_userid=10&md5=4fe038c67c68e5df6e206ecb317cfc59.

Figure VIII-5. A million-tip DPN array fabricated by the Micro Nano Technology Research Group at the University of Illinois.[1176]

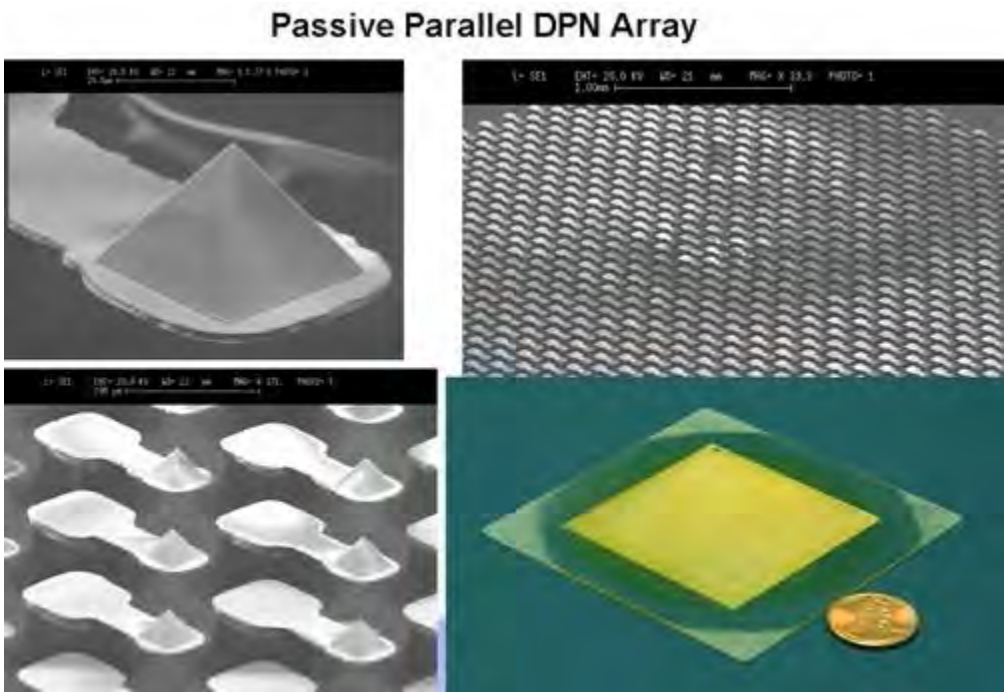

The PALE-based surface remediation effort required in this Task seems to involve lots of surface, lots of remediation, lots of MEMS-based SPMs working in parallel with high reliability, and may require significant funding to develop. However, by this point in our nanofactory program (i.e., ~Year 14-16; Section 4.2) other organizations such as Zyvex Corp. will have accumulated more than a decade of experience developing multi-tip PALE systems, so we believe the technology will be available if/when it is needed, 15 years hence.

3.9.4 Task VIII-3: Replicate NMW-2 on Both Wafers to Full Monolayer Coverage

Task VIII-3 is to exponentially manufacture 10^{11} NMW-2 units on two wafers simultaneously using the plate/plate replication technique that has already been demonstrated in Task VII-5 (Section 3.8.6), Task VII-6 (Section 3.8.7), and Task VII-7 (Section 3.8.8).

[1176] "MNTR Research Focus Slide Show: Passive Parallel DPN Array," 2006, http://mass.micro.uiuc.edu/research/current/nanolithography/2006-focus-intro/slide11.html.

Buildout of 10^{11} NMW-2 units starting from a single unit will require a minimum of $\log_{10}(10^{11})/\log_{10}(2) \sim 37$ replicative generations. Since manufacturing processes are imperfect and may occasionally create nonfunctioning NMW-2 units (Section 3.9.2), and since some units will fail during use, and since even an optimal plate shift sequence will result in some unavoidable waste of replicative cycles, we presume that ~40 replicative generations will suffice to completely build out all available worksites on a wafer. Assuming each replication cycle (operated at 120 MHz) typically requires ~128,700 sec (~1.5 days; Section 3.8.8) to complete, full wafer buildout then requires ~5.15 x 10^6 sec (~60 days).

Note that since some sites will inevitably be ruined and other sites will contain nonfunctional partial or complete replicas due to unavoidable manufacturing error, each wafer will contain a small number of unproductive sites. These locations can be mapped and stored in an on-wafer memory cache, allowing the external control computer to later read this information and adjust its use patterns during subsequent manufacturing operations that employ the wafer.

3.9.5 Task VIII-4: Build Additional Plate Handlers and Replicate 1024 NMW-2 Wafers

Task VIII-4 is to exponentially manufacture 1024 NMW-2 wafers (fully built-out with 10^{11} NMW-2 units on each wafer) using the plate/plate replication technique already demonstrated in Task VIII-3.

Once the first pair of fully built-out NMW-2 wafers has been manufactured in Task VIII-3, one of these two wafers is placed in a second plate handler system. Each plate handler is loaded with a blank wafer oriented with its multielectrode assembly surface (Section 3.9.3) facing the built-out NMW-2 wafer, and then Task VIII-3 is repeated, operating the two plate handlers in tandem. Once the second cycle is completed, we now have four fully built-out NMW-2 wafers. These four wafers are distributed amongst four plate handlers analogous to the previous cycle and the process is repeated again. After a total of 9 cycles of this procedure, we have manufactured a total of 1024 fully built-out NMW-2 wafers that are held in 512 plate handlers.

Since all NMW-2 units on a built-out wafer can be operated simultaneously, the replication time for a built-out wafer is equal to the replication time for a single NMW-2 unit. Assuming each replication cycle (operated at 120 MHz) typically requires ~128,700 sec (~1.5 days; Section 3.8.8) to complete, which includes accelerated pumpdown and plate changeout times, then full wafer replication thus also requires ~128,700 sec (~1.5 days). Thus 9 generations of wafer buildout require 1,158,300 sec (~13.4 days). (Note that operation at 12 MHz rather than 120 MHz using the same accelerated pumpdown and plate changeout times would increase NMW-2 replication time to 250,200 sec, thus requiring ~40(250,200 sec) = 1 x 10^7 sec (~116 days) to build out the first NMW-2 wafer and then ~9(250,200 sec) = 2.25 x 10^6 sec (~26 days) to build out the remainder of the 1024 NMW-2 wafers in 9 generations of plate/plate replication.)

The main process bottleneck in completing Task VIII-4 is the production of 512 plate handler systems. These are macroscale devices that must be produced linearly using macroscale manufacturing systems that are not described in this proposal. The completion of Task VIII-4 will most likely be driven almost entirely by the time required to manufacture 512 plate handlers and their accessory equipment.

In the most optimistic scenario, plate handlers are built and placed into service fast enough not to constrain total buildout time, in which case the buildout of 1024 NMW-2 wafers would require ~5.15 x 10^6 sec (~60 days) for the first two wafers and ~(9)(128,700 sec) = 1,158,300 sec (~13.4 days) to complete the buildout, a total of ~73.4 days (~0.2 year).

In the most pessimistic scenario, plate handlers take so long to build and place into service that just one plate handler is available throughout, in which case the buildout of 1024 NMW-2 wafers would require ~5.15 x 10^6 sec (~60 days) for the first two wafers and ~(1022)(128,700 sec) = 1.32 x 10^8 sec (~4.2 years) to complete the buildout, a total of ~4.4 years.

Once finished, the field of ~10^{14} NMW-2 units present on the 1024 NMW-2 wafers could then fabricate atomically precise nanoparts, and can assemble them into nanodevices and complex nanosystems like the NMW-2, from atoms at the aggregate rate of 10^{14} x 1000 atoms/sec = 10^{17} atoms/sec (~0.06 kg/year). The individual NMW-2 unit is ~200 nm in size with a crane arm that can reach ~200 nm away, and the NMW-2 units can make alternative product objects that are also on the order of (up to) 100-200 nm in size.

Since each plate handler mechanism should fit within a ~20 cm cube or an ~8000 cm^3 volume (Section 3.8.4), 1024 plate-handler-halves represent a total mechanism volume of 8.192 m^3, so to run all plate handlers simultaneously in factory mode probably requires at least ~10 m^3 of pumpable UHV volume with a specific ideal vacuum chamber geometry yet to be determined (see Section 3.11.7).

3.10 Phase IX: Micro-Assembler Manipulator (MAM) and Micro-Assembler Array (MAA)

The key objective of Phase IX is to build a massively parallel array of micron-scale manipulators capable of reliably assembling (with inspection) void-free solid planes of close-fitting submicron-scale nanomachinery, or other micron-scale compound product objects, from submicron-scale product objects manufactured by the NMW-2 wafer. While this may provide an early general-purpose microassembly capability, the immediate need is for a manipulator array that can accept submicron-scale manufacturing modules produced by the NMW-2 Wafers in Phase VIII and efficiently and precisely stack these modules side by side to form a fabricator array that can form the lowest production layers of the first-generation nanofactory to be created in Phase X (Section 3.11).

The Micro-Assembler Manipulator (MAM) and the Micro-Assembler Array (MAA) are briefly described in Section 3.10.1 and illustrated in Figure IX-1. This is followed by an enumeration of the specific tasks required to exponentially manufacture a large number of NMW-2 wafers which include: design and simulation of MAM and MAA (Section 3.10.2), preparation of multielectrode MAM test-assembly surfaces for experimentation (Section 3.10.3), manufacture and operation of the first MAM (Section 3.10.4), preparation of whole-wafer multielectrode MAA wafers (Section 3.10.5), manufacture and operation of one MAA wafer (Section 3.10.6), build-out of 200 MAA wafers (Section 3.10.7), and finally modification needed for high-frequency operation (Section 3.10.8).

3.10.1 Description of the MAM and MAA

The Micro-Assembler Manipulator (MAM) is described in Section 3.10.1.1 and the Micro-Assembler Array (MAA) is described in Section 3.10.1.2 below, followed by a summary of error rates and reliability issues in MAM/MAA manufacture and operation (Section 3.10.1.3).

3.10.1.1 Description of the Micro-Assembler Manipulator (MAM)

The Micro-Assembler Manipulator (MAM) is a 6-DOF (degrees-of-freedom) manipulator of the same basic design as the NAW large crane arm described in Section 3.6.1.1 but ten times larger in every dimension. The MAM thus consists of 7 Stewart platform struts of 4 segments each with a reach envelope of 2000.0 nm (2 microns) when fully extended and 680.0 nm when fully retracted. For the four MAM segments, the 4th segment is a cylinder 50 nm wide and ~435 nm long (solid volume = 854,000 nm^3, passivation surface area = 72,300 nm^2); the 3rd segment is an annulus 100 nm wide of length ~544 nm with radii 25 nm and 50 nm (volume = 3,204,000 nm^3, passivation surface area = 268,100 nm^2); the 2nd segment is an annulus 150 nm wide of length ~680 nm with radii 50 nm and 75 nm (volume = 6,676,000 nm^3, passivation surface area = 553,700 nm^2); and the 1st segment is an annulus 200 nm wide of length ~680 nm with radii 75 nm and 100 nm (volume = 9,346,000 nm^3, passivation surface area = 775,200 nm^2). This means the minimum footprint of a hexagonal strut pattern with the 7th strut placed in the middle would be ~3 x 200 nm ~ 600 nm wide or ~280,000 nm^2; however, we will employ a single 1,000,000 nm^2 foundation block to most easily accommodate the future construction of the MAM array which allocates 1 $micron^2$ per MAM with a 1 micron separation between manipulators in the array (Section 3.10.1.2).

Figure IX-1. Schematic illustration of a single Micro-Assembler Manipulator (MAM), at left, and a completely built-out Micro-Assembler Array (MAA), at right, consisting of 2 x 10^{11} copies of the MAM. Not to scale.

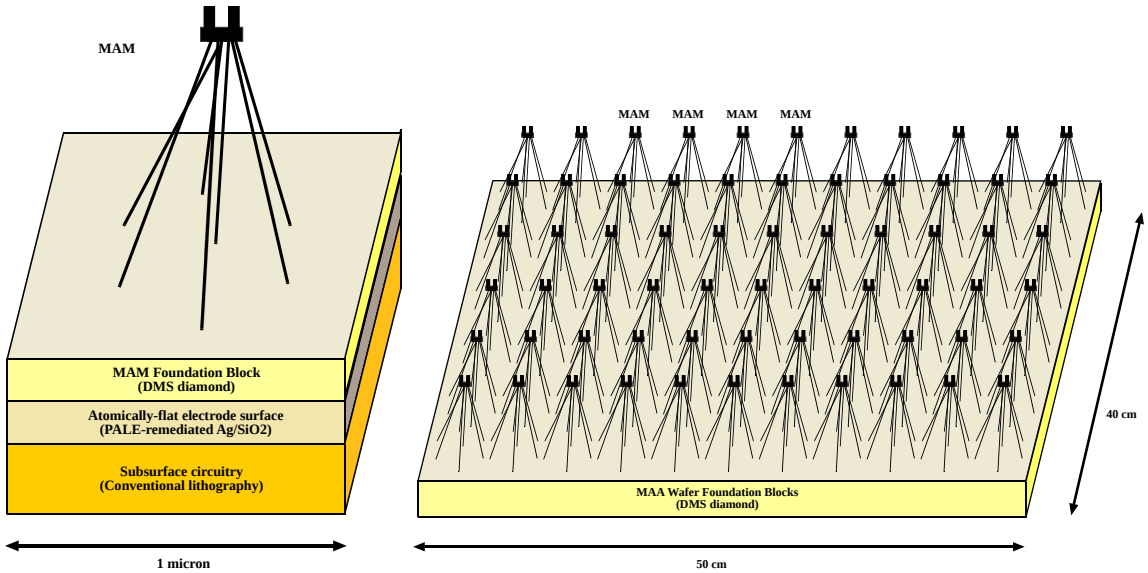

Each segment-driving rotary motor (Section 3.4.1.1) is assumed to be electrically driven, to consist of four parts (rotor, stator, output gear, and housing) and to fit within a box requiring a solid diamondoid material volume of ~200,000 nm^3 and ~50,000 nm^2 of passivated diamondoid surface area per motor. Operating each motor at a frequency of ν_d ~ 1.3 MHz produces a mechanical output power of P_{motor} ~ 20 pW (power density ~10^{11} watts/m^3). The force generated on the slab during Δx = 2 nm displacements is therefore $F_{motor} = P_{motor} / (\Delta x\ \nu_d)$ ~ 10 nN, with each control pulse rotating the threaded screw through a circumferential distance of 2 nm. This rotation produces 0.2 nm of forward motion of the screw (per pulse) with a force of 100 nN applied to the strut (due to the 10:1 mechanical advantage), or a maximum of ~600 nN for all 6 power struts in an ideal geometry, with a maximum MAM tip travel speed of 0.26 mm/sec. Note also that a ~20 pW motor operated at ~1.3 MHz is applying a per pulse energy of ~2 x 10^{-17} J or ~5000 k_BT/pulse at 300 K or ~20,000 k_BT/pulse at 80 K, which is more than sufficient to ensure high reliability. One round trip manipulator motion comprised of two sets of full range strut motions or ~2(2000.0 nm – 680.0 nm) ~ 2640 nm, using 0.2 nm step increments at ~1.3 MHz, would require ~0.01 sec for the MAM to complete (~100 round trip motions/sec) with a pulse budget of 13,200 pulses per round trip. Note that in the final task of Phase IX (Section 3.10.8), the operating frequency is increased from 1.3 MHz to 120 MHz, which in turn increases maximum MAM tip travel speed to 2.6 cm/sec. The current delivered to each motor is $I_{motor} = P_{motor} / V_{cap}$ ~ 2 x 10^{-11} amp.

Each motor is fixed to a foundation block and attached to the universal joint which in turn connects to the base of the sheath (the 1st segment) of each strut; rotating the sheath extends or retracts the other three segments comprising the strut. There is one locking latch (assumed volume ~50,000 nm^3 and ~10,000 nm^2 each, or 200,000 nm^3 and 40,000 nm^2 for all 4 on each

strut) for each of the 4 segments comprising each strut. Each universal joint is assumed to consist of 2 parts and ~40,000 nm^3 of solid diamond structure with ~8,000 nm^2 of passivated diamondoid surface area. Foundation blocks are allocated 10^6 nm^2 x 100 nm thick, but using a honeycomb structure to eliminate 90% of mass, this adds 10^7 nm^3 of solid structure and 2.4 x 10^6 nm^2 of passivated surface; since our maximum fabricable nanopart dimension is 100 nm, a 1 $micron^2$ foundation block must be assembled from 100 subcomponents that each are 100 nm in edge length (i.e., 10^4 nm^2 x 100 nm thick). (A smaller foundation block might suffice for array assembly on the standard multielectrode surface.) The triangular tool chuck is assumed to be a half-square of area (1/2) $(200\ nm)^2$ at its base, 100 nm thick, and to include three integral nanoparts (housing with fixed backstop, a moving rack-mounted gripper plate, and a drive gear), adding 2,500,000 nm^3 of solid structure and ~300,000 nm^2 of passivated diamondoid surface. Electrical leads connecting control lines to each motor are 2 nm diameter unpassivated single-walled carbon nanotube x 500 nm long, adding ~3140 nm^2 x ~0.154 nm thickness ~ 480 nm^3 of unpassivated carbon nanotube wire solid volume, or 960 nm^3 for each hot/ground pair of wires; atom count is ~3140 nm^2 x ~31 C atoms/nm^2 ~ 97,340 C atoms per wire pair. (Note that even at 120 MHz, each wire carries only ~2 nW of power at ~ 1 V or ~ 2 x 10^{-9} amp/wire, or 2.8 x 10^{-8} amps for the common ground line for all 14 control lines, both well below the peak 25-100 x 10^{-6} amp/wire currents observed experimentally[1177] for individual 10-50 nm long single-walled "metallic" carbon nanotubes.)

The MAM also has a force sensor of the type previously described in Section 3.4.1.3, except that the tripped latch will operate (in reverse) an electric motor assumed to be similar to the one described in Section 3.4.1.1, whose mechanical actuation generates an electrical impulse which travels through a wire to a silver electrode and from there back to the semiconductor-based embedded computer where sensor data is processed to provide feedback control to operate the MAM (each MAM is individually controlled, not bus-controlled). The dimensions of these items are also scaled up tenfold from the previous design, with the rod and latch adding 50,000 nm^3 of solid structure and ~29,000 nm^2 of passivated surface. Allowing an additional 2,107,920 nm^3 of material volume and 258,000 nm^2 of passivated surface area (which assumes the stated unallocated volume is divided among ~20 "typical smallest" ~10^5 nm^3 cubic parts) for unallocated diamond lattice structure gives the results for the MAM as shown in Table IX-1.

[1177] Ali Javey, Pengfei Qi, Qian Wang, Hongjie Dai, "Ten- to 50-nm-long quasi-ballistic carbon nanotube devices obtained without complex lithography," PNAS 101(14 September 2004):13408-13410; http://www.pnas.org/cgi/content/abstract/101/37/13408.

Table IX-1. Volume and Parts Estimate for Micro-Assembler Manipulator (MAM)					
Nanopart or Nanodevice	**Number of Com-ponents**	**Solid Volume each (nm^3)**	**# Parts / Com-ponent**	**Solid Volume All (nm^3)**	**Total # of All Parts**
Strut Segment 4	7	854,000	1	5,978,000	7
Strut Segment 3	7	3,204,000	1	22,428,000	7
Strut Segment 2	7	6,676,000	1	46,732,000	7
Strut Segment 1	7	9,346,000	1	65,422,000	7
Locking Latches	28	50,000	1	1,400,000	28
Rotary motors	13	200,000	4	2,600,000	52
Electrical leads	13	960	2	12,480	26
Universal joints	14	40,000	2	560,000	28
Foundation blocks	1	10,000,000	100	10,000,000	100
End-effector	1	2,500,000	3	2,500,000	3
Sensor Assembly:					
Rod and Latch	1	50,000	3	50,000	3
Rotary Motor	1	200,000	4	200,000	4
Electrical Leads	1	9600	2	9600	2
Unallocated structure	1	2,107,920	1	2,107,920	1
TOTALS	**102**			**160,000,000**	**275 parts**

Allocating ~176 C atoms/nm^3 for diamondoid lattice and ~31 H atoms per nm^2 to passivate diamondoid surface gives the scaling results for the entire MAM as shown in Table IX-2. We further allocate 840,000,000 nm^3 of empty space to allow for clearance between struts, giving a total operational volume for the NAW of 1,000,000,000 nm^3 approximating a (1 micron)^3 cube having a ~1,000,000 nm^2 (~1 micron x ~1 micron) footprint on the chip surface, with a total atom count of ~28,648,687,100 atoms (98.3% C atoms, 1.7% H atoms) and a total part count of 275. The "average" part in the MAM has a volume of ~581,818 nm^3 (an ~83.5 nm cube) and is composed of ~104,177,044 atoms. Thus each of the 275 MAM parts may be regarded as a block of nanomachinery very roughly equivalent in size to an entire NMW-2 unit (Section 3.8.1.1 and Table VI-1) and may consist of a single very large simple or compound nanopart or a nanodevice composed of numerous smaller nanoparts. If a train of up to ~8.99 x 10^{13} control pulse cycles is needed to replicate an NMW-2 unit (Section 3.7.1.3), then if each MAM structure of comparable size (~129,194,836 atoms) also requires up to ~8.99 x 10^{13} pulse cycles to build, then building a MAM (28,648,687,100 atoms) requires up to ~2 x 10^{16} control pulse cycles and building out an entire 2000 cm^2 MAA wafer comprised of 2 x 10^{11} MAMs may require up to ~4 x 10^{27} control pulse cycles (though these will be executed massively in parallel by NMW-2 units driven in unison via ganged data buses, not in serial sequence).

Table IX-2. Estimated Atom Counts for Micro-Assembler Manipulator (MAM)						
MAM Nanopart or Nanodevice	**# of prts**	**Total Solid Volume (nm^3)**	**Total Passiv. Area (nm^2)**	**# of C Atoms**	**# of H Atoms**	**Total # of Atoms**
Strut Segment 4	7	5,978,000	506,100	1,052,128,000	15,689,100	1,067,817,100
Strut Segment 3	7	22,428,000	1,876,700	3,947,328,000	58,177,700	4,005,505,700
Strut Segment 2	7	46,732,000	3,875,900	8,224,832,000	120,152,900	8,344,984,900
Strut Segment 1	7	65,422,000	5,426,400	11,514,272,000	168,218,400	11,682,490,400
Locking Latches	28	1,400,000	280,000	246,400,000	8,680,000	255,080,000
Rotary motors	52	2,600,000	650,000	457,600,000	20,150,000	477,750,000
Power/control wire + ground	26	12,480	0	2,196,480	0	2,196,480
Universal joints	28	560,000	112,000	98,560,000	3,472,000	102,032,000
Foundation blocks	100	10,000,000	2,400,600	1,760,000,000	74,400,000	1,834,400,000
End-effector	3	2,500,000	300,000	440,000,000	9,300,000	449,300,000
Force Sensor	9	259,600	79,000	45,689,600	2,449,000	48,138,600
Unallocated structure	1	2,107,920	258,000	370,993,920	7,998,000	378,991,920
TOTALS	**275**	**160,000,000**	**15,764,100**	**28,160,000,000**	**488,687,100**	**28,648,687,100**

There are 13 actuators (individually controlled electrostatic motors) and 1 sensor in the MAM, so we need 14 separate control lines (plus one common ground line for a total of 15) for each MAM to avoid multiplexing and allow direct control of each individual actuator, the conceptually simplest approach. Note that 6 additional sensors (allowing one per strut assembly or DOF; these could include positional, force, or other types of sensors if needed) could easily be added to the existing design if desired, at a minimal extra cost of ~1% more atoms and 6 extra electrical lines per MAM.

3.10.1.2 Description of the Micro-Assembler Array (MAA) and Buildout of the MAA Wafer

The Micro-Assembler Array (MAA) consists of 2 x 10^{11} copies of the Micro-Assembler Manipulator (MAM) arranged in a compact 400,000 x 500,000 manipulator array covering an entire 40 cm x 50 cm MAA electrode wafer surface (Section 3.10.1.3). Each MAM occupies a square 1 $micron^2$ site on the square 2000 cm^2 (2 x 10^{11} $micron^2$) MAA wafer surface, so each electrode wafer surface has a total of 3 x 10^{12} electrodes arranged in 2 x 10^{11} sites with 15 power/control electrodes (13 actuators, 1 sensor, 1 ground) at each 1 $micron^2$ site. Each MAM is comprised of (mostly carbon) 28,648,687,100 atoms (Table IX-2), so building 2 x 10^{11} copies of a MAM on a single MAM electrode wafer surface requires the fabrication and assembly of ~5.72 x 10^{21} atoms. Each replication cycle of a 129,194,836-atom NMW-2 unit requires 128,700 sec (~1.5 days) at the 120 MHz control pulse frequency, including pumpdown and plate changeout (Section 3.8.8), hence each NMW-2 wafer comprised of 10^{11} NMW-2 units can fabricate and assemble ~1.29 x 10^{19} atoms during each ~128,700 sec production cycle. If MAM components can be built and installed via plate/plate assembly at approximately the same rate as NMW-2

components, then a straightforward buildout of an entire MAA wafer would require ~(5.72×10^{21} atoms/MAA wafer) / (1.29×10^{19} atoms/cycle) ~ 444 production cycles of one NMW-2 wafer. Thus a single NMW-2 wafer could assemble a single MAA wafer in (~444)(128,700 sec) ~ 5.71×10^{7} sec (~1.8 years); 200 NMW-2 wafers (out of the 1024 NMW-2 wafers available; Section 3.9.5) if operated in parallel could produce 200 built-out MAA wafers in the same time period (~1.8 years). On the other hand, if 444 NMW-2 wafers are simultaneously employed to manufacture the components of an MAA wafer in parallel, and if components from 444 different NMW-2 wafers can be assembled on a single MAA wafer without significant additional time penalties for plate changeout or other plate-handling activities (since NMW-2 productivity is fabrication-speed limited, not assembly-speed limited; Section 3.7.1) then an entire MAA wafer could be built out in ~128,700 sec. Employing all available 1024 NMW-2 wafers in an effort to build out 200 MAAs would require (444 wafer-cycles/MAA) (200 MAAs) / (1024 wafers) ~ 87 production cycles or ~1.12×10^{7} sec (~130 days).

Each MAM will have sensory feedback. Sensory data is transmitted back through the surface electrodes on the MAM electrode wafer surface upon which each MAM is constructed, and is received by conventional semiconductor-based computer electronics embedded in the wafer surface which can use the sensory data to modify the operating actions of the MAM arm in real time. According to the ITRS semiconductor industry roadmap,[1178] by 2016 the anticipated DRAM cell area (in which a single bit can be reliably transacted (written, stored, and retrieved) is 0.003 micron^2 (~333/micron^2), and 0.002 micron^2 (~500/micron^2) for flash memory – the required surface density of 15/micron^2 for individually addressable electrodes is well within the state of the art, even for 2008 technology (i.e., 53/micron^2 for DRAM, 100/micron^2 for flash).[1179] The semiconductor roadmap also predicts ~185 functions/micron^2 for DRAM and ~850 functions/micron^2 for flash multilevel chips by 2016 (1 function ~ 1 transistor or switch), which should provide sufficient storage and computational capacity to locally process all sensory feedback data and manipulator control signals for each adjacent 1 micron^2 MAM worksite on the MAA wafer.

The MAA wafer surface is a plate of single-crystal ultrapure silicon that is approximately 40 cm x 50 cm square upon which multiple layers of electronic control circuitry have been previously been deposited using conventional lithography, with the topmost layer consisting of atomically

---

[1178] International Technology Roadmap for Semiconductors (ITRS), 2006 Update. "Overview and Working Group Summaries," Tables 1a (Product Generations and Chip Size Model Technology Trend Targets—Near-term Years) and 1b (Product Generations and Chip Size Model Technology Trend Targets—Long-term Years), p.3; http://www.itrs.net/Links/2006Update/FinalToPost/00_ExecSum2006Update.pdf; see also in "Lithography," pp. 7-8; http://www.itrs.net/Links/2006Update/FinalToPost/08_Lithography2006Update.pdf.

[1179] International Technology Roadmap for Semiconductors (ITRS), 2006 Update. "Overview and Working Group Summaries," Tables 1a (Product Generations and Chip Size Model Technology Trend Targets—Near-term Years) and 1b (Product Generations and Chip Size Model Technology Trend Targets—Long-term Years), p.3; http://www.itrs.net/Links/2006Update/FinalToPost/00_ExecSum2006Update.pdf; see also in "Lithography," pp. 7-8; http://www.itrs.net/Links/2006Update/FinalToPost/08_Lithography2006Update.pdf.

flat silicon dioxide insulator interrupted only by fifteen 100 nm x 100 nm atomically flat electrodes arranged in adjacent 1 micron^2 (1,000,000 nm^2) MAM worksites. At 15 electrodes per worksite, the electrodes cover ~15% of the wafer surface. We assume that the wafer surface is oriented parallel to one of the fundamental crystal planes, thus avoiding highly vicinal surfaces (subordinate crystal planes at slight angles to the fundamental planes, imparting to the surface an array of numerous regularly-spaced steps and terraces); unavoidable mid-wafer steps can be herded (via PALE remediation) into the narrow inter-workspace regions of the wafer where they will not affect manufacturing operations within the workspace areas.

A fully built-out MAA wafer will have one working MAM installed at each of the 2 x 10^{11} individual worksites on the wafer, giving a total of 2 x 10^{11} installed MAM units per wafer. The wafer will be controlled by electrical connections leading from the wafer through the plate handling system to an external source of control and power signals (e.g., a macroscale benchtop computer controller). Even assuming a continuous average duty cycle of 100% for each MAM in the MAA and a worst-case continuous power draw of (8 motors x 20 pW/motor) ~ 160 pW per MAM for mechanical operations at a 1.3 MHz pulse control frequency (Section 3.10.1.1), the maximum power draw for the entire 2000 cm^2 MAA wafer is only ~32 watts. This is dwarfed by the maximum allowable power of ~128,000 watts per 2000 cm^2 wafer area for the electronic circuitry on high performance chips with heatsinks (198 watts per 3.1 cm^2 chip area) that is anticipated for 2015-2017 by the semiconductor industry.[1180]

Building and controlling a single ~2000 cm^2 active wafer surface will be technically challenging. However, it may be possible to redesign the Phase X assembly process (Section 3.11.10.3) to employ larger numbers of smaller MAAs, e.g., closer to the 10 cm x 10 cm plates used in earlier Phases.

3.10.1.3 Reliability of MAM/MAA Manufacture and Operation

Each MAM consists of 28,648,687,100 atoms (Table IX-2) and the net per-atom error rate for DMS-based molecular manufacturing by accelerated (120 MHz) NMW-2 modules is ~10^{-15} (Section 3.8.1.3), hence MAMs can be manufactured with an error rate of ~3 x 10^{-5} incorrect atoms per MAM. If we most conservatively assume that a single-atom error that occurs anywhere within a 28,648,687,100-atom MAM structure leads to a nonfunctional MAM, then a fully built-out MAA containing an array of 2 x 10^{11} MAMs will include ~6 x 10^6 (0.003%) nonfunctional MAMs. This number may be slightly reduced because the large majority of atoms in a MAM are not located on or near sliding interfaces where atomically perfect surfaces may be essential for proper functioning, but rather are located internally in bulk structures where atomic precision is not strictly required to achieve specified performance levels. For instance, in the

---

[1180] International Technology Roadmap for Semiconductors (ITRS), 2006 Update. "Overview and Working Group Summaries," Tables 1a (Product Generations and Chip Size Model Technology Trend Targets—Near-term Years) and 1b (Product Generations and Chip Size Model Technology Trend Targets—Long-term Years), p.3; http://www.itrs.net/Links/2006Update/FinalToPost/00_ExecSum2006Update.pdf; see also in "Lithography," pp. 7-8; http://www.itrs.net/Links/2006Update/FinalToPost/08_Lithography2006Update.pdf.

current MAM design there is 15,764,100 nm^2 of passivation area from which may be excluded the surfaces of foundation blocks (2,400,600 nm^2) and the external surfaces of all 7 copies of Strut Segment 1 in each MAM (2,713,200 nm^2), leaving only 10,650,300 nm^2 of critical interfacial surface. Ignoring the risk of error cascades, if random single-atom errors that lie within 3 bond planes (~0.45 nm) of a surface can ruin the interfacial performance of that surface, then (0.45 nm)(10,650,300 nm^2)/(160,000,000 nm^3) ~ 3% of the solid volume of the MAM manipulator comprises critical interfacial atoms whose incorrect placement could cause the MAM to fail, hence on average ~30 random atom placement errors may be required for MAM failure, reducing the manufacturing rate of nonfunctional MAMs to ~10^{-6} – in which case, a fully built-out MAA containing an array of 2 x 10^{11} MAMs may include only ~2 x 10^5 (0.0001%) nonfunctional MAMs.

Each MAM has 14 control lines (Section 3.10.1.1), so operating a MAM at 120 MHz may require up to 1.7 x 10^9 bits/sec, or 3.4 x 10^{20} bits/sec for an entire 2000 cm^2 MAA wafer consisting of 2 x 10^{11} MAM manipulators. Assuming a ~10^{-21} error rate for mechanical actuation operations (Section 3.8.1.3), each MAM has a ~2 x 10^{-12} sec^{-1} single-actuation error rate and each MAA will produce ~0.3 sec^{-1} single-actuator errors in one MAM somewhere on the wafer. Single-actuation errors in a MAM do not necessarily produce a failed operation or product object, especially if MAM step sizes are significantly smaller than the requisite accuracy for parts docking during an assembly operation. Small positioning errors can be prevented from randomly accumulating in the position of each MAM by using the installed sensory feedback mechanism to detect and correct such errors via periodic re-registration of all MAMs against static fiducial markers.

3.10.2 Task IX-1: Design and Simulate MAM and MAA

Task IX-1 is to design and simulate the Micro-Assembler Manipulator (MAM) and the Micro-Assembler Array (MAA). The successful experimental demonstration in Task VIII-2 of the 10 million tip "multitool" for assembly surface remediation writing operations will have provided valuable prior experience in designing, building and operating large manipulator arrays that can now be expanded to a 200 billion manipulator array in Phase IX.

The MAM must be designed, modeled and simulated to be assemblable from nanoparts, nanodevices, or larger compound components up to ~100 nm in size, via plate/plate assembly using an NMW-2 wafer previously demonstrated in Task VIII-4. There is a slight lateral positional mismatch of up to ~0.68 microns between the 10^{11} NMW-2 sites on a 100 cm^2 square NMW-2 wafer and the 10^{10} MAM sites on an opposed 100 cm^2 square MAA wafer, but this variable displacement differential is readily accommodated by the 2 micron reach envelop of the MAMs. An optimized sequence of plate-shift motions similar to those previously described (Section 3.8.1.1), designed (Tasks VII-1 and VIII-1), and demonstrated (Tasks VII-3, VII-6 and VIII-3) can be employed to allow all 10^{11} NMW-2 units on an NMW-2 wafer to participate in the manufacture of the 2 x 10^{11} MAM units comprising a single MAA wafer.

Because the product objects to be assembled into larger product objects will generally not transact new covalent bonds between objects but will adhere solely on the basis of noncovalent bonding, detailed atomistic simulations will probably no longer be required. (Sliding tongue-in-groove interlocks between parts can provide part-part interfaces that are almost as strong as a solid covalently bonded structure of the same shape.) Finite-element and other continuum models should therefore suffice to explore the mechanical responses of wafer plates and machine components to mechanical operations performed during interactions between NMW-2 units on one opposed plate and (1) a MAM electrode wafer surface, (2) an individual partially- or fully-

built MAM, or (3) a growing array of MAMs, on the other opposed plate. Mechanical forces will grow in magnitude as the number of assembled or working MAM units increases toward the full complement of 2 x 10^{11} MAM units on each MAA. Substantial resonance vibrations might develop if all MAM units are operated in unison and the parameter space that would allow these resonances to develop should be thoroughly explored. Control issues will be considerably complicated by the need for localized sensory feedback and must be comprehensively analyzed, modeled, and simulated.

Additional key design, modeling, and simulation subtasks will include:

(1) Design and simulate the basic mechanical workability of a single MAM manipulator arm.

(2) Simulate the assembly of a MAM manipulator from ≤100 nm parts, with the MAM design exemplifying the basic manufacturing engineering philosophy of design-for-assembly. The need to be able to assemble the MAM using the existing NMW-2 wafer manipulator array following the usual plate/plate assembly processes developed in Phases VII and VIII will significantly constrain the details of MAM design and will probably necessitate a highly iterative MAM design process spanning several design cycles.

(3) Define and simulate the entire MAM motion envelope, then analyze all possible mechanical interactions with neighboring manipulators in order to design collision avoidance protocols in regions of the workspace where adjacent motion envelopes overlap). Verify that adjacent MAMs are close enough to provide full manipulator coverage of the entire wafer surface area with no blind spots.

(4) Simulate and verify MAM ability to accept product objects from NMW-2 units on an opposing NMW-2 wafer array.

(5) Determine whether or not the MAM design must be upgraded to include additional sensors and two or more articulated fingers on its end effector in order to satisfy all manipulation requirements as defined in Phases IX and X. Adding fingers and sensors will add some new complexity and a few additional parts and control lines to the design, but should not significantly alter the overall design or atom count as previously enumerated above. Note that multi-fingered end effectors capable of twirling a ball in one hand and performing related delicate motions have been studied and demonstrated experimentally in conventional macroscale robotics.[1181]

[1181] Daniela Rus, "In-Hand Dexterous Manipulation of Piecewise-Smooth 3-D Objects," Intl. J. Robotics Res. 18(1999):355-381; Moëz Cherif, Kamal K. Gupta, "Global Planning for Dexterous Reorientation of Rigid Objects: Finger Tracking with Rolling and Sliding," Intl. J. Robotics Res. 20(2001):57-84; S. Nakamura, K. Tahara, J.H. Bae, M. Sekimoto, S. Arimoro, "Experiments of Grasping and Object-Manipulation by a Pair of Multi-Degrees of Freedom Robot Fingers," Proceedings of 2003 IEEE International Symposium on Computational Intelligence in Robotics and Automation, Kobe, Japan, 2003, pp. 1162-1167; Ikuo Yamano, Takashi Maeno, "Five-fingered Robot Hand using Ultrasonic Motors and Elastic Elements," Proceedings of the 2005 IEEE International Conference on Robotics and Automation, Barcelona, Spain, 18-22 April 2005, pp. 2684-2689, http://www.maeno.mech.keio.ac.jp/English/ICRA2005_yamano.pdf; M. Higashimori, Jeong Hieyong, I. Ishii, M. Kaneko, A. Namiki, M. Ishikawa, "A New Four-Fingered Robot Hand with Dual Turning

(6) Simulate and verify the ability of adjacent MAMs to reliably hand off nanoparts, nanodevices, components and other product objects to neighboring MAMs. Each MAM is separated from its 4 nearest neighbors on the MAA array by 1 micron (measured center-to-center of adjacent sites); since the MAM work envelope includes a 2 micron reach, it should be possible for adjacent MAM arms to engage in joint compound component assembly operations – e.g., where one manipulator holds a workpiece and up to 4 neighboring manipulators participate in component insertion (pushing, pulling, sliding, screwing, locking) operations. The simulated MAM and MAA designs should be demonstrated to have this capability.

(7) Design and simulate a capability for well-sensored MAMs to perform elementary inspections of the external dimensions and surfaces of grasped nanoparts, nanodevices, components and other product objects using sensory feedback.

(8) Simulate and verify the ability of MAMs to set down product objects received from NMW-2 crane arm manipulators in close proximity on an opposing flat surface.

(9) Simulate and verify ability of MAMs to sense the positions and orientations of NMW-2 product objects that have been placed in close proximity on an opposing flat surface, and to nudge or jostle those objects until they are snugly pressed against each other (e.g., in a densely-packed checkerboard pattern, assuming square product objects), and then to verify the integrity of the tight packing using the same MAM sensorium. This and the previous several subtasks will ensure that the micro-assembly systems developed in Phase IX can perform all of the functions that will be required of them in Phase X.

(10) Model and simulate MAA layout and operation.

(11) Model and simulate MAA buildout procedure.

(12) Design, simulate and analyze the optimum plate shift patterns to be executed by the plate handling system during MAA wafer buildout. Simulate an entire construction sequence for building one MAM, using an NMW-2 wafer array to produce the component MAM parts.

(13) Simulations should also explore the limits to increasing operating frequency for the MAM, specifically with an analysis of the impact on MAM design, if any, of increasing pulse frequency ~100 fold from 1.3 MHz to 120 MHz (matching the operating frequency of the fabrication system which has already been demonstrated experimentally in Task VII-7). The MAM design should be modified to allow operation at this higher speed while maintaining adequate reliability. High-speed operation of physical microscale manipulator (MAM/MAA) systems will be required in Task IX-7 to conclude Phase IX.

Mechanism," Proceedings of the 2005 IEEE International Conference on Robotics and Automation, Barcelona, Spain, 18-22 April 2005, pp. 2679-2684; Shadow Robot Company: Air Muscles, accessed March 2008, http://www.shadowrobot.com/gallery.shtml?gallery=handC&img=HandC_Bulb_03.jpg.

3.10.3 Task IX-2: Prepare Multielectrode MAM Test-Assembly Surfaces for Experimentation

Task IX-2 is to prepare a small number of atomically flat surfaces upon which Micro-Assembler Manipulator (MAM) units can be physically constructed and debugged using methods already demonstrated in earlier Phases (e.g., Tasks VI-2 and VII-2). Electrical power and control signals are applied to MAM mechanisms via carbon nanotube wires that connect surface electrode terminals on the atomically smooth assembly surface to electrostatic motors that actuate the manipulators. Nanotube wires from the MAM are joined to the 15 site electrodes by simple van der Waals attraction, or if this is insufficient then by nanotube impalement of the softer metal, by e-beam spot welding,[1182] by using designed mateable connectors, or by other means. Each MAM test-assembly surface is a single-crystal silicon wafer and may include up to 100-1000 worksites each of area ~1 micron^2 each, which should be a sufficient number for experimentation and testing. Each MAM test-assembly surface is fabricated atop a macroscale semiconductor wafer up to 10 cm x 10 cm in size that can be manipulated and precisely positioned using the plate handling system first developed in Task VII-3 (Section 3.8.4). This way, the MAM test-assembly surface can be placed in close parallel juxtaposition with a NMW-2 wafer system within a plate handler mechanism during experimental testing of MAM assembly procedures.

3.10.4 Task IX-3: Build and Operate First MAM

Task IX-3 is to manually assemble the first individual Micro-Assembler Manipulator (MAM) at a designated worksite on the atomically smooth MAM electrode wafer surface of the multielectrode chip created during Task IX-2 (Section 3.10.3), using the NMW-2 wafer-scale manufacturing system created during Phase VIII (Section 3.9). All manipulation tasks are assumed to be performed via blind pick-and-place operations unless it has been deemed necessary to add sensory feedback to the NMW-2 units to ensure adequate manufacturing reliability (Section 3.8.1.3). The design should be tested, iterated and debugged until it is reliable and correct.

To complete Task IX-3, the MAM electrode wafer test surface must first be prepared (Task IX-2), after which a single production cycle of a small number of NMW-2 units on a single NMW-2 wafer will be used to fabricate and assemble, in parallel, all of the assemblable components of a single MAM. The NMW-2 crane arms are used to install the MAM components on the MAM electrode surface via plate/plate manufacture as developed in Phase VII and VIII. Each NMW-2 unit on a Phase VIII wafer can produce 129,194,836 atoms of product objects in a single 128,700 sec (~1.5 day) production cycle at the 120 MHz control pulse frequency, including pumpdown and plate changeout (Section 3.8.8). Each MAM is comprised of 28,648,687,100 atoms (Table IX-2) representing ~275 parts composed of ~104,177,044 atoms each. Thus if one NMW-2 unit builds each of the 275 parts, then 275 NMW-2 units participating in the parallel construction of a

---

[1182] MinFeng Yu, Mark J. Dyer, George D. Skidmore, Henry W. Rohrs, Xue Kun Lu, Kevin D. Ausman, James Von Ehr, Rodney S. Ruoff, "3 Dimensional Manipulation of Carbon Nanotubes under a Scanning Electron Microscope," paper presented at the Sixth Foresight Nanotechnology Conference, November 1998; see also: Robert F. Service, "AFMs Wield Parts for Nanoconstruction," Science 282(27 November 1998):1620-1621; and http://www.foresight.org/Conferences/MNT6/Papers/Yu/index.html.

single MAM can build the first MAM in 128,700 sec (~1.5 day). If more NMW-2 units participate, the work will go faster.

After the first MAM is built, it should be rigorously tested to ensure its basic mechanical workability and smooth functioning throughout its entire designed operating envelope. The MAM should be further tested to demonstrate its ability to accept product objects of a wide range of sizes, shapes, and orientations from NMW-2 units on an opposing NMW-2 wafer array. The MAM has one or more sensors that may allow it to examine handled parts by feel to determine their shape, size, orientation, surface condition, and identity. One or more 3D "test pattern" blocks designed to thoroughly exercise the MAM's sensory capabilities should be manufactured by an NMW-2 unit and then used to test the MAM as described above.

It may be necessary to iterate Tasks IX-1 and IX-3 to fully debug the MAM design and to successfully achieve all desired results.

3.10.5 Task IX-4: Prepare Whole-Wafer Multielectrode MAA Wafer Surfaces

Task IX-4 is to prepare a 3 x 10^{12}-electrode 2000 cm^2 Micro-Assembler Array (MAA) wafer using multi-tip processing methods already demonstrated in Phase VIII (i.e., the substantially similar Task VIII-2), resulting in a remediated atomically smooth MAA electrode wafer surface.

Assuming that the previously estimated (Section 3.9.3) production rate of ~0.06 day/wafer for building NMW-2 wafers can be obtained for the 20-fold larger MAA wafers on an equal-area basis, yielding a fabrication rate of ~1.25 day/wafer for MAA wafers, then preparing 200 MAA electrode wafer surfaces would require ~250 days using the existing wafer processing facility but only ~125 days if the capacity of that system is doubled to 32 wafer processing systems, operated in tandem analogously to the processes described in Section 3.9.3.

3.10.6 Task IX-5: Build and Operate One MAA Wafer

Task IX-5 is to build out the first Micro-Assembler Array (MAA) wafer. As noted in Section 3.10.1.2, buildout of an entire MAA wafer would require ~444 production cycles of a single NMW-2 wafer, thus a single NMW-2 wafer could assemble a single MAA wafer in 5.71 x 10^7 sec (~1.8 years), and 200 NMW-2 wafers could produce 200 built-out MAA wafers in the same time period (~1.8 years) if operated in parallel. Alternatively, if 444 NMW-2 wafers are simultaneously employed to manufacture the components of a single MAA wafer in parallel, and if components from 444 different NMW-2 wafers can be assembled on a single MAA wafer without significant additional time penalties for plate changeout or other plate-handling activities (since NMW-2 productivity is fabrication-speed limited, not assembly-speed limited; Section 3.7.1), then an entire MAA wafer could be fabricated in ~128,700 sec (~1.5 days). Allowing plate handlers to pool manufactured components analogously to exponential manufacturing in the sequence 2 plates, 4 plates, 8 plates, etc., then pooling components from all 444 NMW-2 wafers requires ~9 pooling cycles; allowing ~1 day per pooling cycle requires ~9 days for pooling plus 1.5 days for fabrication, for a total of ~11 days for MAA wafer buildout.

After the first MAA wafer is built out, the manipulator array should be rigorously tested to ensure correct operation of all individual MAMs in the array and to assess the reliability of their manufacture. Additional key validation tests will include:

(1) Validate the optimum plate shift patterns to be executed by the plate handling system during MAA wafer buildout.

(2) Perform a plate/plate test with an NMW-2 wafer that builds 10^{11} copies of 3D "test pattern" blocks which the MAA collects and places into a simple planar array on an atomically flat surface. Afterwards, scan the surface to verify correct placement.

(3) Test all possible mechanical interactions with neighboring manipulators and validate collision avoidance protocols in regions of the workspace where adjacent motion envelopes overlap). Verify that adjacent MAMs are close enough to provide full manipulator coverage of the entire wafer surface area with no blind spots.

(4) Verify the ability of adjacent MAMs to reliably hand off nanoparts, nanodevices, components and other product objects to neighboring MAMs. MAM are separated from their 4 nearest neighbors on the MAA array by 1 micron but each MAM has a 2 micron work envelope, so adjacent MAM arms should be demonstrated to be able to engage in joint compound component assembly operations – e.g., where one manipulator holds a workpiece and up to 4 neighboring manipulators participate in component insertion (pushing, pulling, sliding, screwing, locking) operations.

(5) Verify the ability of well-sensored MAMs to perform elementary inspections of the external dimensions and surfaces of grasped nanoparts, nanodevices, components and other product objects using sensory feedback.

(6) Simulate and verify the ability of MAMs to set down product objects received from NMW-2 crane arm manipulators in close proximity on an opposing flat surface.

(7) Verify the ability of MAMs to sense the positions and orientations of NMW-2 product objects that have been placed in close proximity on an opposing flat surface, and to nudge or jostle those objects until they are snugly pressed against each other (e.g., in a densely-packed checkerboard pattern, assuming square product objects), and then to verify the integrity of the tight packing using the same MAM sensorium. This and the previous several subtasks will ensure that the micro-assembly systems developed in Phase IX can perform all of the functions that will be required of them in Phase X.

Since each MAM can execute ~100 round trip motions/sec (using 0.2 nm step increments at ~1.3 MHz and assuming a pulse budget of 13,200 pulses per round trip; Section 3.10.1.1), a field of ~2 x 10^{11} MAM units on a single MAA plate can perform ~2 x 10^{13} mechanical assembly round-trip motions per second. If each such motion emplaces a ~10^{8} atom component on a surface, the MAA has an assembly capacity of ~10^{21} atoms/sec.

3.10.7 Task IX-6: Build Out 200 MAA Wafers and 200 MAA Handlers

Task IX-6 is to build out 200 Micro-Assembler Array (MAA) wafers. The MAA wafers are built linearly, not exponentially, using NMW-2 wafers developed in Phase VIII. Using all available 1024 NMW-2 wafers and 200 additional plate handlers similar to those developed in Task VIII-4

(but larger), build-out of 200 MAA wafers would require ~87 production cycles or ~1.12 x 10^7 sec (~130 days) as previously estimated in Section 3.10.1.2.

Note that the MAA handlers must be designed to allow virtually contiguous operation of neighboring NMW-2 wafer handlers closely aligned side by side in groups of 20, essentially filling the entire available 2000 cm^2 active surface area of the MAA wafer.

3.10.8 Task IX-7: Modify MAMs and MAA Wafers for High-Frequency Operation

Task IX-7 is to increase the operating pulse frequency for the MAM ~100 fold from 1.3 MHz to 120 MHz to match the operating frequency of the fabrication system (120 MHz operation is demonstrated experimentally in Task VII-7), using a MAM design containing any necessary changes as determined by theoretical studies performed earlier in Task IX-1 (Section 3.10.2(11)).

Task IX-7 concludes with a successful demonstration of a MAM, and an MAA, operated at 120 MHz while maintaining adequate reliability.

3.11 Phase X: First-Generation Nanofactory (FGN)

The key objective of Phase X is to eliminate the Bulk Feedstock Supply System (BFSS) system in favor of a macroscale bulk feedstock supply system and to build a first-generation nanofactory (FGN) capable of mass-producing micron-scale atomically precise diamondoid product objects at ~0.01 kg/hour production rates.

The basic architecture of the first-generation diamondoid nanofactory is briefly described in Section 3.11.1 and illustrated in Figure X-1, including the first production layer for fabrication (Section 3.11.2) and the second production layer for assembly (Section 3.11.3). This is followed by an enumeration of the specific tasks required to design, manufacture, and operate the FGN, which include: design, modeling and simulation of FGN components, operations, and the process of FGN manufacture (Section 3.11.4), manufacture of the FGN base plate (Section 3.11.5), build 24 nanotube wiremaker wafers (Section 3.11.6), building the FGN assembly system and vacuum room (Section 3.11.7), building another 512 NMW-2 plate handlers (Section 3.11.8), improving the plate handling speed by 50-fold (Section 3.11.9), manufacture and installation of 1000 fabrication planes and 4 assembling planes on the FGN base plate (Section 3.11.10), manufacture, attachment and testing of all appurtenant FGN support equipment (Section 3.11.11), and finally the demonstration of FGN production of micron-scale diamondoid product objects in macroscale quantities (Section 3.11.12).

3.11.1 Basic Architecture of the FGN

It is possible to present an exemplar nanofactory architecture that appears to have proper scaling, adequate mass flow, acceptable power consumption, and all necessary fabrication and assembly capabilities (at least on paper) to achieve the objectives of a fully functional diamondoid nanofactory. Several possible architectures have been considered and many would probably work (with differing tradeoffs), but for maximum parsimony of effort we will discuss just one viable architecture that makes maximum use of systems that have previously been described in this proposal and which, by Phase X, will already have been experimentally validated during earlier Phases of this program. While mill-type DMS systems would probably be more energy efficient and might yield higher atom/sec productivity rates than manipulator-type DMS systems, for simplicity in this exemplar first-generation nanofactory design we have opted for a manipulator-type manufacturing system, all the way down to the smallest-scale production level.

We start with a clear statement of the principal objective of Phase X. The objective of Phase X is to build a first-generation nanofactory (FGN) capable of mass-producing micron-scale atomically precise diamondoid product objects at ~0.01 kg/hour production rates. Such micron-scale product objects would include, most notably, medical nanorobots such as respirocytes[1183] and microbivores[1184] (Section 2.3.6) which have long been known[1185] to have revolutionary potential

---

[1183] Robert A. Freitas Jr., "Exploratory Design in Medical Nanotechnology: A Mechanical Artificial Red Cell," Artificial Cells, Blood Substitutes, and Immobil. Biotech. 26(1998):411-430; http://www.foresight.org/Nanomedicine/Respirocytes.html.

[1184] Robert A. Freitas Jr., "Microbivores: Artificial Mechanical Phagocytes using Digest and Discharge Protocol," J. Evol. Technol. 14(April 2005):1-52; http://www.jetpress.org/volume14/freitas.html.

in health care and anti-aging therapeutic applications.[1186] Thus a working FGN would provide enormous economic value (cf. Section 3.12.1) by the end of Phase X – well before the final stage of nanofactory development (Phase XI) was completed.

Figure X-1. Basic architecture of the first-generation nanofactory (FGN); not to scale.

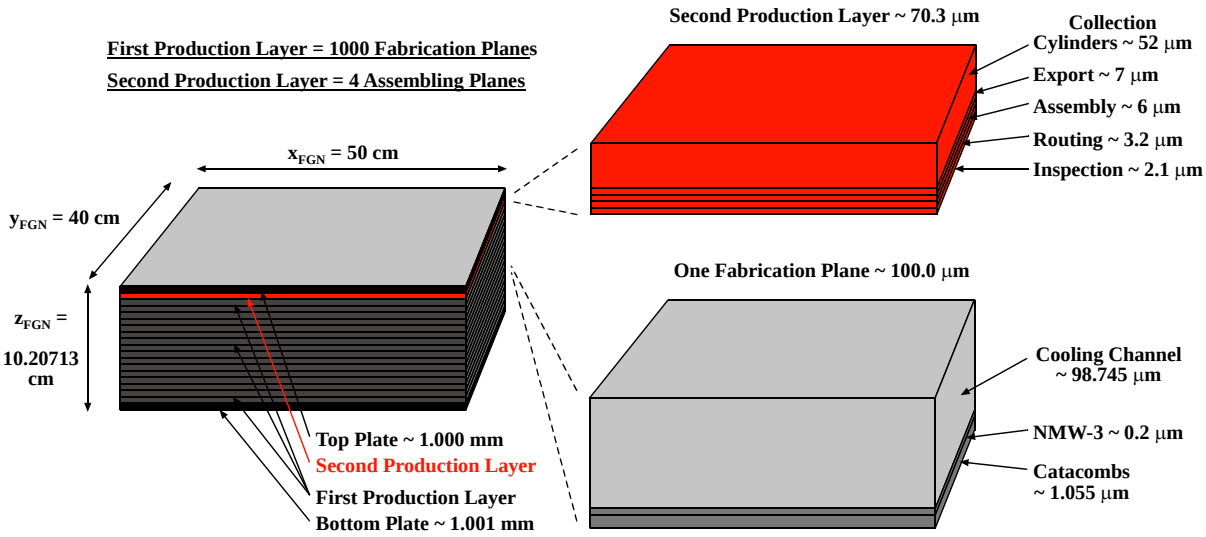

The basic nanofactory architecture is a stack of production layers (Figure X-1), each of which produces components at a given size scale and then passes these completed components up to a higher production layer, there to be assembled into components at the next largest size scale, eventually reaching the size scale of the desired product objects which represent the final output of the highest production layer. We take as our FGN productivity benchmark the very reasonable target mass throughput rate of ~0.01 kg/hour for atomically precise products which is within a factor of 100 of the production target recited for a mature-technology nanofactory in the earliest

---

[1185] Robert A. Freitas Jr., Nanomedicine, Volume I: Basic Capabilities, Landes Bioscience, Georgetown, TX, 1999; http://www.nanomedicine.com/NMI.htm. K. Eric Drexler, Engines of Creation: The Coming Era of Nanotechnology, Anchor Press/Doubleday, New York, 1986. Robert A. Freitas Jr., Nanomedicine, Volume IIA: Biocompatibility, Landes Bioscience, Georgetown, TX, 2003; http://www.nanomedicine.com/NMIIA.htm.

[1186] Robert A. Freitas Jr., "Chapter 15. Comprehensive Nanorobotic Control of Human Morbidity and Aging," in Gregory M. Fahy, Michael D. West, L. Stephen Coles, and Steven B. Harris, eds, The Future of Aging: Pathways to Human Life Extension, Springer, New York, 2008.

nanofactory scaling design.[1187] Assuming that the vast majority of the final product object structure consists of carbon atoms of mass ~2 x 10^{-26} kg/atom, then the required atom processing rate within the FGN production layers at each product size scale must therefore approximate ~10^{20} atoms/sec.

If we consider the NMW-2 manufacturing unit first developed in Phase VII and employed in subsequent Phases VIII and IX, the key production bottleneck is now the Bulk Feedstock Supply System (BFSS) that was first deployed in Phase IV. Although BFSS feedstock/byproduct gas handling and chamber pumpdown cycle times have been reduced from the range of 1-21 days in Phase IV (Section 3.5.1.7) to ~1 day by Phase VII (Section 3.8.8), and plate changeout handling times have been reduced from ~2 weeks in Task VII-4 (Section 3.8.5) to ~8 hours by Task VII-7 (Section 3.8.8) in Phase VII, net productivity of the NMW-2 is still only a ~1000 atom/sec net build rate because a 129,194,836-atom NMW-2 unit can be replicated in a single production cycle of ~128,700 sec (Section 3.8.8). If feedstock molecule handling, vacuum pumpdowns and plate handling could be eliminated entirely by switching to a common piped bulk supply of feedstock and a continuously maintained vacuum, then each production cycle could be reduced to the net serial build time of 1.35 x 10^4 sec for a 129,194,836-atom NMW-2 unit (Section 3.8.1.1) at the 120 MHz control pulse frequency – yielding a continuous ~10,000 atom/sec net fabrication rate per NMW-2 unit, a tenfold improvement in productivity.

Note again (Section 3.7.1) that the aforementioned build rate is (NFW-2; Section 3.5) fabrication-limited, not (NAW; Section 3.6) assembly-limited. The NFW-2 operated at 120 MHz is limited to an ~10,000 atom/sec net build rate, but the time for assembly of a 129,194,836-atom NMW-2 unit is the sum of the nanodevice assembly time of ~1.10 x 10^4 sec (Section 3.7.4) plus an NMW-2 assembly time (from constituent nanoparts and nanodevices) of 5.08 x 10^4 sec (Section 3.7.5) at 1.2 MHz, or just ~618 sec at 120 MHz – yielding a continuous ~200,000 atom/sec net assembly rate for product objects up to ~100 nm in size (e.g., the approximate size of the NMW-2) at the 120 MHz control pulse frequency. Although this mismatch between fabrication and assembly could be eliminated by pairing ~20 fabrication modules with one assembly module (thus in principle allowing the nanofactory to be operated at maximum efficiency), we opt not to do this because doing so would increase nanofactory design complexity while increasing specific productivity only twofold: 20 NMW-2 units operated in parallel at 120 MHz (occupying 400,000 nm^2 of planar surface, ignoring BFSS) would achieve a continuous ~0.48 atom/sec-nm^2 serial build rate, whereas 20 NFW-2 operated in parallel while feeding a single NAW at 120 MHz (occupying 210,000 nm^2 of planar surface, ignoring BFSS) would achieve a continuous ~0.95 atom/sec-nm^2 serial build rate.

The FGN is conceptualized as a box measuring 50 cm wide x 40 cm deep x ~10 cm tall – about the size of a copier machine (Figure X-1). There are two production layers of equal horizontal dimensions, each spanning ~0.2 m^2 of planar surface per layer. In the first production layer there are 1000 fabrication planes, with each plane building nanoscale components up to 100 nm in size at the ~10^{17} atom/sec rate, or ~10^{20} atoms/sec for all 1000 planes. In the second production layer there are four planes of assembly-related machinery that together build finished product objects

---

[1187] K. Eric Drexler, Nanosystems: Molecular Machinery, Manufacturing, and Computation, John Wiley & Sons, New York, 1992, Section 14.4, pp. 421-428.

up to a few microns in size, also at the ~10^{20} atom/sec rate. The operating temperature of the FGN is 109 K (see below).

3.11.2 Description of the First Production Layer

Each fabrication plane is composed of a closely-fitted array of new nanoscale manufacturing workstation (NMW-3) modules (Figure X-2). These new modules are similar in size and function to the NMW-2 units previously demonstrated in Phase VII, except that the old NFW-2 subsystem from Phase IV is upgraded to a new NFW-3 subsystem and the old NAW subsystem from Phase V is upgraded to a new NAW-2 subsystem, for the NMW-3. The NMW-3 units comprising each fabrication plane within the first production layer are 100 nm x 200 nm in horizontal dimensions, so there are 10^{13} of them present in each fabrication plane.

Figure X-2. Schematic illustration of the layout of one fabrication plane in the first production layer of the FGN (not to scale)

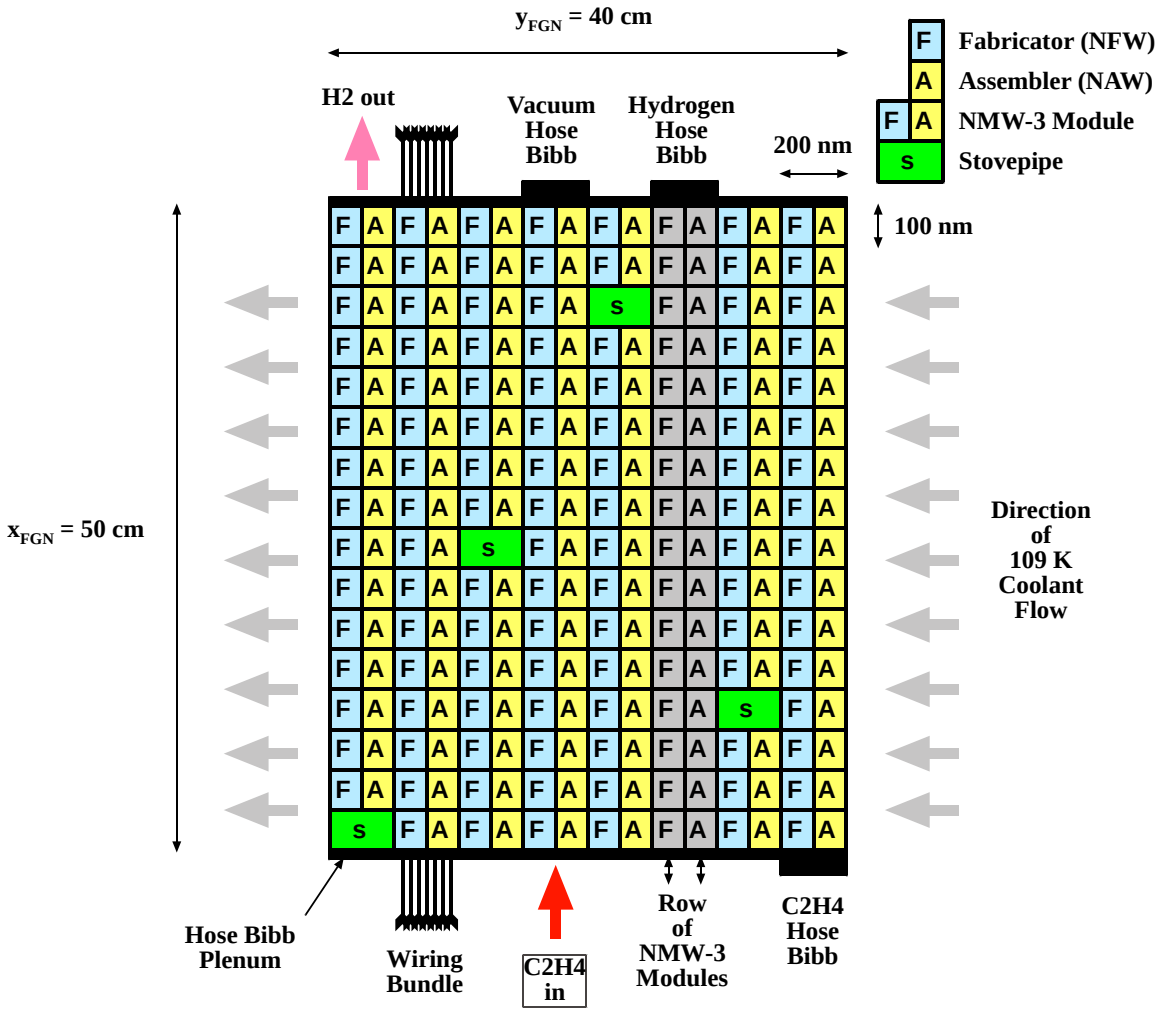

Number of Rows = 40 cm / 200 nm = 2,000,000 rows along y_{FGN} direction

Number of NMW-3 Modules/Row = 50 cm /100 nm = 5,000,000 modules along x_{FGN} direction

The new NMW-3 modules and the 0.2 m^2 fabrication planes that they comprise implement the following important design features and modifications: tanks and rotors (Section 3.11.2.1), manipulators (Section 3.11.2.2), foundation blocks (Section 3.11.2.3), power and control lines (Section 3.11.2.4), support frame (Section 3.11.2.5), catacombs (Section 3.11.2.6), ciliary transport array (Section 3.11.2.7), stovepipes (Section 3.11.2.8), cooling channels (Section 3.11.2.9), and UHV maintenance (Section 3.11.2.10), all of which are summarized in Section 3.11.2.11.

3.11.2.1 Tanks and Rotors

The BFSS gas tank is eliminated in the NFW-3 but some of the non-wall BFSS components are retained, in particular the sorting rotors and transfer units (or their redesigned subsystems with equivalent function). Rather than residing on the BFSS tank wall, the sorting rotors and transfer units now reside within or upon the floor of the new NFW-3 unit, perhaps in the small spaces between the old NFW-2 foundation blocks. Feedstock and waste gases will be passed through the floor of the new NFW-3, eliminating the need for onboard tankage.

3.11.2.2 Manipulators

The NFW-3 manipulators are redesigned as necessary to allow them to reach the floor-mounted sorting rotors and transfer units, so that atomically precise DMS fabrication operations may proceed exactly as before in the old NFW-2 unit. If the NFW-3 unit is operated at the 120 MHz pulse rate, the productivity of each NFW-3 unit is ~10,000 atom/sec in continuous operation. The larger fourth manipulator (Section 3.4.1.1) of the NFW-3 remains the same, able to reach out 113 nm to slightly beyond the normal ~100 nm operating envelope of the NFW-3 unit and retains its ability to pass finished products of the NFW-3 to the adjacent NAW-2 unit. The manipulators of the NAW-2 are the same as for the NAW, but it must be verified that the crane arm manipulator of each NMW-3 module has sufficient reach to pass a product object to any of its four nearest-neighbor NMW-3 modules, so that these arms can participate in the ciliary transport array (Section 3.11.2.7).

3.11.2.3 Foundation Blocks

The foundation blocks on the floor of the old NFW-2 and NAW units are expanded into one continuous solid diamondoid floor, 10 nm thick and 100 nm x 200 nm in size, encompassing both the new 100 nm x 100 nm NFW-3 unit and the new 100 nm x 100 nm NAW-2 unit which together occupy ~20,000 nm^2 of floor area. The sorting rotors are embedded in the foundation block in the NFW-3 space and span the thickness of the block, such that feedstock molecules acquired by a rotor from an open fluid-filled space below the foundation block can be transported to the opposite face of the foundation block and into an NFW-3 transfer unit, from which a DMS manipulator arm can reliably acquire the feedstock molecule for further processing – and *vice versa*, for byproduct molecules to be discharged into the open gas-filled space below the foundation block. The four vertical edge walls of each rectangular foundation block may be designed with complementary ridges and troughs, both to ensure reliable docking and mating with adjacent similar units and to ensure that the interfaces between the adjacent foundation

blocks of tightly juxtaposed neighboring NMW-3 units are leakproof so that feedstock fluid and waste gases cannot diffuse between them.

3.11.2.4 Power and Control Lines

The NMW-2 and NMW-3 have the same number of motors and thus both require ~100 power/control wires (Sections 3.7.1 and 3.8.1.1). The smallest stable single-walled carbon nanotubes are 1.1 nm in outer tube diameter. Double-wall carbon nanotubes (DWCNTs) having an average outer diameter of ~1.4 nm have been synthesized inside zeolites[1188] and DWCNTs in the 1-2 nm range are well known[1189] – DWCNTs combine the electrical and thermal stability of MWNTs with the flexibility of SWNTs[1190] and have already been used to make high-current-carrying field-emission displays (FEDs),[1191] field-effect transistors,[1192] and super-tough fibers.[1193] DWCNTs have even been prepared in macroscale sheets.[1194] Using the atomically precise DMS fabrication capability developed in early Phases it should be possible to build DWCNTs that are <2 nm in diameter in which the inner nanotube has a conductive "metallic" chirality[1195] and the outer nanotube has semiconducting or nonconducting insulator characteristics. (For a given (n,m)

[1188] Naoki Kishi, Tatsuki Hiraoka, Palanisamy Ramesh, Junichi Kimura, Kenichi Sato, Yuji Ozeki, Masahito Yoshikawa, Toshiki Sugai, Hisanori Shinohara, "Enrichment of Small-Diameter Double-Wall Carbon Nanotubes Synthesized by Catalyst-Supported Chemical Vapor Deposition Using Zeolite Supports," Japanese Journal of Applied Physics 46(2007):1797-1802.

[1189] Takeo Yamada, Tatsunori Namai, Kenji Hata, Don N. Futaba, Kohei Mizuno, Jing Fan, Masako Yudasaka, Motoo Yumura, Sumio Iijima, "Size-selective growth of double-walled carbon nanotube forests from engineered iron catalysts," Nature Nanotechnology 1(2006):131-136; http://www.nature.com/nnano/journal/v1/n2/full/nnano.2006.95.html.

[1190] Takeo Yamada, Tatsunori Namai, Kenji Hata, Don N. Futaba, Kohei Mizuno, Jing Fan, Masako Yudasaka, Motoo Yumura, Sumio Iijima, "Size-selective growth of double-walled carbon nanotube forests from engineered iron catalysts," Nature Nanotechnology 1(2006):131-136; http://www.nature.com/nnano/journal/v1/n2/full/nnano.2006.95.html.

[1191] H. Kurachi et al, "FED with double-walled carbon nanotube emitters," IDW Proc. (2001):1237-1240.

[1192] T. Shimada, T. Sugai, Y. Ohno, S. Kishimoto, T. Mizutani, H. Yoshida, T. Okazaki, H. Shinohara, "Double-wall carbon nanotube field-effect transistors: Ambipolar transport characteristics," Appl. Phys. Lett. 84(2004):2412-2414.

[1193] M. Zhang, K.R. Atkinson, R.H. Baughman, "Multifunctional carbon nanotube yarns by downsizing an ancient technology," Science 306(2004):1358-1361.

[1194] M. Endo, H. Muramatsu, T. Hayashi, Y.A. Kim, M. Terrones, M.S. Dresselhaus, " 'Buckypaper' from coaxial nanotubes," Nature 433(2005):476; http://dx.doi.org/10.1038/433476a.

[1195] M. Kociak, K. Suenaga, K. Hirahara, Y. Saito, T. Nakahira, S. Iijima, "Linking chiral indices and transport properties of double-walled carbon nanotubes," Phys. Rev. Lett. 89(2002):155501.

chirality, the nanotube is metallic if n = m.)[1196] Current-carrying carbon nanotubes possess extraordinary thermal stability at high current levels[1197] and have been proposed as the interconnect modality for future VLSI applications.[1198]

[1196] R. Saito, M. Fujita, G. Dresselhaus, M. Dresselhaus, Phys. Rev. B 46(1992):1804; N. Hamada, S. Sawada, A. Oshiyama, Phys. Rev. Lett. 68(1992):1579; J.W. Mintmire, C.T. White, Carbon 33(1995):893.

[1197] G.E. Begtrup, K.G. Ray, B.M. Kessler, T.D. Yuzvinsky, H. Garcia, A. Zettl, "Extreme thermal stability of carbon nanotubes," Physica Status Solidi B 244(2007):3960; http://socrates.berkeley.edu/~tyuz/pub/pssb244.pdf.

[1198] A. Naeemi, R. Sarvari, J.D. Meindl, "Performance comparison between carbon nanotube and copper interconnects for GSI," IEEE IEDM Digest, San Francisco CA, December 2004, pp. 699-702, http://users.ece.gatech.edu/~azad/IEDM04.pdf; A. Naeemi, R. Sarvari, J.D. Meindl, "Performance comparison between carbon nanotube and copper interconnects for gigascale integration (GSI)," IEEE Electron Device Letters 26(February 2005):84-86, http://users.ece.gatech.edu/~azad/EDL-SWNT.pdf; A. Naeemi, J.D. Meindl, "Impact of electron-phonon scattering on the performance of carbon nanotube interconnects for gigascale integration (GSI)," IEEE Electron Device Letters 26(July 2005):476-478, http://users.ece.gatech.edu/~azad/EDL-phonon.pdf; A. Naeemi, J.D. Meindl, "Design and performance modeling for single-wall carbon nanotubes as local, semi-global and global interconnects in gigascale integrated systems," IEEE Trans. Electron Devices 54(January 2007):26-37, http://users.ece.gatech.edu/~azad/TED-SWNT.pdf. B.Q. Wei, R. Vajtai, P.M. Ajayan, "Reliability and current carrying capacity of carbon nanotubes," Appl. Phys. Lett. 79(20 August 2001):1172, http://link.aip.org/link/?APPLAB/79/1172/1; F. Kreupl, A.P. Graham, G.S. Duesberg, W. Steinhögl, M. Liebau, E. Unger, W. Hönlein, "Carbon nanotubes in interconnect applications," Microelectronic Engineering 64(October 2002):399-408, http://dx.doi.org/10.1016/S0167-9317(02)00814-6; J. Li, et al., "Bottom-up Approach for Carbon Nanotube Interconnects," Appl. Phys. Lett. 82(April 2003):2491-2493; N. Srivastava, K. Banerjee, "A Comparative Scaling Analysis of Metallic and Carbon Nanotube Interconnections for Nanometer Scale VLSI Technologies," Proc. VMIC, September 2004, pp. 393-398; N. Srivastava, R.V. Joshi, K. Banerjee, "Carbon Nanotube Interconnects: Implications for Performance, Power Dissipation and Thermal Management," IEDM, 2005, pp. 257-260; N. Srivastava , K. Banerjee, "Performance analysis of carbon nanotube interconnects for VLSI applications," Proceedings of the 2005 IEEE/ACM International Conference on Computer-Aided Design, 6-10 November 2005, San Jose CA, pp. 383-390, http://www.ece.ucsb.edu/Faculty/Banerjee/pubs/ICCAD05_Navin.pdf; A. Raychowdhury, K. Roy, "Modeling of metallic carbon-nanotube interconnects for circuit simulations and a comparison with Cu interconnects for scaled technologies," IEEE Transactions on Computer-Aided Design of Integrated Circuits and Systems 25(January 2006):58-65, http://ieeexplore.ieee.org/search/wrapper.jsp?arnumber=1564304; A. Naeemi, J.D. Meindl, "Compact Physical Models for Multiwall Carbon-Nanotube Interconnects," IEEE Electron Device Letters 27(May 2006):338-340, http://users.ece.gatech.edu/~azad/EDL-MWNT.pdf; K. Banerjee, N. Srivastava, "Are carbon nanotubes the future of VLSI interconnections?" Proceedings of the 43rd Annual Conference on Design Automation (Annual ACM IEEE Design Automation Conference, San Francisco CA), 2006, pp. 809-14, http://www.ece.ucsb.edu/Faculty/Banerjee/pubs/DAC06_invited.pdf and http://videos.dac.com/43rd/papers/47_2.pdf; A. Nieuwoudt, Y. Massoud, "Understanding the Impact of Inductance in Carbon Nanotube Bundles for VLSI Interconnect Using Scalable Modeling Techniques," IEEE Transactions on Nanotechnology 5(2006):758-765; A. Naeemi, J.D. Meindl, "Carbon nanotube interconnect modeling," in: J. Kong, A. Javey, eds., Carbon Nanotube Electronics, Springer, 2007; A. Naeemi, J.D. Meindl, "Carbon nanotube interconnects," ACM International Symposium on Physical Design, Austin TX, USA, May 2007, pp. 77-84, http://doi.acm.org/10.1145/1231996.1232014 and http://users.ece.gatech.edu/~azad/ISPD.pdf; Brajesh Kumar Kaushik, Saurabh Goel, Gaurav Rauthan, "Future VLSI interconnects: optical fiber or carbon nanotube - a review," Microelectronics International 24(2007):53-63, http://dx.doi.org/10.1108/13565360710745601; F. Chen, A. Joshi, V. Stojanovic, A.

On geometric considerations alone, the simplest possible wiring architecture would be to install a 1 x 100 bundle of adjacent ~1.6 nm diameter DWCNT nanowires making a bundle that is ~1.6 nm thick and ~160 nm wide, small enough to fit entirely along the long edge of the 100 nm x 200 nm footprint of the single foundation block of the NMW-3 while leaving 22.4 nm for the occasional stovepipe wire bundle (Section 3.11.2.8), 15 nm for three vertical separation walls each 5 nm thick, and 2.6 nm of open clearance for feedstock fluid and byproduct gas transfer access by embedded sorting rotors. In this scheme, the DWCNT bundle would be built onto the bottom of each foundation block, with every such bundle terminated at either end with a small (e.g., 1 x 1 x 200 nm) connector block to allow adjacent foundation blocks to form secure electrical connections (current methods[1199] are more primitive) between all wires in the bundle when two foundation blocks are firmly pressed together. Tee connectors from each wire would attach to short nanotube leads that travel up through the foundation block and terminate on the motor inside the module that is to receive power and control signals via that wire. Nanotube penetrations of foundation blocks would need to be leaktight to prevent feedstock fluid or waste gases from flowing through or around them to enter the NMW-3 interior space and ruin the high vacuum environment that is maintained there. The row of NMW-3 units connected by a single wire bundle are then operated in unison as a single group, thus simultaneously producing an identical atomically precise product. Rows can be further bundled together as required, then interfaced through a microconnector array fabricated using conventional lithography to connect to an external nanofactory computer process control system. Assuming a maximum possible total power dissipation of 1040 pW for all four NFW-3 manipulators in continuous operation (Sections 3.4.1.1 and 3.4.1.2) at the 120 MHz control pulse frequency (Section 3.9.1), plus an additional 5% (of full duty cycle) when the NAW-2 is operating, a single NMW-3 unit consumes up to ~1100 pW in continuous operation. Each row of 5 x 10^6 NMW-3 units connected in parallel along a single 100-wire bundle therefore would consume up to 5.5 x 10^{-3} W or ~55 x 10^{-6} W per wire in the bundle – or ~55 x 10^{-6} amp/wire at 1 volt – consistent with experimental observations[1200] of individual 10-50 nm long single-walled "metallic" carbon nanotubes conducting 25-100 x 10^{-6} amp/wire electrical currents before failing and a peak burnout threshold of 1000 x 10^{-6} amp/wire reported by others.[1201] Thus at maximum continuous power draw, the electrical system as currently scaled would be operating very close to the nanotube failure limit – although in practice the system would rarely if ever be operated at the maximum power draw,

---

Chandrakasan, "Scaling and Evaluation of Carbon Nanotube Interconnects for VLSI Applications," Proc. Nanonets 2007; G.F. Close, S. Yasuda, B. Paul, S. Fujita, H.-S. P. Wong, "1-GHz Integrated Circuit With Carbon Nanotube Interconnects and Silicon Transistors," Nano Letters 8(13 February 2008):706-709.

[1199] Chuanhong Jin, Kazu Suenaga, Sumio Ijima, "Plumbing carbon nanotubes," Nature Nanotechnology 3(January 2008).

[1200] Ali Javey, Pengfei Qi, Qian Wang, Hongjie Dai, "Ten- to 50-nm-long quasi-ballistic carbon nanotube devices obtained without complex lithography," PNAS 101(14 September 2004):13408-13410; http://www.pnas.org/cgi/content/abstract/101/37/13408.

[1201] Hongjie Dai, Eric W. Wong, Charles M. Lieber, "Probing Electrical Transport in Nanomaterials: Conductivity of Individual Carbon Nanotubes," Science 272(26 April 1996):523-526; Stefan Frank, Philippe Poncharal, Z.L. Wang, Walt A. de Heer, "Carbon Nanotube Quantum Resistors," Science 280(12 June 1998):1744-1746.

which would require all motors to be driving continuously at top speed. If additional safety margin is required, more conservative maximum energy draw ceilings could be imposed with minimal impact on overall system productivity.

However, there is a fundamental problem with this simple scheme that has not appeared in earlier Phases (which have generally employed multielectrode surfaces using larger electrical pathways made of high-conductivity silver metal with fewer connections and lower total current). Carbon nanotubes of metallic chirality possess high conductivity because electronic transport in these nanotubes is ballistic (e.g., like electron waveguides, permitting only a few propagating modes),[1202] with all waste heat being dissipated in the leads to the nanotube element and almost none in the nanotube itself.[1203] To maintain this near-perfect ballistic transport of electrons, the electronic structure of the graphene surface must remain regular and uninterrupted. If a tee joint is integrally fabricated, or mechanically plugged, into an otherwise seamless metallic nanotube wire, an unavoidable quantum "step resistance" of $R_{quantum} \sim h/2e^2 \sim 12{,}900$ ohms is introduced at the tapping point or "defect site".[1204] (Experimentally measured nanotube resistance is nearly zero or very low, on the order of 31 ± 61 ohm/micron even at room temperature,[1205] or 0-12 MΩ for a 12.5 cm length, with the measurement uncertainty probably due to atomic-scale imperfections in the nanotube samples.) Thus a single line interrupted with $N_{tap} = 5 \times 10^6$ taps feeding $N_{motor} = N_{tap}$ nanoscale stepper motors would have a total end-to-end line incremental resistance of $R_{wire} \sim N_{tap}\, R_{quantum} \sim 6.45 \times 10^{10}$ ohms, producing an unacceptably high end-to-end incremental voltage drop of $V_{line} = N_{tap}\, (R_{quantum}\, (N_{motor}\, I_{motor} / 2)) \sim 3.2 \times 10^6$ volts, given that each NMW-3 motor draws a maximum current of $I_{motor} = P_{motor} / V_{motor} \sim 2 \times 10^{-11}$ amp when driven continuously at 120 MHz while drawing $P_{motor} \sim 20$ pW at $V_{motor} \sim 1$ volt (Section 3.4.1.1). Single-nanotube "home run" connections directly from external power source to each nanomotor are theoretically possible but impractical – requiring for each fabrication plane a total of 10^{13} NMW-3 modules x 100 wires/module = 10^{15} individual "home run" wires each measuring ~4 nm^2 in cross-section and average length $x_{FGN}/2 = 25$ cm, giving ~10^{-3} m^3 of wire volume underlying each 2000 cm^2 fabrication plane with a resulting wiring layer thickness of ~5 mm per plane, or ~5 meters of total wiring layer thickness for all 1000 fabrication planes in the FGN.

[1202] Boris I. Yakobson, Richard E. Smalley, "Fullerene Nanotubes: $C_{1,000,000}$ and Beyond," American Scientist 85(July-August 1997):324-337.

[1203] Hongjie Dai, Eric W. Wong, Charles M. Lieber, "Probing Electrical Transport in Nanomaterials: Conductivity of Individual Carbon Nanotubes," Science 272(26 April 1996):523-526; Stefan Frank, Philippe Poncharal, Z.L. Wang, Walt A. de Heer, "Carbon Nanotube Quantum Resistors," Science 280(12 June 1998):1744-1746. Philippe Poncharal, Claire Berger, Yan Yi, Z.L. Wang, Walt A. de Heer, "Room temperature ballistic conduction in carbon nanotubes," J. Phys. Chem. B 106(2002):12104; http://arxiv.org/pdf/cond-mat/0211515.

[1204] Philippe Poncharal, Claire Berger, Yan Yi, Z.L. Wang, Walt A. de Heer, "Room temperature ballistic conduction in carbon nanotubes," J. Phys. Chem. B 106(2002):12104; http://arxiv.org/pdf/cond-mat/0211515.

[1205] Philippe Poncharal, Claire Berger, Yan Yi, Z.L. Wang, Walt A. de Heer, "Room temperature ballistic conduction in carbon nanotubes," J. Phys. Chem. B 106(2002):12104; http://arxiv.org/pdf/cond-mat/0211515.

To solve this problem, a dendritic wiring architecture appears to be a viable scheme for supplying power and control signals to each FGN nanomachinery plane (Figure X-3). Rather than distributing power/control through a single linear wire with N_{motor} taps producing N_{tap} $R_{quantum}$ ~ 6.45 x 10^{10} ohms of total resistance, we can distribute the electricity through a simple binary tree. Each single 50-cm wire interrupted by N_{tap} tee junctions in the original scheme is replaced by two half-plane wire networks 25 cm in extent. Each half-plane wire network is supplied from a power source on either side of the 50-cm wide FGN. The required number of half-plane binary network branchings is $N_{branch} = \log_2(N_{motor}/2) = 21.25 \sim 22$, reducing the incremental electrical resistance along each source-to-motor path from 6.45 x 10^{10} ohms to a modest N_{branch} $R_{quantum}$ ~ 284 Kohms. Each half-plane wire network consists of one "level 1" uninterrupted nanotube wire of length 12.5 cm that bifurcates at a 12,900-ohm resistive junction into two "level 2" nanotube wires of length 6.25 cm, each of which bifurcates at a second 12,900-ohm resistive junction into two "level 3" nanotube wires of length 3.125 cm (giving a total of four "level 3" wires), and so on, down to the "level 21" nanotube wires of length 119.2 nm – which then complete the final connection to the half-plane of $N_{motor}/2$ individual motors by bifurcating into two "level 22" nanotube wires of length 100 nm, exactly spanning the 100 nm separation between adjacent NMW-3 modules in the x_{FGN} direction in each fabrication plane.

Figure X-3. Linear vs. binary tree connectivity for metallic carbon nanotube wiring networks.

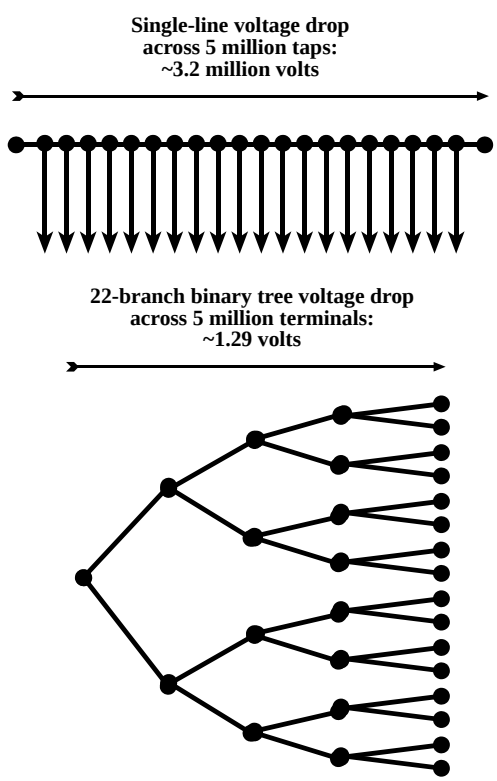

The total length of each half-plane source-to-motor path is: $L_{path} \sim (x_{FGN}/4)\ (1 + 1/2 + 1/4 + ... + 2^{-(Nbranch-1)}) \sim x_{FGN}/2 = 25$ cm. The total length of wire in each half-plane wire network is $L_{network} = (2^0)(x_{FGN}/4)$ meters x 2^0 copies) + $(2^{-1})(x_{FGN}/4)$ meters x 2^1 copies) + $(2^{-2})(x_{FGN}/4)$ meters x 2^2 copies) + ... + $(2^{-(Nbranch-1)})(x_{FGN}/4)$ meters x $2^{(Nbranch-1)}$ copies) = N_{branch} $(x_{FGN}/4)$ = (22)(12.5 cm) =

2.75 meters. The current carried by the level 1 wire is ($N_{motor}/2$) I_{motor} ~ 50 x 10^{-6} amp across a ~12,900 ohm resistance, giving an incremental voltage drop of ~0.645 volts; the level 2 wire carries half the current across the same resistance, giving half the voltage drop; hence the total incremental voltage drop across the entire half-plane source-to-motor electrical path is (0.645 volts) (1 + 1/2 + 1/4 + ... + $2^{-(Nbranch-1)}$) ~ 1.29 volts. Given the experimental observation[1206] that individual single-walled "metallic" carbon nanotubes may fail at electrical current levels of 25-1000 x 10^{-6} amp/wire,[1207] there is a serious risk of failure for the level 1 wire at 50 x 10^{-6} amp and perhaps also the several topmost level wires just below level 1. This may require installing a few somewhat larger-diameter nanotubes that can handle higher currents without failing, or using multiple parallel nanotubes carrying smaller currents instead of single nanotubes at these topmost levels of each half-plane wiring network. Switching speeds should be acceptable because electronic carbon nanotube field-effect transistors are well-known[1208] and have been operated[1209] (along with related nanoelectromechanical components)[1210] at >1 GHz switching frequencies and with no observed degradation of the AC signal up to 200 MHz;[1211] and carbon-nanotube-based electromechanical resonators have been operated from ~200 MHz[1212] up to GHz[1213] frequencies.

[1206] Ali Javey, Pengfei Qi, Qian Wang, Hongjie Dai, "Ten- to 50-nm-long quasi-ballistic carbon nanotube devices obtained without complex lithography," PNAS 101(14 September 2004):13408-13410; http://www.pnas.org/cgi/content/abstract/101/37/13408.

[1207] Ali Javey, Pengfei Qi, Qian Wang, Hongjie Dai, "Ten- to 50-nm-long quasi-ballistic carbon nanotube devices obtained without complex lithography," PNAS 101(14 September 2004):13408-13410; http://www.pnas.org/cgi/content/abstract/101/37/13408. Hongjie Dai, Eric W. Wong, Charles M. Lieber, "Probing Electrical Transport in Nanomaterials: Conductivity of Individual Carbon Nanotubes," Science 272(26 April 1996):523-526; Stefan Frank, Philippe Poncharal, Z.L. Wang, Walt A. de Heer, "Carbon Nanotube Quantum Resistors," Science 280(12 June 1998):1744-1746.

[1208] S. Tans, A.R.M. Verschueren, C. Dekker, "Room-temperature transistor based on a single carbon nanotube," Nature (London) 393(1998):49-52; R. Martel, T. Schmidt, H.R. Shea, T. Hertel, P. Avouris, "Single- and multi-wall carbon nanotube field-effect transistors," Appl. Phys. Lett. 73(26 October 1998):2447-2449; A. Gruneis, M.J. Esplandiu, D. Garcia-Sanchez, A. Bachtold, "Detecting Individual Electrons Using a Carbon Nanotube Field-Effect Transistor," Nano Lett. 7(2007):3766, http://www.nanocat.org/dataeng/recerca/qnepriv/images/nanoletters-2007.pdf.

[1209] J. Chaste, L. Lechner, P. Morfin, G. Fève, T. Kontos, J.-M., Berroir, D.C. Glattli, H. Happy, P. Hakonen, B. Plaçais, "Single Carbon Nanotube Transistor at GHz Frequency," Nano Lett. 8(January 2008):525-528; http://pubs.acs.org/cgi-bin/abstract.cgi/nalefd/2008/8/i02/abs/nl0727361.html.

[1210] Xue Ming, Henry Huang, Christian A. Zorman, Mehran Mehregany, Michael L. Roukes, "Nanoelectromechanical systems: Nanodevice motion at microwave frequencies," Nature 421(30 January 2003):496, http://www.nature.com/nature/journal/v421/n6922/abs/421496a.html.

[1211] D.V. Singh, K.A. Jenkins, J. Appenzeller, "Direct measurements of frequency response of carbon nanotube field effect transistors," Electronics Letters 41(3 March 2005):280-282; http://dx.doi.org/10.1049/el:20057528.

[1212] Vera Sazonova, Yuval Yaish, Hande Üstünel, David Roundy, Tomás A. Arias, Paul L. McEuen, "A tunable carbon nanotube electromechanical oscillator," Nature (London) 431(2004):284-287; https://www.andrew.cmu.edu/user/asurie/15398/nt-oscillator.pdf.

(Burke[1214] predicts a cutoff frequency (due to the influence of quantum capacitance, kinetic inductance, and the effects of parasitic capacitances) for AC nanotube transistors of ~80 GHz/L_{tube} for nanotube transistor gate length L_{tube} in microns, predicting a 120 MHz cutoff at ~0.7 mm length and 1.2 MHz at ~7 cm length, but the corresponding limits for an atomically-precise carbon nanotube binary tree networks, possibly including self-shielding multiwalled "nanocables" (see next paragraph), have not yet been studied.)

The possible utility of switching from a (supply wire + common ground) wiring model to a twisted pair or double-coaxial-type "nanocable" (e.g., 4-walled nanotubes, 2 conducting layers alternating with 2 insulating layers)[1215] wiring model should also be investigated. These alternative models could have several advantages in the later Phases of nanofactory development, including compactness of design, superior high-frequency operating characteristics, and elimination of fan-out from common ground lines exiting the NMW-3 modules that must feed into the parallel grounding binary wiring tree. Note also that the final "level 22" segment of the binary tree has a voltage drop of only I_{motor} $R_{quantum}$ ~ 2.58 x 10^{-7} volts, which means that this tree level (and possibly many others above it) may be highly sensitive to stray environment voltages and crosstalk between adjacent wires, which could add significant noise into the signal traffic and ultimately reduce system reliability. Multitube cables may display a quantum confinement effect that sharply reduces the resistance, possibly giving an electrical conductivity 10-100 times that of copper at room temperatures, and may provide shielding comparable to coax. Single coaxial silicon-based nanocables ~30 nm in diameter have been fabricated in lengths up to 50 microns,[1216] and silicon wires sheathed in diamond-like carbon[1217] and other models including

---

[1213] H.B. Peng, C.W. Chang, S. Aloni, T.D. Yuzvinsky, A. Zettl, "Ultrahigh frequency nanotube resonators," Phys. Rev. Lett. 97(2006):087203; http://socrates.berkeley.edu/~tyuz/pub/prl97.pdf. H.B. Peng, C.W. Chang, S. Aloni, T.D. Yuzvinsky, A. Zettl, "Microwave electromechanical resonator consisting of clamped carbon nanotubes in an abacus arrangement," Phys. Rev. B 76(2007):035405; http://socrates.berkeley.edu/~tyuz/pub/prb76.pdf. J. Chaste, L. Lechner, P. Morfin, G. Fève, T. Kontos, J.-M., Berroir, D.C. Glattli, H. Happy, P. Hakonen, B. Plaçais, "Single Carbon Nanotube Transistor at GHz Frequency," Nano Lett. 8(January 2008):525-528; http://pubs.acs.org/cgi-bin/abstract.cgi/nalefd/2008/8/i02/abs/nl0727361.html. Aaron A. Pesetski, James E. Baumgardner, Erica Folk, John X. Przybysz, John D. Adam, Hong Zhang, "Carbon nanotube field-effect transistor operation at microwave frequencies," Appl. Phys. Lett. 88(13 March 2006):113103; http://link.aip.org/link/?APPLAB/88/113103/1.

[1214] Peter J. Burke, "AC performance of nanoelectronics: towards a ballistic THz nanotube transistor," Solid-State Electronics 48(October-November 2004):1981-1986; http://dx.doi.org/10.1016/j.sse.2004.05.044.

[1215] Christopher Gump (PI), "STTR Phase I: Fabrication of Coaxial Nanowires/Nanocables Using Carbon Nanotubes," Award Number 0539536, ALD NANOSOLUTIONS, INC., 11711 CHASE CT CO 80020, 1 January 2006 to 31 December 2006; http://www.sciencestorm.com/award/0539536.html.

[1216] Y. Zhang, K. Suenaga, C. Colliex, S. Iijima, "Coaxial Nanocable: Silicon Carbide and Silicon Oxide Sheathed with Boron Nitride and Carbon," Science 281(14 August 1998):973-975; http://www.sciencemag.org/cgi/content/full/281/5379/973?ck=nck.

[1217] T. Qiu, X.L. Wu, P.K. Chu, "Coaxial Nanocable Arrays: Si Sheathed With Diamond-like Carbon," Proceedings of the NanoSingapore 2006: IEEE Conference on Emerging Technologies – Nanoelectronics,

carbon nanotube-containing nanocables[1218] have been investigated theoretically and experimentally. One-dimensional coaxial nanocables consisting of a continuous crystalline nanowire encapsulated in a sheath of a different crystalline material have been the focus of extensive research[1219] because these structures are expected to play an important role in the next generation of electrical heterostructured devices as the semiconductor industry attempts to progress below the 22 nm feature level. One advantage of a nanotube coaxial wiring model might be to greatly reduce electronic crosstalk, which is anticipated in dense nanotube networks at close separations.[1220] Reduced-crosstalk nanotube interconnect architectures using DWCNT

Singapore, 10-13 January 2006, p 253-254 (Paper 68-NM-A0182); http://ieeexplore.ieee.org/xpl/freeabs_all.jsp?tp=&arnumber=1609769&isnumber=33794.

[1218] K. Suenaga, C. Colliex, N. Demoncy, A. Loiseau, H. Pascard, F. Willaime, "Synthesis of nanoparticles and nanotubes with well-separated layers of boron nitride and carbon," Science 278(1997):653-655; T. Taguchi, N. Igawa, H. Yamamoto, S. Jitsukawa, "Synthesis of Silicon Carbide Nanotubes," J. Amer. Ceramic Soc. 88(February 2005):459-461, http://www.blackwell-synergy.com/doi/abs/10.1111/j.1551-2916.2005.00066.x; Zhuhua Zhang, Wanlin Guo, Guo'an Tai, "Coaxial nanocable: Carbon nanotube core sheathed with boron nitride nanotube," Appl. Phys. Lett. 90(2007):133103, http://dx.doi.org/10.1063/1.2714997 and http://adsabs.harvard.edu/abs/2007ApPhL..90m3103Z; Shaojun Guo, Lijian Huang, Erkang Wang, "A novel hybrid nanostructure based on SiO_2@carbon nanotube coaxial nanocable," New J. Chem. 31(2007):575-579, http://www.rsc.org/publishing/journals/NJ/article.asp?doi=b616234g.

[1219] L. Dai, X.L. Chen, X. Zhang, T. Zhou, B. Hu, "Coaxial ZnO/SiO 2 nanocables fabricated by thermal evaporation/oxidation," Applied Physics A: Materials Science & Processing 78(March 2004):557-559, http://www.springerlink.com/content/tn9t8qe61e52eabm/fulltext.pdf; Xiaofeng Lu, Qidong Zhao, Xincai Liu, Dejun Wang, Wanjin Zhang, Ce Wang, Yen Wei, "Preparation and Characterization of Polypyrrole/TiO2 Coaxial Nanocables," Macromolecular Rapid Communications 27(6 March 2006):430-434; Brian Daly, Jaideep S. Kulkarni, Donna C. Arnold, Matthew T. Shaw, Sergey Nikitenko, Michael A. Morris, Justin D. Holmes, "Structural investigation of germanium-cobalt core shell nanocable arrays," J. Mater. Chem. 16(2006):3861-3866, http://dx.doi.org/doi:10.1039/b605997j; Brian Daly, Donna C. Arnold, Jaideep S. Kulkarni, Olga Kazakova, Matthew T. Shaw, Sergey Nikitenko, Donats Erts, Michael A. Morris, Justin D. Holmes, "Synthesis and characterization of highly ordered cobalt-magnetite nanocable arrays," Small 2(18 September 2006):1299-1307, http://dx.doi.org/doi:10.1002/smll.200600167; Shaojun Guoa, Erkang Wang, "A novel sensitive solid-state electrochemiluminescence sensor material: $Ru(bpy)_3^{2+}$ doped SiO_2@MWNTs coaxial nanocable," Electrochemistry Communications 9(June 2007):1252-1257, http://dx.doi.org/10.1016/j.elecom.2007.01.030; D.F. Wang, S.Y. Park, Y.S. Lee, Y.P. Lee, J.C. Li, C. Liu, "Synthesis and room-temperature ferromagnetism of $Zn_{0.96}Mn_{0.04}O$/ZnO coaxial nanocable and $Zn_{0.96}Mn_{0.04}O$ film," J. Appl. Phys. 103(2008):07D126, http://link.aip.org/link/?JAPIAU/103/07D126/1.

[1220] A. Naeemi, J.A. Davis, J.D. Meindl, "Compact physical models for multilevel interconnect crosstalk in gigascale integration (GSI)," IEEE Trans. Electron Devices 51(November 2004):1902-1912, http://users.ece.gatech.edu/~azad/TED-04.pdf; François Léonard, "Crosstalk between nanotube devices: contact and channel effects," Nanotechnology 17(2006):2381-2385, http://dx.doi.org/10.1088/0957-4484/17/9/051 and http://www.iop.org/EJ/article/0957-4484/17/9/051/nano6_9_051.pdf; N. Sinha, J.T.W. Yeow, D.A. Jaffray, "Experimental Investigation of the Crosstalk Phenomenon and Current Stability in a Carbon Nanotube Array," Proc. 7th IEEE International Conference on Nanotechnology, Hong Kong, 2-5 Aug 2007.

have been proposed.[1221] A more thorough analysis of the limits of nanotube-based "gigascale integration" or "GSI"[1222] and related issues such as minimizing parasitic capacitance effects in carbon nanotube-based electronic circuits[1223] is warranted but is beyond the scope of this document.

[1221] Daniele Rossi, José Manuel Cazeaux, Cecilia Metra, Fabrizio Lombardi, "Modeling crosstalk effects in CNT bus architectures," IEEE Transactions on Nanotechnology 6(2007):133-145; http://cat.inist.fr/?aModele=afficheN&cpsidt=18606677.

[1222] J.A. Davis, R. Venkatesan, A. Kaloyeros, M. Beylansky, S.J. Souri, K. Banerjee, K.C. Saraswat, A. Rahman, R. Reif, J.D. Meindl, "Interconnect limits on gigascale integration (GSI) in the 21st century," Proceedings of the IEEE 89(March 2001):305-324; http://ieeexplore.ieee.org/search/wrapper.jsp?arnumber=915376. . Naeemi, R. Sarvari, J.D. Meindl, "Performance comparison between carbon nanotube and copper interconnects for GSI," IEEE IEDM Digest, San Francisco CA, December 2004, pp. 699-702, http://users.ece.gatech.edu/~azad/IEDM04.pdf; A. Naeemi, R. Sarvari, J.D. Meindl, "Performance comparison between carbon nanotube and copper interconnects for gigascale integration (GSI)," IEEE Electron Device Letters 26(February 2005):84-86, http://users.ece.gatech.edu/~azad/EDL-SWNT.pdf; A. Naeemi, J.D. Meindl, "Impact of electron-phonon scattering on the performance of carbon nanotube interconnects for gigascale integration (GSI)," IEEE Electron Device Letters 26(July 2005):476-478, http://users.ece.gatech.edu/~azad/EDL-phonon.pdf; A. Naeemi, J.D. Meindl, "Design and performance modeling for single-wall carbon nanotubes as local, semi-global and global interconnects in gigascale integrated systems," IEEE Trans. Electron Devices 54(January 2007):26-37, http://users.ece.gatech.edu/~azad/TED-SWNT.pdf.

[1223] D.V. Singh, K.A. Jenkins, J. Appenzeller, "Direct measurements of frequency response of carbon nanotube field effect transistors," Electronics Letters 41(3 March 2005):280-282; http://dx.doi.org/10.1049/el:20057528. P.J. Burke, "An RF circuit model for carbon nanotubes," IEEE Trans. on Nanotechnology 2(March 2003):55-58; D.L. John, L.C. Castro, D.L. Pulfrey, "Quantum capacitance in nanoscale device modeling," J. Appl. Phys. 96(2004):5180-5184; Chris Dwyer, Moky Cheung, Daniel J. Sorin, "Semi-empirical SPICE Models for Carbon Nanotube FET Logic," Proceedings of the Fourth IEEE Conference on Nanotechnology, Munich, Germany, 17-19 August 2004, http://www.ee.duke.edu/~sorin/papers/ieeenano04_spice.pdf; A. Javey, J. Guo, D.B. Farmer, Q. Wang, E. Yenilmez, R.G. Gordon, M. Lundstrom, H. Dai, "Self-aligned ballistic molecular transistors and electrically parallel nanotube arrays," Nano Letters 4(2004):1319-1322; A. Bansal, B.C. Paul, K. Roy, "Modeling and optimization of fringe capacitance of nanoscale DGMOS devices," IEEE Trans. on Electron Devices 52(2005):256-262, http://portal.acm.org/ft_gateway.cfm?id=1147092&type=pdf&coll=ACM&dl=GUIDE&CFID=26691208&CFTOKEN=11680622; Jing Guo, Sayed Hasan, Ali Javey, Gijs Bosman, Mark S. Lundstrom, "Assessment of high-frequency performance potential of carbon nanotube transistors," November 2005, http://docs.lib.purdue.edu/cgi/viewcontent.cgi?article=1039&context=nanodocs; Xiaolei Liu, Song Han, Daihua Zhang, Koungmin Ryu, Chongwu Zhou, "A Novel Nanotube-on-Insulator (NOI) Approach toward Single-Walled Carbon Nanotube Devices," Mater. Res. Soc. Symp. Proc. Vol. 938, 2006 (0938-N07-10), http://www.mrs.org/s_mrs/bin.asp?CID=6459&DID=176815&DOC=FILE.PDF; Bipul C. Paul, Shinobu Fujita, Masaki Okajima, Thomas Lee, "Impact of geometry-dependent parasitic capacitances on the performance of CNFET circuits," IEEE Electron Device Letters 27(2006):380-382, http://cat.inist.fr/?aModele=afficheN&cpsidt=17769443; Coskun Kocabas, Hoon-sik Kim, Tony Banks, John A. Rogers, Aaron A. Pesetski, James E. Baumgardner, S. V. Krishnaswamy, Hong Zhang, "Radio frequency analog electronics based on carbon nanotube transistors," PNAS 105(5 February 2008):1405-1409, http://rogers.mse.uiuc.edu/files%5C2008%5Cpnasradio.pdf. Peter J. Burke, "AC performance of nanoelectronics: towards a ballistic THz nanotube transistor," Solid-State Electronics 48(October-November 2004):1981-1986; http://dx.doi.org/10.1016/j.sse.2004.05.044.

Using the original wiring model for scaling purposes, the approximate thickness of the wiring bundle underlying each FGN fabrication plane may be estimated as follows. The total length of wire in each half-plane wire network is $L_{network}$ = 2.75 meters, $2L_{network}$ in each full-plane wire network, $4L_{network}$ including parallel ground lines to complete the electrical circuit, $400L_{network}$ for all 100 lines for the $N_{module} = 5 \times 10^6$ NMW-3 modules along a single row of modules in one fabrication plane of the FGN, and $L_{fpWire} = 400\ N_{fpRows}\ L_{network} = 2.2 \times 10^9$ meters of nanotube wires for all $N_{fpRows} = 2 \times 10^6$ rows of modules in one fabrication plane of the FGN, or $L_{fplWires} = 2.2 \times 10^{12}$ meters of nanotube wires for all 1000 fabrication planes. The wiring bundle thickness underlying each fabrication plane is therefore $(4\ nm^2)\ L_{fpWire} / (x_{FGN}\ y_{FGN}) \sim 44$ nm, which we increase by 12% to 50 nm to allow room for necessary openings in the wire bundle (e.g., catacomb support column/wall bypasses, stovepipe bypasses, sorting rotor access ports, etc.) and the few topmost levels of somewhat thicker nanotubes.

The total number of individual wires per half-plane network is $N_{hpn} = (2^{Nbranch} - 1) = 4{,}194{,}303$ wires, so the total number of wires of various sizes to be manufactured and installed in all 1000 fabrication planes of the FGN is $N_{fplWires} \sim (400)\ (N_{fpRows})\ (N_{hpn})$ (1000 planes) = 3.36×10^{18} wires. However, 75% of these wires are 119.2 nm or 100 nm in length and can be manufactured using existing convergent processes, and only a relatively small number of the very long top-level nanotubes must be fabricated (e.g., 800 million of the longest 12.5 cm "level 1" wires per fabrication plane). If 2-nm diameter nanotube wires are used throughout, the total atom count for the nanotube wiring bundle underlying each fabrication plane is $\sim \pi\ (2\ nm)\ L_{fpWire}\ (31.4\ C\ atoms/nm^2) = 4.34 \times 10^{20}$ carbon atoms.

By using one of the two spare wires (Section 3.7.1) among the 100 control lines to connect every other NMW-3 unit in a row, we gain the ability to switch alternating modules into a different mode from their neighbors – e.g., allowing crane arms in adjacent modules within the same row to operate in "mirror mode" 180° out of phase, thus enabling ciliary transport motions (Section 3.11.2.7). Similar use of the other spare wire enables cross-row ciliary capability.

3.11.2.5 Support Frame

Four diamondoid square vertical support columns measuring 5 nm x 5 nm x 200 nm tall (composed of 2 or more strongly interlocked segments of maximum length ≤100 nm to allow their manufacture by the FGN) are added at each of the four corners of the NMW-3 design, along with a ceiling block similar to the foundation block that can provide leaktight mating of adjacent NMW-3 modules, making a rigid wire-frame box capped with ceiling and floor but open sides defining the periphery of the larger $2 \times 10^6\ nm^3$ cubic operating volume of the NMW-3 (Figure X-4). When adjacent NMW-3 units are pressed tightly together, the four vertical columns adhere by van der Waals forces to produce a relatively rigid 10 nm x 10 nm compound column, adding stiffness to the shear walls provided by the foundation and ceiling blocks. The columns are 200 nm tall instead of 100 nm to double the operating volume of the NAW-2 units in the vertical dimension to leave sufficient overhead room for NAW-2 crane arms to pass manufactured components up to 100 nm in size among all four nearest-neighbor NMW-3 modules on the

fabrication plane, using baton-handoff motions of parts between adjacent crane arms (Section 3.11.2.7).

Figure X-4. Schematic illustration of the layout of a single NMW-3 module, along with associated catacombs and cooling channel, in one fabrication plane in the first production layer of the FGN (not to scale)

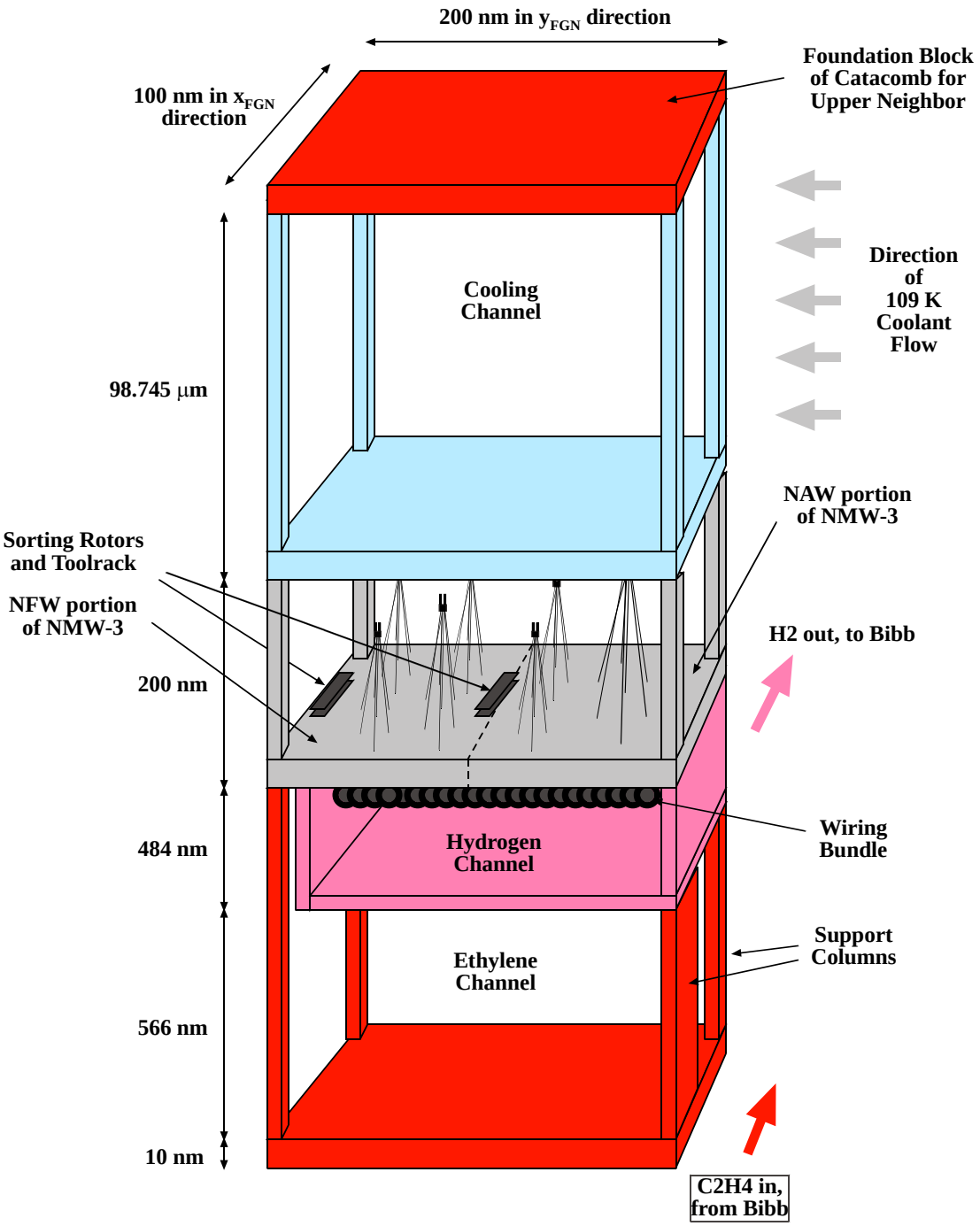

In addition, around the entire 180 cm perimeter we replace the outermost module with a diamondoid vertical wall module, similar in size and shape to a foundation plate (200 nm tall, 10 nm thick), to establishes a vacuum-tight seal between floor and ceiling. This maintains the vacuum environment inside the plate of NMW-3 modules within the fabrication plane and also provides additional mechanical support strength around the perimeter of the FGN.

3.11.2.6 Catacombs

To obtain the highest possible reliability, the FGN will be operated near the lowest possible temperature at which the ethylene feedstock remains a liquid, or ~109 K (Figure IV-2). The ethylene feedstock must include trace concentrations of germane, which will also be present in liquid form since the melting point of GeH_4 lies between 107.15-108.15 K.[1224]

To provide a source of cryogenic feedstock fluids and to carry away byproduct gases, a sealed volume is created underneath the foundation blocks of the array of NMW-3 modules which serve as the leakproof catacomb ceiling (Figure X-4). The catacomb floor (the lowest point in each fabrication plane) is created by laying down a similar plane of NMW-3 foundation blocks (but lacking any NMW-3 wiring or penetrations) directly onto the nanofactory base plate (assumed to be nearly but perhaps not perfectly atomically flat), making a catacomb foundation block 100 nm x 200 nm x 10 nm thick of solid diamond with volume ~200,000 nm^3 and ~46,000 nm^2 of hydrogenated surface area. Next, a set of 4 support columns measuring 5 nm x 5 nm x 1055 nm long (composed of multiple strongly interlocked segments of maximum length ≤100 nm to allow their manufacture by the FGN) are installed at the corners to support the NMW-3 foundation block above the catacomb foundation block. The four columns together total ~105,000 nm^3 of solid diamond with ~21,150 nm^2 of hydrogenated surface area. Note that when adjacent catacomb modules are pressed tightly together, the four vertical columns adhere by van der Waals forces to produce relatively rigid 10 nm x 10 nm compound columns, adding stiffness to the shear walls provided by the upper and lower foundation blocks. Alternatively, the four columns could be fabricated as a single covalent unit if still more stiffness is needed.

Byproduct hydrogen gas is confined to a sealed channel attached to the underside of the NMW-3 foundation blocks. The channel allows flow in the x_{FGN} direction, with the nanotube wiring bundle running in the same direction and occupying the top 50 nm of the hydrogen channel. The open space within the channel through with the hydrogen may flow extends 434 nm below the wiring bundle (see flow calculations, below). The hydrogen channel consists of three walls with docking interfaces that permit neighboring walls to hermetically seal the channel when adjacent catacomb modules are pressed together. The leftmost wall of the hydrogen channel hangs down from the underside of the NMW-3 foundation block and is indented 5 nm to the right of the leftmost edge of the catacomb module, leaving a 5 nm open space through which ethylene

---

[1224] Robert C. Weast, Handbook of Chemistry and Physics, 49th edition, CRC Press, Cleveland OH, 1968. "Germane," Gas Encyclopaedia, Air Liquide, accessed April 2008, http://encyclopedia.airliquide.com/Encyclopedia.asp?GasID=31; see also MSDS at http://encyclopedia.airliquide.com/sds/en/060_AL_EN.pdf. "Germane," MSDS, Voltaix, 1994, http://sauvignon.mit.edu/safety/GeH4.pdf.

feedstock molecules can flow up from below to reach the NMW-3 sorting rotor collection points. The left wall measures (434 nm + 50 nm =) 484 nm tall, 100 nm deep along the x_{FGN} direction, and 1 nm thick, giving ~48,400 nm^3 of solid diamond volume and ~97,968 nm^2 of hydrogenated surface area. The bottom wall of the hydrogen channel is 190 nm wide, 100 nm deep in the x_{FGN} direction, and 1 nm thick, giving ~19,000 nm^3 of solid diamond volume and ~38,580 nm^2 of hydrogenated surface area. The rightmost wall of the hydrogen channel is located flush with the two rightmost support columns, filling the space between them for the topmost 484 nm and also extending another 566 nm all the way to the catacomb foundation block to provide additional floor-to-ceiling structural support filling 46 nm of the 90 nm gap between support columns. The right wall thus measures 1055 nm tall, 90 nm deep along the x_{FGN} direction for 489 nm of height and 46 nm deep for 566 nm of height, and 5 nm thick, giving ~350,230 nm^3 of solid diamond volume and ~140,090 nm^2 of exposed hydrogenated surface area, so the structural total for the entire hydrogen channel is ~417,630 nm^3 of solid diamond volume and ~276,638 nm^2 of hydrogenated surface area. Note that the maximum tolerable gas storage pressure P_{max} (bursting pressure) for a cylindrical tank of radius R ~ (484 nm + 190 nm)/2 = 337 nm, wall thickness t_{wall} ~ 1 nm, and wall material failure strength $\sigma_w = 10^{10}$ N/m^2 for diamond (at a *very* conservative 20% of minimum failure strength), is $P_{max} \sim t_{wall}\ \sigma_w / R = 294$ atm >> 10 atm, for the hydrogen channel.

Liquid ethylene feedstock flows through the 566 nm deep walled-in space beneath the noncommunicating hydrogen channel, called the <u>ethylene channel</u>. This configuration is chosen to prevent possible entry of small H_2 gas molecules into the NMW-3 through the C_2H_4 sorting rotors. The wire bundle is in contact only with molecular hydrogen gas, not with the possibly more reaction liquid ethylene whose molecules contain potentially reactive unsaturated C=C bonds; if deemed necessary, a thin fourth wall can be added to the hydrogen channel to prevent all contact between the wiring bundle and H_2, at minimal increment to the atom count. Around the perimeter only, we replace the catacomb modules with a diamondoid vertical wall module, similar in size and shape to a foundation plate that establishes a sealed subterranean space between floor and ceiling and can be filled with bulk feedstock fluid or byproduct gases at some modest operating pressure (~10 atm).

In the simplest scenario, 4.4% of the perimeter modules are replaced with a hose bib module that permits connection to a microscale feedstock fluid source. This module can be fabricated using conventional MEMS microlithography. Feedstock fluid enters through a rectangular 4 cm x 100 nm x 100 nm (with 100 nm thick walls) hose bib on one side, then is distributed through a narrow plenum running the entire 40 cm width (in the y_{FGN} direction) of the fabrication plane catacomb (comprised of the aforementioned replaced perimeter modules) that allows lateral movement of the fluid to enter into each of the 2×10^6 fluid channels 50 cm in length; byproduct gas exits through an identical coupling on the other side. With each fabrication plane manufacturing diamondoid material at the 10^{17} atom/sec rate, the consumption of ethylene feedstock fluid will approximate 0.5×10^{17} molecules/sec of C_2H_4 liquid ($V_{fluid} \sim 0.00333$ mm^3/sec at 109 K and ~10 atm), and ~10^{17} molecules/sec of H_2 gas ($V_{fluid} \sim 0.144$ mm^3/sec at 109 K and ~10 atm) will be generated as byproduct gas for disposal.

Catacomb scaling is controlled by the flow rates of feedstock consumption and byproduct generation, and by the pressurization required to force liquids and gases through narrow channels. Using the Hagen-Poiseuille equation for laminar pipe flow, fluid circulation requires an estimated driving pressure of $\Delta P_{fluid} = 8\ \eta_{fluid}\ L_{channel}\ \Delta V_{channel} / \pi\ R_h^4 \sim 10$ atm, where the absolute fluid viscosity $\eta_{fluid} \sim 5.82 \times 10^{-4}$ kg/m-sec for liquid ethylene at 109 K and is estimated as $\eta_{fluid} \sim 7.91 \times 10^{-6}$ kg/m-sec for gaseous H_2 at 109 K and ~10 atm pressure (assuming analogous values for N_2

gas).[1225] The total fluid flow V_{fluid} is distributed via the hose bib plenum to each of $N_{channels} = 2 \times 10^6$ parallel rectangular channels of length $L_{channel} = 50$ cm, giving a volume flow rate through each channel of is $\Delta V_{channel} = V_{fluid} / N_{channels} = v_{fluid} A_{channel} \sim 1.67$ micron^3/sec at $v_{fluid} \sim 15.5$ micron/sec for liquid ethylene and 72 micron^3/sec at $v_{fluid} \sim 671$ micron/sec for hydrogen gas, where the channel dimensions are $W_{channel} \sim 190$ nm in width and $H_{channel} = 566$ nm for C_2H_4 and 434 nm for H_2, with $A_{channel} = W_{channel} H_{channel}$ and the hydraulic radius R_h crudely approximated as $\sim(A_{channel}/\pi)^{1/2}$. In this case, the driving power per channel at ~10 atm is $P_{flow} = \pi R_h^4 \Delta P_{fluid}^2 / 8 \eta_{fluid} L_{channel} = 1.75$ pW per ethylene channel and 76.1 pW per hydrogen channel, giving a negligible total power dissipation per fabrication plane for all 2 million ethylene and hydrogen flow channels of ~0.156 milliwatts. Note that the Reynolds number for fluid flow at 109 K for liquid ethylene of density $\rho_{ethylene} = 648.5$ kg/m^3 and absolute viscosity $\eta_{fluid} \sim 5.82 \times 10^{-4}$ kg/m-sec[1226] through an $R_h = 185$ nm channel at $v_{fluid} \sim 15.5$ micron/sec is $N_R = \rho_{ethylene} v_{fluid} R_h / \eta_{fluid} \sim 6 \times 10^{-6}$. Experiments by Reynolds[1227] showed that transition from laminar to turbulent flow typically occurs between $N_R \sim 2000$-13,000, so ethylene fluid flow through the ethylene channels in each fabrication plane should remain fully laminar or very nearly so. Similar results hold for the hydrogen channel which has $N_R \sim 6 \times 10^{-5}$ for density $\rho_{hydrogen} = 2.223$ kg/m^3 at ~10 atm and 109 K.

3.11.2.7 Ciliary Transport Array (CTA)

Because there is a ~20:1 productivity mismatch between NFW-3 and NAW-2 as noted earlier, the duty cycle of the NAW-2 subsystem for assembly operations is only ~5%. The remaining ~95% of the NAW-2 subsystem duty cycle is available for the ciliary transport array, as necessary. The purpose of this array is to receive handoff of completed parts from the crane arm of the NAW-2 unit within each NMW-3 module and then pass those parts along to the nearest stovepipe (Section 3.11.2.8) for transport to another production layer for further processing. (Optimal scheduling of ciliary vs. assembly operations must be carefully analyzed and software must be created to manage this complex workflow planning task.)

Arrays of micron or submicron-scale MEMS manipulator elements can be used to create 1-, 2-, or 3-dimensional programmable motion fields. In the simple 1-dimensional case, a single row of manipulators alternately grasp, transfer, and release a load, passing the payload down the line like a bucket brigade. In the 2-dimensional case, surfaces may be coated with closely-packed

---

[1225] P.M. Holland, B.E. Eaton, H.J.M. Hanley, "A Correlation of the Viscosity and Thermal Conductivity Data of Gaseous and Liquid Ethylene," J. Phys. Chem. Ref. Data 12(1983):917-932; http://www.nist.gov/srd/PDFfiles/jpcrd235.pdf.

[1226] P.M. Holland, B.E. Eaton, H.J.M. Hanley, "A Correlation of the Viscosity and Thermal Conductivity Data of Gaseous and Liquid Ethylene," J. Phys. Chem. Ref. Data 12(1983):917-932; http://www.nist.gov/srd/PDFfiles/jpcrd235.pdf.

[1227] O. Reynolds, "An experimental investigation of the circumstances which determine whether the motion of water shall be direct or sinuous, and of the law of resistance in parallel channels," Phil. Trans. Roy. Soc. 174(1883):935-982.

manipulators, allowing rapid and continuous transfers of multiple payload streams along multiple surface vectors simultaneously.

The prototyping and testing of simple ciliary arrays in MEMS work was an active research area in the 1990s.[1228] Ataka et al.[1229] had fabricated and operated a 1 cm^2 array of 512 cantilever-type bimorph manipulators (each one 500 microns long, 100 microns wide, and 6 microns thick) and operated it at 10 Hz in a coordinated fashion to transport a 2.4 mg piece of silicon wafer at 27-500 micron/sec using ~100 micron strokes and a 4 milliwatt input power to each actuator. Bohringer et al.[1230] had fabricated a prototype array of 1024 cilia called the "cilia chip" that moved silicon chips at speeds up to 200 microns/sec with a placement accuracy of ~3 microns and a lifting capacity of 250 N/m^2. Individual ciliary pixel control allowed movement of multiple components on different trajectories, enabling the performance of various assembly tasks. A larger manipulator chip (M-chip) consisting of ~10,000 microactuator "resonators" (5-micron tall cilia) had also been fabricated on a few cm^2 of silicon substrate and tested at ~5 KHz[1231] – a part dropped onto the array was propelled forward at a constant speed of ~800 microns/sec.[1232] Peter Will et al.[1233] developed a software toolkit to allow researchers to program Intelligent Motion Surfaces[1234] to perform a variety of simple functions including centering parts, spiraling a part to center in a convergent field array, spiraling a part away from the center in a divergent field array, rotating a part about the center using four triangular fields, orienting a part in a programmable field array, and sorting two parts using a hole as a trap for a part being translated past it. Properly

---

[1228] Robert A. Freitas Jr., Nanomedicine, Volume I: Basic Capabilities, Landes Bioscience, Georgetown, TX, 1999; Section 9.3.4, p. 293; http://www.nanomedicine.com/NMI/9.3.4.htm.

[1229] Manabu Ataka, Akito Omodaka, Naohiro Takeshima, Hiroyuki Fujita, "Fabrication and Operation of Polyimide Bimorph Actuators for a Ciliary Motion System," J. Microelectromech. Syst. 2(December 1993):146-150.

[1230] Karl-Fredrich Bohringer, John W. Suh, Bruce Randall Donald, Gregory T.A. Kovacs, "Vector Fields for Task-level Distributed Manipulation: Experiments with Organic Micro Actuator Arrays," Proc. 1997 IEEE International Conference on Robotics and Automation, 20-25 April 1997, IEEE Robotics and Automation Society, pp. 1779-1786. See also: Ivars Peterson, "From microdevice to smart dust," Science News 152(26 July 1997):62-63.

[1231] K. Bohringer, B. Donald, N. MacDonald, "Single-crystal silicon actuator arrays for micro manipulation tasks," IEEE Workshop on Micro Electro Mechanical Systems (MEMS), San Diego CA, February 1996.

[1232] Dan Reznik, Stan Brown, John Camy, "Dynamic Simulation as a Design Tool for a Microactuator Array," Proc. 1997 IEEE International Conference on Robotics and Automation, 20-25 April 1997, IEEE Robotics and Automation Society, pp. 1675-1680.

[1233] Murilo G. Coutinho, Peter M. Will, P. Selvan Viswanathan, "The Intelligent Motion Surface: A hardware/software tool for the assembly of meso-scale devices," Proc. 1997 IEEE International Conference on Robotics and Automation, 20-25 April 1997, IEEE Robotics and Automation Society, pp. 1755-1760.

[1234] P. Will, W. Liu, "Parts Manipulation on a MEMS Intelligent Motion Surface," ISI Research Report -- ISI/RR-94-391, Marina del Rey, CA, May 1994; W. Liu, P. Will, "Parts Manipulation on an Intelligent Motion Surface," Human Robot Interaction and Cooperative Robots, Proc. IEEE/RSJ Intl. Conf. on Intell. Robots and Systems (IROS), August 1995, pp. 399-404.

arrayed, such surfaces could form an assembly pipeline in which parts may enter at one end and be successively sorted, spaced (so parts flow through at a constant rate), centered, aligned and, ultimately, inserted into other parts. However, none of these devices had end-effectors capable of grasping and holding a part, so all of these arrays moved objects with only statistical accuracy.

It is important to point out that the CTA in the present program is a digitally precise manipulator array, not an analog manipulator array as in the MEMS-based ciliary systems of the past. A CTA manipulator will grasp a specific object to be transported, then hand it to another (adjacent) manipulator in a specific and known orientation. Because the NMW-3 modules are making a specific component using a specific series of fabrication and assembly instructions, the progress of a manipulated object along the array, along with its orientation, is entirely deterministic during transit through the FGN.

The top speed of NAW-2 crane arm manipulators is ~1.2 cm/sec at the tip when operated at a 120 MHz electrical control pulse frequency (Section 3.8.8), so if less than one-sixth (<17%) of each round-trip cycle time is consumed for baton-handoff motions of parts between adjacent crane arms then a net forward speed of ~1 cm/sec in the parts flow can be continuously maintained. The center-to-center distance between crane arms in nearest-neighbor NMW-3 modules in a fabrication plane is 100 nm along the row and 200 nm across the row. If the typical scenario involves equal distances traversed in cross-row and along-row transport, then the average distance a part travels during each ciliary arm motion cycle is 150 nm. With stovepipe rows spaced ~0.4 mm apart (Section 3.11.2.8), the maximum transport distance to a stovepipe is ~0.2 mm and the average transport distance is ~0.1 mm within a given fabrication plane, so each part must be handled by an average of (0.1 mm / 150 nm) ~ 667 NAW-2 crane arms before reaching a stovepipe. There are 10^{13} NMW-3 modules and thus 10^{13} crane arm manipulators allocated to the ciliary array in each fabrication plane of the FGN. Each part handling operation requires ~(300 nm round-trip travel / (1 cm/sec)) = 3×10^{-5} sec/part to complete, because adjacent NAW-2 crane arms are 100-200 nm apart (average 150 nm), so round trip distance is 200-400 nm (average 300 nm). As a result, the 10^{13}-arm ciliary array can execute (10^{13} / 3×10^{-5} sec/part) ~ 3×10^{17} part handling operations per second and a total of (3×10^{17} / 667) ~ 5×10^{14} parts/sec could, if necessary, be transported to all stovepipes by the array.

Only a small fraction of this capacity is required by the CTA. While the maximum product object size for the NMW-3 is ~$(100\text{ nm})^3$ and ~10^8 atoms, we more conservatively assume that the "typical smallest" component to be manufactured by the NMW-3 is only ~100,000 nm^3 or ~10^7 atoms. In this case, the output of all 10^{13} NMW-3 modules (each producing at ~10^4 atoms/sec at 120 MHz; see above) in a single fabrication plane is ~10^{17} atoms/sec, or ~10^{10} "typical smallest" parts/sec, still well below the maximum >10^{14} parts/sec capacity of the crane arm array and adding negligibly to the already low existing NAW-2 duty cycle. This leaves a great abundance of spare crane-arm cycles available to the CTA if necessary to execute more complex routing protocols.

Note that in the current design, the ciliary array manipulators do not inspect manufactured components in the first production layer. Rather, inspection is performed by a MAM array as soon as the parts reach the second production layer, before they are passed along for further assembly work (Section 3.11.3). Failed parts are collected in a reject bin in the second production layer. This avoids having to perform testing or to provide a separate reject pathway within each of the 1000 fabrication planes comprising the first production layer. However, if even a small fraction (e.g., 1%) of the 10^{13} NMW-3 modules in a fabrication plane have failed, error cascades may become inevitable. This could be prevented by incorporating fail-stop mechanisms at this stage. (In a fail-stop implementation, we would have an inspection step that

all NMW-3 modules execute. There is a mechanical switch representing a single bit that can be set if an error is detected. This requires a sensor with which parts or tooltips can be brought into physical contact in a specific motion pattern, to determine if they trip the sensor at the right moment due to the presence of a failure condition. If the bit gets set, it controls a set of relays (one for each control line) which turn off all power to the stricken NMW-3 module and deactivates it. In this case, the controls for the crane arm must be reactivated so this larger manipulator can continue to participate in ciliary transport.) Further analysis and detailed future modeling and simulations will be required to determine the need for, and upon need the ideal implementation of, appropriate fail-stop mechanisms in the FGN fabrication planes.

3.11.2.8 Stovepipes

Because achieving the target production rate of ~10^{20} atoms/sec requires multiple fabrication planes, it is necessary to transport completed components through these multiple fabrication planes of the first production layer, up to the second production layer (Section 3.11.3) where those components can later be assembled into finished atomically precise micron-scale product objects.

To accomplish this, each fabrication plane has 10^6 stovepipes through which components from the first production layer may pass to the second production layer (Figure X-5). On a 0.2 m^2 fabrication plane with 10^{13} NMW-3 modules aligned with their 200 nm dimension parallel to the 40 cm dimension of the FGN, there are 2 million rows of modules and 5 million modules in each 50-cm-long row of NMW-3 modules. Thus on average there is one stovepipe located somewhere within every other row of NMW-3 modules to provide a total of 10^6 stovepipes per fabrication plane.

Figure X-5. Stovepipes originate in every fabrication plane comprising the first production layer of the FGN, conveying finished parts upward toward the second production layer for final assembly into end products, where all stovepipes terminate (not to scale).

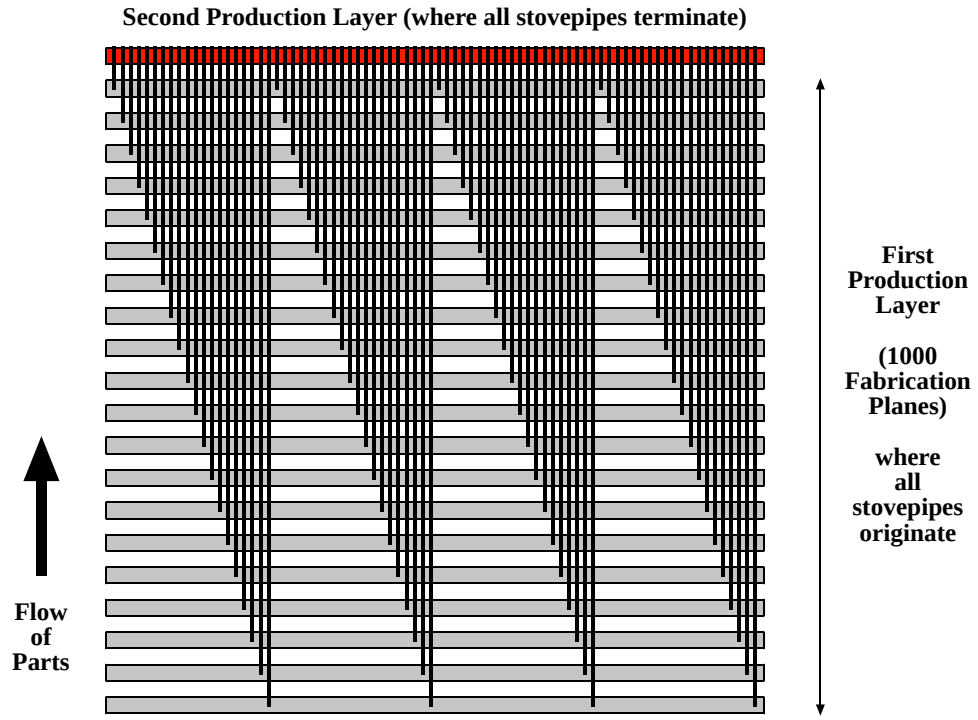

Stovepipes rise up through the 1000 fabrication planes of total thickness 10 cm to arrive at the lowest plane of the second production layer (Section 3.11.3). Stovepipes arriving at that layer are arranged in tight 2x2 groups of 4 pipes called "fourpacks", with each fourpack positioned at the corner junction of four 1 micron^2 MAM foundation blocks in the lowest plane of the second production layer (Figure X-6). All 10^9 stovepipes in the FGN are arranged in 1250 rows with ~0.4 mm between neighboring rows spanning the 50 cm length of the FGN, with each row consisting of 200,000 fourpacks evenly spaced along a line running parallel to the 40 cm dimension of the FGN in the direction of coolant flow.

Figure X-6. Schematic illustration of the layout of the array of stovepipe fourpacks as they enter the lowest assembling plane (Inspection Plane) of the second production layer of the FGN (not to scale). Top view shows the configuration across the entire assembling plane. Bottom view is a closeup showing how each stovepipe feeds parts to a horizontal row of 200 MAMs.

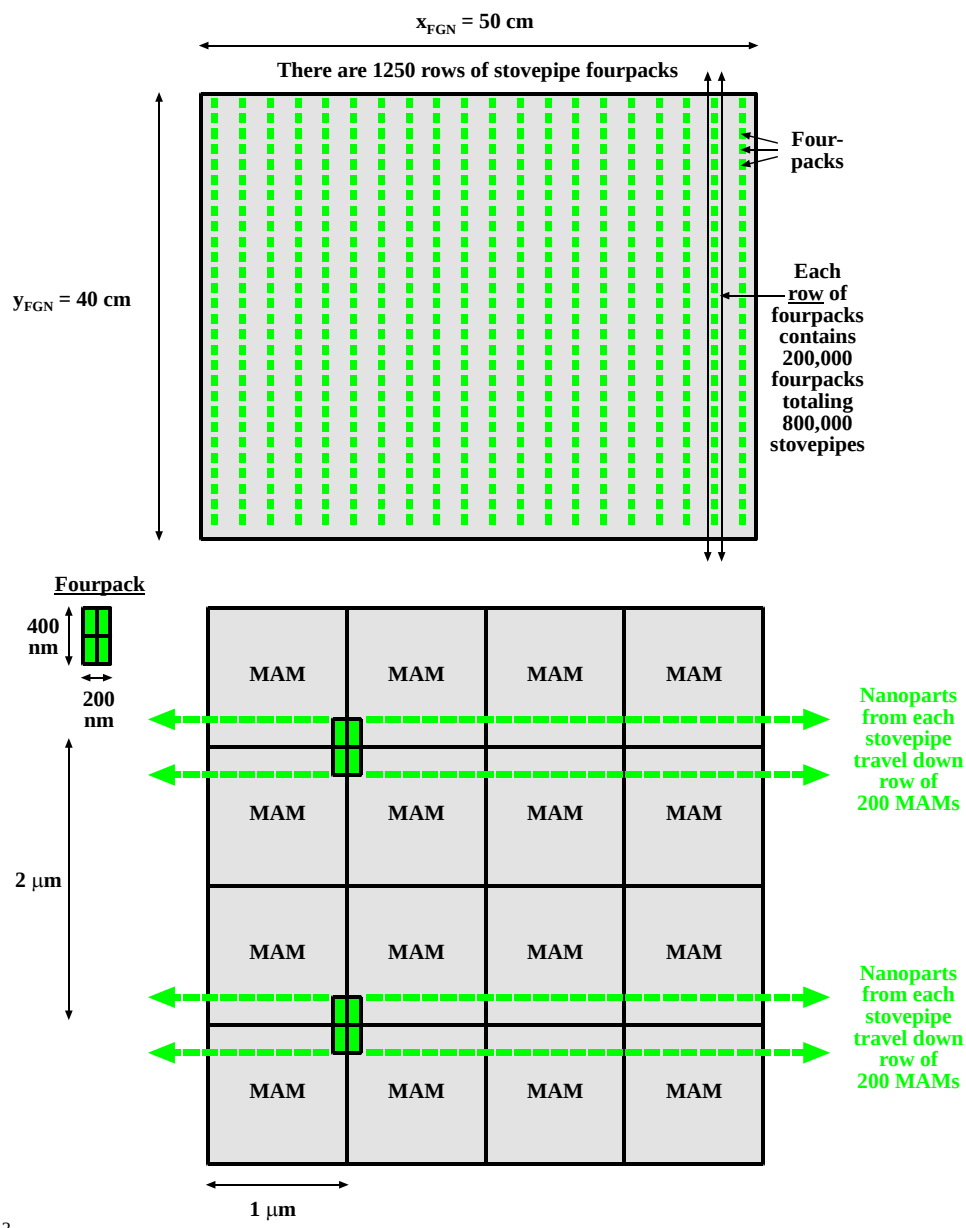

The 10^{13} NMW-3 modules in a single fabrication plane collectively produce output at ~10^{17} atoms/sec or ~10^{10} parts/sec for "typical smallest" ~100,000 nm^3 parts (Section 3.11.2.7), so ~10^4 parts/sec must be transported through each of the 10^6 stovepipes. A line of crane arms spaced 200 nm apart, with each arm having a ±100 nm round trip swing, can hand off transported parts bucket-brigade style while maintaining a constant 400 nm separation between successive parts. The total length of a line of 10^4 parts being transported single-file through a stovepipe with a mean 400 nm spacing between successive parts is ~0.4 cm, so a single-file transport speed of ~1 cm/sec achieves the required ~10^4 parts/sec per stovepipe using just a 40% duty cycle, leaving plenty of space capacity.

Each crane arm manipulator has a solid volume of 161,000 nm^3 (Table V-1), a length of 200.0 nm when fully extended and 68.0 nm when fully retracted (Section 3.6.1.1), and a diameter of 10 nm at the base, but with a 7-strut footprint of ~4000 nm^2 (63 nm x 63 nm) of square area. Allowing 100 nm of overhead clearance for the crane arm (which includes its 10 nm thick foundation block) plus up to another 100 nm of overhead clearance to allow nanoparts of maximum size

~(100 nm)^3 to pass, the stovepipe must be rectangular in cross-section and about 100 nm x 200 nm in size, exactly replacing the footprint of one NMW-3 module in a fabrication plane. If there are 10^6 stovepipes coming up from each of 1000 fabrication planes, then the total stovepipe holing area is (10^6 stovepipes/plane) x (1000 fabrication planes) x (20,000 nm^2/stovepipe) = 20 mm^2, a negligible ~0.01% holing of the entire nanofactory 0.2 m^2 surface area.

Allowing 100 microns (vertical) per fabrication plane (= 100 nm catacomb + 200 nm NMW-3 + 98.745 micron cooling channel), then 1000 fabrication planes are 10 cm thick and the average stovepipe up to the second production layer is 5 cm long and lined with (5 cm / 200 nm) = 250,000 crane manipulators. If each crane arm strut motor consumes 20 pW at 120 MHz (Section 3.6.1.3) and up to 7 motors can operate simultaneously in each arm then the total power draw is 140 pW per crane manipulator arm, so the average stovepipe operated at the indicated 40% duty cycle consumes (40% x 250,000 x 140 pW) = 1.4 x 10^{-5} W, or 14 kW for all 10^9 stovepipes in the FGN, only ~0.1% of total FGN power consumption.

Stovepipes require solid walls (like an elevator shaft) as they traverse (a) the cooling channels, to prevent an influx of coolant molecules into the NMW-3 interior which must be maintained at UHV; (b) the feedstock-fluid/byproduct-gas catacombs, for the same reasons; and (c) each NMW-3 layer, to reduce the random damage that could be caused by a dropped transported part. A jammed stovepipe could be detected by adding a simple force sensor to the stovepipe crane arms, allowing the faulty stovepipe to be shut down and the component traffic rerouted to one of the many other stovepipes on the same fabrication plane. A sufficient number of extra stovepipes can be added to provide the spare capacity needed to accommodate the expected number of stovepipe shutdowns over the estimated working lifetime of the FGN, since it may be difficult to design an FGN architecture that will easily permit mechanical repair and refurbishment of jammed individual stovepipes.

3.11.2.9 Cooling Channels

Assuming a maximum possible total power dissipation of 1040 pW for all four NFW-3 manipulators in continuous operation (Sections 3.4.1.1 and 3.4.1.2) at the 120 MHz control pulse frequency (Section 3.9.1), plus an additional 5% (of full duty cycle) when the NAW-2 is operating, the maximum power draw for an entire fabrication plane containing 10^{13} NMW-3 modules is ~11,000 watts. This is less than 10% of the maximum allowable power of ~128,000 watts per 0.2 m^2 of wafer area for the electronic circuitry on high performance chips with heatsinks (198 watts per 3.1 cm^2 chip area) that is anticipated for 2015-2017 by the semiconductor industry.[1235] Note that nanofactory power consumption is always highest in the lowest production layer where the largest number of very small objects is being handled. Power

---

[1235] International Technology Roadmap for Semiconductors (ITRS), 2006 Update. "Overview and Working Group Summaries," Tables 1a (Product Generations and Chip Size Model Technology Trend Targets—Near-term Years) and 1b (Product Generations and Chip Size Model Technology Trend Targets—Long-term Years), p.3; http://www.itrs.net/Links/2006Update/FinalToPost/00_ExecSum2006Update.pdf; see also in "Lithography," pp. 7-8; http://www.itrs.net/Links/2006Update/FinalToPost/08_Lithography2006Update.pdf.

consumption might be reduced by 2-3 orders of magnitude in the lowest production layer by switching from manipulator-based manufacturing to mill-based manufacturing and by other means (see Phase XI).

To provide a heatsink for each fabrication plane, coolant fluid is flowed in a direction parallel to the 40 cm dimension of the FGN through an $h_{channel}$ = 98.745 micron wide channel above the leaktight ceiling blocks (Section 3.11.2.5) of the NMW-3 array that forms one fabrication plane and the catacomb foundation blocks that form the bottom of the next highest fabrication plane. The presence of up to 10^9 stovepipes crisscrossing the 98.745 micron cooling channel space between each 40 cm x 50 cm plane (with the stovepipes occupying only ≤0.001% of the surface area of that plane) defines a rectangular 98.745 micron x 50 cm channel ($A_{channel} = 4.94 \times 10^{-5}$ m^2) volume through which the coolant may flow through a channel of length $L_{channel}$ = 40 cm before exiting the fabrication plane. The coolant fluid we will use is liquid ethylene at ~109 K, the same substance as the feedstock fluid (though highest purity C_2H_4 may not strictly be required for the coolant fluid).

To carry away a waste heat of P_{plane} = 11,000 W using a coolant fluid of heat capacity $C_V = 9.702 \times 10^5$ J/m^3-K for ethylene at 109 K, with the coolant changing temperature by ΔT = 20 K as it travels between inlet and outlet at a velocity $v_{coolant} = P_{plane} / (C_V \Delta T A_{channel})$ = 11.5 m/sec, which is <0.7% of the 1726 m/sec speed of sound in liquid ethylene at 109 K.[1236] Adding finely divided ethylene ice to the coolant fluid at a volume fraction of f_{ice} = 30% and taking the heat of fusion as $H_{fusion} = 6.81 \times 10^7$ J/m^3 for ethylene ice,[1237] then $v_{coolant} = P_{plane} / ((C_V \Delta T + f_{ice}H_{fusion}) A_{channel})$ ~ 6 m/sec, or 11 m/sec if the FGN is operated at 109 K and a cooling fluid carrying encapsulated ice[1238] is assumed to undergo no net change in temperature between inlet and outlet (ΔT = 0 K) to provide thermal stability to the FGN. Diamond is the most thermally conductive material known so temperatures throughout each fabrication plane are expected to be reasonably uniform with minimal differential expansion of adjoining components and subsystems. The characteristic thermal equilibration time to the midpoint of a cooling channel (conduction path length $X_{path} = h_{channel} / 2$ = 49.3725 microns) filled with liquid ethylene of thermal conductivity $K_{coolant}$ = 0.2645 W/m-K at 109 K[1239] is $t_{EQ} \sim X_{path}^2 C_V / K_{coolant} \sim 0.009$ sec << $L_{channel} / v_{coolant} \sim 0.04$ sec for $v_{coolant}$ ~ 11 m/sec, the time that liquid ethylene coolant takes to traverse the cooling channel from inlet to outlet side with no temperature change.

[1236] B.A. Younglove, "Thermophysical Properties of Fluids. 1. Argon, Ethylene, Parahydrogen, Nitrogen, Nitrogen Trifluoride, and Oxygen," J. Phys. Chem. Ref. Data 11(1982):1-368; http://www.nist.gov/srd/PDFfiles/jpcrdS1Vol11.pdf.

[1237] Heinz Zimmermann, Roland Walzl, "Ethylene," in: Ullmann's Encyclopedia of Industrial Chemistry, 7th Edition, John Wiley and Sons, 2005, http://www.mrw.interscience.wiley.com/ueic/ueic_search_fs.html and http://media.wiley.com/product_data/excerpt/55/35273038/3527303855.pdf.

[1238] K. Eric Drexler, Nanosystems: Molecular Machinery, Manufacturing, and Computation, John Wiley & Sons, New York, 1992, Section 11.5.2, pp. 331-332.

[1239] P.M. Holland, B.E. Eaton, H.J.M. Hanley, "A Correlation of the Viscosity and Thermal Conductivity Data of Gaseous and Liquid Ethylene," J. Phys. Chem. Ref. Data 12(1983):917-932; http://www.nist.gov/srd/PDFfiles/jpcrd235.pdf.

A simple calculation demonstrates that the presence of up to 10^9 stovepipes crisscrossing the 98.745 micron cooling channel space will not provide sufficient structural stability to support the stack of fabrication planes comprising the first production layer. Crudely approximating each stovepipe as a hollow cylinder of inside radius r_{in} = 100 nm, outside radius $r_{out} = r_{in} + t_{wall}$ = 110 nm for wall thickness t_{wall} = 10 nm, length L_{cyl} = 98.745 microns between each fabrication plane, and Young's modulus $E_{cyl} = 1.05 \times 10^{12}$ N/m^2 for diamond, the Euler buckling force is given by $F_{buckle} = \pi^3 E_{cyl} (r_{out}^4 - r_{in}^4) / 4 L_{cyl}^2$ = 40 nN per stovepipe – yielding a buckling strength of $n_{stove}F_{buckle}$ ~ 0.04 N for the $n_{stove} = 10^6$ stovepipes passing between planes 1 and 2, but $n_{stove}F_{buckle}$ ~ 40 N for the $n_{stove} = 10^9$ stovepipes passing between planes 999 and 1000. Each fabrication plane of area A_{plane} = 2000 cm^2 and total thickness h_{plane} = 100 microns (98.745 microns of cooling channel plus 1.255 microns of fabrication machinery plate) has a mean density approximating that of the liquid ethylene coolant fluid at 109 K, $\rho_{plane} \sim \rho_{ethylene}$ = 648.5 kg/m^3,[1240] so each of the n_{plane} = 1000 fabrication planes has a mass of $M_{plane} = \rho_{plane}\, h_{plane}\, A_{plane}$ = 0.013 kg. The entire first production layer mass of $M_{layer} = n_{plane}\, M_{plane}$ = 13 kg will press down upon the perimeter of the lowest fabrication plane with a force of $F_{layerMax} = M_{layer}\, g$ ~ 130 N (g = 9.81 m/sec^2), exceeding its buckling strength by more than 3000-fold.

Note that the weight of the fabrication plane produces a uniform normal gravitational pressure loading of $\Delta P_{plate} = M_{plane}\, g / A_{plane}$ = 0.638 N/m^2 across the surface of the 1.255 micron fabrication machinery plate within each 100 micron thick fabrication plane. Each foundation block of area A_{block} = 20,000 nm^2 for a single NMW-3 module comprising the fabrication machinery plate is supported by 4 support columns of dimensions 5 nm x 5 nm and length 200 nm which each have a buckling strength of $F_{buckle} \sim 1.3 \times 10^{-8}$ N, hence 4 such columns can support a normal pressure of $P_{buckle} = 4\, F_{buckle} / A_{block} = 2.6 \times 10^6$ N/m^2 (~26 atm), which exceeds the gravitational pressure loading from a single fabrication plane (ΔP_{plate}) by $>10^6$ and from all 1000 fabrication planes by $>10^3$. Hence the 1.255 micron thick fabrication machinery plate would be strong enough to support the weight of all the machinery and coolant fluid above it even under 1000-g vertical accelerations, as would the catacombs – catacomb support columns are 1055 nm long but each module includes a floor-to-ceiling support wall with a 5 nm x 46 nm footprint (Section 3.11.2.6), increasing effective support radius by ~2.30-fold while length increases ~5.275-fold, hence buckling strength scales as $\sim(2.30)^4/(5.275)^2 \sim 1$ so the overall catacomb support structure can also withstand ~26 atm of overpressure.

The fabrication machinery plate can also withstand the Poiseuille pressure loading due to the pumping of liquid ethylene through the cooling channel, but the tolerances are very close in the present design. Using the Hagen-Poiseuille equation for laminar pipe flow, adequate coolant circulation requires an estimated driving pressure of $\Delta P_{fluid} = 8\, \eta_{coolant}\, L_{channel}\, \Delta V_{channel} / \pi R_h^4 \sim 2.4 \times 10^6$ N/m^2 (~25 atm), where $\eta_{coolant} \sim 5.82 \times 10^{-4}$ kg/m-sec (absolute viscosity of liquid ethylene at 109 K),[1241] the volume flow rate through a rectangular channel of length $L_{channel}$ = 40

[1240] B.A. Younglove, "Thermophysical Properties of Fluids. 1. Argon, Ethylene, Parahydrogen, Nitrogen, Nitrogen Trifluoride, and Oxygen," J. Phys. Chem. Ref. Data 11(1982):1-368; http://www.nist.gov/srd/PDFfiles/jpcrdS1Vol11.pdf.

[1241] P.M. Holland, B.E. Eaton, H.J.M. Hanley, "A Correlation of the Viscosity and Thermal Conductivity Data of Gaseous and Liquid Ethylene," J. Phys. Chem. Ref. Data 12(1983):917-932; http://www.nist.gov/srd/PDFfiles/jpcrd235.pdf.

cm is $\Delta V_{channel} = v_{coolant} A_{channel} \sim 4 \times 10^{-7}$ m^3/sec for $v_{coolant} \sim 11$ m/sec where the channel is of height $h_{channel} = 98.745$ microns and width $w_{channel} = 0.4$ mm between the 1250 adjacent stovepipe rows along the 50 cm FGN dimension ($A_{channel} = h_{channel}\ w_{channel} = 4 \times 10^{-8}$ m^2), and the hydraulic radius R_h for wide rectangular channels where $h_{channel} << w_{channel}$ is typically approximated by the flow depth,[1242] i.e., $R_h \sim h_{channel} = 98.745$ microns. (Note that the value of ΔP_{fluid} is extremely sensitive to the choice of hydraulic radius ($\sim R_h^{-4}$), slight changes in which could necessitate significant changes in overall system design.)

Ignoring the minor support provided by the stovepipes and the 50 nm thick wiring network, if each fabrication plane was mechanically supported only at the perimeter, then random thermal vibrations would cause the center of the plane to flex and the force of gravity would cause the center of the plane to sag. The bending stiffness of an edge-clamped square plate of thickness h_{plate} and edge length L_{plate} is $k_{bending} = E_{plate}\ h_{plate}^3 / (12\ L_{plate}^2\ (1 - k_{pois}^2))$ and so the positional uncertainty[1243] of the plate surface due to thermal noise is $\Delta x_{bending} \sim (k_B T / k_{bending})^{1/2}$ (Section 3.4.1.2), and the maximum out-of-plane deflection at the center of a rectangular plate that is clamped on all four sides and loaded by uniform normal pressure ΔP_{plate} is $\delta_{plate} = k_{plate}\ (\Delta P_{plate}\ L_{plate}^4 / E_{plate}\ h_{plate}^3)$, where k_{plate} is a constant of order ~0.1 (Section 3.8.1.2). Taking $E_{plate} = 1.05 \times 10^{12}$ N/m^2 for diamond, $L_{plate} = 50$ cm, Poisson's ratio $k_{pois} \sim 0.1$ for diamond, Boltzmann's constant $k_B = 1.381 \times 10^{-23}$ J/K, T = 109 K, $\Delta P_{plate} = M_{plane}\ g / A_{plane} = 0.638$ N/m^2, and $h_{plate} \sim 50$ nm – a compromise estimate for an equivalent solid plate that can be used to represent the 1255 nm thick fabrication machinery plate which contains a 30 nm total thickness of three 10 nm solid diamondoid plates separated by vertical diamondoid stiffening columns) – then $k_{bending} \sim 4.42 \times 10^{-11}$ N/m, $\Delta x_{bending} \sim 6$ microns and $\delta_{plate} >> 10$ microns at the center of the fabrication plane at T = 109 K.

As a result, perimeter-only support will not suffice. The design must be mechanically strengthened by adding an array of stiffener blocks that are attached to the topside surface of the ceiling block of the NMW-3 modules in one fabrication plane and extend across the 98.745 micron cooling channel to attach to the underside surface of the catacomb foundation blocks of the next fabrication plane. If there are n_{cblock} stiffener blocks per fabrication plane and each block is a rectangular prism measuring $L_{cblock} = 98.745$ microns in length with a square cross-section of edge length w_{cblock}, then a basic scaling analysis reveals that $n_{cblock} \sim w_{cblock}^{-4}$, the total volume of all n_{cblock} stiffener blocks $\sim w_{cblock}^{-2}$, and the channel-occluding surface area (in the direction of coolant flow) of all n_{cblock} stiffener blocks $\sim w_{cblock}^{-3}$, which argues for using the smallest possible number of larger blocks. However, the need to evenly distribute the stiffening support across the entire plane to prevent flex and sag argues for using the largest possible number of smaller blocks.

An acceptable design tradeoff may be calculated as follows. If we take as a provisional performance specification that the relative displacement of any two adjacent NMW-3 modules in

---

[1242] Manning Formula, Wikipedia page, accessed February 2008; http://en.wikipedia.org/wiki/Manning_formula.

[1243] K. Eric Drexler, Nanosystems: Molecular Machinery, Manufacturing, and Computation, John Wiley & Sons, New York, 1992; http://www.zyvex.com/nanotech/nanosystems.html.

a fabrication machinery plate due to plate flexure shall not exceed 10% of a single C-C bondlength, or (10%)(1.54 Å) ~ 1.54 x 10^{-11} m, then the maximum allowable flexure along 2 x 10^6 rows along the 40 cm dimension of the FGN is δ_{max} ~ (2 x 10^6)(1.54 x 10^{-11} m) ~ 30 microns. Setting $\delta_{plate} = \delta_{max}$ yields a maximum block separation distance (~plate segment dimension) of $L_{plate} = L_{cplate}$ ~ 0.4 mm, which now yields $k_{bending}$ ~ 6.91 x 10^{-5} N/m and a very modest $\Delta x_{bending}$ ~ 5 nm at the center of each plate segment of the fabrication plane at T = 109 K. Thus we require $n_{cblock} = A_{plane} / L_{cplate}^2$ = 1.25 x 10^6 stiffener blocks. Conservatively taking $n_{cblock} F_{buckle} \sim \pi E_{cyl} n_{cblock} w_{cblock}^4 / 4 L_{cblock}^2$ (for square stiffener blocks) ≥ 100 $F_{layerMax}$ = 13,000 N for an FGN that is designed to sustain 100-g vertical accelerations without damage, then $w_{cblock} \geq 3.35$ microns; we choose w_{cblock} ~ 4 microns.

This scaling exercise yields a design in which each fabrication plane is separated from the next by a cooling channel which is spanned by 1.25 million identical diamondoid 4 micron x 4 micron x 98.745 micron stiffener blocks arranged in a regular grid pattern of 1250 rows (across the FGN 50 cm dimension) with 1000 stiffener blocks per row (of length 40 cm), and ~0.4 mm separating the centers of neighboring stiffener blocks (Figure X-7). Thus a single such row contains 1000 stiffener blocks in a 4-micron wide swath that in the second production layer (Section 3.11.3) aligns with 1 micron^2 MAM foundation blocks in a swath that is 4 MAM modules wide and 400,000 MAM modules long. (To simplify this design exercise, we ignore that 4000 of these modules are covered by stiffener blocks and are thus inaccessible to stovepipe entry.) As noted in Section 3.11.2.8 above, stovepipes arriving in the second production layer are arranged in tight 2x2 groups of 4 pipes called "fourpacks", with each fourpack positioned at the corner junction of four 1 micron^2 MAM foundation blocks in the lowest plane of the second production layer (Figure X-6). Thus the 800,000 stovepipes in each row are collected into fours at 200,000 corner junctions of 4 MAMs, which allows each MAM to carry away the entire output of one stovepipe into a separate linear chain of adjacent MAMs.

Since each row of stiffener blocks is aligned with the coolant flow, the rows occlude just (1250) (4 microns) / (50 cm) ~ 1% of the cross-sectional area of the flow. This is unlikely to cause turbulence or to significantly impede coolant flow because the Reynolds number for fluid flow at 109 K for liquid ethylene of absolute viscosity $\eta_{coolant}$ ~ 5.82 x 10^{-4} kg/m-sec,[1244] through an $h_{coolant}$ = 98.745 micron channel at $v_{coolant}$ ~ 11 m/sec is $N_R = \rho_{ethylene} v_{coolant} h_{coolant} / \eta_{coolant}$ ~ 1210; experiments by Reynolds[1245] showed that transition from laminar to turbulent flow typically occurs between N_R ~ 2000-13,000, so coolant fluid flow through the cooling channel of each fabrication plane is expected to remain laminar or very nearly so.

[1244] P.M. Holland, B.E. Eaton, H.J.M. Hanley, "A Correlation of the Viscosity and Thermal Conductivity Data of Gaseous and Liquid Ethylene," J. Phys. Chem. Ref. Data 12(1983):917-932; http://www.nist.gov/srd/PDFfiles/jpcrd235.pdf.

[1245] O. Reynolds, "An experimental investigation of the circumstances which determine whether the motion of water shall be direct or sinuous, and of the law of resistance in parallel channels," Phil. Trans. Roy. Soc. 174(1883):935-982.

Figure X-7. Schematic illustration of the layout of the array of stiffener blocks crossing the cooling channel between two fabrication planes in the first production layer of the FGN (not to scale).

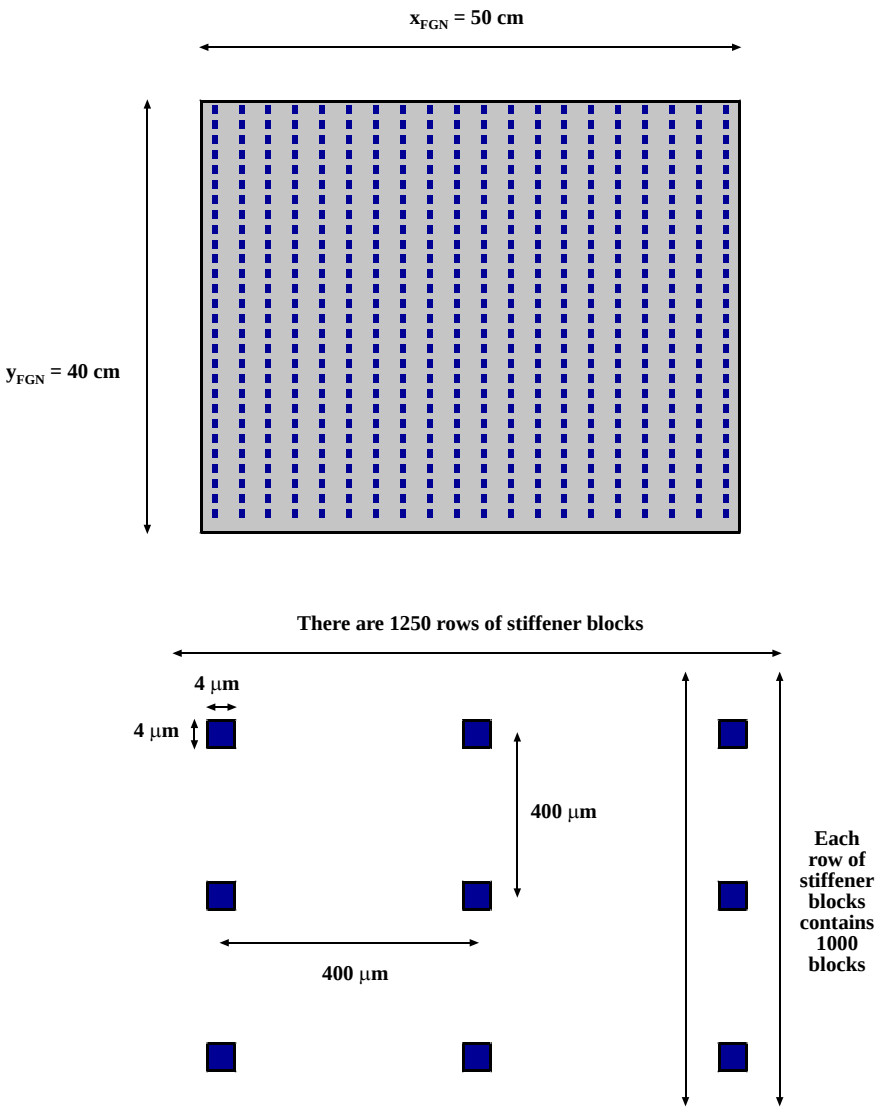

The array of stiffener blocks between adjacent fabrication planes also provides resistance to the Poiseuille pressure loading (due to the pumping of liquid ethylene through the cooling channel) that tends to push the adjacent fabrication planes apart. Pulled in tension, the stiffener blocks in the array can withstand channel pressurization up to $P_{stiffener} \sim (n_{cblock}\ \sigma_w\ A_{stiffener}) / (2\ x_{FGN}\ y_{FGN}) = 2.5 \times 10^6$ N/m^2 (~25 atm) > ΔP_{fluid} (~24 atm estimated coolant driving pressure; see above), taking $n_{cblock} = 1.25 \times 10^6$ stiffener blocks, $\sigma_w = 5 \times 10^{10}$ N/m^2 (working tensile strength for diamond), $A_{stiffener}$ = 16 micron^2 (cross-sectional area of a 4 micron x 4 micron stiffener block), and FGN plate dimensions x_{FGN} = 50 cm and y_{FGN} = 40 cm.

Note that each stovepipe may be regarded as a vacuum-filled square-cylindrical pressure vessel that could be crushed by the external fluid pressure where it traverses the cooling channel.

Stovepipe maximum bursting pressure $P_{stoveburst} = t_{wall}\ \sigma_w / R_{stove} = 6.7 \times 10^9$ N/m^2 (~66,000 atm) >> ΔP_{fluid} (~24 atm estimated coolant driving pressure; see above), taking $t_{wall} = 10$ nm, $\sigma_w \sim 5 \times 10^{10}$ N/m^2 for diamond, and circular-equivalent stovepipe radius $R_{stove} \sim (x_{stove} + y_{stove})/4 = 75$ nm. The four interior walls provide more internal support that additionally resists tank crushing. Since flow is laminar, fluid pressure should be uniform throughout the cooling channel with no pockets of large differential pressures that could give rise to significant bowing, bending, or twisting forces on the stovepipes.

3.11.2.10 Maintaining UHV Inside the FGN During Operation

Even though the FGN will be assembled inside a large vacuum room (Section 3.11.7) (but might subsequently be operated outside of that room), it will be difficult to passively maintain UHV conditions inside the machinery planes of the FGN given the likelihood of slow helium and hydrogen diffusion through the FGN walls over time. Thus it will be necessary to include vacuum bibs that allow external cryopumps to continuously pump down the internal volume of each open machinery plane in each of the 1000 fabrication planes and each of the 4 assembling planes. These vacuum bibs are assumed to be similar in size, number and position to the fluid bibs attached to each catacomb (Section 3.11.2.6) underlying each fabrication plane.

3.11.2.11 Scaling Analysis Summary with Atom Count

Allocating ~176 C atoms/nm^3 for diamondoid lattice and ~31 H atoms per nm^2 to passivate diamondoid surface gives the scaling results for the first production layer as shown in Table X-1. The first production layer (comprised of 1000 fabrication planes and ~3.800 x 10^{24} atoms (93.2% carbons)) is 10 cm thick with a dry mass of ~70.90 grams. If each of 2 x 10^6 rows of NMW-3 modules in each of 1000 fabrication planes receives a separate sequence of 120 x 10^6 control pulses per second (120 MHz operating frequency) on each of ~100 control lines, then operating the first production layer requires a total control data flow of ~2.4 x 10^{19} bits/sec. The first production layer uses 1000 fabrication planes each containing 10^{13} NMW-3 modules that can process ~10^4 atoms/sec to achieve a total processing rate of ~10^{20} atoms/sec or ~10^{13} parts/sec of ~10^5 nm^3 "typical smallest" parts, yielding a mass replication time of ~10.6 hours for the first production layer.

Table X-1. Estimated Atom Count* for Diamondoid Structure of Fabrication Planes Containing 10^{13} NMW-3 Modules Comprising the First Production Layer of the First-Generation Nanofactory (FGN)

FGN Nanofactory Subsystem	Total Solid Volume (m^3)	Total Passiv. Area (m^2)	# of C Atoms	# of H Atoms	Total # of Atoms*
Catacombs			1.27 x 10^{21}	1.07 x 10^{20}	1.377 x 10^{21}
Foundation Blocks	2 x 10^{-9}	4.6 x 10^{-1}			
Support Columns	1.05 x 10^{-9}	2.115 x10^{-1}			
H_2 Channel Walls	4.1763 x 10^{-9}	2.76638			
Perimeter Wall	1.8 x 10^{-15}	3.6 x 10^{-7}			
2 Hose Bibs	3.2 x 10^{-15}	3.2 x 10^{-8}			

NMW-3			1.85×10^{21}	1.50×10^{20}	1.998×10^{21}
Foundation Blocks	2×10^{-9}	4×10^{-1}			
Wiring Bundle†	2.466×10^{-9}	0			
Connector Blocks	4×10^{-12}	1.602×10^{-2}			
Tee Connector Wires	2×10^{-10}	0			
NFW-3 Manipulators	1.45×10^{-9}	1.6383			
NFW-3 Tools/Toolrack	5.28×10^{-11}	6.2×10^{-2}			
NFW-3 Transfer Units	6.25×10^{-11}	5×10^{-3}			
NAW-2 Manipulators	2.19×10^{-9}	2.1463			
Support Columns	1×10^{-10}	1.6×10^{-1}			
Ceiling Blocks	2×10^{-9}	4×10^{-1}			
Perimeter Wall	3.6×10^{-15}	7.2×10^{-7}			
Stovepipes			6.03×10^{19}	2.98×10^{18}	6.328×10^{19}
Shaft Walls	3×10^{-10}	6×10^{-2}			
Wiring Bundle	2.023×10^{-12}	0			
Connector Blocks	1×10^{-13}	4.01×10^{-4}			
Crane Manipulators	4.025×10^{-11}	3.58×10^{-2}			
Cooling Channel			3.43×10^{20}	6.17×10^{16}	3.431×10^{20}
Stiffener Blocks	1.95×10^{-9}	1.99×10^{-3}			
UHV Maintenance					
2 Vacuum Bibs	3.2×10^{-15}	3.2×10^{-8}	5.63×10^{14}	9.92×10^{11}	5.640×10^{14}
Unallocated Structure	1×10^{-10}	1×10^{-2}	1.76×10^{19}	3.10×10^{17}	1.791×10^{19}
TOTALS, 1 Plane	2.015×10^{-8}	8.374	3.541×10^{21}	2.604×10^{20}	3.800×10^{21}
TOTALS, 1000 Planes	2.015×10^{-5}	8.374×10^{3}	3.541×10^{24}	2.604×10^{23}	3.800×10^{24}

* There are also ~10 Ge atoms per NMW-3 module, or ~10^{14} Ge atoms per fabrication plane.
† Reported volume is the volume equivalent to solid diamond for number of atoms in wiring, assuming 176 atoms/nm^3, which should be a generous estimate.

3.11.3 Description of the Second Production Layer and FGN

Four functional assembling planes of manipulator arrays plus the product collection system comprise the second production layer of the FGN (Figure X-8). The first assembling plane is the Inspection Plane (Section 3.11.3.1) – an MAA of the type already demonstrated in Phase IX, using MAMs able to acquire arriving parts from the stovepipes and to inspect them, ejecting defective parts. The second is the Routing Plane (Section 3.11.3.2), which re-routes parts and fills holes left in the parts flow pattern by the ejection of defective parts. The third is the Assembly Plane (Section 3.11.3.3), which assembles the parts into finished atomically precise microscale product objects. The fourth is the Export Plane (Section 3.11.3.4), which acquires finished product objects and transfers them to bulk containers which can be removed from the FGN for use by final consumers. The Section concludes with a scaling analysis and atom count for the FGN (Section 3.11.3.5), followed by a summary of error rates and reliability issues in FGN manufacture and operation (Section 3.11.3.6).

Figure X-8. Schematic illustration of the layout of the four assembling planes comprising the second production layer of the FGN (not to scale)

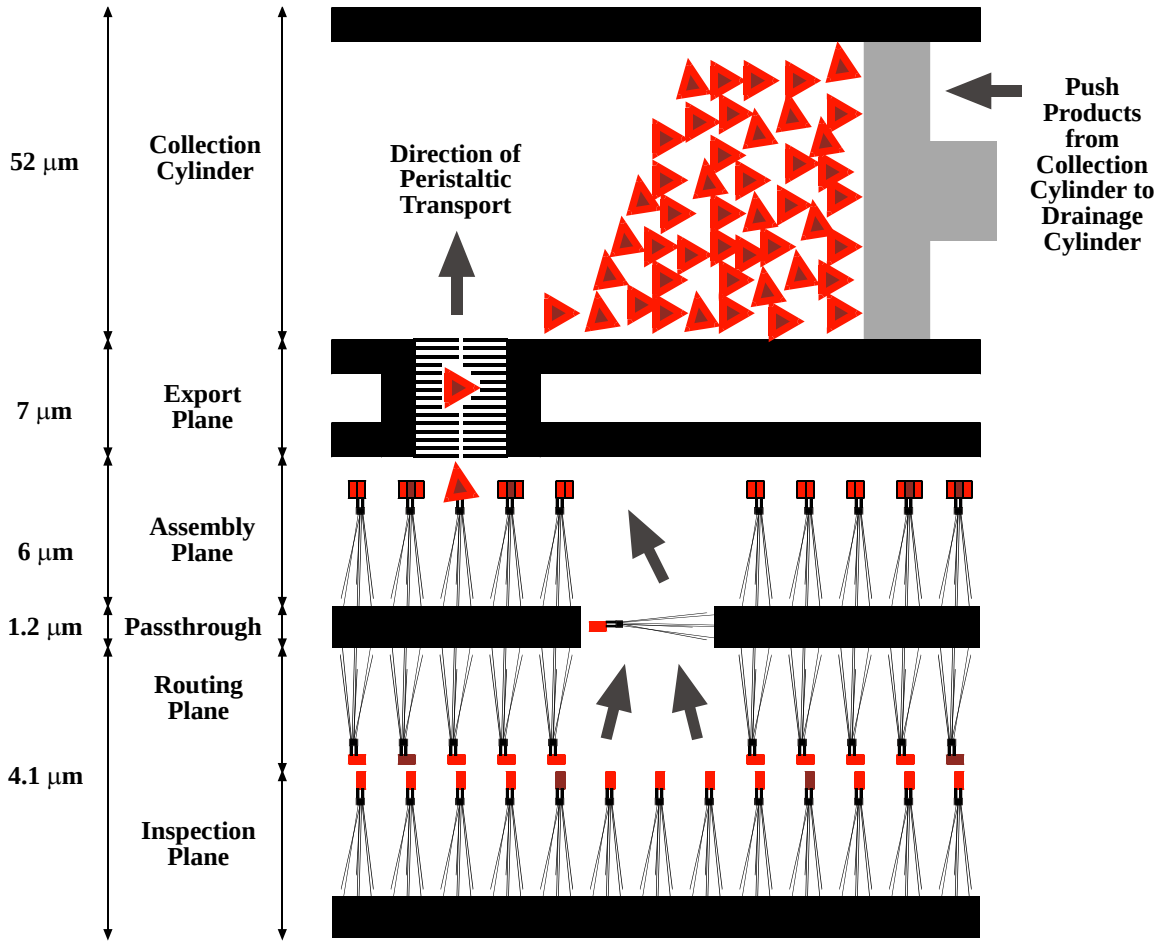

3.11.3.1 Inspection Plane

The Inspection Plane acquires parts arriving through the stovepipes from the fabrication planes in the first production layer (Figure X-6). This plane inspects the arriving parts, sorts them into two categories – accept or reject – then passes the parts along to the overhead Routing Plane (Section 3.11.3.2) for final disposition. Accepted and rejected parts are passed to the Routing Plane along different paths, so parts are already presorted into these two categories upon arriving at the Routing Plane. As a result, the Inspection Plane need not generate "accept" or "reject" signals requiring computational coordination between the Inspection Plane and the Routing Plane manipulator arrays.

The ~0.2 m^2 Inspection Plane is populated by ~2 x 10^{11} MAM manipulators that are essentially identical to the MAMs as described in Section 3.10.1.1. Each Inspection Plane MAM occupies a square 1 $micron^2$ site (Section 3.10.1.2) and operates at 120 MHz (Section 3.10.8). Assuming a continuous 100% duty cycle for 2 x 10^{11} MAM and a worst-case continuous power draw of (8 motors x 2000 pW/motor) ~ 16 nW per MAM at a 120 MHz pulse control frequency (Section 3.10.1.1), the maximum power draw for the entire Inspection Plane is ~3200 W.

There are a few minor changes to the existing MAM design as follows. For all Inspection Plane MAMs, power/control signals are routed through a binary tree nanowire bundle below the MAM foundation blocks in the same manner as described in Section 3.11.2.4 for NMW-3 foundation blocks in a fabrication plane. Because the MAMs draw more power than the NMW-3 modules, each MAM motor is considered for scaling purposes to be supplied by the equivalent of 20 metallic 1.6-nm DWCNT nanotube wires (Section 3.11.2.4). Each set of 20 power/control wires must collectively provide ~2 nW of power to one motor for each of 400,000 MAMs when operated at 120 MHz, drawing a total of 8 x 10^{-4} W or ~40 x 10^{-6} amps/wire at 1 volt – consistent with experimental observations[1246] of individual 10-50 nm long single-walled "metallic" carbon nanotubes conducting 25-1000 x 10^{-6} amp/wire electrical currents before failing. Since each MAM needs 15 control lines (Section 3.10.1.1) and each control line is assumed for scaling purposes to demand 20 wires each 1.6 nm in diameter, the MAM requires a 300-wire bundle which is therefore three times thicker in solid volume than the 100-wire bundle required for the NMW-3 rows and thus measures ~132 nm thick traversing the 40 cm FGN dimension underneath the MAM foundation blocks for each row of 400,000 MAMs which are being operated in unison.

MAM foundation blocks are tightly adjoined to their neighbors to make a solid plate, as described for NMW-3 foundation blocks in Section 3.11.2.3. A support frame of four 50 nm x 50 nm x 3 micron diamondoid columns extends from each of the four corners of the 1 micron^2 MAM foundation block in the Inspection Plane, rising up 3 microns to meet the opposing surface of a 1 micron^2 MAM foundation block of the Routing Plane. A perimeter wall 100 nm thick and 3 microns tall seals the Inspection and Routing Planes against vacuum loss.

Let us now visualize the architecture of the Inspection Plane from the top down (Figure X-9). To start with, the Inspection Plane is organized as an array of 500 million "inspection strips". Each inspection strip consists of a linear array of 400 MAMs measuring 1 micron x 400 microns oriented parallel to the 50 cm FGN dimension. Thus there are 400,000 inspection strips along the 40 cm FGN dimension and 1250 inspection strips along the 50 cm FGN dimension, with each strip spanning the 0.4 mm distance between the 1250 stovepipe/stiffener-block rows in the fabrication planes as previously described in Section 3.11.2.9. Each inspection strip receives parts from two stovepipes, one at either end.

Figure X-9. Schematic illustration of the layout of 10 Inspection Strips consisting, on the left side, one row of 200 MAMs receiving parts from a stovepipe in MAM #1 at far left and inspected parts leaving the Inspection Plane at Inspection MAM #199 for good parts or Reject MAM #200 for failed parts at the rightmost end of the row; and a second row of 200 MAMs on the right side that is the mirror image of the row of MAMs on the left. Heavy arrows show parts flow along each row of MAMs.

[1246] Ali Javey, Pengfei Qi, Qian Wang, Hongjie Dai, "Ten- to 50-nm-long quasi-ballistic carbon nanotube devices obtained without complex lithography," PNAS 101(14 September 2004):13408-13410; http://www.pnas.org/cgi/content/abstract/101/37/13408. Hongjie Dai, Eric W. Wong, Charles M. Lieber, "Probing Electrical Transport in Nanomaterials: Conductivity of Individual Carbon Nanotubes," Science 272(26 April 1996):523-526; Stefan Frank, Philippe Poncharal, Z.L. Wang, Walt A. de Heer, "Carbon Nanotube Quantum Resistors," Science 280(12 June 1998):1744-1746.

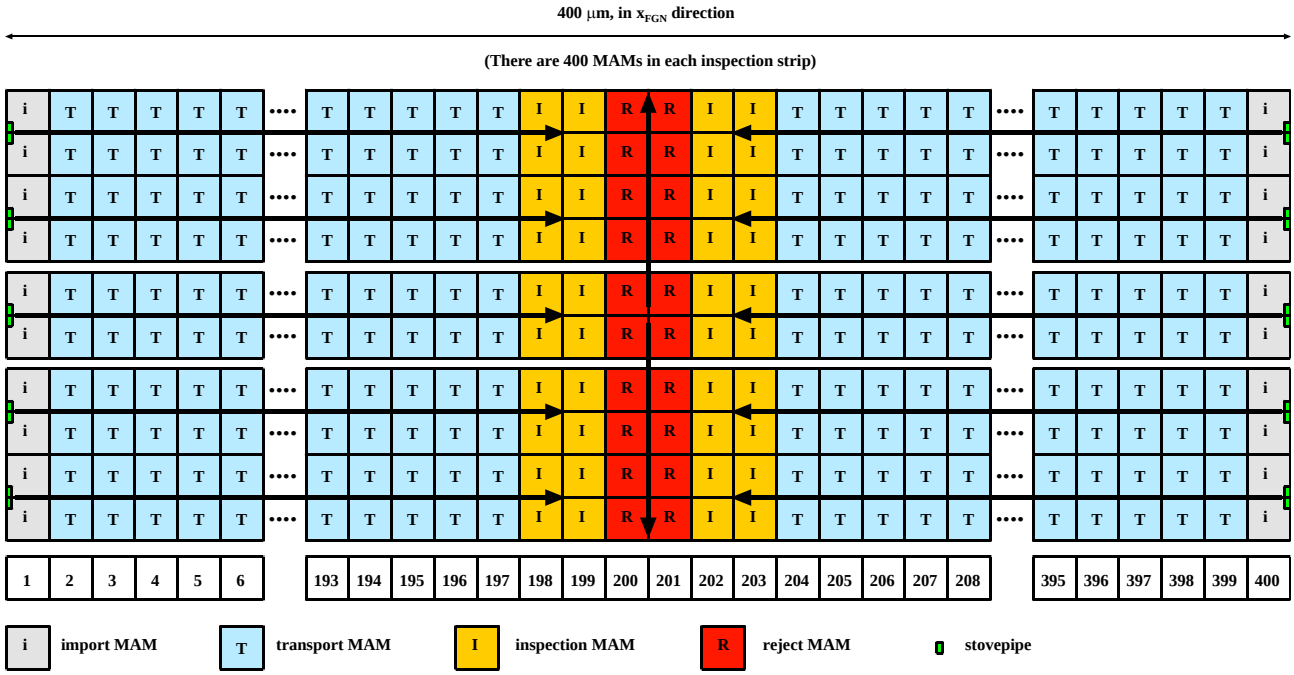

Each inspection strip consists of 400 Inspection Plane MAM modules numbered #1 through #400 from left to right. Module #1 is an "import MAM" containing a penetrating stovepipe through which parts enter the inspection strip at the 10^4 part/sec rate. Modules #2-#197 are high-speed "transport MAMs" that rapidly transport parts left-to-right from module #1 to module #198. Modules #198 and #199 are "inspection MAMs" that perform the parts inspection function. Module #200 is a "reject MAM" that is used to convey rejected parts between neighboring rejection strips. Similarly, module #400 is an import MAM, modules #399-#204 are high-speed transport MAMs to rapidly move parts from right to left, modules #203 and #202 are inspection MAMs and module #201 is a reject MAM. The four types of MAM are described below.

(1) **Import MAMs.** The function of an import MAM is to acquire parts from a stovepipe that penetrates through the MAM foundation block, and then to insert those parts into the inspection processing system. Since the footprint of the 7 struts comprising a MAM is only ~0.68 micron wide at the MAM base to operate correctly (Section 3.10.1.1), there is sufficient room to accommodate the penetration of a 100 nm x 200 nm stovepipe through one corner of the MAM foundation block. The crane arm manipulator at the uppermost terminus of each stovepipe that penetrates a MAM foundation block can hand parts directly to the MAM, which can in turn pass the stream of parts to a row of transport MAMs for inspection purposes (see below). Thus each import MAM gets direct delivery from one stovepipe, allowing each import MAM to convey away the entire 10^4 part/sec output of one stovepipe. The maximum MAM tip travel speed is ~2.6 cm/sec at 120 MHz (Section 3.10.8), so if less than one-fourth (<23%) of each round-trip cycle time is consumed for the baton-handoff motion of parts between stovepipe crane arm and import MAM, then a net forward speed of ~2 cm/sec in the parts flow can be continuously maintained. With MAMs spaced 1 micron apart, each ±0.5 micron round-trip import MAM handoff motion requires 2 microns of MAM tip travel, hence 10^4 handoff motions/sec can be executed, exactly matching the 10^4 parts/sec stovepipe output rate.

(2) **Transport MAMs.** The function of a transport MAM is to acquire parts from an import MAM and to pass those parts at high speed to the end of a line of transport MAMs using reliable hand-to-hand baton-passing motions. Transport MAMs don't need much small-increment repeatability because they are basically just two-state manipulators – they're either grasping a part on the receipt side or releasing a part on the delivery side, and if necessary can use fixed stops to help ensure reliable seating in either terminal position. The exact path taken from the receipt side to the delivery side of the ~1 micron armswing motion is of no concern as long as the path avoids all possible obstacles and cannot cause other mechanical pathologies to occur. Hence we can assume that a transport MAM can be "re-geared" to allow ~2 micron round trips with tenfold larger ~2 nm step increments at 120 MHz with a pulse budget of ~1000 pulses per round trip. With this alteration, transport MAMs can convey parts at a net forward speed of ~20 cm/sec along the line, ten times faster than before. A transport MAM can thus be handed a part up to ~100 nm in size from an import MAM (or from an adjacent transport MAM) and can pass it directly to an adjacent transport MAM (or to an inspection MAM at the end of the line) at the accelerated rate of ~10^5 round trips/sec. To maintain a constant 10^4 part/sec transport rate along the inspection strip, parts must transit the 196 modules separating the import MAM and the first inspection MAM in a net transit time of t_M = (196 modules) x (10^{-4} sec/part-module) = 0.0196 sec/part. But the high-speed transport MAMs allow parts to transit these 196 modules in just t_{TM} = (196 modules) x (10^{-5} sec/part-module) = 0.00196 sec/part. This allows transported parts to pause at the inspection MAMs for an inspection time of $t_{IN} = (t_M - t_{TM})$ = 0.01764 sec/part.

(3) **Inspection MAMs.** The function of an inspection MAM is to acquire parts from a line of transport MAMs and to perform a physical inspection on those parts for quality control purposes, using end-effectors optimized for performing inspection tasks. Since each part travels a pre-planned and fully deterministic pathway from the NMW-3 module where it was manufactured, then through a stovepipe, finally arriving at the MAM that is now inspecting it, the computer that is controlling the actions of the inspecting MAM will know exactly which part is being inspected. At minimum, each part can be checked to ensure that it has the correct geometric dimensions, shape, and topology for that type of part, and no loose, dangling, or protruding elements indicating faulty manufacture. To accomplish this testing, the part may be grasped by one inspection MAM and presented in a particular orientation to a neighboring inspection MAM, which can touch and explore the contours of its surface, producing a stream of force sensor readings that can be compared to the readings expected for that type of part when manipulated in that manner. Any part failing the shape tests can be removed from the parts stream as a reject. If time permits, some limited functionality testing might also be possible, as where an external gear housing is held by one inspection MAM and the central shaft is held by the other inspection MAM, and the resistance to rotation is tested by measuring the force required to turn the shaft through a partial rotation. Comprehensive parts testing will probably not be possible in the limited transit time available, but the testing regimen should suffice to reduce the fraction of bad parts incorporated into final product by many orders of magnitude. Like the original MAM (Section 3.10.1.1), each inspection MAM can execute $n_{motion} \sim 10^4$ round trip motions/sec of ~2.4 microns/motion with 0.2 nm step increments at 120 MHz with a pulse budget of ~12,000 pulses per round trip. If the inspection time available to the inspection MAMs is $t_{IN} = (t_M - t_{TM})$ = 0.01764 sec/part (see above), then within the available inspection time the inspection MAMs can perform ($n_{motion}\ t_{IN}$) ~ 176 motions/part which should suffice to complete the necessary inspection motions. Once the inspection is completed, the part is either handed up to the Routing Plane (Section 3.11.3.2) or over to the reject MAM by the second inspection MAM of the pair.

(4) **Reject MAMs.** The function of a reject MAM is to acquire parts that have been judged defective from an inspection MAM and to pass those parts at high speed to adjacent reject

MAMs in neighboring inspection strips. There are two reject lines in every stovepipe/stiffener-block row and there are 1250 stovepipe/stiffener-block rows in the FGN, so there are 2500 reject lines crossing the Inspection Plane. These 2500 lines of rejected parts are conveyed to 5000 end points at the perimeter of the Inspection Plane, since each reject line breaks into two streams, one transporting parts to the left, the other transporting parts to the right. Rejected parts are then passed up to the Routing Plane (Section 3.11.3.2), there to be placed into 2500 passthroughs which finally convey the defective parts into a single macroscale reject bin. Assuming a ~10^{-7} reject rate (the same as the operating error rate per replication cycle for the NMW-2; Section 3.8.1.3), each stovepipe will place 0.001 parts/sec into each reject line within each inspection strip. Hence the 400,000 inspection strips that are fed by 800,000 stovepipes within a single stovepipe/stiffener-block row will produce 800 reject parts/sec that will be carried off along 2 separate reject lines each having a flow rate of 400 reject parts/sec, which break into 4 separate reject streams each comprising 200,000 reject MAMs and having a typical flow rate of 200 reject parts/sec. Reject MAMs are identical to transport MAMs except that they move twice as fast. Thus in each reject stream, reject MAMs convey parts at a ~40 cm/sec speed (~2 x 10^5 parts/sec rate). Defective parts removal from the Inspection Plane occurs as follows. In the first cycle of reject stream operation, all 200,000 reject MAMs feeding a single reject stream first perform a blind grasping motion in the direction of their nearest inspection MAM. If the inspection MAM transferred no defective part, the reject MAM returns empty; if the inspection MAM did transfer a reject part, then the reject MAM returns grasping a defective part. In the second cycle of reject stream operation, all 200,000 reject MAMs perform 200,000 cycles of hand-over-hand part-passing motions, flushing the entire stream of any reject parts it may contain in ~1 second. (At a 10^{-7} defect rate each flushing cycle will dispose of ~200 defective parts, but the system could accommodate up to 200,000 defective parts per flush cycle, a ~1000-fold higher defect rate.) The FGN has 5000 disposal streams each carrying 200 defect parts/sec, yielding ~10^6 defect parts/sec for the entire FGN which is ~1 mm^3 of defective parts for every ~116 days (~10^7 sec) of FGN operation, assuming the rejects are "typical smallest" ~10^5 nm^3 parts.

The inspection MAMs present a special design challenge because they must process and act upon sensory information gathered during the inspection, and because their actions will serve to remove parts randomly from the flow, ruining the fully deterministic character of that flow. If all parts simultaneously presented to a given line of 400,000 pairs of inspection MAMs associated with a single stovepipe/stiffener-block row (among the 1250 such rows in the Inspection Plane) are the same known part type, then the entire line of inspection MAMs can be operated in unison and can receive a preprogrammed series of inspection motions to execute on the same known kind of part. Once the inspection is complete, some parts will have passed and others will have failed. The inspection MAMs can be designed so that the failure of any inspection test will trip a two-position mechanical latch (essentially a counter that registers 0 for pass, 1 for fail). The two positions of the latch can move mechanical relay elements on the base of the inspection MAM that can actualize any of several possible control strategies, such as: (A) the inspection MAM executes a handoff motion – the latch state flips the signals going to the MAM motors so that the MAM executes a handoff motion to the Routing Plane for latch state 0 or to the reject MAM for latch state 1 – then executes a command to reset the latch to state 0 no matter what state it is currently in; or (B) the inspection MAM executes a handoff motion to the Routing Plane (which is aborted for latch state 1), then a handoff motion to the reject MAM (which is aborted for latch state 0), then resets the latch to state 0. By this means we could avoid requiring the external computer to receive or to send any signals to an individual inspection MAM.

However, detection of a defective part triggers its removal from the deterministic flow pattern. If this event is not reported to the external control computer, the resulting hole in the pattern will be passed forward, eventually reaching the Assembly Plane and causing either a misassembly (if an

assembly manipulator blindly executes an assembly motion with no part in its hand) or a sequencing delay (if the assembly manipulator pauses in executing its planned assembly motion because it has detected no part is present, and waits for a replacement part to arrive in the next cycle, throwing the assembly line out of synchrony).

To allow either external control of sensor-based routing, or Routing Plane compaction of holes in the parts flow pattern with flow pattern updating in the external computer, or both, the two inspection MAMs that perform routing actions in each inspection strip each need at least one outgoing wire to carry the sensor data and one incoming wire to carry a control signal. If a pair of ~1 nm DWCNT low-current wires (Section 3.11.2.4) must be run as "home run" connections to the external control computer from each of 800,000 inspection MAMs that perform parts routing motions from near the centers of the 400,000 inspection strips associated with a single stovepipe/stiffener-block row along the 40 cm dimension of the FGN, and if the wires can connect from either side, then the average such wire runs $(y_{FGN}/2)/2$ ~ 10 cm along the 40 cm dimension of the FGN and up to 0.2 mm on either side of the inspection strip along the 50 cm dimension of the FGN, hence a close-packed plane containing all 800,000 wire pairs would cover an area of A_{wires} ~ (2)(800,000)(10 cm + 0.2 mm)(1 nm) = 1.6 cm^2 which approximately equals the area between two stovepipe/stiffener-block rows or A_{rows} = (0.2 m^2 / 1250) = 1.6 cm^2. This design exercise suggests that running two small-diameter low-current wires to each inspection MAM that performs parts routing motions from the Inspection Plane will require adding a single dense wiring network consisting of ~1 solid sheet of DWCNT wires ~1 nm thick underneath the foundation blocks of the entire 0.2 m^2 Inspection Plane surface. Adding this extra small-wire sheet increases design and signal control complexity but should not significantly increase the total FGN atom count or build time. If each wire in the small-wire sheet carries signal pulses of energy ~1000 k_BT ~ 41 zJ (300 K) at 120 MHz, then each wire draws ~5 pW (~5 x 10^{-12} amp/wire at 1 volt) and the single ~0.2 m^2 sheet of 10^9 DWCNT wires adds a negligible ~0.005 W to the existing 3200 W power requirement for the entire Inspection Plane. The extra wiring sheet and associated snap connectors between foundation blocks can be added to the design for the MAM foundation blocks and can be fabricated at the same time as the MAM foundation blocks.

3.11.3.2 Routing Plane

The Routing Plane acquires inspected parts from the Inspection Plane, alters their positions in the flow pattern if necessary to ensure optimal arrival sequence in the Assembly Plane, then passes them along to the Assembly Plane for further assembly. Defective parts arrive in ~5000 low-number de-patterned streams near the periphery of the Routing Plane and are diverted through the Routing Plane to the reject bin higher up. Nondefective parts that are useful for further assembly arrive in high-number deterministically patterned streams via handoff motions from 2500 lines of 400,000 inspection MAMs (a total of ~10^9 handoff points) in the Inspection Plane below the Routing Plane. The external control computer is informed by the Inspection Plane when individual parts are removed from the flow pattern, allowing it to update the dynamic flow pattern map and then to use the Routing Plane to adjust the positioning of parts in the flow pattern to compensate for gaps and re-establish a flow pattern that is optimal for assembly.

Inspected nondefective parts are passed from 2500 lines of 400,000 inspection MAMs (per line) in the Inspection Plane to 2500 lines of 400,000 transport or routing MAMs (per line) in the Routing Plane. Routing MAMs are identical in size and performance to transport MAMs (Section 3.11.3.1) with two exceptions. First, routing MAMs are four-state manipulators

(backward, forward, left, right), not two-state manipulators. The end-effector of a routing MAMs can grasp a part at one vertex of a square and then release the part upon arrival at one of the other three vertices of the square, where the internal diagonals of the square define the two orthogonal directions of possible parts flow. Second, routing MAMs are individually addressed by the external control computer through a "home run" wire pair connected to each routing MAM. These low-current wires allow the transmission of 2-bit (4-state) words to an individual routing MAM that can command it to execute its powered handoff motions in one of four directions, both on the forward and return strokes of the round-trip handoff motion. The 2-bit input signal can be converted to mechanical action using a small number of electrically actuated relays that re-route the control/power signals flowing to the motors driving each MAM strut. Establishing this control over 4×10^{10} individual routing MAMs requires the addition of a stack of ~40 small-wire sheets to the underside of the Routing Plane foundation blocks. There will be some loss of efficiency due to the need for "home run" wires from sheets higher in the stack to penetrate through sheets lower in the stack to reach the intended individual routing MAM, but a comprehensive design of this wiring pattern is beyond the scope of the present analysis. The stack of small-wire sheets is ~40 nm thick and adds a negligible ~0.2 W to the ~3200 W power requirement for the entire Routing Plane.

The Routing Plane consists of 2×10^{11} MAMs, each occupying 1 micron^2 of Routing Plane surface area and each able to perform part handoff motions at the 10^5 part/sec rate. These MAMs hang down from the ceiling rather than rising up from the floor, and possess end-effectors that are specialized for reliable grasping, transport, and handoff of manufactured parts, not for inspection as with the end-effectors of the inspection MAMs. The Routing Plane is comprised of two subpopulations of manipulators: ~40×10^9 routing MAMs that are individually addressable and ~160×10^9 transport MAMs arranged in short lines that are operated in unison. The exact layout of the two subpopulations of manipulators will depend on the design of the parts flow pattern and the requirements of the Assembly Plane and is beyond the scope of the present analysis, but the overall performance of the Routing Plane can be crudely estimated as follows.

Ignoring removals of a small number of defective parts, there are ~10^{13} parts/sec passing through Routing Plane, with each part moving in some direction across the Plane in a series of 1-micron handoff motions between adjacent MAMs. There are 2×10^{11} MAMs each executing 10^5 part-motions/sec, giving a total Routing Plane handling capacity of 20×10^{15} part motions/sec. Just as in the Inspection Plane we have a line of 200 MAMs separating the stovepipe import point and the inspection MAM export point within each inspection strip, we assume there is a similar arrangement in the Routing Plane in which there are ~200 MAMs between the inspection MAM import point and the "passthrough" (see below) export point. In this case, (200 MAMs)(10^{13} parts/sec) = 2×10^{15} part-motions/sec will be required simply to move all the parts from their import points to their export points without diversion (occupying ~11% of total Routing Plane duty cycle), but this leaves 18×10^{15} part-motions/sec of spare capacity. The subpopulation of ~40×10^9 routing MAMs (occupying another ~20% of total Routing Plane duty cycle) each executing 10^5 part-motions/sec gives a total routing MAM parts handling capacity of 4×10^{15} part motions/sec, which is enough to give every part that is passing through the Routing Plane a displacement of (4×10^{15} part-motions/sec) / (10^{13} parts/sec) = 400 motions, a total displacement of 400 microns or 0.4 mm. This is enough re-routing capacity to displace all 10^{13} parts/sec by the entire 0.4 mm distance between two adjacent 1250 stovepipe/stiffener-block rows (Section 3.11.2.9), in principle allowing all parts to be swapped between adjacent "monoculture" rows.

After the parts flow pattern has been properly adjusted and corrected, nondefective parts are routed to one of ~10^9 "passthroughs" that lead to the Assembly Plane. A passthrough is essentially a short stovepipe, an opening in the Routing Plane that is 1 micron wide, 1 micron

long in the direction of maximum MAM extension, and 1 micron deep (since the separation between the working surfaces of the Routing Plane and the Assembly Plane is ~1 micron). A MAM is mounted on one of the 1 micron^2 faces inside the passthrough hole and receives power/control signals through binary tree nanowire bundles mounted on the backside of the foundation blocks of either the Routing or Assembly Planes, whichever is more convenient. Passthrough MAMs are two-state manipulators identical to transport MAMs (Section 3.11.3.1**)** – they stop either on the Routing side or on the Assembly side of the passthrough hole (with the end-effector either grasping or releasing, respectively, at the end of the motion) and use fixed stops to ensure reliable seating in either terminal position. The exact path taken by the transported part as it moves through the hole is of little concern as long as the path does not impact the side walls of the hole or cause other mechanical pathologies to occur. However, the feed rate into the passthrough must be compatible with what the routing MAMs can deliver and with what the Assembly Plane can accept. Since only 10^{13} parts/sec must be transferred from the Routing Plane via the 10^9 passthroughs to the Assembly Plane, then passthrough MAMs only need be operated at the 10^4 part/sec rate, just 10% of their maximum possible 10^5 parts/sec rate (i.e., the passthroughs need be operated at only ~10% duty cycle). With each of 10^9 passthrough MAMs drawing up to 16 nW of power when operated at 120 MHz (Section 3.10.1.2), the total power draw of the entire passthrough array is just ~16 W.

3.11.3.3 Assembly Plane

The Assembly Plane acquires inspected nondefective parts in a deterministic flow pattern from the Routing Plane, assembles those parts into finished atomically-precise microscale product objects, and then passes the completed product objects to the Export Plane for containerization and transport out of the FGN.

Microscale product objects to be manufactured by the FGN may typically range in size from ~0.5 micron^3 (e.g., for ~1 micron diameter respirocytes)[1247] and 12.1 micron^3 (e.g., for 2-3 micron diameter microbivores)[1248] up to ~69 micron^3 (e.g., for ~4 micron diameter chromallocytes).[1249] For design purposes, the FGN is specified to be able to mass-manufacture atomically precise product objects ranging from 0.5-5 microns in linear dimension and from 0.1-100 micron^3 in displaced volume.

The ~10^9 stovepipes from the first production layer deliver "typical smallest" parts of size ~10^5 nm^3/part at the rate of ~10^{13} parts/sec (Section 3.11.2.11) to the Inspection Plane where all parts

---

[1247] Robert A. Freitas Jr., "Exploratory Design in Medical Nanotechnology: A Mechanical Artificial Red Cell," Artificial Cells, Blood Substitutes, and Immobil. Biotech. 26(1998):411-430; http://www.foresight.org/Nanomedicine/Respirocytes.html.

[1248] Robert A. Freitas Jr., "Microbivores: Artificial Mechanical Phagocytes using Digest and Discharge Protocol," J. Evol. Technol. 14(April 2005):1-52; http://www.jetpress.org/volume14/freitas.html.

[1249] Robert A. Freitas Jr., "The Ideal Gene Delivery Vector: Chromallocytes, Cell Repair Nanorobots for Chromosome Replacement Therapy," J. Evol. Technol. 16(June 2007):1-97; http://jetpress.org/v16/freitas.pdf.

are individually inspected once, then sorted, re-routed and transferred – in an optimal flow pattern designed to enable efficient assembly – through the Routing Plane, finally emerging at the 10^4 part/sec rate from 10^9 passthroughs into the Assembly Plane, again a total flow rate of 10^{13} parts/sec. Hence the Assembly Plane can produce ~0.1 micron^3 (~0.5 micron diameter) product objects each made from ~10^3 "typical smallest" 10^5 nm^3 parts at a ~10^{10} product/sec output rate, or ~100 micron^3 (~5 micron diameter) product objects each made from ~10^6 "typical smallest" 10^5 nm^3 parts at a ~10^7 product/sec output rate.

The ~0.2 m^2 Assembly Plane is populated by ~2 x 10^{11} MAM manipulators that are very similar to the MAMs described in Section 3.11.3.1. Each Assembly Plane MAM occupies a square 1 micron^2 site (Section 3.10.1.2) and operates at 120 MHz (Section 3.10.8). Assuming a continuous 100% duty cycle for 2 x 10^{11} MAM and a worst-case continuous power draw of (8 motors x 2000 pW/motor) ~ 16 nW per MAM at a 120 MHz pulse control frequency (Section 3.10.1.1), the maximum power draw for the entire Assembly Plane is ~3200 W.

As with the Inspection Plane, basic power/control signals for all Assembly Plane MAMs are routed through a binary tree nanowire bundle below the MAM foundation blocks with each MAM motor considered for scaling purposes to be supplied by the equivalent of 20 metallic 1.6-nm DWCNT nanotube wires (Section 3.11.2.4). Each set of 20 power/control wires must collectively provide ~2 nW of power to one motor for each of 400,000 MAMs when operated at 120 MHz, drawing a total of 8 x 10^{-4} W or ~40 x 10^{-6} amps/wire at 1 volt – consistent with experimental observations[1250] of individual 10-50 nm long single-walled "metallic" carbon nanotubes conducting 25-1000 x 10^{-6} amp/wire electrical currents before failing. Since each MAM needs 15 control lines (Section 3.10.1.1) and each control line is assumed for scaling purposes to demand 20 wires each 1.6 nm in diameter, the MAM requires a 300-wire bundle which is therefore three times thicker in solid volume than the 100-wire bundle required for the NMW-3 rows and thus measures ~132 nm thick traversing the 40 cm FGN dimension underneath the MAM foundation blocks for each row of 400,000 MAMs which are being operated in unison. MAM foundation blocks are tightly adjoined to their neighbors to make a solid plate, as described for NMW-3 foundation blocks in Section 3.11.2.3.

Let us now visualize a representative 10:1 convergent assembly architecture (of many possible alternatives that were examined) for the Assembly Plane. Oriented with similar structures below it in the Inspection Plane, the Assembly Plane is organized as an array of 500 million "assembly strips". Each assembly strip (Figure X-10) consists of a linear array measuring 1 micron x 400 microns oriented parallel to the 50 cm FGN dimension. Thus there are 400,000 assembly strips along the 40 cm FGN dimension and 1250 assembly strips along the 50 cm FGN dimension, with each strip spanning the 0.4 mm distance between the 1250 stovepipe/stiffener-block rows in the fabrication planes as previously described in Section 3.11.2.9. Each assembly strip receives parts from two 1 micron^2 passthroughs (Section 3.11.3.2), one at either end of the strip.

[1250] Ali Javey, Pengfei Qi, Qian Wang, Hongjie Dai, "Ten- to 50-nm-long quasi-ballistic carbon nanotube devices obtained without complex lithography," PNAS 101(14 September 2004):13408-13410; http://www.pnas.org/cgi/content/abstract/101/37/13408. Hongjie Dai, Eric W. Wong, Charles M. Lieber, "Probing Electrical Transport in Nanomaterials: Conductivity of Individual Carbon Nanotubes," Science 272(26 April 1996):523-526; Stefan Frank, Philippe Poncharal, Z.L. Wang, Walt A. de Heer, "Carbon Nanotube Quantum Resistors," Science 280(12 June 1998):1744-1746.

Figure X-10. Schematic illustration of the layout of one assembly strip (top) and two groups of 10 assembly half-strips in which parts entering the strip via a passthrough ("P") at far left may pass through up to six assembly sets flowing in the x_{FGN} direction, then completed product objects flow along the column of export MAMs ("E") to a hole MAM which inserts the product object into an export hole in the Export Plane directly above. Heavy arrows show parts flow along each row or column of MAMs. Parts flow from the passthrough at either end towards the export area nearer to the center.

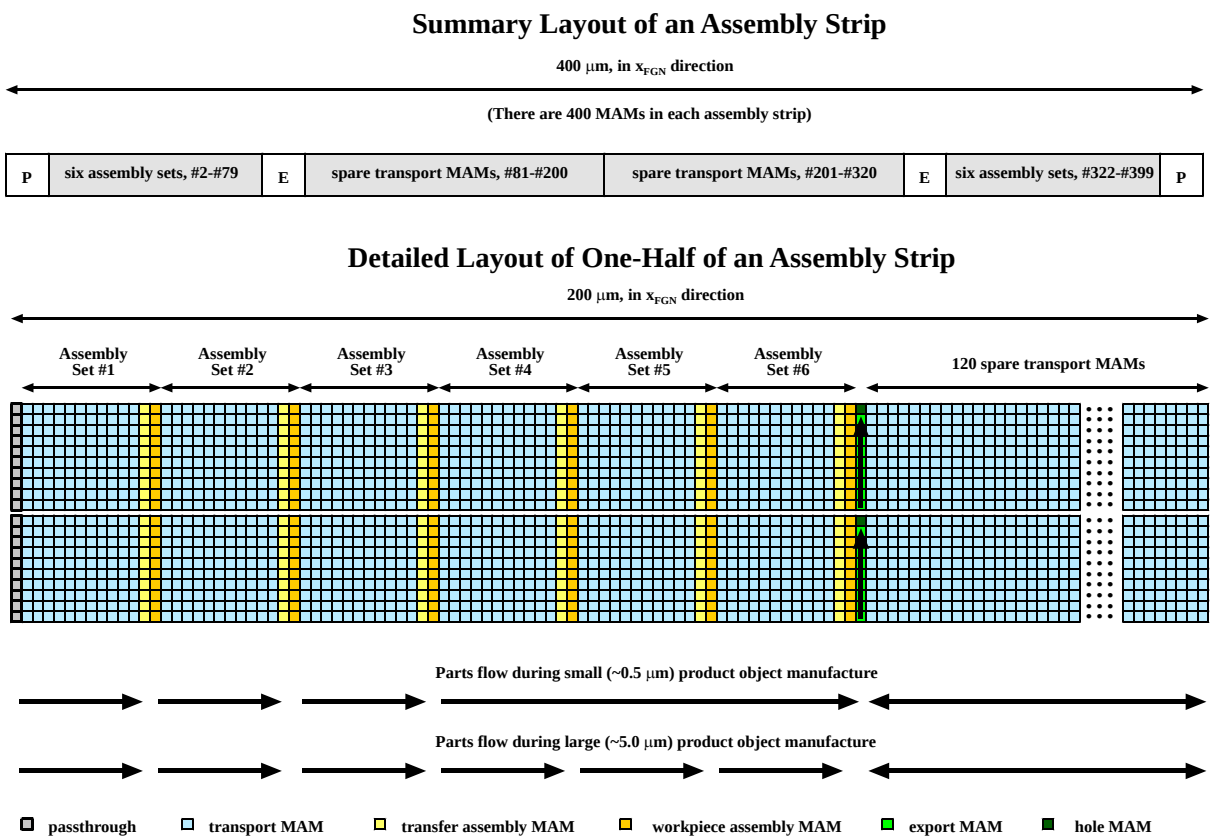

Each assembly strip consists of 400 1 micron^2 spaces numbered #1 through #400 from left to right. Module #1 is a passthrough hole from which parts may enter the assembly strip at the 10^4 part/sec rate. Modules #2-#12 are high-speed two-state "transport MAMs" (Section 3.11.3.1) that rapidly transport parts left-to-right from module #2 to module #12 at the 10^5 parts/sec rate. Modules #13 and #14 are "assembly MAMs" that perform the parts assembly function at the 10^4 parts/sec rate. Assembly MAMs are very similar to inspection MAMs (Section 3.11.3.1) and have end effectors specialized for fine grasping and manipulation motions suitable for assembly work. Assembly MAM #13, called the "transfer assembly MAM," acquires parts from the transport MAM stream (or in some cases from adjacent transfer assembly MAMs) and inserts a new part onto a growing workpiece that is held by the adjacent assembly MAM #14, which is called the "workpiece assembly MAM". When the workpiece is completed, MAM #14 passes the workpiece to module #15 in the next assembly set for further processing.

Modules #2-#14 constitute the first of six assembly sets on the left side of the assembly strip. Assembly of product from parts proceeds along the assembly strip from left to right using the principles of convergent assembly described earlier (Section 2.1.3). Five successive assembly sets identical to assembly set 1 (#2-#14) are comprised of modules #15-#27 (assembly set 2), #28-#40 (assembly set 3), #41-#53 (assembly set 4), #54-#66 (assembly set 5), and #67-#79 (assembly set 6). (It may be advisable to insert a transfer MAM between the transfer assembly MAM (#78) and the workpiece assembly MAM (#79) in assembly set 6 to provide some additional working space when assembling the largest product objects, but for simplicity the present design does not include this feature.) Module #80 is an "export MAM" (see below) that is similar to the "import MAM" (Section 3.11.3.1) except that the export MAM has no foundation-block-penetrating stovepipe. Modules #81-#200 are spare transport MAMs that can be used to temporarily cache parts of various sizes that may be inserted into the growing workpiece, outside of the usual convergent assembly order. Modules #201-#400 are an identical series to #1-#200 but in mirror order (with assembly proceeding from right to left) and an export MAM in module #320, ending with a second passthrough in Module #400, completing the assembly strip.

The same architecture can be used to manufacture either small or large product objects, as follows:

To manufacture the smallest ~0.5 micron product objects (~10^3 parts each) at the ~10^{10} product/sec rate, we define 10^9 assembly arrays each capable of assembling 10 products/sec on the Assembly Plane. There are 500 million assembly strips on the entire Assembly Plane, and each 1 micron x 200 micron assembly array occupies half of an assembly strip as described above. Parts of size ~46.4 nm and ~10^5 nm^3 enter the assembly array from the passthrough hole at the 10^4 parts/sec rate. Thus in 1 second, 10^4 parts enter the array which will be enough to build 10 small product objects per second.

In assembly set 1, the 11 transport MAMs convey the parts to the transfer assembly MAM at the 10^5 parts/sec rate. This transfer is completed in 11 x 10^{-5} sec, which is ~0.001 sec faster than the putative 11 x 10^{-4} sec transfer time that would have been achieved at the slower 10^4 parts/sec transfer rate of the ordinary MAM (the minimum necessary to keep pace with the 10^4 parts/sec feed rate from the passthrough). The saved ~0.001 sec gives the transfer assembly MAM enough time to complete 10 parts assembly motions at the 10^4 parts/sec rate, thus installing 10 parts into the workpiece held by the workpiece assembly MAM. As a result, every ~10^{-3} sec a 10-part component of size ~100 nm and ~10^6 nm^3 is emitted to the right by the workpiece assembly MAM, so that ~10^3 components/sec enter assembly set 2.

In assembly set 2, the 11 transport MAMs convey the 10-part components to the transfer assembly MAM at the 10^5 parts/sec rate, a transfer that is completed in 11 x 10^{-5} sec. Successive components arrive at intervals of ~0.001 sec, giving the transfer assembly MAM ~0.0009 sec to insert these larger components into the workpiece at a more leisurely ~10^3 parts/sec assembly rate and completing a 10-component (100-part) supercomponent in ~0.01 sec. As a result, every ~10^{-2} sec a 100-part supercomponent of size ~215 nm and ~10^7 nm^3 is emitted to the right by the workpiece assembly MAM, so that ~10^2 supercomponents/sec enter assembly set 3.

In assembly set 3, the 11 transport MAMs convey the 100-part supercomponents to the transfer assembly MAM at the 10^5 parts/sec rate, a transfer that is completed in 11 x 10^{-5} sec. Successive components arrive at intervals of ~0.01 sec, giving the transfer assembly MAM ~0.0099 sec to insert the supercomponents into the workpiece at an even more leisurely ~10^2 parts/sec assembly rate and completing a 10-supercomponent (1000-part) product object in ~0.1 sec. As a result,

every ~10^{-1} sec a 1000-part product object of size ~464 nm and ~10^8 nm^3 is emitted to the right by the workpiece assembly MAM, so that ~10 product objects/sec enter assembly set 4.

In assembly set 4, the ~10 product objects/sec completed in assembly set 3 are simply passed through the remaining 39 MAMs without further processing, all the way to the export MAM in module #80 which delivers the finished product objects to the Export Plane at the ~10 product object/sec rate. With all 10^9 assembly arrays manufacturing product objects at the 10 sec^{-1} rate, the target ~10^{10} product/sec rate for the smallest ~0.5 micron product objects is achieved. Note that this small assembly array includes 160 spare transport MAMs that could be used to temporarily cache parts of various sizes that may be inserted into the product object outside of the usual convergent assembly order.

To manufacture the <u>largest ~5 micron product objects</u> (~10^6 parts each) at the ~10^7 product/sec rate, we define 10^7 assembly arrays each capable of assembling 1 products/sec on the Assembly Plane. There are 500 million assembly strips on the entire Assembly Plane, and each 100 micron x 200 micron assembly array occupies one-half of 200 assembly strips. Parts of size ~46.4 nm and ~10^5 nm^3 enter the assembly array from the 100 passthrough holes at the 10^4 parts/sec rate. Thus in 1 second, 10^6 parts enter the array which will be enough to build 1 large product object per second.

In assembly set 1, the transfer assembly MAM completes 10 assembly motions at the 10^4 parts/sec rate, thus installing 10 parts into the workpiece held by the workpiece assembly MAM. As a result, every ~10^{-3} sec a 10-part component of size ~100 nm and ~10^6 nm^3 is emitted to the right by the workpiece assembly MAM, so that ~10^3 10-part components/sec enter assembly set 2 within each assembly strip and a total of ~10^5 10-part components/sec enter assembly set 2 across the entire assembly array spanning 100 assembly strips. Similarly a total of ~10^4 100-part components/sec of size ~215 nm and ~10^7 nm^3 enter assembly set 3 from assembly set 2, ~10^3 1000-part components/sec of size ~464 nm and ~10^8 nm^3 enter assembly set 4 from assembly set 3, and ~10^2 10,000-part components/sec of size ~1 micron and ~10^9 nm^3 enter assembly set 5 from assembly set 4 across the entire assembly array.

In assembly set 5, only ~one 10,000-part component arrives every second which is insufficient for the assembly of a 100,000-part component in within the required 1 second time window. As a result, the transfer assembly MAMs for assembly strips #2-#10 are used to convey hand-over-hand the 9 nearest 10,000-part components to the transfer assembly MAM for assembly strip #1 to be added to the 10,000-part component workpiece already held by the workpiece assembly MAM in assembly strip #1. Since both transfer and assembly operations can occur simultaneously and at the ~10^4 component/sec rate, assembly is completed in ~1.001 sec; the same process occurs simultaneously within the other 9 assembly strip decades (e.g., #11-#20, #21-#30, etc.). As a result, every ~1 sec a 100,000-part component of size ~2.15 microns and ~10^{10} nm^3 is emitted to the right from assembly set 5 into assembly set 6, from each of 10 of the 100 assembly strips in assembly set 5, so that a total of ~ten 100,000-part components/sec enter assembly set 6.

In assembly set 6 a similar process of lateral component supply occurs as in assembly set 5, except that in assembly set 6 the assembly of the one 1,000,000-part product object of size ~4.64 microns and ~10^{11} nm^3 is completed after the conveyance of ten 100,000-part components from as far as 100 microns away, requiring ~1.01 sec to complete when transfer and assembly operations are performed by transfer assembly MAMs at the 10^4 sec^{-1} rate. The one 1,000,000-part product object is then handed to the export MAM in module #80, which delivers the finished product object to the Export Plane at the ~1 product object/sec rate. With all 10^7 assembly arrays

manufacturing product objects at the 1 sec^{-1} rate, the target ~10^7 product/sec rate for the largest ~5 micron product objects is achieved. Note that this large assembly array includes 16,000 spare transport MAMs that could be used to temporarily cache parts of various sizes that may be inserted into the product object outside of the usual convergent assembly order.

In the entire Assembly Plane there are ~1 x 10^9 passthroughs and ~186 x 10^9 transport MAMs that can be arranged in linear control rows and operated in unison. There are also a total of 12 x 10^9 assembly MAMs, including 6 x 10^9 workpiece assembly MAMs that can be arranged in control rows and operated in unison. But there are 6 x 10^9 transfer assembly MAMs that upon occasion will be called upon to operate in a different mode than their immediate neighbors, and the module numbers of the MAMs that must operate in a different mode will vary according to the size and nature of the product object being produced by the FGN. If attaching one pair of ~1 nm DWCNT low-current "home run" control wires (Section 3.11.2.4) and a few small switching relays to each of 6 x 10^9 transfer assembly MAMs will suffice to switch the MAMs between two different modes, then we must add 6 small-wire sheets (Section 3.11.3.1) totaling 6 nm thick underneath the foundation blocks of the 0.2 m^2 Assembly Plane surface. Adding these extra small-wire sheets increases design and signal control complexity but should not significantly increase the total FGN atom count or build time. If each wire in the small-wire sheet carries signal pulses of energy ~1000 k_BT ~ 41 zJ (300 K) at 120 MHz, then each wire draws ~5 pW (~5 x 10^{-12} amp/wire at 1 volt) and the six ~0.2 m^2 sheets of 10^9 DWCNT wires adds a negligible ~0.03 W to the existing 3200 W power requirement for the entire Inspection Plane. The extra wiring sheet and associated snap connectors between foundation blocks can be added to the design for the MAM foundation blocks and can be fabricated at the same time as the MAM foundation blocks.

In the entire Assembly Plane there are ~1 x 10^9 export MAMs that must also be individually addressable and controllable. That's because in the Export Plane, there is only one export hole ~ 5 microns in diameter located above every tenth export MAM – the export holes are spaced 10 microns apart, directly above the line of export MAMs below. When the smallest ~0.5 micron product objects are being manufactured, these product objects arrive at every export MAM in the assembly strip at the ~10 product objects/sec rate. One of every ten of these export MAMs, called the "hole MAM", lies underneath an export hole. The nearest line of 10 export MAMs has 0.1 sec to pass their 9 additional product objects hand-over-hand to the hole MAM, and the hole MAM has the same amount of time to pass all 10 product objects up to the export hole. Export MAMs operating at the 10^4 sec^{-1} rate should achieve all these tasks in just 0.001 sec, easily satisfying the product flow requirement. Similarly, when the largest ~5 micron product objects are being manufactured, these product objects arrive at just one of ten hole MAMs at the ~1 product object/sec rate. In this case no hand-over-hand motions from neighboring export MAMs are necessary and the hole MAM need only pass the one product object up into the export hole within the 1 second time allotment – a very leisurely pace.

Export MAMs are similar to import MAMs (Section 3.11.3.1) – though lacking, of course, foundation-block-penetrating stovepipes – but are usually operated as five-state devices (backward, forward, left, right, and up). An export MAM can receive a finished product object from the workpiece assembly MAM to one side, then rotate the object into the vertical position and insert the finished product up into an overhead export hole in the Export Plane (Section 3.11.3.4), including a special ejection motion (see below). Export MAMs can also move objects up or down the line of adjacent export MAMs to position product objects under the nearest export hole. Export MAMs can also pass parts to or from the 160-micron-long cache arrays within each assembly strip. To properly control all these tasks, all export MAMs must be directly addressable, requiring the attachment of two pairs of ~1 nm DWCNT low-current control wires

(Section 3.11.2.4) and a few small switching relays to each of ~10^9 export MAMs, resulting in the addition of 2 small-wire sheets (Section 3.11.3.1) ~2 nm thick underneath the foundation blocks of the 0.2 m^2 Assembly Plane surface – making a total of 8 of such sheets that are required in the present design.

Given that export MAMs can easily transition between 1-2 microns of vertical reach and product objects may lie between 0.5-5 microns in diameter, normal operations will require a clearance of at least ~6 microns between opposing surfaces of the Assembly Plane and the Export Plane. Providing support between these two planes are 1.25 x 10^6 support columns spaced 0.4 mm apart and measuring 1 $micron^2$ x 6 micron in size – the footprint of each support column replaces one cache array space in every 400 assembly strips, and support columns are located maximally distant from export holes to minimize geometric interference. Additionally, hole MAMs must be able to lift the smallest 0.5 micron product at least 6 microns up from the Assembly Plane floor in order to guarantee full reliable insertion into the export hole. Therefore the reach of the hole MAMs must be extended from the usual 2 micron maximum to at least 5.5 microns. This appears feasible by adding just three additional segments (increasing their number from 4 to 7) to each of the 7 struts comprising the basic crane arm design (Section 3.6.1.1) from which the MAM design was originally derived (Section 3.10.1.1). A perimeter wall 100 nm thick and 6 microns tall seals the Inspection and Routing Planes against vacuum loss.

3.11.3.4 Export Plane

The Export Plane (Figure X-8) acquires finished atomically-precise microscale product objects from the Assembly Plane and passes these products into a macroscale collection system that accumulates the product in bulk form inside sealed vials that can be removed from the FGN for external consumption.

Microscale products to be accumulated through the Export Plane will include objects ranging in size from ~0.5 micron diameter (~0.1 $micron^3$) produced at a ~10^{10} sec^{-1} rate up to ~5 micron diameter (~100 $micron^3$) produced at a ~10^7 sec^{-1} rate by the Assembly Plane. The ~0.2 m^2 Export plane consists of two flat 0.1 micron thick diamondoid parallel plates each comprised of 2 x 10^{11} foundation blocks similar to the 1 $micron^2$ MAM foundation blocks. The opposing faces of the two plates are separated by 7 microns and are perforated with a total of 10^8 square export holes measuring 5 micron x 5 micron in size, thus displacing (counting the open area plus an identical blade area) ~5.0 x 10^9 or 2.5% of the 2 x 10^{11} 1-$micron^2$ foundation blocks in each plate. The holes lie in rows, with holes spaced 10 microns apart center-to-center. The rows run parallel to the 40 cm dimension of the FGN. Each row has 40,000 export holes. There are 2500 rows of export holes, spaced alternately 240 microns and 160 microns apart along the 50 cm dimension of the FGN, aligned with every tenth assembly strip in the Assembly Plane below.

On each side of each square export hole along the 50 cm dimension of the FGN, a stack of ~35 blades are spaced 0.2 microns apart across the entire 7 micron distance between the two parallel plates comprising the Export Plane. The blades are rectangular in shape measuring 5 microns x 2.5 microns, and are 0.1 micron thick. Each of the 35 blade pairs is free to slide along a 5 micron long groove such that when the blade pair is fully inserted and touching along one common edge, the 25 $micron^2$ export hole is completely closed off, but when the blade pair is fully retracted, the 25 $micron^2$ export hole is completely open. One reversible blade motor drives each blade forward or backward along the 5 micron groove in 5 nm steps, thus requiring 1000 steps to completely close or open the hole but allowing the hole aperture size to be selected in 5 nm increments.

There are 70 blade motors controlling each export hole and thus 7 x 10^9 blade motors to control in the entire Export Plane. The power dissipated by two atomically-smooth sliding diamondoid surfaces may be crudely approximated[1251] by $P_{slide} \sim k_1 S_{contact} v_{slide}^2 \sim 0.4$ pW for $k_1 = 400$ kg/m^2-sec,[1252] relative interfacial velocity $v_{slide} = 2.5$ cm/sec, and mutual contact area $S_{contact} \sim 1.5$ micron^2 for a two grooves each of length 2.5 microns and groove wall height 0.1 micron on either side, when driven primarily by shear-reflection drag and band-stiffness scattering. This implies that all 70 blade motors controlling each export hole will dissipate ~28 pW when in operation at 2.5 cm/sec, or ~0.003 W for all 7 x 10^9 blade motors (for 10^8 holes) in the Export Plane if simultaneously actuated. Simultaneous row actuation allows each of the 2500 rows to be powered by 5000 full-plane binary tree networks (power + ground), with each network delivering power to 2.8 x 10^6 nodes, requiring a binary tree with $\log_2(2.8 \times 10^6) \sim 22$ branches, about the same as the fabrication plane networks previously described (Section 3.11.2.4). Each such full-plane network requires $2L_{network} \sim 5.5$ meters of wires of ~4 nm^2 cross-section, so 5000 networks gives a total wire volume of ~1.1 x 10^{-13} m^3 running parallel to the rows along one of the two facing plate surfaces of the two parallel plates comprising the Export Plane.

Initially, all blade pairs for all export holes are set to the fully open position except for the first blade pair, which is set so as to define a hole aperture just slightly larger than the clearance needed to insert the 0.5-5 micron product object into the hole. When a hole MAM inserts a product object into the hole, a short ~100 nm wide rod is extended outward through the end-effector of the hole MAM, forcing the product object to detach from the end-effector. The lowest blade pair is then moved forward into the hole, causing the hole to become narrower and trapping the product object on the inside of the hole. The end-effector rod is then fully retracted as the blade pair completes its motion in ~10^{-4} sec and seals off the hole. Note that actuating the 35 blade pairs in sequence produces a peristaltic-like motion which gently pushes the product object through the export hole until it is ejected out the other side, with the last blade pair remaining fully closed to prevent re-entry of the product object back into the export hole. Actuating each successive blade pair at intervals of ~2.9 x 10^{-6} sec (with time intervals as small as ~0.01 x 10^{-6} sec addressable using a 120 MHz pulse rate) causes the product object to be propelled through the export hole in ~10^{-4} sec, matching the fastest possible product object feed rate for small products from the Assembly Plane (Section 3.11.3.3).

All 40,000 export holes along one row open onto a smooth-walled 50 micron x 50 micron square collection cylinder with ~1 micron thick walls that runs the entire length of the 40 cm FGN dimension. There are 2500 such collection cylinders, one for each row. Each square collection cylinder has an internal volume of ~10^{18} nm^3 and receives (~10^{18} nm^3/sec) / 2500 rows ~ 4 x 10^{14} nm^3/sec of product, hence fills to capacity every ~2500 sec (~0.7 hour). Thus about twice an

---

[1251] Robert A. Freitas Jr., Nanomedicine, Volume I: Basic Capabilities, Landes Bioscience, Georgetown, TX, 1999, Section 4.3.4.2, p. 101, http://www.nanomedicine.com/NMI/4.3.4.2.htm; K. Eric Drexler, Nanosystems: Molecular Machinery, Manufacturing, and Computation, John Wiley & Sons, New York, 1992, Section 10.4.6, pp. 290-293.

[1252] Robert A. Freitas Jr., Nanomedicine, Volume I: Basic Capabilities, Landes Bioscience, Georgetown, TX, 1999, Section 4.3.4.2, p. 101, http://www.nanomedicine.com/NMI/4.3.4.2.htm; K. Eric Drexler, Nanosystems: Molecular Machinery, Manufacturing, and Computation, John Wiley & Sons, New York, 1992, Section 10.4.6, pp. 290-293.

hour, each square collection cylinder must be swept by a tight-fitting 50 micron x 50 micron x 10 micron thick piston block that pushes the bulk product into a much larger atomically imprecise ~10^{23} nm^3 (~100 cm^3) drainage cylinder into which all the 50 micron collection cylinders empty their pushed contents. Nanofactory manufacturing operations are briefly halted (for a few seconds) during each such sweep.

The larger drainage cylinder measures ~2 cm^2 in cross-section and runs the entire length of the 50 cm FGN dimension. A larger piston pushes the contents of the drainage cylinder (which takes ~10^5 sec or ~1 day to fill) into a collection bottle, which when full and capped is passed out of the FGN through an airlock mechanism that can avoid breaking the vacuum inside the FGN.

The FGN is now manufacturing ~100 cm^3/day (~240 gm/day) of atomically precise microscale product having a mean density of ~2.4 gm/cm^3 (i.e., products are about two-thirds (~68%) solid diamond and about one-third (~32%) vacuum, by volume).

3.11.3.5 Scaling Analysis Summary with Atom Count

Allocating ~176 C atoms/nm^3 for diamondoid lattice and ~31 H atoms per nm^2 to passivate diamondoid surface gives the scaling results for the second production layer as shown in Table X-2. The second production layer (comprised of four assembling planes and ~6.789 x 10^{22} atoms (99.4% carbons)) is 67.6 microns thick with a dry mass of ~1.34 grams. If each of 5 x 10^5 rows of MAMs in each of 3 assembly planes and each of 2500 rows of export holes receives a separate sequence of 120 x 10^6 control pulses per second (120 MHz operating frequency) on each of ~100 control lines, and if 49 small-wire sheets with 10^9 wires/sheet conduct ~10^5 pulses/sec, then operating the second production layer requires a total control data flow of ~5.1 x 10^{15} bits/sec.

Allowing ~3200 W power dissipation for each of the four Assembly Planes gives a total heat generation of 12,800 W for the entire second production layer. This heat may be conducted away by (a) increasing the coolant flow velocity in the topmost cooling channel above the 1000th fabrication plane by 5-fold, or in the topmost 4 cooling channels by 2-fold (since diamond is the most thermally conductive material known), (b) increasing the width of just the topmost cooling channel from 98.745 microns to 498.745 microns, or (c) adding an external cooling jacket around the perimeter of four assembling planes.

Table X-2. Estimated Atom Count* for Diamondoid Structure of Four Assembling Planes Comprising the Second Production Layer of the First-Generation Nanofactory (FGN)

FGN Nanofactory Subsystem	Total Solid Volume (m^3)	Total Passiv. Area (m^2)	# of C Atoms	# of H Atoms	Total # of Atoms*
Inspection Plane			8.026 x 10^{21}	1.13 x 10^{20}	8.139 x 10^{21}
200 x 10^9 MAMs	3.2 x 10^{-8}	3.1528			
Wiring Bundle	7.398 x 10^{-9}	0			
Support Frame	6 x 10^{-9}	4.8 x10^{-1}			
1 Small-Wire Sheet	2 x 10^{-10}	0			
Snap Connectors	4 x 10^{-12}	1.602 x 10^{-2}			
Perimeter Wall	5.4 x 10^{-13}	1.08 x 10^{-5}			

Routing Plane			8.469×10^{21}	1.18×10^{20}	8.587×10^{21}
199×10^{9} MAMs	3.2×10^{-8}	3.1528			
Wiring Bundle	7.398×10^{-9}	0			
10^{9} Passthrough MAMs	1.6×10^{-10}	1.576×10^{-2}			
Passthrough Walls	4×10^{-10}	8×10^{-3}			
40 Small-Wire Sheets	8×10^{-9}	0			
Snap Connectors	1.6×10^{-10}	6.408×10^{-1}			
Assembly Plane			7.223×10^{21}	1.02×10^{20}	7.325×10^{21}
199×10^{9} MAMs	3.2×10^{-8}	3.1528			
Wiring Bundle	7.398×10^{-9}	0			
8 Small-Wire Sheets	1.6×10^{-9}	0			
Snap Connectors	3.2×10^{-11}	1.282×10^{-1}			
Support Columns	7.5×10^{-12}	3×10^{-5}			
Perimeter Wall	1.08×10^{-12}	2.16×10^{-5}			
Export Plane			4.362×10^{22}	4.23×10^{19}	4.366×10^{22}
2 Parallel Plates	3.9×10^{-8}	7.8×10^{-1}			
Blade Stacks	8.75×10^{-9}	1.855×10^{-1}			
Blade Motors	7×10^{-12}	4.2×10^{-6}			
Wiring Bundle	1.1×10^{-13}	0			
2500 Square Cylinders	2×10^{-7}	4×10^{-1}			
2500 Square Pistons	6.25×10^{-11}	1.25×10^{-5}			
Unallocated Structure	1×10^{-9}	1×10^{-1}	1.760×10^{20}	3.10×10^{18}	1.791×10^{20}
TOTALS, Second Production Layer	3.836×10^{-7}	12.213	6.751×10^{22}	3.784×10^{20}	6.789×10^{22}
TOTALS, First Production Layer	2.015×10^{-5}	8.374×10^{3}	3.541×10^{24}	2.604×10^{23}	3.800×10^{24}
TOTALS for FGN	2.053×10^{-5}	8.386×10^{3}	3.609×10^{24}	2.608×10^{23}	3.869×10^{24}

* There are also ~10^{14} Ge atoms per fabrication plane, hence ~10^{17} Ge atoms in all 1000 fabrication planes comprising the first production layer, hence ~10^{17} Ge atoms in the entire FGN.

It should be noted that a sheet of tightly packed nanoscale diamond blocks with opposed hydrogen-terminated interfacial surfaces will be somewhat less thermally conductive than a solid sheet of diamond lacking such interfaces. The effects of this on cooling efficiency is an issue requiring further investigation (e.g., design, modeling and simulation studies) in the context of system design for both of the production layers in the FGN (and all three such layers in the SGN; Section 3.12).

Note also that more inspection planes can be added to the second production layer design if needed to achieve adequate manufacturing reliability with acceptably low defect rates.

The FGN as a whole has ~3.869×10^{24} atoms (93.3% carbons) and measures 50 cm x 40 cm x 10.20713 cm tall with a dry mass of ~72.24 gm of atomically precise components. Power consumption and control signal traffic are both dominated by the first production layer, which requires a data flow of ~2.4×10^{19} bits/sec compared to only ~5.1×10^{15} bits/sec for the second production layer. The FGN produces ~11 MW of waste heat while manufacturing atomically

precise products at ~10^{20} atoms/sec, ~10^{18} nm^3/sec, or ~0.01 kg/hour, giving the FGN a mass replication time of ~7.2 hours (or, similarly, ~10.7 hours by atom count).

Ignoring capital and human labor costs, the production cost of FGN products is driven primarily by the cost of material inputs, which includes: (1) electrical power at today's typical $0.10/kW-hr rate, or (~11 x 10^6 W) ($2.78 x 10^{-8}/W-sec) / ((~240 gm/day) / (86,400 sec/day)) ~ $110/gm, plus (2) high-purity 5N ethylene feedstock gas at ~$1/gm (based on 18 March 2008 quotes from Praxair[1253] of $4.63/gm for 150 gm lecture bottles, and from ST Gas Ltd.[1254] of $1.37/gm for 110 gm lecture bottles and $0.0848/gm for 16 kg cylinders, which is ~1000 times the typical ~$0.5/lb wholesale price of 98.5% (1N) commercial grade ethylene in 2007[1255]). This implies an FGN materials production cost for atomically precise microscale product objects of C_{FGNgm} ~ $111/gm.

3.11.3.6 Reliability of FGN Manufacture and Operation

A detailed and comprehensive analysis of molecular manufacturing error rates will be required to properly assess the defect rate likely to occur when building various components and subsystems of the FGN, especially since the equipment and procedures for manufacturing the FGN are very complex and involve mole-quantities of moving parts (see below).

However, as a crude estimate, at a 109 K operating temperature the error rate for DMS-related fabrication operations is ~10^{-10} per NMW-3 replication cycle (Section 3.8.1.3) or ~10^{-18} per atom, so the systemic error rate will probably be driven by the mechanical/control error rate and by the imperfect-vacuum radical poisoning rate which have been estimated (Section 3.8.1.3) as ~10^{-7} per NMW-3 replication cycle or ~10^{-15} per atom. The FGN consists of 3.869 x 10^{24} atoms, so we may logically assume that the FGN as initially manufactured will include ~4 million erroneously placed atoms and will have suffered ~4 billion radical poisoning events and ~4 billion erroneous mechanical/control events. In its 1000 fabrication planes the FGN includes ~10^{16} NMW-3 modules, of which it must be assumed that (10^{16} modules) (10^{-7} error rate per module) ~ 10^9 of them are nonfunctional from the outset. Clearly the FGN must incorporate error tolerance as a critical design feature (Section 3.11.4), and ideally the FGN should remain moderately functional even when a random distribution of perhaps up to ~1% of its NMW-3 modules have become incapacitated (a ~1% failed-module threshold).

Once the FGN has been built and is operating in production mode, similar error rates will apply. At 109 K, the error rate for DMS-related operations is ~10^{-10} per NMW-3 replication cycle or

---

[1253] Gloria Winters, Praxair Distrib. Inc., personal communication to Robert A. Freitas Jr., 18 March 2008.

[1254] Stephen Haywood, Scientific and Technical Gas Ltd., UK, personal communication to Robert A. Freitas Jr., 18 March 2008.

[1255] "ICIS Students, Indicative Chemical Prices A-Z," http://www.icis.com/StaticPages/A-E.htm; Tom Stundza, "Benzene prices slide; ethylene prices rise," Purchasing.com, 8 August 2007, http://www.purchasing.com/article/CA6466597.html; "Petrochemicals firms take a stand against oil price volatility" Market Focus, www.eprm.com, May 2003, pp. 54-55; http://www.gvsi.com/download/editorials/Mrktfocs-May-03.pdf.

~10^{-18} per atom (Section 3.8.1.3), so again the systemic error rate is driven by the mechanical/control error rate (presumed to be ~10^{-7} per NMW-3 replication cycle or ~10^{-15} per atom; Section 3.8.1.3) and by the imperfect-vacuum radical poisoning rate which is ~10^{-7} per NMW-3 replication cycle or ~10^{-15} per atom (Section 3.8.1.3). Obtaining this low radical poisoning rate requires maintaining a 10^{-18} atm vacuum environment inside each of the 1000 fabrication planes. To get a sense of how good a vacuum this is, consider that each fabrication plane has a gross interior volume of (2000 cm^2 XY area) (200 nm height) ~ 4 x 10^{-8} m^3, from which we may subtract the solid volume of the vertical support columns (~1 x 10^{-10} m^3, Table X-1) and the solid volume of all the NMW-3 machinery including the NFW-3 manipulators, tools/toolrack, and transfer units, and the NAW-2 manipulators (~3.7553 x 10^{-9} m^3, Table X-1), leaving 3.61447 x 10^{-8} m^3 of vacuum volume. From the ideal gas law with P = 10^{-18} atm, V = 3.61447 x 10^{-8} m^3, R_{gas} = 8.206 x 10^{-5} m^3-atm/mole-K, T = 109 K, and N_A = Avogadro's number (6.023 x 10^{23} molecules/mole), the number of molecules of contaminant gas present in the entire open vacuum volume of each fabrication plane is $n_{contam} = (PV / R_{gas}T)\ N_A$ ~ 2.4 contaminant gas molecules. Thus the FGN must maintain in its interior working volumes very nearly a perfect vacuum.

The productive lifetime of an FGN is a function both of the NMW-3 module failure rates and of the tolerance of the FGN for accumulated failed modules (Section 3.11.4), and other factors. As previously noted, the 1000 fabrication planes of the FGN (subsuming the vast majority of active failure-prone mechanisms inside the FGN) collectively contain 10^{16} NMW-3 modules (Section 3.11.2) with an assumed failure rate from all causes of ~3 x 10^{-11} sec^{-1} (Section 3.8.1.3), so during continuous operation ~300,000 NMW-3 modules fail every second, on average, somewhere inside the FGN. After 1 year of FGN operation, ~10^{13} modules or ~0.1% of all NMW-3 modules in the FGN will have failed, so a ~10 year FGN operating lifetime (the ~1% failed-module threshold) does not seem unreasonable.

3.11.4 Task X-1: Design, Model and Simulate FGN Components, Operations, and Process of Manufacture

Task X-1 is to design, model, and simulate the components and operations of the FGN Assembly System and of the First-Generation Nanofactory (FGN) itself.

Components of the FGN to be designed, modeled and simulated include the FGN base plate and its method of manufacture (Section 3.11.5), the first production layer (Section 3.11.2), the second production layer (Section 3.11.3), and the appurtenant FGN support equipment (Section 3.11.11) including FGN sidewall connections to feedstock gas supply and byproduct gas exhaust hose bibs, sidewall connections to the extensive electrical wiring coming from each productive machinery plane, and cooling fluid supply lines to be mated to the ~1000 cooling channels passing through the FGN (including simulations of adequate coolant flow).

Components of the first production layer include tanks and rotors (Section 3.11.2.1), manipulators (Section 3.11.2.2), foundation blocks (Section 3.11.2.3), power and control lines (Section 3.11.2.4), support frame (Section 3.11.2.5), catacombs (Section 3.11.2.6), ciliary transport array (Section 3.11.2.7), stovepipes (Section 3.11.2.8), and cooling channels (Section 3.11.2.9). The physical structure of the stack of 1000 fabrication planes and its operation as a complete subsystem must also be modeled and simulated.

Components of the second production layer include the inspection plane (Section 3.11.3.1), the routing plane (Section 3.11.3.2), the assembly plane (Section 3.11.3.3) and the export plane (Section 3.11.3.4). The physical structure of the stack of 4 assembling planes and its operation as a complete subsystem must also be modeled and simulated, along with its operation in concert with the first production layer.

Components of the FGN Assembly System to be designed, modeled and simulated include the NMW-2 Wafer Plate Handlers previously described in Section 3.9.5, the MAA Wafer Plate Handlers previously described in Section 3.10.7, and the new components of the FGN Assembly System and their operation as described in Section 3.11.7 and Section 3.11.10 including the Inspection Rack Gantry, the Inspection Rack, the FGN Assembly Gantry, the airlock passthrough and human access corridors.

The physical integrity and stability of the growing FGN as it exists during numerous intermediate stages of construction must also be modeled, simulated, and validated.

Parallel control algorithms must be investigated for operating the FGN nanofactory. One approach is to send identical instructions to large numbers of manufacturing modules at a time, analogous to how a SIMD (Single Instruction Multiple Data) processor works.[1256] Engineers at Thinking Machines studied these algorithms extensively in the 1980s to build the first supercomputers, and more recently nVidia has been building pseudo-SIMD graphics cards that have been described as "stunningly fast, fun to program,[1257] and involve lots of advanced (proprietary) compiler technology." Parallel manufacturing systems can in principle have many possible control/configuration architectures, analogous to convergent[1258] or fractal[1259] assembly; agoric algorithms;[1260] stigmergy,[1261] swarm,[1262] amorphous computing,[1263] or agent-based

---

[1256] "Welcome to SIMD," SIMD Tech, 2003; http://www.simdtech.org/home.

[1257] http://developer.nvidia.com/object/gpu_gems_home.html.

[1258] Ralph C. Merkle, "Convergent assembly," Nanotechnology 8(1997):18-22; http://www.zyvex.com/nanotech/convergent.html.

[1259] J. Parkinson, R. Gordon, "Beyond micromachining: the potential of diatoms," Trends in Biotechnol. 17(1999):190-196; K.H. Sandhage, M.B. Dickerson, P.M. Huseman, M.A. Caranna, J.D. Clifton, T.A. Bull, T.J. Heibel, W.R. Overton, M.E.A. Schoenwaelder, "Novel, bioclastic route to self-assembled, 3-D, chemically tailored meso-nanostructures: Shape-preserving reactive conversion of biosilica (diatom) microshells," Advanced Mater. 14(2002):429-433; A. Carbone, N.C. Seeman, "A route to fractal DNA-assembly," Natural Computing 1(2002):469-480, http://www.ihes.fr/PREPRINTS/M02/Resu/resu-M02-24.html (abstract), http://www.ihes.fr/PREPRINTS/M02/M02-24.pdf (paper).

[1260] M.S. Miller, K.E. Drexler, "Markets and computation: agoric open systems," in Bernardo A. Huberman, ed., The Ecology of Computation, Elsevier Science Publ., Amsterdam, 1988, http://www.agorics.com/Library/agoricpapers/aos/aos.0.html; K.E. Drexler, M.S. Miller, "Incentive engineering for computational resource management," in Bernardo A. Huberman, ed., The Ecology of Computation, Elsevier Science Publ., Amsterdam, 1988, http://www.agorics.com/Library/agoricpapers/ie/ie0.html; M.S. Miller, K.E. Drexler, "Comparative ecology: a computational perspective," in Bernardo A. Huberman, ed., The Ecology of Computation, Elsevier Science Publ., Amsterdam, 1988, http://www.agorics.com/Library/agoricpapers/ce/ce0.html; Oliver Guenther, Tad Hogg, Bernardo A. Huberman, "Market organizations for controlling smart matter,"

approaches;[1264] kinematic cellular automaton assembly lines;[1265] or other manufacturing analogs taken from high-performance parallel computing[1266] such as SMP (Symmetric

---

in R. Conte, R. Hegselmann, P. Terna, eds., Simulating Social Phenomena, Lecture Notes in Economics and Mathematical Systems, Springer, 1997, pp. 241-257; Oliver Guenther, Tad Hogg, Bernardo A. Huberman, "Power markets for controlling smart matter," arXiv:cond-mat/9703078 v1 7 March 1997, 20 December 2001, http://arxiv.org/pdf/cond-mat/9703078; Tad Hogg, Bernardo A. Huberman, "Controlling Smart Matter," Smart Materials and Structures 7(1998):R1-R1, http://www.arxiv.org/abs/cond-mat/9611024; J. Storrs Hall, Louis Steinberg, Brian D. Davison, "Combining agoric and genetic methods in stochastic design," Nanotechnology 9(September 1998):274-284, http://www.cs.rutgers.edu/~davison/pubs/chsmith/chsmith.html; Tihamer Toth-Fejel, "Agents, assemblers, and ANTS: scheduling assembly with market and biological software mechanisms," Nanotechnology 11(June 2000):133-137, http://www.erim.org/cec/papers/NanoAgents.pdf.

[1261] Pierre-Paul Grasse, "La reconstruction du nid et les coordinations inter-individuelles chez Bellicoitermes natalenis et Cubitermes sp. La theorie de la stigmergie: Essai d'interpretation des termites constructeurs," Insect Societies 6(1959):41-83; Guy Theraulaz, Eric Bonabeau, J.L. Deneubourg, "The algorithmic beauty of stigmergic patterns in social insects," Math. Sci. 435(1999):52-65; E. Bonabeau, S. Guerin, D. Snyers, P. Kuntz, G. Theraulaz, "Three-dimensional architectures grown by simple 'stigmergic' agents," BioSystems 56(2000):13-32; M. Dorigo, E. Bonabeau, G. Theraulaz, "Ant algorithms and stigmergy," Future Generation Computer Systems 16(2000):851-871.

[1262] Guy Theraulaz, Eric Bonabeau, "Coordination in distributed building," Science 269(4 August 1995):686-688; Guy Theraulaz, Eric Bonabeau, "Modeling the collective building of complex architectures in social insects with lattice swarms," J. Theor. Biol. 177(1995):381-400; Guy Theraulaz, Eric Bonabeau, J.L. Deneubourg, "The origin of nest complexity in social insects," Complexity 3(1998):15-25; Guy Theraulaz, Eric Bonabeau, J.L. Deneubourg, N. Franks, O. Rafelsberger, J.L. Joly, S. Blanco, "A model for the emergence of pillars, walls and royal chamber in termite nests," Phil. Trans. R. Soc. London Ser. B Biol. Sci. 353(1998):1561-1576; E. Bonabeau, M. Dorigo, G. Theraulaz, Swarm Intelligence: From Natural to Artificial Systems, Santa Fe Institute Sciences of Complexity Series, Oxford University Press, New York, 1999.

[1263] Amorphous Computing HomePage, http://www.swiss.ai.mit.edu/projects/amorphous/; Radhika Nagpal, Gerry Sussman, "Robust Engineering Using Biologically-inspired Models of Cell Differentiation and Morphogenesis," MIT Artificial Intelligence Lab, 2003, http://www.swiss.ai.mit.edu/projects/amorphous/Robust/.

[1264] Tihamer Toth-Fejel, "Agents, assemblers, and ANTS: scheduling assembly with market and biological software mechanisms," Nanotechnology 11(June 2000):133-137, http://www.erim.org/cec/papers/NanoAgents.pdf; Catie Chang, "Self-assembling two-dimensional shapes," UROP, Summer 2002, http://swiss.csail.mit.edu/projects/amorphous/Robust/catie/; Rebecca Bloom, Catherine Chang, Attila Kondacs, "Compilation and biologically-inspired self-assembly of two-dimensional shapes," Final Project Paper, Biologically Motivated Programming Technology for Robust Systems, MIT Course 6.978, December 2002, http://www.swiss.ai.mit.edu/projects/amorphous/6.978/final-papers/attila-catie-rebecca-final.pdf; Attila Kondacs, "Biologically-inspired self-assembly of 2-D shapes, using global-to-local compilation," Intl. Joint Conf. on Artif. Intell. (IJCAI'03), 2003, http://www.swiss.ai.mit.edu/projects/amorphous/papers/IJCAI-03.pdf; Radhika Nagpal, Attila Kondacs, Catherine Chang, "Programming methodology for biologically-inspired self-assembling systems," AAAI Spring Symposium on Computational Synthesis: From Basic Building Blocks to High Level Functionality, March 2003, http://www.swiss.ai.mit.edu/projects/amorphous/papers/aaai-symp03.pdf.

MultiProcessors),[1267] MPP (Massively Parallel Processors),[1268] and NOWs/COWs (Networks/Clusters of Workstations).[1269]

Another key challenge will be the detailed design of a complex nanofactory system that can tolerate the occurrence of large numbers of random-located failures among its constituent population of productive NMW-3 modules. Note that the 1000 fabrication planes of the FGN (subsuming the vast majority of active failure-prone mechanisms inside the FGN) collectively contain 10^{16} NMW-3 modules (Section 3.11.2) with an assumed radiation-induced failure rate of ~3×10^{-11} sec^{-1} (Section 3.8.1.3), so on average ~300,000 NMW-3 modules fail every second, somewhere inside the FGN. After 1 year of FGN operation, ~10^{13} modules or ~0.1% of all NMW-3 modules in the FGN will have failed. A detailed analysis of all likely failure modes of NMW-3 modules must be undertaken to allow the design of subsystems and procedures that can limit the resulting damage to the product stream or to the FGN structure itself. There appear to be many dozens of such possible failure modes to be analyzed. It seems likely that each one of these failure modes can be dealt with by the judicious addition of negligible quantities of sensors or control wire mass to the baseline FGN design.

For example, product objects manufactured by each fabrication plane are examined for correctness by the Inspection Plane (Section 3.11.3.1) prior to being incorporated in subsequent downstream assemblies, eliminating the potential failure cascade from that source of manufacturing error. Erroneous product objects can be traced back to the individual NMW-3

[1265] Tihamer Toth-Fejel, "LEGOs™ to the stars: Active mesostructures, kinematic cellular automata, and parallel nanomachines for space applications," The Assembler 4(Third Quarter 1996):2-12; http://www.islandone.org/MMSG/9609lego.htm.

[1266] Tihamer Toth-Fejel, "LEGOs™ to the stars: Active mesostructures, kinematic cellular automata, and parallel nanomachines for space applications," The Assembler 4(Third Quarter 1996):2-12; http://www.islandone.org/MMSG/9609lego.htm.

[1267] W.W. Gropp, E.L. Lusk, "A taxonomy of programming models for symmetric multiprocessors and SMP clusters," Programming Models for Massively Parallel Computers (PMMP '95), 9-12 October 1995, Berlin, Germany, 1995, http://www-unix.mcs.anl.gov/~gropp/bib/papers/1995/taxonomy.pdf; David E. Culler, Jaswinder Pal Singh, Anoop Gupta, Parallel Computer Architecture: A Hardware/Software Approach, Morgan-Haufmann Publishers, 1999; William E. Johnston, "Rationale and strategy for a 21st century scientific computing architecture: The case for using commercial symmetric multiprocessors as supercomputers," Information and Computing Sciences Division, Lawrence Berkeley National Laboratory, LBNL Report No. 37661, http://www-itg.lbl.gov/~johnston/Scientific.Comp.Arch/Scientific.Comp.Arch.fm.html; "Cluster of SMPs," High Performance Computing Laboratory, University of New Mexico, 2003, http://hpc.eece.unm.edu/cluster.html.

[1268] J.L. Potter, The Massively Parallel Processor, MIT Press, Cambridge, MA, 1985.

[1269] Thomas E. Anderson, David E. Culler, David A. Patterson, NOW Team, "A case for NOW (Networks of Workstations)," IEEE Micro. 15(February 1995):54-64, http://www.cs.cornell.edu/Courses/cs614/2003SP/papers/ACP94.pdf; David E. Culler, Jaswinder Pal Singh, Anoop Gupta, Parallel Computer Architecture: A Hardware/Software Approach, Morgan-Haufmann Publishers, 1999.

module that made them because routing of product objects into the Inspection Plane is completely deterministic, so the detection of a statistically improbable sequence of failed components coming from the same NMW-3 will alert the external control computer that a particular NMW-3 module in a given fabrication plane has likely failed and should be shut down. A 2D grid of 1.6-nm-diameter control-signal nanowires (Section 3.11.2.4) crisscrossing the underside of each plane of foundation blocks in each fabrication plane will allow the control computer to send a shutdown signal to any selected individual NMW-3 module (which shuts down only when a signal is received on both X and Y lines to which it is attached). This signal could simply lock the feed rotors thus disabling only the fabrication operations of the NMW-3 while leaving it free to continue participating in the ciliary array without adding failed output into the product stream, or it could take other possible actions too numerous to list here. The proposed 2D wire grid will increase FGN solid volume by $(1.6\ \text{nm})^2$ $((2 \times 10^6$ wires)(50 cm/wire) + $(5 \times 10^6$ wires)(40 cm/wire)) = $7.68 \times 10^{-12}\ \text{m}^3$ per plane, or $7.68 \times 10^{-9}\ \text{m}^3$ for all 1000 fabrication planes in the FGN, adding a negligible ~0.04% to the total solid volume of the FGN.

A crude nanowire grid was constructed as a 160-kilobit memory device smaller than a white blood cell was fabricated by Stoddart's group in 2007[1270] by laying down a series of perpendicular crossing nanowires with 400 bottom wires and 400 crossing top wires. Sitting at each intersection of the tic-tac-toe structure and serving as the storage element were approximately 300 bistable rotaxane molecules that could be switched between two different states, and each junction of a crossbar could be addressed individually by controlling the voltages applied to the appropriate top and bottom crossing wires, forming a bit at each nanowire crossing.

Design, modeling and simulation of proposed microscale products (see also Section 3.12.3.8) which can be constructed using convergent assembly processes must be undertaken to define appropriate products for the FGN to manufacture, and to ensure that the identified products are buildable and will perform as desired once they are built.

3.11.5 Task X-2: Manufacture FGN Base Plate

Task X-2 is to manufacture a smooth 40 cm x 50 cm surface upon which the first fabrication plane may be set down, inside a large bulk-made FGN support frame which has previously been assembled using conventional macroscale technologies. The FGN base plate would ideally be atomically smooth because this would prevent "rocking" in the frame and would allow a maximally even distribution of the downward gravitational force due to FGN mass. Of course, base plate atomic smoothness is not strictly required because the catacomb floor of the first fabrication plane will be a strong diamond sheet that is a minimum of 10 nm thick and could easily be made up to ~1000 nm thick if necessary at a cost of adding only ~3×10^{22} atoms (~1% of total FGN mass) to the present design. Such a ~1 micron thick lower foundation should readily tolerate nonuniformities of up to 10-100 nm in the base plate surface. However, if the base plate can be made atomically smooth, this will allow the use of a thinner foundation in the lowest fabrication plane, possibly as thin as 10 nm in the case of a perfectly atomically smooth base plate. Note that the crystal planes need not be perfectly aligned because no atomically

---

[1270] J.E. Green, J.W. Choi, A. Boukai, et al. "A 160-kilobit molecular electronic memory patterned at 10(11) bits per square centimetre," Nature 445(2007):414-417.

precise fabrication will be taking place on the base plate surface. The sole purpose of the base plate is to provide physical support and to evenly distribute across the lowest catacomb foundation plane the relatively small (~2 kg)(100)(9.81 m/sec^2)/(0.2 m^2) = 9810 N/m^2 (~0.1 atm) pressure that will result from a 2 kg FGN mass sustaining a 100-g vertical acceleration without damage (Section 3.11.2.9). The catacomb support columns can withstand without buckling up to ~26 atm (Section 3.11.2.9) – which is the same localized pressure that would result if only ~10^{-3} of the base plate surface was in close contact with the catacomb foundation plane, the result of using an *extremely* unsmooth base plate surface.

The most logical material for the base plate is probably diamond, or diamond-coated materials over a silicon, tungsten, or other underlayment at least ~1 mm thick. An identical top plate should seal the top of the FGN, and should be joined to the FGN in a leaktight manner but need not be atomically precise. Diamond wafers are already commercially available whose surface consists of ~5 nm ultramicrodiamonds,[1271] and it should be possible to remediate 5 nm rough diamond surface to near atomic smoothness using the array-based PALE methods already demonstrated in Task VIII-1.

3.11.6 Task X-3: Build 24 Nanotube Wiremaker Wafers

Task X-3 is to manufacture a small number of wafers of the usual size, capable of being manipulated by existing large-wafer plate handlers, that contain both NMW-2 modules and MAM modules capable of manufacturing nanotube wires (Section 3.11.2.4) in continuous lengths from 238 nm up to 12.5 cm, and of installing them in binary tree full-plane networks underlying the fabrication planes and other manufacturing nanomachinery planes in the FGN.

Each NMW-2 module can fabricate a product object having ~10^8 carbon atoms using a single BFSS-full of feedstock in a manufacturing cycle lasting t_{fab} ~ 1.29 x 10^5 sec (Section 3.8.8), with each module producing a 0.5 mm length of 2-nm-diameter nanotube assuming ~200 carbon atoms per nanometer of linear run. If a 2000 cm^2 (40 cm x 50 cm) wiremaker wafer surface is 65% occupied by NMW-2 modules each occupying ~0.1 micron^2/worksite, then each wafer can produce (65% wafer) (0.2 m^2/wafer) (10^{13} modules/m^2) (~10^8 atoms/module-cycle) / (1.29 x 10^5 sec/cycle) ~ 10^{15} atoms/sec of nanotube wiring. Since the total atom count for the nanotube wiring bundle underlying each fabrication plane is ~4.34 x 10^{20} carbon atoms (Section 3.11.2.4), then one wiremaker wafer can fabricate a sufficient length of nanotube wiring for one fabrication plane in ~4.34 x 10^5 sec (~5 days); to fabricate the necessary wiring for 1000 fabrication planes in an entire FGN will take 24 wiremaker wafers about (1000 planes)(4.34 x 10^{20} atoms/plane)/(24 wafers)(10^{15} atoms/wafer-sec) ~ 1.81 x 10^7 sec (~209 days).

Individual wires may be fabricated with small nanoscale connectors at both ends, so wires can be readily snapped together into a network like tinkertoys.

The total wire count for the nanotube wiring bundle underlying all 1000 fabrication planes in the FGN is ~3.36 x 10^{18} wires (Section 3.11.2.4), with 75% of these wires either 100 nm or 119.2 nm

---

[1271] Advanced Diamond Technologies, Inc., "Diamond Wafers," accessed March 2008; http://www.thindiamond.com/Diamond_Wafers.asp.

in length; the smallest 14 levels of the wiring network or 99.994% of all the wires measure 0.5 mm or shorter. We assume that only 5% of a 2000 cm^2 (40 cm x 50 cm) wiremaker wafer surface is covered by MAM units with each unit occupying ~1 $micron^2$/worksite and performing ~10^4 round trip motions per second at the 120 MHz operating frequency (Section 3.10.1.1), with ~12,930 full-range motions assumed necessary to acquire two wire segments, complete one joining operation, then pass the joined wires on to the next step or into an on-wafer depot. In this case, each wafer can produce (5% wafer) (0.2 m^2/wafer) (10^{12} modules/m^2) (12,930 module-motions/join)$^{-1}$ (10^4 motions/sec) ~ 7.73 x 10^9 joins/sec on nanotube wiring segments comprising a binary tree wiring network. If 3.36 x 10^{18} wire joins must be made to complete ~1000 wiring bundles for the entire FGN, then assembling all necessary wiring will take 24 wiremaker wafers about (3.36 x 10^{18} joins)/(24 wafers)(7.73 x 10^9 joins/wafer-sec) ~ 1.81 x 10^7 sec (~209 days).

Hence all nanotube wiring bundles for the FGN can be fabricated and assembled into network bundles in ~209 days. Since the total buildout time for the FGN is 3.48 x 10^7 sec (~403 days) (Section 3.11.10.5), this leaves up to ~194 days, or ~48% of the total buildout cycle time, for installation operations in which the wiring networks are installed on the fabrication planes comprising the FGN.

The manufacture of all wiring bundles for 1000 fabrication planes in the FGN incorporates ~4.34 x 10^{23} atoms in 2-nm-diameter wires having an approximate displaced volume of ~π(2 nm / 2)^2 (4.34 x 10^{23} atoms) / (200 x 10^9 atoms/meter) (1000 planes) = 6.82 x 10^{-9} m^3 per fabrication plane, a volume of wires which could be stacked on 10% of the wafer surface to a depth of only 341 nm in on-wafer harnesses, racks, or other jigs that are used to depot initial, intermediate and finished wiring structures prior to installation in the FGN. The remaining 20% of wafer surface is reserved for on-wafer MAM-class manipulators that may be used to withdraw wire networks from the depots and install them as wiring bundles on an opposing plate surface.

An alternative manufacturing method could make use of the presence of DMS-capable NMW-2 modules on the same wafer as the MAMs: Short (100 nm) segments of nanotube wire could be manufactured with reactive (unterminated) ends which could then be butted against each other and should fuse to form a single continuous length of nanotube. This latter approach should be further investigated because it could be the most convenient way to install the stovepipe wiring bundles which must run vertically as well as horizontally throughout the FGN.

What about wire manufacturing reliability? The DMS fabrication error rate is 3.2 x 10^{-19} at 109 K (Section 3.8.1.3); a 2-nm-diameter metallic carbon nanotube wire has ~200 atoms/nm of linear run, so DMS-related error misplaces one atom every ((3.2 x 10^{-19}/atom)(200 atoms/nm))$^{-1}$ = 1.56 x 10^7 meters of nanotube wire. In the FGN, 1000 fabrication planes have $N_{fplWires}$ ~ 3.36 x 10^{18} wires of total length $L_{fplWires}$ = 2.2 x 10^{12} meters, hence average wire length is $L_{fplWires}$ / $N_{fplWires}$ ~ 655 nm; so we expect wires containing one misplaced atom to occur at the (655 nm / 1.59 x 10^7 m) ~ 4.12 x 10^{-14} rate, which implies the presence of ~138,000 single-atom-misplacement wires (out of 3.36 x 10^{18} wires total) in the first production layer (1000 fabrication planes) of the FGN. Further analysis is required to determine if this misplacement error rate will significantly degrade FGN performance, or whether an intermediate inspection stage should be added to the process.

3.11.7 Task X-4: Build FGN Assembly System and Vacuum Room

The FGN Assembly System includes at least the following mechanical subsystems, all of which must be capable of operating for extended periods of time inside a UHV vacuum environment:

(1) **NMW-2 Wafer Plate Handlers**. Each plate handler mechanism should fit within a ~20 cm cube or an ~8000 cm^3 volume, so 1024 NMW-2 plate handlers represent a total mechanism volume of 8.192 m^3, so to run all plate handlers simultaneously in factory mode probably requires at least ~10 m^3 of pumpable UHV volume (Section 3.9.5).

(2) **MAA Wafer Plate Handlers**. Each plate handler mechanism should fit within a 40 cm x 50 cm x 10 cm rectangular prism; allowing a 1 cm clearance between plates, that's ~22,000 cm^3 volume per handler, so 200 MAA plate handlers represent a total mechanism volume of 440 m^3 of pumpable UHV volume.

(3) **Inspection Rack Gantry**. This is a manipulator mechanism that can acquire an MAA wafer from the MAA plate handlers and transfer it to the Inspection Rack. A rack containing 200 MAA plate handlers that are 10 cm thick and have a 1 cm separation between handlers can be arranged in square cubbyhole pattern measuring ~(200)(10 cm + 1 cm)(40 cm) ~ 8.8 m^2 in area. Allowing ~57 cm clearance in front of the rack to include 7 cm for gantry mechanism provides (8.8 m^2)(57 cm) ~ 5 m^3 for clearance and gantry mechanism.

(4) **Inspection Rack**. The Inspection Rack should occupy a cylindrical volume measuring roughly 1 m in diameter and 1 m in height (volume ~ 1 m^3), plus another ~1 m^3 to account for the defective parcel removal mechanism, giving a total Rack volume of 2 m^3.

(5) **FGN Assembly Gantry**. This gantry acquires MAA wafers from the Inspection Rack and positions them over the FGN for module installation, then returns the empty MAA wafers to the Rack. We allocate ~2 m^3 for this mechanism.

(6) **FGN Under Construction**. The FGN under construction has a finished volume of 40 cm x 50 cm x 10 cm or ~0.02 m^3. Including appurtenant structures such as gas, electrical, and coolant fluid connections, piping and pumps, and allowing additional clearance to allow easy access to the nanomachinery planes during FGN assembly, we allocate a total of ~10 m^3 for the FGN and its immediate neighborhood. This gives a clearance of ~1 m in every direction around the perimeter of the FGN, which seems sufficient.

(7) **Airlock Passthrough**. We allocate ~1 m^3 for an "airlock" mechanism to allow materials to be transferred into or out of the main vacuum room without breaking vacuum.

(8) **Human Access Corridors**. We allocate ~10 m^3 to allow additional clearance for human access to the machinery inside the FGN factory room.

The total volume of the aforementioned mechanisms and clearances totals 480 m^3. This is equivalent to a factory room with a floor space ~10 m (~33 ft) wide and ~16 m (~52 ft) long, with a ceiling height of ~3 m (~10 ft).

The entire room must be pumped down to, and maintained under, UHV conditions for extended periods of time. Critical issues for maintaining vacuum inside a factory room of such large volume include potentially long pumpdown times due to the large material surface areas that must be allowed sufficient time to degas, possible leakage at equipment joints and seams where walls

join inside the factory room (e.g., the leakage rate through ferro-fluidic rotating shaft seals to be used in ITER is ~10^{-15} atm-m^3/sec),[1272] and the need to design macroscale robotic machinery without hydraulics or exposed joints using potentially volatizable lubricants. Careful attention to the selection of materials with low vapor pressures such as glass, stainless steel, and ceramics will be required.

A 480 m^3 vacuum chamber is certainly very large but not beyond current practice. Large laboratory UHV vacuum chambers typically range from 2 m^3,[1273] to 10 m^3,[1274] in volume. 10^{-10} torr is typical for large nuclear beamline facilities,[1275] but much larger systems such as the 1080 m^3 internal UHV vacuum volume of the proposed ITER fusion reactor[1276] are well-known. ITER requires a base pressure no higher than ~10^{-8} torr during operation but ~10^{-10} torr for non-fuel components,[1277] and there is also ~80 km of cabling inside the ITER vacuum volume.[1278] The world's largest vacuum chamber belongs to NASA: the Space Power Facility (originally built in 1969 and since refurbished several times) that resides at NASA Glenn Research Center's Plum Brook Station in Sandusky, Ohio. The SPF measures 100 feet (~30.5 m) in diameter and 122 feet (~37.2 m) tall giving a total enclosed high-vacuum chamber volume of ~27,000 m^3 (Figure X-11).[1279]

[1272] Nick Balshaw, "Vacuum for Fusion – ITER," Vacuum KTN Meeting, London, March 2007, N.H. Balshaw, UKAEA; http://www.scitech.ac.uk/Resources/PDF/Balshaw.pdf.

[1273] "Ultrahigh Vacuum Chambers – a New Service from ITL," J. Synchrotron Rad. 2(1995):75; http://journals.iucr.org/s/issues/1995/01/00/a28079/a28079.pdf.

[1274] P. Sonato, W.R. Baker, P. Fiorentin, G. Marchiori, P. Zaccaria, G. Zollino, V. Antoni, M. Bagatin, D. Desideri, G. Serianni, L. Tramontin, R. Bertoncello, "The wall conditioning techniques in RFX," Vacuum 47(June-August 1996):977-980.

[1275] "Preliminary Design Report for the VESPERS Beamline at the Canadian Light Source Inc.," 22 November 2005; http://www.uwo.ca/ssw/research/vespers/resources/vespers_pdr_rev0.pdf.

[1276] R.J.H. Pearce, M.E.P. Wykes, C. Lowry, C. Day, V. Hauer, "Requirements and progress in vacuum conductance modeling on ITER," paper 051, 51st IUVSTA Workshop, 9-12 July 2007, Djuronaset, Varmdo, Sweden; http://www.vgd07.dl.ac.uk/Presentaions/Program%20and%20Abstracts.pdf.

[1277] Nick Balshaw, "Vacuum for Fusion – ITER," Vacuum KTN Meeting, London, March 2007, N.H. Balshaw, UKAEA; http://www.scitech.ac.uk/Resources/PDF/Balshaw.pdf.

[1278] Nick Balshaw, "Vacuum for Fusion – ITER," Vacuum KTN Meeting, London, March 2007, N.H. Balshaw, UKAEA; http://www.scitech.ac.uk/Resources/PDF/Balshaw.pdf.

[1279] "World's Largest Vacuum Chamber to Test Orion," 19 June 2007, http://www.nasa.gov/mission_pages/constellation/orion/vacuum_chamber.html; "NASA Space Power Facility – Quick Facts," 24 January 2007; http://facilities.grc.nasa.gov/spf/quick.html.

Figure X-11. World's largest vacuum chamber, the Space Power Facility at NASA Glenn Research Center's Plum Brook Station in Sandusky, Ohio, has a ~27,200 m^3 volume of vacuum.[1280]

External view of facility

Inside the vacuum chamber

The SPF pumping system includes sixteen 48-inch diameter LN_2-baffled electrically heated oil diffusion pumps (pumping speed ~700,000 liters/s) and ten 48-inch diameter cryopumps with vacuum isolation gate valves (pumping speed ~600,000 liters/s), giving a pumpdown time of 2 hours from atmospheric pressure down to 20 torr, 4 hours from 20 torr down to 10^{-3} torr, and another 2-6 hours from 10^{-3} torr down to 10^{-6} torr.[1281] Adding more cryopumps or using longer pumpdown times presumably would allow the NASA system to reach UHV conditions inside this extremely large volume.

Note that after construction, the FGN might be operated outside the large FGN Assembly System vacuum room. An isolated FGN would probably occupy at least ~10 m^3 of physical volume including appurtenant support structures and equipment such as feedstock gas supply cylinders,

---

[1280] "World's Largest Vacuum Chamber to Test Orion," 19 June 2007, http://www.nasa.gov/mission_pages/constellation/orion/vacuum_chamber.html; "NASA Space Power Facility – Quick Facts," 24 January 2007; http://facilities.grc.nasa.gov/spf/quick.html.

[1281] "NASA Space Power Facility – Facility Capabilities," 24 January 2007; http://facilities.grc.nasa.gov/spf/capabilities.html.

coolant fluid pumps and associated fluid reservoirs and plumbing, electrical connections and associated wiring and conventional support electronics, external control computers and data caches, and so forth.

3.11.8 Task X-5: Build another 512 NMW-2 Plate Handlers

Task X-5 is to build another 512 NMW-2 plate handlers as previously demonstrated in Task VIII-4 (Section 3.9.5). This allows us to manufacture 1024 platefuls of modules at once, instead of just 512.

3.11.9 Task X-6: Improve Plate Handling Speed by 50-fold

Task X-6 is to reduce the previously-stated ~8 hour plate changeout time (Section 3.8.8) approximately 50-fold to a ~0.18 hour (~640 sec) plate changeout time by improving process efficiencies based on engineering experience, most likely by incorporating significant automation. This speedup seems feasible because all the plates have to do is align, and then grab, and all operations are automated and will take place in a continuously-maintained UHV environment. No sophisticated nanoscale DMS fabrication or assembly operations must be performed by the plate handling systems that might otherwise require significant amounts of extra processing time.

3.11.10 Task X-7: Manufacture and Install 1000 Fabrication Planes and 4 Assembling Planes on FGN Base Plate

Task X-7 is to demonstrate one complete manufacturing and installation cycle for the stack of 1000 fabrication planes comprising the first production layer of the FGN, atop the FGN base plate, followed by the manufacturing and installation of the 4 assembly layers comprising the second production layer of the FGN, atop the first production layer. Our description here ignores the possible need for a slightly thicker catacomb foundation plane on the first (lowest) fabrication plane if an atomically smooth base plate cannot be made available (Section 3.11.5), since installing such a plane one at the bottom of the first production layer stack would add negligible time to the entire process. Our summary description also omits installation details for the stovepipes between fabrication planes, although the mass of the stovepipe subsystem is accounted for in the calculations.

3.11.10.1 Manufacturing NMW-3 Modules

Each of the fabrication planes is assumed to consist of 3.800 x 10^{21} atoms (93.2% of them carbon; Table X-1). Each NMW-2 wafer contains 10^{11} NMW-2 modules each able to fabricate atomically precise modules as complex as themselves (e.g., ~275.1 million-atom NMW-3 modules; Section 3.11.2) at a ~1000 atom/sec net build rate (Section 3.8.8), giving a ~10^{14} atom/sec build rate per wafer. Operating all available 1024 NMW-2 wafers using 1024 plate handlers (512 built in Section 3.9.5, another 512 built in Section 3.11.8) yields a net build rate of ~10^{17} atoms/sec, allowing the components of the first four fabrication planes to be manufactured in (4 planes)(3.800 x 10^{21} atoms/plane) / (10^{17} atoms/sec) ~ 152,000 sec, closely matching the ~128,700 sec cycle of operation for NMW-2 modules (Section 3.8.8) and thus also for the NMW-

2 wafers (Section 3.9). For computational convenience in the following description we'll assume a 4-plane NMW-3 module build time of ~128,700 sec as before.

3.11.10.2 Loading the MAAs with NMW-3 Modules

Every ~128,700 seconds there are ~4 x 10^{13} NMW-3 modules to be manufactured to fill out four complete fabrication planes. Running the 1024 NMW-2 wafers (each containing ~10^{11} NMW-2 units) for one full 128,700 sec cycle produces ~4 x 10^{13} NMW-3 modules along with all appurtenant structures including catacombs, stovepipes, cooling channels and other unallocated structure. Each one of the 100 MAM arrays (MAAs; Section 3.10.1.2) is 40 cm x 50 cm in size and has 2 x 10^{11} MAMs, with each MAM able to pick up one finished NMW-3 module from an NMW-2 wafer and carry it away for installation on the FGN base plate.

The assembly of a fabrication plane begins with the Inspection Rack Gantry reaching into the Inspection Rack and withdrawing an empty MAA. This MAA is brought into contact with 20 of the ~1024 NMW-2 wafers and picks up from those 20 wafers a total of 2 x 10^{11} NMW-3 modules. We presume this transfer can occur as quickly as the NMW-2 wafer plateholders and the MAA plateholders can be mated and calibrated. The MAMs themselves can perform transfer operations at a tip velocity of ~2.6 cm/sec when operated at 120 MHz (Section 3.10.1.1), so a grasping motion across a ~1 micron gap might require only (1 micron)/(2.6 cm/sec) ~ 4 x 10^{-5} sec, but this time will increase up to ~10^{-4} sec (e.g., using ~10^{4} handoff motions/sec; Section 3.11.3.1) when grasp/ungrasp times are added to the transfer time requirement. In Task X-6, the previously-stated ~8 hour plate changeout time (Section 3.8.8) was decreased to ~300 sec (Section 3.11.9). With this improvement, the pickup of the first ~2 x 10^{11} NMW-3 modules by the first MAA requires ~300 sec. Pickup of all ~4 x 10^{13} NMW-3 modules needed to fill out four complete fabrication planes by 200 MAAs is completed in ~60,000 sec, well within the available 128,700 sec production cycle of the NMW-2 wafers.

3.11.10.3 Loading MAAs into the Inspection Rack

The Inspection Rack is a circular rack that can hold up to 4 MAAs at a time in an edgewise vertical orientation, in a "+" pattern viewed from above. The Rack completes ~50 revolutions every 128,700 sec. During each revolution, the Inspection Rack Gantry places a fresh NMW-3-loaded MAA into an open slot in the Rack every ~640 sec. After ~128,000 sec, all 200 MAAs have been placed in the Inspection Rack. As each NMW-2 wafer is emptied, it can be removed and rejoined with another empty NMW-2 wafer and their next 128,700-sec production cycle may begin. When the last (the 200th) MAA is loaded at the ~128,000 sec mark, the last of the empty NMW-2 wafers can begin its next 128,700-sec production cycle, and from then on, production is essentially continuous.

The Inspection Rack turns in 90° increments, once every ~640 sec. The first position is occupied by the newly-arrived fresh MAA. The MAA in the second position is being tested. The MAA in the third position is being removed full, then returned empty ~640 sec later. The MAA in the fourth position is empty, awaiting removal to be refilled with cargo elsewhere. The surplus of MAA wafers are transported by the Inspection Rack Gantry to the MAA wafer handlers that were created in Task IX-6.

After inspection at the second position (see below), the MAA moves to the third position and is presented to the FGN Assembly Gantry, which removes the MAA for further processing elsewhere. Over the course of a 128,700-sec revolution, each of the 200 MAAs in succession is similarly removed, one after the other, until all have been removed full and returned empty. One MAA is removed from the Rack every (128,700 sec)/(201) ~ 640 sec. This allows the first MAA to reside in the Rack for t_1 ~ 640 sec before being removed for further processing elsewhere. Thereafter, one MAA is removed from the Rack every ~640 sec. The last MAA enters the Rack at t_{enter} ~ 127,420 sec and exits the Rack at t_{exit} ~ 128,060 sec, hence has a total residence time in the Rack of $t_{200} = (t_{exit} - t_{enter})$ ~ 640 sec. Hence t_1 ~ 640 sec is the residence time for an MAA in the Rack.

While each MAA resides in the Inspection Rack, the Rack mechanism performs three important functions within the 640-second minimum available time window at the second position:

(1) **Parcel Assembly**. The MAMs on each MAA are instructed to push together their NMW-3 module cargoes into separate parcels containing 10,000 modules per parcel. Each parcel measures 10 microns x 20 microns. Upon pushing the NMW-3 modules together, their electrical connectors are mated, establishing full electrical connectivity between adjacent modules. Transporting one module across the longest 50 cm plate dimension – whether alone or after being incorporated into a module parcel, with MAMs operated as a CTA (Section 3.11.2.7) – at the ~2.6 cm/sec MAM tip speed requires only ~20 sec.

(2) **Parcel Testing**. Each parcel is then tested to make sure it is functional. At minimum, electrical connectivity is verified by sending electric pulses down each control line. All NMW-3 modules connected along a given control line must perform correctly. Other tests may be applied to each parcel, possibly employing specialized testing jigs that are built into the Inspection Rack and assembled using manufacturing systems already demonstrated in Phase VIII and Phase IX. Parcels that do not successfully pass all the tests are flagged as defective. We allocate ~600 sec for this activity.

(3) **Removal of Defective Parcels**. A macroscale manipulator possibly containing MEMS-scale end-effector components reaches across the open face of the MAA being tested on the Inspection Rack and plucks from that MAA surface each parcel that has been flagged as defective. The manipulator removes the defective parcel either for disposal or for rework (if rework is deemed feasible). We allocate ~20 sec for this activity.

A failure rate of 10^{-7} per 10^5 nm^3 "typical smallest" part was assumed for the Inspection Plane subsystem described in Section 3.11.3.1. The NMW-3 module including all component subsystems plus its share of the catacombs and other structures has a volume of (1.461×10^{-8} m^3/plane) / (10^{13} NMW-3 modules/plane) ~ 1.461×10^6 nm^3/module (Table X-1) though this includes a higher 200 nm ceiling to provide greater overhead clearance so the NMW-3 module has a bit more empty space than the "typical smallest" part. Adopting the same failure rate per nm^3 as before and assuming a ~10^6 nm^3 volume for NMW-3 modules, the failure rate for NMW-3 modules is expected to be ~10^{-6}. Therefore we expect a per-parcel failure rate of ~10^{-2} with ~1% of all parcels removed for disposal or rework, giving a ~99% pass rate on all parcels.

Thus the full mass flow of ~4×10^{13} NMW-3 modules are processed through the Inspection Rack every 128,700 sec, and all surviving parcels of modules have been tested and are known to be functional.

If 40 cm x 50 cm MAA wafers prove too unwieldy, the Inspection Rack can be redesigned to handle ~200 smaller 10 cm x 10 cm wafers using a 20-fold faster processing speed.

3.11.10.4 Unloading the Rack and Installing NMW-3 Parcels

Every ~640 sec, the FGN Assembly Gantry removes one MAA from the Inspection Rack and applies that MAA to the growing FGN. Since each MAA is ~2000 cm^2 in area and the FGN base plate is ~2000 cm^2 in area with the same dimensions, each loaded/inspected MAA can be applied directly to the FGN base plate to deliver its cargo of ~2 x 10^{11} NMW-3 modules that have been pre-assembled into ~2 x 10^7 parcels and tested. After positioning over, and alignment with, the FGN base plate or the fabrication plane currently under construction using the Assembly Gantry, the MAMs on the MAA are operated as a digitally precise ciliary array (e.g., a Ciliary Transport Array; Section 3.11.2.7) so as to install all ~2 x 10^7 parcels into a ~40 cm^2 section measuring 8 cm (8000 parcels extending in the 10-micron direction, parallel to y_{FGN}) x 5 cm (2500 parcels extending in the 20-micron direction, parallel to x_{FGN})) of one fabrication plane on the growing FGN. Completion of 50 such deliveries installs one complete ~2000 cm^2 of fabrication plane surface, and 200 deliveries completes the assembly of 4 fabrication planes in 128,700 sec.

We allow ~640 sec of MAA-handling time for cargo delivery to the FGN base plate, including all necessary parcel positioning, joining, testing, and other handling operations to assure correct installation. Once a cycle is complete, the discharged MAA is returned empty to the Inspection Rack to await refilling during the next production cycle while the FGN Assembly Gantry picks up the next MAA and repeats the 640 sec cycle. The buildout time for four fabrication planes may therefore be approximated as (4 fabrication planes)(10^{13} NMW-3 modules/fabrication plane)(640 sec/delivery cycle) / (2 x 10^{11} NMW-3 modules/delivery cycle)} ~ 128,000 sec, closely matching the 128,700 sec production cycle of the NMW-2 wafers.

A small number of MAA-size wiremaking wafers (Section 3.11.6) are employed at the end of each fabrication plane installation cycle to lay down all wiring bundles for the next plane that is to be installed.

3.11.10.5 Assembly of FGN Production Stacks and Total Assembly Time

First, we require ~128,700 sec to manufacture the first batch of 4 x 10^{13} NMW-3 modules to initiate the FGN-building process.

After that the installation process proceeds continuously at the rate of 128,700 sec per 4 fabrication planes installed, for a total 250 cycles to make 1000 fabrication planes to complete the first production layer of the FGN. The last (250th) production cycle of the NMW-2 wafers is used to build components to start the second production layer of the FGN.

The second production layer of the FGN consists of an additional four assembling planes totaling 6.789 x 10^{22} atoms, roughly equivalent to ~18 fabrication planes (each of which totals ~3.800 x 10^{21} atoms).

Hence the total buildout time for the FGN is ~(268 production cycles)(128,700 sec/cycle) / (99% pass rate) = 3.48 x 10^7 sec (~13 months). Buildout time can be reduced in direct linear proportion

to any simultaneous proportional reduction in both (a) the 128,700 sec production cycle time (e.g., by increasing pulse frequency higher than 120 MHz) and (b) the 640-sec MAA handling and inspection time (e.g., by improving automation efficiencies).

It may be desirable to design and build the collection cylinders in the Export Plane to be detachable, to facilitate their easy removal in Phase XI (allowing MAAs to pick up finished micron-scale product objects directly from the Export Plane) to facilitate the completion of Task XI-2 (Section 3.12.5) and avoid the need for rebuilding a second FGN to assist in the construction of the first SGN during Phase XI.

3.11.11 Task X-8: Manufacture, Attach and Test Appurtenant FGN Support Equipment

Task X-8 is to manufacture and complete the attachment of support equipment to the completed FGN. FGN sidewall connections to feedstock gas supply and byproduct gas exhaust hose bibs must be made. Additional sidewall connections to the extensive electrical wiring coming from each productive machinery plane must be established and tested. Finally, cooling fluid supply lines must be mated to the ~1000 cooling channels passing through the FGN.

Feedstock and byproduct gas flows and electrical connectivity must be tested and verified.

If the coolant fluid includes a suspension of microscale or nanoscale ice particles at a volume fraction of f_{ice} ~ 20% (Section 3.11.2.9), then the method for producing this fluid suspension in macroscale quantities must be specified, simulated, and demonstrated experimentally.

Coolant fluid channel leaktightness may be verified by testing first with low-pressure gas, intrusion of which through a leak can be detected using a small number of sensors installed in every fabrication plane throughout the FGN. Once leaktightness is verified, coolant fluid flows through the device can then be tested and validated at the anticipated temperatures and flow rates that will normally occur during FGN operation.

3.11.12 Task X-9: Demonstration of Diamondoid FGN Production

Task X-9 is to operate the FGN, once it is completed, in full production mode to verify that it can manufacture atomically precise micron-scale product objects at the desired total mass-flow rate of ~0.01 kg/hour (~1 mole/hour).

3.12 Phase XI: Second-Generation Nanofactory (SGN)

The key objective of Phase XI is to build out the first desktop nanofactory capable of manufacturing atomically precise diamondoid macroscale product objects at ~0.01 kg/hour production rates. A description of one typical high-value product, along with estimates of overall SGN productivity and the potential profitability of manufacturing the exemplar high-value product using the SGN, are given in Section 3.12.1.

The basic architecture of the (diamondoid) second-generation nanofactory (SGN) is briefly described in Section 3.12.2 (Figure XI-1), incorporating into the FGN design the third production layer for macroscale assembly for the SGN (Section 3.12.3). This is followed by an enumeration of the specific tasks required to design, manufacture and operate the SGN, which include: design, modeling and simulation of FGN components, operations, and the process of SGN manufacture (Section 3.12.4), manufacturing a new FGN with an open export plane (Section 3.12.5), building or updated an SGN assembly system and vacuum room similar to the system previously used for the FGN (Section 3.12.6), manufacturing and installing the four macroassembling planes and the VES on a modified FGN base (Section 3.12.7), manufacturing, attaching and testing the appurtenant SGN support equipment (Section 3.12.8), and finally the demonstration of SGN production of macroscale diamondoid product objects in macroscale quantities (Section 3.12.9).

The possibility of designing and building a more compact and energy-efficient diamondoid desktop nanofactory as an industrial product of the SGN is discussed briefly in Section 3.12.10.

3.12.1 SGN Productivity, Products, and Profitability

The second-generation nanofactory (SGN) will be capable of manufacturing atomically precise diamondoid macroscale product objects at ~0.01 kg/hour (e.g., ~10^{20} atoms/sec, ~10^{18} nm^3/sec, ~1 mole/hour) production rates. Like the FGN, the SGN will produce ~100 cm^3/day (~240 gm/day) of atomically precise high-density macroscale product having a mean density of ~2.4 gm/cm^3 (i.e., products are about two-thirds (~68%) solid diamond and about one-third (~32%) vacuum, by volume).

What sorts of representative product objects might the SGN manufacture? One notable example is high-performance ~1 exaflop (~10^{18} floating-point operations/sec)[1282] "CPU dice" that could serve as the computational heart of a handheld supercomputer measuring 8 cm x 12 cm x 1.04 cm (~100 cm^3 in volume) that could fit in your pocket. Leading supercomputers already achieving ~10^{14} flops in 2008 are projected to reach ~10^{18} flops by 2028 assuming a constant 18-month doubling time, following Moore's Law, but such computers typically fill large rooms. The SGN's ability to manufacture a handheld exaflop supercomputer by 2028 would represent a substantial improvement over traditional Moore's Law progress. It would be possible to

---

[1282] "One million trillion 'flops' per second targeted by new institute," Science blog, 21 February 2008, http://www.scienceblog.com/cms/one-million-trillion-flops-second-targeted-new-institute-15534.html; "Fastest Computer: One Million Trillion 'Flops' Per Second Targeted," 22 February 2008, http://www.nccs.gov/2008/02/22/fastest-computer-one-million-trillion-flops-per-second-targeted/.

manufacture one such handheld exaflop supercomputer per day using the SGN, but most of the components of the pocket supercomputer such as batteries, keypad, I/O connections, and the display need not be manufactured to atomic precision. These components would more economically be produced using conventional semiconductor lithography and other legacy microscale or macroscale manufacturing technologies such as the ~micron-resolution solid printing and 3D fabbing techniques previously described in Section 2.2.3.

Figure XI-1. Basic architecture of the second-generation nanofactory (SGN); not to scale.

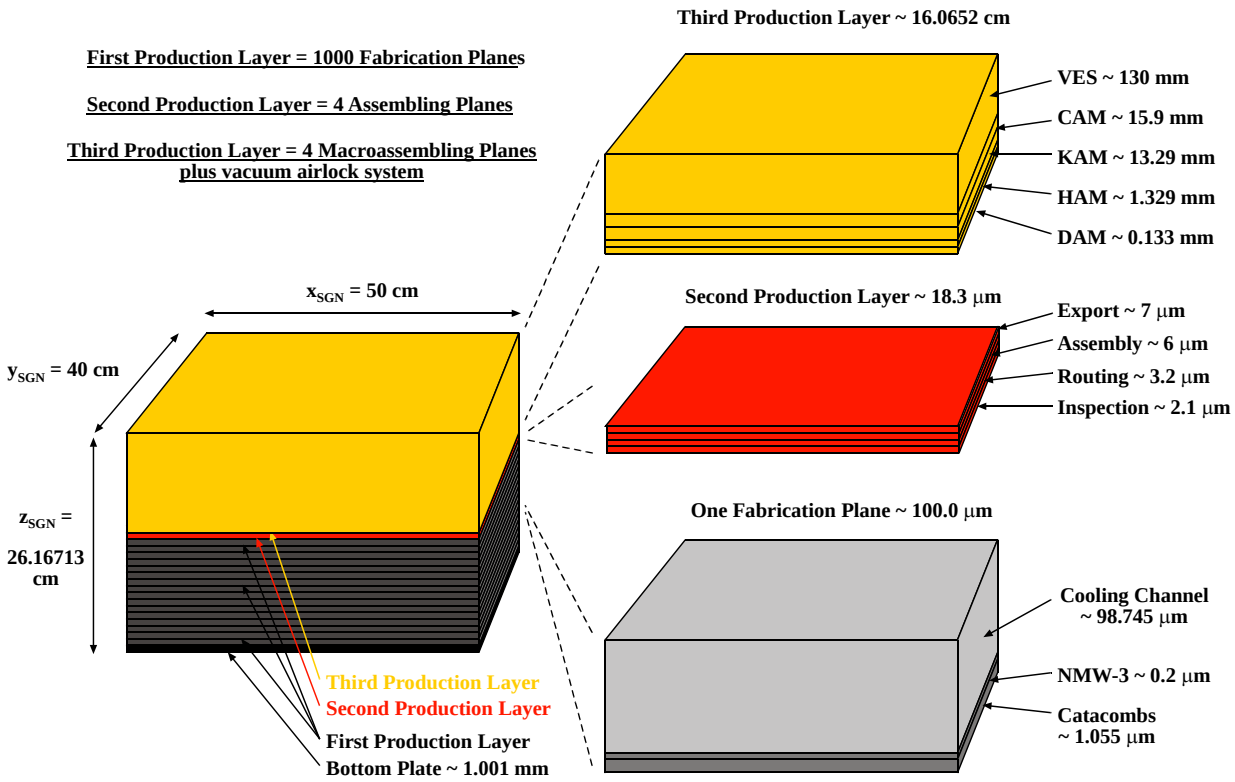

A single ~1 exaflop CPU dice entirely composed of mechanical computational elements for CPU and memory[1283] should exhibit performance on the order of ~2 x 10^{16} operations/sec-W and ~10^{28} operations/sec-m^3,[1284] hence each exaflop CPU dice dissipates ~50 W of waste heat and has a computational kernel ~10^{-10} m^3 (~10^{17} nm^3, ~0.1 mm^3) in volume, consisting of 10^9 CPU cores

---

[1283] K. Eric Drexler, Nanosystems: Molecular Machinery, Manufacturing, and Computation, John Wiley & Sons, New York, 1992, Chapter 12, pp. 342-371.

[1284] Robert A. Freitas Jr., Nanomedicine, Volume I: Basic Capabilities, Landes Bioscience, Georgetown, TX, 1999; Section 10.2.1, pp. 343-345; http://www.nanomedicine.com/NMI/10.2.1.htm#p6.

per dice assuming ~10^8 nm^3 and 10^6 interlocks (transistor-equivalents) per ~1 GHz CPU core.[1285] We allow an additional ~0.9 mm^3 for atomically precise diamondoid interfaces, interconnects, cooling channels and other support structure, giving ~1 mm^3 volume (or ~0.0024 gm) for each 1-exaflop CPU dice. Since electrons can be moved faster than atoms, electronic or even quantum[1286] supercomputer cores should be smaller and more efficient than mechanical computational systems[1287] – the latter is adopted here only to provide a conservative estimate of likely capabilities and because sufficient system-level mechanical nanocomputer architectural details have been published[1288] to permit a valid scaling calculation. (By 2008: (a) carbon nanotube transistors having an ~18 nm channel line (Figure XI-2) had been built,[1289] which is somewhat larger than the proposed ~16 nm^3 interlock volume[1290] for a mechanical CPU assumed above, and transistor action has been observed in single-walled graphene quantum dots in nanometer-scale quantum confinement regions (current experimental processes permit ~10 nm feature sizes; devices smaller than ~30 nm are dominated by quantum confinement effects),[1291]

[1285] K. Eric Drexler, Nanosystems: Molecular Machinery, Manufacturing, and Computation, John Wiley & Sons, New York, 1992, Chapter 12, pp. 342-371.

[1286] M.V.G. Dutt, L. Childress, L. Jiang, E. Togan, J. Maze, F. Jelezko, A.S. Zibrov, P.R. Hemmer, M.D. Lukin, "Quantum register based on individual electronic and nuclear spin qubits in diamond," Science 316(1 June 2007):1312-1316.

[1287] K. Eric Drexler, Nanosystems: Molecular Machinery, Manufacturing, and Computation, John Wiley & Sons, New York, 1992, Chapter 12, pp. 342-371. C.P. Lutz, A.J. Heinrich, J.A. Gupta, D.M. Eigler, "Molecule cascades: nanometer-scale molecular architectures that compute," TRANSDUCERS, Solid-State Sensors, Actuators and Microsystems 1(June 2003):5-8, http://ieeexplore.ieee.org/xpl/freeabs_all.jsp?tp=&arnumber=1215239&isnumber=27333; D.M. Eigler, C.P. Lutz, M.F. Crommie, H.C. Mahoran, A.J. Heinrich, J.A. Gupta, "Information transport and computation in nanometre-scale structures," Phil. Trans. R. Soc. Lond. A 362(2004):1135-1147. Laura Pescini, Heribert Lorenz, Robert H. Blick, "Mechanical gating of coupled nanoelectromechanical resonators operating at radio frequency," Appl. Phys. Lett. 82(2003):352-354, http://www2.nano.physik.uni-muenchen.de/publikationen/2003/03_01_Pescini_APL.pdf; Robert L. Badzey, Guiti Zolfagharkhani, Alexei Gairdazhy, P. Mohanty, "A Controllable Nanomechanical Memory Element," Appl. Phys. Lett. 85(18 October 2004):3587-3589; R.H. Blick, H. Qin, H.S. Kim, R. Marsland, "A nanomechanical computer: Exploring new avenues of computing," New Journal of Physics 9(2007):241-249, http://www.iop.org/EJ/article/1367-2630/9/7/241/njp7_7_241.pdf; H.S. Kim, H. Qin, R.H. Blick, "Direct mechanical mixing in a nanoelectromechanical diode," Appl. Phys. Lett. 91(2007):143101.

[1288] K. Eric Drexler, Nanosystems: Molecular Machinery, Manufacturing, and Computation, John Wiley & Sons, New York, 1992, Chapter 12, pp. 342-371.

[1289] "World's smallest nanotube transistor," The Engineer Online, 22 November 2004, http://secure.theengineer.co.uk/Articles/266769/World's+smallest+nanotube+transistor.htm; "Infineon Unveils World's Smallest Nanotube Transistor," Nanotechnology Now, 22 November 2004, http://www.nanotech-now.com/news.cgi?story_id=06788.

[1290] K. Eric Drexler, Nanosystems: Molecular Machinery, Manufacturing, and Computation, John Wiley & Sons, New York, 1992, Chapter 12, pp. 342-371.

[1291] L.A. Ponomarenko, F. Schedin, M.I. Katsnelson, R. Yang, E.W. Hill, K.S. Novoselov, A.K. Geim, "Chaotic Dirac Billiard in Graphene Quantum Dots," Science 320(18 April 2008):356-358;

so molecular manufacturing should make it possible to build very small electronic devices; (b) nanotube transistors[1292] and related nanoelectromechanical components[1293] had been operated at >1 GHz switching frequencies, even up to 23 GHz for CNFETs;[1294] and (c) diamond semiconductor devices had been operated up to 81 GHz.[1295]) A ~10^{17} nm^3 CPU dice kernel composed of ~10^{11} modules each measuring ~10^6 nm^3 in volume and ~2.4 x 10^{-18} kg in mass has a mean time to failure of ~3000 years per module due to radiation damage[1296] – after ~1 year of operation, ~0.03% of the modules in the CPU dice kernel will have failed, so the supercomputer architecture must incorporate sufficient redundancy to remain functional given the predicted module failure rate.

Figure XI-2. A carbon nanotube transistor having an ~18 nm channel line has been demonstrated experimentally.[1297]

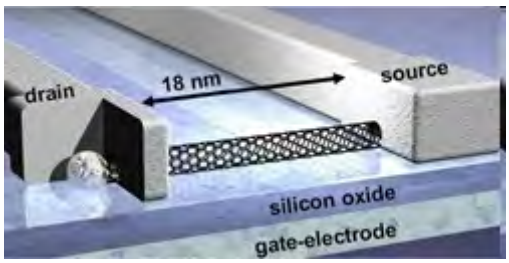

---

http://www.sciencemag.org/cgi/content/abstract/320/5874/356 and http://onnes.ph.man.ac.uk/nano/Publications/Science_QD_2008.pdf.

[1292] J. Chaste, L. Lechner, P. Morfin, G. Fève, T. Kontos, J.-M., Berroir, D.C. Glattli, H. Happy, P. Hakonen, B. Plaçais, "Single Carbon Nanotube Transistor at GHz Frequency," Nano Lett. 8(January 2008):525-528; http://pubs.acs.org/cgi-bin/abstract.cgi/nalefd/2008/8/i02/abs/nl0727361.html.

[1293] Xue Ming, Henry Huang, Christian A. Zorman, Mehran Mehregany, Michael L. Roukes, "Nanoelectromechanical systems: Nanodevice motion at microwave frequencies," Nature 421(30 January 2003):496, http://www.nature.com/nature/journal/v421/n6922/abs/421496a.html.

[1294] Aaron A. Pesetski, James E. Baumgardner, Erica Folk, John X. Przybysz, John D. Adam, Hong Zhang, "Carbon nanotube field-effect transistor operation at microwave frequencies," Appl. Phys. Lett. 88(13 March 2006):113103; http://link.aip.org/link/?APPLAB/88/113103/1.

[1295] Yoshiko Hara, "NTT verifies diamond semiconductor operation at 81 GHz," EE Times, 22 August 2003, http://www.eetimes.com/story/OEG20030822S0005.

[1296] K. Eric Drexler, Nanosystems: Molecular Machinery, Manufacturing, and Computation, John Wiley & Sons, New York, 1992, Section 6.6 "Radiation Damage," pp. 154-156.

[1297] "World's smallest nanotube transistor," The Engineer Online, 22 November 2004, http://secure.theengineer.co.uk/Articles/266769/World's+smallest+nanotube+transistor.htm; "Infineon Unveils World's Smallest Nanotube Transistor," Nanotechnology Now, 22 November 2004, http://www.nanotech-now.com/news.cgi?story_id=06788.

The potential profitability of nanofactory manufacturing using the SGN is nothing short of astonishing. Consider the following crude estimate of revenue, cost and profit for the exaflop CPU dice product.

The proposed SGN can manufacture (100 cm^3/day) / (1 mm^3/CPU dice) ~ 10^5 exaflop CPU dice every day. We further assume that each SGN can be operated 92.1% of the time with 7.9% reserved for downtime and maintenance (e.g., a typical target in the semiconductor industry is <5% unscheduled downtime for equipment availability,[1298] or ~2% median equipment downtime among the top 4% of world-class manufacturers[1299]). If each CPU dice can be sold for ~$744 – the same price as the 64-bit 1-GHz 62-watt low-voltage Itanium-2 CPU "Deerfield" chip manufactured by Intel in 2008[1300] – as the key data processing component inside a handheld supercomputer that retails for ~$2000, then a gross revenue of R_{SGN} = (10^5 CPU dice/day) (365 days/year) ($744/CPU dice) (92.1% SGN duty cycle) = $25.01 billion/year could be generated by one SGN on total pocket-supercomputer sales of ~$67 billion/year.

The cost of material inputs to operate the SGN is low. Specifically, the cost of the ethylene feedstock gas is C_{SGNgas} = ($1/gm) (240 gm/day) (365 days/year) = $87,600/year, assuming a ~$1/gm cost for 5N ethylene gas (based on 18 March 2008 quotes from Praxair[1301] of $4.63/gm for 150 gm lecture bottles, and from ST Gas Ltd.[1302] of $1.37/gm for 110 gm lecture bottles and $0.0848/gm for 16 kg cylinders) which was ~1000 times the typical ~$0.5/lb wholesale price of 98.5% (1N) commercial grade ethylene in 2007.[1303] The cost of electrical power to run the ~11 MW nanofactory is $C_{SGNelect}$ = (~11 x 10^6 W) ($2.78 x 10^{-8}/W-sec) (3.14 x 10^7 sec/year) = $9.60 x 10^6/year, taking the cost of electrical power at today's typical $0.10/kW-hr rate. Therefore the total material production costs for operating one SGN are $C_{SGNprod}$ ~ C_{SGNgas} + $C_{SGNelect}$ = $9.6876 million/year to produce 87,600 gm/year, a unit materials production cost (excluding capital and human labor costs) of C_{SGNgm} ~ $111/gm. This implies an annual net operating income for one SGN, excluding amortized capital outlays and human labor, of I_{SGN} = R_{SGN} – $C_{SGNprod}$ = $25.00 billion/year when manufacturing the CPU dice product.

[1298] Joseph J. Chamberlain, John Nunes, "Service Parts Management: A Real-life Success Story," Supply Chain Management Review, 1 September 2004; http://www.scmr.com/article/CA477303.html.

[1299] "A Manager's Guide to Overall Equipment Effectiveness (OEE)," MMS Online, 2003; http://www.mmsonline.com/articles/ac050505.html.

[1300] Vladimir Romanchenko, "Intel Deerfield: Low Voltage Itanium 2," 7 March 2008; http://www.digit-life.com/articles2/intel/intel-sep-2k3.html.

[1301] Gloria Winters, Praxair Distrib. Inc., personal communication to Robert A. Freitas Jr., 18 March 2008.

[1302] Stephen Haywood, Scientific and Technical Gas Ltd., UK, personal communication to Robert A. Freitas Jr., 18 March 2008.

[1303] "ICIS Students, Indicative Chemical Prices A-Z," http://www.icis.com/StaticPages/A-E.htm; Tom Stundza, "Benzene prices slide; ethylene prices rise," Purchasing.com, 8 August 2007, http://www.purchasing.com/article/CA6466597.html; "Petrochemicals firms take a stand against oil price volatility" Market Focus, www.eprm.com, May 2003, pp. 54-55; http://www.gvsi.com/download/editorials/Mrktfocs-May-03.pdf.

The productive lifetime of an SGN is a function both of the NMW-3 module failure rates and of the tolerance of the SGN for accumulated failed modules (Section 3.11.4), and other factors. As previously noted, the 1000 fabrication planes of the SGN (subsuming the vast majority of active failure-prone mechanisms inside the SGN) collectively contain 10^{16} NMW-3 modules (Section 3.12.2) with an assumed failure rate from all causes of ~3 x 10^{-11} sec^{-1} (Section 3.8.1.3), so during continuous operation ~300,000 NMW-3 modules fail every second, on average, somewhere inside the SGN. After 1 year of SGN operation, ~10^{13} modules or ~0.1% of all NMW-3 modules in the SGN will have failed, so an SGN operating lifetime up to ~10 years (the ~1% failed-module threshold) does not seem unreasonable. In principle, the materials replacement and energy cost to build a new SGN containing ~31.54 kg of atomically precise components (Section 3.12.3.7), using an SGN, is only (31.54 kg/SGN)($111/gm) ~ $3.5 million/SGN – though this ignores the ($310,000/gm)(31.54 kg) ~ $9.8 billion opportunity cost incurred while the SGN was not manufacturing the high-value CPU dice product to be sold at market prices.

3.12.2 Basic Architecture of the SGN

The second-generation nanofactory (SGN) is almost identical to the first-generation nanofactory (FGN) in shape, size, method of manufacture, and operation. The SGN is conceptualized as a box measuring 50 cm wide x 40 cm deep x ~44 cm tall – a reasonable size for a "desktop" unit, about the size of a copier machine (Figure XI-1). The SGN has the same mass throughput as the FGN but can manufacture atomically precise macroscale product objects up to 10,000 cm^3 in volume within a 40 cm x 25 cm x 10 cm product dimensional size envelope. Like the FGN (Section 3.11.1), the operating temperature of the SGN is 109 K.

The SGN has three production layers of equal horizontal dimensions, each spanning ~0.2 m^2 of planar surface per layer.

In the first production layer, identical to the FGN (Section 3.11.2), there are 1000 fabrication planes, with each plane building nanoscale components up to 100 nm in size at the ~10^{17} atom/sec rate, or ~10^{20} atoms/sec for all 1000 planes. The entire first production layer of the SGN contains 10^{16} NMW-3 modules, as in the FGN.

In the second production layer, almost identical to the FGN (Section 3.11.3), there are four planes of assembly-related machinery that together can build larger-scale components up to ~5 microns in size, also at the ~10^{20} atom/sec rate. The second production layer of the SGN differs from the same layer in the FGN only in the Export Plane (Section 3.11.3.4): in the SGN, the square collection cylinders, square pistons, and drainage cylinders on the topside surface of the Export Plane are replaced with a third production layer that lies above.

Unique to the SGN, the third production layer consists of 4 pairs of macroassembling planes topped off with a vacuum airlock mechanism to allow export of finished macroscale products without breaking vacuum and contaminating the internal UHV environment. The function of the third production level is to assemble ~5 micron (~100 $micron^3$) parts into macroscale product objects up to ~10,000 cm^3 in size. For simplicity the current design for the third production layer does not include an inspection plane. One or more inspection planes could readily be added to the third production layer design without significantly altering SGN size, atom count, or mass throughput, if needed to achieve adequate manufacturing reliability with acceptably low defect rates.

3.12.3 Description of the Third Production Layer and SGN

Four functional planes of manipulator arrays of tenfold larger scale in each successively higher machinery plane comprise the manufacturing core of the third production layer of the SGN. The first macroassembling plane is the Dekamicro-Assembly Manipulator (DAM) plane (Section 3.12.3.2), which is followed by the Hectomicro-Assembly Manipulator (HAM) plane (Section 3.12.3.3), the Kilomicro-Assembly Manipulator (KAM) plane (Section 3.12.3.4) and the Centimeter-Assembly Manipulator (CAM) plane (Section 3.12.3.5). Each of the four manipulator planes is paired with a scale-matched export plane, analogous to the Assembly Plane (Section 3.11.3.3) and Export Plane (Section 3.11.3.4) pair in of the FGN. Above the topmost manipulator plane lies the Vacuum Export System (Section 3.12.3.6), which has an output port that can accommodate a finished macroscale product object having physical dimensions up to 40 cm (running parallel to the y_{SGN} = 40 cm dimension) x 25 cm (running parallel to the x_{SGN} = 50 cm dimension) x 10 cm tall. The SGN structure is summarized in Section 3.12.3.7.

3.12.3.1 Parts Feed Into the Third Production Layer

The third production layer receives microscale parts from the second production layer (Section 3.11.3) that arrive through 10^8 export holes in the Export Plane (Section 3.11.3.4). The export holes are arranged in rows of 40,000 holes per row, with holes within each row spaced 10 microns apart center-to-center. The rows run parallel to the 40 cm dimension of the SGN and there are 2500 rows of export holes, spaced alternately 240 microns and 160 microns apart along the 50 cm dimension of the SGN. For simplicity in this design exercise, we shall assume that all parts arriving from the second production layer are the largest size possible, namely ~5 micron (~100 micron^3) parts. In this case, parts arrive at the Dekamicro-Assembly Manipulator (DAM) Plane (Section 3.12.3.2) from the Export Plane at the rate of 10^7 parts/sec, which means that 1 part/sec emerges from every tenth export hole along a row of export holes.

3.12.3.2 Dekamicro-Assembly Manipulator (DAM) Plane

The Dekamicro-Assembly Manipulator (DAM) Plane acquires 10^7 parts/sec of input parts of size ~5 micron (~100 micron^3) from the 10^8 holes in the Export Plane (Section 3.11.3.4) of the second production layer, assembles 1000 of them into a 10 x 10 x 10 array making output parts of size ~50 micron (~10^5 micron^3), then exports these output parts at a 10^4 parts/sec rate to the HAM Plane (Section 3.12.3.3) through the DAM Export Plane which has 10^6 holes spaced 1000 microns apart center-to-center within each row of holes. There are 400 holes per row running parallel to the 40 cm dimension of the SGN, and there are 2500 rows of holes spaced 200 microns apart along the 50 cm dimension of the SGN. Hence 0.1 input parts/sec enter the DAM Plane from every Export Plane hole and 0.01 output parts/sec exit the DAM Plane through every DAM Export Plane hole.

The DAM Plane consists of an array of ~2 x 10^9 DAMs, each of which is assumed to be a 6-DOF (degrees-of-freedom) manipulator similar to the MAM (Section 3.10.1.1) but ten times larger in every dimension, allowing a 6.8 micron-20 micron reach envelope with a 10 micron x 10 micron footprint on the DAM Plane floor and ~1 micron thick foundation blocks. Each DAM has a solid volume of 160 micron^3, a passivated surface area of ~1576.41 micron^2, a tip speed of ~2.6 cm/sec with 2 nm step increments, and a worst-case continuous power draw of (8 motors x 200 nW/motor) ~ 1600 nW per DAM at a 120 MHz pulse control frequency, giving a total power

draw of ~3200 W for the entire DAM Plane. Like the Export Plane (Section 3.11.3.4), the DAM Export Plane consumes negligible power (~0.003 W) during operation.

The flow of input parts across the DAM Plane follows the same basic pattern as three successive planar 10:1 convergent assembly sets analogous to those previously described for the Assembly Plane of the FGN (Section 3.11.3.3). These assembly sets include a large number (~186 x 10^7) of high-speed transport DAMs, a smaller number (~12 x 10^7) of assembly DAMs, ~6 x 10^7 transfer assembly DAMs, and ~1 x 10^7 export DAMs that are individually addressable and controllable in the entire DAM Plane.

The DAM Export Plane must accommodate ~50 micron output parts and thus lies 60 microns above the DAM Plane to provide adequate clearance between planes. The ~0.2 m^2 DAM Export Plane consists of two flat 1 micron thick diamondoid parallel plates each comprised of 2 x 10^9 foundation blocks each 100 $micron^2$ in area similar in design to the 1 $micron^2$ MAM foundation blocks. The opposing faces of the two plates are separated by 70 microns and are perforated with a total of 10^6 square DAM Export holes measuring 50 micron x 50 micron in size, thus displacing (counting the open area plus an identical blade area) ~5.0 x 10^7 or 2.5% of the 2 x 10^9 100-$micron^2$ foundation blocks in each plate. Providing support between these two planes are 1.25 x 10^5 support columns spaced 0.4 mm apart in the x_{SGN} dimension and 4 mm apart in the y_{SGN} dimension, and measuring 100 $micron^2$ x 60 micron in size – the footprint of each support column replaces one DAM foundation block, and support columns are located maximally distant from DAM Export Plane holes to minimize geometric interference. Additionally, hole DAMs must be able to lift the 50 micron output part at least 60 microns up from the DAM Plane floor in order to guarantee full reliable insertion into the DAM Export Plane hole. Therefore the reach of the hole DAMs must be extended from the usual 20 micron maximum to ~60 microns, using a design similar to that previously described for the hole MAMs (Section 3.11.3.3). A perimeter wall 1 micron thick and 60 microns tall seals the DAM and DAM Export Planes against vacuum loss.

3.12.3.3 Hectomicro-Assembly Manipulator (HAM) Plane

The Hectomicro-Assembly Manipulator (HAM) Plane acquires 10^4 parts/sec of input parts of size ~50 micron (~10^5 $micron^3$) from the 10^6 holes in the DAM Export Plane (Section 3.12.3.2), assembles 1000 of them into a 10 x 10 x 10 array making output parts of size ~500 micron (~0.1 mm^3), then exports these output parts at a 10 parts/sec rate to the KAM Plane (Section 3.12.3.4) through the HAM Export Plane which has 10^4 holes spaced 10 mm apart center-to-center within each row of holes. There are 40 holes per row running parallel to the 40 cm dimension of the SGN, and there are 250 rows of holes spaced 2000 microns apart along the 50 cm dimension of the SGN. Hence 0.01 input parts/sec enter the HAM Plane from every DAM Export Plane hole and 0.001 output parts/sec exit the HAM Plane through every HAM Export Plane hole.

The HAM Plane consists of an array of ~2 x 10^7 HAMs, each of which is assumed to be a 6-DOF (degrees-of-freedom) manipulator similar to the DAM (Section 3.12.3.2) but ten times larger in every dimension, allowing a 68 micron-200 micron reach envelope with a 100 micron x 100 micron footprint on the HAM Plane floor and ~10 micron thick foundation blocks (which includes the 1 micron thickness of the topmost DAM Export Plane plate; Section 3.12.3.2). Each HAM has a solid volume of 160,000 $micron^3$, a passivated surface area of ~157,641 $micron^2$, a tip speed of ~2.6 cm/sec with 20 nm step increments, and a worst-case continuous power draw of (8 motors x 20,000 nW/motor) ~ 160,000 nW per HAM at a 120 MHz pulse control frequency, giving a total power draw of ~3200 W for the entire HAM Plane. Like the DAM Export Plane

(Section 3.12.3.2), the HAM Export Plane consumes negligible power (~0.003 W) during operation.

The flow of input parts across the HAM Plane follows the same basic pattern as the three successive planar 10:1 convergent assembly sets previously described for the DAM Plane (Section 3.12.3.2). These assembly sets include a large number (~186 x 10^5) of high-speed transport HAMs, a smaller number (~12 x 10^5) of assembly HAMs, ~6 x 10^5 transfer assembly HAMs, and ~1 x 10^5 export HAMs that are individually addressable and controllable in the entire HAM Plane.

The HAM Export Plane must accommodate ~500 micron output parts and thus lies 600 microns above the HAM Plane to provide adequate clearance between planes. The ~0.2 m^2 HAM Export Plane consists of two flat 10 micron thick diamondoid parallel plates each comprised of 2 x 10^7 foundation blocks each 10,000 $micron^2$ in area similar in design to the 100 $micron^2$ DAM foundation blocks. The opposing faces of the two plates are separated by 700 microns and are perforated with a total of 10^4 square HAM Export holes measuring 500 micron x 500 micron in size, thus displacing (counting the open area plus an identical blade area) ~5.0 x 10^5 or 2.5% of the 2 x 10^7 10,000-$micron^2$ foundation blocks in each plate. Providing support between these two planes are 1.25 x 10^4 support columns spaced 4 mm apart in the x_{SGN} dimension and 4 mm apart in the y_{SGN} dimension, and measuring 10,000 $micron^2$ x 600 micron in size – the footprint of each support column replaces one HAM foundation block, and support columns are located maximally distant from HAM Export Plane holes to minimize geometric interference. Additionally, hole HAMs must be able to lift the 500 micron output part at least 600 microns up from the HAM Plane floor in order to guarantee full reliable insertion into the HAM Export Plane hole. Therefore the reach of the hole HAMs must be extended from the usual 200 micron maximum to ~600 microns, using a design similar to that previously described for the hole DAMs (Section 3.12.3.2). A perimeter wall 10 micron thick and 600 microns tall seals the HAM and HAM Export Planes against vacuum loss.

3.12.3.4 Kilomicro-Assembly Manipulator (KAM) Plane

The Kilomicro-Assembly Manipulator (KAM) Plane acquires 10 parts/sec of input parts of size ~500 micron (~0.1 mm^3) from the 10^4 holes in the HAM Export Plane (Section 3.12.3.3), assembles 1000 of them into a 10 x 10 x 10 array making output parts of size ~5 mm (~100 mm^3), then exports these output parts at a 0.01 parts/sec rate to the CAM Plane (Section 3.12.3.5) through the KAM Export Plane which has 100 holes spaced 10 cm apart center-to-center within each row of holes. There are 4 holes per row running parallel to the 40 cm dimension of the SGN, and there are 25 rows of holes spaced 2 cm apart along the 50 cm dimension of the SGN. Hence 0.01 input parts/sec enter the KAM Plane from every HAM Export Plane hole and 0.001 output parts/sec exit the KAM Plane through every KAM Export Plane hole.

The KAM Plane consists of an array of ~2 x 10^5 KAMs, each of which is assumed to be a 6-DOF (degrees-of-freedom) manipulator similar to the HAM (Section 3.12.3.3) but ten times larger in every dimension, allowing a 680 micron-2000 micron reach envelope with a 1 mm x 1 mm footprint on the KAM Plane floor and ~100 micron thick foundation blocks (which includes the 10 micron thickness of the topmost HAM Export Plane plate; Section 3.12.3.3). Each KAM has a solid volume of 0.16 mm^3, a passivated surface area of ~15.7641 mm^2, a tip speed of ~2.6 cm/sec with 200 nm step increments, and a worst-case continuous power draw of (8 motors x 2 mW/motor) ~ 16 mW per KAM at a 120 MHz pulse control frequency, giving a total power draw

of ~3200 W for the entire KAM Plane. Like the HAM Export Plane (Section 3.12.3.3), the KAM Export Plane consumes negligible power (~0.003 W) during operation.

The flow of input parts across the KAM Plane follows the same basic pattern as the three successive planar 10:1 convergent assembly sets previously described for the HAM Plane (Section 3.12.3.3). These assembly sets include a large number (~186 x 10^3) of high-speed transport KAMs, a smaller number (~12 x 10^3) of assembly KAMs, ~6 x 10^3 transfer assembly KAMs, and ~1 x 10^3 export KAMs that are individually addressable and controllable in the entire KAM Plane.

The KAM Export Plane must accommodate ~5 mm output parts and thus lies 6 mm above the KAM Plane to provide adequate clearance between planes. The ~0.2 m^2 KAM Export Plane consists of two flat 100 micron thick diamondoid parallel plates each comprised of 2 x 10^5 foundation blocks each 1 mm^2 in area similar in design to the 10,000 $micron^2$ HAM foundation blocks. The opposing faces of the two plates are separated by 7 mm and are perforated with a total of 10^2 square KAM Export holes measuring 5 mm x 5 mm in size, thus displacing (counting the open area plus an identical blade area) ~5.0 x 10^3 or 2.5% of the 2 x 10^5 1-mm^2 foundation blocks in each plate. Providing support between these two planes are 1.25 x 10^3 support columns spaced 4 mm apart in the x_{SGN} dimension and 40 mm apart in the y_{SGN} dimension, and measuring 1 mm^2 x 6 mm in size – the footprint of each support column replaces one KAM foundation block, and support columns are located maximally distant from KAM Export Plane holes to minimize geometric interference. Additionally, hole KAMs must be able to lift the 5 mm output part at least 6 mm up from the KAM Plane floor in order to guarantee full reliable insertion into the KAM Export Plane hole. Therefore the reach of the hole KAMs must be extended from the usual 2 mm maximum to ~6 mm, using a design similar to that previously described for the hole HAMs (Section 3.12.3.3). A perimeter wall 100 micron thick and 6 mm tall seals the KAM and KAM Export Planes against vacuum loss.

3.12.3.5 Centimeter-Assembly Manipulator (CAM) Plane

The Centimeter-Assembly Manipulator (CAM) Plane acquires 0.01 parts/sec of input parts of size ~5 mm (~100 mm^3) from the 10^2 holes in the KAM Export Plane (Section 3.12.3.4), assembles 1000 of them into a 10 x 10 x 10 array making output parts of size ~5 cm (~100 cm^3), then exports these output parts at a 10^{-5} parts/sec rate to the Vacuum Export System (VES; Section 3.12.3.6) through the CAM Export Plane which has 1 central hole measuring 25 cm along the x_{SGN} = 50 cm dimension of the SGN and the full 40 cm along the y_{SGN} = 40 cm dimension of the SGN. Hence 0.001 input parts/sec enter the CAM Plane from every KAM Export Plane hole and 0.0001 output parts/sec exit the CAM Plane through the single large CAM Export Plane hole. By continuing the assembly process for ~100 times longer, the CAM can manufacture a final product object of up to ~100 times greater volume (~10,000 cm^3) in ~10^7 sec (~100 days), consistent with the ~100 cm^3/day output of the SGN. Smaller product objects can be routed directly through the CAM Export Plane if so desired.

The CAM Plane consists of an array of ~2000 CAMs, each of which is assumed to be a 6-DOF (degrees-of-freedom) manipulator similar to the KAM (Section 3.12.3.4) but ten times larger in every dimension, allowing a 0.68 cm-2 cm reach envelope with a 1 cm x 1 cm footprint on the CAM Plane floor and ~1 mm thick foundation blocks (which includes the 100 micron thickness of the topmost KAM Export Plane plate; Section 3.12.3.4). Each CAM has a solid volume of 160 mm^3, a passivated surface area of ~15.7641 cm^2, a tip speed of ~2.6 cm/sec with 2 micron

step increments, and a worst-case continuous power draw of (8 motors x 200 mW/motor) ~ 1.6 W per CAM at a 120 MHz pulse control frequency, giving a total power draw of ~3200 W for the entire CAM Plane. When manufacturing large product objects it may be necessary for some CAMs to hold the product object aloft while other CAMs install input parts along the undersurface of the product object.

The flow of input parts across the CAM Plane largely follows a similar pattern as the three successive planar 10:1 convergent assembly sets previously described for the KAM Plane (Section 3.12.3.4), although here the entire assembly of the product object takes place underneath the CAM Export Plane hole which spans about half (~1000 cm^2) of the entire ~2000 cm^2 SGN plane. These assembly sets may include a large number (~1820) of high-speed transport CAMs, a smaller number (~120) of assembly CAMs and ~60 transfer assembly CAMs, with all CAMs individually addressable and controllable in the CAM Plane.

The CAM Export Plane must accommodate the passage of output product objects up to ~10 cm thick but these objects are assembled entirely under the open space of the single CAM Export hole, hence a vertical separation from the CAM Plane of only ~1.5 cm should provide adequate clearance for handoffs of ~0.5 cm input parts held by CAMs having a minimum retracted length of 0.68 cm. The ~0.2 m^2 CAM Export Plane is considered to be a part of the VES (described in Section 3.12.3.6) because it is always operated as part of the VES largely independent of the activities of the CAM Plane. Additionally, hole CAMs must be able to lift the 5-100 mm tall output product object at least 2.5 cm up from the CAM Plane floor in order to guarantee full reliable insertion through the CAM Export Plane hole into the VES. The previously noted maximum reach of 2 cm for CAMs needs only minor alteration to satisfy the 2.5 cm requirement. A perimeter wall 1 mm thick and 1 cm tall seals the CAM and CAM Export Planes against vacuum loss.

3.12.3.6 Vacuum Export System (VES)

The function of the Vacuum Export System is to accept finished product objects from the CAM Plane and export them out of the second-generation nanofactory (SGN) without breaking the internal vacuum of the SGN. The VES provides an output port that can accommodate a finished macroscale product object having physical dimensions up to 25 cm (running parallel to the x_{SGN} = 50 cm dimension) x 40 cm (running parallel to the y_{SGN} = 40 cm dimension) x 10 cm tall (~10,000 cm^3), or as small as ~5 cm (~100 cm^3).

The VES consists of four principal structures, listed from topmost to bottommost structure, as follows:

(1) **SGN Casing Top and Walls**. The SGN Casing Top (~1184 cm^3, ~2594 cm^2) is a single diamondoid plate measuring about 52 cm x 42 cm x 1 cm with a hole measuring ~25 cm x 40 cm removed from it on one side, which is manufactured by assembling numerous small diamondoid blocks. This size is sufficient to accommodate the SGN Casing Walls (~2068 cm^3, 4136 cm^2), which consists of ~1 cm thick vertical support walls that extend down ~11 cm from the SGN Casing Top to the CAM Export Plane and seal the top of the SGN against vacuum leakage.

(2) **VES Export Plane**. This is another diamondoid plate of similar manufacture to the SGN Casing Top, measuring ~25 cm x 40 cm x 1 cm (~1000 cm^3, ~2130 cm^2). The sides of the

plate are mounted in a groove along the vertical support walls of the SGN Casing Walls, allowing the plate to be slid from one side of the SGN to the other, alternately completely exposing (when fully retracted) or completely covering (when fully extended) the export hole. When the plate is fully extended, its forward edge that has come into contact with a vertical support wall forms a leaktight seal with that wall. The plate also has several lengthwise tongues that ride in several complementary grooves in the underside of the SGN Casing Top, which holds the two plates in firm contact and maintains a leaktight sliding seal between them.

(3) **VES Vacuum Piston**. This is a hollow box measuring ~25 cm x 40 cm x 10 cm in size, with 1 cm thick diamondoid walls. The box has vacuum in its interior, and is internally crossed by 10 evenly-spaced internal support pillars measuring 1 cm^2 x 8 cm long to provide additional stiffness to the structure, giving ~3120 cm^3 (~6660 cm^2) of solid diamondoid structure. The sides of the piston are mounted in several grooves along the vertical support walls of the SGN Casing Walls, allowing the piston to be slid from one side of the SGN to the other, alternately completely exposing (when fully retracted) or completely covering (when fully extended) the export hole. When the piston is fully extended, its forward edge that has come into contact with a vertical support wall forms a leaktight seal with that wall. The piston also has several lengthwise tongues that ride in several complementary grooves in the underside of the VES Export Plane, which holds the two structures in firm contact and maintains a leaktight sliding seal between them.

(4) **CAM Export Plane**. This is another diamondoid plate almost identical to the VES Export Plane, measuring ~25 cm x 40 cm x 1 cm (~1000 cm^3, ~2130 cm^2). The sides of the plate are mounted in a groove along the vertical support walls of the SGN Casing Walls, allowing the plate to be slid from one side of the SGN to the other, alternately completely exposing (when fully retracted) or completely covering (when fully extended) the export hole. When the plate is fully extended, its forward edge that has come into contact with a vertical support wall forms a leaktight seal with that wall. The plate also has several lengthwise tongues that ride in several complementary grooves in the underside of the VES Vacuum Piston, which holds the two structures in firm contact and maintains a leaktight sliding seal between them. The underside of the CAM Export Plane lies ~1.5 cm above the opposing surface of the CAM Plane (Section 3.12.3.5).

The three diamond plates described above will not be unitary covalently-bonded diamond but rather arrays of tightly interlocked diamond prisms each measuring ~10^6 nm^3 in volume (Section 3.12.3.8), the largest solid objects that the fabrication planes can produce. Such interlocking arrays can be: (a) atomically smooth on each exterior face, (b) almost as strong as a unitary diamond solid, and (c) virtually leakproof to gases in the cross-plate direction (Section 3.12.3.8).

The VES will operate using a 9-step export cycle that allows export of a finished product object without breaking the internal SGN vacuum. The following description of the VES export cycle includes a 3-digit binary code in which the three digits signify the states of the CAM Export Plane door, the VES Vacuum Piston, and the VES Export Plane door (0 = plate retracted, hole open; 1 = plate extended, hole closed), respectively:

Step 1: (1, 1, 1) All three doors are closed.

Step 2: (1, 0, 1) The VES Vacuum Piston door is opened. Pulling the piston away from the wall creates a ~10 cm high export space, and this export space contains only vacuum.

Step 3: (0, 0, 1) Retraction of the door in the CAM Export Plane allows access to the export space from below. The CAM Plane can now build into the export space.

Step 4: (0, 0, 1) The CAM Plane assembles the product object into the export space, then elevates it 2.5 cm above the CAM Plane floor.

Step 5: (1, 0, 1) Extension of the door in the CAM Export Plane seals off access to the export space from below. The product object now resides entirely in the export space.

Step 6: (1, 0, 0) Opening the door in the VES Export Plane lets air into the export space but not into the SGN interior because the CAM Export Plane door is closed.

Step 7: (1, 0, 0) Manually remove the product object from the export space. The SGN-manufactured product object is now available for external consumption.

Step 8: (1, 1, 0) The VES Vacuum Piston "door" is now closed. Forcing the piston against the far wall forces all air out of the export space and reduces the export space to zero volume.

Step 9: (1, 1, 1) Closing the door in the VES Export Plane forces out the remaining air and seals the SGN. All three doors are now closed. The export cycle may now repeat.

The power dissipated by two atomically-smooth sliding interlocked diamondoid surfaces may be crudely approximated[1304] by $P_{slide} \sim k_1 S_{contact} v_{slide}^2 \sim 4$ watts for $k_1 = 400$ kg/m^2-sec,[1305] relative interfacial velocity $v_{slide} = 1$ mm/sec, and mutual contact area $S_{contact} \sim 10{,}000$ cm^2 which assumes that two hydrogen-passivated diamondoid plates of area ~1000 cm^2 are in tight contact and that the tongue-in-groove design increases the total contact area by approximately tenfold. In this case, product export (Steps 5-7) following the completion of CAM Plane manufacturing operations (Steps 3-4) will require (2) (25 cm) / (1 mm/sec) ~ 500 sec (~8 min).

Although 1 cm thick diamond plates for the CAM Export or VES Export plane doors may seem excessive, we probably need such thick plates because plate deflection scales with the cube of plate thickness. By analogy to a rectangular 1.5:1 clamped plate[1306] or to a >2:1 clamped strip plate,[1307] the 1-atm pressure loading of an isolated CAM Export Plane door or a VES Export Plane door will produce a maximum out-of-plane deflection of $\delta_{plate} = k_{plate} (\Delta P_{plate} L_{plate}^4 / E_{plate} h_{plate}^3) \sim 38$ microns at the center of a rectangular plate of shortest edge $L_{plate} = 25$ cm, thickness $h_{plate} = 1$ cm and Young's modulus $E_{plate} = 1.05 \times 10^{12}$ N/m^2 for diamond, when clamped on all four sides and loaded by uniform normal pressure $\Delta P_{plate} = 1$ atm, where k_{plate} is a constant of

---

[1304] Robert A. Freitas Jr., Nanomedicine, Volume I: Basic Capabilities, Landes Bioscience, Georgetown, TX, 1999, Section 4.3.4.2, p. 101, http://www.nanomedicine.com/NMI/4.3.4.2.htm; K. Eric Drexler, Nanosystems: Molecular Machinery, Manufacturing, and Computation, John Wiley & Sons, New York, 1992, Section 10.4.6, pp. 290-293.

[1305] Robert A. Freitas Jr., Nanomedicine, Volume I: Basic Capabilities, Landes Bioscience, Georgetown, TX, 1999, Section 4.3.4.2, p. 101, http://www.nanomedicine.com/NMI/4.3.4.2.htm; K. Eric Drexler, Nanosystems: Molecular Machinery, Manufacturing, and Computation, John Wiley & Sons, New York, 1992, Section 10.4.6, pp. 290-293.

[1306] Samuel Levy, Samuel Greenman, "Bending with large deflection of a clamped rectangular plate with length-width ratio of 1.5 under normal pressure," National Advisory Committee for Aeronautics (NACA), Washington DC, Technical Note 853, 1942; http://naca.larc.nasa.gov/reports/1942/naca-tn-853/

[1307] Prof. Dr.-Ing. Kai-Uwe Bletzinger, "Theory of Plates, Part II: Plates in bending," Lehrstuhl fur Statik, Technische Universitat Munchen, Lecture Notes, Winter Semester 2000/2001; http://www.statik.bauwesen.tu-muenchen.de/vorlesungen/plates.dir/plates_part2.pdf.

order ~0.1.[1308] The thermal uncertainty of such a plate at 300 K (Section 3.4.1.2) is $\Delta x_{bending}$ ~ 0.02 Å, creating transient gaps that are much too small to allow gas molecules to pass. The 1-atm out-of-plane deflection for a CAM Export Plane or a VES Export Plane door plate in full contact with a VES Vacuum Piston having 10 internal support pillars is conservatively estimated as δ_{plate} ~ 36 nm, or δ_{plate} ~ 15 nm when all three "door" structures are in full contact.

It will probably be prudent to include an auxiliary UHV pumping system to remove any stray contaminant molecules that might make their way into the space between the CAM Plane and the CAM Export Plane, despite all precautions. Laser-induced desorption or related means (Section 3.5.1.7) might also be required to eliminate physisorbed atmospheric molecules such as water or hydrocarbons from the interior surfaces of VES structures after their brief exposure to atmosphere during removal of the product object from the SGN. Opening the VES only under a low-humidity low-pressure contaminant-free "clean room" type atmosphere would further reduce the probability of contamination of the internal vacuum environment of the SGN. Better still, opening the VES to remove final product only under external UHV conditions (e.g., Section 3.11.7) could entirely eliminate the need for leaktight seals above the CAM Export Plane. This might then allow most of the VES to be constructed out of atomically-imprecise non-leaktight structures that would not need to be manufactured by the FGN, thus reducing SGN buildout time by a factor of ~5.6 (i.e., see "SGN–VES+CAMEP" option in Table XI-1) using the FGN.

3.12.3.7 SGN Scaling Analysis Summary with Atom Count

Allocating ~176 C atoms/nm^3 for diamondoid lattice and ~31 H atoms per nm^2 to passivate diamondoid surface gives the scaling results for the third production layer of the SGN as shown in Table XI-1. The third production layer (comprised of five assembly subsystems and ~1.592 x 10^{27} atoms (99.99996% carbons)) is 0.133 mm (DAM; Section 3.12.3.2) + 1.329 mm (HAM; Section 3.12.3.3) + 1.329 cm (KAM; Section 3.12.3.4) + 1.59 cm (CAM; Section 3.12.3.5) + VES (13 cm; Section 3.12.3.6) = 16.0652 cm thick with a dry mass of ~31.68 kg. Although the third production layer is ~600 times more massive than the first and second production layers combined, the third layer is large enough and stiff enough to be independently supported by massive external (atomically imprecise) support columns, thus enabling the 100-g vertical acceleration design goal (Section 3.11.2.9) to be maintained for the entire SGN. If each of the 2 x 10^9 DAMs, 2 x 10^7 HAMs, 2 x 10^5 KAMs, and 2000 CAMs receives a separate sequence of 120 x 10^6 control pulses per second (120 MHz operating frequency) on each of ~100 control lines, and if each of the 10^6 DAM Export holes, 10^4 HAM Export holes, and 10^2 KAM Export holes each with 2 x 70 blade motors receives a separate sequence of 120 x 10^6 control pulses per second (120 MHz operating frequency) on each of ~2 control lines per motor, then operating the third

---

[1308] Prof. Dr.-Ing. Kai-Uwe Bletzinger, "Theory of Plates, Part II: Plates in bending," Lehrstuhl fur Statik, Technische Universitat Munchen, Lecture Notes, Winter Semester 2000/2001; http://www.statik.bauwesen.tu-muenchen.de/vorlesungen/plates.dir/plates_part2.pdf. Samuel Levy, Samuel Greenman, "Bending with large deflection of a clamped rectangular plate with length-width ratio of 1.5 under normal pressure," National Advisory Committee for Aeronautics (NACA), Washington DC, Technical Note 853, 1942; http://naca.larc.nasa.gov/reports/1942/naca-tn-853/.

production layer requires a total control data flow of (2.424×10^{19} bits/sec) + (1.697×10^{16} bits/sec) ~ 2.426×10^{19} bits/sec.

Allowing ~3200 W power dissipation for each of the four macroscale assembling planes (DAM, HAM, KAM and CAM) plus ~4 watts for the VES (during the brief periods when it is operating) gives a total heat generation of 12,804 W for the entire third production layer. This heat may be conducted away by similar means as has previously been described for the second production layer (Section 3.11.3.5).

Table XI-1. Estimated Atom Count* for the Diamondoid Structure of the Third Production Layer of the Second-Generation Nanofactory (SGN), and Totals for the SGN

SGN Nanofactory Subsystem	Total Solid Volume (m^3)	Total Passiv. Area (m^2)	# of C Atoms	# of H Atoms	Total # of Atoms*
DAM Plane			1.644×10^{23}	1.431×10^{20}	1.645×10^{23}
2×10^9 DAMs	3.2×10^{-7}	3.1528			
Wiring Bundle	7.398×10^{-8}	0			
Support Frame	6×10^{-8}	4.8×10^{-1}			
Small-Wire Sheet	2×10^{-9}	0			
Snap Connectors	4×10^{-11}	1.602×10^{-2}			
Perimeter Wall	1.08×10^{-10}	2.16×10^{-4}			
DAM Export Plane					
2 Parallel Plates	3.9×10^{-7}	7.8×10^{-1}			
Blade Stacks	8.75×10^{-8}	1.855×10^{-1}			
Blade Motors	7×10^{-11}	4.2×10^{-6}			
Wiring Bundle	3.584×10^{-12}	0			
HAM Plane			1.646×10^{24}	1.431×10^{20}	1.646×10^{24}
2×10^7 HAMs	3.2×10^{-6}	3.1528			
Wiring Bundle	7.398×10^{-7}	0			
Support Frame	6×10^{-7}	4.8×10^{-1}			
Small-Wire Sheet	2×10^{-8}	0			
Snap Connectors	4×10^{-10}	1.602×10^{-2}			
Perimeter Wall	1.1×10^{-8}	2.16×10^{-3}			
HAM Export Plane					
2 Parallel Plates	3.9×10^{-6}	7.8×10^{-1}			
Blade Stacks	8.75×10^{-7}	1.855×10^{-1}			
Blade Motors	7×10^{-10}	4.2×10^{-6}			
Wiring Bundle	3.584×10^{-11}	0			

KAM Plane			1.665×10^{25}	1.437×10^{20}	1.665×10^{25}
2×10^{5} KAMs	3.2×10^{-5}	3.1528			
Wiring Bundle	7.398×10^{-6}	0			
Support Frame	6×10^{-6}	4.8×10^{-1}			
Small-Wire Sheet	2×10^{-7}	0			
Snap Connectors	4×10^{-9}	1.602×10^{-2}			
Perimeter Wall	1.2×10^{-6}	2.16×10^{-2}			
KAM Export Plane					
2 Parallel Plates	3.9×10^{-5}	7.8×10^{-1}			
Blade Stacks	8.75×10^{-6}	1.855×10^{-1}			
Blade Motors	7×10^{-9}	4.2×10^{-6}			
Wiring Bundle	3.584×10^{-10}	0			
CAM Plane			8.343×10^{25}	1.142×10^{20}	8.343×10^{25}
2×10^{3} CAMs	3.2×10^{-4}	3.1528			
Wiring Bundle	7.398×10^{-5}	0			
Support Frame	6×10^{-5}	4.8×10^{-1}			
Small-Wire Sheet	2×10^{-6}	0			
Snap Connectors	4×10^{-8}	1.602×10^{-2}			
Perimeter Wall	1.8×10^{-5}	3.6×10^{-2}			
Vacuum Export System			1.473×10^{27}	5.472×10^{19}	1.473×10^{27}
Casing Top	1.184×10^{-3}	0.2594			
Casing Walls	2.068×10^{-3}	0.4136			
VES Export Plane	1×10^{-3}	0.2130			
VES Vacuum Piston	3.120×10^{-3}	0.6660			
CAM Export Plane	1×10^{-3}	0.2130			
Unallocated Structure	1×10^{-4}	1	1.76×10^{25}	3.10×10^{19}	1.76×10^{25}
TOTALS, Third Production Layer	$8.970374712 \times 10^{-3}$	20.3167686	1.592×10^{27}	6.298×10^{20}	1.592×10^{27}
Deleted Portions of Export Plane:					
2500 Square Cylinders	2×10^{-7}	4×10^{-1}			
2500 Square Pistons	6.25×10^{-11}	1.25×10^{-5}			
TOTALS, Revised Second Production Layer	$1.83516230 \times 10^{-7}$	11.8127466	3.230×10^{22}	3.662×10^{20}	3.267×10^{22}
TOTALS, First Production Layer	2.015×10^{-5}	8.374×10^{3}	3.541×10^{24}	2.604×10^{23}	3.800×10^{24}
TOTALS for SGN	8.991×10^{-3}	8.406×10^{3}	1.596×10^{27}	2.614×10^{23}	1.596×10^{27}
SGN–VES+CAMEP†	1.619×10^{-3}	8.405×10^{3}	2.986×10^{26}	2.611×10^{23}	2.988×10^{26}

* There are also ~10^{14} Ge atoms per fabrication plane, hence ~10^{17} Ge atoms in all fabrication planes comprising the first production layer, hence ~10^{17} Ge atoms in the entire SGN.

† CAMEP = CAM Export Plane as the highest atomically-precise level in the SGN; the VES is still present but is no longer leaktight, thus may be assumed to be made using non-atomically precise techniques that do not require manufacture by the SGN.

The SGN as a whole has ~1.596 x 10^{27} atoms (99.98% carbons) and measures 50 cm x 40 cm x 26.16713 cm tall with a total "dry" mass of ~31.75 kg of atomically precise components – a total SGN volume of 87,130.4 cm^3 giving a "dry" nanomachinery density of ~362 kg/m^3. The first production layer is ~10 cm tall (~70.9 gm)), the second production layer with export cylinders deleted is ~18.3 microns tall (~0.643 gm), and the third production layer is 16.0652 cm tall (~31.68 kg), all atop the 1.001 mm atomically imprecise base plate. SGN control signal traffic is dominated by the first and third production layers, requiring a data flow of ~2.4 x 10^{19} bits/sec for the first production layer, ~5.1 x 10^{15} bits/sec for the second production layer, and ~2.426 x 10^{19} bits/sec for the third production layer, giving a total requirement of ~5 x 10^{19} bits/sec for the entire SGN (minimum total irreversible bit-erasure power draw ~ 0.2 W assuming ~k_BT/bit at T = 300 K). Power consumption is ~11 MW for the first production layer (Section 3.11.2.9), ~12,800 W for the second production layer (Section 3.11.3.5) and ~12,804 W for the third production layer (Section 3.12.3.7), so the SGN produces ~11.03 MW of waste heat while manufacturing atomically precise products at ~10^{20} atoms/sec, ~10^{18} nm^3/sec, or ~0.01 kg/hour. This gives the nominal SGN a mass replication time of ~132 days, or ~25 days using the ~5.943 kg "SGN–VES+CAMEP" option in Table XI-1.

3.12.3.8 Characteristics and Limitations of SGN-Buildable Products

All products which can be built by the SGN must be manufacturable via the process of convergent assembly. Thus the SGN cannot build macroscale chunks of clear flawless diamond such as might be suitable for wedding ring gemstones or other hypothetical interface-free macroscale objects such as transparent windshields for cars, crystal faces for wristwatches, picture windows for houses, or large busts or trophies for display on the fireplace mantle (unless it can be shown that the presence of numerous submicroscale interfaces will not destroy optical transparency). This requirement for convergent assemblability of SGN products means that all macroscale SGN products will be comprised of many trillions of modular components that have been assembled together into a macroscale whole. Alternative manufacturing architectures will be required for the positional assembly of atomically precise unitary objects comprised solely of covalent bonds that exceed ~100 nm in any dimension, up to macroscale sizes. The SGN can also fabricate products only from C/Ge/H atoms, plus a few other supplementary elements if any such are deemed essential to program success (e.g., Section 3.2.2.5(F)), but probably not including metallic or radioactive atoms.

The largest purely-covalent modular component that can be fabricated by the lowest-level fabrication plane in the SGN would be a solid ~100 nm cube of seamless diamondoid crystal measuring ~10^6 nm^3 in volume and incorporating ~10^8 atoms (Section 3.11.2.7). (Many SGN products will be composed of even smaller modules – e.g., "typical smallest" components of only ~100,000 nm^3 or ~10^7 atoms (Section 3.11.2.7), with these components often including

assemblies of nanoparts each as tiny as a few nm in size or ~1000 atoms, or even smaller.) A 1 cm^3 cube-shaped macroscale product assembled from ~10^6 nm^3 nanoscale modules would thus contain ~10^{15} of them. Products made in this manner can approach the physical strength of pure diamond, because, for example, modules can be fabricated with tight-fitting complementary tongue-in-groove features on their opposing surfaces, allowing the modules to be slid together in one direction during assembly but to strongly resist separation when pulled or compressed in any other direction because of the interlocking grooves. Since the ends of joint lines on opposing faces can be positioned to occur only across unbroken covalently-bonded diamondoid surfaces of neighboring modules elsewhere in the array, such tightly interlocking arrays can be designed to possess no continuous pathways through which gas molecules could readily diffuse, thus creating a virtually leaktight material.

Product objects consisting of smooth-faced ~10^6 nm^3 cubes held together only by van der Waals forces between opposing flat faces will be considerably weaker, typically on the order of ~5% of the strength of solid diamond,[1309] and will possess discontinuous interfaces between each cube. However, it should be possible to seamlessly covalently bond two 100 nm cubes if their opposed faces consist solely of a regular lattice of depassivated C(110) surfaces, because these surfaces do not reconstruct when depassivated. However, the requirements for performing such covalent joining are rather stringent:

(1) The current SGN architecture has no ability to depassivate cube (module) surfaces post-fabrication, so each cube to be joined in this manner must be fabricated with one or more clean C(110) surfaces from the outset, and then the ciliary transport mechanisms within the fabrication plane, the stovepipes, etc. must be able to handle the cube without touching (and likely ruining) the chemically active cube face(s) and without ruining the transport mechanisms themselves.

(2) Prior to joining, the dimer troughs and ridges of the opposed faces must be precisely parallel and aligned so that the ridges of one face lie above the troughs of the opposing face, and the opposing faces must also be oriented approximately parallel (but see (4) below).

(3) During joining, the maximum tolerable lateral positioning error to avoid misreaction is of the order 20-50 pm,[1310] so the two rather large ~10^6 nm^3 cubes must be held and positioned to the same high accuracy as is required for the much smaller toolheads during DMS fabrication.

[1309] K. Eric Drexler, Nanosystems: Molecular Machinery, Manufacturing, and Computation, John Wiley & Sons, New York, 1992, Section 3.5.1.b, p. 66.

[1310] Jingping Peng, Robert A. Freitas Jr., Ralph C. Merkle, "Theoretical Analysis of Diamond Mechanosynthesis. Part I. Stability of C_2 Mediated Growth of Nanocrystalline Diamond C(110) Surface," J. Comput. Theor. Nanosci. 1(March 2004):62-70; http://www.MolecularAssembler.com/JCTNPengMar04.pdf. Jingping Peng, Robert A. Freitas Jr., Ralph C. Merkle, James R. Von Ehr, John N. Randall, George D. Skidmore, "Theoretical Analysis of Diamond Mechanosynthesis. Part III. Positional C_2 Deposition on Diamond C(110) Surface using Si/Ge/Sn-based Dimer Placement Tools," J. Comput. Theor. Nanosci. 3(February 2006):28-41; http://www.MolecularAssembler.com/Papers/JCTNPengFeb06.pdf.

(4) Also during joining, heat is released as cross-interface C-C bonds are formed because the reaction is exoergic, approximating the C(110) plane cleavage energy of E_{cleave} = 13.0 J/m^2,[1311] or $\Delta E = A_{face}\ E_{cleave}$ ~ 0.13 pJ when two 100 nm x 100 nm (L_{cube} = 100 nm, A_{face} ~ 10^4 nm^2) cube faces are joined. Instantly thermalizing this energy into an isolated 10^6 nm^3 cube of pure diamond would raise the cube temperature by $\Delta T = \Delta E / C_V\ V_{cube}$ = (0.13 pJ) / ((1.82 x 10^6 J/m^3-K) (10^6 nm^3)) ~ 71 K in an equilibration time of $t_{EQ} \sim A_{face}\ C_V / K_{diamond}$ = (10^4 nm^2) (1.82 x 10^6 J/m^3-K) / (2000 W/m-K) ~ 9 x 10^{-12} sec. Since $\Delta T \sim L_{cube}^{-1}$, joining smaller cubes can produce unacceptable temperature increases during interfacial bonding and thus may require joining the two surfaces by commencing the join with the opposing faces slightly off-parallel and then slowly tilting the faces together to "zip up" the surface, allowing covalent bonding to proceed at a controlled rate. If it were possible to convergently assemble in ~10 sec a 1 cm^3 cube-shaped seamless macroscale product from ~10^{15} nanoscale modules each ~10^6 nm^3 in size requiring ~6 x 10^{15} interfacial joins, this would produce (0.13 pJ/join) (6 x 10^{15} joins) / (10 sec) ~ 78 watts of waste heat, a small fraction of the ~11 megawatt SGN power consumption (but see (6) below).

(5) After joining, the resulting product object must be small enough to travel through the internal transit spaces that are available inside the SGN. A slightly modified SGN could provide for separate routing of a few oversize objects through the system, but to obtain any significant mass throughput of such objects the SGN would require a major redesign.

(6) Since C(111) surfaces cannot be joined in this manner because such surfaces reconstruct when large contiguous areas are depassivated, it is unclear how seamless solid diamond constructions could be assembled from modules in all three lattice dimensions.

The bulk appearance of SGN products made from submicroscale module arrays is largely unexplored but can probably be simulated and engineered once the basic parameters are established. It is currently unknown if a macroscale 3D regular array of ~100 nm H-passivated transparent diamond cubic modules can produce an optically transparent bulk material. Somewhat analogous to the case of randomly sized and oriented component modules, samples of commercial-grade diamond grit purchased from Crystalite Corporation appear black in the particle size range from 77-250 microns, gray in color from 3-42 microns, and white from 0.25-2 microns (and presumably smaller as well), suggesting that surface feature sizes of ~100 nm and smaller in a module array should also produce a predominantly white surface. This is not surprising, given that the wavelengths of visible light range from 700 nm (red) to 400 nm (blue), so light passing through submicron-featured otherwise colorless material should be completely scattered (like light passing through a fog of micron-size water droplets). However, if the modules are fabricated and positioned so as to produce raised parallel linear surface ridges spaced ~0.4-0.7 microns apart (i.e., ~half a dozen 100-nm-module widths) similar to dispersive optical reflection gratings, an otherwise white bulk surface could be engineered to partake an opalescence sheen displaying a rainbow of colors that shifts with viewing angle, like the surface of a CD or DVD disk when tilted under white light (Figure XI-3(A)).

[1311] J.E. Field, "Chapter 9. Strength and Fracture Properties of Diamond," in J.E. Field, ed., The Properties of Diamond, Academic Press, New York, 1979, pp. 281-324; R.H. Telling, C.J. Pickard, M.C. Payne, J.E. Field, "Theoretical Strength and Cleavage of Diamond," Phys. Rev. Lett. 84(May 2000):5160-5163, http://www.tcm.phy.cam.ac.uk/~cjp20/publications/PRL84_5160.pdf.

Figure XI-3. Iridescent surface coloration can be engineered into SGN products if desired, using nanoscale structures analogous to those found on (A) CD/DVD disks, (B) peacock feathers,[1312] (C) mother-of-pearl,[1313] or (D) the scales on butterfly wings.[1314]

(A)

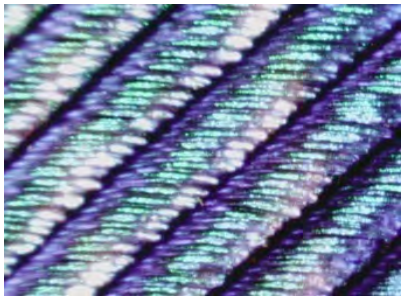

(B)

(C)

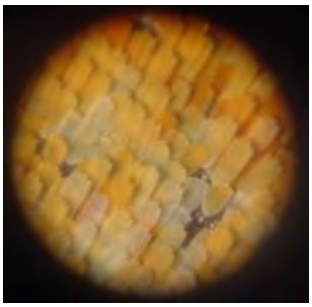

(D)

[1312] Shinya Yoshioka, Shuichi Kinoshita, "Effect of Macroscopic Structure in Iridescent Color of Peacock Feathers," Forma 17(2002):169-181; J. Zi, Y. Xindi, Y. Li, et al, "Coloration strategies in peacock feathers," PNAS 100(2003):12576-12578. See also: R. Nave, "Peacock Feather Colors," HyperPhysics, Light and Vision, accessed 30 March 2008; http://hyperphysics.phy-astr.gsu.edu/Hbase/vision/peacock.html.

[1313] A. Lin, M.A. Meyers, "Growth and structure in abalone shell," Materials Science and Engineering A 390(2005):27-41; G. Mayer, "Rigid biological systems as models for synthetic composites," Science 310(2005):1144-1147, http://www.sciencemag.org/cgi/content/abstract/310/5751/1144. See also: "Nacre," Wikipedia, accessed 30 March 2008; http://en.wikipedia.org/wiki/Mother-of-pearl.

[1314] C.W. Mason, "Structural colors in insects. II. Iridescent colors," J. Phys. Chem. 31(1927):321-354; P. Vukusic, J.R. Sambles, H. Ghiradella, "Optical Classification of Microstructure in Butterfly Wing-scales," Photonics Science News 6(2000):61-66; Richard O. Prum, Tim Quinn, Rodolfo H. Torres, "Anatomically diverse butterfly scales all produce structural colours by coherent scattering," J. Exp. Biol. 209(31 January 2006):748-765, http://jeb.biologists.org/cgi/content/full/209/4/748.

Similar iridescent coloration effects are commonly observed in nature – e.g., in peacock feathers (which contain a photonic lattice with a 150-nm array spacing)[1315] (Figure XI-3(B)), nacre or mother-of-pearl (continuous parallel lamina of hexagonal aragonite ($CaCO_3$) crystal plates 10-20 microns wide and 500 nm thick)[1316] (Figure XI-3(C)), opals (a regular 3D crystalline array of colloidal silica spheres several hundred nanometers in size) and "inverse opals" (a "cubic graphite" structure with a unit cell of several hundred nanometers),[1317] and butterfly wings (coated with photonic crystal scales producing multilayer interference and coherent scattering from complex 3D nanostructures ~200 nm in diameter)[1318] (Figure XI-3(D)).

3.12.3.9 Reliability of SGN Manufacture and Operation

A detailed and comprehensive analysis of molecular manufacturing error rates will be required to properly assess the defect rate likely to occur when building various components and subsystems of the SGN, especially since the equipment and procedures for manufacturing the SGN are very complex and involve mole-quantities of moving parts (see below).

However, as a crude estimate, at a 109 K operating temperature the error rate for DMS-related fabrication operations is ~10^{-10} per NMW-3 replication cycle (Section 3.8.1.3) or ~10^{-18} per atom, so the systemic error rate will probably be driven by the mechanical/control error rate and by the imperfect-vacuum radical poisoning rate which have been estimated (Section 3.8.1.3) as ~10^{-7} per NMW-3 replication cycle or ~10^{-15} per atom. The SGN consists of 2.988 x 10^{26} atoms (in the SGN–VES+CAMEP option; Table XI-1), so we may logically assume that the SGN as initially manufactured will include ~300 million erroneously placed atoms and will have suffered ~300 billion radical poisoning events and ~300 billion erroneous mechanical/control events. In its 1000 fabrication planes the SGN includes ~10^{16} NMW-3 modules, of which it must be assumed that (10^{16} modules) (10^{-7} error rate per module) ~ 10^{9} of them are nonfunctional from the outset.

[1315] Shinya Yoshioka, Shuichi Kinoshita, "Effect of Macroscopic Structure in Iridescent Color of Peacock Feathers," Forma 17(2002):169-181; J. Zi, Y. Xindi, Y. Li, et al, "Coloration strategies in peacock feathers," PNAS 100(2003):12576-12578. See also: R. Nave, "Peacock Feather Colors," HyperPhysics, Light and Vision, accessed 30 March 2008; http://hyperphysics.phy-astr.gsu.edu/Hbase/vision/peacock.html.

[1316] A. Lin, M.A. Meyers, "Growth and structure in abalone shell," Materials Science and Engineering A 390(2005):27-41; G. Mayer, "Rigid biological systems as models for synthetic composites," Science 310(2005):1144-1147, http://www.sciencemag.org/cgi/content/abstract/310/5751/1144. See also: "Nacre," Wikipedia, accessed 30 March 2008; http://en.wikipedia.org/wiki/Mother-of-pearl.

[1317] Anvar A. Zakhidov, Ray H. Baughman, Zafar Iqbal, Changxing Cui, Ilyas Khayrullin, Socrates O. Dantas, Jordi Marti, Victor G. Ralchenko, "Carbon Structures with Three-Dimensional Periodicity at Optical Wavelengths," Science 282(30 October 1998):897-901.

[1318] C.W. Mason, "Structural colors in insects. II. Iridescent colors," J. Phys. Chem. 31(1927):321-354; P. Vukusic, J.R. Sambles, H. Ghiradella, "Optical Classification of Microstructure in Butterfly Wing-scales," Photonics Science News 6(2000):61-66; Richard O. Prum, Tim Quinn, Rodolfo H. Torres, "Anatomically diverse butterfly scales all produce structural colours by coherent scattering," J. Exp. Biol. 209(31 January 2006):748-765, http://jeb.biologists.org/cgi/content/full/209/4/748.

Clearly the SGN must incorporate error tolerance as a critical design feature (Section 3.11.4), and ideally the SGN should remain moderately functional even when a random distribution of perhaps up to ~1% of its NMW-3 modules have become incapacitated.

Once the SGN has been built and is operating in production mode, similar error rates will apply. At 109 K, the error rate for DMS-related operations is ~10^{-10} per NMW-3 replication cycle or ~10^{-18} per atom (Section 3.8.1.3), so again the systemic error rate is driven by the mechanical/control error rate (presumed to be ~10^{-7} per NMW-3 replication cycle or ~10^{-15} per atom; Section 3.8.1.3) and by the imperfect-vacuum radical poisoning rate which is ~10^{-7} per NMW-3 replication cycle or ~10^{-15} per atom (Section 3.8.1.3). Obtaining this low radical poisoning rate requires maintaining a 10^{-18} atm vacuum environment inside each of the 1000 fabrication planes – very nearly a perfect vacuum (Section 3.11.3.6). The productive lifetime of the SGN should be in the range of 1-10 years (Section 3.12.1).

3.12.4 Task XI-1: Design, Model and Simulate SGN Components, Operations, Process of Manufacture, and Products

Task XI-1 is to design, model, and simulate the components and operations of the SGN Assembly System and of the First-Generation Nanofactory (SGN) itself. This task is substantially identical to Task X-1, except that Task XI-1 must also incorporate an analysis of the third production layer which is comprised of four macroassembling planes including the Dekamicro-Assembly Manipulator (DAM) Plane (Section 3.12.3.2), the Hectomicro-Assembly Manipulator (HAM) Plane (Section 3.12.3.3), the Kilomicro-Assembly Manipulator (KAM) Plane (Section 3.12.3.4) and the Centimeter-Assembly Manipulator (CAM) Plane (Section 3.12.3.5), along with the Vacuum Export System or VES (Section 3.12.3.6).

The physical integrity and stability of the growing SGN as it exists during numerous intermediate stages of construction must also be modeled, simulated, and validated, along with detailed studies of error tolerances extending the analysis previously undertaken in Task X-1.

Design, modeling and simulation of proposed macroscale products (Section 3.12.3.8) which can be constructed using convergent assembly processes must be undertaken to define appropriate products for the SGN to manufacture, and to ensure that the identified products are buildable and will perform as desired once they are built.

Other general design-related issues may include:

(1) Need comprehensive simulations of all nanofactory operations. If individual DMS operations in a mature manufacturing system can be made as simple and reliable as primitive transistor operations in a modern electronic computer chip that flawlessly performs ~10^{24} transistor operations per day, then the level of complexity inherent in nanofactory operations may be regarded as considerable but not inconceivable.

(2) The design space of basic nanofactory architectures should be surveyed and evaluated, though the space is probably too large for a comprehensive assessment. A good nanofactory design should be a bootstrap-capable system, should exhibit ease of reprogramming, should allow maximum geometric accessibility to workpieces during manufacture, should exhibit maximum reliability during operation, should be "safe" and exhibit nonevolvability, should be "buildable", and should enable clean manufacturing and pollution-free operation.

(3) Need to investigate possible requirements for macroscale-equivalent process control and monitoring instrumentation in nanofactories, including sensors, limit switches, and the like, constituting sensory feedback loops that permitting conditional actuation. If DMS fabrication sequences and parts assembly sequences can be design to minimize or eliminate unwanted reconstructions or other structural pathologies, then the need for conventional inline sensing is greatly reduced (along with the number of possible failure modes).

(4) Need to investigate designs for multiply redundant production lines, with quantification of performance and design tradeoffs including number of parallel production lines, mean-time-to-breakdown of a given production line, the optimal number of alternative workpiece pathways through the nanofactory, the optimal number and location of production flow shunts, and so forth, to determine the reliability and efficiency of the overall manufacturing operation.

(5) Need a formal study and analysis of the effects of external vibration on nanofactory operation, including cyclical moderate- and high-frequency mechanical vibrations that arise from internal operations or which arrive from external sources.

(6) Studies of advanced nanofactories generally should include: (A) design and control of intricate trillion unit systems, where each unit has complex behaviors and physical interactions with other units that must be studied, prototyped, tested, and reworked at various levels of aggregation; (B) design and control of complex flowthrough pathways for feedstock, energy, information, waste intermediates, materials recycling, and so forth; and (C) analysis and design for system reliability including (i) redundancy analysis and design, (ii) analysis and design of switching/handoff schemes among multiple alternate production lines, (iii) analysis of the accumulation rate of dead production lines and the effect of such dead lines on system architecture and operation, and (iv) provision for parts testing and handling/reworking of reject parts and their buffer storage and rerouting through the system.

3.12.5 Task XI-2: Manufacture New FGN with Open Export Plane

Task XI-2 is to manufacture an exact new copy of the FGN (Sections 3.11.5, 3.11.10, and 3.11.11) except that the Export Plane of the second production layer is left incomplete – specifically, the collection cylinders and drainage cylinder are deleted from the design.

The FGN may be manufactured in the manner described in Section 3.11, apparently requiring a ~13 month build time (Section 3.11.10.5). Alternatively, this ~9800 hour build time may be significantly reduced by taking advantage of the ability of the existing FGN to manufacture NMW-3 modules more quickly because this is the principal build-time bottleneck. In particular, the first production layer requires the fabrication and assembly of 10^{16} NMW-3 modules and appurtenant structures for all 1000 fabrication planes totaling 3.800 x 10^{24} atoms of total mass ~70.9 gm (Section 3.11.2.11). A working FGN capable of ~0.01 kg/hour (Section 3.11.3.5) can manufacture this mass of NMW-3 modules and their appurtenant structures in just ~7.1 hours (or in just ~10.6 hours assuming a ~10^{20} atom/sec production rate; Section 3.11.3.5). To this end, the collection cylinders and drainage cylinder of the FGN Export Plane may be removed or deleted, and replaced with a routing plane that collects finished NMW-2 modules into a configuration that facilitates their efficient loading onto MAAs as described in Section 3.11.10.2. The old FGN thus modified now manufactures NMW-3 modules a 1000-fold more quickly than the NMW-2 wafer system (Section 3.11.10.1) and therefore may efficiently replace it in the task of producing new NMW-3 modules for the new FGN.

This substitution being made, the new bottleneck in the efficient manufacture of the new FGN (having an open Export Plane) now becomes the loading of the NMW-3 modules onto the MAAs and the downstream handling of the MAAs. Each MAA can hold 2 x 10^{11} NMW-3 modules, but the old FGN is now producing this many modules every 0.37 sec, which is 1000-fold faster than the ~300 sec MAA loading time realized in Section 3.11.10.2. Further analysis is required to determine how fast MAAs can be processed through subsequent manufacturing stages including inspection (Section 3.11.10.3) and NMW-3 parcel installation (Section 3.11.10.4), but if a fairly modest tenfold increase in processing speed can be achieved then the replication time for the modified FGN should also fall by tenfold, to ~1.3 months.

3.12.6 Task XI-3: Build SGN Assembly System and Vacuum Room

Task XI-3 is to build a macroscale factory for constructing the SGN. The Vacuum Room should be built large enough from the start to accommodate the additional equipment and clearances necessary to use a first FGN to build a second FGN (which will form the base of the first SGN) – perhaps an increase in size from 480 m^3 to ~500 m^3 of useable UHV volume will be sufficient.

The SGN Assembly System is a revised version of the FGN Assembly System (Section 3.11.7) using equipment and procedures that have been modified to include both the accelerated production of the first and second production layers using the old FGN, and also to include the new methods of adding the third production layer using MAAs as described in Section 3.12.7.

3.12.7 Task XI-4: Manufacture and Install 4 Macroassembling Planes and VES on Modified FGN Base

Task XI-4 is to install the third production layer. The manipulators, foundation blocks and associated wiring will be constructed from smaller modules of a type and size that can be manipulated and laid down by the MAAs as described in the Phase X task sequence (e.g., Section 3.11.10).

Assuming that the manufacture of these modules is no longer the process-limiting constraint because module manufacturing is now done by the existing FGN as described in Section 3.12.5, then the primary manufacturing constraint is the rate at which the MAAs can lay down the modules in order to build out the manipulator arrays for each of the four macroassembling planes, plus the VES. We shall assume for this analysis that the manipulators are constructed out of machinery components that are ~1 micron (~1 $micron^3$) in size, or ~2 x 10^{11} atoms per component (assuming Fabrication-Plane equivalent number density of atoms per unit volume; Table X-1). Each MAA can emplace 2 x 10^{11} micron-size components/$micron^3$ during each emplacement cycle because each MAA has 2 x 10^{11} MAMs.

The Dekamicro-Assembly Manipulator (DAM) Plane (Section 3.12.3.2) includes ~1.6 x 10^{23} atoms which demands the emplacement of (1.6 x 10^{23} atoms) / (2 x 10^{11} atoms/component) ~ 8 x 10^{11} machinery components, in turn requiring (8 x 10^{11} components) / (2 x 10^{11} components/MAA-cycle) ~ 4 MAA-cycles to emplace all machinery components of the DAM Plane. If each MAA cycle takes ~640 sec to complete (Section 3.11.10), then construction of the DAM Plane is finished in (4 MAA-cycles) (640 sec/MAA-cycle) ~ 2560 sec (~0.7 hours).

The Hectomicro-Assembly Manipulator (HAM) Plane (Section 3.12.3.3) includes ~1.6 x 10^{24} atoms which demands the emplacement of (1.6 x 10^{24} atoms) / (2 x 10^{11} atoms/component) ~ 8 x 10^{12} machinery components, in turn requiring (8 x 10^{12} components) / (2 x 10^{11} components/MAA-cycle) ~ 40 MAA-cycles to emplace all machinery components of the HAM Plane. If each MAA cycle takes ~640 sec to complete (Section 3.11.10), then construction of the HAM Plane is finished in (40 MAA-cycles) (640 sec/MAA-cycle) ~ 25,600 sec (~7 hours).

The Kilomicro-Assembly Manipulator (KAM) Plane (Section 3.12.3.4) includes ~1.67 x 10^{25} atoms which demands the emplacement of (1.67 x 10^{25} atoms) / (2 x 10^{11} atoms/component) ~ 8 x 10^{13} machinery components, in turn requiring (8 x 10^{13} components) / (2 x 10^{11} components/MAA-cycle) ~ 400 MAA-cycles to emplace all machinery components of the KAM Plane. If each MAA cycle takes ~640 sec to complete (Section 3.11.10), then construction of the KAM Plane is finished in (400 MAA-cycles) (640 sec/MAA-cycle) ~ 256,000 sec (~71 hours).

The Centimeter-Assembly Manipulator (CAM) Plane (Section 3.12.3.5) includes ~8 x 10^{25} atoms which demands the emplacement of (8 x 10^{25} atoms) / (2 x 10^{11} atoms/component) ~ 4 x 10^{14} machinery components, in turn requiring (4 x 10^{14} components) / (2 x 10^{11} components/MAA-cycle) ~ 2000 MAA-cycles to emplace all machinery components of the CAM Plane. If each MAA cycle takes ~640 sec to complete (Section 3.11.10), then construction of the CAM Plane is finished in (2000 MAA-cycles) (640 sec/MAA-cycle) ~ 1.28 x 10^{6} sec (~15 days).

Finally, we must install in the SGN the Vacuum Export System or VES (Section 3.12.3.6). Since virtually all components of the VES are effectively macroscale bulk diamond plates having atomically flat and atomically precise external surfaces, various efficiencies of manufacture can be employed to greatly hasten the assembly process. For example, the usual ~1 micron^3 machinery components can be aggregated into larger ~100 micron^3 blocks by the FGN production system before being passed to the MAAs for final assembly. In this case, each machinery block now incorporates ~2 x 10^{13} atoms/block. The VES plus other unallocated structure of the SGN (Table XI-1) includes ~1.6 x 10^{27} atoms which now demands the emplacement of only (1.6 x 10^{27} atoms) / (2 x 10^{13} atoms/block) ~ 8 x 10^{13} blocks, in turn requiring (8 x 10^{13} blocks) / (2 x 10^{11} blocks/MAA-cycle) ~ 400 MAA-cycles to emplace all blocks comprising the VES. If each MAA cycle takes ~640 sec to complete (Section 3.11.10), then construction of the VES is finished in (400 MAA-cycles) (640 sec/MAA-cycle) ~ 256,000 sec (~71 hours).

Total assembly time for the SGN is therefore the sum of: 1.3 months (FGN base; Section 3.12.5) + 0.7 hours (DAM) + 7 hours (HAM) + 71 hours (KAM) + 15 days (CAM) + 71 hours (VES) ~ 1455 hours (~61 days).

3.12.8 Task XI-5: Manufacture, Attach and Test Appurtenant SGN Support Equipment

Task XI-5 is to manufacture and complete the attachment of support equipment to the completed SGN. This Task is essentially identical to Task X-8 and may proceed in a similar manner, as previously described in Section 3.11.11.

3.12.9 Task XI-6: Demonstration of Diamondoid SGN Production

Task XI-6 is to operate the SGN, once it is completed, in full production mode to verify that it can manufacture atomically precise macroscale product objects at the desired total mass-flow rate of ~0.01 kg/hour (~1 mole/hour).

3.12.10 Task XI-7: Design and Build an Efficient Third-Generation Nanofactory (TGN)

Task XI-7 is to design and build an efficient third-generation nanofactory (TGN). A mill-based low-energy-dissipation nanofabrication system will probably be required to reduce energy usage by 3-4 orders of magnitude to make practical a mature high-throughput ~1 kg/hour diamondoid nanofactory system with a ~1 kW power dissipation as described in Section 2.1.3 and quantified in Table 2-2. Alternative power/control architectures might also be required, since the binary tree architecture employed in the FGN (Section 3.11.2.4) and SGN requires continuous nanotube wires that are too lengthy for the FGN or SGN to manufacture themselves, hence these nanofactories are not strictly capable of complete self-replication because they require some nanotube wires to be provided and installed as "vitamin parts" by the external factory (e.g., the FGN Assembly System; Section 3.11.7).

Room temperature operation at a mechanosynthetic reliability equivalent to that available at T_{SGN} = 109 K operation (Section 3.8.1.3) as assumed here for the FGN (Section 3.11.1) and SGN (Section 3.12.2) may require finding an alternative set of DMS reactions with minimum exoergicities and minimum barriers to accessible pathologies exceeding ΔE_{alt} ~1.10 eV for T_{alt} = 300 K (room temperature operation) or ΔE_{alt} ~ 1.00 eV for T_{alt} ~ 273 K (ice-water coolant operation) where $\exp(-\Delta E_{MinToolset} / k_B T_{SGN}) = \exp(-\Delta E_{alt} / k_B T_{alt})$ – a major challenge, since this is significantly higher than the $\Delta E_{MinToolset}$ = 0.40 eV value available using the minimal DMS toolset[1319] that has been assumed in all prior Phases. Using T_{SGN} = 127 K – which would yield a DMS-related error rate of similar magnitude to other error sources (Section 3.8.1.3) – requires a minimum of ΔE_{alt} ~0.95 eV for T_{alt} = 300 K or ΔE_{alt} ~ 0.86 eV for T_{alt} ~ 273 K, still a significant technical challenge.

Energy efficiency is another paramount challenge: It is well known that molecular machines can operate arbitrarily close to chemical equilibrium at every instant of the cycle, and still perform work at the rate of several micrometers per second against piconewton loads.[1320] (Notes

---

[1319] Robert A. Freitas Jr., Ralph C. Merkle, "A Minimal Toolset for Positional Diamond Mechanosynthesis," J. Comput. Theor. Nanosci. 5(May 2008):760-861.

[1320] R. Dean Astumian, "Adiabatic operation of a molecular machine," Proc. Natl. Acad. Sci. 104(11 December 2007):19715-19718. See also: Lisa Zyga, " 'Kind and Gentle' Molecular Machine Could Operate at Near-Equilibrium," PhysOrg.com, 20 December 2007, http://www.physorg.com/news117366760.html.

Astumian:[1321] "In the molecular world, we can truly have motors that operate with nearly 100% efficiency.") This energy-efficient nanofactory system would be a third-generation nanofactory (TGN) and perhaps the most valuable product of the SGN.

The total mass of the diamondoid TGN components listed in Table 2-2 is only <0.112 kg. Drexler[1322] adds: "Allowing 1 kg/m^3 for internal compressive structure to support external atmospheric pressure adds ~0.05 kg; allowing 0.1 kg/m^2 to provide for a sturdy case, rubber feet, and the like adds ~0.08 kg. These masses sum to <0.25 kg. Allowing as much as 0.75 kg for other subsystems yields an estimated total system mass <1 kg." If a TGN can be designed using a modular architecture for easy convergent assembly, this high-throughput desktop system could be manufactured very quickly using the SGN if its mass lies in the ~1 kg range and if the SGN has a mass throughput of ~0.01 kg/hour – giving, for example, a build time for a mature diamondoid nanofactory of (1 kg) / (0.01 kg/hour) ~ 100 hours (~4 days) using the SGN.

A typical diamondoid nanomachinery density, using ~3510 kg/m^3 diamond building materials, is ~2400 kg/m^3, as specified for typical FGN or SGN products which are about two-thirds (~68%) solid diamond and about one-third (~32%) vacuum, by volume (Section 3.11.3.4). The overall "dry" nanomachinery density is only ~362 kg/m^3 for the entire SGN (Section 3.12.3.7) because the SGN includes large hollow internal volumes for cooling channels, overhead parts clearances, parts stovepipes, parts passthroughs, and the like. Taking a similar ~362 kg/m^3 for a ~1 kg TGN gives a total nanofactory volume (including ~90% empty space as in the SGN) of: (1 kg) / (362 kg/m^3) ~ 2762 cm^3. Allowing ~4 times more empty space (i.e., another ~7238 cm^3) for additional parts clearances raises TGN volume to ~10,000 cm^3, consistent with the ~100 kg/m^3 nanomachinery density figure cited in *Nanosystems*[1323] that yields the same result.[1324] A 10,000 cm^3 TGN would thus include ~2.85% (~285 cm^3) of solid diamond and ~97.15% (~9,715 cm^3) of empty space.

A ~10,000 cm^3 TGN can have dimensions of 25 cm x 40 cm x 10 cm, a product object footprint identical to the maximum product size that can be manufactured by the SGN (Section 3.12.3). A ~10 cm height for the TGN is roughly consistent with (a) the sum of all ten product scales of ~10.51 cm, or (b) the sum of all ten mechanism scales of ~21.02 cm from Table 2-2, assuming all

---

[1321] R. Dean Astumian, "Adiabatic operation of a molecular machine," Proc. Natl. Acad. Sci. 104(11 December 2007):19715-19718. See also: Lisa Zyga, " 'Kind and Gentle' Molecular Machine Could Operate at Near-Equilibrium," PhysOrg.com, 20 December 2007, http://www.physorg.com/news117366760.html.

[1322] K. Eric Drexler, Nanosystems: Molecular Machinery, Manufacturing, and Computation, John Wiley & Sons, New York, 1992, Section 14.4.4 "Mass and volume", pp. 424-425.

[1323] K. Eric Drexler, Nanosystems: Molecular Machinery, Manufacturing, and Computation, John Wiley & Sons, New York, 1992, Section 14.4.4 "Mass and volume", pp. 424-425.

[1324] *Nanosystems* additionally – and apparently unnecessarily – allowed for an extra ~10,000 cm^3 of workspace volume to accommodate low-density (~100 kg/m^3) product objects or their intermediates for each of three highest-level manipulator stages, then multiplied the resulting ~30,000 cm^3 allowance by an additional factor of 1.66 "to allow for packing inefficiencies, cooling channels, and so forth," yielding an excessively large nanofactory volume of ~50,000 cm^3.

such products or mechanisms are vertically stacked inside the nanofactory. One TGN could then be manufactured every ~4 days by one SGN (see above).

4. Program Development Timelines

The speed at which the Nanofactory Development Program can be executed is of great interest to researchers and investors alike. The pace of development will be determined by many factors both tangible and intangible, and cannot be precisely calculated in advance because the program is a very long-term effort and may face currently unforeseeable obstacles during its execution. The duration of the program is also dependent upon the magnitude and timing of financial resources that are directed toward completing program tasks, the tightness of focus on the program agenda that can be maintained by the program directors, the availability of scientific and engineering personnel qualified to participate in the program, and the possible emergence of competing efforts once it becomes clear to the mainstream nanoscience community that program goals are both technically feasible and economically worthy of aggressive pursuit.

4.1 Four Scenarios for Nanofactory Development

In view of the above uncertainties, at least four basic scenarios for diamondoid nanofactory development are readily conceived:

(1) **Aggressive**. In the aggressive scenario, all tasks are pursued in parallel whenever possible. This scenario assumes that (a) the pathway outlined in this proposal is exactly correct and can be executed essentially as described, and (b) all necessary human and financial resources are made available to pursue all program objectives at the greatest possible speed (i.e., the program has effectively unlimited funding). Estimated time to completion: 15-20 years.

(2) **Efficient**. In the efficient scenario, resources are allocated to program objectives in a rational manner designed to keep the entire program moving forward smoothly. Multiple tasks are pursued in parallel and some efforts are devoted to multiple Phases simultaneously, but there is a strong emphasis on completing the current Phase to the extent necessary to enable the successful completion of subsequent Phases. This scenario assumes that (a) the pathway outlined in this proposal is largely correct and can be executed essentially as described, but (b) human and financial resources are limited and thus are insufficient to allow pursuit of numerous multiple program objectives simultaneously. Estimated time to completion: 20-25 years.

(3) **Conservative**. In the conservative scenario, each program Phase is required to be completed essentially in full before performing any significant work on the next program Phase – that is, proof is demanded and provided that each Phase is successful before any resources are committed to the next Phase of development. This scenario assumes that (a) the funding source is uncertain as to the technical feasibility of each Phase and wants proof before committing additional funds, or (b) the funding source seeks to generate some level of economic return from the completed Phase, perhaps for the purpose of offsetting some of the costs anticipated to be incurred in the next Phase of the work. Estimated time to completion: 30-40 years.

(4) **Supine**. In the supine scenario, the nanofactory development program is not directly pursued with any significant dedicated resources by any organization. The program objectives are achieved only randomly with the slow accumulation of relevant theoretical and experimental successes as the inevitable outcome of the natural evolutionary pace of research in mainstream nanoscience and nanoengineering. This scenario assumes that (a) the proposed program as described is not regarded as technically feasible or fund-worthy, and as a result (b) the program is

not directly funded. The supine scenario is the passive "do nothing" benchmark for the three active scenarios described earlier. Estimated time to completion: 40-50 years.

4.2 An Efficient Timeline for Nanofactory Development

Table 4-1 provides a summary timeline for nanofactory development, based on a prioritized list of subtasks compiled from the text of this proposal.

Table 4-1. An Efficient Timeline for the Diamondoid Nanofactory Development Program

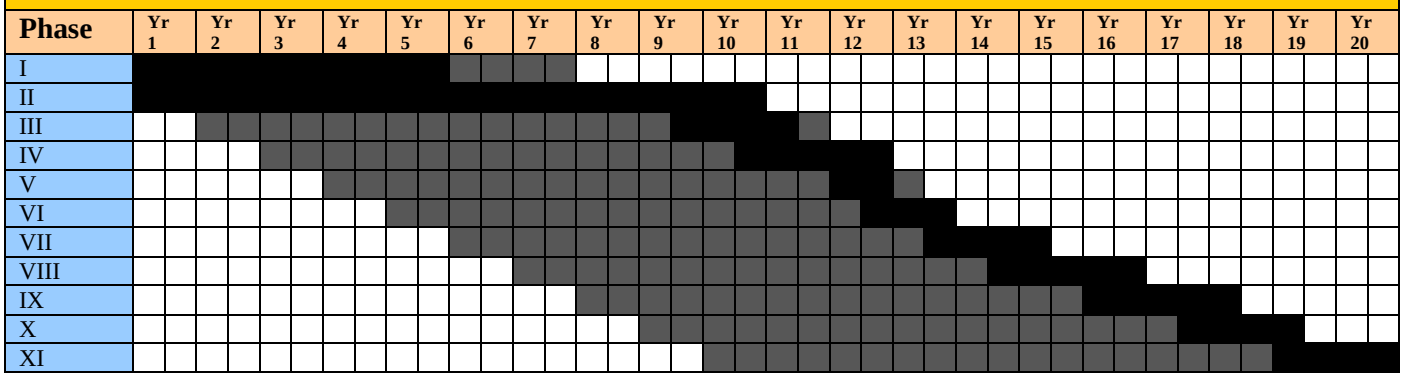

4.3 Summary and Conclusions

We have presented a development program for the Phase XI nanofactory. The Phase XI nanofactory, while energy intensive and requiring significant external support infrastructure (cooling, power, high purity feedstock, vacuum system, computer control system, and more) both to build and to operate, will be able to manufacture a wide range of hydrocarbons, including diamond, graphite, fullerenes, single and multi-walled nanotubes of controlled chirality, lonsdaleite, polyynes, and other products with atomically precise control of shape and structure. The nanofactory is designed to build individual parts (single molecules) that are atomically precise up to 100 nanometers in linear dimension and assemblies of parts of a size up to several centimeters. Total production capacity of an individual Phase XI nanofactory is estimated to be ~0.01 kg/hour. Besides using hydrogen and carbon, the system also uses small amounts of germanium for catalytic purposes. The ability to manufacture atomically precise structures that include other elements, though desirable (and likely to occur for a few additional elements during the development process), is not specifically required for the manufacture of the Phase XI system.

In each Phase of this program, we analyze the total mass output of the system (production capacity in atoms or kilograms per unit time); the power requirements; heat dissipation (including thermal and cooling issues); speed of operation; control requirements and frequency of control signals; the positional accuracy of the positional devices in the face of thermal noise at the appropriate operating temperature; temperature of mechanosynthesis and consequent reliability of unit synthesis operations (based on the reactions described in *A Minimal Toolset for Diamond Mechanosynthesis*); the vacuum required; feedstock requirements and feedstock feed mechanisms appropriate to each phase; the specific temperatures of operation in each Phase

required to maintain feedstock as either gas or liquid, as required; the flow of parts, sub-assemblies and assemblies; the size, organization, and forces exerted by the required manipulators; the required infrastructure of non-atomically-precise mechanisms (refrigeration systems, vacuum systems, power supplies, handling and manipulation of modules); the apparent overall system reliability; the ability to manufacture each Phase N system using only capabilities demonstrated in Phases N-1 and earlier (for N = I to XI); and various other issues that seem critical to the feasibility of the overall development program.

We conclude that a multi-year development program for the Phase XI (or similar) system is feasible and should be pursued.